

Advanced Combustion Engines and Fuels

2018 Annual Progress Report

Vehicle Technologies Office

(This page intentionally left blank)

Disclaimer

This report was prepared as an account of work sponsored by an agency of the United States government. Neither the United States government nor any agency thereof, nor any of their employees, makes any warranty, expressed or implied or assumes any legal liability or responsibility for the accuracy, completeness, or usefulness of any information, apparatus, product, or process disclosed or represents that its use would not infringe privately owned rights. Reference herein to any specific commercial product, process, or service by trade name, trademark, manufacturer, or otherwise does not necessarily constitute or imply its endorsement, recommendation, or favoring by the United States government or any agency thereof. The views and opinions of authors expressed herein do not necessarily state or reflect those of the United States government or any agency thereof.

Acknowledgements

We would like to express our sincere appreciation to Alliance Technical Services, Inc., and Oak Ridge National Laboratory for their technical and artistic contributions in preparing and publishing this report.

In addition, we would like to thank all the participants for their contributions to the programs and all the authors who prepared the project abstracts that comprise this report.

Acronyms

List of Abbreviations, Definitions, and Nomenclature

0D	zero-dimensional
124 TMB	1,2,4-trimethylbenzene
1D	one-dimensional
2D	two-dimensional
3D	three-dimensional
6AU	six-speed automatic transmission
6-PPD	antioxidant N-(1,3-dimethylbutyl)-N'-phenyl-p-phenylenediamine
8AU	eight-speed automatic transmission
A30	Co-Optima gasoline blend containing 30% aromatics, by volume
ACEC	Advanced Combustion and Emissions Control
ACI	advanced compression ignition
ACS	Advanced Combustion Systems
ADC	advanced distillation curve
ADM	actuator driver module
AEC	Advanced Engine Combustion
AF	air-fuel ratio
AFIDA	Advanced Fuel Ignition Delay Analyzer
AFR	air-fuel ratio
aHR	accumulated heat release
AHRR	apparent heat release rate
AIAA	American Institute of Aeronautics and Astronautics
AKI	anti-knock index
Al	aluminum
ALE	arbitrary Lagrangian-Eulerian
ALK	Predominantly alkylate-containing Co-Optima gasoline blend
AMFI	additive mixing fuel injection (new low-temperature gasoline combustion control system)
ANL	Argonne National Laboratory
ANN	artificial neural network
Ar	argon

ASME	American Society of Mechanical Engineers
ASOI	after the start of injection
ASTM	ASTM International, formerly American Society for Testing and Materials
atdc	after top dead center
aTDC	after top dead center
ATDC	after top dead center
aTDC _f	after top dead center firing
atm	atmosphere(s)
a.u.	arbitrary units
AVFL	Advanced Vehicles/Fuels/Lubricants
bar(a or -a)	bar (absolute)
BDC	bottom dead center
BMEP	brake mean effective pressure
BOB	blendstock for oxygenate blending
BP	boiling point
BP	band pass
BSFC	brake specific fuel consumption
BTDC	before top dead center
BTE	brake thermal efficiency
BTU	British thermal unit
BW	beam warming
C	carbon
C	Celsius
C ₂	hydrocarbon with two carbon atoms
C ₄	hydrocarbon with four carbon atoms
Ca	capillary number
CA	California
CA	crank angle
CA10	crank angle at 10% mass fraction burned
CA25	crank angle at 25% mass fraction burned
CA50	crank angle at 50% mass fraction burned

CA75	crank angle at 75% mass fraction burned
CA90	crank angle at 90% mass fraction burned
CAD	crank angle degree(s)
CB	carbon black
CC	close-coupled
CCD	charged-coupled device
CCV	cycle-to-cycle variation
CDA	cylinder deactivation
CDC	conventional diesel combustion
cDPF	catalyzed diesel particulate filter
Ce	cerium
CEI	controlled electronic ignition
CFA	certification Fuel A
CFD	computational fluid dynamics
CFH	Central Fuel Hypothesis
CFL	Courant–Friedrichs–Lewy
CFP	capillary flow porometry
CFPH	central fuel property hypothesis
CFR	Cooperative Fuel Research
CH ₄	methane
CHA	chabazite
CH ₂ O	formaldehyde
cHOV	cumulative heat of vaporization
CHT	conjugate heat transfer
CI	compression ignition
CLEERS	Cross-Cut Lean Exhaust Emissions Reduction Simulations
CLSVOF	combined level-set volume of fluid
cm	centimeter(s)
cm ³	cubic centimeter(s)
CMC	conditional moment closure
CNG	compressed natural gas

CO	Colorado
CO	carbon monoxide
CO ₂	carbon dioxide
Co-Optima	Co-Optimization of Fuels and Engines
CoV	coefficient of variation
COV IMEP	coefficient of variation in indicated mean effective pressure
CPD	cells per diameter
CPFR	constant pressure flow rig
CPOX	Catalytic Partial Oxidation
CPU	central processing unit
CR, cr	compression ratio
CRADA	cooperative research and development agreement
CRC	Coordinating Research Council
CS	catalytic stripper
CT	computed tomography
Cu	copper
CV	cross validation
cyc	cycle
d	day
dATDC	degrees above top dead center
dB	decibel(s)
DBE	double bond equivalent
dbTDC	degrees before top dead center
dBTE	delta brake thermal efficiency
DC	District of Columbia
DCN	derived cetane number
DDI-PFS	double direct injection partial fuel stratification
deg	degrees
DeG	degreened
D-EGR	dedicated exhaust gas recirculation
DENOX	an active selective catalytic reduction system

DFI	ducted fuel injection
DI	direct injection
DIB	diisobutylene
DSC	differential scanning calorimetry
DISI	direct injection spark ignition
DLC	diamond-like carbon
D_{nozz}	injector nozzle diameter
DNPH	2,4-dinitrophenylhydrazine
DNS	direct numerical simulation
DOC	diesel oxidation catalyst
DOE	U.S. Department of Energy
DOI, doi	digital object identifier
DOSY	diffusion ordered spectroscopy, an NMR spectroscopic technique for measuring diffusion coefficients
DPF	diesel particulate filter
DRFF	deactivation roller finger follower
DSF	Dynamic Skip Fire
DSR	dynamic species reduction
E0	gasoline
E10	10% ethanol, 90% gasoline blend
E20	20% ethanol, 80% gasoline blend
E30	30% ethanol, 70% gasoline blend
E50	50% ethanol, 50% gasoline blend
E85	85% ethanol, 15% gasoline blend
EA IMEP	electronically assisted indicated mean effective pressure
ECN	Engine Combustion Network
EC	elemental carbon
EEE	certification gasoline
EEPS	engine exhaust particle sizer
EFA	Exhaust Filtration Analysis
e.g.	exempli gratia, (Latin, meaning for example)
EGR	exhaust gas recirculation

EPA	U.S. Environmental Protection Agency
EINO _x	emissions index of nitrous oxide
EOC	end of compression
EPA	Environmental Protection Agency
ERC	Engine Research Center at University of Wisconsin–Madison
et al.	et alii (Latin, meaning and others)
etc.	et cetera (Latin, meaning and the rest)
EtOH	ethanol
eV	electronvolt
EVC	exhaust valve closing
EVO	exhaust valve opening
eVOF	evaporation submodel
FACE	Fuels for Advanced Combustion Engines
FBP	final boiling point
FDF	filtered density function
Fe	iron
FE	fuel efficiency
FEARCE	Fast, Easy, Accurate and Robust Continuum Engineering (formerly KIVA-hpFE)
FEM	finite element method
FID	flame ionization detector
FMEP	friction mean effective pressure
FPF	front propagation formulation
FREI	Flames with Repetitive Extinction and Ignition
FSN	filter smoke number
ft	foot, feet
ft-lb	foot pounds
FTE	freight ton efficiency
FTIR	Fourier-transform infrared spectroscopy
FTP	Federal Test Procedure
ft/s	feet per second
FWG	Fuels Working Group

FY	Fiscal Year
g	gravity
g	gram(s)
G'	dynamic stiffness
gal	gallon
GCI	gasoline compression ignition
GDI	gasoline direct injection
GDCI	gasoline direct injection compression ignition
GHG	greenhouse gas
GHRR	gross heat release rate
GM	General Motors
GMRES, gmres	generalized minimal resolution method
GO	graphene oxide
GOC	gas oxidation catalyst
GP	Gaussian process
GPF	gasoline particulate filter
GPU	graphics processing unit
GTL1	gas-to-liquids derived fuel number one
GWU	George Washington University
GVW	gross vehicle weight
h	hour(s)
H ₂	diatomic hydrogen
H ₂ O	water
H ₂ O ₂	hydrogen peroxide
H-bonding	hydrogen bonding
H/C	hydrogen-to-carbon ratio
HC	hydrocarbon
HCCI	homogeneous charge compression ignition
HD	heavy-duty
HDD	heavy-duty diesel
HDR	high dynamic range

HECO-SING	High-Efficiency Cost-Optimized, Spark-Ignited Natural Gas
HEGO	exhaust oxygen sensor
HFIR	High Flux Isotope Reactor
HFS	high fuel stratification
HHDDT	heavy heavy-duty diesel truck
HiDos	high use of controlled ammonia dosing
HMN	hepta-methyl-nonane
HO	high-olefin gasoline (a Co-Optima core fuel)
HO ₂	hydroperoxyl radical
HOV, HoV	heat of vaporization
hp	horsepower
HPC	high-performance computing
HPF	high-performance fuel
hp-hr	horsepower-hour
HP PTWA	high porosity plasma transfer wire arc
hr	hour(s)
HRA	heat release analysis
HRR	heat release rate
HT	high temperature
HVAC	heating, ventilation, and air conditioning
HWFET	Highway Fuel Economy Test
Hz	Hertz
IBP	initial boiling point
ICCD	intensified charge-couple device
ICE	internal combustion engine
ICLASS	International Conference on Liquid Atomization and Spray Systems
ID	ignition delay
IDT	ignition delay time
i.e.	id est, (Latin meaning that is)
IL	Illinois
IMEP	indicated mean effective pressure

IMEPg	gross indicated mean effective pressure
IMEPn	net indicated mean effective pressure
in	inch(es)
IQR	interquartile range
IQT	ignition quality tester
IR	infrared
IS	indicated specific
ISBN	International Standard Book Number
ISCO	indicated specific carbon monoxide
ISFC	indicated specific fuel combustion
ISG	integrated starter generator
ISHC	indicated specific hydrocarbon
ISNO _x	indicated specific nitrogen oxides
ISSoot	indicated specific soot
IVC	intake valve closing
IVO	intake valve opening
J	joule
K	Kelvin
K	empirically determined coefficient that varies with operating conditions
KC	kinetically controlled
kg	kilogram(s)
KH	Kelvin Helmholtz
KH-RT	Kelvin Helmholtz–Rayleigh Taylor
kHz	kilohertz
kJ	kilojoule(s)
KLSA	knock limited spark advance
kPa	kilopascal(s)
kV	kilovolt(s)
kW	kilowatt(s)
kWh, kW-hr	kilowatt-hour(s)
L	liter(s)

LANL	Los Alamos National Laboratory
LB	lattice-Boltzmann
lbs	pounds
LD	long-dwell
LD	light-duty
LDR	low dynamic range
LE	Lagrangian–Eulerian
LED	light-emitting diode
LES	large eddy simulation
LFS	laminar flame speed
LIF	lasar induced fluorescence
LHT	low heat transfer
LHV	lower heating value
Li	lithium
LIVC	late intake valve closing
LLC	Limited Liability Company
LLNL	Lawrence Livermore National Laboratory
LMC	lean Miller cycle
LNF	lean NO _x filter
LNT	lean NO _x trap
LPG	liquefied petroleum gas
L-S	Lean-Stoich (operating either full lean or stoichiometric)
LS	lean stratified
LSPI	low speed pre-ignition
LSU	Louisiana State University
LT	low temperature
LTC	low-temperature combustion
LTGC	low-temperature gasoline combustion
LTHR	low-temperature heat release
LTP	low-temperature plasma
LVF	liquid volume fraction

LWP	long wave pass
m ²	square meter(s)
m ³	cubic meter(s)
MAP	manifold absolute pressure
MAPO	maximum amplitude pressure oscillation
MCCI	mixing-controlled compression ignition
MCE	multi-cylinder engine
MCP	methylcyclopentane
MD	Maryland
MD	medium-duty
MEMS	micro-electromechanical system
MF	merit function
MFB	mass fraction burned
Mg	magnesium
mg	milligram(s)
M/G	motor/generator
mi	mile(s)
MI	Michigan
min	minute(s)
MIP	mercury intrusion porosimetry
mJ	millijoule(s)
mL	milliliter(s)
mm	millimeter(s)
mo	month(s)
mol	mole, molar
mol%	mole fraction
MON	Motor Octane Number
MPa	megapascal(s)
mpg	mile(s) per gallon
mph	mile(s) per hour
MPI	Message Passing Interface

ms	millisecond(s)
m/s	meter(s) per second
MS	mail stop
MSS	microsoot sensor
MTU	Michigan Technological University
MW	megawatt(s)
N	nitrogen
N30	Co-Optima gasoline blend containing 30% naphthenes by volume
NG	natural gas
NH ₃	ammonia
Ni	nickel
NIOSH	National Institute of Occupational Safety and Health
nm	nanometer(s)
NMEP	net mean effective pressure
NMOG	non-methane organic gases
NMR	nuclear magnetic resonance spectroscopy
NO	nitric oxide
NO _x	oxides of nitrogen
NR	natural rubber
NREL	National Renewable Energy Laboratory
ns	nanosecond(s)
NSC	NO _x storage catalyst
NSFC	net specific fuel consumption
NTC	negative temperature coefficient
NVO	negative valve overlap
O	atomic oxygen
O ₂	diatomic oxygen
[O ₂]	oxygen mole fraction
O ₃	ozone
O30	Co-Optima gasoline blend containing 30% olefins by volume
OC	organic carbon

OC	oxidation catalyst
OD	optical density
OD	optical depth
OEM	original equipment manufacturer
OH	hydroxyl radical
OHC	oxidation half cycle
OI	octane index
ON	octane number
ORC	organic Rankine cycle
ORNL	Oak Ridge National Laboratory
OS	octane sensitivity
OXYL	o-xylene
P	phosphorus
P	pressure
P&D	production and delivery
PAH	polycyclic aromatic hydrocarbon
P_{amb}	ambient pressure
PB	particulate blackening
PB	production bore
P_c	compressed pressure
PCG	Los Alamos National Laboratory's Parallel Conjugate Gradient solver package
PCP	peak cylinder pressure
PCV	positive crankcase ventilation
P_{cyl}	cylinder pressure
Pd	palladium
PF	particulate filter
PFI	port fuel injection
PFS	partial fuel stratification
PGM	platinum group metal
phr	part(s) per hundred rubber
P_{in}	intake pressure

P_{inj}	injection pressure
PIONA	paraffins, iso-paraffins, olefins, naphthenes, and aromatics
PLIF	planar laser-induced fluorescence
PLII	planar laser-induced incandescence
PM	particulate matter
PMI	Particulate Matter Index
PN	particulate number
PNA	passive NO _x adsorber
PNNL	Pacific Northwest National Laboratory
POSF	fuels designator
ppm	parts per million
PRF	primary reference fuel
PSD	partical size distribution
psi	pound(s) per square inch
psig	pound(s) per square inch gauge
Pt	platinum
PT	pressure–temperature
PTWA	plasma transfer wire arc
PVD	physical vapor deposition
Q1	first quarter
Q2	second quarter
Q3	third quarter
Q4	fourth quarter
r/min	revolutions per minute
RANS	Reynolds-averaged Navier–Stokes
Rc	compression ratio
RCCI	reactivity controlled compression ignition
RCM	rapid compression machine
R&D	research and development
RD5-87	research-grade regular E10 gasoline
RD5-87A	research-grade regular E10 gasoline, AKI = 88, RON = 92.0

RD5-87B	research-grade regular E10 gasoline, AKI = 87, RON = 90.6
Re	Reynolds number
rGO	reduced graphene oxide
Rh	rhodium
RHC	reduction half cycle
RI	ringing intensity
RIM	refractive index matching
RMCSET	ramped model cycle supplemental emissions test
RON	Research Octane Number
rpm, RPM	revolution(s) per minute
RSD	rainbow schlieren deflectometry
RVP	Reid vapor pressure
s	second(s)
S	sensitivity
S	sulfur
S	octane sensitivity ($S = \text{RON} - \text{MON}$)
S1	existing surrogate blends based on matching RON, S, H/C, and stoichiometric air/fuel ratio
S2	new surrogate blends, based on matching the hydrocarbon classes in the detailed hydrocarbon analyses
SAE	SAE International, formerly the Society of Automotive Engineers
SAMR	scattering-absorption measurement ratio
SBR	styrene-butadiene-rubber
SBS	styrene-butadiene-styrene
sccm	standard cubic centimeters per minute
SCE	single cylinder engine
SCO	selective catalytic oxidation
SCR	selective catalytic reduction
SCRE	single-cylinder research engine
SCRF	integrated selective catalytic reduction and diesel particulate filter
sec	second(s)
SEM	scanning electron microscopy

Si	silicon
SI	spark ignition
SIDI	spark ignition direct injection
SI-MF	spark ignition merit function
S'_{\max}	maximum torque from rheometer cure test
S'_{\min}	minimum torque from rheometer cure test
SMC	stoichiometric Miller cycle
SMD	Sauter mean diameter
SNL	Sandia National Laboratories
SOI	start of injection
SPH	smoothed particle hydrodynamics
S/S	start–stop
SS	steady-state
SSE	start of solenoid energizing
SSZ-13	aluminosilicate zeolite
ST1	SuperTruck 1
ST2	SuperTruck 2
SUV	sport-utility vehicle
SV	space velocity
SWI	spray–wall interaction
T	temperature
T	time
T_{50}	temperature at which a catalyst achieves 50% conversion of a particular species
T_{90}	temperature at which a catalyst achieves 90% conversion of a particular species
TBC	thermal barrier coating
TBD	to be determined
T_{BDC}	temperature at bottom dead center
T_c	compressed temperature
TC	turbocharger
TCC	transparent combustion chamber
TCO	total cost of ownership

T_{coolant}	coolant temperature
TCR	thermochemical recuperation
TDC	top dead center
TE	thermal efficiency
TEM	transmission electron microscopy
TFM	tabulated flamelet model
TGA	thermogravimetric analysis
THC	total hydrocarbons
T_{in}	intake temperature
TN	Tennessee
TPD	temperature programmed desorption
TPR	temperature programmed reduction
TPRF	toluene primary reference fuel
TS	thermal stratification
TSF	toluene standardization fuel
TWC	three-way catalyst
UA	University of Alabama
UBHC	unburned hydrocarbons
UDDS	Urban Dynamometer Driving Schedule
UDF	user defined function
UEGO	exhaust oxygen sensor
UM	University of Michigan
UPS	United Parcel Service
U.S.	United States
US06	Supplemental Federal Test Procedure
USAX	Sultra-small angle X-ray scattering
USC	University of South Carolina
USCAR	United States Council for Automotive Research LLC
U.S. DRIVE	United States Driving Research and Innovation for Vehicle Efficiency and Energy Sustainability
UV	ultraviolet
V	volt

V0b	version 0b diesel fuel surrogate
viz.	videlicet (Latin meaning namely, in other words)
VN	vanadium nitride
VOF	volume of fluid
vol%	percent by volume
VP	vice president
VP (443K)	vapor pressure at 443 K
vs.	versus
WA	Washington
WBG	wood-based biogasoline
WCAC	water charge air cooler
WGS	water-gas-shift
WHR	waste heat recovery
wk	week(s)
wt%	weight of the component divided by total sample weight, multiplied by 100
XPS	X-ray photoelectron spectroscopy
XRD	X-ray diffraction
YSI	yield sooting index
Zero-RK	Zero-Order Reaction Kinetics combustion software package

List of Symbols

Å	angstrom
°	degree(s)
°aTDC, °ATDC	degree(s) after top dead center
°C	degree(s) Celsius
°CA	degree(s) crank angle
°F	degree(s) Fahrenheit
ΔMerit	change in merit score
ΔP	pressure difference
ΔRON	change in research octane number
ΔS	change in octane sensitivity
ΔS	S' max - S' min, change in torque from rheometer cure test
f	impingement frequency
γ	ratio of specific heats
η _f	fuel-conversion efficiency
>	greater than
<	less than
μ	micron(s)
μg	microgram(s)
μL	microliter(s)
μL/min	microliter(s) per minute
μm	micrometer(s)
μs	microsecond(s)
%	percent
Ø	diameter
λ	equivalence ratio (ratio of actual air-to-fuel ratio to stoichiometric air-to-fuel ratio)
φ _m	fuel/charge-mass equivalence ratio (the same as φ, but the fuel is normalized by the total charge mass rather than only the air mass (Sjoberg II.5 definition: mass-based fuel-air equivalence ratio))
Φ	phi-sensitivity metric
Φ _S *	normalized phi-sensitivity
ρ _{amb}	ambient density

Executive Summary

On behalf of the Vehicle Technologies Office of the U.S. Department of Energy, we are pleased to introduce the Fiscal Year 2018 Annual Progress Report for the Advanced Combustion Engines and Fuels Program. In support of the Vehicle Technology Office's goal for future U.S. economic growth, the Program focuses early-stage research and development on improving the understanding of combustion processes, fuel properties, and emissions control technologies, generating knowledge and insight necessary for industry to develop the next generation of engines and fuels for the efficient, cost-effective, and secure transportation of people and goods across America.

One of the most promising and cost-effective approaches to improving the fuel economy of the U.S. vehicle fleet is to introduce the next generation of higher-efficiency, very-low-emission combustion engines that meet future federal emissions regulations into the passenger and commercial vehicle markets. Advanced fuel formulations that can incorporate non-petroleum-based blending agents could further enhance engine efficiency, reduce greenhouse gas emissions, and provide fuel diversification. Also, innovations in combustion, fuels, emissions control, air control, turbomachinery, and energy recovery could potentially increase fuel economy considerably compared to today's vehicles. The expected national economic, environmental, and energy security benefits from these next-generation engines and fuels would be significant inasmuch as the majority of vehicles sold over the next several decades will still include an engine.

The Program has set the following goals for passenger and commercial vehicle fuel economy improvements.

- By 2025, improve light-duty engine efficiency to demonstrate 35% improvement in passenger vehicle fuel economy (25% improvement from engine efficiency and 10% from fuel co-optimization), relative to a 2015 baseline vehicle, while meeting U.S. Environmental Protection Agency Tier 3 emissions standards
- By 2025, improve heavy-duty engine efficiency by 35% relative to a 2009 baseline vehicle and identify cost-effective high-performance fuels that can further increase efficiency up to an additional 4%, while meeting prevailing U.S. Environmental Protection Agency emissions standards

This report highlights progress achieved by the Advanced Combustion Engines and Fuels Program during Fiscal Year 2018. The nature, current focus, and recent progress of the Program are described together with summaries of national laboratory, industry, and university projects that provide an overview of the exciting work being conducted to address critical technical barriers and challenges to commercializing the next generation of higher-efficiency engine, emissions control, and fuel technologies for passenger and commercial vehicles.

Gurpreet Singh, Program Manager
Advanced Combustion Engines and Fuels Program
Vehicle Technologies Office

Kenneth C. Howden
Vehicle Technologies Office

Kevin Stork
Vehicle Technologies Office

Roland M. Gravel
Vehicle Technologies Office

Michael Weismiller
Vehicle Technologies Office

Table of Contents

Acknowledgements.....	ii
Acronyms.....	iii
List of Abbreviations, Definitions, and Nomenclature	iii
List of Symbols.....	xxi
Executive Summary	xxii
List of Figures.....	xxviii
List of Tables.....	lii
Vehicle Technologies Office Overview.....	1
Organization Chart.....	1
Advanced Combustion Engines and Fuels Program Overview	2
Introduction	2
Goals	2
State of the Art	2
Current Technical Focus Areas and Objectives.....	4
Technical Highlights	7
Invention and Patent Disclosures	28
I. Combustion Research	30
I.1 Light- and Medium-Duty Diesel Combustion (Sandia National Laboratories).....	30
I.2 Heavy-Duty Low-Temperature and Diesel Combustion and Heavy-Duty Combustion Modeling (Sandia National Laboratories)	36
I.3 Spray Combustion Cross-Cut Engine Research (Sandia National Laboratories)	45
I.4 Low-Temperature Gasoline Combustion (LTGC) Engine Research (Sandia National Laboratories).....	51
I.5 Gasoline Combustion Fundamentals (Sandia National Laboratories).....	60
I.6 Advancements in Fuel Spray and Combustion Modeling with High Performance Computing Resources (Argonne National Laboratory).....	68
I.7 Fuel Injection and Spray Research Using X-Ray Diagnostics (Argonne National Laboratory)	75
I.8 RCM Studies to Enable Gasoline-Relevant Low Temperature Combustion (Argonne National Laboratory)	81
I.9 Advances in High Efficiency Gasoline Compression Ignition (Argonne National Laboratory)	88
I.10 Advanced Ignition Systems for Gasoline Direct Injection (GDI) Engines (Argonne National Laboratory)	93
I.11 Stretch Efficiency for Combustion Engines: Exploiting New Combustion Regimes (Oak Ridge National Laboratory)	99
I.12 Neutron Imaging of Advanced Transportation Technologies (Oak Ridge National Laboratory).....	105

I.13	Chemical Kinetic Models for Advanced Engine Combustion (Lawrence Livermore National Laboratory).....	111
I.14	Model Development and Analysis of Clean and Efficient Engine Combustion (Lawrence Livermore National Laboratory).....	116
I.15	2018 FEARCE Development: A Robust and Accurate Engine Modeling Software (Los Alamos National Laboratory).....	121
I.16	Accelerating Predictive Simulation of Internal Combustion Engines with High Performance Computing (Oak Ridge National Laboratory).....	129
I.17	Development and Validation of Predictive Models for In-Cylinder Radiation and Wall Heat Transfer (The Pennsylvania State University).....	135
I.18	Model Development for Multi-Component Fuel Vaporization and Flash Boiling (University of Illinois at Urbana-Champaign).....	141
I.19	Spray-Wall Interaction at High-Pressure and High-Temperature Conditions (Michigan Technological University).....	146
I.20	Development and Validation of a Lagrangian Soot Model Considering Detailed Gas Phase Kinetics and Surface Chemistry (University of Wisconsin).....	154
I.21	Development and Validation of Physics-Based Submodels of High Pressure Supercritical Fuel Injection at Diesel Conditions (The University of Alabama).....	160
I.22	Development of a Physics-Based Combustion Model for Engine Knock Prediction (The Ohio State University).....	166
I.23	Development and Multiscale Validation of Euler-Lagrange-Based Computational Methods for Modeling Cavitation within Fuel Injectors (Boston University).....	172
I.24	Turbulent Spray Atomization Model for Diesel Engine Simulations (Georgia Institute of Technology).....	178
II.	Co-Optimization of Fuels and Engines.....	183
II.1	Co-Optima (National Renewable Energy Laboratory).....	183
II.2	Engine Efficiency Potential of High-Octane Renewable Fuels in Multi-Cylinder Engines (Oak Ridge National Laboratory).....	190
II.3	Developing a Better Understanding of Octane Index (Oak Ridge National Laboratory).....	196
II.4	Characterizing BOB Impacts and Limits within Octane Index (Oak Ridge National Laboratory).....	203
II.5	Advanced Light-Duty SI Engine Fuels Research (Sandia National Laboratories).....	209
II.6	Effect of Properties/Injection Schedule on Fuel Spray Mixing (Sandia National Laboratories).....	216
II.7	Low-Temperature Gasoline Combustion (LTGC) Engines: Fuel Effects and Fuel Co-Optimization (Sandia National Laboratories).....	221
II.8	Thermophysical Property Impact on Spray Formation (Sandia National Laboratories).....	229
II.9	Multi-Mode SI/ACI: Stratification/Fuel/Dilute (Oak Ridge National Laboratory).....	235
II.10	Fuel Effects on Low Speed Pre-Ignition (Oak Ridge National Laboratory).....	240
II.11	Fuel Property Effects on Abnormal Combustion (Oak Ridge National Laboratory).....	246

II.12	Fuel Properties Enhancing Multi-Mode ACI/SI Engine Operation (Argonne National Laboratory)	253
II.13	X-Ray Imaging of GDI Sprays with Alcohol Blends (Argonne National Laboratory)	259
II.14	Fuel Properties Effects on Auto-Ignition in Internal Combustion Engines (Argonne National Laboratory)	263
II.15	RCM for Kinetic Mechanism Development (Argonne National Laboratory).....	270
II.16	Mixing-Controlled Compression-Ignition Combustion and Fuel-Effects Research: Ducted Fuel Injection (Sandia National Laboratories).....	277
II.17	Flow Reactor Autoignition Kinetic Mechanism Development and Validation and Understanding How Fuels Blend for Autoignition (National Renewable Energy Laboratory)	282
II.18	Fuel Autoignition Behavior (National Renewable Energy Laboratory)	288
II.19	Modification of PMI to Include Oxygenate Effects (National Renewable Energy Laboratory)	294
II.20	Virtual Properties, Reduced Mechanism, Blending of Kinetics Properties, and Modeling of Fuel Properties (National Renewable Energy Laboratory).....	305
II.21	Scenario Co-Optimizer (Lawrence Berkeley National Laboratory).....	309
II.22	Fuel Property Blending Model (Pacific Northwest National Laboratory).....	313
II.23	Fuel Impacts on Emissions Control Performance and Durability (Oak Ridge National Laboratory)	319
II.24	Fuel Impacts on ACI PM Formation (Oak Ridge National Laboratory)	325
II.25	Kinetic Mechanism Development (Lawrence Livermore National Laboratory).....	331
II.26	Fuel Property Blending Model (Lawrence Livermore National Laboratory).....	336
II.27	Virtual Properties, Reduced Mechanism, Blending of Kinetics Properties, and Modeling of Fuel Properties (Lawrence Livermore National Laboratory)	341
II.28	Engine Simulations in Support of Co-Optima (Argonne National Laboratory).....	347
II.29	Characterization of Biomass-Based Fuels and Fuel Blends for Low-Emissions, Advanced Compression Ignition Engines (The University of Alabama).....	353
II.30	Dynamic Species Reduction for Multi-Cycle CFD Simulations (University of Michigan)	358
II.31	Micro-liter Fuel Characterization and Property Prediction (Louisiana State University)	362
II.32	The Development of Yield-Based Sooting Tendency Measurements and Modeling to Enable Advanced Combustion Fuels (Yale University)	368
III.	Alternative Fueled Engines.....	375
III.1	Single-Fuel Reactivity Controlled Compression Ignition Combustion Enabled by Onboard Fuel Reformation (Stony Brook University)	375
III.2	High-Efficiency Cost-Optimized Spark-Ignited Natural Gas (HECO-SING) Engines–2018 (Robert Bosch LLC)	381
III.3	Innovative Dual Fuel Aftermarket Emissions Solution (CALSTART)	389
III.4	Reduced Petroleum Use through Easily-Reformed Fuels and Dedicated Exhaust Gas Recirculation (Southwest Research Institute).....	392

III.5	Improving the Fundamental Understanding of Opportunities Available from Direct Injected Propane in Spark Ignited Engines (Oak Ridge National Laboratory)	395
III.6	Direct Injection Propane for Advanced Combustion (National Renewable Energy Laboratory)	401
III.7	Direct Injection 4.3-L Propane Engine Research Development and Testing (Blossman Services, Inc.)	406
IV.	Emission Control R&D.....	412
IV.1	Joint Development and Coordination of Emission Control Data and Models: Cross-Cut Lean Exhaust Emissions Reduction Simulations (CLEERS) Analysis and Coordination (Oak Ridge National Laboratory)	412
IV.2	CLEERS Aftertreatment Modeling and Analysis (Pacific Northwest National Laboratory).....	419
IV.3	Low-Temperature Emission Control to Enable Fuel-Efficient Engine Commercialization (Oak Ridge National Laboratory)	426
IV.4	Emissions Control for Lean-Gasoline Engines (Oak Ridge National Laboratory)	432
IV.5	Cummins-ORNL SmartCatalyst CRADA: NO _x Control and Measurement Technology for Heavy-Duty Diesel Engines (Oak Ridge National Laboratory)	437
IV.6	Fuel-Neutral Studies of PM Transportation Emissions (Pacific Northwest National Laboratory).....	443
IV.7	Advanced Emission Control for High-Efficiency Engines (Pacific Northwest National Laboratory).....	449
IV.8	Development and Optimization of Multi-Functional SCR-DPF Aftertreatment for Heavy-Duty NO _x and Soot Emission Reduction (Pacific Northwest National Laboratory).....	454
IV.9	Enabling Lean and Stoichiometric Gasoline Direct Injection Engines through Mitigation of Nanoparticle Emissions (University of Minnesota).....	460
V.	High Efficiency Engine Technologies	467
V.1	Volvo SuperTruck 2: Pathway to Cost-Effective Commercialized Freight Efficiency (Volvo Group North America)	467
V.2	Cummins/Peterbilt SuperTruck II (Cummins Inc.).....	473
V.3	Development and Demonstration of a Fuel-Efficient Class 8 Tractor and Trailer SuperTruck (Navistar, Inc.)	478
V.4	Improving Transportation Efficiency through Integrated Vehicle, Engine, and Powertrain Research – SuperTruck 2 (Daimler Trucks North America).....	484
V.5	Development and Demonstration of Advanced Engine and Vehicle Technologies for Class 8 Heavy-Duty Vehicle – SuperTruck II (PACCAR Inc.)	490
V.6	Ultra-Efficient Light-Duty Powertrain with Gasoline Low-Temperature Combustion (Delphi Technologies, PLC)	497
V.7	Lean Miller Cycle System Development for Light-Duty Vehicles (General Motors LLC)	504
V.8	Cummins 55% BTE Project (Cummins Inc.)	510
V.9	A High Specific Output Gasoline Low-Temperature Combustion Engine (General Motors).....	514

V.10 Solenoid Actuated Cylinder Deactivation Valve Train for Dynamic Skip Fire
(Delphi Technologies, PLC) 519

V.11 Temperature-Following Thermal Barrier Coatings for High-Efficiency Engines
(HRL Laboratories, LLC) 525

VI. Lubricant Technologies..... 530

VI.1 Power Cylinder Friction Reduction through Coatings, Surface Finish, and Design
(Ford Motor Company)..... 530

VI.2 Integrated Friction Reduction Technology to Improve Fuel Economy Without Sacrificing
Durability (George Washington University)..... 535

VII. System-Level Efficiency Improvement 539

VII.1 Improved Tire Efficiency through Elastomeric Polymers Enhanced with Carbon-Based
Nanostructured Materials (Oak Ridge National Laboratory) 539

VII.2 Advanced Non-Tread Materials for Fuel-Efficient Tires (PPG Industries, Inc.)..... 544

VIII. Index of Principal Investigators..... 550

IX. Project Listings by Organizations..... 554

List of Figures

Figure 1. Research areas within Advanced Combustion Engines and Fuels Program	5
Figure 2. Schematic of energy balance considered in the derivation of the new cavitation erosion metric (Som, I.6)	8
Figure 3. Impact of electrode geometry and electron seeding on low-temperature plasma discharge (Scarcelli, I.10).....	9
Figure 4. Log plot of ignition delay versus ambient temperature for n-dodecane at Spray A conditions. Larger detailed mechanisms are able to capture the ignition delay at low temperature and high temperature better than the smaller reduced mechanisms tested. (Whitesides, I.14)	10
Figure 5. Back-illumination images of sprays with different ethanol–iso-octane blend ratios (top row labels: E0 is pure iso-octane, E30 is 30–70 ethanol–iso-octane blend, and E100 is pure ethanol) under various ambient pressure conditions (left column labels) (Lee, I.18).....	11
Figure 6. Measured particle size distributions for ACI combustion (Kokjohn, I.20)	11
Figure 7. Fuel properties impacting boosted SI engine efficiency (Farrell, II.1).....	12
Figure 8. Knock-limited combustion phasing as a function of octane index for each fuel at the ACI condition (Szybist, II.3).....	13
Figure 9. A comparison between two different modeling approaches to spray formation (Arienti, II.8)	15
Figure 10. Mean apparent heat release rate plotted for intake temperatures from 40–180°C for 2,000 r/min operation; arrow denotes spark timing, shaded region denotes one standard deviation of data at each condition (Splitter, II.11)	16
Figure 11. Natural luminosity image from experiment with single-duct holder confirms that conventional diesel combustion spray produces significantly more incandescence from hot soot than ducted fuel injection spray (Mueller, II.16)	17
Figure 12. Molecular-level solution structure and Reid vapor pressure (RVP). The average number of molecules in clusters was determined by using nuclear magnetic resonance diffusion measurements in (a) ethanol in iso-octane, (b) ethanol in n-heptane, and (c) iso-butanol in n-heptane. Reid vapor pressure for the ethanol–n-heptane solution compared with cluster size is shown in (b). (Mueller, II.21).....	18
Figure 13. Prediction of RON and octane sensitivity (OS) for the simulated blending of nine high-performance fuels into the Co- Optima core fuels (Pitz, II.26)	19
Figure 14. Demonstration of simultaneous two-color pyrometry, rainbow schlieren deflectometry, and OH* chemiluminescence measurements using a simple Bunsen burner (Agrawal, II.29).....	20
Figure 15. Cut-plane equivalence ratio distribution and temperature distribution from the CFD simulations of single-fuel reactivity-controlled compression ignition combustion with diesel and its reformat (Lawler, III.1)	21
Figure 16. Custom high-efficiency research engine with 1:5:1 stroke-to-bore ratio and high compression ratio (Szybist, III.5)	22

Figure 17. CO oxidation light-off performance showing excellent low-temperature activity and stability of the hydrothermally treated Pt/CeO₂ catalyst under exhaust conditions ([O₂] = 10%, [CO] = 0.4%, gas hourly space velocity = 200 L (gcat hr)⁻¹) (Wang, IV.2)..... 23

Figure 18. SCR-onset conversion inflections for (a) a commercial Cu-CHA (chazabite) and (b) a model Cu-Beta SCR catalyst (Partridge, IV.5)..... 24

Figure 19. Pathway toward improved NO_x reduction performance by a surface-active NO_x species (Rappe, IV.8) 25

Figure 20. Baseline Model Year 2009 vehicle (left) and VEV3 text mule (right) at rest stop during fuel economy test (Amar, V.1) 25

Figure 21. Complete dynamic skip fire cylinder head assembly on test stand (Fernandez, V.10)..... 27

Figure I.1.1. Combustion image velocimetry results show the evolution of the azimuthally averaged radial component of flow (red/blue false color strips; note the piston profile on the right side). The left portion is for a main injection starting shortly before top dead center, and the right plot shows data for a main injection starting approximately 9 crank angle degrees (CAD) above top dead center (ATDC), when the stepped-lip piston shows significant advantages over the conventional piston. Inward flow (blue regions) is evidence of a vortex in the outer portion of the stepped-lip combustion chamber. The strength and longevity of the vortex corresponds to faster mixing-controlled combustion (line plots) and reduced soot emissions (bar plots) for the stepped-lip piston. 32

Figure I.1.2. CFD results shown on a vertical cutting plane containing one spray axis. False color represents the fuel–air equivalence ratio; the black contour represents the stoichiometric iso-contour, which has an equivalence ratio of 1.0. Colored vectors are shown to indicate the velocity field components projected onto the plane. Top: main injection starts near top dead center. Bottom: main injection starts approximately 9 CAD ATDC..... 33

Figure I.1.3. Components of the radial acceleration equation visualized on a vertical cutting plane containing a spray axis. Bottom: the radial acceleration; blue colors represent acceleration inward toward the cylinder axis and red colors represent outward acceleration. Top left: the contribution of the radial pressure gradient to the radial acceleration. Top right: the contribution of vertical convection of radial momentum to radial acceleration. Note the units are 1/°CA: a value of 2 corresponds to an outward acceleration equal to the local velocity magnitude in the time it takes the crankshaft to rotate one degree..... 34

Figure I.2.1. Optical engine schematic showing the orientation of the PAH-PLIF and soot-PLII laser sheets in the combustion chamber and the orientation of the cameras and beamsplitter for imaging through the piston-crown window..... 37

Figure I.2.2. Representative instantaneous images of simultaneous 633-nm PAH-PLIF (false-colored green) and soot-PLII (red) at an elevation of 15 mm below the firedeck for single injections over a range of intake O₂ mole fractions. Each row of images is acquired at a different CAD timing and from separate engine cycles. Each image is a partial view of the whole combustion chamber, capturing one of the eight jets, penetrating from left to right, with the injector near the left, indicated by a white dot, while the curved white line represents the piston bowl. The laser sheet penetrates from right to left..... 38

Figure I.2.3. Cylinder pressure (top) and injection schedules (bottom) for CC or LD double-injection conditions at 10% intake O₂. Single-injection pressure data using only the first injection of either the CC or the LD conditions are shown for reference. 39

Figure I.2.4. Representative instantaneous images of simultaneous 633-nm PAH-PLIF and soot-PLII at three laser-sheet elevations for the CC condition (top three sets of images, each outlined in red) and at the lowest elevation for the LD condition (bottom set of images, outlined in blue), both at 10% intake O₂. The crank angle of image acquisition is in the top-left corner of each composite image. Other details of the images are as in Figure I.2.2. 40

Figure I.2.5. Ensemble-averaged images of simultaneous PAH-PLIF for excitation at 355 nm (false-colored blue), 532 nm (green), and 633 nm (red) and soot-PLII (grayscale) at three laser-sheet elevations for the CC condition (left side) and for the LD condition (right side), both at 362 CAD (top row) and 366 CAD (bottom row) and with 10% intake O₂. Details of the field of view of images are as in Figure I.2.2. 41

Figure I.2.6. Predictions of multi-dimensional computational fluid dynamics simulations of the residual jet of the first injection of a double-injection condition with either negative ignition-dwell (900 K ambient gas) or positive ignition-dwell (760 K ambient)..... 42

Figure I.3.1. (left) Normalized liquid-length and (right) lift-off length measurements for surrogate fuels at different temperatures. Spray A conditions, but with 80 MPa fuel injection pressure. 47

Figure I.3.2. (left) Extinction measurement at various times after the start of injection. (right) Tomographic reconstruction of extinction measurement for fuel mass fraction, compared to model (Musculus/Kattke) predictions. Spray D experimental conditions, except the fuel is C70-doped toluene. 47

Figure I.3.3. Extinction imaging of Spray G (Spray G injector and ambient conditions) with three different injection durations. Blue dashed lines show the line-of-sight projection of the hole drill angle. 48

Figure I.3.4. Measured plume direction (defined at right) for different injection durations or with multiple injections. Same conditions as Figure I.3.3. 49

Figure I.4.1. A comparison of temperature-map images of the thermal stratification in a vertical cut-plane for CONVERGE-LES simulations of the all-metal engine, which has a shallow, broad bowl (top), and experimental vertical-plane images derived from calibrated planar laser-induced fluorescence images acquired in the optically accessible engine, which has a flat piston top (bottom) [1] 53

Figure I.4.2. Comparison of CHEMKIN single-zone internal combustion engine results with experimental data for well pre-mixed LTGC engine operation (i.e., HCCI). Figure I.4.2a shows a comparison of the TBDC values for the experiment and the CHEMKIN simulations with the S1 and S2 surrogates. Figure I.4.2b compares the early stages of the heat release for the S1 and S2 surrogates against experimental data for Pin = 1.6 and 2.0 bar. All Pins are absolute..... 55

Figure I.4.3. A comparison of the f-sensitivity of the proposed fuel blend given at the top of the plot (Blend 4) with that of RD5-87A (regular E10 gasoline) for intake pressures from 1.0 to 2.5 bar 56

Figure I.4.4. A series of cylinder-pressure traces that show how the AMFI system can adjust the combustion phasing from retarded to advanced by increasing the amount of EHN additive supplied. Base fuel = RD5-87A, Pin = 1.0 bar, Tin = 60°C, fm = 0.40, speed = 1,200 rpm..... 56

Figure I.4.5. Demonstration of the ability of the AMFI system to control CA50 through a load sweep. (a) Required changes in CA50 with load change and the change in the amount of EHN additive required to make the CA50 changes. (b) Thermal efficiencies (TE) and required Tin through the load sweep for the AMFI system (solid lines) and for Tin control (dashed lines). fm = 0.3–0.46 for both the AMFI-controlled and heated, Tin-controlled sweeps. Pin = 1.0 bar, 1,200 rpm, base fuel = RD5-87A; 0°CA (crank angle) = TDC-intake. 57

Figure I.5.1. Schlieren image of post-discharge transient plasma streamers for a 19.2 kV discharge in 2.0 bar ambient air along with an image of O atom distributions from complementary simulation results. A comparison of the predicted and measured O atom concentrations at the anode tip is also provided for two conditions.	62
Figure I.5.2. Image of the groundless partial DBD electrode and complementary filtered imaging of excited-state O from resultant negative coronas that surround the insulator during transient plasma discharges in air. Also included is a plot of post-discharge products that form in non-flammable mixtures of propane and air.....	62
Figure I.5.3. Sequence of images showing ignition kernel development for pin-to-pin and groundless partial DBD TPI as compared to inductive spark ignition for different voltages and pulse repetition rates	63
Figure I.5.4. Comparison of ISFC as a function of load for lean conditions with and without O ₃ addition for engine speeds between 800 rpm and 1,400 rpm.....	64
Figure I.5.5. Plots of IMEP, CA50, and coefficient of variation of IMEP as a function of spark timing for a sweep of intake temperatures (42–80°C) and a fixed 1,000 rpm engine speed	65
Figure I.5.6. Comparison of measured in-cylinder O ₃ concentration and early-stage apparent heat release rate profiles for a sweep of intake temperatures	66
Figure I.6.1. Schematic of energy balance considered in the derivation of the new cavitation erosion metric, which considers the transfer and storage of energy in the solid material due to repeated impacts from cavitation cloud collapse events.....	70
Figure I.6.2. Comparison of erosion patterns between experimental images from Skoda et al. [4] (top) and homogeneous relaxation model predictions of local maximum pressure (middle) and accumulated stored energy (bottom) at the top channel wall.....	71
Figure I.6.3. (a) Ignition delay and (b) flame liftoff as a function of ambient temperature conditions with LES models using ANNs. (c) Memory consumption over all nodes for a conventional interpolation vs. ANN method.....	72
Figure I.6.4. Temporal evolution of CH ₂ O mass fraction contours predicted by the TFM-ANN LES model (right) is compared against the CH ₂ O PLIF data (left) from a single shot injection	72
Figure I.7.1. Near-nozzle spray surface area in ECN Spray C (a) and Spray D (b) injectors measured using ultra-small-angle X-ray scattering	76
Figure I.7.2. Near-nozzle spray surface area in ECN Spray D as a function of transverse position, shown for several distances from the injector nozzle.....	77
Figure I.7.3. A view of the outside surface and hole counter bores of an ECN Spray G injector	77
Figure I.7.4. Measurements of the ECN Spray C injector, including nozzle geometry (left), high-speed X-ray imaging of cavitation inside the nozzle (center), and a cross-section of the fuel density as it first emerges from the injector nozzle (right).....	78
Figure I.8.1. Calculated normalized HRRs for PRF90/O ₂ /diluent mixture at T _c = 735 K, presented as a function of aHR, illustrating exothermic trends across a range of P _c for (a) experimental measurements and (b) LLNL model predictions [6]. Insets highlight preliminary exothermicity, e.g., LTHR before transition to high-temperature heat release. Two experimental tests conducted at each condition demonstrate very good consistency.	84

Figure I.9.1. Results of pilot injection quantity sweep at constant 90 dB combustion noise 90

Figure I.9.2. Overview of single-, double-, and triple-injection strategy injection timings and combustion phasings..... 90

Figure I.9.3. Comparison of single-, double-, and triple-injection results with constant 90 dB combustion noise 91

Figure I.9.4. Effects of EGR on combustion and emissions while maintaining constant 90 dB combustion noise 91

Figure I.10.1. Impact of electrode geometry and electron seeding on LTP discharge..... 95

Figure I.10.2. Comparison between simulations and experiments in terms of post-discharge plasma regime 95

Figure I.10.3. VizGlow results highlighting the distribution of atomic oxygen (O) and temperature..... 96

Figure I.10.4. Impact of number of pulses on LTP ignition as calculated using CONVERGE..... 97

Figure I.10.5. CONVERGE results showing the impact of number of pulses on the flame kernel growth 97

Figure I.11.1. Schematic of the in-cylinder reforming process in which one cylinder has an isolated intake and exhaust, feeds the reforming catalyst, and is incorporated into the intake for the other three cylinders. Intake and exhaust systems have been modified to accommodate boosted operation in 2018..... 100

Figure I.11.2. Brake thermal efficiency as a function of catalyst inlet O₂ concentration and Φ_{catalyst} at 2,000 rpm and 4 bar BMEP 101

Figure I.11.3. Axial temperature profile of reforming catalyst at 2,000 rpm, 4 bar BMEP over a range of catalyst inlet O₂ concentrations and catalyst Φ conditions 101

Figure I.11.4. Schematic of two possibilities of reaction zones in reforming catalyst. In scheme (a), the oxidation and steam reforming occur sequentially. In scheme (b), the partial oxidation and steam reforming reactions occur simultaneously over a portion of the catalyst. 102

Figure I.11.5. Axial temperature profile for increasing engine load, from 4 bar to 10 bar BMEP, at an engine speed of 2,000 rpm. Catalyst inlet O₂ was held constant at 1.8%, and catalyst Φ was held constant at 5..... 103

Figure I.11.6. Exhaust temperature, intake manifold pressure, BMEP, and intake manifold pressure as a function of load for the reforming strategy and the baseline engine operation. 103

Figure I.12.1. (a) Mass-attenuation coefficients versus atomic number, and (b) schematic of neutron-imaging apparatus (Sources: [a] Nikolay Kardjilov [2006], [b] ORNL)..... 105

Figure I.12.2. System used to study intra-nozzle dynamics of fuel injection include (a) high-pressure fuel delivery system and (b) the aluminum spray chamber with optical viewport. The spray chamber is designed with (c) directed fans to minimize fuel buildup on the chamber walls and the fuel injector.... 106

Figure I.12.3. Normalized neutron radiographs of fuel injection from a single-hole GDI-style injector (ECN Spray G) highlight ability to see opening and closing of the check ball as well as deflection of the injector both during and after injection. Top row shows subtraction-normalized images, which provide a qualitative understanding of the needle motion. Bottom row shows log-ratio-normalized images, which provide quantitative information on how the neutron path lengths change through the different materials during the needle motion.	107
Figure I.12.4. (a) Approach for fitting normalized image data to analytical path length model. (b) Needle displacement results show oscillation during injection and large movement after ball is seated. Results show low sensitivity to image filtering.	108
Figure I.12.5. Slices of neutron and X-ray CT reconstructions of large-bore Bosch injector performed in collaboration with Argonne National Laboratory	109
Figure I.12.6. Soot cake thickness down GPF channel length extracted from neutron CT scans shows continuous decrease with regeneration percent with E0 particulate matter (left) and staggered decrease with E30 particulate matter (right).....	109
Figure I.13.1. Comparison of old and new trimethyl benzene (red) and ortho-xylene (blue) LLNL kinetic model simulations with ignition delay times (IDTs) measured in the ANL RCM [1]. Symbols: experimental data. Dashed lines: old LLNL kinetic model predictions. Solid lines: new LLNL model predictions.	112
Figure I.13.2. Evolution of major PAHs during the pyrolysis of toluene primary reference fuel 97.5 (n-heptane/iso-octane/toluene = 14.5/8.0/77.5, by mole, respectively, 97.5 research octane number [RON]) in a flow reactor. Symbols: experimental data, Shao et al. [4]. Lines: LLNL PAH kinetic model predictions.....	113
Figure I.13.3. Comparison of LLNL gasoline surrogate model results with IDTs measured in the Stanford high-pressure shock tube for a high-octane, moderate sensitivity (RON = 101, OS 7) gasoline [3]. ϕ is fuel/air equivalence ratio. Symbols: experimental data. Lines: simulations. Dashed line and open squares: first-stage IDT. Solid lines and filled symbols: total IDT.....	114
Figure I.14.1. Log plot of ignition delay versus ambient temperature for n-dodecane at Spray A conditions. Larger detailed mechanisms are able to capture the ignition delay at low temperature and high temperature better than the smaller reduced mechanisms tested.	117
Figure I.14.2. Total simulation time for Spray A simulation with detailed reaction model [9], colored by time spent in chemistry and non-chemistry routines	118
Figure I.15.1. Four-valve DISI engine: (a) turbulent structures shown by magnitude of vorticity (1/s) during intake; (b) pressure rise as a function of crank angle as compared to experimental data	124
Figure I.15.2. The ECN Spray A case: (a) injection of diesel in quiescent nitrogen at 2.2 MPa, KH-RT spray model; (b) the penetration depth of the spray compared to ECN experimental data.....	124
Figure I.15.3. Multiphase flow simulation with VOF method, gasoline injected into quiescent air at 3 bar: (a) gasoline jet primary break-up into ligaments and (b) primary break-up and w-component of velocity of air showing recirculation.....	125
Figure I.16.1. Model transitioned from cylinder sector to full-cylinder geometry with positionable intake swirl flap for improved simulation of charge motion and mixing	131

Figure I.16.2. Simulation results from full-cylinder model show improved local mixing, resulting in increased oxidation of CO and soot late in the cycle.....	131
Figure I.16.3. For the full-cylinder model, improved charge motion and detailed piston geometry with valve cut-outs results in earlier and faster combustion within the squish region, leaving less residual CO.....	131
Figure I.16.4. Comparison of predictions for key combustion metrics and engine-out emissions.....	132
Figure I.16.5. Flow chart for iterative strategy used with CHT model.....	133
Figure I.16.6. Initial results with CHT model predict higher combustion chamber wall temperatures than assumed values used in simulations with uniform, constant wall temperatures, resulting in lower heat losses.....	133
Figure I.17.1. Time-resolved (at intervals of two crank angle degrees of rotation) measured IR spectral radiative intensities in the transparent combustion chamber engine at 40 kPa manifold absolute pressure, 1,300 r/min.....	137
Figure I.17.2. Comparison of measured and simulated spectral intensities for the transparent combustion chamber engine operating at 40 kPa manifold absolute pressure, 1,300 r/min. The comparisons are made at 30° aTDC.	137
Figure I.17.3. AHRR of the knocking operating condition for each temperature and three diluents at 10%: (a) N ₂ , (b) H ₂ O, and (c) CO ₂ . All AHRR plots represent a single engine operating condition where the black line represents the median engine cycles, the red line represents one standard deviation advanced cycles, and the blue line represents one standard deviation retarded cycles.	138
Figure I.17.4. Computed root-mean-square temperature profiles for a fully developed turbulent channel flow between parallel plates held at different fixed temperatures, with and without consideration of radiative heat transfer. Left: DNS results from [1]. Right: Current LES results.	139
Figure I.18.1. Back-illumination images of sprays with different ethanol-iso-octane blend ratios (top row labels: E0 is pure iso-octane, E30 is 30–70 ethanol-iso-octane blend, and E100 is pure ethanol) under various ambient pressure conditions (left column labels).....	143
Figure I.18.2. Time-resolved liquid penetration lengths for ethanol-iso-octane fuel blend sprays (E100 is pure ethanol, E30 is 30% ethanol plus 70% iso-octane, and E0 is pure iso-octane) at chamber pressures of (a) 100 kPa, (b) 50 kPa, and (c) 20 kPa	143
Figure I.18.3. Droplet distribution curves for ethanol-iso-octane fuel blend sprays (E100 is pure ethanol, E30 is 30% ethanol plus 70% iso-octane, and E0 is pure iso-octane) at chamber pressures of (a) 100 kPa, (b) 50 kPa, and (c) 20 kPa.....	144
Figure I.18.4. Graphical visualization of the simulated spray result (left) and ethanol mass fraction profile on the plume centerline (right) at 1 ms after start of injection time for ethanol injection at $P_{\text{ambient}} = 50$ kPa.....	144
Figure I.18.5. Iso-octane injection at $P_{\text{ambient}} = 50$ kPa. Experimental spray image (left), simulated spray (center), and fuel vapor mass fraction profile (right) at 1 ms after start of injection time.....	145
Figure I.19.1. (a) n-Heptane film thickness at $P_{\text{inj}} = 150$ MPa, (b) n-heptane film thickness at density = 22.8 kg/m ³ , and (c) Sauter mean diameter of diesel spray at $P_{\text{inj}} = 150$ MPa and density = 22.8 kg/m ³ ; subfigure shows measurement positions.....	148

Figure I.19.2. Splashing criteria of diesel, water, n-dodecane, n-heptane, and diesel	148
Figure I.19.3. Gas velocity fields and spray shape for the hydro-dynamically smooth plate (left figures) and rough plate (right figures).....	149
Figure I.19.4. Experiments vs. CFD comparison of liquid penetration (left), rebound radii (center), and rebound heights (right).....	150
Figure I.19.5. Splashed mass ratio results for simulations at $u = 15, 16, 17,$ and 24 . Comparison of the splashed mass ratios at $u = 15, 16,$ and 17 shows the transition to splashing between $u = 15$ and 16 . Splashed mass at $u = 24$ is presented for three resolutions, showing second-order convergence in the splashed mass ratio. The subfigure shows the highly resolved lamella and cusp formation from the 160 CPD simulation.	150
Figure I.19.6. Time-averaged secondary droplet characterization of the 80 CPD diesel droplet train impingement simulation with a pre-existing liquid film at the nondimensional velocity $u = 24$. D is impinging droplet diameter and d is secondary droplet diameter.	152
Figure I.20.1. Comparisons of measured and predicted particle size distributions for mixing controlled compression ignition combustion	155
Figure I.20.2. Measured particle size distributions for advanced compression ignition combustion.....	156
Figure I.20.3. (left) Simulated and (right) measured particle size distributions for neat diesel fuel and 52% syngas.....	156
Figure I.20.4. Comparisons of measured and predicted PSDs and representative simulated soot aggregates for several different sized particles	157
Figure I.20.5. Ensemble-averaged 633-nm PAH PLIF and soot PLII images for the long dwell operating condition	158
Figure I.21.1. Detection method illustrating liquid, two-phase, and vapor regions of the spray based on RSD measurements from 95 injections: (a) instantaneous RSD image showing dark region near injector and (b) time sequence of contours of number of reliable hue readings	162
Figure I.21.2. Gas-phase adiabatic mixing of fuel and air as a function of fuel molar mixture fraction using real-fluid properties and real-fluid mixing models for Engine Combustion Network Spray A conditions.....	163
Figure I.21.3. Relationship between the mixture's normalized refractive index and equivalence ratio and temperature for the Engine Combustion Network Spray A conditions.....	163
Figure I.21.4. Density contours for n-dodecane/nitrogen mixtures at various fuel mole fractions	164
Figure I.21.5. Comparison of simulation and experimental (left) vapor and liquid penetration results and (right) ignition delay behavior for n-heptane injected at 1,000 bar, 363 K into air at 28 bar, 825 K	165
Figure I.21.6. Comparison of experimental RSD images (top in each pair) and synthetic RSD images (bottom in each pair) processed from CFD results for n-heptane injected at 1,000 bar, 363 K into air at 28 bar, 825 K.....	165

Figure I.22.1. (left) Multi-cycle LES using FPF reproduces CCV of in-cylinder pressure in an engine experiment under a non-knocking condition (colored thick lines: 15 LES cycles, black thin lines: 50 representative cycles from the experiment, dashed-dotted lines: the fastest and slowest cycles in the experiment, triangles: 5% and 95% bounds from 5,000 cycles in the experiment, circles: measured mean pressure). (right) Comparison of the predicted COV with the experimental data. 168

Figure I.22.2. Comparison of the flame front evolution in fast and slow cycles in LES. Also shown is the subfilter kinetic energy at top dead center. In the fast cycle, where the flame propagates faster, the subfilter kinetic energy is higher near the spark plug as compared with that in the slow cycle. 168

Figure I.22.3. Verification of the coupling of CMC with Converge CFD. The evolution of species mass fractions is linear both in time and in scalar (conditioning variable) space. The predicted filtered fuel mass fractions in two-dimensional LES of idealized ignition in homogeneous isotropic turbulence closely follow the specified profile (exact solution). 170

Figure I.22.4. Test of CMC-FPF-Converge in a simple configuration. A premixed flame kernel is deposited initially at the center of the computational domain and grows in homogenous isotropic turbulence. The initial temperature field is inhomogeneous. The ignition in the end-gas region is observed at $t = 1.5$ ms. 170

Figure I.23.1. Comparisons of terminal bubble shape for a range of parameter space from SPH (BU), VOF (BU), front tracking (Hua), and experiments (Bhaga)..... 174

Figure I.23.2. The differences between VOF and SPH simulations for low Reynolds numbers..... 174

Figure I.23.3. Time-averaged velocity field from numerical simulations of nozzle flow for varying cylindrical outlet diameters..... 175

Figure I.23.4. Normalized neutron radiographs comparing the max-cavitating (flash boiling) and non-cavitating (non-flash) conditions in the single-hole, large-bore injector 176

Figure I.23.5. Normalized neutron intensity in sac region for non-flash and flash boiling conditions. Shaded bands represent one standard deviation..... 176

Figure I.24.1. Predicted path-integrated SMD along the centerline of ECN Spray D ($d_{nozz} = 180$ mm, dodecane fuel) using the newly developed KH-Faeth model. Comparison is shown against measurement (USAXS) and benchmark KH breakup model..... 180

Figure I.24.2. Near-nozzle surface area measurements for ECN Spray D at several distances 181

Figure I.24.3. SAMR measurements of path-integrated SMD in ECN Spray D at three different viewing angles. Measurements are at an axial position of 10 mm from the nozzle exit. $P_{amb} = 1$ bar, $P_{inj} = 500$ bar. 181

Figure II.1.1. Fuel properties impacting boosted SI engine efficiency. Figure by John Farrell, NREL. . 185

Figure II.2.1. Projected volumetric fuel economy improvements offered by Co-Optima Tier 3 blendstocks 194

Figure II.3.1. Pressure-temperature trajectories for the five engine operating conditions investigated for three of the Co-Optima core fuels..... 197

Figure II.3.2. Knock-limited combustion phasing as a function of octane index for each fuel investigated at (a) the boosted SI condition, (b) the RON-like condition, and (c) the MON-like condition 199

Figure II.3.3. Knock-limited combustion phasing as a function of octane index for each fuel at the ACI condition	199
Figure II.3.4. Constant-volume ignition delay in milliseconds, calculated from kinetic modeling, as a function of pressure and temperature for each of the five fuels investigated at stoichiometric conditions.....	200
Figure II.3.5. Ignition delay differences between the alkylate fuel and either aromatic, E30, or the Tier III fuel at stoichiometric conditions ($\Phi = 1.0$). Red areas indicate that the alkylate fuel has a shorter ignition delay and blue areas indicate that the alkylate fuel has a longer ignition delay.	201
Figure II.4.1. SI merit function for fuel properties developed in Co-Optima [4].....	204
Figure II.4.2. Structure, RON, and S for the fuels investigated in this study	205
Figure II.4.3. RON of 20 vol% blends of the fuel components investigated, as well as lines of linear blending for the BOB and each of the pure components. Amylene and prenol exhibit synergistic blending while MCP exhibits linear blending.....	205
Figure II.4.4. S of 20 vol% blends of the fuel components investigated, as well as lines of linear blending for the BOB and each of the pure components. Amylene and prenol exhibit synergistic blending while MCP exhibits nearly linear blending.	206
Figure II.4.5. Pressure-temperature trajectories of each of the operating conditions investigated.....	207
Figure II.4.6. Knock-limited combustion phasing as a function of octane index for each fuel investigated at (a) the boosted SI condition, (b) the RON-like condition, and (c) the MON-like condition.....	207
Figure II.5.1. For naturally aspirated stratified-charge, direct-injection SI operation at 1,000 rpm, smoke emissions for E30 are much higher than the average trend line due to the formation of pool fires. For boosted operation at 2,000 rpm, E30 suppresses soot formation. Intake $[O_2] = 17\%$, $\phi_m = 0.33$, $T_{coolant} = 75^\circ C$. PMI values were provided by [4] and [5]. Figure by Magnus Sjöberg, SNL.	210
Figure II.5.2. Effect of engine coolant temperature on piston-top wall wetting and associated formation of sooting pool fires and exhaust smoke emissions. Intake $[O_2] = 18\%$. Figure by Magnus Sjöberg, SNL, and Xu He, Beijing Institute of Technology.	211
Figure II.5.3. Schematic of diffused back-illumination setup for in-cylinder soot quantification.....	211
Figure II.5.4. Detection of in-cylinder soot for stratified operation with a RON98 fuel containing 19.6% DIB by volume. Figure by Namho Kim, SNL.....	212
Figure II.5.5. Effect of intake oxygen mole fraction on combustion phasing rendering “trace autoignition” for lean SI operation with $\phi_m = 0.50$ in the end-gas. Figure by Magnus Sjöberg, SNL.....	213
Figure II.5.6. Example of the application of the octane-index framework for lean mixed-mode combustion utilizing end-gas autoignition. $P_{in} = 100$ kPa. Figure by Magnus Sjöberg, SNL.....	213
Figure II.6.1. (left) Cross-section of continuous-flow heated spray chamber, with capabilities depicted; (right) spray chamber installed in laboratory on optical table and behind operator safety barrier.....	217
Figure II.6.2. Schematic illustrating the geometry of Spray G and the process of plume interaction and spray collapse.....	218

Figure II.6.3. (Top) LVF simulations at axial distance cut plane of $z = 15$ mm. Middle is with injector at 0° rotation; left at 22.5° rotation. Right is tomographic reconstruction at 0° rotation. (Bottom left, middle) Projected liquid volume, the integral of the liquid volume along a line of sight indicated at the top. (Bottom right) Profile of original LVF compared to tomographic reconstruction using projection data taken from only two views (0° and 22.5° rotation)..... 218

Figure II.6.4. Time sequence of schlieren images from the same injection. Spray G fuel injector with iso-octane fuel and 0.8 ms injection duration. Injector is oriented at 0° rotation in the continuous-flow chamber. Time given relative to the start of injection..... 219

Figure II.7.1. Combustion phasing (CA50) as a function of intake temperature (T_{in}) for various fuels for fully premixed LTGC operation at $P_{in} = 1.0$ bar, $\phi = 0.4$, 1,200 rpm. For the scale on the y-axis, $0^\circ\text{CA} = \text{top dead center (TDC)-intake}$ and $360^\circ\text{CA} = \text{TDC-compression}$ 223

Figure II.7.2. TBDC required for a CA10 of 368.7°CA (solid lines) or 371.5°CA (dashed lines) as a function of P_{in} for the Co-Optima high-cycloalkane, high-aromatic, and E30 fuels, and for the two regular E10 fuels. $\phi_m = 0.38$, 1,200 rpm. All fuels are fully premixed (i.e., HCCI), which requires $T_{in} \geq 60^\circ\text{C}$ to prevent fuel condensation in the intake system. The points where T_{in} reaches this minimum value of 60°C are noted on the plot..... 224

Figure II.7.3. Comparisons of CA50 as a function of TBDC for computational results using the S1 and S2 surrogates with experimental data at $P_{in} = 1.0$ bar for the E30, high-cycloalkane, and high-aromatic Co-Optima fuels and the RD5-87A regular gasoline. $\phi = 0.4$, 1,200 rpm. 225

Figure II.7.4. Comparison of the TBDC values required for simulations with the S1 (dotted lines) and S2 (dashed lines) surrogates to match the CA50 values of the experimental data (solid lines) for intake pressures from 1.0 bar to 2.4 bar absolute. Figure II.7.4a shows results for the high-aromatic fuel with RI held constant at 5 MW/m^2 , and Figure II.7.4b shows the high-cycloalkane fuel for which CA10 = 368.7°CA except for $P_{in} = 2.4$ bar, where CA10 = 371.5°CA 226

Figure II.8.1. Cavitation interaction with time-accurate, resolved, liquid surface dynamics. Shown from left to right: a schematic of the experiment [5]; three snapshots at increasing injection pressure from the experiments; and the corresponding CLSVOF simulations, where the vapor cloud due to cavitation is marked in red. Hydraulic flipping is intermittently observed in the simulation. 231

Figure II.8.2. Spray G geometry seen through a mid-plane cut. The mesh used in the CFD simulation is a blend between the high-resolution tomography of the holes ($1.7 \mu\text{m}$) and counterbores and a lower-resolution tomography of the fuel passages and the ball ($5.1 \mu\text{m}$). 231

Figure II.8.3. A comparison between two different modeling approaches to spray formation. Left: snapshot of the liquid surface, colored by temperature, from the time-resolved CLSVOF simulation. Right: a cross-section of the liquid volume fraction (from 0-blue to 1-red) from the solution obtained with CONVERGE [6]. The same injector model (Spray G [4]) and fuel (iso-octane) were used for the two simulations. 232

Figure II.8.4. Plot of vapor quality (non-dimensional units) from a data slice through one of the orifices in the simulation with BOB4. The black line marks the intersection of the liquid surface with the plane. Note how cavitation causes the fuel to impinge on the inner wall of the counterbore. Much lower levels of vapor quality are found in the simulation with iso-octane at the same injection conditions. 233

Figure II.9.1. Multi-mode concept showing ACI at part-load with engine running in SI mode for low loads and near idle and at higher engine loads and speeds 236

Figure II.9.2. Schematic of single-cylinder engine (left) and picture of engine installed (right)	237
Figure II.9.3. A single-zone temperature model is used to present experimental results of partially stratified ACI with gasoline-range primary reference fuels (PRFs), highlighting areas for two-stage heat release	237
Figure II.9.4. Examples of range of conditions considered across ACI range and locations examined. The left figure shows a smaller ACI range and the different load locations (from low-load to high-load centroids). The figure on the right shows an expanded ACI range and the different locations examined.....	238
Figure II.9.5. Results showing diminishing returns as ACI range is increased with different ACI efficiencies	238
Figure II.10.1. Engine oil pressure reduction as a function of LSPI segment for various engine loads and injector orientations; the reduced engine load conditions required increased fuel-wall targeting to match oil pressure drop present at higher engine load operation	242
Figure II.10.2. Recorded LSPI events per segment for matched load, varied injector orientation operation	243
Figure II.10.3. Oil pressure reduction for different engine loads and fuel distillation (left) and corresponding LSPI event counts (right)	243
Figure II.10.4. Lubricant additive metal content (left) and corresponding LSPI number count, color coded to lubricant (right)	244
Figure II.10.5. Oil pressure reduction for different engine loads and fuels (left) and corresponding LSPI event counts (right)	245
Figure II.11.1. Mean apparent heat release rate plotted for intake temperatures of 40–180°C for 2,000 r/min operation; arrow denotes spark timing, shaded region denotes one standard deviation of data at each condition.....	249
Figure II.11.2. Quantified trends in PSHR and CA50 phasing for 2,000 r/min operation (black, circle markers) and 1,000 r/min operation (grey, diamond markers) as a function of intake temperature; whiskers denote one standard deviation (SD) of the respective property	250
Figure II.11.3. Quantified trends in KLSA CA50 and bulk gas temperature at CA2 of the deflagration as functions of PSHR for 2,000 r/min operation (black, circle markers) and 1,000 r/min operation (grey, diamond markers); whiskers denote one standard deviation of the respective property	250
Figure II.11.4. Pressure-temperature trajectory up to 2% of heat release (CA2) of the deflagration (blue star marker); spark discharge timing denoted (red circle markers) for an intake temperature sweep with boosted operation at 2,000 r/min engine speed plotted on constant-volume ignition delay simulation results in milliseconds (grey numbers), with ignition delay defined as a 50 K rise.....	251
Figure II.12.1. Knock intensity as a function of intake air temperature at 1,500 rpm, 9 bar net IMEP, and constant CA50 (crank angle at 50% mass fraction burned) of 20 crank angle degrees (CAD) after top dead center (aTDC)	255
Figure II.12.2. Intake air temperature requirement as a function of intake manifold pressure at 12.6:1 and 15.3:1 compression ratio. Combustion phasing maintained at CA50 = 12 CAD aTDC and 3 bar net IMEP.	256

Figure II.12.3. Intake air temperature change for knock-limited SI operation at 9 bar net IMEP and ACI operation at 3 bar net IMEP.....	257
Figure II.12.4. Motored compression trajectories during ACI operation for A30 and O30 test fuels	257
Figure II.13.1. The projected density distribution in sprays emerging from an eight-hole GDI injector. At left is a non-evaporating spray of gasoline-type calibration fluid; at right is a spray from the same injector using iso-octane fuel.	260
Figure II.13.2. Synchrotron X-ray radiography measurements of iso-octane injection. The measurements were taken 2 mm from the fuel injection nozzle (left). Under conditions designed to inhibit flash boiling, injection plume density was relatively high, with narrow, well-defined individual plumes (middle). Under flash-boiling conditions, local fuel density decreased, plume spread increased, and the overlap between adjacent spray plumes increased (right).....	261
Figure II.13.3. Plot showing slices through the density distributions 1 mm downstream of the fuel injector for three fuels: iso-octane, iso-octane with 20% butanol, and iso-octane with 20% ethanol. The density distribution is dramatically different for the ethanol blend.....	261
Figure II.14.1. Ethanol and isobutanol effects on the required base fuel RON to obtain constant RON 98 of the final fuel blends and the effects on the cylinder-pressure-transducer-based MAPO knock intensities	265
Figure II.14.2. Effective octane ratings of non-PRF fuels between their peak knocking lambdas and stoichiometry based on the CFR knockmeter knock intensities (A and B) and the cylinder-pressure-transducer-based MAPO knock intensities (C and D).....	266
Figure II.14.3. Three PRF 90 test conditions with the standard knockmeter knock intensity, using variations to intake temperature (T_{in}) and pressure (P_{in})	267
Figure II.15.1. Isoleths of RCM-measured and chemical kinetically modeled ignition delay times under static (i.e., constant volume) conditions compared against isopleths of ACI engine top dead center conditions (with CA50 = +12 °aTDC). Shaded regions indicate the range of pressures covered in the RCM experiments; points beyond this are extrapolations of observed trends.....	272
Figure II.15.2. Comparison of relative fuel reactivities where static conditions (in RCM and model) are ranked against engine-intake requirements at $\phi = 0.38$. Baseline fuel is ALK. Intake pressure (P_{in}) of engine adjusted at each T_{in} to maintain CA50 = +12 °aTDC. T_c of RCM and model selected using engine-estimated, motored top dead center conditions; P_c of RCM and model adjusted to achieve $\tau_{ig} = 4$ ms. Parity conditions shown as dashed line; departures from this indicate inconsistencies with ACI engine data.	273
Figure II.15.3. Comparison of RCM-measured and model-computed HRRs (normalized by mixture lower heating value), plotted as functions of accumulated heat release. Experiments indicate little fuel-to-fuel differences; model predicts significant differences.....	274
Figure II.15.4. Normalized phi-sensitivity vs. temperature for RD5-87 measured under two pressure protocols. Model results utilize a multi-component surrogate for the E10 full boiling-range fuel.	275
Figure II.16.1. Schematic of the DFI concept on one fuel spray within an engine	278
Figure II.16.2. Single-duct holder (left) and two-duct holder (right) attached to cylinder head. All ducts have an inside diameter, length, and standoff distance from the injector orifice of 2 mm, 12 mm, and 3 mm, respectively.	278

Figure II.16.3. Natural luminosity image from experiment with single-duct holder. Camera is viewing the cylinder head through a window in the piston (compare to left side of Figure II.16.2). Duct has an inside diameter, length, and standoff distance from the injector orifice of 2 mm, 12 mm, and 3 mm, respectively.	279
Figure II.16.4. CDC results show trade-off between soot and NO _x emissions as dilution increases, whereas DFI breaks the soot/NO _x trade-off by simultaneously attenuating soot and NO _x formation. For DFI, duct has an inside diameter, length, and standoff distance from the injector orifice of 2 mm, 12 mm, and 3 mm, respectively.	280
Figure II.16.5. DFI dramatically lowers soot at constant dilution and combustion phasing. Plot shows the change in indicated-specific emissions of soot, NO _x , hydrocarbons, and carbon monoxide (CO) and the fuel-conversion efficiency (η_f) for DFI vs. CDC at 16 mol% O ₂ . For a given parameter X, the bar plot shows $(X_{DFI} - X_{CDC}) / \min(X_{DFI}, X_{CDC})$. Inset shows AHRR.....	280
Figure II.17.1. Example autoignition products of isooctane: reactor versus model results.....	283
Figure II.17.2. Autoignition products of ethanol: model versus experimental data	284
Figure II.17.3. Autoignition products from dimethylfuran: model versus experimental data	285
Figure II.17.4. Retro-Diels-Alder pathways for the three isomers of methyl cyclohexenes	286
Figure II.17.5. Experimental data for methyl cyclohexene isomers and formation of the soot precursor cyclopentadiene.....	286
Figure II.18.1. Arrhenius plot of ignition delay (log scale) versus inverse temperature (1,000/K) for iso-octane at 10 bar initial pressure in the AFIDA. The AFIDA simulations with full CFD simulation with a 127-species reduced mechanism (purple squares) fit well against the experimental points (black circles). 0D simulations with the detailed Co-Optima mechanism (red line) and the 127-species reduced mechanism (blue line) are also plotted. Note how well the 0D simulations match experimental data for longer ignition delay times. (Figure: Mohammad Rahimi, NREL).....	290
Figure II.18.2. Correlation of RON predicted from AFIDA ignition delay to RON measured by CFR engine method. AFIDA-predicted RON vs. RON measured on the CFR engine, showing excellent agreement. Red points are oxygenated blends in primary reference fuels, toluene standardization fuels, and complex gasoline surrogates. Blue points are oxygenated candidates blended into the core Co-Optima boosted SI fuels. (Figure: Jon Luecke, NREL).....	291
Figure II.19.1. Raw mass spectrometer ion current data for several species: (a) E0-10% cumene blends and (b) E30-10% cumene blends in FACE B gasoline.....	297
Figure II.19.2. (a) Predicted time-dependent droplet diameter, (b) droplet temperature, and (c) liquid aromatic additive mass during evaporation of droplets of FACE B blends with 4-t-butyl toluene, at constant ambient temperature and pressure of 371 K and 1 atm	299
Figure II.19.3. PN concentration as a function of particle diameter at Condition A for fuels blended with aromatics at 20 vol%. Error bars are 95% confidence intervals.	300
Figure II.19.4. Comparison of particle size distributions between Conditions A and B for the 20 vol% 4-t-butyl toluene blends. Error bars are 95% confidence intervals.....	300

Figure II.19.5. Results of the linear model using optimal combined explanatory variables determined through regularized regression. Large dots indicate the mean experimental PM mass in mg/m³ with individual data points plotted as smaller circles (a slight jitter has been added to the y-values to prevent overlap in this illustration). 302

Figure II.20.1. Ignition delay time calculation using FACE A multi-component surrogate, PRF surrogate, and TPRF surrogate..... 308

Figure II.21.1. Tradeoff curves for bi-objective optimization with uncertainty in fuel component cost (synthetic cost data used to only show capabilities) 311

Figure II.21.2. Tradeoff curves for data-informed GP bi-objective optimization..... 312

Figure II.22.1. Molecular-level solution structure and Reid vapor pressure. The average number of molecules in clusters was determined by using NMR diffusion measurements in (a) ethanol in iso-octane, (b) ethanol in n-heptane, and (c) iso-butanol in n-heptane. Reid vapor pressure for the ethanol–n-heptane solution compared with cluster size is shown in (b). (Kee Sung Han) 315

Figure II.22.2. Hydrogen-bond clustering of alcohols in n-heptane determined by molecular dynamics simulations. Left: Number of hydrogen bonds per alcohol with increasing alcohol content. Middle: Ethanol molecule clustering distributions. Right: Molecular depictions of ethanol–n-heptane mixtures from molecular dynamics simulations. (Amity Andersen)..... 315

Figure II.22.3. Comparison of the solid-liquid equilibria for mixtures of diesel surrogate fuel V0b with complex diesel fuels, CFA or GTL1. Volume percentages of diesel surrogate fuel V0b are shown along the lower x-axis, increasing from left to right, and volume percentages of diesel fuels CFA or GTL1, as appropriate, are shown along the upper x-axis, increasing from right to left. Data points and trendlines for mixtures of V0b+CFA are shown as hollow symbols and dashed lines, while mixtures of V0b+GTL1 are shown as filled symbols and solid lines. Trendlines are second-order polynomials that represent isobars, distinguished by color, for each set of mixtures. Each material can be expected to remain a liquid at temperatures above its respective trendline at a given pressure. Below its respective trendline, a pure material will solidify, and a multicomponent material will have at least one component freeze out. (Tim Bays and Margaret Jones) 316

Figure II.23.1. T_{50} and T_{90} of surrogate BOB (baseline); 10%, 20%, and 30% ethanol blended into the BOB; unblended (100%) ethanol; 10%, 20%, and 30% isobutanol blended into the BOB; unblended (100%) isobutanol; 10%, 20%, and 30% of an aromatic mixture blended into the BOB; unblended (100%) aromatic mixture; 10%, 20%, and 30% di-isobutylene blended into the BOB; and unblended (100%) di-isobutylene. Error bars represent 95% confidence intervals calculated from three replicate runs..... 322

Figure II.23.2. Comparison of CO light-off temperatures (T_{50} and T_{90}) over the hydrothermally aged commercial TWC for all the fuel blends investigated. Error bars represent 95% confidence intervals calculated from three replicate runs. 322

Figure II.23.3. Comparison of NO_x light-off temperatures (T_{50} and T_{90}) over the hydrothermally aged commercial TWC for all the fuel blends investigated. Error bars represent 95% confidence intervals calculated from three replicate runs. 323

Figure II.24.1. (a) Explains the labeling format for this report in reference to the different conditions studied. The shape indicates which fuel, the shading indicates the % EGR, the color indicates for which type of air-fuel stratification the condition would be classified. (b) A plot of the conditions tested in this project. 327

Figure II.24.2. (a) Plot comparison of PM mass rate for each condition tested. PM mass rates were calculated from both gravimetric (black lines) and EC/OC (gray lines) filter analyses. Solid lines indicate RON 87 fuel test points and dashed lines indicate RON 70 fuel test points. (b) Mass rate data from the EC/OC analyses showing fraction speciated as EC (gradient black) and OC (colored) compared to the microsoot sensor mass rate data (solid black to right or comparable EC/OC data). Fuels are differentiated by the OC fill color (RON 70, white; RON 87, shaded color), as indicated in the legend. 327

Figure II.24.3. Stacked bar graphs in (a) compare C1 HC emissions in order of increasing air-fuel stratification. The open bars represent the hydrocarbons measured by a FID, and the blue bars represent the aldehyde contribution measured using DNPH cartridges. Percent values above the bars indicate the aldehyde fraction of the total C1 HC emissions. Graph (b) shows breakdowns in the aldehyde composition, measured with DNPH, in terms of C_x (x = number of carbons). No significant presence of aldehydes was measured by DNPH for the RON 70, 15% EGR (HFS) conditions; confirmation of this is still under way. Symbols at the bottom of each bar in (a) and (b) graphs indicate the engine conditions (see Figure II.24.2a). 328

Figure II.24.4. Size distribution plots for particulate flux at each condition tested. (a) RON 87 fuel and (b) RON 70 fuel from EEPS real-time exhaust sampling downstream of 2-stage dilution tunnel, which included a denuder. HCCI (red), PFS (orange), HFS (green). Arrow shows direction conditions with increasing air-fuel stratification. 329

Figure II.24.5. The particle flux (a) sum of all particle sizes measured by EEPS at each engine condition. The stacked bar graph (b) shows the fraction distribution of the total particle flux values associated with sub-25-nm, nuclei mode particulate (bottom, darker gray) and those that fall in the accumulation mode region above 25 nm (top, lighter gray). 329

Figure II.25.1. Experimental (symbols) and simulated (lines) ignition delay times of cyclopentanone in air at $\phi = 0.5, 1.0, \text{ and } 2.0$, and $P = 15$ bar. Solid and open symbols are shock tube and RCM experimental results, respectively [2]. 333

Figure II.25.2. Experimental (symbols) and simulated (lines) ignition delay times of cyclopentanone in air at $\phi = 0.5, 1.0, \text{ and } 2.0$, and $P = 30$ bar. Solid and open symbols are shock tube and RCM experimental results, respectively [2]. 333

Figure II.25.3. Experimental and simulated pressure histories from the autoignition of an E10 research-grade 87 anti-knock index gasoline at various pressures at the end of compression (EOC) in the Argonne National Laboratory RCM. 334

Figure II.26.1. Prediction of RON and OS for the simulated blending of nine HPFs into the Co-Optima core fuels. 338

Figure II.26.2. Predicted (curves) and measured (symbols) laminar flame speeds of cyclopentanone at different fuel-air equivalence ratios and unburned gas temperatures. Experiments: University of Central Florida, black symbols; Lund University, red and blue symbols. 339

Figure II.26.3. Predicted (curves) and measured (symbols) laminar flame speeds of methyl acetate and ethyl acetate at different fuel-air equivalence ratios and unburned gas temperatures. Experiments: Lund University [2]. 339

Figure II.27.1. Composition of the four-component Co-Optima BOB and the five virtual BOBs that maximize the volume fraction of each of the PIONA classes. The octane numbers predicted by the neural network match the Co-Optima BOB (90.3 RON and 84.7 MON) to within 0.1 octane numbers. 343

Figure II.27.2. Variation of the merit score across the four-component Co-Optima BOB and the five virtual BOBs as a function of blending level of four blendstocks: (a) ethanol, (b) iso-butanol, (c) 3-pentanone, and (4) methylacetate	344
Figure II.28.1. (left) CFR engine geometry (red: knockmeter port cavity; green: intake valve with 180° shroud; blue: spark plug and cavity). (right) Temporal evolution of in-cylinder pressure for both experiment and simulation (spark timing: -13 CAD ATDC).	349
Figure II.28.2. Contour plots of OH and CH ₂ O mass fractions and local pressure difference on a horizontal cut plane passing through the spark plug electrode, at knock onset. Intake and exhaust valves are located on the left and right sides, respectively. Knockmeter port cavity can be seen at the bottom.	349
Figure II.28.3. (left) Knock intensity as a function of spark timing. Grey dot: knock intensity from each cycle CFD result with Mach CFL 50; red dot: maximum knock intensity at each spark timing with Mach CFL 50; blue dot: maximum knock intensity divided by two at each spark timing with Mach CFL 5. CFL number controls CFD time-stepping method, and larger value indicates large time step and faster simulation time. (right) Sensitivity index indicated thermal efficiency.	351
Figure II.28.4. (left) Maximum knock intensity for different HoV values. KLSA predicted by the slope change point is highlighted by red dot. (right) Relative difference in BSFC for two HoVs. Negative value means lower BSFC for 115% HoV.	351
Figure II.29.1. Updated two-color pyrometer design illustrating equal path lengths and equal number of components (left) and sample images of a sooting n-heptane flame with the bandpass filters removed (right). Note the images appear horizontally flipped due to beam splitter reflecting 50% of light and letting 50% pass straight.	355
Figure II.29.2. Computer-aided drafting illustration of how the three diagnostics are set up in relation to the CPFR.	355
Figure II.29.3. Demonstration of simultaneous two-color pyrometry, rainbow schlieren deflectometry, and OH* chemiluminescence measurements using a simple Bunsen burner.	356
Figure II.29.4. New high-pressure air compressor that can supply up to 150 bar continuous air flow and enables testing at the full capacity of the current CPFR at 60 bar.	356
Figure II.29.5. Demonstration of neural network prediction of liquid length data from the Engine Combustion Network hosted by Sandia National Laboratories. Symbols are data from experiments and lines represent predictions from the neural network.	357
Figure II.30.1. Cycle diagram showing gas exchange and open valve periods where species reduction is applied.	360
Figure II.30.2. (a) CONVERGE mesh for CFR combustion chamber; (b) Direct injection (DI)/ACI chamber mesh based on Ford 1.6 L, 4-valve pent roof design	360
Figure II.31.1. Microcombustion results for Co-Optima fuel blends with matched RON and partially matched octane sensitivity. Fuel samples courtesy of Szybist/Oak Ridge National Laboratory [1]. Results presented at 2018 Annual Merit Review (I. Schoegl/LSU).	364
Figure II.31.2. Uncertainty quantification for temperature measurements via pyrometry (Schoegl/LSU)	365

Figure II.31.3. Operating conditions tested for nano-liter fuel delivery at ambient and elevated pressures (S. Menon/LSU).....	366
Figure II.32.1. Sooting tendencies of amines ($C_4H_{11}N$ isomers) compared with structurally analogous alcohols and ethers ($C_4H_{10}O$ isomers). The sooting tendencies of the oxygenates were either measured directly or they were estimated with the National Renewable Energy Laboratory (NREL) structure-property model (red asterisks); see Key Publication 1.....	370
Figure II.32.2. Soot yields for mixtures of a conventional diesel fuel and the optimal NREL acid-upgrading blendstock. The results are normalized to the pure diesel fuel. Each mixture was added to the flame at a fixed flow rate of 100 μ l/hour.....	370
Figure II.32.3. YSIs predicted for dioxolanes and related hydrocarbons with the NREL structure-property model. The panel on the left is with the original database, while the panel on the right shows improved predictions after measurements of the dioxolanes synthesized at Los Alamos National Laboratory were added to the database.	371
Figure II.32.4. Measured YSI versus reference-case YSI for various air-fuel ratios (λ) and adiabatic flame temperatures (T_{ad}). The reference-case YSI for each fuel is the YSI measured with $\lambda = 0$ and $T_{ad} = 2,224$ K.	371
Figure II.32.5. YSIs for n-alkanes (left panel) and aromatic hydrocarbons (right panel) predicted with computational simulations at pressures from 1–15 atm.....	372
Figure II.32.6. YSI predictions for 20 Co-Optima Tier 2 and Tier 3 blendstocks using chemical-kinetic-based simulations.....	372
Figure III.1.1. Single-cylinder engine RCCI results with diesel fuel as the DI fuel and PRF80 as the premixed fuel for varying injection timings as an example result of a fuel reactivity separation study.....	378
Figure III.1.2. An experimental comparison between diesel-reformate RCCI and diesel-gasoline RCCI collected on a fully instrumented, single-cylinder research engine.....	379
Figure III.1.3. Cut-plane equivalence ratio distribution and temperature distribution from the CFD simulations of single-fuel RCCI combustion with diesel and its reformate.....	379
Figure III.2.1. CCV comparison between two ignition systems, each over two operating conditions....	383
Figure III.2.2. CCV comparison between two ignition systems, each over two operating conditions....	383
Figure III.2.3. Images are binarized and compared to adjacent pixels and relation to the ignited spark image, to assess if they are valid images or noise.....	383
Figure III.2.4. Validation of automated to manual ignition processing techniques over two different types of ignition systems (evaluated at the same operating point and condition).....	384
Figure III.2.5. Hencken burner test set-up for igniter plasma imaging under atmospheric conditions ...	385
Figure III.2.6. Image of corona plasma during the 350 μ s duration corona generation phase is visible in the UV band with the Hencken burner, while the combustion flame front can be seen in the subsequent images.....	385
Figure III.3.1. Trending PM concentrations for all tests with OEM aftertreatment average PM mg/m^3	391

Figure III.4.1. Dedicated EGR engine configuration.....	393
Figure III.4.2. Updated engine configuration for dedicated cylinder testing.....	394
Figure III.5.1. Knock-limited phasing of propane and isooctane at two compression ratios and various intake temperatures	397
Figure III.5.2. Custom high-efficiency research engine with 1.5:1 stroke-to-bore ratio and high compression ratio	397
Figure III.5.3. Enthalpy ratio of reformed products to initial products in the synthetic exhaust flow reactor for three different engine conditions	398
Figure III.5.4. Modified gasoline direct injection pump with bleed port for propane	399
Figure III.5.5. (a) Spark-to-CA10 combustion duration and (b) COV of IMEP for both gasoline and propane as a function of the cam overlap at 2,000 rpm and 4 bar brake mean effective pressure (BMEP)	399
Figure III.5.6. Combustion efficiency for both gasoline and propane as a function of the cam overlap at 2,000 rpm and 4 bar BMEP	400
Figure III.6.1. Bench-scale fuel injector flow rig for flow studies through the OEM piezoelectric fuel injector from a Ford 6.7-L diesel engine (Figure: Jacob Barson, NREL)	403
Figure III.7.1. Kinetic intensity vs. average speed for the NREL package delivery cycle vs. various standard drive cycles.....	408
Figure III.7.2. Schematic of the GT-SUITE injection system model developed for the 4.3-L engine	409
Figure III.7.3. Representative pressure oscillations in Injector Bank #1 of the injection system of the 4.3-L engine for indolene (gasoline) operation at a nominal inlet pressure of 200 bar.....	410
Figure IV.1.1. 2018 CLEERS Workshop registrations by type of organization	414
Figure IV.1.2. 2018 CLEERS Workshop presentation topics	414
Figure IV.1.3. (a) Core sample temperatures, (b) outlet NO concentration, (c) outlet CO concentration, and (d) outlet CO ₂ concentration measured during a synthetic exhaust flow reactor experiment conducted with a Pd-exchanged ZSM-5 catalyst sample	415
Figure IV.1.4. Impact of changing CO concentration on NO uptake and release measured in a synthetic exhaust flow reactor over a Pd-exchanged ZSM-5 PNA core sample. NO concentration during (a) isothermal uptake and (b) TPD; CO concentration during (c) isothermal NO uptake and (d) TPD; (e) integrated NO adsorption and desorption.....	417
Figure IV.1.5. Schematic of NO storage and release on a Pd-exchanged ZSM-5 PNA	417
Figure IV.2.1. NO _x conversions as a function of temperature during standard SCR for selected Cu, H/SSZ-13 and Cu, Na/SSZ-13 degreened catalysts. Reactant feed contains 360 ppm NO _x (containing ~20 ppm NO ₂), 360 ppm NH ₃ , 14% O ₂ , 2.5% H ₂ O balanced with N ₂ at a gas hourly space velocity of 100,000 h ⁻¹	421

Figure IV.2.2. PNA performance of 1 wt% and 1.9 wt% Pd/SSZ-13 with Si/Al = 6. NO _x adsorption at 100°C for 10 min (after 10 min bypass) followed with temperature-programmed desorption (10°C/min). The feed gas mixture contains 200 ppm of NO _x , 14% O ₂ , 3% H ₂ O with 200 ppm CO. Note that for 1.9 wt% Pd/SSZ-13, more time was needed for the NO _x to get back to the initial level due its high effectiveness at abating NO _x ; the desorption of NO _x , therefore, was started after ~23 min.	422
Figure IV.2.3. Low-Temperature Three-Way Catalyst Test Protocol, the third protocol prepared by the LTAT group of the ACEC Tech Team and released to the technical community at https://cleers.org/low-temperature-protocols	423
Figure IV.2.4. CO oxidation light-off performance showing excellent low-temperature activity and stability of the hydrothermally treated Pt/CeO ₂ catalyst under exhaust conditions ([O ₂] = 10%, [CO] = 0.4%, gas hourly space velocity = 200 L (gcat hr) ⁻¹)	423
Figure IV.2.5. Pore size distributions in samples from three axial regions in a commercial SCR-filter	424
Figure IV.3.1. (a) 2% Pt catalysts supported on a 20% SiO ₂ /80% Al ₂ O ₃ support from Solvay show exceptionally low THC light-off behavior in the fresh state using the U.S. DRIVE evaluation protocol, but even mildly aging at 700°C for 4 h (degreened) results in lost activity. (b) Of all the samples evaluated, Pt-based catalysts (+) show the lowest light-off temperatures, while aging up to 800°C continues to degrade performance.	427
Figure IV.3.2. Varying the Si content of the primarily alumina support material results in a decrease in THC light-off temperature in the 10–30% Si content range. One of the samples contained 4% La, which increases the THC light-off temperature.....	428
Figure IV.3.3. (a) In the degreened state, the Pd/ZSM-5 stores significant concentrations of C ₃ H ₆ , C ₁₀ H ₂₂ , and NO following the U.S. DRIVE trapping protocol. (b) Upon aging at 800°C, only C ₁₀ H ₂₂ is stored, but it is in large quantities, thus illustrating the ability of ZSM-5 to be useful as a HC trap material.	428
Figure IV.3.4. (a) Fully hydrothermally aging the oxidation catalysts according to the U.S. DRIVE protocol results in significant losses in activity. (b) Including a hydrothermally aged trap material, Pd/ZSM-5, in front of the oxidation catalyst results in significant improvements of the catalytic activity.....	429
Figure IV.3.5. Summary of T ₅₀ and T ₉₀ light-off temperatures at each of the different aging steps for the dual-bed Pd/ZSM-5 and oxidation catalyst combination.....	429
Figure IV.3.6. (a) Dual-bed configuration with Pd/ZSM-5 HC-trap in front of the oxidation catalysts while heating at a rate of 40°C/min. Significant HC quantities are trapped at low temperature and then released at 194°C before being oxidized at higher temperatures. (b) When physically mixing the trap and the oxidation catalyst in the same bed, the released HCs are more readily converted over the oxidation catalyst.	430
Figure IV.4.1. Tail-pipe emissions from a lean gasoline engine equipped with a passive SCR system over a pseudo-transient drive cycle using different operating strategies	434
Figure IV.4.2. (a) H ₂ production from CO + H ₂ O and (b) NH ₃ production from NO + CO + H ₂ O using catalysts with different Ce loading. Blue lines are catalyst activities at 350°C, yellow lines are activities at 450°C, and red lines are activities at 550°C.	435

Figure IV.4.3. NH ₃ production from NO + H ₂ + H ₂ O (left), NH ₃ production from NO + CO + H ₂ O (middle), and H ₂ production from CO + H ₂ O (right) on Malibu-1 (top) and ORNL-1 (bottom) evaluated clean, while flowing SO ₂ , and after sulfation.....	435
Figure IV.5.1. SCR-onset conversion inflections for (a) a commercial Cu-CHA SCR catalyst and (b) a model Cu-Beta [1] SCR catalyst	438
Figure IV.5.2. Conceptual model of Cu-SCR CI origin [4].....	439
Figure IV.5.3. Five-Step Protocol for characterizing onset transients for the individual and combined Cu-redox half cycles [4].....	440
Figure IV.5.4. (a) Variation in r-ratio ($r_{\text{RHC}}/r_{\text{OHC}}$) with temperature; (b) variation in N ₂ CI with increasing r-ratio.....	440
Figure IV.5.5. Kinetic model results for varying NO (50, 100, 150, 200, 250 ppm) at constant 200 ppm NH ₃ for (a) N ₂ , (b) NO CI, and (c) r_{RHC} and r_{OHC} . (d) Spatiotemporal CI distribution for a field-aged commercial Cu-SCR catalyst and 200 ppm standard SCR; L is total catalyst length, e.g., 1/8L is 1/8th along the catalyst length.....	441
Figure IV.5.6. Kinetic-model predictions of the (a) NO, NH ₃ and N ₂ onset transients for fast SCR, and (b) corresponding N ₂ -specific NO and NH ₃ transients	441
Figure IV.6.1. Comparison of controlling pore size distributions for the C1 and A2 substrates found using a custom-built CFP system	445
Figure IV.6.2. Reconstructed microstructure (left), flow solution (center), and simulated concentration field (right)	445
Figure IV.6.3. Comparison between measured initial penetration of 50-nm particles through various filter materials and predictions made by microscale lattice-Boltzmann simulations	446
Figure IV.6.4. Comparison between measured initial penetration of 50-nm particles through various filter materials and predictions made by a modified spherical unit collector model.....	446
Figure IV.6.5. Size-resolved filtration efficiency predicted by a classical spherical unit collector model and by a new constricted tube collector model compared to experimental data for the C2 filter substrate ...	447
Figure IV.7.1. NO _x uptake and release for 1 wt% Pd/SSZ-13 with Si/Al = 6, 12, and 30, before and after hydrothermal aging	451
Figure IV.7.2. Transmission electron microscopy images of 1 wt% Pd/SSZ-13 with Si/Al = 6 after hydrothermal aging	451
Figure IV.7.3. ²⁷ Al NMR spectra of fresh and hydrothermally aged 1 wt% Pd/SSZ-13 with Si/Al = 6, 12, and 30.....	452
Figure IV.7.4. Methane conversion as a function of time on stream for 3 wt% Pd/SSZ-13 with Si/Al = 6, 12, 24, and 36.....	452
Figure IV.7.5. Comparison of 3 wt% Pd/SSZ-13 (Si/Al = 36) with Pd/Al ₂ O ₃	453
Figure IV.8.1. SCR standard (NO only) performance of Cu-SSZ-13 and Cu-SSZ-13 + 10 wt% ZrO ₂ catalyst	456

Figure IV.8.2. NH ₃ oxidation (by O ₂ , i.e., without NO _x) activity of Cu-SSZ-13 and Cu-SSZ-13 + 10 wt% ZrO ₂ at varying proximity of SCR and SCO catalyst phases	457
Figure IV.8.3. TPR behavior of Cu-SSZ-13 + 10 wt% ZrO ₂ catalyst compared to that of Cu-CHA alone and ZrO ₂ alone	458
Figure IV.8.4. Pathway towards improved NO _x reduction performance by a surface-active NO _x species	458
Figure IV.8.5. Thermally induced ion-exchange aging mechanism of Cu-CHA + Ba/ZrO ₂ binary catalyst	459
Figure IV.9.1. Engine and instrumentation schematic showing dilution system and instruments used in the experimental study	462
Figure IV.9.2. Engine-out PSDs for the lean homogenous combustion mode at the four different engine conditions for each of the seven fuels tested. From top left to bottom right: LH1, LH2, LH3, and LH4.	464
Figure IV.9.3. Correlation between PN and the PMI for the lean homogenous combustion mode at the 2,000 rpm 7 bar BMEP engine condition with the E50 fuel omitted.....	464
Figure IV.9.4. PN > 23 nm filtration efficiency as a function of non-oxidized soot mass loading on the GPF per filter substrate volume	465
Figure V.1.1. Project schedule and phasing (Volvo)	467
Figure V.1.2. Baseline Model Year 2009 vehicle (left) and VEV3 test mule (right) at rest stop during fuel economy test (Volvo)	468
Figure V.1.3. Synthetic exhaust gas flow reactor rig at Oak Ridge National Laboratory (Volvo).....	470
Figure V.2.1. Mule vehicle WHR system integration. This system will be applied in stages in late 2019, finishing in 2020.	476
Figure V.3.1. Effects of cylinder deactivation on BSFC.....	479
Figure V.3.2. Turbocharger optimization	480
Figure V.3.3. Advanced fuel injection strategy simulation.....	480
Figure V.3.4. Schematic of intent ORC system	481
Figure V.3.5. Effects of oil temperature on BTE of high-temperature and baseline pistons	481
Figure V.3.6. Efficiency breakdown and loss comparison at peak BTE for diesel, EEE, and E85 with a new injector.....	482
Figure V.4.1. Phases of SuperTruck 2 project.....	484
Figure V.4.2. ST2 collaboration model	485
Figure V.4.3. ST2 updated validation methodology	486
Figure V.4.4. Detroit roadmap to reach the 55% BTE target.....	487

Figure V.4.5. Daimler Trucks North America updated pathway to reach 115% freight efficiency target	488
Figure V.4.6. A-Sample impacted bills of material.....	488
Figure V.5.1. Route selection to evaluate SuperTruck technologies.....	491
Figure V.5.2. Forecasted freight efficiency	492
Figure V.5.3. Aerodynamic development (computational fluid dynamics)	493
Figure V.5.4. Vehicle velocity vs. grade to determine power requirement	494
Figure V.5.5. Engine roadmap to 55% BTE	495
Figure V.6.1. Gen 3X GDCI engine.....	499
Figure V.6.2. Preliminary load sweep at 1,500 rpm for the Gen 3X GDCI engine	500
Figure V.6.3. Initial BSFC contour map for Gen 3X GDCI engine.....	501
Figure V.6.4. Engine compartment of completed Gen 3 vehicle	501
Figure V.6.5. Simulated vehicle fuel economy results for the 2.2 L Gen 3X GDCI engine with various powertrain technologies compared to baseline engine and full hybrid engines (Argonne).....	502
Figure V.7.1. Fuel consumption improvement achieved during SCE calibration optimization on final MCE hardware set	506
Figure V.7.2. First steady-state engine (fixed-drive supercharger) and dyno installation.....	507
Figure V.7.3. BSFC reduction of LMC engine running in SMC mode with external EGR, naturally aspirated key points.....	507
Figure V.7.4. Cycle fuel economy predictions based on weighted test points.....	508
Figure V.7.5. Transient dyno hardware package.....	509
Figure V.8.1. Revised path to 55% BTE from project's demonstrated peak BTE.....	513
Figure V.9.1. UDDS and HWFET drive cycle test results.....	515
Figure V.9.2. Efficiency gain of LTC	516
Figure V.9.3. Effects of fuel mass injected for second injection.....	516
Figure V.9.4. Coefficient of variation of IMEP at 50 V/1,000 ms, 55 V/1,000 ms, and 60 V/1,500 ms	517
Figure V.9.5. Coefficient of variation of IMEP and crank angle at 50% mass fraction burned for voltage from 50 V to 70 V.....	517
Figure V.9.6. Igniter-by-igniter variation.....	517
Figure V.10.1. Locking mechanism friction comparison.....	521
Figure V.10.2. Final engine build DRFF hardware.....	521

Figure V.10.3. GEN 5 solenoid force vs. stroke throughout durability test.....	522
Figure V.10.4. Complete DSF cylinder head assembly on test stand	522
Figure V.10.5. Actuator driver module	523
Figure V.10.6. Baseline engine installed in dyno cell.....	523
Figure V.11.1. Surface roughness is greatly improved by filtering spheres for size and using a top layer of small-diameter spheres sintered under pressure; this results in a more robust sealing layer.....	526
Figure V.11.2. Valve prototypes with microshell TBC applied to the face were fabricated by (1) machining stainless steel valves with a pocket in the face, (2) filling the pocket with nickel microshells and sintering, (3) bonding a nickel foil to the surface, and (4) final heat treatment and clean-up	527
Figure V.11.3. Exhaust port liner coating process begins with (1) plating a core with solid nickel to form a shell once the core is dissolved, (2) spraying the shell with a TBC microshell and binder slurry and sintering, and (3) spraying over the TBC with a ceramic protective coating and curing	527
Figure V.11.4. Exhaust temperatures in the center (left) and near the wall (right) at the exhaust port exit	527
Figure V.11.5. Pre- and post-test conditions of Generation 2 coated valves vs. Generation 1	528
Figure VI.1.1. HP PTWA coating shows friction benefits with DLC, PVD, and nitride ring face coatings	532
Figure VI.1.2. Cranktrain friction as a function of engine speed at 100°C oil temperature for various HP PTWA coatings.....	532
Figure VI.1.3. Cranktrain friction as a function of engine speed at 100°C oil temperature for various piston ring face coatings with HP PTWA 3 coating.....	533
Figure VI.1.4. Cranktrain friction as a function of engine speed at 100°C oil temperature for various piston ring face coatings with HP PTWA 3 coating.....	533
Figure VI.1.5. Motored engine friction tests showed HP PTWA coatings offer friction benefit	534
Figure VII.1.1. High-resolution C1s XPS analysis of the functionalized GO fillers before the reduction	541
Figure VII.1.2. High-resolution C1s XPS analysis of the functionalized GO fillers after the reduction	541
Figure VII.1.3. High-resolution N1s XPS analysis of the functionalized GO fillers (a) before and (b) after the reduction.....	541
Figure VII.1.4. SBS samples filled with rGO at several weight contents.....	542
Figure VII.1.4. SBS samples filled with rGO at several weight contents.....	542
Figure VII.2.1. Example of sampling data for determination of diffusion coefficients.....	547

List of Tables

Table 1. Hybrid Technology Approach Risk Assessment (Hergart, V.5)	26
Table I.3.1. Physical and Chemical Properties of CRC AVFL-18a Diesel Surrogates	46
Table I.9.1. Engine Operating Conditions of 90 dB Constant Combustion Noise Parametric Sweeps....	89
Table I.10.1. Comparison of Plasma Properties between Modeling and Experiments	95
Table II.2.1. Results of Engine Experimental and Vehicle Modeling Study	193
Table II.2.2. Fleet-Average On-Road Driving Results for All Fuels	194
Table II.3.1. Fuels Working Group Expanded Matrix Fuel Formulations	198
Table II.10.1. Tested Fuels	242
Table II.11.1. Tested Fuels	248
Table II.12.1. Fuel Properties.....	254
Table II.19.1. Properties of Aromatics Blended into FACE B Gasoline.....	295
Table II.19.2. Measured Compositions of Fuels, HOV, and PMI (computed from detailed hydrocarbon analysis)	296
Table II.19.3. Engine Operating Conditions for PM Measurements; Intake Air Temperature Fixed at 35°C	296
Table II.19.4. Results of Linear Regression Analysis for Condition A Using Mole Percent Concentrations of Ethanol and Aromatics in the Blends	301
Table II.19.5. Regularized Regression Results and Statistics	302
Table II.20.1. Reduced Component Surrogates for FACE A Fuel Corresponding to Multi-Component Surrogate from Sarathy et al. [4].....	307
Table II.22.1. Composition of Diesel Fuels/Diesel Fuel Surrogate*	316
Table II.23.1. Surrogate BOB Composition.....	321
Table II.23.2. Synthetic Engine Exhaust Gas Composition.....	321
Table II.27.1. Comparison of the Neural Network Model Predictions for Octane Numbers and the ASTM Standard Measurements D2699 and D2700	345
Table II.28.1. Mean Knock Characteristics from Experiments and Simulations.....	349
Table III.1.1. Diesel-Reformate RCCI Compared to Diesel-Gasoline RCCI at an Example Operating Condition.....	378
Table III.2.1. Aftertreatment Simulation Emissions and Fuel Economy Projected Attainment	386
Table III.2.2. Partial Example of Early TCO Calculation Tool	386
Table III.2.3. Preliminary System Payback Scenarios Comparison	387

Table III.6.1. Estimated Volumetric Blending for Propane/Natural Gasoline	403
Table IV.1.1. Experiment Parameters.....	416
Table IV.2.1. Apparent Activation Energy and Turn-Over Rate Summary of Cu, H/SSZ-13, and Cu, Na/SSZ-13 Catalysts. Reaction feed contains 360 ppm NO _x (containing ~20 ppm NO ₂), 360 ppm NH ₃ , 14% O ₂ , 2.5% H ₂ O balanced with N ₂ at a gas hourly space velocity of 667,000 h ⁻¹ . Temperatures were varied from 180°C to 100°C.....	420
Table IV.4.1. Compositions of the Synthesized Catalysts for Evaluation of the Effect of Ce Loading.....	434
Table IV.6.1. Summary of Simulation and Modeling Approaches Applied throughout the Project.....	447
Table IV.9.1. Fuel Property Data and PMI.....	462
Table IV.9.2. Engine Conditions Including Operating Mode and Equivalence Ratio	463
Table V.11.1. Milestone Status.....	528
Table VI.2.1. Percent Improvement of Fuel Efficiency of 0W-16 Formulations.....	537
Table VII.2.1. Compound Data of Silica Prototypes with Different Surface Treatments.....	546
Table VII.2.2. Compound Data of Silica Prototypes with Different Morphologies	547
Table VII.2.3. Resistance to Degradation of Silica Prototypes with Different Morphologies.....	548

(This page intentionally left blank)

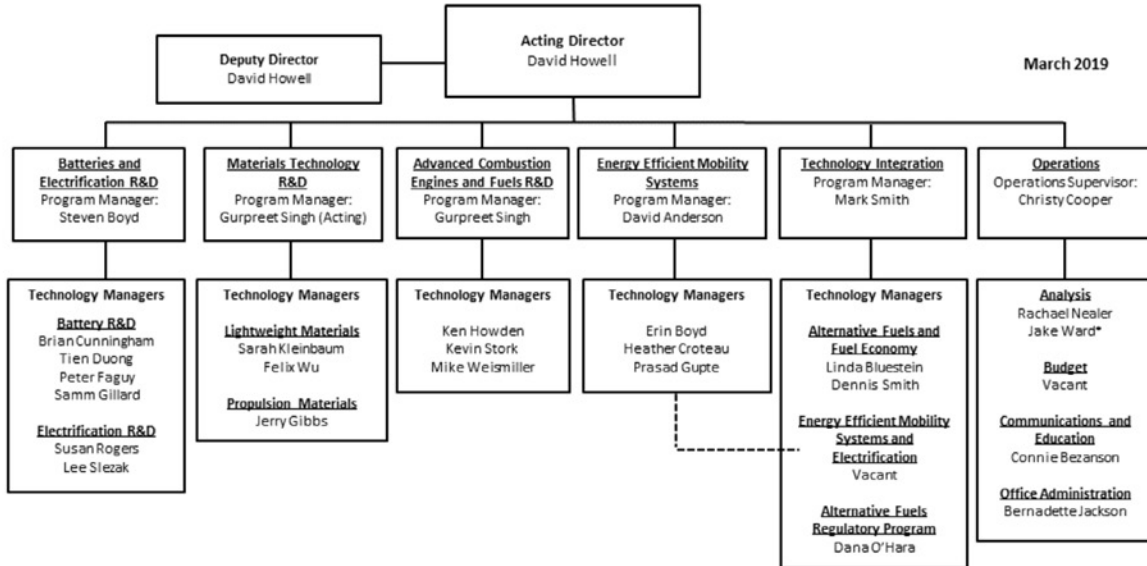
Vehicle Technologies Office Overview

Vehicles move our national economy. Annually, vehicles transport 11 billion tons of freight – more than \$32 billion worth of goods each day – and move people more than 3 trillion vehicle-miles. Growing our national economy requires transportation and transportation requires energy. The transportation sector accounts for 70% of U.S. petroleum use. The United States imports 20% of the petroleum consumed – sending more than \$15 billion per month overseas for crude oil. The average U.S. household spends nearly one-sixth of its total family expenditures on transportation, making transportation the most expensive spending category after housing.

To strengthen national security, enable future economic growth, improve energy efficiency, and increase transportation energy affordability for Americans, the Vehicle Technologies Office (VTO) funds early-stage, high-risk research on innovative vehicle and transportation technologies. VTO leverages the unique capabilities of the national laboratory system and engages private sector partners to develop innovations in electrification, including advanced battery technologies; advanced combustion engines and fuels, including co-optimized systems; advanced materials for lighter-weight vehicle structures; more efficient powertrains; and energy efficient mobility systems.

VTO is uniquely positioned to address early-stage challenges due to strategic public-private research partnerships with industry (e.g. U.S. DRIVE, 21st Century Truck Partnership) that leverage relevant expertise. These partnerships prevent duplication of effort, focus DOE research on critical R&D barriers, and accelerate progress. VTO focuses on research that industry does not have the technical capability to undertake on its own, usually due to a high degree of scientific or technical uncertainty or is too far from market realization to merit industry resources.

Organization Chart



¹ Bureau of Transportation Statistics, DOT, 2016. Table 3-1 Weight and Value of Shipments by Transportation Mode https://www.bts.gov/archive/publications/transportation_statistics_annual_report/2016/tables/ch3/table3_1

² Ibid.

³ Transportation Energy Data Book 37th Edition, ORNL, 2018. Table 3.8 Shares of Highway Vehicle-Miles Traveled by Vehicle Type, 1970-2016.

⁴ EIA Monthly Energy Review <https://www.eia.gov/totalenergy/data/monthly/pdf/mer.pdf>

⁵ Bureau of Labor Statistics, Consumer Expenditure Survey, 2017. Average annual expenditures and characteristics of all consumer units, 2013-2017. <https://www.bls.gov/cex/2017/standard/multiyr.pdf>

Advanced Combustion Engines and Fuels Program Overview

Introduction

The Advanced Combustion Engines and Fuels Program supports the Vehicle Technology Office's goal and focuses early-stage research and development (R&D) to improve understanding of the combustion processes, fuel properties, and emission control technologies while generating knowledge and insight necessary for industry to develop the next generation of engines and fuels.

Cutting-edge research using unique capabilities and expertise at the national laboratories, done in close collaboration with academia and industry, will strengthen the knowledge base of the next generation of higher-efficiency, very-low-emissions combustion engines for passenger and commercial vehicles. In addition, a science-based understanding of how engine efficiency and emissions are impacted by fuel properties, and conversely, how engines can be modified to take advantage of desirable fuel properties, could enable further efficiency improvements. The fundamental knowledge and new understanding developed by this program can be used to co-optimize engines, fuels, and emission controls (exhaust aftertreatment). Market introduction of these co-optimized high-performance fuels and advanced engines that meet prevailing emissions regulations could expeditiously reduce petroleum use in U.S. highway transportation over the next several decades, during which time the Energy Information Administration reference case forecasts that the vast majority of vehicles sold will still include an engine.¹

Goals

The Advanced Combustion Engines and Fuels R&D Program set the following goals for improvement of the fuel economy of passenger and commercial vehicles.

- By 2025, improve light-duty engine efficiency to demonstrate 35% improvement in passenger vehicle fuel economy (25% improvement from engine efficiency and 10% from fuel co-optimization) relative to a 2015 baseline vehicle, while meeting U.S. Environmental Protection Agency Tier 3 emissions standards
- By 2030, improve heavy-duty engine efficiency by 35% relative to a 2009 baseline vehicle and identify cost-effective high-performance fuels that can further increase efficiency up to an additional 4%, while meeting prevailing U.S. Environmental Protection Agency emissions standards

The U.S. Environmental Protection Agency Tier 3 Bin 30 emissions standard for passenger vehicles represents a greater than 80% reduction in combined emissions of nitrogen oxides (NO_x) and non-methane organic gases and a 70% reduction in particulate matter (PM) emissions (to less than 3 mg/mi) compared to the previous Tier 2 Bin 5 standard. Future catalyst and emission control systems must be able to operate efficiently at the lower exhaust temperatures of advanced combustion engines (i.e., greater than 90% conversion of criteria pollutants at 150°C) to achieve these extremely low criteria pollutant emission levels.

State of the Art

Gasoline and diesel engines continue to be attractive options to power transportation vehicles due to significant advances in engine combustion, emission control, and fuel technologies that continue to increase the thermal efficiency of these engines and simultaneously reduce regulated emissions. Also, these engines can be readily adapted to use natural gas and biofuels such as ethanol and biodiesel. Integrated with hybrid and plug-in hybrid electric vehicle powertrains, these engines can be operated at fuel-efficient speed-load conditions. This next-generation hybrid engine-electric drivetrain could offer a cost-competitive and fuel-efficient powertrain as the U.S. transportation sector transitions to full electrification.

¹Energy Information Administration, *Annual Energy Outlook 2018*. Reference case scenario forecasts that even in 2050, over 96% of all highway transportation vehicles sold will still have internal combustion engines.

Spark-ignition (SI) gasoline engines power the majority of the U.S. light-duty vehicle fleet. They generally operate with stoichiometric combustion to allow use of highly efficient and cost-effective three-way catalysts for emission control. Engine technology advances in recent years contributing to substantial improvements in gasoline engine efficiency include direct fuel injection, flexible valve timing and lift systems, improved combustion chamber design, and reduced mechanical friction losses.

Boosted air handling systems and direct injection fueling systems have enabled gasoline SI engine downsizing, which has been a major trend during the last decade to improve light-duty vehicle fuel economy. Further efficiency improvement of these higher-power-density downsized engines through higher compression ratios, however, has been constrained by current fuel properties. Fuel autoignition, which causes engine knock, is limiting the compression ratio of SI engines.

Lean-burn (or dilute) gasoline combustion engines have higher efficiencies at part load but require lean- NO_x emission controls to meet the more stringent U.S. emissions regulations. They have been introduced in countries with less stringent emissions regulations. Advances in lean-burn gasoline combustion and emission controls are critical for introducing this higher-efficiency technology in the U.S. market.

Achieving high efficiency in lean-burn gasoline engines depends on creating combustible mixtures near the spark plug and away from cylinder walls in an overall lean environment. A comprehensive understanding of the dynamics of fuel–air mixture preparation is required, i.e., intake air flows and fuel sprays, as well as their interactions with the combustion chamber surfaces over a wide operating range and generating appropriate turbulence to enhance flame speed. Improved simulation tools are being developed for optimizing the lean-burn systems over the wide range of potential intake systems, piston geometries, and injector designs. Also, robust, high-energy ignition systems and mixture control methods are being investigated to reduce combustion variability at lean, highly boosted conditions, and achieve reliable ignition and combustion; examples include high-energy plugs, plasma, corona, and laser ignition systems.

Low-temperature combustion (LTC) strategies such as homogeneous charge compression ignition, pre-mixed charge compression ignition, and reactivity-controlled compression ignition exhibit high efficiency with engine-out emissions of NO_x and PM at very low levels, thereby reducing exhaust aftertreatment requirements. Significant R&D efforts have focused on air handling and conditioning of intake air, fuel–air mixing, fuel property impacts, combustion timing control, and transient response. Progress in LTC strategies continues to expand the operational range, covering speed and load combinations consistent with light- and heavy-duty drive cycles.

Multi-mode combustion strategies combine two operating modes to achieve overall higher efficiency compared to SI-only operation: (a) boosted spark ignition during starting and high-load operation to achieve suitable power density and (b) LTC modes under low and medium loads for high efficiency. R&D efforts will focus on controlling transitions between the two operating modes, expanding the speed and load range during LTC, improving cold operation, and reducing combustion noise.

Diesel engines are also well-suited for light- and medium-duty vehicle applications, delivering fuel economies that are considerably higher than those of comparable SI engines. Key developments in combustion and emission controls have enabled manufacturers to achieve the mandated emissions levels and introduce new diesel-powered models to the U.S. market. U.S. Department of Energy (DOE) research has contributed to all of these areas. However, diesels in passenger cars have limited market penetration in the United States, primarily due to the cost of the added components required to reduce emissions; hence, research was focused on increasing engine efficiency and reducing the cost of emissions compliance.

The heavy-duty diesel is the most common engine for commercial vehicles because of its high efficiency and outstanding durability. Efficiency gains were modest in the early 2000s, when R&D efforts focused on meeting increasingly stringent heavy-duty engine emissions standards. After the U.S. Environmental Protection Agency 2010 emissions standards for NO_x and PM were met, efforts turned to further improving the engine efficiency. Continued R&D to improve boosting, thermal management, and the reduction and/or recovery of rejected thermal energy has resulted in current heavy-duty diesel engine efficiencies in the 43–45% range. Advanced

combustion regimes and demonstrated waste heat recovery technologies can potentially improve overall engine efficiency to 57%.

The Co-Optimization of Fuels and Engines (“Co-Optima”) initiative, which kicked off in 2016, is a collaboration between the Advanced Combustion Engines and Fuels Program and the Bioenergy Technologies Office. A national laboratory R&D consortium was formed to investigate the co-development of advanced fuels and engines, which offers a great opportunity to improve engine efficiency and diversify the fuel supply. Research focused on identifying fuel properties that enable optimized engine performance and on developing a fuel-property-based approach that could provide the technical information required to define future fuel requirements that are not based on composition. Market introduction of advanced fuel and engine technologies can be accelerated by addressing the fuel property limitations and barriers to more efficient light-duty and heavy-duty engines. The market will define the best means to blend and provide these fuels.

Although NO_x and PM engine-out emissions are significantly lower for advanced LTC strategies and lean-burn technologies such as conventional and advanced diesel combustion strategies for light- and heavy-duty engines as well as lean-burn gasoline engines, further reductions are needed to meet future more stringent regulations. Also, higher hydrocarbon and carbon monoxide emissions require additional controls, which are often a challenge with the low exhaust temperatures (about 150°C).

Urea selective catalytic reduction (urea-SCR) technology has been used for NO_x control in Tier 3 light- and medium-duty vehicles, heavy-duty engines, and other diesel engine applications in the United States. All diesel vehicle manufacturers have adopted urea-SCR since it has a broader temperature range of effectiveness than competing means of NO_x reduction and allows the engine/emission control system to achieve higher fuel efficiency. Although urea-SCR is a relatively mature catalyst technology, more support research to aid formulation optimization and minimize degradation effects, such as hydrocarbon fouling, was conducted.

Particulate matter produced by direct injection technology utilized for most advanced gasoline engines, although smaller in mass than diesel particulates, may still represent significant emissions in terms of particulate number counts. PM emissions from dilute combustion gasoline engines are not fully understood; their morphology and chemical composition are also affected by combustion. Research has been conducted to develop filtration systems (for smaller diameter PM) that are durable and with low fuel economy penalties caused by increased backpressure and the need to regenerate the filter.

Complex and precise engine and emission controls require sophisticated feedback systems employing new types of sensors. NO_x and PM sensors are under development and require additional advances to be cost-effective, accurate, and reliable. Upcoming regulations with increased requirements for onboard diagnostics will be a challenge for manufacturers trying to bring advanced fuel-efficient solutions to market. Sensors and catalyst diagnostic approaches will be a key element of emission control research in the next few years.

The higher overall costs of current light- and medium-duty diesel engine systems in comparison to conventional gasoline systems are partly due to complex engine and exhaust gas recirculation (EGR) systems and the catalyst expense and volume associated with urea-SCR systems and diesel particulate filters. Aggressive research has substantially reduced the combined fuel penalty for SCR/diesel particulate filter systems, but further reductions are possible. Another improvement being pursued is to pair NO_x trap technology with SCR catalysts. The advantage is that the SCR catalyst uses the NH_3 produced by the NO_x trap, so no urea is needed. Formulation and system geometries have been researched to reduce cost by reducing the overall precious metal content of the NO_x trap+SCR systems, making the systems more feasible for light-duty vehicles.

Current Technical Focus Areas and Objectives

The Advanced Combustion Engines and Fuels Program supports early-stage R&D to improve the understanding of, and ability to manipulate, combustion processes, generating knowledge and insight necessary for industry to develop the next generation of engines and fuels. Unique facilities and capabilities at the national laboratories are used in cutting-edge research, in close collaboration with academia and industry, to strengthen the knowledge base of high-efficiency, advanced combustion engines and fuels.

The program objectives are as follows:

- Further the fundamental understanding of advanced combustion strategies that simultaneously show higher efficiencies and very low emissions, elucidating the effects of critical factors such as fuel spray characteristics, in-cylinder air motion, heat transfer, and others
- Develop science-based understanding of how engine efficiency and emissions are impacted by fuel properties, and conversely, how engines can be modified to take advantage of desirable fuel properties and control of emissions from co-optimized fuels/engines to meet future emissions regulations
- Improve the effectiveness and durability of emission control (exhaust aftertreatment) devices to complement advanced combustion strategies and high-performance fuels, as well as reduce their use of precious metals to reduce cost, which is another barrier to penetration of advanced combustion engines in the passenger and commercial vehicle markets
- Develop precise and flexible engine controls, and sensors for control systems and engine diagnostics, to facilitate adjustments of parameters that allow advanced combustion engines to operate over a wider range of engine speed and load conditions
- Further advance engine technologies such as turbo-machinery, flexible valve systems, advanced combustion systems, and fuel system components to reduce parasitic losses and other losses to the environment, and incorporate technologies such as bottoming cycles to recover energy from the engine exhaust

The Program maintains close collaboration with industry through a number of working groups and teams and utilizes these networks to identify and address critical issues and for setting goals, adjusting priorities of research, and tracking progress. These collaborative groups, which include auto manufacturers, engine companies, fuel suppliers, national laboratories, and universities, are organized as follows: (a) the Advanced Combustion and Emission Control Technical Team and the Fuels Working Group of the U.S. DRIVE (Driving Research and Innovation for Vehicle efficiency and Energy sustainability) Partnership, and (b) the Engine Powertrain Team of the 21st Century Truck Partnership. Focused efforts are carried out under the Advanced Engine Combustion Memorandum of Understanding and the Cross-Cut Lean Exhaust Emission Reduction Simulation (CLEERS) activity of the Advanced Engine Cross-Cut Team. In the fuels and engines co-optimization effort, the Program works closely with a broad range of stakeholders representing vehicle and engine manufacturers, energy companies, biofuel producers, manufacturers of catalysts and emission control systems, fuel distributors, and retailers.

The Advanced Combustion Engines and Fuels Program focuses on the following research areas (Figure 1): combustion fundamentals, co-optimization of fuels and engines, alternative fuel engines, emission control R&D, high-efficiency engine technologies, lubricant technologies, and system-level efficiency improvement. Projects competitively selected and awarded through Funding Opportunity Announcements are fully funded through the duration of the project in the year the funding is awarded. Directly funded work at the national laboratories is subject to change based on annual appropriations.

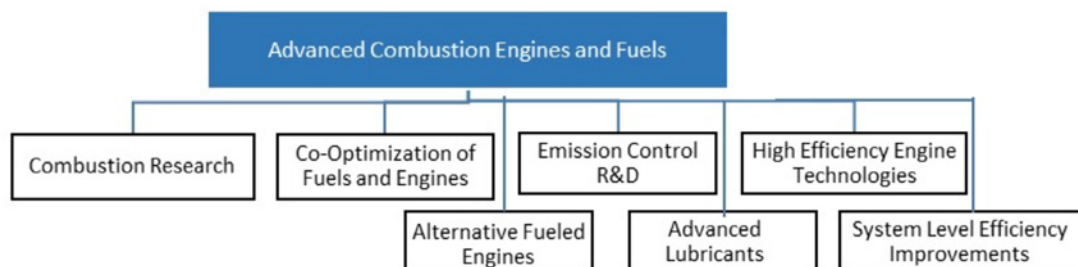


Figure 1. Research areas within Advanced Combustion Engines and Fuels Program

Combustion Research

Combustion fundamentals research uses unique diagnostic tools, including advanced laser, high-intensity X-ray, and neutron-based optical diagnostics, to determine how fuel injection, air mixing, and combustion take place in the engine and how emissions are formed. Experimental data are used to establish quantitative relationships between in-cylinder processes and efficiency improvement potential for both current and next-generation engines. Predictive, high-fidelity models that simulate the fundamental physics of fuel injection sprays, heat transfer, turbulence, and combustion phenomena are developed using high-performance computing resources at the national laboratories to achieve results comparable to the detailed experiments. Detailed and accurate chemical kinetics models of different fuel molecules are used to simulate surrogate fuels and determine their impact on combustion efficiency and emissions. Numerical routines for models that can reduce the computational time are developed to enable high-fidelity engine models as viable engine design tools for industry. Knowledge from experiments, in combination with predictive engine simulation, will enable companies to develop a new generation of advanced combustion engines.

Co-Optimization of Fuels and Engines

Early-stage research is on fuel property impacts on combustion and determining fuel characteristics that enable higher efficiency in advanced combustion strategies. Research focus is on performance of tailored blend stocks including bio-derived, synthetic, and petroleum-based blend stocks that will increase engine efficiency, specifically on advanced fuels that enable maximum performance of advanced conventional and kinetically controlled combustion strategies.

Alternative Fueled Engines

R&D activities focus on overcoming technical barriers to the implementation of petroleum-displacing fuels. Alternative fuels such as natural gas, and renewable fuels such as drop-in biofuels, frequently have technical barriers that impede their implementation in traditional, petroleum-fuels equipment and infrastructure. Work to overcome these barriers will include support for new, alternative-fuel engine offerings, testing and evaluation of refueling infrastructure, and evaluation of the emissions impact of novel alternative fuels.

Emission Control R&D

The lower exhaust temperatures of advanced combustion engines make conventional aftertreatment systems unsuitable. Research on exhaust aftertreatment systems for these advanced combustion engines will be on catalyst technologies that are active at the lower exhaust temperatures, namely those that provide greater than 90% conversion efficiency at about 150°C. Early-stage fundamental research at the national laboratories, in close collaboration with industry and academia, addresses barriers to achieving key performance metrics such as catalyst activity, selectivity, durability, and cost-effectiveness.

High Efficiency Engine Technologies

Projects research and develop technologies for more efficient clean advanced engine/powertrain systems to improve passenger and commercial vehicle fuel economy.

Lubricant Technologies

Projects focus on R&D of technologies that can reduce friction losses in new and legacy vehicles to improve fuel economy.

System-Level Efficiency Improvement

R&D projects focus on system-level improvements to achieve vehicle performance targets. These include improvements in drivetrain efficiency and reducing aerodynamic drag and tire rolling resistance.

Technical Highlights

Combustion Research

Sandia National Laboratories is providing the scientific understanding needed to design, optimize, and calibrate the next generations of light- and medium-duty diesel engines that comply with increasingly stringent pollutant emissions regulations while achieving thermal efficiencies approaching 50%. In FY 2018 they (1) provided a mechanistic understanding of how spray-wall interactions promote the formation of recirculating flow structures in a stepped-lip diesel combustion chamber and (2) began conception and design of a new medium-duty diesel research platform. (Busch, I.1)

Sandia National Laboratories diesel combustion research and University of Wisconsin combustion modeling combined in FY 2018 to (1) image a second injection penetrating into the residual jet from a first injection to build conceptual-model understanding of multiple-injection schemes and (2) analyze simulation predictions to complement conceptual-model understanding of multiple-injection interactions affecting ignition gained through experiments. (Musculus, I.2)

Sandia National Laboratories facilitated improvement of engine spray combustion modeling in FY 2018 by (1) organizing workshop activities for the Engine Combustion Network, including monthly web meetings, standards, and topic organization; (2) investigating spray and combustion behavior of AVFL-18a diesel surrogates relative to a commercial diesel fuel; (3) developing a high-speed imaging extinction diagnostic for spray mixture quantification; and (4) characterizing plume interaction and mixing for multiple-injection gasoline direct injection conditions. (Pickett, I.3)

Sandia National Laboratories is providing and exploring fundamental understandings for development of low-temperature gasoline combustion (LTGC) engines. In FY 2018 they (1) completed an uncertainty quantification analysis of cylinder-pressure measurements in collaboration with Lawrence Livermore National Laboratory, (2) initiated a collaborative project with the State University of New York at Stony Brook to apply computational fluid dynamics (CFD) modeling to the Sandia LTGC research engine, (3) developed an improved surrogate mixture for modeling regular E10 gasoline (10% ethanol, 90% gasoline blend) and collaborated with Lawrence Livermore National Laboratory to validate and improve their chemical-kinetic mechanism for gasoline, (4) completed a study of the capabilities and limits of spark-assist for controlling combustion timing for well-mixed LTGC (i.e., homogeneous charge compression ignition), (5) investigated the chemistry of ϕ -sensitivity and its relationship to octane sensitivity—a critical study because ϕ -sensitivity combined with controlled mixture stratification can provide combustion-timing control and extend the load range, and (6) developed and demonstrated an advanced combustion-timing control system for LTGC engines. (Dec, I.4)

Sandia National Laboratories is investigating phenomenological aspects related to advanced ignition, which is accomplished through targeted experiments performed in a single-cylinder optically accessible research engine and in-house-developed ignition/combustion vessels. In FY 2018 they (1) quantified transient plasma discharge products and ignition behavior at engine-relevant conditions, (2) fabricated new igniters and optical test vessels, (3) demonstrated improved low-load engine emissions and efficiency with O_3 -enhanced advanced compression ignition (ACI), and (4) identified O_3 addition mechanisms that increase fuel reactivity. (Ekoto, I.5)

Argonne National Laboratory is advancing fuel spray modeling research through accurate representation of the fluid dynamics and thermodynamics leading to cavitation inception, cavitation cloud shedding, and collapse that can lead to cavitation-induced erosion. In FY 2018 they (1) identified existing cavitation erosion metrics in the literature; (2) implemented and evaluated existing cavitation erosion metrics; (3) developed, implemented, and validated an improved cavitation erosion metric into CONVERGE; (4) developed an automated multi-dimensional manifold bifurcation algorithm; (5) validated artificial neural networks manifold methodology for Engine Combustion Network Spray A; (6) implemented artificial neural networks flamelet code in CONVERGE CFD code; and (7) demonstrated validation and speed-up of CFD code and reduction in memory consumption of the code. (Som, I.6)

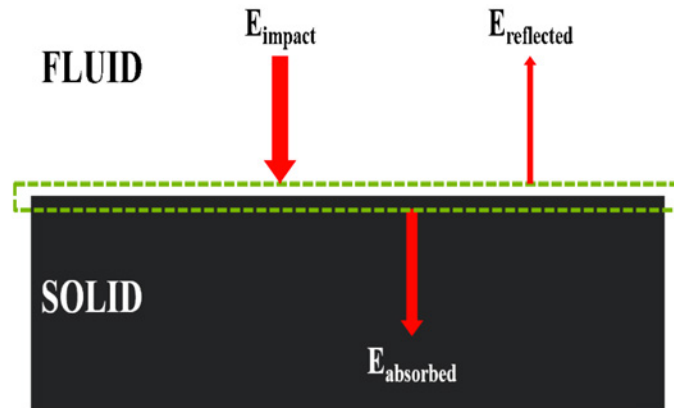


Figure 2. Schematic of energy balance considered in the derivation of the new cavitation erosion metric (Som, I.6)

Argonne National Laboratory is measuring near-nozzle surface area in diesel sprays covering a range of injector geometries and operating conditions and collaborating with simulation groups to incorporate this data in their simulations. They are optimizing the workflow for data collection and analysis of X-ray tomography measurements of fuel injectors and delivering a high-resolution three-dimensional (3D) model of a production gasoline injector nozzle that is ready for CFD. They are also completing measurements and analysis of a cavitating diesel nozzle, including high-resolution measurements of its geometry, valve motion, internal cavitation, and external fuel distribution. In 2018 ultra-small-angle X-ray scattering was used to measure near-nozzle surface area for diesel sprays using two Engine Combustion Network diesel injectors at several operating conditions. (Powell, I.7)

Argonne National Laboratory continued its rapid compression machine (RCM) studies in FY 2018 to enable gasoline-relevant LTC by (1) acquiring new ignition measurements for multi-component surrogate blends to mimic 'neat' and ethanol-blended gasolines and evaluating and quantifying performance of surrogate formulation approaches; (2) acquiring autoignition measurements for a full-boiling-range, market-representative E10 gasoline (fuel blend with 90% gasoline, 10% ethanol); (3) quantifying autoignition behavior of neat and bi-component blends of selected aromatic and olefinic compounds found in commercial gasolines covering a range of thermodynamic and fuel loading conditions; and (4) coordinating RCM Workshop activities and organizing the 4th International RCM Workshop. (Goldsborough, I.8)

Argonne National Laboratory is improving the knowledge of cylinder conditions necessary for stable part-load gasoline compression ignition combustion with low combustion noise, emissions, and fuel consumption by developing better understanding of injection strategies to control mixture conditions, minimizing the level of EGR to maintain a fixed NO_x emissions level, and minimizing the boost level required for stable engine operation. In FY 2018 they (1) performed multiple parametric sweeps at constant combustion noise to identify opportunities for reduced emissions and fuel consumption and (2) identified a triple-injection strategy that demonstrated consistently lower emissions and indicated specific fuel consumption with increasing EGR. (Kolodziej, I.9)

Argonne National Laboratory is improving the basic knowledge and computational tools to properly characterize advanced ignition strategies for gasoline direct injection (GDI) engines. In 2018 they (1) resolved discrepancies concerning low-temperature plasma (LTP)-to-arc transition between modeling and experiments on a quantitative basis by removing some uncertainties in both the experiments and the plasma model; (2) delivered very close agreement between their model and experiments performed at Sandia National Laboratories in terms of chemical and thermal plasma properties; (3) initialized LTP calculations using CFD combustion simulations; and (4) performed first-ever LTP ignition simulations with CONVERGE, providing valuable insight into the ignition mechanism from a LTP deposition. (Scarcelli, I.10)

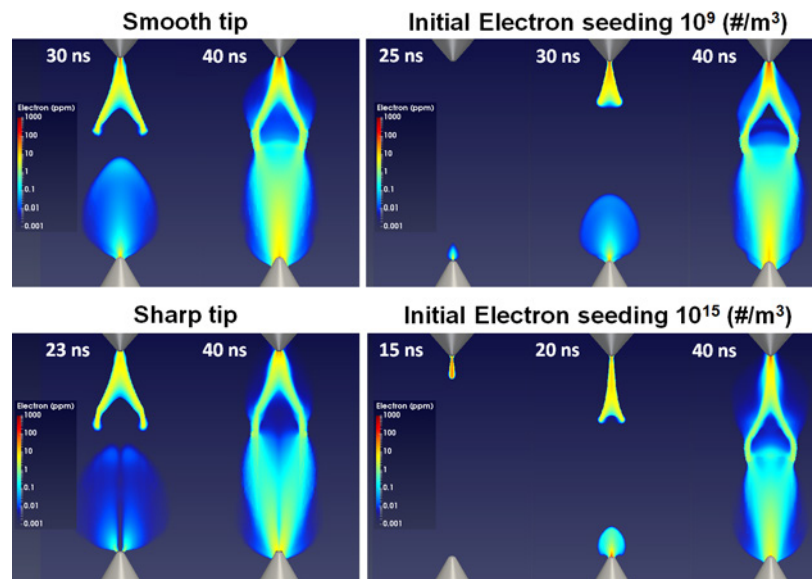


Figure 3. Impact of electrode geometry and electron seeding on low-temperature plasma discharge (Scarcelli, I.10)

Oak Ridge National Laboratory is using a thermodynamics-based approach to identify and pursue opportunities for improved efficiency in internal combustion engines. In FY 2018 they (1) determined whether the Oak Ridge National Laboratory EGR-loop catalytic reforming strategy is compatible with expanded load operation and (2) quantified the impacts of expanded load operation on the catalyst thermal conditions and the overall brake thermal efficiency (BTE) of the engine. (Szybist, I.11)

Oak Ridge National Laboratory is using the unique neutron imaging capability at their High Flux Isotope Reactor to advance the understanding of two components being employed in modern vehicles: the gasoline direct injector and the particulate filter. In FY 2018 they (1) implemented high-fidelity neutron imaging capabilities using the High Flux Isotope Reactor for advanced transportation research, (2) employed technique to aid improved design and control of complex advanced combustion systems and help to guide model validation and input, and (3) reported findings to the research community and worked with industrial partners to ensure research is focused on the most critical topics. (Wissink, I.12)

Lawrence Livermore National Laboratory is developing predictive chemical kinetic models for gasoline, diesel, and next-generation fuels, as well as for fuel components used in surrogate fuels; combining component models into surrogate fuel models to represent real transportation fuels; and using these models to simulate advanced combustion strategies in engines. In FY 2018 they (1) validated the gasoline surrogate model up to pressures of 220 bar for a representative research-grade, full-boiling, mid-octane gasoline; (2) developed a new polycyclic aromatic hydrocarbon kinetic model and linked it to a sectional soot model to predict soot; (3) improved kinetic models for diesel surrogate components; and (4) developed and validated new reaction-rate rules for iso-alkanes. (Pitz, I.13)

Lawrence Livermore National Laboratory is advancing the state of the art in engine simulation through the development of fast and accurate models and working with industry partners to prove capability and impact of combustion chemistry software. In FY 2018 they (1) accelerated detailed kinetics coupled to engine CFD, (2) implemented fast solution methods for one-dimensional (1D) laminar flames, and (3) deployed web application for kinetic model testing and debugging. (Whitesides, I.14)

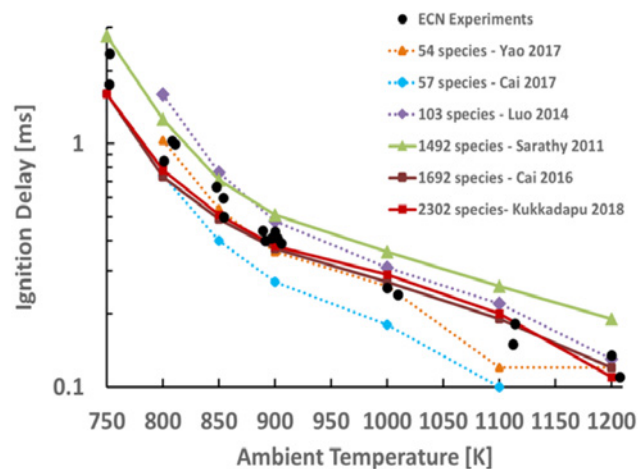


Figure 4. Log plot of ignition delay versus ambient temperature for n-dodecane at Spray A conditions. Larger detailed mechanisms are able to capture the ignition delay at low temperature and high temperature better than the smaller reduced mechanisms tested. (Whitesides, I.14)

Los Alamos National Laboratory is providing better understanding of engine combustion processes in order to enhance the ability to minimize fuel use and unwanted emissions. In FY 2018 they (1) developed a four-valve direct injection, spark ignition engine system for validation of FEARCE; (2) validated progress of FEARCE on experimental data of the four-valve direct injection, spark ignition engine; (3) constructed systems to use ChemKin II/III and Chemkin-Pro reactive chemistry software; (4) added the Kelvin Helmholtz – Rayleigh Taylor spray model to the code and began validation against Engine Combustion Network test cases; (5) developed faster linear solver systems by implementing a multigrid solution system of linear equations that improves our current implicit solutions methods by more than a factor of two; and (6) began the process of commercialization of FEARCE. (Carrington, I.15)

Oak Ridge National Laboratory supports rapid advancements in engine design, optimization, and control through the development and application of advanced simulation tools and novel techniques to best utilize high-performance computing resources and detailed predictive models. In FY 2018 they (1) transitioned to a full-cylinder geometry model and full-cycle simulation with gas exchange to better capture mixing and turbulence effects, (2) coupled combustion model with conjugate heat transfer model of metal engine components to provide better thermal boundary conditions including temporal and spatial variations, and (3) evaluated impacts of these model refinements on predictive accuracy and computational requirements. (Edwards, I.16)

The Pennsylvania State University is developing, implementing, and providing to the community open submodels for radiation and boundary-layer wall heat transfer in medium-resolution large eddy simulation and unsteady Reynolds-averaged Navier–Stokes that (when coupled with models of equal fidelity for other key physical processes, such as liquid fuel sprays) provide truly predictive capability for CFD of in-cylinder processes in engines, including couplings between different modes of heat transfer. In FY 2018 they (1) performed quantitative comparisons between measured and computed spectral infrared radiation for an optical engine; (2) analyzed experimental data from a metal engine to determine if an influence of in-cylinder radiation on knock can be found; and (3) investigated the coupling between turbulent boundary-layer wall heat transfer and radiative heat transfer, toward developing a CFD-based model that captures that coupling. (Haworth, I.17)

University of Illinois at Urbana-Champaign is improving the multi-component fuel droplet and film vaporization models used in internal combustion engine simulation through the use of discrete and continuous thermodynamics methods and developing a comprehensive model to predict the characteristics of multi-component flash boiling spray. In FY 2018 they (1) obtained experimental measurements of non-boiling and flash-boiling sprays; (2) developed, validated, and integrated discrete method vaporization models for multi-component fuel droplets; and (3) developed, validated, and integrated continuous method vaporization models for multi-component fuel droplets. (Lee, I.18)

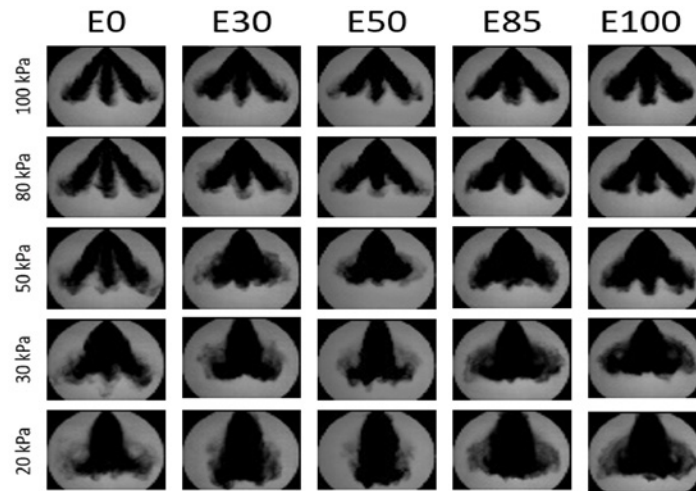


Figure 5. Back-illumination images of sprays with different ethanol–iso-octane blend ratios (top row labels: E0 is pure iso-octane, E30 is 30–70 ethanol–iso-octane blend, and E100 is pure ethanol) under various ambient pressure conditions (left column labels) (Lee, I.18)

Michigan Technological University has developed, implemented, and validated a volume of fluid approach for modeling evaporation, which is integrated into CFD codes to provide accurate and predictive simulation of spray–wall interactions without extensive need of parameter tunings. In FY 2018 they (1) quantified film thickness and heat flux on the heated surface for a single-hole nozzle spray impingement, (2) optimized the spray–wall interaction model in high-fidelity Lagrangian–Eulerian spray model, (3) validated Lagrangian–Eulerian spray model with experiments and generated boundary conditions for direct numerical simulation framework studies, and (4) demonstrated the droplet direct numerical simulation impingement criteria for splashing and non-splashing cases and formulated the evaporation direct numerical simulation submodel. (Lee, I.19)

University of Wisconsin is developing a new soot model that is validated under conditions ranging from conventional, mixing-controlled compression ignition to ACI combustion. In FY 2018 they (1) measured particle size distributions in an engine operating under conventional, mixing-controlled compression ignition combustion and ACI combustion modes; (2) compared soot model predictions to measured particle size distribution data; and (3) packaged the soot model for inclusion in government-sponsored and commercial codes. (Kokjohn, I.20)

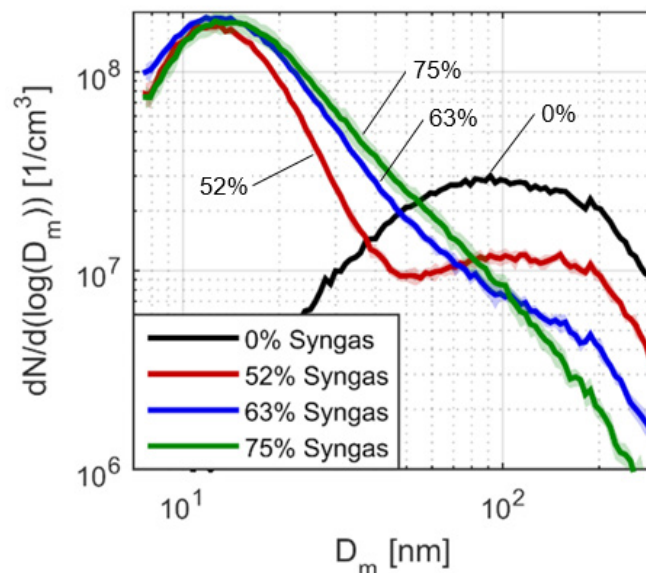


Figure 6. Measured particle size distributions for ACI combustion (Kokjohn, I.20)

The University of Alabama is developing a CFD code integrated with real-gas property models to predict fuel-air mixing at diesel conditions, and generating high-quality experimental data on fuel-air mixing in the near field of the jet to validate the code. In FY 2018 they (1) applied CFD code integrated with real-gas property models to predict fuel-air mixing in diesel sprays, (2) generated experimental data for comparison with CFD predictions, and (3) made comparisons. (Agrawal, I.21)

The Ohio State University is improving the predictive capability for CFD simulation of engine knock phenomena. In FY 2018 they (1) reproduced cycle-to-cycle variations under non-knocking conditions using multi-cycle large eddy simulation and (2) implemented the developed combustion model for engine knock prediction into CONVERGE CFD as a user-defined function. (Kim, I.22)

Boston University is developing and validating more accurate, physics-based, mathematical submodels for use in CFD software to enable better prediction of cavitation within fuel injectors. In FY 2018 they (1) completed a second High Flux Isotope Reactor imaging campaign of cavitation in fuel injectors, (2) populated a cavitation database with experimental data on cavitation under different flow and geometry conditions, and (3) developed a more accurate Reynolds-averaged Navier-Stokes model based on the improved cavitation model. (Ryan, I.23)

Georgia Institute of Technology is developing a new spray atomization model for engine CFD codes with improved prediction accuracy for local spray morphology and global spray characteristics over a wide range of engine operating conditions, improving understanding of fundamental physics governing atomization in diesel fuel sprays, and developing and applying a new diagnostic called scattering-absorption measurement ratio for spatially resolved measurement of diesel spray morphology. In 2018 they (1) developed a primary breakup model for diesel spray simulations; (2) performed near-nozzle measurements of liquid surface area; and (3) made improvements to the scattering-absorption measurement ratio diagnostic. (Genzale, I.24)

Co-Optimization of Fuels and Engines

The U.S. Department of Energy Co-Optimization of Fuel and Engines (Co-Optima) initiative brings together the U.S. Department of Energy’s Office of Energy Efficiency and Renewable Energy, nine national laboratories, 13 universities, and numerous industry and government stakeholders to explore near-term improvements to the types of fuels and engines found in most vehicles currently on the road, as well as the development of potential long-term solutions using revolutionary new combustion technologies. The primary near-term objective is to identify how co-optimized fuel/engine innovations can achieve a 35% increase in light-duty fuel economy. For medium- and heavy-duty vehicles, Co-Optima is pursuing a 4% increase in fuel economy through fuel/engine innovations capable of delivering nearly 60% brake thermal efficiency. In FY 2018 Co-Optima (1) concluded a standalone light-duty boosted SI project, (2) developed an R&D and analysis framework for a light-duty multimode project, and (3) completed fuel screening for a medium- and heavy-duty mixing-controlled compression ignition project. (Farrell, II.1)

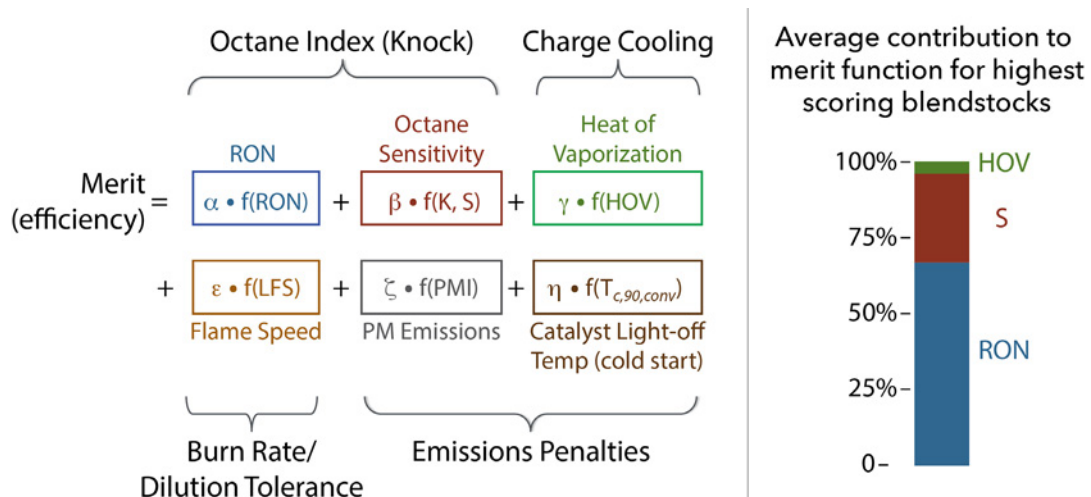


Figure 7. Fuel properties impacting boosted SI engine efficiency (Farrell, II.1)

Oak Ridge National Laboratory provides assessments of the potential benefits offered by improving gasoline octane ratings to support techno-economic evaluations of potential future biofuel formulations in the United States. In FY 2018 they (1) quantified impacts of biofuels with increased octane rating on vehicle energy consumption, volumetric fuel economy, and tailpipe CO₂ emissions to support life-cycle analysis of the potential of these fuels if implemented nationwide; (2) completed a draft report documenting engine experimental and vehicle model evaluations of U.S. DRIVE (Driving Research and Innovation for Vehicle Efficiency and Energy Sustainability) Fuels Working Group fuels; and (3) estimated potential impacts of Co-Optima Tier 3 blendstocks on vehicle energy consumption, volumetric fuel economy, and tailpipe CO₂ emissions. (Sluder, II.2)

Oak Ridge National Laboratory is investigating how the pressure and temperature conditions at the start of compression determine the autoignition tendency for a range of gasoline-boiling-range fuels, including a number of high-interest fuel blendstocks identified by the Co-Optima initiative. In FY 2018 they (1) determined if the octane index sufficiently characterizes the performance of 19 different fuel blends across five different pressure-temperature trajectories, from boosted SI to ACI; and (2) determined whether there is a kinetic basis for the octane index by performing kinetic modeling across the range of operating conditions investigated experimentally. (Szybist, II.3)

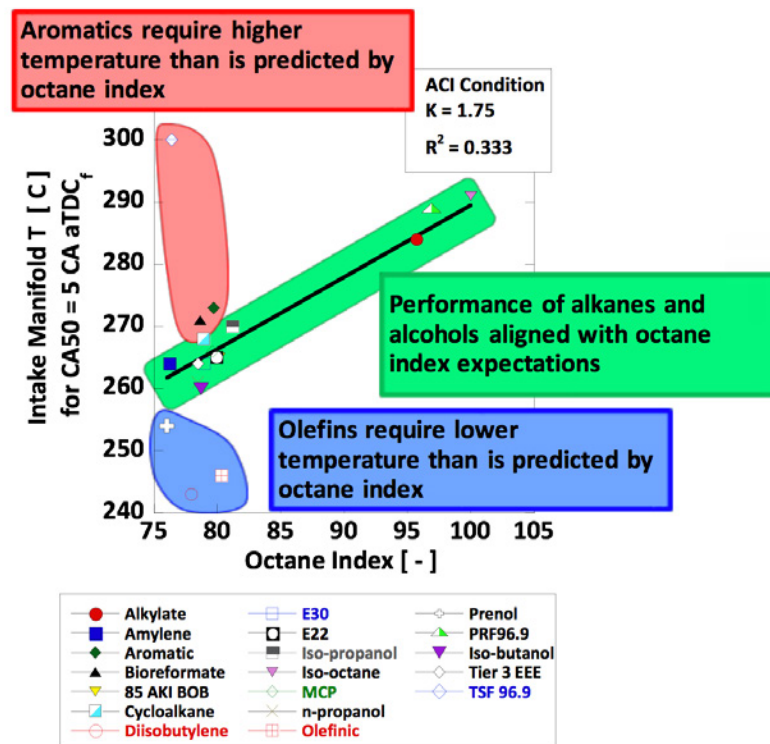


Figure 8. Knock-limited combustion phasing as a function of octane index for each fuel at the ACI condition (Szybist, II.3)

Oak Ridge National Laboratory is co-developing engines and fuels to accelerate the development of efficient combustion modes and the utilization of diverse fuel sources. In FY 2018 they (1) identified fuel candidates that can provide a modest research octane number (RON) and high octane sensitivity; (2) quantified the blending performance of the fuel candidate, specifically the extent of synergistic or antagonistic blending; and (3) determined whether the performance in a modern engine is indicative of the predicted fuel properties of the blend, particularly with the fuels with modest RON and high octane sensitivity. (Szybist, II.4)

Sandia National Laboratories is providing the science base needed to understand how emerging alternative fuels impact highly efficient direct injection spark ignition light-duty engines being developed by industry, elucidating how engine design and operation can be optimized for clean and efficient use of future fuels, and

developing and applying advanced optical diagnostics for probing in-cylinder processes. In FY 2018 they (1) assessed the relevance of the Particulate Matter Index for nine fuels across three stoichiometric well-mixed and two lean stratified operating conditions; (2) developed in-cylinder soot diagnostics based on diffused back-illumination, and used them to quantify in-cylinder soot mass distributions for key operating points; (3) used wall-wetting diagnostics based on refractive index matching to determine the role of fuel films for in-cylinder soot production; (4) showed that high smoke emissions for cold-start stratified-charge operation with an E30 fuel (70% gasoline, 30% ethanol blend) can be traced to increased fuel films on the piston top, with associated sooting pool fires; (5) acquired lean mixed-mode combustion data for five fuels, spanning a range of equivalence ratio, intake pressure, intake temperature, and intake oxygen mole fraction conditions; and (6) performed an initial assessment of the efficacy of octane-index framework for lean conditions. (Sjöberg, II.5)

Sandia National Laboratories is identifying differences in fuel spray mixing, evaporation, plume interaction, droplet atomization, and liquid film formation with respect to proposed candidate fuels. In FY 2018 they (1) completed a new spray chamber facility with continuous-flow operation; (2) applied a suite of high-speed optical diagnostics to measure vapor, liquid, plume direction, and spray collapse at representative engine conditions; and (3) used different injection durations and multiple injections to understand methods to limit liquid penetration and prevent wall impingement. (Pickett, II.6)

Sandia National Laboratories is providing fundamental understanding of the autoignition behavior of fuels at conditions relevant to low-temperature gasoline combustion (LTGC)/ACI operation to support the co-development of LTGC/ACI engines and fuels that optimize their performance. In FY 2018 they (1) acquired LTGC performance data for the high-cycloalkane fuel from the Co-Optima core fuels matrix over the suite of previously established LTGC operating conditions for fuel evaluation; (2) acquired similar LTGC performance data for a second regular E10 (gasoline containing 10% ethanol) reference fuel; (3) compared the autoignition reactivity of the high-cycloalkane fuel to that of the E30 (gasoline containing 30% ethanol) and high-aromatic Co-Optima fuels and to both the original regular E10 (RD5-87A) and second regular E10 (RD5-87B) fuels over a range of conditions; (4) determined the validity/usefulness of the octane index as a means of correlating the autoignition behavior of these fuels and other fuels for LTGC engine operation; (5) obtained ϕ -sensitivity and intermediate-temperature heat release data for the high-cycloalkane Co-Optima fuel and RD5-87B fuel and compared with previous data for the E30, high-aromatic, and RD5-87A fuels; (6) developed more accurate surrogate blends for computational simulations of the high-cycloalkane, E30, and high-aromatics Co-Optima core fuels, and validated them against fully premixed LTGC/homogeneous charge compression ignition engine data over a range of intake temperatures and pressures; and (7) supported the development of a merit function for ACI fuels. (Dec, II.7)

Sandia National Laboratories is providing guidance on the suitability of new fuel candidates as drop-in replacements for GDI engines. In FY 2018 they (1) demonstrated the value of high-resolution CFD simulation and developed analysis methodologies to differentiate composition-dependent effects (as opposed to the current empirical/calibrated spray models) and (2) tested a new cavitation model and investigated modes of cavitation (bulk vs. wall cavitation) for a specific GDI configuration. (Arienti, II.8)

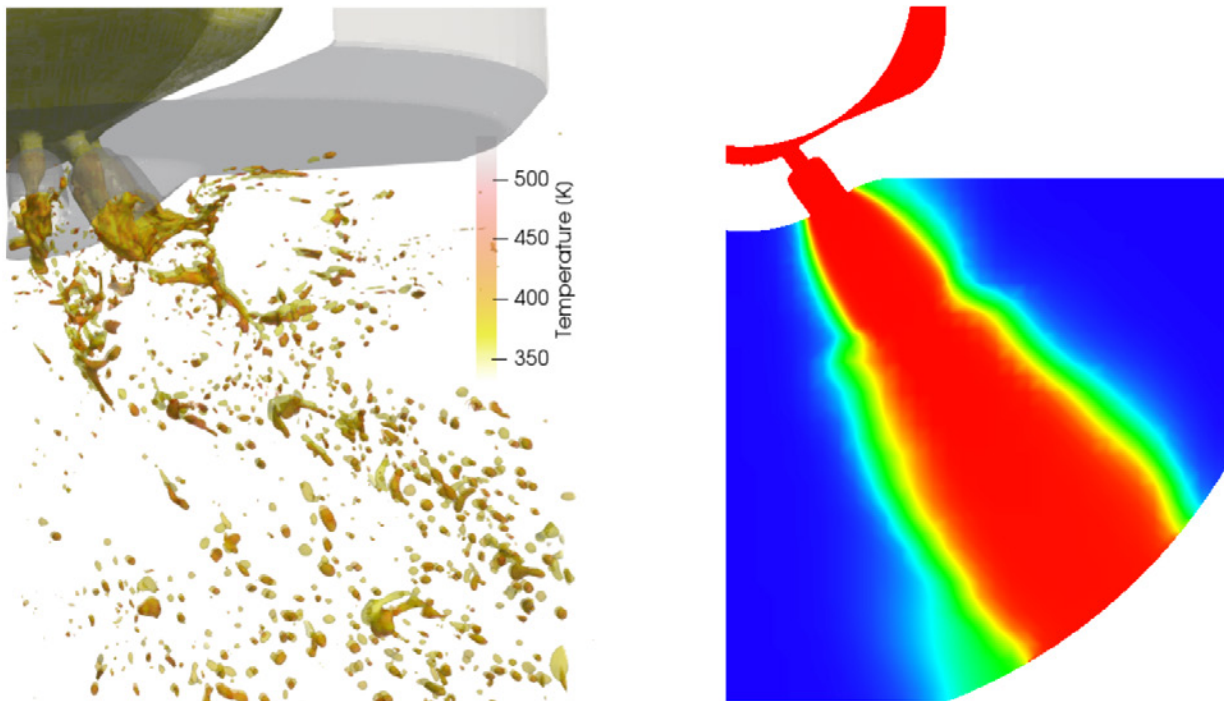


Figure 9. A comparison between two different modeling approaches to spray formation (Arienti, II.8)

Oak Ridge National Laboratory is quantifying the role of fuel properties in enabling ACI performance, as well as the impact on SI performance, using a single-cylinder, center mount, boosted GDI engine platform. In FY 2018 they (1) performed an assessment of fuel economy potential as a function of speed and load range/location of the ACI portion of the engine operating map, (2) configured a specialized multi-mode single-cylinder research platform, and (3) facilitated knowledge discovery and additional insights through modeling in collaboration with the Co-Optima Toolkit development project. (Curran, II.9)

Oak Ridge National Laboratory is providing more clarity on the relationship between fuel properties and low-speed pre-ignition, with fuel properties being specifically studied. In FY 2018 they (1) quantified the relationship between fuel properties and low-speed pre-ignition frequency with respect to fuel distillation and molecular properties and (2) determined if specific fuel properties affect low-speed pre-ignition intensity. (Splitter, II.10)

Oak Ridge National Laboratory is expanding the understanding of the role of low-temperature heat release and pre-spark heat release on knock at relevant engine conditions by studying the knock propensity of an alkane-based fuel over a wide range of intake temperatures at knock-prone conditions in a spark-ignited engine. In FY 2018 they (1) developed a phenomenological understanding of molecular structure and fuel property effects on abnormal stochastic ignition and combustion event frequency and intensity and (2) quantified effects. (Splitter, II.11)

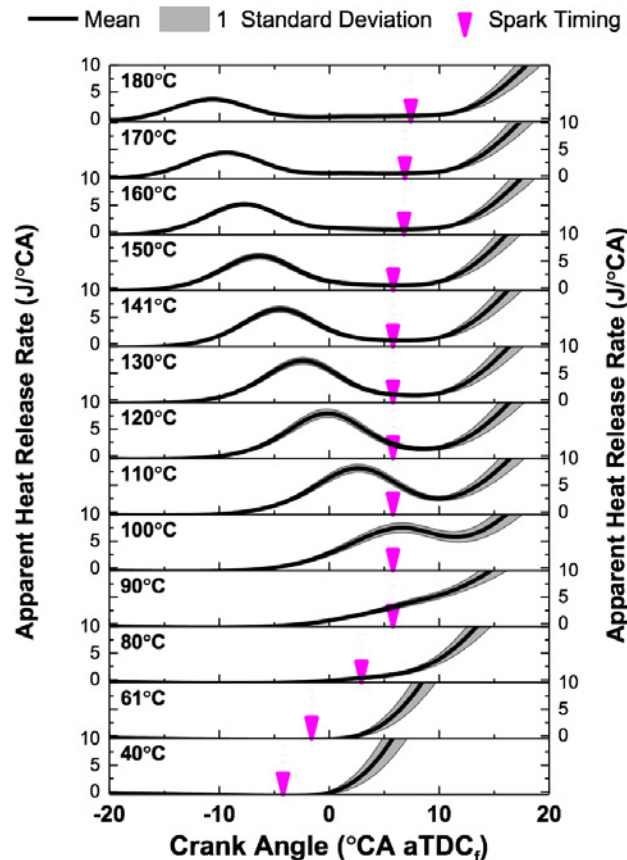


Figure 10. Mean apparent heat release rate plotted for intake temperatures from 40–180°C for 2,000 r/min operation; arrow denotes spark timing, shaded region denotes one standard deviation of data at each condition (Splitter, II.1.1)

Argonne National Laboratory is investigating the effect of octane sensitivity on the intake temperature swing required to achieve both knock-free high-load SI and stable low-load ACI operation in a GDI engine for five RON 98 full-boiling-range gasolines. In 2018 they (1) operated a single-cylinder GDI engine in compression ignition mode at two geometric compression ratios utilizing the five Co-Optima fuels with RON 98, (2) quantified the delta between minimum cylinder temperature increase required for stable low-load ACI and temperature reduction required for knock-free high-load SI, (3) determined how octane sensitivity impacts the cylinder temperature swing needed to achieve both knock-free high-load SI and stable low-load ACI operation, and (4) identified fuels with the lowest temperature delta required for multi-mode ACI/SI operation. (Rockstroh, II.12)

Argonne National Laboratory is studying how the physical properties of the fuel affect mixture formation in a spray chamber under conditions that mimic a GDI engine. In FY 2018 they (1) performed X-ray radiography measurements that quantify the near-nozzle fuel distributions from a GDI injector for two fuels: a non-evaporating calibration fluid and iso-octane; (2) performed X-ray radiography measurements that quantify the near-nozzle fuel distributions from a GDI injector for neat iso-octane, iso-octane with 20% ethanol, and iso-octane with 20% butanol under non-vaporizing conditions; and (3) performed X-ray tomography measurements that quantify the spray breakup under flash-boiling conditions for neat iso-octane, iso-octane with 20% ethanol, and iso-octane with 20% butanol. (Powell, II.13)

Argonne National Laboratory is identifying the effects of fuel composition and engine intake conditions and using the trends observed on the Cooperative Fuel Research engine to correlate with fuel knock propensity on modern boosted SI engines. In FY 2018 they (1) developed fuel blends of constant RON 98 and investigated

the effects of ethanol concentration and base fuel chemical composition on combustion characteristics; and (2) with one fuel blend, investigated the effects of compression ratio, intake pressure, and intake temperature on its end-gas autoignition and knocking characteristics. (Kolodziej, II.14)

Argonne National Laboratory is acquiring experimental autoignition data that will (a) support the development, validation, and improvement of robust chemical kinetic mechanisms for real and surrogate fuels; and (b) provide insight into the chemical effects of fuel performance in boosted SI and ACI engines. In FY 2018 they (1) acquired additional data for five compositionally diverse, high-RON Co-Optima Core fuels over an extended range of thermodynamic and fuel-loading conditions beyond FY 2017 efforts; (2) acquired autoignition data for select high-performance fuels over a range of fuel loadings and thermodynamic conditions, and blends of these with a research-grade full-boiling-range fuel; (3) amended RCM database of iso-olefins to facilitate formulation of robust rate rules for such fuel constituents; and (4) demonstrated experimental, RCM-based approach to measure ϕ -sensitivity of fuels. (Goldsborough, II.15)

Sandia National Laboratories is developing advanced combustion strategies for mixing-controlled compression ignition engines that are synergistic with renewable and/or unconventional fuels in a manner that enhances domestic energy security, economic competitiveness, and environmental quality. In FY 2018 they (1) designed, fabricated, installed, and tested hardware to enable the first-ever ducted fuel injection (DFI) experiments in an engine; (2) conducted DFI experiments in an engine with a single duct to determine whether the technology works as expected; and (3) conducted DFI experiments in an engine with two ducts to quantify the effects of DFI on regulated emissions and efficiency, including whether DFI can break the longstanding soot/ NO_x tradeoff. (Mueller, II.16)

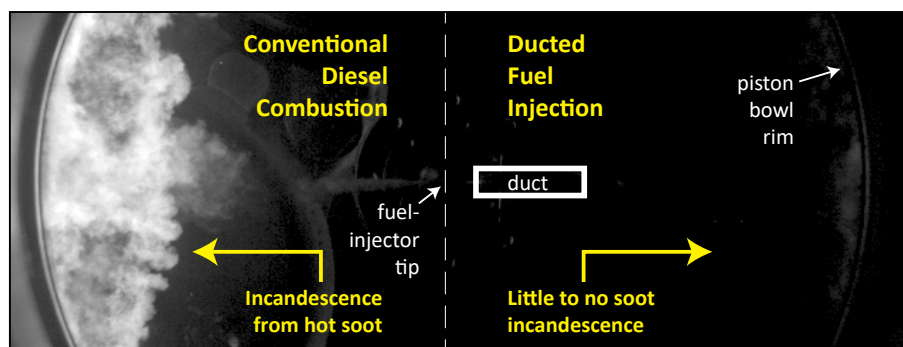


Figure 11. Natural luminosity image from experiment with single-duct holder confirms that conventional diesel combustion spray produces significantly more incandescence from hot soot than ducted fuel injection spray (Mueller, II.16)

National Renewable Energy Laboratory upgraded an existing reactor system with improved analytical capability in FY 2018 and is applying this capability to reveal important aspects of autoignition and soot precursor formation mechanisms. In FY 2018 (1) the upgraded analysis system was validated using isooctane; (2) the system was utilized to study the skeletal autoignition mechanisms of promising bioblendstocks, as well as prenil and methyl acetate; and (3) the reactor was utilized to show that a key degradation pathway was missing from reaction mechanisms for the three isomers of methyl cyclohexenes. (Fioroni, II.17)

National Renewable Energy Laboratory is developing experimental and simulation tools to characterize fuel ignition behavior in support of advanced combustion engine development; supporting the development of research fuels, surrogates, and blends, and related reduced kinetic mechanisms to further enable co-development of advanced combustion engines and high performance fuels; linking bench-scale constant volume combustion chamber-based fuel ignition measurements to single-cylinder research engine studies to enable rapid predictive feedback of engine performance for complex fuel blends; and (4) developing understanding of fuel chemical and physical properties that enable co-optimization of high-performance fuels and high-efficiency engines. In FY 2018 they (1) quantified fuel component, surrogate blend, and full-boiling-range gasoline ignition performance over engine-relevant parametric space using constant volume combustion chamber ignition kinetics experiments; (2) acquired unique data from their Advanced Fuel Ignition Delay

Analyzer; (3) and performed extensive characterization and experimental methodology development with the Advanced Fuel Ignition Delay Analyzer. (Zigler, II.18)

National Renewable Energy Laboratory is developing understanding of and predicting the effects of blending alcohols into gasoline on PM emissions. In FY 2018 they (1) quantified PM emissions from a full-factorial designed experiment fuel matrix having the variables of aromatic vapor pressure, aromatic concentration, and ethanol concentration; (2) analyzed PM emission and fuel property data, as well as droplet evaporation modeling results to identify and characterize the fuel property interactions affecting PM; and (3) developed improved predictive models for PM emissions based on better understanding of fuel property effects and interactions. (Ratcliff, II.19)

National Renewable Energy Laboratory is identifying computational surrogates that represent more complicated fuels for the purposes of detailed ignition delay calculations. In FY 2018 they (1) identified the potential for using a detailed kinetic mechanism as a surrogate for fuels not appearing in the usual inputs for that mechanism, (2) demonstrated the feasibility of fitting reactant composition to product speciation based on a limited set of notional experiments, and (3) implemented and verified correct operation of relevant analytics pipeline. (Grout, II.20)

Lawrence Berkeley National Laboratory is extending its capabilities from simple multi-objective optimization of analytically given merit functions to data-informed surrogate optimization that exploits statistical models and other approximation models. In FY 2018 they (1) implemented capability for simulation optimization, (2) modeled and implemented capability for sensitivity analysis, (3) developed simple user interface to improve tool usability, and (4) defined proof of concept with synthetic cost data and spark ignition merit function. (Mueller, II.21)

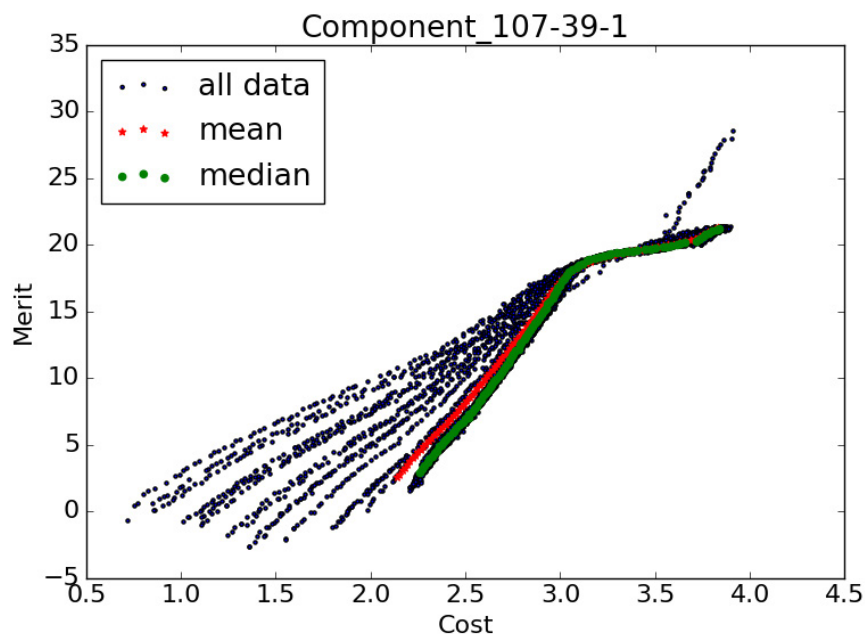


Figure 12. Molecular-level solution structure and Reid vapor pressure (RVP). The average number of molecules in clusters was determined by using nuclear magnetic resonance diffusion measurements in (a) ethanol in iso-octane, (b) ethanol in n-heptane, and (c) iso-butanol in n-heptane. Reid vapor pressure for the ethanol–n-heptane solution compared with cluster size is shown in (b). (Mueller, II.21)

Pacific Northwest National Laboratory is developing a fundamental attribution of the effects of molecular-level solution structures, such as clustering, hydrogen-bonding networks, and crystallization, on fuel properties in a finished fuel. In FY 2018 they (1) related nuclear magnetic resonance spectroscopic measurements and molecular dynamics simulations of alcohol clusters in model fuel systems to Reid vapor pressure, (2) measured the changes in phase behavior resulting from the introduction of complex fuel mixtures on diesel surrogate fuels at high pressures simulating those of vehicle fuel injection systems and attempted to mitigate fuel

solidification, and (3) completed phase change behavior measurements for four Coordinating Research Council diesel surrogate fuels and three Co-Optima diesel surrogate fuels. (Bays, II.22)

Oak Ridge National Laboratory is investigating the compatibility of Co-Optima fuel candidates with emissions control systems and identifying opportunities for alternative emissions control strategies based on novel fuel chemistry. In FY 2018 they (1) measured the catalyst light-off of Co-Optima blendstock candidates in the context of fuel blends similar to what would be used in vehicles and (2) published results from prior blendstock light-off measurements. (Pihl, II.23)

Oak Ridge National Laboratory is investigating the effects of fuel chemistry and combustion strategies on emissions and the functionality of the emissions control system to identify potential challenges as well as opportunities created by new fuel compositions. In FY 2018 they (1) collected condensable and solid exhaust PM species as well as gaseous emissions as fuel and air–fuel stratification were changed, (2) quantified how air–fuel stratification and fuel RON influence PM mass production, and (3) quantified the change in hydrocarbon gaseous emissions as the elemental carbon component of PM increased. (Debusk, II.24)

Lawrence Livermore National Laboratory is developing and improving chemical kinetic models for high-performance fuels (HPFs) and base fuels and using the models to simulate combustion properties at boosted SI, ACI, and mixing-controlled compression ignition engine conditions. In FY 2018 they (1) developed and improved chemical kinetic models for HPFs; (2) developed, improved, and validated kinetic models for surrogate components and surrogate mixtures to represent base fuels for gasoline and diesel fuels; and (3) improved diesel surrogate kinetic models to represent Coordinating Research Council diesel surrogates using RCM experimental data from University of Connecticut. (Pitz, II.25)

Lawrence Livermore National Laboratory is discovering promising HPF and base-fuel blends that provide the desired engine combustion properties under advanced combustion engine conditions. In FY 2018 they (1) provided accurate fuel property values for HPF/base-fuel blends and (2) identified base-fuel compositions that improve blending behavior with HPFs in terms of RON and/or octane sensitivity. (Pitz, II.26)

Lawrence Livermore National Laboratory is demonstrating new Co-Optima tools for stakeholders to evaluate a blendstock's potential with respect to their market estimates. In FY 2018 they (1) assessed the validity of the Central Fuel Hypothesis with respect to using the octane rating of a blendstock for oxygenate blending to capture its blending performance with oxygenates and bio-derived hydrocarbons; (2) quantified the potential to optimize the blendstock for oxygenate blending and finished fuel performance using a chemical kinetic model for the inputs to the boosted spark ignition merit function—specifically, the RON and the octane sensitivity; (3) coordinated with the Co-Optima Fuel Properties Team to test the blendstock for oxygenate blending and blendstock combinations found in the virtual fuel search to have the largest variation in the

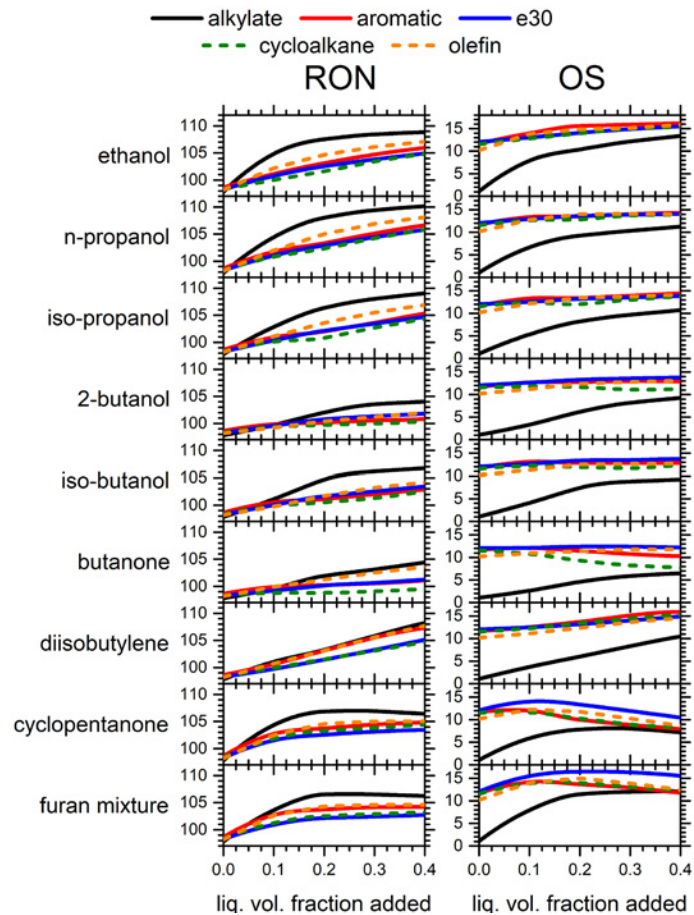


Figure 13. Prediction of RON and octane sensitivity (OS) for the simulated blending of nine high-performance fuels into the Co-Optima core fuels (Pitz, II.26)

boosted spark ignition merit score; and (4) validated the model octane predictions using new test data collected for the ASTM standard measurements for RON (D2699) and motor octane number (D2700). (McNenly, II.27)

Argonne National Laboratory is gaining a better understanding of fuel–engine interactions in order to develop robust knock mitigation strategies. In FY 2018 they (1) validated the 3D CFD model against experimental data, (2) performed a numerical investigation of Co-Optima Central Fuel Property Hypothesis, (3) validated the 3D CFD model and developed an efficient approach for knock-limited spark advance prediction, and (4) investigated fuel property effects with local sensitivity and global sensitivity analysis. (Som, II.28)

The University of Alabama is experimentally evaluating fuel–air mixing and subsequent ignition and combustion processes and properties in different fuel injection regimes; identifying synergistic opportunities offered by biofuels and their blends with conventional fuels; performing experiments in a flexible, modular, and optically accessible flow rig with a continuous supply of preheated compressed air; utilizing a suite of time-resolved optical diagnostic techniques; and developing a neural network to model functional relationships between fuels' physical/chemical properties and ignition/combustion characteristics. In FY 2018 they (1) integrated time-resolved diagnostics systems to the test facility, (2) developed image post-processing techniques, and (3) developed a neural network model framework. (Agrawal, II.29)

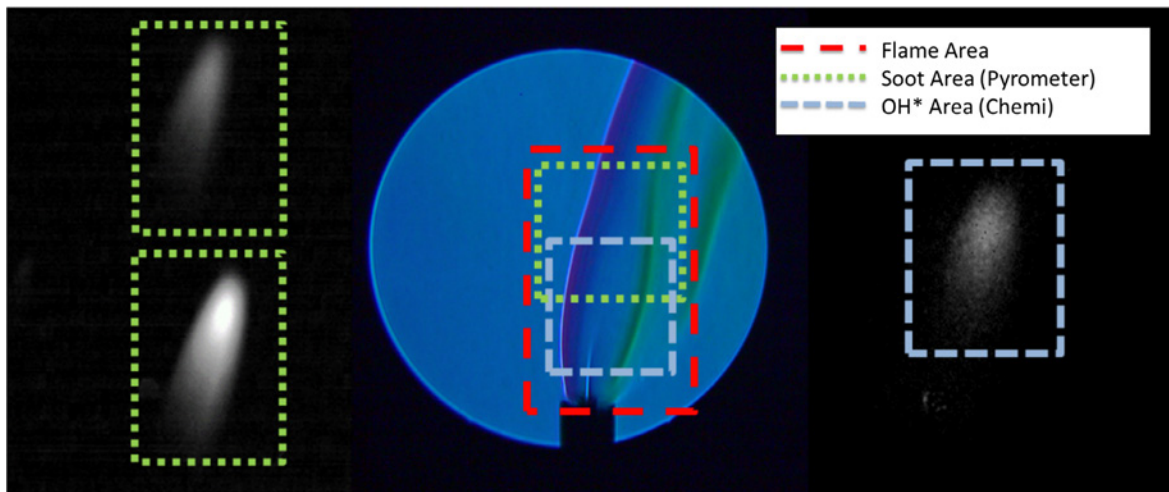


Figure 14. Demonstration of simultaneous two-color pyrometry, rainbow schlieren deflectometry, and OH* chemiluminescence measurements using a simple Bunsen burner (Agrawal, II.29)

University of Michigan is providing CFD tools that will reduce the computational expense of a full engine cycle simulation with chemistry by 80% relative to the state of the art and enable the Co-Optima team to efficiently perform multi-cycle simulations to capture prior cycle compositional and thermal effects while improving numerical accuracy. In FY 2018 they (1) obtained engine and operating conditions for simulation, chemical mechanisms, and surrogates to be used for project simulations; (2) obtained Cooperative Fuel Research and ACI meshes from national lab activities; (3) completed baseline ACI and Cooperative Fuel Research multi-cycle simulations with chemistry active throughout cycle; (4) completed implementation of dynamic species reduction routines into CONVERGE; (5) identified Cooperative Fuel Research and ACI conditions with cyclic coupling; and (6) validated the dynamic species reduction model. (Lavoie, II.30)

Louisiana State University seeks to establish a foundation for small-volume, high-throughput fuel testing, where relevant fuel metrics are quantified in a micro combustion experiment. In FY 2018 they (1) demonstrated capability to operate at elevated pressure, (2) validated core assumptions, and (3) quantified uncertainty of key measurements. (Schoegl, II.31)

Yale University is developing information for stakeholders that describes the effects of biofuel composition on soot formation. In FY 2018 they (1) measured the sooting tendencies of at least 25 commercially available hydrocarbons and 25 blendstock samples that have been produced by the Co-Optima High Performance Fuels

Team, (2) determined whether the laboratory-scale sooting tendencies measured in this work apply to the full range of air-fuel equivalence ratios (λ) and pressures that exist in real engines, and (3) validated at least one detailed chemical kinetic mechanism for each of the nine specific hydrocarbons in the Co-Optima Tier 3 SI blendstocks. (Pfefferle, II.32)

Alternative Fueled Engines

Stony Brook University is reforming gasoline, diesel, and natural gas to varying levels and characterizing the constituent species of their reformat mixtures as well as the autoignition tendency of the reformat mixtures to evaluate potential efficiency, emissions, operating range, and burn characteristics as compared to conventional gasoline and diesel fuels. In FY 2018 they (1) utilized the models that were validated in the previous fiscal year to better understand the combustion chemistry and performance characteristics of single-fuel reactivity-controlled compression ignition. (2) investigated the effects of increasing reactivity separation between the high- and low-reactivity fuels on reactivity-controlled compression ignition combustion; and (3) used the CFD and experimental research engines to determine the operating strategy, operating range, efficiency, and emissions characteristics of single-fuel reactivity-controlled compression ignition. (Lawler, III.1)

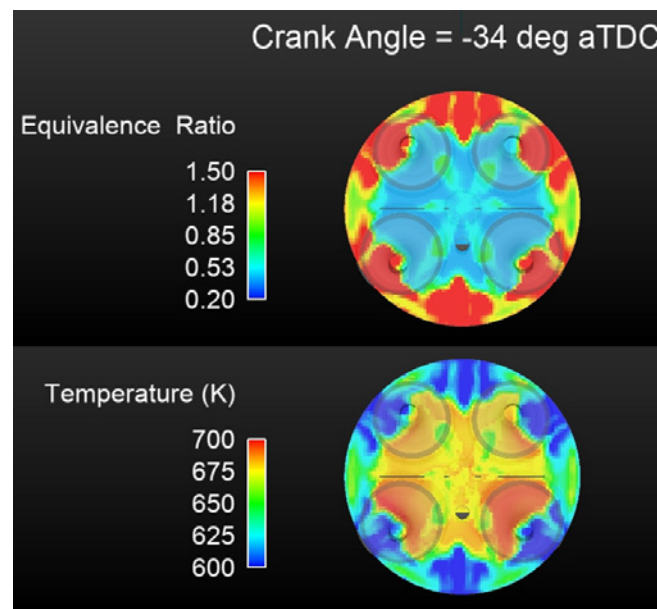


Figure 15. Cut-plane equivalence ratio distribution and temperature distribution from the CFD simulations of single-fuel reactivity-controlled compression ignition combustion with diesel and its reformat (Lawler, III.1)

Robert Bosch LLC is developing and demonstrating a high-efficiency cost-optimized spark-ignited natural gas heavy-duty engine capable of approaching current near-diesel efficiency while achieving current U.S. Environmental Protection Agency emissions regulations. In FY 2018 they (1) processed ignition imaging and analyzed results/correlated image differences to engine results, (2) performed simulations of various aftertreatment and control systems/developed recommendation for optimal system, (3) developed total cost of ownership evaluation balancing performance results versus cost impact, (4) developed a projected ignition system wear (maintenance) assessment, and (5) generated the final project report. (White, III.2)

CALSTART is developing an advanced emission control system for Class 7 and Class 8 heavy-duty dual-fuel vehicles that eliminates or mitigates the negative effects of currently used diesel particulate filter and selective catalytic reduction emissions-treatment systems. In 2018 they (1) demonstrated steady improvement in PM compared to the baseline engine, (2) developed a mechanism to reduce the hydrogen production for a single-cylinder engine, (3) determined the optimal testing equipment for continual on track emissions testing, (4) produced 100% of the required parts, and (4) initiated the baseline engine testing of the one-cylinder stock engine. (Sokolsky, III.3)

Southwest Research Institute is improving the efficiency of a gasoline engine by using advanced petroleum and bio-derived fuels in a dedicated EGR engine. In FY 2018 they (1) quantified impacts of fuel chemistry on hydrogen production in the dedicated cylinder of a dedicated EGR engine and (2) demonstrated improved hydrogen production through hardware optimization of a dedicated cylinder. (Briggs, III.4)

Oak Ridge National Laboratory is expanding the understanding of propane as a motor fuel using direct injection in advanced SI engines. In FY 2018 they (1) designed and built a custom long-stroke engine with high compression ratio for use with propane, (2) quantified reforming performance with propane over Rh-based catalyst over multiple simulated operating points in a synthetic exhaust flow reactor, and (3) baselined multi-cylinder engine with propane and compared with gasoline operation. (Szybist, III.5)

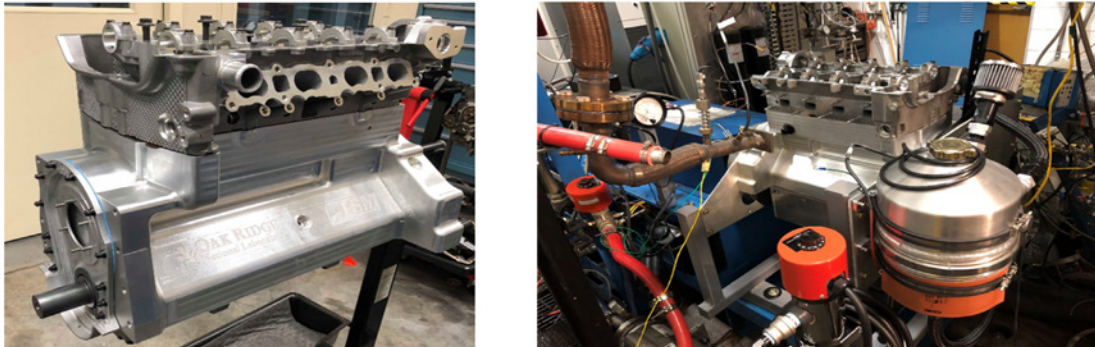


Figure 16. Custom high-efficiency research engine with 1:5:1 stroke-to-bore ratio and high compression ratio (Szybist, III.5)

National Renewable Energy Laboratory is conducting early-stage research to understand fundamental challenges and potential for propane blends to support ACI using direct injection. In FY 2018 they (1) completed initial lower technology readiness level studies to explore direct injection of propane with more advanced combustion engine strategies, (2) conducted bench-scale injector studies focused on challenges with controlling injection of propane blends through existing direct injection injectors, (3) provided guidance on evaporation and mixing differences for propane blends through initial CFD studies, and (4) initiated modifications to the Advanced Fuel Ignition Delay Analyzer to enable propane blend ignition studies. (Zigler, III.3)

Blossman Services, Inc., is developing a propane-fueled spark ignition, direct injection engine and emissions control system based on a current production General Motors 4.3-L spark ignition, direct injection V6 engine that is certification-ready and supports a plan to commercialize it for package delivery trucks. In FY 2018 they (1) developed a custom package delivery truck drive cycle; (2) used the package delivery truck drive cycle to create a greenhouse gas baseline using the 6.0-L port fuel injection gasoline variant; (3) conducted baseline vehicle-level evaluations to determine greenhouse gas targets for the new 4.3-L direct injection propane engine in the P1000 package delivery truck; (4) projected 4.3-L direct injection propane engine performance and incorporated results in P1000 package delivery vehicle simulations to compare performance against the 6.0-L port fuel injection gasoline baseline; (5) began engine baseline studies of a 4.3-L spark ignition, direct injection gasoline engine from Chevrolet Silverado pickup; (6) developed 1D models using GT-SUITE to simulate typical GDI systems similar to the one used on the General Motors 4.3-L spark ignition, direct injection gasoline engine; and (7) began initial aftertreatment three-way catalyst studies to focus on propane mono-fuel operation. (Denton, III.7)

Emission Control R&D

Oak Ridge National Laboratory is supporting industry in the development of accurate simulation tools for the design of catalytic emissions control systems that will enable advanced high-efficiency combustion engines to meet emissions regulations while maximizing fuel efficiency through (1) coordinating the CLEERS activity for the DOE Advanced Engine Crosscut Team; (2) supporting precompetitive collaborative interactions and

providing a consistent framework for sharing information among the emissions control R&D community; (3) identifying emissions control R&D needs and priorities; (4) collaborating with Pacific Northwest National Laboratory to develop mechanistic insights, modeling strategies, benchmark data sets, and representative device parameters for catalytic emissions control devices; and (5) utilizing the CLEERS framework to share the resulting insights, strategies, data sets, and parameters with the emissions control community. (Pihl, IV.1)

Pacific Northwest National Laboratory is promoting the development of improved computational tools for simulating realistic full-system performance of lean-burn engines and the associated emissions control systems. In 2018 they (1) provided detailed atomic-level understanding on the beneficial or detrimental roles of alkali and alkaline co-cations on the activity and durability of Cu/SSZ-13 SCR catalysts, (2) prepared Pd/SSZ-13 passive NO_x adsorber materials with well-defined structure to provide molecular-level insight into passive NO_x adsorber chemistry using combined spectroscopic and density functional theory approach, (3) finalized low-temperature three-way catalyst test protocol, (4) discovered a Pt-based single-atom catalyst that exhibits the elusive combination of low-temperature activity and high-temperature durability for CO oxidation, (5) characterized the catalyst composition and distribution in a commercial multi-functional exhaust filter, and (6) effectively disseminated the technical results in 14 peer-reviewed publications in lead scientific journals. (Wang, IV.2)

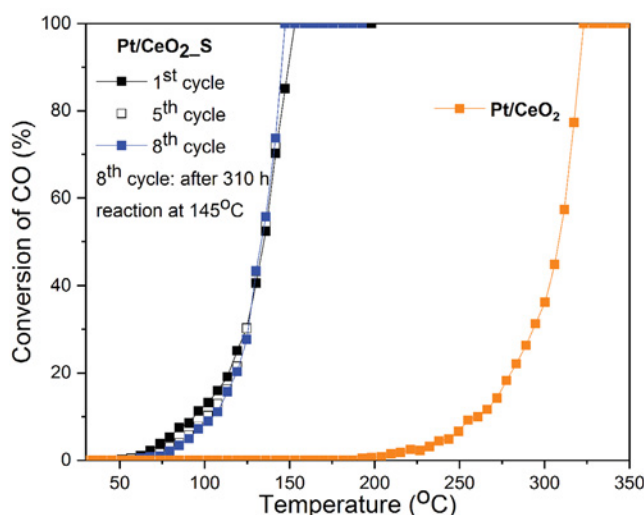


Figure 17. CO oxidation light-off performance showing excellent low-temperature activity and stability of the hydrothermally treated Pt/CeO₂ catalyst under exhaust conditions ([O₂] = 10%, [CO] = 0.4%, gas hourly space velocity = 200 L (gcat hr)⁻¹) (Wang, IV.2)

Oak Ridge National Laboratory is (1) developing emission control technologies that achieve >90% reduction of pollutants at low temperatures (<150°C) to enable fuel-efficient engines with low exhaust temperatures to meet new U.S. Environmental Protection Agency Tier 3 emissions regulations that require ~80% less NO_x and hydrocarbon emissions than current standards, (2) identifying advancements in technologies that will enable commercialization of advanced combustion engine vehicles, and (3) understanding fundamental surface chemistry mechanisms that either enable or limit low-temperature emission control. In FY 2018 they (1) concluded a collaborative catalyst oxidation behavior and silica content optimization study with University of South Carolina and Solvay, (2) studied trap materials and the impact of aging, (3) studied promising materials in combination with each other to overcome drawbacks resulting from using the individual materials alone, and (4) implemented a fast ramping protocol to understand the impact of the proximity of the trap material. (Toops, IV.3)

Oak Ridge National Laboratory is conducting research on an emissions control concept known as passive SCR. In FY 2018 it (1) identified engine operating strategies to meet Tier 3 emission levels (0.03 g/mi NO_x + hydrocarbons) with a passive SCR system (three-way catalyst + SCR) over pseudo-transient cycle, (2) assessed the effect of Ce loading on NH₃ formation on a bench flow reactor, and (3) determined impacts of sulfur on isolated reactions in three-way catalysts on a bench flow reactor. (Parks, IV.4)

Oak Ridge National Laboratory is conducting R&D to understand the fundamental chemistry of automotive catalysts, identify strategies for enabling self-diagnosing catalyst systems, and address critical barriers to market penetration. In FY 2018 they (1) developed a conceptual model describing the origin of Cu selective catalytic reduction onset conversion inflections, (2) developed a five-step protocol to probe half-cycle kinetic parameters, (3) developed a new kinetic model describing conversion inflections, and (3) developed a new methodology for guiding kinetic model development and determining kinetic parameters. (Partridge, IV.5)

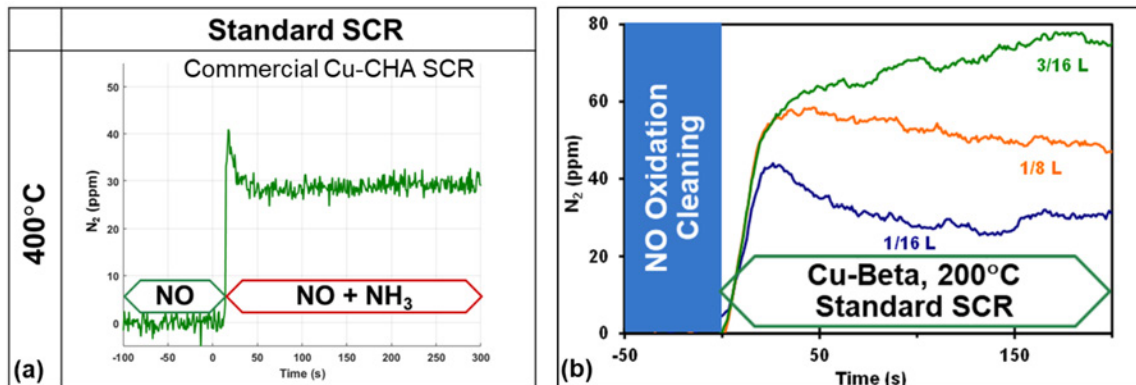


Figure 18. SCR-onset conversion inflections for (a) a commercial Cu-CHA (chabazite) and (b) a model Cu-Beta SCR catalyst (Partridge, IV.5)

Pacific Northwest National Laboratory provides fundamental insight and tools to support the development and optimization of exhaust filter solutions for a variety of future high-efficiency engines, running on a broad spectrum of fuels. In FY 2018 they (1) developed a specialized capillary flow porometry system for characterization of ceramic exhaust filter media, (2) performed detailed 3D simulations of ultra-fine particle capture in exhaust filters using the lattice-Boltzmann method, (3) evaluated methods of improving the standard spherical unit collector filter model, and (4) developed a new transient filter simulation model based on constricted tube collectors. (Stewart, IV.6)

Pacific Northwest National Laboratory is conducting R&D on advanced emission control for high-efficiency engines, specifically focusing on passive NO_x absorbers, oxidation of methane and short alkanes, and improved understanding of particulates. In FY 2018 they (1) finished synthesis, characterization, and evaluation of Pd/SSZ-13 materials with 100% or close to 100% atomic dispersions; (2) finished hydrothermal aging tests of these new materials; (3) initiated sulfur poisoning tests of the Pd/SSZ-13 materials and particle-size-dependent investigations of Pd/beta passive NO_x adsorber materials; (4) synthesized Pd/SSZ-13 catalysts with varying Si/Al ratios; and (5) initiated research on Pd loading dependence of Pd/SSZ-13 catalysts. (Wang, IV.7)

Pacific Northwest National Laboratory is developing a novel active SCR phase that, when employed in the SCR on diesel particulate filter configuration, will enable sufficient passive soot oxidation capacity while retaining the necessary NO_x reduction performance efficiency to be attractive for the heavy-duty diesel application. In FY 2018 they (1) defined critical catalyst design parameters for a ZrO₂-based selective catalytic oxidation (SCO) phase combined with a Cu-chabazite SCR phase forming an SCR-SCO binary catalyst system, in relation to NO_x reduction performance and SCR durability; (2) developed understanding of the impact of secondary oxide or heteroatom additives to ZrO₂ employed to improve NO oxidation (to NO₂) behavior on NO_x reduction performance and SCR durability; and (3) explored the optimized pathway towards SCO impact on fast-SCR contribution to NO_x reduction. (Rappe, IV.8)

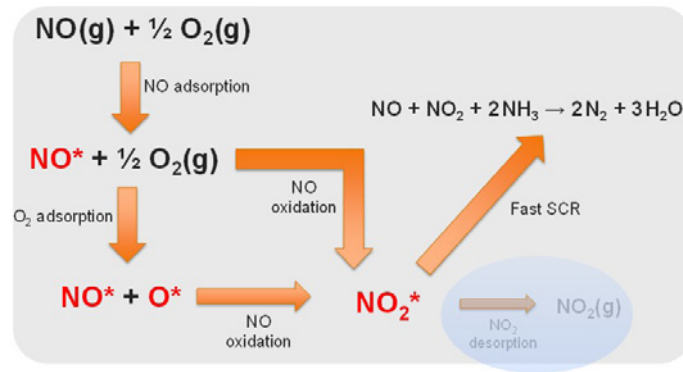


Figure 19. Pathway toward improved NO_x reduction performance by a surface-active NO_x species (Rappe, IV.8)

University of Minnesota–Twin Cities is developing system-level strategies by seeking synergies between fuel and lubricant properties, engine calibration, and next-generation aftertreatment strategies for particulate mass and particulate number reduction. In FY 2018 they (1) completed a full-factorial screening of seven fuels over lean and stoichiometric GDI operating modes, (2) revealed fuel and aftertreatment synergies to achieve low particulate number and particulate mass emissions, and (3) determined effective density as a function of diameter for lean and stoichiometric GDI particles. (Northrop, IV.9)

High Efficiency Engine Technologies

Volvo Group North America continues its SuperTruck research to demonstrate >100% improvement in vehicle ton-miles per gallon compared with a best-in-class 2009 truck, demonstrate 55% brake thermal efficiency on an engine dynamometer, and develop technologies that are commercially cost-effective in terms of a simple payback. In FY 2018 it (1) finalized complete vehicle requirements, (2) completed road tests with technology mule truck (VEV3), and (3) identified all components and technologies for integration in a demonstrator. (Amar, V.1)



Figure 20. Baseline Model Year 2009 vehicle (left) and VEV3 text mule (right) at rest stop during fuel economy test (Amar, V.1)

Cummins Inc. is designing, developing, and demonstrating a very-high-efficiency engine optimized around the drive cycle that will yield a very high increase in vehicle freight efficiency compared to the 2009 baseline vehicle. In FY 2018 they (1) completed design and procurement of the CERD, a transmission-coupled motor/generator with provisions for a waste heat recovery turbine connection for future system coupling; (2) completed testing of the CERD in a powertrain test cell; (3) demonstrated a base engine performance of 49% brake thermal efficiency on a new engine platform; (4) completed build of a mule vehicle to be used for powertrain technology development; (5) completed layout and design of a comprehensive waste heat recovery

system; and (6) completed build of mule tires that represents approximately 50% of the goal for rolling resistance improvement over the 2009 baseline. (Ruth, V.2)

Navistar, Inc., is researching, developing, and demonstrating a heavy-duty engine that can meet 2010 federal emission standards and can achieve 55% brake thermal efficiency demonstrated in an operational engine at a 65-mph cruise point on a dynamometer. In FY 2018 they (1) evaluated cylinder deactivation technology to achieve elevated exhaust temperatures efficiently, (2) improved air system efficiency for SuperTruck 2 engines, (3) investigated novel fuel system configuration to increase combustion burn rates, (4) identified organic Rankine cycle waste heat recovery system that contributes to achieving 55% brake thermal efficiency, (5) evaluated new technologies for engine thermal management, and (6) continued gasoline compression ignition investigation at Argonne National Laboratory. (Zukouski, V.3)

Daimler Trucks North America is developing and demonstrating a greater than 100% improvement in overall freight efficiency on a heavy-duty Class 8 tractor-trailer measured in ton-miles per gallon. In FY 2018 they (1) performed selection and defined scope of work for each of the work stream areas; (2) simulated multiple concepts for the engine, vehicle cooling, and aerodynamics; (3) performed design engineering for A-Sample (75% complete); (4) solidified the A-Sample build schedule and moved resources into the program; (5) completed the first program audit and action items to remain compliant, and (6) agreed on the final SuperTruck 2 validation testing cycle. (Yee, V.4)

PACCAR Inc. is researching, developing, and demonstrating a Class 8 long-haul truck and trailer combination that can meet prevailing federal emission standards and applicable safety and regulatory requirements. In FY 2018 they (1) determined the engine power required for the SuperTruck II vehicle to meet performance targets while meeting or exceeding the performance of the 2009 baseline vehicle; (2) assessed the average road load required for the SuperTruck II vehicle in order to complete representative drive cycles and the Environmental Protection Agency Phase 2 greenhouse gas regulatory cycles; (3) defined the appropriate level of powertrain electrification/hybridization needed in order to achieve the required freight efficiency improvement target while optimizing the balance between system cost and added weight of components; (4) selected the drive and duty cycles for the demonstration of freight efficiency improvement; and (5) completed simulation and analysis of engine, powertrain, and vehicle to define the technical path. (Hergart, V.5)

Table 1. Hybrid Technology Approach Risk Assessment (Hergart, V.5)

eMotor Power	15 kW	30 kW	45 kW	60 kW	90 kW	120 kW	120kW
Battery (e = energy, p = power)	e 10 kWh	e 10 kWh	p 10 kWh	p 10 kWh	p 10 kWh	p 10 kWh	e 60 kWh*
System Voltage	48 V	48 V	650 V	650 V	650 V	650 V	650 V
Integration	PTO	PTO	PTO	Integrated	Integrated	Integrated	Integrated
Contribution to ST-II Freight Efficiency	G	G	G	G	G	G	R
Customer Payback	G	Y	R	R	R	R	R
GHG2 Credit Potential	G	G	G	G	G	G	G
Serviceability	G	G	Y	Y	Y	Y	Y
Volume Potential	G	G	Y	R	R	R	R
Customer Cost	G	Y	Y	Y	R	R	R
Commercialization Cost	Y	Y	Y	R	R	R	R
Proof Of Concept Cost	G	G	Y	R	R	R	R
Zero Emission Zone Capable	R	R	R	R	R	R	G

Delphi Technologies is addressing technical risks and issues that must be overcome for gasoline direct-injection compression ignition to become a production-viable technology, with the ultimate deliverable being demonstration of a 35% fuel economy improvement over a baseline vehicle with a port fuel injection engine, while simultaneously meeting Tier 3 emissions levels. In FY 2018 they (1) characterized a benchmark GDI SI engine; (2) characterized and mapped a Generation (Gen) 3 gasoline direct-injection compression ignition engine on a performance dynamometer; (3) developed improved strategies for high-load gasoline

direct-injection compression ignition operation; (4) performed Gen 3 vehicle simulation for fuel economy and emissions; and (5) refined controls, algorithms, and software for the Gen 3 gasoline direct-injection compression ignition vehicle. (Confer, V.6)

General Motors is researching, developing, and demonstrating the new lean Miller cycle combustion concept. In FY 2018 they (1) finalized calibration on a single-cylinder engine of the final combustion hardware set deployed to a multi-cylinder engine, (2) finalized hardware procurement for the first multi-cylinder engine design and built two engines, (3) finalized control architecture for a steady-state dyno engine and commissioned multi-cylinder engine on dyno to support validation of fuel efficiency projections, (4) refined simulation toolsets to project cycle fuel economy and emissions potential, and (5) designed and procured multi-cylinder engine upgrades and after-treatment systems for transient development phases. (Battiston, V.7)

Cummins Inc. is using a diesel engine system to demonstrate peak engine efficiency of 55% brake thermal efficiency in a test cell and is developing and demonstrating an advanced, highly integrated combustion and after-treatment system to achieve 2010 emissions compliance. In FY 2018 they (1) demonstrated in a test cell peak engine efficiency of the diesel engine system, (2) demonstrated emissions compliance of the system, and (3) completed the final technical report. (Kocher, V.8)

General Motors is developing a high-output, low-temperature gasoline combustion engine system demonstrating a 15–17% fuel economy improvement relative to a contemporary stoichiometric combustion engine. In FY 2018 they (1) conducted a homogeneous stoichiometric SI combustion assessment of the LTC engine with the prototype controller, (2) developed and demonstrated LTC performance at key steady-state points in conjunction with the novel low-temperature plasma ignition system, (3) developed LTC control system architecture and calibration control system models and algorithms, and (4) developed and demonstrated full LTC engine calibrations and simplified combustion control system. (Yun, V.9)

Delphi Technologies is developing solenoid actuated valve train hardware that will allow dynamic skip fire technology to be more easily commercialized with current overhead cam production engines. In FY 2018 they (1) demonstrated actuator control, (2) confirmed operation of the deactivation system, (3) baselined dyno engine performance, and (4) confirmed control system functionality. (Fernandez, V.10)

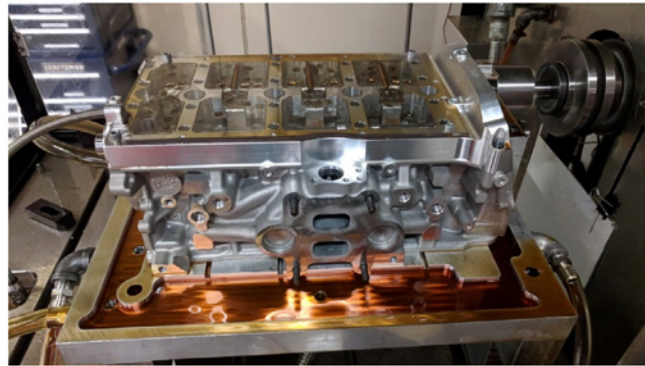


Figure 21. Complete dynamic skip fire cylinder head assembly on test stand (Fernandez, V.10)

HRL Laboratories, LLC, is increasing internal combustion engine efficiency and decreasing heat loss from the combustion chamber with temperature-following thermal barrier coatings. In FY 2018 they (1) demonstrated >2% efficiency gain and thermal barrier coating survival of first-generation valves, pistons, and exhaust ports in a successful engine test; (2) defined a scalable low-cost process for microshell fabrication; and (3) defined processes to coat valves, pistons, and port liners. (Schaedler, V.11)

Lubricant Technologies

Ford Motor Company is demonstrating friction reduction potential using advanced high-porosity plasma transfer wire arc coatings, surface finish, and design on power cylinder systems containing cylinder bore, piston rings, piston skirt, bearings and crankshaft, and advanced engine oils. In FY 2018 they (1) demonstrated

friction benefits of high-porosity plasma transfer wire arc coatings in engine cranktrain; (2) demonstrated friction benefit of ring face coating technologies in laboratory bench, motored single cylinder, and motored engine cranktrain tests; and (3) demonstrated friction benefit in a motored engine. (Gangopadhyay, VI.1)

George Washington University is developing a prototype 0W-20 low-viscosity oil and demonstrating that it can improve fuel economy by 2%, is backward compatible, and is suitable for use by current cars and light trucks. In FY 2018 they (1) fabricated surface textures on the new 2018 platform engine for fuel economy testing and (2) developed vehicle test protocols to confirm fuel economy improvement using the new engine. (Hsu, VI.2)

System Level Efficiency Improvement

Oak Ridge National Laboratory is reducing the hysteretic losses of elastomers that are used for manufacturing vehicle tires. In FY 2018 they (1) scaled up the synthesized filler material, (2) dispersed the filler material in the elastomer matrix using industrial techniques, and (3) tested the properties of the composite elastomers using industrial techniques. (Polyzos, VII.1)

PPG Industries, Inc., is developing a new silica filler that can increase tire fuel efficiency by 2% while maximizing key performance properties in non-tread tire components compared to current carbon black-filled sidewall compounds. In FY 2018 they (1) developed a database with custom-made silica fillers to enable statistical analysis of the results and (2) identified the surface chemistry and morphology variables that optimize the wide range of required sidewall performance metrics. (Dos Santos Freire, VII.2)

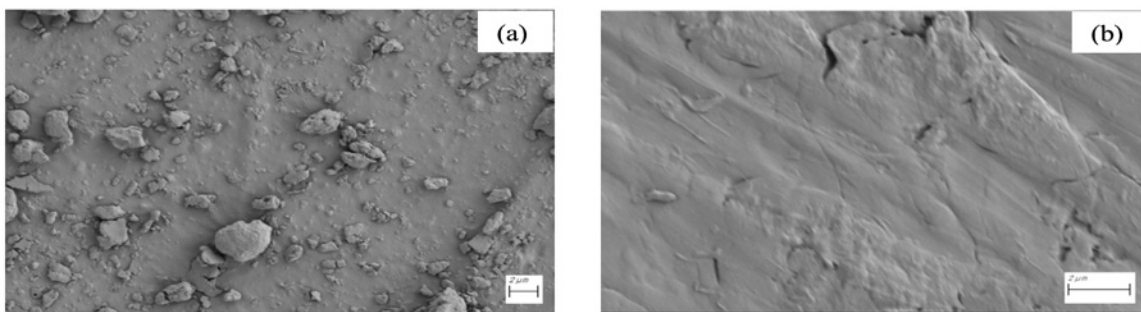


Figure 22. Scanning electron micrograph images of the abraded surface of (a) unfilled styrene-butadiene-styrene and (b) styrene-butadiene-styrene-graphene oxide samples after 100 abrading cycles (Dos Santos Freire, VII.2)

Invention and Patent Disclosures

1. Invention Disclosure: Waters, J., and D.B. Carrington. 2016. “A Parallel Large Eddy Simulation in a Finite Element Projection Method for All Flow Regimes.” *Numerical Heat Transfer, Part A* 70 (2): 117–131. (Carrington, I.15)
2. Invention Disclosure: Carrington, D.B. 2009. “A Characteristic-Based Split hp-Adaptive Finite Element Method for Combustion Modeling in KIVA-hpFE.” LANL Scientific Report no. LA-UR-09-06527. (Carrington, I.15)
3. Invention Disclosure: Carrington, D.B., X. Wang, and D.W. Pepper. 2014. “A Predictor-Corrector Split Projection Method for Turbulent Reactive Flow.” *Journal of Computational Thermal Sciences* 5 (4): 333–352. (Carrington, I.15)
4. Invention Disclosure: Carrington D.B., X. Wang, and D.W. Pepper. 2014. “An hp-Adaptive Predictor-Corrector Split Projection Method for Turbulent Compressible Flow.” *Proceedings of the 15th International Heat Transfer Conference, IHTC-15, Kyoto, Japan, August 10–15, 2014.* (Carrington, I.15)

5. Invention Disclosure: Carrington, D.B., M. Mazumder, and J.C. Heinrich. 2018. "Three-Dimensional Local ALE-FEM Method for Fluid Flow in Domains Containing Moving Boundaries/Objects Interfaces." *Progress in Computational Fluid Dynamics* 18 (4): 199–215. (Carrington, I.15)
6. Invention Disclosure: Carrington, D.B., and J. Waters. 2018. "Turbulent Reactive Flow Modeling in Engines: A Robust and Accurate Toolkit/Software for Simulating Engine Dynamics." *Proceedings of the ASME 2018 Internal Combustion Engine Fall Technical Conference, ICEF2018, San Diego, CA, USA, November 4–7, 2018.* (Carrington, I.15)
7. Invention Disclosure: Waters J., D.B. Carrington, and D.W. Pepper. 2016. "An Adaptive Finite Element Method with Dynamic LES for Incompressible and Compressible Flows." *Journal of Computational Thermal Sciences* 8 (1): 57–71. (Carrington, I.15)
8. Invention Disclosure: Waters, J., D.B. Carrington, and M.M. Francois. 2017. "Modeling Multi-phase Flow: Spray Break-up Using Volume of Fluids in a Dynamic LES FEM Method." *Numerical Heat Transfer, Part B* 72 (4): 285–299. (Carrington, I.15)
9. Mueller, C.J. 2018. "Ducted Fuel Injection." U.S. Patent #9,909,549; issued March 6, 2018. (Mueller, II.16)
10. Invention Disclosure: Mariuz, Robert M., Kevin R. Keegan, Peter Charles, and Hermes A. Fernandez. 2018. S-N/A, Docket No. DP-324785, eDEAC Z STRAP patent application submitted on 07/09/2018. (Fernandez, V.10)
11. Invention Disclosure: Keegan, Kevin R., Hermes A. Fernandez, Robert M. Mariuz, Catherine C. Vavonese, and Jacob Daniels. 2018. S-N/A, Docket No. DP-324738, "Non Magnetic Centering Sleeve." submitted on 04/19/2018. (Fernandez, V.10)
12. Invention Disclosure: Keegan, Kevin R., Hermes A. Fernandez, Robert M. Mariuz, Catherine C. Vavonese, and Peter R. Charles. 2018. S-N/A, Docket No. DP-324748, "Control Rod Trigger." submitted 05/02/2018. (Fernandez, V.10)
13. Invention Disclosure: Mariuz, Robert, Kevin R. Keegan, Hermes A. Fernandez, and Richard B. Roe. 2017. S-149,210, iEdison Invention 10042275-18-0002, Docket No. DP-324592, "Side Lock Mechanism for Rocker Finger Follower." originally submitted on 11/15/2017 was resubmitted on 1/24/2018. (Fernandez, V.10)
14. Invention Disclosure: Walker, Michael, Paul Najt, and Russell Durrett. 2018. "A Method to Cast Thermal Barrier Coatings in Sand or Granular Media Casting Processes." Submitted August 2018. (Schaedler, V.11)

I. Combustion Research

I.1 Light- and Medium-Duty Diesel Combustion (Sandia National Laboratories)

Stephen Busch, Principal Investigator

Sandia National Laboratories
PO Box 969, MS 9053
Livermore, CA 94551-0969
E-mail: sbusch@sandia.gov

Michael Weismiller, DOE Technology Development Manager

U.S. Department of Energy
E-mail: Michael.Weismiller@ee.doe.gov

Start Date: March 1, 2018

End Date: September 30, 2018

Project Funding (FY18): \$620,000

DOE share: \$620,000

Non-DOE share: \$0

Project Introduction

Diesel engines remain a cost-effective, efficient, powerful propulsion source for many light- and medium-duty vehicle applications. Modest efficiency improvements in these engines can eliminate millions of tons of CO₂ emissions per year, but these improvements will require improved understanding of how diesel combustion chamber geometry influences mixture preparation, combustion, and pollutant formation processes.

The research focus for this performance period is to provide insight into spray-wall interactions in stepped-lip combustion chambers. These interactions are believed to promote the formation of recirculating flow structures that improve thermal efficiency and reduce soot emissions, but these benefits are only fully realized for late main injection timings. A detailed mechanistic understanding of these processes can lead to cleaner, more efficient combustion chamber designs.

Objectives

This project will provide scientific understanding needed to design, optimize, and calibrate the next generations of light- and medium-duty diesel engines that comply with increasingly stringent pollutant emission regulations while achieving thermal efficiencies approaching 50%.

Overall Objectives

- Develop conceptual models for spray-wall interactions, combustion, and pollutant formation in direct injection diesel engines
- Develop conceptual models that describe fuel injection, mixture formation, combustion, and pollutant formation during catalyst heating operation

Fiscal Year 2018 Objectives

- Provide a mechanistic understanding of how spray-wall interactions promote the formation of recirculating flow structures in a stepped-lip diesel combustion chamber
- Begin conception and design of a new medium-duty diesel research platform

Approach

The approach of this research project involves carefully coordinated experimental and numerical simulation efforts. Detailed optical measurements provide quantitative information about flow, mixture preparation, and combustion processes inside the combustion chamber of Sandia's small-bore direct injection diesel research engine. The three-dimensional engine geometry and experimental data are made publically available and support the development and evaluation of computational fluid dynamics (CFD) simulation codes and

numerical models. A new medium-duty diesel research platform is being developed to ensure the relevance of future research.

Close collaboration with numerical simulation experts from Wisconsin Engine Research Consultants (subcontractors) provides a much needed complement to the optical engine experiments. The experimental results are used to evaluate the predictive abilities of computational simulations. In turn, analysis of the simulation results generates a deeper understanding of in-cylinder flow and combustion physics. The results of this combined approach are not possible to obtain with experimental data alone, and the analyses provide fundamental, science-based understanding of in-cylinder phenomena. This knowledge will be embodied in conceptual models that guide the development and calibration of the next generations of diesel engines.

Results

Key accomplishments:

- Provided experimental evidence correlating the strength and persistence of recirculating flow with increased heat release rates and decreased soot emissions with the stepped-lip combustion chamber
- Developed mechanistic understanding of how fuel sprays interact with the stepped-lip piston to promote the formation of beneficial recirculating flow structures
- Completed conception of a new medium-duty thermal/optical diesel research platform

Faster mixing-controlled combustion was identified as a key to thermal efficiency improvement with stepped-lip diesel piston bowls in the previous year's activities. Additionally, CFD simulations inside both the conventional and stepped-lip combustion chambers predicted the formation of two additional recirculation zones above the stepped-lip piston that are not predicted for the conventional piston [1]. Research performed in this fiscal year was focused on providing experimental evidence for the recirculating flow structures and on in-depth analysis of the CFD results to better understand the physics responsible for the evolution of turbulent flow resulting from spray-piston bowl interactions. Finally, the initial concept for a new medium-duty diesel research engine has been developed.

Combustion image velocimetry is an experimental technique used to provide information about the evolution of turbulent, combusting flow based on high-speed natural combustion luminosity images [2]. This technique has been applied in Sandia's small-bore optical diesel engine to characterize the flow evolution in the stepped-lip combustion chamber for two different main injection timings [3]. The radial component of the flow provides evidence of vertical-plane flow structures that form as a result of interactions between the fuel spray and the stepped-lip combustion chamber. The azimuthally averaged flow velocity is shown as a function of crank angle and radius with a red-white-blue color map in the bottom portion of Figure I.1.1. The line plots in the top portion of Figure I.1.1 indicate that faster, more efficient combustion results with the stepped-lip piston at the later main injection timing. The later main injection also results in a more significant reduction in engine-out soot emissions. Both the differences in the slopes of the mass-fraction-burned (MFB) lines and the reduction in soot emissions correspond with the strength and longevity of the recirculating flow structures.

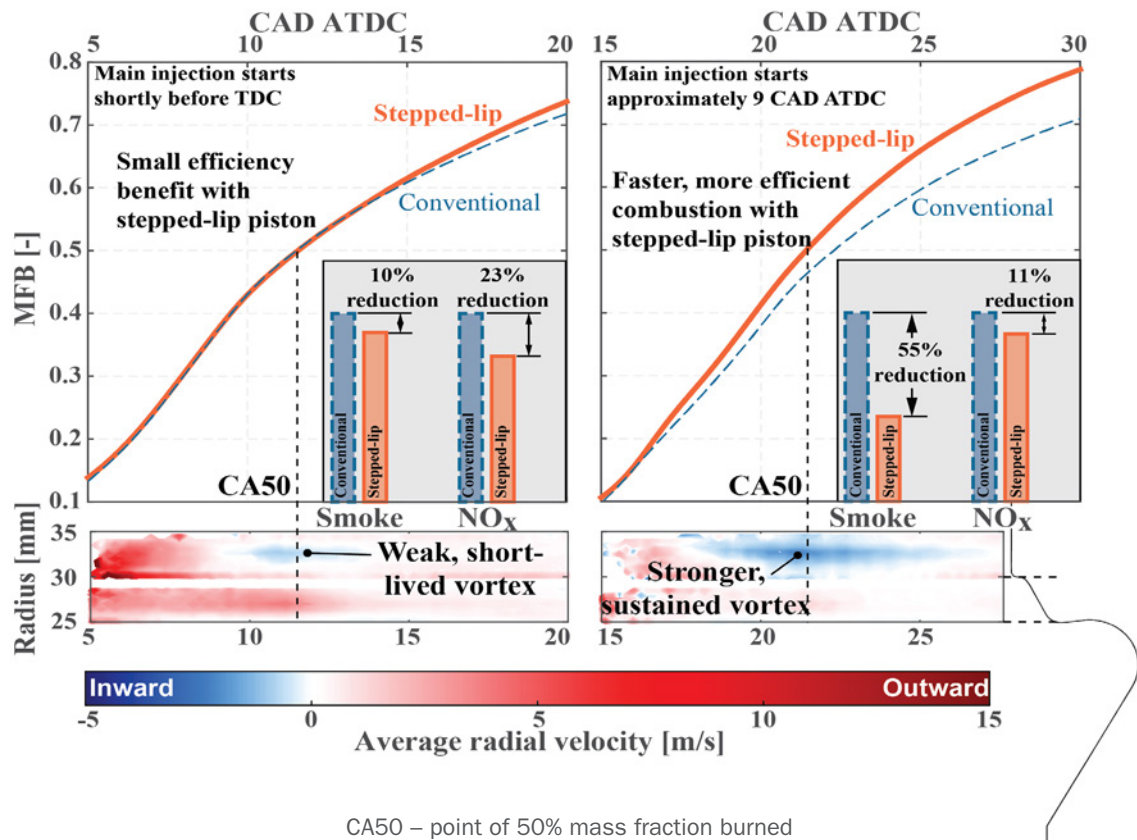


Figure I.1.1. Combustion image velocimetry results show the evolution of the azimuthally averaged radial component of flow (red/blue false color strips; note the piston profile on the right side). The left portion is for a main injection starting shortly before top dead center, and the right plot shows data for a main injection starting approximately 9 crank angle degrees (CAD) above top dead center (ATDC), when the stepped-lip piston shows significant advantages over the conventional piston. Inward flow (blue regions) is evidence of a vortex in the outer portion of the stepped-lip combustion chamber. The strength and longevity of the vortex corresponds to faster mixing-controlled combustion (line plots) and reduced soot emissions (bar plots) for the stepped-lip piston.

CFD simulations have been performed by solving the Reynolds-averaged Navier-Stokes equations on a three-dimensional mesh representing the complete single-cylinder engine to simulate the evolution of turbulent flow in the stepped-lip combustion chamber. Simulations are performed for both injection timings mentioned above under non-combusting conditions in order to isolate the effects of spray-wall interactions [4]. Examination of a vertical cutting plane containing the fuel injector's seven spray axes provides insight into spray-wall interactions and the formation of vortices. Figure I.1.2 shows the fuel-air equivalence ratio with false color projected on the vertical cutting plane with velocity vectors indicating the components of the flow field as they are projected onto the plane. The top image depicts a crank angle after the end of the main injection that started shortly before top dead center. The simulation does not predict the formation of strong, long-lived recirculation zones above the squish region for this injection timing, which supports the experimental findings shown in Figure I.1.1. The bottom of Figure I.1.2 depicts the same vertical cutting plane shortly after the end of the main injection that started approximately 9 CAD ATDC. In this case, a strong flow pattern has developed along the step, and flow patterns consistent with recirculation are observed; flow is directed inward along the cylinder head and outward into the top of the outer region of the combustion chamber. This prediction also supports the experimental finding that energetic flow structures persist late into the cycle for the later main injection timing.

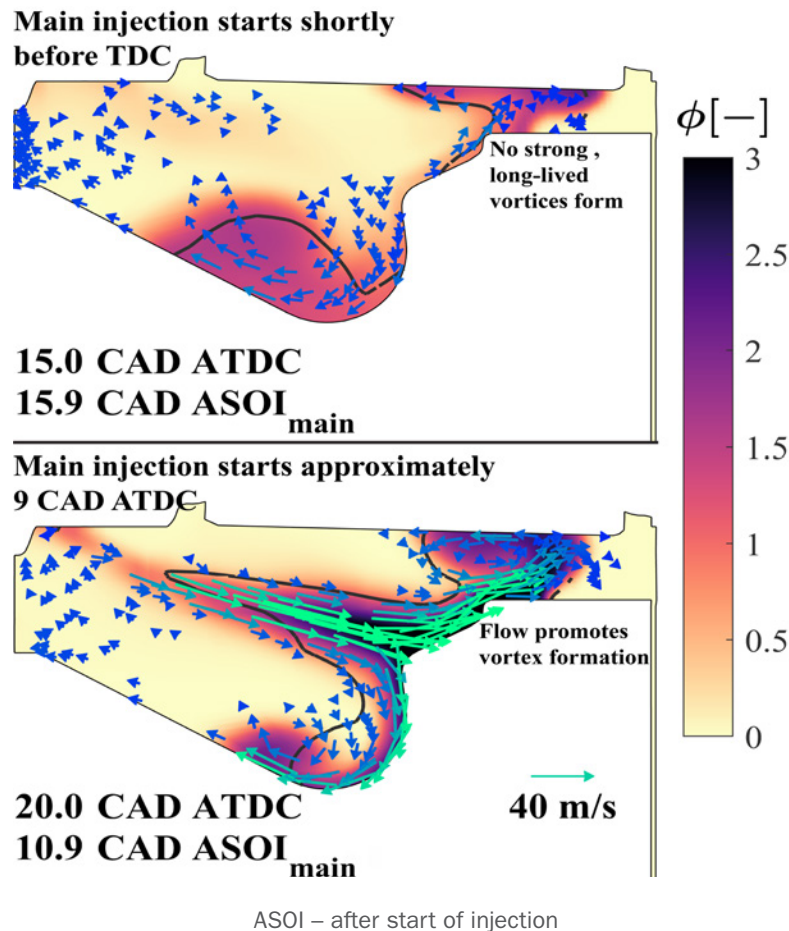


Figure I.1.2. CFD results shown on a vertical cutting plane containing one spray axis. False color represents the fuel–air equivalence ratio; the black contour represents the stoichiometric iso-contour, which has an equivalence ratio of 1.0. Colored vectors are shown to indicate the velocity field components projected onto the plane. Top: main injection starts near top dead center. Bottom: main injection starts approximately 9 CAD ATDC.

Because the CFD simulations show good qualitative agreement with the experimental findings, a deeper analysis of the simulation results is performed to provide additional insight into the physics responsible for the behavior depicted in Figure I.1.2. To this end, the terms of the Reynolds-averaged Navier-Stokes equations for fluid motion are evaluated by converting the Cartesian-based simulation results into polar coordinates. The radial component of Reynolds-averaged acceleration is normalized by the local velocity magnitude and depicted on a vertical cutting plane in Figure I.1.3. Each image represents the point in time when the spray begins to separate from the piston surface for the main injection that starts approximately 9 CAD ATDC.

The outward acceleration in the central portion of the jet is the result of one term in the Reynolds-averaged Navier-Stokes equation for radial momentum: the vertical convection of outward radial momentum. As the spray impacts the surface of the piston step, the surface imparts an upward velocity to the spray. The spray penetrates upward and outward and eventually separates from the piston surface. Penetration then continues into the outer portion of the combustion chamber, the so-called “squish” region. As the spray penetrates outward, a high-pressure region builds up in front of it. This high pressure, combined with the low pressure in the center of the chamber associated with air entrainment into the spray and vaporization, creates an adverse pressure gradient that acts to accelerate the spray inward. This is depicted at the top left of Figure I.1.3 and is the dominant force acting on the fluid near the cylinder head. As a result, flow near the head accelerates inward toward the center of the combustion chamber. The combination of this inward flow and outward flow contributes to the formation of beneficial vortices above the stepped-lip combustion chamber.

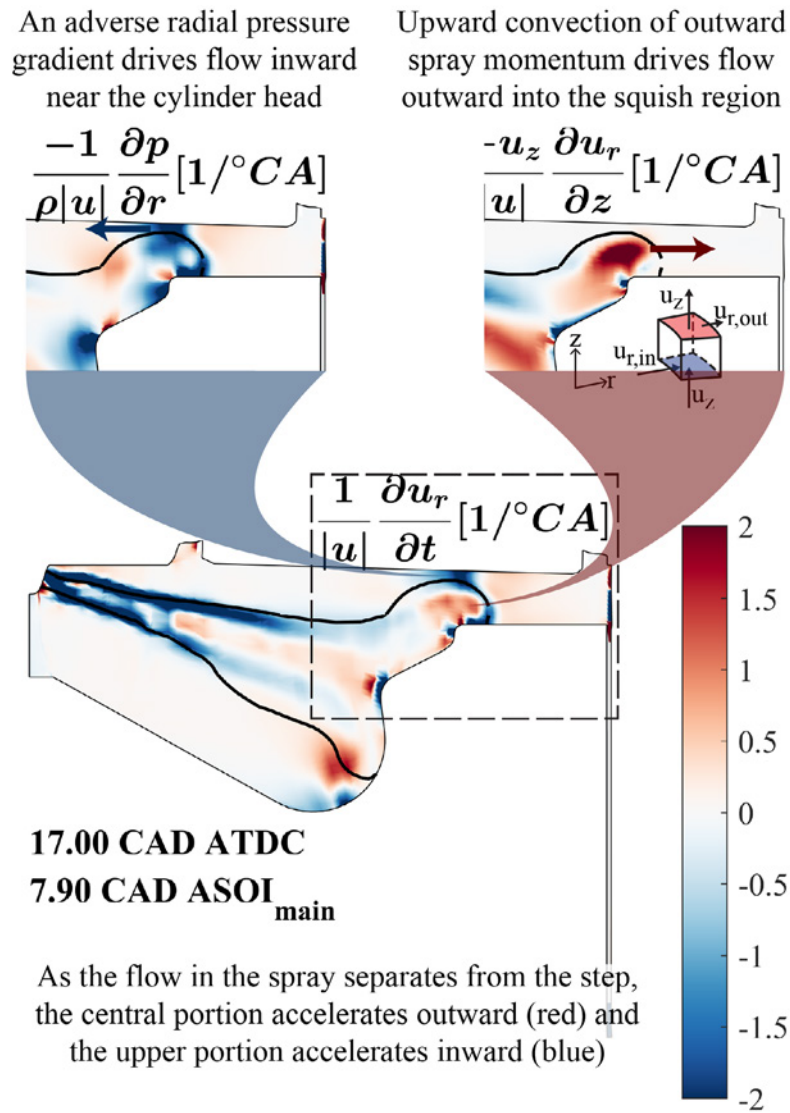


Figure I.1.3. Components of the radial acceleration equation visualized on a vertical cutting plane containing a spray axis. Bottom: the radial acceleration; blue colors represent acceleration inward toward the cylinder axis and red colors represent outward acceleration. Top left: the contribution of the radial pressure gradient to the radial acceleration. Top right: the contribution of vertical convection of radial momentum to radial acceleration. Note the units are 1/°CA: a value of 2 corresponds to an outward acceleration equal to the local velocity magnitude in the time it takes the crankshaft to rotate one degree.

While the impact of light-duty diesel research is expected to be limited by the relatively low market penetration of diesel passenger cars in the United States, medium-duty diesel engines are widely used in a large variety of commercial and vocational vehicles. Improving the efficiency and emissions of these engines requires a scientific understanding of phenomena such as turbulent mixing, heat transfer, and exhaust catalyst warm-up strategies. For these reasons, a new medium-duty diesel research engine has been conceived to replace Sandia’s small-bore diesel engine. This new engine will be designed for two configurations, an all-metal engine for thermodynamic measurements and an optical engine for optical combustion diagnostic measurements.

Conclusions

The focus of this year's work has been on experimental characterization and numerical analysis of spray-wall interactions in stepped-lip combustion chambers. Two factors that help create beneficial flow structures in the stepped-lip combustion chamber have been identified.

- Vertical convection of the spray momentum upward and outward into the squish region
- Adverse radial pressure gradients drive flow inward along the cylinder head surface

Key Publications

1. Zha, K., S. Busch, A. Warey, R.C. Peterson, and E. Kurtz. 2018. "A Study of Piston Geometry Effects on Late-Stage Combustion in a Light-Duty Optical Diesel Engine Using Combustion Image Velocimetry." SAE Technical Paper 2018-01-0230, DOI: 10.4271/2018-01-0230.
2. Busch, S. 2018. "Light Duty Diesel Combustion." In *Advanced Combustion Systems and Fuels: 2017 Annual Progress Report*, 29–35. Department of Energy, Office of Energy Efficiency and Renewable Energy, Vehicle Technologies Office.
3. Busch, S., K. Zha, F. Perini, R. Reitz, E. Kurtz, A. Warey, and R. Peterson. 2018. "Bowl Geometry Effects on Turbulent Flow Structure in a Direct Injection Diesel Engine." SAE Technical Paper 2018-01-1794, DOI: 10.4271/2018-01-1794.

References

1. Busch, S. 2018. "Light Duty Diesel Combustion." In *Advanced Combustion Systems and Fuels: 2017 Annual Progress Report*, 29–35. Department of Energy, Office of Energy Efficiency and Renewable Energy, Vehicle Technologies Office.
2. Dembinski, H.W.R., and H.-E. Angstrom. 2012. "Optical Study of Swirl during Combustion in a CI Engine with Different Injection Pressures and Swirl Ratios Compared with Calculations." SAE Technical Paper 2012-01-0682, DOI: 10.4271/2012-01-0682.
3. Zha, K., S. Busch, A. Warey, R.C. Peterson, and E. Kurtz. 2018. "A Study of Piston Geometry Effects on Late-Stage Combustion in a Light-Duty Optical Diesel Engine Using Combustion Image Velocimetry." SAE Technical Paper 2018-01-0230, DOI: 10.4271/2018-01-0230.
4. Busch, S., K. Zha, F. Perini, R. Reitz, E. Kurtz, A. Warey, and R. Peterson. 2018. "Bowl Geometry Effects on Turbulent Flow Structure in a Direct Injection Diesel Engine." SAE Technical Paper 2018-01-1794, DOI: 10.4271/2018-01-1794.

Acknowledgements

Ford Motor Company is acknowledged for their engineering support and for the loan of critical engine hardware for Sandia's new medium-duty diesel engine. Dr. Kan Zha is acknowledged for her work to perform the combustion image velocimetry experiments and process the imaging data.

Sandia National Laboratories is a multi-mission laboratory managed and operated by National Technology and Engineering Solutions of Sandia, LLC, a wholly owned subsidiary of Honeywell International, Inc., for the U.S. Department of Energy's National Nuclear Security Administration under contract DE-NA-0003525.

I.2 Heavy-Duty Low-Temperature and Diesel Combustion and Heavy-Duty Combustion Modeling (Sandia National Laboratories)

Mark PB Musculus, Principal Investigator

Sandia National Laboratories
PO Box 969, MS 9053
Livermore, CA 94551-0969
E-mail: mpmuscu@sandia.gov

Michael Weismiller, DOE Technology Development Manager

U.S. Department of Energy
E-mail: Michael.Weismiller@ee.doe.gov

Start Date: October 1, 2017	End Date: September 30, 2018	
Project Funding (FY18): \$310,000	DOE share: \$310,000	Non-DOE share: \$0

Project Introduction

Regulatory drivers and market demands for lower pollutant emissions, lower carbon dioxide emissions, and lower fuel consumption motivate the development of clean and fuel-efficient engine operating strategies. Most current production engines use a combination of both in-cylinder and exhaust emission control strategies to achieve these goals. The emissions and efficiency performance of in-cylinder strategies depend strongly on flow and mixing processes associated with fuel injection.

Both heavy- and light-duty engine/vehicle manufacturers use multiple-injection strategies to reduce noise, emissions, and fuel consumption. For both conventional and low-temperature diesel combustion, the state of knowledge and modeling tools for multiple injections are far less advanced than for single-injection strategies. Engine efficiency is limited to some degree by tradeoffs that must be accepted to meet particulate matter (including soot) emissions limits. Recent work on this project has filled some knowledge gaps on soot oxidation with multiple injections, and the current work for Fiscal Year (FY) 2018 addresses knowledge gaps on soot formation for multiple injections. While total in-cylinder soot is readily measured, discerning formation from oxidation is difficult. The FY 2018 experiments are designed to create in-cylinder conditions at the threshold of soot formation, where processes that affect soot formation can be more readily discerned. Soot formation pathways under such conditions are fraught with uncertainties [1], and soot models significantly overpredict polyaromatic hydrocarbon (PAH) and soot [2], so experimental data at these conditions will provide much needed data for improvements to PAH and soot models.

Objectives

This project includes diesel combustion research at Sandia National Laboratories and combustion modeling at the University of Wisconsin.

Overall Objectives

- Develop fundamental understanding of how in-cylinder controls can improve efficiency and reduce pollutant emissions of advanced low-temperature combustion (LTC) technologies
- Quantify the effects of fuel injection, mixing, and combustion processes on thermodynamic losses and pollutant emission formation
- Improve computer modeling capabilities to accurately simulate these processes

FY 2018 Objectives

- Image a second injection penetrating into the residual jet from a first injection to build conceptual-model understanding of multiple-injection schemes

- Analyze simulation predictions to complement conceptual-model understanding of multiple-injection interactions affecting ignition gained through experiments

Approach

This project uses an optically accessible, heavy-duty, direct-injection diesel engine (Figure I.2.1). A large window in the piston crown provides primary imaging access to the piston bowl, and other windows at the cylinder wall provide cross-optical access for laser diagnostics.

The optical setup in Figure I.2.1 uses two cameras to record simultaneous images of planar laser-induced fluorescence of polyaromatic hydrocarbons (PAH-PLIF) and planar laser-induced incandescence of soot (soot-PLII). The PAHs are chemical precursors to soot that start with a small number of aromatic rings and grow to molecules with a greater number of rings prior to the formation of soot particles. Different size-classes of PAH can be probed by using different laser wavelengths. Here, a laser wavelength of 355 nm probes PAH with ~3–6 rings, 532 nm likely probes approximately 10 rings, and 633 nm probes very large PAH—well over 10 rings [3]. The PAH-PLIF laser beams are formed into thin (<1 mm) sheets for the planar imaging diagnostics and are utilized one excitation wavelength at a time. Each is paired with a second laser sheet at a wavelength of 1,064 nm to simultaneously excite soot-PLII. The overlapping beam-sheets are introduced at three different elevations relative to the firedeck (see Figure I.2.1). A beamsplitter reflects a portion of the laser-induced signals to one intensified charge-coupled device (ICCD) camera for soot-PLII imaging and transmits the remainder of the light to a second ICCD camera for PAH-PLIF imaging.

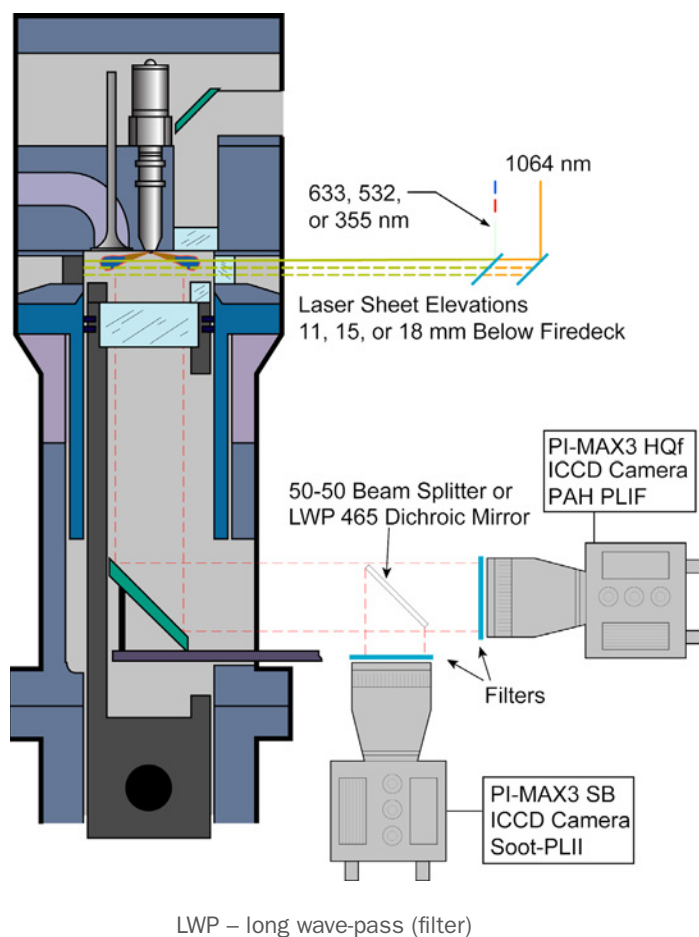


Figure I.2.1. Optical engine schematic showing the orientation of the PAH-PLIF and soot-PLII laser sheets in the combustion chamber and the orientation of the cameras and beamsplitter for imaging through the piston-crown window.

Results

Figure I.2.2 shows a composite of representative instantaneous images of simultaneous 633-nm PAH-PLIF and soot-PLII at an elevation of 15 mm below the firedeck for single injections over a range of increasing dilution of the intake air by nitrogen, with intake oxygen (O₂) mole fractions from 15% down to 7.5%. The PAH-PLIF is false-colored green, while soot-PLII is red, and overlap regions appear yellow. At each O₂ condition, a series of images acquired at different crank angle degree (CAD) timings from different engine cycles is shown, referenced to 360 CAD at top-dead-center (TDC) of the compression stroke. The inception of large PAH (using 633-nm PLIF excitation) ranges from 358 CAD for 15% intake O₂ to as late as 370 CAD for 9% intake O₂. The 7.5% intake O₂ condition has no PAH, nor any soot, though ignition and combustion do occur even at this low oxygen concentration. The 9% intake O₂ condition shows PAH but no detectable soot, while the 10% intake O₂ condition has large PAH and threshold soot formation, with earlier and/or greater soot formation at 12.5% and 15% intake O₂. Although 10% intake O₂ is not suitable for practical engine operation, it is interesting for studying multiple-injection effects on soot formation, since it is at the threshold of sooting, such that multiple-injection effects on soot formation may be more readily observed than at other conditions where small changes to formation are difficult to separate from changes in soot oxidation. Hence, this condition is selected for further study using multiple injections.

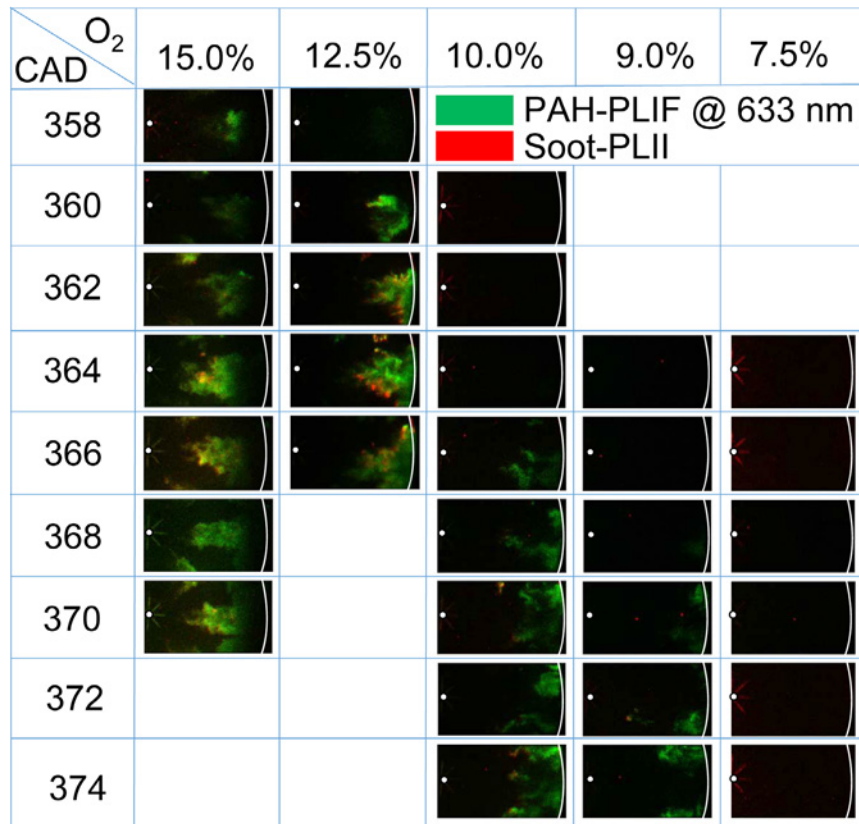


Figure I.2.2. Representative instantaneous images of simultaneous 633-nm PAH-PLIF (false-colored green) and soot-PLII (red) at an elevation of 15 mm below the firedeck for single injections over a range of intake O₂ mole fractions. Each row of images is acquired at a different CAD timing and from separate engine cycles. Each image is a partial view of the whole combustion chamber, capturing one of the eight jets, penetrating from left to right, with the injector near the left, indicated by a white dot, while the curved white line represents the piston bowl. The laser sheet penetrates from right to left.

To study multiple-injection effects on soot formation, two different double-injection conditions were utilized. The first is a close-coupled (CC) double injection, with a first injection of 0.8 ms duration, followed by a second injection of duration 2 ms, placed as close as practically possible without merging injections. Figure I.2.3 shows the injection schedule (bottom, red) and resulting cylinder pressure (top, red) at 10%

intake O_2 . A second condition was created using larger (1.1 ms) first injection that was timed much earlier, to create a long-dwell (LD) condition (see blue injection schedule and pressure data in Figure I.2.3). These conditions were specifically designed according to two criteria. First, the LD condition creates a well-mixed residual from the first injection by the time of the second injection, while the CC condition creates a much more heterogeneous residual mixture into which the second injection penetrates. Second, the duration of the first injection for the LD condition was increased to 1.1 ms so that the pressure trajectories during the early PAH and soot formation period, identified by the shaded region in Figure I.2.3, would be similar for the two conditions. In-cylinder temperature is known to be very important for soot and PAH formation [4], so matching the pressure trajectory is important to achieve similar bulk temperatures so that multiple-injection effects on soot formation can be studied without the confounding effects of bulk in-cylinder temperature differences.

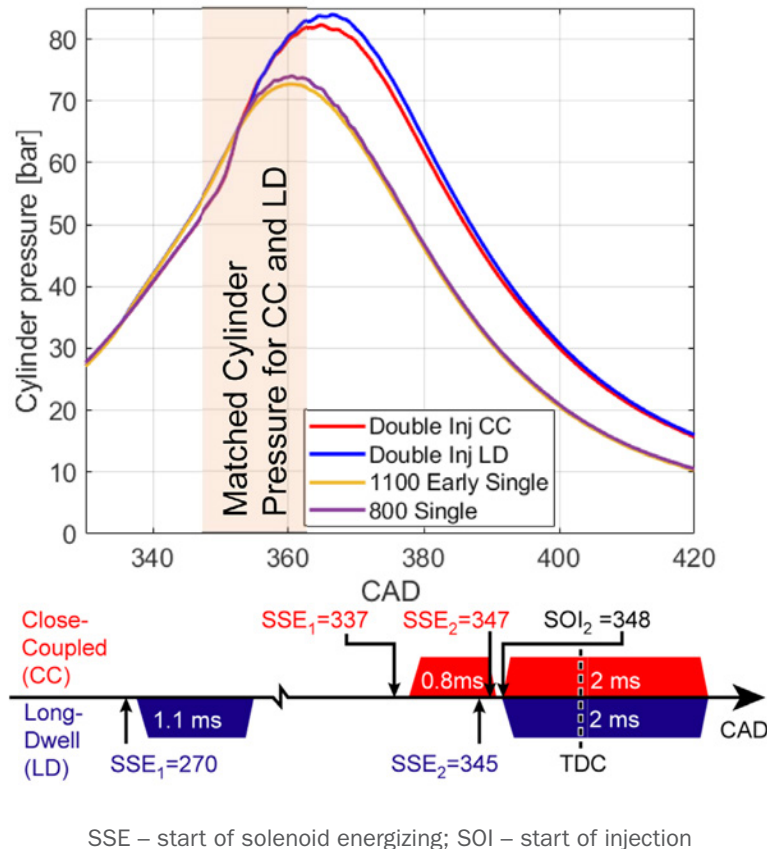


Figure I.2.3. Cylinder pressure (top) and injection schedules (bottom) for CC or LD double-injection conditions at 10% intake O_2 . Single-injection pressure data using only the first injection of either the CC or the LD conditions are shown for reference.

Figure I.2.4 shows four sets of composite 633-nm PAH-PLIF and soot-PLII images for the operating conditions in Figure I.2.3, with the same field of view and false-colored green and red in the same way as the images in Figure I.2.2. The top three sets of two rows of images are acquired at three different laser-sheet elevations for the close-coupled condition, and at various CAD timings as indicated in the upper-left corner of each image. The three-dimensional shape of the jet can be discerned to some degree by comparing images at the three elevations. The bottom set of images, outlined in blue, is for the long-dwell condition at a sheet elevation of 18 mm below the firedeck.

The images in Figure I.2.4 show that for the CC conditions, large PAHs (green, 633-nm PLIF excitation) fill the downstream jet all the way to the bowl wall (right side of images), especially for the uppermost elevation. Soot (red) appears after the PAH and generally farther upstream (left), closer to the injector, on the jet periphery, and with little overlap with the PAH, which appears yellow where there is overlap. Given

the importance of temperature for soot formation at these threshold conditions [4], soot may form on the jet periphery, which is where the diffusion flame is located, because that is where temperatures are high enough for soot formation under these diluted conditions. The lack of overlap (yellow color) may also indicate that large PAHs are mostly consumed when soot formation occurs. One other curious observation is a gap in the PAH distribution at the lowest elevation, as indicated by the dashed white ellipses in Figure I.2.4. PAH fluorescence is detected upstream (left) of the gap, so it is unlikely to be caused by laser-sheet attenuation (the laser sheet propagates from right to left). It is possible that the gap is due to jet-wall interactions at the elevation of the laser sheet, such that soot moves out of the plane of the laser sheet in the recirculation region at the bottom of the bowl. Whatever the cause, it seems to be correlated with the close coupling between injections, as the bottom set of images for the LD condition does not display such a repeatable gap in the PAH distribution.

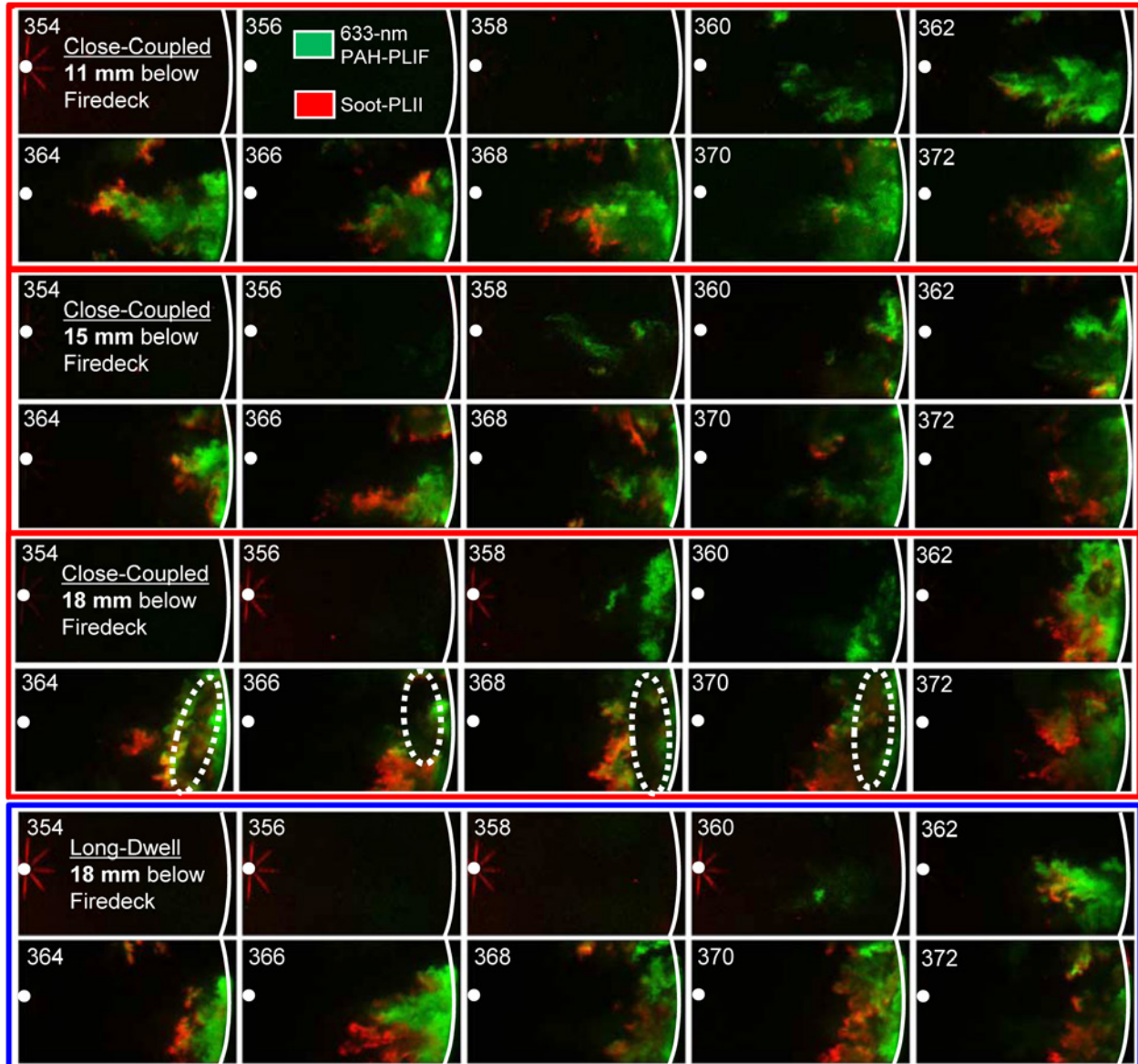


Figure I.2.4. Representative instantaneous images of simultaneous 633-nm PAH-PLIF and soot-PLII at three laser-sheet elevations for the CC condition (top three sets of images, each outlined in red) and at the lowest elevation for the LD condition (bottom set of images, outlined in blue), both at 10% intake O_2 . The crank angle of image acquisition is in the top-left corner of each composite image. Other details of the images are as in Figure I.2.2.

While Figure I.2.2 and Figure I.2.4 show representative instantaneous images at a series of CAD for only one PAH-PLIF excitation wavelength (633 nm), Figure I.2.5 shows ensemble-averaged images to indicate the mean behavior for all three wavelengths, at three different laser-sheet elevations, side-by-side with soot, for both the CC (left side) and LD (right side) operating conditions at 362 CAD (top) and 366 CAD (bottom) for the 10% intake O₂ condition. The PAH-PLIF images are false-colored blue (355 nm), green (532 nm), and red (633 nm) according to the excitation wavelength of the laser sheet. Regions of overlap are colored according to the red-green-blue colormap. The soot-PLII images are shown in grayscale beside the composite PAH-PLIF images.

The images at 362 CAD show that in the mean behavior, initial soot formation is weaker for the LD condition (less bright soot-PLII images), which is a consequence of delayed PAH formation in the images at earlier CAD (not shown here). Additionally, the PAH-PLIF signals for all three excitation wavelengths are weaker within the central sheet elevation for the CC condition, but not for the LD condition. This apparent structural difference in the PAH formation may be due to a real physical effect associated with the injection dwell, or it may be due at least in part to optical effects including laser-sheet attenuation and/or signal trapping.

The images at 366 CAD show that the weak swirl flow (0.5 swirl number), with direction indicated by the arrows in the LD images, transports an adjacent jet into the field of view for the LD condition, but not for the CC condition (indicated by the dashed-white ellipses in Figure I.2.5). Such a separate and distinct shape in ensemble-averaged images indicates a repeatable occurrence, for both PAH and soot. This observation suggests that multiple-injection interactions along the bowl wall for the CC condition create a narrower PAH and soot distribution in the downstream jet than for the more well-mixed LD condition. This also shows that the formation of PAHs and soot depends on the dwell between injections, indicating that the residual jet created by the first injection has a significant effect on PAH and soot formation in the second injection.

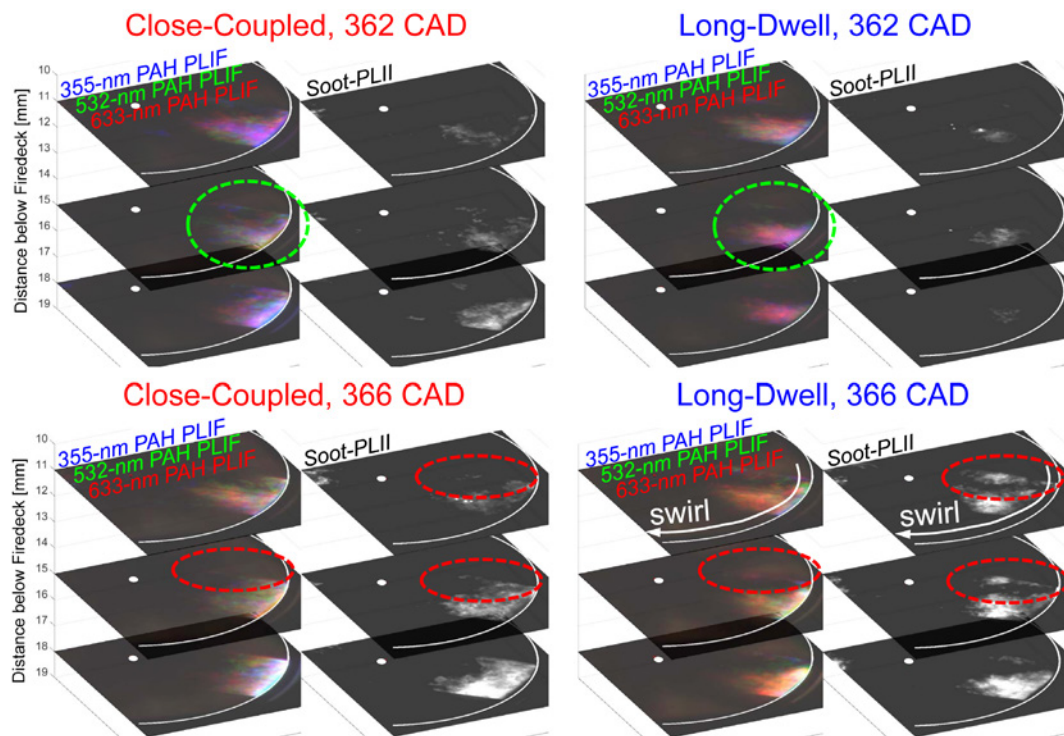
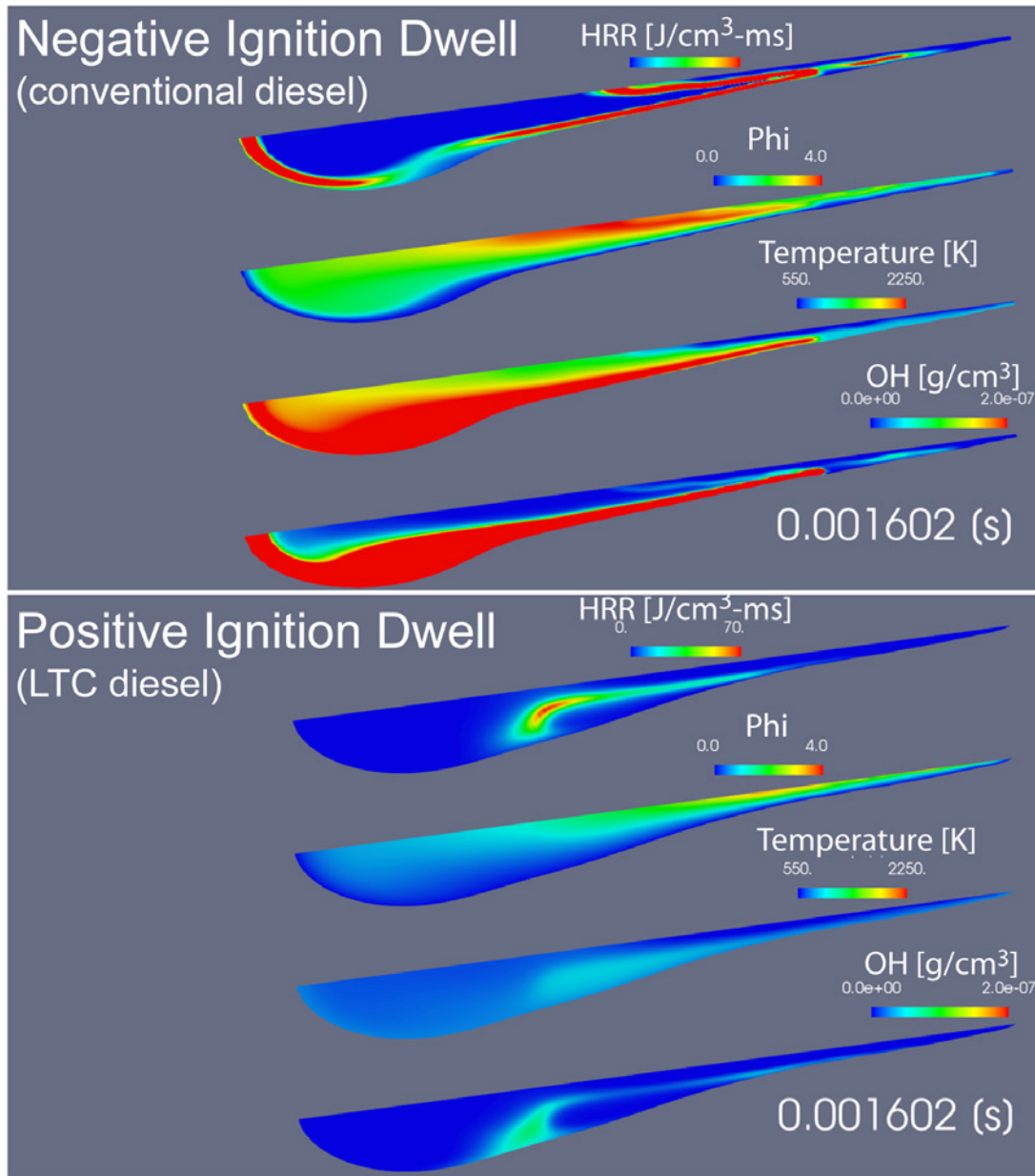


Figure I.2.5. Ensemble-averaged images of simultaneous PAH-PLIF for excitation at 355 nm (false-colored blue), 532 nm (green), and 633 nm (red) and soot-PLII (grayscale) at three laser-sheet elevations for the CC condition (left side) and for the LD condition (right side), both at 362 CAD (top row) and 366 CAD (bottom row) and with 10% intake O₂. Details of the field of view of images are as in Figure I.2.2.

To gain further insight into the structure of the residual jet than can be derived from experimental measurements, Figure I.2.6 shows a snapshot of computational fluid dynamics simulation predictions of diesel jets under conditions with a negative ignition dwell, i.e., with ignition occurring before the end of injection as in conventional diesel combustion (top), and conditions with a positive ignition dwell, with ignition after the end of injection, as is typical of LTC conditions. The ignition timing for the simulations was varied by changing the in-cylinder gas temperature from 900 K for negative ignition dwell to 760 K for positive ignition dwell.



HRR – heat release rate

Figure I.2.6. Predictions of multi-dimensional computational fluid dynamics simulations of the residual jet of the first injection of a double-injection condition with either negative ignition-dwell (900 K ambient gas) or positive ignition-dwell (760 K ambient)

The simulations predict that the residual jet for the negative ignition-dwell condition is much higher temperature (red color) than for the positive ignition-dwell condition (blue color), and with a well-established diffusion-flame structure on the jet periphery, as evident in the OH distribution. The jet interior is filled with CO and soot precursors, whereas the positive ignition-dwell jet is filled with formaldehyde and other products of first-stage ignition only. These results provide guidance to upcoming experiments to measure key species in the residual jet that likely affect the multiple-injection interactions that change soot-formation processes as observed in the experiments.

Conclusions

- Demonstrated how intake-air dilution can create threshold-formation conditions for PAH and soot to gain insight into how ignition processes in multiple injections may disrupt or enhance pollutant-formation processes
- Comparison of multiple-injection conditions with injections that are close coupled or long dwell showed enhanced PAH and soot formation in the second injection jet even with delayed first-stage ignition, pointing to important local mixture and/or turbulence interactions
- Multi-sheet planar imaging of PAH and soot reveals structural differences after ignition and combustion in second-injection jets, providing further evidence of residual-jet mixtures and/or turbulence effects
- Jet simulations provide additional insight into residual jet dynamics for ignition dwells that are negative (as in conventional diesel) or positive (as in LTC), demonstrating a dynamic progression of ignition and combustion during the injection dwell, helping guide future experiments

Key Publications and Presentations

1. Wissink, M.L., S.J. Curran, G. Roberts, M.P.B. Musculus, and C. Mounaïm-Rousselle. 2017. "Isolating the Effects of Reactivity Stratification in Reactivity-Controlled Compression Ignition with Iso-Octane and n-Heptane on a Light-Duty Multi-Cylinder Engine." Accepted to *Int. J. Engine Research*.
2. Roberts, G., C. Mounaïm-Rousselle, M.P.B. Musculus, M. Wissink, S. Curran, and W.E. Eagle. 2017. "RCCI Combustion Regime Transitions in a Single-Cylinder Optical Engine and a Multi-Cylinder Metal Engine." *SAE Int. J. Engines* 10 (5).
3. "The In-Cylinder Intersection of Thermofluids and Chemistry as Revealed by Optical Diagnostics." Cummins Tech Center, Thermal and Fluid Sciences Functional Excellence (TSFE) Conference, Columbus, IN, April 2017.
4. Eagle, Ethan. 2017. "Comparing Hydrocarbon C-H Stretch Infrared Emission during Direct Injection with and without Combustion in an Optical Diesel Engine." National Meeting of the Combustion Institute, April 2017.
5. Roberts, Greg. 2017. "A First Application of Quantitative Soot Extinction Measurements within a Heavy-Duty Diesel Engine with Optical Access." CRF Research Highlight Series, April 2017.
6. "Fuel Property and Engine Combustion Research of the US Co-Optima Initiative." Tailor-Made Fuels from Production to Propulsion, 5th Int. Conference, RWTH Aachen U., Germany, June 2017.
7. "US DOE Co-Optimization of Fuels and Engines (Co-Optima) Initiative: Recent Progress on Advanced Compression-Ignition." ERC – 2017 Symposium: Impact of Future Regulations on Engine Technology, Madison, WI, June 2017.
8. Roberts, Greg, and Mark Musculus. 2017. "Insight into In-Cylinder Processes that Limit RCCI Combustion Phasing Control Authority, Using Visible and Infrared Imaging." AEC Meeting, Southfield, MI, August 2017.

9. “The Co-Optimization of Fuels and Engines: Chemical Kinetics and Optical Research.” University Seminar Series, Lund University, Sweden, October 2017.
10. Roberts, Greg, and Mark Musculus. 2018. “The Roles of Large-Scale Mixing Structures and Wall Wetting on Ignition and Combustion over a Wide Range of DI SOI in a Dual-Fuel, Heavy-Duty Optical Diesel Engine.” AEC Meeting, Southfield, MI, January 2018.

References

1. Violi, A., N. Hansen, and H. Michelsen. 2017. “Developing a Predictive Model for the Chemical Composition of Soot Nanoparticles.” <https://www.osti.gov/biblio/1351404>.
2. Vishwanathan, G., and R.D. Reitz. 2015. “Application of a Semi-Detailed Soot Modeling Approach for Conventional and Low Temperature Diesel Combustion – Part I: Model Performance.” *Fuel* 139: 757–770.
3. Bobba, M.K., and M.P.B. Musculus. 2011. “Laser Diagnostics of Soot Precursors in a Heavy-Duty Diesel Engine at Low-Temperature Combustion Conditions.” *Combust. Flame* 159, no. 2: 832–843.
4. Ciajolo, A., A. D’anna, R. Barbella, A. Tregrossi, and A. Violi. 1996. “The Effect of Temperature on Soot Inception in Premixed Ethylene Flames.” *Proc. Combust. Inst.* 26, no. 2: 2327–2333.

Acknowledgements

This research was sponsored by the U.S. Department of Energy Office of Energy Efficiency and Renewable Energy. Optical engine experiments were conducted at the Combustion Research Facility, Sandia National Laboratories, Livermore, California. Sandia National Laboratories is a multi-mission laboratory managed and operated by National Technology and Engineering Solutions of Sandia, LLC., a wholly owned subsidiary of Honeywell International, Inc., for the U.S. Department of Energy’s National Nuclear Security Administration under contract DE-NA0003525.

I.3 Spray Combustion Cross-Cut Engine Research (Sandia National Laboratories)

Lyle M. Pickett, Principal Investigator

Sandia National Laboratories
PO Box 969, MS 9053
Livermore, CA 94551-9053
E-mail: Impicke@sandia.gov

Michael Weismiller, DOE Technology Development Manager

U.S. Department of Energy
E-mail: Michael.Weismiller@ee.doe.gov

Start Date: October 1, 2017	End Date: September 20, 2018	
Project Funding (FY18): \$845,000	DOE share: \$845,000	Non-DOE share: \$0

Project Introduction

All future high-efficiency engines will have fuel directly sprayed into the engine cylinder. Engine developers agree that a major barrier to the rapid development and design of these high-efficiency, clean engines is the lack of accurate fuel spray computational fluid dynamics (CFD) models. The spray injection process largely determines the fuel-air mixture processes in the engine, which subsequently drive combustion and emissions in both direct-injection gasoline and diesel systems. More predictive spray combustion models will enable rapid design and optimization of future high-efficiency engines, providing more affordable vehicles and also saving fuel.

Objectives

Overall Objectives

- Facilitate improvement of engine spray combustion modeling, accelerating the development of cleaner, more efficient engines
- Lead a multi-institution, international research effort on engine spray combustion called the Engine Combustion Network (ECN), with focus on diesel and gasoline sprays

Fiscal Year 2018 Objectives

- Organize workshop activities for the ECN, including monthly web meetings, standards, and topic organization
- Investigate spray and combustion behavior of AVFL-18a diesel surrogates relative to a commercial diesel fuel
- Develop high-speed imaging extinction diagnostic for spray mixture quantification
- Characterize plume interaction and mixing for multiple-injection gasoline direct-injection conditions

Approach

To accelerate the progression of predictive CFD modeling capabilities and leverage the expertise of the global spray research community, a multi-institution collaboration, called the Engine Combustion Network, has been established. By providing highly vetted, quantitative datasets available online [1] for both diesel and gasoline targets, CFD models may be evaluated more critically and in a manner that has not happened to date. Productive CFD evaluation requires new experimental data with better quantification for the spray and the relevant boundary conditions, but it also includes a working methodology to evaluate the capabilities of current modeling practices. Activities include the gathering of experimental and modeling results at target conditions to allow a side-by-side comparison and expert review of the current state of the art for diagnostics and engine modeling.

Experiments are performed in a high-temperature, high-pressure spray facility prepared at conditions that represent either diesel or gasoline engine conditions at the time of injection. Target conditions, such as the ECN diesel “Spray A” or “Spray D” operating condition, which uses an n-dodecane (single-component) fuel, or the gasoline “Spray G” operating condition for an eight-hole injector, are chosen as baseline conditions. Activities this year included expansion of the operating conditions to include other fuels and injector operating conditions.

Results

Seeking to extend the database and understanding to practical diesel fuels, a new dataset for spray mixing, ignition, and lift-off stabilization was developed. The diesel fuel target and surrogates were developed by Coordinating Research Council (CRC) through extensive study and property evaluation [2]. By selecting surrogates with known physical and chemical composition, it is possible to develop CFD spray and combustion models most applicable to real diesel fuels and to provide a fuel standard that will not change with time. Based upon a certification fuel target (CFA), four different surrogates were chosen, consisting of four to nine components. The detailed compositions are provided by Mueller, et al. [2], but a summary of the properties is given in Table I.3.1. Experiments were performed at Spray A conditions using a single hole nozzle of 0.090 mm diameter orifice (#0766-603-04).

Table I.3.1. Physical and Chemical Properties of CRC AVFL-18a Diesel Surrogates

Fuel	CFA	V0a	V0b	V1	V2
Number of components	~5,000	4	5	8	9
Fuel density [kg/m^3]	848	818	837.5	828.4	853
Derived cetane number (DCN)	43.7	46.2	44.4	45.5	42.6
90% distillation temperature [K]	603	548	578	578	578
Heat of vaporization [kJ/mol]	–	73.1	75.4	74.2	–

Detailed measurements of the mean liquid penetration and lift-off length for these fuels are shown in Figure I.3.1 [3]. A spline fit is provided along with the scatter data to guide interpretation. The data for the surrogate fuels have been normalized to that of the CFA fuel at 900 K. For all conditions of the study, including different injection pressures and ambient oxygen concentrations, the liquid length decreases in the order of: $\text{CFA} > \text{V2} \approx \text{V0b} \geq \text{V1} > \text{V0a}$. The trend in liquid length for the surrogate fuels appears to be strongly correlated with the 90% distillation temperature given in Table I.3.1. Notably, the V0b, V1, and V2 fuels are characterized by very similar liquid lengths owing to consistency in their 90% distillation temperatures. While the liquid length for the surrogate fuels falls short of the CFA target, the variance is only approximately 10%, which is much less than single-component surrogates like n-heptane or n-dodecane.

The measured ignition delay for the surrogate fuels is scattered about the CFA target, suggesting success in generating surrogates that are chemically similar to the target. Although significant scatter is observed in the ignition delay and lift-off length data, especially at lower ambient temperatures, the DCN does not correlate well with experimental ignition delay measurements. These results show the limitations of a cetane number test, which produces different conditions than those typical of injection for a modern engine, and different than the pressures (60–70 bar) and temperatures of this study. Lift-off length trends followed similar trends as ignition delay, with no strong correlation to DCN.

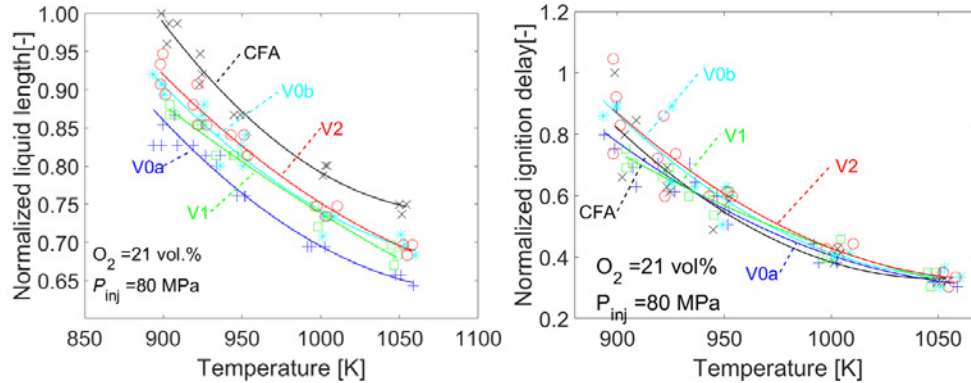


Figure I.3.1. (left) Normalized liquid-length and (right) lift-off length measurements for surrogate fuels at different temperatures. Spray A conditions, but with 80 MPa fuel injection pressure.

The next phase of research sought to develop a high-temporal resolution, line-of-sight extinction imaging diagnostic that could be applied for quantitative, time-resolved mixture fraction measurements in vaporizing sprays. While past research in our laboratory has shown success using planar Rayleigh scattering for mixture fraction measurement [4], the diagnostic is limited in that liquid regions and spurious particles must be completely avoided. An alternative is to apply an absorption diagnostic proportional to fuel concentration, and one that is tolerant to liquid. Ultra-violet back-illumination extinction imaging has been applied for this purpose, but it requires use of image intensifiers that render the images noisy and difficult to quantify. Fuels commonly used as gasoline or diesel fuel surrogates do not scatter significant light in their vapor state and are not typically strong absorbers at visible wavelengths.

For this study, toluene fuel was doped with parts-per-million levels of fullerene-C70 for absorption imaging measurement at 406 nm (violet wavelength) using a high-speed un-intensified complementary metal oxide semiconductor camera. Measurements were performed using diffused back-illumination imaging and using an ECN Spray D diesel injector, as shown in Figure I.3.2.

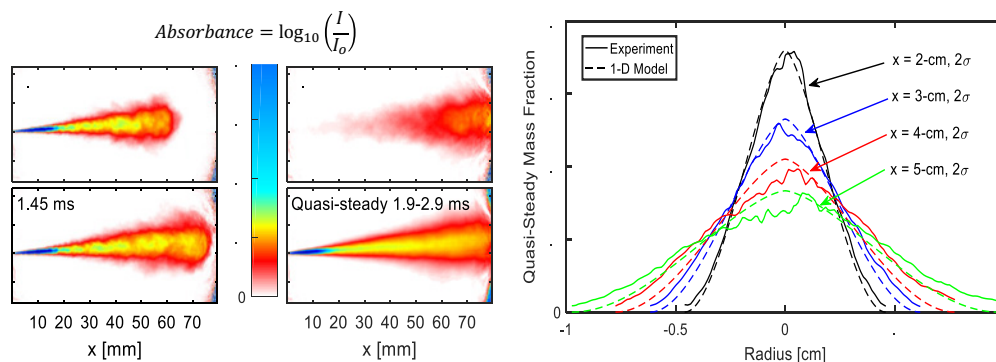


Figure I.3.2. (left) Extinction measurement at various times after the start of injection. (right) Tomographic reconstruction of extinction measurement for fuel mass fraction, compared to model (Musculus/Kattke) predictions. Spray D experimental conditions, except the fuel is C70-doped toluene.

The left of the figure shows instantaneous absorbance images during and after the end of injection, as well as an average during the quasi-steady period of injection. For toluene fuel at these Spray D conditions, the liquid penetrates less than 20 mm from the injector. Without C70 doped into the fuel, no extinction is measured where only fuel vapor is present (downstream of 20 mm). But with C70 added, there is ample extinction in vapor regions (and liquid regions), providing an opportunity to quantify the fuel/air mixture. Quantification requires understanding the absorption coefficient of the fuel tracer at the conditions of the experiment. Rather than performing a direct calibration, model jet predictions for mixture fraction are used in comparison to the

experiment. The average line-of-sight extinction signal from the doped fuel was converted to fuel mixture fraction distribution at different axial distances via computed tomography, as shown at the right of Figure I.3.2. By applying a scaling factor of two times the C70-doped fuel extinction coefficient in liquid at room temperature, the experimental data follows the model predictions. Significantly, the same scaling factor appears to apply at very different mixture fractions, which would correspond to different vapor mixture temperatures. While further work is needed to understand the effect of local conditions (e.g., temperature) on the measurement, the technique shows excellent potential compared to other diagnostics (such as laser-induced fluorescence).

Aspects of gasoline direct-injection and fuel–air mixing were investigated by performing experiments with different injection duration, or by using multiple injections. A reference fuel injector with eight stepped holes, the ECN “Spray G” [1,5], was chosen for initial experiments because of the vast dataset developed for this particular injector and operating condition. Figure I.3.3 shows diffused back-illumination extinction imaging of the fuel spray rotated with plume pairs in alignment along a line of sight.

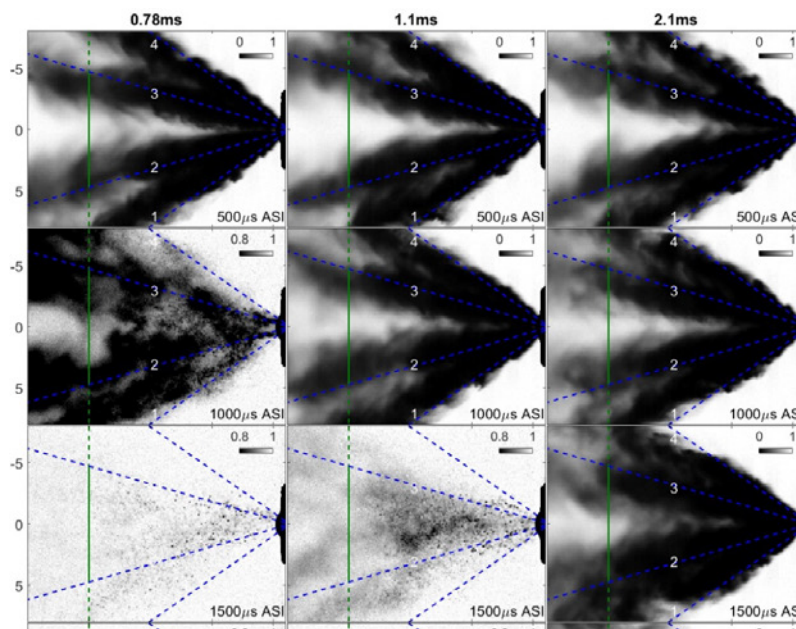


Figure I.3.3. Extinction imaging of Spray G (Spray G injector and ambient conditions) with three different injection durations. Blue dashed lines show the line-of-sight projection of the hole drill angle.

Analysis of the measured extinction, and the overall spray geometry, permitted identification of the actual plume direction [6], as shown in Figure I.3.4. The figure shows that the plumes begin penetration at angles slightly less than the drill angle, but the plumes bend towards the injector with increasing time of injection. The data show indications of strong plume interaction, with the interaction completely dependent upon the duration of injection. Velocity measurements between plumes confirm this observation [5].

Although a longer injection duration is found to promote plume collapse, a potential solution is to stage fuel delivery with multiple, shorter injections. Figure I.3.4 shows that when a second injection is performed, with some dwell after the first injection, the fuel is delivered at a very similar plume direction as the first injection. Therefore, the fuel is delivered in a more disperse fashion with less tendency for plume collapse. For example, the total fuel delivered for the multiple-injection condition in Figure I.3.4 is the same as that of the 1.1-ms continuous injection, with very different outcomes in fuel delivery. The significance of this research is that it identifies techniques to control/prevent wall-wetting and film formation in an engine.

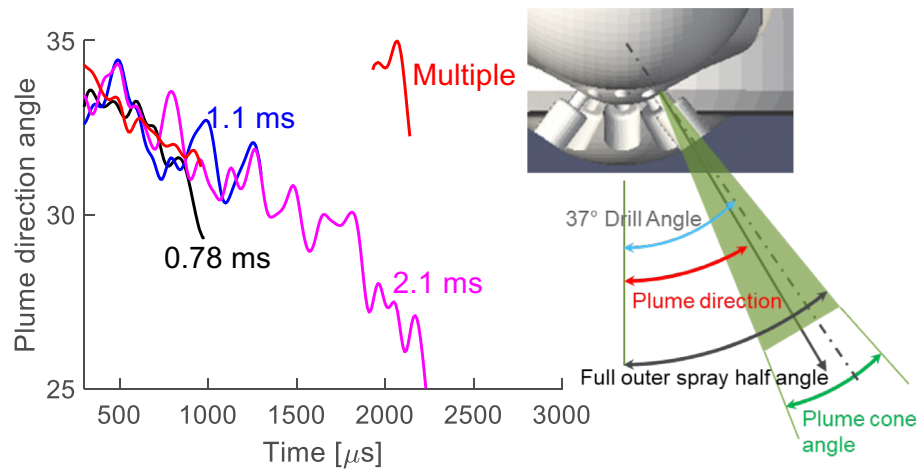


Figure I.3.4. Measured plume direction (defined at right) for different injection durations or with multiple injections. Same conditions as Figure I.3.3.

Conclusions

Research in spray combustion this year has provided new information and diagnostics important for both diesel and gasoline fuel injection. The gasoline and diesel targets are used by the ECN, and the experimental data provided is now being used by the ECN community to improve CFD models that will be used to optimize future engine designs. Key activities for FY 2018 include:

- Generation of a new dataset for CRC diesel surrogates. The dataset includes time-resolved liquid length, penetration, ignition delay, lift-off length, and soot concentration.
- Development of a new mixing diagnostic based upon visible-wavelength extinction imaging, offering the potential to better understand fuel–air mixing, particularly in co-existent liquid and vapor regions.
- Characterization of multiple-injection gasoline direct-injection events, showing promise to limit plume collapse and liquid penetration.

Please see the references below and ECN proceedings [1] for details about many other achievements/activities for FY 2018.

Key Publications

1. Skeen, S.A., and K. Yasutomi. 2018. “Measuring the Soot Onset Temperature in High-Pressure n-Dodecane Spray Pyrolysis.” *Combustion and Flame* 188: 483–487.
2. Sphicas, P., L.M. Pickett, S.A. Skeen, and J.H. Frank. 2017. “Inter-Plume Aerodynamics for Gasoline Spray Collapse.” *International Journal of Engine Research*. doi:10.1177/1468087417740306.
3. Duke, D.J., A.L. Kastengren, K.E. Matusik, A.B. Swantek, C.F. Powell, R. Payri, D. Vaquerizo, L. Itani, G. Bruneaux, R.O. Grover, S. Parrish, L. Markle, D. Schmidt, J. Manin, S.A. Skeen, and L.M. Pickett. 2017. “Internal and Near Nozzle Measurements of Engine Combustion Network “Spray G” Gasoline Direct Injectors.” *Experimental Thermal and Fluid Science* 88: 608–621.
4. Crua, C., J. Manin, and L.M. Pickett. 2017. “On the Transcritical Mixing of Fuels at Diesel Engine Conditions.” *Fuel* 208: 535–548.
5. Westlye, F.R., K. Penney, A. Ivarsson, L.M. Pickett, J. Manin, and S.A. Skeen. 2017. “Diffuse Back-Illumination Setup for High Temporally Resolved Extinction Imaging.” *Appl. Opt.* 56 (17): 5028–5038.

References

1. Engine Combustion Network data archive < <https://ecn.sandia.gov/> >, 2018.
2. Mueller, C.J., et al. 2016. “Diesel Surrogate Fuels for Engine Testing and Chemical-Kinetic Modeling: Compositions and Properties.” *Energy and Fuels* 30 (2): 1445–1461.
3. Yasutomi, K., C.J. Mueller, L.M. Pickett, and S.A. Skeen. 2018. “Investigation of the Spray and Combustion Characteristics of Four Multi-Component Diesel Surrogate Fuels Relative to Their Commercial Target Fuel.” *THIESEL*.
4. Manin, J., L.M. Pickett, S.A. Skeen, and J.H. Frank. 2017. “Time-Resolved Measurements of Mixing Quantities in Diesel Jets.” *COMODIA*.
5. Sphicas, P., L.M. Pickett, S.A. Skeen, J.H. Frank, and S.E. Parrish. 2018. “Inter-Plume Velocity Measurements to Understand Spray Collapse When Varying Injection Duration or Number of Injections.” In press *Atom. Sprays*.
6. Duke, D.J., A.L. Kastengren, K.E. Matusik, A.B. Swantek, C.F. Powell, R. Payri, D. Vaquerizo, L. Itani, G. Bruneaux, R.O. Grover, S. Parrish, L. Markle, D. Schmidt, J. Manin, S.A. Skeen, and L.M. Pickett. 2017. “Internal and Near Nozzle Measurements of Engine Combustion Network ‘Spray G’ Gasoline Direct Injectors.” *Experimental Thermal and Fluid Science* 88: 608–621.

Acknowledgements

We thank Koji Yasutomi, Shane Daly, Emre Cenker, Julien Manin, Jonathan Frank, Dave Cicone, and Aaron Czeszynski for their devoted research. Studies were performed at the Combustion Research Facility. Sandia National Laboratories is a multi-mission laboratory managed and operated by National Technology and Engineering Solutions for Sandia LLC, a wholly owned subsidiary of Honeywell International, Inc., for the U.S. Department of Energy’s National Nuclear Security Administration under contract DE-NA0003525.

Thanks also to Scott A. Skeen of Sandia National Laboratories.

I.4 Low-Temperature Gasoline Combustion (LTGC) Engine Research (Sandia National Laboratories)

John E. Dec, Principal Investigator

Sandia National Laboratories
MS 9053, P.O. Box 969
Livermore, CA 94550
E-mail: jedec@sandia.gov

Michael Weismiller, DOE Technology Development Manager

U.S. Department of Energy
E-mail: Michael.Weismiller@ee.doe.gov

Start Date: October 1, 2017	End Date: September 30, 2018	
Project Funding (FY18): \$675,000	DOE share: \$675,000	Non-DOE share: \$0

Project Introduction

Improving the efficiency of internal combustion engines is critical for meeting global needs to reduce petroleum consumption and CO₂ emissions. Engines using low-temperature gasoline combustion (LTGC) (which includes homogeneous charge compression ignition [HCCI]) have a strong potential for contributing to these goals since their thermal efficiencies meet or exceed those of diesel engines. They also have very low NO_x and particulate emissions. LTGC can be applied either as a full-time operating strategy or for light-duty engines, as part of a multi-mode combustion strategy where the engine switches to conventional spark ignition (SI) at high loads. This multi-mode approach provides high efficiencies during LTGC operation at low and intermediate loads where light-duty engines operate most of the time and maintains high power density by switching to SI for high loads. Full-time LTGC provides high efficiencies at all loads as required for medium- and heavy-duty applications. LTGC engines are potentially lower-cost than diesels, and by providing medium- and heavy-duty engines that use gasoline with high efficiency, LTGC could help balance the demand for gasoline and diesel fuel, a problem that is expected to worsen if only conventional technologies are used. In all applications, LTGC allows gasoline to be used with high efficiency for more effective use of crude-oil supplies and lower overall CO₂ production.

Although substantial progress has been made in understanding LTGC, several important aspects require additional research. In particular, rapid control of combustion timing remains a key technical barrier to the commercialization of these engines. Studies in Fiscal Year (FY) 2018 addressed four of these research needs, including the development of a new combustion-timing control system. First, a computational fluid dynamics (CFD) modeling study provided key insights into the mechanism responsible for producing the thermal stratification that largely controls the heat release rate (HRR) for well-premixed operation. Second, a new method has been developed for determining surrogate mixtures that more accurately reproduce the behavior of real distillate fuels when applied in chemical-kinetic models. Also, an improved methodology was developed for validating these surrogates and the chemical-kinetic mechanisms against LTGC engine data. Third, a chemical-kinetic analysis was conducted in order to understand the chemistry responsible for making autoignition reactions sensitive to variations in the local equivalence ratio (ϕ -sensitive), which allows mixture stratification to provide important benefits for LTGC. Based on this understanding, new fuel blends are proposed that can provide higher ϕ -sensitivity, and at the same time, have high research octane number (RON) and octane-sensitivity values for good performance under boosted-SI conditions. Fourth, and perhaps most importantly, a new device that provides direct control of combustion timing in LTGC engines has been developed and demonstrated to control combustion timing well over large variations of fueling rate, intake boost pressure, and engine speed.

Objectives

Overall Objectives

- Provide the fundamental understanding (science-base) required to overcome the technical barriers to the development of LTGC engines for light-, medium-, and heavy-duty applications
- Explore methods of exploiting this fundamental understanding to develop practical techniques that can overcome these barriers to LTGC engines

FY 2018 Objectives

- Complete an uncertainty quantification analysis of cylinder-pressure measurements, in collaboration with Lawrence Livermore National Laboratory (LLNL)
- Initiate a collaborative project with the State University of New York at Stony Brook to apply CFD modeling to the Sandia LTGC research engine
- Develop an improved surrogate mixture for modeling regular E10 gasoline (10% ethanol, 90% gasoline blend), and collaborate with LLNL to validate and improve their chemical-kinetic mechanism for gasoline
- Complete a study of the capabilities and limits of spark-assist for controlling combustion timing for well-mixed LTGC (i.e., HCCI)
- Investigate the chemistry of ϕ -sensitivity and its relationship to octane sensitivity—a critical study because ϕ -sensitivity combined with controlled mixture stratification can provide combustion-timing control and extend the load range
- Develop and demonstrate an advanced combustion-timing control system for LTGC engines

Approach

Studies were conducted in the Sandia dual-engine LTGC laboratory, which is equipped with both an all-metal engine and a matching optically accessible single-cylinder LTGC research engine (displacement = 0.98 liters). This facility allows operation over a wide range of conditions, and it has been designed to provide precise control of virtually all operating parameters, allowing well-characterized experiments. These research engines were derived from Cummins B-series diesel engines. The cylinder head has been modified to accommodate a spark plug (with assistance from Cummins), and the diesel piston was replaced with a custom LTGC piston having an open combustion chamber and a broad, shallow bowl. The compression ratio was 14:1 for all data presented in this report. The engine is equipped with a centrally located gasoline-type direct injector capable of 300 bar injection pressures supplied by General Motors. A research-grade E10 gasoline that is representative of regular-grade gasolines sold in the United States (called RD5-87A) was used for these studies.

To gain insight into the in-cylinder processes, two modeling efforts have been initiated: (1) a collaborative CFD modeling effort was initiated with State University of New York at Stony Brook, with initial efforts directed at understanding the mechanism for thermal stratification; and (2) a CHEMKIN modeling capability has been established to investigate the chemical kinetics of autoignition and the chemical origins of ϕ -sensitivity, as well as to validate surrogate mixtures and the detailed chemical-kinetic mechanism for gasoline from LLNL against experimental LTGC engine data. Finally, a new technique to control combustion timing in an LTGC engine had good potential, but considerable development efforts were required, so a proposal was written for internal Sandia funds to develop this technique over a three-year period prior to FY 2018. After a basic demonstration, the control device required to implement this technique was transferred to the DOE Vehicle Technologies Office-funded LTGC research program (near the start of FY 2018), where it has been tested over a wide range of operating conditions.

Results

Previous studies have shown that naturally occurring thermal stratification causes the charge in a LTGC engine to autoignite sequentially, even for a well-premixed charge (i.e., HCCI). This reduces the peak HRR,

allowing higher loads without knock. Moreover, enhancing the thermal stratification has potential to extend LTGC operation to higher loads and to further improve efficiency. Our laser-imaging studies [1] indicated that the thermal stratification was produced by wall heat transfer combined with large-scale turbulent structures that transport the colder gases from the near-wall region into the central part of the charge. However, the source of this large-scale turbulence or how it might be controlled was unknown. CFD modeling has good potential to improve our understanding of these and other critical in-cylinder processes, so a collaboration with State University of New York at Stony Brook was initiated to apply the CONVERGE CFD code to our LTGC research engine. The CONVERGE calculations to investigate thermal stratification were made using the large eddy simulation (LES) option to preserve the larger-scale turbulent structures. Figure I.4.1 shows a comparison of the development of the temperature distribution near top dead center (TDC) for CONVERGE-LES (top) and experimental measurements (bottom). The LES computations modeled the all-metal LTGC engine, which has a broad, shallow piston bowl, while the experimental temperature-map images were derived from calibrated planar laser-induced fluorescence images in the optically accessible research engine, which has a flat piston top that produces a pancake combustion chamber, as evident in the images. Despite these differences in the combustion-chamber geometry, the results are remarkably similar. Both image sets show that the thermal stratification results from large-scale turbulent structures that distribute colder fluid throughout the bulk gases. Moreover, careful examination of the LES images at earlier crank angles (not shown here) shows that the large-scale turbulent structures are already present shortly after bottom dead center, when temperature inhomogeneities first become sufficient for the turbulence to be seen in the images. This finding suggests that the large-scale turbulence responsible for the thermal stratification may persist from turbulence generated by the intake flows. Additional research is needed to confirm this finding, but if it is correct, it may lead to methods of altering the intake flows to control the amount of thermal stratification in the charge.

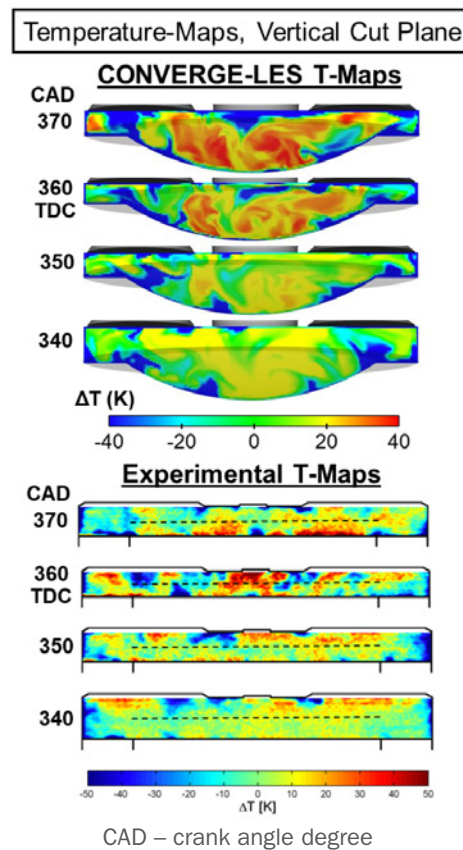
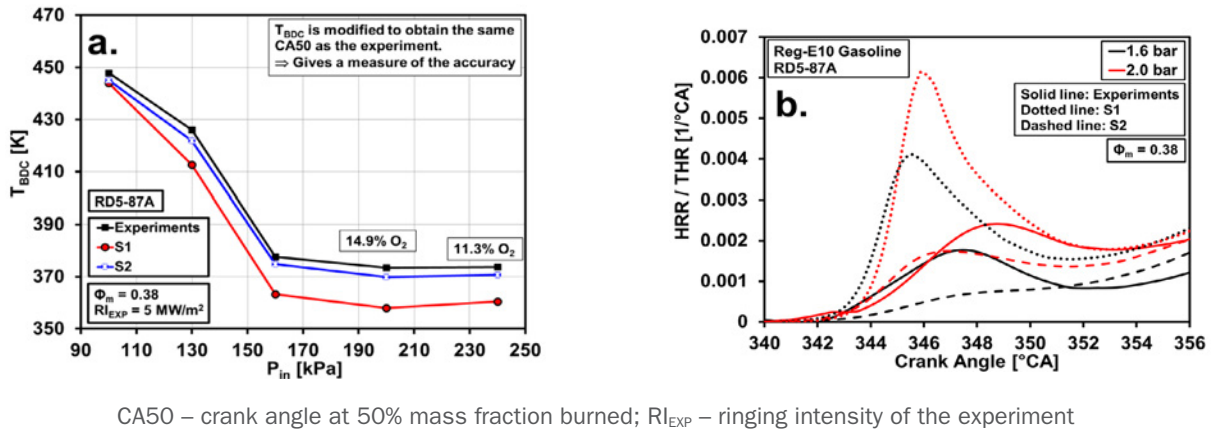


Figure I.4.1. A comparison of temperature-map images of the thermal stratification in a vertical cut-plane for CONVERGE-LES simulations of the all-metal engine, which has a shallow, broad bowl (top), and experimental vertical-plane images derived from calibrated planar laser-induced fluorescence images acquired in the optically accessible engine, which has a flat piston top (bottom) [1]

Modeling of the combustion processes in an LTGC engine (or any engine) requires an accurate chemical-kinetic mechanism and a surrogate blend that correctly reproduces the behavior of the distillate gasoline being used. To determine whether the LLNL detailed chemical-kinetic mechanism and the surrogate blend for RD5-87A regular E10 gasoline (called S1 here) were sufficiently accurate, an investigation was conducted to compare well-premixed LTGC (i.e., HCCI) data against CHEMKIN calculations using the single-zone internal-combustion-engine reactor model that is supplied with this software. This single-zone model was used because the chemical-kinetic mechanism is very large (2,878 species and 12,839 reactions), so it is not practical to run CFD simulations; however, with a single-zone model, a methodology must be applied to account for the heat transfer that affects the compressed-gas temperatures and pressures, and therefore the autoignition timing, in the real LTGC engine. In the current work, the Woschni heat-transfer model [2] supplied with CHEMKIN, which accounts for the average heat transfer, was applied and found to work well. Initial computational results conducted with the LLNL gasoline mechanism from June 2017 gave only a poor match, but the new LLNL mechanism, made available to selected research partners in December 2017, was found to give very good performance.

Comparisons of the CHEMKIN results using this latest chemical-kinetic mechanism and the original S1 surrogate with the experimental data showed a reasonable match for naturally aspirated operation, but significant discrepancies as the intake pressure (P_{in}) was increased above 1.0 bar, simulating turbocharged operation. As shown in Figure I.4.2a, the bottom dead center temperatures (T_{BDC}) for the CHEMKIN calculations had to be reduced well below the experimental values for $P_{in} \geq 1.3$ bar when the S1 surrogate was used, indicating that the autoignition chemistry with S1 was too reactive. An investigation revealed that S1 had been formulated using only five standard fuel-component species whose concentrations were tuned to match the RON and motor octane number (MON) values of the fuel, and that these concentrations did not match well with the concentrations of the respective hydrocarbon classes in the fuel based on a detailed hydrocarbon analysis. Therefore, as part of the current project, a new seven-component surrogate blend was developed based on the detailed hydrocarbon analysis. As Figure I.4.2a shows, the T_{BDC} values obtained with CHEMKIN using this new surrogate (called S2) match closely with the experimental values at all intake pressures. An examination of the early stages of the combustion heat release shows the reason for the poor performance of S1 and the improved performance of S2, as illustrated in Figure I.4.2b for the $P_{in} = 1.6$ and 2.0 bar cases. Note that in Figure I.4.2b, the HRR is normalized by the total heat release (THR) so that the data for both $P_{in} = 1.6$ and 2.0 bar can be plotted on the same scale. At these higher P_{in} s, the fuel exhibits low-temperature heat release (LTHR), which occurs from 342 to 352 CAD in Figure I.4.2b. This LTHR drives the charge more quickly into hot autoignition, reducing the required T_{BDC} values as P_{in} is increased (see Figure I.4.2a). As Figure I.4.2b shows, the S1 surrogate greatly overpredicts the amount of LTHR (dotted lines) compared to the experiment (solid lines), causing autoignition to occur at much lower T_{BDC} values than the experiment. In contrast, the S2 surrogate (dashed lines) matches the experimental LTHR values much more closely, resulting in a good match for T_{BDC} . The S2 surrogate also gives a better match to the measured RON and MON values of the fuel than the S1 surrogate.

Similar to the effect of naturally occurring thermal stratification discussed above, fuel stratification can also cause the charge in an LTGC engine to autoignite sequentially, reducing the peak HRR. Also like thermal stratification, reducing the HRR with fuel stratification allows higher loads without knock and/or more advanced combustion timing for higher efficiencies. Additionally, fuel stratification can be used to provide rapid combustion-timing control. Perhaps most importantly, fuel stratification is readily controlled by changes in the fuel-injection strategy, unlike thermal stratification, which is difficult to control or to enhance. Realizing these benefits of fuel stratification requires that an appropriate fuel/charge-gas mixture be produced and that the fuel's autoignition timing be sensitive to variations in the local equivalence ratio (ϕ) within the stratified charge (ϕ -sensitive). Typically, gasoline has only weak or moderate ϕ -sensitivity at naturally aspirated conditions, but it becomes strongly ϕ -sensitive as the intake pressure is boosted, as occurs with turbocharging.



CA50 – crank angle at 50% mass fraction burned; RI_{EXP} – ringing intensity of the experiment

Figure I.4.2. Comparison of CHEMKIN single-zone internal combustion engine results with experimental data for well pre-mixed LTGC engine operation (i.e., HCCL). Figure I.4.2a shows a comparison of the T_{BDC} values for the experiment and the CHEMKIN simulations with the S1 and S2 surrogates. Figure I.4.2b compares the early stages of the heat release for the S1 and S2 surrogates against experimental data for $P_{in} = 1.6$ and 2.0 bar. All P_{in} s are absolute.

If the ϕ -sensitivity of gasoline could be increased at naturally aspirated and low-boost conditions, fuel stratification could be used much more effectively for improving LTGC-engine operation. However, the chemical-kinetics responsible for ϕ -sensitivity were not previously known, so an investigation was conducted using the LLNL detailed gasoline mechanism in CHEMKIN for a variety of compounds that are representative of the various hydrocarbon classes in gasoline. The results showed that only compounds with significant negative temperature coefficient (NTC) behavior exhibited strong ϕ -sensitivity. The ϕ -sensitivity was greatest in the NTC region, but significant ϕ -sensitivity persisted on the hot side of the NTC region where autoignition typically occurs in LTGC engines. This latter finding is important because gasoline composition should also be tuned to avoid passing through the NTC region during the compression stroke so that the fuel exhibits a high octane sensitivity (i.e., RON – MON). Thus, shifting the gasoline composition to include more compounds whose NTC region extends closer to, but not into the LTGC autoignition temperature–pressure range should enhance the ϕ -sensitivity while allowing octane sensitivity to remain at acceptable values. These compounds can then be blended with aromatics or other compounds that do not exhibit NTC behavior to raise the RON to an acceptable level.

Following this logic, several fuel blends were tested using CHEMKIN with the goal of developing a fuel with increased ϕ -sensitivity at naturally aspirated and low-boost conditions compared to regular E10 (RD5-87A), but one that also has higher RON and octane-sensitivity values than regular E10 for good performance under boosted SI conditions. A blend of 17.5% 1-hexene, 28.5% n-pentane, 8% iso-octane, 30% p-xylene, and 16% iso-butanol gave the best performance, and it meets current U.S. Environmental Protection Agency requirements for maximum olefin, aromatic, and iso-butanol content. A comparison of this proposed blend with RD5-87A, presented in Figure I.4.3, shows that the new blend has significantly higher ϕ -sensitivity than RD5-87A at $P_{in} = 1.0, 1.3,$ and 1.6 bar, where it was relatively low with RD5-87A. The lower ϕ -sensitivities at higher boost are inconsequential because the values are still quite high. This blend also has RON = 101.5 and octane-sensitivity = 11.5, compared to RON = 92 and octane-sensitivity = 7.3 for RD5-87A. With these ratings, it should be a very good LTGC fuel for full-time LTGC, mixed-mode LTGC and SI, or boosted SI engines.

Rapid, robust control of combustion timing is perhaps the single biggest challenge to developing commercial LTGC engines. To overcome this problem, a new device was developed that works by metering and mixing tiny amounts (\sim tenths of a mm^3) of an ignition-enhancing additive into the fuel each engine cycle. Because the additive amounts are so small, it is estimated that a gallon-sized reservoir would only require refilling at service intervals of \sim 7,000 miles (cost \sim \\$20, about seven times less than the cost of the fuel saved). Essentially, this additive-mixing fuel injection (AMFI) system controls combustion timing (as measured by the crank angle of the 50% burn point, CA50) by rapidly changing the reactivity of the fuel. Although this technique

is conceptually straightforward, building the hardware for metering and mixing these very small amounts of additive and ensuring that it consistently delivers the desired amount each engine cycle required expertise in micro-fluidics and involved a considerable development effort that was beyond the scope of our Vehicle Technologies Office-funded LTGC research program. A successful proposal was written to Sandia’s laboratory-directed research and development program to obtain the funding required to develop this technique over a three-year period prior to FY 2018. The laboratory-directed research and development project ended with a basic demonstration of the device, and after filing a patent, the AMFI system was transferred to our Vehicle Technologies Office-funded program, where it has been tested over a wide range of conditions.

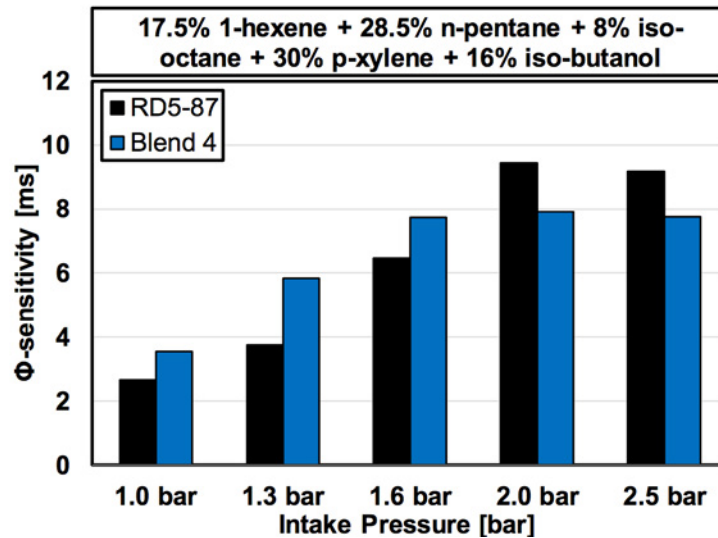


Figure I.4.3. A comparison of the ϕ -sensitivity of the proposed fuel blend given at the top of the plot (Blend 4) with that of RD5-87A (regular E10 gasoline) for intake pressures from 1.0 to 2.5 bar

Figure I.4.4 demonstrates the ability of the AMFI system to control the combustion phasing at an otherwise fixed operating condition. The additive used for these studies was 2-ethylhexyl nitrate (EHN), a common, inexpensive diesel-fuel ignition improver. As can be seen, increasing the additive from 0.24 to 0.32 mm³/cycle advances CA50 sufficiently to increase the ringing intensity (RI) from 0.7 to 7.5 MW/m² [3], i.e., from very retarded to advanced beyond the knock limit of RI = 5 MW/m². Moreover, this CA50 change can be accomplished in a matter of seconds using the AMFI system, whereas for thermal control, the intake temperature (T_{in}) would have to be increased from 149°C to 158°C for this same CA50 advancement, which would take much longer.

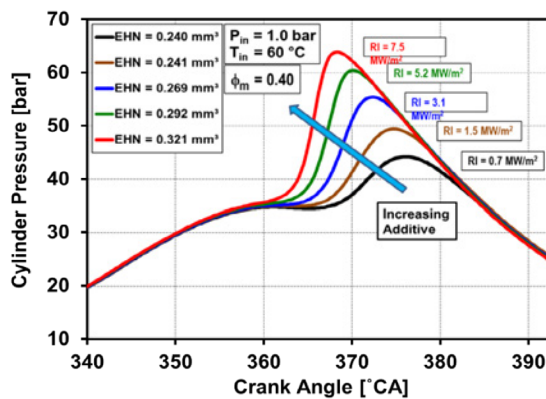


Figure I.4.4. A series of cylinder-pressure traces that show how the AMFI system can adjust the combustion phasing from retarded to advanced by increasing the amount of EHN additive supplied.

Base fuel = RD5-87A, P_{in} = 1.0 bar, T_{in} = 60°C, ϕ_m = 0.40, speed = 1,200 rpm.

A more challenging test of combustion-timing control capability is to maintain the desired CA50 for large changes in operating conditions. Figure I.4.5 presents a demonstration of the AMFI system's ability to control CA50 as the fueling rate is increased to sweep the load from a gross-indicated mean effective pressure (IMEP_g) of 410 kPa to 610 kPa. As Figure I.4.5a shows, by adjusting the amount of additive, CA50 can be readily adjusted to the desired value. The AMFI system has also been tested for CA50 control through sweeps of intake boost pressure and engine speed, and it performed very well.

Another very important advantage of the AMFI system is that the additive can enhance the overall reactivity of the fuel in addition to changing the reactivity to maintain the desired CA50 as operating conditions vary. As a result, autoignition can be achieved without significant intake heating or large amounts of retained hot residuals, even at naturally aspirated ($P_{in} = 1.0$ bar) conditions. For example, Figure I.4.5b shows that T_{in} was held constant at 60°C (representative of intercooler-outlet temperatures) for the AMFI-controlled load sweep, compared to T_{in} s from 144°C to 181°C being required for the heated T_{in} -controlled sweep with no additive. This large reduction (or elimination) of the need for intake heating or retained hot residuals greatly simplifies LTGC operation, and it increases the thermal efficiency and maximum load for a given P_{in} , as also shown in Figure I.4.5b. For both sweeps, ϕ_m was increased from 0.3 to 0.46, but the charge density is higher for the AMFI-controlled sweep with $T_{in} = 60^\circ\text{C}$, which shifts the sweep to higher loads as shown. Thermal efficiencies are also substantially higher for the AMFI sweep because the lower T_{in} results in lower combustion temperatures that increase the specific-heat ratio (γ) for greater work extraction, and they reduce heat transfer losses. These results show that the AMFI system can greatly improve CA50 control, simplify LTGC operation, and increase both efficiency and load; thus, it offers substantial benefits for overcoming the challenges to commercializing LTGC engines.

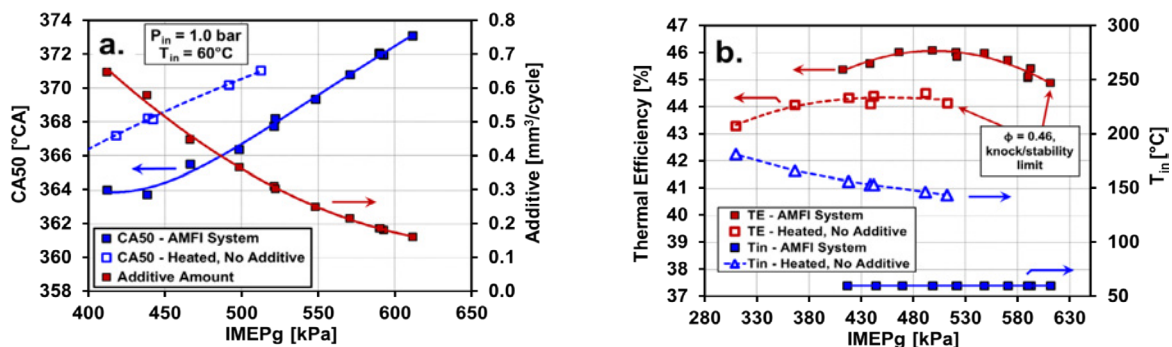


Figure I.4.5. Demonstration of the ability of the AMFI system to control CA50 through a load sweep. (a) Required changes in CA50 with load change and the change in the amount of EHN additive required to make the CA50 changes. (b) Thermal efficiencies (TE) and required T_{in} through the load sweep for the AMFI system (solid lines) and for T_{in} control (dashed lines). $\phi_m = 0.3$ – 0.46 for both the AMFI-controlled and heated, T_{in} -controlled sweeps. $P_{in} = 1.0$ bar, 1,200 rpm, base fuel = RD5-87A; 0°CA (crank angle) = TDC-intake.

Conclusions

- LES modeling of in-cylinder flows in our LTGC engine provided substantial insight into the mechanism causing the thermal stratification required for good LTGC performance. The thermal stratification is produced by large-scale turbulence that appears to persist from turbulence generated by the intake flows, but additional research is needed to verify that this is the source of the turbulence.
- A new seven-component surrogate blend has been developed for regular E10 gasoline (RD5-87A) based on matching the detailed hydrocarbon analysis of the real distillate fuel. This new computational surrogate is shown to give a much closer match to experimental data than the previously available surrogate when applied using the latest detailed chemical-kinetic mechanism from LLNL.

- Chemical-kinetic analyses provided an understanding of the chemistry that produces ϕ -sensitivity, a fuel property that allows fuel stratification to reduce HRRs and to rapidly control CA50 in LTGC engines.
- Based on this understanding, the potential for developing a fuel blend with an increased ϕ -sensitivity was examined computationally. The best blend, consisting of five typical gasoline components, increases the ϕ -sensitivity by 45% (average increase at $P_{in} = 1.0$ bar and 1.3 bar) compared to regular gasoline, has a RON = 101.5 and an octane sensitivity = 11.5, and does not exceed U.S. Environmental Protection Agency blending limits.
- A new device has been developed that provides direct control of combustion timing in LTGC engines.
 - o The AMFI system works by metering and mixing tiny amounts (tenths of a mm^3) of an ignition-enhancing additive into the fuel each engine cycle.
 - o For automotive use, the additive would only need to be replenished at service intervals ($\sim 7,000$ mi) at a cost of $\sim \$20$, far less than the cost of the fuel saved compared to conventional SI combustion.
 - o The AMFI system has been demonstrated to control combustion timing well for large variations of fueling rate, intake boost pressure, and engine speed.
 - o The AMFI system also greatly reduces (or eliminates) the need for intake heating or retained hot residuals, simplifying LTGC operation, increasing thermal efficiency, and increasing the maximum load at a given intake boost level.

Key Publications, Presentations, and Awards

1. Lopez-Pintor, D., and J.E. Dec. 2018. "Phi-Sensitivity for LTGC / ACI Engines: Understanding the Fundamentals & Tailoring Fuel Blends to Maximize this Property." AEC Working Group Meeting, Argonne National Laboratory, January 29 – February 1, 2018.
2. Gentz, G., J. Dernette, C. Ji, and J.E. Dec. 2018. "Spark Assist for CA50 Control & Improved Robustness in a Premixed LTGC Engine – Effects of Equivalence Ratio and Intake Boost." SAE Technical Paper 2018-01-1252, doi:10.4271/2018-01-1252, SAE 2018 World Congress.
3. Petitpas, G., R. Whitesides, J.E. Dec, and J. Dernette. 2018. "Refining Measurement Uncertainties in HCCI/LTGC Engine Experiments." SAE Technical Paper 2018-01-1248, doi:10.4271/2018-01-1248, SAE 2018 World Congress.
4. Sofianopoulos, A., M.R. Boldaji, B. Lawler, S. Mamalis, and J.E. Dec. 2018. "Effect of Engine Size, Speed, and Dilution Method on Thermal Stratification of Premixed HCCI Engines – A Large Eddy Simulation Study." Submitted to *Int. J. Engine Research* (IJER-18-0174) August 2018.
5. Dec, J. E., G. Gentz, and D. Lopez-Pintor. 2018. "A Device for Rapid, Robust Combustion-Timing Control of LTGC Engines." AEC Working Group Meeting, US-Car, Detroit, MI, August 2018.
6. Lopez-Pintor, D., J.E. Dec, and G. Gentz. 2018. "Development and Validation of Improved Computational Surrogates for Distillate Fuels in LTGC Engines." AEC Working Group Meeting, US-Car, Detroit, MI, August 2018.
7. Dec, J.E. 2018. "Low-Temperature Gasoline Combustion (LTGC) Engine Research." DOE Annual Merit Review, Office of Vehicle Technologies, June 2018.
8. ASME Soichiro Honda Medal: Dec, J.E., November 2017.
9. SAE Lloyd L. Withrow Distinguished Speaker Award: Dec, J.E., April 2018.

References

1. Dronniou, N., and J.E. Dec. 2012. "Investigating the Development of Thermal Stratification from the Near-Wall Regions to the Bulk-Gas in an HCCI Engine with Planar Imaging Thermometry." *SAE Int. J. Engines* 5 (3): 1046–1074, doi:10.4271/2012-01-1111.
2. Heywood, J.B. 1988. *Internal Combustion Engine Fundamentals*. New York: McGraw-Hill.
3. Eng, J.A. 2002. "Characterization of Pressure Waves in HCCI Combustion." SAE Technical Paper 2002-01-2859, doi:10.4271/2002-01-2859.

I.5 Gasoline Combustion Fundamentals (Sandia National Laboratories)

Isaac W. Ekoto, Principal Investigator

Sandia National Laboratories
7011 East Ave.
Livermore, CA 94551
E-mail: iekoto@sandia.gov

Michael Weismiller, DOE Technology Development Manager

U.S. Department of Energy
E-mail: Michael.Weismiller@ee.doe.gov

Start Date: October 1, 2017	End Date: September 30, 2018	
Project Funding (FY18): \$920,000	DOE share: \$920,000	Non-DOE share: \$0

Project Introduction

Next-generation automotive gasoline engines have the potential to meet aggressive DOE Vehicle Technologies Office fuel economy and pollutant emission targets through a combination of reduced heat transfer, lower throttling losses, shorter combustion durations, and higher compression ratios. A major challenge for spark-ignited engines that use conventional inductor coil spark igniters at low power conditions is poor combustion stability when large amounts of charge dilution by air or external gas recirculation are introduced. These igniters also often operate poorly under elevated charge motions and high in-cylinder densities present during high-speed boosted conditions. As a result, there is tremendous desire for advanced ignition technology that can expand the operability range. Desired features include larger and more energetic ignition volumes, tolerance to elevated cylinder densities and charge motions, and excellent durability. There is also opportunity for ignition systems to be an important source of radicals and heat that are used to tailor gasoline reactivity for advanced compression ignition (ACI) strategies. However, there is a lack of foundational understanding of igniter mechanisms for new technologies, which inhibits the development of production-ready systems.

The primary research objective in the Gasoline Combustion Fundamentals project is to investigate phenomenological aspects related to advanced ignition, which is accomplished through targeted experiments performed in a single-cylinder optically accessible research engine and in-house developed ignition/combustion vessels. In situ optical diagnostics and ex situ gas sampling measurements are performed to elucidate important details of ignition and combustion processes, and then are further used to develop and validate complementary high-fidelity ignition simulations. The primary project audience is automotive manufacturers, Tier 1 suppliers, and technology startups—close cooperation has resulted in the development and execution of project objectives that address crucial mid- to long-range research challenges.

Objectives

Overall Objectives

- Identify ignition technologies that enable effective combustion control for advanced gasoline engines
- Investigate phenomenological aspects related to advanced ignition
- Expand the knowledge base of ACI and multi-mode combustion systems over the full load range
- Develop models of fundamental engine combustion and in-cylinder emissions formation processes

Fiscal Year 2018 Objectives

- Quantify transient plasma discharge products and ignition behavior at engine-relevant conditions
- Fabricate new igniters and optical test vessels
- Demonstrate improved low-load engine emissions and efficiency with O₃-enhanced ACI
- Identify O₃ addition mechanisms that increase fuel reactivity

Approach

Performed research leverages experimental and numerical capabilities from multiple partners to characterize different aspects of advanced ignition and associated engine combustion. Based on industry guidance, an investigation was performed into the fundamental characteristics of transient plasma ignition (TPI)—a form of low-temperature plasma formed by very short-pulse, high-voltage electrical discharges. An in-house built ignition testing facility was used to characterize thermal energy deposition, ignition volume, and radical formation for a range of electrode configurations. Impactful results were shared with Riccardo Scarcelli of Argonne National Laboratory, who modeled TPI for both inert and combustion conditions using the high-fidelity non-equilibrium plasma solver, VizGlow, and the computational fluid dynamics solver, CONVERGE. An additional ignition research topic is to explore fundamental mechanisms for fueled pre-chambers. For this project, a larger ignition test facility was designed and fabricated in FY 2018 that can replicate in-cylinder conditions at the time of ignition and has extensive optical access for non-invasive in situ diagnostics of relevant ignition phenomena.

An industry call for low-cost, efficient, and onboard means of tailoring ACI fuel properties has also motivated research into the use of ozone (O₃), a powerful oxidizing chemical agent generated through coronal discharges in intake air. A combination of Sandia National Laboratories experiments in a direct injected optical engine and PRISME Laboratory rapid compression machine experiments at the University of Orléans, France, was used to investigate the change in gasoline reactivity with O₃ addition. Measurements were complemented by kinetics modeling that utilized Lawrence Livermore National Laboratory gasoline surrogate mechanisms to clarify the dominant chemical pathways responsible for augmented reactivity. Optical measurements of in-cylinder O₃ concentration along with performance and emissions data were shared with General Motors R&D to directly support their own internal projects.

Results

Increased electric fields for TPI relative to other plasma ignition technologies (e.g, microwave or radio frequency corona discharges) lead to strong ionization and dissociation rates as a result of limited collisional electron energy transfer effects [1,2]. As a result, TPI can extend dilution tolerance limits through the formation of active radicals and rapid volumetric heating via electron energy transfer processes. An important radical generated by transient plasma discharges is atomic oxygen (O), which can both increase flame speeds and accelerate the onset of auto-ignition chemical reactions. Ground-state O number density from transient plasma discharges at engine-relevant densities was measured via two-photon laser-induced fluorescence just after the discharge, with results quantified by a developed signal model. All measurements were performed in a custom-built, optically accessible spark calorimeter with a fixed-gap (5.2 mm) pin-to-pin electrode configuration and gas pressures of 1.5 bar to 3.4 bar absolute (Figure I.5.1). Pressure-rise calorimetry and schlieren imaging were used to estimate the global discharge temperature as a function of ambient pressure and applied voltage. Experimental measurements at select conditions are compared to numerical modeling results of the discharge that were generated using VizGlow, a general-purpose, self-consistent, multi-species, multi-temperature, non-equilibrium plasma solver.

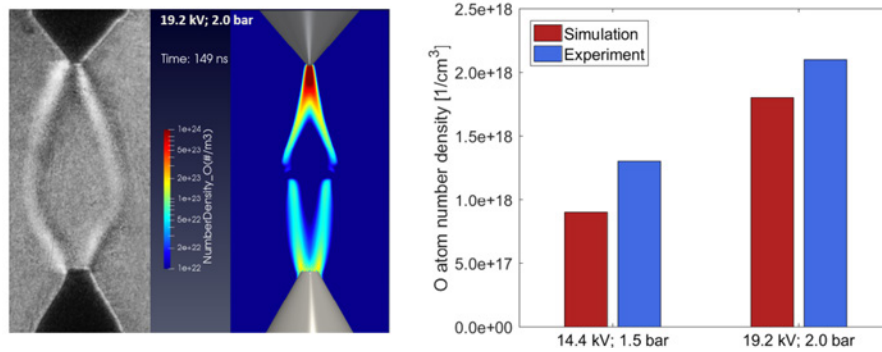


Figure I.5.1. Schlieren image of post-discharge transient plasma streamers for a 19.2 kV discharge in 2.0 bar ambient air along with an image of O atom distributions from complementary simulation results. A comparison of the predicted and measured O atom concentrations at the anode tip is also provided for two conditions.

Major findings are as follows:

- Twin streamers observed for a broad range of initial pressures (1.5–3.4 bar) were joined at the upper anode and lower cathode tips, but repelled from each other near the electrode gap center.
- Molecular excited-state relaxation processes resulted in measured streamer temperatures shortly after the discharge (~100 μs) of up to 1,500 K, which are expected to aid ignition.
- Extensive O-atom mole fractions of up to 3% were measured near the anode tip.
- Qualitative and quantitative measurements of streamer characteristics were closely matched for a broad range of initial pressures.

A major issue for the pin-to-pin electrode configuration from Figure I.5.1 is the propensity for transition to inter-electrode breakdown that results in substantial electrode erosion due to elevated discharge currents. To inhibit undesirable breakdown transition, the electrode was redesigned in a groundless partial dielectric barrier discharge (DBD) configuration. For this electrode, a central anode was surrounded by approximately 1.5 mm of a dielectric alumina ceramic in the shape of a cone frustum, with the anode surface exposed and flush mounted with the ceramic tip. Ignition was expected to happen at the exposed anode, with significant enhancement of the flame speeds that resulted from negative corona surface discharges that surround the insulator. An image sequence in Figure I.5.2 illustrates the groundless partial DBD electrode (upper left) and includes complementary images of excited-state O for various initial pressure and voltage discharge combinations in desiccated air. Also in Figure I.5.2 is a plot of post-discharge constituents from non-flammable mixtures of propane and air that were collected using bulk sampling and speciated via gas chromatography.

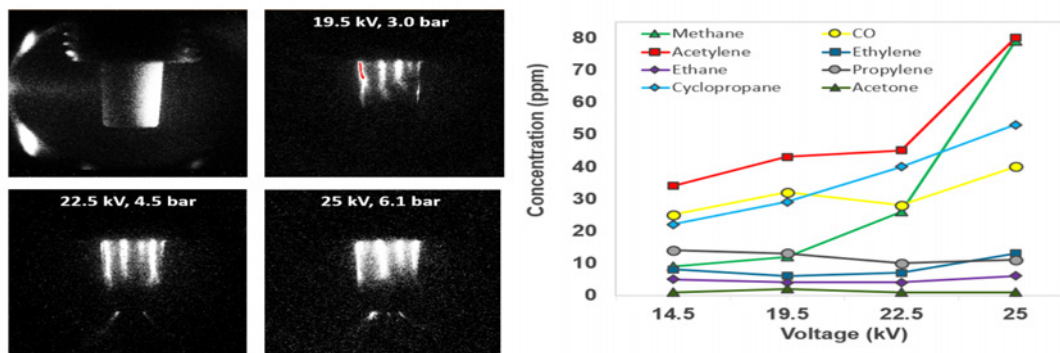


Figure I.5.2. Image of the groundless partial DBD electrode and complementary filtered imaging of excited-state O from resultant negative coronas that surround the insulator during transient plasma discharges in air. Also included is a plot of post-discharge products that form in non-flammable mixtures of propane and air.

Major findings are as follows:

- Voltage breakdown transition boundaries increased relative to the pin-to-pin electrodes.
- Significant excited-state O luminosity was observed from negative corona streamers that originated at the grounded electrode body and propagated along the insulator surface toward the exposed anode.
- The strong luminosity indicates a high degree of molecular ionization and dissociation in this region.
- Large measurements of fuel fragment concentrations are believed to originate in the same region.
- Complementary modeling indicates the discharge products can increase flame speeds by up to 20%.

Schlieren image sequences of ignition kernel development and subsequent flame propagation at discrete times after the discharge are plotted in Figure I.5.3 for the pin-to-pin and groundless partial DBD electrodes, along with a comparison to ignition from a high-energy (93 mJ) inductor coil spark plug igniter. The fuel was propane, while the oxidizer was desiccated air. Concentrations were fixed at stoichiometric conditions (6.45% propane in air). The initial pressure was 1.3 bar absolute. Pulse bursts of five and ten pulses were examined for TPI (ignition was not achieved for a five-pulse burst for either TPI igniter at the conditions examined). In all cases, the dwell between successive pulses was 100 μ s. Peak voltage and pulse number are tabulated at the end of the respective sequence. Note that for the groundless partial DBD electrode, two sets of images were acquired: (1) electrode tip in view to examine ignition processes along the insulator and (2) electrode tip at the upper edge of the image to examine flame propagation processes in detail.

Inductive spark plug						V (kV)	# of pulses
Spark Ignition							1
Pin-to-pin electrode configuration							
Arc ignition						18	10
TPI						15	10
TPI						15	5
Groundless DBD electrode							
Arc ignition						29	10
TPI						24	10
TPI close up						24	10
TPI quench						24	5

Figure I.5.3. Sequence of images showing ignition kernel development for pin-to-pin and groundless partial DBD TPI as compared to inductive spark ignition for different voltages and pulse repetition rates

Major findings are as follows:

- For both TPI electrodes, a 10-pulse burst was required for stable ignition, which suggests kernel energy must be systematically replenished in the earliest phases.
- The pin-to-pin TPI electrode initiated ignition at both the anode and cathode, with the initial flame kernel quickly propagating up along one or both discharge streamers.
- The groundless partial DBD electrode initiated ignition at the electrode tip, with outward flame propagation into the bulk gas and rapidly up along the insulator surface.
- Flame propagation rates for both TPI igniters roughly doubled relative to a conventional inductor coil ignition system (93 mJ).

Pure ACI modes are challenging at elevated engine loads and speeds due to large pressure rise rates that lead to increased engine knock [3]. A viable solution is the so-called dual- or mixed-mode strategy where ACI is employed for low-to-moderate loads, with conventional spark ignition used at higher loads [4]. For intermediate loads and speeds, spark-assisted compression ignition (SACI) can be used where compression heating from a spark-initiated flame kernel leads to end-gas auto-ignition. Unthrottled operation and low heat transfer losses preserve high thermal efficiencies from ACI, while slower pressure rise rates due to significant fuel consumption by the deflagration inhibit engine knock. For spray-guided direct injection combustion chambers, a combination of early- and late-cycle injections can stabilize combustion for a wide range of loads by controlling the fuel fraction consumed by the deflagration. However, some amount of charge pre-heat is generally required, which can come at the cost of increased heat transfer losses and poor transient response. In FY 2018, the use of 30 ppm of intake seeded O_3 in the spray-guided, single-cylinder, optically accessible engine was investigated as a way to replace charge pre-heating for stable SACI operation. Figure I.5.4 plots indicated specific fuel consumption (ISFC) with and without O_3 addition for a broad range of loads (1.5–5.5 bar indicated mean effective pressure [IMEP]) and engine speeds (800–1,400 rpm).

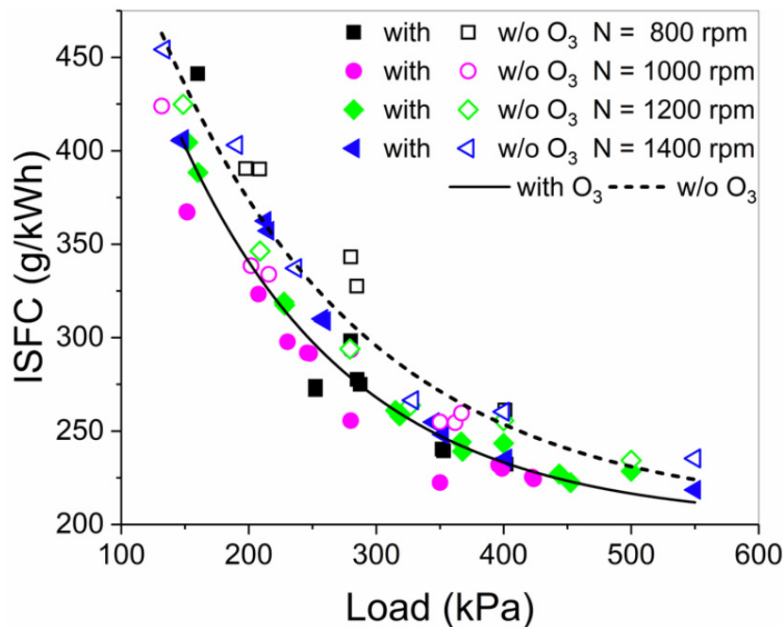


Figure I.5.4. Comparison of ISFC as a function of load for lean conditions with and without O_3 addition for engine speeds between 800 rpm and 1,400 rpm

Major findings are as follows:

- Stable end-gas auto-ignition without intake pre-heat was achieved across the range of loads and engine speeds examined for an engine with a moderate compression ratio (13:1).
- A 6–9% decrease in ISFC was achieved relative to conditions without O₃ due to an increase in combustion efficiency and shorter overall combustion durations.
- Emissions of NO_x were below 5 g/kg-fuel provided that the spark timing preceded the 2nd injection. However, this came at the expense of elevated particulate matter emissions.

To simultaneously minimize elevated particulate matter or NO_x emissions from the double injection strategy, exclusive use of early direct injection is possible provided that end-gas temperatures exceed ~1,000 K. However, achieving these temperatures in a moderate compression ratio engine typically requires extensive charge pre-heating from retained residuals generated during negative valve overlap strategies that add cost and complexity to the engine architecture. Accordingly, a study was performed to see if heavy intake O₃ seeding (50 ppm) could partially replace charge pre-heat for early direct injection SACI operation. Moderate engine loads of between 4 bar and 5 bar IMEP were investigated for engine speeds between 800 and 1,400 rpm, with the intake temperatures swept between 42°C and 80°C. Intake and exhaust pressures were fixed at 1.0 bar and 1.1 bar, respectively, with moderate positive valve overlap used to keep internal residuals between 12% and 20%. For each condition, the fueling rate at maximum brake torque spark timing was adjusted until the minimum achievable load was met, provided that the coefficient of variation of IMEP was below 3%, the ringing intensity was below 1 MW/m², and NO_x emissions were below 1 g/kg-fuel. In Figure I.5.5, IMEP, 50% mass fraction burn angle (CA50), and coefficient of variation of IMEP are plotted as a function of spark timing for a sweep of intake temperatures at a fixed 1,000 rpm engine speed.

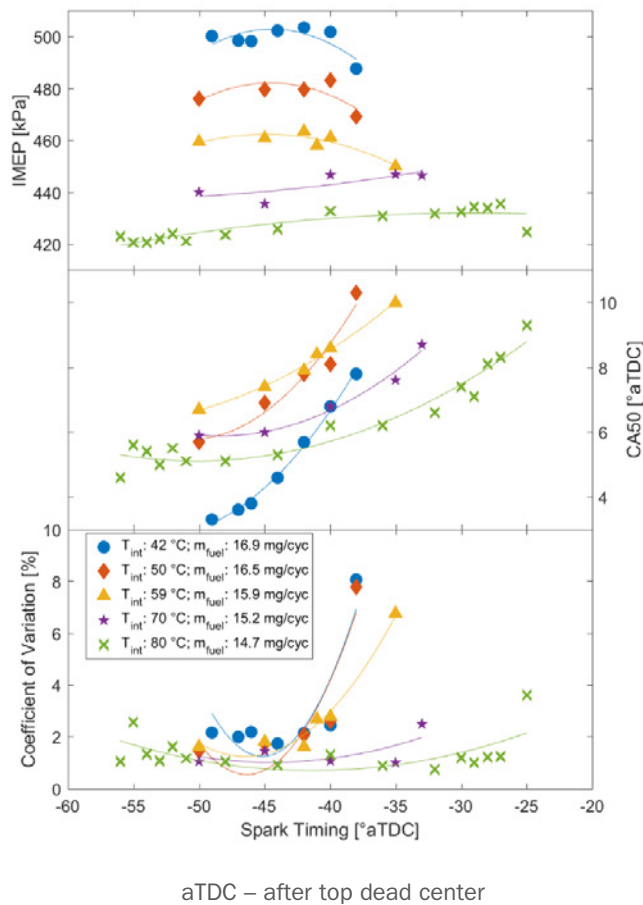


Figure I.5.5. Plots of IMEP, CA50, and coefficient of variation of IMEP as a function of spark timing for a sweep of intake temperatures (42–80°C) and a fixed 1,000 rpm engine speed

Major findings are as follows:

- Combustion without O_3 led to immediate and sustained misfire for all conditions.
- As intake temperature increased, the lowest achievable load decreased and combustion was less sensitive to spark timing as a result of the increased charge reactivity.
- Peak efficiencies for all loads were above 39%, while particulate matter and NO_x emissions were both negligible.
- As engine load or speed increased, combustion became increasingly dependent on higher deflagration fractions, and hence spark timing.

Finally, to examine the impact of O_3 decomposition on auto-ignition kinetics, measured O_3 profiles with intake valve closure temperatures of 361 K and 384 K are plotted in Figure I.5.6 alongside close-up apparent heat release rate profiles that focus on the low-temperature heat release (LTHR) periods for fired conditions that match the range of intake valve closure temperatures for select conditions from Figure I.5.5. The range of intake valve closure temperatures for the O_3 measurements was matched to the fired experiment values. Ozone profiles are plotted on a semi-log scale to more clearly highlight when rapid thermal decomposition into O and O_2 occurs. Near the conclusion of decomposition, there was increased absorbance that was likely from hydroperoxyl (HO_2) formed during LTHR reactions that was not present in the reference datasets. Although this spurious absorbance was not desired, it nonetheless is a convenient marker of LTHR onset.

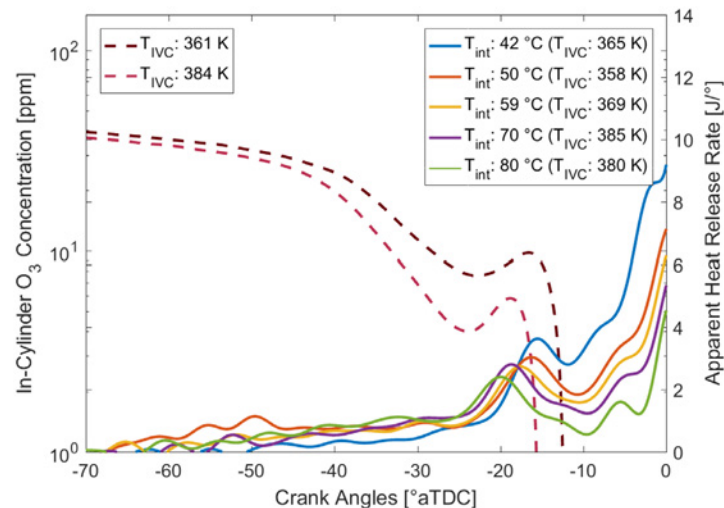


Figure I.5.6. Comparison of measured in-cylinder O_3 concentration and early-stage apparent heat release rate profiles for a sweep of intake temperatures

Based on the combined optical and kinetic modeling results, the following process is proposed to explain enhanced auto-ignition with O_3 addition:

- During compression, O_3 rapidly decomposes into O_2 and O at temperatures above 600 K.
- For alkanes—the major fuel class in gasoline—the burst of O abstracts fuel hydrogen to form hydroxyl (OH) and alkyl radical, with the OH abstracting fuel hydrogen to make more alkyl radical.
- At the high-density, low-temperature conditions present in the engine, the alkyl radicals combine with O_2 to form an excited adduct that abstracts more fuel hydrogen to make alkylhydroperoxide.
- Decomposition of alkylhydroperoxide into alkyloxy radical and OH then becomes a sustaining source of LTHR radicals [5].
- Depending on initial intake O_3 concentration, these early LTHR reactions can advance combustion phasing by more than 20 crank angles.

Conclusions

- Relative to conventional inductor coil ignition systems, multi-pulse TPI was found to augment initial flame growth rates through a combination of reduced electrode heat losses, large ignition volumes, and the formation of reactive species and fuel fragments.
- Ozone addition—a powerful oxidizing agent that can be generated through onboard coronal discharges in intake air—was found to be an effective way to replace intake charge heating for high-efficiency and low-emitting SACI operating modes.
- A combination of engine experiments, quantitative in-cylinder O₃ measurements, and a literature survey of prominent LTHR mechanisms was used to propose a mechanism that describes how O₃ addition enhances charge reactivity for gasoline engine combustion.

Key Publications

1. Scarcelli, R., T. Wallner, S. Som, S. Biswas, I. Ekoto, D. Breden, A. Karpatne, and L. Raja. “Modeling Non-Equilibrium Discharge and Validating Transient Plasma Characteristics at Above-Atmospheric Pressure.” *Plasma Sources Science and Technology*, (In Press).
2. Ekoto, I., and F. Foucher. 2018. “Mechanisms of Enhanced Reactivity with Ozone Addition for Advanced Compression Ignition.” SAE World Congress Experience, Detroit, MI, SAE International 2018-01-1249.
3. Scarcelli, R., A. Zhang, T. Wallner, D. Breden, A. Karpatne, L. Raja, I. Ekoto, and B. Wolk. 2018. “Multi-Dimensional Modeling of Non-equilibrium Plasma for Automotive Applications.” SAE Technical Papers, April 2018.
4. Zhang, A., R. Scarcelli, T. Wallner, D. Breden, A. Karpatne, L.L. Raja, I. Ekoto, and B. Wolk. 2018. “Numerical Investigation of Nanosecond Pulsed Discharge in Air at Above-Atmospheric Pressures.” *Journal of Physics D: Applied Physics* 51 (34).

References

1. Starikovskiy, A., and N. Aleksandrov. 2013. “Plasma-Assisted Ignition and Combustion.” *Prog Energy Combust* 39 (1): 61–110.
2. Wolk, B., and I. Ekoto. 2017. “Calorimetry and Imaging of Plasma Produced by a Pulsed Nanosecond Discharge Igniter in EGR Gases at Engine-Relevant Densities.” *SAE International Journal of Engines* 10 (3).
3. Dec, J.E. “Advanced Compression-Ignition Engines—Understanding the In-Cylinder Processes.” *P. Combust. Inst.* 32 (2): 2727–42.
4. Olesky, L.M., J.B. Martz, G.A. Lavoie, J. Vavra, D.N. Assanis, and A. Babajimopoulos. 2013. “The Effects of Spark Timing, Unburned Gas Temperature, and Negative Valve Overlap on the Rates of Stoichiometric Spark Assisted Compression Ignition Combustion.” *Appl Energy* 105: 407–17.
5. Zádor, J., C.A. Taatjes, and R.X. Fernandes. 2011. “Kinetics of Elementary Reactions in Low-Temperature Autoignition Chemistry.” *Prog Energy Combust* 37 (4): 371–421.

Acknowledgements

Work was performed at the Combustion Research Facility, Sandia National Laboratories, Livermore, California. Financial support was provided by the U.S. Department of Energy, Vehicle Technologies Office. Sandia National Laboratories is a multi-mission laboratory managed and operated by National Technology and Engineering Solutions of Sandia, LLC, a wholly owned subsidiary of Honeywell International, Inc., for the U.S. Department of Energy’s National Nuclear Security Administration under contract DE-NA0003525.

I.6 Advancements in Fuel Spray and Combustion Modeling with High Performance Computing Resources (Argonne National Laboratory)

Sibendu Som, Principal Investigator

Argonne National Laboratory
9700 S. Cass Avenue
Argonne, IL 60439
E-mail: ssom@anl.gov

Michael Weismiller, DOE Technology Development Manager

U.S. Department of Energy
E-mail: Michael.Weismiller@ee.doe.gov

Start Date: October 1, 2017

End Date: September 31, 2018

Project Funding (FY18): \$400,000

DOE share: \$400,000

Non-DOE share: \$0

Project Introduction

In this project, significant efforts have been dedicated towards advancing the capabilities in multiphase and turbulent combustion models to improve predictive capability of diesel engine simulations. Cavitation erosion has been noted in diesel injector hardware, namely within the needle seat region and along the injector needle, as well as the entrance to nozzle holes [1]. Ideally, an injector hardware designer would be able to utilize a computationally efficient design tool to accurately predict cavitation and to inform improved designs that mitigate the severity of cavitation-induced erosion. However, developing a predictive erosion index is a challenge due to the disparate timescales characterizing cavitation impacts and the gradual material fatigue and erosion process. Although several cavitation erosion indicators have been proposed in the literature [2,3], no single metric has been identified as universally applicable across all injector geometries and injection conditions. For example, the maximum local pressure [2] provides an efficient means to represent the extrema of impact stresses on the neighboring walls. Although this metric can characterize the potential for plastic deformation and pitting from impacts in excess of the material yield stress, the maximum local pressure does not provide insight into the material response from repeated hydrodynamic impacts. Therefore, there exists an opportunity to formulate an improved erosion metric that can bridge the existing gap in how repeated cavitation cloud implosions are represented and linked to the material erosion process.

Incorporation of realistic fuel surrogates and detailed chemistry is a fundamental step towards predictive engine simulations. However, the use of the latest multi-component diesel surrogates and detailed hydrocarbon chemistry with a few thousand species is still not tractable. The development work at Argonne comprising of higher-fidelity flamelet models and leveraging fast chemistry solvers has been used to address this challenge. This effectively brings the use of the latest surrogates into the realm of diesel engine simulations. Unsteady flamelet methods are being increasingly used to include complex chemistry in engine simulations. However, memory costs increase non-linearly with an increase in the dimensionality of flamelet manifolds. The aim of this work is to develop a novel methodology that can reduce multi-dimensional flamelet manifolds, maintaining the same level of fidelity using deep artificial neural networks (ANNs). This new approach allows the implementation of large dimensional manifolds at significantly lower memory costs. This approach improved the scalability, speed, and fidelity of diesel engine simulations in the CONVERGE computational fluid dynamics (CFD) code. This approach has now been validated over a range of applications and conditions.

Objectives

In order to advance fuel spray modeling research, there remains a need to link the influence of injection conditions and parameters on the lifetime of the injector. This can only be made possible through accurate representation of the fluid dynamics and thermodynamics leading to cavitation inception, cavitation cloud shedding and collapse that can lead to cavitation-induced erosion. The objectives of these efforts are summarized below.

Overall Objectives

For the Cooperative Research and Development Agreement with Cummins and Convergent Science, the overall objectives of the project are as follows.

- Integrate flash-boiling approach with advanced turbulence model
- Validate flash-boiling model predictions against experimental data
- Develop in-nozzle cavitation erosion model for diesel injectors
- Validate erosion model against optical data from the literature and new data from the Advanced Photon Source

Fiscal Year (FY) 2018 Objectives

For the Cooperative Research and Development Agreement with Cummins and Convergent Science, the specific objectives for FY 2018 are as follows.

- Identify existing cavitation erosion metrics in the literature
- Implement and evaluate existing cavitation erosion metrics
- Develop, implement, and validate an improved cavitation erosion metric into CONVERGE

In order to advance the state of art in tabulated models, a deep neural network based algorithm was developed and validated for diesel engine applications. The overall objectives are summarized here.

Overall Objectives

For the turbulent combustion modeling work, the overall objectives of the project are as follows.

- Demonstrate the use of detailed chemistry mechanisms and realistic fuel surrogates for diesel engines
- Demonstrate the feasibility of using ANNs for replacing multi-dimensional unsteady flamelet manifolds
- Demonstrate the use of complex surrogates for engine simulations

FY 2018 Objectives

- Develop an automated multi-dimensional manifold bifurcation algorithm
- Validate ANN manifold methodology for Engine Combustion Network Spray A
- Implement ANN flamelet code in CONVERGE CFD code
- Demonstrate validation and speed-up of CFD code and reduction in memory consumption of the code

Approach

CONVERGE is utilized to model cavitation within the PREVERO Channel “K” geometry from the experimental work of Skoda et al. [4] for diesel fuel with pressure drops ranging from 150 bar to 265 bar. Because the experimental data set includes characterization of erosion events within this geometry, this case serves as the starting point to validate the current cavitation modeling approach and evaluate pertinent cavitation erosion metrics. Key features of the channel geometry include a constant diameter of 303 μm , channel length of 994 μm , and an inlet radius of curvature of 40 μm . It is important to note that in the experiments of Skoda et al. [4], the channel was constructed from aluminum in order to accelerate the expected incubation period before material erosion. Cavitation and condensation are represented using the homogeneous relaxation model [5].

The turbulent combustion modeling work investigates the use of deep ANNs to replace lookup tables in order to reduce the memory footprint and increase computational speed of tabulated flamelets. The proposed framework is validated by applying it to an n-dodecane spray flame and comparing global flame characteristics for different ambient conditions using a well-established large-eddy simulation framework. A novel speed-up technique is introduced, which takes advantage of the ability of ANNs to predict multiple outputs with one network model by classifying the species based on their correlation to one another. The same framework is then extended to the simulations of methyl-decanoate combustion in a compression ignition engine with a five-dimensional manifold. The validation studies show that the use of ANNs is able to accurately capture flame liftoff, autoignition, two-stage heat release, and other quantitative trends over a range of conditions. The use of neural networks in conjunction with the grouping mechanism produces a significant reduction in the memory footprint and computational costs for the code, and these metrics are investigated in detail. This model is integrated and tested within the CONVERGE CFD code.

Results

In order to link the effect of repeated impacts, of varying stress and strain rates, with the eventual material fatigue and rupture, a new metric, called the accumulated stored energy, E_{stored} , was proposed and implemented into CONVERGE based on an energy analysis of a control volume at the fluid-solid interface, as depicted in Figure I.6.1. More details on this metric can be found in [6], but a summary is provided here. For a given impact characterized by a pressure above the yield stress, the amount of energy absorbed by the material from a given impact, $E_{absorbed}$, is assumed to equal the energy of that impact, E_{impact} . To represent the progressive damage to the material from repeated impacts, the stored energy, E_{stored} , by the material is calculated by a cumulative sum of $E_{absorbed}$ from all impacts. In this approach, material failure would then be predicted when E_{stored} exceeds a critical threshold. In its current form, E_{stored} is used as a qualitative measure of cavitation erosion. However, based on its ability to capture the effect of repeated impacts on the material state and current progress within the incubation period, the newly derived E_{stored} provides an improved characterization of cavitation erosion over existing metrics in the literature.

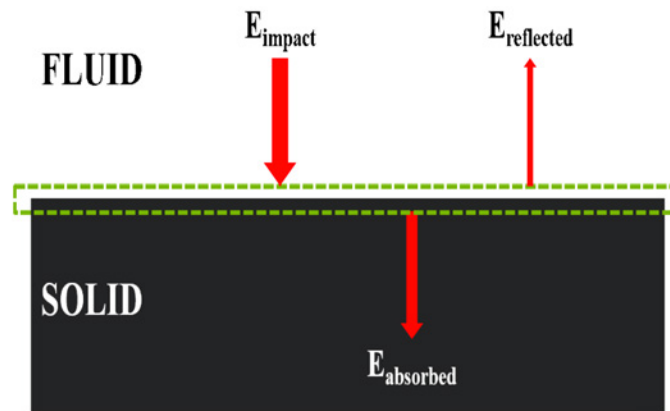


Figure I.6.1. Schematic of energy balance considered in the derivation of the new cavitation erosion metric, which considers the transfer and storage of energy in the solid material due to repeated impacts from cavitation cloud collapse events

This newly derived metric was then implemented into CONVERGE and compared with one of the popular erosion metrics from the literature, namely the maximum local pressure recorded at the wall. Comparison of the measured and predicted cavitation erosion is shown in Figure I.6.2 for two different pressure drop, ΔP , conditions. The experimental results from Skoda et al. [4] highlight that as ΔP increases, the cavitation erosion locations move further downstream, as indicated with the red arrows, and that the incubation period, T , or time before first material removal, also increases. These experimental results indicate that with increasing ΔP , cavitation erosion severity decreases.

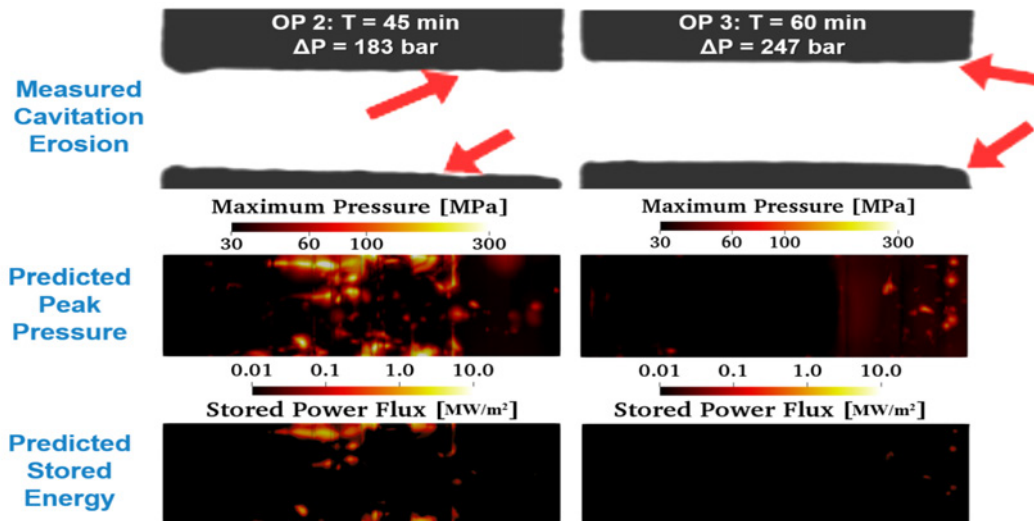


Figure I.6.2. Comparison of erosion patterns between experimental images from Skoda et al. [4] (top) and homogeneous relaxation model predictions of local maximum pressure (middle) and accumulated stored energy (bottom) at the top channel wall

Our current cavitation modeling approach is able to reproduce these trends, although the two employed metrics provide different information about the cavitation erosion process. Results for the OP2 condition indicate several locations with impact stresses in excess of 30 MPa at locations between 34% and 70% of the total channel length, which is in acceptable agreement with the experimentally indicated location at approximately 70% of the channel length. At the OP3 condition, lower peak pressures are recorded at the channel exit. While the maximum local pressure metric provides an indication of potential sites for pitting and material rupture from single impact events, no additional information can be determined regarding the incubation period or critical locations where material erosion is likely. To gain further insight into the predicted cavitation erosion process, the amount of stored energy in the material due to repeated impacts can be evaluated. For both conditions, several of the impacts indicated by the maximum local pressure metric in Figure I.6.2 (middle) are filtered out, and only impacts with stresses in excess of the material yield strength (60 MPa) are shown. Comparison of the predicted stored energy distributions for the OP2 condition and at the channel exit for the OP3 condition provides a qualitative assessment of relative incubation period before material rupture. The larger average stored energy for the OP2 condition in comparison to the OP3 condition suggests that the incubation period would be shorter under the OP2 condition. This result is consistent with the experimental findings, where the incubation period for the OP3 condition was found to be relatively longer. These findings using the newly developed cavitation erosion metric highlight its utility in quantifying both the energy of single impact events, as well as the influence of repeated impacts on the incubation period before material rupture. Future work will evaluate longer simulated times in order to quantify the rate of energy storage, and how this information can be used to extrapolate behavior dictating the incubation period, which occurs over a much longer period of time than can be feasibly simulated.

As part of the turbulent combustion modeling effort, a neural network based flamelet approach was developed. This code can automatically bifurcate a multi-dimensional unsteady flamelet manifold and subsequently train multiple ANNs to generate a final ANN-based flamelet manifold that has significantly lower memory compared to a multi-dimensional table. The ANN comprises multiple hidden layers, and sensitivity analyses with respect to training parameters were carried out to ensure accuracy of retrieval. The tabulated flamelet model (TFM) [7], previously developed in the lab, was used to validate and demonstrate the efficacy of this approach. A constant volume spray flame, the Engine Combustion Network Spray A, was simulated using the conventional multi-dimensional manifold interpolation and compared against the results obtained from the ANN approach. These are large-eddy simulations (LES) with 62 μm minimum cell size with a peak cell-count of 22 million. A four-dimensional manifold was generated for this problem and further reduced using the ANN algorithm. Figure I.6.3 shows the model validation against experimental data and comparison against conventional

interpolation technique. The results demonstrate that the model is able to accurately predict autoignition and flame stabilization for spray flames at diesel-relevant conditions. This approach was further validated against formaldehyde planar laser-induced fluorescence (PLIF) data [8]. Figure I.6.4 shows that the ANN approach is able to satisfactorily capture the formation of intermediate species. This approach was further extended to the modeling of methyl-decanoate combustion in an optical direct injection engine. The simulations were run for an open cycle simulation with LES turbulence model that resulted in a peak cell-count of 25 million. The chemistry mechanism is the most detailed mechanism available for methyl-decanoate with 3,299 species and 10,804 reactions. The LSODES solver, in conjunction with the developed ANN strategy, was used in the model. The flamelet manifold comprised of a five-dimensional manifold that comprises of nine pressure levels. These are some of the most detailed compression ignition engine simulations carried out using detailed mechanisms. These studies also showed a significant reduction in memory usage and 37% speed-up of the CFD code on account of the ANN algorithm.

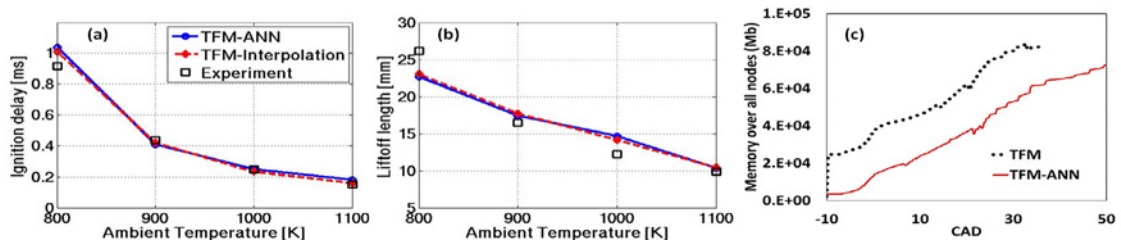


Figure I.6.3. (a) Ignition delay and (b) flame liftoff as a function of ambient temperature conditions with LES models using ANNs. (c) Memory consumption over all nodes for a conventional interpolation vs. ANN method.

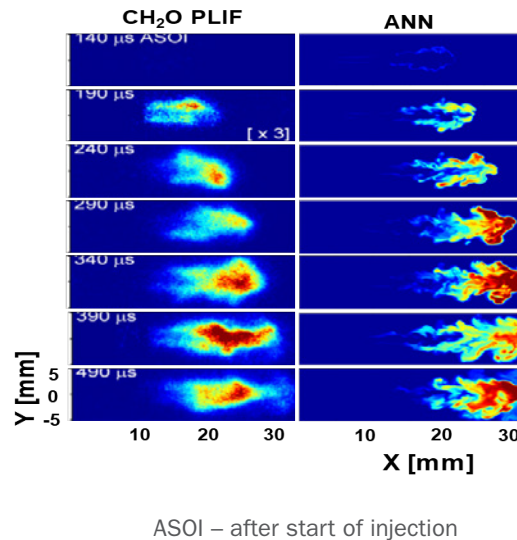


Figure I.6.4. Temporal evolution of CH₂O mass fraction contours predicted by the TFM-ANN LES model (right) is compared against the CH₂O PLIF data (left) from a single shot injection

Conclusions

To improve the link between predicted cavitation cloud collapse events and the incubation period leading to material rupture and erosion, a new computational metric was derived based on the fluid-solid energy transfer from impact events. Through comparison of predicted cavitation development and cloud collapse events in a channel geometry under two different pressure drop conditions with available experimental data, the stored energy metric revealed the following findings.

- While the maximum local pressure metric provides an indication of potential sites for pitting and material rupture for single impact events, no additional information could be determined regarding the incubation period or critical locations where material erosion is likely.
- The stored energy metric provides an indication of the influence of flow conditions on the incubation period before material erosion. These findings using the newly developed cavitation erosion metric highlight its utility in quantifying both the energy of single impact events, as well as the influence of repeated impacts on the incubation period before material rupture.

In order to improve combustion models, a novel deep neural network based code was developed. This code can reduce multi-dimensional flamelet manifolds in an automated fashion and significantly reduce computational costs. Moreover, significantly complex chemistry mechanisms with large dimensional manifolds can now be used for engine simulations. A comprehensive validation of the models and performance assessment has been carried out over multiple conditions and the findings are summarized as follows:

- The ANN methodology was validated extensively over Engine Combustion Network experiments, and the model is able to capture global as well as local characteristics over a range of conditions.
- It was demonstrated that this method is generic in nature and can be extended to other complex fuels and chemistry mechanisms with higher manifold dimensionality.
- The new method reduced memory consumption of the code by 30% and reduced computational costs by 37% for high-fidelity diesel engine simulations.
- Complex flamelet manifolds with >9 pressure levels can now be easily accommodated within diesel engine simulations.

Key Publications

1. Magnotti, Gina M., Michele Battistoni, Kaushik Saha, and Sibendu Som. 2018. "Exploration of Cavitation-Induced Erosion Metrics in Throttle Flow Simulations." Paper presented at 10th International Cavitation Symposium, Baltimore, MD, (May 14–16).
2. Magnotti, Gina M., Michele Battistoni, Kaushik Saha, and Sibendu Som. 2018. "Evaluation of a New Cavitation Erosion Metric Based on Fluid-Solid Energy Transfer in Channel Flow Simulations." Paper presented at 14th International Conference on Liquid Atomization & Spray Systems, Chicago, IL, (July 22–26).
3. Owoyele, Opeoluwa, et al. 2017. "Unsteady Flamelet Modelling of Spray Flames Using Deep Artificial Neural Networks." In APS Division of Fluid Dynamics Meeting Abstracts.
4. Owoyele, Opeoluwa, et al. "Application of Deep Artificial Neural Networks to Multi-Dimensional Flamelet Libraries and Spray Flames." *International Journal of Engine Research* (under review).

References

1. Koukouvinis, P., I.K. Karathanassis, and M. Gavaises. 2018. "Prediction of Cavitation and Induced Erosion Inside a High-Pressure Fuel Pump." *International Journal of Engine Research* 9: 360–373.
2. Koukouvinis, P., M. Gavaises, J. Li, and L. Wang. 2015. "Large Eddy Simulation of Diesel Injector Opening with a Two Phase Cavitation Model." *Journal of Physics: Conference Series* 656.
3. Franc, Jean-Pierre. 2009. "Incubation Time and Cavitation Erosion Rate of Work-Hardening Materials." *ASME J. Fluids Eng.* 131.

4. Skoda, Romuald, Uwe Iben, Alexander Morozov, Michael Mihatsch, Steffen Schmidt, and Nikolaus Adams. 2011. "Numerical Simulation of Collapse Induced Shock Dynamics for the Prediction of the Geometry, Pressure and Temperature Impact on the Cavitation Erosion in Micro Channels." Paper presented at WIMRC 3rd International Cavitation Forum, University of Warwick, UK, (July 4–6).
5. Bilicki, Z., and J. Kestin. 1990. "Physical Aspects of the Relaxation Model in Two-Phase Flow." *Proc. R. Soc. Lond. A.* 428: 379–397.
6. Magnotti, Gina M., Michele Battistoni, Kaushik Saha, and Sibendu Som. 2018. "Evaluation of a New Cavitation Erosion Metric Based on Fluid-Solid Energy Transfer in Channel Flow Simulations." Paper presented at 14th International Conference on Liquid Atomization & Spray Systems, Chicago, IL, (July 22–26).
7. Kundu, Prithwish, Muhsin M. Ameen, and Sibendu Som. 2017. "Importance of Turbulence-Chemistry Interactions at Low Temperature Engine Conditions." *Combustion and Flame* 183: 283–298.
8. Skeen, Scott A., Julien Manin, and Lyle M. Pickett. 2015. "Simultaneous Formaldehyde PLIF and High-Speed Schlieren Imaging for Ignition Visualization in High-Pressure Spray Flames." *Proceedings of the Combustion Institute* 35, no. 3: 3167–3174.

Acknowledgements

The principal investigator gratefully acknowledges the contributions of Dr. Prithwish Kundu on developments related to turbulent combustion modeling and Dr. Gina Magnotti on two-phase flow and cavitation erosion modeling. We gratefully acknowledge the computing resources provided by the Laboratory Computing Resource Center at Argonne National Laboratory, and Convergent Science Inc., for providing the CONVERGE CFD software licenses. We would also like to acknowledge Prof. Tarek Echehki and Opeoluwa Owoyele from North Carolina State University for their collaborative efforts on developing the flamelet model.

I.7 Fuel Injection and Spray Research Using X-Ray Diagnostics (Argonne National Laboratory)

Christopher F. Powell, Principal Investigator

Argonne National Laboratory
9700 S. Cass Ave.
Lemont, IL 60439
E-mail: powell@anl.gov

Michael Weismiller, DOE Technology Development Manager

U.S. Department of Energy
E-mail: Michael.Weismiller@ee.doe.gov

Start Date: October 1, 2017	End Date: September 30, 2018	
Project Funding (FY18): \$505,000	DOE share: \$505,000	Non-DOE share: \$0

Project Introduction

Fuel injection systems are one of the most important components in the design of combustion engines with high efficiency and low emissions. A detailed understanding of the fuel injection process and the mechanisms of spray atomization is needed to implement advanced combustion strategies with improved engine performance. X-ray diagnostics can provide unique data in the study of fuel injection; they are highly penetrative and can generate quantitative, unambiguous measurements of useful spray properties, even in the optically opaque region very near the nozzle. This project uses X-ray diagnostics of sprays to provide insight into the fundamentals of sprays and to generate quantitative data for development and validation of advanced injection simulations.

Objectives

- Complete measurements of near-nozzle surface area in diesel sprays covering a range of injector geometries and operating conditions; collaborate with simulation groups to incorporate this data in their simulations
- Optimize the workflow for data collection and analysis of X-ray tomography measurements of fuel injectors; deliver a high-resolution, three-dimensional (3D) model of a production gasoline injector nozzle that is ready for computational fluid dynamics (CFD)
- Complete measurements and analysis of a cavitating diesel nozzle, including high-resolution measurements of its geometry, valve motion, internal cavitation, and external fuel distribution

Approach

The aim of this project is to develop and perform high-precision measurements of fuel injection and sprays to further the development of accurate computational spray models. These measurements are performed at the Advanced Photon Source at Argonne National Laboratory. This source provides a very-high-flux beam of X-rays, enabling quantitative, time-resolved measurements of sprays with very high spatial resolution. The X-rays are used for five different measurement techniques: tomography to measure injector nozzle geometry, radiography to measure spray density, phase contrast imaging to acquire high-speed images, fluorescence to track atomic elements, and small-angle scattering to measure droplet size [1]. Each of these techniques complements other diagnostics by providing unique and useful information that cannot be obtained in other ways.

In the process of making these measurements, Argonne collaborates with industrial partners including engine and fuel injection system manufacturers. Industry access to these diagnostics increases the understanding of the fundamental science behind their products. The group also collaborates with spray modelers to incorporate this previously unknown information about the spray formation region into new models. This leads to an

improved understanding of the mechanisms of spray atomization and facilitates the development of fuel injection systems designed to improve efficiency and reduce pollutants.

In addition to measurements of injectors and sprays, the group explores other applications of X-ray diagnostics for combustion research. Measurements of cavitating flows provide unique data to improve the fundamental understanding of internal fuel flow and its role in spray atomization, as well as the relationship between injector geometry, cavitation, and nozzle damage. Recent measurements have also evaluated the use of X-rays as a diagnostic for shock tubes, natural gas injectors, and spark ignition. These new applications broaden the impact of the work and help to improve the fundamental understanding in other areas important to advanced combustion, including fundamental chemistry, gas jets, and ignition.

Results

A significant amount of effort over the last several years has been spent performing experiments in collaboration with the Engine Combustion Network (ECN) [2,3,4]. This collaboration is led by Sandia National Laboratories, who have defined a specific set of operating conditions and procured a set of shared hardware. Argonne uses its full suite of unique injector and spray diagnostics to contribute to the ECN community. This partnership puts Argonne's data in the hands of simulation groups worldwide and maximizes the impact of the work on improving computational simulations of sprays, combustion, and engines.

In Fiscal Year 2018, the near-nozzle surface area was measured for diesel sprays using two ECN diesel injectors at several operating conditions. Measurements were performed using ultra-small-angle X-ray scattering, which measures the angular distribution of X-ray scattering to quantify the surface area in the spray [5]. These measurements are unique; other diagnostics of surface area or drop size are restricted by the high number density of droplets in the near-nozzle region. Ultra-small-angle X-ray scattering measurements were used to make a comparison between the ECN Spray C and Spray D injectors. Both Sprays C and D are single-hole, heavy-duty diesel injectors, but while D is close to a production geometry with smoothed interior surfaces and a tapered hole, C is designed to promote cavitation, with sharp corners and a cylindrical hole. The effects of the internal geometry and cavitation are manifested in the near-nozzle surface area, as shown in Figure I.7.1. Spray C shows a higher surface area near-nozzle than Spray D, presumably because cavitation inside the nozzle promotes breakup in the near-nozzle region. As the spray moves downstream, Spray C shows a lower surface area. This is because the more highly atomized Spray C has spread more rapidly, and there is less fuel in the probe volume.

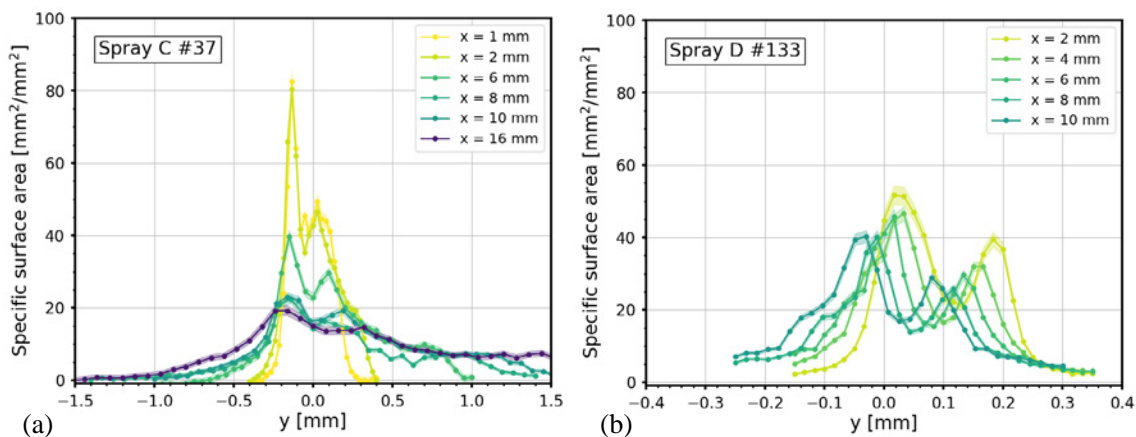


Figure I.7.1. Near-nozzle spray surface area in ECN Spray C (a) and Spray D (b) injectors measured using ultra-small-angle X-ray scattering

In Figure I.7.2, the surface area for the non-cavitating Spray D is shown for several distances downstream of the nozzle exit. The valley at the center of the surface area distributions in Figure I.7.2 (also apparent in Figure I.7.1) is likely caused by ligament structures in the core of the spray, which have lower surface area compared to atomized droplets. These ligaments break up as the spray moves downstream, and the surface area distributions evolve to approximate a normal distribution indicative of a well-atomized jet. While not shown in these figures, this core breakup has been found to occur closer to the nozzle with higher injection or ambient

pressure. Nozzle geometry, needle motion, near-nozzle spray density, and near-nozzle surface area have now all been measured for both Sprays C and D. These have been shared with ECN modeling groups, and the results were used extensively for model validation at the recent ECN6 Workshop [6].

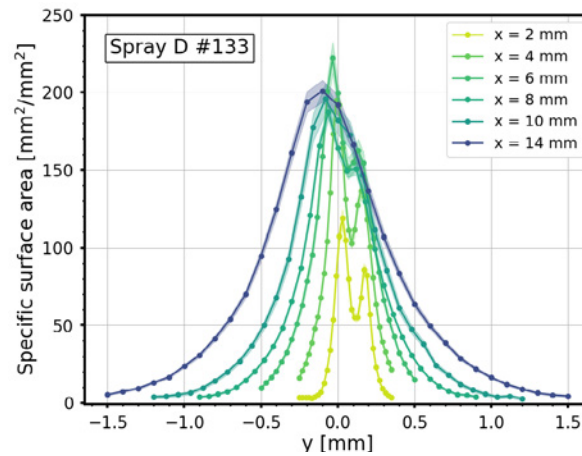


Figure I.7.2. Near-nozzle spray surface area in ECN Spray D as a function of transverse position, shown for several distances from the injector nozzle

Figure I.7.3 shows a 3D rendering of the tip of a gasoline direct injector based on X-ray tomography measurements. While the measurement capability was demonstrated in 2017, the geometries that were delivered were not suitable for importing directly into CFD simulation software. Instead, there were several flaws. The geometries contained gaps, the vectors that define surface normals were not consistently oriented, and the file sizes were intractable for typical computer workstations. This year, significant effort was put into refining the workflow for generating 3D nozzle geometries based on the high-precision measurements. Procedures have been developed to repair the geometries, the file size has been decreased by eliminating superfluous information, and inlet plenums for flow development have been added. The geometries that are now being delivered are ready for CFD, with minimal work required by simulation groups. It is expected that these improvements will increase the number of groups that use the injector geometries that are delivered. Perhaps more importantly, CFD groups will no longer need to make modifications to the geometries. This will help to ensure that simulation results performed by different institutions are directly comparable to one another. This will allow simulation approaches to be compared side-by-side, without the ambiguity introduced by different nozzle geometries.

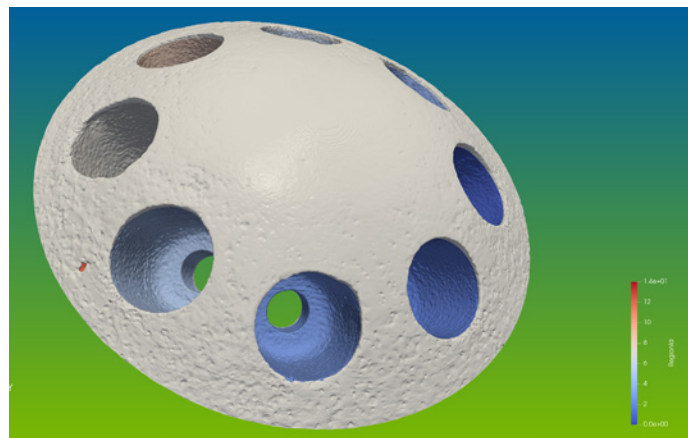


Figure I.7.3. A view of the outside surface and hole counter bores of an ECN Spray G injector

Figure I.7.4 shows a series of measurements performed on the ECN Spray C injector. At left is a rendering of the view from inside the sac looking out the spray nozzle. It can be seen that the boundary between sac and nozzle has a relatively sharp corner. In Spray C, this inlet corner radius is intentionally kept small in order to promote cavitation. Our measurements found, however, that the inlet corner radius varied by a factor of two depending on location. This causes cavitation to form preferentially at the locations where this corner is most sharp, with minimal cavitation where the corner is more rounded. This is seen in the center of Figure I.7.4, which is an X-ray image through the steel nozzle, with the sac at left and outlet at right. Along the upper edge of the nozzle, the white band shows a large region of cavitation vapor formed by fuel passing over the sharpest corner. This region of very intense cavitation extends the full length of the nozzle, and even manifests itself in the emerging liquid jet, as seen at the right of Figure I.7.4. This is an X-ray tomography measurement of the liquid jet's density distribution in a plane 100 μm downstream of the nozzle exit. The bright orange shows regions of high liquid density, while darker colors indicate low density. It can be seen that the distribution has a large region of low density at the upper part of the jet. This region corresponds with the region of cavitation imaged inside the injector, and with the sharpest corner measured in the nozzle geometry. These data have been openly shared with the modeling community and were used extensively for model validation at the ECN6 Workshop [6].

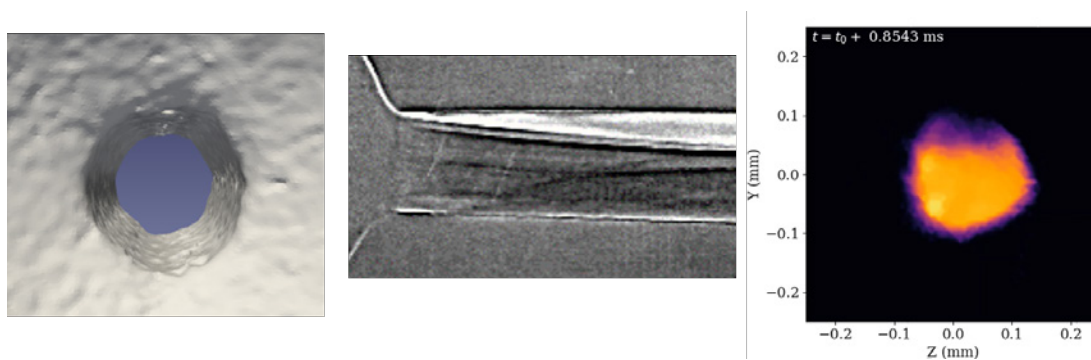


Figure I.7.4. Measurements of the ECN Spray C injector, including nozzle geometry (left), high-speed X-ray imaging of cavitation inside the nozzle (center), and a cross-section of the fuel density as it first emerges from the injector nozzle (right)

Conclusions

X-ray diagnostics can reveal the flows inside fuel injectors as well as diagnose the mixing of fuel and air. Such measurements are not possible using other imaging techniques and represent a powerful data set for development and validation of computational models of fuel flow. This data is crucial for the development of accurate spray models and for the detailed understanding of spray behavior. Improvements to these models will speed the development of cleaner, more efficient engines.

Key Publications

1. Matusik, Katarzyna E., Daniel J. Duke, Alan L. Kastengren, Nicholas Sovis, Andrew B. Swantek, and Christopher F. Powell. 2017. "High-Resolution X-Ray Tomography of Engine Combustion Network Diesel Injectors." *International Journal of Engine Research*, <https://doi.org/10.1177/1468087417736985>.
2. Battistoni, Michele, Gina M. Magnotti, Caroline L. Genzale, Marco Arienti, Katarzyna E. Matusik, Daniel J. Duke, Jhoan Giraldo, Jan Ilavsky, Alan L. Kastengren, Christopher F. Powell, and Pedro Marti-Aldaravi. 2018. "Experimental and Computational Investigation of Subcritical Near-Nozzle Spray Structure and Primary Atomization in the Engine Combustion Network Spray D." *International Journal of Fuels and Lubricants*, <https://doi.org/10.4271/2018-01-0277>.

3. Kim, Sayop, Gabrielle Martinez, Gina Magnotti, Benjamin Knox, Alan Kastengren, Katarzyna E. Matusik, Brandon A. Sforzo, Christopher F. Powell, Tommaso Lucchini, Gianluca D'Errico, and Caroline Genzale. 2018. "Validation of a New Turbulence-Induced Lagrangian Primary Breakup Model for Diesel Spray Atomization." 14th International Conference on Liquid Atomization and Spray Systems, Chicago, IL, July 2018.
4. Torelli, Roberto, Brandon A. Sforzo, Katarzyna E. Matusik, Alan L. Kastengren, Kamel Fezzaa, Christopher F. Powell, Sibendu Som, Yuanjiang Pei, Tom Tzanetakis, Yu Zhang, and Michael Traver. 2018. "Numerical Study of Shot-to-Shot Variability in a Diesel Injector Using Real Geometry, Gasoline-Like Fuels, and Short Injection Durations." 14th International Conference on Liquid Atomization and Spray Systems, Chicago, IL, July 2018.
5. Matusik, Katarzyna E., Brandon A. Sforzo, Hee Je Seong, Alan L. Kastengren, Jan Ilavsky, and Christopher F. Powell. 2018. "X-Ray Measurements of Fuel Spray Specific Surface Area and Sauter Mean Diameter for Cavitating and Non-Cavitating Diesel Sprays." 14th International Conference on Liquid Atomization and Spray Systems, Chicago, IL, July 2018.
6. Sforzo, Brandon A., Katarzyna E. Matusik, Christopher F. Powell, Alan L. Kastengren, Shane Daly, Scott Skeen, Emre Cenker, Lyle M. Pickett, Cyril Crua, and Julien Manin. 2018. "Fuel Nozzle Geometry Effects on Cavitation and Spray Behavior at Diesel Engine Conditions." 10th International Symposium on Cavitation, Baltimore, MD, May 2018.
7. Torelli, Roberto, Katarzyna E. Matusik, Brandon A. Sforzo, Alan L. Kastengren, Christopher F. Powell, Sibendu Som, Yuanjiang Pei, Tom Tzanetakis, and Michael Traver. 2018. "In-Nozzle Cavitation-Induced Orifice-to-Orifice Variations Using Real Injector Geometry and Gasoline-Like Fuels." 10th International Symposium on Cavitation, Baltimore, MD, May 2018.
8. Torelli, Roberto, Katarzyna Matusik, Kyle Nelli, Alan L. Kastengren, Kamel Fezzaa, Christopher F. Powell, Sibendu Som, Yuanjiang Pei, Tom Tzanetakis, Yu Zhang, Michael Traver, and David J. Cleary. 2018. "Evaluation of Shot-to-Shot In-Nozzle Flow Variations in a Heavy-Duty Diesel Injector Using Real Nozzle Geometry." SAE Paper No. 2018-01-0303, SAE 2018 World Congress, Detroit, MI, April 2018.
9. Battistoni, Michele, Gina M. Magnotti, Caroline L. Genzale, Marco Arienti, Katarzyna E. Matusik, Daniel J. Duke, Jhoan Giraldo, Jan Ilavsky, Alan L. Kastengren, Christopher F. Powell, and Pedro Marti-Aldaravi. "Experimental and Computational Investigation of Subcritical Near-Nozzle Spray Structure and Primary Atomization in the Engine Combustion Network Spray D." SAE Paper No. 2018-01-0277, SAE 2018 World Congress, Detroit, MI, April 2018.

References

1. Kastengren, A.L., and C.F. Powell. 2014. "Synchrotron X-Ray Techniques for Fluid Dynamics." *Experiments in Fluids* 55: 1686.
2. Kastengren, A.L., F.Z. Tilocco, C.F. Powell, J. Manin, L.M. Pickett, R. Payri, and T. Bazyn. 2012. "Engine Combustion Network (ECN): Measurements of Nozzle Geometry and Hydraulic Behavior." *Atomization & Sprays* 22 (12): 1011–1052.
3. Battistoni, M., G.M. Magnotti, C.L. Genzale, M. Arienti, K.E. Matusik, D.J. Duke, J. Giraldo, J. Ilavsky, A.L. Kastengren, C.F. Powell, and P. Marti-Aldaravi. 2018. "Experimental and Computational Investigation of Subcritical Near-Nozzle Spray Structure and Primary Atomization in the Engine Combustion Network Spray D." *International Journal of Fuels and Lubricants*, <https://doi.org/10.4271/2018-01-0277>.

4. Matusik, K.E., D.J. Duke, N. Sovis, A.B. Swantek, C.F. Powell, R. Payri, D. Vaquerizo, S. Giraldo-Valderrama, and A.L. Kastengren. 2017. "A Study on the Relationship between Internal Nozzle Geometry and Injected Mass Distribution of Eight ECN Spray G Nozzles." ILASS–Europe 2017, 28th Annual Conference on Liquid Atomization and Spray Systems, Valencia, Spain, September 2017.
5. Kastengren, A.L., J. Ilavsky, J. Viera, R. Payri, D. Duke, A. Swantek, F.Z. Tilocco, N. Sovis, and C.F. Powell. 2017. "Measurements of Droplet Size in Shear-Driven Atomization Using Ultra-Small Angle X-Ray Scattering." *International Journal of Multiphase Flow* 92: 131–139, <http://dx.doi.org/10.1016/j.ijmultiphaseflow.2017.03.005>.
6. 6th Workshop of the Engine Combustion Network:
<https://ecn.sandia.gov/ecn-workshop/ecn6-workshop/>

Acknowledgements

Measurements were performed at the 7BM, 9ID, and 32ID beamlines of the Advanced Photon Source at Argonne National Laboratory. Use of the Advanced Photon Source is supported by the U.S. Department of Energy under Contract No. DEAC0206CH11357. Thanks also to Alan Kastengren, Katarzyna Matusik, Brandon Sforzo, and Aniket Tekawade of Argonne National Laboratory.

I.8 RCM Studies to Enable Gasoline-Relevant Low Temperature Combustion (Argonne National Laboratory)

S. Scott Goldsborough, Principal Investigator

Argonne National Laboratory
9700 S. Cass Avenue
Argonne, IL 60439
E-mail: scott.goldsborough@anl.gov

Michael Weismiller, DOE Technology Development Manager

U.S. Department of Energy
E-mail: Michael.Weismiller@ee.doe.gov

Start Date: October 1, 2017	End Date: September 30, 2018	
Project Funding (FY18): \$370,000	DOE share: \$370,000	Non-DOE share: \$0

Project Introduction

Accurate, predictive combustion models are necessary towards the reliable design and control of next-generation engines able to meet mandated fuel economy and emissions standards, with associated reductions in development times and costs for new configurations [1]. The imprecision of available models prevents adoption of detailed simulation techniques within current design processes. Existing engineering-scale models can achieve satisfactory performance at some operating points; however, they are not sufficiently robust to cover complete ranges of conventional engine operation, or when novel/advanced combustion concepts are utilized. Towards this, there is a critical need to improve the understanding of the multiple physical and chemical processes that occur within combustion engines, including chemical ignition, fluid-chemistry interactions, and pollutant formation/decomposition. To advance these understandings, fundamental data are necessary which can be acquired at conditions that are representative of engine combustion chambers, and can be acquired with sufficiently low experimental uncertainties. In particular, there is a lack of data to quantify the autoignition behavior of full-boiling-range fuels, to formulate robust multi-component surrogate blends to replicate these fuels, and to develop/validate chemical kinetic models for individual constituents and blends. Moreover, the capability to accurately estimate and reduce uncertainties in kinetic models of transportation fuels is not satisfactorily advanced.

Objectives

Overall Objectives

- Acquire autoignition data using Argonne National Laboratory's (ANL's) rapid compression machine (RCM) at conditions representative of today's and future internal combustion engines, including high pressure ($P = 15\text{--}80$ bar), low-to-intermediate temperatures ($T = 650\text{ K--}1,100\text{ K}$), and a range of fuel loadings
- Improve understandings of advanced compression ignition phenomena and develop modeling capabilities for full-boiling-range fuels
- Collaborate with combustion researchers within DOE's Vehicle Technologies Office and Basic Energy Science programs to accurately quantify uncertainties in chemical kinetic models in order to improve their predictability for a range of fuels

Fiscal Year (FY) 2018 Objectives

- Acquire new ignition measurements for multi-component surrogate blends to mimic "neat" and ethanol-blended gasolines; evaluate and quantify performance of surrogate formulation approaches

- Acquire autoignition measurements for a full-boiling-range, market-representative E10 (fuel blend with 90% gasoline, 10% ethanol) gasoline
- Quantify autoignition behavior of neat and bi-component blends of selected aromatic and olefinic compounds found in commercial gasolines covering a range of thermodynamic and fuel loading conditions
- Coordinate RCM Workshop activities (2nd Characterization Initiative, CFD [Computational Fluid Dynamics] Study); organize 4th International RCM Workshop

Approach

RCMs are sophisticated experimental tools that can be employed to acquire fundamental insight into fuel ignition and pollutant formation chemistry, as well as fluid-chemistry interactions, especially at conditions that are relevant to advanced, low-temperature combustion concepts, as well as boosted spark-ignition strategies [2]. They are capable of creating and maintaining well-controlled, elevated temperature and pressure environments (e.g., $T = 600\text{ K}–1,100\text{ K}$, $P = 5–80\text{ bar}$), where the chemically active period preceding autoignition can be monitored and probed via advanced in situ and ex situ diagnostics. The ability to utilize wide ranges of fuel and oxygen concentrations within RCMs, from ultra-lean to over-rich (e.g., $\phi = 0.2–2.0+$), and span dilute to oxy-rich regimes (e.g., $O_2 = 5\%$ to $>21\%$) offers specific advantages relative to other laboratory apparatuses such as shock tubes and flow reactors, where complications can arise. The exothermic behavior of fuels at such conditions is not well characterized, even though this is important towards a range of combustion engine phenomena. Furthermore, the understanding of interdependent, chemico-physical phenomena, like “non-uniform ignition,” that can occur at some conditions within RCMs is a topic of ongoing investigation within the combustion community, while interpretation of facility influences on datasets is also being addressed [3]. Approaches to implement novel diagnostics that can provide more rigorous constraints for model validation compared to integrated metrics such as ignition delay times, e.g., quantification of important radical and stable intermediates such as H_2O_2 and C_2H_4 [4,5], are under development by combustion researchers.

ANL’s twin-piston RCM is utilized in this project to acquire data necessary for a broad range of fuels, while improvements to the facility’s hardware and data analysis protocol are performed to extend its capabilities and fidelity. Multi-disciplinary collaborations are undertaken at ANL and other U.S. laboratories, as well as with researchers at national and international institutions, including complementary RCM facilities.

Results

Key accomplishments for FY 2018:

- Formulated a novel methodology to quantify heat release rates and accumulated heat release for pressure-based, RCM autoignition measurements to facilitate evaluation of chemical kinetic model predictions of preliminary and main exothermicity, and for fuel-to-fuel comparisons; demonstrated the technique using a primary reference fuel (PRF) blend across wide ranges of temperature and pressure
- Expanded database of autoignition measurements for RD5-87, a research-grade, full-boiling-range, U.S. market representative E10 regular gasoline (research octane number [RON] = 92, motor octane number [MON] = 84.5), over wide ranges of temperature and pressure
- Acquired RCM data for an E10 regular gasoline as part of the Coordinating Research Council (CRC) Fuels for Advanced Combustion Engines Working Group’s AVFL31b project
- Acquired autoignition data for three single-ring methylated aromatics, including toluene, o-xylene, and 1,2,4-trimethyl benzene, across a range of temperatures at two engine-representative pressures
- Acquired autoignition data for a prototypical iso-olefin, 2-methyl 2-butene, covering a wide range of stoichiometry and temperature/pressure conditions
- Organized the 4th International RCM Workshop at Trinity College Dublin in conjunction with the 37th International Symposium on Combustion

Heat release analysis (HRA) has a long history in application to both internal combustion engines and fundamental apparatuses, providing a means to derive insight into governing chemical and physical processes in situations where direct measurement is challenging or not practical. Applications exist also for numerical simulations. As discussed in Goldsborough, et al. [6], significant potential exists to extract a wealth of information from RCM pressure-time histories via HRA, including (a) providing additional targets for evaluation and improvement of chemical kinetic models; (b) quantifying the evolution and trends of preliminary and main exothermicity, i.e., low-, intermediate-, and high-temperature heat release, for various fuels; and (c) detecting the existence of non-uniform ignition phenomena during an RCM test. Past works have discussed challenges with application of HRA to RCM datasets and how to achieve rigorous, quantitative results. Challenges include properly representing physical phenomena in the reaction chamber (e.g., heat loss to the walls, growth of the boundary layer, gas flow to the crevice, and condensation of heavy fuels near cold surfaces); describing the thermophysical properties of the reacting mixture, including changes in composition; and adequately recording the time-varying conditions in the reaction chamber, with minimal perturbation by the data acquisition system.

A novel methodology to apply HRA to RCM measurements was formulated through this project, and experiments were conducted to demonstrate the approach. A PRF blend (90% iso-octane, 10% n-heptane vol/vol) was used at stoichiometric fuel/O₂ ratios, diluted in nitrogen/argon gas to 11.5% O₂, where the compressed temperature range covered $T_c = 715\text{--}940\text{ K}$ ($\Delta T_c \sim 27\text{ K}$), with compressed pressures of $P_c = 20\text{--}70\text{ bar}$ ($\Delta P_c = 10\text{ bar}$) [6]. Simulations were also conducted at the same conditions using an updated version of the Lawrence Livermore National Laboratory (LLNL) gasoline surrogate model [7]. Figure I.8.1 presents representative heat release rates (HRRs) plotted as a function of the time-integrated, or accumulated, heat release (aHR) for (a) experiment and (b) model results. The parameters are normalized against the heating value of the mixture. The trajectories start at the origin and progress in a clockwise manner, where heat loss eventually absorbs all of the chemical energy. Immediately evident in Figure I.8.1a is that none of the experimental cases achieves an aHR greater than 0.8, meaning that 20% of the fuel energy is not properly taken into account in the HRA framework. This is due to an incorrect tracking of the physical losses in the current formulation, which can be influenced by the exothermic events and resulting higher gas temperature/pressure. The situation is most severe at $P_c = 20\text{ bar}$, where the time lag between the first-stage and main ignition is the longest, allowing for greater energy loss from the mixture, especially in the crevice. At the highest T_c 's in this dataset, though, the HRRs are rapid enough so that peak aHRs are > 0.9 . Also discernable in Figure I.8.1a is that the peak aHRs for $P_c \geq 60\text{ bar}$ are consistent with the $P_c = 50\text{ bar}$ case, highlighting that piston rebound, which occurs at the higher pressures, does not significantly alter the HRR calculations as discussed in [1]. Finally, there is excellent shot-to-shot repeatability in the HRR-aHR curves. This is found to be true, even for conditions where preliminary exothermicity occurs before the end of piston compression. The inset in Figure I.8.1a highlights early exothermic behavior. Low-temperature heat release (LTHR) is identifiable as a “bump,” where the HRR first increases and then decreases. The end of first-stage ignition can be demarcated at the second inflection point; for instance, at $P_c = 20\text{ bar}$, the end of first-stage ignition occurs at $\text{aHR} = 3.9\%$, while at $P_c = 70\text{ bar}$, it occurs at close to $\text{aHR} = 6.8\%$. Thus, as pressure is increased, there is an increase in the rapidity of LTHR, as well as the magnitude of integrated heat release. These trends are similar to those observed in engine measurements [8]. At first order, the shifts should be expected due to higher reactant concentrations; however, there is also a change in the flux through low-temperature chemical pathways, such as $\dot{R} + \text{O}_2(+M) = \text{RO}\dot{\text{O}}(+M)$.

The model results presented in Figure I.8.1b indicate that, while the global trends are very similar to the experiments, there are noticeable differences in the preliminary and main heat release processes. For instance, the shapes of the HRR curves are distinctive compared to those seen in Figure I.8.1a where the influence of pressure is more substantial in the model. Furthermore, $\text{aHR} \rightarrow 1.0$ for nearly all of the model results, though dissociation of CO₂, etc., after ignition can reduce these values. More rigorous accounting of the physics in the experiment would ensure quantitative comparisons between the two results. Nevertheless, it is now possible to conduct perturbation/sensitivity analyses for additional parameters beyond ignition delay times. For instance, using the temperature at the starts of intermediate- and high-temperature heat release, across the range of T_c

and P_c , could lead to better understanding of kinetic features, such as HO_2 chemistry, that cause the observed trends, and could result in more robust models for gasoline.

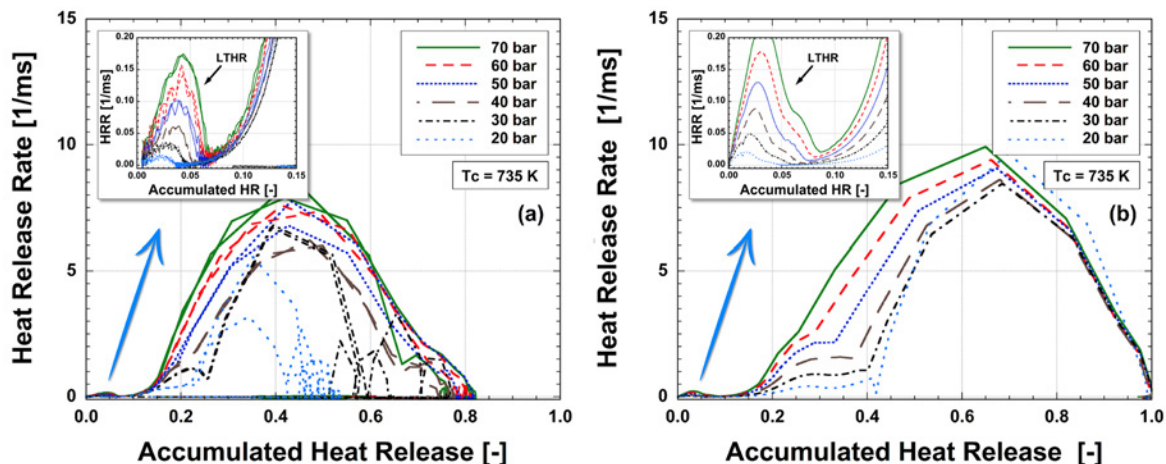


Figure I.8.1. Calculated normalized HRRs for PRF90/ O_2 /diluent mixture at $T_c = 735$ K, presented as a function of aHR, illustrating exothermic trends across a range of P_c for (a) experimental measurements and (b) LLNL model predictions [6]. Insets highlight preliminary exothermicity, e.g., LTHR before transition to high-temperature heat release. Two experimental tests conducted at each condition demonstrate very good consistency.

Experiments were also conducted in FY 2018 towards improving the formulation methodology for multi-component surrogate mixtures of full-boiling-range gasolines. Of particular interest is the capability to capture perturbation effects of ethanol, covering a range of blend ratios. This ability, for ethanol or other blending agents, is critical for creating robust empirical correlations, as well as accurately simulating fuel effects in advanced combustion engines. Previously, bi- to multi-component surrogates for FACE-F, one of the mid-octane gasolines created by the CRC [9], were evaluated using autoignition measurements in the ANL RCM. The four surrogates, which exhibited similar behavior as the neat gasoline, demonstrated poor response to ethanol, however [10]. A new collaboration was initiated with Trinity College Dublin to evaluate functional group approaches for surrogate formulation [11]. Two iterations for FACE-F, including a seven-component FGF-TCD1 and a nine-component FGF-TCD3, were tested along with ethanol blends. The results, while not completely successful, were encouraging, and this effort is continuing in FY 2019 with adjustments to surrogate component selection, as well as compositional adjustment.

A sweep of experiments was conducted with RD5-87, a research-grade, U.S. market representative E10 gasoline (RON = 92, MON = 84.5), to extend the database of autoignition measurements begun in FY 2017. The new tests in FY 2018 covered temperatures, pressures, and fuel loadings representative of the operating conditions in Sandia's low-temperature gasoline combustion engine, specifically $T_c = 700$ K–950 K and $P_c = 15$ –80 bar. This will facilitate direct comparisons between the RCM database and trends observed in the engine data. The new RCM measurements also provide useful targets for the updated LLNL gasoline surrogate model, while being useful for additional targets of multi-component surrogates.

Experiments were conducted with another E10 full-boiling-range gasoline as part of the CRC Fuels for Advanced Combustion Engines Working Group's AVFL31b project. The fuel matrix for that work utilizes nineteen gasoline-type fuels of varying RON, sensitivity, and ethanol content formulated for CRC AVFL20 [12]. Fuel #1 (RON = 91, MON = 84.5) was used in the FY 2018 tests with conditions selected for direct comparison against analogous measurements made at the Massachusetts Institute of Technology's Sloan Automotive Laboratory.

An extensive sweep of tests was also performed to quantify the autoignition behavior of three single-ring methylated aromatics, including toluene, *o*-xylene (OXYL), and 1,2,4-trimethyl benzene (124TMB). A recently updated chemical kinetic model from LLNL, where low-temperature chemistry for OXYL and 124TMB was

added, was used for comparisons against the RCM measurements. The tests employed stoichiometric and lean mixtures of fuel/O₂/diluent, where the O₂ concentration was diluted to near 12.5%. Temperatures spanned 830–1,100 K, with pressures of 25 bar and 45 bar. Unlike in previous works, there was little evidence of non-uniform ignition phenomena across all of the test conditions explored. As expected, toluene was found to be least reactive at test conditions below about 1,000 K. This lower level of reactivity for toluene, relative to OXYL and 124TMB, was well predicted by the kinetic mechanism. An interesting trend was observed in the experiments where OXYL was more reactive than 124TMB at low temperatures while 124TMB became more reactive at high temperatures. The cross-over in reactivity observed around 900 K was captured by the kinetic mechanism. Besides properly replicating the relative reactivity of OXYL and 124TMB, the mechanism also appeared to do a good job in quantitatively matching the measured ignition delays, with differences in experimental and simulated values generally within $\pm 20\%$. The experimental and simulated discrepancies were slightly higher for toluene ($\pm 30\text{--}35\%$) at the test conditions investigated.

Autoignition data were acquired for a prototypical iso-olefin, 2-methyl 2-butene, with the test conditions covering a range of stoichiometry, temperature, and pressure ($\phi = 0.5\text{--}2.0$, $T_c = 685\text{--}1,000\text{ K}$, $P_c = 25\text{ bar}$ and 45 bar). Collaborations are ongoing with LLNL to utilize these new data for improvements to the alkene sub-mechanism of the gasoline surrogate model. These data will also be used in FY 2019 as a benchmark to quantify and understand how aromatics and olefins chemically interact during autoignition at engine-relevant conditions.

Finally, coordinating activities were undertaken in FY 2018 for the International RCM Workshop. The Workshop is a collaborative forum where experimentalists, modelers, and theoreticians work synergistically to better understand the chemical and physical processes that occur within low-temperature combustion and other engine regimes via RCM and related experimental platforms. A 2nd Characterization Initiative was begun in FY 2018 to better understand facility-to-facility and platform-to-platform influences on the measurements. Ethanol was selected for use as the fuel, with experimental tests performed at ten institutions covering two fuel loadings, two compressed pressures, and a range of compressed temperatures. The Workshop also began collaborative CFD investigations of RCM dynamics. The 4th Meeting was organized and held at Trinity College Dublin in conjunction with the 37th International Symposium on Combustion and four other workshops (Turbulent Non-premixed Flame, Premixed Turbulent Flame, International Sooting Flame, and Flame Chemistry). The meeting was attended by more than 60 participants and covered industrial viewpoints, the 2nd Characterization Initiative, and CFD applications, as well as best practices for measurements, repositories and standards, and translating RCM measurements to engine combustion.

Conclusions

- A novel methodology was formulated to apply HRA to RCM measurements, demonstrated via experiments conducted using PRF90 across a wide range of compressed conditions.
- Two surrogate mixtures for FACE-F were created using functional-group-based approach, and tests were conducted using neat and ethanol-blended fuels.
- ANL's RCM has been used to acquire additional autoignition data for a research-grade, U.S. market representative, E10 gasoline over a range of conditions representative of Sandia's low-temperature gasoline combustion engine.
- ANL's RCM has been used to acquire autoignition data for three single-ring methylated aromatics, including toluene, OXYL, and 124TMB.
- ANL's RCM has been used to acquire autoignition data for a prototypical iso-olefin, 2-methyl 2-butene.
- RCM Workshop activities were coordinated (2nd Characterization Initiative, CFD Study), and the 4th International RCM Workshop was organized and held at Trinity College Dublin.

Key Publications

1. Goldsborough, S.S., J. Santner, D. Kang, A. Fridlyand, T. Rockstroh, and M.C. Jespersen. 2018. "Heat Release Analysis for Rapid Compression Machine Experiments: Challenges and Opportunities." *Proc. Combust. Inst.*, <https://doi.org/10.1016/j.proci.2018.05.128>.
2. Kang, D., A. Fridlyand, S.S. Goldsborough, M. Mehl, S. Wagnon, W.J. Pitz, and M.J. McNenly. 2018. "Autoignition Study of FACE-F Gasoline and Its Surrogates at Advanced IC Engine Conditions." *Proc. Combust. Inst.*, <https://doi.org/10.1016/j.proci.2018.08.053>.
3. Kukkadapu, G., D. Kang, S.W. Wagnon, K. Zhang, M. Mehl, M. Monge-Palacios, H. Wang, S.S. Goldsborough, C.K. Westbrook, and W.J. Pitz. 2018. "Kinetic Modeling Study of Surrogate Components for Gasoline, Jet and Diesel Fuels: C7 – C11 Methylated Aromatics." *Proc. Combust. Inst.*, <https://doi.org/10.1016/j.proci.2018.08.016>.
4. Santner, J., and S.S. Goldsborough. 2018. "Hot-Spot Induced Mild Ignition: Numerical Simulation and Scaling Analysis." Submitted to *Combust Flame*.
5. Santner, J., and S.S. Goldsborough. 2018. "Perturbations in Reacting Flows: New Scaling Analyses." WSSCI Spring Technical Meeting, Corvallis, OR.
6. Kodavasal, J., and S.S. Goldsborough. 2018. "A Machine Learning Based Ignition Delay Model for Gasoline-Type Fuels with a Range of Reactivity." CSSCI Spring Technical Meeting, Minneapolis, MN.
7. Santner, J., and S.S. Goldsborough. 2018. "Perturbations in Reacting Flows: New Scaling Analyses." CSSCI Spring Technical Meeting, Minneapolis, MN.
8. Kang, D., and S.S. Goldsborough. 2018. "Progress Quantifying Fuel Reactivity for Model Validation and Fuel Ranking, across a Range of Combustion Scenarios." AEC Winter Review Meeting, Argonne, IL.
9. Kang, D., B. Wagner, and S.S. Goldsborough. 2018. "Progress Quantifying Fuel Reactivity for Model Validation and Fuel Ranking, across a Range of Combustion Scenarios." AEC Summer Review Meeting, Southfield, MI.
10. Goldsborough, S.S., and J. Santner. 2018. "From Mild Ignition to Mixed-Mode Combustion: Parameterizing Flame Dynamics and End Gas Response." AEC Summer Review Meeting, Southfield, MI.

References

1. Basic Research Needs for Clean and Efficient Combustion of 21st Century Transportation Fuels. (http://science.energy.gov/~media/bes/pdf/reports/files/ctf_rpt.pdf)
2. Goldsborough, S.S., S. Hochgreb, G. Vanhove, M.S. Wooldridge, H.J. Curran, and C.-J. Sung. 2017. *Prog. Energy Combust. Sci.* 63: 1–78,
3. Goldsborough, S.S., and J. Santner. "Mining an Experimental Autoignition Database to Hierarchically Identify Facility Influences on the Measurements." In preparation.
4. Bahrini, C., O. Herbinet, P.-A. Glaude, C. Schoemaeker, C. Fittschen, and F. Battin-Leclerc. 2012. *J. Am. Chem. Soc.* 139: 11944–11947.
5. Stranic, I., S.H. Pyun, D.F. Davidson, and R.K. Hanson. 2012. *Combust. Flame* 159: 3242–3250.
6. Goldsborough, S.S., J. Santner, D. Kang, A. Fridlyand, T. Rockstroh, and M.C. Jespersen. "Heat Release Analysis for Rapid Compression Machine Experiments: Challenges and Opportunities." *Proc. Combust. Inst.*, <https://doi.org/10.1016/j.proci.2018.05.128>.

7. Mehl, M., S. Wagnon, K. Tsang, G. Kukkadapu, W.J. Pitz, C.K. Westbrook, Y. Tsang, H.J. Curran, N. Atef, M.A. Rachidi, M.S. Sarathy, and A. Ahmed. 2017. "A Comprehensive Detailed Kinetic Mechanism for the Simulation of Transportation Fuels." LLNL-CONF-725343.
8. Dec, J.E., and Y. Yang. 2010. "Boosted HCCI for High Power without Engine Knock and Ultra-Low NOx Emissions." *SAE Int. J. Engines* 3: 750–767.
9. Cannella, W., M. Foster, G. Gunter, and W. Leppard. 2014. "FACE Gasolines and Blends with Ethanol: Detailed Characterization of Physical and Chemical Properties." CRC Report No. AVFL-24.
10. Kang, D., A. Fridlyand, S.S. Goldsborough, M. Mehl, S. Wagnon, W.J. Pitz, and M.J. McNenly. 2018. "Autoignition Study of FACE-F Gasoline and Its Surrogates at Advanced IC Engine Conditions." *Proc. Combust. Inst.*, <https://doi.org/10.1016/j.proci.2018.08.053>.
11. Won, S.H., F.M. Haas, S. Dooley, T. Edwards, and F.L. Dryer. 2017. "Reconstruction of Chemical Structure of Real Fuel by Surrogate Formulation Based on Combustion Property Targets." *Combust. Flame* 183: 39–49.
12. Sluder, C.S., D.E. Smith, M. Wissink, J.E. Anderson, T.G. Leone, and M.H. Shelby. 2017. "Effects of Octane Number, Sensitivity, Ethanol Content, and Engine Compression Ratio on GTDI Engine Efficiency, Fuel Economy and CO2 Emissions: Final Report." CRC Report No. AVFL-20.

Acknowledgements

This work was performed under the auspices of the U.S. Department of Energy by Argonne National Laboratory under Contract DE-AC02-06CH11357. Experimental measurements were conducted with the assistance of Dongil Kang, Mahir Rafi, Brianna Wagner, Omar Ahmed, and Danielle Markovich. Chemical kinetic modeling was conducted with the assistance of Scott Wagnon, Goutham Kukkadapu, Marco Mehl, William Pitz, and Russell Whitesides (Lawrence Livermore National Laboratory).

I.9 Advances in High Efficiency Gasoline Compression Ignition (Argonne National Laboratory)

Christopher P. Kolodziej, Principal Investigator

Argonne National Laboratory
9700 S. Cass Ave.
Argonne, IL 60439
E-mail: ckolodziej@anl.gov

Michael Weismiller, DOE Technology Development Manager

U.S. Department of Energy
E-mail: Michael.Weismiller@ee.doe.gov

Start Date: October 1, 2017	End Date: September 30, 2018	
Project Funding (FY18): \$390,000	DOE share: \$390,000	Non-DOE share: \$0

Project Introduction

Gasoline is a fuel characterized by higher volatility and lower reactivity than diesel fuel. Typical gasoline-fueled commercial vehicles use an engine with a positive ignition source, such as a spark plug. The maximum compression ratio, and maximum potential indicated thermal efficiency, of gasoline spark ignition engines is limited by knocking combustion at high loads [1]. Gasoline compression ignition (GCI) allows the engine to operate on gasoline fuels with diesel-like efficiency through higher compression ratio, leaner air-fuel ratio, and lower heat transfer losses than gasoline spark ignition engines [2].

The mixture conditions of GCI can vary from fully premixed to partially premixed to mixing-controlled combustion. Mixing-controlled GCI offers the highest injection-based combustion control and lowest emissions of hydrocarbons and carbon monoxide, while fully premixed and partially premixed GCI allow for lower combustion temperatures and therefore lower emissions of oxides of nitrogen (NO_x) and soot [3]. The challenge for mixing-controlled combustion is the relatively high soot and NO_x emissions due to the lack of fuel and air premixing, while for partially to fully premixed combustion the challenges are relatively higher hydrocarbon and carbon monoxide emissions and combustion noise. Mixing-controlled combustion is difficult to achieve with gasoline at low and medium loads due to the relatively long ignition delay (low reactivity) of the fuel compared to diesel. Therefore, some form of partially to fully premixed GCI is generally used in the low- to medium-load range. The reactivity of the fuel-air mixture for partially premixed GCI at low and medium loads is generally controlled by the level of stratification (local richness reduces ignition delay), boost pressure, cylinder temperature, and exhaust gas recirculation (EGR) to maintain stable engine operation under the combustion noise requirements.

Objectives

Overall Objectives

- Increase the efficient use of gasoline
- Reduce the soot and NO_x emissions of compression ignition engines relative to diesel operation

Fiscal Year 2018 Objectives

Improve the knowledge of cylinder conditions necessary for stable part-load GCI combustion with low combustion noise, emissions, and fuel consumption through the following objectives.

- Develop better understanding of injection strategies to control mixture conditions
- Minimize the level of EGR to maintain a fixed NO_x emissions level
- Minimize the boost level required for stable engine operation

Approach

Since the announcement of Mazda’s multi-mode SKYACTIV-X engine in August 2017 and an updated United States Driving Research and Innovation for Vehicle efficiency and Energy sustainability (U.S. DRIVE) Advanced Combustion and Emissions Control Roadmap in March 2018, light-duty GCI research has been refocused on the low- and medium-load areas of the engine operating map [4,5]. To support GCI research in the low- to medium-load range, a 2,000 rpm, 6 bar indicated mean effective pressure (IMEP) test condition was chosen based on recommendations from the Advanced Combustion and Emissions Control Tech Team, based on where light-duty engines most frequently operate in the vehicle drive cycle. A multi-cylinder light-duty diesel engine with a 17.5:1 compression ratio was used to carry out this investigation. While this compression ratio is significantly higher than that of current light-duty gasoline spark ignition engines, it is not too much higher than the expected 15:1–16:1 geometric compression ratio of the Mazda SKYACTIV-X engine [4]. The engine used the stock Bosch CRIP2 common-rail fuel injection system to control the injection pressure, number of injections, and fuel quantity per injection. The fuel used was an 87 AKI (anti-knock index) E10 (90% gasoline, 10% ethanol blend) gasoline.

Combustion noise level has typically been one of the biggest challenges for GCI engines to overcome. It has also been shown that allowing increased combustion noise can increase the efficiency potential of a GCI engine [6]. In this work, parametric sweeps of all tested combustion controls were performed at constant 90 dB combustion noise to develop a method to quickly characterize a given speed-load condition in GCI with a certain piston geometry (compression ratio), injection system, and fuel combination. The soot emissions needed to be less than 0.1 FSN (filter smoke number) for a test point to be considered in the analysis. First, parametric sweeps were performed with the number of injections, timings, and fuel quantity per injection to find the lowest possible indicated specific fuel consumption (ISFC) and indicated specific hydrocarbon (ISHC) and indicated specific carbon monoxide (ISCO) emissions. This first step was performed with no EGR, the minimum boost to maintain each condition to a combustion stability of 3% coefficient of variance of IMEP, and the minimum injection pressure possible for this fueling system (400 bar) for highest fuel stratification. Second, an EGR sweep was performed with a double- and triple-injection strategy to find the required EGR level for a given engine-out NO_x emissions requirement.

Results

The first phase of testing on injection strategies was performed without EGR to allow the widest range of injection parameters to be tested. Combustion noise of 90 dB, less than 0.1 FSN soot emissions, and less than 3% coefficient of variance of IMEP was achieved with the conditions outlined in Table I.9.1 with a single injection. This set the baseline intake temperature and pressure to be used for the remaining parametric sweeps.

Table I.9.1. Engine Operating Conditions of 90 dB Constant Combustion Noise Parametric Sweeps

Parameter	Value
Engine Speed [rpm]	2,000
Engine Load [bar IMEP]	6
Fuel	87 AKI, E10
Injection Pressure [bar]	400
EGR [%]	0
Boost Pressure [bar(a)]	1.44
Intake Air Temp [°C]	50

After setting the baseline conditions with a single-injection strategy, a double-injection strategy was investigated by performing a sweep of pilot-injection quantity and timing. A fixed pilot-injection timing of -70 degrees after top dead center (°aTDC) was chosen for the pilot-injection quantity sweep based on testing from the previous year at 10 bar IMEP. The pilot injection ratio was swept from 40% to 25% (0.6 ms to 0.3 ms injection duration). The combustion noise was maintained at 90 dB at each pilot-injection quantity by adjusting the main injection timing. As can be seen in Figure I.9.1, ISFC, ISHC, and ISCO all decreased with lower pilot-injection quantity, while maintaining a constant combustion noise of 90 dB and less than 0.1 FSN

soot emissions. The pilot-injection quantity of 0.3 ms was the lowest possible with the fuel injection equipment tested. Using the pilot-injection quantity of 0.3 ms, a pilot-injection timing sweep was performed from -70 °aTDC to -24 °aTDC. Over this range of pilot-injection timings, the combustion, emissions, and efficiency were only affected from -70 °aTDC to -65 °aTDC, where ISHC decreased from 5 g/kWh to 3.5 g/kWh. As a result of the pilot-injection quantity and timing sweeps at constant 90 dB, the lowest pilot-injection quantity and a timing of -65 °aTDC were chosen as the optimum injection parameters.

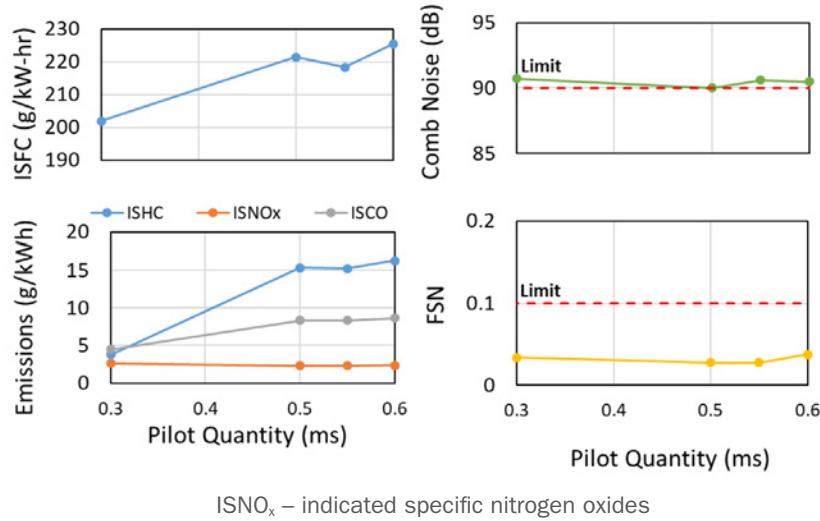


Figure I.9.1. Results of pilot injection quantity sweep at constant 90 dB combustion noise

To test a triple-injection strategy, a third injection was added shortly after the main injection. Figure I.9.2 shows the injector current traces (narrow lines), heat release rates (HRRs, wide lines), and cylinder pressures (medium-thickness lines) of the single-, double-, and triple-injection strategies. The single-injection (blue lines) and double-injection (black lines) strategies had almost the same main injection timing (\approx -16.5 °aTDC) and combustion phasing. The triple-injection (orange line) shows a third injection occurring at 0 °aTDC, which could describe this strategy as an early pilot injection with a late double injection. The pilot duration remained 0.3 ms, but the main (second) injection was reduced because of the addition of the third injection. As a result, the main (second) injection timing could be advanced to -17.4 °aTDC for the same combustion noise level. The overall effect of the added third injection was the combustion phasing could be advanced for the same combustion noise level, which reduced the ISFC, ISHC, and ISCO, while retaining less than 0.1 FSN, compared to both the single- and double-injection strategies (Figure I.9.3).

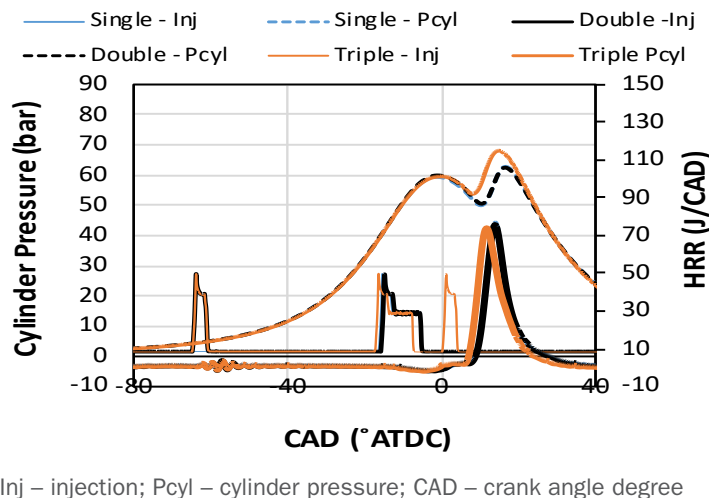


Figure I.9.2. Overview of single-, double-, and triple-injection strategy injection timings and combustion phasings

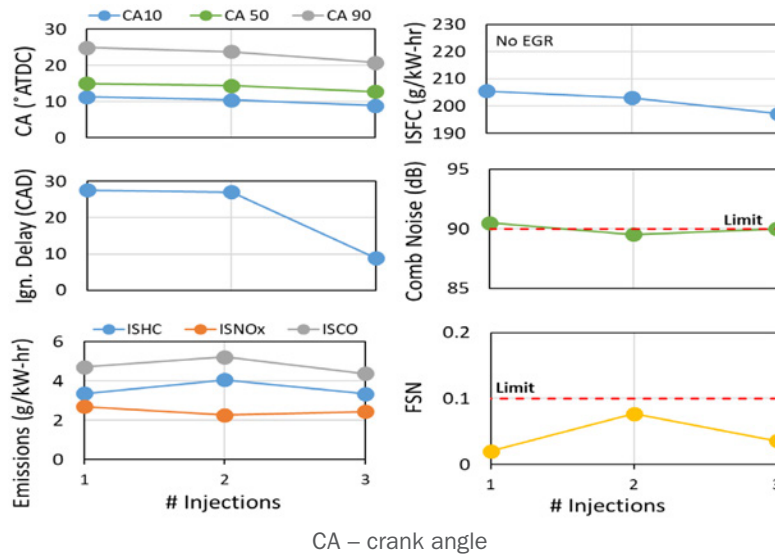


Figure I.9.3. Comparison of single-, double-, and triple-injection results with constant 90 dB combustion noise

Without EGR, ISNO_x emissions were approximately 2–3 g/kWh, depending on injection parameters. Figure I.9.4 shows the effect of EGR on combustion and emissions for both the double- and triple-injection strategies while sweeping EGR at a constant 90 dB combustion noise level. The main (second) injection timing was adjusted earlier with increasing EGR to maintain the combustion noise level. At each EGR level, the triple-injection strategy had earlier autoignition (CA10) and centroid of combustion (CA50), along with lower ISHC, ISCO, and ISFC. With 30% EGR, ISNO_x decreased to 0.6 g/kWh, and it decreased to 0.3 g/kWh with 35% EGR. At a constant combustion noise level, increasing EGR caused a slight reduction in ISHC and ISCO while maintaining ISFC due to the possibility of advancing the main injection timing.

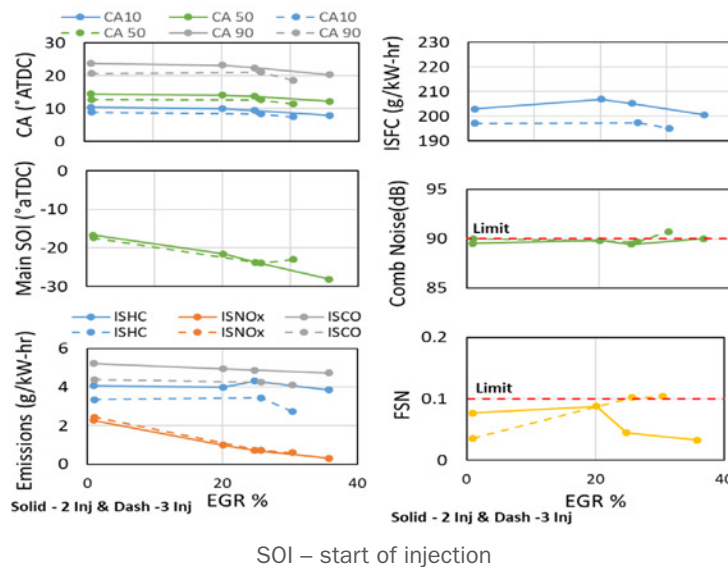


Figure I.9.4. Effects of EGR on combustion and emissions while maintaining constant 90 dB combustion noise

As a result of the 90 dB constant combustion noise parametric sweeps at 2,000 rpm and 6 bar IMEP, ISFC was decreased from 215 g/kWh to 195 g/kWh with a triple-injection strategy and 30% EGR. This was achieved while simultaneously meeting the 0.1 FSN soot emissions target and reducing ISNO_x to 0.6 g/kWh, ISHC to 2.7 g/kWh, and ISCO to 4 g/kWh.

Conclusions

- Given that combustion noise is the most restrictive parameter for higher efficiency with partially premixed GCI, multiple parametric sweeps were performed at constant 90 dB combustion noise to identify opportunities for reduced emissions and fuel consumption.
- Sweeps of single-, double-, and triple-injection strategy parameters led to a triple-injection strategy where one early injection occurs at -65° aTDC and a double injection occurs closer to engine top dead center.
- While increasing EGR to reduce ISNO_x emissions, the triple-injection strategy had consistently lower emissions and ISFC.
- Using the triple-injection strategy with a well-timed late double injection at 90 dB combustion noise, ISFC was reduced from 215 g/kWh to 195 g/kWh while meeting the soot and NO_x emissions targets and achieving lower ISHC and ISCO emissions.

Key Publications

1. Cung, K., and S. Ciatti. 2017. "A Study of Injection Strategy to Achieve High Load Points for Gasoline Compression Ignition (GCI) Operation." ASME ICEF2017-3625.
2. Cung, K., S. Ciatti, S. Tanov, and O. Andersson. 2017. "Low-Temperature Combustion of High Octane Fuels in a Gasoline Compression Ignition Engine." *Front. Mech. Eng.* 21, December 2017.

References

1. Leone, T.G., J.E. Anderson, R.S. Davis, A. Iqbal, R.A. Reese, M.H. Shelby, and W.M. Studzinski. 2015. "The Effect of Compression Ratio, Fuel Octane Rating, and Ethanol Content on Spark-Ignition Engine Efficiency." *Environmental Science & Technology* 49 (18): 10778–10789.
2. Sellnau, M., K. Hoyer, W. Moore, M. Foster, et al. 2018. "Advancement of GDCI Engine Technology for US 2025 CAFE and Tier 3 Emissions." SAE Technical Paper 2018-01-0901, doi:10.4271/2018-01-0901.
3. Zhang, Y., S. Sommers, Y. Pei, P. Kumar, et al. 2017. "Mixing-Controlled Combustion of Conventional and Higher Reactivity Gasolines in a Multi-Cylinder Heavy-Duty Compression Ignition Engine." SAE Technical Paper 2017-01-0696, doi:10.4271/2017-01-0696.
4. Adcock, Ian. 2017. "ICE BREAKER!" *Automotive Engineering*, October 2017, 24.
5. U.S. DRIVE. 2018. "Advanced Combustion and Emission Control Roadmap." March 2018.
6. Ciatti, S. 2013. "Use of Low Cetane Fuel to Enable Low Temperature Combustion." U.S. Department of Energy Vehicle Technologies Office Annual Merit Review.

Acknowledgements

Vasudha Patri, Timothy Rutter, Steve Ciatti, and Doug Longman all played critical roles in the progress of this project.

I.10 Advanced Ignition Systems for Gasoline Direct Injection (GDI) Engines (Argonne National Laboratory)

Riccardo Scarcelli, Principal Investigator

Argonne National Laboratory
9700 S. Cass Avenue
Lemont, IL 60439
Email: rscarcelli@anl.gov

Michael Weismiller, DOE Technology Development Manager

U.S. Department of Energy
E-mail: Michael.Weismiller@ee.doe.gov

Start Date: October 1, 2016	End Date: September 30, 2019	
Project Funding (FY18): \$400,000	DOE share: \$400,000	Non-DOE share: \$0

Project Introduction

Due to the United States' heavy reliance on gasoline engines for automotive transportation, efficiency improvements of advanced gasoline direct injection (GDI) combustion concepts have the potential to dramatically reduce foreign oil consumption. However, combustion strategies such as stratified, dilute, and boosted operation present challenging conditions for conventional ignition systems, thereby limiting the attainable benefits of these advanced combustion concepts.

Advanced ignition systems for GDI engines enable the continued use of conventional combustion systems (reducing cost/risk) while providing potentially substantial benefits to fuel economy. In-depth understanding of the ignition physics and advanced ignition models will aid the development of dilution-tolerant, high-efficiency, and low-emissions GDI combustion systems

Objectives

This research project addresses the technological barrier of limited attainable GDI engine efficiency due to the lack of robust spark ignition dilute combustion technology and controls, which is essentially caused by:

- Limited GDI engine dilute operation.
- Limited assessment of advanced ignition systems enabling dilute combustion in GDI engines.
- Limited availability of modeling tools to evaluate and improve advanced ignition systems.

While the ultimate benefit is the improvement of GDI engine efficiency, the goal of this project is to expand the tools (knowledge and models) to enable significant improvement of the current ignition technology.

Approach

This is a simulation effort that aims at improving the fundamental understanding of advanced ignition processes and building comprehensive models that can be leveraged to potentially simulate any ignition system of interest.

Advanced diagnostics from project partners Sandia National Laboratories and Michigan Technological University are leveraged with the intent to enhance the fundamental understanding of ignition processes of conventional as well as non-conventional technologies and provide datasets for model validation. Non-equilibrium plasma simulations are carried out using the commercial solver VizGlow through a collaboration with Esgee Technologies Inc. The goal of these simulations is to provide proper understanding of the low-temperature plasma (LTP) physics. Novel ignition modeling capabilities are implemented into the computational fluid dynamics (CFD) engine code CONVERGE that is largely used in the automotive industry. The main tasks planned at Argonne are as follows.

- Expand the capabilities of conventional spark ignition models to improve the predictive nature of these models at challenging (boosted and dilute) engine operation
- Improve the fundamental understanding of non-conventional ignition technologies that are being evaluated by the automotive industry
- Build and develop comprehensive models that can be used to simulate non-conventional ignition processes in internal combustion engines
- Use the developed models to guide the research and development of advanced ignition systems to achieve highly dilute and highly efficient combustion in GDI engines

Results

Major accomplishments in FY 2018 can be summarized as follows.

- Sensitivity analysis performed on non-equilibrium plasma simulations
- Improved non-equilibrium plasma simulations quantitatively validated against experiments
- Non-equilibrium plasma simulations coupled with CFD combustion simulations
- LTP ignition processes simulated using the CFD engine code CONVERGE

Sensitivity Analysis Performed on Non-Equilibrium Plasma Simulations

In FY 2017, the non-equilibrium plasma multi-dimensional modeling effort was initiated to numerically study the LTP regime and transition to arc. The VizGlow solver was used to mimic the experiments carried out at Sandia and simulate the non-equilibrium plasma generated from a pin-to-pin electrode configuration at different ambient pressure values. Simulations qualitatively matched the experimental observations consisting of slower, thinner, and increasingly branching streamers at increasing pressure values and correctly captured the transition from LTP regime to undesired arcing at lower pressure values. Simulations predicted the transition to happen at 1.6 bar versus 2.2 bar from experiments. The impact of mesh size on VizGlow simulations was also evaluated.

In FY 2018, several potential causes for the off-set between experiments and simulations were investigated, including gas composition, electrode geometry, and initial electron seeding. Gas composition was found to be the only parameter affecting the LTP-to-arc transition pressure threshold. However, large quantities of combustion residuals (CO_2 and H_2O) had to be added to the stoichiometric mixture to significantly affect the post-discharge regime. Electrode geometry irregularities—locally enhancing the electric field—and initial electron seeding showed significant impact on the streamer induction and propagation process; nevertheless, the post-discharge plasma regime and properties were not affected (Figure I.10.1). Therefore, in an attempt to try to reduce the discrepancy between modeling and experiments, other features of the plasma model were investigated such as the kinetics and, in particular, the cross sections of electronic impact reactions.

Improved Non-Equilibrium Plasma Simulations Quantitatively Validated against Experiments

In FY 2017, simulations captured the chemical (atomic oxygen, O) and thermal (temperature) properties of LTP qualitatively, meaning in terms of distributions and trends. However, an apple-to-apple comparison of the same quantities between modeling and experiments was not possible. Also, the off-set between simulations and experiments in terms of LTP-to-arc transition pressure threshold persisted.

In FY 2018, the improved characterization of the experiments, better control on mixture composition and electrode geometry, and the evaluation of model uncertainties related to the electron impact kinetics allowed improving the quantitative agreement between numerical and experimental data in terms of post-discharge regime (Figure I.10.2). Moreover, the apple-to-apple comparison in terms of plasma chemical and thermal properties between simulation and experiments shown in Table I.10.1 indicates a very close quantitative agreement.

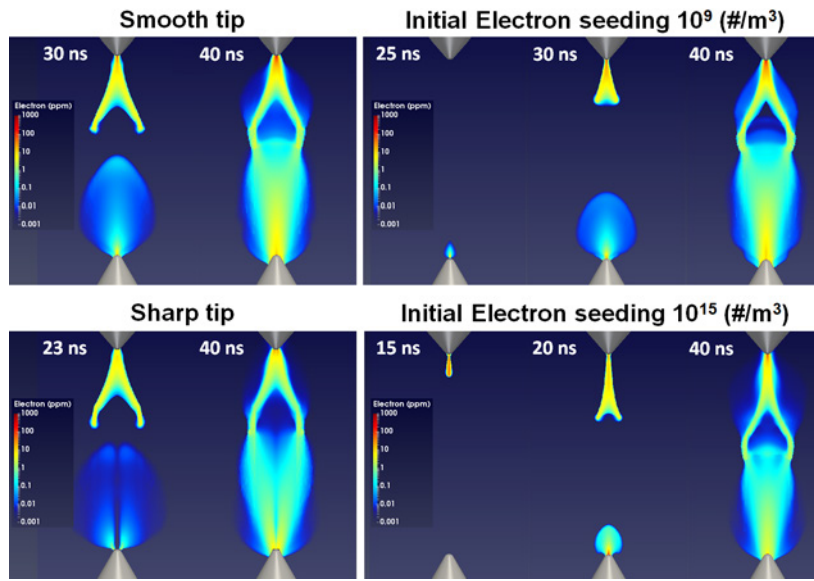


Figure I.10.1. Impact of electrode geometry and electron seeding on LTP discharge

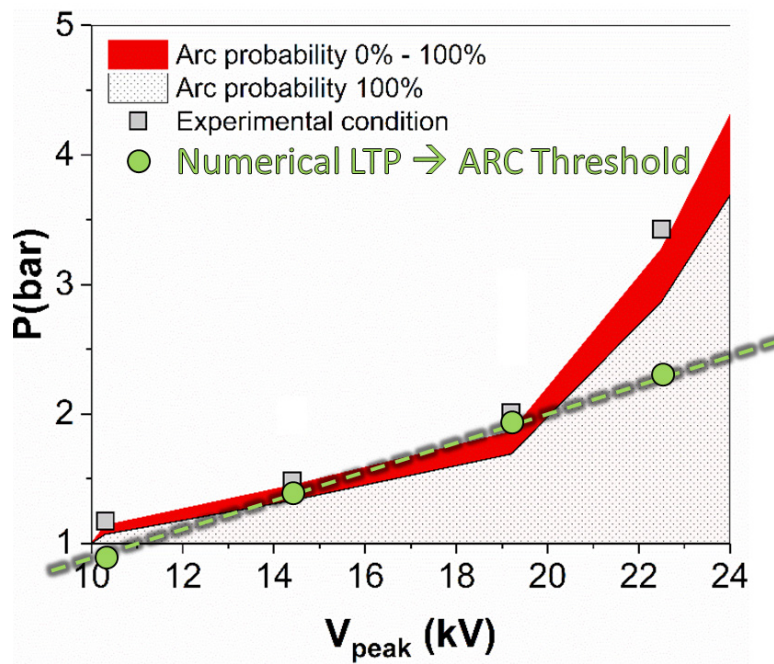


Figure I.10.2. Comparison between simulations and experiments in terms of post-discharge plasma regime

Table I.10.1. Comparison of Plasma Properties between Modeling and Experiments

Test condition	Simulation		Experiments	
	O (1/cm ³)	T (K)	O (1/cm ³)	T (K)
14.4 kV, 1.5 bar	0.9 x 10 ¹⁸	770	1.3 x 10 ¹⁸	779
19.2 kV, 2.0 bar	1.8 x 10 ¹⁸	938	2.1 x 10 ¹⁸	1094

Non-Equilibrium Plasma Simulations Coupled with CFD Combustion Simulations

In FY 2018, a step forward was made to convey the improved LTP knowledge into the development of an LTP ignition model for CFD engine simulations. The information generated using VizGlow was used to initialize the post-discharge plasma characteristics in CONVERGE. The regions where the production of O and the increase of temperature were the most significant (see Figure I.10.3) were used to deposit a mix of thermal energy and species in CONVERGE at the end of the LTP discharge. The mixed deposition (O and thermal energy) was meant to represent the LTP properties that were measured experimentally.

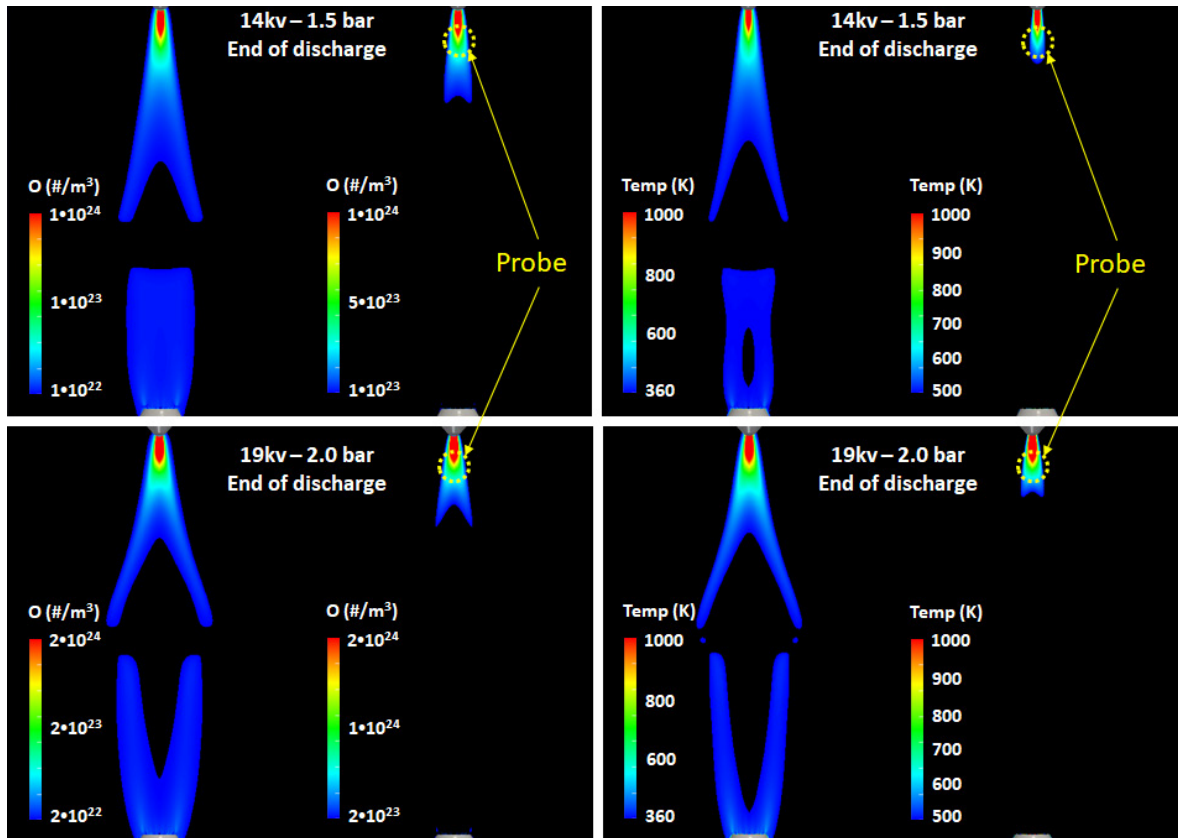


Figure I.10.3. VizGlow results highlighting the distribution of atomic oxygen (O) and temperature

LTP Ignition Processes Simulated Using the CFD Engine Code CONVERGE

In FY 2018, the first attempt, to the best of our knowledge, to simulate ignition from LTP using a CFD engine code (CONVERGE) was made. A number of pulses were simulated at the two operating conditions shown in Table I.10.1 (14 kV, 1.5 bar and 19 kV, 2.0 bar). Figure I.10.4 shows the impact of the number of pulses on the maximum temperature calculated in CFD simulations. The LTP ignition mechanism showed substantial differences with respect to thermal deposition. The ignition is the result of the local accumulation of active species that trigger the fuel kinetics above a certain threshold. Therefore, a minimum number of pulses to generate ignition is expected depending on the specific conditions in the gap. For a near-arc LTP condition such as 19 kV, 2.0 bar, a fairly low number (two) of consecutive pulses is required to trigger ignition, as can be seen in Figure I.10.5. These preliminary LTP ignition simulations were conducted at stoichiometric and quiescent conditions. It is expected that lean/dilute operation and the presence of non-quiescent flow conditions will alter the number of pulses required to trigger ignition from a LTP deposition.

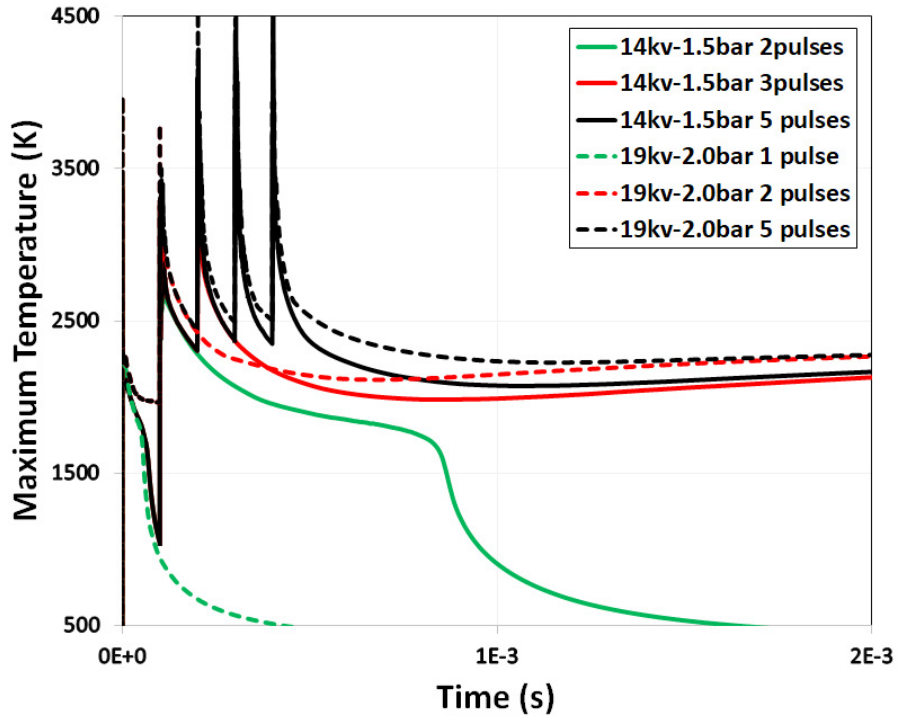


Figure I.10.4. Impact of number of pulses on LTP ignition as calculated using CONVERGE

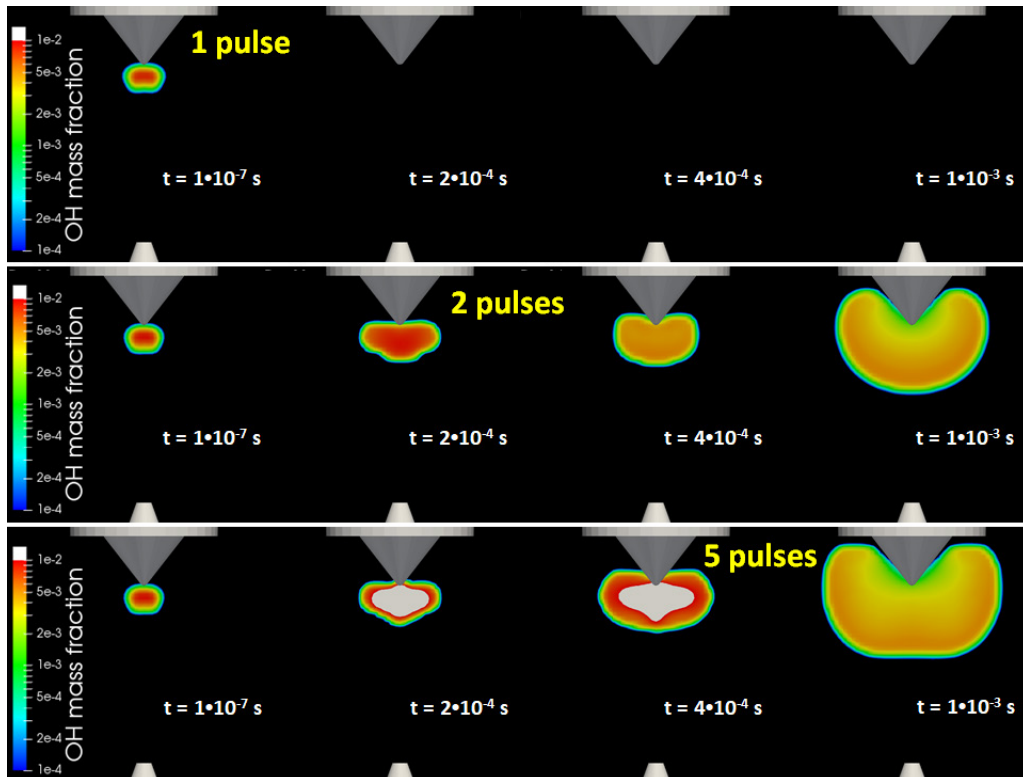


Figure I.10.5. CONVERGE results showing the impact of number of pulses on the flame kernel growth

Conclusions

This research project has continued to improve basic knowledge and computational tools to properly characterize advanced ignition strategies for GDI engines. The main conclusions are listed below.

- The discrepancies concerning LTP-to-arc transition between modeling and experiments on a quantitative basis were resolved by removing some uncertainties in both the experiments (better control of mixture and geometry) and the plasma model (sensitivity analysis and model tuning).
- When the model matched experiments performed at Sandia National Laboratories, the apple-to-apple comparison in terms of chemical (O) and thermal (temperature) plasma properties delivered a very close quantitative agreement.
- The information from the non-equilibrium plasma model VizGlow could be trusted with a good confidence and was used to initialize LTP ignition calculations using CFD combustion simulations.
- LTP ignition simulations were performed—for the first time, to the best of our knowledge—with the CFD engine software CONVERGE, thus providing valuable insight into the ignition mechanism from a LTP deposition.

Future research work will validate LTP ignition CFD simulations against experiments and continue to develop predictive models for advanced ignition technologies that enable high-efficiency GDI engines.

Key Publications

1. Scarcelli, R., et al. “Modeling Non-Equilibrium Discharge and Validating Transient Plasma Characteristics at Above-Atmospheric Pressure.” Approved for publication in *Plasma Sources Science & Technology*.
2. Scarcelli, R., et al. 2018. “Multi-Dimensional Modeling of Non-Equilibrium Plasma for Automotive Applications.” SAE Technical Paper 2018-01-0198.
3. Zhang, A., R. Scarcelli, et al. 2018. “Numerical Investigation of Nanosecond Pulsed Discharge in Air at Above-Atmospheric Pressures.” *Journal of Physics D: Applied Physics* 51, no. 34.
4. Scarcelli, R., et al. 2018. “Development of a Hybrid Lagrangian-Eulerian Model to Describe Spark-Ignition Processes at Engine-like Turbulent Flow Conditions.” ASME-ICEF 2018-9690.
5. Scarcelli, R. 2018. “Modeling Advanced Ignition Systems in CONVERGE.” 2018 CONVERGE User Conference, September 2018, Madison, WI, USA (oral presentation).
6. Scarcelli, R. 2018. “Recent Progress in Low-Temperature Plasma Ignition Modeling.” 2018 Fall AEC Program Review Meeting, August 2018, Southfield, MI, USA (oral presentation).
7. Scarcelli, R. 2017. “GDI Combustion Work at Argonne - The Impact of Ignition Characteristics on Combustion Stability at Lean and EGR Dilute Operation.” 2017 VERIFI Workshop, November 2017, Lemont, IL, USA (oral presentation).

I.11 Stretch Efficiency for Combustion Engines: Exploiting New Combustion Regimes (Oak Ridge National Laboratory)

James P. Szybist, Principal Investigator

Oak Ridge National Laboratory
2360 Cherahala Blvd.
Knoxville, TN 37932
E-mail: szybistjp@ornl.gov

Michael Weismiller, DOE Technology Development Manager

U.S. Department of Energy
E-mail: Michael.Weismiller@ee.doe.gov

Start Date: October 1, 2016	End Date: September 30, 2018	
Project Funding (FY18): \$300,000	DOE share: \$300,000	Non-DOE share: \$0

Project Introduction

The overarching goal of this project is to use a thermodynamics-based approach to identify and pursue opportunities for improved efficiency in internal combustion engines. The combustion strategy identified as the most promising approach to improving light-duty engine efficiency is high dilution from exhaust gas recirculation (EGR) for spark-ignited combustion enabled by fuel reforming through thermochemical recuperation. The overall efficiency advantages for high-EGR conditions are summarized in a thermodynamic modeling study by Caton [1] and include decreased pumping work, decreased heat transfer, and increased ratio of specific heats (γ). The amount of EGR that can be used is limited due to combustion instabilities, but the dilution limit can be extended for additional efficiency improvements with the use of high-flame-speed components, namely H_2 . This project is pursuing fuel reforming to generate H_2 in an effort to extend the EGR dilution limits for spark-ignited combustion in the most thermodynamically favorable way possible. Ideally, this involves using exhaust heat to drive endothermic reforming reactions to increase the chemical fuel energy to achieve thermochemical recuperation, a form of waste heat recovery.

Objectives

Overall Objectives

- Identify and characterize the potential of catalytic EGR-loop reforming to achieve waste heat recovery through thermochemical recuperation and extend the dilution limit of an engine
- Perform thermodynamics-focused analysis to determine the efficiency potential of this strategy relative to other emerging combustion strategies

Fiscal Year 2018 Objectives

- Determine whether the Oak Ridge National Laboratory EGR-loop catalytic reforming strategy is compatible with expanded load operation
- Quantify the impacts of expanded load operation on the catalyst thermal conditions and the overall brake thermal efficiency (BTE) of the engine

Approach

This project is focused on increasing engine efficiency for light-duty engines with a focus on waste heat recovery and engine thermodynamics. Specifically, an EGR-loop catalytic fuel reforming combustion strategy has been developed to achieve higher efficiency. This strategy brings together three complementary features that can provide thermodynamic efficiency benefits. The first of these is operating with high levels of EGR dilution, which provides reduced pumping work, a higher ratio of specific heats (γ), and reduced heat transfer [1]. The second is thermochemical recuperation waste heat recovery by catalytically reforming fuel, so that

waste engine heat can be converted to chemical energy that can subsequently be consumed in the engine [2]. Finally, this strategy is focused on maintaining overall stoichiometric conditions in the engine exhaust so that the fuel penalty associated with lean emissions control devices can be avoided.

In the 2017 annual report for this project, the development of the engine operating strategy was detailed, from bench-flow reactor results to on-engine catalyst performance, and finally, for full-engine combustion. Those efforts are now documented in three 2018 publications listed in the Publications section. In addition, thermodynamic modeling of reforming equilibrium and computational fluid dynamics simulations were also provided to illustrate the efficiency gains that could be achieved with this operating strategy. While a fuel consumption benefit of nearly 10% was demonstrated, the results were for a moderate engine operating condition of 2,000 rpm and 4 bar brake mean effective pressure (BMEP). In 2018, efforts were focused on determining whether this operating strategy was applicable to a broader portion of the engine operating map. Specifically, efforts were focused on determining whether the catalytic reforming strategy would be accompanied by excessively high catalyst temperatures at high loads that would damage the engine, and whether the increased intake manifold pressure at high loads would cause efficiency penalties due to air handling.

Results

A schematic of the engine configuration used for the EGR-loop reforming strategy is shown in Figure I.11.1. In this strategy, one of the cylinders has an isolated intake and exhaust manifold. The entirety of the exhaust from this cylinder is fed directly to the reforming catalyst, which then mixes with fresh air to feed the three remaining cylinders. This configuration allows control of the reforming catalyst boundary conditions, specifically the catalyst inlet O_2 concentration and the catalyst equivalence ratio (Φ_{catalyst}), which we have previously shown is essential to achieving thermodynamically efficient reforming with robust performance. Figure I.11.1 is an updated version of the schematic shown in the 2017 annual report and represents modifications made for 2018 to enable boosted operation to achieve the load expansion objective for 2018, specifically mass air flow controllers, a rupture disc, and a backpressure valve.

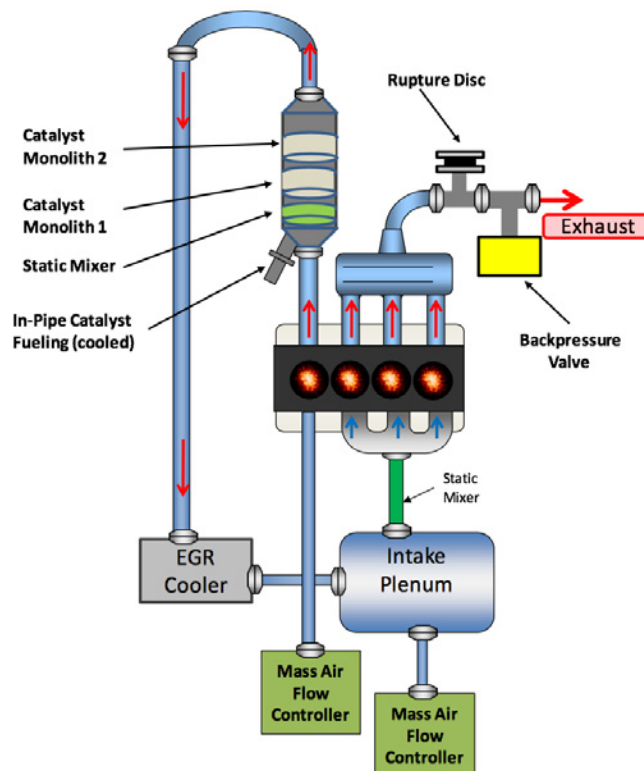


Figure I.11.1. Schematic of the in-cylinder reforming process in which one cylinder has an isolated intake and exhaust, feeds the reforming catalyst, and is incorporated into the intake for the other three cylinders. Intake and exhaust systems have been modified to accommodate boosted operation in 2018.

Figure I.11.2 shows a contour plot of BTE as a function of catalyst inlet conditions, namely O_2 concentration and Φ_{catalyst} . The highest BTE at 2,000 rpm and 4 bar BMEP, 30.1%, occurs at cylinder $\Phi_{\text{cylinder 4}} = 0.91$ and $\Phi_{\text{catalyst}} = 8.5$. For comparison purposes, the baseline engine operating strategy at this speed and load operating point produces a BTE of 28.5%; thus, all of the operating points in Figure I.11.2 represent an efficiency advantage over the baseline condition (which equates to reduced fuel consumption of ~5%). The highest BTE does not coincide with the highest levels of reformat, as measured by H_2 and CO . These species have peak concentrations when the catalyst inlet O_2 concentrations are highest, or the leanest $\Phi_{\text{cylinder 4}}$. The reduced BTE at the higher H_2 and CO concentrations can be attributed to thermodynamically unfavorable fuel reforming reactions (partial oxidation). This illustrates the importance of controlling the boundary conditions of the reforming catalyst.

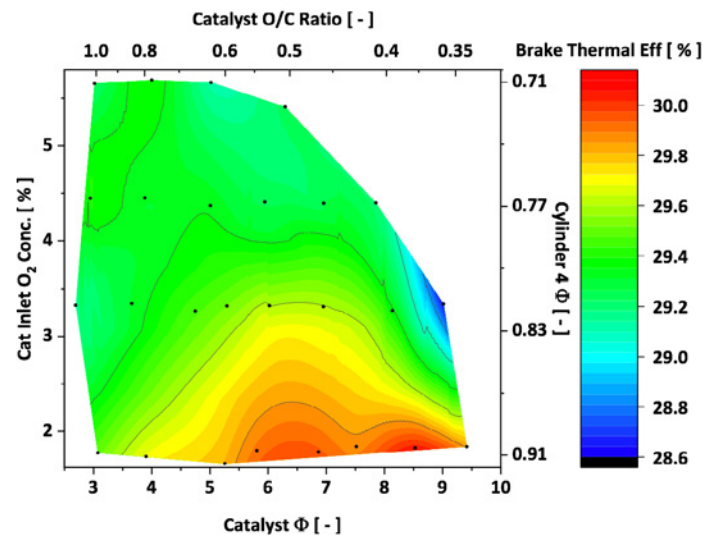


Figure I.11.2. Brake thermal efficiency as a function of catalyst inlet O_2 concentration and Φ_{catalyst} at 2,000 rpm and 4 bar BMEP

The axial temperature profiles for two of the inlet O_2 concentrations are shown over a sweep of Φ_{catalyst} in Figure I.11.3, where the tan boxes represent the catalyst monoliths. The left-most thermocouple measures the temperature approximately 1 mm upstream of the first catalyst monolith. Immediately downstream of the front face of the catalyst, there is a rapid increase in temperature, reaching a local peak temperature at an axial position of 10 mm for most conditions. This is followed by temperature decreases throughout the remainder of the catalyst (note the thermocouple located at 60 mm gave anomalous measurements, but the data are included for completeness). The initial rise in temperature can be interpreted as exothermic oxidation reactions at the front of the catalyst followed by endothermic reforming reactions downstream. The magnitude of the exotherm in the catalyst is dependent on both Φ_{catalyst} and on catalyst inlet O_2 concentration.

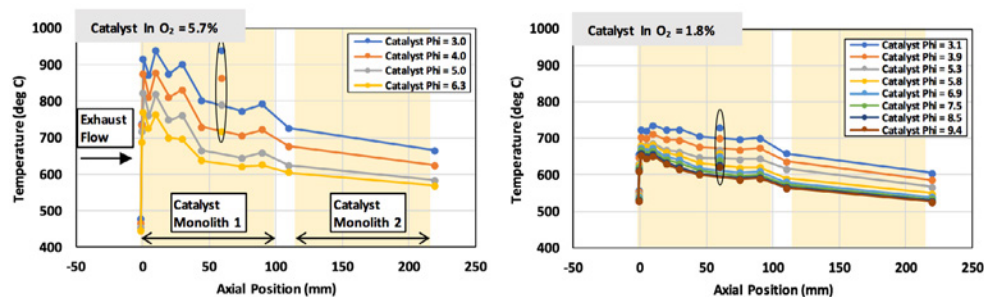


Figure I.11.3. Axial temperature profile of reforming catalyst at 2,000 rpm, 4 bar BMEP over a range of catalyst inlet O_2 concentrations and catalyst Φ conditions

The observations about the exotherm in the catalyst in Figure I.11.3 can provide insight into the reactions occurring within the catalyst, and particularly, the relative competitiveness of the exothermic oxidation reactions and the endothermic reforming reactions. To assist with the insights that can be inferred, Figure I.11.4 presents schematics of two possible reforming scenarios where O_2 is the limiting reactant, as it is for all conditions in this study. Figure I.11.4a represents a scenario where oxidation reactions are favored over reforming reactions so long as any oxygen is present. In this scenario, the catalyst temperature continues to rise until all of the oxygen has been consumed, at which point endothermic reactions can begin and H_2O can be consumed through reforming reactions. In contrast, Figure I.11.4b represents a scenario where reforming and oxidation reactions are competitive with one another and occur simultaneously. Thus, the consumption of O_2 through partial oxidation occurs coincident with the consumption of H_2O through steam reforming, thereby attenuating the peak temperature that the catalyst experiences. By examining the experimental results, we can determine that the scenario depicted in Figure I.11.4b supports the experimental findings because Φ_{catalyst} is effective at decreasing the exotherm magnitude at a given inlet O_2 concentration. This is an important finding that provides confidence to increase the engine load, because as the engine load increases, so too does the O_2 flux through the catalyst.

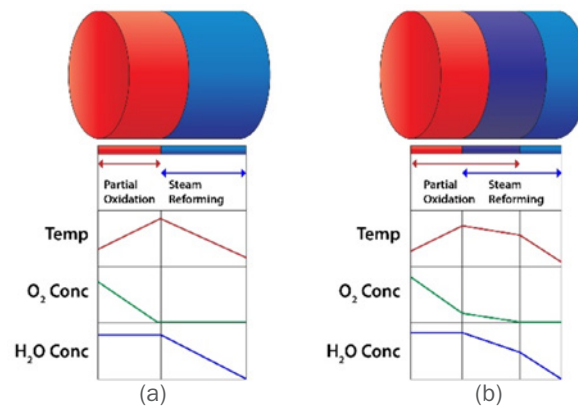


Figure I.11.4. Schematic of two possibilities of reaction zones in reforming catalyst. In scheme (a), the oxidation and steam reforming occur sequentially. In scheme (b), the partial oxidation and steam reforming reactions occur simultaneously over a portion of the catalyst.

Figure I.11.5 shows the catalyst inlet temperature and peak catalyst temperature as a function of engine load. While the catalyst inlet temperature increases with engine load, the temperature rise associated with the reforming process in the catalyst remains approximately constant. Thus, the higher O_2 and fuel energy flux through the catalyst do not increase the catalyst temperature. Instead, the increase in temperature is associated with the higher inlet temperature, and the catalyst inlet O_2 concentration of 1.8% and Φ_{catalyst} are the controlling factors for the catalyst exotherm.

Figure I.11.6 shows BTE as a function of load for both the Oak Ridge National Laboratory catalytic EGR-loop reforming strategy and conventional spark ignition operation. The reforming strategy provides a BTE benefit of one to two efficiency points at all points in the engine load sweep. Together, these results show that (1) this operating strategy is applicable over large portions of the engine operating map, and (2) this operating strategy provides an efficiency benefit over the entire operating range, not just light load. There are potentially further efficiency benefits that can be realized with increases in compression ratio to take advantage of the knock resistance that EGR provides [1].

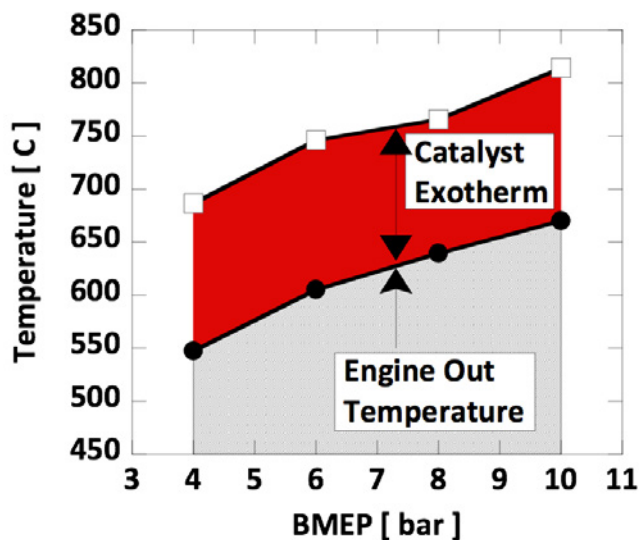


Figure I.11.5. Axial temperature profile for increasing engine load, from 4 bar to 10 bar BMEP, at an engine speed of 2,000 rpm. Catalyst inlet O₂ was held constant at 1.8%, and catalyst Φ was held constant at 5.

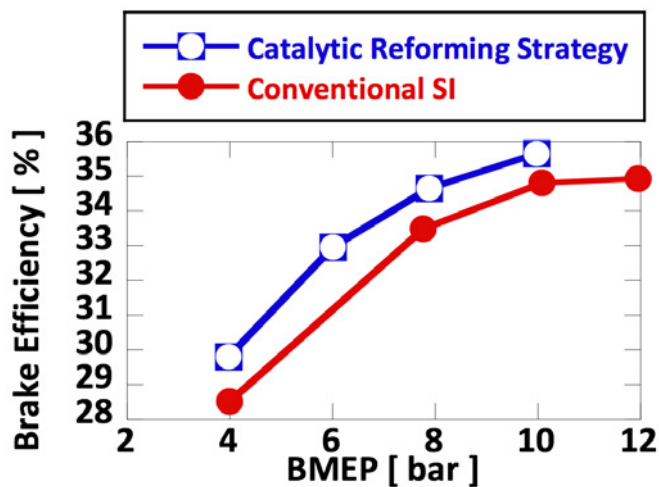


Figure I.11.6. Exhaust temperature, intake manifold pressure, BMEP and intake manifold pressure as a function of load for the reforming strategy and the baseline engine operation.

Conclusions

In 2018, the Oak Ridge National Laboratory EGR-loop catalytic reforming combustion strategy was further developed by extending its applicability to higher loads, increasing the engine operation from 4 bar to 10 bar BMEP. In doing so, the following conclusions have been made.

- The magnitude of the temperature rise in the reforming catalyst can be controlled by the inlet boundary conditions, namely Φ_{catalyst} and the inlet O_2 concentration.
- The inlet boundary conditions are effective at limiting the reforming exotherm because the endothermic steam reforming reactions are competitive with the exothermic partial oxidation reactions. As a result, the engine load could be operated to 10 bar BMEP without excessive catalyst temperatures.
- The catalytic reforming strategy provided efficiency benefits at all loads investigated, accounting for a fuel consumption decrease of up to 5%. Further efficiency benefits are likely possible with increases in compression ratio that can take advantage of the improved knock resistance of the reformat mixture.

The results presented in this annual report will be reported on in more detail in an SAE technical paper that will be presented at the 2019 SAE WCX meeting.

Key Publications

1. Brookshear, D.W., J.A. Pihl, and J.P. Szybist. 2018. "Catalytic Steam and Partial Oxidation Reforming of Liquid Fuels for Application in Improving the Efficiency of Internal Combustion Engines." *Energy Fuels* 32 (2): 2267–2281. DOI: 10.1021/acs.energyfuels.7b02576.
2. Chang, Y., J.P. Szybist, J.A. Pihl, and D.W. Brookshear. 2018. "Catalytic Exhaust Gas Recirculation-Loop Reforming for High Efficiency in a Stoichiometric Spark-Ignited Engine through Thermochemical Recuperation and Dilution Limit Extension, Part 1: Catalyst Performance." *Energy Fuels* 32 (2): 2245–2256. DOI: 10.1021/acs.energyfuels.7b02564.
3. Chang, Y., J.P. Szybist, J.A. Pihl, and D.W. Brookshear. 2018. "Catalytic Exhaust Gas Recirculation-Loop Reforming for High Efficiency in a Stoichiometric Spark-Ignited Engine through Thermochemical Recuperation and Dilution Limit Extension, Part 2: Engine Performance." *Energy Fuels* 32 (2): 2257–2266. DOI: 10.1021/acs.energyfuels.7b02565.

References

1. Caton, J.A. 2013. "A Comparison of Lean Operation and Exhaust Gas Recirculation: Thermodynamic Reasons for the Increases of Efficiency." SAE Technical Paper 2013-01-0266, doi:10.4271/2013-01-0266.
2. Fennell, D., M. Herreros, A. Tsolakis, H. Xu, K. Cockle, and P. Millington. 2013. "GDI Engine Performance and Emissions with Reformed Exhaust Gas Recirculation (REGR)." SAE Technical Paper 2013-01-0537.

Acknowledgements

The authors gratefully acknowledge John Nunan of Umicore for providing catalyst samples and Galen Fisher of the University of Michigan for supporting our efforts to obtain substrates and catalysts. Thanks also to Josh Pihl, Shean Huff, and Brian Kaul of Oak Ridge National Laboratory.

I.12 Neutron Imaging of Advanced Transportation Technologies (Oak Ridge National Laboratory)

Martin L. Wissink, Principal Investigator

Oak Ridge National Laboratory (ORNL)
 P.O. Box 2008
 Oak Ridge, TN 37831
 E-mail: wissinkml@ornl.gov

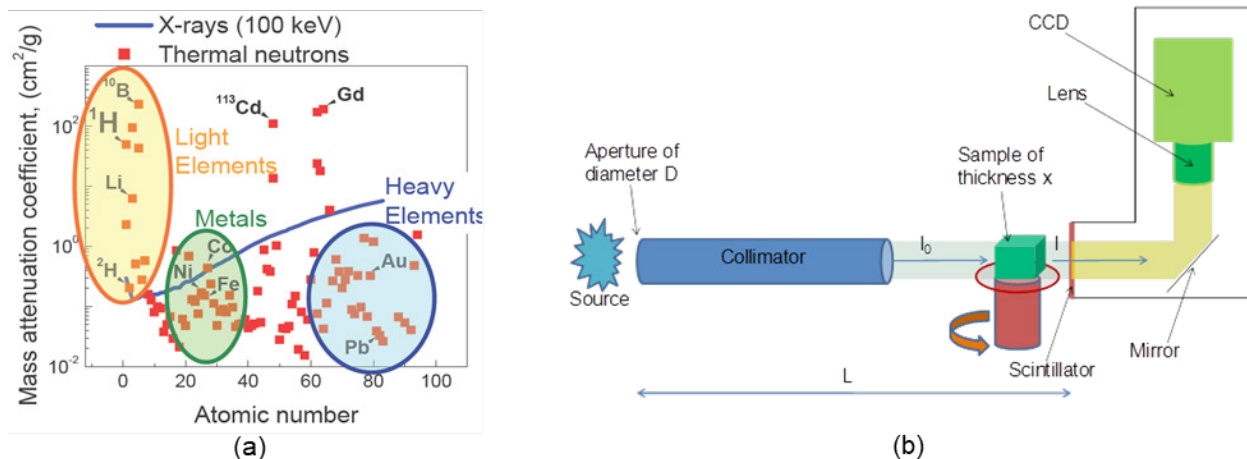
Michael Weismiller, DOE Technology Development Manager

U.S. Department of Energy
 E-mail: Michael.Weismiller@ee.doe.gov

Start Date: October 1, 2017	End Date: September 30, 2018	
Project Funding (FY18): \$282,000	DOE share: \$282,000	Non-DOE share: \$0

Project Introduction

Unlike X-rays, neutrons are very sensitive to light elements such as hydrogen (H) atoms and can penetrate through thick layers of metals (Figure I.12.1a). These two properties suggest neutrons are well suited to probe engine parts such as diesel particulate filters, exhaust gas recirculation coolers, fuel injectors, oil in engines, oil residues in filters, batteries, advanced materials, etc. Neutron imaging is based on the interactions of a sample with a neutron beam. The interactions are dependent on sample thickness/density and elemental make-up and result in absorption and scattering of neutrons within the sample. A two-dimensional position-sensitive detector placed behind the sample can measure the transmitted neutron flux (Figure I.12.1b). When combined with a high-precision (~1/100 of a degree) rotational stage, it is possible to perform computed tomography (CT) scans and thus generate three-dimensional images of working fluids inside real devices. Samples can be analyzed at one position or a complete reconstruction can provide a cross-section of the entire sample at a resolution of the detector; the detector resolution is currently at ~50–80 microns (at the detector).



CCD – charge-coupled device

Figure I.12.1. (a) Mass-attenuation coefficients versus atomic number, and (b) schematic of neutron-imaging apparatus (Sources: [a] Nikolay Kardjilov [2006], [b] ORNL)

Objectives

- Implement high-fidelity neutron imaging capabilities using the High Flux Isotope Reactor (HFIR) for advanced transportation research. Once fully developed, this advanced capability will allow the imaging of a range of processes that occur in advanced vehicle systems.
- Employ technique to aid improved design and control of complex advanced combustion systems and help to guide model validation and input.
- Report findings to research community and work with industrial partners to ensure research is focused on the most critical topics.

Approach

This project is focused on using the unique neutron imaging capability at ORNL's HFIR to advance the understanding of two components being employed in modern vehicles: the gasoline direct injector (GDI) and the particulate filter. Recent efforts are aimed at investigating intra-nozzle fuel injector fluid dynamics while spraying. A specialized fuel delivery system and spray chamber are employed in this study that mesh well with the neutron beamline and GDI-style injectors (Figure I.12.2). These efforts are designed to improve understanding of how injector design, external conditions, and fuel properties influence internal dynamics, especially as it relates to advanced combustion regimes and injector durability. Particulate filters are a key component of the emissions control system for modern diesel engines, and possibly gasoline engines in the future, yet there remain significant questions about the basic behavior of the filters. In particular, understanding how ash, or non-regenerable metal oxide-based particulate, fills the particulate filter and interacts with the wall is a focus of this effort. The results of these measurements will provide important data to the aftertreatment modeling community on the soot and ash profiles, which change over the course of the vehicle's lifetime. In carrying out these studies, we work closely with industrial partners to obtain relevant systems and devices. The proximity of our research facility to the neutron beam allows for iterative studies when appropriate.

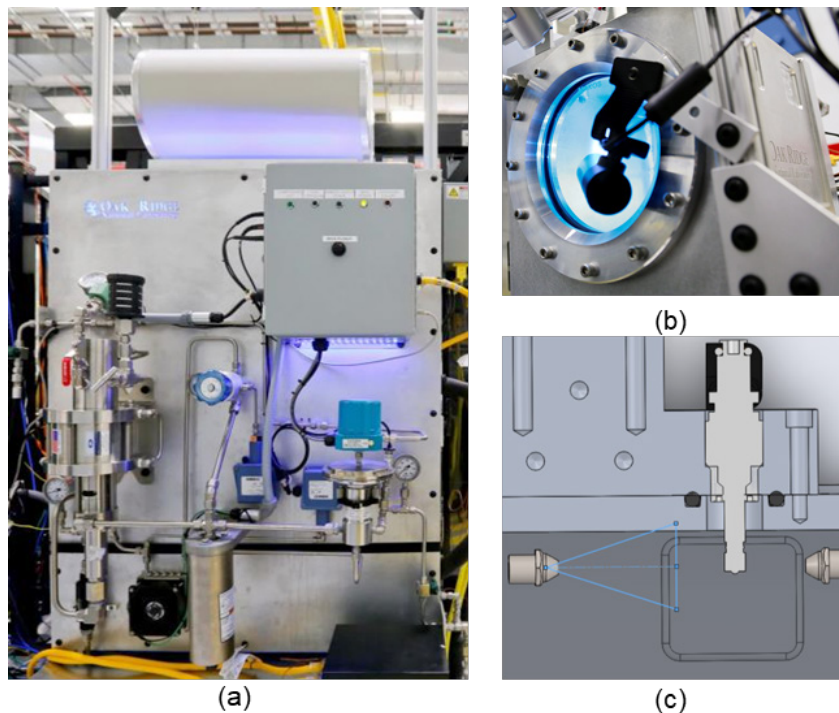


Figure I.12.2. System used to study intra-nozzle dynamics of fuel injection include (a) high-pressure fuel delivery system and (b) the aluminum spray chamber with optical viewport. The spray chamber is designed with (c) directed fans to minimize fuel buildup on the chamber walls and the fuel injector.

There has been collaboration with researchers from several institutions during this project, including Argonne National Laboratory; General Motors; Bosch; Continental Automotive; the University of Tennessee; the University of California, Berkeley; Boston University; and a Massachusetts Institute of Technology consortium on particulate filters.

Results

The dynamic imaging effort has continued to focus on coordination with the Engine Combustion Network (ECN). This global community has set guidelines as to which baseline experimental conditions should be employed and even goes as far as supplying injectors and other hardware. The experimental results can then be shared with the modeling community to help accelerate findings. While not part of the official collection of ECN injectors, General Motors has provided single-hole and eight-hole versions of the ECN Spray G, which is the common benchmark for GDI-style injectors. Bosch also donated a single-hole, large-bore injector, which was used as part of a cavitation study with collaborators at Boston University. During the November 2017 neutron imaging campaign, all three of the injectors were operated using the ECN-preferred fuel, iso-octane, at operating conditions similar to the ECN-specified G2 and G3 conditions, including cases with both single and multiple injections. Neutron images were collected for each condition over 1–3 million injection cycles to produce an ensemble-average movie of the injection process.

The dynamic imaging analysis performed in Fiscal Year (FY) 2018 focused on quantifying needle motion observed during and after injection, as shown in Figure I.12.3 for the single-hole Spray G-style injector. Through the dynamic normalization approach, it is possible to see regions in the injector where the relative quantity of fuel varies from the static reference condition, as the fuel attenuates neutrons significantly more than the steel parts of the injector. This allows for visualization of the opening and closing of the check ball, as well as deflection or displacement of the needle both during and after injection based on the relative absence or abundance of fuel.

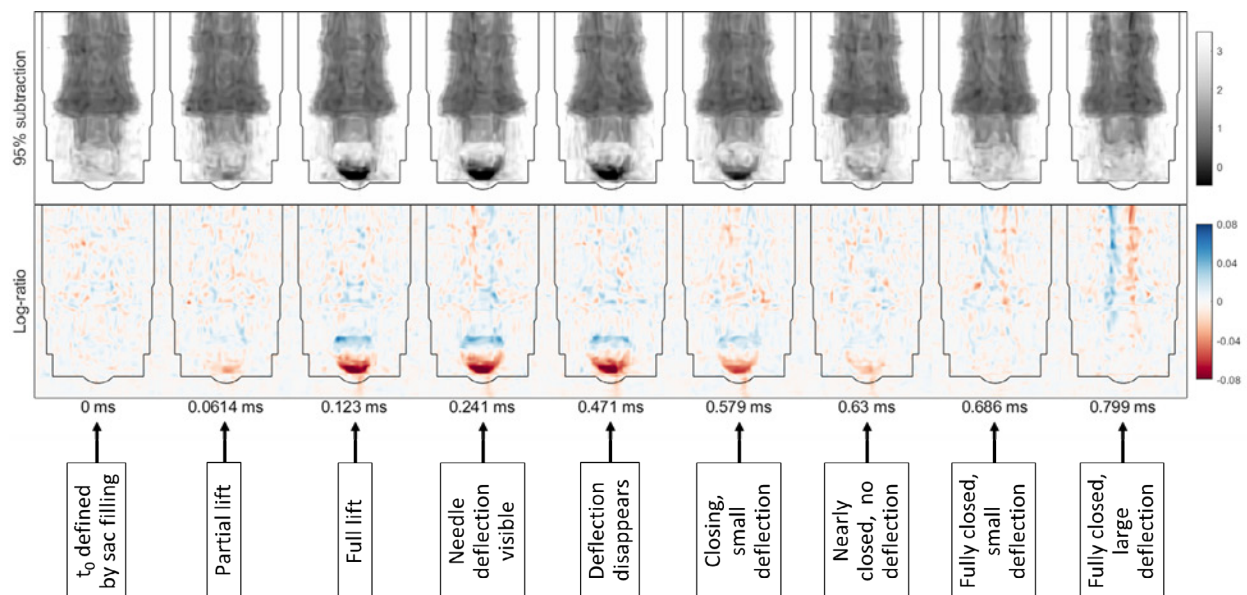


Figure I.12.3. Normalized neutron radiographs of fuel injection from a single-hole GDI-style injector (ECN Spray G) highlight ability to see opening and closing of the check ball as well as deflection of the injector both during and after injection. Top row shows subtraction-normalized images, which provide a qualitative understanding of the needle motion. Bottom row shows log-ratio-normalized images, which provide quantitative information on how the neutron path lengths change through the different materials during the needle motion.

The quantification approach is based on modeling the neutron attenuation through the known geometry of the injector and how the neutron path length through the injector needle at a given pixel on the detector would change when the needle is displaced. This model is then fit to the normalized neutron imaging data by

vertically averaging a region of the image with a strong indication of needle motion, as shown in Figure I.12.4(a). This procedure is then performed for each image in the sequence, and the resulting model fits produce a result of displacement vs. time over the averaged region, as shown in Figure I.12.4(b). The model fit indicates oscillations during injection, as well as a large displacement immediately after the ball is seated at the end of injection, which agrees with the qualitative assessment from the normalized images. This analysis is being further refined to include the effects of detector blurring and needle location variation during the ensemble image collection, and a manuscript describing the approach and results is in preparation. Results to date have been shared with the ECN at the ECN 6 Workshop.

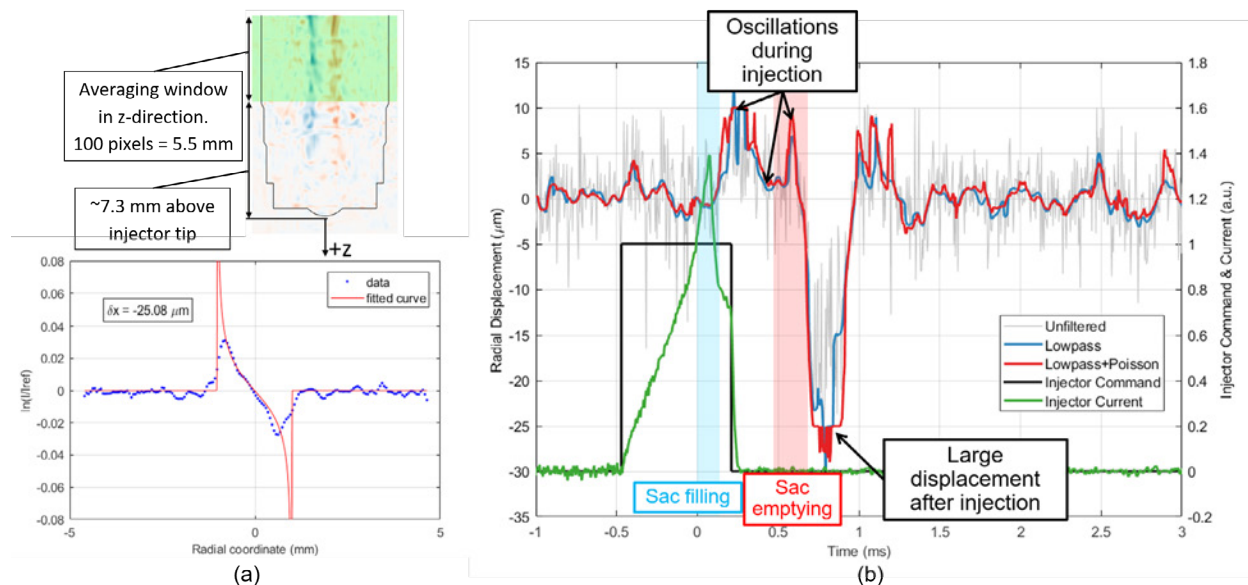


Figure I.12.4. (a) Approach for fitting normalized image data to analytical path length model. (b) Needle displacement results show oscillation during injection and large movement after ball is seated. Results show low sensitivity to image filtering.

Other injector-related efforts in FY 2018 included performing a two-part CT scan of the Bosch large-bore injector to obtain full internal flow geometry. As in previous FYs, collaboration continued with Argonne National Laboratory in which high-resolution X-ray CT was performed in the nozzle region, and neutron CT was performed on the entire geometry, which includes thicker metal features that are difficult to penetrate with X-rays. Figure I.12.5 shows slices of the neutron CT of the injector, obtained at the HFIR at ORNL, with an area surrounding the nozzle which was the focus of the high-resolution X-ray CT, obtained at the Advanced Photon Source at Argonne National Laboratory.

Another area of focus continues to be particulate layers that are observed in gasoline particulate filters (GPFs). GPFs that were filled with particulate from a GDI-based engine using gasoline blended with 0% and 30% ethanol (E0 and E30, respectively) were imaged at HFIR using CT techniques. The GPFs were originally filled to 4 g/L and then sequentially regenerated, followed by imaging. In previous FYs, several imaging campaigns were performed for regeneration levels up to 80%, and that work was concluded in FY 2018 by performing imaging at 100% regeneration. In contrast to the particulate layers typically seen in diesel particulate filters, there is minimal decrease in thickness until 40% of the particulate is regenerated, as seen in Figure I.12.6 for both E0 and E30. Differences between the E0 and E30 are also apparent, as the soot thickness decreased continuously as the E0 diesel particulate filters were regenerated, whereas the soot cake thickness appeared to stall multiple times during the E30 diesel particulate filter regeneration.

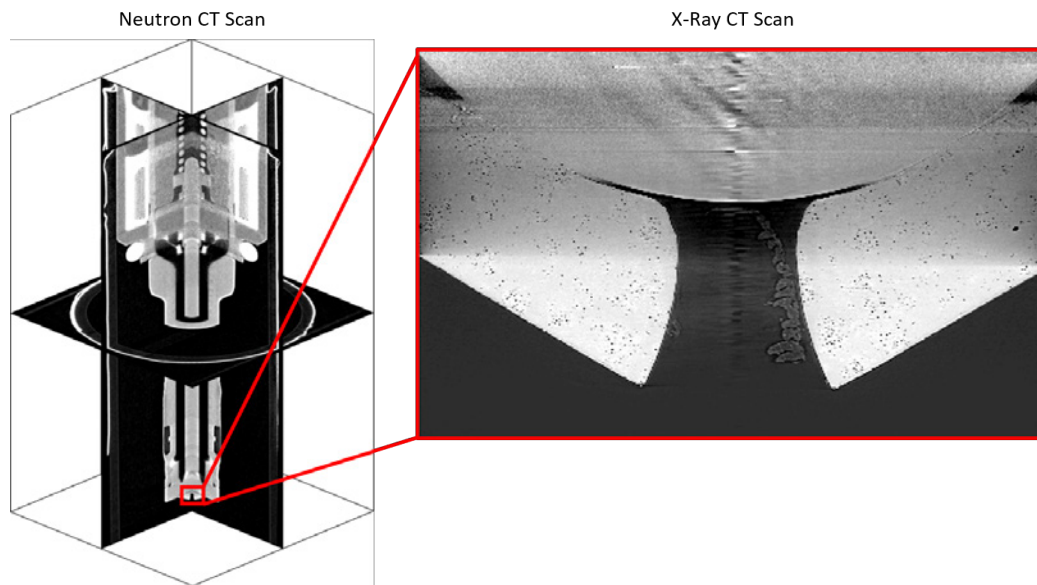


Figure I.12.5. Slices of neutron and X-ray CT reconstructions of large-bore Bosch injector performed in collaboration with Argonne National Laboratory

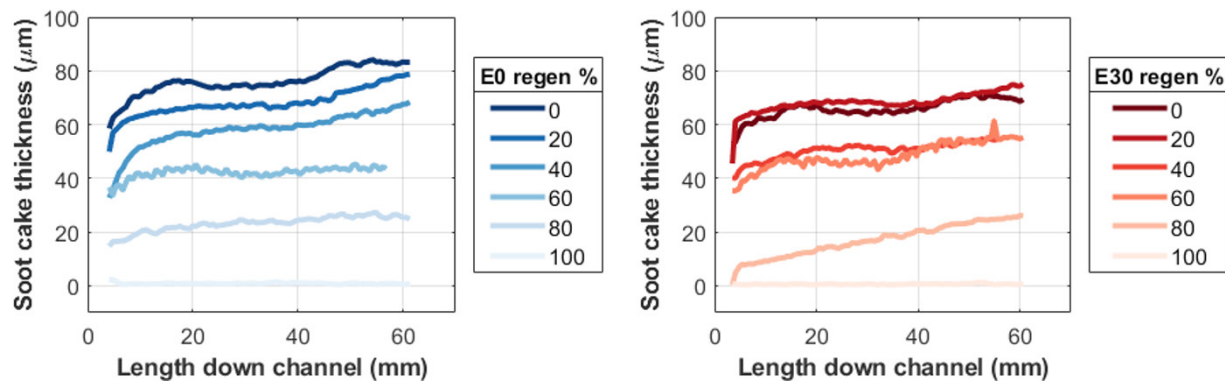


Figure I.12.6. Soot cake thickness down GPF channel length extracted from neutron CT scans shows continuous decrease with regeneration percent with E0 particulate matter (left) and staggered decrease with E30 particulate matter (right)

Conclusions

- Neutron imaging is a non-destructive, non-invasive diagnostic approach to improve understanding of advanced vehicle and combustion systems, targeting fuel economy improvements and durability. Efforts to date have focused on fuel injectors and particulate filters.
- Neutron imaging of fuel injection in a dynamic capacity has been demonstrated at the HFIR CG-1D imaging beamline and has shown the ability to both visualize and quantify the internal injector dynamics, including fluid motion and needle deflection/displacement. Dynamic imaging was performed with three injectors using iso-octane at multiple chamber conditions with both single and multiple injections. All injectors exhibited oscillation of the ball and needle during injection, with significant effects seen in cases with multiple injections.
- Continuing the ongoing collaboration with Argonne National Laboratory, a two-part CT scan of the Bosch large-bore injector was completed using both X-ray and neutron approaches to combine their complementary abilities to obtain well-defined internal geometry of these devices.

- The imaging campaign for GPFs loaded with soot from E0 and E30 was completed at 100% regeneration. Gasoline particulate differs in behavior from diesel particulate and also varies with the ethanol fraction in the gasoline. The successive regeneration and imaging strategy employed in this project is yielding unique insights not otherwise attainable with other methodologies.

Future directions could include the following:

- Publication of quantitative dynamic GDI imaging approach and results to date.
- A beamtime award of 6 d on the HFIR CG-1D imaging beamline has been scheduled for November 2018. Efforts for this campaign will be focused on needle and fluid motions, higher throughout the entire GDI-based injector, including interactions between the needle and the upper stops and solenoid armature. A new spray chamber has been designed and built to enable these measurements as well as operation at more extreme conditions and with higher throughput.
- A new detector is being developed to enable measurements with higher signal-to-noise ratio and improved resolution and data throughput. Commissioning is anticipated in FY 2019.

Key Publications

1. Wissink, Martin, Charles Finney, Eric Nafziger, Derek Splitter, and Todd Toops. 2018. "Internal GDI-Based Injector Dynamics Employing Neutron Radiography." Poster presented at THIESEL2018: Thermo and fluid dynamic processes in direct injection engines, Valencia, Spain (September).
2. Wissink, Martin, Todd Toops, Charles Finney, Derek Splitter, and Eric Nafziger. 2018. "Attenuation Modeling Approach to Dynamic Neutron Imaging of Gasoline Direct Injectors." Presentation at Engine Combustion Network ECN6 Workshop, Valencia, Spain (September).
3. Barnard, Richard C., Hassina Bilheux, Todd Toops, Eric Nafziger, Charles Finney, Derek Splitter, and Rick Archibald. 2018. "Total Variation-Based Neutron Computed Tomography." *Review of Scientific Instruments* 89, no. 5: 053704.
4. Wissink, Martin, Todd Toops, Charles Finney, Eric Nafziger, Derek Splitter, and Jonathon Willocks. 2018. "Neutron Imaging of Advanced Transportation Technologies." Presentation at DOE VTO Annual Merit Review (June).
5. Wissink, Martin, Todd Toops, Charles Finney, Eric Nafziger, Derek Splitter, Hassina Bilheux, and Louis Santodonato. 2018. "An Update on Neutron Diagnostics of Transportation Technologies." Presentation at AEC Program Review Meeting, Argonne National Laboratory (January).

Acknowledgements

Tyler Ambrico contributed to the dynamic imaging analysis over the summer of FY 2018 as a part of DOE's Science Undergraduate Laboratory Internship program. This research used resources at the High Flux Isotope Reactor, which is a DOE Office of Science User Facility. Thanks also to Todd J. Toops, Charles E.A. Finney, Eric J. Nafziger, Derek Splitter, and Hassina Bilheux of ORNL.

I.13 Chemical Kinetic Models for Advanced Engine Combustion (Lawrence Livermore National Laboratory)

William J. Pitz, Principal Investigator

Lawrence Livermore National Laboratory (LLNL)
P. O. Box 808, L-372
Livermore, CA 94551
E-mail: pitz1@llnl.gov

Michael Weismiller, DOE Technology Development Manager

U.S. Department of Energy
E-mail: Michael.Weismiller@ee.doe.gov

Start Date: October 1, 2017	End Date: September 30, 2019	
Project Funding: \$500,000	DOE share: \$500,000	Non-DOE share: \$0

Project Introduction

Predictive engine simulation models are needed to make rapid progress towards DOE's goals of increasing combustion engine efficiency and reducing pollutant emissions. To assess the effect of fuel composition on engine performance and emissions, these engine simulations need to couple fluid dynamic and fuel chemistry submodels. Reliable chemical kinetic submodels representative of conventional and next-generation transportation fuels need to be developed and improved to fulfill these requirements.

Objectives

Overall Objectives

- Develop predictive chemical kinetic models for gasoline, diesel, and next-generation fuels so that simulations can be used to overcome technical barriers to advanced combustion regimes in engines and achieve needed gains in engine efficiency and reductions in pollutant emissions
- Develop detailed chemical kinetic models for fuel components used in surrogate fuels for spark-ignition engines, diesel engines, and kinetically controlled compression-ignition engines
- Combine component models into surrogate fuel models to represent real transportation fuels; use them to model advanced combustion strategies in engines that lead to low emissions and high efficiency

Fiscal Year 2018 Objectives

- Validate and improve diesel surrogate fuel component and mixture models using new experimental data from University of Connecticut's rapid compression machine (RCM)
- Improve gasoline surrogate model with new data on blends of olefins and aromatics from the Argonne National Laboratory (ANL) RCM

Approach

Gasoline and diesel fuels consist of complex mixtures of hundreds of different components. These components can be grouped into chemical classes including n-alkanes, iso-alkanes, cyclo-alkanes, alkenes, oxygenates, and aromatics. Since it is not feasible to develop chemical kinetic models for hundreds of components, specific components need to be identified to represent each of these chemical classes. Then detailed chemical kinetic models can be developed for these selected components. These component models are subsequently merged together to produce a "surrogate" fuel model for gasoline, diesel, and next-generation transportation fuels. This approach creates realistic surrogates for gasoline or diesel fuels that can reproduce experimental behavior of the practical real fuels that they represent. Detailed kinetic models for surrogate fuels can then be simplified as needed for inclusion in multidimensional computational fluid dynamics simulations of engine combustion.

Results

Key accomplishments for Fiscal Year 2018:

- Developed and improved the kinetic mechanisms of 1,2,4 trimethyl benzene (124TMB), iso-dodecane, and iso-cetane
- Developed a new polycyclic aromatic hydrocarbon (PAH) model
- Developed a preliminary soot model using sectional method
- Established that LLNL gasoline surrogate model matches ignition properties at very high pressures in shock tube (up to 220 atm)
- Developed a detailed kinetic model which describes the ignition chemistry of n-alkanes (C8–C20), including those found in diesel fuel
- Evaluated LLNL gasoline surrogate model using new ANL RCM data on FACE F research-grade gasoline
- Developed a new mechanism for a C6 branched olefin (2-methyl-2-pentene) that is more representative of olefins in gasoline fuels

The LLNL kinetic models for diesel components were improved to enhance the predictability of diesel surrogate mixture models. The kinetic models for 124TMB, iso-cetane (2,2,4,4,6,8,8-heptamethylnonane), and iso-dodecane (2,2,4,6,6-pentamethylheptane) were improved. The kinetic model of 124TMB was revised heavily to add the missing reaction pathways and update the reaction rate constants based on information from fundamental computational chemistry studies. Specifically, significant improvements were made to the low-temperature reaction chemistry of 124TMB. The kinetic submodels of xylene isomers and toluene, which are building blocks for the 124TMB model, were also updated. The improved mechanism was validated against new experimental data obtained from the RCM from ANL to ensure that the mechanism successfully captures the ignition propensity of 124TMB [1] (Figure I.13.1). It was also validated against speciation data from the shock tube at University of Illinois, Chicago, and against high-temperature shock-tube ignition data from Rensselaer Polytechnic Institute.

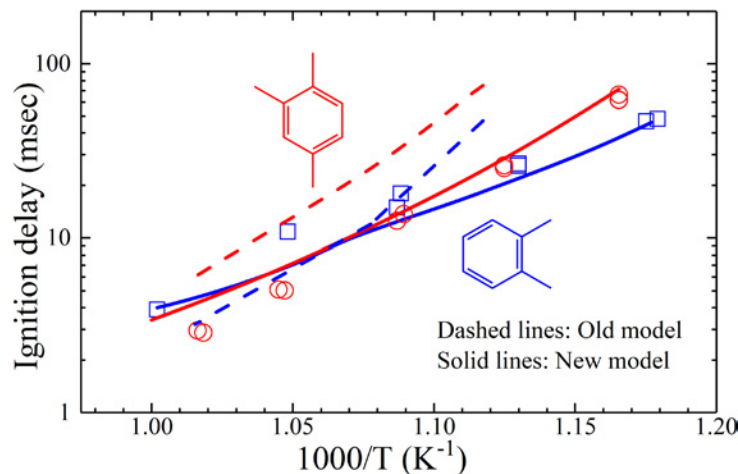


Figure I.13.1. Comparison of old and new trimethyl benzene (red) and ortho-xylene (blue) LLNL kinetic model simulations with ignition delay times (IDTs) measured in the ANL RCM [1].

Symbols: experimental data. Dashed lines: old LLNL kinetic model predictions.

Solid lines: new LLNL model predictions.

Developing a predictive kinetic model for iso-cetane is challenging due to the high number of methyl substitutions that make estimations difficult for reaction-rate constants and thermodynamic properties. In order to capture the effect of methyl substitutions, the ignition properties of the isomers of hexane (five isomers

with varying degree of substitutions) and iso-dodecane have been simulated and compared to those measured experimentally in RCMs from the National University of Ireland, Galway, and University of Connecticut. Using the ignition delay data of the hexane isomers, iso-octane, and iso-dodecane, a set of reaction rate rules has been developed for use in improving the kinetic models for other iso-alkanes. These new reaction rate rules, when used in the iso-cetane kinetic model, helped to improve its performance. Further improvements are still needed for the iso-cetane model to accurately predict the full range of IDTs in the RCM.

Predictive soot models are needed in engine simulation codes to predict the effects of fuel properties and engine-design changes on soot emissions. Formation of soot involves various physical and chemical processes, which include PAH formation, nucleation, surface growth, coagulation, and oxidation. The complex processes after PAH formation are largely captured by employing a soot-sectional method. The sectional method is built hierarchically on the PAH mechanism, which describes the formation of soot precursors during oxidation and pyrolysis of hydrocarbons. However, accurate prediction using PAH kinetic models has been a long-time challenge for the combustion community. During this project, the LLNL kinetics team has developed a detailed PAH model using newly available PAH formation reaction rates and reaction product channels from the literature. The PAH mechanism describes the formation and consumption of large PAHs from two (naphthalene) to seven (coronene) rings and can be used to simulate the PAHs produced during oxidation/pyrolysis of gasoline and diesel fuels. Predictions of the PAH model have been compared against experimental pyrolysis data with encouraging results (Figure I.13.2). This PAH model has been linked to a soot sectional model so that preliminary soot predictions can be made and compared to measured soot data in reacting systems.

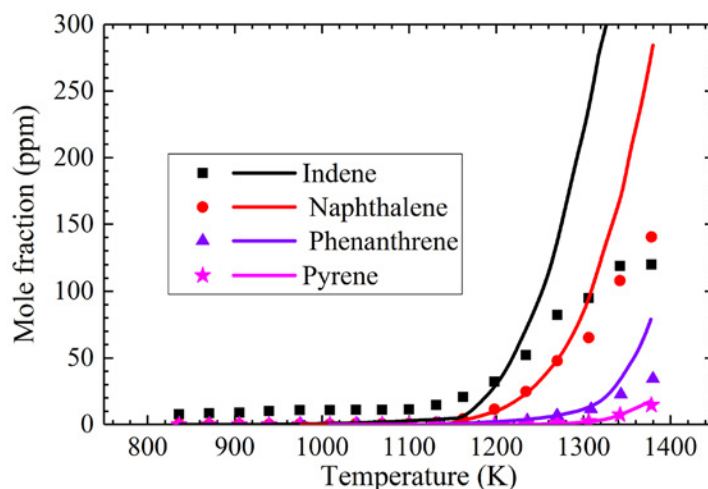


Figure I.13.2. Evolution of major PAHs during the pyrolysis of toluene primary reference fuel 97.5 (n-heptane/iso-octane/toluene = 14.5/8.0/77.5, by mole, respectively, 97.5 research octane number [RON]) in a flow reactor. Symbols: experimental data, Shao et al. [4]. Lines: LLNL PAH kinetic model predictions.

The LLNL gasoline surrogate model was evaluated using new experimental data from the RCM at ANL on FACE F, which is a research-grade, full-boiling, mid-octane gasoline with an antiknock index of 91.5 and octane sensitivity (OS) of 5.6 [2]. A gasoline surrogate mixture using five representative components was developed to represent FACE F. The RCM data covered a pressure range of 20–70 bar and a temperature range of 700 K–1,000 K, and included equivalence ratios of 0.3 and 1. For a stoichiometric equivalence ratio, the LLNL chemical kinetic model with the five-component surrogate mixture was generally in good agreement with the IDTs over a temperature range of 700 K–1,000 K and pressures of 20–41 bar. The simulated pressure histories also matched well the experimentally measured ones at 750 K, which show two-stage ignition behavior and first-stage heat release. For the fuel-lean equivalence ratio of 0.3, where the pressure range was increased up to 70 bar, the chemical kinetic model was generally more reactive than experimentally observed. Sensitivity analysis of the gasoline surrogate mechanism indicated that improvements may be needed for the submodel of cyclopentane, a component used in the surrogate mixture to represent cycloalkanes present in FACE F. Improvements to the cyclopentane kinetic model are underway.

The LLNL kinetic model for gasoline was used to simulate shock tube experiments on ignition of high-octane gasolines [3]. The measured IDTs allowed testing of the kinetic model at much higher pressures than previously available in a shock tube. The experimental conditions included pressures from 40 atm to 220 atm and fuel/air equivalence ratios of 0.7 to 1. The RON and OS of the high-octane gasolines ranged from 101 to 106 and 7 to 15, respectively. Surrogate mixtures were developed to match as closely as possible the properties of each gasoline in terms of RON, OS, and chemical-class composition. The surrogate mixtures were used to simulate the ignition behavior of the high-octane gasolines. Comparisons of the measured and simulated ignition behavior are shown for one of the high-octane gasolines in Figure I.13.3. Good agreement was obtained between the measured and simulated IDTs, showing that the kinetic model performs well at very high pressures like those encountered under internal combustion engine conditions.

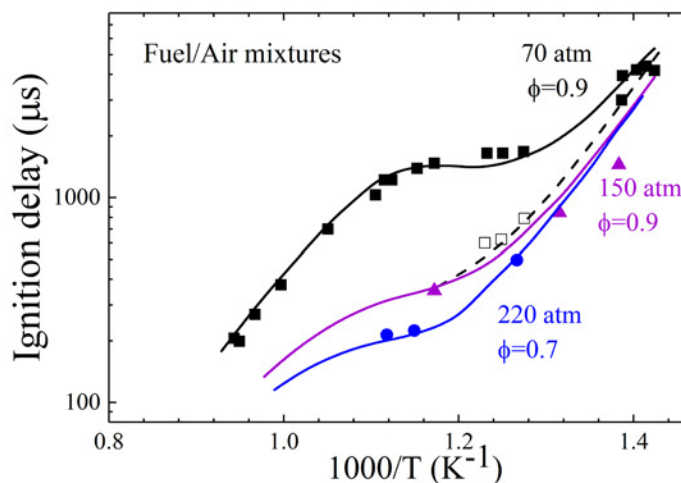


Figure I.13.3. Comparison of LLNL gasoline surrogate model results with IDTs measured in the Stanford high-pressure shock tube for a high-octane, moderate sensitivity (RON = 101, OS 7) gasoline [3]. ϕ is fuel/air equivalence ratio. Symbols: experimental data. Lines: simulations. Dashed line and open squares: first-stage IDT. Solid lines and filled symbols: total IDT.

Conclusions

- The LLNL gasoline surrogate model was shown to be valid up to pressures of 220 bar for a representative research-grade, full-boiling, mid-octane gasoline (FACE F).
- A new PAH kinetic model was developed and linked to a sectional soot model to predict soot.
- Kinetic models were improved for diesel surrogate components 1,2,4 trimethyl benzene, iso-dodecane, and iso-cetane.
- New and validated reaction-rate rules for iso-alkanes were developed.

Key Publications

1. Kukkadapu, G., D. Kang, S.W. Wagnon, K. Zhang, M. Mehl, M.M. Palacios, H. Wang, S.S. Goldsborough, C.K. Westbrook, and W.J. Pitz. 2018. "Kinetic Modeling Study of Surrogate Components for Gasoline, Jet and Diesel Fuels: C7-C11 Methylated Aromatics." *Proceedings of the Combustion Institute*. <https://doi.org/10.1016/j.proci.2018.08.016>.
2. Kang, D., A. Fridlyand, S.S. Goldsborough, S.W. Wagnon, M. Mehl, W.J. Pitz, and M.J. McNenly. 2018. "Auto-Ignition Study of FACE Gasoline and Its Surrogates at Advanced IC Engine Conditions." 37th International Symposium on Combustion. <https://doi.org/10.1016/j.proci.2018.08.053>.

3. Davidson, D.F., J.K. Shao, R. Choudhary, M. Mehl, N. Obrecht, and R.K. Hanson. 2018. "Ignition Delay Time Measurements and Modeling for Gasoline at Very High Pressures." *Proceedings of the Combustion Institute*. <https://doi.org/10.1016/j.proci.2018.08.032>.
4. Wang, M., K. Zhang, G. Kukkadapu, S.W. Wagon, M. Mehl, W.J. Pitz, and C.-J. Sung. 2018. "Autoignition of Trans-Decalin, a Diesel Surrogate Compound: Rapid Compression Machine Experiments and Chemical Kinetic Modeling." *Combustion and Flame* 194: 152–163.

References

1. Kukkadapu, G., D. Kang, S.W. Wagon, K. Zhang, M. Mehl, M.M. Palacios, H. Wang, S.S. Goldsborough, C.K. Westbrook, and W.J. Pitz. 2018. "Kinetic Modeling Study of Surrogate Components for Gasoline, Jet and Diesel Fuels: C7-C11 Methylated Aromatics." *Proceedings of the Combustion Institute*. <https://doi.org/10.1016/j.proci.2018.08.016>.
2. Cannella, W., M. Foster, G. Gunter, and W. Leppard. 2014. "FACE Gasolines and Blends with Ethanol: Detailed Characterization of Physical and Chemical Properties." Coordinating Research Council, Inc., CRC Report No. AVFL-24, <http://www.crao.org/Publications/advancedVehiclesFuelsLubricants/index.html>.
3. Davidson, D.F., J.K. Shao, R. Choudhary, M. Mehl, N. Obrecht, and R.K. Hanson. 2018. "Ignition Delay Time Measurements and Modeling for Gasoline at Very High Pressures." *Proceedings of the Combustion Institute*. <https://doi.org/10.1016/j.proci.2018.08.032>.
4. Shao, C., H. Wang, N. Atef, Z. Wang, B. Chen, M. Almalki, Y. Zhang, C. Cao, J. Yang, and S.M. Sarathy. 2018. "Polycyclic Aromatic Hydrocarbons in Pyrolysis of Gasoline Surrogates (n-Heptane/iso-Octane/Toluene)." *Proc. Combust. Inst.* doi: <https://doi.org/10.1016/j.proci.2018.06.087>.

Acknowledgements

This work was performed under the auspices of the U.S. Department of Energy by Lawrence Livermore National Laboratory under Contract DE-AC52-07NA27344.

I.14 Model Development and Analysis of Clean and E (Lawrence Livermore National Laboratory)

Russell Whitesides, Principal Investigator

Lawrence Livermore National Laboratory (LLNL)
L-792, 7000 East Ave.
Livermore, CA 94551
E-mail: whitesides1@llnl.gov

Michael Weismiller, DOE Technology Development Manager

U.S. Department of Energy
E-mail: Michael.Weismiller@ee.doe.gov

Start Date: October 1, 2017	End Date: September 30, 2018	
Project Funding (FY18): \$925,000	DOE share: \$925,000	Non-DOE share: \$0

Project Introduction

Internal combustion engine design is increasingly driven by computational models used to predict performance metrics, which previously would have been predicted by limited design intuition or expensive and time-consuming physical testing. Improved model capabilities shorten design cycles and enable the production of cleaner and more efficient engines. This project focuses on advancing the state of the art in internal combustion engine simulations. The overarching goal is to enable predictive models and reduced time to solution for simulations that impact combustion engine design.

Objectives

Overall Objectives

- Advance state of the art in engine simulation through the development of fast and accurate models
- Work with industry partners to prove capability and impact of combustion chemistry software

Fiscal Year 2018 Objectives

- Accelerate detailed kinetics coupled to engine computational fluid dynamics (CFD)
- Implement fast solution methods for one-dimensional (1D) laminar flames
- Deploy web application for kinetic model testing and debugging

Approach

This project is an ongoing research effort under DOE's Advanced Combustion Engines subprogram with annual feedback and direction from program managers and memorandum of understanding partners. During the current performance period, this project has focused on three areas: (1) fast chemical solution for engine CFD, (2) efficient solvers for 1D flames with detailed chemistry, and (3) deployment of a web application for kinetic model testing and debugging.

Results

Fast Chemical Solution for Engine CFD

Detailed reaction kinetics are vital for prediction of ignition and emissions phenomena, two of the most important aspects of advanced engine development. This project has developed methods for efficient solution of large chemical systems in engine CFD simulations. In the current year, a new extrapolation-based ordinary differential equations solver, SEULEX [1], was incorporated into the LLNL-developed Zero-RK chemistry solver suite [2]. The current effort was motivated by a study done by Imren and Haworth [3], which showed

that SEULEX can be more efficient than the commonly used backward differential formula methods when coupled to CFD simulations. The present work leverages the existing LLNL fast chemistry tools work as part of a flexible framework that can interface to industry standard codes, such as CONVERGE CFD, as well as open source codes, like OpenFOAM, often favored in academia.

The Engine Combustion Network (ECN) Spray A condition [4] was used to test the performance of the solver and investigate the impact of highly detailed chemistry on engine-relevant phenomena. Multiple groups have run experiments and simulations under the agreed-upon Spray A conditions, so there is a wealth of data for validation and comparison. Despite this previous effort, a gap remains in agreement between the simulations and experiments at lower temperatures. Previous simulation efforts have been limited to chemical reaction models containing up to around 100 species due to the impact of mechanism size on simulation time. At these smaller sizes, chemical models omit or over-simplify low-temperature chemical reactions [5]. In the present work, simulations were run using six chemical mechanisms ranging from 54 to 2,300 species, with three smaller mechanisms [6–8] that have been used before for this problem and three highly detailed (more than 1,000 species) [9,10].

Figure I.14.1 shows a plot of the ignition delay versus ambient temperature for Spray A conditions with n-dodecane as the fuel simulated with each of the six chemical mechanisms. The plot shows that the two most recent detailed mechanisms match the experimental data best. The two smallest mechanisms are too reactive at higher temperatures while they fail to predict ignition at 750 K. The 103-species mechanism is not quite reactive at all temperatures and also fails to predict ignition at the lowest temperature. Only the large detailed mechanisms correctly predict ignition at 750 K. This first-of-its-kind result is possible due to the capability of the fast chemistry solvers developed in this project.

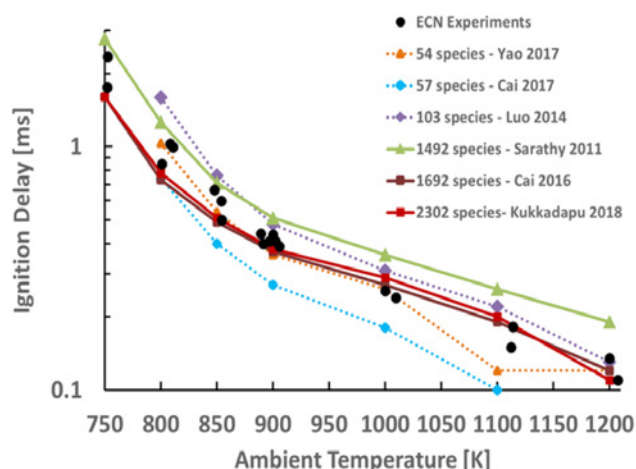


Figure I.14.1. Log plot of ignition delay versus ambient temperature for n-dodecane at Spray A conditions. Larger detailed mechanisms are able to capture the ignition delay at low temperature and high temperature better than the smaller reduced mechanisms tested.

As an example of the reduction in simulation time using the newly developed solver, solution times were compared for the Spray A simulations using three different chemical solvers for the 1,492-species n-dodecane model. The three solvers are SAGE (the default solver built into CONVERGE CFD), Zero-RK CVODE (the LLNL solver that has been previously developed in this program), and Zero-RK SEULEX (the extrapolation-based ordinary differential equations solver that has been implemented this year). The comparisons in simulation time for both chemistry and total solution time are shown in Figure I.14.2. The new Zero-RK SEULEX solver shows significant improvement in time-to-solution and is able to cut the simulation time from over two weeks to about three days.

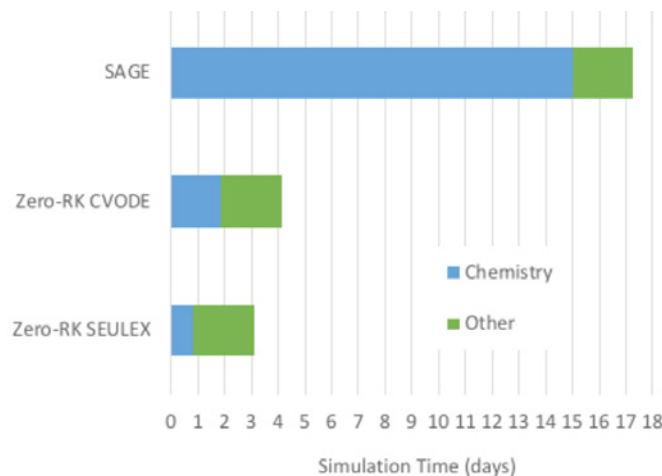


Figure I.14.2. Total simulation time for Spray A simulation with detailed reaction model [9], colored by time spent in chemistry and non-chemistry routines

Efficient Solvers for One-Dimensional Laminar Flames

Simulations of 1D laminar flames using detailed kinetic mechanisms are useful in a wide variety of engine combustion applications. The most common use is in the computation of laminar flame speeds, which are useful for chemical mechanism validation, as inputs to turbulent flame speed correlations, and to predict knocking in spark-ignition engines. Other applications include generation of flamelet libraries for CFD simulations and prediction of combustion dynamics in micro-flow reactors. These fundamental combustion simulations are an important component in the study of realistic transportation fuel models in boosted spark-ignition and multi-mode engine configurations.

The fast chemistry methods developed for Zero-RK [2] have been adapted to accelerate fully coupled fluid-chemistry models for steady and unsteady laminar, premixed flames. The adaptive preconditioner method was extended to include convective and diffusive terms and to take advantage of parallel computing architectures when solving the chemical system at multiple spatial locations. The key to the approach developed here is an iterative solver with approximate Jacobians that allow for efficient matrix factorization. The result is a set of solvers with solution time that scales linearly with the number of chemical species included in the reaction mechanism. For highly detailed reaction models, this linear scaling results in significant cost savings. For example, computing a single laminar flame speed for the gasoline reaction model developed under the Co-Optima program, containing 2,878 species, the current solver is approximately 50 times faster than the previous state of the art. In addition, the solver has been parallelized to be able to take advantage of multi-core computing systems and shows good parallel scaling up to 16 central processing unit cores, further reducing time to solution for these calculations. For the common case of evaluating flame speed as a function of equivalence ratio for a single fuel, a speedup of over 100 times can be achieved with our solvers compared with the commonly used Chemkin Pro software. The new solvers were verified to produce the same results, subject to numerical accuracy, as those by Chemkin Pro [11], FlameMaster [12] and NGA [13]. The unsteady solver has also been experimentally validated against measurements made in a millimeter-scale flow reactor as part of a separate project [14].

The solvers are already being applied in collaboration with multiple Advanced Combustion Systems and Co-Optima partners, and a manuscript describing the methodology is in preparation. Furthermore, the approach of direct coupling of detailed chemical kinetics with advection and diffusion has the potential to achieve significant speedup over the range of applications and simulations used in the Advanced Combustion Systems program and the larger high-efficiency clean combustion research community, including fully coupled CFD and reduced-order engine models [15].

Combustion Tools Web Application

In previous years, work under this task resulted in the development of software tools to identify errors in large chemical kinetic mechanisms and their associated thermochemistry files. These tools were only available on the LLNL network and required training to use. To allow outside users access and improve utilization of these tools, LLNL researchers collaborated with information technology professionals at LLNL to develop a web application that provides a user-friendly interface and cloud-based environment to run them. This implementation gives users around the world access to the tools without the need to install any software or perform updates. The web application is available at <https://combustiontools.llnl.gov>. The chemical analysis tools are able to identify non-physical behavior, which is then flagged so that researchers can find and fix problems with model's reaction rates. A thermochemistry repair tool is also available that checks for any discontinuous thermodynamic functions and can make automatic repairs. The presence of discontinuous thermodynamic functions in the fuel chemistry model can cause simulations to take extremely small time steps, which leads to unnecessary increases in the computational cost. Improved access to these tools will help improve the accuracy and performance of detailed chemical mechanisms and improve the work flow of fuel and engine researchers throughout the Advanced Combustion Systems program and its industry partners.

Conclusions

Key Accomplishments for Fiscal Year 2018

- New chemistry solver coupled to engine CFD enables new simulation regime, which pushes the predictive envelope for low-temperature combustion
- Efficient 1D flame solvers dramatically reduce simulation time for detailed kinetics, opening a door to a wide variety of engine applications, including improved kinetic model development and fuel kinetic effects on engine knock
- Combustion tools web application brought online for use by industry and academic partners to improve the models used throughout the combustion community

Key Publications

1. Killingsworth, Nick J., Matthew J. McNenly, and Russell A. Whitesides. "Cloud Based Tool for Analysis of Chemical Kinetic Mechanisms." In preparation.
2. Lapointe, Simon, Russell A. Whitesides, and Matthew J. McNenly. "Sparse, Iterative Simulation Methods for One-Dimensional Laminar Flames." *Combust. Flame*, under review.

References

1. Hairer, Ernst. "Solving Ordinary Differential Equations II - Stiff and Differential - Algebraic Problems." Springer, n.d. [//www.springer.com/us/book/9783662099476](http://www.springer.com/us/book/9783662099476) (accessed April 2, 2018).
2. McNenly, M.J., R.A. Whitesides, and D.L. Flowers. 2015. "Faster Solvers for Large Kinetic Mechanisms Using Adaptive Preconditioners." *Proc. Combust. Inst.* 35: 581–587. doi:10.1016/j.proci.2014.05.113.
3. Imren, A., and D.C. Haworth. 2016. "On the Merits of Extrapolation-Based Stiff ODE Solvers for Combustion CFD." *Combust. Flame* 174: 1–15. doi:10.1016/j.combustflame.2016.09.018.
4. Pickett, L.M., C.L. Genzale, G. Bruneaux, L-M. Malbec, L. Hermant, C. Christiansen, and J. Schramm. 2010. "Comparison of Diesel Spray Combustion in Different High-Temperature, High-Pressure Facilities." *SAE Int. J. Engines* 3: 156–181. doi:10.4271/2010-01-2106.
5. Engine Combustion Network ECN5 Proceedings, (n.d.). <https://ecn.sandia.gov/ecn-workshop/ecn5-workshop/> (accessed April 2, 2018).

6. Yao, T., Y. Pei, B.-J. Zhong, S. Som, T. Lu, and K.H. Luo. 2017. "A Compact Skeletal Mechanism for n-Dodecane with Optimized Semi-Global Low-Temperature Chemistry for Diesel Engine Simulations." *Fuel* 191: 339–349. doi:10.1016/j.fuel.2016.11.083.
7. Davidovic, M., T. Falkenstein, M. Bode, L. Cai, S. Kang, J. Hinrichs, and H. Pitsch. 2017. "LES of n-Dodecane Spray Combustion Using a Multiple Representative Interactive Flamelets Model." *Oil Gas Sci Technol – Rev IFP Energ. Nouv.* 72. doi:10.2516/ogst/2017019.
8. Luo, Z., S. Som, S.M. Sarathy, M. Plomer, W.J. Pitz, D.E. Longman, and T. Lu. 2017. "Development and Validation of an n-Dodecane Skeletal Mechanism for Spray Combustion Applications." *Combust. Theory Model* 18: 187–203. doi:10.1080/13647830.2013.872807.
9. Sarathy, S.M., C.K. Westbrook, M. Mehl, W.J. Pitz, C. Togbe, P. Dagaut, H. Wang, M.A. Oehlschlaeger, U. Niemann, K. Seshadri, P.S. Veloo, C. Ji, F.N. Egolfopoulos, and T. Lu. 2011. "Comprehensive Chemical Kinetic Modeling of the Oxidation of 2-Methylalkanes from C7 to C20." *Combust. Flame* 158: 2338–2357. doi:10.1016/j.combustflame.2011.05.007.
10. Cai, L., H. Pitsch, S.Y. Mohamed, V. Raman, J. Bugler, H. Curran, and S.M. Sarathy. 2016. "Optimized Reaction Mechanism Rate Rules for Ignition of Normal Alkanes." *Combust. Flame* 173: 468–482. doi:10.1016/j.combustflame.2016.04.022.
11. ANSYS Chemkin Theory Manual 18.0 (15180), Reaction Design: San Diego, 2017.
12. Pitsch, H. 2017. "FlameMaster: A C++ Computer Program for 0D Combustion and 1D Laminar Flame Calculations." <https://www.itv.rwth-aachen.de/index.php?id=flamemaster>.
13. Desjardins, O., G. Blanquart, G. Balarac, and H. Pitsch. 2008. "High Order Conservative Finite Difference Scheme for Variable Density Low Mach Number Turbulent Flows." *J. Comput. Phys* 227: 7125–7159. doi:10.1016/j.jcp.2008.03.027.
14. Lapointe, S., C.L. Druzgalski, and M.J. McNenly. "Numerical Study of a Micro Flow Reactor at Engine Pressures: Flames with Repetitive Extinction and Ignition and Simulations with a Reduced Chemical Model." *Combust. Flame* 197: 102–110. doi:10.1016/j.combustflame.2018.07.020.
15. Kodavasal, Janardhan, Matthew J. McNenly, Aristotelis Babajimopoulos, Salvador M. Aceves, Dennis N. Assanis, Mark A. Havstad, and Daniel L. Flowers. 2013. "An Accelerated Multi-Zone Model for Engine Cycle Simulation of Homogeneous Charge Compression Ignition Combustion." *Int. J. Engine Res.* 14: 416–433. doi:10.1177/1468087413482480.

Acknowledgements

This work was performed under the auspices of the U.S. Department of Energy by Lawrence Livermore National Laboratory under Contract DE-AC52-07NA27344.

LLNL Document Number: LLNL-TR-761325

Significant contributions to the work reported here were made by Nick Killingsworth, Simon Lapointe, and Matthew McNenly of Lawrence Livermore National Laboratory.

I.15 2018 FEARCE Development: A Robust and Accurate Engine Modeling Software (Los Alamos National Laboratory)

David B. Carrington, Principal Investigator

Los Alamos National Laboratory (LANL)
 P.O. Box 1663
 MS-B216
 Theoretical Division, T-3 Fluid Dynamics and Solid Mechanics
 Los Alamos, NM 87544
 E-mail: dcarrington@lanl.gov

Michael Weismiller, DOE Technology Development Manager

U.S. Department of Energy
 E-mail: Michael.Weismiller@ee.doe.gov

Start Date: October 1, 2017	End Date: September 30, 2018	
Project Funding (FY18): \$200,000	DOE share: \$200,000	Non-DOE share: \$0

Project Introduction

Research and development of **F**ast, **E**asy, **A**ccurate and **R**obust Continuum Engineering (**FEARCE**, formerly KIVA-hpFE) for turbulent reactive and multiphase flow, particularly as related to engine modeling, is relevant to the DOE Vehicle Technologies Office efforts at addressing national energy security. Less dependence on petroleum products leads to greater energy security. By U.S. Environmental Protection Agency standards, some vehicles are now reaching the 42–50 mpg mark. These are conventional gasoline engines. With continued investment and research into new technical innovations, the potential exists to save more than 4 million barrels of oil per day, or approximately \$200 to \$400 million per day. This would be a significant decrease in emissions and use of petroleum and a very large stimulus to the U.S. economy.

Better understanding of fuel injection and fuel–air mixing, thermodynamic combustion losses, and combustion/emission formation processes enhances our ability to minimize fuel use and unwanted emissions. Helping to accomplish this understanding, the FEARCE or KIVA development project is providing a state-of-the-art capability for accurately simulating combustion processes: to have a predictive methodology in software helping industry and researchers not only meet national goals on fuel usage and emissions, but global goals. In addition, a predictive, robust, and accurate capability for simulating the engine combustion process helps to minimize time and labor for development of new engine technology.

Objectives

A main goal of the FEARCE or KIVA development project is to help provide better understanding of engine combustion processes in order to enhance the ability to minimize fuel use and unwanted emissions. The FEARCE development project is providing a state-of-the-art capability for accurately simulating combustion processes and is providing a more predictive methodology than currently available in software to supply industry and researchers a tool to help meet national goals on emissions and engine efficiencies. In addition, a predictive, robust, and accurate capability for simulating engine combustion processes helps to minimize time and labor for development of new engine technology. To meet these goals, our project objectives are listed as follows.

Overall Objectives

- Develop mathematical and computer algorithms and software for the advancement of speed, accuracy, robustness, and range of applicability of FEARCE, an internal engine combustion modeling software package, to be a more predictive computer code. This is to be accomplished by employing higher-order, spatially accurate methods for reactive turbulent flow and more predictive spray injection, combined

with a robust and accurate actuated parts simulation along with more appropriate turbulence modeling. In addition, we seek to understand the effect of heat transfer and the variation of temperatures on the internal combustion engine by creating easy-to-use numerical methods that eliminate all usual assumptions about such phenomena, such as assumed heat transfer processes at chamber and part boundaries. The code combines state-of-the-art chemical reaction simulators, such as Chemkin-Pro.

- Provide engine modeling software that is easier to maintain and easier to add models to than the current KIVA codes, and reduce code development costs into the future via more modern code architecture. In addition, FEARCE is being developed to be a commercially available software package, where DOE and LANL are doing the very difficult longer-term research for better modeling software which is best done using the types of capabilities available at the national laboratories.
- Provide software capable of producing fast turn-around times needed by industry. The code not only functions well on small computer platforms but addresses high-performance computing aspects required for high-fidelity and more predictive solutions. These objectives require extensive use of high-performance computing, thereby requiring our work to employ modern frameworks and methods that take advantage of computer resources very effectively, which FEARCE has accomplished by scaling to the size of the problem in a super-linear manner, the holy grail of high-performance computing.

Fiscal Year 2018 Objectives

- Develop a four-valve direct injection, spark ignition (DISI) engine system for validation of FEARCE
- Validate progress of FEARCE on experimental data of the four-valve DISI engine; collaborate with Dr. Magnus Solberg of Sandia National Laboratories (SNL) on the DISI setup and experimental data
- Construct systems to use ChemKin II and III and ChemKin-Pro reactive chemistry software
- Continue spray model development for both predictive spray break-up and subsequent droplet transport and fate; implement the Kelvin Helmholtz – Rayleigh Taylor (KH-RT) spray model and perform validation against data stored on the Engine Combustion Network (ECN) website from various experimentalists
- Develop faster linear solver system by implementing a multigrid solution system of linear equations that improves our current implicit solutions methods by more than a factor of two
 - o Invented a method for implementing Message Passing Interface (MPI) for today's and future platforms [1] that is super-linear
- Begin the process of commercialization of FEARCE

Approach

Our approach is founded in designing, inventing, and developing new modeling methods and software. The design is a finite element method (FEM). Many beneficial and salient attributes of the software stem from the FEM formulation. We invented and developed the following systems to date (details are provided in the referenced publications).

- Developed the FEM predictor–corrector scheme projection method for high accuracy and all the benefits the FEM system brings to computational fluid dynamics (CFD) modeling of engines [2,3]
- Developed the hp-adaptive system for higher-order accuracy, where ‘h-adaptive’ is automatic grid refinement and ‘p-adaptive’ is higher-order approximation as driven by the error measure of the simulation [4]
- Invented the local-arbitrary Lagrangian–Eulerian (ALE) method for moving bodies [5]
 - o Invented a moving marker system to track any chosen interfaces and reconstruct intersected elements to match the interface

- Developed immersed boundary methods for moving bodies [6]
- Developed new dynamic large eddy simulation (LES), specifically designed for wall-bounded flows [7]
 - o Self-damping turbulence at the walls negates the need for a law-of-the-wall system
- Invented and developed volume-of-fluid (VOF) methods in FEM for true multi-phase compressible flow to fully represent the spray break-up process and to have predictive spray modeling [8]
- Developed a fast linear solver system
 - o Developed parallel solution method [1]
 - Delivered 30× speed-up over serial code given the same problem and settings
 - Implicit solutions methods for 10× speed-up over serial parallel for an overall 300× speed-up
 - o Added Trilinos [9] Multigrid matrix solution, further improving solution speed and parallel scaling by order of magnitude (8×) over Implicit Beam-Warming system in FEARCE (that delivers 300×) for a total of 2,400× speed-up over explicit serial version
 - o Delivers super-linear scalability
- Invented a method for implementing MPI for today's and future platforms [1]

We are building models and code so that they meet all the objectives in easy-to-maintain software that easily handles addition of others' submodels. Careful verification and validation of the methods and code is required. The development of this technology utilizes many areas of expertise, including multi-species turbulent reactive flow modeling with liquid sprays, modeling of immersed moving bodies, and the extensive numerical methods for the solution of the model and governing equations developed in the software.

Results

Our efforts this year continue to push toward a comprehensive tool for the future with the accomplishment of more grid generation improvements, validation of immersed moving parts including four-valve DISI engine, the KH-RT spray model, and an algebraic multigrid linear equation solver implementation for even greater computational speed. We've also begun the process of commercializing the software to be able to fully support the requirements of industries and researchers for a simulation software.

Grid Generation

- In conjunction with Program Development Company, who developed GridPro, we are working on providing high quality grids for the engine system with an eye toward ease of use. The overset parts system used in the moving parts algorithm allows for easy grid generation of the cylinders and ports, with the spark and injector modules easily inserted. The piston and valves surfaces simply are also inserted by overlaying their surface representations after a quality grid is automatically generated.
- The overset gridding greatly simplifies the gridding process, removing the need to work around immersed bodies employed in traditional gridding methods. The injector and spark systems are built separately with the idea of making various types of injectors and spark plug modules that are simply connected to the engine cylinder grid. It cannot be overstated: a quality grid is needed to produce reliable simulations. Gridding is a major component of CFD, where we seek to provide that quality with a minimum of labor.

Engine Simulation and Continued Validation of Immersed Moving Parts for the Engine System

- We developed an immersed boundary method and are developing the immersed FEMs for moving bodies using FEARCE's surface marker system. This work is partially based on methods used in our local-ALE system for moving bodies.
- The moving marker system utilizes track-moving boundary interfaces [5].

- Immersed boundary employs interpolation and projection of nearest nodal values normal to the surface. Immersed FEM utilizes the shape or basis functions for interpolation and a projection system to place a point along the normal to the surface, from which the nearest node is projected, to calculate the fluid's motion and thermodynamic state.
- A four-valve engine test case is functioning as shown in Figure I.15.1 using the immersed boundary methods, showing turbulent flow structures (by vorticity).

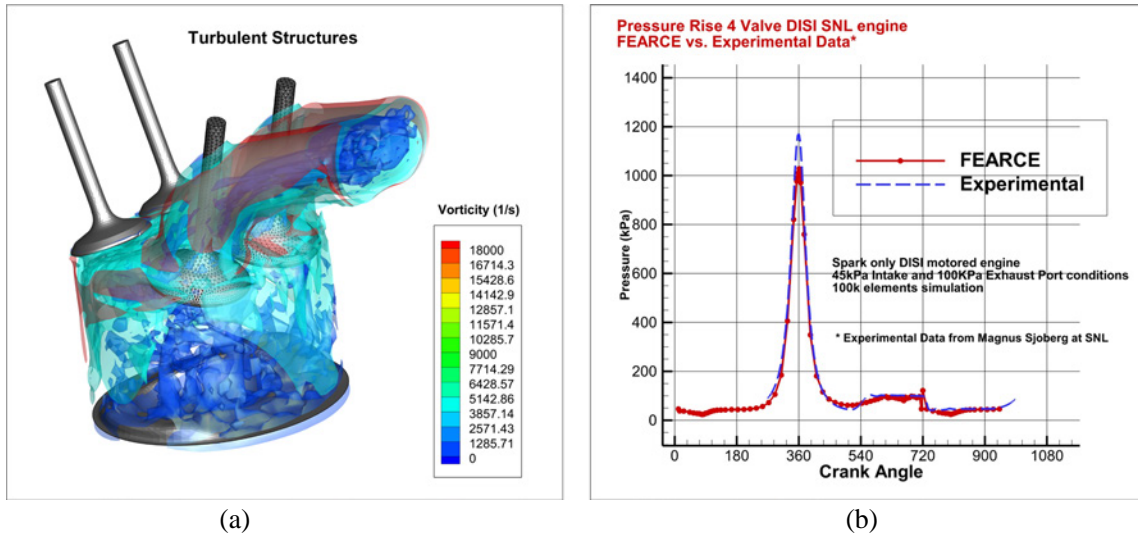


Figure I.15.1. Four-valve DISI engine: (a) turbulent structures shown by magnitude of vorticity (1/s) during intake; (b) pressure rise as a function of crank angle as compared to experimental data

Spray Modeling

- We implemented the KH-RT spray model into FEARCE. Tests have been conducted on Spray A and Spray G ECN test cases to date with the following results. The KH-RT spray model [10] for the Spray A case simulates injection of diesel into quiescent nitrogen at 2.2 MPa, as shown in Figure I.15.2. Figure I.15.2a shows the droplets at 2 μ s. Figure I.15.2b shows the penetration (mass moment distribution) of the spray droplets over time compared with experimental data from ECN.

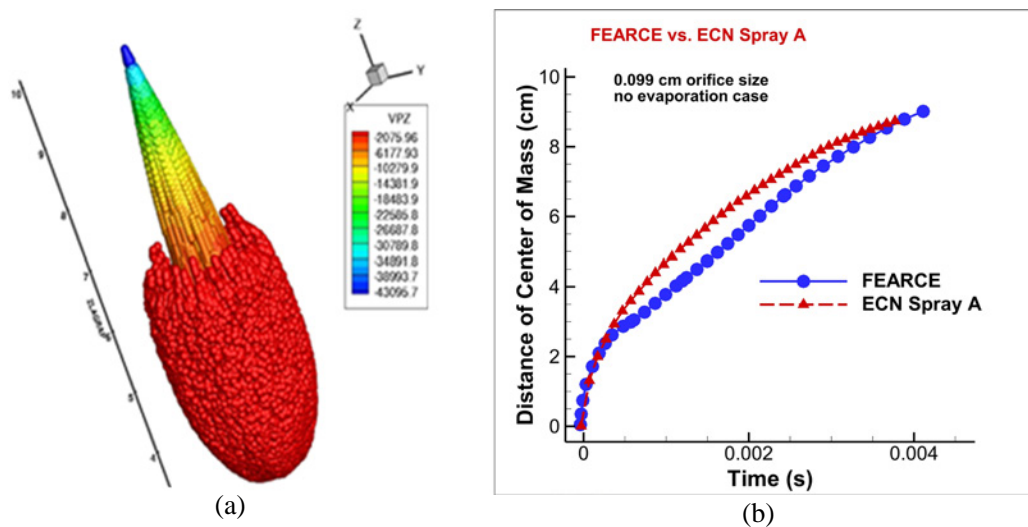


Figure I.15.2. The ECN Spray A case: (a) injection of diesel in quiescent nitrogen at 2.2 MPa, KH-RT spray model; (b) the penetration depth of the spray compared to ECN experimental data

- We are developing a system for fully representing the injection process from our current predictive spray break-up process using VOF, as shown in Figure I.15.3. The system hands off the predicted spray break-up into ligaments and subsequent droplet transport modeling and evaporation, allowing true spray break-up transition to the Lagrangian particle and Rayleigh–Taylor secondary break-up systems, thereby producing more accurate engineering modeling for the injection system. Figure I.15.3 shows liquid being injected into air at 3 bar through an orifice of 0.01-mm diameter early in time. The break-up length where the wave instabilities are large enough to cause ligamentation is five orifice diameters downstream of inlet, which is near the results obtained by direct numerical simulation (DNS) as reported in Waters et al. [8].

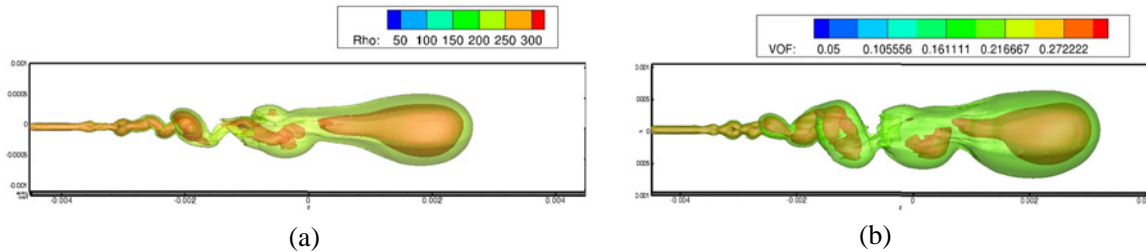


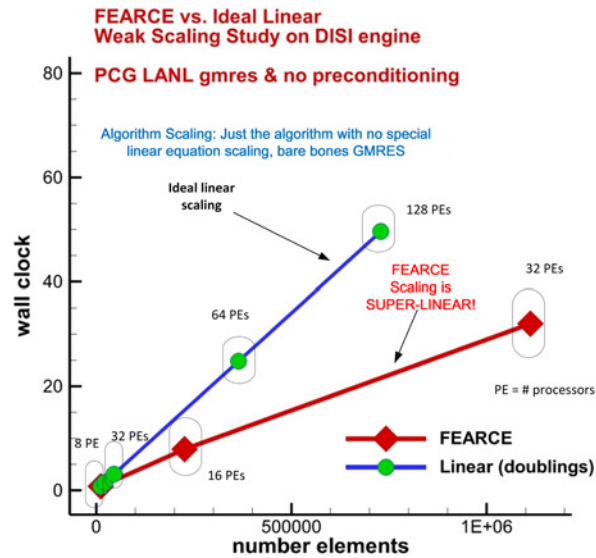
Figure I.15.3. Multiphase flow simulation with VOF method, gasoline injected into quiescent air at 3 bar: (a) gasoline jet primary break-up into ligaments and (b) primary break-up and w-component of velocity of air showing recirculation

Computational Efficiency

We continued work on parallel solution method and reducing wall-clock time by adding the Trilinos Multigrid preconditioning. Previously, we had developed a 10× speed-up with the implicit solve related to increased time step size. Additionally, we produced a 30× speed-up over the serial version with the implementation of a shared-node FEM system that reduces communication cost and produces a super-linear scaling for an over 300× speed-up [1]. We installed systems to access the Trilinos solver package where the multigrid preconditioning is providing about 8× speed-up for a total of 2,400× speed-up over the serial version of FEARCE. Multigrid improves the already good parallel scaling when running on a large number of processors. Keeping in mind that the parallel version of FEARCE is significantly faster than KIVA-4mpi, the parallel version of KIVA-4, significant strides have been made at the speed of solution.

- We are delivering super-linear scalability, as was demonstrated in Waters and Carrington [1], in a strong scaling experiment on standard CFD benchmark problems such as the backward-facing step or flow over a cylinder. Shown in Figure I.15.4 is the scaling of FEARCE's algorithm (without special linear equation solver treatments such as preconditioning or multigrid), besting the ideal linear scaling.
- We implemented access to the Algebraic Multigrid Preconditioning and linear equation solvers from Trilinos (<https://trilinos.org/>).
 - o We improved wall-clock times by a factor of 8 over our original 300× speed-up, beyond 2,400× speed-up over our explicit serial solver, as shown in Figure I.15.5. We are now encroaching on exceptional high-performance computing performance. Note that optimal performance usually requires some domain distribution alteration, not simply the doubling shown in the scaling analysis in Figure I.15.4 and Figure I.15.5.
 - o Further gains in the wall-clock times are expected for the super-linear system by employing greater vectorization and use of graphic processing units (use of Kukkos with Trilinos).
- It is significant to note that FEARCE requires far fewer elements to achieve the same accuracy as older KIVA codes, allowing for much faster solution on the same resolution with higher accuracy. This is the idea of high-performance computing, getting the most solution accuracy and speed from the least amount of computational work, utilizing the least of a computer and getting better accuracy, allowing for high-resolution systems having extremely good accuracy.

- FEARCE produces better accuracy than previous codes and on coarser grids. Hence, the new code is capable of being faster on the same resolution as old codes but is more accurate even on less resolved problems, providing additional advantages. Previous reports show ever increasing computational speed versus KIVA-4mpi.



GMRES – generalized minimal resolution method; PCG – LANL’s Parallel Conjugate Gradient solver package

Figure I.15.4. FEARCE’s super-linear algorithm scaling versus the ideal scaling curve

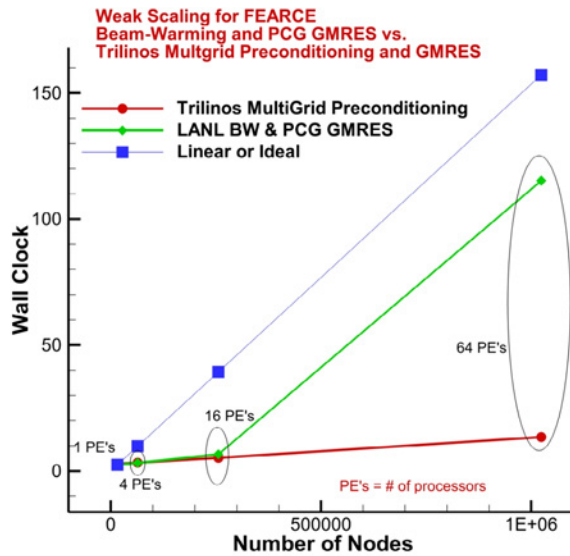


Figure I.15.5. FEARCE’s beam-warming (BW) system versus use of Trilinos Multigrid preconditioned GMRES, a weak scaling study

Conclusions

The KIVA development project at LANL is nearing the objective of having robust state-of-the-art CFD software for turbulent reactive flow, particularly well-suited for combustion modeling in engines or machines where immersed moving boundaries are involved, all with an eye toward solutions produced on quality grids created with a minimal amount of labor.

- Fast grid generation: computer-aided drawing to CFD grid in nearly a single step
- Four-valve DISI engine experimental data used to validate the robust moving immersed FEM method
- KH-RT spray model added to the code with validation ongoing via the ECN test cases
 - o Spray A case with KH-RT for validation
 - o Spray G cases with evaporation proceeding
- Predictive spray modeling with the addition of VOF method
 - o Developing transition to Lagrangian particle transport from predictive spray break-up for engineering-type simulations
- Highly scalable parallel solution system, with multigrid preconditioning producing nearly perfect scaling, 2,400 times faster than serial version of FEARCE, eight times faster than just the super-linear FEARCE and only GMRES Krylov linear equation solver
 - o Researching Exascale possibilities by using vectorizable Cuda friendly sections of code for graphic processing nested into the MPI parallel framework
- ChemKin II/III and also Chemkin-Pro added for faster, larger, and more robust reactive chemistry

Key Publications

1. Carrington, D.B., and J. Waters. 2018. “Turbulent Reactive Flow Modeling in Engines: A Robust and Accurate Toolkit/Software for Simulating Engine Dynamics.” *Proceedings of the ASME 2018 Internal Combustion Engine Fall Technical Conference, ICEF2018*, San Diego, CA, USA, November 4–7, 2018.
2. Hatamipour, V.D., D.B. Carrington, and J.C. Heinrich. 2018. “Accuracy and Convergence of Arbitrary Lagrangian-Eulerian Finite Element Simulations based on a Fixed Mesh.” *Progress in Computational Fluid Dynamics*, an Int. Jour., vol. 18, no. 4, pp. 215–231.
3. Carrington, D.B., M. Mazumder, and J.C. Heinrich. 2018. “Three-Dimensional Local ALE-FEM Method for Fluid Flow in Domains Containing Moving Boundaries/Objects Interfaces.” *Progress in Computational Fluid Dynamics*, an Int. Jour., vol. 18, no. 4, pp. 199–215.
4. Waters, J., D.B. Carrington, X. Wang, and D.W. Pepper. 2018. “A Dynamic LES Model for Turbulent Reactive Flow with Parallel Adaptive Finite Elements.” In *Energy for Propulsion, Chapter 3: Turbulent Combustion Modeling and Simulations*, 217–235. Singapore: Springer.
5. Waters, J., and D.B. Carrington. 2018. “Modeling Multi-Phase Flow: Spray Break-up Using Volume of Fluids in a Dynamic LES FEM Method.” 2018 AIAA Aerospace Sciences Meeting, AIAA Science and Technology Forum and Exposition 2018, Kissimmee, FL, January 8–12, 2018.
6. Waters, J., D.B. Carrington, and M.M. Francois. 2017. “Modeling Multi-phase Flow: Spray Break-up Using Volume of Fluids in a Dynamic LES FEM Method.” *Numerical Heat Transfer, Part B*, vol. 72, no. 4, pp. 285–299.

References

1. Waters, J., and D.B. Carrington. 2016. "A Parallel Large Eddy Simulation in a Finite Element Projection Method for All Flow Regimes." *Numerical Heat Transfer, Part A* 70 (2): 117–131.
2. Carrington, D.B. 2009. "A Characteristic-Based Split hp-Adaptive Finite Element Method for Combustion Modeling in KIVA-hpFE." LANL Scientific Report no. LA-UR-09-06527.
3. Carrington, D.B., X. Wang, and D.W. Pepper. 2014. "A Predictor-Corrector Split Projection Method for Turbulent Reactive Flow." *Journal of Computational Thermal Sciences* 5 (4): 333–352.
4. Carrington D.B., X. Wang, and D.W. Pepper. 2014. "An hp-Adaptive Predictor-Corrector Split Projection Method for Turbulent Compressible Flow." Proceedings of the 15th International Heat Transfer Conference, IHTC-15, Kyoto, Japan, August 10–15, 2014.
5. Carrington, D.B., M. Mazumder, and J.C. Heinrich. 2018. "Three-Dimensional Local ALE-FEM Method for Fluid Flow in Domains Containing Moving Boundaries/Objects Interfaces." *Progress in Computational Fluid Dynamics* 18 (4): 199–215.
6. Carrington, D.B., and J. Waters. 2018. "Turbulent Reactive Flow Modeling in Engines: A Robust and Accurate Toolkit/Software for Simulating Engine Dynamics." *Proceedings of the ASME 2018 Internal Combustion Engine Fall Technical Conference, ICEF2018*, San Diego, CA, USA, November 4–7, 2018.
7. Waters J., D.B. Carrington, and D.W. Pepper. 2016. "An Adaptive Finite Element Method with Dynamic LES for Incompressible and Compressible Flows." *Journal of Computational Thermal Sciences* 8 (1): 57–71.
8. Waters, J., D.B. Carrington, and M.M. Francois. 2017. "Modeling Multi-phase Flow: Spray Break-up Using Volume of Fluids in a Dynamic LES FEM Method." *Numerical Heat Transfer, Part B* 72 (4): 285–299.
9. Trilinos: <https://trilinos.org/>
10. Reitz, R.D. 1987. "Modeling Atomization Processes in High-Pressure Vaporizing Sprays." *Atomization and Sprays Technology* 3: 309–337.

Acknowledgements

Jiajia Waters, LANL: Co-Principal Investigator

Brad Philpbar, LANL: Graduate Research Assistant

Michael Weismiller and Gurpreet Singh, U.S. Department of Energy's Vehicle Technologies Office: Managers of the Advanced Combustion Engines and Fuels research portfolio

I.16 Accelerating Predictive Simulation of Internal Combustion Engines with High Performance Computing (Oak Ridge National Laboratory)

K. Dean Edwards, Principal Investigator

Oak Ridge National Laboratory (ORNL)
National Transportation Research Center
2360 Cherahala Blvd.
Knoxville, TN 37932
E-mail: edwardskd@ornl.gov

Michael Weismiller, DOE Technology Development Manager

U.S. Department of Energy
E-mail: Michael.Weismiller@ee.doe.gov

Start Date: October 1, 2017	End Date: September 30, 2019	
Project Funding (FY18): \$450,000	DOE share: \$450,000	Non-DOE share: \$0

Project Introduction

This project supports rapid advancements in engine design, optimization, and control through the development and application of advanced simulation tools and novel techniques to best utilize high-performance computing (HPC) resources and detailed predictive models. This project couples ORNL's experimental and modeling expertise for engine and emissions-control technologies with DOE's Advanced Scientific Computing Research leadership, HPC resources, and fundamental research tools. Access to these resources is allocated primarily via a competitive process for the DOE Advanced Scientific Computing Research Leadership Computing Challenge (ALCC) program. Specific focus areas evolve according to the needs of industry and DOE, with the project typically supporting one or more tasks in close collaboration with industry partners.

During Fiscal Year (FY) 2018, this project primarily supported a multi-year collaborative effort between General Motors, ORNL, Lawrence Livermore National Laboratory (LLNL), and Convergent Science, Inc., which is using HPC resources and graphic processing unit (GPU)-enabled numerical solvers to evaluate the impact of increased simulation detail on the predictive accuracy and computational needs of computational fluid dynamics (CFD) engine simulations. Current commercially available computing resources provide capability for reasonably detailed engine simulations when the field of study is relatively narrow and fast turn-around time is not crucial. However, for applications such as virtual engine design and calibration where hundreds or thousands of individual simulations are needed with rapid throughput, CFD engine simulations must be overly simplified, resulting in a trade-off between accuracy and speed. The use of massively parallel HPC resources and faster, GPU-enabled numerical solvers provides a more favorable trade-off, enabling highly detailed (and hopefully more accurate) simulations with more acceptable computational times. Under this project, the team is using ORNL's Titan supercomputer and LLNL's Zero-RK chemistry solvers to systematically increase the level of simulation detail and add more first-principle, predictive submodels. The resulting impact on simulation accuracy and computational time is then evaluated.

Objectives

Overall Objectives

- Use massively parallel HPC resources and GPU-enabled numerical solvers to enable use of CFD engine models with significantly increased levels of detail and predictive submodels
- Evaluate impact of model refinements on predictive accuracy, computational speed, and extent of operational space covered without further tuning and calibration

Fiscal Year 2018 Objectives

- Transition to a full-cylinder geometry model and full-cycle simulation with gas exchange to better capture mixing and turbulence effects
- Couple combustion model with conjugate heat transfer (CHT) model of metal engine components to provide better thermal boundary conditions, including temporal and spatial variations
- Evaluate impact of these model refinements on predictive accuracy and computational requirements

Approach

As part of a multi-year collaborative effort between General Motors, ORNL, LLNL, and Convergent Science, Inc., the project team is using HPC and GPU-enabled numerical solvers to enable increased levels of simulation detail in CFD engine models. Our approach involves systematically adding increased detail and first-principles-based submodels to improve the predictive accuracy of combustion performance and emissions over more of the engine operating range while reducing the need for tuning and calibration. The baseline model for this effort is a closed-valve cylinder-sector diesel engine model in CONVERGE with skeletal chemistry. Initial efforts under this multi-year project used LLNL's Zero-RK chemistry solvers to take advantage of Titan's GPUs and enable use of highly detailed chemical mechanisms to simulate the combustion process, resulting in significant improvements in predicted engine-out emissions. During FY 2018, efforts focused on converting the engine model to a full-cylinder geometry with full-cycle simulation and gas exchange to provide more accurate modeling of mixing effects and coupling with a CHT model to provide better thermal boundary conditions.

Results

Results with the full-cylinder geometry model showed continued improvement in the accuracy of engine-out emissions predictions. Previous efforts refining the kinetic mechanism used to simulate combustion produced good agreement with experimental measurements of engine-out nitrogen oxide (NO_x) and hydrocarbon emissions but over-predicted carbon monoxide (CO) and soot emissions at many operating conditions. In those simulations, which used the cylinder-sector model, in-cylinder charge motion was imposed using an average swirl ratio value. The full-cylinder geometry model includes gas exchange through the intake and exhaust manifold with a fully positionable swirl valve in the intake runner (Figure I.16.1) to provide more accurate charge motion. As shown in Figure I.16.2, the full-cylinder model predicts higher kinetic energy and decreased swirl motion late in the cycle, which promotes local mixing, resulting in intensification of combustion late in the cycle and increased oxidation of CO and soot. Furthermore, due to the improved charge motion and accurate piston geometry with valve cut-outs, combustion is observed to occur earlier and faster within the squish region, resulting in a significant decrease in residual CO concentration in this area, as shown in Figure I.16.3. Focusing our analysis on twenty down-selected cases at operating points across the full speed-load range of the engine, Figure I.16.4 compares key combustion metrics and engine-out emissions for the full-cylinder model to the best cylinder-sector results and experimental data. As shown, substantial improvement in CO predictions is achieved with the full-cylinder model at high load (Cases 8 and 10–14). While significant error still exists at these conditions, refined simulation of charge motion and mixing produced levels of improvement in CO accuracy not seen with previous refinements to the combustion chemistry and computational mesh. Future efforts in FY 2019 under a new ALCC project awarded in July 2018 will seek to further refine simulation of small-scale mixing impacts on CO and soot oxidation by replacing the current Reynolds averaged Navier Stokes turbulence model with a large-eddy simulation model.

Additional refinements made to the engine model include coupling with a CHT model to provide spatially and temporally varying thermal boundary conditions. Due to the difficulty of measuring combustion chamber wall temperatures and heat fluxes, thermal boundary conditions for engine simulations are poorly known and understood. Coupling the combustion model to a CHT model of key solid components (including the piston, liner, and head) expands the domain of the model beyond the poorly known conditions at the cylinder walls to boundaries with the cooling jacket, where conditions are better known.

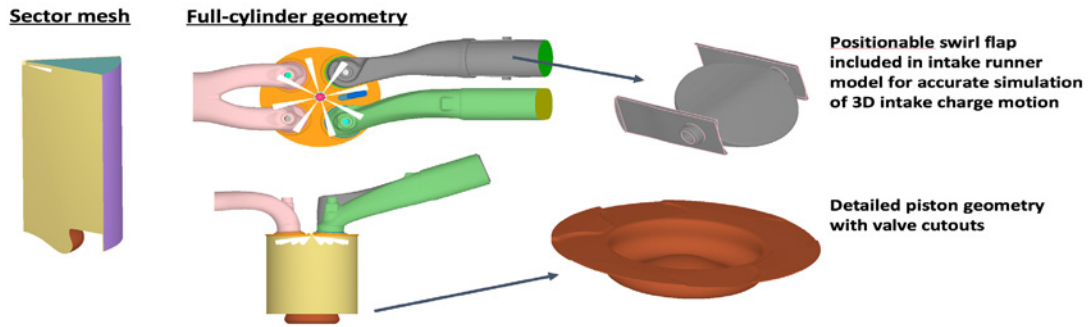
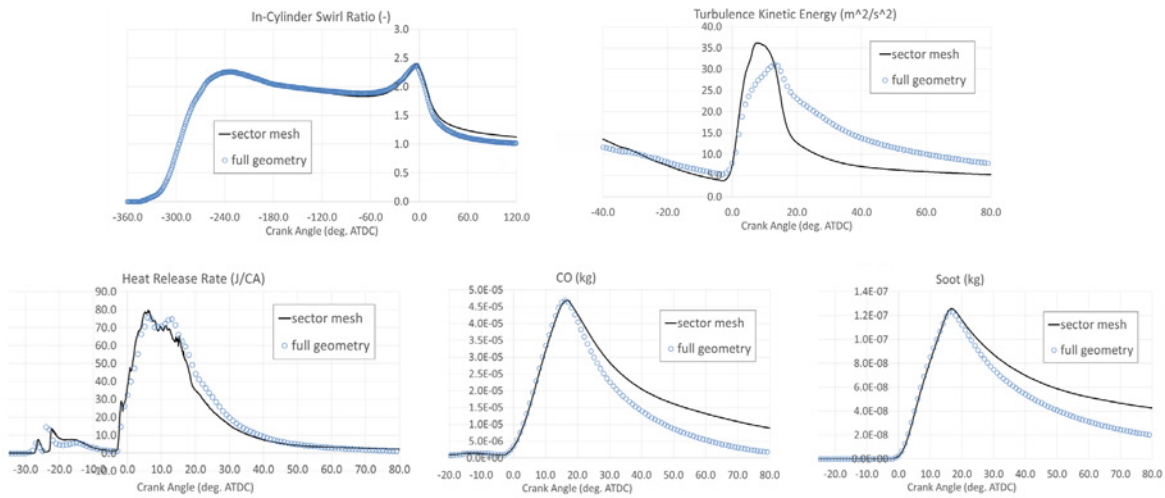
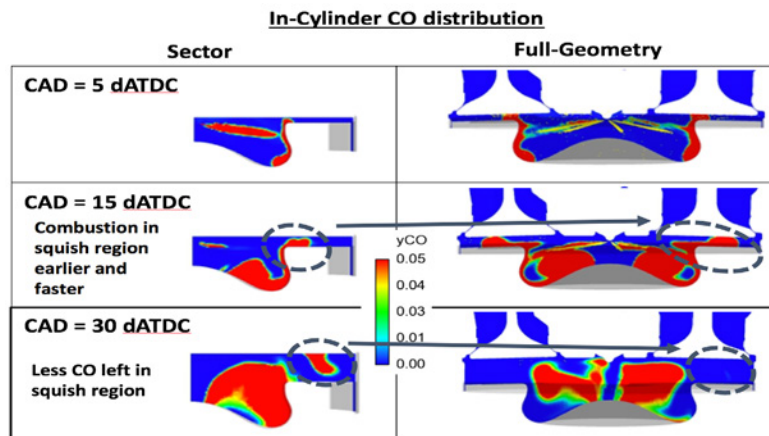


Figure I.16.1. Model transitioned from cylinder sector to full-cylinder geometry with positionable intake swirl flap for improved simulation of charge motion and mixing



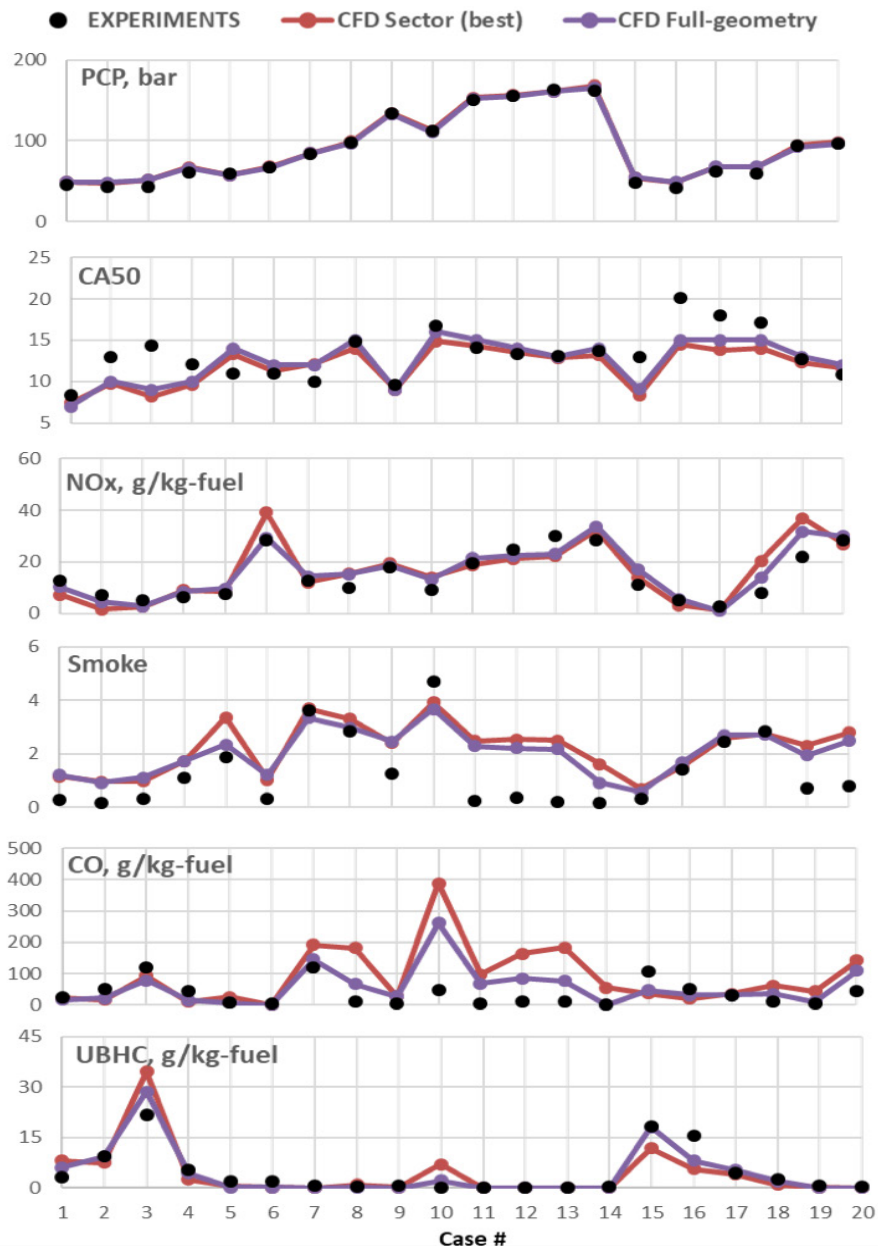
ATDC – after top dead center

Figure I.16.2. Simulation results from full-cylinder model show improved local mixing, resulting in increased oxidation of CO and soot late in the cycle



CAD – crank angle degree; dATDC – degrees after top dead center

Figure I.16.3. For the full-cylinder model, improved charge motion and detailed piston geometry with valve cut-outs results in earlier and faster combustion within the squish region, leaving less residual CO



UBHC – unburned hydrocarbons; PCP – peak cylinder pressure; CA50 – crank angle when combustion is 50% complete

Figure I.16.4. Comparison of predictions for key combustion metrics and engine-out emissions

Using CONVERGE v2.4.20, which includes one-dimensional and three-dimensional (3D) CHT capabilities, a coupled model of the full, four-cylinder engine was constructed, which includes all cylinders (with pistons and liners), the head, and the cooling jackets for the liner and head. An iterative approach is used involving separate models for the cooling jacket and the combined combustion chamber and solid components, as outlined in Figure I.16.5. As an initial step, a steady-state simulation is performed on the cooling jacket model with imposed constant, uniform wall temperatures at the interface with the solid/gas model. The resulting heat flux solution from the jacket model is then imposed as boundary conditions on the solid/gas model. To reduce computational demands, combustion is solved within a single engine cylinder, with resulting thermal loads mapped to the remaining cylinders. Heat flux results from the coupled combustion and CHT model are then mapped back to the coolant jacket to complete the iterative loop. Multiple engine cycles must be simulated for solution convergence. Because the solid conduction model converges much more slowly than the combustion

model, a supercycling approach is used. At user-defined intervals, the combustion model is paused while the solid model is run to steady-state using a full cycle of heat flux data stored in memory. This approach greatly accelerates time-to-solution.

Initial simulations with the CHT model are predicting higher combustion chamber wall temperatures (Figure I.16.6), suggesting that the values used in previous simulations were underestimated. As a result, less heat is lost, resulting in higher gas temperatures, which could further improve CO oxidation rates but also increase predicted NO_x . Further analysis and refinement of the CHT model is underway and will continue in FY 2019 under the new ALCC project on Titan.

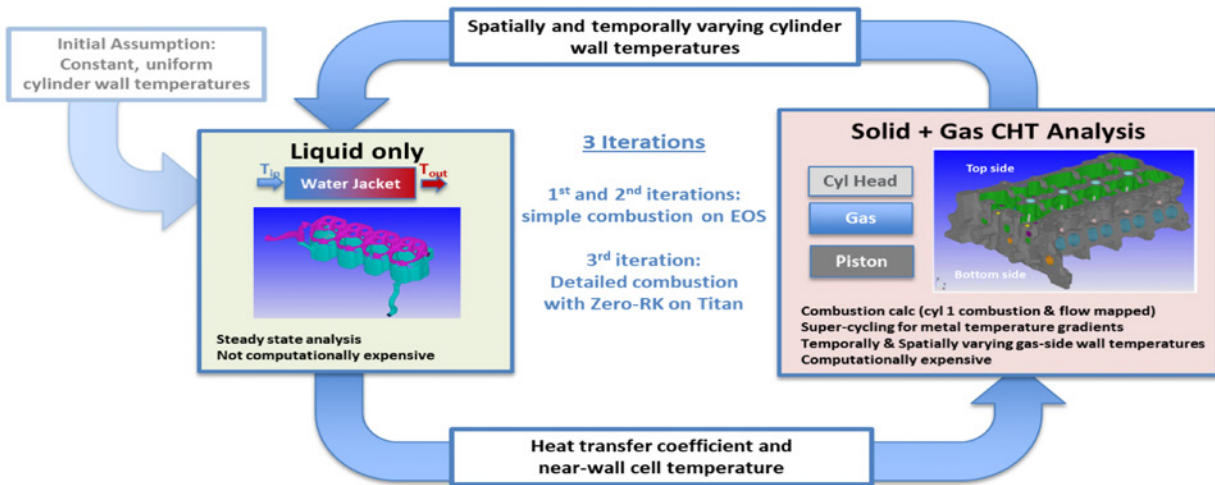


Figure I.16.5. Flow chart for iterative strategy used with CHT model

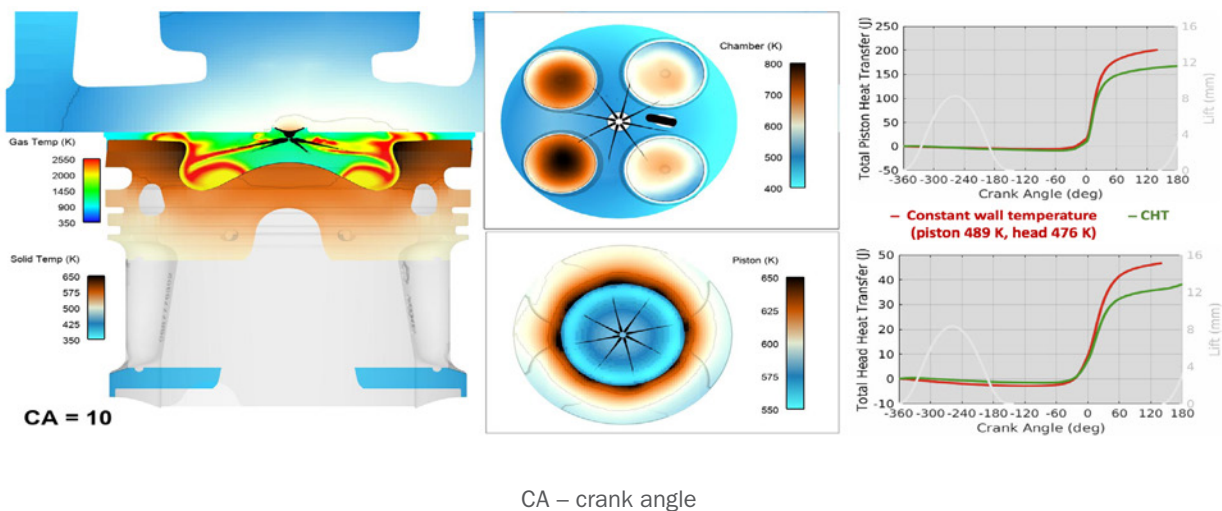


Figure I.16.6. Initial results with CHT model predict higher combustion chamber wall temperatures than assumed values used in simulations with uniform, constant wall temperatures, resulting in lower heat losses

Conclusions

- Compared to the cylinder-sector model, the full-geometry model with gas exchange predicts significantly different charge motion with improved small-scale mixing, resulting in enhanced late-cycle combustion and increased oxidation of CO and soot.
- Improved charge motion and detailed piston geometry allow earlier and faster combustion in the squish region, reducing residual CO.
- Initial CHT simulations suggest that thermal boundary conditions used in previous simulation efforts may have underestimated combustion chamber wall temperatures, resulting in an overprediction of heat transfer losses.
- Improved predictive accuracy achieved with these model refinements is somewhat offset by increased computational demands, as time-to-solution on Titan increases from approximately 5 h for the sector model, to 86 h for the full-geometry model, to 3 wk for the multi-cycle CHT model.

Key Publications

1. Gao, J., R.O. Grover, Jr., V. Gopalakrishnan, R. Diwakar, W.R. Elwasif, K.D. Edwards, C.E.A. Finney, and R.A. Whitesides. 2017. “Steady-State Calibration of a Diesel Engine in CFD Using a GPU-Based Chemistry Solver.” *ASME Journal of Engineering for Gas Turbines and Power* 140: 10.
2. Edwards, K.D., C.E.A. Finney, and W.R. Elwasif. 2018. “Accelerating Predictive Simulation of IC Engines with High Performance Computing.” DOE VTO 2018 Annual Merit Review.
3. Grover, R.O., Jr. 2018. “User of HPC to Drive Development of Advanced, More Fuel-Efficient Engines.” HPC User Forum. (September). Dearborn, MI, USA.
4. Grover, R.O., Jr. 2018. “Steady-State Calibration Development for Passenger-Car Diesel Engines Leveraging Graphical Processing Units (GPUs).” 2018 CONVERGE User Conference. (September). Madison, WI, USA.
5. Finney, C.E.A., C.S. Daw, B.C. Kaul, K.D. Edwards, and R.M. Wagner. 2017. “Deterministic Cyclic Variability: Modeling and Simulation.” VERIFI 2017 Workshop. (November). Chicago, IL, USA.

Acknowledgements

This project was performed in close collaboration with our colleagues and fellow researchers at General Motors (Ron Grover, Jian Gao, Vankatesh Gopalakrishnan, Ramachandr Diwakar), LLNL (Russell Whitesides), and Convergent Science, Inc., (Tristan Burton, Nitesh Attal). Thanks also to Charles E.A. Finney and Wael R. Elwasif at ORNL.

Portions of this work used resources of the Oak Ridge Leadership Computing Facility at ORNL, which is supported by the DOE Office of Science under Contract No. DE-AC05-00OR22725.

I.17 Development and Validation of Predictive Models for In-Cylinder Radiation and Wall Heat Transfer (The Pennsylvania State University)

Daniel C. Haworth, Principal Investigator

The Pennsylvania State University
140 Research East Building
University Park, PA 16802
E-mail: dch12@psu.edu

Volker Sick, Principal Investigator

University of Michigan
1231 Beal Ave.
Ann Arbor, MI 48109
E-mail: vsick@umich.edu

James P. Szybist, Principal Investigator

Oak Ridge National Laboratory
2360 Cherahala Blvd.
Knoxville, TN 37932
E-mail: szybistjp@ornl.gov

Michael Weismiller, DOE Technology Development Manager

U.S. Department of Energy
E-mail: Michael.Weismiller@ee.doe.gov

Start Date: January 1, 2016	End Date: December 31, 2018	
Project Funding: \$716,660	DOE share: \$639,236	Non-DOE share: \$77,424

Project Introduction

The lack of accurate submodels for in-cylinder radiation and heat transfer has been identified as a key shortcoming in developing truly predictive, physics-based computational fluid dynamics (CFD) models that can be used to develop and design combustion systems for advanced high-efficiency, low-emissions engines. Recent measurements of wall layers in engines show discrepancies of up to 100% with respect to standard CFD boundary layer models. And, recent analysis of in-cylinder radiation based on the most recent spectral property databases and high-fidelity radiative transfer equation solvers has shown that at operating pressures and exhaust-gas recirculation levels typical of modern compression-ignition truck engines, radiative emission can be as high as 40% of the wall heat losses, that molecular gas radiation (mainly carbon dioxide and water vapor) can be more important than soot particle radiation, and that a significant fraction of the emitted radiation (50% or more) can be reabsorbed before reaching the walls.

A hierarchical modeling approach is adopted that ranges from high-resolution “scientific” large-eddy simulation (LES) to medium-resolution “engineering” LES to low-resolution time-dependent Reynolds-averaged Navier Stokes. The submodels are being implemented in a code-neutral manner to facilitate implementation into CFD codes other than the ones that are used to carry out the research. Experimental data for model validation are being generated in single-cylinder research engines, and additional data for model development and validation are being derived using high-resolution LES.

Objectives

The overarching goal of this project is to develop, implement, and provide to the community open submodels for radiation and boundary layer wall heat transfer in medium-resolution LES and unsteady Reynolds-averaged Navier Stokes that (when coupled with models of equal fidelity for other key physical processes, such as

liquid fuel sprays) provide truly predictive capability for CFD of in-cylinder processes in engines, including couplings between different modes of heat transfer.

Overall Objectives

- Quantify the relative importance of turbulent boundary layer wall heat transfer, radiative heat transfer, and boundary layer/radiation couplings in engines
- Provide new experimental datasets that can be used to provide physical insight into heat transfer processes in engines and to validate models
- Augment the experimental measurements with data from high-resolution numerical simulations
- Develop, implement, and validate a hierarchy of CFD-based models that can be used as part of predictive engine simulations to develop new high-efficiency, low-emissions engines

Fiscal Year 2018 Objectives

- Perform quantitative comparisons between measured and computed spectral infrared (IR) radiation for an optical engine
- Analyze experimental data from a metal engine to determine if an influence of in-cylinder radiation on knock can be found
- Investigate the coupling between turbulent boundary layer wall heat transfer and radiative heat transfer, toward developing a CFD-based model that captures that coupling

Approach

Four different engine configurations are being explored experimentally and/or computationally: (1) a canonical engine configuration that is an idealized version of a two-valve, single-cylinder optical research engine; (2) the two-valve, single-cylinder optical research engine itself; (3) a four-valve, single-cylinder optical research engine; and (4) a four-valve metal engine. The program builds on the efforts of projects that have been funded through the National Science Foundation/DOE Advanced Engine Combustion Program and on other ongoing projects and collaborations among the investigators.

The research program has three novel elements that, together, will enable significant advances in predictive CFD submodels for in-cylinder heat transfer: (1) explicit accounting for couplings between radiation and wall heat transfer modeling; (2) tight collaboration between modeling and experiment, including new experimental measurements and high-resolution LES data for model validation; and (3) a hierarchical modeling approach that includes high-fidelity modeling for physics discovery (high-resolution LES) to augment the experimental measurements, and predictive models that can be used for medium-resolution LES and unsteady Reynolds-averaged Navier Stokes for engine combustion system development and design.

Results

Work continued on making quantitative comparisons between measured and computed IR spectral radiative intensities in an engine. The engine is the transparent combustion chamber optical engine at the University of Michigan. Recent efforts have focused on a 40 kPa manifold absolute pressure, 1,300 r/min operating condition. This is an operating condition that has been used in previous experimental and simulation studies for this engine. Because of the strong and irregular absorptance by the quartz engine liner in the IR, the comparisons are currently limited to a wavenumber range of $\sim 1.4\text{--}2.5\ \mu\text{m}$. This captures some of the key CO_2 and H_2O bands but misses an important CO_2 band that peaks at approximately $4.3\ \mu\text{m}$. At 1,300 r/min, time-resolved spectra can be obtained at intervals of two crank angle degrees of rotation. An example of measured time-resolved spectra is shown in Figure I.17.1. These measurements provide information about the relative weights of different emission features throughout the engine cycle, which may be used to extract temperature and/or composition information from measured spectral radiative intensities.

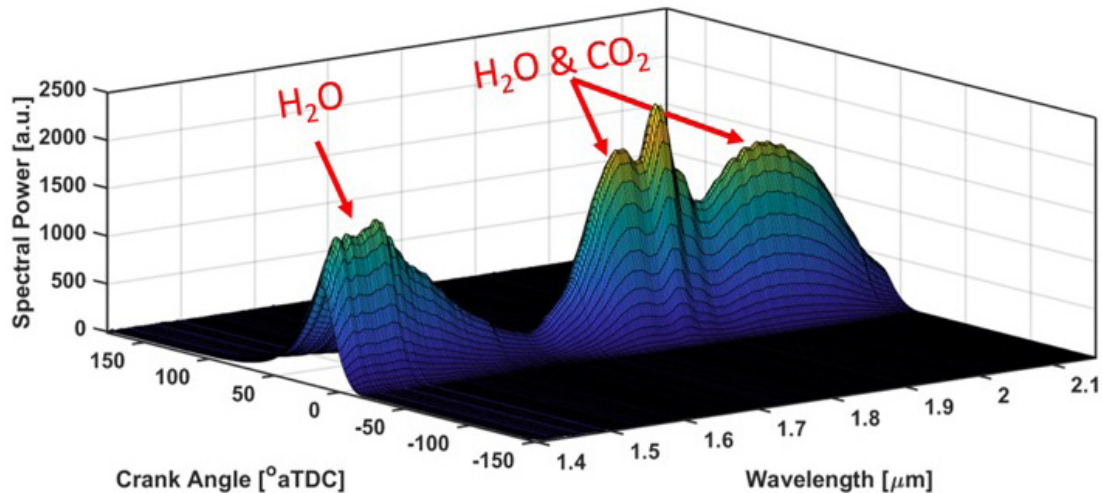


Figure I.17.1. Time-resolved (at intervals of two crank angle degrees of rotation) measured IR spectral radiative intensities in the transparent combustion chamber engine at 40 kPa manifold absolute pressure, 1,300 r/min

Figure I.17.2 is a comparison between simulated and experimental IR spectra for the transparent combustion chamber engine at the same operating condition. This plot compares spectra at 30° after top-dead-center (aTDC) combustion. The simulated spectrum was obtained from an instantaneous snapshot of the in-cylinder computed temperature, pressure, and composition fields, which were post-processed using a photon Monte Carlo radiation solver with line-by-line spectral resolution. Both spectra have been normalized to the spectral feature from 1.7–2.2 μm . There is large discrepancy between simulation and experiment for wavelengths longer than approximately 2.5 μm because of the strong attenuation of the measured signal at those wavelengths by the quartz cylinder liner in the optical engine. Other than that, the quantitative agreement between the two spectra is quite good. A sapphire piston window has been procured, which will allow measurements to be made at wavelengths as long as 5.5 μm , corresponding to the upper wavelength limit of the IR camera that is available. With that, quantitative comparisons can be made over the full near-to-mid IR range that is of interest for radiative heat transfer in the engine.

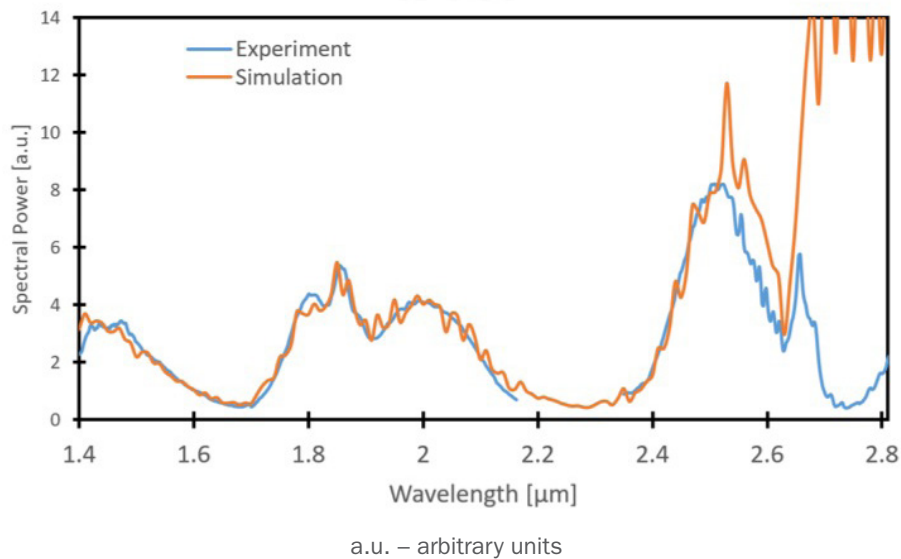


Figure I.17.2. Comparison of measured and simulated spectral intensities for the transparent combustion chamber engine operating at 40 kPa manifold absolute pressure, 1,300 r/min. The comparisons are made at 30° aTDC.

At Oak Ridge National Laboratory, experiments in a metal engine were conducted to investigate whether or not an influence of in-cylinder radiation on knock can be seen. This experimental study investigated the knocking propensity of iso-octane and Primary Reference Fuel 90 fuels at a constant fueling rate under boosted operation. At this condition, 10% dilution was added to the mixture with three gases that differed in their optical thickness: N_2 , H_2O , and CO_2 . Because these gases also have different thermodynamic properties, the end-of-compression temperatures are different. To account for the temperature differences, a sweep of intake temperatures was done for each diluent. The experimental apparent heat-release rates (AHRRs) for each diluent are shown in Figure I.17.3. The AHRR plots each have three lines, where these lines collectively represent the distribution for a single operating condition. The black line represents the median operating condition, whereas the red and blue lines represent one standard deviation for advanced and retarded cycles, respectively. For both N_2 diluent (Figure I.17.3) and H_2O diluent (Figure I.17.3b), the advanced combustion cycles (red) show engine knock, where there is a second local spike in AHRR that is more abrupt than the initial spike caused by deflagration. There continues to be some evidence of knock, characterized by a second local peak in AHRR, for the later engine cycles (black and blue lines), but the engine knock is significantly attenuated. For the CO_2 diluent (Figure I.17.3c), there are some clear differences. First, when knock occurs in the red cycles, the AHRR from the knock event is typically lower than the AHRR from the deflagration portion of combustion. Second, for the CO_2 diluent, knock does not appear to be as attenuated as it was for the N_2 and H_2O diluents. This can be observed in the late engine cycles (blue), where the knock event is apparent for CO_2 but is visible for a smaller number of conditions with N_2 and H_2O diluents. Further analysis is underway to determine whether or not the in-cylinder radiation environment can be separated sufficiently from the thermochemical environment to say anything conclusive regarding a potential influence of radiation on knock. The CFD models that have been developed under this project are being exercised toward that end.

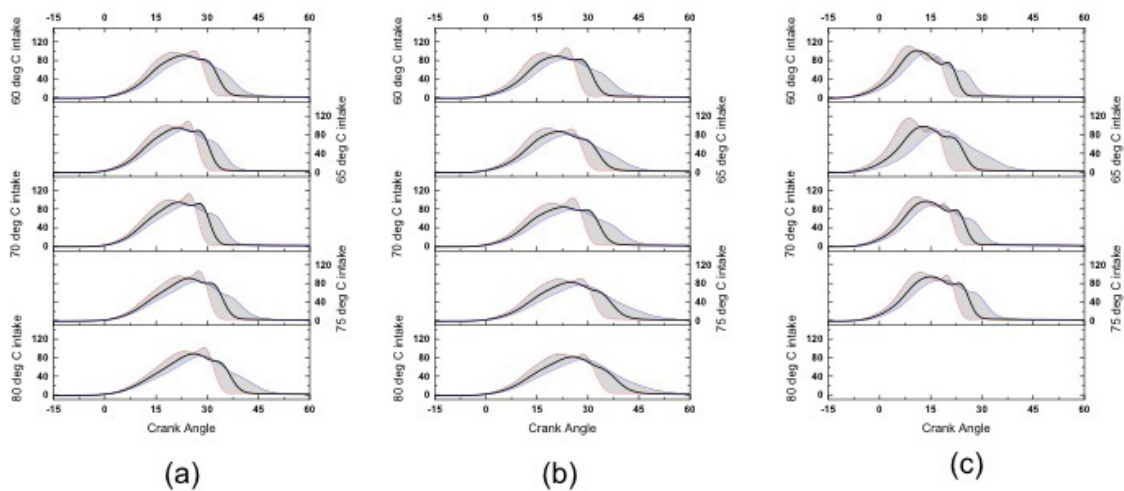


Figure I.17.3. AHRR of the knocking operating condition for each temperature and three diluents at 10%: (a) N_2 , (b) H_2O , and (c) CO_2 . All AHRR plots represent a single engine operating condition where the black line represents the median engine cycles, the red line represents one standard deviation advanced cycles, and the blue line represents one standard deviation retarded cycles.

Finally, couplings between turbulent boundary layer wall heat transfer and radiative heat transfer were explored using LES. There is evidence in the literature that the structure of an equilibrium turbulent boundary layer can be altered in the presence of radiation. In [1], direct numerical simulation (DNS) was performed for a fully developed turbulent channel flow with different fixed temperatures at the two walls, where the working fluid was a radiatively participating molecular gas. By comparing results for cases where radiative heat transfer was ignored with those for cases where radiation was considered, it was shown that radiation significantly altered the structure of the turbulent velocity and temperature boundary layers. Here, the same configuration has been simulated using LES. DNS and LES root-mean-square temperature profiles, with and without consideration of radiative heat transfer, are compared in Figure I.17.4. Radiative transfer redistributes energy in the channel, thereby suppressing turbulent fluctuations in temperature. This effect is captured in both

the DNS and the LES. Quantitative differences between the DNS and the LES are largest close to the walls. That is because a wall model is used in the LES, whereas all scales are fully resolved in the DNS. The degree of agreement between DNS and LES results is encouraging. This suggests that the key couplings between boundary layer wall heat transfer and radiative heat transfer can be captured in LES, at a small fraction of the computational effort required for DNS. This will facilitate model development and validation. The DNS data show that the value of turbulent Prandtl number in the vicinity of the wall increases by as much as a factor of two with consideration of radiation (not shown). This suggests that a relatively simple model might be devised to account for boundary layer/radiation couplings, where the value of the turbulent Prandtl number is modified in the vicinity of the walls.

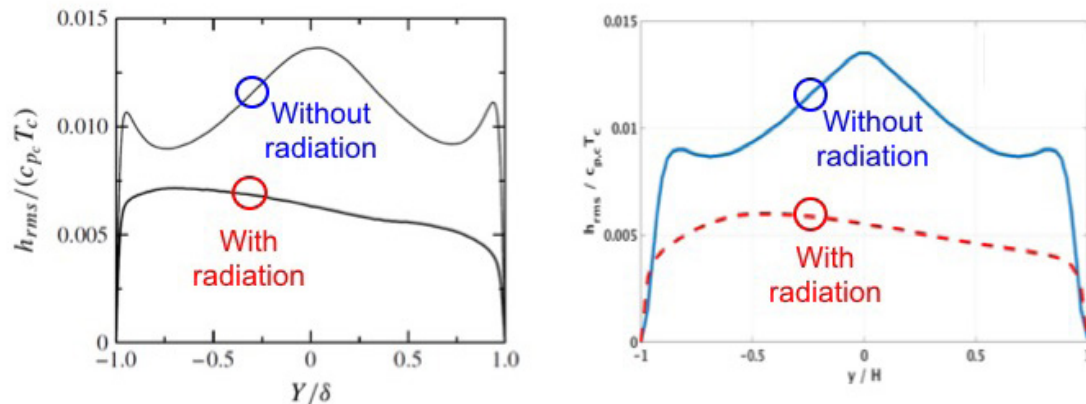


Figure I.17.4. Computed root-mean-square temperature profiles for a fully developed turbulent channel flow between parallel plates held at different fixed temperatures, with and without consideration of radiative heat transfer. Left: DNS results from [1]. Right: Current LES results.

Conclusions

In this third year of the project, the focus has been on (1) making quantitative comparisons between computed and measured spectral IR radiative intensities in an optical engine; (2) analyzing experimental data from a metal engine to determine if an influence of radiation on engine knock can be discerned; and (3) exploring couplings between turbulent boundary layer wall heat transfer and radiative heat transfer.

- Spectral IR radiative intensities in an optical engine can be measured and computed with good temporal resolution and high spectral precision. A sapphire (versus quartz) window will allow measurements to longer wavelengths.
- It remains unclear whether or not it will be possible to identify a conclusive influence of radiation on engine knock from the metal engine data. Further analysis using the high-fidelity CFD-based radiation models is being performed toward that end.
- Couplings between turbulent boundary layer wall heat transfer and radiative heat transfer that had been identified in the literature using DNS have been reproduced using LES. It is anticipated that this will lead to a relatively simple model based on a modified turbulent Prandtl number to account for this coupling.

Key Publications

1. Haworth, D.C., and S. Ferreyro Fernandez. 2017. "Modeling Soot Formation in High-Pressure Turbulent Spray Flames." *70th Annual Meeting of the American Physical Society - Division of Fluid Dynamics*, Denver, CO (19–21 November 2017).
2. Ferreyro Fernandez, S., and D.C. Haworth. 2018. "Simulations of Soot Formation in High-Pressure Transient Spray Flames." *Spring Technical Meeting of the Eastern States Section of the Combustion Institute*, State College, PA (4–7 March 2018).

3. Paul, C., D.C. Haworth, S. Roy, and M.F. Modest. 2018. "Influence of Turbulence-Radiation Interactions in Engine Radiation Heat Transfer." *Spring Technical Meeting of the Eastern States Section of the Combustion Institute*, State College, PA (4–7 March 2018).
4. Sircar, A., and D.C. Haworth. 2018. "CFD-Based Non-Equilibrium Wall Heat Transfer Models for Engine-Relevant Conditions." *Spring Technical Meeting of the Eastern States Section of the Combustion Institute*, State College, PA (4–7 March 2018).
5. Haworth, D.C., and C. Paul. 2018. "A Simplified CFD Model for Radiative Heat Transfer in Engines." *International Multidimensional Engine Modeling User's Group Meeting at the SAE Congress*, Detroit, MI (9 April 2018).
6. Henrion, L., M.C. Gross, and V. Sick. 2018. "An Infrared Spectroscopic Diagnostic of Radiative Heat Transfer in Internal-Combustion Engines." *Journées d'Étude, Belgian Section of the Combustion Institute*, Mons, Belgium (15–16 May 2018).
7. Sick, V., L. Henrion, A. Mazacioglu, and M.C. Gross. 2018. "Time-Resolved Infrared Imaging and Spectroscopy for Engine Diagnostics." *13th AVL International Symposium on Propulsion Diagnostics*, Kurhaus, Baden-Baden, Germany (26–27 June 2018), invited lecture.
8. Paul, C. 2018. "An Open-Source Framework for Advanced Turbulent Combustion and Radiation Modeling in IC Engines." Ph.D. thesis, The Pennsylvania State University, University Park, PA.
9. Paul, C., D.C. Haworth, and M.F. Modest. 2018. "A Simplified CFD Model for Spectral Radiative Heat Transfer in High-Pressure Hydrocarbon-Air Combustion Systems." *Proc. Combust. Inst.* 37. In press.
10. Ferreyro Fernandez, S., C. Paul, A. Sircar, A. Imren, D.C. Haworth, S. Roy, and M.F. Modest. 2018. "Soot and Spectral Radiation Modeling for High-Pressure Turbulent Spray Flames." *Combust. Flame* 190: 402–415.

References

1. Vicquelin, R., Y.F. Zhang, O. Gicquel, and J. Taine. 2014. "Effects of Radiation in Turbulent Channel Flow: Analysis of Coupled Direct Numerical Simulations." *J. Fluid Mech.* 753: 360–401.

Acknowledgements

This material is based upon work supported by the Department of Energy, Office of Energy Efficiency and Renewable Energy and the Department of Defense, Tank and Automotive Research, Development, and Engineering Center, under Award Number DE-EE0007278.

I.18 Model Development for Multi-Component Fuel Vaporization and Flash Boiling (University of Illinois at Urbana-Champaign)

Chia-fon Lee, Principal Investigator

University of Illinois at Urbana-Champaign
1206 W. Green St.
Urbana, IL 61801
E-mail: cflee@illinois.edu

Sibendu Som, Principal Investigator

Argonne National Laboratory Energy Systems Division
9700 S. Cass Avenue
Argonne, IL 60439
Email: ssom@anl.gov

Michael Weismiller, DOE Technology Development Manager

U.S. Department of Energy
E-mail: Michael.Weismiller@ee.doe.gov

Start Date: January 1, 2016	End Date: December 31, 2018	
Project Funding: \$761,000	DOE share: \$685,000	Non-DOE share: \$76,000

Project Introduction

Modern internal combustion engines are designed to maximize efficiency and minimize pollutant emissions. One factor that can greatly deteriorate engine performance is poor fuel atomization, which is characterized by incomplete fuel vaporization and spray impingement on cylinder walls. Residual fuel in the cylinder causes high levels of unburned hydrocarbons and carbon monoxide emissions while altering engine fuel dilution. Thus, enhancing fuel vaporization is crucial for improving engine performance. The design process to increase engine efficiency is done through numerical model simulations that search for optimal parameters. However, the performance of available sub-models for fuel vaporization is limited by the complexity of fuel representation that is both computationally efficient and quantitatively accurate. The lack of experimental data to support and validate the numerical models is another key factor impeding model development. The current project aims to overcome the barriers of inadequate predictive tools and data for (1) fuel property effects on combustion and engine efficiency optimization and (2) fuel effects on emissions and emission control system impacts.

The key innovation of this work is to apply novel approaches to represent the complexity of fuel composition in models, and to validate these approaches through experimental observation. Under engine environments, flash boiling may also take place during the vaporization process of multi-component fuels. Promoting the occurrence of flash boiling can dramatically improve the spray atomization process, which is closely tied to the parameters that govern vaporization. Hence, a unified model to predict the occurrence of flash boiling is developed in this work. These phenomena are important for improving engine design through fuel vaporization enhancement. The appropriate methodologies for evaluating mixing rules and saturation properties of the multi-component fuel are examined and validated through experiments. The outcome of this project will advance current design processes to achieve greater efficiency and accuracy for internal combustion engines and related applications.

Objectives

The goals of this project are to improve the multi-component fuel droplet and film vaporization models used in internal combustion engine simulation through the use of discrete and continuous thermodynamics methods and to develop a comprehensive model to predict the characteristics of multi-component flash-boiling spray.

These models will be verified and validated with experimental observation of vaporization in the forms of spray, droplet, and wall films.

Overall Objectives

- Design and develop a multi-component fuel droplet and wall film vaporization model using two approaches: discrete and continuous thermodynamics methods
- Design and develop an analytical model for multi-component flash boiling
- Integrate the multi-component droplet and film model into multi-dimensional engine calculations to predict the fuel vaporization process under engine operation conditions
- Conduct multi-component droplet and fuel film vaporization experiments in a non-combusting chamber to verify the proposed vaporization models
- Characterize flash-boiling phenomena of multi-component fuel sprays by optical and laser diagnostic techniques

Fiscal Year 2018 Objectives

- Obtain experimental measurements of non-boiling and flash-boiling sprays
- Develop, validate, and integrate discrete method vaporization models for multi-component fuel droplet
- Develop, validate, and integrate continuous method vaporization models for multi-component fuel droplet

Approach

To develop a state-of-the-art numerical model for predicting the multi-component fuel vaporization process, two numerical approaches are implemented and tested: discrete and continuous methods. The discrete method keeps track of key surrogate species, while the continuous method uses a probability distribution function to represent thermodynamic properties of multi-component fuel. Fuel droplet, spray, and film vaporizations are the model applications examined in this work. A comprehensive numerical model to predict the occurrence of flash boiling for multi-component fuel is constructed in collaboration with Dr. Sibendu Som's group at Argonne National Laboratory. Due to the high computational cost from the complexity of multi-component fuel simulations, the world-leading computing resource center at Argonne National Laboratory is invaluable in the success of this work. Extensive parametric studies of flash-boiling phenomenon are executed through both experimental and numerical endeavors.

Parallel to the model development endeavor, experiments are performed to verify the proposed models, where an extensive dataset is created to bridge the gap between single-component and multi-component combustion. More specifically, measurements of multi-component fuel spray characteristics under flash-boiling and non-flash-boiling conditions are made, along with observations of droplet and film vaporization trends. New spray, droplet, and film chambers are designed and assembled to obtain datasets of multi-component fuel vaporization characteristics, including temperature and concentration histories, temporal droplet size evolution, and fuel film thickness evolution. These experiments employ optical and laser diagnostic techniques. These validated sub-models are implemented into engine simulation models for final testing and validation. Comprehensive multi-component fuel datasets will provide invaluable information for model development and engine design.

Results

High-speed back-illumination images of the spray in a temperature- and pressure-controlled chamber are utilized to perform visual assessment of the spray behavior for different fuel blends under various operating conditions. Flash-boiling events can be detected through the merging of spray plumes. For instance, pure iso-octane (E0) at the pressure of 100 kPa (Figure I.18.1, top left panel) is an example of spray not undergoing flash boiling, where distinct spray jet plumes can be identified. For pure ethanol (E100) at the pressure of 20 kPa, on the other hand, all the spray jets merge into a single plume (Figure I.18.1, bottom right panel). Besides merging of the jet plumes, flash boiling is also observed to create spray collapse, where the width

of the spray decreases. 50-50 ethanol-iso-octane blend (E50) at 20 kPa pressure is an example of such a case (Figure I.18.1, bottom middle panel), where the spread of the spray is significantly smaller than other scenarios. Another interesting phenomenon observed by changing fuel blend ratios and ambient pressure is the back circulation of the spray at the end of the jet, which can be identified by the swirls near the end of the jet plumes (e.g., Figure I.18.1, bottom left panel). All these characteristics can be utilized to create optimal jet characteristics to improve engine performance and efficiency.

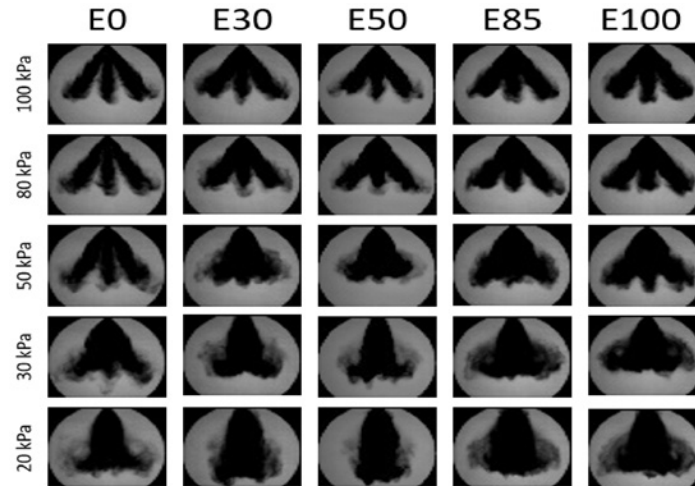


Figure I.18.1. Back-illumination images of sprays with different ethanol-iso-octane blend ratios (top row labels: E0 is pure iso-octane, E30 is 30–70 ethanol-iso-octane blend, and E100 is pure ethanol) under various ambient pressure conditions (left column labels)

One of the time-series spray behaviors examined is spray liquid penetration length. Different fuel blend sprays under the ambient pressure of 100 kPa (Figure I.18.2a) have similar trends, but as the ambient pressure decreases to 50 kPa (Figure I.18.2b) and 20 kPa (Figure I.18.2c), the impact of blend ratios is observed. Sprays with higher ethanol content have the longest liquid penetration length at the end of the spray event when the pressure is at 50 kPa, while blends of E30 and E50 have the longest final penetration length at 20 kPa. The non-linear trend with respect to pressure is the result of complex interactions between the change in fuel properties from blending, spray mechanics, and the occurrence of flash-boiling events, which favor different blend ratios at different pressures. All these parameters are key to developing and assessing the numerical model for engine design optimization.

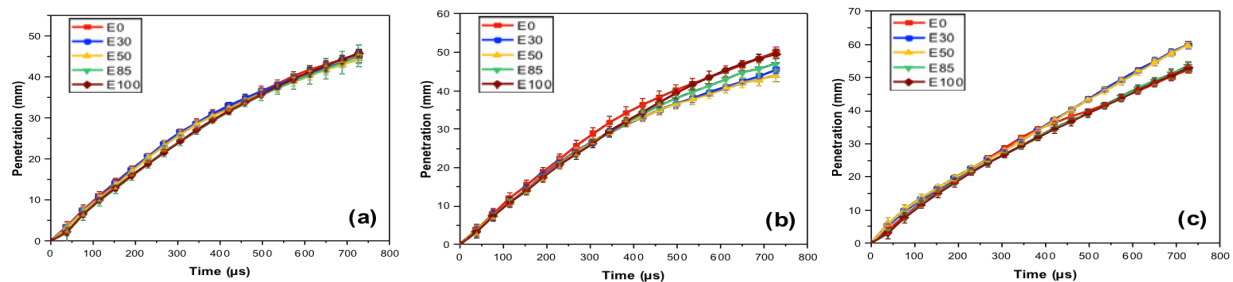


Figure I.18.2. Time-resolved liquid penetration lengths for ethanol-iso-octane fuel blend sprays (E100 is pure ethanol, E30 is 30% ethanol plus 70% iso-octane, and E0 is pure iso-octane) at chamber pressures of (a) 100 kPa, (b) 50 kPa, and (c) 20 kPa

One venue to improve spray performance is through reducing droplet size. The droplet size distributions for all the spray blend and ambient pressure cases are measured through Phase Doppler Anemometry. Figure I.18.3 shows the droplet distribution curves for sprays with fuel blends of pure iso-octane, 30-70 ethanol-iso-octane blend (E30), and pure ethanol under different ambient pressures. When flash-boiling events occur

(e.g., Figure I.18.3a blue line), enhanced atomization causes spray to have smaller droplets compared to non-flashing sprays (e.g., Figure I.18.3a red line). When ethanol is added to iso-octane, the peak value of droplet distribution curves shifts to the left, signifying more small droplets and less large droplets are found in ethanol-iso-octane sprays (Figure I.18.3 blue lines) than pure iso-octane sprays (Figure I.18.3 red lines). A reason for such shift in distribution includes the change in fuel properties such as latent heat of vaporization by blending, which can change the environment temperature as the spray droplets evaporate. These observations provide important parameters for numerical models to consider when making fuel blend and operating condition design choices.

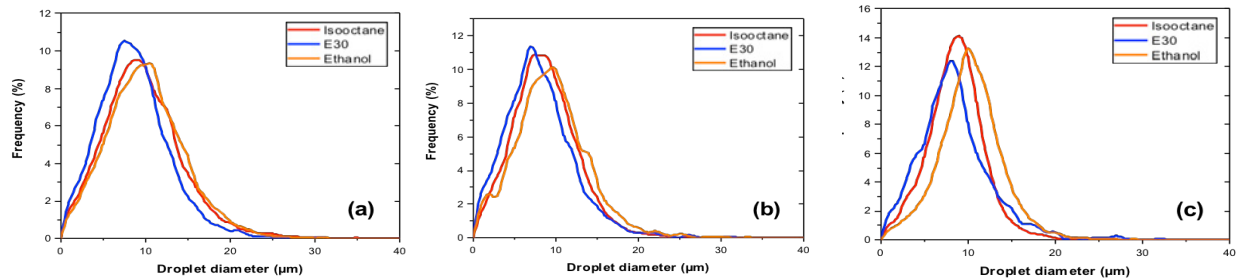


Figure I.18.3. Droplet distribution curves for ethanol-iso-octane fuel blend sprays (E100 is pure ethanol, E30 is 30% ethanol plus 70% iso-octane, and E0 is pure iso-octane) at chamber pressures of (a) 100 kPa, (b) 50 kPa, and (c) 20 kPa

For numerical model development, a broad spectrum of features, such as turbulence modeling, mesh size, and break-up parameters, have been investigated and compared to the experimental results gathered within this project. A significant test has been carried out for pure ethanol injection in a chamber at 50 kPa (Figure I.18.4). The simulation results demonstrate the capabilities of the newly developed model well. The flashing-driven breakup sub-model is one of the areas identified as a crucial component in future spray model development.

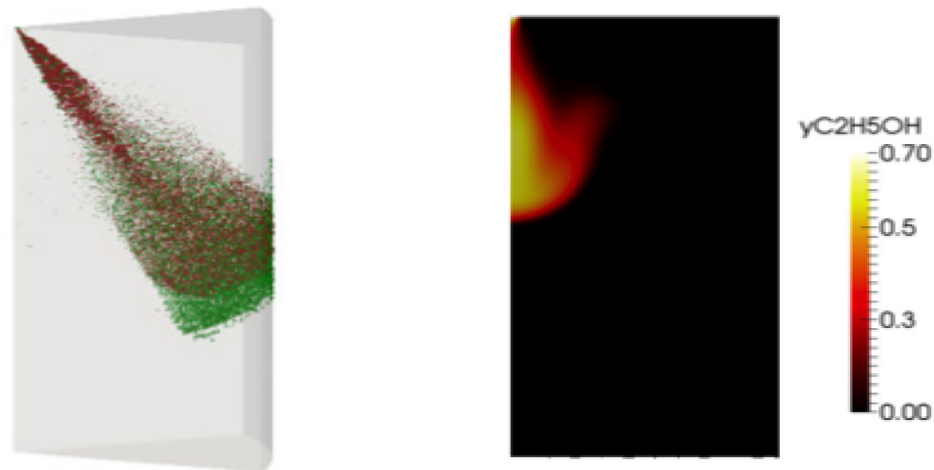


Figure I.18.4. Graphical visualization of the simulated spray result (left) and ethanol mass fraction profile on the plume centerline (right) at 1 ms after start of injection time for ethanol injection at $P_{\text{ambient}} = 50 \text{ kPa}$

The performance of the newly developed model is evaluated through the simulation of the eight-hole injector used in the experimental portion of this project. The numerical setup parameters (e.g., ambient temperature, ambient pressure, and injection pressure) are exactly the same as the experimental setup, using iso-octane as the test fuel. There is reasonable qualitative agreement between the experimental spray image and the simulated spray, as shown in Figure I.18.5.

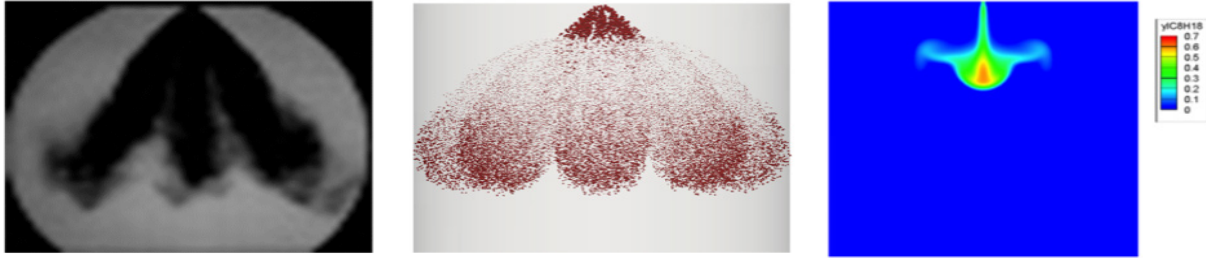


Figure I.18.5. Iso-octane injection at $P_{\text{ambient}} = 50$ kPa. Experimental spray image (left), simulated spray (center), and fuel vapor mass fraction profile (right) at 1 ms after start of injection time

Conclusions

- Decreasing spray chamber pressure promotes the occurrence of flash boiling that reduces the droplet sizes of fuel spray.
- Adding volatile fuel (e.g., ethanol) into less volatile fuel (e.g., iso-octane) can improve spray atomization through bubble generation and bubble bursting that creates small droplets.
- Blending fuels that alter the latent heat of vaporization of pure fuels can enhance spray vaporization.
- Flashing-based break-up sub-model is crucial for future spray model improvement, as it can greatly impact the accuracy of engine design outcome.

Key Publications

1. Chen, Tairan, Junhao Yan, Timothy H. Lee, Biao Huang, Guoyu Wang, and Chia-fon F. Lee. 2019. "Spray Characteristics of Gasoline-Ethanol Fuel Blends under Flash-Boiling Conditions." SAE Technical Paper. Submitted.
2. Gao, Suya, Junhao Yan, Mianzhi Wang, and Chia-fon F. Lee. 2018. "Modeling of Quasi-1D Multi-Component Fuel Droplet Vaporization Using Discrete Approach with Experimental Validation." SAE Technical Paper 2018-01-0287.
3. Liang, Zhengxing, Junhao Yan, Gang Li, Timothy H. Lee, Zhang Li, and Chia-fon F. Lee. 2018. "Measurement of the Evaporation Behavior of the Film of Fuel Blends." SAE Technical Paper 2018-01-0290.
4. Yan, Junhao, Tairan Chen, Suya Gao, and Chia-fon F. Lee. 2019. "Macroscopic and Microscopic Study of Effect of Fuel Properties on Flash Boiling Spray with Isooctane-Ethanol Fuel Blends." SAE Technical Paper. Submitted.

I.19 Spray–Wall Interaction at High-Pressure and High-Temperature Conditions (Michigan Technological University)

Seong-Young Lee, Principal Investigator

Michigan Technological University (MTU)
815 R.L. Smith Bldg. 1400 Townsend Drive
Houghton, MI 49931
E-mail: sylee@mtu.edu

Michael Weismiller, DOE Technology Development Manager

U.S. Department of Energy
E-mail: Michael.Weismiller@ee.doe.gov

Start Date: January 1, 2016	End Date: December 30, 2018	
Project Funding: \$653,790	DOE share: \$570,000	Non-DOE share: \$83,790

Project Introduction

The goals of this research project are to develop, implement, and validate a volume of fluid (VOF) approach for modeling evaporation, which is integrated into computational fluid dynamics (CFD) codes to provide accurate and predictive simulation of spray–wall interactions without extensive need of parameter tunings. This is accomplished by development and inclusion of an evaporation submodel in the existing VOF modeling framework. This submodel will be validated through extensive experimentation of the spray–wall interaction and film formation, spreading, and vaporization dynamics.

Objectives

Overall Objectives

- Develop and validate an advanced spray–wall interaction (SWI) and associated film formation and vaporization modeling approach using a VOF method with evaporation submodel
- Perform accurately predictive simulations of sprays and their impingement without the need of extensive parameters tuning using the direct numerical simulation (DNS) of spray–wall impingement
- Develop submodels for droplet formation characteristics post-wall impingement via detailed DNS and large eddy simulation models that are supported by accurate experimentation
- Conduct experimentation of the SWI and liquid wall film under conditions matching the thermodynamic charge state and surface temperatures to those of engines

Fiscal Year 2018 Objectives

- Quantify film thickness and heat flux on the heated surface for a single-hole nozzle spray impingement
- Optimize the SWI model in high-fidelity Lagrangian–Eulerian (LE) spray model
- Validate LE spray model with experiments and generate boundary conditions for DNS framework studies
- Demonstrate the droplet DNS impingement criteria for splashing and non-splashing cases and formulate the evaporation DNS submodel

Approach

First, targeted experimentation of the spray–wall interactions and liquid wall film under conditions matching the thermodynamic charge state and surface temperatures to those of engines is performed. Second, the experimental data is used to support development and validation of an advanced SWI and associated film formation and vaporization modeling approach via application of a VOF method with an integrated evaporation submodel. With the inclusion of a vaporization submodel for the film and the results of the DNS analysis of spray–wall impingement, accurately predictive simulations of spray impingement can be eventually performed without the need of parameters tuning.

Results

Fiscal Year 2018 Accomplishments

- Performed the n-heptane new film thickness measurement based on the CFD feedback
- Completed the additional droplet sizing measurement and data analysis
- Conducted the splashing criteria of single droplet impinging on wall
- Evaluated influence of surface roughness on the prediction of gas velocities near the wall to correctly assess the gas–liquid interaction in the rebound/splashed portion of the spray in LE simulations
- Conducted DNS model of contact angle, spread factor, etc., under MTU single droplet impingement
- Developed a DNS model of train droplets on dry/wet walls and developed a droplet evaporation model
- Developed a secondary droplet characterization algorithm in DNS simulation
- Implemented SWI model in CONVERGE with modified splash criteria and surface roughness model

Measurement of Film Thickness and Droplet Size

The project team found that the film thickness data reported in the 2017 Annual Report did not match very well with LE simulation results due to residual diesel in the n-heptane fuel system. We noticed that it is necessary to switch fuel with a sufficiently proper purging procedure. The updated film thickness results in a 2.4 mm² x 2.4 mm² area zone around the impinging point are shown in Figure I.19.1. Tests were repeated five times at each condition. The initial rising part of the film thickness was caused by the presence of the fuel mist. Therefore, the film thickness data are believed to be accurate only after the mist disappeared. At each condition, the film thickness continually decreases after impingement due to the evaporation of n-heptane. The average film thickness decreases as the ambient density is increased (cf. Figure I.19.1a). The higher ambient density suppresses the spray penetration velocity and spray cone angle, which leads to a delayed impingement time and to the formation of a smaller initial film area. The influence of the injection pressure is shown in Figure I.19.1b. In general, the averaged film thickness decreases as the injection pressure is increased, also showing a shift of the peak values to earlier times with increasing injection pressure. The higher injection pressure leads to high impact momentum, which benefits the splash rather than the tendency of the fuel to adhere to the wall, resulting in thinner liquid film and faster evaporation.

The team also conducted the drop size measurement for diesel spray with conditions of 150 MPa and 22.8 kg/m³ and Figure I.19.1c shows the Sauter mean diameter evolution at five different positions. Before the end of injection (~2.7 ms), Position 3 (near impinging point) has the largest Sauter mean diameter. After the injection, the Sauter mean diameter at Position 4 and Position 5 surpass size at Position 3.

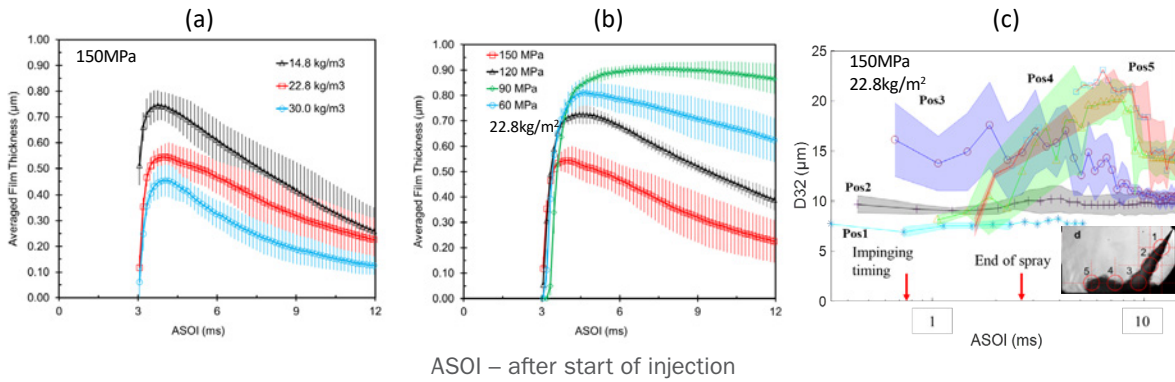


Figure I.19.1. (a) n-Heptane film thickness at $P_{inj} = 150$ MPa, (b) n-heptane film thickness at density = 22.8 kg/m^3 , and (c) Sauter mean diameter of diesel spray at $P_{inj} = 150$ MPa and density = 22.8 kg/m^3 ; subfigure shows measurement positions

Single Drop Wall Impingement

Yarin and Weiss [1] suggested a splashing threshold defined by capillary number (Ca) and dimensionless viscosity length (λ). Ca represents the relative effect of viscous forces versus surface tension acting across an interface between a liquid and a gas. Figure I.19.2 provides the correlation between Ca and λ , together with the black solid line representing the splashing criteria from Yarin and Weiss [1]. The data points represent our experimental results at various conditions, including variation of liquid viscosity, surface tension, smooth and roughened surfaces, and heated plate (400 K). The roughened surface is the BK-7 window, while the smooth, heated surface is the heat-treated stainless steel. The red symbols in Figure I.19.2 denote splashing events, while the blue symbols signify non-splashing events. Overall, our experimental results follow the same trend in predicting non-splashing and splashing phenomena with the literature for water, diesel, and n-dodecane, but not for n-heptane. The data points from non-splashing cases with n-heptane are observed to shift towards the splashing region. The reason for this fact might be due to the liquid properties of n-heptane such as viscosity and surface tension. Nevertheless, Yarin and Weiss’s criterion may not work for many cases since the derived splashing threshold provides an explanation only for corona splash mechanism. Moreover, this correlation posed under an assumption of no interaction of droplet with the solid dry surface instead of a thin liquid film; therefore, it may not be applied for droplet impingement directly on a dry surface. The best fit for the current experimental data is found to be between a dashed line showing $Ca\lambda^{3/4} = 12$ and a dotted line exhibiting $Ca\lambda^{3/4} = 10$ in Figure I.19.2.

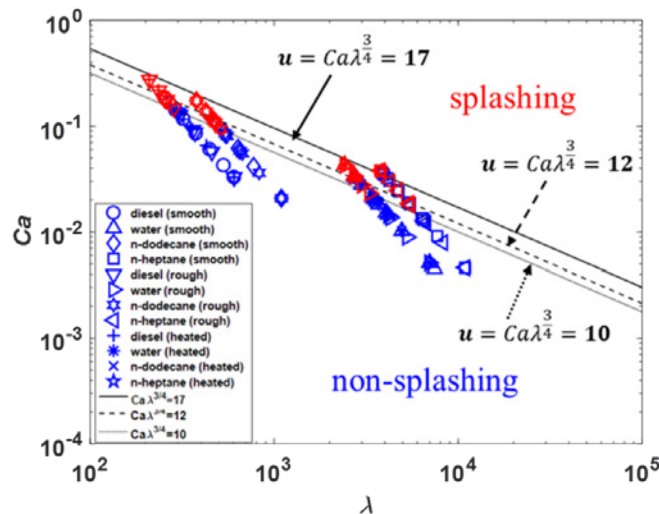


Figure I.19.2. Splashing criteria of diesel, water, n-dodecane, n-heptane, and diesel

LE Simulation Study

Most of the Lagrangian–Eulerian simulation activity carried out during the third year was focused on improving the numerical results. This was achieved through the following three steps, which were found to be fundamental to achieve better prediction of the spray impingement.

- The influence of surface roughness on the prediction of gas velocities near the wall was evaluated, and it allowed for a better assessment of the gas–liquid interaction in the rebound/splashed portion of the spray. The recirculation region at the leading edge of the impinged spray was successfully predicted when accounting for the roughness of the impinged wall (cf. Figure I.19.3).

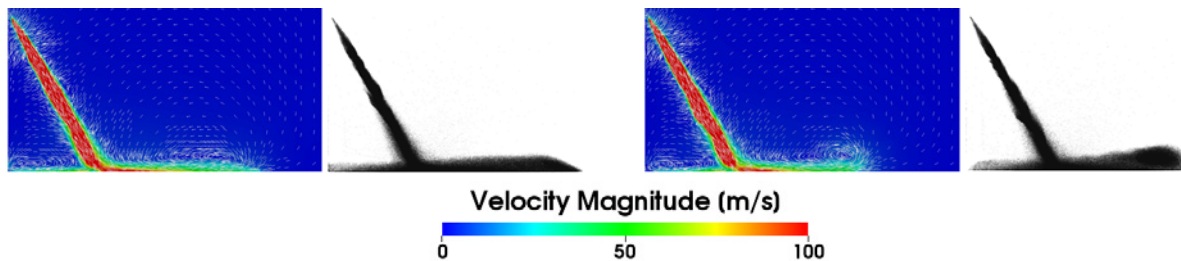


Figure I.19.3. Gas velocity fields and spray shape for the hydro-dynamically smooth plate (left figures) and rough plate (right figures)

- Droplet size distributions at specified locations pre- and post-impingement were extracted and compared against MTU experiments (cf. Figure I.19.1c). Within this activity, the setup of break-up and coalescence/collision models was further improved as a result of the droplet size study.
- Conjugate heat transfer modeling was included to achieve a more accurate representation of the interaction and energy exchange between the wall film and the heated plate. Within this activity, new tools for the calculation of selected wall film properties (mass, area, and thickness) were developed, and the results were compared against MTU’s experiments. The experimental data of film mass and film area were successfully matched, while areas of improvement in the film thickness prediction were identified (in terms of film evaporation).

The findings from surface roughness, droplet size, and conjugate heat transfer studies were combined with the use of the modified Stanton & Rutland SWI model implemented in the second year. Improved prediction of impingement-related quantities was achieved while reducing the need for tunable parameters, as the current implementation of the SWI model does not require any inputs from the user (cf. Figure I.19.4).

A three-million core-hour allocation on Argonne National Laboratory’s Mira supercomputer was requested and obtained as a joint effort with the University of Massachusetts Dartmouth team. This time allocation will be used to run a matrix of DNS calculations that will investigate the impingement characteristics of a train of droplets under multiple conditions relevant to internal combustion engine fuel sprays. To this aim, pre-impingement data (liquid and gas properties as well as droplet sizes and velocities) were extracted for 12 operating conditions and five locations in the impingement regions. These data will serve as boundary and initial conditions for the DNS test matrix.

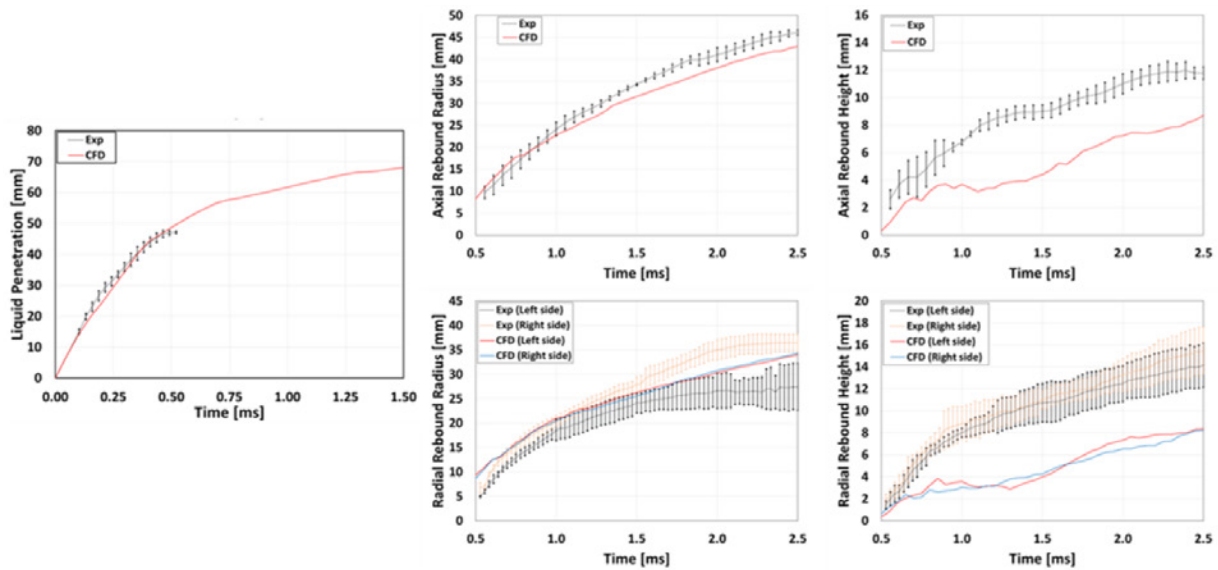


Figure I.19.4. Experiments vs. CFD comparison of liquid penetration (left), rebound radii (center), and rebound heights (right)

Direct Numerical Simulation Study

The areas of focus for the DNS studies have been (a) the impingement of spray droplets on solid surfaces under non-evaporating conditions and (b) development and testing of an accurate VOF-based evaporation modeling approach and solver. In an effort to reduce the turnaround time of diesel droplet train simulations, a pre-existing liquid film was introduced. When simulating droplet train impingements with an initially dry surface, the asymptotic splashed mass ratio is not reached until after a liquid film is established and the impingements reach pseudo-steady state. To avoid the transient film formation period, a pre-existing liquid film was initialized for the diesel droplet train impingement at $u = 24$ at two resolutions, 40 and 80 cells per droplet diameter (CPD). The representative diesel droplet extracted from LE simulations performed by the Argonne group was used ($d = 5.97 \mu\text{m}$, $v = 77 \text{ m/s}$). The splashed mass ratio was quantified and compared to the initially dry surface results. It was determined the pre-existing film produces the same splashing dynamics and splashed mass ratio while reducing the runtime by approximately 40%. Using the new pre-existing film framework, a convergence test was performed by running a highly resolved 160 CPD diesel droplet train simulation. The splashed mass ratios of the simulations at 40, 80, and 160 CPD were compared and showed second-order convergence. The results are shown in Figure I.19.5 along with a subfigure from the highly resolved 160 CPD simulation showing detailed cusp formation and secondary droplets.

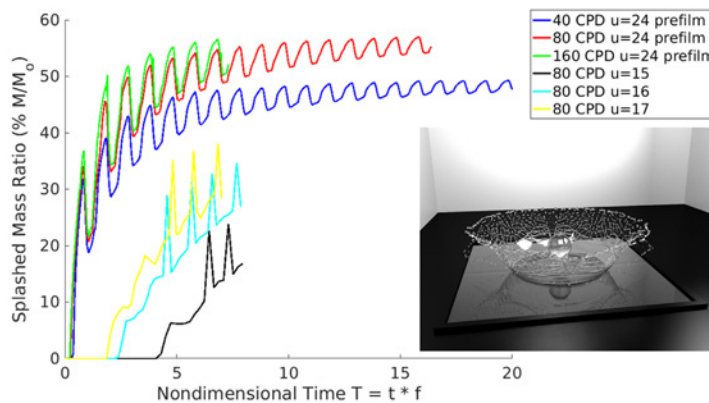


Figure I.19.5. Splashed mass ratio results for simulations at $u = 15, 16, 17,$ and 24 . Comparison of the splashed mass ratios at $u = 15, 16,$ and 17 shows the transition to splashing between $u = 15$ and 16 . Splashed mass at $u = 24$ is presented for three resolutions, showing second-order convergence in the splashed mass ratio. The subfigure shows the highly resolved lamella and cusp formation from the 160 CPD simulation.

The difference in splashed mass between 80 CPD and 160 CPD was found to be only 2%; therefore, 80 CPD was selected as an optimal balance between resolution and runtime. At 160 CPD the computational expense is too large, requiring over three months of runtime on 400 cores to capture the impingement of seven droplets, while at 80 CPD the impingement of 16 droplets was simulated in just over two weeks. The simulation results show that the currently implemented splashing model of O'Rourke and Amsden [2] still over-predicts the splashed mass ratio by approximately 20%, stressing the unmet need for an improved SWI model.

Once an optimal simulation framework and resolution was selected, diesel droplet train simulations were performed near the splashing threshold proposed by Yarin and Weiss [1] ($u = 17$) to determine the splashing threshold for micron-sized diesel droplets. Simulations were run at $u = 15, 16,$ and 17 and captured the transition from droplet deposition to splashing. The transition to splashing was determined based on the signal in splashed mass ratio, shown in Figure I.19.5. A dimensionless time ($T = t \cdot f$) was used for plotting, where t is physical time and f is the impingement frequency. Any time, T , corresponds to the $T-1$ droplet impingement. At $u = 15$ it is not until the impingement of the fifth droplet that splashed mass is seen. This splashed mass is not due to secondary droplets crossing the splashing threshold height; rather, it is due to the lamella leaving the open boundaries of the domain and therefore is not representative splashing. At $u = 16$ and 17 , splashing is seen after the impingement of the third and second droplets, respectively, and is due to secondary droplets crossing the splashing threshold height. In the simulations, we also see stable lamellae at $u = 15$, while at $u = 16$ and 17 unstable lamellae are seen, which lead to cusp formation and secondary droplet ejection. Based on this qualitative and quantitative analysis, it was determined the transition to splashing occurs between $u = 15$ and 16 for micron-sized diesel droplets, proving the robustness of Yarin and Weiss's [1] splashing model with respect to changes in droplet size and liquid.

To gain further insight into the post-impingement dynamics, a robust VOF-based algorithm was developed that characterizes the number and size of secondary droplets as a function of time. The algorithm analyzes the volume fractions in computational cells above the splashing threshold height to locate isolated liquid structures and calculate their volume. After rigorously testing the algorithm with complex liquid geometries, a secondary droplet analysis was performed on the pre-existing film diesel droplet train simulation at $u = 24$. The time-averaged number of secondary droplets and percent of secondary droplet volume are presented in Figure I.19.6, where the secondary droplet diameter, d , is non-dimensionalized by the impinging droplet diameter, D (d/D). Although the majority of secondary droplets have a diameter of $0.375 \mu\text{m}$ or less, they represent a negligible percent of the splashed mass. The majority of the splashed liquid mass is composed of droplets with a diameter between $0.3 \mu\text{m}$ and $1.05 \mu\text{m}$. A second peak in splashed mass is seen at $d/D = 0.4$; this is due to the lamella rim as it crosses the splashed mass threshold height before breaking into secondary droplets. This was confirmed by observing the secondary droplet characterization as a function of time while comparing the results to the simulation at each time. This observation further showed the robustness of the algorithm. Such analyses will be used to develop a highly accurate SWI model that will accurately predict the size and distribution of secondary droplets in LE simulations.

Significant progress has been made in the development of the VOF-based evaporating modeling approach and solver. The six main steps in the algorithm, presented in the previous annual report, have been completed. The evaporation solver has now been validated for the evaporation of a stationary droplet and a droplet which rises due to buoyancy effects in two dimensions [3]. The solver was found to perform very well during all validation tests and is currently being extended to three dimensions.

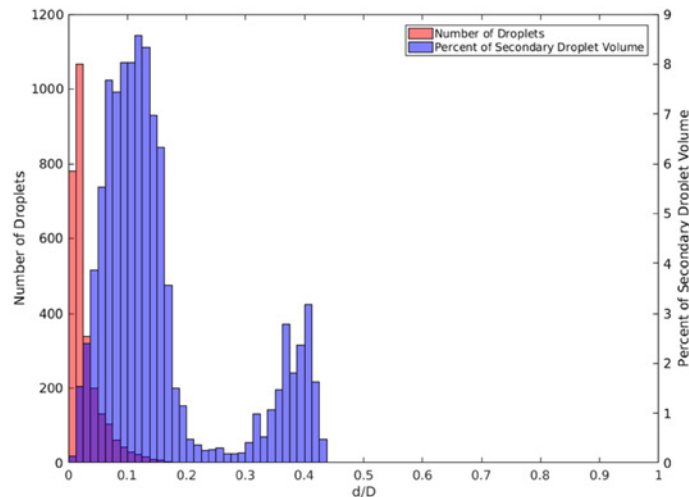


Figure I.19.6. Time-averaged secondary droplet characterization of the 80 CPD diesel droplet train impingement simulation with a pre-existing liquid film at the nondimensional velocity $u = 24$. D is impinging droplet diameter and d is secondary droplet diameter.

Conclusions

- *Experiment work:* (1) Completed impinging spray test with n-heptane for new film thickness measurement, showing the trend of decreasing thickness by increasing ambient density and injection pressure. (2) Provided new splashing criteria for various fuels with ambient and elevated surface temperatures, showing the deviation of Yarin & Weiss's formulation.
- *LE work:* (1) Spray-wall interaction prediction in the LE CFD model was improved from previous year results. (2) Including the effect of surface roughness, predicting free-spray droplet sizes correctly, and including conjugate heat transfer modeling were fundamental to achieve more accurate pre-impingement conditions of both liquid droplets and surrounding gas. (3) The splashing criterion as well as the film evaporation model need to be revised based on the feedback that the DNS test matrix study will provide.
- *DNS work:* (1) By performing a highly resolved 160 CPD resolution simulation of a diesel droplet train impingement using the representative droplet from the Argonne LE simulation analysis, convergence of splashed mass was shown to be second-order. Therefore, 80 CPD has been selected as a balance between resolution and runtime. (2) The splashing threshold was found to be between $u = 15$ and 16 for micron-sized diesel droplets based on DNS results. (3) A robust VOF-based secondary droplet analysis algorithm was developed that characterizes the number and size of secondary droplets as a function of time. These results can now be implemented into a SWI model to accurately predict the secondary droplet distribution resulting from diesel droplet impingements. (4) The VOF-based evaporation model and solver has been completed and validated in two dimensions and is now being extended to three dimensions.

Key Publications

1. Zhao, L., N. Ahuja, X. Zhu, Z. Zhao, et al. 2018. "Splashing Criterion and Topological Features of a Single Droplet Impinging on the Flat Plate." SAE Technical Paper 2018-01-0289.
2. Zhao, L., Z. Zhao, X. Zhu, N. Ahuja, et al. 2018. "High Pressure Impinging Spray Film Formation Characteristics." SAE Technical Paper 2018-01-0312.
3. Zhao, L., R. Torelli, X. Zhu, J. Naber, et al. 2018. "Evaluation of Diesel Spray-Wall Interaction and Morphology around Impingement Location." SAE Technical Paper 2018-01-0276.

4. Markt, D.P., R. Torelli, A. Pathak, M. Raessi, S. Som, R. Scarcelli, S.-Y. Lee, and J. Naber. 2018. "Using a DNS Framework to Test a Splashed Mass Sub-Model for Lagrangian Spray Simulations." SAE Technical Paper 2018-01-0297.
5. Zhu, X., R. Torelli, L. Zhao, et al. 2018. "Film Formation Characteristics of N-Heptane Spray-Wall Impingement at Engine-Like Conditions." ICLASS 2018.
6. Markt Jr., D., L. Zhao, X. Zhu, et al. 2018. "An Experimental and Computational Study of a Single Diesel Droplet Impinging on a Dry Surface." ICLASS 2018.
7. Markt, D.P., A. Pathak, and M. Raessi. 2018. "Advanced Computational Simulations of Surface Impingement of a Train of Ethanol Drops: A Pathway to Developing Spray-Wall Interaction Sub-Models." *Computing in Science Engineering* 20 (4): 56–65.
8. Pathak, A., and M. Raessi. 2018. "Steady-State and Transient Solutions to Drop Evaporation in a Finite Domain: Alternative Benchmarks to the d2 Law." *Int. J. Heat & Mass Transfer* 127: 1147–1158.

References

1. Yarin, A.L., and D.A. Weiss. 1995. "Impact of Drops on Solid Surfaces: Self-Similar Capillary Waves, and Splashing as a New Type of Kinematic Discontinuity." *Journal of Fluid Mechanics* 283: 141–173.
2. O'Rourke, P., and A. Amsden. 2000. "A Spray/Wall Interaction Submodel for the KIVA-3 Wall Film Model." SAE Technical Paper 2000-01-0271.
3. Pathak, A., and M. Raessi. 2016. "A 3D, Fully Eulerian, VOF-Based Solver to Study the Interaction between Two Fluids and Moving Rigid Bodies Using the Fictitious Domain Method." *Journal of Computational Physics* 311: 87–113.

Acknowledgements

Thanks to Jeffrey Naber, Riccardo Scarcelli, Sibendu Som, Roberto Torelli, and Mehdi Raessi for integral contributions to the project.

I.20 Development and Validation of a Lagrangian Soot Model Considering Detailed Gas Phase Kinetics and Surface Chemistry (University of Wisconsin)

Sage Kokjohn, Principal Investigator

University of Wisconsin System
21 N Park St., Suite 6401
Madison, WI 53715
E-mail: kokjohn@wisc.edu

Michael Weismiller, DOE Technology Development Manager

U.S. Department of Energy
E-mail: Michael.Weismiller@ee.doe.gov

Start Date: January 1, 2016	End Date: December 31, 2018	
Project Funding: \$501,919	DOE share: \$441,727	Non-DOE share: \$60,192

Project Introduction

Computational fluid dynamics (CFD) modeling is used to develop current and future production engines. A key shortcoming of CFD-driven engine design is the ability to predict soot emissions. The objective of this project is to improve soot modeling capabilities to enable the engine industry to design advanced combustion engines. A focus of the project is developing and validating a detailed reaction mechanism including polycyclic aromatic hydrocarbon (PAH) chemistry up to benzo[a]pyrene. The model will be rigorously validated through comparisons with experimental data. The model will be developed in a Lagrangian framework that will use a statistical representation of the soot aggregates to allow detailed tracking of soot makeup without the need to assume a fractal dimension. Optical and metal engine experiments necessary to validate PAH growth and soot formation will be conducted. The final outcome of the project will be a new soot model that is validated under conditions ranging from conventional, mixing controlled compression ignition to advanced compression ignition combustion.

Objectives

Overall Objectives

- Improve soot modeling capabilities in government-sponsored and commercial CFD codes to enable the engine industry to design high-efficiency clean engines for transportation applications
- Identify, develop, and validate a semi-detailed reaction mechanism capable of predicting PAH chemistry up to at least benzo[a]pyrene
- Perform high-fidelity experiments to measure in-cylinder PAH and engine-out soot mass and particle size distributions to improve the combustion community's fundamental understanding of soot formation

Fiscal Year 2018 Objectives

- Measure particle size distributions in an engine operating under conventional, mixing controlled compression ignition combustion and advanced compression ignition combustion modes
- Compare soot model predictions to measured particle size distribution data
- Package the soot model for inclusion in government-sponsored and commercial codes

Approach

An advanced soot modeling framework is being developed in the government-sponsored CFD code (KIVA) and commercial CFD code (CONVERGE), and a targeted validation effort is being undertaken to ensure the computational tools are able to adequately capture all of the upstream processes influencing soot formation (spray, mixing, ignition, combustion). Simultaneously, optical and metal engine experiments are being

performed to enable detailed characterization of PAH formation and soot production. The final effort will combine the validation experiments and simulation framework development to test the soot model and make comparisons to existing models.

Results

- Coupled a detailed solution of the population balance equations to an engineering-level CFD model and demonstrated the ability to reproduce measured particle size distributions (PSDs)
- Used multi-wavelength laser-based imaging to measure PAH growth in an optical engine
- Developed a post-processing-based coupling approach to enable the detailed soot model to be used in any open source or commercial CFD code

Experimental data was collected in two engines, and simulations were performed to evaluate soot model performance and provide insight into the soot formation process. The first engine was a GM 1.9-L small bore, light-duty automotive engine, and the second was a Caterpillar C15 large bore, heavy-duty engine. The GM 1.9-L engine was run at five different operating conditions with sweeps of start of injection timing (SOI) and rail pressure. Rail pressure sweeps were performed with a SOI timing of -8.5° after top dead center (ATDC), and the SOI sweep was performed at a rail pressure of 950 bar. An engine speed of 2,300 r/min, gross indicated mean effective pressure of 8 bar, and equivalence ratio of 0.33 were kept constant.

Figure I.20.1 shows PSDs grouped by injection timing and injection pressure. Measured and simulated PSDs are in parallel plots for trend comparison. The quantity of accumulation mode particles increases as the SOI timing is retarded from -8.5° to -3° ATDC, but in general, the PSD shape is rather insensitive to SOI timing. As injection pressure is increased, the number of nucleation mode particles increases and the number of accumulation mode particles decreases. In general, the simulations show very good agreement with both the trends and magnitudes of the measured particle size distributions. Namely, the simulations show that changes in SOI timing result in similar shapes of the PSD, while changes in injection pressure cause changes in the shape of the distributions and the balance between nucleation mode and accumulation mode particles. The simulations accurately capture the increase in the nucleation mode particles (and decrease in accumulation mode) as injection pressure is increased. For all cases the profiles match to within an order of magnitude for the entire measured domain, excepting the smallest particles of the -3° , 950 bar case. Note that no model constants were adjusted for these comparisons.

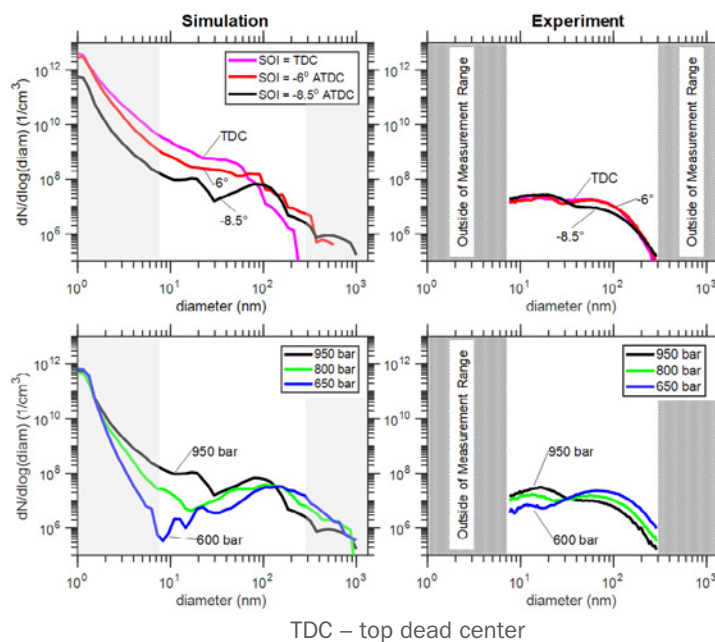


Figure I.20.1. Comparisons of measured and predicted particle size distributions for mixing controlled compression ignition combustion

The heavy-duty (Caterpillar C15) engine was used to study advanced compression ignition combustion by operating on premixed syngas (a 50-50 blend of H₂ and CO) and direct-injected diesel fuel. Figure I.20.2 shows the measured PSDs for a sweep of different syngas energy percentages. Clearly, as the percentage of syngas is increased, the population of accumulation mode particles is reduced while the inception mode population is increased.

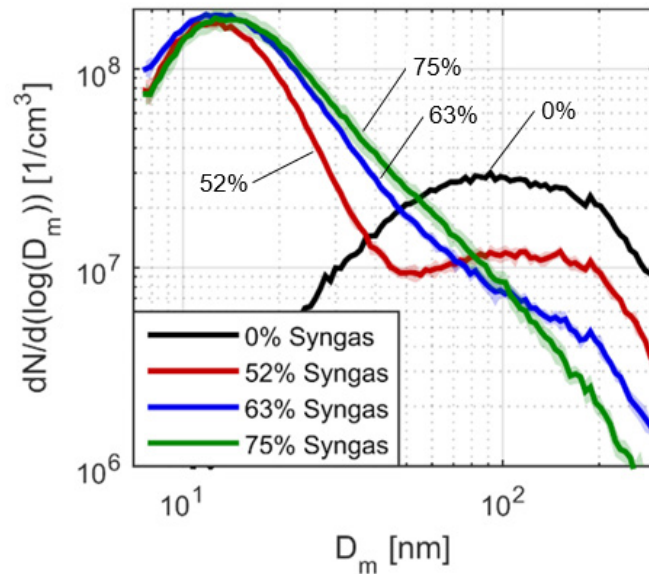


Figure I.20.2. Measured particle size distributions for advanced compression ignition combustion

The neat diesel fuel and 52% syngas mix cases were chosen as a foundation for comparison because, although they have significantly different PSD profiles, they both have an accumulation mode. The accumulation mode population is a useful feature that can be utilized in comparisons. Figure I.20.3 shows a comparison between the measured and predicted PSDs for the neat diesel and mixed syngas cases. The neat diesel case has a larger inception mode population but lacks an independent inception mode, while the mixed syngas case has a prominent inception mode. The simulation captures both cases' accumulation mode shapes and the neat diesel's higher accumulation mode numbers. Quantitatively, the neat diesel simulation predicts all particles larger than 20 nm to within an order of magnitude. For the mixed syngas case, the large inception mode with a smaller and distinct accumulation mode trends are predicted well and to within an order of magnitude throughout the size domain excepting particles surrounding 60 nm, where the dwell in population is over-predicted. In the simulated neat diesel results, there is an identifiable inception mode that is not present in the measured results. These small particles may be missing in the measured data as a result of the measurement process, in which smaller particles may diffuse to the wall or agglomerate with larger particles. Similar to the study in the small bore engine, no model constants were adjusted.

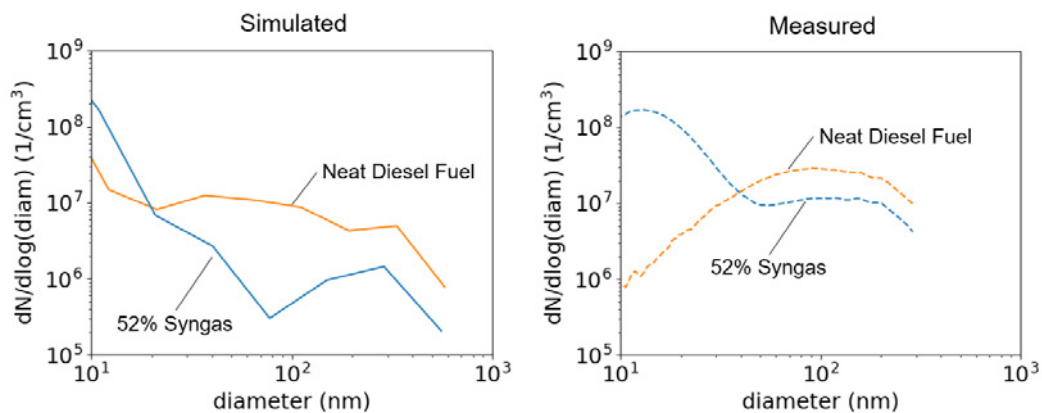


Figure I.20.3. (left) Simulated and (right) measured particle size distributions for neat diesel fuel and 52% syngas

In addition to the ability to predictively simulate PSD, a benefit of the current model is the substantial amount of information available regarding not only mass, particle size, and number, but also features of the soot particles that cannot be derived from other models. We are beginning to use this information to generate simulated soot aggregates that are representative of a size or type of particle. To generate the soot aggregate, the number of primary particles, C and H atoms for each particle, and size of each particle are taken from the detailed soot model. The fractal dimension, radius of gyration, and mobility diameter are calculated using correlations of Park et al. [1], Lall et al. [2], and Rogak and Flagan [3]. The ballistic cluster-cluster aggregate method [4] is then used to randomly connect two clusters with the correct primary particle size. The process is repeated until the aggregate contains the desired number of primary particles. The fractal dimension, radius of gyration, and mobility diameter of the ballistic cluster-cluster aggregate generated particle is then compared to the desired values. If they agree, the particle is used as a representative aggregate.

Figure I.20.4 shows the measured and predicted PSDs for the small bore engine operating with an SOI timing of -8.5° ATDC and an injection pressure of 950 bar. The soot aggregates were simulated for several different particle sizes. Two-dimensional projections of the soot aggregates are shown by the call-outs on the plot. To the authors' knowledge, this is the first CFD-based prediction of transmission electron microscope style soot aggregates under diesel engine conditions. Future efforts will use this analysis to provide fundamental insight into soot morphology and growth. Additionally, the ability to predict the soot structure will open up substantial opportunities to contribute the technology to other areas (e.g., manufacturing, coating development/application).

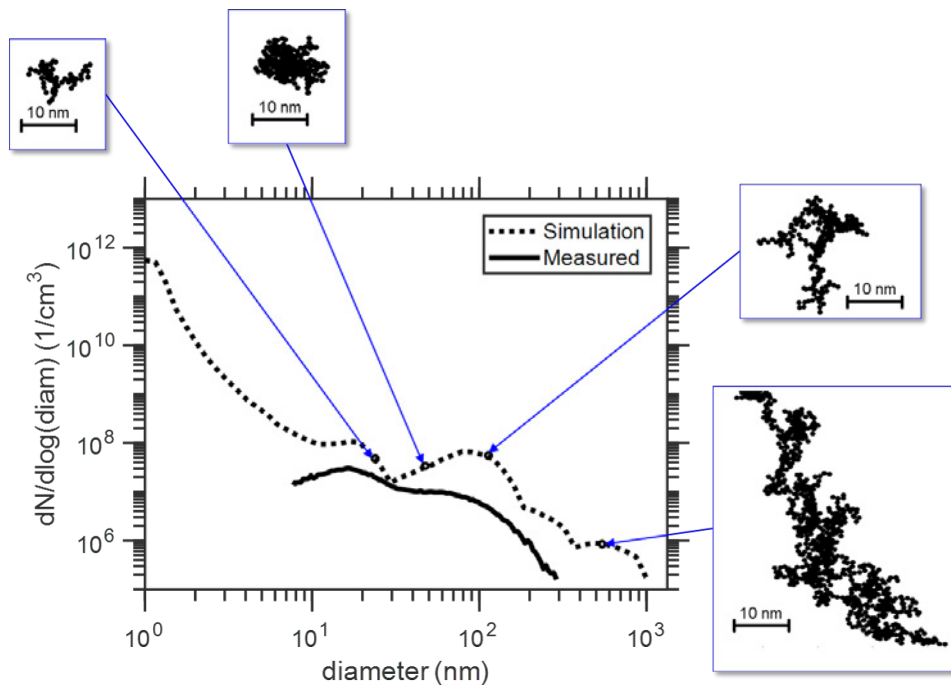


Figure I.20.4. Comparisons of measured and predicted PSDs and representative simulated soot aggregates for several different sized particles

To support the model development effort, in-cylinder soot and PAH were imaged in an optical engine operating under low-temperature advanced compression ignition combustion conditions. The laser for probing PAH provided a ~ 70 mJ beam pulsed at 10 Hz with a wavelength of either 355 nm, 532 nm, or 633 nm. Each of these wavelengths is absorbed by different size ranges of PAH molecules, from small to large as the wavelength is increased, thereby probing the growth of in-cylinder PAH. The laser for probing soot provides a beam at ~ 250 mJ pulsed at 10 Hz with a wavelength of 1,064 nm, which is too long to be absorbed by PAH but is absorbed by soot, heating it to near its vaporization temperature, vastly increasing its incandescent emission. The resulting planar laser-induced fluorescence (PLIF) of PAH and planar laser-induced incandescence (PLII) of soot were imaged by two intensified charge coupled device cameras using appropriate filters. The two laser

beams were formed into thin sheets and were spatially overlapped with each other. Temporally, the 1,064 nm laser pulse was 2.5 μ s later than the PAHs laser pulse, which is long enough to avoid any cross-talk or interference between the PAH PLIF and soot PLII signals. Three different laser sheet heights were employed, at 11 mm, 15 mm, or 18 mm below the cylinder fire deck.

Figure I.20.5 shows an example of false-colored simultaneous PAH PLIF and soot PLII for a double injection operating condition. On the left are PAH PLIF images for 633-nm laser excitation at three different laser heights, and on the right are the corresponding soot PLII images. The z-axis indicates the heights of each sheet below the fire deck. Each slice image is the ensemble averaged of 12 instantaneous images from different engine cycles. The injector is near the left corner of the image, and the jet penetrates from left to right, with the piston bowl wall at the curved boundary on the right side of the images. Only one of the eight jets was visualized. These data will be used in the continuing efforts to provide further insight into model performance and improve our understanding of soot formation and growth under engine-relevant conditions.

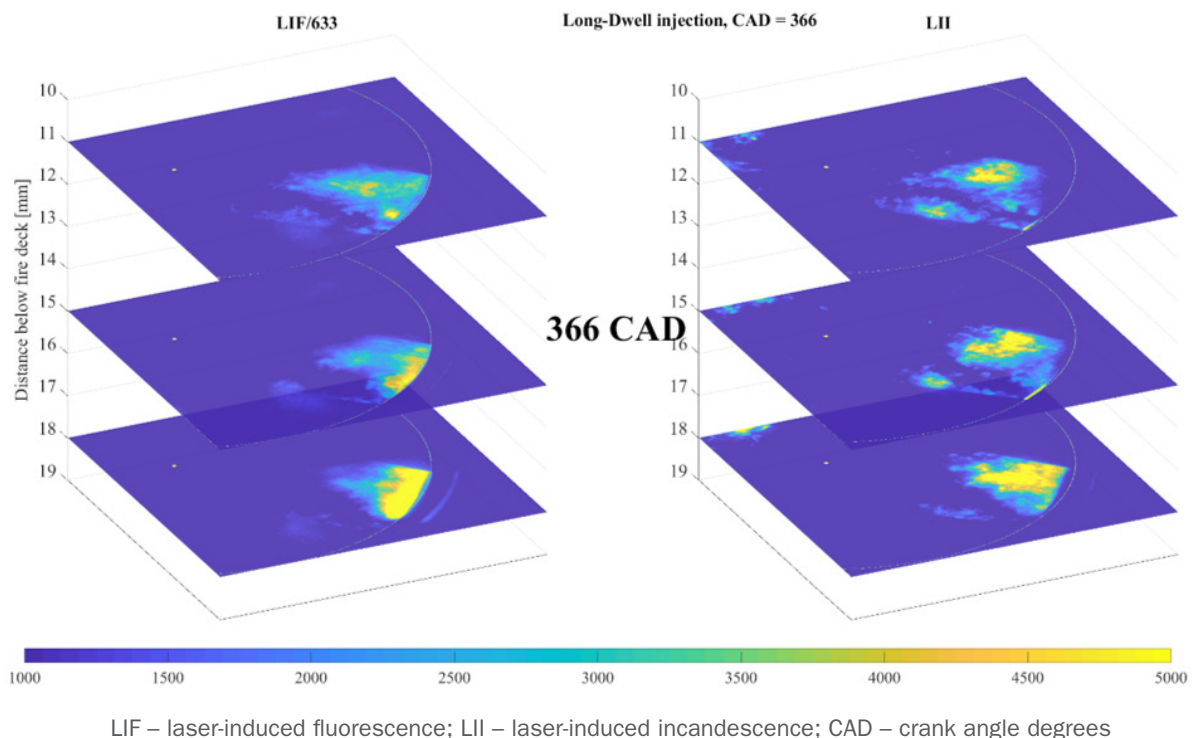


Figure I.20.5. Ensemble-averaged 633-nm PAH PLIF and soot PLII images for the long dwell operating condition

Conclusions

- The detailed soot model was shown to reproduce the measured particle size distribution from multiple engines over a range of operating conditions in both conventional mixing controlled combustion and advanced compression ignition combustion without adjustment of model constants.
- The detailed soot model is capable of providing substantial insight into the soot morphology and particle structure that cannot be obtained using simplified models. This information may be useful for design of future engine systems (e.g., considering interactions between the engine combustion process and aftertreatment).
- PAH and soot imaging have been completed and will be used to assess the robustness of the model predictions and provide insight into the soot formation process.

Key Publications

1. Chuahy, F., T. Strickland, N.R. Walker, and S.L. Kokjohn. 2018. “Effects of Reformed Fuel on Dual-Fuel Combustion Particulate Morphology.” 2018 Spring Technical Meeting, Central States Section of The Combustion Institute, May 20–22, 2018, Minneapolis, MN.
2. Strickland, T., and S.L. Kokjohn. 2018. “Simulation of a Diesel Fuel Jet with a 3D Stochastic Soot Model.” 2018 Spring Technical Meeting, Central States Section of The Combustion Institute, May 20–22, 2018, Minneapolis, MN.
3. Kokjohn, S.L. 2018. “Advanced Combustion: Challenges and Opportunities.” University of Michigan–Ann Arbor, August 16, 2018.
4. Strickland, T., and S.L. Kokjohn. 2018. “Simulated Soot Aggregates under Diesel Combustion Conditions.” In preparation to be submitted, Fall 2018.

References

1. Park, Kihong, Feng Cao, David B. Kittelson, and Peter H. McMurry. 2003. *Env. Sci. Tech.* 37 (3): 577–583.
2. Lall, A.A., W. Rong, L. Madler, and S. Friedlander. 2008. *J. Aerosol Sci.* 39 (5): 403–417.
3. Rogak, Steven N., and Richard C. Flagan. 1990. *J. Colloid Interface Science* 134 (1): 206–218.
4. Meakin, P. 1988. *J. Chem. Phys.* 89 (1).

Acknowledgements

The in-cylinder PAH and soot data were collected by Dr. Mark Musculus’ group from Sandia National Laboratories’ Combustion Research Facility. Convergent Science, Inc., is thanked for supplying CONVERGE CFD licenses and technical assistance on the implementation of new routines into CONVERGE.

I.21 Development and Validation of Physics-Based Submodels of High Pressure Supercritical Fuel Injection at Diesel Conditions (The University of Alabama)

Ajay K. Agrawal, Principal Investigator

The University of Alabama
359 H.M. Comer Hall
Tuscaloosa, AL 35487
Email: aagrawal@eng.ua.edu

Sibendu Som, Principal Investigator

Argonne National Laboratory
9700 S. Cass Ave.
Argonne, IL 60439
Email: ssom@anl.gov

Michael Weismiller, DOE Technology Development Manager

U.S. Department of Energy
E-mail: Michael.Weismiller@ee.doe.gov

Start Date: January 1, 2016	End Date: December 31, 2018	
Project Funding (FY18): \$542,487	DOE share: \$476,012	Non-DOE share: \$66,475

Project Introduction

The project seeks to develop and validate accurate, physics-based, numerical submodels and implement them in computational fluid dynamics (CFD) software codes to enable accurate predictions of diesel sprays at pressures higher than the current systems. The combined experimental-computational effort has four main objectives: (1) acquire spatially and temporally resolved scalar measurements of fuel-oxidizer mixing in the near field of the fuel jet; (2) develop software modules to calculate thermo-physical properties of diesel surrogates and their mixtures with oxidizer of interest in real-gas operating regime; (3) integrate the real-fluid model into a commercial and an open-source CFD code to simulate fuel-air mixing in high-pressure diesel sprays; and (4) assess the robustness, accuracy, and uncertainty of the integrated CFD solvers in computing diesel sprays.

A constant pressure flow rig was developed and integrated with rainbow schlieren deflectometry (RSD) optical diagnostics to acquire statistically significant fuel-air mixing data from multiple injections in quick succession possible with the facility. Methods to process schlieren images were developed to compute mixture fraction (or equivalence ratio) and temperature contours in the whole field of the jet. Real-gas property models were developed to create tables of thermo-physical properties at real-gas conditions, which were then integrated into two software codes. Robustness of the CFD codes was assessed by comparing with experimental data, and a more comprehensive plan to compare experimental and computational results is currently in progress.

Objectives

Develop a CFD code integrated with real-gas property models to predict fuel-air mixing at diesel condition, and generate high-quality experimental data on fuel-air mixing in the near field of the jet to validate the code.

Overall Objective

- Produce a validated real-fluid property code which can be integrated with CFD solvers to improve their accuracy in simulating high-pressure diesel sprays
- Integrate the real-fluid property code with CFD solvers to compute fuel-air mixing at supercritical conditions using the Eulerian-Eulerian approach

- Generate an extensive experimental data set to validate CFD models for high-pressure diesel sprays
- Assess the accuracy of the Eulerian-Eulerian approach to simulate fuel spray at high-pressure diesel engine operating conditions

Fiscal Year 2018 Objectives

- Apply CFD code integrated with real-gas property models to predict fuel-air mixing in diesel sprays
- Generate experimental data for comparison with CFD predictions, and make comparisons

Approach

Experiments were conducted in a constant pressure flow rig, a newly developed test facility at The University of Alabama. In the constant pressure flow rig, a low-speed flow of heated, pressurized air is continuously supplied to the test chamber, and the fuel is injected against this flow to perform fuel-air mixing experiments in quick succession to acquire statistically significant measurements. High-speed RSD, a novel optical diagnostics technique pioneered in our laboratory to acquire quantitative scalar measurements in jets and flames, was utilized to resolve the highly dynamic features of the mixing process. Experiments were conducted for several test conditions to develop and verify the RSD technique, and preliminary comparison with CFD predictions has been completed.

A real-fluid model developed at The University of Alabama to account for the compressibility effects was integrated by the Argonne National Laboratory team with CFD code CONVERGE, and the functionality of integrated code has been demonstrated. We identified that an accurate real-gas mixing model is necessary, and thus, completed the relevant mixing model analysis. Plans include extending the CFD code to include the real-gas mixing model, and then systematically comparing CFD predictions with experimental results obtained by the RSD technique for a range of test conditions.

Results

Four key accomplishments of the project during this year, two experimental and two computational, are described next. With these results, we have gained confidence in our methodologies, which have been significantly refined from their earlier versions. Mainly, both experimental and computational analyses required an in-depth investigation of real-gas mixing models and how they can affect the results. We have resolved related issues, and presently, we are well on our way to perform systematic comparisons. The four key accomplishments discussed in this section are as follows:

- Accurately identified liquid, two-phase, and vapor regions of the jet from RSD measurements.
- Accurately converted refractive index measurements into mixture temperature and equivalence ratio using higher-order models verified for real-gas mixtures rather than the simplified Dale-Gladstone relationship applicable to ideal gas mixtures but used commonly in the literature.
- Developed accurate mixture models to account for real-gas effects at high-pressure diesel conditions, resulting in three-dimensional (3D) property tables for integration with CFD codes. In the past, we evaluated properties as a function of pressure and temperature. To account for the mixing model, we now create 3D property tables in terms of pressure, temperature, and mixture fraction.
- Post-processed CFD predictions to generate synthetic RSD images for comparison with experimental RSD images. In this way, one-to-one comparison between predictions and experiments is possible in all regions of the spray, including the mixing region, ignition zone, and the combustion zone.

Liquid Boundary Detection Algorithm

A robust technique to identify the liquid jet region as opposed to the vapor region was developed. The liquid region of the spray must be identified to distinguish it from the vapor region, where the RSD technique can be reliably used to quantify the local mixture properties. The present technique leverages the large number of injections that are acquired in quick succession in the constant pressure flow rig integrated with the high-speed

RSD system. Experiment yields over 95 videos of RSD images depicting the jet evolution. The RSD images are processed to transform RGB (red, green, and blue) readings to HSI (hue, saturation, and intensity), and saturation and/or intensity at a pixel location below specified threshold values are considered to indicate presence of liquid at that position. The results from this processing are shown in Figure I.21.1, which includes both an instantaneous RSD image and the time evolution of the reliable hue reading contour plots. In the RSD image, the near injector region is clearly dark and the downstream region shows distinctly visible colors. In the near injector region, the time evolution shows that there are zero reliable hue readings, while in the downstream region, nearly all hue readings are reliable. Between approximately 20 mm and 25 mm downstream of the injector exit, the number of reliable readings increases rapidly, indicating the presence of two-phase region. Effectively, RSD technique can be used to identify the liquid region, the two-phase spray region, and the outer vapor region, where the fuel-air mixing can be quantified from RSD-based hue data.

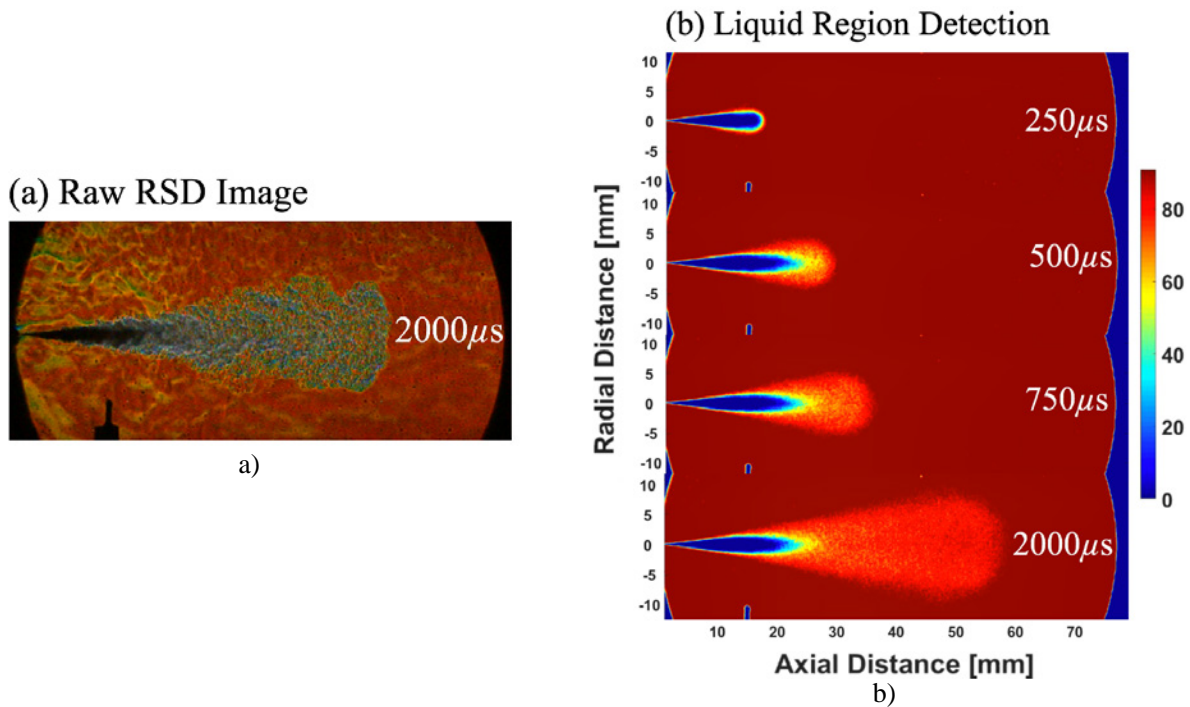


Figure I.21.1. Detection method illustrating liquid, two-phase, and vapor regions of the spray based on RSD measurements from 95 injections: (a) instantaneous RSD image showing dark region near injector and (b) time sequence of contours of number of reliable hue readings

Real-Gas Mixture Model to Acquire Mixture Properties from RSD Measurements

The conversion of RSD measurements of refractive index into mixture properties such as temperature, mixture fraction, etc., requires relationship between optical properties of a mixture and its thermodynamic state. Thus, the thermodynamic mixing states for given ambient air temperature/pressure and the fuel injection conditions must be determined. We assume adiabatic mixing between fuel and air and apply real-fluid properties and real-fluid mixing models to establish the adiabatic mixing line, as shown in Figure I.21.2 for Spray A condition from the Engine Combustion Network at Sandia National Laboratories—that is, n-dodecane fuel injected at 1,500 bar and 363 K into ambient nitrogen at 60 bar and 900 K. The dotted line shows that as the fuel concentration in the mixture increases (higher mixture fraction), the fuel-nitrogen mixture temperature decreases until the point when the mixture enters the two-phase region. After this point, at fuel mole fraction of approximately 0.25, the two-phase mixture behavior is not well characterized and is therefore not shown. The relationship between mixture fraction and temperature is a function of the initial conditions and fuel type, and it can be determined in the vapor region using real properties and real-gas mixing models, while assuming adiabatic mixing for a given experiment.

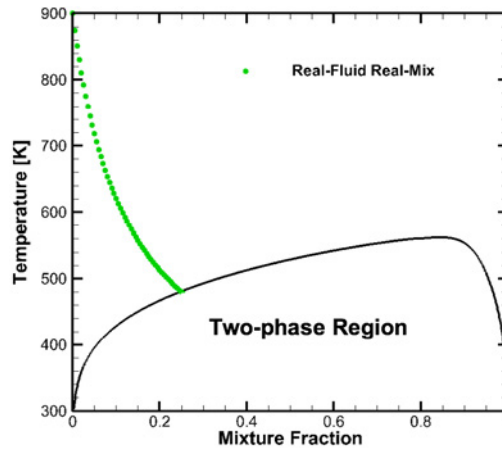


Figure I.21.2. Gas-phase adiabatic mixing of fuel and air as a function of fuel molar mixture fraction using real-fluid properties and real-fluid mixing models for Engine Combustion Network Spray A conditions

The relationship between the fuel mixture fraction and temperature can be used to develop the relationship with the refractive index of the mixture. In past applications of RSD, we utilized the Dale-Gladstone formulation ($n=1+\sum\kappa\rho$), which is valid for ideal-gas mixtures with refractive indices near unity. However, for real-fluid mixtures of components with refractive index much greater than unity, the original formulation given by Lorenz-Lorentz in Equation 1 is more accurate. The important variables in this equation are mixture molecular polarizability and density. The mixture density can be determined from the real-fluid mixing models using real-fluid properties and adiabatic mixing assumption, as discussed above. The mixture molecular polarizability is determined by applying a mixing law that has been validated against measurements published in literature.

$$\frac{(n^2-1)}{(n^2+2)} = \frac{\rho N_a}{3\epsilon} \frac{\alpha}{MW} = \frac{\rho_{mix} N_a}{3\epsilon} \sum \frac{x_i \alpha_i}{MW_i} \quad (1)$$

Applying Equation 1 after replacing the mixture refractive index, n , with the normalized refractive index difference, $\delta = (n - n_o) / n_o$, where n_o is the refractive index at the ambient conditions, and with the known relationship between mixture fraction and mixture temperature, we can obtain accurate relationships between optical properties and thermodynamic properties, as shown in Figure I.21.3. Here, refractive index difference is the scalar property measured by RSD, and equivalence ratio and mixture temperature are the corresponding thermodynamic properties for given fuel injection and chamber conditions of the experiment. Note that RSD measurements require multiple injections so that the acquired data can be averaged to ensure axisymmetry required for Abel inversion. Combining this discussion with the ability to detect the liquid boundary and two-phase region, as described above, makes RSD a unique diagnostic tool to investigate engine-relevant fuel sprays.

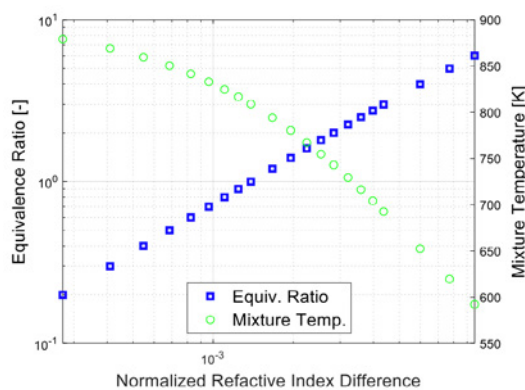


Figure I.21.3. Relationship between the mixture's normalized refractive index and equivalence ratio and temperature for the Engine Combustion Network Spray A conditions

Real-Gas Properties and Real-Gas Mixture Models for Integration with CFD Codes

Previously developed real-fluid property models must be combined with real-fluid mixing models to account for real-gas effects at diesel conditions. Briefly, it is not appropriate to use volume- or mass-weighted combinations of pure component real-gas properties when considering a real-gas mixture. Thus, we have undertaken the development of a user-defined function that reads in three-dimensional property tables based on real-gas mixing models and interpolates as needed to return the desired thermal or transport properties at specified values of pressure, temperature, and mixture fraction. For example, Figure I.21.4 shows the calculated density contours for n-dodecane/nitrogen mixtures as a function of pressure, temperature, and mixture fraction; similar plots are generated for other thermo-physical properties (viscosity, thermal conductivity, etc.). This additional complexity (three-dimensional vs. two-dimensional property tables) required reworking the user-defined function developed in the previous year of the project. Current efforts include understanding the required resolution in each dimension (i.e., pressure, temperature, mixture fraction), as even a relatively coarse resolution can result in a 100–500 megabyte file, which can burden the random-access memory of the CONVERGE CFD software.

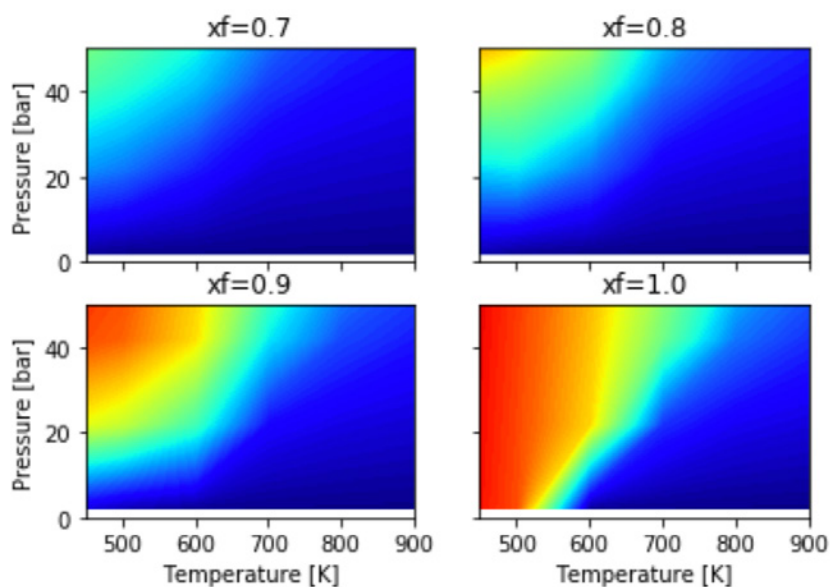


Figure I.21.4. Density contours for n-dodecane/nitrogen mixtures at various fuel mole fractions

Comparison between CONVERGE CFD Predictions and RSD Measurements

A previously presented experimental test condition—n-heptane injected at 1,000 bar, 363 K into air at 28 bar, 825 K—was simulated by Argonne National Laboratory collaborators using CONVERGE CFD software. Figure I.21.5 shows comparisons between vapor and liquid penetration data from simulation and experiments as well as the comparison of experimental and simulated ignition delay data. Good agreement between the simulations and experiments can be seen for both parameters. The CFD data were post-processed to generate synthetic RSD images for direct comparison with experimental RSD images. This approach is not limited by the requirement of the axisymmetry, and thus, instantaneous realizations can be compared with each other. Figure I.21.6 shows a few comparisons between experimental RSD images and synthetic RSD images generated from the CFD density fields. The synthetic RSD images show good agreement of the first-stage reaction behavior both spatially and temporally. This gives strong support to previous postulation about the behavior of the experimental RSD images disappearing as the temperature increased during the first-stage reactions. Again, this preliminary comparison shows good agreement in spatial and temporal evolution of the spray, including the ignition behavior. The next steps in this work will be to directly compare the simulated and measured equivalence ratio field prior to ignition.

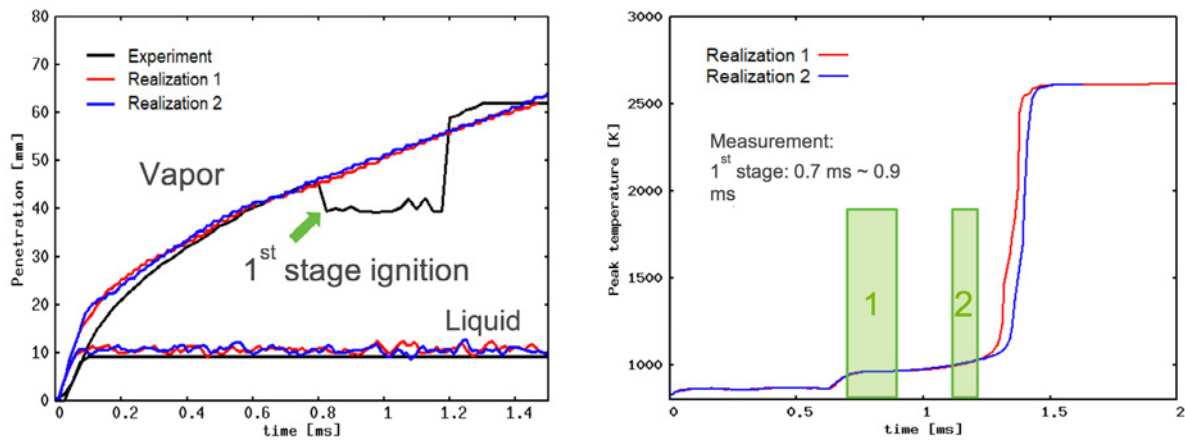


Figure I.21.5. Comparison of simulation and experimental (left) vapor and liquid penetration results and (right) ignition delay behavior for n-heptane injected at 1,000 bar, 363 K into air at 28 bar, 825 K

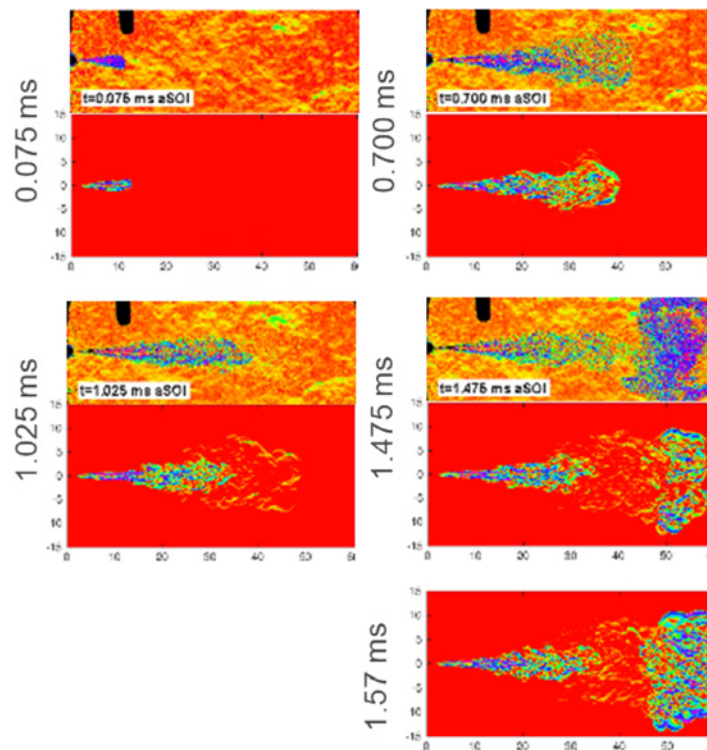


Figure I.21.6. Comparison of experimental RSD images (top in each pair) and synthetic RSD images (bottom in each pair) processed from CFD results for n-heptane injected at 1,000 bar, 363 K into air at 28 bar, 825 K

Conclusions

Experimental and computational capabilities have been developed, and verification of each capability has been completed independently. Initial comparisons between experiments and CFD predictions show encouraging results. The project is ready to move forward to the next step of systematic comparisons.

Acknowledgements

Nicholas D'Amico, National Energy Technology Laboratory

I.22 Development of a Physics-Based Combustion Model for Engine Knock Prediction (The Ohio State University)

Seung Hyun Kim, Principal Investigator

The Ohio State University
201 W. 19th Ave.
Columbus, OH 43210
E-mail: kim.5061@osu.edu

Michael Weismiller, DOE Technology Development Manager

U.S. Department of Energy
E-mail: Michael.Weismiller@ee.doe.gov

Start Date: February 1, 2016	End Date: July 31, 2019	
Project Funding: \$715,933	DOE share: \$643,839	Non-DOE share: \$72,094

Project Introduction

Engine knock is a primary factor to limit the fuel efficiency of passenger cars. It is caused by undesired ignition of fuel/air mixture before spark-ignited (SI) premixed flame fronts consume the fresh gas, and it is accompanied by rapid rise and oscillation of in-cylinder pressure and potential engine damage. Approaches to increase the fuel efficiency of SI engines, such as increasing the compression ratio and downsizing, often generate thermodynamic conditions that are more prone to autoignition and thus engine knock.

The ultimate goal of this project is to improve the predictive capability for computational fluid dynamics (CFD) simulation of engine knock phenomena. Toward this goal, this project will develop a physics-based combustion model for large eddy simulation (LES) of engine knock processes. The model is developed in the context of LES to reproduce the stochastic nature of knocking phenomena. To advance the predictive capability of knock models, the emphasis of the model development is placed on turbulence-chemistry interactions during end-gas ignition and high-fidelity chemistry description. In typical engine conditions, in-cylinder flows are highly turbulent. Complex turbulent motions substantially affect heat release rates and end-gas ignition. The physics-based and accurate modeling of such turbulence-chemistry interactions is necessary, in particular to predict processes in high scalar dissipation layers. Accurate description of end-gas ignition requires the use of a high-fidelity chemical mechanism. This project aims to enable engine knock LES where ignition chemistry is described by a reduced mechanism that contains about 100 species, while employing a physics-based model for turbulence-chemistry interactions.

Objectives

Overall Objectives

- Develop a combustion model that improves the predictive capability for engine knock by capturing turbulence-chemistry interactions in a physics-based way and incorporating high-fidelity chemistry into LES of in-cylinder turbulent reacting flows
- Advance a fundamental understanding of turbulence-chemistry interactions during end-gas ignition through engine LES, high-fidelity direct numerical simulation (DNS), and engine experiments

Fiscal Year (FY) 2018 Objectives

- Reproduce cycle-to-cycle variations (CCV) under non-knocking conditions using multi-cycle LES
- Implement the developed combustion model for engine knock prediction into CONVERGE CFD as a user-defined function (UDF)

Approach

The overall approach includes joint computational and experimental efforts focusing on the model development and validation with high-fidelity numerical and experimental data. The physics-based and mathematically consistent modeling framework consists of separate models for SI premixed flame propagation and end-gas ignition processes to consider fundamentally different turbulence-chemistry interactions during the two processes. Conditional moment closure (CMC) [1] is used to model end-gas ignition, while the front propagation formulation (FPF) [2] is used to model SI premixed flame propagation. The model is developed in the context of LES to reproduce the stochastic nature of the knocking phenomena. For thorough validation, DNS and engine experiments are performed to provide high-fidelity datasets. DNS data guides the model development by providing detailed statistical information.

Results

FY 2018 Accomplishments

- Reproduced CCV in an engine experiment under a non-knocking condition using multi-cycle LES
- Implemented the CMC-FPF model into CONVERGE CFD
- Acquired in-cylinder pressure data from single-cylinder engine experiments
- Developed and assessed the mixing model used in the knock CMC model

Multi-Cycle LES under Non-Knocking Condition

In FY 2018, a major effort has been devoted to reproduce CCV in an Oak Ridge experiment using multi-cycle LES. CCV of in-cylinder pressure and of temperature play a key role in knocking since the end-gas ignition is sensitive to those thermodynamic properties. A non-knocking case is firstly considered before moving to knocking conditions. The premixed combustion model, FPF, and an associated kernel model are further developed to reproduce CCV in multi-cycle LES. In the following, improvements in the premixed combustion modeling over the FY 2017 version are described before presenting multi-cycle LES results.

In FY 2017, the core part of the premixed combustion model FPF was implemented into CONVERGE CFD as a UDF. The improvements made in FY 2018 include the development of a low dissipative numerical scheme to evaluate a chemical reaction source term in FPF in the framework of CONVERGE CFD, coupling with the CEQ software [3], to reproduce the dissociation effects in high temperature and pressure conditions, estimation of the subfilter flame speed, and laminar-to-turbulent flame transition modeling. Among these, the LES results presented here suggest that the laminar-to-turbulent flame transition plays an important role in reproducing CCV in LES under non-knocking, stoichiometric operation conditions. Thus, more details of the role played by the laminar-to-turbulent flame transition are discussed below.

Many studies on CCV report that variations in the initial growth of a flame kernel formed by spark discharge account for a major portion of CCV and that turbulence plays a key role in variations in the initial flame kernel growth [4–7]. Of these, the recent experimental studies by Zeng et al. [6] and Schiffmann et al. [7] suggest the importance of the laminar-to-turbulent flame transition. Zeng et al. [6] observed substantial variations in the flame surface area during the early stage of the burning process where the laminar-to-turbulent flame transition occurs. Schiffmann et al. [7] performed a statistical analysis of their particle image velocimetry and OH fluorescence data obtained in an optical engine in order to look for a root cause of CCV in an SI engine. Among many quantities, the laminar-to-turbulent flame transition time is found to have strong correlation with CCV. In their study, the laminar-to-turbulent flame transition time, which is the time required for an initial laminar kernel to develop as a fully turbulent flame, is estimated by considering the change in the slope of the flame surface area vs. crank angle degree (CAD) curve. To capture variations in the laminar-to-turbulent flame transition time, a kernel model is developed in this project.

Multi-cycle LES was performed with the improved FPF-CONVERGE model. The engine considered is a single-cylinder version of the General Motors lean NO_x filter (LNF) 2.0-L four-cylinder design turbocharged gasoline direct injection engine from the 2007 Pontiac Solstice, for which in-cylinder pressure measurements

were made at Oak Ridge. The engine operating conditions used in the simulation include the speed of 2,006 rpm, stoichiometric iso-octane fueling (gaseous fuel/air mixture from the intake manifold), the spark timing of 2.2 CAD before the top dead center, and the compression ratio 9:1. The simulation of fifteen cycles has been performed. One equation dynamic model is used to solve for the subfilter kinetic energy. The LES version of Peters' turbulent flame speed model [8] with modified model parameters is used for the evaluation of the subfilter turbulent flame speed. A laminar-to-turbulent transition model is used to capture the effects of turbulence on the initial flame kernel growth. The predicted in-cylinder pressure is compared with the experimental data in Figure I.22.1. Overall, CCV predicted by LES is comparable to that in the experiment, although the predicted coefficient of variance (COV) is larger than that in the experiment. It is to be noted that without the laminar-to-turbulent flame transition model, the level of predicted CCV is much lower. It is also noted that the predicted peak pressure is consistently higher than the experimental data, which is also observed in other engine LES results using CONVERGE CFD [9]. This is probably because a flame-wall interaction model is currently not supported in CONVERGE CFD. Shown in Figure I.22.2 is the flame front evolution in the fast cycle, defined as the cycle with the highest peak pressure, and in the slow cycle, defined as the cycle with the lowest peak pressure. The flame burns much faster in the fast cycle, resulting in much higher pressure rise. As can be seen in Figure I.22.2, in the fast cycle, turbulence at top dead center is much more intense than that in the slow cycle. The observed dependence of CCV on the turbulence field is consistent with the previous studies [4,5].

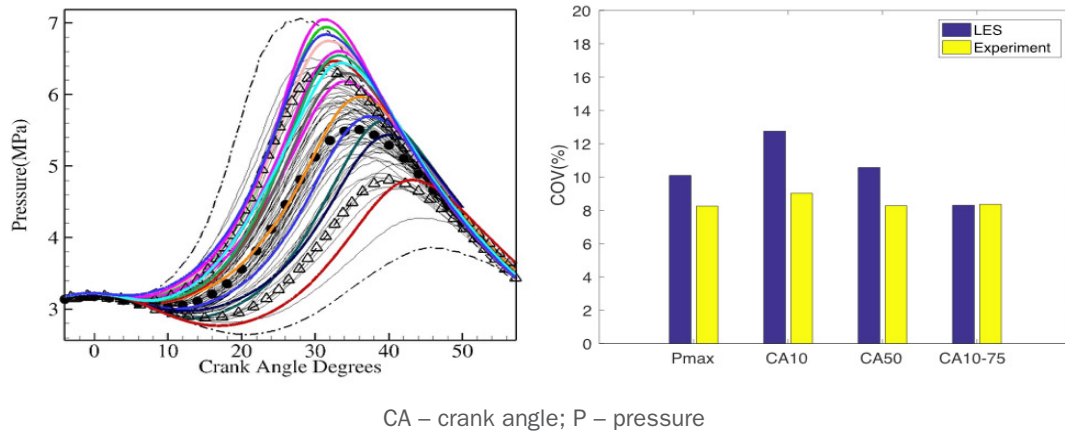


Figure I.22.1. (left) Multi-cycle LES using FPF reproduces CCV of in-cylinder pressure in an engine experiment under a non-knocking condition (colored thick lines: 15 LES cycles, black thin lines: 50 representative cycles from the experiment, dashed-dotted lines: the fastest and slowest cycles in the experiment, triangles: 5% and 95% bounds from 5,000 cycles in the experiment, circles: measured mean pressure). (right) Comparison of the predicted COV with the experimental data.

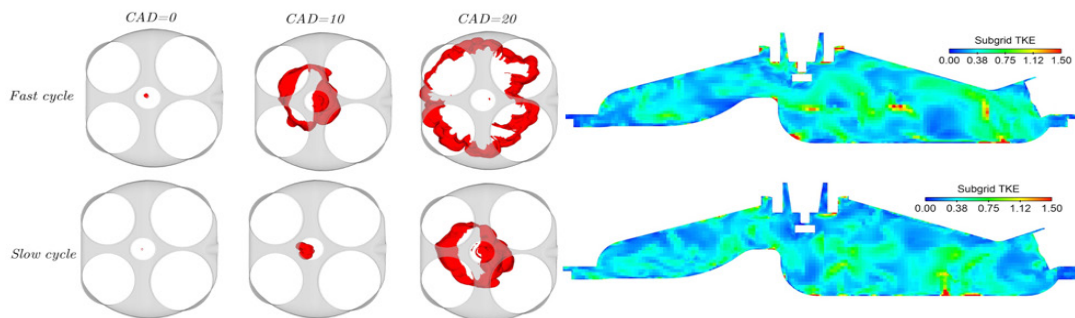


Figure I.22.2. Comparison of the flame front evolution in fast and slow cycles in LES. Also shown is the subfilter kinetic energy at top dead center. In the fast cycle, where the flame propagates faster, the subfilter kinetic energy is higher near the spark plug as compared with that in the slow cycle.

Validation of Knock CMC Using DNS Data

In FY 2018, the mapping method to model the mixing-related terms in sensible-enthalpy-based CMC [10] was validated using the DNS data generated in this project. The mapping approach utilizes scalar structures solved in CMC to model the filtered density function and scalar dissipation rates of sensible enthalpy, a reacting scalar. Results have shown that the mapping method for modeling filtered density function works well for fresh and ignited mixtures, while it leads to errors near ignition fronts. The LES cells with the relative errors larger than 25% are found to be around 10% of the total LES cells when the error is based on the evaluated mean from the modeled filtered density function. The error in the mapping method for filtered density function modeling is related to large conditional fluctuations in total-enthalpy-based CMC and associated inaccuracy in reaction rate estimation. Since the filtered density function is used to evaluate quantities necessary for the density evaluation in the flow solver, accuracy in the reaction rate prediction in sensible-enthalpy-based CMC appears to outweigh the compromise in the mixing submodel.

Implementation of CMC-FPF into CONVERGE CFD

In FY 2018, the combustion model, CMC-FPF, has been implemented into CONVERGE CFD as a UDF. It was reported in FY 2017 that the solver for CMC-FPF was developed and coupled with NGA [11]. A UDF module to couple the CMC-FPF solver with CONVERGE CFD was developed in FY 2018. In CMC-FPF, the spark-ignited premixed flame propagation is described by FPF, which is similar to the widely-used level set method when applied to the flamelet regime. End-gas ignition is described by CMC, which adopts surface filtering (averaging) to preserve small-scale scalar structures and thus account for small-scale turbulence-chemistry interactions. Overall, the combustion models feed chemical source terms into CONVERGE CFD, while CONVERGE CFD feeds turbulence and mixing-related quantities into the combustion models. Currently, a single-cell version of the total-enthalpy-based CMC solver, which assumes that the spatial dependence of the conditionally filtered species mass fractions, the scalar structure in enthalpy space, in the end-gas region is negligible, is implemented. The conditionally filtered/averaged quantities are known to have much weaker spatial dependence than their unconditional counterparts, which are quantities solved in LES or Reynolds averaged Navier-Stokes simulations. Before moving to the engine geometry, the implementation was tested in simple configurations in FY 2018.

The coupling in CONVERGE UDF was first tested for an idealized ignition problem, where the scalar structure in enthalpy space is specified. The purpose is to test the coupling model in a case where the exact solution is known. Two-dimensional LES of ignition in homogeneous isotropic turbulence was performed using the UDF interface module. In this test case, the CMC solver is not included, but the CMC solutions are prescribed to change linearly both with time and in scalar space. Due to the linearity, the filtered species mass fractions from CONVERGE CFD should follow the specified solution in CMC. The internal energy, which is solved in CONVERGE CFD, is taken as the conditioning variable. There should be no fundamental difference between the enthalpy and the internal energy when adopted as a conditioning variable for CMC. The subfilter variance is modeled using an algebraic model. In order to verify the implementation, the LES results are compared with the prescribed profile (exact solution) in Figure I.22.3. It can be seen that the fuel mass fractions closely follow the exact solution, which is linear in the scalar space. The reaction progress with time during a designed ignition process is well reproduced. The UDF interface for coupling CMC-FPF with CONVERGE CFD was then tested in two-dimensional LES of end-gas ignition in homogeneous isotropic turbulence. A flame kernel is deposited at the center of the computational domain. The development of the initial kernel and the propagation of the SI premixed flame fronts are described by the FPF model, while the end-gas ignition is described by the CMC model. A reduced mechanism for the primary reference fuel/air mixture [12], which consists of 116 species, is used to describe ignition of the stoichiometric iso-octane/air mixture. The initial temperature inhomogeneity is assigned using a scalar spectrum function. Figure I.22.4 shows the time evolution of the temperature fields in the test case. The end-gas ignition is observed after 1.5 ms. After the ignition, the ignition fronts develop quickly.

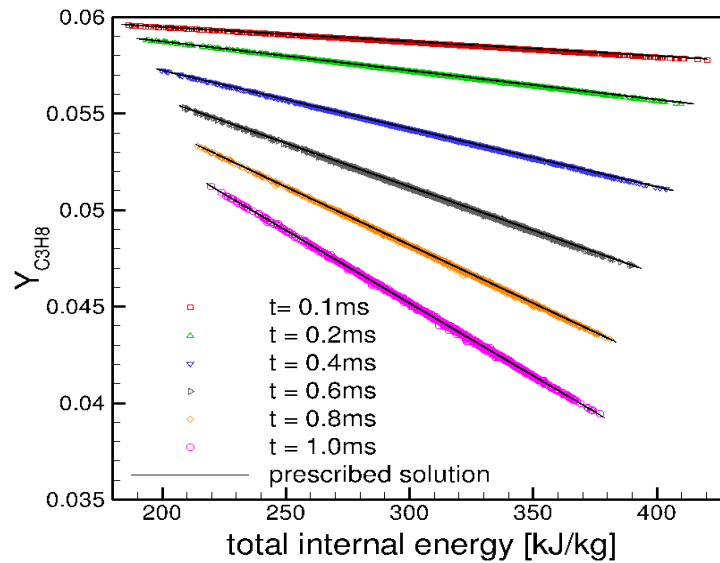


Figure I.22.3. Verification of the coupling of CMC with CONVERGE CFD. The evolution of species mass fractions is linear both in time and in scalar (conditioning variable) space. The predicted filtered fuel mass fractions in two-dimensional LES of idealized ignition in homogeneous isotropic turbulence closely follow the specified profile (exact solution).

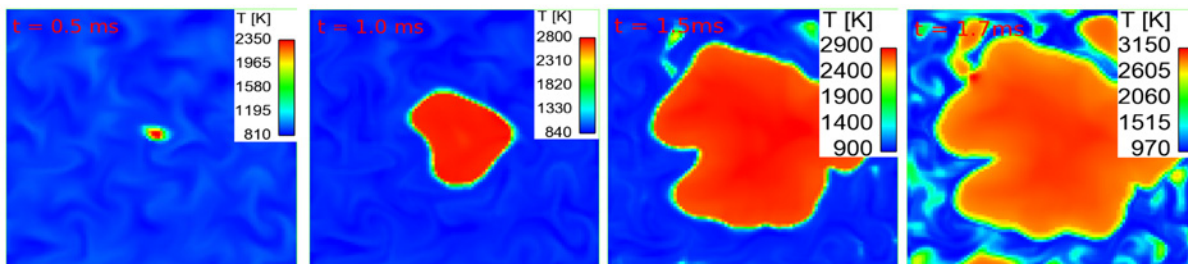


Figure I.22.4. Test of CMC-FPF-CONVERGE in a simple configuration. A premixed flame kernel is deposited initially at the center of the computational domain and grows in homogeneous isotropic turbulence. The initial temperature field is inhomogeneous. The ignition in the end-gas region is observed at $t = 1.5$ ms.

Conclusions

The summary of the progress and the key findings for FY 2018 is the following.

- Multi-cycle LES using the premixed combustion model, FPF, with the kernel model has reproduced CCV in an Oak Ridge engine experiment under a non-knocking condition. The laminar-to-turbulent flame transition is found to play an important role in reproducing the degree of CCV observed in the experiment.
- A mapping method to predict the mixing terms in sensible-enthalpy-based CMC is being developed. The mixing submodel in sensible-enthalpy-based CMC has been validated using the end-gas ignition DNS database produced previously in this project.
- The base solver for the CMC-FPF model has been implemented into CONVERGE CFD. Initial tests for simple configurations have been performed. Application to an engine configuration is in progress.

Key Publications

1. Su, Y., and S.H. Kim. 2018. “An Improved Consistent, Conservative, Non-Oscillatory and High Order Finite Difference Scheme for Low Mach Number Turbulent Flow Simulation.” *J. Comput. Phys.* 372: 202–219.
2. Wang, W., and S.H. Kim. 2018. “Sensible-Enthalpy-Based Conditional Moment Closure for Homogeneous Charge Compression Ignition with Temperature Inhomogeneity.” *Flow, Turbulence and Combustion*. <https://doi.org/10.1007/s10494-018-9985-4>.

References

1. Klimenko, A.Y., and R.W. Bilger. 1999. *Prog. Energy Combust. Sci.* 25: 595–687.
2. Kim, S.H. 2015. *J. Comput. Phys.* 285: 193–207.
3. Pope, S.B. 2003. Cornell University Report FDA 03-02, <http://tcg.mae.cornell.edu/CEQ>.
4. Vermorel, O., S. Richard, O. Colin, C. Angelberger, A. Benkenida, and D. Veynante. 2009. *Combust. Flame* 156: 1525–1541.
5. Truffin, K., C. Angelberger, S. Richard, and C. Pera. 2015. *Combust. Flame* 162: 4371–4390.
6. Zeng, W., S. Keum, T-W. Kuo, and V. Sick. 2018. *Proc. Combust. Inst.* <https://doi.org/10.1016/j.proci.2018.07.081>.
7. Shiffmann, P., D. Reuss, and V. Sick. 2018. *Int. J. Engine Research* 19: 491–508.
8. Pitsch, H. 2005. *Combust. Flame* 143: 587–598.
9. Zhao, L., A.A. Moiz, S. Som, N. Fogla, M. Bybee, W. Wahiduzzaman, M. Mirzaeian, F. Millo, and J. Kodavasal. 2018. *Int. J. Engine Research* 19: 886–904.
10. Wang, W., and S.H. Kim. 2018. *Flow, Turbulence and Combustion*. <https://doi.org/10.1007/s10494-018-9985-4>.
11. Desjardins, O., G. Balnquart, G. Balarac, and H. Pitsch. 2008. *J. Comput. Phys.* 227: 7125–7159.
12. Luong, M.B., Z. Luo, T.F. Lu, S.H. Chung, and C.S. Yoo. 2013. *Combust. Flame* 160: 2038–2047.

Acknowledgements

This material is based upon work supported by the DOE Office of Energy Efficiency and Renewable Energy and the Department of Defense Tank and Automotive Research, Development, and Engineering Center under Award Number DE-EE0007334. The computational resources are provided by the Oak Ridge Leadership Computing Facility and the Ohio Supercomputer Center. The principal investigator thanks Convergent Science for its help in using CONVERGE CFD. Thanks also to Derek Splitter and K. Dean Edwards of Oak Ridge National Laboratory and Nicholas D’Amico, Program Manager at National Energy Technology Laboratory.

I.23 Development and Multiscale Validation of Euler-Lagrange-Based Computational Methods for Modeling Cavitation within Fuel Injectors (Boston University)

Emily Ryan, Principal Investigator

Boston University (BU)
110 Cummington Mall
Boston, MA 02215
E-mail: ryanem@bu.edu

Michael Weismiller, DOE Technology Development Manager

U.S. Department of Energy
E-mail: Michael.Weismiller@ee.doe.gov

Start Date: February 1, 2016

End Date: January 30, 2019

Project Funding (FY18): \$215,169

DOE share: \$210,186

Non-DOE share: \$4,983

Project Introduction

The main objective of this research project is to develop and validate more accurate, physics-based, mathematical submodels for use in computational fluid dynamics (CFD) software to enable better prediction of cavitation within fuel injectors. The outcome of the research will be two new submodels for cavitation that can be used in conjunction with CFD, one for preliminary design and the second for final design analysis.

Controlled cavitation in fuel injectors can improve the atomization of the spray, which improves combustion and reduces emissions. However, excess cavitation can be detrimental to efficiency and can damage the injector. Therefore, the global motivation for research into cavitation in fuel injectors stems from the fact that improvements in fuel injection systems will increase fuel efficiency, reduce the emission of harmful pollutants, and improve the lifetime and reliability of nozzles.

Objectives

Overall Objectives

- Develop and validate physics-based, mathematical submodels for use in standard multiphase CFD software to enable better prediction of cavitation within fuel injectors
- Develop a small-scale experimental setup to investigate cavitation in a canonical nozzle over a range of flow and geometry conditions
- Image cavitation in a fuel injector using the high flux isotope reactor (HFIR) at Oak Ridge National Laboratory (ORNL)

Fiscal Year 2018 Objectives

- Complete second HFIR imaging campaign of cavitation in fuel injector
- Populate cavitation database with experimental data on cavitation under different flow and geometry conditions
- Develop more accurate Reynolds-averaged Navier-Stokes model based on improved cavitation model

Approach

This project is developing methods for simulating cavitation dynamics in a fuel injector that can be used in preliminary design and for final design analysis, and performing experiments for validation of the models. Research focuses on three specific thrusts: computational model development, small-scale cavitation experiments, and HFIR imaging of a real fuel injector.

Computational Model Development

The computational submodels that are being developed rely on cavitation analysis performed with a high-resolution model of bubble dynamics and use both a Lagrangian frame solver in the form of the smoothed particle hydrodynamics (SPH) method and the Eulerian CFD solver OpenFOAM. One submodel will create constitutive relations for inclusion in a CFD solver using an upscaling process based on the results from detailed computational studies of canonical injectors. Detailed simulations of cavitation in nozzles using SPH and OpenFOAM will form a database from which an upscaling method will be used to define a new submodel that can be integrated into a Reynolds-averaged Navier-Stokes based multiphase CFD code (much like turbulence models are used in CFD). The second submodel will consist of the SPH model itself by defining the two-way coupling interface equations for use with unsteady Reynolds-averaged Navier-Stokes CFD. Using a two-way coupled SPH and CFD approach will create a more detailed and accurate model but will be much more computationally expensive than upscaling and as such is proposed for final design analysis. Development and validation of the SPH tool and the subsequent full simulation capabilities based on the new submodels relies on outcomes from experimental studies of detailed flow characteristics for canonical and real-geometry injectors performed at BU and ORNL.

Small-Scale Cavitation Experiments

Small-scale cavitation experiments are being conducted at BU using a canonical nozzle setup with both optical and passive acoustical measurements. Untreated tap water is forced through the nozzle at various flow rates to investigate cavitation onset. Initial experiments were run continuously, with no valving between the pump and test section, and the pump was run continuously at a range of target voltages. Newer experiments are also using a real fuel injector (provided by ORNL) with an actuator to simulate fuel injection events.

HFIR Imaging

In performing dynamic studies of fuel injector operation, a heated and pressure-controlled spray chamber is employed. A closed-loop fuel injection system with heated spray chamber is installed at the neutron imaging beamline at ORNL's HFIR. The sophisticated system is designed to operate with commercial and prototype injectors and deliver fuel to the injectors at rail pressures up to 150 bar. The spray chamber can be operated at absolute pressures as low as 0.2 bar, currently has a maximum pressure of approximately 4 bar, and can be heated to over 100°C while also flowing 10–40 L/min of directed sweep gas to further eliminate condensation build-up. These conditions are necessary to avoid condensation of the fuel in the chamber, since it will block neutron flux.

Results

Fiscal Year 2018 Accomplishments

- Investigated ability of Euler and Lagrangian methods to simulate bubble dynamics
- Demonstrated that cavitation-inducing conditions can exist within a nozzle even when conditions downstream of the nozzle do not indicate cavitation should occur
- Analyzed data from second ORNL HFIR campaign, which show a significant difference in neutron attenuation between flashing and non-flashing conditions

Bubble Dynamics

Volume-of-fluid (VOF) and SPH simulations of buoyantly rising bubbles have been studied. Results show that both VOF and SPH can be used to predict terminal bubble shape and rise velocity for a wide range of parameters, but that for low Reynolds numbers, VOF and SPH simulations have different transient behavior. The discrepancies appear to be due to differences in viscosity implementation between the two methods. Figure I.23.1 illustrates the agreement between BU SPH and VOF simulations, as well as numerical simulations from the literature [1] and experimental results from the literature [2]. Figure I.23.2 shows the differing transient model results for low Reynolds numbers.

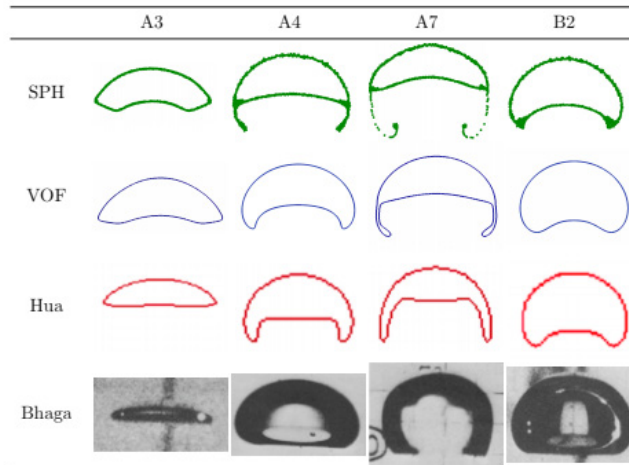


Figure I.23.1. Comparisons of terminal bubble shape for a range of parameter space from SPH (BU), VOF (BU), front tracking (Hua), and experiments (Bhaga)

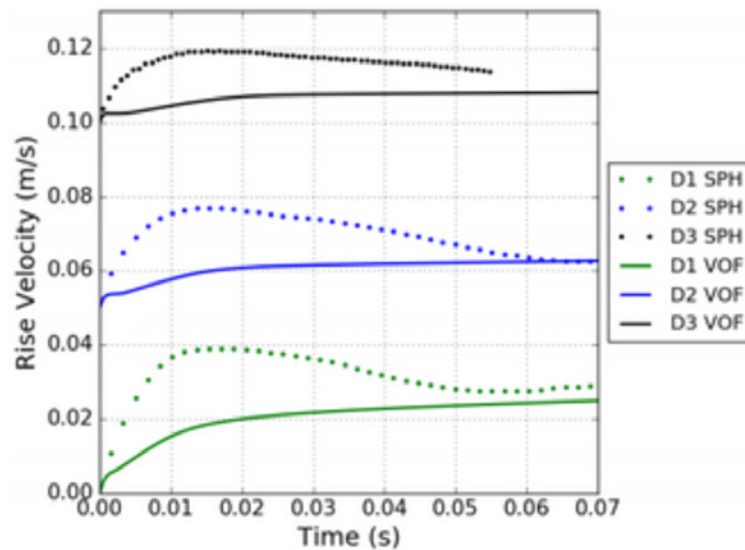


Figure I.23.2. The differences between VOF and SPH simulations for low Reynolds numbers

Detecting Cavitation

The optical and acoustic cavitation detection methods used in nozzle experiments at BU have determined nozzle outlet flow velocities where cavitation is seen to first onset. It is known from cavitation theory that the maximum velocity at which cavitation can be expected is related to the vapor pressure. Similarly, a minimum velocity at which cavitation is expected can be calculated using the critical pressure, which is related to the average nuclei size in the fluid.

Table I.23.1 shows the determined onset velocities for cavitation for various circular nozzle outlet diameters. It can be seen that the velocity determined by experiments for cavitation onset, v_2 , is lower than the minimum velocity at which cavitation is expected as predicted by theory. In order to further study this, axis-symmetric simulations were conducted to fully study the velocity profile within the nozzle section. It was hypothesized that localized velocities in the nozzle were greater than those required for cavitation to occur. Figure I.23.3 shows the time-averaged velocity field results from the CFD simulations. The simulations show that the

maximum velocity occurs in the upper section of the nozzle outlet. These higher velocities would not be recorded by a flow meter placed downstream. As such, the determined velocities from experiment differ with the expected velocities from theory. Table I.23.1 shows quantitatively the maximum velocities seen in each respective nozzle section via CFD modeling (CFD v_{max}).

It can be seen from the results in Table I.23.1 that the maximum velocities as predicted by the CFD are indeed higher than the onset velocities calculated by theory. This confirms the hypothesis that localized velocities are inducing cavitation in the system and not velocities recorded by the outlet flow meter.

Table I.23.1. Parameters for Nozzles Studied in Experiment. Determined onset velocities do not meet minimum velocities determined for cavitation.

D_1 (mm)	24.3	24.3	24.3
D_2 (mm)	2.5	4.0	8.8
Q (m ³ /s)x 10 ⁻⁴	0.415	1.89	5.52
p_1 (kPa)	224.11	189.63	155.15
Re_{onset}	21430	59918	79586
$v_{2,onset}$ (m/s)	8.46	15.06	9.07
v_{min} (m/s)	21.18	19.48	17.62
v_{max} (m/s)	26.66	25.33	23.95
CFD v_{max} (m/s)	17.48	34.60	27.77

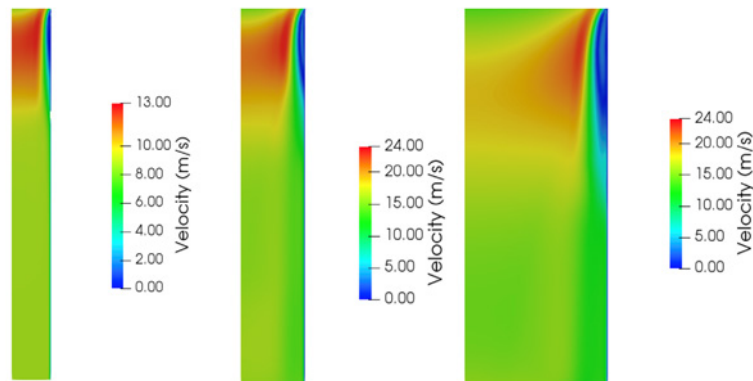


Figure I.23.3. Time-averaged velocity field from numerical simulations of nozzle flow for varying cylindrical outlet diameters

HFIR Imaging

Dynamic normalization of the neutron imaging data shows lower density of fuel in both the spray and nozzle regions in the max-cavitating (flash boiling) condition, as indicated by the blue regions in the rightmost panels of Figure I.23.4. A zoomed-in panel on the far right highlights differences in the spray development for the two cases beginning just inside the nozzle. To quantify relative differences in sac (void below the ball and above the nozzle) filling and emptying rates, a pixel region representing the sac was selected. The mean pixel intensities of this region in the log-ratio normalized images are shown as a function of time at both conditions in Figure I.23.5 along with injection command and current for reference. This result is analogous to normalized optical depth, in which changes to neutron attenuation relative to a static reference condition are shown. In the

case of Figure I.23.5, the normalized intensity decreases rapidly as the sac fills due to the influx of fuel, which strongly attenuates neutrons. The sac filling and emptying rates and the normalized intensity during injection are virtually identical between the two cases, indicating that the rate of fuel entering the sac is not significantly affected by the downstream condition in this configuration.

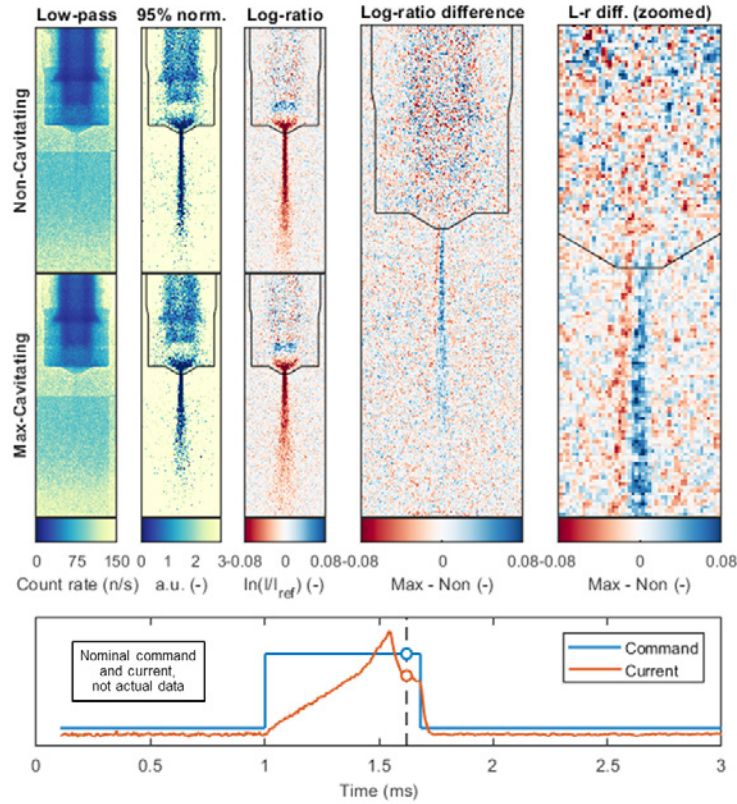


Figure I.23.4. Normalized neutron radiographs comparing the max-cavitating (flash boiling) and non-cavitating (non-flash) conditions in the single-hole, large-bore injector

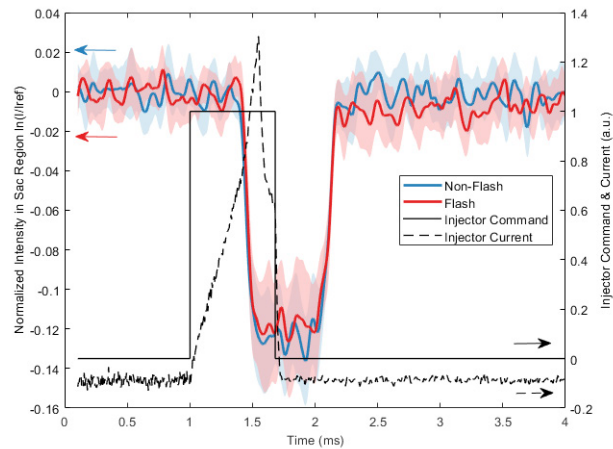


Figure I.23.5. Normalized neutron intensity in sac region for non-flash and flash boiling conditions. Shaded bands represent one standard deviation.

Conclusions

- Demonstrated how CFD Reynolds-averaged Navier-Stokes simulations can be used to explain and inform experimental data on cavitation
- Analyzed HFIR imaging data, which shows rate of fuel entering the sac is not significantly affected by the downstream condition

Key Publications

1. Do, Huy. 2018. "Cavitation Detection and Characterization for Small Scale Nozzles and Fuel Injectors." M.S. Thesis, Boston University (May).
2. Villafranco, D.O., H.K. Do, S.M. Grace, E.M. Ryan, and R. Holt. "Assessment of Cavitation Models in the Prediction of Cavitation in Nozzle Flow." ASME Fluids Engineering Division Summer Meeting, *Volume 2: Development and Applications in Computational Fluid Dynamics; Industrial and Environmental Applications of Fluid Mechanics; Fluid Measurement and Instrumentation; Cavitation and Phase Change*. V002T16A003. doi: 10.1115/FEDSM2018-83223.

References

1. Hua, Jinsong, and Jing Lou. 2007. "Numerical Simulation of Bubble Rising in Viscous Liquid." *Journal of Computational Physics* 222.2: 769–795.
2. Bhaga, Dahya, and M.E. Weber. 1981. "Bubbles in Viscous Liquids: Shapes, Wakes and Velocities." *Journal of Fluid Mechanics* 105: 61–85.

Acknowledgements

Thanks to Sheryl Grace, Glynn Holt, and James Bird at Boston University; Todd Toops, Eric Nafziger, Derek Splitter, and Charles Finney of subcontractor ORNL; and Nicholas D'Amico of National Energy Technology Laboratory.

I.24 Turbulent Spray Atomization Model for Diesel Engine Simulations (Georgia Institute of Technology)

Caroline L. Genzale, Principal Investigator

Georgia Institute of Technology (Georgia Tech)
GW Woodruff School of Mechanical Engineering,
771 Ferst Drive
Atlanta, GA 30332
E-mail: caroline.genzale@me.gatech.edu

Christopher Powell, Principal Investigator

Argonne National Laboratory
9700 South Cass Avenue
Lemont, IL 60439
Email: powell@anl.gov

Michael Weismiller, DOE Technology Development Manager

U.S. Department of Energy
E-mail: Michael.Weismiller@ee.doe.gov

Start Date: January 18, 2016	End Date: January 17, 2019	
Project Funding: \$576,597	DOE share: \$492,807	Non-DOE share: \$83,790

Project Introduction

This project aims to improve the predictive capabilities of spray submodels used in engine computational fluid dynamics (CFD) codes. The objective is to develop a new spray submodel that appropriately captures the role of injected liquid turbulence on diesel jet breakup, addressing shortcomings in the widespread adoption of submodels that treat atomization as a process primarily governed by aerodynamic inertial forces at the injected fluid interface. Our objective is motivated by (1) a significant body of literature that demonstrates the importance of internal injector flows on atomization, (2) experimental data indicating that liquid turbulence plays a fundamental role in spray atomization when gas inertial forces are low, and (3) a systematic lack of predictive capabilities for current aerodynamic-governed spray submodels. Even when global spray characteristics are well predicted, current spray submodels can vary widely in predictions of local spray morphology (e.g., local drop sizes). These inaccuracies suggest a fundamental mismatch of the modeled atomization physics and the actual physics governing the atomization process.

Modeling inaccuracies can largely be attributed to a lack of quantitative measurements to guide fundamental understanding and submodel development. Measurements of local spray morphology are needed within practical diesel sprays, especially under engine-relevant operating conditions. This project aims to fill this measurement gap. An innovative experimental approach is under development, which leverages the joint capabilities of Georgia Tech's high-pressure continuous-flow spray chamber and Argonne National Laboratory's near-nozzle X-ray diagnostics at the Advanced Photon Source. Joint measurements at the two institutions yield two-dimensional (2D) liquid volume fraction and drop size distribution within practical diesel sprays.

Objectives

Overall Objectives

- Develop a new spray atomization model for engine CFD codes with improved prediction accuracy for local spray morphology and global spray characteristics over a wide range of engine operating conditions, including conditions relevant for advanced combustion engines

- Improve understanding of fundamental physics governing atomization in diesel fuel sprays, especially for advanced combustion regimes
- Develop and apply a new diagnostic, scattering-absorption measurement ratio (SAMR), for spatially resolved measurement of diesel spray morphology, including spatially resolved distributions of Sauter mean diameter and liquid volume fraction, over a wide range of engine-relevant operating conditions

Fiscal Year 2018 Objectives

- Implement diagnostic improvements to SAMR to improve spatial resolution and accuracy and establish viability of measurement technique in high-optical-thickness regions of spray
- Extend validation of new spray atomization model to conventional diesel and advanced combustion regimes

Approach

Two new droplet measurement diagnostics are developed to address the existing spray measurement gaps in real-world fuel injection sprays at engine-relevant operating conditions. These new measurements then provide the necessary physical insight to formulate and validate a new, more predictive spray atomization submodel for engine CFD codes. First, a new X-ray scattering diagnostic under recent development at Argonne National Laboratory, ultra-small-angle X-ray scattering (USAXS), is applied to diesel sprays to quantify droplet sizes within optically thick regions near the injector nozzle and along the spray centerline. Second, a new 2D measurement technique is developed to quantify the spatially resolved atomization of diesel sprays. The new diagnostic, termed the scattering-absorption measurement ratio (SAMR), results from coupling two measurements performed at two institutions: (1) 2D measurements of optical thickness via liquid-scattering extinction, performed at Georgia Tech and (2) 2D measurements of liquid volume fraction via X-ray radiography, performed at Argonne National Laboratory. A ratio of the two measurements yields the spatially resolved Sauter mean diameter (SMD). Diesel spray experiments are replicated at the two institutions using shared Engine Combustion Network (ECN) Spray D and Spray A injectors. Several existing spray atomization submodels are then benchmarked against this data to identify model formulation inaccuracies, leading to the formulation of a new modeling approach that incorporates fundamental understanding gleaned from the USAXS and SAMR measurement campaigns. The measurement campaign and new spray atomization modeling approach are formulated based on the hypothesis that liquid turbulence plays an important contributing role in spray breakup, especially under low ambient density conditions of relevance for advanced combustion engines.

Results

Key Accomplishments for Fiscal Year 2018

- Demonstrated new spray atomization CFD model for diesel sprays that accurately responds to changes in ambient density and injection pressure without model tuning
- Demonstrated quantitative near-nozzle measurements of liquid surface area within the initial liquid core breakup region of a diesel spray for the first time
- Increased spatial extent of viable SAMR droplet size measurements by more than 50%, including regions of high optical depth >1 along centerline of diesel spray

Spray Atomization Model Development

A new hybrid-physics spray breakup model introduced last year, termed the KH-Faeth model, was further improved and validated against new USAXS and SAMR measurements of SMD in ECN Spray D ($d_{\text{nozz}} = 180 \mu\text{m}$). These recent validation studies demonstrate that the model significantly improves prediction accuracy in droplet size magnitude, centerline axial breakup rate, and response to changes in operating condition. Predictions of SMD are compared against the benchmark Kelvin-Helmholtz (KH) breakup model and against USAXS measurements of centerline SMD from Argonne National Laboratory in Figure I.24.1. SMD prediction errors are less than $5 \mu\text{m}$ along the spray centerline at all validation conditions, which cover

a broad range of operating conditions relevant for low-temperature combustion engine operation ($P_{\text{amb}} = 1, 2$ bar) and conventional diesel operation ($P_{\text{amb}} = 20$ bar). Non-monotonic fluctuations seen in the USAXS measurement are believed to result from noise. Conversely, the benchmark KH model predicts SMD errors as large as $\sim 40 \mu\text{m}$ ($P_{\text{amb}} = 1$ bar, $P_{\text{inj}} = 500$ bar). Indeed, at an ambient pressure of 1 bar, with an injection pressure of 500 bar, prediction error is improved from about 300% with the KH model to about 25% with the new KH-Faeth model. The KH-Faeth model also demonstrates appropriate decay of SMD along the centerline where measurements are available. Perhaps most importantly, the KH-Faeth model demonstrates appropriate response to change in operating conditions without model tuning as operating conditions are transitioned through conventional diesel and low-temperature combustion regimes. The KH-Faeth model includes liquid turbulence properties as a competing breakup mechanism to the commonly employed Kelvin-Helmholtz aerodynamic jet instability. The new model adopts primary droplet sizing equations developed by Faeth and co-workers from holographic imaging experiments of turbulent primary breakup in round liquid jets [1]. Further validation of the KH-Faeth model is ongoing against the growing database of spatially resolved SMD measurements resulting from this project.

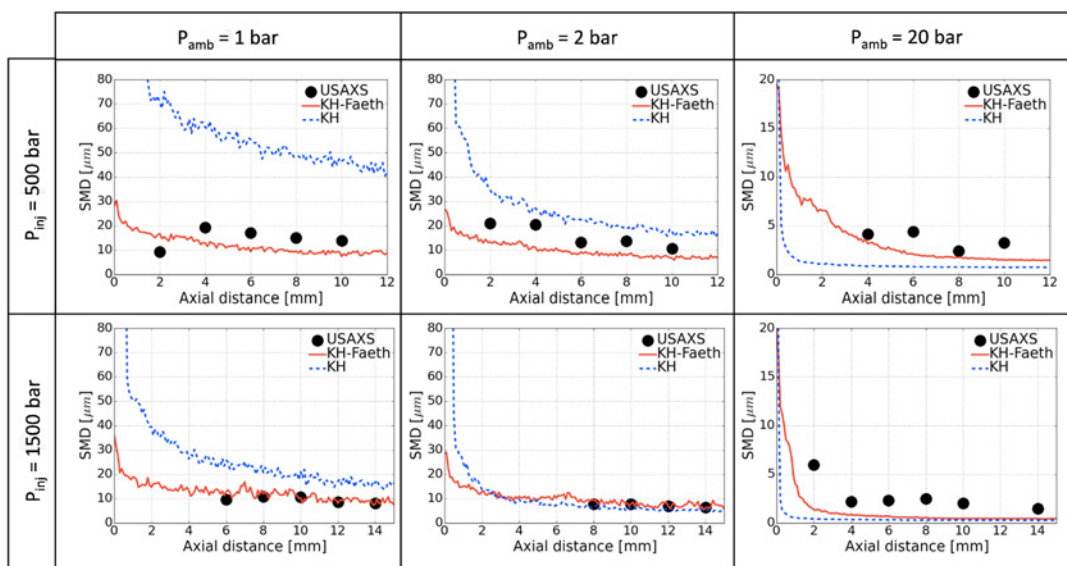


Figure I.24.1. Predicted path-integrated SMD along the centerline of ECN Spray D ($d_{\text{nozz}} = 180$ mm, dodecane fuel) using the newly developed KH-Faeth model. Comparison is shown against measurement (USAXS) and benchmark KH breakup model.

Spatially Resolved Diesel Spray Morphology Measurements

As an integral part of this project, two new spray measurement diagnostics are developed to provide needed quantitative atomization data in diesel sprays for model validation. Without such data available to date, diesel spray models have been historically under-validated, relying largely on validation against large-scale spray quantities such as the spray head penetration rate. As demonstrated previously in Figure I.24.1, these new spray measurements allow for a more rigorous assessment of model physics and have enabled the development of a model with improved physical response and prediction accuracy, without model tuning.

Near-nozzle measurements of liquid surface area were accomplished via USAXS in ECN Spray D to quantify the surface area at several locations in the flow field, tracking the breakup of larger droplets or ligaments into smaller droplets. These measurements contribute an unprecedented level of quantitative spray morphology detail to available diesel spray measurements for model validation. Figure I.24.2 shows measured surface area distributions perpendicular to the spray axis for several distances from the spray nozzle, acquired at an injection pressure of 1,500 bar and ambient pressures of 1 bar and 20 bar ($\mu_{\text{amb}} = 1.2 \text{ kg/m}^3$ and 22.8 kg/m^3 , respectively). It can be seen that at a distance of 10 mm from the nozzle, the surface area shows a local minimum near the center of the spray. This may reflect the presence of poorly atomized structures in the

center of the spray in this region nearest the injector. As the fuel moves downstream, the distributions show a shape resembling a Gaussian distribution that would be expected for a well-atomized spray. This behavior is more clearly exhibited for the 22.8 kg/m³ ambient condition case.

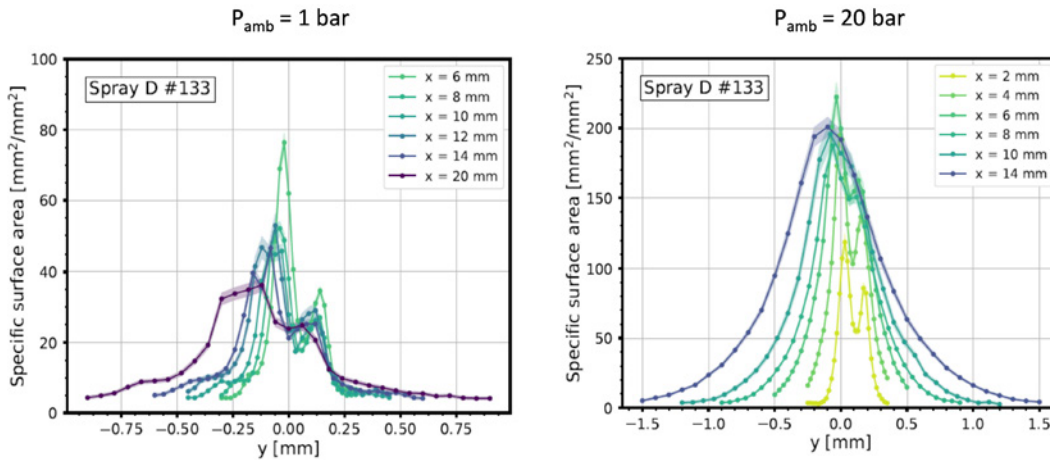


Figure I.24.2. Near-nozzle surface area measurements for ECN Spray D at several distances from the nozzle exit (x). $P_{inj} = 1,500$ bar, $P_{amb} = 1$ bar (left) and 20 bar (right).

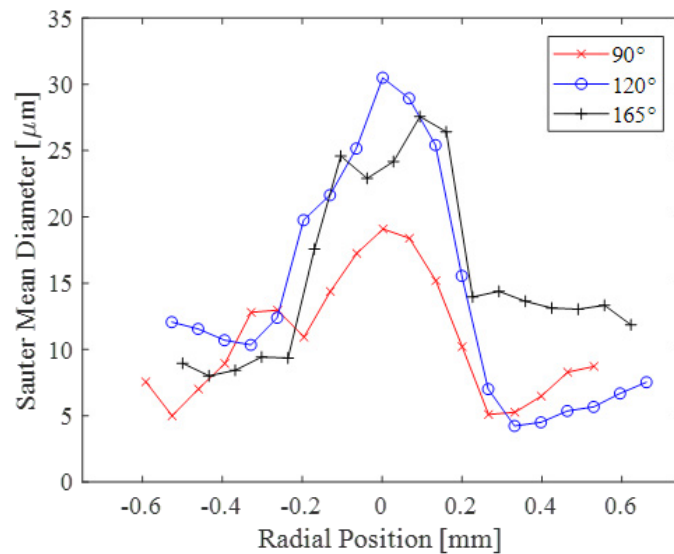


Figure I.24.3. SAMR measurements of path-integrated SMD in ECN Spray D at three different viewing angles. Measurements are at an axial position of 10 mm from the nozzle exit.
 $P_{amb} = 1$ bar, $P_{inj} = 500$ bar.

Radial measurements of SMD were accomplished via SAMR in ECN Spray D. Extending from the proof-of-concept measurements demonstrated last year, recent measurements demonstrate improved spatial resolution, multiple viewing angles to assess spray asymmetries, and measurements within the optically thick centerline region. Light scattering measurements with visible-wavelength illumination, such as those used in SAMR, suffer from multiple scattering errors in regions of high optical depth. Thus, in previously reported measurement campaigns, SMD measurements were not calculated or reported for optical depth >2.0 , eliminating available measurements from the centerline region. As a result, roughly half of the spray width was unresolved. In the last fiscal year, a multiple scattering correction was developed and applied to enable quantification of SMD in these regions. The most recent measurements at an ambient pressure of 1 bar and injection pressure of 500 bar are shown in Figure I.24.3, including measurements from multiple viewing

angles. As shown, significant spray asymmetries influence the path-integrated radial SMD distribution. While the overall spray dispersion is similar for different viewing angles, the peak path integrated SMD can vary by about 10 μm . These asymmetries likely arise from asymmetries in the nozzle geometry and internal nozzle flow. Because the current work employs engineering-level CFD simulations with a symmetrical spray assumption, the multiple viewing angle measurements must be averaged to yield a statistically symmetric spray for model validation. However, in their fully resolved form, these measurements also offer a new quantitative data set for rigorous validation of three-dimensional simulations of coupled nozzle flow and spray. The new KH-Faeth model is being validated against these measurements in continuing work.

Conclusions

- A newly developed primary breakup model for diesel spray simulations, termed the KH-Faeth model, significantly improves prediction accuracy in drop size magnitude, centerline axial breakup rate, and response to changes in operating condition. At an ambient pressure of 1 bar and an injection pressure of 500 bar, prediction error is improved from about 300% with the benchmark model to about 25% with the new KH-Faeth model. The KH-Faeth model also demonstrates appropriate decay of SMD along the centerline and appropriate response to a wide change in operating conditions without model tuning, including transition through conventional diesel and low-temperature combustion regimes.
- Near-nozzle USAXS measurements of liquid surface area track the breakup of larger droplets or ligaments into smaller droplets and contribute an unprecedented level of quantitative spray morphology detail to available diesel spray measurements for model validation.
- Improvements to the SAMR diagnostic have enabled measurements of SMD throughout the entire cross-section of optically thick diesel sprays, improving the spatial extent of viable measurements by more than 50%. This new capability revealed significant asymmetries in the spray breakup when measurements were conducted from multiple viewing angles. These measurements offer a new quantitative data set for rigorous validation of three-dimensional simulations of coupled nozzle flow and spray. Further validation of the KH-Faeth model is also in process.

Key Publications

1. Martinez, G.L., F. Poursadegh, G.M. Magnotti, K.E. Matusik, D.J. Duke, B.W. Knox, C.L. Genzale, C.F. Powell, and A.L. Kastengren. "Measurement of Sauter Mean Diameter in Diesel Sprays Using Scattering-Absorption Measurement Ratio Technique." *International Journal of Engine Research*. Accepted for publication.
2. Martinez, G.L., F. Poursadegh, G.M. Magnotti, K.E. Matusik, D.J. Duke, B.W. Knox, C.L. Genzale, C.F. Powell, and A.L. Kastengren. 2018. "Measurement of Sauter Mean Diameter (SMD) in Diesel Sprays Using a Scattering-Absorption Measurement Ratio Technique." Conference on Thermo- and Fluid Dynamic Processes in Direct Injection Engines (THIESEL 2018). September 2018.
3. Kim, S., G.L. Martinez, B.F. Yraguen, G.M. Magnotti, K.E. Matusik, B.A. Sforzo, A.L. Kastengren, C.F. Powell, T. Lucchini, G. D'Errico, B.W. Knox, and C.L. Genzale. 2018. "Validation of a New Turbulence-Induced Lagrangian Primary Breakup Model for Diesel Spray Atomization." International Conference on Liquid Atomization and Spray Systems (ICLASS). July 2018.

References

1. Wu, P.-K., and G.M. Faeth. 1993. "Aerodynamic Effects on Primary Breakup of Turbulent Liquids." *Atomization and Sprays* 3: 265–289.

II. Co-Optimization of Fuels and Engines

II.1 Co-Optima (National Renewable Energy Laboratory)

John Farrell, Principal Investigator

National Renewable Energy Laboratory (NREL)
15013 Denver West Parkway
Golden, CO 80401
E-mail: john.farrell@nrel.gov

Dan Gaspar, Principal Investigator

Pacific Northwest National Laboratory (PNNL)
902 Battelle Boulevard
Richland, WA 99354
E-mail: daniel.gaspar@pnnl.gov

Chris Moen, Principal Investigator

Sandia National Laboratories (SNL)
7011 East Avenue
Livermore, CA 94550
E-mail: cmoen@sandia.gov

Robert Wagner, Principal Investigator

Oak Ridge National Laboratory (ORNL)
1 Bethel Valley Road
Oak Ridge, TN 37831
E-mail: wagnerrm@ornl.gov

Kevin Stork, DOE Technology Development Manager

U.S. Department of Energy
E-mail: Kevin.Stork@ee.doe.gov

Start Date: October 1, 2015	End Date: September 30, 2018	
Project Funding (FY18): \$10,639,000	DOE share: \$10,639,000	Non-DOE share: \$0

Project Introduction

The U.S. Department of Energy (DOE) Co-Optimization of Fuels and Engines (Co-Optima) initiative is conducting research and analysis to accelerate the introduction of efficient, clean, affordable, and scalable high-performance fuels and engines. This effort is simultaneously tackling fuel and engine research to maximize light-, medium-, and heavy-duty vehicle fuel economy and performance, while mapping lower-cost pathways to reduce emissions, leveraging diverse domestic fuel resources, boosting U.S. economic productivity, and enhancing national energy security.

Co-Optima collaboration brings together DOE's Office of Energy Efficiency and Renewable Energy, nine national laboratories, 13 universities, and numerous industry and government stakeholders to explore near-term improvements to the types of fuels and engines found in most vehicles currently on the road, as well as the development of potential long-term solutions using revolutionary new combustion technologies.

Co-Optima research and development (R&D) is testing the following two hypotheses:

Central Engine Hypothesis

There are engine architectures and strategies that provide higher thermodynamic efficiencies than are available from modern internal combustion engines; new fuels are required to maximize efficiency and operability across a wide speed/load range.

Central Fuel Hypothesis

If we identify target values for the critical fuel properties that maximize efficiency and emissions performance for a given engine architecture, then fuels that have properties with those values (regardless of chemical composition) will provide comparable performance.

Co-Optima is jointly funded by the DOE Office of Energy Efficiency and Renewable Energy's Vehicle Technologies Office and Bioenergy Technologies Office. This report focuses only on the Vehicle Technologies Office-funded work carried out in Fiscal Year (FY) 2018.

Objectives

Overall Objectives

Co-Optima R&D is taking aim at the following near-term (2025–2030 target date) and long-term (2030+ target date) improvements relative a 2015 baseline vehicle:

- The primary near-term objective for Co-Optima is to identify how co-optimized fuel/engine innovations can achieve a 35% increase in light-duty (LD) fuel economy. This represents an improvement 10% greater than that expected from engine improvements alone.
- For medium- and heavy-duty (MD/HD) vehicles, Co-Optima is pursuing a 4% increase in fuel economy through fuel/engine innovations capable of delivering near 60% brake thermal efficiency, along with potential lower-cost paths to meeting the next tier of criteria emissions regulations by achieving reductions in engine-out particulate matter, NO_x, and hydrocarbon/CO emissions of 50%.

Fiscal Year 2018 Objectives

Co-Optima objectives for FY 2018 included the following:

- Concluding standalone LD boosted spark-ignition (SI) project.
- Developing an R&D and analysis framework for LD multimode project.
- Completing fuel screening for MD/HD mixing-controlled compression ignition (MCCI) project.

Approach

Co-Optima encompasses near-term and longer-term LD and MD/HD innovations. The LD research is focused on near-term boosted SI combustion to improve high-load engine efficiency, and multimode combustion—which makes use of advanced compression ignition (ACI) combustion under part-load conditions and boosted SI combustion under high-load conditions—to increase engine efficiency across the operational range and overall fuel economy. The MD/HD research is focused on conventional MCCI combustion in the near term and kinetically controlled (KC) combustion in the long term for even more efficiency and emissions improvements.

These interconnected areas of research take a common approach, with a focus on identification of:

- Fuel property impacts on engine performance through combustion experiments and simulations.
- Blendstocks (including but not limited to those sourced from biomass) with fuel properties needed to deliver specific LD or MD/HD improvements (including fuel economy, performance, and emissions) through a tiered screening approach.

- Barriers to commercial introduction of new blendstocks (including technical factors of materials compatibility, emissions, and engine knock, as well as sustainability, economics, and scalability) through life-cycle analysis across a wide spectrum of metrics.

The overall objective of Co-Optima is to provide data, tools, and objective knowledge to support informed decision-making by stakeholders. Co-Optima efforts are focused on identifying blendstocks to blend into a liquid petroleum base fuel at levels of up to 30%. Although research is investigating blendstocks derived from a range of sources, the only bioblendstocks under consideration are those sourced from non-food-based feedstocks. Engine/fuel technologies are considered for eventual use in both hybridized and non-hybridized powertrains.

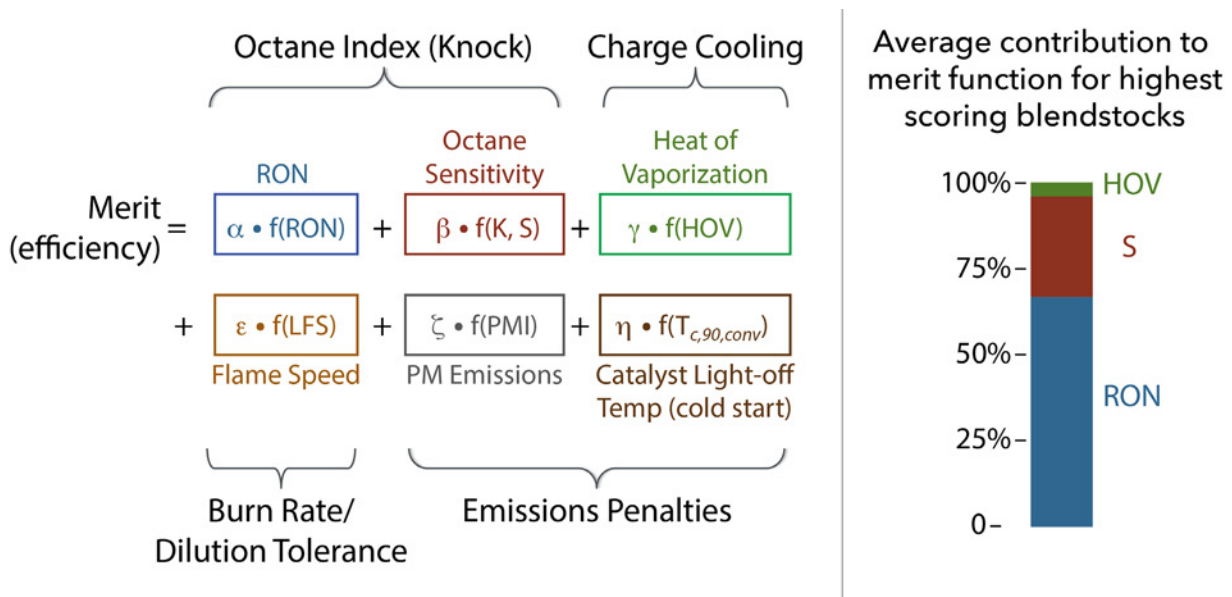
Results

Detailed results from individual Co-Optima projects will be covered in separate project reports. This document will discuss high-level national laboratory accomplishments for each of the research areas shown in Figure II.1.1, as well as crosscutting R&D that spans multiple research areas.

A. LD Boosted SI Project

The most significant FY 2018 Co-Optima accomplishment was completion of the boosted SI LD project, which encompassed identification of fuel property impacts on engine performance; blendstocks that offer desired fuel properties; and possible barriers to blendstocks’ commercial introduction. These areas will be discussed in more detail in other reports.

As detailed in the formula in Figure II.1.1, a revised engine efficiency merit function was released in FY 2018 [1]. This mathematical equation quantifies fuel efficiency potential and weighs the relative importance of critical fuel properties in relation to SI engine efficiency.



RON – research octane number; LFS – laminar flame speed; HOV – heat of vaporization; K – an empirically determined coefficient that varies with operating conditions; S – octane sensitivity; PMI – Particulate Matter Index

Figure II.1.1. Fuel properties impacting boosted SI engine efficiency. Figure by John Farrell, NREL.

In FY 2018, Co-Optima researchers also clarified and quantified engine–fuel interactions, leading to an update to the merit function and better understanding of fuel property impacts on engine performance. The team also conducted an analysis of the uncertainty in the merit function and determined that the uncertainty in a given

score is +/- 2 merit function points. After further analysis, RON, S, and HOV remain the fuel properties with the greatest impact on engine efficiency for boosted SI engines.

Co-Optima's FY 2017 systematic study of more than 400 potential blendstocks provided additional insights into the fuel properties imparted by 14 chemical families, supplying valuable guidelines for identification of new fuels for boosted SI engines. Interim results were published in FY 2018 [2], and a revised list of blendstocks with the potential to improve the efficiency of boosted SI engines was developed. Eight representative blendstocks from five chemical families were identified as candidates for more detailed investigation: alcohols (ethanol, iso-propanol, n-propanol, and iso-butanol), ketones (cyclopentanone), furans (a 40:60 mixture by weight of methylfuran: 2,4-dimethylfuran), alkenes (di-isobutylene), and high-aromatics mixtures.

Co-Optima researchers explored a broad and diverse range of chemical functional groups and production routes, assessing possible blendstocks based on criteria including physical properties as well as potential health effects, engine efficiency improvements, and viability for commercial introduction by 2025–2030.

Efforts during FY 2018 focused on refining the fuel property data and blending models, as well as addressing key scientific lines of inquiry, such as identifying the molecular basis for non-linear octane blending. Co-Optima researchers discovered that two fuel properties—RON and S—are responsible for the majority (>80%) of the efficiency benefit for the highest-performing blendstocks. While HOV can contribute improvements, only small alcohols (those with four carbon atoms or fewer) can increase HOV significantly enough when blended with petroleum blendstocks (e.g., by 100–200 kJ/kg) to result in an appreciable efficiency improvement. Researchers determined that the other fuel properties included in the merit function are relatively less effective, though the Particulate Matter Index debit can be significant for highly aromatic blendstocks.

The only chemical family that demonstrates potential to increase all three major fuel properties is small alcohols. Many cycloalkanes, ketones, aromatics, alkenes, and furans conferred meaningful increases in RON and S. Iso-alkanes, ethers, and esters primarily contributed higher RON when blended into petroleum (hydrocarbon) base fuels. FY 2018 research revealed unexpected benefits from co-blending esters with ethanol, increasing S in ways that do not occur when esters are blended into a petroleum blendstock for oxygenate blending.

At the end of FY 2018, Co-Optima researchers developed a final list of ten blendstocks from four chemical families that have the greatest potential to increase boosted SI efficiency:

- Alcohols – iso-butanol, ethanol, fusel alcohol, methanol, prenol;
- Olefins – di-isobutylene;
- Furans – mixture of methylfuran and 2,4-dimethylfuran; and
- Ketones – cyclopentanone.

Researchers also identified key barriers to their near-term commercialization and shared this information with the stakeholder community [3].

Through a combination of engine experiments and simulations, researchers showed that engine parameters (compression ratio, downsizing) and fuel property improvements (higher RON, S, and HOV) can contribute boosted SI fuel economy improvements up to 10% for certain stretch cases [4,5].

B. LD Multimode SI/ACI Project

One major FY 2018 accomplishment of the LD multimode project—which is examining combinations of different ignition, combustion, and/or fuel preparation strategies—was identification of a theoretical framework. ACI combustion has well-documented potential for improved efficiency and emissions under part-load operation but poses challenges that limit speed/load range. The new Co-Optima approach uses boosted SI

combustion under high-load operation and ACI combustion under part-load operation to maintain the power density and efficiency gains achieved through downsizing and downspeaking.

The Co-Optima team is making use of this framework to bound highly boosted SI operation and aggressive part-load ACI strategy, considering a broad range of engine speed and gas composition variations (exhaust-gas recirculation, air dilutions, etc.), as well as phi sensitivity variations in-cylinder. Researchers are conducting engine experiments that span this wide spectrum of varying conditions to collect data on fuel property and engine parameter impacts. Next, the team plans to develop and validate simulations that reproduce experimental data across this range of conditions, allowing exploration of fuel property and engine parameter impacts through techniques such as global sensitivity analysis.

Researchers also showed that while the autoignition performance of a broad range of fuels operating in the SI regime aligns with octane index, under ACI conditions, the correlation of performance to octane index is poor and appears to correlate with molecular composition. Further work is underway to develop a better understanding of which fuel properties have the greatest impact on ACI operation.

C. MD/HD MCCI Project

Co-Optima's near-term MD/HD research is focusing on co-optimization of fuels with the MCCI combustion technology used in today's commercial diesel engines, with plans for subsequent exploration of new and innovative combustion approaches. Today's MCCI engines are highly efficient but require sophisticated and costly emissions-control technologies. Co-Optima MCCI research is working to reduce the total cost of ownership of MD/HD vehicles by decreasing expenses related to fuel and emissions-control systems. Key scientific challenges include identifying novel combustion approaches and blendstocks with the potential to make significant contributions to industry targets of 60% efficiency improvement and 50% reductions in particulate matter, NO_x, and hydrocarbon/CO emissions.

MCCI blendstock identification and evaluation activities have explored a broad and diverse range of chemical functional groups and production routes. In FY 2018, Co-Optima researchers performed a targeted screening of potential MCCI blendstocks from 18 chemical families, assessing physical properties, cetane numbers, cold-flow properties, energy densities, and abilities to reduce particulate matter.

Novel combustion technologies such as ducted fuel injection were investigated for potential to improve combustion efficiency and the soot–NO_x trade-off, allowing greater freedom in adjusting other parameters. Researchers are now working to grow their understanding of basic ducted fuel injection operation, fuel property dependencies, potential efficiency, and emissions. Current research is identifying possible sensitivity of particulate matter formation from ducted fuel injection to fuel properties.

D. MD/HD KC Combustion Project

KC combustion holds the promise of very high thermodynamic efficiencies—as high as 60% brake thermal efficiency—combined with simultaneous low emissions. Co-Optima transformative KC engine combustion and fuel research to enable long-term MD/HD solutions is at an early stage. The team is tackling significant science and engineering challenges, including identification of key fuel properties and engine parameters needed for optimal efficiency, power density, and wide operability; development of effective control strategies; and development of effective aftertreatment to enable low-temperature NO_x/particulate matter control.

In FY 2018 Co-Optima researchers initiated efforts to identify key fuel properties, define appropriate metrics for fuel ignition, and better understand reactivity, combustion phasing, and emissions formation for full-time KC operation. This improved understanding and control will make it possible to expand the operable range of the KC regime to cover the entire required speed/load range, leading to a potential MD/HD fuel economy improvement of 4% over 2030 business-as-usual scenarios.

E. Crosscutting Research

A multidisciplinary approach serves as the foundation of the Co-Optima initiative, and researchers have developed a suite of state-of-the-art facilities and computational tools to advance crosscutting fuels and

engine innovations. A broad arsenal of laboratory experimental capabilities supply the highly accurate data on reaction kinetics for fuel ignition and soot formation needed for validation of detailed kinetic models and insights into how molecular structure impacts fuel properties. Computational tools extend this understanding to help identify new blendstocks capable of greater performance, as well as feasible production routes from biomass. The combined insights from experiments, simulation, and analyses are being used with a new Co-Optimizer software tool that makes it possible to assess candidate blendstocks in relation to tradeoffs involving a number of complex variables, including blendstock production scale, economics, life-cycle emissions, and infrastructure compatibility.

Conclusions

- Engine parameters (compression ratio, downsizing) and fuel property improvements (higher RON, S, HOV) can contribute boosted SI fuel economy improvements up to 10% for certain stretch cases.
- Ten blendstocks from four chemical families have been identified that have the greatest potential to increase boosted SI efficiency by conferring increased RON, S, and HOV to fuels when blended into petroleum blendstocks for oxygenate blending at levels up to 30%.
- The autoignition performance of a broad range of fuels operating in the SI regime aligns with octane index, but under ACI conditions, the correlation of performance to octane index is poor, and performance appears to correlate with molecular composition.
- Many oxygenated blendstocks exhibit light-off performance lower than an E10 (fuel blend with 90% gasoline and 10% ethanol) surrogate, which could result in reduced cold-start emissions.

Key Publications

Below are representative publications from FY 2018; please reference the individual Co-Optima project reports for a detailed and comprehensive list of FY 2018 publications.

1. Szybist, J.P., and D.A. Splitter. 2018. "Understanding Chemistry-Specific Fuel Differences at a Constant RON in a Boosted SI Engine." *Fuel* 217: 370–81, <https://doi.org/10.1016/j.fuel.2017.12.100>.
2. Fioroni, G.M., L. Fouts, and R.L. McCormick. "Heat of Vaporization and Species Evolution During Gasoline Evaporation Measured by DSC/TGA/MS for Blends of C1 to C4 Alcohols in Commercial Gasoline Blendstocks." Submitted.
3. Van Dam, N., M. Sjoberg, and S. Sibendu. 2018. "Large-Eddy Simulations of Spray Variability Effects on Flow Variability in a Direct-Injection Spark-Ignition Engine under Non-Combusting Operating Conditions." SAE Technical Paper 2018-01-0196 10.4271/2018-01-0196.
4. Westbrook, C.K., M. Mehl, W.J. Pitz, G. Kukkadapu, S. Wagnon, and K. Zhang. 2018. "Multi-Fuel Surrogate Chemical Kinetic Mechanisms for Real World Applications." *Physical Chemistry Chemical Physics* 20 (16): 10588–10606, 10.1039/c7cp07901j.

References

1. Miles, Paul. 2018. "Efficiency Merit Function for Spark Ignition Engines: Revisions and Improvements Based on FY16–17 Research." Technical Report. U.S. Department of Energy, Washington, DC. DOE/GO-102018-5041.
2. Farrell, John, John Holladay, and Robert Wagner. 2018. "Fuel Blendstocks with the Potential to Optimize Future Gasoline Engine Performance: Identification of Five Chemical Families for Detailed Evaluation." Technical Report. U.S. Department of Energy, Washington, DC. DOE/GO-102018-4970.
3. Gaspar, Dan, et al. "Top Ten Bioblendstocks for Higher Engine Efficiency in Boosted Spark Ignition Engines." Manuscript in preparation.

4. Sluder, C.S., and D.E. Smith. “U.S. DRIVE Fuels Working Group Engine and Vehicle Modeling Study to Support Life-Cycle Analysis of High-Octane Fuels.” Report in press.
5. Sluder, C.S. “Estimation of the Fuel Efficiency Potential of Six Gasoline Blendstocks Identified by the U.S. Department of Energy’s Co-Optimization of Fuels and Engines Program.” Submitted.

Acknowledgements

The authors gratefully acknowledge the contributions from the Co-Optima researchers and the extended leadership team: Mary Bidy (NREL), John Dec (SNL), Jennifer Dunn (Argonne National Laboratory), Anthe George (SNL), Ray Grout (NREL), Doug Longman (Argonne National Laboratory), Robert McCormick (NREL), Matt McNenly (Lawrence Livermore National Laboratory), Paul Miles (SNL), Bill Pitz (Lawrence Livermore National Laboratory), Todd Pray (Lawrence Berkeley National Laboratory), Magdalena Ramirez Corredores (Idaho National Laboratory), Sibendu Som (Argonne National Laboratory), Andy Sutton (Los Alamos National Laboratory), Jim Szybist (ORNL), and Derek Vardon (NREL).

II.2 Engine Efficiency Potential of High-Octane Renewable Fuels in Multi-Cylinder Engines (Oak Ridge National Laboratory)

Scott Sluder, Principal Investigator

Oak Ridge National Laboratory (ORNL)
2360 Cherahala Boulevard
Knoxville, TN 37932
E-mail: sluders@ornl.gov

Kevin Stork, DOE Technology Development Manager

U.S. Department of Energy
E-mail: Kevin.Stork@ee.doe.gov

Start Date: October 1, 2017

End Date: September 30, 2018

Project Funding: \$440,000

DOE share: \$440,000

Non-DOE share: \$0

Project Introduction

Engine downsizing is an important facet of increasing vehicle fuel efficiency while maintaining performance at a level that customers demand. As original equipment manufacturers have begun to increase the power density of smaller displacement engines, the onset of knock has emerged as an important challenge that currently limits the degree to which engine displacement (and fuel consumption) can be reduced in a practical automobile. A recent study by researchers from AVL, BP, John Deere, Ford Motor Company, and ICM has shown that increasing the fuel octane rating can allow substantial engine efficiency improvements at the knock limit [1]. Improvements were shown to be enabled through both a chemical octane effect as well as a charge-cooling effect derived from the heat of vaporization of the fuel. The charge-cooling effect was shown to be approximately the same order-of-magnitude improvement as the octane increase effect. Other studies have begun to show similar results.

The U.S. certification driving cycles on which fuel economy ratings are based typically result in engines operating well away from their peak efficiency values. Engine downsizing results in engines operating at higher loads more often during normal driving, thus reducing throttling and other losses and moving towards higher-efficiency areas of their operating maps. However, in order to satisfy consumer demands, these engines must be able to deliver performance similar to non-downsized engines. These performance demands can cause downsized engines to operate in knock-limited regimes more frequently. In the past, some vehicles have utilized premium fuel for its potential to improve performance, but these engines were not typically downsized to use the added anti-knock capability of the premium-grade fuel to increase efficiency.

When engines reach the knock limit, one common technique that is used to protect the engine from damage is to retard the ignition timing. Retarding the timing has the effect of moving the onset of combustion to a cooler, lower-pressure point, thus removing the knocking condition. However, this technique also results in a loss in fuel efficiency. Thus, when an engine reaches the knock limit, fuel efficiency is reduced in favor of engine durability. Increasing the knock limit through changes in fuel formulation, such as increasing the octane rating, offers the potential to improve fuel efficiency under these conditions and enable further engine downsizing. This project will study how differing high-octane fuel formulations can be used to enable increased engine efficiency and to estimate the magnitude of the effect that increased engine efficiency has on vehicle fuel economy.

Objectives

Overall Objective

- The objective of this project is to provide assessments of the potential benefits offered by improving gasoline octane ratings to support techno-economic evaluations of potential future biofuel formulations in the United States.

Fiscal Year 2018 Objectives

- Quantify impacts of biofuels with increased octane rating on vehicle energy consumption, volumetric fuel economy, and tailpipe CO₂ emissions to support life-cycle analysis of the potential of these fuels if implemented nationwide
- Complete a draft report documenting engine experimental and vehicle model evaluations of U.S. DRIVE (United States Driving Research and Innovation for Vehicle efficiency and Energy sustainability) Fuels Working Group fuels
- Estimate potential impacts of Co-Optima Tier 3 blendstocks on vehicle energy consumption, volumetric fuel economy, and tailpipe CO₂ emissions

Approach

ORNL will investigate the potential fuel economy impacts of the use of higher-octane gasoline blends. ORNL is partnering with Ford Motor Company to make use of an EcoBoost 1.6-L engine to examine the potential fuel efficiency benefits of octane improvement in a downsized engine application. Ford has provided ORNL with the engine and engineering support for the 1.6-L engine. Vehicle modeling in Autonomie will be used to estimate vehicle-level impacts from data gathered during engine-based studies. Hybridization presents opportunities to improve market penetration of engines designed to use high-octane fuels. These opportunities are possible through the use of hybridization strategies that can mitigate the performance penalties that occur when an engine designed for use with high-octane fuels is operated using a fuel with lower octane rating. These strategies will be investigated alongside conventional vehicles using vehicle models to estimate the potential fuel economy benefits that are possible. In the studies for the project, data will be collected using fuel formulations that explore the co-optimization program central fuel hypothesis, that fuel performance and engine efficiency derive from the measured combustion properties of the fuel. The project will also study fuels blended using the Tier 3 blendstock candidates identified by the program and provide data in support of the Tier 3 evaluations by other teams.

Results

The U.S. DRIVE Fuels Working Group (FWG) fuels matrix was developed to include non-ethanol biofuel formulations as well as ethanol at 20% volumetric blend level. Results from fuels studied in the Coordinating Research Council project AVFL-20 Phase 3 are included in the life-cycle analysis report [1]. In that study, 10% ethanol (E10) and 30% ethanol (E30) fuels were assessed for vehicle efficiency, while 20% ethanol (E20) fuels were only investigated at a screening level. The FWG matrix addresses additional fuel blends not included in AVFL-20 to enable a more complete study of the potential impacts of increasing octane ratings.

Engine studies were performed at ORNL using a model year 2013 Ford EcoBoost 1.6-liter, 4-cylinder engine. This engine incorporates twin-independent cam phasing, center-mount direct fuel injection, and a single-stage turbocharger. In addition to the production 10.5 compression ratio (CR) pistons, pistons were machined by ORNL from blanks with a reduced bowl volume to increase the compression ratio to 11.4 and 13.2 [1,3].

The nominal 97 research octane number (RON) fuels in the FWG fuel matrix were studied using the CR11.4 pistons. Experiments for the present study were conducted in accordance with methods used and previously reported for the AVFL-20 study. Engine fuel consumption maps were developed by collecting data at engine speeds of 1,000 rpm, 1,500 rpm, 2,000 rpm, 2,500 rpm, and 5,000 rpm, capturing the full range of engine torque output. Additionally, maximum torque points were collected at 3,000–4,500 rpm. Although studies with the 101 RON fuels in the FWG matrix were originally planned, these studies were discontinued because of performance issues with the CR13.2 pistons that were discovered during the AVFL-20 project plus an engine failure not related to the pistons that required an engine replacement [3].

Vehicle modeling allows the engine data gathered during this project to be used to estimate the energy consumption, volumetric fuel economy, and tailpipe CO₂ emissions from vehicles that might use engines with the different compression ratios and fuels studied in this project. This study adopted the vehicle models used for AVFL-20 to assure compatibility of results from the two projects. The Autonomie vehicle simulation

software package was used to develop models for a mid-size sedan and a small sport-utility vehicle (SUV) [1]. Autonomie has been extensively benchmarked and offers the advantage of being a non-proprietary modeling tool designed to assess fuel consumption for conventional and hybrid vehicle designs. The drive cycles studied include the urban dynamometer driving schedule (UDDS), the highway fuel economy test (HWFET), and the US06 cycle. Results for the US06 cycle were divided into results for both the city and highway portions of the cycle.

Vehicle energy consumption over a drive cycle is a metric that provides insight into directional changes in engine efficiency afforded by different fuels and compression ratios. For the nominal 97 RON fuels studied at 11.4 CR, the results show that the range of improvements in energy consumption on a given cycle are between 0.4% and 2.3% for the sedan and between 0.9% and 3.1% for the SUV, depending on the test cycle. The similarity in results is expected, given that the fuels had very similar RON and sensitivity and were tested at constant CR. Volumetric fuel economy depends both on the vehicle energy consumption for a given cycle and on the volumetric heating value of the fuel. Differences among the volumetric fuel economy values for the non-ethanol fuels were small relative to the difference between these fuels and the E20 fuel, consistent with their volumetric heating values. These trends were observed for both the mid-size sedan and small SUV. Compared to fuel WBG4 (a nominal 97 RON fuel blend with 27% by volume wood-based biogasoline), the E20 (also nominally 97 RON) fuel has about 7% lower (poorer) fuel economy on the UDDS and HWFET drive cycles for both the sedan and SUV and 4.7% to 6.7% lower (poorer) fuel economy on the US06 drive cycle. Tailpipe CO₂ emissions for a given drive cycle depend on both the vehicle energy consumption for the cycle and the carbon intensity of the fuel. In this case, the carbon intensity is defined as the mass of tailpipe CO₂ emitted per unit fuel energy combusted (in British thermal units), not to be confused with CO₂ emissions during production of the fuel. The E20 fuel provided the lowest overall tailpipe CO₂ emissions. The difference between maximum and minimum values of tailpipe CO₂ emissions among these fuels ranged from 2.0% to 3.7% for the sedan and from 2.3% to 0.3% for the SUV over the four cycles. Table II.2.1 shows the results of the engine experimental and vehicle modeling study.

The engine and vehicle modeling study outlined previously was used in combination with other published results to establish energy consumption metrics that represent effects on the light-duty U.S. fleet. Higher-octane-number fuel enables increased compression ratio and therefore higher efficiency. The required increase in fuel RON to enable a one-number increase in CR is engine-dependent and can be expressed as a ratio, octane number (ON)/CR. For this study, ON/CR values of 5.6, 3.7, and 3.0 were used in combination with the measured RON values for the fuels in both the AVFL-20 Phase 3 and the FWG matrices to project the efficiency benefit of CR increase expected to be enabled by each fuel. The methodology detailed in a USCAR (United States Council for Automotive Research LLC) study was used for this purpose [4]. The vehicle modeling conducted for both the AVFL-20 and FWG studies focused on the UDDS cycle, the HWFET cycle, and the US06 cycle. Two additional cycles, the SC03 and cold CO tests, are used in calculation of the 5-cycle fuel economy value that is considered representative of “on-road” consumer driving (and is included on the window sticker of new vehicles). As the SC03 and cold CO tests cannot be reliably modeled, the UDDS results were used in their place in the 5-cycle calculation. For the purpose of the life-cycle analysis study, the small-SUV results from the vehicle modeling study were selected to approximate the energy use impacts of each fuel on the entire U.S. light-duty fleet. Baseline results consisted of the two 91 RON E10 fuels at CR10.5. The fuel-specific vehicle efficiency gains, including an engine downsizing factor for turbocharged engines, were used in combination with the fleet-average on-road energy consumption value to calculate fuel-specific fleet-average energy use for each fuel.

Table II.2.1. Results of Engine Experimental and Vehicle Modeling Study

Changes with CR11.4 relative to baseline (avg. of AVFL-20 fuels #1 and #10 at CR10.5)											
	Drive Cycle	#20 97.3 RON, 10.1 S, E20		BRS1 97.3 RON, 9.9 S, 9% Bio		BRS2 97.1 RON, 9.8 S, 27% Bio		WBG2 97.6 RON, 9.3 S, 9% Bio		WBG4 97.6 RON, 9.4 S, 27% Bio	
		Sedan	SUV	Sedan	SUV	Sedan	SUV	Sedan	SUV	Sedan	SUV
		Energy Use Reduction	UDDS	0.9%	1.3%	-0.9%	-0.6%	0.3%	0.6%	0.5%	0.8%
HWFET	0.5%		1.5%	0.1%	0.6%	0.2%	0.6%	0.2%	0.7%	0.4%	1.1%
US06 City	4.3%		5.0%	1.6%	2.0%	2.1%	2.1%	3.4%	3.3%	3.5%	2.8%
US06 Hwy	2.5%		3.8%	1.4%	1.9%	1.1%	2.0%	1.9%	2.1%	2.1%	3.0%
Fuel Economy Increase	UDDS	-1.9%	-1.6%	3.3%	3.5%	4.6%	4.9%	4.7%	5.0%	5.1%	5.4%
	HWFET	-2.3%	-1.4%	4.3%	4.8%	4.4%	4.8%	4.4%	4.9%	4.6%	5.4%
	US06 City	1.5%	2.0%	5.9%	6.1%	6.4%	6.3%	7.8%	7.6%	7.9%	7.1%
	US06 Hwy	-0.4%	0.9%	5.6%	6.2%	5.3%	6.3%	6.1%	6.4%	6.3%	7.5%
CO ₂ Emissions Reduction	UDDS	0.2%	0.5%	-2.5%	-2.3%	-1.9%	-1.6%	-1.8%	-1.5%	-1.8%	-1.5%
	HWFET	-0.4%	0.7%	-1.7%	-1.0%	-2.2%	-1.6%	-2.2%	-1.6%	-2.4%	-1.5%
	US06 City	3.5%	4.2%	-0.1%	0.3%	-0.2%	-0.2%	1.0%	1.0%	0.8%	0.2%
	US06 Hwy	1.7%	2.8%	-0.3%	0.1%	-1.2%	-0.4%	-0.4%	-0.4%	-0.7%	0.2%

S – octane sensitivity

All the fuels provided a decrease in total energy consumption relative to the baseline, ranging from 1.5% to 6.0%. Impacts to volumetric fuel economy are impacted both by the total energy consumption of the vehicle and the heating value of the fuel. Volumetric fuel economy ranged from 6.6% lower to 10.7% higher than the baseline, depending on the fuel and the test cycle. The efficiency improvements projected for 3.0 ON/CR were 1.4% –1.8% greater than those projected for 5.6 ON/CR, depending upon the fuel. Most fuels were projected to provide a volumetric fuel economy increase (improvement) for at least one of the ON/CR values studied. Improvements (increases) in volumetric fuel economy ranged from 0.4% to 10.7%. E30 fuels were an exception, as they showed a decrease in volumetric fuel economy despite decreased energy consumption. Most of the fuels were projected to provide a decrease (improvement) in total tailpipe CO₂ emissions for at least one of the ON/CR values studied. The ethanol-blended fuels provided the greatest reductions (improvements) in total tailpipe CO₂ emissions, ranging from 1.5% to 6.9%. The ethanol-free blends were projected to provide a range of impacts, ranging from 1.2% higher (worse) to 1.5% lower (improvement) in total tailpipe CO₂ emissions, depending on ON/CR ratio. These results are shown in Table II.2.2.

A synergistic study was conducted with fuel blends containing Co-Optima Tier 3 blendstocks. Blends of ethanol, n-propanol, isopropanol, isobutanol, diisobutylene, and a bioreformate surrogate were produced at a fixed RON of 97. The hydrocarbon base stock for the fuels was an 85 anti-knock index blendstock for oxygenate blending, similar to that used for regular-grade 10% ethanol blends in the marketplace. The blends were analyzed and the results used to facilitate modeling the properties of these blends at differing blend levels. This information in turn allowed estimation of the fuel efficiency impact of these blends in vehicles. The results demonstrated that ethanol was the most effective octane-boosting compound of the blendstocks that were studied. Hence, it produced the greatest improvement in efficiency at any given blend level. Oxygenate blending reduces the volumetric heating value of gasoline blends, and as a result, volumetric fuel economy is degraded at high blending levels despite improvements in engine efficiency. While all the alcohols studied exhibited this tendency, ethanol blending produced a relatively narrow range of blend levels where volumetric fuel economy increased at the same time as energy consumption decreased. Projected volumetric fuel economy improvements are shown in Figure II.2.1.

Table II.2.2. Fleet-Average On-Road Driving Results for All Fuels

Fuel	Total Energy Consumption Decrease			Volumetric Fuel Economy Increase			Total Tailpipe CO ₂ Emissions Decrease				
	3.0 ON/CR	3.7 ON/CR	5.6 ON/CR	3.0 ON/CR	3.7 ON/CR	5.6 ON/CR	3.0 ON/CR	3.7 ON/CR	5.6 ON/CR		
Nominal RON 96 - 98	14	3.2%	2.6%	1.8%	3.8%	3.1%	2.3%	2.9%	2.3%	1.5%	
	20	4.0%	3.4%	2.5%	1.2%	0.5%	-0.4%	3.2%	2.6%	1.7%	
	6	3.9%	3.3%	2.6%	-5.3%	-5.9%	-6.6%	6.0%	5.5%	4.8%	
	15	4.2%	3.6%	2.8%	-3.9%	-4.5%	-5.3%	4.0%	3.4%	2.6%	
	BRS1	3.2%	2.5%	1.6%	7.5%	6.8%	5.8%	1.5%	0.9%	-0.1%	
	BRS2	3.0%	2.4%	1.5%	7.4%	6.7%	5.8%	0.8%	0.1%	-0.8%	
	WBG2	3.2%	2.6%	1.6%	7.6%	6.9%	5.9%	0.9%	0.2%	-0.7%	
	WBG4	3.0%	2.4%	1.5%	7.4%	6.7%	5.8%	0.3%	-0.3%	-1.2%	
	101-102	7	4.7%	4.0%	2.9%	1.5%	0.8%	-0.3%	7.7%	7.1%	6.0%
		16	5.0%	4.3%	3.2%	5.8%	5.1%	3.8%	4.5%	3.8%	2.6%
18		5.5%	4.8%	3.7%	2.4%	1.7%	0.4%	4.7%	4.1%	2.9%	
19		6.0%	5.3%	4.2%	-3.1%	-3.8%	-5.0%	6.9%	6.2%	5.1%	
BRS3		4.6%	3.9%	2.8%	10.2%	9.4%	8.1%	1.2%	0.5%	-0.7%	
BRS4		4.6%	4.0%	2.8%	10.7%	10.0%	8.7%	1.8%	1.2%	0.0%	

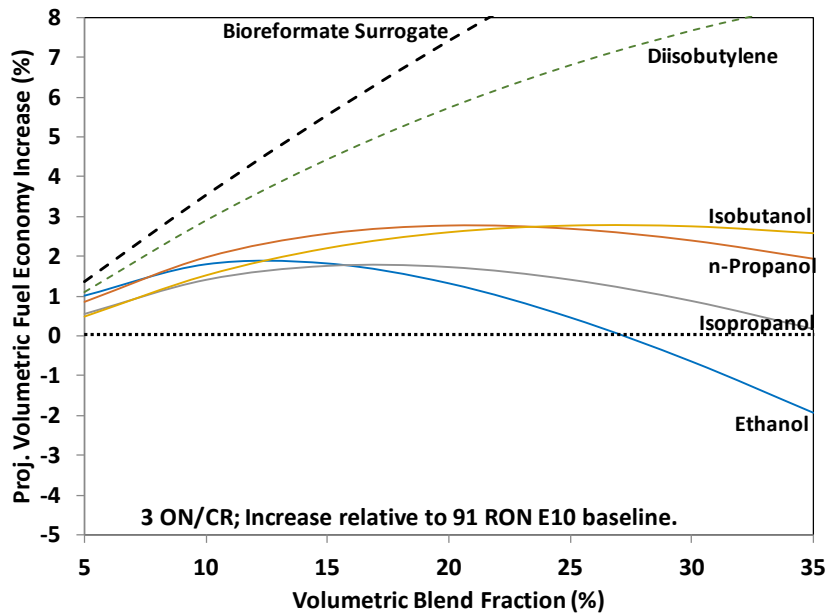


Figure II.2.1. Projected volumetric fuel economy improvements offered by Co-Optima Tier 3 blendstocks

Conclusions

- Engine experiments and vehicle modeling to support the U.S. DRIVE Fuels Working Group life-cycle analysis of high-octane fuel pathways were completed. Projections of the impact of these fuels on the U.S. light-duty fleet are that all the fuels provide reductions in energy use. Ethanol-blended fuels provided the greatest opportunities for tailpipe CO₂ reductions, but the 30% ethanol blends could not provide volumetric fuel economy improvements relative to the baseline case.
- Evaluation of the Co-Optima Tier 3 blendstocks as 97 RON blends in a full-boiling-range blendstock for oxygenate blending shows that ethanol is the most effective octane booster. Ethanol also therefore offers the greatest potential efficiency improvement at any given blend level, but only provides a volumetric fuel economy improvement at levels just less than 30%. Other blendstocks provide a lesser improvement in energy consumption but can provide volumetric fuel economy improvement over a wider range of blend levels.

Key Publications

1. Sluder, C. Scott, David E. Smith, James E. Anderson, Thomas G. Leone, and Michael H. Shelby. “U.S. DRIVE Fuels Working Group Engine and Vehicle Modeling Study to Support Life-Cycle Analysis of High Octane Fuels.” Draft submitted report for publication by the U.S. Department of Energy.
2. Sluder, C. Scott. “Estimation of the Fuel Efficiency Potential of Six Gasoline Blendstocks Identified by the U.S. Department of Energy’s Co-Optimization of Fuels and Engines Program.” Draft 19FFL-0027 submitted for the 2019 SAE International Powertrain, Fuels, and Lubricants Meeting.

References

1. Sluder, C. Scott, David E. Smith, James E. Anderson, Thomas G. Leone, and Michael H. Shelby. “U.S. DRIVE Fuels Working Group Engine and Vehicle Modeling Study to Support Life-Cycle Analysis of High-Octane Fuels.” Draft report submitted for publication by the U.S. Department of Energy.
2. Stein, Robert A., Dusan Polovina, Kevin Roth, Michael Fost, Michael Lynskey, Todd Whiting, James E. Anderson, Michael H. Shelby, Thomas G. Leone, and Steve Vandergriend. 2012. “Effect of Heat of Vaporization, Chemical Octane, and Sensitivity on Knock Limit for Ethanol – Gasoline Blends.” *SAE Int. J. Fuels Lubr.* 5 (2), doi: 10.4271/2012-01-1277.
3. Sluder, C. Scott, David E. Smith, Martin Wissink, James E. Anderson, Thomas G. Leone, and Michael H. Shelby. 2017. “Effects of Octane Number, Sensitivity, Ethanol Content, and Engine Compression Ratio on GTDI Engine Efficiency, Fuel Economy, and CO₂ Emissions.” Coordinating Research Council Report #AVFL-20.
4. Leone, T., J. Anderson, R. Davis, A. Iqbal, R. Reese, M. Shelby, et al. 2015. “The Effect of Compression Ratio, Fuel Octane Rating, and Ethanol Content on Spark-Ignition Engine Efficiency.” *Environ. Sci. Technol.* 49.

II.3 Developing a Better Understanding of Octane Index (Oak Ridge National Laboratory)

James Szybist, Principal Investigator

Oak Ridge National Laboratory
2360 Cherahala Blvd.
Knoxville, TN 37922
E-mail: szybistjp@ornl.gov

Kevin Stork, DOE Technology Development Manager

U.S. Department of Energy
E-mail: Kevin.Stork@ee.doe.gov

Start Date: October 1, 2017

End Date: September 30, 2018

Project Funding (FY18): \$280,000

DOE share: \$280,000

Non-DOE share: \$0

Project Introduction

An organizing principle of the Co-Optimization of Fuels and Engines (Co-Optima) initiative is the central fuel properties hypothesis, which states that fuel properties provide an indication of the performance of the fuel, regardless of the fuel's chemical composition. However, it is not yet understood whether traditional fuel properties for spark ignition (SI) engines are sufficient at characterizing autoignition performance under all of the relevant engine conditions for multi-mode engines. Multi-mode engine operation encompasses conventional SI engine operation under boost for full-load operation, moderate-load SI conditions, and advanced compression ignition (ACI) strategies at light engine loads. ACI operation relies on fuel autoignition rather than flame propagation in-cylinder and has the potential to increase engine efficiency because of fuel-lean operation and reduced pumping work. Each of these strategies has unique pressure-temperature (PT) conditions in-cylinder at the start of compression, and these result in distinct trajectories through the PT domain, which govern the kinetic reactions important to autoignition for that particular case. As a result, the fuel that is most prone to autoignite under one PT trajectory may be the most resistant at a different PT trajectory. In this project, a combined experimental and kinetic modeling approach is used to investigate how the pressure and temperature conditions at the start of compression determine the autoignition tendency for a range of gasoline-boiling-range fuels, including a number of high-interest fuel blendstocks identified by the Co-Optima initiative, to better understand whether the central fuel properties hypothesis is sufficient using fuel properties as they are currently defined.

Objectives

Overall Objectives

- Determine if existing fuel properties are predictive of engine performance in accordance with the central fuel properties hypothesis for both conventional and advanced combustion strategies
- Where conventional fuel properties are insufficient, demonstrate the need for different fuel properties and characterize the phenomena that need to be more accurately described

Fiscal Year 2018 Objectives

- Determine if the octane index (OI) sufficiently characterizes the performance of 19 different fuel blends across five different PT trajectories, from boosted SI to ACI
- Determine whether there is a kinetic basis for the OI by performing kinetic modeling across the range of operating conditions investigated experimentally

Approach

Prior work within Co-Optima has shown that the rank ordering of a given set of fuels' resistance to autoignition can change as engine operating condition changes. In some ways this has been known for nearly a century because the two octane number tests, the research octane number (RON) and motor octane number (MON), produce different rankings for a given set of fuels. To relate the specific performance of an engine and fuel to the RON and MON tests, Kalghatgi [1,2] pioneered a practical method to correlate the RON and MON values to knock-limited spark advance. This method requires a parameter, K , which is dependent on the engine operating conditions, to act as a weighting factor between RON and MON. The resultant OI, see Equation 1, correlates to the actual knock propensity of the fuel much more strongly than either RON or MON [1–3]. This allows the relative knock resistance of fuels to be determined at conditions in real engines which differ from the RON and MON tests.

$$OI = RON - K * S \quad (1)$$

The experimental effort within this project was to determine whether the OI framework is sufficiently predictive over a wide range of PT domain operation, including both boosted SI and lean-burn ACI conditions. This was done by including 19 different fuels with a wide range of fuel properties in an experimental matrix in a single-cylinder engine at Oak Ridge National Laboratory that spanned five operating conditions. The second part of this project was to determine whether there is a kinetic basis for the OI framework within the PT domain. This portion of the project was done in collaboration with Lawrence Livermore National Laboratory, who supplied the kinetic mechanisms, defined surrogate compositions for five of the fuel blends that were included in the experimental effort, and performed ignition delay calculations.

Results

The intent of this investigation was to experimentally investigate PT trajectories that spanned the range from “beyond RON” to “beyond MON” condition. A beyond RON PT trajectory is one that has a lower temperature at a given pressure than the RON test, and a beyond MON PT trajectory is one that has a higher temperature at a given pressure than the MON test, as described in reference [4]. Experiments were performed for 19 fuels spanning a wide range of properties to determine if conventional fuel properties could accurately predict the rank-ordering of the fuels with the OI, Equation 1. The PT trajectories generated from the conditions investigated are shown in Figure II.3.1 for three of the Co-Optima core fuels: alkylate, aromatic, and E30 (gasoline blend with 30% ethanol). These were chosen to illustrate that the chosen experimental conditions and hardware configurations successfully spanned the range of intended PT trajectories. In addition, fuel-specific differences in the PT trajectories are minor compared to the differences in PT trajectory caused by changes in operating condition. Note that the PT trajectories depicted in Figure II.3.1 are plotted for the compression process up to the time of ignition and thus do not represent the continuation of the PT trajectory for the unburned gas once flame propagation begins.

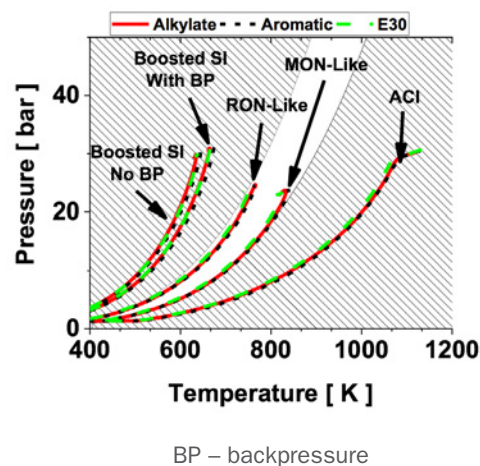


Figure II.3.1. Pressure-temperature trajectories for the five engine operating conditions investigated for three of the Co-Optima core fuels

In order to span such a wide range of operating conditions and investigate the propensity of the fuels to autoignite, both the engine load and operating condition had to be manipulated significantly. In particular, the boosted SI operation required a relatively low compression ratio, and because it operated under a boosted intake pressure, had a high engine load. The RON-like and MON-like conditions required a higher compression ratio to encounter knock at the lighter engine loads. Finally, because the ACI operating condition is fuel-lean, a high compression ratio with a very light engine load was required. The engine operating conditions and mechanical compression ratio of the engine at each of these PT trajectories is shown in Table II.3.1.

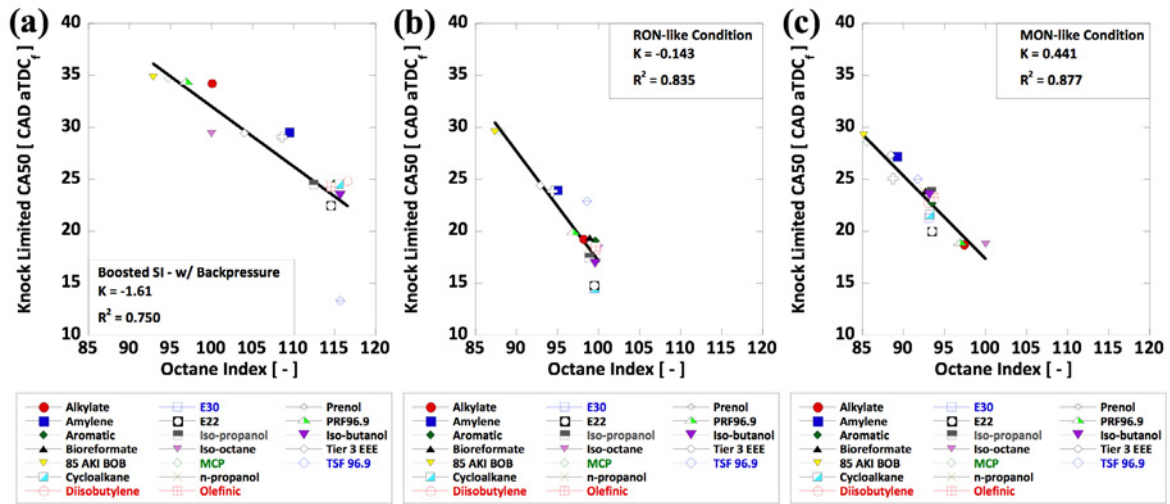
Table II.3.1. Fuels Working Group Expanded Matrix Fuel Formulations

	Boosted SI No Backpressure	Boosted SI With Backpressure	RON-like	MON-like	ACI
Compression Ratio	9.2:1	9.2:1	11.85:1	11.85:1	13.66:1
Engine Speed [RPM]	2,000	2,000	2,000	2,000	2,000
Intake T [C]	50	50	50	150	240–300
Air Flow [g/min]	900	900	475	420	400
Intake Pressure [kPa absolute]	154–157	159–162	98–101	98–101	105–115
Exhaust Pressure [kPa absolute]	133–137	154–157	104–107	104–107	103–105
Engine Load [IMEPg, kPa]	1,500–2,000	1,500–2,000	800–1,100	700–900	235
CA50 Phasing [CAD aTDCf]	8–40	8–40	12–40	13–40	5–9
Equivalence Ratio	1.00	1.00	1.00	1.00	0.3

IMEPg – gross indicated mean effective pressure; CA50 – crank angle at 50% mass fraction burned; CAD – crank angle degrees; aTDCf – after top dead center firing

The knock-limited CA50 combustion phasing is plotted as a function of OI for the boosted SI condition, the RON-like condition, and the MON-like condition in Figure II.3.2. As described in the Approach section, the OI is a mathematical combination of RON and MON as well as constant K to serve as weighting factor for the engine operating condition, Equation 1. Among the 19 fuels investigated, there is a good correlation between the actual knock-limited CA50 combustion phasing and OI. The notable exception is that one fuel, TSF 96.9, enables much earlier combustion phasing than is predicted by the OI. It is worth pointing out that this fuel, while interesting, has a very high concentration of toluene and is not representative of commercially available fuels. The results in Figure II.3.2 agree well with previous researchers who have shown that OI is a superior way to rate the performance relative to other metrics for SI combustion, namely RON, MON, or anti-knock index (AKI, the average of RON and MON) [1–3].

Figure II.3.3 shows the OI correlation for the ACI operating condition, using the required intake manifold temperature to maintain constant CA50 combustion phasing instead of using the combustion phasing at a constant operating condition. This technique was required because the ACI operating point was only operable under a small CA50 combustion phasing window, from 4 to 10 crank angle degrees aTDCf, and the different fuels would not all operate in this narrow window with the same intake temperature. Unlike the SI conditions, the OI provides a poor correlation coefficient. Further inspection shows that the operating trends correspond to chemical family instead of OI. Specifically, alkanes and alcohols perform as expected based on OI, aromatics require a higher temperature than predicted by OI, and olefins require a lower temperature than predicted by OI.



BOB – blendstock for oxygenate blending; E22 – gasoline blend with 22% ethanol; MCP – methylcyclopentane; PRF – primary reference fuel; EEE – certification gasoline; TSF – toluene standardization fuel

Figure II.3.2. Knock-limited combustion phasing as a function of octane index for each fuel investigated at (a) the boosted SI condition, (b) the RON-like condition, and (c) the MON-like condition

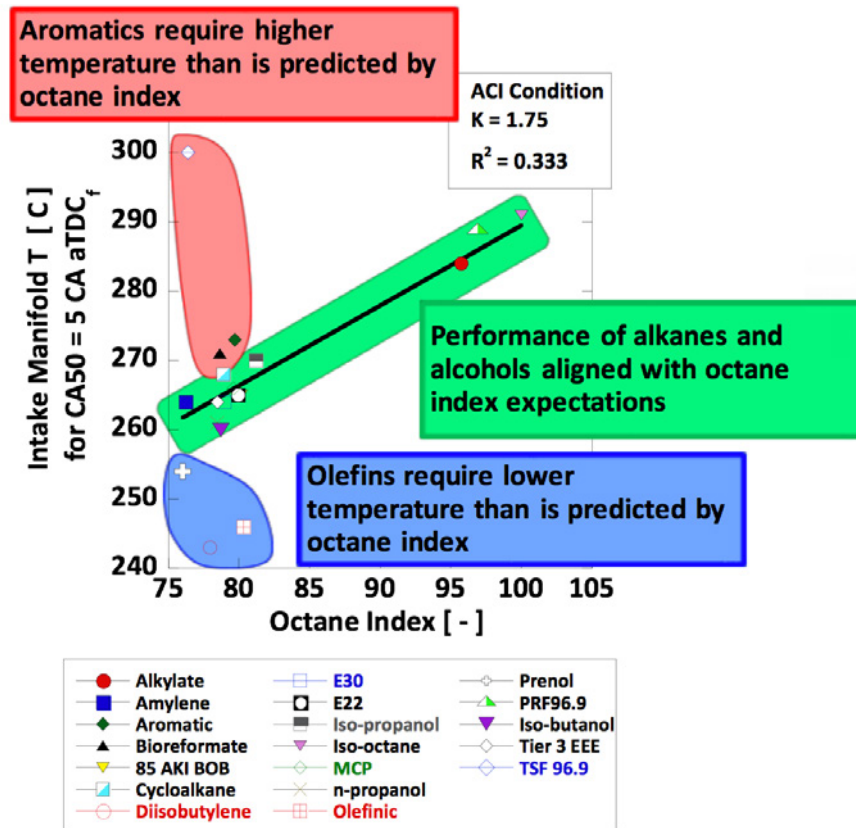


Figure II.3.3. Knock-limited combustion phasing as a function of octane index for each fuel at the ACI condition

To better understand these results, chemical kinetic modeling was performed to provide insight into whether or not there is a fundamental kinetic basis for the OI framework. This was done in collaboration with Lawrence Livermore National Laboratory, who provided the chemical kinetic mechanisms, surrogate formulations for five of the experimental fuels investigated, and constant-volume ignition delay calculations. Constant-volume ignition delays are shown in Figure II.3.4 as functions of pressure and temperature for the five surrogate formulations under stoichiometric conditions. It is apparent that there are fuel-specific differences, but these differences are difficult to quantify.

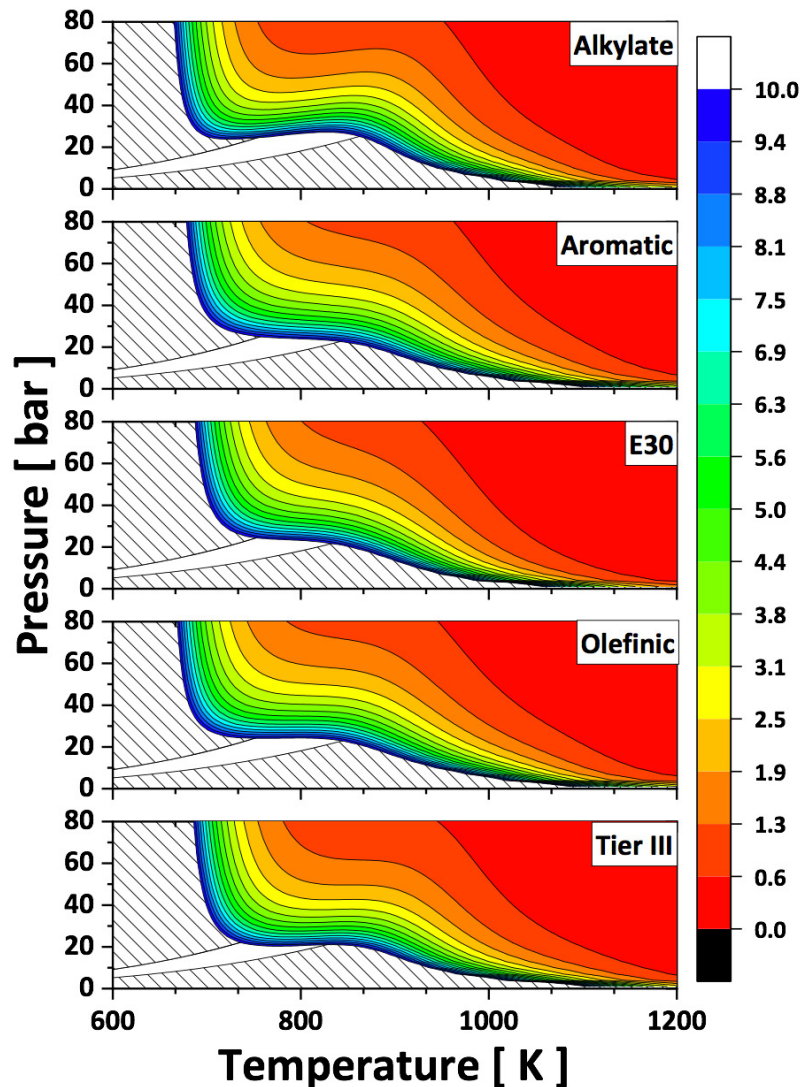


Figure II.3.4. Constant-volume ignition delay in milliseconds, calculated from kinetic modeling, as a function of pressure and temperature for each of the five fuels investigated at stoichiometric conditions

Figure II.3.5 shows ignition delay differences between the alkylate fuel and each of the four remaining surrogates. The alkylate fuel has a low octane sensitivity; thus, according to OI theory, it should be more reactive in the beyond RON region and less reactive in the beyond MON region relative to the other fuels. The color coding in Figure II.3.5 shows red when the alkylate fuel is more reactive and blue when the alkylate fuel is less reactive. With this knowledge, it can be seen that in the beyond RON region, the alkylate fuel is more reactive, as denoted by the red coloring. However, in the beyond MON region, only the E30 fuel is consistently more reactive. Thus, in the beyond MON region in the PT domain, the fundamental kinetics basis for the OI breaks down and there are fuel-specific differences that appear. This finding is consistent with the experimental results shown in Figure II.3.3 for the ACI condition.

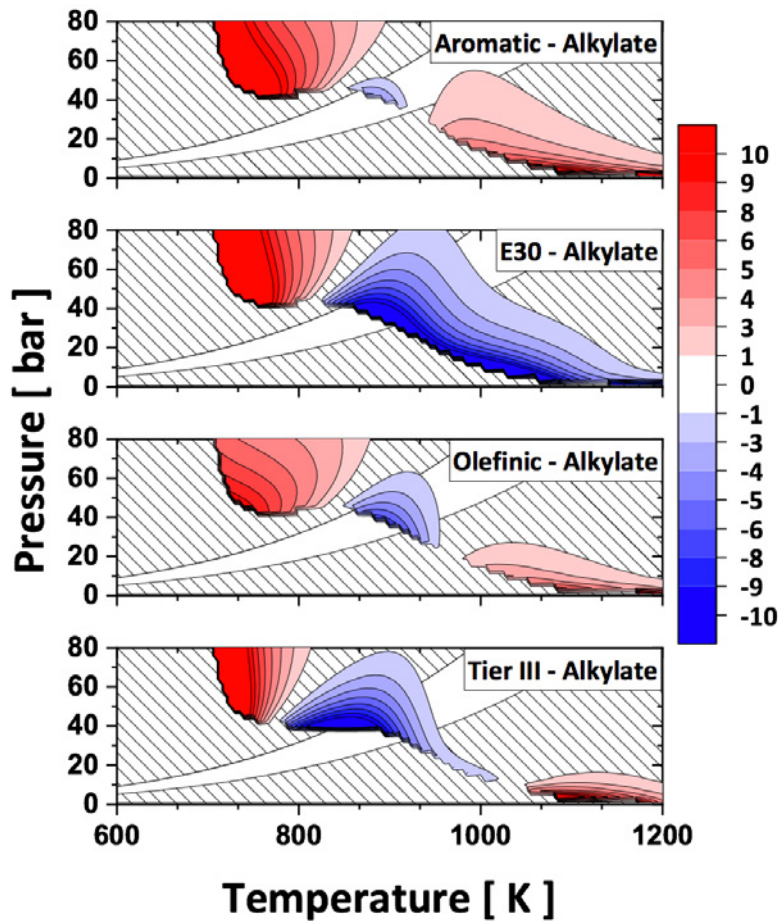


Figure II.3.5. Ignition delay differences between the alkylate fuel and either aromatic, E30, or the Tier III fuel at stoichiometric conditions ($\Phi = 1.0$). Red areas indicate that the alkylate fuel has a shorter ignition delay and blue areas indicate that the alkylate fuel has a longer ignition delay.

Conclusions

This project combines experimental and kinetic modeling efforts to investigate whether the central fuel properties hypothesis, as it pertains to fuel autoignition, is capable of predicting the rank-ordering of 19 fuels across a wide range of fuel properties and across a wide range of PT trajectories.

- The OI framework, which combines the RON and MON fuel properties with a weighting factor for engine operating condition, provides a much better correlation to performance than RON or MON alone.
- Among the SI operating conditions, OI does a reasonably good job of predicting the autoignition propensity between the different fuels investigated.
- For the ACI operating condition, the correlation to OI is poor. Instead of autoignition occurring in accordance with fuel properties, the chemical family of the fuel played a significant role; alkanes and alcohols behaved as expected based on OI, aromatics required a higher temperature than expected based on OI, and olefins required a lower temperature than expected based on OI.
- Kinetic modeling illustrated that there was kinetic basis for the OI in the beyond RON regime, but this breaks down in the beyond MON regime.

Key Publications

1. Szybist, J.P., and D.A. Splitter. 2018. “Understanding Chemistry-Specific Fuel Differences at a Constant RON in a Boosted SI Engine.” *Fuel* 217: 370–381. DOI: 10.1016/j.fuel.2017.12.100.
2. Splitter, D.A., A. Gilliam, J. Szybist, and J. Ghandhi. 2018. “Effects of Pre-Spark Heat Release on Engine Knock Limit.” *Proc. Comb. Inst.* DOI: 10.1016/j.proci.2018.05.145.
3. Jatana, G., D.A. Splitter, B. Kaul, and J.P. Szybist. 2018. “Fuel Property Effects on Low-Speed Pre-Ignition.” *Fuel* 230: 474–482. DOI: 10.1016/j.fuel.2018.05.060.

References

1. Kalghatgi, G.T. 2001. “Fuel Anti-Knock Quality - Part I. Engine Studies.” SAE Technical Paper 2001-01-3584. DOI: 10.4271/2001-01-3584.
2. Kalghatgi, G.T. 2001. “Fuel Anti-Knock Quality-Part II. Vehicle Studies - How Relevant is Motor Octane Number (MON) in Modern Engines?” SAE Technical Paper 2001-01-3585. DOI: 10.4271/2001-01-3585.
3. Kalghatgi, G.T, K. Nakata, and K. Moga. 2005. “Octane Appetite Studies in Direct Injection Spark Ignition (DISI) Engines.” SAE Technical Paper 2005-01-0244. DOI: 10.4271/2005-01-0244.
4. Szybist, J., and D. Splitter. 2017. “Pressure and Temperature Effects on Fuels with Varying Octane Sensitivity at High Load in SI Engines.” *Combustion and Flame* 177: 49–66. DOI: 10.1016/j.combustflame.2016.12.002.

Acknowledgements

The authors gratefully acknowledge Bill Pitz and Scott Wagon at Lawrence Livermore National Laboratory for their support of the kinetic modeling efforts in this investigation. Thanks also to Derek Splitter of Oak Ridge National Laboratory.

II.4 Characterizing BOB Impacts and Limits within Octane Index (Oak Ridge National Laboratory)

James Szybist, Principal Investigator

Oak Ridge National Laboratory
2360 Cherahala Blvd.
Knoxville, TN 37922
E-mail: szybistjp@ornl.gov

Kevin Stork, DOE Technology Development Manager

U.S. Department of Energy
E-mail: Kevin.Stork@ee.doe.gov

Start Date: October 1, 2017	End Date: September 30, 2018	
Project Funding (FY18): \$200,000	DOE share: \$200,000	Non-DOE share: \$0

Project Introduction

An organizing principle of the Co-Optimization of Fuels and Engines (Co-Optima) initiative is the central fuel properties hypothesis, which states that fuel properties provide an indication of the performance of the fuel, regardless of the fuel's chemical composition. By adopting this framework for spark ignition (SI) engines, it was possible to quantify the relative value of the different fuel properties as they relate to potential efficiency improvements through the use of an efficiency merit function (MF). The MF considers potential efficiency improvements, meaning that in most cases the engine design would have to be modified to improve efficiency through increased compression ratio, high exhaust gas recirculation rates, or similar. Specifically, research octane number (RON) and octane sensitivity (S), which is the difference between RON and the motor octane number (MON), can be traded for one another to maintain an equivalent MF score. Such an exercise is attractive because it is a way to create a value proposition for refiners if, for example, it is more cost-effective to produce a lower-RON, high-S blendstock for oxygenate blending (BOB). It can further create a value proposition by providing refiners and biofuel manufacturers flexibility if there are multiple pathways to meet the required fuel specifications. While this tradeoff can be identified and quantified through the MF from a mathematical standpoint, the extent to which these properties can be traded in modern engines is not well known. Specifically, previous research has demonstrated that the fuel properties that influence the MF provide an incomplete description of fuel performance in an engine. The goal of this project is to determine whether RON and S can actually be traded for comparable performance in a modern engine under multiple operating conditions. To determine this, an experimental approach was used with fuel components that stretched the boundary of common fuels by having a modest RON with a high S.

Objectives

Overall Objective of Co-Optima

- Co-develop engines and fuels to accelerate the development of efficient combustion modes and the utilization of diverse fuel sources

Fiscal Year 2018 Objectives

- Identify fuel candidates that can provide a modest RON and high S
- Quantify the blending performance of the fuel candidate, specifically the extent of synergistic or antagonistic blending
- Determine whether the performance in a modern engine is indicative of the predicted fuel properties of the blend, particularly with the fuels with modest RON and high S

Approach

While prior work within Co-Optima has shown that the rank ordering of a given set of fuels' resistance to autoignition can change as engine operating condition changes, knock typically only limits operation at the highest engine loads. Thus, as long as the knock resistance is sufficient under these conditions, the knock resistance at the lighter loads is not as important. To relate the specific performance of an engine and fuel to the RON and MON tests, Kalghatgi [1,2] pioneered a practical method to correlate the RON and MON values to knock-limited spark advance. This method requires a parameter, K , which is dependent on the engine operating conditions, to act as a weighting factor between RON and MON. The resultant octane index (OI), Equation 1, correlates to the actual knock propensity of the fuel much more strongly than either RON or MON [1–3]. This allows the relative knock resistance of fuels to be determined at conditions in real engines which differ from the RON and MON tests.

$$OI = RON - K * S \quad (1)$$

For conditions where $K = -1$, which is empirically representative of boosted SI conditions, a one-point increase in RON and a one-point increase in S are equally valuable and thus provide the same performance increase. In this investigation, fuels that have a modest RON but high S are identified as a way to provide these types of tradeoffs. Importantly, since the RON and MON tests are not representative of modern engine conditions, actual engine performance needs to be verified with these conditions. In this study, three such fuel components are identified, their fuel blending assessed, and finally, their performance in a modern engine is assessed to determine if fuel property tradeoffs between RON and S can be done to realize equivalent engine performance.

Results

One of the key group contributions from the Co-Optima initiative has been the development of the SI merit function, as reported in reference [4] and shown in Figure II.4.1. This framework allows the contribution of each fuel property to be individually weighted with regards to engine efficiency relative to a regular-grade E10 fuel (gasoline blend with 10% ethanol). Specifically, the first two terms quantify the OI impact, which takes into consideration RON and S , the next two terms take into account the latent heat of vaporization, the fourth term quantifies the flame speed effect, and the last two terms quantify the efficiency impact of particulate matter and catalyst light-off, respectively.

$$\begin{aligned} Merit = & \frac{(RON_{mix} - 91)}{1.6} - K \frac{(S_{mix} - 8)}{1.6} \\ & + \frac{0.085[ON / kJ / kg] \cdot ((HoV_{mix} / (AFR_{mix} + 1)) - (415[kJ / kg] / (14.0[-] + 1)))}{1.6} \\ & + \frac{((HoV_{mix} / (AFR_{mix} + 1)) - (415[kJ / kg] / (14.0[-] + 1)))}{15.2} \\ & + \frac{(S_{Lmix} - 46[cm / s])}{5.4} \\ & - H(PMI_{mix} - 1.6)[0.7 + 0.5(PMI_{mix} - 1.4)] \\ & + 0.008^{\circ}C^{-1}(T_{c,90,conv} - T_{c,90,mix}) \end{aligned}$$

Figure II.4.1. SI merit function for fuel properties developed in Co-Optima [4]

The magnitude of each term in the MF is quantified such that each point increase approximates a relative efficiency increase of 1% [4]. With the development of this tool came with the realization that fuel properties could be traded off for one another to produce engine performance with equivalent efficiency. Specifically of interest to this project was that RON could be traded off for S . In other words, the same engine performance could be realized from a fuel with high RON (~98) and modest octane sensitivity (~8), or from a fuel with modest RON (~94) and high octane sensitivity (~12). Knowing the extent to which these properties could be traded off for each other could make the economics of a co-optimized fuel more attractive to both conventional energy companies (petroleum) and the bio-fuels industry.

Two chemical families were initially identified that provide high octane sensitivity with modest RON: alkylated cycloalkanes and branched-chain olefins. From these, methylcyclopentane (MCP) and amylene were procured as representative samples. It is noteworthy that amylene has a higher RON than would be ideal for this study, but other higher-molecular-weight branched-chain olefins that had the lower RON were either not available in sufficient quantities from chemical supply companies or were cost prohibitive. Later, prenil was identified by the high-performance fuels team within the Co-Optima initiative as being an attractive molecule that met these requirements. Prenil is a branched-chain olefin with an alcohol group. These compounds are shown in Figure II.4.2.

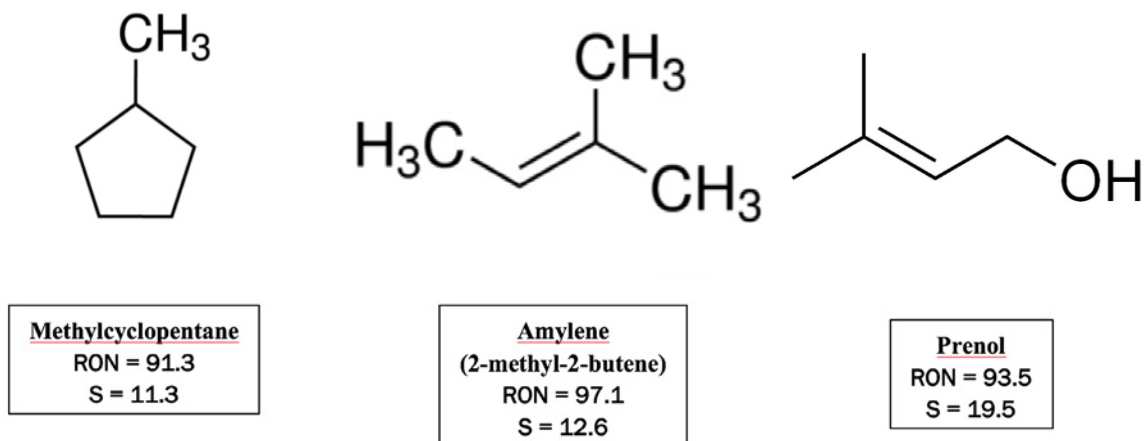


Figure II.4.2. Structure, RON, and S for the fuels investigated in this study

These species were blended at 20 vol% in a BOB. BOBs are sub-octane refinery streams that do not yet contain ethanol or other oxygenates, but are intended to meet the gasoline requirements for octane number, vapor pressure, distillation, and other properties after 10% ethanol has been added to them. Blending at a 20 vol% level revealed non-linear synergistic blending with regards to RON for both amylene and prenil. On the other hand, the blending response of MCP was linear on a volume basis, as shown in Figure II.4.3.

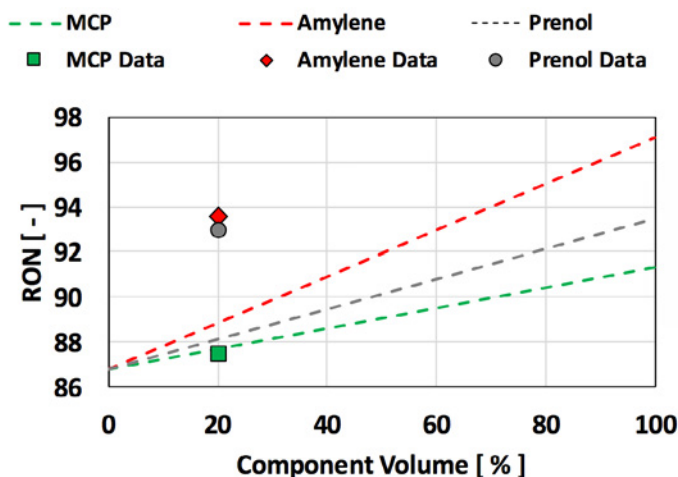


Figure II.4.3. RON of 20 vol% blends of the fuel components investigated, as well as lines of linear blending for the BOB and each of the pure components. Amylene and prenil exhibit synergistic blending while MCP exhibits linear blending.

In addition to a non-linear synergistic blending for RON, there was also non-linear synergistic blending for S for both amylene and prenil, shown in Figure II.4.4. Or, since S is the difference between RON and MON, synergistic blending with regards to S could also be considered to be synergistic blending with regards to RON but not MON. The magnitude of the synergistic blending with regards to S is higher for amylene than it is for prenil, though the synergism for both is significant. The MCP, again, does not show a synergistic blending response and may even show antagonistic blending behavior.

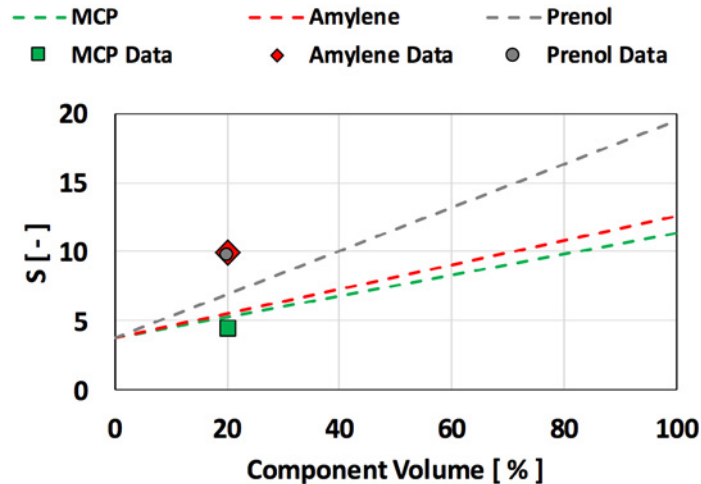


Figure II.4.4. S of 20 vol% blends of the fuel components investigated, as well as lines of linear blending for the BOB and each of the pure components. Amylene and prenil exhibit synergistic blending while MCP exhibits nearly linear blending.

It is significant that, at only a 20 vol% blend level, the prenil and amylene components were able to upgrade a sub-octane BOB to such a large extent. In fact, the RON of the prenil blend at a 20 vol% level was nearly the same as it is at 100 vol%. This illustrates that the non-linear blending phenomena needs to be considered, and why it has been a focus of research within Co-Optima [5].

The MF tradeoffs and the non-linear blending phenomena discussed thus far have used the RON and MON tests as a basis. These tests are not representative of typical operating conditions for modern engines; thus, actual engine performance measurements can provide additional confidence that these property measurements are indicative of actual engine performance and not just an anomaly at the conditions of the RON and MON tests. To investigate modern engine conditions, another Co-Optima project [6] was leveraged to include these fuel blends in a larger investigation that, combined, included 19 fuel blends. The experimental investigation focused on autoignition characteristics as a function of the pressure-temperature trajectory, considering boosted SI conditions, naturally aspirated SI conditions, and advanced compression ignition conditions. The wide range of operating conditions were chosen because they represent a wide range of pressure-temperature trajectories, which dictate which kinetic reactions will be most important to autoignition. The range of pressure-temperature trajectories investigated can be seen in Figure II.4.5.

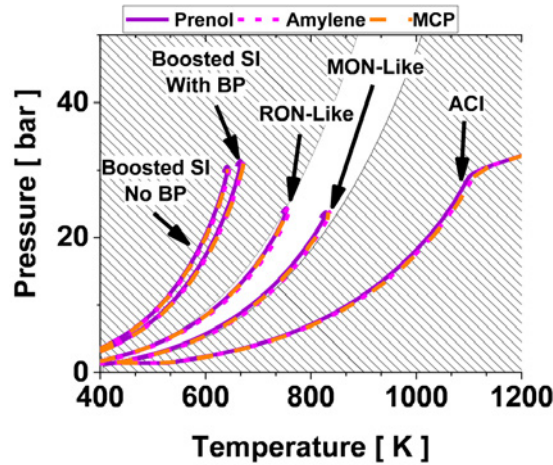
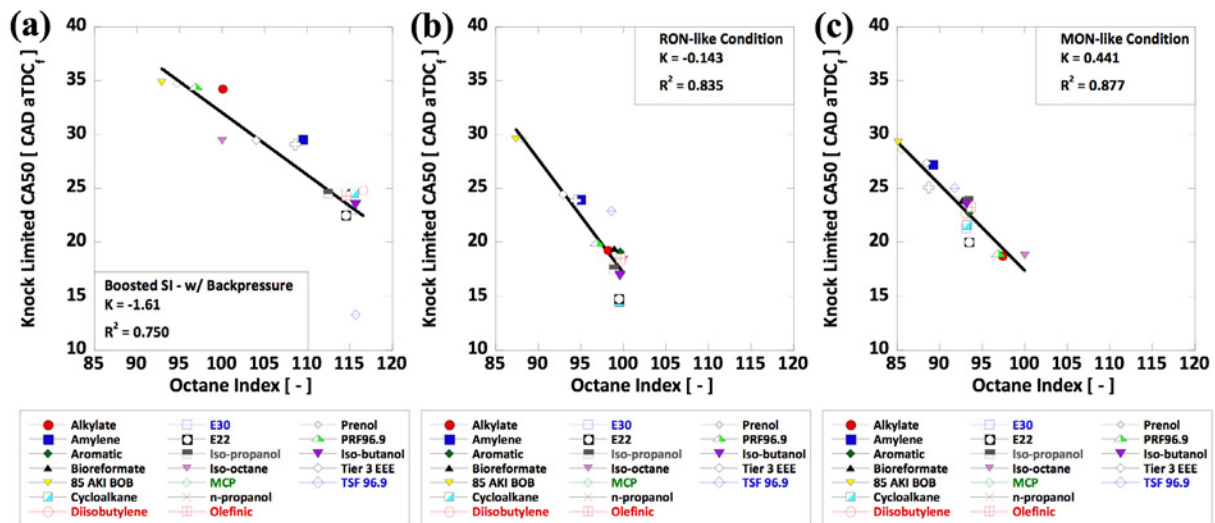


Figure II.4.5. Pressure-temperature trajectories of each of the operating conditions investigated

Figure II.4.6 shows the knock-limited crank angle at 50% mass fraction burned (CA50) combustion phasing as a function of OI. OI is the combined impact of the first two terms of the merit function shown in Figure II.4.1 and has been shown to be the most impactful part of the merit function [4]. Earlier CA50 combustion phasing (lower number) means that the fuel is more resistant to knock and therefore generates more power and higher efficiency at a constant fueling rate. The results in Figure II.4.6 show that the knock-limited CA50 combustion phasing for the amylene, prenol, and MCP blends all agree reasonably well with their OI and are not outliers compared with the remaining fuels. This provides evidence that these fuel components behave in accordance with the fuel properties of the blends. As a result, this demonstrates that these fuel properties derived from blending modest-RON and low-S fuel blends do translate to engine performance. Thus, RON and S can be traded off against one another for equivalent engine performance to minimize the cost of fuel production.



CAD – crank angle degrees; aTDC_f – after top dead center firing; AKI – anti-knock index;
 E30 – gasoline blend with 30% ethanol; E22 – gasoline blend with 22% ethanol; PRF – primary reference fuel;
 EEE – certification gasoline; TSF – toluene standardization fuel

Figure II.4.6. Knock-limited combustion phasing as a function of octane index for each fuel investigated at (a) the boosted SI condition, (b) the RON-like condition, and (c) the MON-like condition

Conclusions

In this investigation, three fuel candidates were identified that have modest RON and high S. They were identified as potential candidates for which high S could be traded off for modest RON to provide equivalent performance in boosted SI engines, which could provide a value proposition for both conventional fuel producers and biofuel producers. The following conclusions were made.

- The olefin (amylene) and olefinic alcohol (prenol) both experienced synergistic blending with the BOB. As a result, at a 20 vol% blend level, the RON of the blends was approaching the RON of the pure component. In contrast, MCP behaved in a much more linear manner. The fuels with the synergistic blending are much more valuable for blending.
- Engine experiments confirmed that the operation of these fuel blends was in line with their fuel property predictions. Thus, even though the RON and MON are not representative of modern engine operating conditions, the tradeoffs quantified by RON and MON are predictive of actual engine performance.

Key Publications

1. Szybist, J.P., and D.A. Splitter. 2018. "Understanding Chemistry-Specific Fuel Differences at a Constant RON in a Boosted SI Engine." *Fuel* 217: 370–381. DOI: 10.1016/j.fuel.2017.12.100.
2. Splitter, D.A., A. Gilliam, J. Szybist, and J. Ghandhi. 2018. "Effects of Pre-Spark Heat Release on Engine Knock Limit." *Proc. Comb. Inst.* DOI: doi.org/10.1016/j.proci.2018.05.145.
3. Jatana, G., D.A. Splitter, B. Kaul, and J.P. Szybist. 2018. "Fuel Property Effects on Low-Speed Pre-Ignition." *Fuel* 230: 474–482. DOI: 10.1016/j.fuel.2018.05.060.

References

1. Kalghatgi, G.T. 2001. "Fuel Anti-Knock Quality - Part I. Engine Studies." SAE Technical Paper 2001-01-3584. DOI:10.4271/2001-01-3584.
2. Kalghatgi, G.T. 2001. "Fuel Anti-Knock Quality-Part II. Vehicle Studies - How Relevant is Motor Octane Number (MON) in Modern Engines?" SAE Technical Paper 2001-01-3585. DOI:10.4271/2001-01-3585.
3. Kalghatgi, G.T., K. Nakata, K. Moga. 2005. "Octane Appetite Studies in Direct Injection Spark Ignition (DISI) Engines." SAE Technical Paper 2005-01-0244. DOI:10.4271/2005-01-0244.
4. Miles, P. 2018. "Efficiency Merit Function for Spark Ignition Engines: Revisions and Improvements Based on FY16–17 Research." Technical Report. U.S. Department of Energy, Washington, DC. DOE/GO-102018-5041.
5. McCormick, R., G. Fioroni, L. Fouts, E. Christensen, et al. 2017. "Selection Criteria and Screening of Potential Biomass-Derived Streams as Fuel Blendstocks for Advanced Spark-Ignition Engines." *SAE Int. J. Fuels Lubr.* 10 (2): 442–460, <https://doi.org/10.4271/2017-01-0868>.
6. Szybist, J. 2018. "Developing a Better Understanding of Octane Index." Contribution in the DOE VTO FY 2018 Annual Report.

II.5 Advanced Light-Duty SI Engine Fuels Research (Sandia National Laboratories)

Magnus Sjöberg, Principal Investigator

Sandia National Laboratories (SNL)
MS9053, P.O. Box 969
Livermore, CA 94551-0969
E-mail: mgsjobe@sandia.gov

Kevin Stork, DOE Technology Development Manager

U.S. Department of Energy
E-mail: Kevin.Stork@ee.doe.gov

Start Date: October 1, 2017	End Date: September 30, 2018	
Project Funding (FY18): \$708,000	DOE share: \$708,000	Non-DOE share: \$0

Project Introduction

This project furthers the science-base needed by industry stakeholders to co-evolve the next generations of highly efficient direct injection spark ignition (DISI) engines and new gasoline-type fuels. Here, the research emphasis is on lean operation, which can provide high efficiency, using fuels that also support traditional non-dilute stoichiometric operation for peak load and power. Lean operation induces challenges with ignition stability, slow flame propagation, and low combustion efficiency. Therefore, techniques that can overcome these challenges are studied. Specifically, fuel stratification is used to ensure ignition and completeness of combustion, but this technique has soot- and NO_x-emissions challenges. For ultra-lean well-mixed operation, turbulent deflagration can be combined with controlled end-gas autoignition to render mixed-mode combustion for sufficiently fast heat release. However, such mixed-mode combustion requires appropriate autoignition reactivity, motivating fuel studies of autoignition under lean conditions.

Objectives

- Provide the science-base needed to understand how emerging alternative fuels impact highly efficient DISI light-duty engines being developed by industry
- Elucidate how engine design and operation can be optimized for clean and efficient use of future fuels
- Develop and apply advanced optical diagnostics for probing in-cylinder processes

Approach

The Alternative Fuels DISI Engine Lab at Sandia houses an engine that is capable of both performance testing and in-cylinder optical diagnostics. First, performance testing with an all-metal engine configuration is conducted over wide ranges of operating conditions and alternative fuel blends. This allows quantifying fuel-efficiency and exhaust-emissions behavior. Second, in-cylinder processes are examined with high-speed optical diagnostics, including advanced laser-based techniques. This reveals the mechanisms that govern the combustion process and exhaust-emissions formation. Computer modeling provides additional insight of the governing combustion fundamentals. The combination of performance testing, exhaust-emissions measurements, optical diagnostics, and modeling allows building a comprehensive science-base.

Results

Key Accomplishments for Fiscal Year 2018

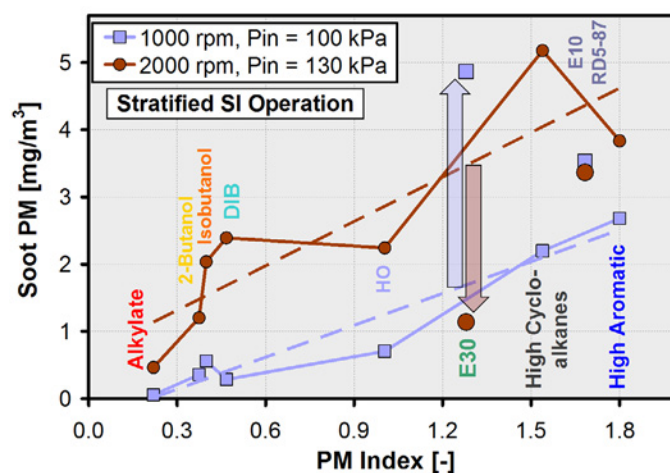
- Assessed the relevance of the Particulate Matter Index (PMI) for nine fuels across three stoichiometric well-mixed and two lean stratified operating conditions
- Developed in-cylinder soot diagnostics based on diffused back-illumination, and used them to quantify in-cylinder soot mass distributions for key operating points

- Used wall-wetting diagnostics based on refractive index matching to determine the role of fuel films for in-cylinder soot production
- Showed that high smoke emissions for cold-start stratified-charge operation with an E30 fuel (70% gasoline, 30% ethanol blend) can be traced to increased fuel films on the piston top, with associated sooting pool fires
- Acquired lean mixed-mode combustion data for five fuels, spanning a range of equivalence ratio (ϕ), intake pressure (P_{in}), intake temperature (T_{in}), and intake oxygen mole fraction [O_2] conditions
- Performed an initial assessment of the efficacy of octane-index framework for lean conditions

In the following sections, selected examples of the Fiscal Year 2018 accomplishments are presented.

Fully Stratified Operation

Spray-guided, stratified-charge spark ignition (SI) operation can provide high thermal efficiency for low and mid loads, where a light-duty automotive engine typically spends a large fraction of time. However, while enabling high-efficiency operation, fuel stratification can cause unacceptably high engine-out smoke levels, depending both on the fuel injection and combustion strategy, and the fuel composition. A commonly used metric for a fuel's sooting propensity is the PMI, which originally was developed for port fuel injection engines [1]. In the current effort, the efficacy of PMI is assessed for a direct injection engine operating in either stratified-lean or well-mixed stoichiometric mode. This work includes the use of fuel components that were not emphasized during the original development of the PMI metric, such as various alcohols. For brevity, only results for stratified operation are presented in this report. For stratified naturally aspirated operation at 1,000 revolutions per minute (rpm), the light-blue squares in Figure II.5.1 show that for most fuels, the measured engine-out soot (as derived from paper darkening in an AVL 415S Smoke Meter) scales relatively well with PMI. However, the two ethanol-containing fuels, E30 and RD5-87 (E10, a blend of 90% gasoline with 10% ethanol), fall well above the dashed linear trend line, which was based on the seven non-ethanol fuels (shown connected by solid lines). In-cylinder optical diagnostics reveal that under these conditions, the E30 fuel impinges on the piston top, causing wall-wetting and associated pool fires, as discussed in [2] and [3]. The elevated smoke emissions with E30 become even more severe for operation with a reduced coolant temperature, such as during warm-up, as shown in the top row of Figure II.5.2. The imaging presented in this figure shows that the liquid fuel films become thicker and larger with a reduction of the coolant temperature. As a result, the combustion becomes more strongly sooting, explaining the increased smoke emissions.

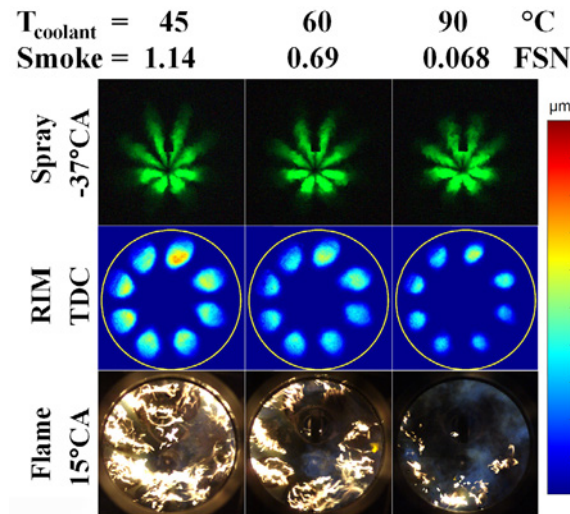


PM – particulate matter; HO – high-olefin gasoline (a Co-Optima RON98 core fuel)

Figure II.5.1. For naturally aspirated stratified-charge, direct-injection SI operation at 1,000 rpm, smoke emissions for E30 are much higher than the average trend line due to the formation of pool fires.

For boosted operation at 2,000 rpm, E30 suppresses soot formation. Intake [O_2] = 17%, $\phi_m = 0.33$,

$T_{coolant} = 75^\circ\text{C}$. PMI values were provided by [4] and [5]. Figure by Magnus Sjöberg, SNL.

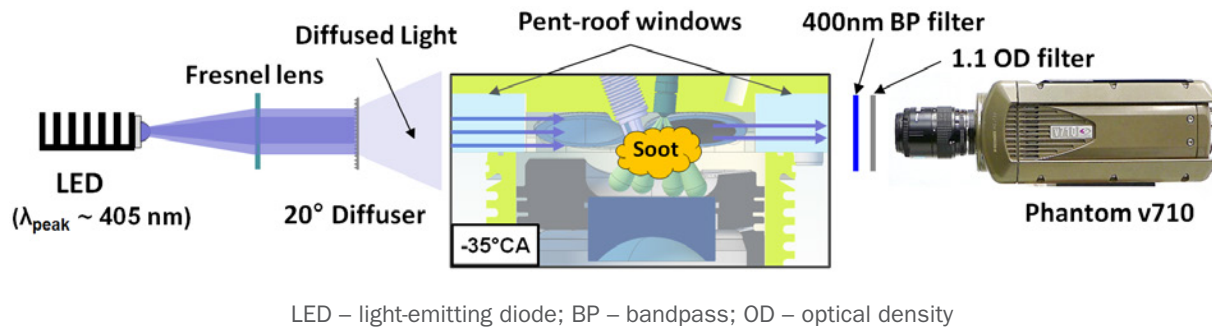


FSN – filter smoke number; RIM – refractive index matching; TDC – top dead center

Figure II.5.2. Effect of engine coolant temperature on piston-top wall wetting and associated formation of sooting pool fires and exhaust smoke emissions. Intake $[\text{O}_2] = 18\%$. Figure by Magnus Sjöberg, SNL, and Xu He, Beijing Institute of Technology.

Furthermore, Figure II.5.1 shows that when the operating conditions change to a higher-speed, boosted condition, represented by brown circles, the effect of ethanol reverses. Here, the E30 fuel falls well below the dashed linear trend line. At this slightly boosted operating point, optical diagnostics reveal that both the wall-wetting and pool-fire activity are strongly reduced for all fuels. As a result, it is hypothesized that the soot-formation pathway becomes dominated by bulk-gas soot processes, partly augmented by a tumble-induced fuel-vapor asymmetry [6]. In this situation, the fuel-borne oxygen of the ethanol in the E30 fuel helps to suppress soot formation. It should be noted that the calculation of PMI does not take the oxygen content of the fuel into account.

For a better understanding of fuel effects on bulk-gas soot-formation processes, a new in-cylinder soot diagnostic was developed and used, as depicted in Figure II.5.3. Using diffused back-illumination, the amount of in-cylinder soot can be quantified on a crank-angle resolved basis. The initial results indicate strong fuel effects, and also substantial cycle-to-cycle variations. Figure II.5.4 provides an example of a strongly sooting cycle for a fuel that contains diisobutylene (DIB), with elevated soot concentration on the intake side of the combustion chamber. Looking back at Figure II.5.1, it can be seen that the DIB blend falls well above the average trend line for operation at 2,000 rpm. In combination with direct flame imaging, the diffused back-illumination diagnostics confirm that the DIB fuel produces elevated in-cylinder soot to a degree that is inconsistent with its low PMI.



LED – light-emitting diode; BP – bandpass; OD – optical density

Figure II.5.3. Schematic of diffused back-illumination setup for in-cylinder soot quantification.

Figure by Namho Kim, SNL.

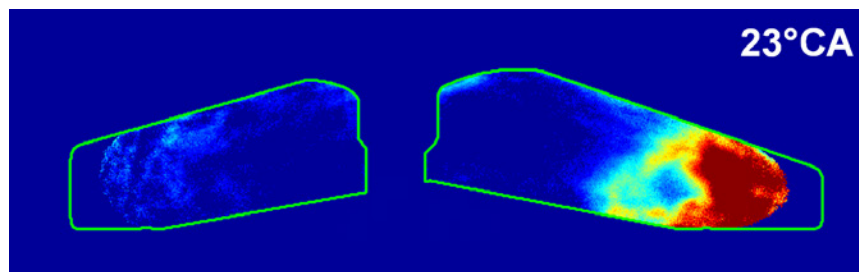


Figure II.5.4. Detection of in-cylinder soot for stratified operation with a RON98 fuel containing 19.6% DIB by volume. Figure by Namho Kim, SNL.

Lean Autoignition Studies

Lean or dilute well-mixed SI engine operation can improve thermal efficiency, but a key challenge is to maintain a 10–90% burn duration shorter than 30 degrees crank angle ($^{\circ}\text{CA}$), which is needed to realize efficiency gains of lean combustion [7]. Lean deflagration has a tendency to cause a slow burn-out process, but a speed-up can be achieved via the use of mixed-mode combustion, which features a combination of turbulent deflagration and end-gas autoignition [8]. Practical implementation of mixed-mode combustion (or other advanced compression ignition strategies) requires that suitable fuels are available in the marketplace and that appropriate autoignition metrics are available to specify the fuels being used. Consequently, the applicability of research octane number (RON) and motor octane number (MON) for autoignition under lean conditions is currently being assessed for a range of fuels. For these experiments, several injections during the intake stroke create a well-mixed fuel–air charge. However, to stabilize flame development for these lean conditions, a small amount of extra fuel (1.6 mg \approx 10% of the total fuel mass) is injected at the time of spark to enrich the mixture near the spark plug. This injection strategy is called partial fuel stratification (PFS).

Figure II.5.5 shows a comparison of lean autoignition reactivity for five fuels over a range of intake $[\text{O}_2]$. The autoignition metric used here is based on a determination of the combustion phasing (crank angle at 50% mass fraction burned, CA50) where the amount of end-gas autoignition is marginal, as outlined in [9]. It can be observed that the autoignition reactivity varies substantially between fuels, with the RON91 fuel being the most reactive and therefore requiring a less advanced combustion phasing for the beneficial end-gas autoignition to take place. These well-controlled tests utilize electric intake air heating to promote autoignition. In a practical implementation, elevated charge temperature can be achieved by retaining hot residual gases, which would lower $[\text{O}_2]$ of the reactants. Figure II.5.5 shows that the response to changes of the intake $[\text{O}_2]$ varies between fuels, with the high-cycloalkane fuel being the least sensitive. The differences in $[\text{O}_2]$ sensitivity could have consequences for a practical engine implementation that uses retained residuals or exhaust-gas recirculation.

Figure II.5.6 provides an example of the ability of the octane index to rank-order the fuels' autoignition reactivity. The best-fit K-factor is 0.51 for operation with $[\text{O}_2] = 15.5\%$, notionally placing the autoignition regime right in between the RON ($K = 0$) and the MON ($K = 1$) tests. The quality of the fit is good over this selection of fuels, with an R2 value of 0.92. Future work will expand the assessment of the octane index to other conditions and will include fuels that contain alcohols and other classes of molecules.

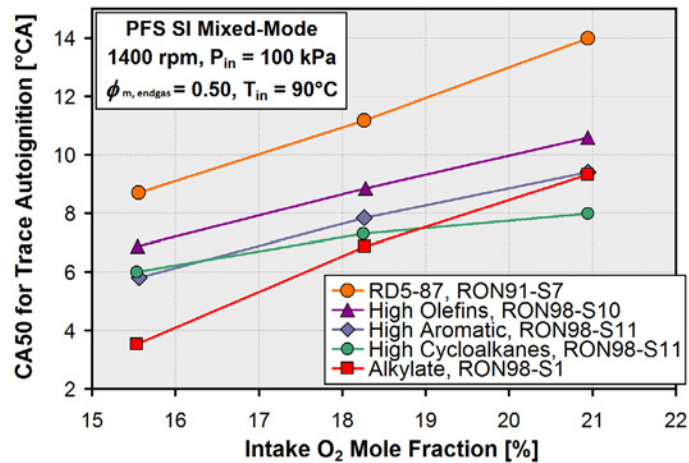


Figure II.5.5. Effect of intake oxygen mole fraction on combustion phasing rendering “trace autoignition” for lean SI operation with $\phi_m = 0.50$ in the end-gas. Figure by Magnus Sjöberg, SNL.

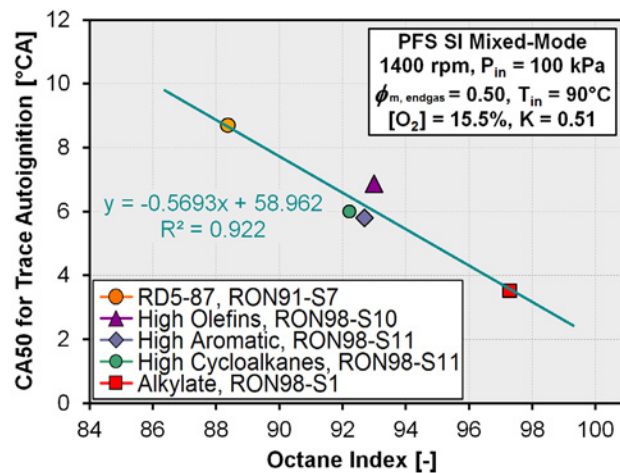


Figure II.5.6. Example of the application of the octane-index framework for lean mixed-mode combustion utilizing end-gas autoignition. $P_{in} = 100$ kPa. Figure by Magnus Sjöberg, SNL.

Conclusions

These research tasks are contributing strongly to both the Co-Optima project and to the fundamental science of fuel/combustion interactions for advanced SI engine combustion.

For advanced lean stratified-charge operation, the smoke/soot emissions can be reasonably well correlated with the fuels' PMI values, but with some noteworthy exceptions. For conditions that are prone to wall wetting, the ethanol content of an E30 fuel can cause pool fires and smoke emissions that are strongly elevated relative to expectations based on PMI. In contrast, for boosted conditions dominated by bulk-gas soot formation, the oxygen content of the E30 fuel acts to suppress soot formation. Also, for these boosted conditions, a fuel containing DIB shows higher-than-expected in-cylinder soot and exhaust smoke emissions. These findings with regards to wall wetting, pool fires, and bulk-gas soot formation highlight the need to further develop fuel-property metrics that can better predict the effect of fuel on engine PM emissions, even for advanced stratified-charge operation utilizing non-conventional gasoline-type fuels.

For lean mixed-mode combustion, fuels can exhibit different responses to changes of the intake oxygen mole fraction, implying differences in the response to retained residuals or exhaust gas recirculation for a practical

implementation. Using a small set of fuels, it was demonstrated that the octane-index framework can be applicable for rank-ordering fuels in terms of their lean autoignition reactivities. However, both the fuels matrix and experimental matrix need to be expanded for future studies.

Key Publications

1. Sjöberg, M., and X. He. 2018. “Combined Effects of Intake Flow and Spark-Plug Location on Flame Development, Combustion Stability and End-Gas Autoignition for Lean Spark-Ignition Engine operation Using E30 Fuel.” *International Journal of Engine Research* 19, no. 1 (January): 86–95.
2. Ding, C.P., M. Sjöberg, D. Vuilleumier, D.L. Reuss, X. He, and B. Böhm. 2018. “Fuel-Film Thickness Measurements Using Refractive Index Matching in a Stratified-Charge SI Engine Operated on E30 and Alkylate Fuels.” *Experiments in Fluids* 59: 59.
3. Westbrook, C.K., M. Sjöberg, and N.P. Cernansky. 2018. “A New Chemical Kinetic Method of Determining RON and MON Values for Single Component and Multicomponent Mixtures of Engine Fuels.” *Combustion and Flame* 195: 50–62, doi: 10.1016/j.combustflame.2018.03.038.
4. Van Dam, N., M. Sjöberg, and S. Som. 2018. “Large-Eddy Simulations of Spray Variability Effects on Flow Variability in a Direct-Injection Spark-ignition Engine under Non-Combusting Operating Conditions.” SAE Paper 2018-01-0196.
5. He, X., Y. Li, M. Sjöberg, D. Vuilleumier, C.P. Ding, F. Liu, and X. Li. 2019. “Impact of Coolant Temperature on Piston Wall-Wetting and Smoke Generation in a Stratified-Charge DISI Engine Operated on E30 Fuel.” *Proceedings of the Combustion Institute* 37 (4): 4955–4963, doi: 10.1016/j.proci.2018.07.073.
6. Vuilleumier, D., X. Huan, T. Casey, and M. Sjöberg. 2018. “Uncertainty Assessment of Octane Index Framework for Stoichiometric Knock Limits of Co-Optima Gasoline Fuel Blends.” *SAE International Journal of Fuels and Lubricants* 11 (3): 247–269, doi: 10.4271/04-11-03-0014.

References

1. Aikawa, K., T. Sakurai, and J. Jetter. 2010. “Development of a Predictive Model for Gasoline Vehicle Particulate Matter Emissions.” *SAE Int. J. Fuels Lubr.* 3 (2): 610–622, doi: 10.4271/2010-01-2115.
2. Ding, C.P., M. Sjöberg, D. Vuilleumier, D.L. Reuss, X. He, and B. Böhm. 2018. “Fuel-Film Thickness Measurements Using Refractive Index Matching in a Stratified-Charge SI Engine Operated on E30 and Alkylate Fuels.” *Experiments in Fluids* 59: 59.
3. He, X., Y. Li, M. Sjöberg, D. Vuilleumier, C.P. Ding, F. Liu, and X. Li. 2019. “Impact of Coolant Temperature on Piston Wall-Wetting and Smoke Generation in a Stratified-Charge DISI Engine Operated on E30 Fuel.” *Proceedings of the Combustion Institute* 37 (4): 4955–4963, doi: 10.1016/j.proci.2018.07.073.
4. Fouts, L., G.M. Fioroni, E. Christensen, M. Ratcliff, R.L. McCormick, B.T. Zigler, S. Sluder, J.P. Szybist, J.E. Dec, P.C. Miles, S. Ciatti, J.T. Bays, W. Pitz, and M. Mehl. 2018. “Properties of Co-Optima Core Research Gasolines.” Technical Report NREL/TP-5400-71341. Golden, CO: National Renewable Energy Laboratory.
5. Christensen, E., L. Fouts, G.M. Fioroni, and R.L. McCormick, Private communication, March 2018.
6. Zeng, W., M. Sjöberg, D.L. Reuss, and Z. Hu. 2017. “High-Speed PIV, Spray, Combustion Luminosity, and Infrared Fuel-Vapor Imaging for Probing Tumble-Flow-Induced Asymmetry of Gasoline Distribution in a Spray-Guided Stratified-Charge DISI Engine.” *Proc. Comb. Inst.* 36 (3): 3459–3466, doi: 10.1016/j.proci.2016.08.047.

7. Ayala, F., and J. Heywood. 2007. "Lean SI Engines: The Role of Combustion Variability in Defining Lean Limits." SAE Technical Paper 2007-24-0030, doi: 10.4271/2007-24-0030.
8. Sjöberg, M., and W. Zeng. 2016. "Combined Effects of Fuel and Dilution Type on Efficiency Gains of Lean Well-Mixed DISI Engine Operation with Enhanced Ignition and Intake Heating for Enabling Mixed-Mode Combustion." *SAE Int. J. Engines* 9 (2): 750–767, doi:10.4271/2016-01-0689.
9. Sjöberg, M., D. Vuilleumier, N. Yokoo, and K. Nakata. 2017. "Effects of Gasoline Composition and Octane Sensitivity on the Response of DISI Engine Knock to Variations of Fuel-Air Equivalence Ratio." COMODIA 2017, July 25–28, Okayama, Japan.

Acknowledgements

The work was performed at the Combustion Research Facility, Sandia National Laboratories, Livermore, California. Sandia National Laboratories is a multi-mission laboratory managed and operated by National Technology and Engineering Solutions of Sandia, LLC., a wholly owned subsidiary of Honeywell International, Inc., for the U.S. Department of Energy's National Nuclear Security Administration under contract DE-NA0003525.

The principal investigator thanks David Vuilleumier and Namho Kim for their contributions to this project.

II.6 Effect of Properties/Injection Schedule on Fuel Spray Mixing (Sandia National Laboratories)

Lyle M. Pickett, Principal Investigator

Sandia National Laboratories
P.O. Box 969, MS 9053
Livermore, CA 94551-9053
E-mail: LMPicke@sandia.gov

Kevin Stork, DOE Technology Development Manager

U.S. Department of Energy
E-mail: Kevin.Stork@ee.doe.gov

Start Date: October 1, 2017	End Date: September 30, 2018	
Project Funding (FY18) \$380,000	DOE share: \$380,000	Non-DOE share: \$0

Project Introduction

The DOE project for Co-Optimization of Fuels and Engines seeks to define both fuel properties and engine hardware to create cleaner and more fuel-efficient engines. Fuel spray technologies are central to this goal as the spray injection determines the combustible mixtures formed within the engine. Sprays are known to affect burn rate and efficiency, particulate formation and emissions, as well as temperature and engine knock sites. Computational fluid dynamics (CFD) models must predict complicated interaction between plumes and vaporization to be useful as design tools for industry.

Changes in fuel properties are expected to affect fuel delivery. While Co-Optima fuels may be selected for chemical criteria, such as high octane number rating, an understanding of how the physical properties affect spray performance is necessary to optimize fuel delivery. Many of the selected Co-Optima fuels have properties that are different than standard gasoline, requiring investigations for their performance. A new continuous-flow spray chamber facility has been completed, offering capability to control the pressure and temperature of the gases at engine-relevant conditions at the time of injection as well as a massive increase in data throughput. Direct-injection multi-hole gasoline sprays for different Co-Optima fuels are investigated in this chamber.

Objectives

Overall Objectives

- Identify differences in fuel spray mixing, evaporation, plume interaction, droplet atomization, and liquid film formation with respect to proposed candidate fuels

Fiscal Year 2018 Objectives

- Complete new spray chamber facility with continuous-flow operation
- Apply suite of high-speed optical diagnostics to measure vapor, liquid, plume direction, and spray collapse at representative engine conditions
- Use different injection durations and multiple injections to understand methods to limit liquid penetration and prevent wall impingement

Approach

An optically accessible spray chamber designed for operation at pressures ranging from 0.25 bar (vacuum) to 150 bar and gas temperatures from 300 K to 1,100 K was installed in a new laboratory. A well-characterized gasoline fuel injector (Engine Combustion Network Spray G) was installed in a temperature-controlled port.

The same injector is also used by Argonne National Laboratory for X-ray spray characterization. High-speed schlieren and extinction imaging were applied to measure liquid and vapor characteristics of the spray. New methods for post-processing line-of-sight diagnostics to reveal local plume characteristics were developed. The facility and diagnostics provide excellent capabilities for the study of fuel spray mixing and deliver key datasets important for CFD validation.

Results

A laboratory was reconditioned and a new high-pressure, high-temperature temperature vessel was installed as shown in Figure II.6.1. This chamber utilizes a continuous flow of pressurized, high-temperature gases to an optically accessible test section. Fused-silica windows of 140-mm diameter act as the pressure window, while inner fused silica blanks act as a thermal barrier. Air, nitrogen, or air/nitrogen mixtures flow through heaters encased inside the pressure vessel and enter the spray test section at temperatures as high as 1,100 K and pressures as high as 150 bar. The pressure vessel is insulated from the heaters and test section, and the vessel is water-cooled to maintain temperatures below 200°C, temperatures at which the duplex 2205 stainless material maintains strength. Exhaust gases are water-cooled with a heat-exchange capacity matching the supply heaters. Fuel is delivered to temperature-controlled gasoline or diesel fuel injectors. Injections may be repeated after fuel vapor is scavenged downstream, and a fresh charge of gas is available in the spray test section. The facility represents a major step forward in research capabilities, with an expected 300× increase in data throughput compared to a premixed-burn style spray chamber [1].

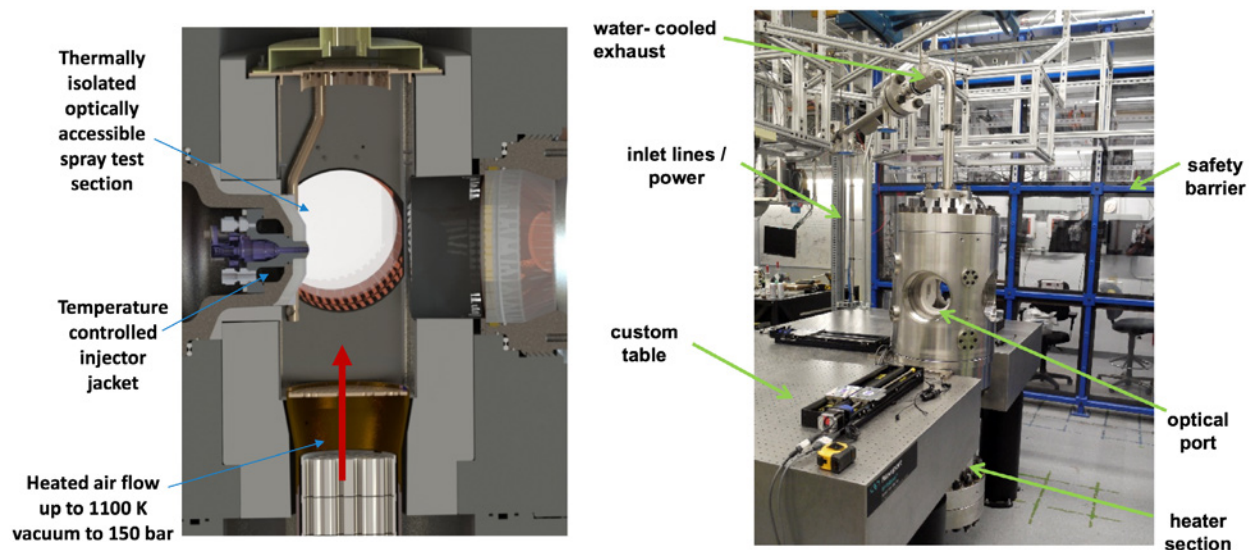


Figure II.6.1. (left) Cross-section of continuous-flow heated spray chamber, with capabilities depicted; (right) spray chamber installed in laboratory on optical table and behind operator safety barrier

New experiments were designed to characterize the fuel spray mixing and evaporation processes. A reference fuel injector with eight stepped holes, the Engine Combustion Network Spray G [2], was chosen for initial experiments because of the vast dataset developed for this particular injector and operating condition. Past work has shown that the interaction between plumes is complicated and difficult to predict [3]. Plumes may redirect from the manufactured drill angle, interact strongly, and cause the entire spray to collapse. The net effect is vastly different fuel delivery and wall impingement targeting depending upon the degree of interaction.

The manner of plume interaction and terminology for this process is depicted in Figure II.6.2. The plume cone angle may grow because of internal nozzle flow behavior, but it also responds to changes in gas temperature and pressure, as well as the fuel itself. The plume growth and air entrainment create intense aerodynamic forces that can redirect the entire plume far away from the drill angle. The resulting plume direction may change during the injection event [3], showing a sensitivity to the injection duration. CFD researchers that vary

either plume direction or plume cone angle find that varying the cone angle provides better overall agreement compared to the various experimental results, including gas and liquid velocity [3]. An experiment that could readily measure both the plume cone angle and plume direction would provide key information about the degree of interaction between plumes and how these parameters depend upon fuel properties and injection duration.

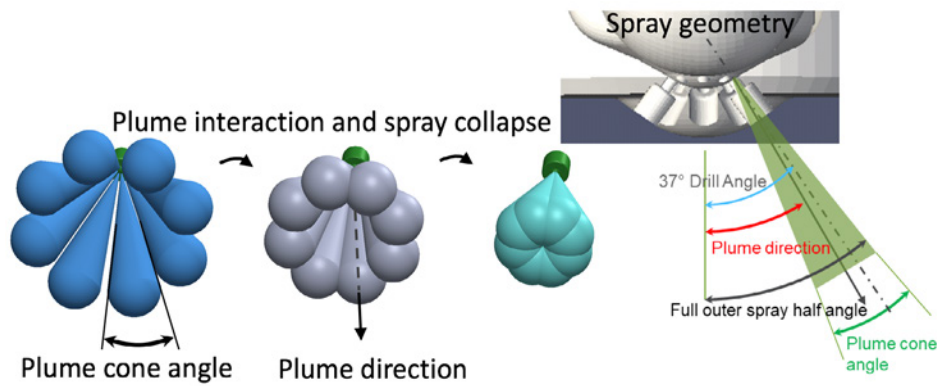


Figure II.6.2. Schematic illustrating the geometry of Spray G and the process of plume interaction and spray collapse

The experiment utilizes two different high-speed imaging diagnostics, both line-of-sight measurements. The first is diffused back-illumination imaging, applied to measure extinction from liquid. The second is schlieren imaging, applied to measure the outer envelope of the spray containing both liquid and vapor. The diffused back-illumination diagnostic is sensitive to only liquid extinction, rather than vapor-phase beam steering, by nature of the diffused lighting and large collection angle. The diagnostic is used to measure the maximum axial and radial liquid penetration, for example, which is directly related to in-cylinder wall wetting and film formation. But by performing measurement with different injector orientations, it is also possible to identify the plume center at planes at different axial distances away from the injector, and thus the plume direction. The technique is demonstrated using synthetic spray liquid volume fraction (LVF) data as shown in Figure II.6.3.

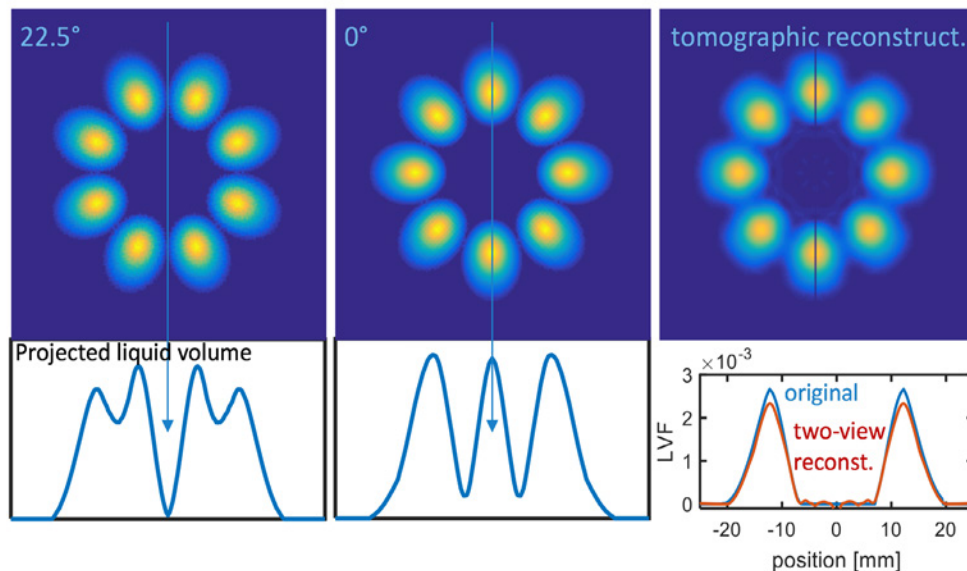


Figure II.6.3. (Top) LVF simulations at axial distance cut plane of $z = 15$ mm. Middle is with injector at 0° rotation; left at 22.5° rotation. Right is tomographic reconstruction at 0° rotation. (Bottom left, middle) Projected liquid volume, the integral of the liquid volume along a line of sight indicated at the top. (Bottom right) Profile of original LVF compared to tomographic reconstruction using projection data taken from only two views (0° and 22.5° rotation).

The synthetic LVF data is from Gaussian-shaped plumes directed at the drill angle of the nozzle (37°). Sampled on a plane at a fixed axial distance from the injector, z , the plumes appear skewed towards the centerline, but this is a consequence of the distance of the plume relative to the hole origin. As shown in Figure II.6.2, the left side of the plume (at a fixed z) has a shorter distance from the hole compared to the right side and will therefore appear more fuel-rich. The middle of Figure II.6.3 shows the LVF distribution with the injector oriented in the primary position at 0° rotation, where the entire spray is at its widest orientation. The left shows results with the injector in the secondary position at 0° rotation, where plume pairs are in direct alignment with each other and the total spray is at its thinnest width.

The bottom left and middle simulate what is measured by line-of-sight extinction imaging at these two orientations. Experimental measurements in these two orientations demonstrate that it is possible to extract a plume direction from the measurement [3,4], although the data are seriously limited with respect to the number of injections and operating conditions where the plumes are distinct from one another. Without the usual data limitations, it is possible to collect images for many injections at many orientations using the new high-throughput spray chamber. To determine the minimum number of acceptable injector rotations, projection data from only two different orientations (as shown) were utilized to apply tomographic reconstruction of the spray footprint. A linear weighting function was applied to create artificial projections based upon different injector orientations. For example, the projection at 11° rotation is the mean (equal weighting) of the two projections shown in Figure II.6.4, while the projection at 3° rotation is weighted 87% to that of the projection at 0° rotation and so forth.

The tomographic reconstruction using data from the two views given at the bottom right in Figure II.6.3 shows nice agreement for plume center location and width of the liquid region, albeit the peak LVF and sharpness of features are degraded. Ultimately, the reconstruction is acceptable despite using only two different projection views. This exercise demonstrates the potential to use high-quality liquid extinction data to more exactly define the plume position in three-dimensional space. By coupling this method to high-speed imaging with the injector at several rotation positions, the primary outcome is identification of the plume direction at every instant in time during an injection event, including time after the end of injection.

Extinction imaging provides a measurement of plume direction, but as mentioned above, the plume cone angle can be the catalyst for plume interaction and redirection, and it is critical for predictive CFD. Plume cone angle measurements are obtained using high-sensitivity schlieren imaging, as demonstrated in Figure II.6.4. These line-of-sight images show sensitivity to any refractive index gradient, including vaporized fuel or even shock waves propagating through the gas during the injection event. With the injector oriented at 0° rotation, the outer edges of plumes at the top or bottom of the images are exposed and distinct. In addition, the measurement is sensitive to vapor fuel to provide a true measurement of mixture fraction at the edge of the spray. If measuring only liquid, fuel-air mixtures at the periphery of the spray are not well represented, particularly for gasoline sprays at elevated temperature where fuel vaporization is rapid.

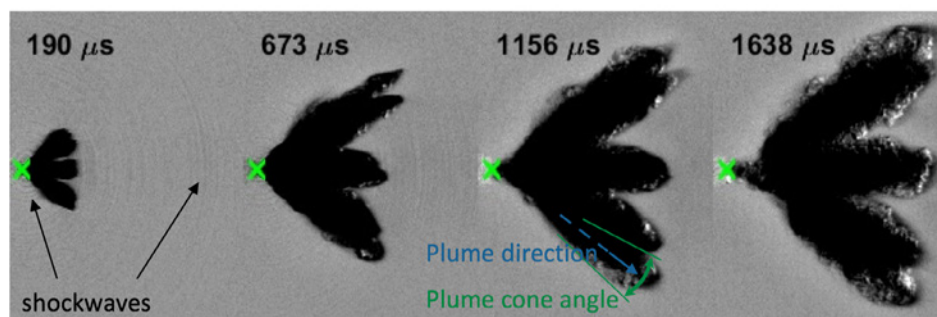


Figure II.6.4. Time sequence of schlieren images from the same injection. Spray G fuel injector with iso-octane fuel and 0.8 ms injection duration. Injector is oriented at 0° rotation in the continuous-flow chamber. Time given relative to the start of injection.

As depicted in Figure II.6.4, the exposed edge of the plume cone is measured with schlieren, which, combined with the plume-direction measurement obtained using other diffused back-illumination measurements, provides a measurement of the outer one-half of the plume cone angle. The measurement can be repeated for each plume by rotating the injector by 45° increments. Measurements are performed during injection as well as after the end of injection to characterize dynamics of plume interaction and vaporization after the end of injection or with multiple injections.

Conclusions

To provide fundamental understanding of fuel spray mixing with alternative Co-Optima target fuels, a new spray chamber and new optical diagnostics have been developed. The datasets for liquid penetration, plume direction, and plume cone angle provide key data needed to improve CFD modeling of direct-injection fuel sprays. This work hastens the optimization of fuels and engines for low-emission, high-efficiency technologies. Key activities for Fiscal Year 2018 included:

- Commissioning of a new high-temperature, high-pressure spray chamber facility with continuous-flow operation, capable of reproducing thermodynamic conditions at the start of injection for the entire engine operating cycle.
- Development of critical optical diagnostics for liquid penetration and motion of interacting plumes, including methods for tomographic reconstruction of plume position in three dimensions throughout the injection event.
- Detection of the spray vapor envelope for quantification of the plume cone angle, which has been identified as a key driver for plume interaction and redirection and of fundamental importance for CFD prediction.

Together, the new spray chamber and diagnostics for plume cone angle and plume direction provide a powerful diagnostic to assess the effects of fuel properties. The diagnostics are currently being applied and analyzed for Tier-3-selected Co-Optima fuels.

References

1. Meijer, M., B. Somers, J. Johnson, J. Naber, S.-Y. Lee, L.-M. Malbec, G. Bruneaux, L.M. Pickett, M. Bardi, R. Payri, and T. Bazyn. 2012. “Engine Combustion Network (ECN): Characterization and Comparison of Boundary Conditions for Different Combustion Vessels.” *Atom. Sprays* 22 (9): 777–806.
2. Engine Combustion Network data archive < <https://ecn.sandia.gov/gasoline-spray-combustion/target-condition/spray-g-operating-condition/>>, 2018.
3. Sphicas, P., L.M. Pickett, S. Skeen, J. Frank, T. Lucchini, D. Sinoir, G. D’Errico, K. Saha, and S. Som. 2017. “A Comparison of Experimental and Modeled Velocity in Gasoline Direct-Injection Sprays with Plume Interaction and Collapse.” *SAE Int. J. Fuels and Lubricants* 10 (1): 184–201.
4. Duke, D.J., A.L. Kastengren, K.E. Matusik, A.B. Swantek, C.F. Powell, R. Payri, D. Vaquerizo, L. Itani, G. Bruneaux, R.O. Grover, S. Parrish, L. Markle, D. Schmidt, J. Manin, S.A. Skeen, and L.M. Pickett. 2017. “Internal and Near Nozzle Measurements of Engine Combustion Network “Spray G” Gasoline Direct Injectors.” *Experimental Thermal and Fluid Science* 88: 608–621.

Acknowledgements

The Principal Investigator acknowledges Scott A. Skeen for his contributions to this report and the project. We thank Tim Gilbertson, Alberto Garcia, Nathan Harry, Sam Fairbanks, Chris Ingwerson, Aaron Czeszynski, Laurie Bell, Paul Abers, and Joonsik Hwang for their extraordinary efforts for the design and construction of the laboratory. The study was performed at the Combustion Research Facility. Sandia National Laboratories is a multi-mission laboratory managed and operated by National Technology and Engineering Solutions for Sandia LLC, a wholly owned subsidiary of Honeywell International, Inc., for the U.S. Department of Energy’s National Nuclear Security Administration under contract DE-NA0003525.

II.7 Low-Temperature Gasoline Combustion (LTGC) Engines: Fuel Effects and Fuel Co-Optimization (Sandia National Laboratories)

John E. Dec, Principal Investigator

Sandia National Laboratories
MS 9053, P.O. Box 969
Livermore, CA 94550
E-mail: jedec@sandia.gov

Kevin Stork, DOE Technology Development Manager

U.S. Department of Energy
E-mail: Kevin.Stork@ee.doe.gov

Start Date: October 1, 2017	End Date: September 30, 2018	
Project Funding: \$170,000	DOE share: \$170,000	Non-DOE share: \$0

Project Introduction

Engines using low-temperature gasoline combustion (LTGC), including homogeneous charge compression ignition (HCCI), have a strong potential to reduce fuel costs and CO₂ emissions by 30% or more over current spark ignition (SI) engines due to their high thermal efficiencies and very low NO_x and particulate emissions. Because the LTGC combustion process is largely controlled by the chemical kinetics of autoignition, the fuel properties are closely coupled to the engine performance, and co-optimization of LTGC engines and their fuels has a strong potential to improve performance. Toward this larger goal, it is critical to understand fuel autoignition characteristics under LTGC-like conditions, including the temperatures, pressures, and high dilution levels (either lean or dilute with exhaust gas recirculation/residuals) typical of these engines. When operated in a well-mixed LTGC mode (i.e., HCCI), the Sandia LTGC research engine, with its precise controls, provides an excellent platform for determining these required fuel autoignition characteristics. LTGC operating conditions are also similar to those proposed for other advanced compression ignition (ACI) concepts and for the low-temperature combustion in multi-mode LTGC/SI engines for light-duty applications. These LTGC/HCCI studies also have relevance to fuel performance with respect to avoiding knock in SI engines [1].

For these reasons, fundamental fuel autoignition studies have been conducted for well-premixed LTGC over a wide range of intake temperatures and pressures, and several fuels have been investigated to better understand the effects of various classes of hydrocarbons and to determine whether the standard gasoline autoignition metrics (research octane number [RON] and motor octane number [MON]) are adequate for LTGC/ACI engines, or if additional autoignition metrics will be required. One of the two main efforts for Fiscal Year 2018 was focused on evaluating the LTGC performance of the Co-Optima core fuels and comparing their performance against regular gasoline. The core fuels have been designed to determine whether differences in fuel composition affect the autoignition if the RON and MON values are the same. Thus, the core fuels tested in this study all have significantly different compositions but the same high RON \approx 98 and a high octane sensitivity ($S = \text{RON} - \text{MON} \approx 10.5$), as desirable for boosted SI engines. Understanding the performance of these fuels for LTGC operation is important for multi-mode engines that use LTGC at low-to-intermediate loads and switch to boosted SI for high loads, and also for full-time LTGC for medium- and heavy-duty applications that would need to operate on gasoline from the same pump. The second objective for Fiscal Year 2018 was to investigate the potential of developing new, more accurate surrogate blends for these fuels for use in computational analyses of both LTGC/ACI and SI engines. These new surrogate compositions are based on the detailed hydrocarbon analysis (DHA) of each fuel, and comparisons against the well-characterized fully premixed experimental LTGC engine data from this study showed them to be much more accurate than previously available surrogates.

Objectives

Overall Objectives

- Provide fundamental understanding of the autoignition behavior of fuels at conditions relevant to LTGC/ACI operation to support the co-development of LTGC/ACI engines and fuels that better optimize their performance, including:
 - The performance of high-RON, high-S fuels for LTGC operation as part of a multi-mode strategy that switches to boosted SI at high loads, for light-duty applications
 - Determining the fuel properties required for co-optimization of full-time LTGC for medium- and heavy-duty applications
- Provide data for chemical-kinetic model and computational surrogate development and validation

Fiscal Year 2018 Objectives

- Acquire LTGC performance data for the high-cycloalkane fuel from the Co-Optima core fuels matrix over the suite of previously established LTGC operating conditions for fuel evaluation
- Acquire similar LTGC performance data for a second regular E10 (gasoline containing 10% ethanol) reference fuel
- Compare the autoignition reactivity of the high-cycloalkane fuel to that of the E30 (gasoline containing 30% ethanol) and high-aromatic Co-Optima fuels and to both the original regular E10 (RD5-87A) and second regular E10 (RD5-87B) fuels over a range of conditions
- Determine the validity/usefulness of the octane index as a means of correlating the autoignition behavior of these fuels and other fuels for LTGC engine operation
- Obtain ϕ -sensitivity and intermediate-temperature heat release data for the high-cycloalkane Co-Optima fuel and RD5-87B fuel and compare with previous data for the E30, high-aromatic, and RD5-87A fuels
- Develop more accurate surrogate blends for computational simulations of the high-cycloalkane, E30, and high-aromatic Co-Optima core fuels, and validate them against fully premixed LTGC/HCCI engine data over a range of intake temperatures and pressures
- Support the development of a merit function for ACI fuels

Approach

The performance of these fuels was evaluated in the Sandia LTGC Engine Laboratory using the all-metal, single-cylinder LTGC research engine (displacement = 0.98 L) fitted with a 14:1 compression-ratio piston that provides an open combustion chamber. This facility allows operation over a wide range of conditions, and it has been designed to provide precise control of virtually all operating parameters for well-characterized experiments.

To determine the autoignition characteristics of the high-cycloalkane Co-Optima fuel and the RD5-87B regular E10 fuel, the engine was operated in a well-premixed HCCI mode across a wide range of intake temperatures ($T_{in,s}$) at an intake pressure (P_{in}) of 1.0 bar and for $P_{in,s}$ from 1.0 bar to 2.4 bar absolute. Additionally, some data were acquired using early direct-injection fueling to investigate the effects of differences in the heat of vaporization between fuels. Data were also acquired to measure key parameters relevant to LTGC operation, including the sensitivity of autoignition to variations in the local fuel/air equivalence ratio within the cylinder (ϕ -sensitivity) and the amount of intermediate-temperature heat release. These datasets result in a fairly large engine-operation test matrix for each fuel, and they cover the same range of conditions as previous datasets for the E30, high-aromatic, and RD5-87A fuels.

New computational surrogate blends were developed for each fuel based on their DHAs, with representative compounds being included in the surrogate for each hydrocarbon class present in the fuel, including

cycloalkanes, which were not included in previous surrogates. Concentrations of these representative compounds were set to match those of their respective classes of hydrocarbons in the DHAs. Also, multiple n-alkane and iso-alkane compounds were included to match those of the real fuel because reactivity can vary significantly between shorter- and longer-chain n- and iso-alkanes. CHEMKIN simulations using the latest detailed chemical-kinetic mechanism from Lawrence Livermore National Laboratory were conducted to validate these surrogates against well-premixed LTGC engine data over a range of conditions.

Results

The Co-Optima core fuels test matrix was designed to determine whether the gasoline SI autoignition metrics, RON and MON, are adequate for predicting autoignition in LTGC engines and knock in boosted SI engines for fuels with widely varying composition. To this end, the high-cycloalkane fuel tested this year and the E30 and high-aromatic fuels tested previously have very different compositions but nearly identical high RON (RON \approx 98) and high octane sensitivity ($S = \text{RON} - \text{MON} \approx 10.5$) values that were chosen because they are advantageous for boosted SI engines. Figure II.7.1 shows a comparison of the autoignition reactivity of these three Co-Optima core fuels and the two regular E10 gasolines for well-premixed, naturally aspirated operation ($P_{\text{in}} = 1.0$ bar) in the LTGC engine at an equivalence ratio (ϕ) of 0.4. At these conditions, intake heating was required to achieve autoignition for all the fuels tested, and for each fuel, T_{in} was swept over a wide range to shift combustion phasing (i.e., the 50% burn point [CA50]) from being highly retarded to overly advanced. As can be seen, for the high-cycloalkane fuel, the T_{in} required for a given CA50 is intermediate between the $T_{\text{in,s}}$ for the E30 and high-aromatic fuels, indicating that its autoignition reactivity is intermediate at this operating condition, even though all three fuels have the same RON and S. Figure II.7.1 also shows that the $T_{\text{in,s}}$ required for the E30 fuel are closely bracketed by the $T_{\text{in,s}}$ of the two regular E10 gasolines, RD5-87A (acquired previously) and RD5-87B (acquired this year). Thus, the autoignition reactivity of E30 is similar to that of fuels with RON values of 92.0 and 90.6, at these naturally aspirated conditions, despite it having a RON of \sim 98. Taken together, these comparisons show that RON and S are not sufficient to determine the autoignition quality of these fuels for LTGC or LTGC-like ACI engines at these operating conditions.

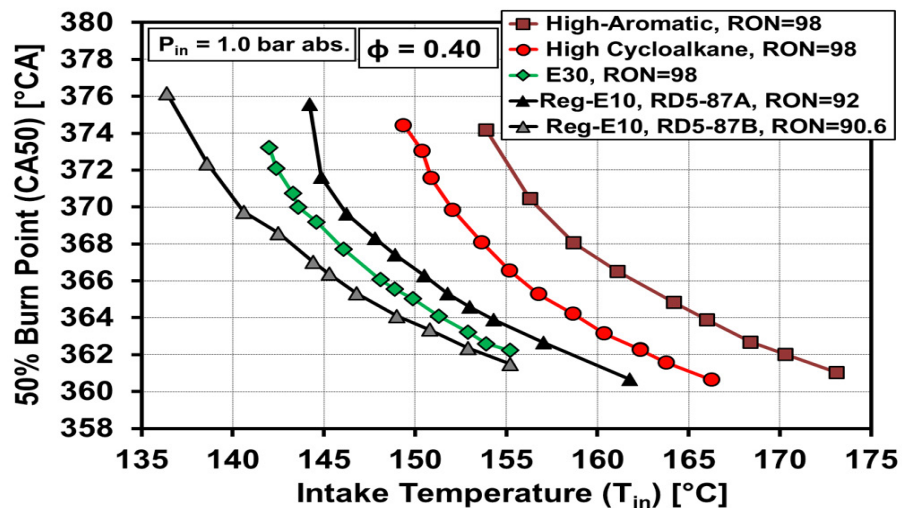


Figure II.7.1. Combustion phasing (CA50) as a function of intake temperature (T_{in}) for various fuels for fully premixed LTGC operation at $P_{\text{in}} = 1.0$ bar, $\phi = 0.4$, 1,200 rpm. For the scale on the y-axis, 0 °CA = top dead center (TDC)-intake and 360 °CA = TDC-compression.

The octane index (OI) has been suggested as a method for extending the use of RON and MON to determine the autoignition quality of fuels under LTGC conditions [2]. Accordingly, the $\text{OI} = \text{RON} - K \cdot S$ (where S is the octane sensitivity and K is an empirically determined coefficient that varies with operating conditions) was computed for the data in Figure II.7.1 combined with data for some other fuels at this same operating condition. Even with K adjusted for the best fit, the OI gives a poor correlation for these data, resulting in an $R^2 = 0.515$, as might have been expected since the three Co-Optima fuels have significantly different CA50s

for the same T_{in} in spite of their nearly identical RON and S values. This shows that even if RON and S are adapted using the OI, they are not adequate to predict LTGC autoignition at this operating condition.

It is also important to understand the effect of intake pressure boost on the autoignition reactivity of fuels for both LTGC and advanced SI engines. Figure II.7.2 shows the effect of increased P_{in} (simulated turbo or super charging) on the autoignition reactivity for the same five fuels shown in Figure II.7.1. In this figure, the autoignition reactivity metric is the bottom dead center temperature at the end of the intake stroke (T_{BDC}) required to obtain autoignition with a 10% burn point timing (CA10) of ≈ 368.7 degrees crank angle ($^{\circ}CA$) (continuous lines) or 371.5 $^{\circ}CA$ (dashed lines). A more retarded CA10 was required for the higher boost pressures to prevent engine knock. The reactivity of all the fuels increases with increased P_{in} , as evident from the lower required T_{BDC} s. For the two regular E10 fuels, a sharp increase in reactivity occurs as P_{in} is increased above 130 kPa. Examination of the heat release rates shows that this is due to the onset of low-temperature heat release as the increased pressure shifts the fuel into the negative temperature coefficient region.

However, this behavior is not seen for the high-cycloalkane and E30 Co-Optima fuels, and it occurs only weakly for the high-aromatic fuel (between $P_{in} = 180$ and 200 kPa), because these fuels have a reduced propensity for low-temperature heat release reactions due to their higher octane sensitivity ($S \approx 10.5$) and higher RON (~ 98). The reactivity of these three Co-Optima fuels still increases with boost, but it occurs more progressively, and T_{BDC} doesn't reach the 105 – $110^{\circ}C$ range until $P_{in} = 200$, 220 , or 240 kPa for the E30, high-aromatic, and high-cycloalkane fuels, respectively. These results demonstrate why these high-RON, high-S fuels are beneficial for allowing higher boost without knock in SI engines, and why they require less exhaust gas recirculation to control autoignition in boosted LTGC engines. Although Figure II.7.2 shows that the general trends in T_{BDC} with boost are similar for the three Co-Optima fuels, E30 is consistently more reactive (lower T_{BDC}) across the range of P_{in} s presented, and it reaches $T_{in} = 60^{\circ}C$ (the minimum- T_{in} limit for premixed fueling) at a lower P_{in} than the other two Co-Optima fuels. At naturally aspirated and low-boost conditions, the reactivity of the high-cycloalkane fuel is intermediate between the E30 and high-aromatic fuels, in agreement with the data in Figure II.7.1. However, the high-cycloalkane fuel shows the least reactivity increase with increased intake pressure, which causes it to cross the high-aromatic curve, so that for $P_{in} \geq 180$ kPa, it is the least reactive fuel. The low autoignition reactivity of the high-cycloalkane fuel at high boost pressures indicates that it would likely have a low propensity for knock (i.e., end-gas autoignition) under boosted SI operation, making it a very good fuel for those engines.

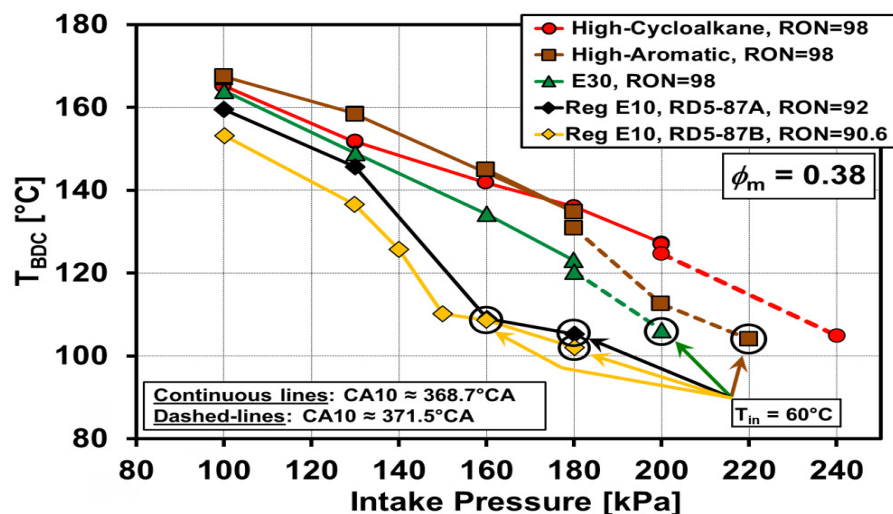


Figure II.7.2. T_{BDC} required for a CA10 of 368.7 $^{\circ}CA$ (solid lines) or 371.5 $^{\circ}CA$ (dashed lines) as a function of P_{in} for the Co-Optima high-cycloalkane, high-aromatic, and E30 fuels, and for the two regular E10 fuels. $\phi_m = 0.38$, $1,200$ rpm. All fuels are fully premixed (i.e., HCCI), which requires $T_{in} \geq 60^{\circ}C$ to prevent fuel condensation in the intake system. The points where T_{in} reaches this minimum value of $60^{\circ}C$ are noted on the plot.

Modeling of engine combustion requires accurate chemical-kinetic mechanisms combined with appropriate surrogate blends to represent real distillate fuels. These computational surrogates contain only a limited number of species (typically 5–10), and they are necessary because including the great number of species present in real fuels would make the computational cost of modeling them prohibitively high. Well-premixed LTGC engine data are completely kinetically controlled and provide a very good database for validating chemical-kinetic mechanisms and surrogate blends. To perform these validations, the single-zone internal combustion engine module of the CHEMKIN software package was applied for three reasons: (1) computations with detailed chemical-kinetic mechanisms require relatively little time to execute, (2) it uses the slider-crank formula to vary the reactor volume in the same manner as the combustion chamber of an internal combustion engine, and (3) it contains a submodel to determine the average heat transfer and to account for its effect on the temperature and pressure history of the charge. Using this approach, a series of initial tests was conducted that confirmed the need to account for the heat transfer and that the most recent detailed chemical-kinetic mechanism for gasoline from Lawrence Livermore National Laboratory, made available to Co-Optima participants in December 2017, gives significantly better results than the previous version. Accordingly, this recent kinetic mechanism (containing 2,878 species and 12,839 reactions) and the heat transfer submodel were used in all subsequent tests of the surrogate blends presented below.

After completing these initial tests, the CHEMKIN internal combustion engine module was applied to investigate the performance of the previously existing surrogate blends developed by Lawrence Livermore National Laboratory (referred to as S1 surrogates), which were based mainly on matching the RONs, MONs, H/C ratios, and stoichiometric air/fuel ratios of the various fuels. Figure II.7.3 presents a comparison of the well-premixed, naturally aspirated ($P_{in} = 1.0$ bar) experimental data from Figure II.7.1 for the three Co-Optima fuels and RD5-87A (solid lines and square symbols) with the computational results using the existing S1 surrogates (dotted lines and triangle symbols), and with computational results using new surrogate blends developed under the current project (referred to as S2 surrogates) as discussed below (dashed lines and circle symbols). In this plot, the data from Figure II.7.1 have been re-plotted in terms of T_{BDC} on the x-axis rather than T_{in} , to facilitate comparison with model results. As can be seen, computations using the existing S1 surrogates match the general trends in the experimental data, but they show significant discrepancies at some conditions. In particular, they overpredict the reactivity of the fuels (i.e., CA50s are too advanced) at the lower T_{BDC} s of each sweep, with the error being especially large for the high-aromatic fuel, where the surrogate gives a CA50 that is 5 °CA advanced from the experimental value for $T_{BDC} = 445$ K.

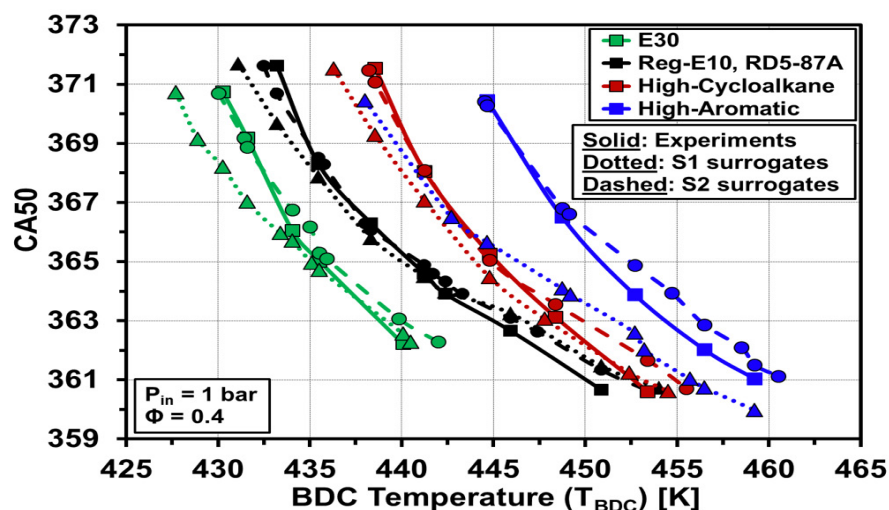


Figure II.7.3. Comparisons of CA50 as a function of T_{BDC} for computational results using the S1 and S2 surrogates with experimental data at $P_{in} = 1.0$ bar for the E30, high-cycloalkane, and high-aromatic Co-Optima fuels and the RD5-87A regular gasoline. $\phi = 0.4$, 1,200 rpm.

Because of these discrepancies with the S1 surrogates at $P_{in} = 1.0$ bar and even greater discrepancies for intake-boosted conditions presented below, new S2 surrogate formulations were developed for the E30, high-cycloalkane, and high-aromatic Co-Optima fuels based on the actual composition of these fuels as determined from their DHAs. This surrogate development method follows the same approach recently applied with good success to RD5-87A (regular E10) as part of our core-program research [3]. For these Co-Optima fuels, making S2 surrogates that closely matched the DHAs required adding one or two additional species and making some significant adjustments to the concentrations of the various species, compared to the respective S1 surrogates. The resulting S2 surrogates contain molecules representing all the hydrocarbon classes (n-alkanes, iso-alkanes, cyclo-alkanes, aromatics, olefins, and ethanol), and they more correctly account for the molecular size distribution of the n-alkanes and iso-alkanes. As Figure II.7.3 shows, computations with these new S2 surrogates match very closely with the experimental data for all the fuels, particularly for CA50s ≥ 365 °CA, which are the CA50s of interest for LTGC engines, because the engine starts to knock as CA50 is advanced earlier than ~ 365 °CA. The largest improvement over the S1 surrogate is for the high-aromatic fuel, but the S2 surrogates give significant improvements for the other fuels as well.

The performance of the S1 and S2 surrogates was also tested for intake pressures up to 2.4 bar absolute. Figure II.7.4 compares the results of CHEMKIN simulations using the S1 and S2 surrogates with experimental data for the Co-Optima high-aromatic (Figure II.7.4a) and high-cycloalkane (Figure II.7.4b) fuels. For both fuels, the autoignition reactivity increased with P_{in} , resulting in lower required T_{BDC} s, as was observed in Figure II.7.2. However, for the experimental high-aromatic data in Figure II.7.4a, the T_{BDC} at each P_{in} was adjusted to obtain a ringing intensity (RI, defined in Eng 2002 [4]) of 5 MW/m² (which corresponds to the most advanced CA50 without knock in this LTGC research engine [5]), rather than holding CA10 constant as was done for the data in Figure II.7.2. The experimental data for the high-cycloalkane fuel in Figure II.7.4b are the same as in Figure II.7.2, with CA10 = 368.7 °CA except for $P_{in} = 2.4$ bar, where CA10 = 371.5 °CA. For both fuels, T_{BDC} s for the simulations were adjusted until CA50 matched that of the experiments, so the difference between the T_{BDC} s of the simulations and the experiments provides a metric for the accuracy of the simulations.

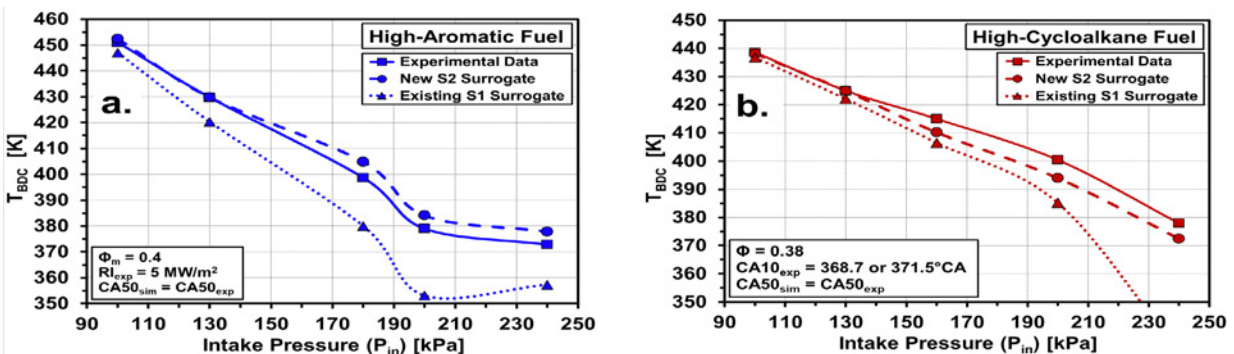


Figure II.7.4. Comparison of the T_{BDC} values required for simulations with the S1 (dotted lines) and S2 (dashed lines) surrogates to match the CA50 values of the experimental data (solid lines) for intake pressures from 1.0 bar to 2.4 bar absolute. Figure II.7.4a shows results for the high-aromatic fuel with RI held constant at 5 MW/m², and Figure II.7.4b shows the high-cycloalkane fuel for which CA10 = 368.7 °CA except for $P_{in} = 2.4$ bar, where CA10 = 371.5 °CA.

As Figure II.7.4a shows, the existing S1 surrogate for the high-aromatic fuel overpredicts the autoignition reactivity, so T_{BDC} values below those of the experiment were required to compensate. The S1 surrogate is already somewhat overly reactive at $P_{in} = 1.0$ bar (in agreement with Figure II.7.3), and this discrepancy increases significantly with increased P_{in} . Detailed examination of the heat release rates shows that this occurs because the S1 surrogate produces an overly strong intermediate-temperature heat release for $P_{in} \leq 180$ kPa and both an overly strong intermediate-temperature heat release and overly strong low-temperature heat release for $P_{in} > 180$ kPa, which drive the charge more quickly into the main hot ignition. In contrast, the new S2 surrogate, which more closely matches the actual fuel composition, provides a close match with the experiment for all the P_{in} s examined. For the high-cycloalkane fuel, shown in Figure II.7.4b, the S1 surrogate

is only slightly over-reactive for $P_{in} \leq 130$ kPa, but its deviation from the experiment becomes progressively greater as P_{in} is increased from 130 kPa to 200 kPa. For $P_{in} > 200$ kPa, the reactivity of the S1 surrogate increases rapidly, leading to a T_{BDC} deviation of 46 K at $P_{in} = 2.4$ bar. The S2 surrogate gives a much closer match to the experiment across the P_{in} sweep. For both this high-cycloalkane fuel and the high-aromatic fuel, the T_{BDC} s are nearly identical to the experimental values for $P_{in} \leq 130$ kPa, and they remain within 6 K of the experimental values for all P_{in} s examined. Similar improvements in the match of CHEMKIN simulations with the experiments for the S2 surrogates were also found for the E30 and RD5-87A fuels (RD5-87A results are presented in Dec 2018 [3]).

Conclusions

- The autoignition characteristics of the high-cycloalkane Co-Optima fuel and a second regular E10 gasoline (RD5-87B) have been investigated for a wide range of operating conditions to determine their performance relative to previous data for the E30 and high-aromatic Co-Optima fuels and previous data for a different regular E10 gasoline (RD5-87A).
- For naturally aspirated operation ($P_{in} = 1.0$ bar), data acquired for a wide range of intake temperatures showed the following:
 - o Autoignition reactivity of the high-cycloalkane fuel is intermediate between the reactivity of the high-aromatic and E30 fuels, which are the least-reactive and one of the most-reactive fuels tested, respectively. This occurs even though all three fuels have the same RON of ~ 98 and $S \approx 10.5$.
 - o The newer RD5-87B regular E10 gasoline is more reactive than the previously tested RD5-87A regular E10, in agreement with its lower RON of 90.6 compared to $RON = 92.0$ for RD5-87A.
 - o Autoignition reactivity of the E30 Co-Optima fuel ($RON \approx 98$) falls between that of the two regular E10 fuels that have RONs of 90.6 and 92.0.
 - o The octane index ($OI = RON - K*S$), with K adjusted for the best fit to the $P_{in} = 1.0$ bar data, gives only a poor correlation with the LTGC autoignition data at this condition, $R^2 = 0.515$.
 - o Overall, these results show that RON, MON, S, and OI are not adequate autoignition metrics for LTGC. The only correlation was that the relative reactivity of the two regular E10 gasolines, which have similar compositions, corresponded to their relative RON values.
- With increased intake pressure (simulated turbocharging), all fuels showed increased autoignition reactivity, but the increase was much more gradual for the $RON \approx 98$ Co-Optima fuels than for the regular E10 fuels due to their much lower propensity for low-temperature heat release.
 - o Although the trends in increased reactivity with intake-pressure boost are similar for the three Co-Optima fuels, E30 is consistently the most reactive of the three across the range of intake pressures investigated.
 - o The high-cycloalkane fuel shows the least reactivity increase with increased intake pressure. As a result, it is more reactive than the high-aromatic fuel at naturally aspirated and low-boost conditions, but for $P_{in} \geq 180$ kPa, it is the least reactive fuel tested. This suggests that it might make a very good fuel for boosted SI engines.
- The high-cycloalkane fuel has low intermediate-temperature heat release, and its autoignition is little affected by variations in equivalence ratio (i.e., it is not ϕ -sensitive) except at high boost pressures ($P_{in} \geq 2.0$ bar). As a result, it is not a good fuel for LTGC operation.
- The well-characterized measurements acquired for these studies provide a very good database for the validation of chemical-kinetic mechanisms and computational surrogate blends. Comparing computational results using the latest detailed chemical-kinetic mechanism from Lawrence Livermore National Laboratory with these data showed:

- o The computational surrogate blends existing prior to this study (based on matching RON, MON, H/C ratio, and the stoichiometric air/fuel ratio) do not match the data well, particularly at higher intake-boost pressures and for lower intake temperatures at $P_{in} = 1$ bar.
- o New surrogate blends were developed as part this project for the E30, high-cycloalkane, and high-aromatic fuels. Computations using these new surrogates (which are based on the actual composition of these fuels as determined from their DHAs) closely matched the experimental LTGC/HCCI engine data.

Key Publications

1. Dec, J.E., G. Gentz, and D. Lopez-Pintor. 2018. "Performance of the High-Cycloalkane RON98 Fuel." GM/Sandia Working Group Meeting, February 16, 2018.
2. Dec, J.E., and W.J. Pitz. 2018. "Medium/Heavy-Duty Kinetically Controlled ACI." Co-Optima All Hands Meeting, Argonne National Laboratory, March 21–22, 2018.
3. Lopez-Pintor, D., and J.E. Dec. 2018. " Φ -Sensitivity for LTGC/ACI Engines: Understanding the Fundamentals and Tailoring Fuel Blends to Maximize this Property." Co-Optima All Hands Meeting, April 18, 2018.
4. Arienti, M., J.E. Dec, C.J. Mueller, L.M. Pickett, and C.F. Powell. 2018. "Co-Optima: Mixing-Controlled and Kinetically Controlled Compression-Ignition Combustion and Spray Research." Team Report for the DOE Annual Merit Review, Office of Vehicle Technologies, FT056, June 2018.
5. Dec, J.E., and D. Lopez-Pintor. 2018. " Φ -Sensitivity for LTGC/ACI Engines: Understanding the Fundamentals and Tailoring Fuel Blends to Maximize this Property." Co-Optima High Performance Fuels Team Meeting, July 25, 2018.
6. Lopez-Pintor, D., J.E. Dec, and G. Gentz. 2018. "Development and Validation of Improved Computational Surrogates for Distillate Fuels in LTGC Engines." AEC Working Group Meeting, Detroit, MI, August 14–17, 2018.
7. ASME Soichiro Honda Medal: Dec, J.E., November 2017.

References

1. Yang, Y., J.E. Dec, M. Sjöberg, and C. Ji. 2015. "Understanding Fuel Anti-Knock Performances in Modern SI Engines Using Fundamental HCCI Experiments." *Combustion and Flame* 162: 4006–4013.
2. Risberg, P., G. Kalghatgi, and H.-E. Ångström. 2003. "Autoignition Quality of Gasoline-Like Fuels in HCCI Engines." SAE Technical Paper 2003-01-3215, doi:10.4271/2003-01-3215.
3. Dec, J.E. 2018. "Low-Temperature Gasoline Combustion (LTGC) Engine Research." U.S. Department of Energy, Office of Vehicle Technologies 2018 Annual Merit Review Presentation for Project ACS004, Washington D.C, June 2018.
4. Eng, J.A. 2002. "Characterization of Pressure Waves in HCCI Combustion." SAE Technical Paper 2002-01-2859, doi:10.4271/2002-01-2859.
5. Dernotte, J., J.E. Dec, and C. Ji. 2015. "Energy Distribution Analysis in Boosted HCCI-like / LTGC Engines – Understanding the Trade-offs to Maximize the Thermal Efficiency." *SAE Int. J. Engines* 8 (3): 956–980, doi:10.4271/2015-01-0824.

II.8 Thermophysical Property Impact on Spray Formation (Sandia National Laboratories)

Marco Arienti, Principal Investigator

Sandia National Laboratories
7011 East Avenue
Livermore, CA 94550
E-mail: marient@sandia.gov

Kevin Stork, DOE Technology Development Manager

U.S. Department of Energy
E-mail: Kevin.Stork@ee.doe.gov

Start Date: September 15, 2017	End Date: September 15, 2018	
Project Funding (FY18): \$345,000	DOE share: \$345,000	Non-DOE share: \$0

Project Introduction

Understanding the impact of new fuels on engine performance requires in-depth analysis of the charge formation process and of its dependence on thermophysical properties such as viscosity, surface tension, and heat of vaporization. The project aims to quantify the sensitivity of the gasoline direct injection (GDI) primary atomization process to fuel blend properties while generating a reference database of the near-field fuel spray for integration with engine-level computational fluid dynamics (CFD) simulation tools.

Objectives

In order to expand advanced compression ignition operating range, the project will provide guidance on the suitability of new fuel candidates as drop-in replacements for GDI engines by reaching the following objectives.

- Demonstrate a predictive capability for spray and mixture formation that can support combustion strategies requiring control of fuel stratification
- Quantify impact on charge preparation in terms of thermophysical properties of blends with high levels of ethanol
- Capture effects linked to transient operation of the fuel injector, particularly filming/dribbling tendencies; these processes are identified as sources of incomplete evaporation and suboptimal combustion
- Generate a reference database of the near-field fuel spray for integration with engine-level CFD simulation tools

Fiscal Year 2018 Objectives

- Demonstrate the value of high-resolution CFD simulation and develop analysis methodologies to differentiate composition-dependent effects (as opposed to the current empirical/calibrated spray models)
- Test new cavitation model and investigate modes of cavitation (bulk vs. wall cavitation) for a specific GDI configuration

Approach

A new computational approach was introduced to Co-Optima in 2018 to investigate internal injector flow dynamics and the early stages of primary atomization in multi-component fuels. This approach is embodied by the multiphase CFD research code combined level-set volume of fluid (CLSVOF) [1,2]. The high-performance computing architecture of the code is maintained by the Center for Computational Sciences

and Engineering of Lawrence Berkeley National Laboratory; the core multiphase algorithms were developed at Florida State University. Because it includes the injector's geometry and it captures the fuel–liquid interface, this computational approach is the most accurate for evaluating charge preparation [3]. Co-Optima simulations are carried out on Sandia National Laboratories' Capacity Clusters in New Mexico, on Peregrine (Argonne National Laboratory), and at the Combustion Research Facility cluster in California. Details of the injector geometry and validation data, including fuel density and spray size distribution, are obtained from X-radiography scans at the Advanced Photon Source facility at Argonne.

Results

- Increased accuracy of run-time thermodynamic state calculations of mixed state (vapor and liquid) for a multi-component fuel
- Successfully tested the coupling between cavitation model and interface capturing
- Completed Spray G (eight holes, GDI [4]) simulation using National Renewable Energy Laboratory's four-component blendstock for oxygenate blending (BOB) surrogate; spray characteristics are being compared to the baseline simulation with iso-octane

In the case of CFD simulation of a multi-component fluid, it is of particular importance to correctly determine the saturation boundaries at the thermodynamic conditions of every computational cell. In addition to temperature, saturation curves depend on the composition of the fuel blend, making tabulation cumbersome. Saturation boundaries can be evaluated by iteration under the constraint of equal pressures and equal Gibbs energies of the two phases. In this scenario, increased accuracy is obtained by dynamically linking the CLSVOF code to the Reference Fluid Thermodynamic and Transport Properties Database (REFPROP) library of National Institute of Science and Technology (NIST) [6]; the thermophysical properties of the fuel blend are then obtained in a computational cell as a function of the Helmholtz energy and using mixture rules of non-ideal fluids.

The most salient algorithm introduced in the code is the determination of temperature and phase composition given the density and internal energy of the computational cell. This problem is solved by first assuming the cell state corresponds to single phase, then by comparing the input density with the saturated density at that estimated temperature. If the first is lower than the latter, then the two-phase composition is calculated by the more expensive but general two-phase REFPROP subroutine.

In general cavitation models, only liquid and vapor phases of one species are considered, whereas the application to spray formation (atomization) problems requires accounting for the non-condensable gas phase. In the approach developed for Co-Optima, when the fluid pressure equals the saturation pressure of the mixture, liquid and vapor phases are allowed to coexist under the assumption of thermodynamic equilibrium. At the same time, the liquid surface is discretized with the CLSVOF interface-capturing method that avoids numerical diffusion while still allowing physical diffusion between different species in the gas. With this capability in place, one can study the effect of cavitation on primary atomization. Figure II.8.1 (left panel) illustrates the setting of the experiments by Biçer and Sou [5] that were used to test this concept. As the pictures from the experiment suggest, cavitation takes place in the recirculation zone past the sharp inlet of the nozzle. The repeated shedding of the cavitation cloud observed in the experiment is reproduced in the calculation (Figure II.8.1, right panels); this is an important result because of the effect it might have on the liquid jet trajectory outside of the injector. A quantitative comparison with experimental measurements is discussed in a forthcoming paper.

The Spray G simulations include detailed features of the eight holes and their counterbores obtained by X-ray tomography at Argonne National Laboratory. The smallest resolution of the inner walls from X-ray tomography is 1.7 μm , which allows the emergence of details of surface roughness, as shown in Figure II.8.2. Nominally, the injector's hole diameter is 165 μm , with length-to-diameter ratio of 1.4 and drill angle of 37° [4]. An embedded boundary method based on the level-set function is used to translate the nozzle geometry into the data structure of CLSVOF. Pressure boundary conditions are applied at the injector's inlet ($P_{\text{in}} = 200$ bar) and at the free outer boundaries ($P_{\text{out}} = 6$ bar).

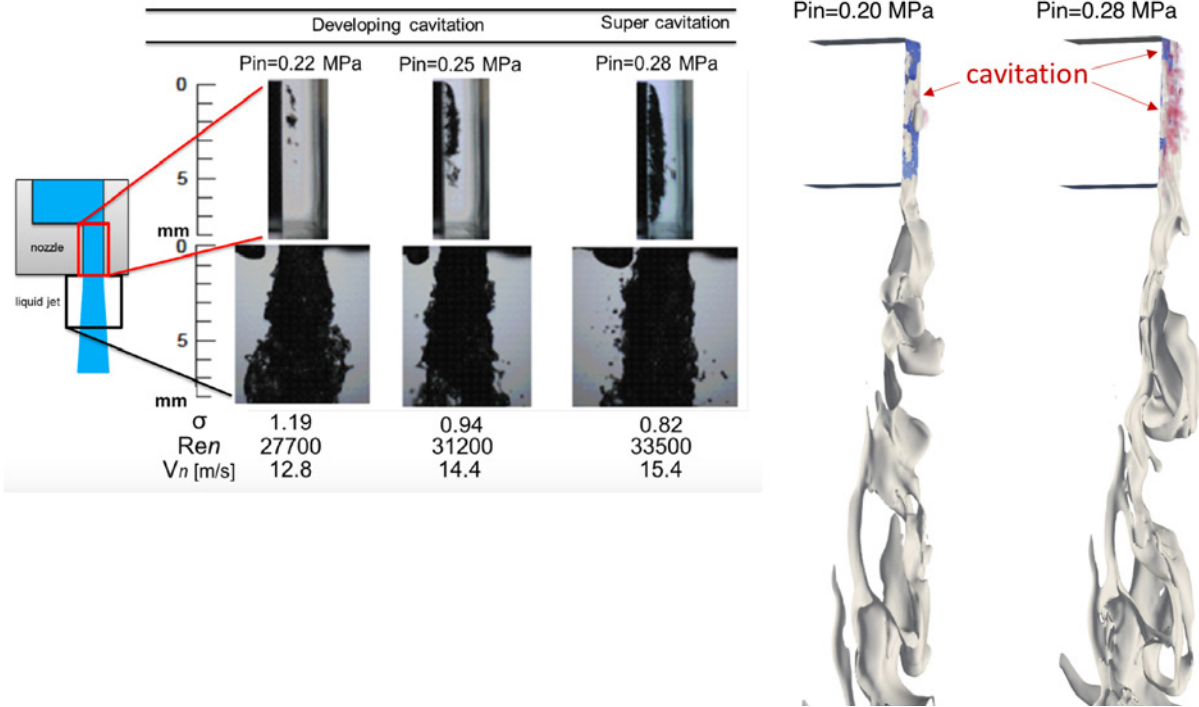


Figure II.8.1. Cavitation interaction with time-accurate, resolved, liquid surface dynamics. Shown from left to right: a schematic of the experiment [5]; three snapshots at increasing injection pressure from the experiments; and the corresponding CLSVOF simulations, where the vapor cloud due to cavitation is marked in red. Hydraulic flipping is intermittently observed in the simulation.

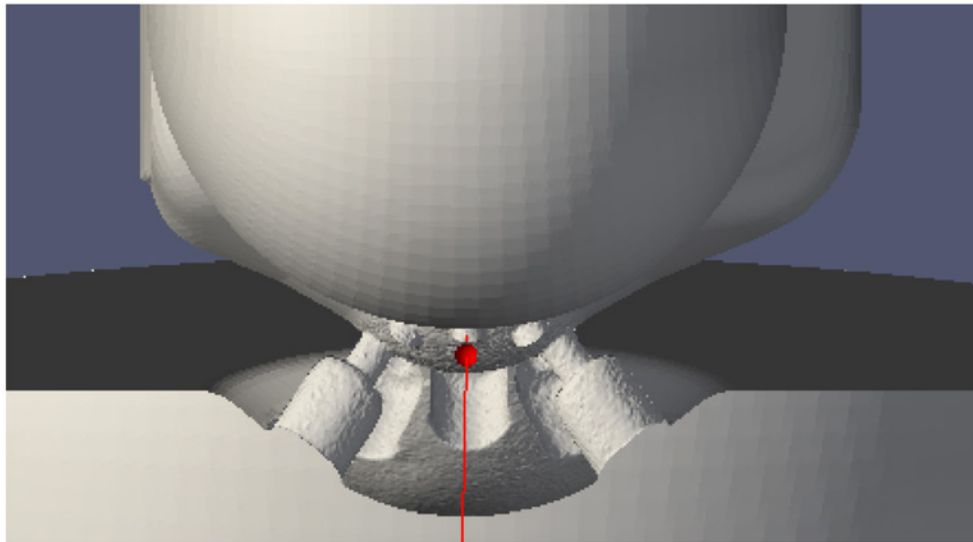


Figure II.8.2. Spray G geometry seen through a mid-plane cut. The mesh used in the CFD simulation is a blend between the high-resolution tomography of the holes (1.7 μm) and counterbores and a lower-resolution tomography of the fuel passages and the ball (5.1 μm).

Turbulent flow in CLSVOF is represented in the large eddy simulation (LES) framework following the wall-adapting local eddy-viscosity (WALE) model [7]. Particularly suited for complex internal geometries, this model is based on the square of the velocity gradient tensor to account for the effects of both the strain and the rotation rate of the smallest resolved turbulent fluctuations. WALE recovers the proper $O(y^3)$ near-wall scaling for the eddy viscosity without requiring dynamic procedure and is therefore preferred to the Smagorinsky model. Two additional levels of refinement were added to the 256^3 base grid to achieve minimum grid resolution of $5.8 \mu\text{m}$.

Two fuels were considered in this study, iso-octane and the blendstock BOB4. For iso-octane, the close-up visualization of the orifices, shown in Figure II.8.3, illustrates key differences between the new proposed approach and the approach commonly used in industry: the CLSVOF result (with LES) is shown in the left panel, whereas a diffused-interface Reynolds-averaged Navier-Stokes (RANS) (in practice, time-averaged) calculation is shown in the right panel. The RANS simulation was carried out with the commercial software CONVERGE [8]. The CLSVOF simulation captures several details of the atomization process, including the partial filling of the counterbores; moreover, transient interacting vortices result in perturbations of spray angle and direction that are absent from lower-resolution, engineering-level simulations. For the BOB4 blendstock, higher levels of cavitation are recognized at the same injection condition, causing a further deflection of the fuel jet (see Figure II.8.4). Quantification of these effects, validation with Engine Combustion Network (ECN) data for iso-octane, and analysis of droplet distribution will be carried out in 2019 with carryover funds from 2018 (35% of the total).

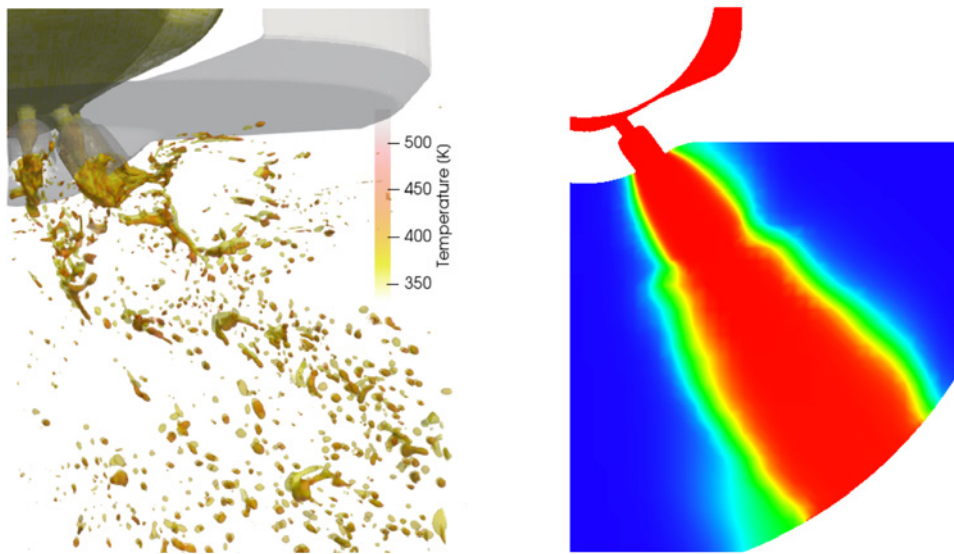


Figure II.8.3. A comparison between two different modeling approaches to spray formation. Left: snapshot of the liquid surface, colored by temperature, from the time-resolved CLSVOF simulation. Right: a cross-section of the liquid volume fraction (from 0-blue to 1-red) from the solution obtained with CONVERGE [6]. The same injector model (Spray G [4]) and fuel (iso-octane) were used for the two simulations.

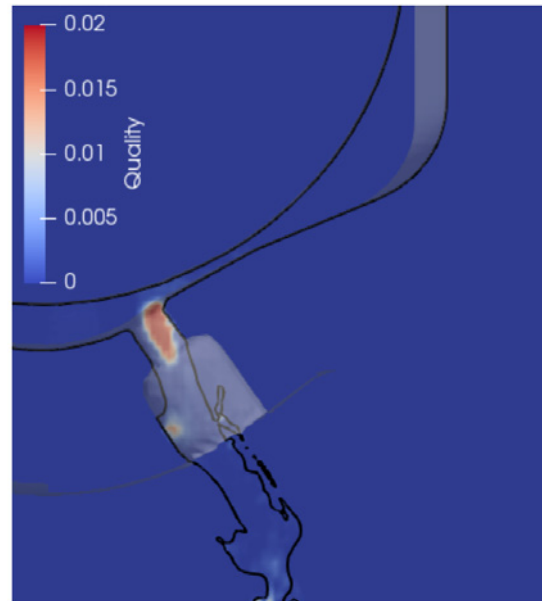


Figure II.8.4. Plot of vapor quality (non-dimensional units) from a data slice through one of the orifices in the simulation with BOB4. The black line marks the intersection of the liquid surface with the plane. Note how cavitation causes the fuel to impinge on the inner wall of the counterbore. Much lower levels of vapor quality are found in the simulation with iso-octane at the same injection conditions.

Conclusions

Activity in 2018 was focused on enabling multi-component simulations in a new research code and on exploring the GDI spray characteristics within the LES framework. As expected, the computational cost of LES is substantially higher with respect to a RANS simulation, and the interface-capturing algorithm contributes to the increase in this cost. However, the results show that the increased spatial and temporal resolution make it possible to discriminate spray characteristics based on fuel properties. It is expected that this difference can be most appreciated during the transient operation of the injector. By resolving the formation of individual droplets, CLSVOF can also provide boundary condition data in case the internal flow simulation is altogether skipped and the modeler resorts to a Lagrangian approach for the spray.

Key Publication

“Cavitation in Multi-Component Fuel: GDI Applications.” In preparation for SAE Journal.

References

1. Jemison, M., M. Sussman, and M. Arienti. 2014. “Compressible, Multi-Phase Semi-Implicit Method with Moment of Fluid Interface Representation.” *Journal of Computational Physics* 279: 182–217.
2. Arienti, M., and M. Sussman. 2017. “A Numerical Study of the Thermal Transient in High-Pressure Diesel Injection.” *International Journal of Multiphase Flow* 88: 205–221.
3. Battistoni, M., G. Magnotti, C. Genzale, M. Arienti, et al. 2018. “Experimental and Computational Investigation of Subcritical Near-Nozzle Spray Structure and Primary Atomization in the ECN Spray D.” SAE 2018-01-0277.
4. Engine Combustion Network. “Spray G Operating Condition.” <https://ecn.sandia.gov/gasoline-spray-combustion/target-condition/spray-g-operating-condition/> (accessed October 29, 2018).

5. Biçer, B., and A. Sou. 2016. “Application of the Improved Cavitation Model to Turbulent Cavitating Flow in Fuel Injector Nozzle.” *Applied Mathematical Modeling* 40: 4712–4726.
6. Lemmon, E.W., I.H. Bell, M.L. Huber, M.O. McLinden. 2018. “NIST Standard Reference Database 23: Reference Fluid Thermodynamic and Transport Properties-REFPROP, Version 10.0.” National Institute of Standards and Technology, Standard Reference Data Program, Gaithersburg, MD.
7. Convergence Science Inc. “Internal Combustion Engine FAQs.” <https://convergecdf.com/support/faqs>.
8. Nicoud, F., and F. Ducros. 1999. “Subgrid-Scale Stress Modelling Based on the Square of the Velocity Gradient Tensor.” *Flow, Turbulence and Combustion* 62: 183–200.

II.9 Multi-Mode SI/ACI: Stratification/Fuel/Dilute (Oak Ridge National Laboratory)

Scott Curran, Principal Investigator

Oak Ridge National Laboratory
2360 Cherahala Blvd.
Knoxville, TN 37922
E-mail: curransj@ornl.gov

Kevin Stork, DOE Technology Development Manager

U.S. Department of Energy
E-mail: Kevin.Stork@ee.doe.gov

Start Date: October 1, 2017	End Date: September 30, 2018	
Project Funding (FY18): \$325,000	DOE share: \$325,000	Non-DOE share: \$0

Project Introduction

This project has an overall goal of quantifying the role of fuel properties in enabling advanced compression ignition (ACI) performance, as well as the impact on spark-ignition (SI) performance using a single-cylinder, center mount, boosted gasoline direct injection engine platform. This project aims to bridge foundational DOE Co-Optima research into fuel property impacts on SI-mode efficiency, ACI-mode efficiency, and multi-mode impacts. Co-evolution of these emerging technologies and biofuels represents an opportunity to reduce petroleum consumption in future engines and vehicles in a mutually beneficial way. Further understanding of fuel property impacts on maximizing ACI operation with additional requirements of being able to run in SI-mode part-time is important to the objectives within the DOE Co-Optimization of Fuels and Engines initiative. Knowledge discovery and additional insights through modeling in collaboration with the Co-Optima Toolkit development project are key to furthering these goals.

Objectives

Overall Objectives

- Quantify fuel effects on multi-mode constraints and the impact of range/location of ACI mode
- Understand fuel property impacts on achieving ACI with requirements of being able to run in SI-mode part-time
- Characterize the impact of ACI range and location on potential improvements to fuel economy

Fiscal Year 2018 Objectives

- Perform assessment of fuel economy potential as a function of speed and load range/location of the ACI portion of the engine operating map; the map can have improvements on fuel economy
- Configure specialized multi-mode single-cylinder research platform
- Facilitate knowledge discovery and additional insights through modeling in collaboration with Co-Optima Toolkit development project

Approach

This is a new project for Fiscal Year 2018 that is focused on understanding the ability for multi-mode ACI operation to increase fuel economy and understanding the fundamental challenges and opportunities for expanding ACI operation over the engine speed and load map via enabling fuel properties. For this work, a strategy of operating the engine in ACI-mode at part-load and using conventional SI outside the operational boundaries of ACI is used, as illustrated in Figure II.9.1. To improve the fundamental understanding of the

opportunities for multi-mode ACI/SI operating strategies, a combination of experimental engine research and modeling and simulation is used. It is important to understand fuel property impacts on achieving high-efficiency ACI with the additional requirements of being able to run the engine in SI-mode part-time as well over a drive cycle.

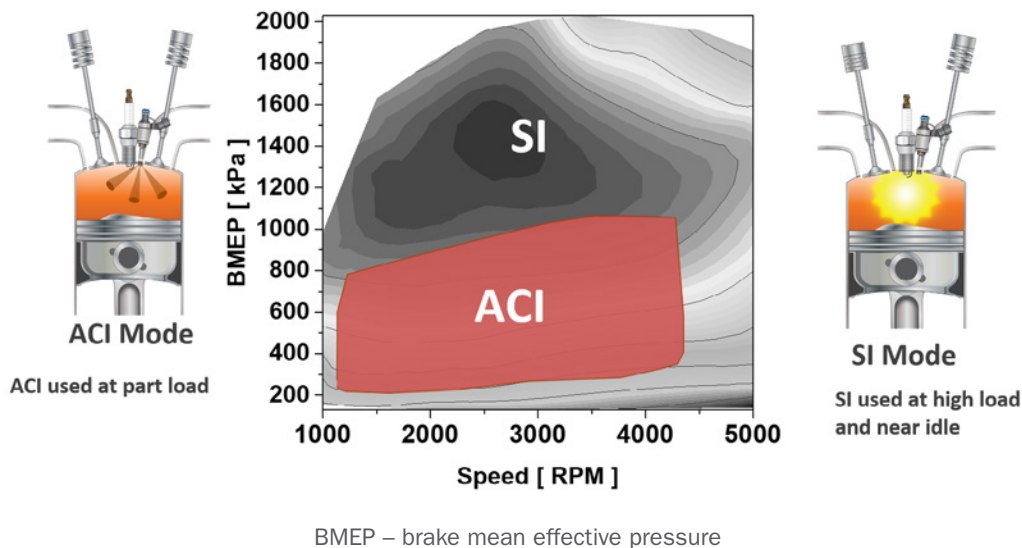


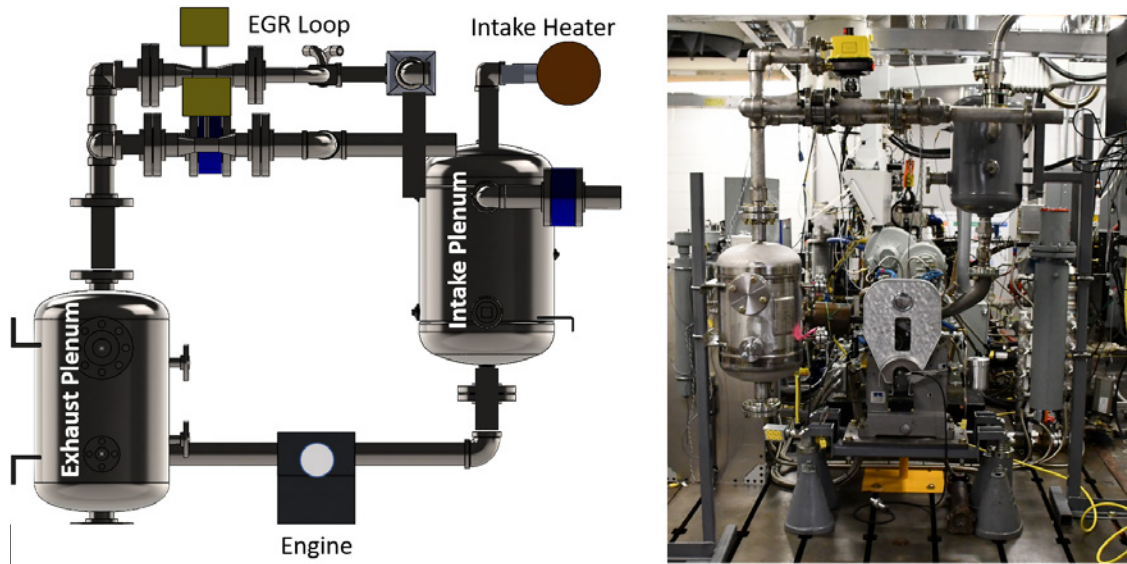
Figure II.9.1. Multi-mode concept showing ACI at part-load with engine running in SI mode for low loads and near idle and at higher engine loads and speeds

A unique single-cylinder research platform that is purpose-built for SI/ACI research was acquired in collaboration with General Motors and uses a Ricardo Hydro bottom end and a custom head that is used at both Sandia National Laboratories and the University of Wisconsin. The engine features an 86 mm bore, 94/6 mm stroke. This unique General Motors single-cylinder metal engine research platform equipped with enabling technologies for a multi-mode combustion strategy will allow for further control over the pressure-temperature space. Additional authority over the combustion process will be enabled through advanced features of this engine (advanced cam phasing, fuel stratification, high-energy nonthermal plasma ignition systems). The matched geometry will enable collaborations for further knowledge discovery for ACI multi-mode combustion fundamentals to complement the metal engine experiments at Oak Ridge National Laboratory. A key focus of this work on the single-cylinder platform is developing multi-mode constraints and accounting for realistic boundary conditions.

To accelerate the research and development of multi-mode strategies, simulation studies were completed to understand the impact of multi-mode efficiency and range considerations. Understanding the impact not only of the efficiency while in multi-mode operation but also the multi-mode speed/load range and subsequent location within the drive-cycle is expected to have tradeoffs on fuel economy improvements.

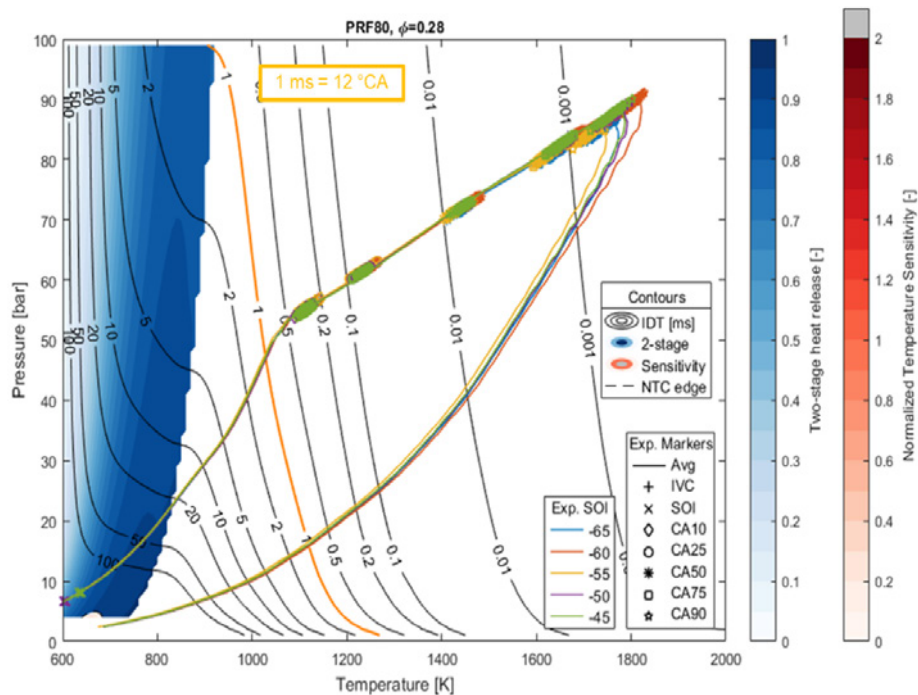
Results

A schematic of the single-cylinder engine is shown in Figure II.9.2. Special consideration in the design of the air handling system included an advanced intake heating for beyond motor octane number conditions needed for ACI operation. The ability for this engine to navigate the pressure-temperature trajectories for achieving stable ACI is important to the objectives of this project. Building off the foundational pressure-temperature (P-T) analysis by Szybist and Splitter [1], ACI P-T analysis using partially stratified ACI combustion data was performed to understand any additional requirements, as shown in Figure II.9.3.



EGR – exhaust gas recirculation

Figure II.9.2. Schematic of single-cylinder engine (left) and picture of engine installed (right)



IDT – ignition delay time; NTC – negative temperature coefficient; IVC – intake valve closing; SOI – start of injection; CA – crank angle; CA10 – crank angle at 10% mass fraction burned; CA25 – crank angle at 25% mass fraction burned; CA50 – crank angle at 50% mass fraction burned; CA75 – crank angle at 75% mass fraction burned; CA90 – crank angle at 90% mass fraction burned

Figure II.9.3. A single-zone temperature model is used to present experimental results of partially stratified ACI with gasoline-range primary reference fuels (PRFs), highlighting areas for two-stage heat release

The multi-mode simulation studies to understand the impact of the location and range of the ACI region within the speed and load map were conducted using vehicle system simulations for a mid-size passenger sedan vehicle with a conventional five-speed transmission. The base engine map used for the study was a 2.2 L

gasoline direct injection engine that has been validated in Autonomie. The multi-mode study assumed the base engine was modified to run in a multi-mode ACI strategy, where the ACI mode had a constant brake specific fuel consumption to examine the effect on fuel economy. A range of ACI brake specific fuel consumption from 180 g/kW-hr to 260 g/kW-hr was examined across different load ranges of ACI operation and different minimum loads, as shown in Figure II.9.4. While a consistent brake specific fuel consumption is not expected in practice, being able to hold it constant gave a more comparable approach for the study.

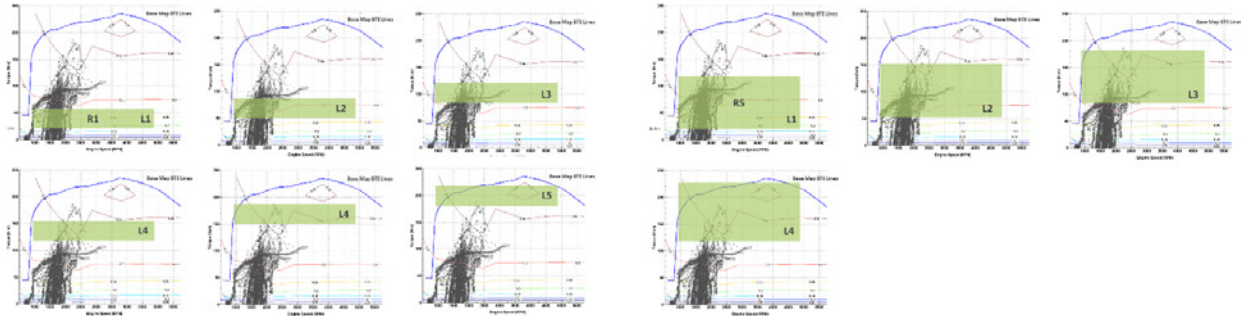
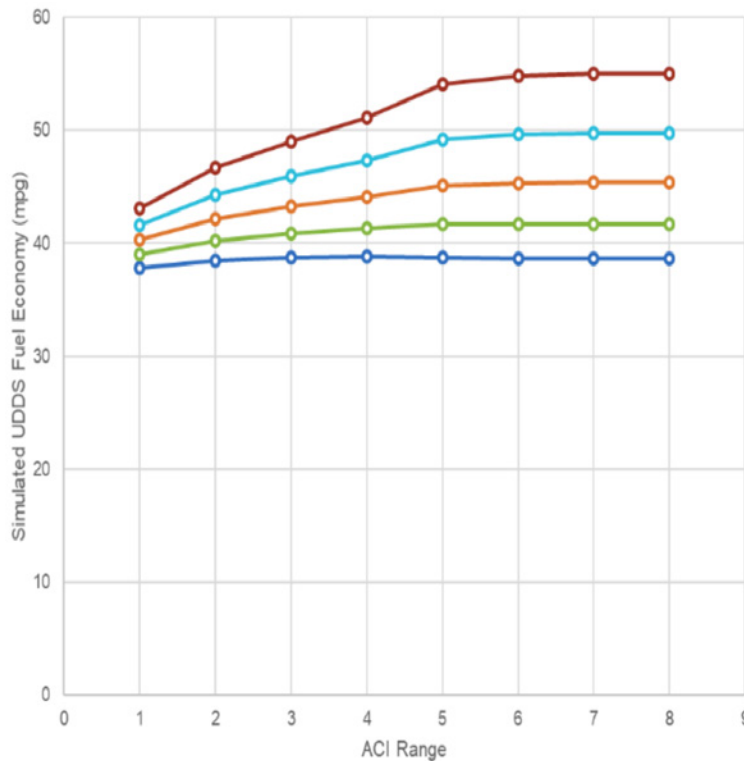


Figure II.9.4. Examples of range of conditions considered across ACI range and locations examined. The left figure shows a smaller ACI range and the different load locations (from low-load to high-load centroids). The figure on the right shows an expanded ACI range and the different locations examined.

The modeling results showed a clear point of diminishing returns for improvements in modeled fuel economy as the ACI region was increased and that modest fuel economy gains could be realized for moderate ACI ranges and locations, as shown in Figure II.9.5. This type of analysis will be important in determining constraints of multi-mode operation and the impact on potential fuel economy gains with different fuels.



UDDS – Urban Dynamometer Driving Schedule

Figure II.9.5. Results showing diminishing returns as ACI range is increased with different ACI efficiencies

Conclusions

In 2018, a new multi-mode ACI/SI project was begun with the goal of quantifying the role of fuel properties in enabling ACI performance and the impacts on SI performance to accelerate the development of multi-mode strategies enabled by fuel properties. A unique single-cylinder engine was acquired and installed to support these goals. The ability for multi-mode strategies to improve fuel economy was better understood using modeling and analysis. The following conclusions can be made.

- Findings of multi-mode simulations illustrate the effect of ACI speed and load regions on improving fuel economy and show a point of diminishing returns for load expansion depending on drive cycle.
- A unique General Motors single-cylinder metal engine research platform, equipped with enabling technologies for a multi-mode combustion strategy, has been acquired for the project and will allow for further control over the pressure-temperature space.

Together, the new spray chamber and diagnostics for plume cone angle and plume direction provide a powerful diagnostic to assess the effects of fuel properties. The diagnostics are currently being applied and analyzed for Tier-3-selected Co-Optima fuels.

Key Publications

1. Drallmeier, J., M. Wissink, S. Curran, and R. Wagner. 2018. "Ignition Delay in Low Temperature Combustion." SAE Technical Paper 2018-01-1125. DOI:10.4271/2018-01-1125.
2. Wissink, M., S. Curran, C. Kavuri, and S. Kokjohn. 2018. "Spray-Wall Interactions in a Small-Bore, Multicylinder Engine..." *ASME. J. Eng. Gas Turbines Power* 140 (9): 092808–092808-8. DOI:10.1115/1.4039817.

References

1. Szybist, J., and D. Splitter. 2017. "Pressure and Temperature Effects on Fuels with Varying Octane Sensitivity at High Load in SI Engines." *Comb and Flame* 177: 49–66. DOI: 10.1016/j.combustflame.2016.12.002.

Acknowledgements

The principal investigator acknowledges co-authors Martin Wissink and Robert Wagner. The authors also gratefully acknowledge General Motors for providing a specialized research platform for the project.

II.10 Fuel Effects on Low Speed Pre-Ignition (Oak Ridge National Laboratory)

Derek Splitter, Principal Investigator

Oak Ridge National Laboratory
2360 Cherahala Blvd.
Knoxville, TN 37922
E-mail: splitterda@ornl.gov

Kevin Stork, DOE Technology Development Manager

U.S. Department of Energy
E-mail: Kevin.Stork@ee.doe.gov

Start Date: October 1, 2017

End Date: September 30, 2018

Project Funding (FY18): \$150,000

DOE share: \$150,000

Non-DOE share: \$0

Project Introduction

Downsized and turbocharged spark-ignited engines are being increasingly used by engine manufacturers to improve vehicle efficiency while reducing CO₂ emissions [1,2]. While greatly effective at improving fuel economy, the increased specific outputs of these engines make them more prone to damaging phenomena such as pre-ignition. Although pre-ignition is not a novel process or unique to downsized boosted engines [3], the high-load, low-speed operating conditions of these engines result in a particularly intense pre-ignition process, which is typically referred to as low-speed pre-ignition (LSPI). LSPI events often consist of very strong knock events that can cause significant damage to engine hardware, including catastrophic engine failure.

LSPI typically occurs during very high load operation at engine speeds around 2,000 rpm or below, wherein the flame initiates before the spark is fired and leads to flame propagation at a significantly advanced combustion phasing. The increased pressure rise due to the advanced combustion phasing often causes violent end-gas knock or even “super-knock” for events that transition to developing detonation [4], all of which can result in catastrophic engine damage. The fundamental causes of LSPI still remain poorly understood, and there is a lack of firm consensus on the underlying mechanisms that promote LSPI, but recent findings by Splitter et al. highlight that fundamental fuel properties are important to LSPI event occurrence [5], and previous findings by Jatana et al. [6] highlighted that there are fuel property effects on LSPI beyond those of fuel distillation alone. Although there has been significant recent work to understand LSPI processes, a gap still exists in the understanding of the impact of fuel properties, both physical and chemical, on LSPI behavior. This project aims to provide more clarity on the relationship between fuel properties and LSPI, with fuel properties being specifically studied.

Objectives

- Quantify the relationship between fuel properties and LSPI frequency with respect to fuel distillation and molecular properties
- Determine if specific fuel properties affect LSPI intensity

Approach

The engine used in this study is based on a 1.6 L Ford EcoBoost engine equipped with the production center-mounted direct injection fueling system. The engine was converted to a single-cylinder engine by disabling Cylinders 2, 3, and 4, where Cylinder 1 is closest to the crank snout and Cylinder 4 is closest to the flywheel. The combustion chamber geometry and camshaft profiles on Cylinder 1 were unchanged from the stock configuration. The engine was operated using standalone laboratory fueling and air handling systems. The engine was controlled through a custom Driven-based engine controller, with automatic engine controls developed at Oak Ridge National Laboratory with calibration based on manual engine mapping. The controller used a mass airflow based control feedback enabled tabular based engine map for fully automatic control of fuel, air, spark timing, and camshaft phasing. All measurements presented in this study were acquired in

automated operation using time varying load square-wave segments at 2,000 rpm. Each segment consisted of 5 min of operation at low load (5 bar gross indicated mean effective pressure [IMEPg]), followed by 25 min of high-load (13–16 bar IMEPg) operation. Note these loads are typically lower than those of previous LSPI work, as the fuel used in the present work is of a reduced octane number, 70 RON (research octane number). This fuel obtains pre-ignition and heavy knock retard at reduced loads. The first 5 min of each 25-min high-load segment were thermally transient in boundary conditions and were discarded from the analysis such that only the last 20 min of data (20,000 cycles) of each high-load segment were used for the study of LSPI behavior. Finally, eight to ten such consecutive low-high-low load square wave segments were run for each experiment to ensure sufficient LSPI event count for consistent statistical analysis. Fresh engine oil was used for each experiment, and the lubricant pressure was monitored to verify fuel-oil dilution was occurring. To reproduce fuel-oil dilution, the injector was oriented such that the fuel-linear impingement could be increased or decreased to maintain similar fuel-oil dilution for various fuels/load throughout the LSPI segments.

The fuels used were based on a reduced octane number gasoline acquired from Haltermann products. One fuel was baseline fuel from previous high-load experiments, product code HFO437 (hereby referred to as EEE); the other fuels used were lower octane number and operated at reduced load (hereby referred to as 70RON). Two lots of 70RON were used, with various fuel distillation points, which differed in distillation as determined by the ASTM D86 test by approximately 20°F for most of the fuel distillation. In the more volatile 70RON fuel, 6.5% by volume nitromethane (CH_3NO_2) was added to some experiments to explore fuel effects on promotion of LSPI.

A cycle was identified as LSPI if the peak recorded cylinder pressure and four percentage of mass fraction burned (CA04) were both more than 3.85 standard deviations greater than the median maximum cylinder pressure of all the cycles. The approach is similar to that described in detail by Mansfeild et al. [7].

Results

- Confirmed that LSPI number count is highly correlated with fuel–wall interaction
- Illustrated that lubricant effects are independent of only fuel–wall interaction, a critical aspect for fuel property formulations
- Revealed that at reduced fuel–wall interaction conditions, adverse fuel properties, like fuel nitration, can enable expression of lubricant effects that are traditionally suppressed at lower load operating conditions

The fuels tested in this project are reported in Table II.10.1, which highlights that the RON and distillation of the fuels were very similar for the fuels based on 70RON gasoline, and the distillation of EEE (certification gasoline) and the low-volatility 70RON fuel are very similar. The EEE gasoline was used as a reference fuel for a baseline comparison for the reduced octane fuels, which are the major focus of the work for this year. The reduced octane fuels were used as they have similar fuel kinetics at reduced engine load, and thus reduced engine damage potential, increasing the repeatability of the experiments. However, although this was the intent, there were additional discoveries that reveal added information to the fundamentals of LSPI that are also revealed from this approach.

Table II.10.1. Tested Fuels

Fuel Name	EEE	70RON low vol.	70RON high vol.	70RON + CH ₃ NO ₂
Blended molecule	-	-	-	CH ₃ NO ₂
Blended (% vol.)	100%	100%	100%	6.5%, bal. 70RON
RON (ASTM D2699)	96.3	71.0	71.2	69.5
MON (ASTM D2700)	88.8	67.7	66.9	62.7
IBP (°F) (ASTM D86)	87	100	96	96
T5 (°F) (ASTM D86)	114	143	132	128
T10 (°F) (ASTM D86)	127	162	146	142
T20 (°F) (ASTM D86)	148	185	167	161
T30 (°F) (ASTM D86)	171	202	184	180
T40 (°F) (ASTM D86)	200	216	199	197
T50 (°F) (ASTM D86)	220	227	211	210
T60 (°F) (ASTM D86)	231	238	222	222
T70 (°F) (ASTM D86)	241	251	233	233
T80 (°F) (ASTM D86)	257	269	246	246
T90 (°F) (ASTM D86)	315	293	271	271
T95 (°F) (ASTM D86)	340	309	298	297
FBP (°F) (ASTM D86)	411	335	331	330

MON – motor octane number; IBP – initial boiling point; FBP – final boiling point

As shown in Figure II.10.1, the 70RON fuel (black data in Figure II.10.1) could attain similar oil pressure drop as a function of LSPI segment number at the reduced load (13 bar IMEP_g) operating condition as compared to the EEE fuel at high load (20 bar IMEP_g, red data in Figure II.10.1). The similar oil pressure drop was used as a surrogate to determine fuel-oil dilution, and at the lower load condition, injector orientation was required to increase fuel-linear impingement to replicate oil pressure drop. Note that for all tests, new oil was used, and the 70RON and EEE fuels are both knock limited with similar combustion phasing, with both fuels resulting in a crank angle at 50% mass fraction burned of ~36 degrees crank angle after top dead center firing at the respective loads.

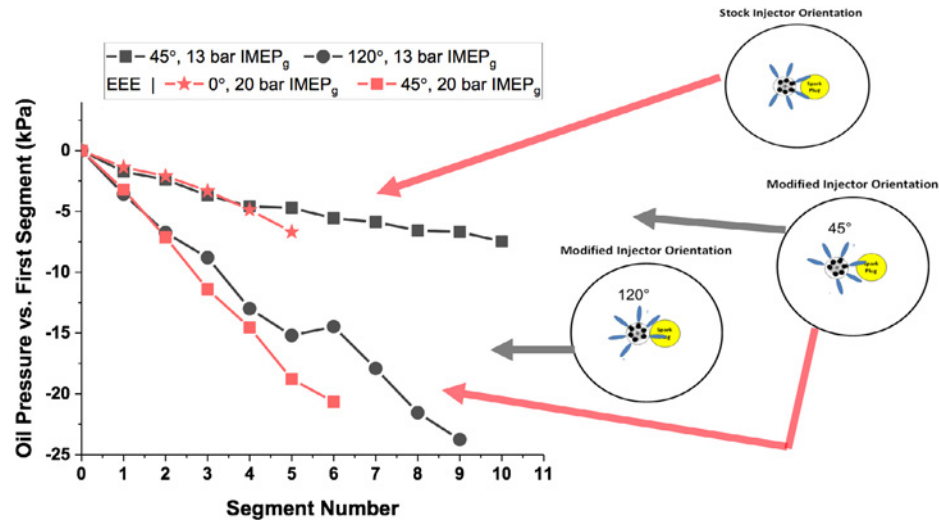


Figure II.10.1. Engine oil pressure reduction as a function of LSPI segment for various engine loads and injector orientations; the reduced engine load conditions required increased fuel-wall targeting to match oil pressure drop present at higher engine load operation

At the 13 bar IMEP_g operating condition, it was found that the increased oil pressure drop with the 120° injector orientation (circles marker data in Figure II.10.1) also correlated to statistically significant increase in the number count of LSPI events, approximately double the events, as shown in Figure II.10.2.

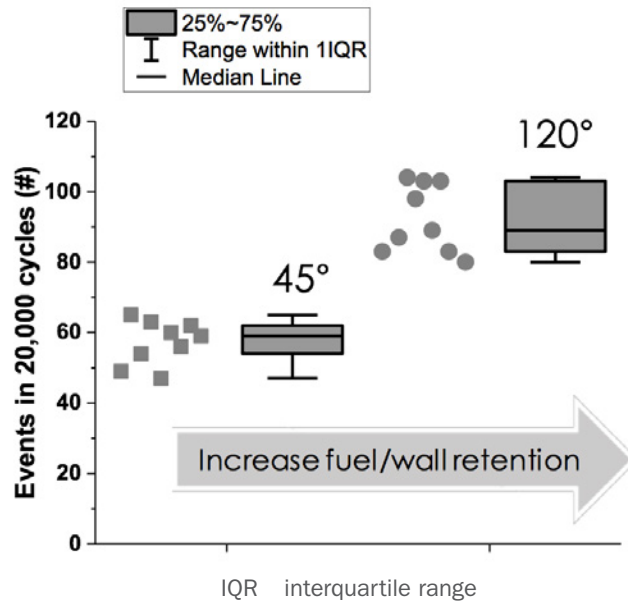


Figure II.10.2. Recorded LSPI events per segment for matched load, varied injector orientation operation

The results of Figure II.10.1 and Figure II.10.2 highlight that fuel mass (i.e., load) and fuel spray orientation affect fuel retention in the top ring zone and, correspondingly, LSPI event count. Using this as a working theory, the fuel volatility was intentionally decreased. This was performed at a near similar octane number of 71 RON. In these experiments, the LSPI count and oil pressure drop per segment were monitored. If there were reductions in either quantity, the engine load (i.e., mass of fuel injected) was increased until the LSPI count was similar to that of the lower volatility 70RON fuel. The results of this approach are presented in Figure II.10.3, where it is seen that the increased volatility fuel has almost no LSPI activity at matched operating conditions and that load increase of 3 bar IMEP_g (16 bar vs. 13 bar) was required to match the LSPI activity and oil pressure drop of the lower volatility fuel. Interestingly, for a given oil pressure drop trend, the LSPI count seems to be very similar, suggesting that the fuel retention of the cases in the top ring zone is similar between the fuels.

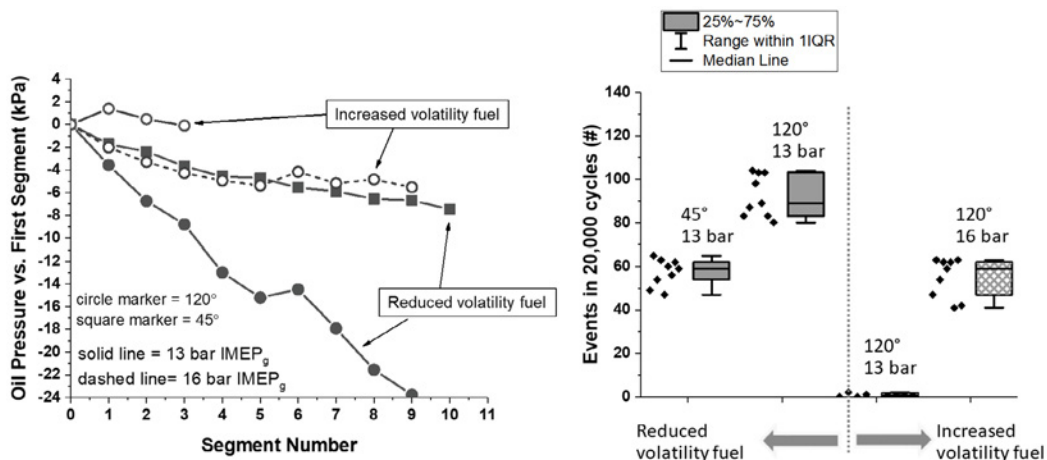


Figure II.10.3. Oil pressure reduction for different engine loads and fuel distillation (left) and corresponding LSPI event counts (right)

Using the results presented in Figure II.10.3, a series of experiments was conducted with various lubricants. The lubricants were used because there is an established relationship in the literature on detergent effects on LSPI (specifically, calcium and sodium content of the lubricant tend to promote LSPI in several reported studies). However, in the present work, very interesting findings occurred. Specifically, at the lower load condition (13 bar), there was no effect from the lubricant detergent package, although there were LSPI events occurring. However, at the high load condition with the more volatile fuel, there was sensitivity to the lubricant additive package. Figure II.10.4 highlights these findings, where significant lubricant effect is seen at only the higher load operating condition, suggesting that a chemically or possibly thermally driven chemical process could be present for lubricant detergent activity, affecting LSPI propensity.

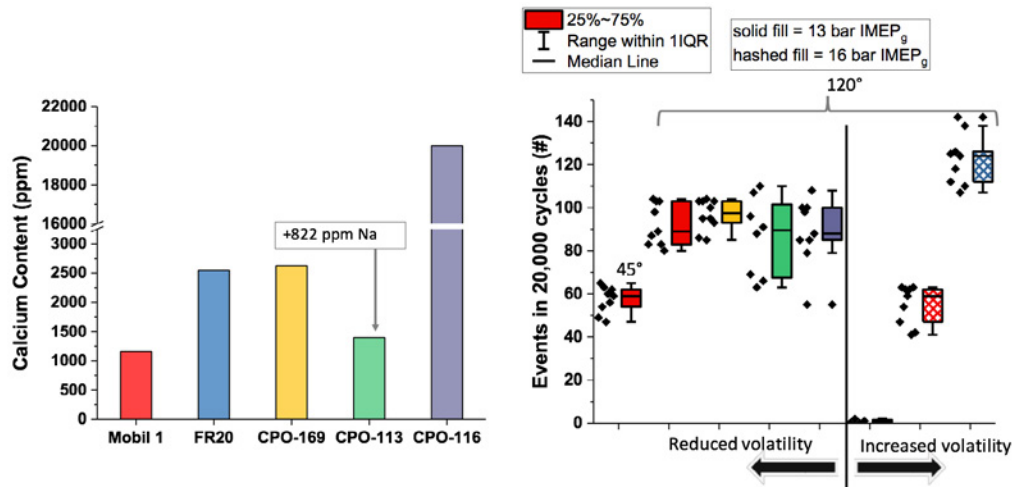


Figure II.10.4. Lubricant additive metal content (left) and corresponding LSPI number count, color coded to lubricant (right)

Based on the interesting results in Figure II.10.4, the fuel was cut with 6.5% by volume nitromethane (CH_3NO_2), a fuel that is a monopropellant and known to exhibit a high degree of pre-ignition propensity. This fuel was used because it was suspected that processes like oil nitration could be possible in the detergent-based effect on lubricant promotion of LSPI. Thus, the nitromethane was an attempt to chemically alter the fuel such that there could be increased activity from the fuel and lubricant effects. As shown in Table II.10.1, the nitromethane-cut 70RON fuel had virtually no effect on the RON or fuel distillation. However, as shown in Figure II.10.5, unlike the near zero LSPI count with the uncut high volatility fuel, the nitromethane-cut fuel exhibited significant LSPI activity at the 13 bar IMEP_g operating condition. Moreover, the nitromethane-cut fuel also exhibited a lubricant-based effect on LSPI propensity at the lower load operating condition, something not observed with either of the uncut 70RON fuels, suggesting that there could be evidence for chemical effects on lubricant effect on LSPI present that occur at high loads, which were simulated with CH_3NO_2 addition.

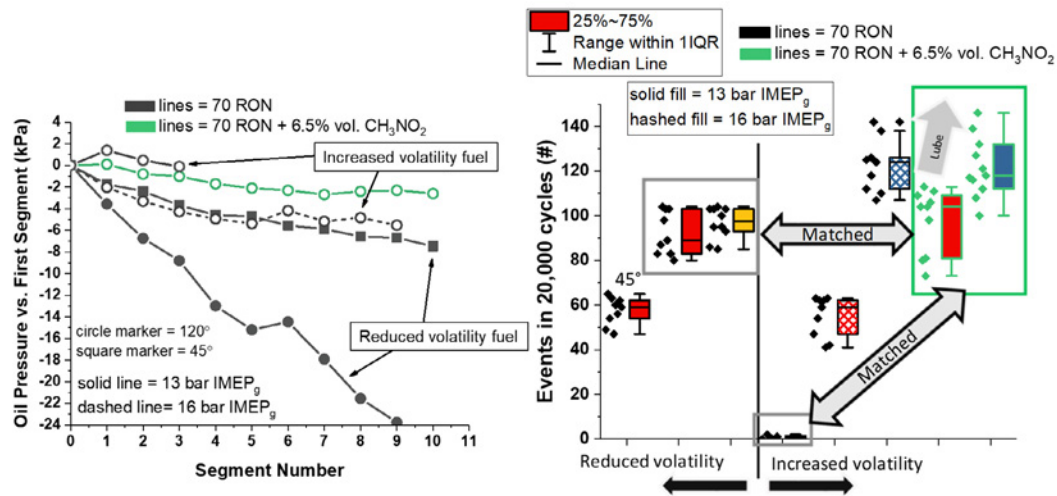


Figure II.10.5. Oil pressure reduction for different engine loads and fuels (left) and corresponding LSPI event counts (right)

Conclusions

- Confirmed that LSPI number count is highly correlated with fuel distillation and fuel retention in the top ring zone
- Illustrated that fuel retention is insufficient to describe all generalized LSPI phenomena and has virtually no correlation to lubricant activity at reduced engine loads (even if the fuel is preceptive to LSPI at those conditions)
- Revealed that additional fuel and possibly lubricant properties are present that could be influenced by engine load and required for LSPI

Key Publications

1. Jatana, Gurneesh S., Derek A. Splitter, Brian Kaul, and James P. Szybist. 2018. "Fuel Property Effects on Low-Speed Pre-Ignition." *Fuel* 230: 474–482.

References

1. Pawlowski, Alexander, and Derek Splitter. 2015. "SI Engine Trends: A Historical Analysis with Future Projections." SAE Technical Paper No. 2015-01-0972.
2. Splitter, Derek, Alexander Pawlowski, and Robert Wagner. 2016. "A Historical Analysis of the Co-Evolution of Gasoline Octane Number and Spark-Ignition Engines." *Frontiers in Mechanical Engineering* 1: 16.
3. Chapman, Elana M., and Vincent S. Costanzo. 2015. "A Literature Review of Abnormal Ignition by Fuel and Lubricant Derivatives." *SAE International Journal of Engines* 9, no. 2015-01-1869: 107–142.
4. Wang, Zhi, Yunliang Qi, Xin He, Jianxin Wang, Shijing Shuai, and Chung K. Law. 2015. "Analysis of Pre-Ignition to Super-Knock: Hotspot-Induced Deflagration to Detonation." *Fuel* 144: 222–227.
5. Splitter, Derek, Brian Kaul, James Szybist, and Gurneesh Jatana. 2017. "Engine Operating Conditions and Fuel Properties on Pre-Spark Heat Release and SPI Promotion in SI Engines." *SAE International Journal of Engines* 10, no. 2017-01-0688.
6. Jatana, Gurneesh S., Derek A. Splitter, Brian Kaul, and James P. Szybist. 2018. "Fuel Property Effects on Low-Speed Pre-Ignition." *Fuel* 230: 474–482.
7. Mansfield, Andrew B., Elana Chapman, and Kenneth Briscoe. 2016. "Impact of Fuel Octane Rating and Aromatic Content on Stochastic Pre-Ignition." SAE Technical Paper No. 2016-01-0721.

II.11 Fuel Property Effects on Abnormal Combustion (Oak Ridge National Laboratory)

Derek Splitter, Principal Investigator

Oak Ridge National Laboratory
2360 Cherahala Blvd.
Knoxville, TN 37922
E-mail: splitterda@ornl.gov

Kevin Stork, DOE Technology Development Manager

U.S. Department of Energy
E-mail: Kevin.Stork@ee.doe.gov

Start Date: October 1, 2017	End Date: September 30, 2018	
Project Funding (FY18): \$150,000	DOE share: \$150,000	Non-DOE share: \$0

Project Introduction

Spark ignition engine efficiency and operation are fundamentally limited by knock, a process observed via cylinder-pressure measurements as early as late 1910 [1]. Knock is an unwanted and uncontrolled autoignition of the fuel, which, if not avoided, can lead to engine damage and therefore is impermissible in almost all engine applications. Although knock is a fundamental barrier and has been studied for over a century, a fully detailed understanding of knock and other autoignition phenomena has proven elusive. Knock continues to be the primary barrier to achieving higher efficiency in spark ignition engines, and the recent automotive trends of downsizing and down-speeding engines have exacerbated the issue. Therefore, improving the understanding of knock and fuel-specific effects on knock remains a high priority in engine and combustion research. Knock is highly fuel-dependent; the fuel octane number tests are used to define a fuel's knocking tendency relative to reference fuels (isooctane and n-heptane, both alkanes).

One of the most insightful understandings of knock was presented by Leppard [2], who showed that for alkanes, there is a two-stage ignition process that includes low-temperature heat release (LTHR) followed by a negative temperature coefficient region wherein the reaction rate becomes inversely proportional to temperature. Following these processes is a high-temperature heat release event, which in spark ignition combustion is a pre-mixed flame deflagration combustion process, where knock also can occur. Many fundamental studies in shock tubes and rapid compression machines have been carried out on the fuel kinetic processes of LTHR, but to date, much of the understanding and observation of LTHR in engines has come from compression ignition combustion processes, with many being kinetically controlled and thus at vastly different conditions than production engines (e.g., homogeneous charge compression ignition [3]).

The goal of this project is to expand the understanding of the role of LTHR and pre-spark heat release (PSHR) on knock at relevant engine conditions by studying the knock propensity of an alkane-based fuel over a wide range of intake temperatures at knock-prone conditions in a spark-ignited engine. The results are analyzed as functions of PSHR and intake temperature independently and also are compared with constant-volume ignition delay simulations to support the observed trends. The results of this work highlight the importance of LTHR processes on knocking propensity, and the corresponding effect that PSHR has on bulk gas kinetic state and knock.

Objectives

- Develop a phenomenological understanding of molecular structure and fuel property effects on abnormal stochastic ignition and combustion event frequency and intensity
- Quantify fuel effects on PSHR and endgas knock

Approach

The engine used in this study is based on a 2.0 L GM Ecotec engine equipped with the production side-mounted direct injection fueling system. The engine was converted to a single-cylinder engine by disabling Cylinders 1, 2, and 3, where Cylinder 1 is closest to the crank snout and Cylinder 4 is closest to the flywheel. The combustion chamber geometry and camshaft profiles on Cylinder 4 were unchanged from the stock configuration. The engine was operated using standalone laboratory fueling and air handling systems. The engine was controlled through a custom Driven-based engine controller. All measurements presented in this study were acquired in automated operation using 1,000 r/min or 2,000 r/min engine speed, where intake temperature was swept from 40°C in 20°C increments up to first indication of PSHR and 10°C increments after PSHR was observable; the maximum intake temperature was the lower of 180°C or when repeatable and excessive pre-ignition was encountered. At each intake temperature condition, spark timing was adjusted to maintain knock-limited spark advance (KLSA) phasing. For each condition tested, cylinder pressure, spark discharge, and camshaft position data were recorded at 0.2°CA (degrees crank angle) resolution for 5,000 sequentially fired cycles. Fuel injection timing was held constant at 280°CA before firing top dead center. Spark timing was adjusted as needed to achieve the desired KLSA combustion phasing as determined by visual inspection of the indicated pressure trace, which was also observed to correspond to an abrupt increase in measured combustion noise. Engine fuel flow was measured with a Coriolis fuel flow meter and cross checked with a laboratory-grade wideband oxygen sensor installed in the engine exhaust. Throughout the study, engine coolant and sump oil temperatures were maintained at 90°C and 95°C, respectively.

A central analysis of the present work is separation of experimentally measured heat release into high-temperature deflagration and low-temperature volumetric heat release processes. There is little literature that has reported PSHR phenomena to date, with no accepted techniques to partition volumetric and flame propagation combustion processes based on experimental pressure data. The approach developed herein employs fitting a spline to the measured PSHR. The approach developed in this project assumes that LTHR can be separated from the deflagration processes and that LTHR starts and ends with zero slope. Using these assumptions, the experimental apparent heat release was fit with a spline up to the spark discharge timing in one crank angle (CA) degree increments to reduce fitting artifact noise, whereafter the spline was fit by a three-point approach constrained to tangency with the measured heat release at spark discharge, and tangency to zero apparent heat release at both endpoints. The endpoint condition crank angle was determined by finding the local maximum of the second derivative of the apparent heat release, within a local search space between spark discharge and CA10 of the total (i.e., un-partitioned) heat release. Thus, this approach assumes that the low-temperature reactions cannot encompass more than 10% of the total heat release. The spline fit was then subtracted from the measured total apparent heat release to solve for the deflagration-based heat release. Subsequent analysis of the results uses this result to partition the heat release mechanisms and determine the effect of PSHR on abnormal combustion processes such as knock.

Results

- Confirmed that fuel property effects exist on PSHR
- Illustrated that PSHR expression coincides with reduced intake temperature sensitivity to knock
- Revealed that PSHR is an indicator for fundamental kinetic pathways that exist in end-gas knock

The fuel used was an alkylate-based fuel, designed for the DOE Vehicle Technologies Office Co-Optima effort, with properties listed in Table II.11.1

Table II.11.1. Tested Fuels

Parameters	Test Method	Test Fuel	Simulation Surrogate
Research Octane Number (-)	ASTM D2699	98.0	98.5
Motor Octane Number (-)	ASTM D2700	96.7	96.3
Octane Sensitivity (-)	Calculated	1.3	2.2
Aromatics (vol%)	ASTM D1319	0	2
Saturates (vol%)	ASTM D1319	100	98
Olefins (vol%)	ASTM D1319	0	0
Ethanol (vol%)	ASTM D4815mod	0	0
Carbon (wt%)	ASTM D5291	83.75	84.37
Hydrogen (wt%)	ASTM D5291	15.80	15.63
Oxygen (wt%)	ASTM D5599	0	0
Stoichiometric Air-Fuel Ratio (-)	Calculated	15.07	15.04
# of Components in Surrogate	-	NA	4

The stack plot of Figure II.11.1 illustrates the trends in apparent heat release rate for 2,000 r/min operation from 40°C to 180°C intake temperature, where in each subplot the mean apparent heat release rate is the black line, one standard deviation of apparent heat release rate is the grey shaded region, KLSA spark timing is the vertical arrow, and the intake temperature is noted in the upper left. For conditions without PSHR (intake temperatures between 40°C and 80°C), KLSA requires a nearly linear retard totaling 8°CA. However, for conditions when PSHR is observed, i.e., intake temperatures 90°C and above, KLSA (and CA50, discussed later) is nearly constant despite the 90°C intake temperature change. Throughout this temperature range PSHR is present and is seen to advance with intake temperature; at 180°C PSHR starts nearly 25°CA before and ends 10°CA before KLSA spark timing, illustrating complete negative temperature coefficient behavior. This atypical non-linear relationship between KLSA and intake temperature is quantified more fully in Figure II.11.2, where PSHR and the CA50 of the deflagration are plotted as a function of intake temperature for both 2,000 r/min and 1,000 r/min; note that at 1,000 r/min, the intake temperature was limited to a maximum of 90°C due to the onset of pre-ignition events. Consistent with the qualitative findings in Figure II.11.1, Figure II.11.2 shows that both engine speeds exhibit an initial increase in PSHR, but since the 2,000 r/min condition did not exhibit excessive pre-ignitions, it was able to be operated at intake up to and beyond maximum PSHR, expression. The CA50 trends of Figure II.11.2 highlight that prior to PSHR, near-linear retard in KLSA CA50 combustion phasing is required with increasing intake temperature, but once PSHR occurs, additional KLSA CA50 retard is not required.

The results of Figure II.11.2 highlight that the presence of PSHR (not necessarily the magnitude of PSHR) coincides with constant KLSA CA50 phasing. Moreover, the results show that the general trends in PSHR and CA50 are similar for both engine speeds, suggesting that PSHR is rate-limited by time and the absolute magnitude of PSHR expression could be less important than simply the presence of PSHR. The trends in Figure II.11.2 highlight that the dependency of KLSA changes from intake-temperature-dominant before PSHR is expressed, to completely insensitive to intake temperature after PSHR is expressed. This behavior is highly unusual for knock-prone conditions, as it is well established that for a given fuel and engine operating speed, knock is directly dependent on the end-gas kinetic state, which is a function of the temperature history of the fuel, which is affected only by compression ratio and initial conditions.

Building on the findings of PSHR, the deflagration portion of the heat release was analyzed, as presented in Figure II.11.3, which directly illustrates the relation of KLSA CA50 and the bulk gas temperature at CA2 of the deflagration as a function of PSHR at both 2,000 r/min and 1,000 r/min. Note, the calculation of the bulk gas temperature at CA2 of the deflagration is based on the assumption that the burned volume at CA2 is minimal and using the full chamber volume zone for bulk gas temperature determination is still valid.

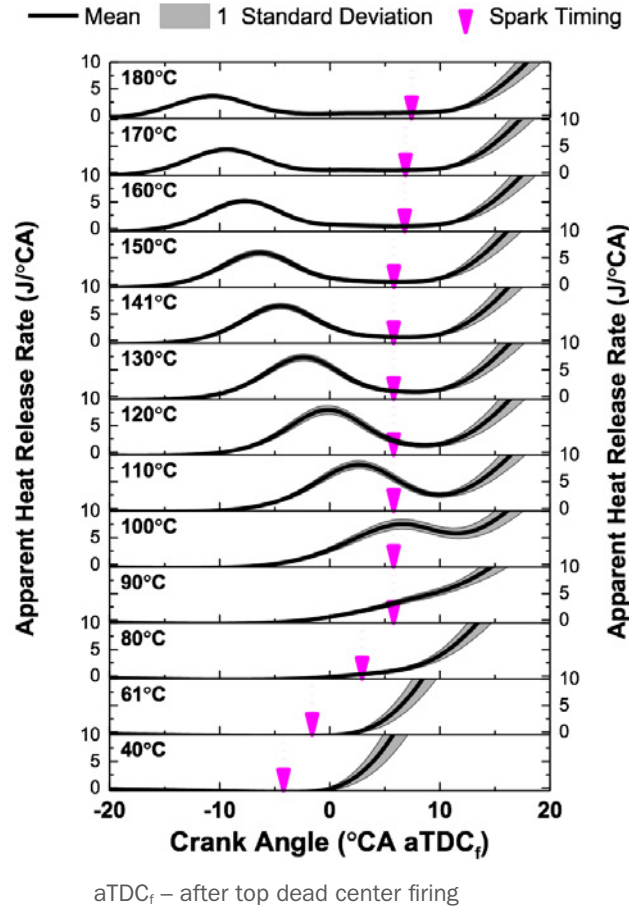


Figure II.11.1. Mean apparent heat release rate plotted for intake temperatures of 40–180°C for 2,000 r/min operation; arrow denotes spark timing, shaded region denotes one standard deviation of data at each condition

The CA50 trends in Figure II.11.3 highlight that once PSHR is expressed, the KLSA CA50 is constant, regardless of PSHR amount. This is somewhat counterintuitive, as Figure II.11.1 and Figure II.11.2 demonstrated that the magnitude of PSHR first increased with increasing intake temperature, but then actually began to decrease as a function of further increasing intake temperature. Thus, by inspection of the PSHR alone, at the highest intake temperatures, the reduced PSHR magnitude would suggest reduced bulk gas temperature. However, as indicated by the gas temperature at CA2 trends in the upper plot of Figure II.11.3, once sufficient PSHR occurs, the bulk gas temperature at CA2 is a constant, plateauing at a temperature of approximately 800 K, a value that was also independent of engine speed. Moreover, for conditions without PSHR, the temperature at CA2 of the deflagration is also approximately constant; but at these conditions the temperature at CA2 does show speed dependency, which can be attributed to increased time for heat transfer at reduced engine speed. These combined trends illustrate two findings. First, without PSHR, the temperature at the start of the deflagration process (i.e., CA2) for KLSA operation is approximately constant. Second, the PSHR process is somewhat self-regulating, in that the in-cylinder temperature at the start of the deflagration (i.e., CA2) reaches a maximum value irrespective of whether the temperature rise is from PSHR or intake temperature. What is interesting from this perspective is that without PSHR, combustion phasing needs to be retarded to maintain a constant bulk gas temperature at CA2. However, what is not obvious is why the 800 K plateau in CA2 bulk gas temperature occurs for conditions with PSHR.

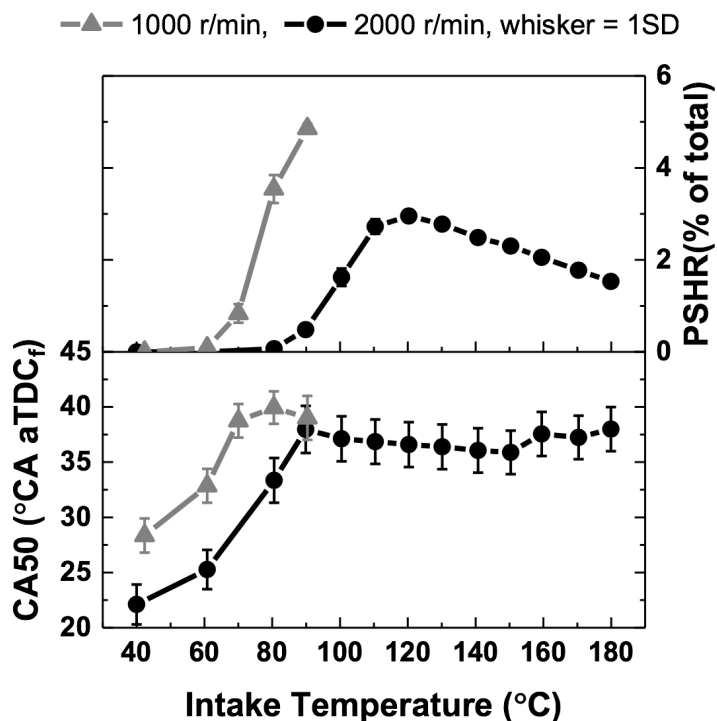


Figure II.11.2. Quantified trends in PSHR and CA50 phasing for 2,000 r/min operation (black, circle markers) and 1,000 r/min operation (grey, diamond markers) as a function of intake temperature; whiskers denote one standard deviation (SD) of the respective property

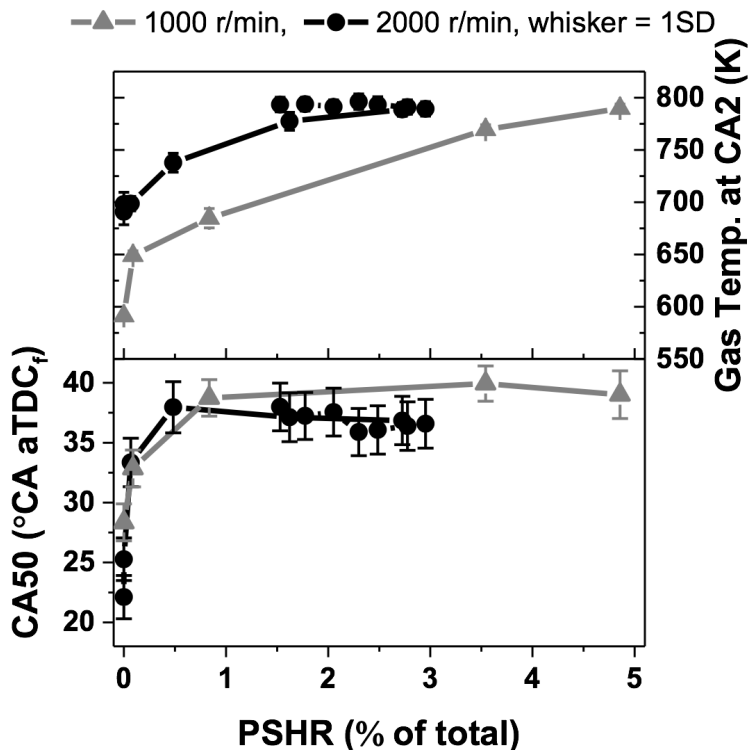


Figure II.11.3. Quantified trends in KLSA CA50 and bulk gas temperature at CA2 of the deflagration as functions of PSHR for 2,000 r/min operation (black, circle markers) and 1,000 r/min operation (grey, diamond markers); whiskers denote one standard deviation of the respective property

To highlight the source of the 800 K plateau, the in-cylinder pressure-temperature history was plotted up to CA2 and overlaid on top of contours of the constant-volume ignition delay in Figure II.11.4, where ignition delay was defined as a 50 K temperature rise. Also indicated in Figure II.11.4 are the spark timing and CA2 pressure-temperature conditions by red dots and blue stars, respectively.

Figure II.11.4 also illustrates that for conditions without PSHR, as deflagration occurs, the end-gas region will traverse a very similar path to conditions with PSHR, suggesting that bulk-gas LTHR reaction in the end gas is highly probable, and understanding these could be critical for knock. However, experimentally observing LTHR in the end gas with conventional pressure-based diagnostics is much more difficult due to the much larger deflagration exotherm conflating direct measurement of the end-gas LTHR process. Nonetheless, the findings in this project suggest that LTHR can exist in the end gas of fuels and could affect knock. Although the effects of PSHR and LTHR on knock still require more research and insight, the current work demonstrates that knock sensitivity changes when LTHR occurs in the bulk gas. Moreover, the current work highlights that fuels with strong negative temperature coefficient behavior can exhibit a self-regulating temperature rise and, correspondingly, a decoupling of intake temperature dependency on when knock occurs.

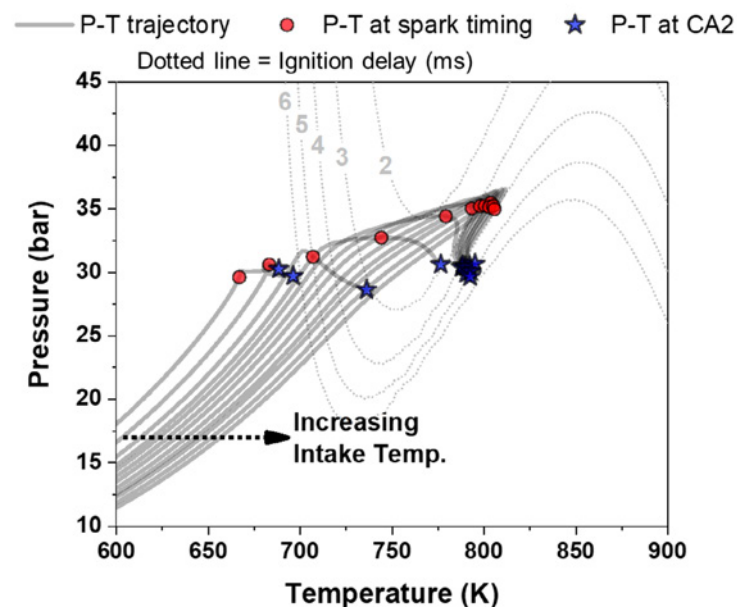


Figure II.11.4. Pressure-temperature trajectory up to 2% of heat release (CA2) of the deflagration (blue star marker); spark discharge timing denoted (red circle markers) for an intake temperature sweep with boosted operation at 2,000 r/min engine speed plotted on constant-volume ignition delay simulation results in milliseconds (grey numbers), with ignition delay defined as a 50 K rise

Conclusions

- Results suggested that LTHR processes are likely present in the end gas of spark ignition engines, but that they are not readily observable with conventional pressure-based combustion diagnostics
- Illustrated that engine operating conditions with pre-spark heat release actually improve the knock tolerance of a fuel
- Revealed that PSHR could offer benefits for knock-limited engine operation at conditions relevant to downsized, boosted spark ignition engines

Key Publications

1. Splitter, Derek A., Arthur Gilliam, James Szybist, and Jaal Ghandhi. 2018. "Effects of Pre-Spark Heat Release on Engine Knock Limit." *Proceedings of the Combustion Institute*.
2. Gilliam, Arthur, Derek A. Splitter, James P. Szybist, and Jaal B. Ghandhi. 2018. "Fuel Kinetic Effects on Pre-Spark Heat Release and Engine Knock Limit." *THIESEL conference*, <https://www.osti.gov/servlets/purl/1468190>.

References

1. Splitter, D., A. Pawlowski, and R. Wagner. 2016. *Frontiers in Mechanical Engineering* 1, <https://doi.org/10.3389/fmech.2015.00016>.
2. Leppard, W.R. 1990. "The Chemical Origin of Fuel Octane Sensitivity." SAE Technical Paper 902137, <https://doi.org/10.4271/902137>.
3. Najt, P.M., and D.E. Foster. 1983. "Compression-Ignited Homogeneous Charge Combustion." SAE Technical Paper. 830264, <https://doi.org/10.4271/830264>.

II.12 Fuel Properties Enhancing Multi-Mode ACI/SI Engine Operation (Argonne National Laboratory)

Toby Rockstroh, Principal Investigator

Argonne National Laboratory
9700 S. Cass Avenue
Argonne, IL 60439
E-mail: trockstroh@anl.gov

Kevin Stork, DOE Technology Development Manager

U.S. Department of Energy
E-mail: Kevin.Stork@ee.doe.gov

Start Date: October 1, 2017	End Date: September 30, 2018	
Project Funding (FY18): \$350,000	DOE share: \$350,000	Non-DOE share: \$0

Project Introduction

The potential efficiency benefits of advanced compression ignition (ACI) in four-stroke gasoline engines are well recognized [1]. However, it has also been acknowledged that the operational limits of ACI required switching to conventional spark ignition (SI) operation for idle conditions and to obtain high specific power output [2–4]. For ACI operation, the temperature and pressure at the end of compression needs to be high enough to initiate auto-ignition, while the high-load SI operation is constrained by the onset of knock.

Similarly, the gasoline fuel for a multi-mode engine needs to fulfill two seemingly contradicting requirements. For ACI operation at low load, a fuel with a moderate auto-ignition propensity is desired, while the high-load SI operation demands a fuel with high auto-ignition resistance in order to prevent knock. Historically, gasoline knock resistance (or conversely, the auto-ignition propensity) has been described by the research octane number (RON) and the motor octane number (MON). It has since been shown that octane number does not adequately describe knock resistance in modern SI engines, and the octane index has been implemented as a practical means to utilize RON and octane sensitivity ($S = \text{RON} - \text{MON}$), as well as engine operating parameters, to more accurately describe the “octane appetite” both in modern SI [5,6] as well as ACI engines [7].

For the purpose of this investigation, five full boiling range gasolines with a RON of 98 were investigated. One of the test fuels had a low octane sensitivity of $S = 3$ while the remaining fuels had a high sensitivity of $S = 10$, albeit utilizing different chemical classes to generate the octane sensitivity. The aim of the study was to investigate the effect of octane sensitivity on the intake temperature swing required to achieve both knock-free high-load SI and stable low-load ACI operation in a gasoline direct injection engine.

Objectives

- Test high-octane-sensitivity fuels (high and low heat of vaporization) vs. low-sensitivity fuels (low heat of vaporization) at two geometric compression ratios
- Quantify the delta between minimum cylinder temperature increase required for stable low-load ACI and temperature reduction required for knock-free high-load SI using the Co-Optima RON 98 fuels
- Determine how octane sensitivity impacts the cylinder temperature swing needed to achieve both knock-free high-load SI as well as stable low-load ACI operation
- Identify fuels with the lowest temperature delta required for multi-mode ACI/SI operation

Approach

All Co-Optima RON 98 fuels were tested on a single-cylinder direct injection SI engine at two compression ratios: 12.6:1 (“low”) and 15.3:1 (“high”). Details of the core fuels are listed in Table II.12.1.

Table II.12.1. Fuel Properties

Property	Method	O30 ^e	E30 ^f	A30 ^g	ALK ^h	N30 ⁱ
PHYSICAL PROPERTIES						
RON (R)	D2699	98.2	97.4	98.1	98.0	98.0
MON (M)	D2700	88.0	86.6	87.8	96.6	87.1
S ^a	R-M	10.2	10.8	10.3	1.4	10.9
LHV ^b	D4809	44.071	38.170	42.952	44.524	43.208
HoV ^c		337	565	412	309	393
COMPOSITION ANALYSIS						
Aromatic ^d	D1319	10.6	8.1	30.8	0	28.2
Olefin ^d	D1319	31.3	5	4.2	0	1.5
Saturate ^d	D1319	58.1	57.1	65	100	70.3
Ethanol ^d	D5599	<0.1	30.59	<0.1	<0.1	<0.1

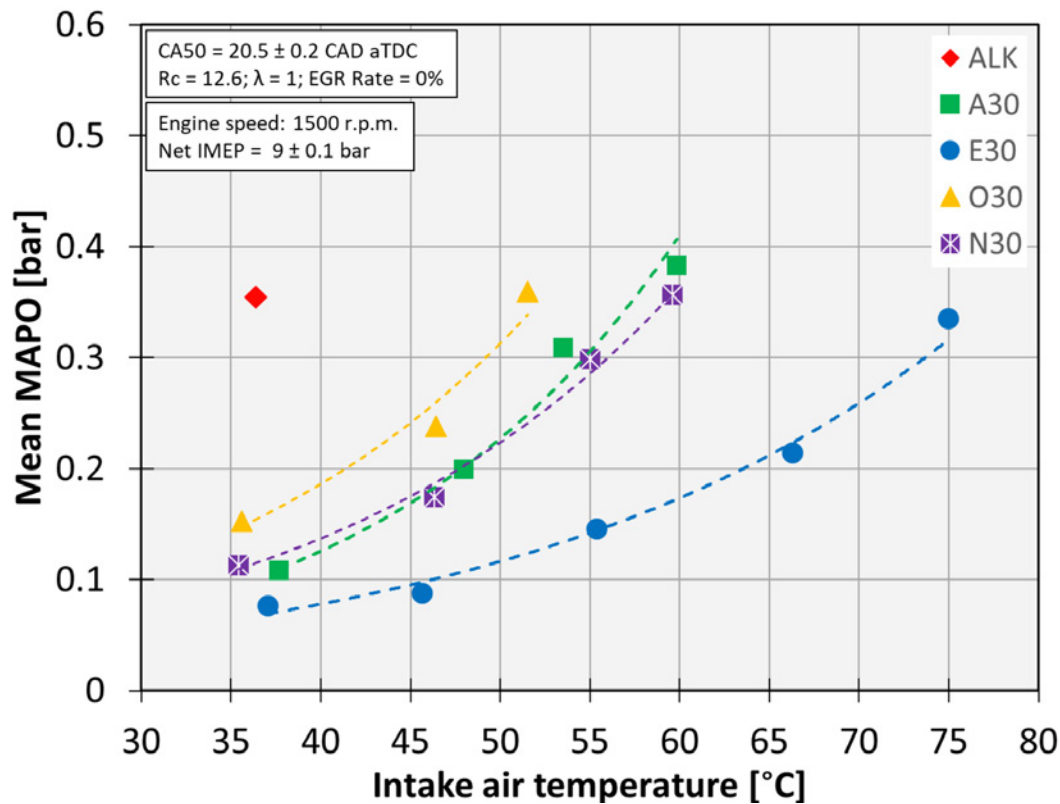
^aS = octane sensitivity, ^bLHV [MJ/kg] = lower heating value, ^cHoV [kJ/kg] = heat of vaporization, ^dvolume fraction, ^eCo-Optima gasoline blend containing 30% olefins by volume, ^fCo-Optima gasoline blend containing 30% ethanol by volume, ^gCo-Optima gasoline blend containing 30% aromatics by volume, ^hPredominantly alkylate-containing (i.e., iso-octane) Co-Optima gasoline blend, ⁱCo-Optima gasoline blend containing 30% naphthenes by volume

At the low compression ratio, the fuels were tested on the engine under conventional SI mode at 9 bar net indicated mean effective pressure (net IMEP) load, as a representative high-load operating condition, and under compression ignition mode at 3 bar net IMEP load, as a representative low-load operating condition. These tests were conducted in order to establish the intake temperature change required to operate the engine at the said “multi-mode” condition with the various fuels, and to test the hypothesis that fuels with higher octane sensitivity require a lower temperature change. The 9 bar net IMEP tests were conducted at constant combustion phasing to determine the highest intake temperature allowable for each fuel for identical knock intensity. Following these high-load tests, the engine was operated under ACI mode with an intake boost pressure of 1 bar (hence intake pressure of 2 bar-a) at constant combustion phasing to determine the intake air temperature required for identical combustion phasing. The data obtained from these tests is used to determine the cylinder temperature change required for “multi-mode” operation at the low compression ratio of 12.6:1.

At the high compression ratio, the initial plan was to repeat the previous study in order to understand the effect of compression ratio on multi-mode operation characteristics of the core fuels, but the engine could not be operated under high-load SI mode due to extremely late combustion phasing resulting in high cyclic variability, and hence abnormal knock behavior from cycle to cycle. Hence, only low-load ACI tests were conducted at moderately boosted intake air conditions (intake pressure in the range 1.05–1.15 bar-a) to determine the intake air temperature required for identical combustion phasing.

Results

The SI engine operation with the ALK fuel at the low compression ratio was found to be knock-limited at the baseline intake temperature of 35°C, as shown in Figure II.12.1. Among the octane-sensitive fuels, the O30 fuel was found to have the lowest knock-limited air temperature of 52°C, while E30 had the highest air temperature of 75°C. The N30 and A30 fuels were found to be knock-constrained at a moderate 60°C. Engine tests using the high compression ratio revealed that the 9 bar operating case was not attainable for any of the test fuels due to excessive knock activity.



MAPO – maximum amplitude pressure oscillation; Rc – compression ratio; EGR – exhaust gas recirculation

Figure II.12.1. Knock intensity as a function of intake air temperature at 1,500 rpm, 9 bar net IMEP, and constant CA50 (crank angle at 50% mass fraction burned) of 20 crank angle degrees (CAD) after top dead center (aTDC)

Due to intake air temperature heating limitations, an intake manifold pressure of 2 bar was required to operate the engine in ACI mode at the lower compression ratio, as shown in the right-hand side segment of Figure II.12.2. The O30 fuel required the lowest intake air temperature of 152°C to enable stable compression ignition, while the A30 fuel needed 170°C. The E30 and ALK fuels required a slightly lower temperature of 167°C, while the N30 fuel needed 163°C intake air heating to maintain the desired combustion phasing CA50 = 12 CAD aTDC. Since a constant intake manifold pressure was maintained, the lambda was adjusted to maintain a constant load of 3 bar net IMEP. The intake boost requirement (due to inadequate heating) at the lower compression ratio shifted the ACI operating range into the RON operating range, as will be discussed later. The high compression ratio was investigated next, as shown in the left-hand side segment of Figure II.12.2. ACI operation was now enabled at near naturally aspirated intake air conditions. At 1.05 bar intake pressure, the ALK fuel required the highest intake air temperature of 182°C, while O30 only needed 150°C. The A30 fuel required approximately 24°C higher intake temperature than O30, despite having similar RON and octane sensitivity. E30 and N30 needed roughly 165°C intake air temperature. The intake pressure was swept to 1.15 bar, resulting in a near-linear reduction of intake air temperature to maintain combustion phasing. The temperature sensitivity ranking of the fuels remained consistent, although a slight change in slope was noticed for the E30 fuel.

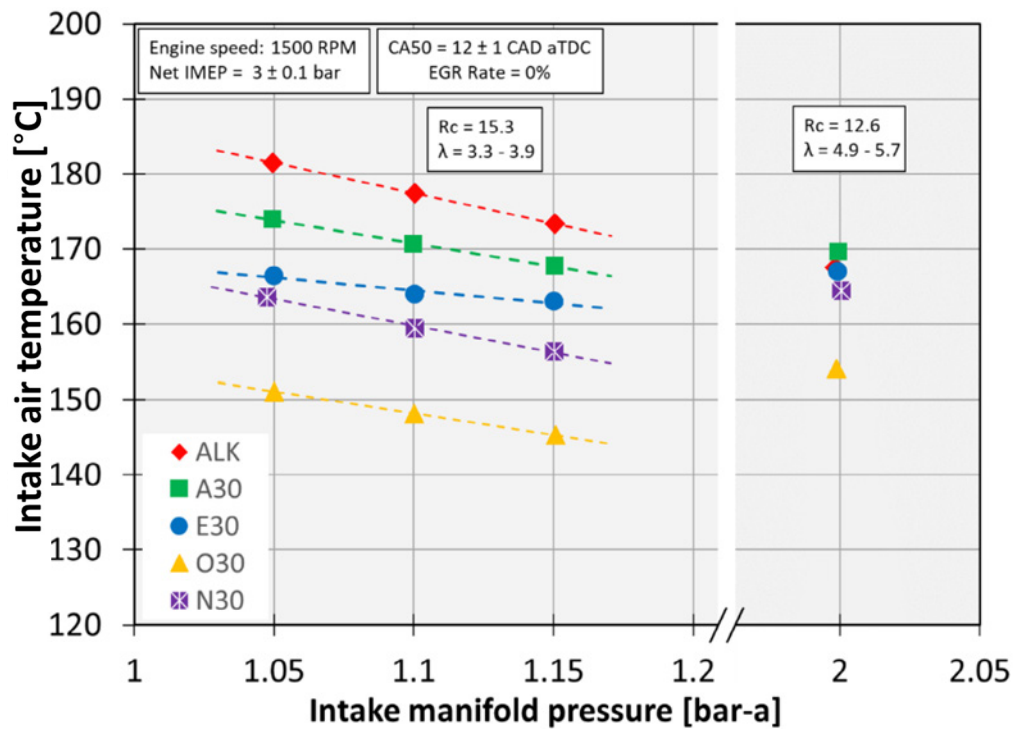


Figure II.12.2. Intake air temperature requirement as a function of intake manifold pressure at 12.6:1 and 15.3:1 compression ratio. Combustion phasing maintained at CA50 = 12 CAD aTDC and 3 bar net IMEP.

The temperature deltas between minimum intake air temperature for ACI and maximum air temperature for knock-limited SI operation are summarized for the five test fuels in Figure II.12.3. The highest temperature change was required for the ALK fuel to enable multi-mode operation, where the higher auto-ignition resistance in ACI mode appears to correlate with the high MON 95 rating. Furthermore, the increased knock propensity of the ALK fuel agrees with previous findings in literature highlighting the benefits of high octane sensitivity in modern gasoline direct injection engines [5–7]. However, the benefits of octane sensitivity at a given RON cannot be universally applied, as indicated by the knock-limited intake air temperatures of the four test fuels with similar RON and octane sensitivity. While O30 was found to exhibit the lowest intake air temperature requirement for ACI operation, it also resulted in a lower knock-limited intake air temperature in SI mode. The A30 and N30 fuels, on the other hand, required significantly higher intake air heating for ACI operation but also enabled a higher knock-limited intake air temperature in SI mode. Overall, E30 was found to require the lowest temperature swing between SI and ACI engine operation.

The inconsistencies in assessing a fuel's suitability for ACI operation in terms of its octane sensitivity are highlighted by investigating the motored compression trajectories in the temperature-pressure diagram shown in Figure II.12.4. Representative compression trajectories are depicted for the A30 and O30 fuels at both geometric compression ratios. The low compression ratio required an intake pressure of 2 bar-a and pushed the cylinder conditions near those of RON. With the high compression ratio, the cylinder conditions were more closely represented by the MON trajectory. It is clearly evident that, despite having the same MON of 88, the O30 fuel required roughly 40 K lower compressed temperature than A30 to maintain the same combustion phasing.

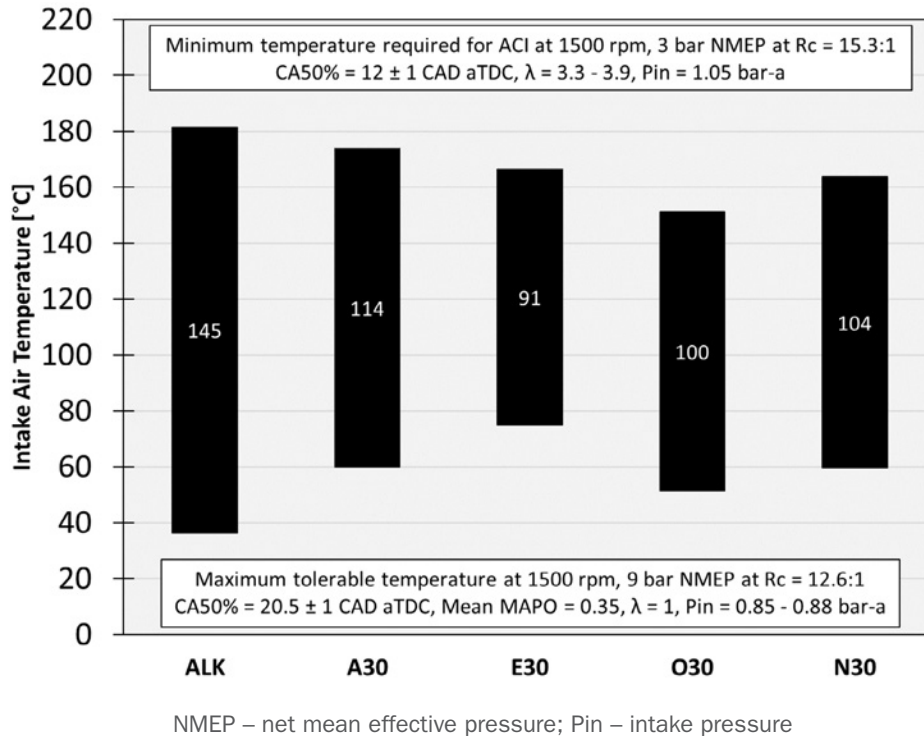


Figure II.12.3. Intake air temperature change for knock-limited SI operation at 9 bar net IMEP and ACI operation at 3 bar net IMEP

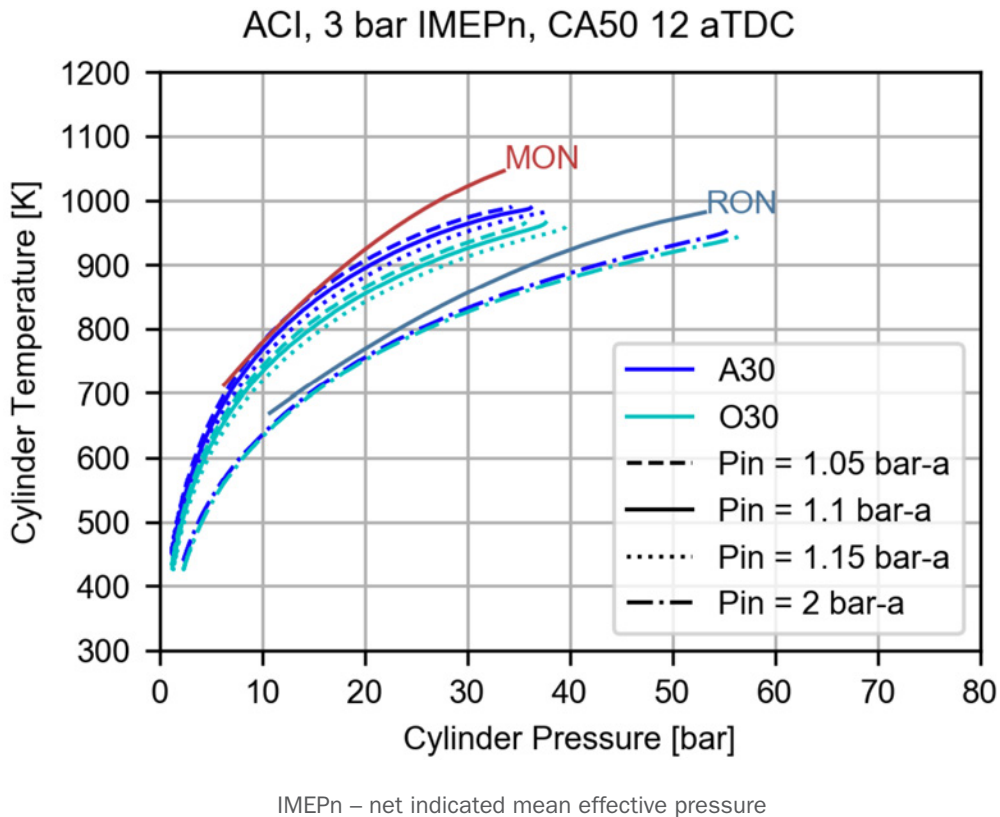


Figure II.12.4. Motored compression trajectories during ACI operation for A30 and O30 test fuels

Conclusions

- A single-cylinder gasoline direct injection engine was successfully operated in compression ignition mode at two geometric compression ratios utilizing the five Co-Optima 98 RON fuels
- With a compression ratio of 12.6:1, an intake temperature sweep was conducted in SI mode at 9 bar net IMEP; however, ACI operation required intake air boosting of 2 bar
- A compression ratio of 15.3:1 enabled near naturally aspirated ACI operation, but knock-free operation at 9 bar net IMEP was not attainable for any of the test fuels
- While the low-octane-sensitive ALK fuel did correlate with the highest multi-mode temperature delta, high octane sensitivity was shown not to be a direct indicator of a fuel's multi-mode temperature delta
- Appreciable variation in the temperature swing required to enable knock-limited SI and low-load ACI was found between all test fuels
- The E30 fuel was found to have the lowest temperature delta

Key Publications

1. Pulpeiro Gonzalez, J., C.P. Kolodziej, and T. Rockstroh. "Statistical Analysis of Fuel Effects on Cylinder Conditions Leading to End-Gas Autoignition in SI Engines." *Proceedings of the SAE 2019 World Congress*, (submitted October 2018, under review).
2. Shah, A., C. Kolodziej, D. Longman, and T. Rockstroh. 2018. "Effect of Octane Sensitivity of Gasoline-like Fuels on Cylinder Temperature Sensitivity towards Mode Switching in a Multi-mode SI Engine." *Fuel* (in preparation).

References

1. Zhao, F., and D. Assanis. 2003. "Homogeneous Charge Compression Ignition (HCCI) Engines." Published by SAE International with a Product Code of PT-94, ISBN of 978-0-7680-1123-4.
2. Milovanovic, N., D. Blundell, S. Gedge, and J. Turner. 2005. "SI-HCCI-SI Mode Transition at Different Engine Operating Conditions." SAE Technical Paper 2005-01-0156, <https://doi.org/10.4271/2005-01-0156>.
3. Milovanovic, N., R. Chen, and J. Turner. 2004. "Influence of the Variable Valve Timing Strategy on the Control of a Homogeneous Charge Compression (HCCI) Engine." SAE Technical Paper 2004-01-1899, <https://doi.org/10.4271/2004-01-1899>.
4. Kulzer, A., A. Christ, M. Rauscher, C. Sauer, et al. 2006. "Thermodynamic Analysis and Benchmark of Various Gasoline Combustion Concepts." SAE Technical Paper 2006-01-0231, <https://doi.org/10.4271/2006-01-0231>.
5. Kalghatgi, G. 2001. "Fuel Anti-Knock Quality - Part I. Engine Studies." SAE Technical Paper 2001-01-3584, <https://doi.org/10.4271/2001-01-3584>.
6. Kalghatgi, G. 2001. "Fuel Anti-Knock Quality- Part II. Vehicle Studies - How Relevant is Motor Octane Number (MON) in Modern Engines?" SAE Technical Paper 2001-01-3585.
7. Kalghatgi, G., K. Nakata, and K. Mogi. 2005. "Octane Appetite Studies in Direct Injection Spark Ignition (DISI) Engines." SAE Technical Paper 2005-01-0244, <https://doi.org/10.4271/2005-01-0244>.

Acknowledgements

Christopher Kolodziej is a principle investigator for this project, and Ashish Shah co-authored this report. This work was made possible with the support of the following: Timothy Rutter, Jorge Pulpeiro and Doug Longman.

II.13 X-Ray Imaging of GDI Sprays with Alcohol Blends (Argonne National Laboratory)

Christopher F. Powell, Principal Investigator

Argonne National Laboratory
9700 S. Cass Ave.
Lemont, IL 60439
E-mail: powell@anl.gov

Kevin Stork, DOE Technology Development Manager

U.S. Department of Energy
E-mail: Kevin.Stork@ee.doe.gov

Start Date: October 1, 2017	End Date: September 30, 2018	
Project Funding (FY18): \$150,000	DOE share: \$150,000	Non-DOE share: \$0

Project Introduction

The introduction of new cleaner-burning fuels into the marketplace must overcome several hurdles. One of these is the fuel's impact on the injection and mixing of fuel and air. It is well known that changing the physical properties of the fuel has an impact on injector performance and combustion [1]. However, the link between engine performance and the fuel's density, viscosity, volatility, and other properties is not well understood. This project aims to determine how the physical properties of the fuel affect the mixture preparation.

The mixture formation will be studied in a spray chamber under conditions that mimic a gasoline direct-injection (GDI) engine. The fuel distributions will be measured for several different operating conditions, including low-load conditions that cause flash boiling and possibly spray collapse. Studies of mixing under these extreme cases will help in the development and validation of computational spray models that establish a scientific link between the fuel properties and the injection, combustion, and engine performance.

Objectives

- Perform two-dimensional (2D) X-ray radiography measurements that quantify the near-nozzle fuel distributions from a GDI injector for two fuels: a non-evaporating calibration fluid and iso-octane. This measurement will quantify the impact of the fuel's volatility on the spray's density distribution.
- Perform 2D X-ray radiography measurements that quantify the near-nozzle fuel distributions from a GDI injector for three alcohol fuel blends at non-evaporating conditions. Comparison of these distributions will show how the fuel composition impacts the spray density.
- Perform three-dimensional X-ray tomography measurements that quantify the spray breakup under flash-boiling conditions for three alcohol fuel blends.

Approach

A detailed understanding of the impact that fuel properties have on the fuel injection process and the mechanisms of spray atomization is needed to spur the adoption of low-carbon fuels. Near-nozzle measurements of sprays using visible light are difficult because of strong scattering from the high number of droplets in this region. For this reason, X-ray diagnostics will be used for these studies. X-rays are highly penetrative and can generate quantitative, unambiguous measurements of useful spray properties, even in the optically opaque region very near the nozzle [2].

Quantitative X-ray measurements of the near-nozzle fuel distribution from GDI injection will be performed. Alcohol fuel blends will be used to vary the physical properties of the fuel, such as density and viscosity, to assess the effect of these properties on the mixture preparation. The first series of measurements will be done

under non-vaporizing conditions, so that phase change does not impact the results and the physical properties are specifically isolated. In this way, the effect that the fuels have on the fuel and air mixing can be quantified and understood based on their physical properties.

In addition to the non-vaporizing studies, a second series of measurements will quantify the near-nozzle fuel distributions under flash-boiling conditions. Flash boiling and spray collapse cause a very abrupt change in the fuel–air mixing and are a big challenge for GDI engines at low loads. The measurements will study phenomena such as spray collapse across a range of fuels and assess how the properties of the fuels impact the mixture preparation and the initial conditions of combustion.

The measurements will quantify the near-nozzle fuel distribution using several alcohol blends. Specifically, this year researchers investigated three fuels: neat iso-octane, iso-octane with 20% ethanol, and iso-octane with 20% butanol. Together, these fuels give a broad span of density and viscosity and allow the impact of those properties on the fuel/air mixing to be assessed. These measurements will be done under non-vaporizing conditions, so that the chemistry of the fuels doesn't matter, and specifically focus on the physical properties.

Results

Quantitative X-ray radiography measurements of the near-nozzle fuel distribution have been performed to study the effect that the physical properties of the fuel, such as density and viscosity, have on the mixture preparation. Time-resolved 2D density projections of the fuel sprays from an eight-hole GDI injector are shown in Figure II.13.1. These plots compare the density distributions between gasoline calibration fluid and iso-octane. The more volatile iso-octane shows reduced peak density and increased spray dispersion.

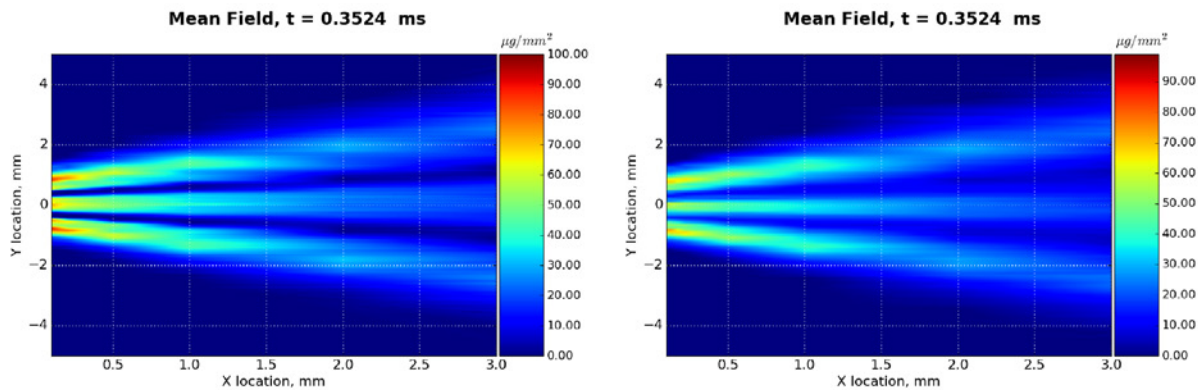


Figure II.13.1. The projected density distribution in sprays emerging from an eight-hole GDI injector. At left is a non-evaporating spray of gasoline-type calibration fluid; at right is a spray from the same injector using iso-octane fuel.

In Figure II.13.2, the effects of flash boiling on GDI sprays are shown for iso-octane fuel. Synchrotron X-ray radiography was used to quantify the density distributions of fuels injected under conditions simulating a GDI engine. Iso-octane was injected at conditions designed to either promote or inhibit flash boiling. Flash boiling is a poorly understood phenomenon that can occur when hot injected fuel encounters partial vacuum in the engine. As shown in Figure II.13.2, when flash boiling occurred, the fuel evaporated more readily, local fuel density decreased, the spread of the injection plumes increased, and the overlap between adjacent spray plumes increased.

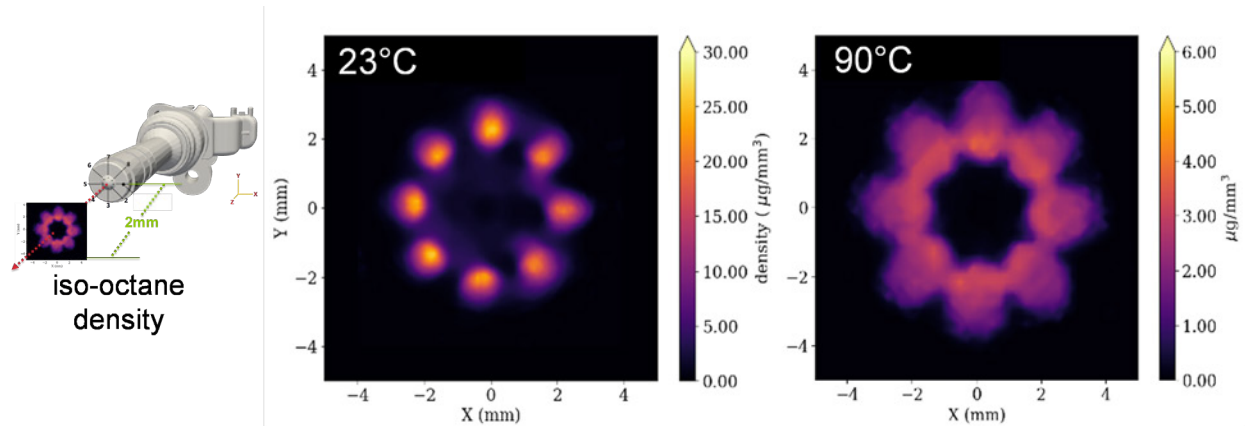


Figure II.13.2. Synchrotron X-ray radiography measurements of iso-octane injection.

The measurements were taken 2 mm from the fuel injection nozzle (left). Under conditions designed to inhibit flash boiling, injection plume density was relatively high, with narrow, well-defined individual plumes (middle). Under flash-boiling conditions, local fuel density decreased, plume spread increased, and the overlap between adjacent spray plumes increased (right).

Blends of iso-octane with 20% ethanol (EtOH) or butanol (BuOH) were also studied under flashing and non-flashing conditions. Figure II.13.3 shows a slice across the density distributions measured one mm from the spray nozzle. While the fuel distributions for iso-octane and BuOH are nearly identical, the peak mass for the EtOH blend is significantly lower and the distribution is broader, indicating that the lower boiling point of EtOH is causing the spray to evaporate and diffuse more quickly. This quantitative data can be compared with simulations to improve our knowledge of the impact of fuel properties on sprays under these extreme conditions.

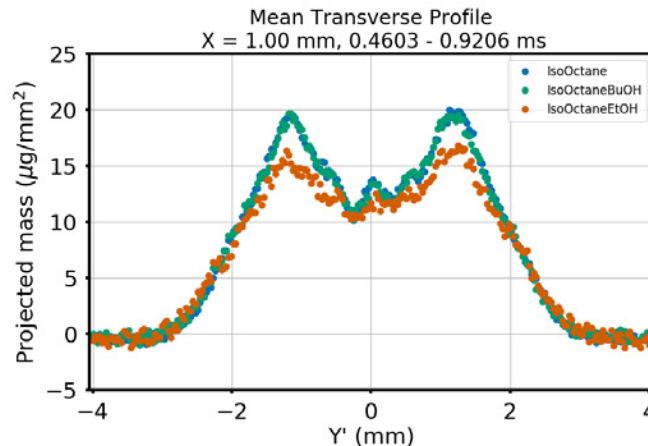


Figure II.13.3. Plot showing slices through the density distributions 1 mm downstream of the fuel injector for three fuels: iso-octane, iso-octane with 20% butanol, and iso-octane with 20% ethanol. The density distribution is dramatically different for the ethanol blend.

Conclusions

Experiments have quantified the near-nozzle fuel density distribution of flash-boiling sprays for the first time, and have done so across a range of fuel properties. The precise measurements will provide other Co-Optima researchers with data for validating computational models that predict the links among fuel properties, fuel density distribution, engine conditions, and combustion characteristics.

References

1. Lešnik, L., B. Vajda, Z. Žunič, L. Škerget, and B. Kegl. 2013. “The Influence of Biodiesel Fuel on Injection Characteristics, Diesel Engine Performance, and Emission Formation.” *Applied Energy* 111: 558–570.
2. Kastengren, L., and C.F. Powell. 2014. “Synchrotron X-Ray Techniques for Fluid Dynamics.” *Experiments in Fluids* 55: 1686.

Acknowledgements

Measurements were performed at the 7BM beamline of the Advanced Photon Source at Argonne National Laboratory. Use of the Advanced Photon Source is supported by the U.S. Department of Energy under Contract No. DEAC0206CH11357. Thanks also to Alan Kastengren, Katarzyna Matusik, Brandon Sforzo, and Aniket Tekawade of Argonne National Laboratory for contributions to this project.

II.14 Fuel Properties Effects on Auto-Ignition in Internal Combustion Engines (Argonne National Laboratory)

Christopher P. Kolodziej, Principal Investigator

Argonne National Laboratory
9700 S. Cass Avenue
Argonne, IL 60439
E-mail: ckolodziej@anl.gov

Kevin Stork, DOE Technology Development Manager

U.S. Department of Energy
E-mail: Kevin.Stork@ee.doe.gov

Start Date: October 2017

End Date: September 2018

Project Funding (FY18): \$350,000

DOE share: \$350,000

Non-DOE share: \$0

Project Introduction

Gasoline octane number is measured on a variable compression ratio Cooperative Fuel Research (CFR) engine under the conditions described by ASTM methods D2699 (research octane number) and D2700 (motor octane number) [1,2]. However, it has been shown that neither of these octane numbers, nor the average of the two (pump octane number), is capable of predicting the knock propensity of fuels with various chemical compositions with modern automotive down-sized boosted direct-injection spark ignition (SI) engines [3–6].

Yates and Swarts have proposed that the cause for this disconnect has to do with variances in the cylinder pressure and temperature conditions experienced by the fuel leading up to end gas autoignition between the octane tests and modern boosted SI engines, as well as the technique for quantifying knock intensity [3,7]. Boosted operation shifts the pressure-temperature trajectory towards higher pressures (at a given temperature) than the research octane number (RON) or motor octane number (MON) methods, which could impact the low-temperature chemistry leading to high-temperature end gas autoignition. The CFR engine also uses a standard “knockmeter” as opposed to the high-speed cylinder pressure transducers typically used for knock intensity quantification on modern SI engines. Hauber et al. have proposed a new method for rating gasoline knock propensity that quantifies knock intensity in the same way as modern SI engines, based on the knocking maximum amplitude of pressure oscillations (MAPO) as measured by a high-speed cylinder pressure transducer [8].

This project has used a well-instrumented standard CFR octane rating engine to investigate the effects of fuel composition and engine intake pressure and temperature on the MAPO knock intensities as measured by CFR knockmeter and cylinder pressure transducer.

Objectives

Overall Objectives

- Identify the effects of fuel composition and engine intake conditions on combustion, end gas autoignition, and knocking characteristics
- Use the trends observed on the CFR engine to correlate with fuel knock propensity on modern boosted SI engines

Fiscal Year 2018 Objectives

- Develop fuel blends of constant RON 98 and investigate the effects of ethanol concentration and base fuel chemical composition on combustion characteristics
- With one fuel blend, investigate the effects of compression ratio, intake pressure, and intake temperature on its end gas autoignition and knocking characteristics

Approach

A standard CFR F1/F2 octane rating engine was outfitted with modern engine combustion research instrumentation: thermocouples, high-speed pressure transducers (intake, cylinder, and exhaust), intake air humidity sensor, electronic knockmeter data logging, wide-range lambda sensor, Coriolis fuel rate meter, compressed air mass flow controller for throttled/boosted operation, Fourier transform infrared spectroscopy emissions (residual gas) characterization, etc. A three-pressure analysis GT-Power model of the CFR engine was developed and validated for estimating cylinder gas temperatures [9].

Two sets of constant RON 98 fuel blends were developed with 0 vol% to 50 vol% ethanol. One set used isooctane and n-heptane primary reference fuels (PRFs) as base fuels and adjusted the proportion of these two components such that RON 98 was achieved for the final blend with increasing levels of ethanol. The other fuel set used toluene standardization fuel (TSF) blends from ASTM D2699 as the base fuels, and the required amount of ethanol was added to reach RON 98. The aromatic (toluene) content ranged from 50 vol% to 74 vol% (depending on the TSF), all representing a significantly higher aromatic content than commercial blendstock for oxygenate blending fuels. It has been shown that base fuel aromatic content reduces ethanol's ability to increase the octane number of the final blend [10,11]. Therefore, the PRF–ethanol blends were studied as the “zero aromatic content” fuel blends, while the TSF–ethanol blends maximized the effects of base fuel aromatic content. Isobutanol blends were also prepared with PRF and TSF base fuels to compare the effects on constant RON 98 splash blending versus ethanol, with and without aromatic (toluene) content. A comparison was made of knock intensities based on the CFR knockmeter and the cylinder-pressure-transducer-based MAPO at both the lambda of highest knock intensity (typically slightly rich) and at stoichiometry, where modern SI engines normally operate. Full boiling range gasoline blends from the Co-Optima RON 98 fuels matrix were also tested for comparison with the surrogate blends.

Through the course of the RON splash-blending studies, it was found that isoparaffinic fuels had unique knocking characteristics compared to fuels with higher aromatic and alcohol content. Therefore, a single isoparaffinic fuel (PRF 90) was selected to explore how intake air temperature, intake pressure, and compression ratio affected its knocking characteristics at stoichiometry. This approach allowed for one fuel to be exposed to a range of cylinder pressure and temperature trajectories, comparable to those found with modern boosted SI engines.

Results

Several PRF and TSF base fuels were blended with ethanol and isobutanol under constant RON 98 splash-blended conditions to understand the effect of base fuel aromatic content on each alcohol's ability to increase the RON of the fuel blend to RON 98. It can be seen in the top graph of Figure II.14.1 that the starting RON of the isoparaffinic PRF base fuels (solid symbols) needed to be significantly lower for a given alcohol blend level than that of the high-aromatic-content TSF base fuels. This shows that the ability to increase octane rating of both alcohols was reduced due to aromatic content in the base fuel. The RON of pure ethanol is estimated to be between 107 (Heywood) and 109 (Hunwartz et al.), and 105 for isobutanol (Christensen, et al.) [12–14]. This could help explain why ethanol was more effective at raising the octane of the base fuel blend than isobutanol, shown by the lower base fuel RON requirement at a given alcohol volume blend level with ethanol. However, it is possible that the two alcohols may also have different blending RON behaviors.

The bottom graph of Figure II.14.1 shows the cylinder-pressure-transducer-based MAPO knock intensity at standard RON 98 test conditions for all fuel blends. It should be noted that these fuels were all blended to RON 98 based on achieving the same CFR knockmeter-based standard knock intensity. At 0 vol% alcohol, a six-fold higher MAPO was observed with the highly isoparaffinic PRF (1.2 bar) compared to the highly aromatic toluene-based fuel (0.2 bar). As alcohol content (ethanol or isobutanol) increased, the MAPO-based knock intensities of the isoparaffinic PRF-based fuels decreased significantly, while the MAPOs of the aromatic TSF-based fuels were not affected. The PRF–alcohol blends reached the same low MAPO values as the TSF–alcohol blends (0.2 bar) for approximately 25 vol% to 30 vol% alcohol levels and higher. As a reminder, all test points in Figure II.14.1 were at the lambda of maximum knockmeter knock intensity, slightly richer than stoichiometry, of each fuel during standard RON testing.

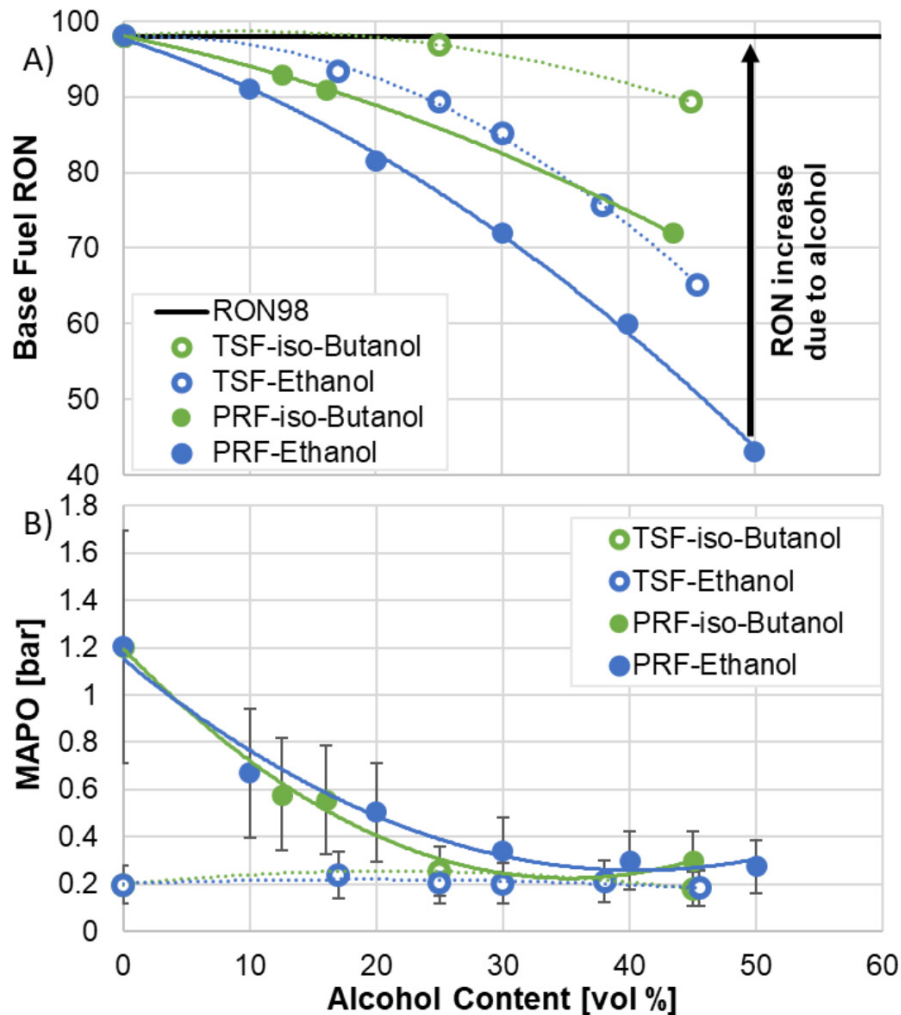


Figure II.14.1. Ethanol and isobutanol effects on the required base fuel RON to obtain constant RON 98 of the final fuel blends and the effects on the cylinder-pressure-transducer-based MAPO knock intensities

Lambda sweeps were performed at RON test conditions with several RON 98 fuels, including PRF 98 and PRF 96.9, to investigate the effects of rating the octane of fuels based on their lambda of highest knock intensity, per D2699, or at stoichiometry, where modern SI engines typically operate. The lambda of peak knock was slightly richer than stoichiometry for all fuel blends. So knock intensities decreased as the lambda was swept from slightly rich to stoichiometry. In order to perform an effective RON rating at each lambda, the knock intensity of PRF 98 was defined as that of an effective RON 98, and the knock intensity of PRF 96.9 as that of an effective RON 96.9. Based on those reference knock intensities, the effective RON of the other fuels could be calculated by the octane bracketing method at each lambda based on either the CFR knockmeter knock intensity (Figure II.14.2A and Figure II.14.2B) or the cylinder-pressure-transducer-based MAPO knock intensity (Figure II.14.2C and Figure II.14.2D). Figure II.14.2A and Figure II.14.2B show that at each fuel's peak knocking lambda, their RON ratings were all approximately RON 98 based on the CFR knockmeter. However, the effective RON ratings decreased for the PRF-ethanol blends, TSF, and the Co-Optima RON 98 E30 (gasoline blend with 30% ethanol by volume) and high-aromatic fuels as the lambda swept from peak knocking lambda to stoichiometry. This means that the knockmeter knock intensities of those fuels diverged from the knock intensities of the PRFs as lambda approached stoichiometry. The only gasoline blend that seemed to maintain its effective RON rating at stoichiometry was the highly isoparaffinic Co-Optima RON 98 alkylate fuel. This shows similar knock intensity behavior with the isoparaffinic fuels, such as PRF and the Co-Optima alkylate fuel, compared to the aromatic and ethanol blends. Based on the CFR knockmeter at

stoichiometric conditions, the effective stoichiometric RON of the non-isoparaffinic fuels decreased by three to six octane numbers.

The effective RON ratings were also calculated using the cylinder-pressure-transducer-based MAPO knock intensities. As shown in Figure II.14.1B, fuels with the same RON can have very different MAPO-based knock intensities. Figure II.14.2C and Figure II.14.2D show the effective MAPO-based RON values of the test fuels at each lambda. The MAPO-based knock intensities of PRF 98 and PRF 96.9 were again chosen as reference values at each lambda. At peak knocking lambda, the lower MAPO-based knock intensities of the PRF-ethanol blends compared to those of the PRFs caused their MAPO-based RON rating to be two to five octane higher than that of PRF 98 (Figure II.14.2C). A similar trend was found with the TSF and the Co-Optima RON 98 E30 and high-aromatic fuels. Interestingly, the MAPO-based knock intensities of all fuels converged as lambda approached stoichiometry, causing their MAPO-based RON ratings to also converge. This shows, perhaps coincidentally, that fuels blended to have the same CFR knockmeter-based RON values may still have the same knock propensities on modern SI engines, operating at stoichiometry and evaluating knock intensity based on cylinder-pressure-transducer-based MAPO.

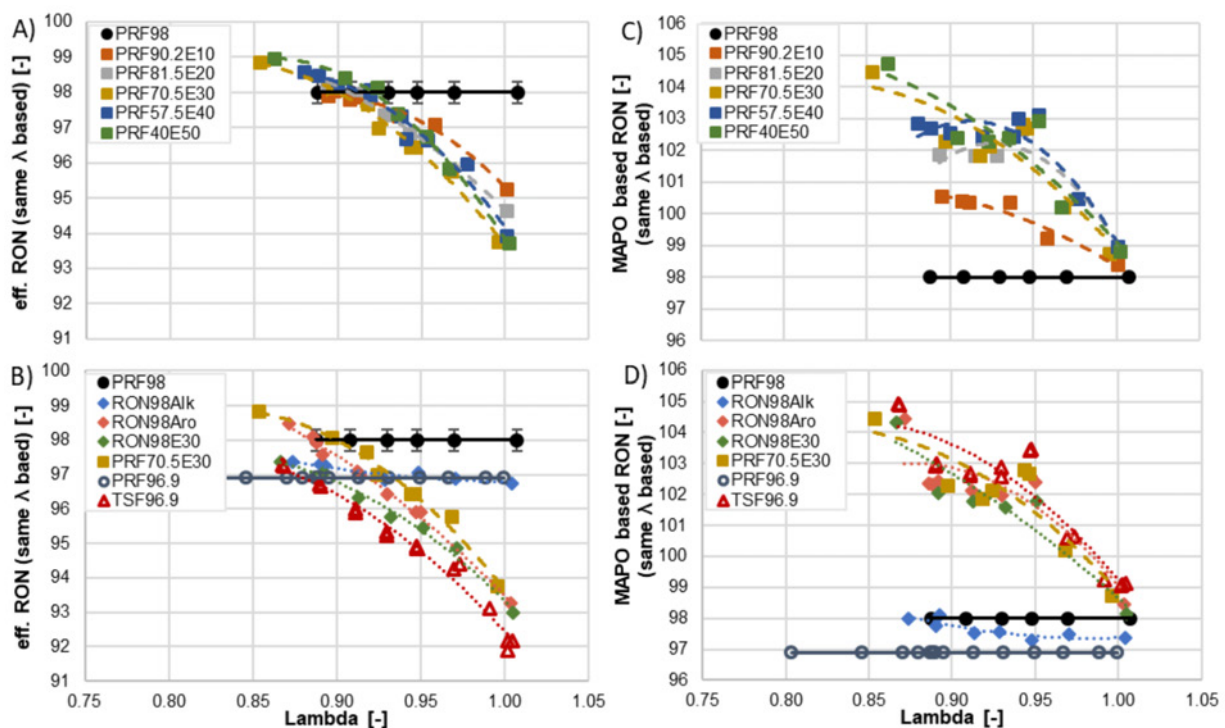


Figure II.14.2. Effective octane ratings of non-PRF fuels between their peak knocking lambdas and stoichiometry based on the CFR knockmeter knock intensities (A and B) and the cylinder-pressure-transducer-based MAPO knock intensities (C and D)

Seeing the unique knockmeter and MAPO-based knock intensity behavior of isoparaffinic fuels compared to aromatic and ethanol blends, one isoparaffinic fuel (PRF 90) was chosen for a detailed study of the effects of intake pressure and temperature. Starting from RON test conditions, the lambda was adjusted to stoichiometry, and the intake pressure was increased to 1.1, 1.2, and 1.3 bar absolute to achieve similar cylinder conditions as a modern boosted SI engine. The effects of temperature were also tested by increasing the intake temperature to 90°C and 150°C. To note, the mixture intake temperature of the MON test (ASTM D2700) is 149°C.

Figure II.14.3 shows the cylinder pressure traces of three PRF test conditions, which all had the same knockmeter knock intensities. It can be seen that the knocking characteristics varied significantly. Between the three test conditions, the timing and pressure of the knock point, where end gas autoignition occurs, was earliest and at the lower pressure with the highest intake pressure and temperature. At lower temperatures

(33°C and 45.3°C), the knock point occurred at similar timings, but at higher cylinder pressure with higher intake pressure. The MAPO in the pressure trace was significantly reduced with increased boost pressure at the relatively lower intake temperatures. However, MAPO increased when the temperature was raised at higher intake pressure.

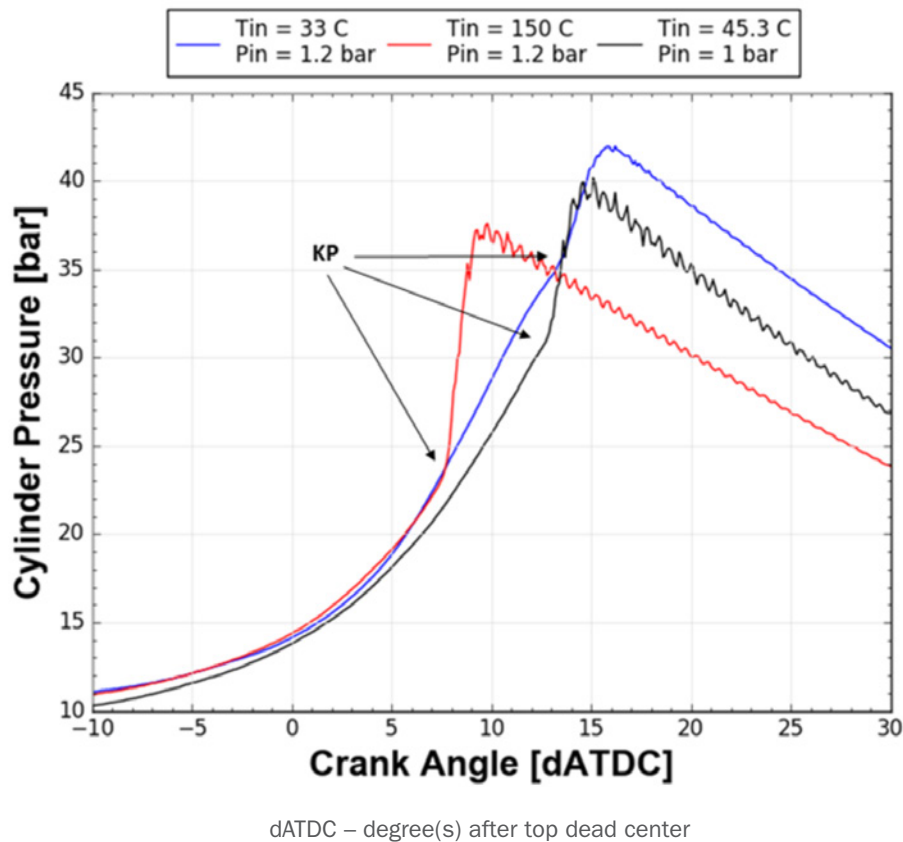


Figure II.14.3. Three PRF 90 test conditions with the standard knockmeter knock intensity, using variations to intake temperature (T_{in}) and pressure (P_{in})

Conclusions

- Under constant RON 98 splash-blended conditions, aromatic (toluene) content in the base fuel reduced the octane-enhancing capability of ethanol and isobutanol.
- Isoparaffinic fuels have an approximately six-fold increase in cylinder-pressure-transducer-based MAPO knock intensity compared to fuels with high aromatic or alcohol content at the same RON 98 level, rated by the CFR knockmeter-based knock intensity.
- For constant RON 98 fuel blends, cylinder-pressure-transducer-based MAPO knock intensities converge regardless of PRF and TSF base fuel composition once ethanol or isobutanol content exceeds 25–30 vol%.
- Starting from peak knocking lambda and moving towards stoichiometry, knockmeter-based knock intensities diverge between isoparaffinic fuels and those with aromatic and ethanol content, causing their effective knockmeter-based stoichiometric RON ratings to diverge.
- Starting from peak knocking lambda and moving towards stoichiometry, cylinder-pressure-transducer-based MAPO knock intensities converge between isoparaffinic fuels and those with aromatic and ethanol content, causing their MAPO-based stoichiometric RON ratings to be coincidentally similar to their original standard RON ratings.
- Intake pressure and temperature also have important effects on the cylinder-pressure-transducer-based MAPO knock intensity and location of knock point for a given isoparaffinic fuel (PRF 90).

Key Publications

1. Rockstroh, T., C. Kolodziej, M. Jespersen, et al. 2018. "Insights into Engine Knock: Comparison of Knock Metrics across Ranges of Intake Temperature and Pressure in the CFR Engine." SAE Technical Paper 2018-01-0210, doi:10.4271/2018-01-0210.
2. Choi, S., C.P. Kolodziej, A. Hoth, and T. Wallner. 2018. "Development and Validation of a Three Pressure Analysis (TPA) GT-Power Model of the CFR F1/F2 Engine for Estimating Cylinder Conditions." SAE Technical Paper 2018-01-0848, doi:10.4271/2018-01-0848.
3. Hoth, A., C. Kolodziej, T. Rockstroh, et al. 2018. "Combustion Characteristics of Match-Blended PRF and TSF Fuels with Ethanol in an Instrumented CFR Engine." SAE Technical Paper 2018-01-1672.

References

1. ASTM International. 2015. "Standard Test Method for Research Octane Number of Spark-Ignition Engine Fuel." ASTM D2699-15a.
2. ASTM International. 2016. "Standard Test Method for Motor Octane Number of Spark-Ignition Engine Fuel." ASTM D2700-16.
3. Swarts, A., A. Yates, C. Viljoen, and R. Coetzer. 2005. "A Further Study of Inconsistencies between Autoignition and Knock Intensity in the CFR Octane Rating Engine." SAE Technical Paper 2005-01-2081, doi:10.4271/2005-01-2081.
4. Mittal, V., and J. Heywood. 2008. "The Relevance of Fuel RON and MON to Knock Onset in Modern SI Engines." SAE Technical Paper 2008-01-2414, doi:10.4271/2008-01-2414.
5. Mittal, V., and J. Heywood. 2010. "The Shift in Relevance of Fuel RON and MON to Knock Onset in Modern SI Engines Over the Last 70 Years." *SAE Int. J. Engines* 2 (2): 1–10, doi:10.4271/2009-01-2622.
6. Kalghatgi, G. 2001. "Fuel Anti-Knock Quality- Part II. Vehicle Studies - How Relevant is Motor Octane Number (MON) in Modern Engines?" SAE Technical Paper 2001-01-3585, doi:10.4271/2001-01-3585.
7. Yates, A., A. Swarts, and C. Viljoen. 2005. "Correlating Auto-Ignition Delays and Knock-Limited Spark-Advance Data for Different Types of Fuel." SAE Technical Paper 2005-01-2083, doi:10.4271/2005-01-2083.
8. Hauber, J., K. Huber, and R. Nell. 2018. "New GKI - Gasoline Knock Index for Rating of Fuel's Knock Resistance on an Upgraded CFR Test Engine." SAE Technical Paper 2018-01-1743.
9. Choi, S., C.P. Kolodziej, A. Hoth, and T. Wallner. 2018. "Development and Validation of a Three Pressure Analysis (TPA) GT-Power Model of the CFR F1/F2 Engine for Estimating Cylinder Conditions." SAE Technical Paper 2018-01-0848, doi:10.4271/2018-01-0848.
10. Foong, T., K. Morganti, M. Brear, G. Silva, et al. 2014. "The Octane Numbers of Ethanol Blended with Gasoline and its Surrogates." *Fuel* 115: 727–739, doi:10.1016/j.fuel.2013.07.105.
11. Hoth, A., C. Kolodziej, T. Rockstroh, et al. 2018. "Combustion Characteristics of Match-Blended PRF and TSF Fuels with Ethanol in an Instrumented CFR Engine." SAE Technical Paper 2018-01-1672.
12. Hunwartz, I. 1982. "Modification of CFR Test Engine Unit to Determine Octane Numbers of Pure Alcohols and Gasoline-Alcohol Blends." SAE Technical Paper 820002, doi:10.4271/820002.
13. Heywood, J. 1998. *Internal Combustion Engine Fundamentals*. New York: McGraw-Hill. ISBN: 0-07-028637-X.

14. Christensen, Earl, Janet Yanowitz, Matthew Ratcliff, and Robert L. McCormick. 2011. “Renewable Oxygenate Blending Effects on Gasoline Properties.” *Energy & Fuels* 25 (10): 4723–4733, doi:10.1021/ef2010089.

Acknowledgements

Toby Rockstroh is the co-principal investigator for this project. Several people assisted in making this work successful, including Alexander Hoth, Timothy Rutter, Dave Bell, and Doug Longman.

II.15 RCM for Kinetic Mechanism Development (Argonne National Laboratory)

S. Scott Goldsborough, Principal Investigator

Argonne National Laboratory (ANL)
9700 S. Cass Avenue
Argonne, IL 60439
E-mail: scott.goldsborough@anl.gov

Kevin Stork, DOE Technology Development Manager

U.S. Department of Energy
E-mail: Kevin.Stork@ee.doe.gov

Start Date: October 1, 2017	End Date: September 30, 2018	
Project Funding (FY18): \$150,000	DOE share: \$150,000	Non-DOE share: \$0

Project Introduction

Fuel performance in modern spark ignition and advanced compression ignition (ACI) engines depends on many fuel properties. Although autoignition chemistry is a primary driver, heat of vaporization and flame speed, as well as chemical kinetic sensitivities to thermal and compositional stratification, are also important. Furthermore, the development and propagation/amplification of pressure waves after localized autoignition events leading to structural damage can also be dependent on the fuel. The capability to model, and thus predict, fuel performance based on fundamental measurements could significantly reduce the costs and time associated with co-optimizing fuels and engines.

The efforts of this project are primarily focused on acquiring experimental autoignition data that will (a) support the development, validation and improvement of robust chemical kinetic mechanisms for real and surrogate fuels; and (b) provide insight into the chemical effects of fuel performance in boosted spark ignition and ACI engines.

Objectives

Overall Objectives

- Acquire autoignition data for a variety of conventional and potential high-performance fuels using ANL's rapid compression machine (RCM) facilities, at conditions relevant to boosted spark ignition and ACI engines, necessary for the development/validation of chemical kinetic models and the interpretation of fuel-engine interactions
- Investigate fuel-dependent chemical kinetic processes which influence fuel performance

Fiscal Year (FY) 2018 Objectives

- Acquire additional data for five compositionally diverse, high research octane number (RON) Co-Optima core fuels over an extended range of thermodynamic and fuel-loading conditions beyond FY 2017 efforts
- Acquire autoignition data for select high-performance fuels over a range of fuel loadings and thermodynamic conditions, and blends of these with a research-grade full boiling-range fuel
- Expand RCM database of iso-olefins to facilitate formulation of robust rate rules for such fuel constituents
- Demonstrate experimental, RCM-based approach to measure ϕ -sensitivity of fuels

Approach

The work pursued for this project seeks to address challenges associated with measuring the autoignition properties of potential future fuels and fuel blends, interpreting their performance in combustion engines (in terms of knock and combustion phasing), and properly modeling their behavior in zero- and multi-dimensional

simulation frameworks. The approach used in this project is based on ANL's RCM, where this device is able to access experimental conditions that are directly relevant to modern spark ignition and ACI engines, e.g., $T = 650\text{--}1,100\text{ K}$, $P = 10\text{--}100\text{ bar}$, $O_2 = 10\text{--}21\%$, $\phi = 0.2\text{--}2.0+$. ANL's RCM typically uses 10–20 mL of fuel to conduct tests covering a wide range of conditions, with the autoignition chemistry studied over the low-temperature, negative-temperature-coefficient, and intermediate-temperature regimes. Smaller volumes can be used to explore focused operating regimes.

RCMs have been used for nearly 100 years to investigate autoignition phenomena at engine-relevant conditions, and they have continually become more sophisticated [1,2]. They are capable of creating and maintaining well-controlled, elevated-temperature and -pressure environments where the chemically active period preceding autoignition can be decoupled from physical interactions that occur in an engine and some combustion vessels, e.g., spray breakup, turbulent fuel/air mixing, thermal/compositional stratification. Furthermore, the operating conditions, e.g., T , P , ϕ , and O_2 , can be independently varied, unlike in internal combustion engines, and this provides necessary insight. The ability to utilize wide ranges of fuel and oxygen concentrations within RCMs, from ultra-lean to over-rich, and spanning dilute to undiluted regimes, offers specific advantages relative to other laboratory apparatuses such as shock tubes and flow reactors, where complications can arise under such conditions. ANL's twin-piston RCM is utilized in this project where ignition times are measured and heat release rates are quantified.

Results

Key accomplishments for FY 2018 include:

- Acquiring data for five compositionally diverse, high RON Co-Optima core fuels at thermodynamic and fuel-loading conditions relevant to ACI engine operation; evaluating experimental trends against ACI engine data and comparing to chemical kinetic model predictions using Lawrence Livermore National Laboratory (LLNL) Co-Optima mechanism;
- Acquiring autoignition data for $C_2\text{--}C_4$ high-performance alcohol fuels (unblended) covering a range of fuel loadings and thermodynamic conditions;
- Acquiring new autoignition data for 2-methyl 2-pentene, a C_5 iso-olefin, over a range of experimental conditions for comparison against the 2-methyl 2-butene dataset;
- Evaluating normalized ϕ -sensitivity (Φ_s^*) of research-grade, full boiling-range E10 (10% ethanol, 90% gasoline fuel blend) gasoline over a range of conditions based on Sandia National Laboratories-defined Φ_s^* , and comparing experimental trends to model predictions.

Experiments were conducted to further characterize the autoignition behavior of the five high RON, full boiling-range fuels blended for the Co-Optima program in FY 2017. One fuel has near-zero sensitivity (i.e., the difference between RON and motor octane number [MON]), while the others have MON near 87. The fuels are ALK, E30, A30, O30, and N30, where the first is a predominantly alkylate-containing (i.e., iso-octane) mixture, while the remaining four are blended at 30% vol./vol. ethanol, aromatics, olefins, and naphthenes, respectively. The compositions of the four base fuels were adjusted by the supplier to meet octane number specifications, so the base blendstocks are unique and compositionally diverse. Combustion engine performance (e.g., phasing) under ACI scenarios has been demonstrated to be significantly influenced by fuel composition, rather than conventional fuel specifications, and efforts this year further clarified this.

Tests were conducted at compressed temperature (T_c) = 875–1,000 K and compressed pressure (P_c) = 15– 80 bar, with a focus on undiluted, lean fuel loadings, $\phi = 0.28$ and 0.38. These conditions are relevant to future ACI and spark ignition/ACI multi-mode engines but are well beyond the test protocols of RON and MON. Experiments were undertaken with the compressed pressures targeted at each compressed temperature to achieve ignition times of 2–20 ms. These timescales are relevant to operating piston engines. Comparisons were made directly against data from a single-cylinder, direct-injection engine, which was operated under nearly homogeneous charge compression ignition conditions, with the injection timing set just after intake valve closing (i.e., -300 degrees after top dead center [$^\circ$ aTDC]). The engine speed was fixed

at 1,500 rpm, and for three intake temperatures ($T_{in} = 100^{\circ}\text{C}$, 135°C , and 170°C), the corresponding intake pressures were adjusted to hold the combustion phasing (crank angle of 50% accumulated heat release, CA50) fixed at 12°aTDC . Chemical kinetic modeling at the RCM test conditions was also undertaken for comparison against the measurements, where the LLNL Co-Optima model was employed with multi-component surrogates used to represent the five, full boiling-range fuels [3].

Representative results are presented in Figure II.15.1, where reactivity maps are shown for ALK at the two fuel loadings and covering the range of compressed conditions experienced in the engine. Isoleths of ignition delay time are shown at 2 ms, 4 ms, 8 ms, and 16 ms, with symbols indicating the data and lines the model results. The trends illustrate how, as temperature increases, the test mixtures become more reactive, such that lower pressures are needed to achieve the same autoignition times. Conversely, there is an appearance of negative-temperature-coefficient behavior at lower temperature and higher pressure. Evident in Figure II.15.1 is that the kinetic model does a fairly good job replicating the ALK fuel reactivity, though there are some discrepancies. For instance, at cooler temperatures, the model does not align as well with the data points, while the spacings between the isopleths become larger than observed in the experiment. The latter feature indicates that the model is not as ‘pressure-sensitive’ as the real fuel. Finally, as the mixture becomes richer (i.e., $\phi = 0.28 \rightarrow 0.38$), the fuel is more reactive, with, again, lower pressures required for the same autoignition times.

The engine measurements are also shown in Figure II.15.1, where the top dead center pressure and temperature conditions are plotted, with the temperatures calculated using a mass-averaged approximation. Non-reactive (i.e., motored) conditions are used to be analogous to the RCM reporting protocol. It can be seen that the isopleth of $\text{CA}_{50} = +12^{\circ}\text{aTDC}$ falls generally close to the 4 ms experimental points, while there are some differences in apparent reactivity.

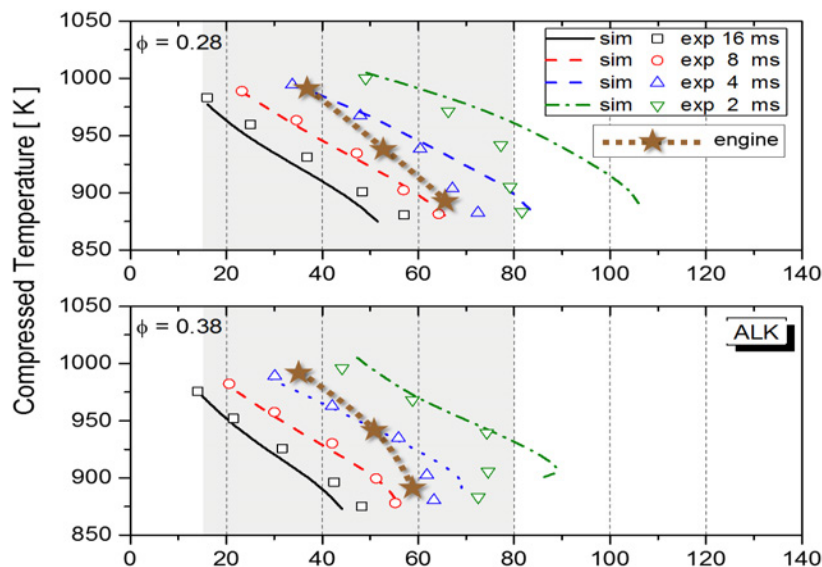


Figure II.15.1. Isoleths of RCM-measured and chemical kinetically modeled ignition delay times under static (i.e., constant volume) conditions compared against isopleths of ACI engine top dead center conditions (with $\text{CA}_{50} = +12^{\circ}\text{aTDC}$). Shaded regions indicate the range of pressures covered in the RCM experiments; points beyond this are extrapolations of observed trends.

Figure II.15.2 next summarizes the RCM and model results for the five fuels where the relative reactivities are plotted directly against relative reactivities observed during engine operation. The ALK fuel is used as a baseline here since it has near-zero sensitivity. The intake pressures required to hold combustion phasing fixed at the three intake temperature conditions are used on the x-axis, while the pressures required to achieve autoignition times of 4 ms are used on the y-axis. Fuel-to-fuel differences visible here highlight shortcomings of octane rating for characterizing ACI operation since the four fuels have identical ratings.

A parity line is drawn in Figure II.15.2 to indicate a situation of perfect correlation between the static measurements in the RCM/model and the data from the dynamic, variable-volume engine. In general, it can be seen that the RCM trends correspond fairly well with the engine data, though there are some inconsistencies. On the other hand, it appears that the model reactivity trends are quite different from the data. For instance, the E30 and O30 are predicted to be much more and less reactive, respectively.

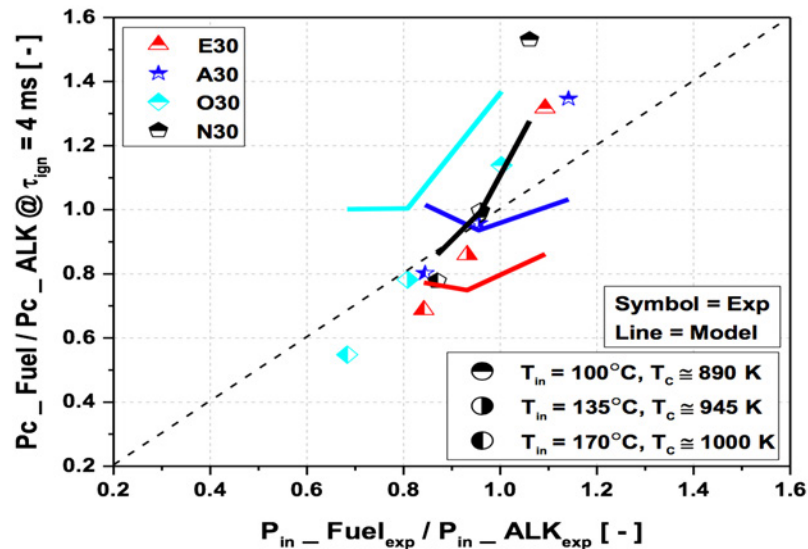


Figure II.15.2. Comparison of relative fuel reactivities where static conditions (in RCM and model) are ranked against engine-intake requirements at $\phi = 0.38$. Baseline fuel is ALK. Intake pressure (P_{in}) of engine adjusted at each T_{in} to maintain CA50 = +12 °aTDC. T_c of RCM and model selected using engine-estimated, motored top dead center conditions; P_c of RCM and model adjusted to achieve $\tau_{ig} = 4$ ms. Parity conditions shown as dashed line; departures from this indicate inconsistencies with ACI engine data.

Figure II.15.3 next compares the RCM-based, experimentally measured (apparent) heat release rates (HRRs) against calculated ones for the five fuels and multi-component surrogates, respectively. Quantification of discrepancies has implications for model-based fuel co-optimization, as well as a range of modeling approaches covering reduced-order, as well as multi-dimensional, ones. Disagreements in exothermicity progress can influence fuel–engine interactions and associated control strategies. Recent work has described how RCM measurements can be used to derive important information from pressure-time datasets towards quantifying the evolution and trends of preliminary exothermicity, i.e., low- and intermediate-temperature heat release, as well as high-temperature heat release, and how these can be utilized for the evaluation and improvement of chemical kinetic models [4].

Direct comparisons are presented at one representative temperature and reactivity ($T_c = 940$ K, 4 ms) for a fuel loading of $\phi = 0.38$. The HRRs are shown as functions of accumulated heat release, as in [5]. In Figure II.15.3, it can be seen that no low-temperature heat release is observed, but there is appreciable intermediate-temperature heat release, while the high-temperature heat release process appears to occur in two phases, covering accumulated heat release of ~ 0.1 – 0.75 , with a slow final period, to ~ 0.8 . The last portion is difficult to visualize in this presentation due to measurement noise contained within the HRR calculation, but it is readily distinguished at time-based representations. The maximum accumulated heat release recorded for the tests is near 70–80% of the lower heating value of the mixture. This is due to exothermicity-induced heat loss in the RCM’s reaction chamber relative to the non-reacting experiments used to parameterize the HRR calculation. Specifically, there is a pressure/temperature rise in the gas, causing steeper thermal gradients near the walls, while additional gas flow is driven into the piston crevices by the pressure rise. These features are not properly captured by the methodology to derive HRRs [4]. The peak HRRs seen in Figure II.15.3 are much higher than at the $\phi = 0.28$ condition (not shown here), while only slight fuel-to-fuel differences are evident.

There are significant discrepancies seen between the measurements and the model. Some challenges related to such comparisons include sampling frequency and filtering of the datasets that need to be considered [4]. At the $\phi = 0.38$ condition, the simulations, like the measurements, indicate two high-temperature heat release phases, but this depends on the fuel. In general, this occurs at accumulated heat release $\sim 0.1\text{--}0.5$, $0.5\text{--}0.9$, and $0.9\text{--}1.0$, with the middle portion the most explosive. There are significant fuel-to-fuel differences. For instance, simulations for ALK and E30 have the most intense HRRs, while the other three have slower rates across the first portion of the high-temperature heat release process. The magnitude and extent of the phase distinctions seem to follow the extent of 1,2,4-trimethyl benzene contained in the surrogate blend.

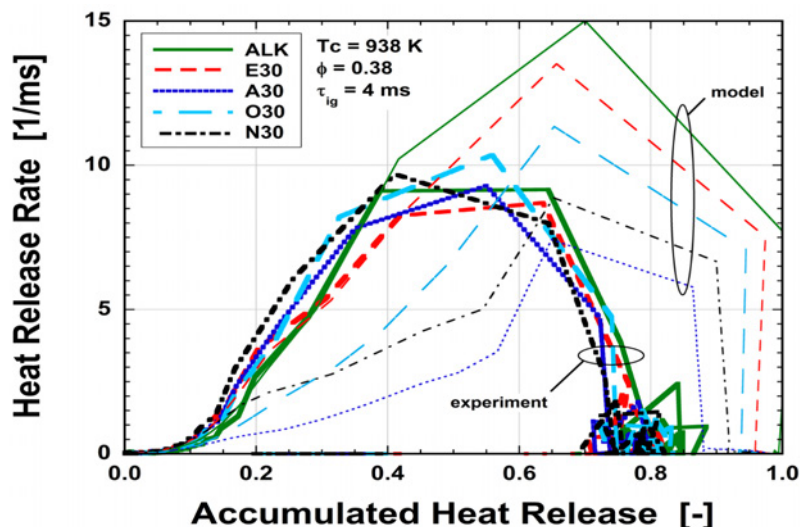


Figure II.15.3. Comparison of RCM-measured and model-computed HRRs (normalized by mixture lower heating value), plotted as functions of accumulated heat release. Experiments indicate little fuel-to-fuel differences; model predicts significant differences.

Measurements were also conducted with $C_2\text{--}C_4$ high-performance alcohol fuels, including ethanol, n-propanol, iso-propanol, 2-butanol, and iso-butanol, covering a range of fuel loadings and thermodynamic conditions. Collaborations are ongoing with LLNL to utilize these additional data for improvements to the alcohol sub-mechanism of the Co-Optima kinetic model, while the two iso-alcohols will be blended with a full boiling-range gasoline for tests in FY 2019.

Autoignition data were acquired for a second iso-olefin, 2-methyl 2-pentene, to augment the dataset of 2-methyl 2-butene. The test conditions covered a range of stoichiometry, temperature, and pressure ($\phi = 0.5\text{--}2.0$, $T_c = 685\text{ K--}1,000\text{ K}$, $P_c = 25\text{ bar and }45\text{ bar}$). Collaborations are ongoing with LLNL to utilize these additional data for improvements to the alkene sub-mechanism of the gasoline surrogate model.

Finally, tests were conducted in an effort to establish a methodology to experimentally characterize the phi-sensitivity of fuels. Phi-sensitivity quantifies the change in a fuel's reactivity as the fuel/air ratio varies across an engine's combustion chamber due to non-uniformities, e.g., via early fuel injection. Although the development of fundamental understandings of phi-sensitivity is critical, no standardized ways to measure phi-sensitivity have been reported previously. To this end, RCM tests were conducted with RD5-87, a research-grade E10 gasoline representative of market fuels. Different fuel/air ratios were used ($\phi = 0.4\text{--}1.0$) under two pressure protocols (fixed and varying pressure) covering a range of temperatures. Sandia National Laboratories' definition of a normalized phi-sensitivity, $\Phi_s^* = (1/\tau)(\partial\tau/\partial\phi)$, was utilized. The results, which are presented in Figure II.15.4, demonstrated good consistency across the test conditions and showed negative phi-sensitivity for RD5-87. This property would enable combustion control via fuel stratification in an ACI engine. The measurement results were compared to predictions using the Co-Optima kinetic model, where these exhibited substantially different results. Efforts in FY 2019 will be undertaken to measure the phi-sensitivity of various Co-Optima fuel blends.

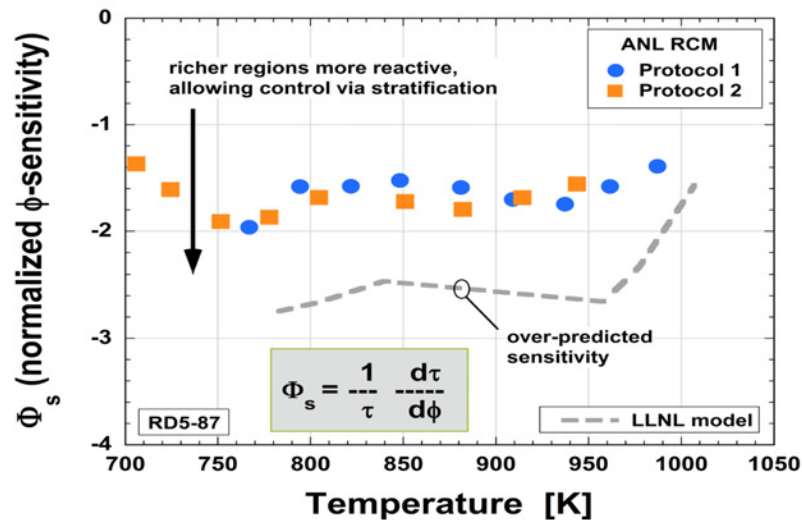


Figure II.15.4. Normalized phi-sensitivity vs. temperature for RD5-87 measured under two pressure protocols. Model results utilize a multi-component surrogate for the E10 full boiling-range fuel.

Conclusions

- ANL's RCM has been used to acquire autoignition data for five compositionally diverse, high RON Co-Optima core fuels, with the measurements compared directly against experimental trends in an ACI engine and to LLNL chemical kinetic model predictions, where the model indicated notable inconsistencies with the measurements.
- Autoignition data has been acquired for C2–C4 high-performance alcohol fuels (unblended) covering a range of fuel loadings and thermodynamic conditions.
- Autoignition data has been acquired for 2-methyl 2-pentene, a C₅ iso-olefin, over a range of experimental conditions for comparison against the 2-methyl 2-butene dataset and validation of chemical kinetic rate rules for branched olefins.
- Normalized ϕ -sensitivity (Φ_s^*) of research-grade, full boiling-range E10 gasoline was evaluated over a range of conditions using Sandia National Laboratories' Φ_s^* definition; experimental trends were directly compared to chemical kinetic model predictions.

Key Publications

1. Goldsborough, S.S., J. Santner, D. Kang, A. Fridlyand, T. Rockstroh, and M.C. Jespersen. 2018. "Heat Release Analysis for Rapid Compression Machine Experiments: Challenges and Opportunities." *Proc. Combust. Inst.* <https://doi.org/10.1016/j.proci.2018.05.128>.
2. Rockstroh, T., C. Kolodziej, S.S. Goldsborough, and T. Wallner. 2018. "Insights into Engine Knock: Comparison of Knock Metrics across a Range of Intake Temperature and Pressure in the CFR Engine." SAE Technical Paper 2018-01-0210.
3. Rockstroh, T., C. Kolodziej, M. Jespersen, S.S. Goldsborough, and T. Wallner. 2018. "Insights into Knock: Comparison of Knock Metrics across Ranges of Intake Temperature and Pressure in the CFR Engine." AEC Winter Review Meeting, Argonne, IL.
4. Kang, D., and S.S. Goldsborough. 2018. "Progress Quantifying Fuel Reactivity for Model Validation and Fuel Ranking, across a Range of Combustion Scenarios." AEC Winter Review Meeting, Argonne, IL.

5. Kang, D., B. Wagner, and S.S. Goldsborough. 2018. "Progress Quantifying Fuel Reactivity for Model Validation and Fuel Ranking, across a Range of Combustion Scenarios." AEC Summer Review Meeting, Southfield, MI.
6. Goldsborough, S.S., and J. Santner. 2018. "From Mild Ignition to Mixed-Mode Combustion: Parameterizing Flame Dynamics and End Gas Response." AEC Summer Review Meeting, Southfield, MI.

References

1. Basic Research Needs for Clean and Efficiency Combustion of 21st Century Transportation Fuels. (http://science.energy.gov/~media/bes/pdf/reports/files/ctf_rpt.pdf)
2. Goldsborough, S.S., S. Hochgreb, G. Vanhove, M.S. Wooldridge, H.J. Curran, and C.-J. Sung. 2017. *Prog. Energy Combust. Sci.* 63: 1–78. <https://doi.org/10.1016/j.pecs.2017.05.002>.
3. Kang, D., A. Shah, T. Rockstroh, and S. Goldsborough. 2019. "Utilizing Static Autoignition Measurements to Estimate Intake Air Condition Requirements for Compression Ignition in a Multi-Mode Engine – Application of Chemical Kinetic Modeling." SAE Paper 2019-01-0955. <https://doi.org/10.4271/2019-01-0955>.
4. Goldsborough, S.S., J. Santner, D. Kang, A. Fridlyand, T. Rockstroh, and M.C. Jespersen. "Heat Release Analysis for Rapid Compression Machine Experiments: Challenges and Opportunities." *Proc. Combust. Inst.* <https://doi.org/10.1016/j.proci.2018.05.128>.
5. Sjoberg, M., and W. Zeng. 2016. "Combined Effects of Fuel and Dilution Type on Efficiency Gains of Lean Well-Mixed DISI Engine Operation with Enhanced Ignition and Intake Heating for Enabling Mixed-Mode Combustion." *SAE Int. J. Engines* 9: 750–767. <https://doi.org/10.4271/2016-01-0689>.

Acknowledgements

This work was performed under the auspices of the U.S. Department of Energy by Argonne National Laboratory under Contract DE-AC02-06CH11357. Experimental measurements were conducted with the assistance of Dongil Kang, Mahir Rafi, Brianna Wagner, Omar Ahmed, and Danielle Markovich. Chemical kinetic modeling was conducted with the assistance of Scott Wagnon, Goutham Kukkadapu, Marco Mehl, William Pitz, and Russell Whitesides (LLNL).

II.16 Mixing-Controlled Compression-Ignition Combustion and Fuel-Effects Research: Ducted Fuel Injection (Sandia National Laboratories)

Charles J. Mueller, Principal Investigator

Sandia National Laboratories
PO Box 969, MS 9053
Livermore, CA 94551-0969
E-mail: cjmuell@sandia.gov

Kevin Stork, DOE Technology Development Manager

U.S. Department of Energy
E-mail: Kevin.Stork@ee.doe.gov

Start Date: October 1, 2017

End Date: September 30, 2018

Project Funding (FY18): \$335,000

DOE share: \$335,000

Non-DOE share: \$0

Project Introduction

This project is focused on developing advanced combustion strategies for mixing-controlled compression-ignition (i.e., diesel-cycle) engines that are synergistic with renewable and/or unconventional fuels in a manner that enhances domestic energy security, economic competitiveness, and environmental quality. During this reporting period, the focus was on ducted fuel injection (DFI), a technology that involves injecting fuel along the axis of one or more small cylindrical ducts within the combustion chamber. Each duct performs a function similar to the tube on a Bunsen burner, helping to premix the fuel with the intake gas before ignition, creating a stable flame that does not form soot. Soot is a regulated toxic emission that is second in importance only to carbon dioxide as a climate-forcing species. The purpose of the work conducted during Fiscal Year (FY) 2018 is to enhance the understanding of DFI and its potential to lower the emissions from mixing-controlled compression-ignition engines without adversely affecting other regulated emissions or efficiency.

Objectives

Overall Objectives

- Provide new technologies like DFI to increase the performance per unit cost, mass, and volume of future high-efficiency engine/fuel systems
- Provide high-quality experimental data for computational fluid dynamics model development to facilitate the accurate, rapid, and cost-effective computational optimization of new technologies
- Provide a fundamental understanding of fuel composition and property effects by formulating and studying the performance of chemically and physically well-characterized reference fuels made from blending stocks as well as pure compounds

Fiscal Year 2018 Objectives

- Design, fabricate, install, and test hardware to enable the first-ever DFI experiments in an engine
- Conduct DFI experiments in an engine with a single duct to determine whether the technology works as expected
- Conduct DFI experiments in an engine with two ducts to quantify the effects of DFI on regulated emissions and efficiency, including whether DFI can break the longstanding soot/nitrogen oxides (NO_x) tradeoff

Approach

This project aims to deliver an improved understanding of mixing-controlled compression-ignition combustion and fuel effects through experimental observation employing optical and conventional diagnostics, combined with careful analysis of the results. Building from the work conducted in FY 2017 and before [1,2], which used constant-volume combustion-vessel experiments to show that DFI is a promising soot-attenuation technology for mixing-controlled compression-ignition applications, efforts in FY 2018 were focused on conducting the first DFI experiments in an engine. To achieve this, modifications were made to the cylinder head of an optically accessible heavy-duty engine to facilitate the installation and alignment of DFI ducts, and high-speed in-cylinder imaging diagnostics were combined with measurements of efficiency and engine-out emissions to characterize the effects of DFI [3].

Results

A schematic of the DFI concept implemented in an engine is shown in Figure II.16.1. The first step toward enabling DFI to be tested in the optical engine was to design ducts and a duct-holder assembly that incorporated the knowledge gained from previous DFI experiments conducted in constant-volume combustion vessels [1,2]. One requirement of the new duct assembly was that it must enable precise alignment of one or more ducts with their corresponding spray(s) in the axial, radial, tangential, and azimuthal directions. A second requirement was that it must be retrofittable onto the existing cylinder head. Figure II.16.2 shows renderings of the resultant one- and two-duct holders as attached to the cylinder head. Once the duct-holder designs were finalized, they were detailed, fabricated, and assembled into the optical engine.

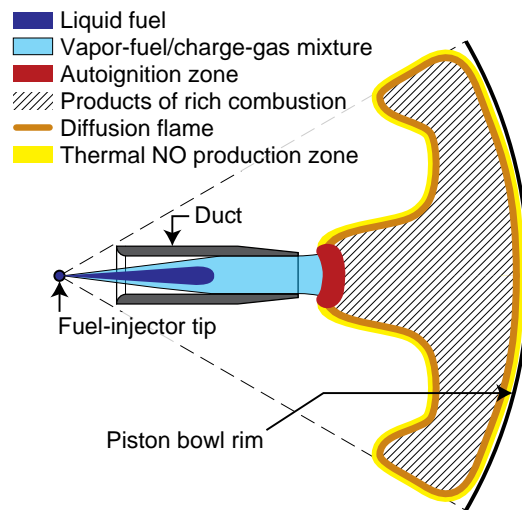


Figure II.16.1. Schematic of the DFI concept on one fuel spray within an engine

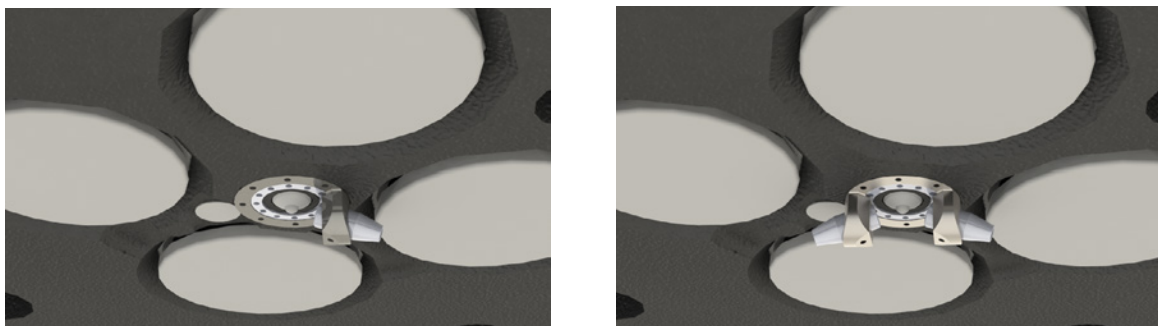


Figure II.16.2. Single-duct holder (left) and two-duct holder (right) attached to cylinder head. All ducts have an inside diameter, length, and standoff distance from the injector orifice of 2 mm, 12 mm, and 3 mm, respectively.

The single-duct holder was tested first because it enabled a simultaneous, side-by-side comparison of a DFI spray vs. a conventional diesel combustion (CDC) spray, and because it was the simplest geometry to align. Figure II.16.3 shows a single frame from a high-speed movie of natural luminosity during the combustion event with the one-duct holder. When hot soot is present, the natural luminosity signal is dominated by incandescence therefrom. Figure II.16.3 confirms that the CDC spray on the left produces significantly more incandescence from hot soot than the DFI spray on the right. All experiments were conducted with a commercial No. 2 ultra-low-sulfur diesel fuel containing ~30 wt% aromatics.

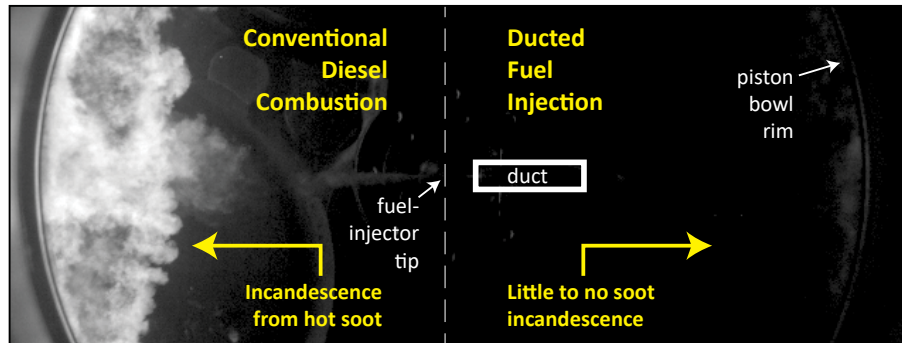


Figure II.16.3. Natural luminosity image from experiment with single-duct holder. Camera is viewing the cylinder head through a window in the piston (compare to left side of Figure II.16.2). Duct has an inside diameter, length, and standoff distance from the injector orifice of 2 mm, 12 mm, and 3 mm, respectively.

With the single-duct holder, it was difficult to determine what fraction of each of the regulated emissions was originating from the DFI spray vs. the CDC spray. To overcome this uncertainty, the single-duct holder was replaced by a two-duct holder, the two-duct holder was aligned with the sprays, DFI experiments were conducted, and results were compared to those from CDC with two free sprays (i.e., no ducts). These experiments were conducted at two dilution levels (21 mol% and 16 mol% oxygen) to elucidate whether DFI is compatible with exhaust-gas recirculation for the simultaneous suppression of both soot and NO_x emissions.

In a typical diesel engine, dilution is used to lower the temperatures and oxygen (O_2) concentrations in the reacting mixtures to attenuate the formation of NO_x . Unfortunately, this almost universally results in increased soot formation, a problem generally known as the soot/ NO_x tradeoff. This effect can be observed in Figure II.16.4, the upper plot of which shows the indicated-specific (IS) soot and ISNO_x emissions measured during the CDC experiments. The lower plot of Figure II.16.4 shows that when the same level of dilution (16 mol% O_2) is used in the engine equipped with DFI, NO_x is attenuated by a similar amount as for CDC, while the measured soot is not only significantly lower than for CDC, it decreases compared to DFI without dilution. The latter observation indicates that DFI breaks the soot/ NO_x tradeoff with dilution.

Figure II.16.5 shows that the engine-out soot emissions are 19 times lower for DFI vs. for CDC at the constant dilution level of 16 mol% O_2 , while the other regulated emissions, efficiency, and apparent heat-release rate (AHRR) are not significantly degraded by DFI. In fact, the indicated-specific hydrocarbon (ISHC) emissions are lower and the AHRR is shorter with DFI. These results indicate that DFI holds significant promise for substantially improving the performance of mixing-controlled compression-ignition engines. Research is planned for FY 2019 to explore whether DFI combined with renewable, oxygenated fuels can further extend this performance benefit while displacing imported petroleum.

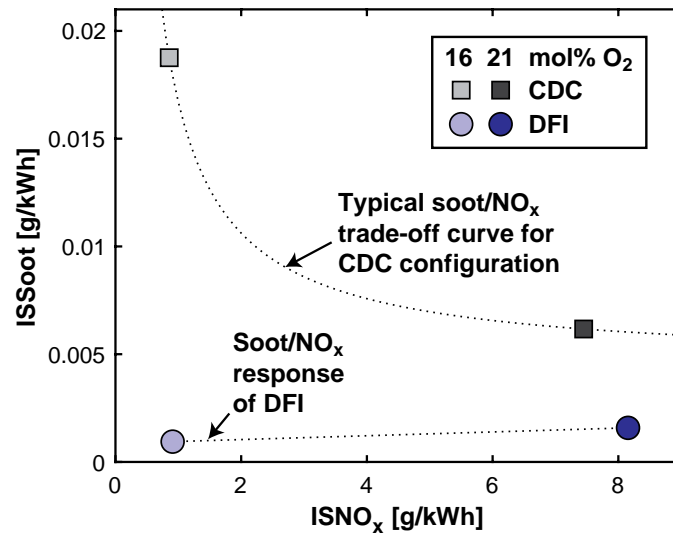


Figure II.16.4. CDC results show trade-off between soot and NO_x emissions as dilution increases, whereas DFI breaks the soot/NO_x trade-off by simultaneously attenuating soot and NO_x formation. For DFI, duct has an inside diameter, length, and standoff distance from the injector orifice of 2 mm, 12 mm, and 3 mm, respectively.

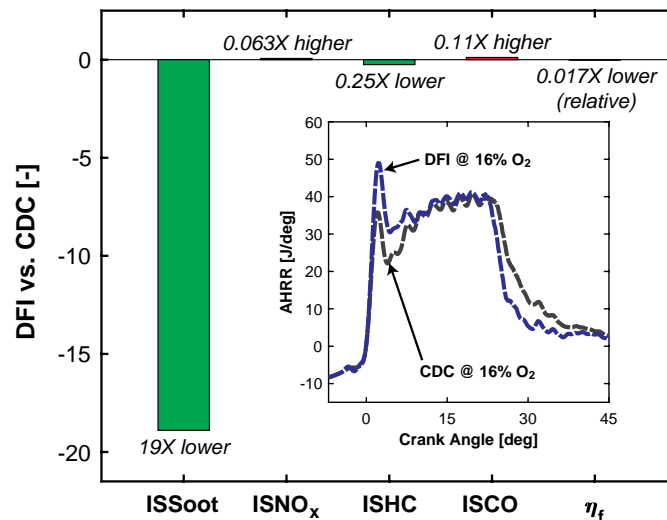


Figure II.16.5. DFI dramatically lowers soot at constant dilution and combustion phasing. Plot shows the change in indicated-specific emissions of soot, NO_x, hydrocarbons, and carbon monoxide (CO) and the fuel-conversion efficiency (η_f) for DFI vs. CDC at 16 mol% O₂. For a given parameter X, the bar plot shows $(X_{DFI} - X_{CDC}) / \min(X_{DFI}, X_{CDC})$. Inset shows AHRR.

Conclusions

Based on the conducted work and the observations summarized in the preceding section, the following conclusions are drawn:

- A DFI duct assembly was made small enough to be installed in a heavy-duty diesel engine, and adequate spray/duct alignment was achieved by hand and without the use of precision instrumentation in this first-ever study of DFI in an engine.
- DFI is effective at attenuating engine-out soot emissions relative to conventional mixing-controlled compression-ignition (i.e., diesel) combustion.
- DFI has been observed to break the soot/NO_x tradeoff with increasing dilution.

Key Publications

1. Gehmlich, R.K., C.J. Mueller, D.J. Ruth, C.W. Nilsen, S.A. Skeen, and J. Manin. 2018. “Using Ducted Fuel Injection to Attenuate or Prevent Soot Formation in Mixing-Controlled Combustion Strategies for Engine Applications.” *Applied Energy* 226: 1169–86, doi:10.1016/j.apenergy.2018.05.078.
2. Yasutomi, K., C.J. Mueller, L.M. Pickett, and S.A. Skeen. 2018. “Investigation of the Spray and Combustion Characteristics of Four Multi-Component Diesel Surrogate Fuels Relative to Their Commercial Target Fuel.” THIESEL 2018 *Conference on Thermo- and Fluid-Dynamic Processes in Direct Injection Engines*, Valencia, Spain, September 11–14, 2018.
3. Mueller, C.J. 2018. “Improved Mixing-Controlled Combustion Technologies and Fuels for High-Efficiency Compression Ignition Engines.” In U.S. Department of Energy Report DOE/EE-1708: *Vehicle Technologies Office FY 2017 Annual Progress Report, Advanced Combustion Systems and Fuels*, May 2018.
4. Yasutomi, K., C.J. Mueller, L.M. Pickett, and S.A. Skeen. 2018. “Investigation of Spray Characteristics for Multi-Component Fuel.” In Proc. of the *Western States Section of the Combustion Institute Spring Meeting*, Paper #1C02, Bend, Oregon, March 25–27, 2018.
5. Mueller, C.J. 2018. “Ducted Fuel Injection.” U.S. Patent #9,909,549; issued March 6, 2018.
6. Mueller, C.J. 2017. “Experiments Enable Optimization of Ducted Fuel Injection.” *Co-Optimization of Fuels & Engines FY17 Year in Review*.

References

1. Mueller, C.J., C.W. Nilsen, D.J. Ruth, R.K. Gehmlich, L.M. Pickett, and S.A. Skeen. 2017. “Ducted Fuel Injection: A New Approach for Lowering Soot Emissions from Direct-Injection Engines.” *Applied Energy* 204: 206–220, doi:10.1016/j.apenergy.2017.07.001.
2. Gehmlich, R.K., C.J. Mueller, D.J. Ruth, C.W. Nilsen, S.A. Skeen, and J. Manin. 2018. “Using Ducted Fuel Injection to Attenuate or Prevent Soot Formation in Mixing-Controlled Combustion Strategies for Engine Applications.” *Applied Energy* 226: 1169–86, doi:10.1016/j.apenergy.2018.05.078.
3. Nilsen, C.W., D.E. Biles, and C.J. Mueller. 2018. “Using Ducted Fuel Injection to Attenuate Soot Formation in a Mixing-Controlled Compression-Ignition Engine.” Manuscript in preparation for submission to *SAE Int. J. Engines*.

Acknowledgements

The principal investigator gratefully acknowledges major contributions to FY 2018 research efforts by interns Christopher W. Nilsen (University of California, Davis) and Drummond E. Biles (University of New Hampshire).

II.17 Flow Reactor Autoignition Kinetic Mechanism Development and Validation and Understanding How Fuels Blend for Autoignition (National Renewable Energy Laboratory)

Gina Fioroni, Principal Investigator

National Renewable Energy Laboratory (NREL)
15013 Denver West Parkway
Golden, CO 80401
E-mail: gina.fioroni@nrel.gov

Kevin Stork, DOE Technology Development Manager

U.S. Department of Energy
E-mail: Kevin.Stork@ee.doe.gov

Start Date: October 1, 2017	End Date: September 30, 2018	
Project Funding (FY18): \$750,000	DOE share: \$750,000	Non-DOE share: \$0

Project Introduction

The purpose of this project was first, to upgrade an existing reactor system with improved analytical capability, and second, to apply this capability to reveal important aspects of autoignition and soot precursor formation mechanisms that are not revealed by other experiments. The concept is to use a straight quartz tube flow reactor coupled to a dual gas chromatograph system that can accurately measure the autoignition products generated over a wide temperature range while simultaneously identifying them via a mass spectrometer. The system combines five detectors to quantitate a wide range of products, including oxygenates, hydrocarbons, light gases (such as methane and acetylene), carbon dioxide, and carbon monoxide (CO). Various residence times as well as oxygen ratios can also be investigated in this apparatus. An older version of this reactor developed in Fiscal Year 2017 was used to develop a small-volume approach to predict research octane number and octane sensitivity [1]. The project was jointly funded by DOE's Vehicle Technologies and Bioenergy Technologies Offices.

Objectives

- Validate the ability of the upgraded flow reactor to measure autoignition kinetics using isooctane, a well-studied molecule with well-known kinetics
- Examine the skeletal autoignition mechanisms for the light-duty spark-ignition Co-Optima blendstocks, as well as methyl acetate and prenol, to try to understand synergistic and antagonistic blending effects
- Investigate soot precursor formation—elucidate degradation pathways of the three isomers of methyl cyclohexenes to investigate the yield sooting index differences between the isomers and the measured versus predicted values

Approach

The reactor consists of a straight quartz tube that is 75 cm in length and is uniformly heated inside a ceramic tube furnace to temperatures between 473 K and 1,200 K. Various diameter quartz tubes can be employed depending on the desired residence time. Fuel (via a syringe pump), helium, and oxygen (via mass flow controllers) are all introduced at the inlet of the reactor and mix at the point of the syringe needle where the fuel is introduced. Helium is used as an inert dilution gas that is also the carrier gas flow utilized in the carrier gas systems. Fuel flow rates vary from 5 $\mu\text{L}/\text{min}$ up to 20 $\mu\text{L}/\text{min}$ depending on the run conditions but are kept low to ensure very dilute conditions for safety. The flow of oxygen can be adjusted to assess the effect of various air-to-fuel ratios as desired.

Analysis is performed via a dual gas chromatograph system. The upgraded system contains five detectors that can be used to accurately quantitate oxygenates, hydrocarbons, light gases, carbon dioxide, and CO. The outlet of the reactor is sampled using an inert steel, heated transfer line that uses a vacuum pump to draw 0.5 L/min of gas from the reactor into two identical sample loops in the gas chromatographs.

Results

Validation of the Upgraded Reactor System Using Isooctane

To validate this system for autoignition kinetic work, we chose to re-run the model compound isooctane as its reaction kinetics are well known [2]. Isooctane was run from 800 K up to 1,100 K at stoichiometric air-to-fuel conditions, and the reaction products were measured using the dual system and compared to the mechanism from Lawrence Livermore National Laboratory (LLNL) (S. Wagnon, private communication to the Principal Investigator, August 15, 2017), which was modeled using a one-dimensional plug flow model. Figure II.17.1 shows the results for some of the autoignition products of isooctane. In all cases (including those not shown), the concentrations of the products measured were very close to those predicted by the mechanism. These results demonstrate that the upgraded reactor system can be used to study autoignition mechanisms with very good accuracy.

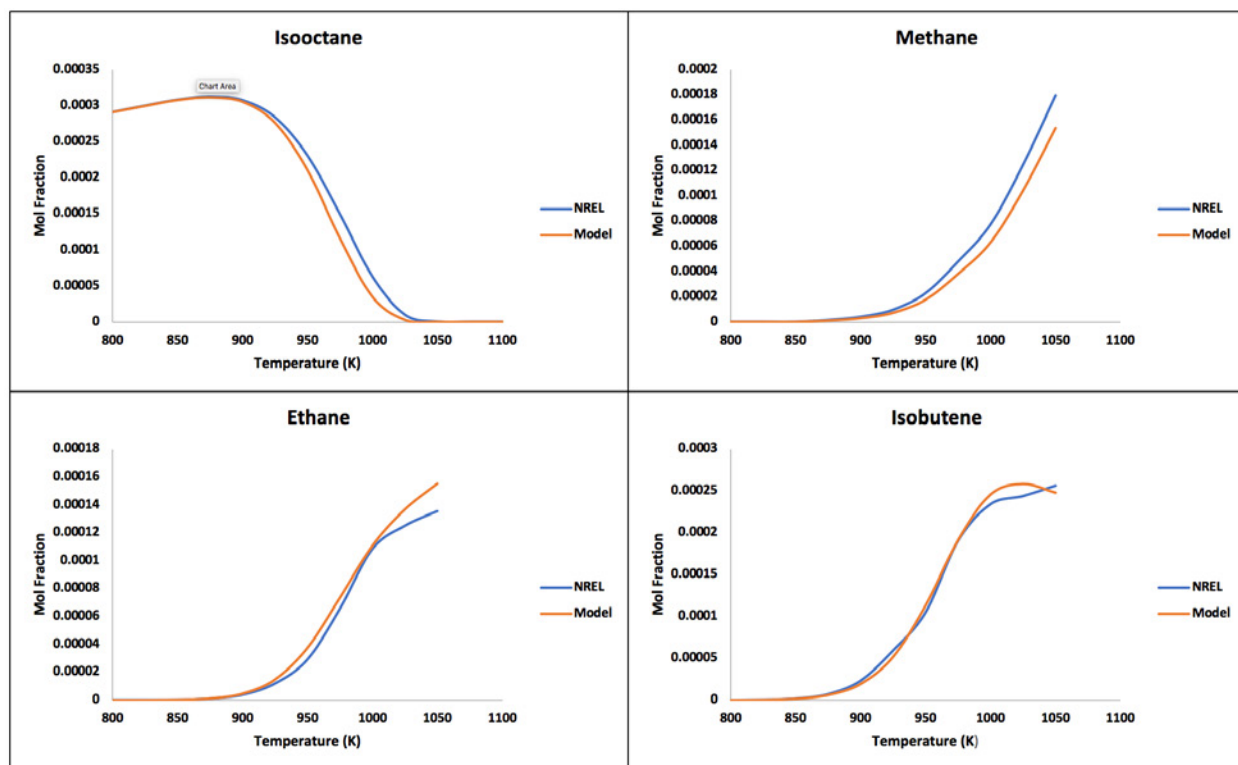


Figure II.17.1. Example autoignition products of isooctane: reactor versus model results

Study of Autoignition Reaction Mechanisms of Light-Duty Spark-Ignition Co-Optima Compounds

Several oxygenated species were identified under the Co-Optimization of Fuels and Engines project as potential bioblendstocks for use in spark-ignition engines, and their skeletal autoignition mechanisms were studied in the upgraded reactor system [3,4]. All but one (high-aromatic bioreformate) of these were investigated; they include ethanol, isopropanol, 1-propanol, isobutanol, diisobutylene, dimethyl furan, and cyclopentanone. Additionally, prenol and methyl acetate were investigated as they displayed interesting blending behavior with gasoline [5]. The Co-Optima mechanism developed at LLNL (S. Wagnon and W. Pitz, Co-Optima Mechanism, personal communication, 2018) was used to model the reactor under one-dimensional plug flow conditions. The results for all the compounds investigated are too extensive to include here; however, a couple of interesting cases will be examined.

Alcohols: For these compounds, the results were similar for all the cases. Results for ethanol are shown in Figure II.17.2 as an example. For the parent compound and formation of its aldehyde autoignition product (in this case ethanol and acetaldehyde), there was a clear discrepancy in the consumption of the alcohol and the formation of the aldehyde, which appear to be in direct correlation with each other. In all cases, the experimental data showed reaction of the alcohol at lower temperatures and formation of the aldehyde at lower temperatures and in higher concentration than what was predicted by the model. This was also the case for 1-propanol and its aldehyde products, propanal and 2-propenal; for isobutanol and its aldehyde products, 2-methyl propanal and methacrolein; and lastly, for isopropanol and its product acetone (which is a ketone). In all cases the low-molecular-weight gases were well predicted by the model. For example, in Figure II.17.2, ethane and CO have good agreement between the experimental results and the model; however, the experimental data clearly show ethanol reacting by 750 K, while the model predicts ethanol to begin reacting at 950 K, a 200 K discrepancy. The formation of acetaldehyde begins by about 775 K in the reactor, while the model predicts it to begin forming at 950 K. Additionally, the concentration of acetaldehyde is measured at much higher concentration than the model predicts. These data point to a possible reaction rate issue within the predictive model, or alternatively, to some experimental factor that causes increased reactivity at low temperature. A joint effort between NREL and LLNL is investigating this discrepancy.

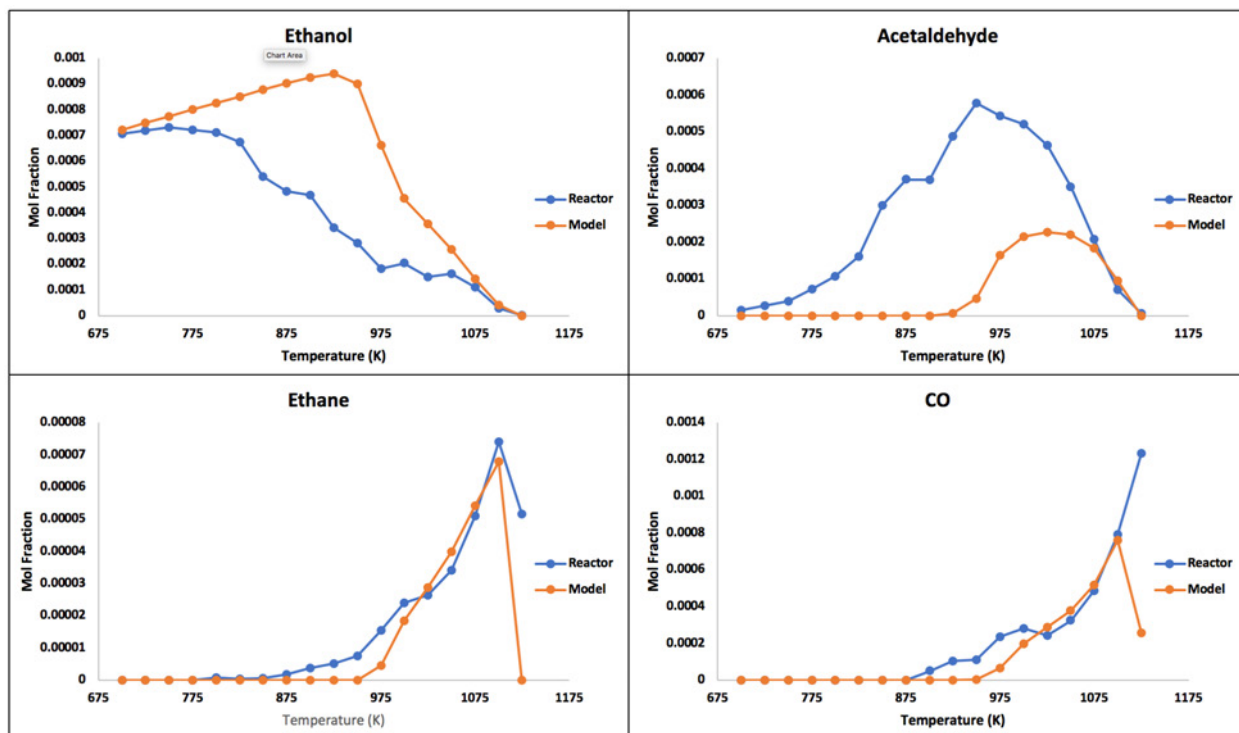


Figure II.17.2. Autoignition products of ethanol: model versus experimental data

Cyclopentanone: This was very similar to the alcohol case, where the experimental data showed cyclopentanone reacting at much lower temperatures than what was predicted by the model. Additionally, the formation of the aldehyde product 2-propenal was observed at lower temperatures and at higher concentrations than were predicted by the model, similar to the alcohol cases. Another interesting observation for cyclopentanone was the detection of cyclopentadiene, which was not predicted to be a predominant product in the model. Potentially, a pathway to form this intermediate is not captured in the model. As with the alcohols, the formation of the low-molecular-weight gases was well predicted by the model.

Diisobutylene: Similar to the alcohols and cyclopentanone, diisobutylene reacted at lower temperatures than what was predicted by the model. Consistent with the other compounds, the permanent gases were well predicted. One compound that was observed in much higher concentration than predicted was 1-pentene.

Dimethylfuran: Unlike the other potential fuel blendstocks studied, dimethylfuran appears to match well with the model predictions as far as consumption of the dimethylfuran (Figure II.17.3). In agreement with the other compounds studied, the low-molecular-weight-gases were well predicted. There were discrepancies noted in the formation of aromatics from dimethylfuran: phenol was measured in higher concentration than predicted. Further, benzene and toluene were noted to be increasing in concentration at higher temperatures (1,100 K), while the model predicts that concentrations of these components is decreasing at higher temperatures.

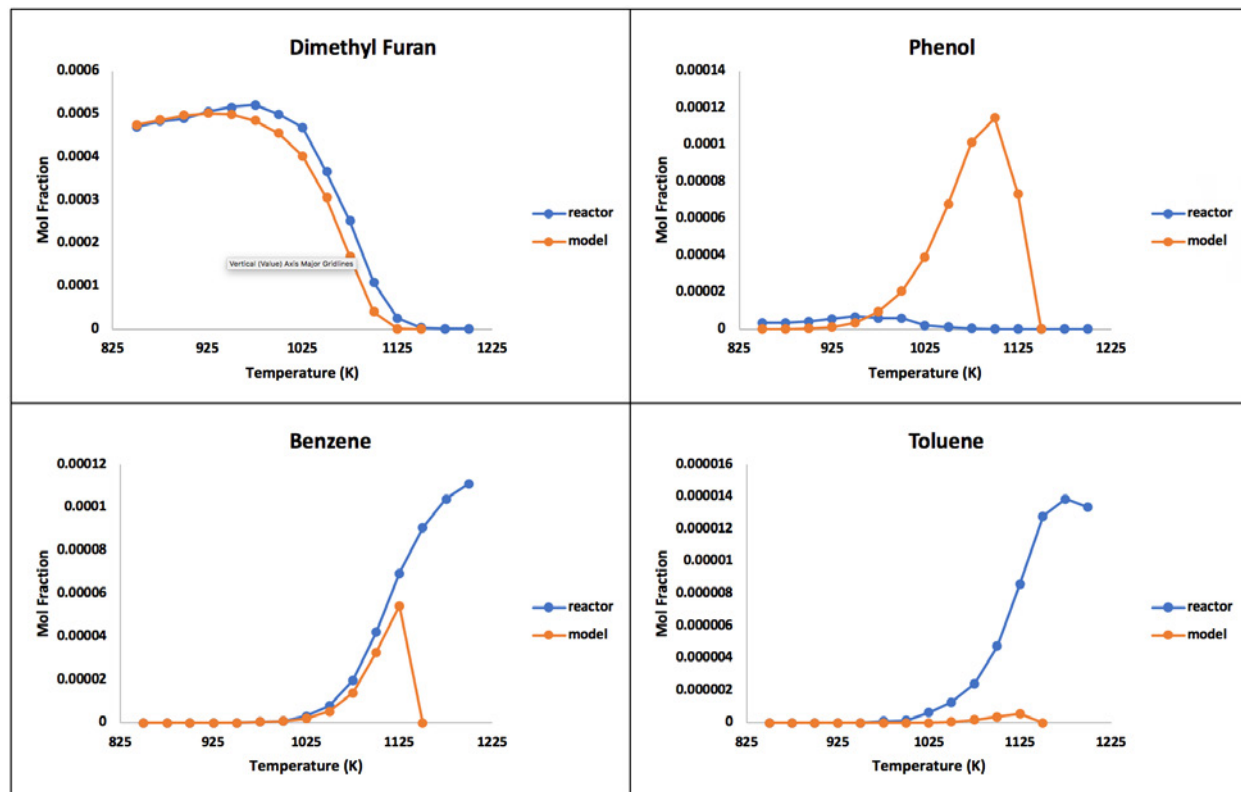


Figure II.17.3. Autoignition products from dimethylfuran: model versus experimental data

Prenol and methyl acetate: These compounds were run to investigate synergistic and antagonistic blending behavior. To accomplish this, observation of the low-temperature reaction of heptane is required. At this point, we were not able to observe heptane reaction products at low temperatures (600 K to 800 K). This could be due to the formation of products in lower concentration than can currently be measured or, possibly, residence times used in these experiments were not long enough for significant reactions to occur. Current work is focused on improving detection limits by increasing the amount of fuel fed and extending the residence time range we can run. Additionally, a larger sample loop was installed in the gas chromatograph system.

Degradation Pathways of the Three Isomers of Methyl Cyclohexenes

The yield sooting index is an experimentally determined measure of a compound's inherent chemical tendency to form soot [6]. The yield sooting index for the three isomers of methyl cyclohexenes was both predicted from a group contribution method [6] and measured. Predicted yield sooting index values for two of the three methyl cyclohexene isomers were much lower than the measured yield sooting index values. Quantum mechanics calculations revealed that a retro-Diels-Alder reaction pathway was likely an important path for two of the three isomers and that this pathway had not been captured in the model. The retro-Diels-Alder reaction involves ring opening and the formation of lower-molecular-weight products rather than formation of aromatic soot precursors, as shown in Figure II.17.4 for 1-methyl and 4-methyl cyclohexene. This is in contrast to the 3-methyl isomer, which reacts preferentially via dehydrogenation, retaining the ring structure of the molecule and leading to the formation of higher-molecular-weight molecules and soot precursor molecules such as cyclopentadiene. These theoretical results were validated in the flow reactor, as shown in Figure II.17.5 [7].

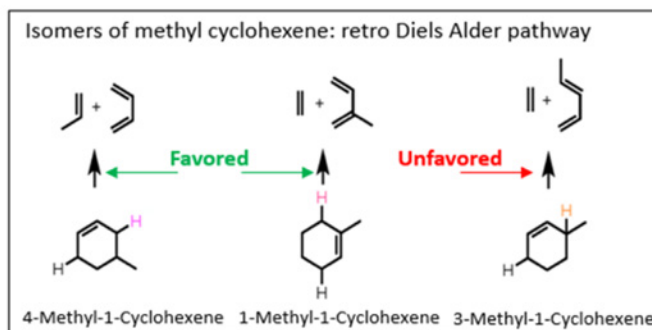


Figure II.17.4. Retro-Diels-Alder pathways for the three isomers of methyl cyclohexenes

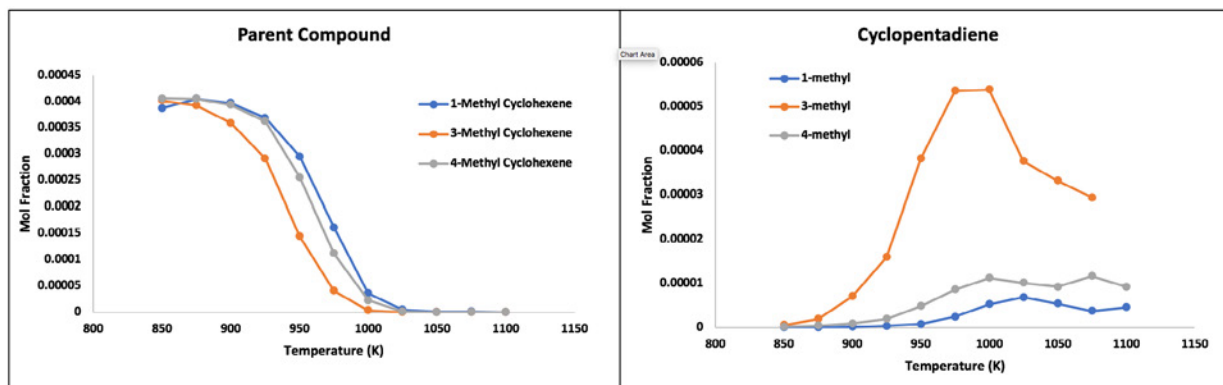


Figure II.17.5. Experimental data for methyl cyclohexene isomers and formation of the soot precursor cyclopentadiene

Conclusions

The NREL flow reactor was upgraded in Fiscal Year 2018 with expanded product analysis capability. The reactor was used to investigate autoignition and soot precursor formation mechanisms. The conclusions are as follows.

- The upgraded analysis system was validated using isooctane, demonstrating that the system can accurately measure autoignition kinetics.
- The system was utilized to study the skeletal autoignition mechanisms of the promising bioblendstocks, as well as prenol and methyl acetate.
- The reactor was utilized to show that a key degradation pathway was missing from reaction mechanisms for the three isomers of methyl cyclohexenes. Along with quantum mechanics calculations, a retro-Diels-Alder pathway was identified for two of the three isomers of methyl cyclohexenes, explaining the differences in their yield sooting index values.

In Fiscal Year 2019, research utilizing this reactor will focus on further development of autoignition mechanisms and blending effects. Additionally, the reactor will be employed to study phi sensitivity.

Key Publications

1. Kim, S., G.M. Fioroni, J.-W. Park, D.J. Robichaud, D.D. Das, P.C. St. John, T. Lu, C.S. McEnally, L.D. Pfefferle, R.S. Paton, T.D. Foust, and R.L. McCormick. 2018. "Experimental and Theoretical Insight into the Soot Tendencies of the Methylcyclohexene Isomers." *Proc. Comb. Inst.* doi.org/10.1016/j.proci.2018.06.095.

2. Lunderman, S., G.M. Fioroni, R.L. McCormick, M.R. Nimlos, M.J. Rahimi, R.W. Grout. 2018. "Screening Fuels for Autoignition with Small Volume Experiments and Gaussian Process Classification." *Energy Fuels* 32: 9581–9591.

References

1. Lunderman, S., G.M. Fioroni, R.L. McCormick, M.R. Nimlos, M.J. Rahimi, and R.W. Grout. 2018. "Screening Fuels for Autoignition with Small Volume Experiments and Gaussian Process Classification." *Energy Fuels* 32: 9581–9591.
2. Mehl, M., S. Wagnon, K. Tsang, G. Kukkadapu, W.J. Pitz, C.K. Westbrook, Y. Tsang, H.J. Curran, N. Atef, M.A. Rachidi, M.S. Sarathy, and A. Ahmed. 2017. "A Comprehensive Detailed Kinetic Mechanism for the Simulation of Transportation Fuels." LLNL-CONF-725343, February 28, 2017.
3. McCormick, R.L., G.M. Fioroni, L. Fouts, E. Christensen, J. Yanowitz, E. Polikarpov, K. Albrecht, D.J. Gaspar, J. Gladden, and A. George. 2017. "Selection Criteria and Screening of Potential Biomass-Derived Streams as Fuel Blendstocks for Advanced Spark-Ignition Engines." *SAE Int. J. Fuels Lubr.* 10 (2), doi:10.4271/2017-01-0868.
4. Farrell, J., J. Holladay, and R. Wagner. 2018. "Fuel Blendstocks with the Potential to Optimize Future Gasoline Engine Performance: Identification of Five Chemical Families for Detailed Evaluation." Technical Report. U.S. Department of Energy, Washington, DC. DOE/GO-102018-4970.
5. Fioroni, G.M., M. Rahimi, L. Fouts, R. Grout, and R.L. McCormick. "Analysis of Co-Optima LDSI Blendstock Autoignition Chemistry in a Plug Flow Reactor and Preliminary Comparison to Simulation Results." NREL Q3 Milestone Report.
6. Das, D., P. St. John, C. McEnally, S. Kim, and L. Pfefferle. 2018. "Measuring and Predicting Sooting Tendencies of Oxygenates, Alkanes, Alkenes, Cycloalkanes, and Aromatics on a Unified Scale." *Combustion and Flame* 190: 349–364.
7. Kim, S., G.M. Fioroni, J.-W. Park, D.J. Robichaud, D.D. Das, P.C. St. John, T. Lu, C.S. McEnally, L.D. Pfefferle, R.S. Paton, T.D. Foust, and R.L. McCormick. 2018. "Experimental and Theoretical Insight into the Soot Tendencies of the Methylcyclohexene Isomers." *Proc. Comb. Inst.* doi.org/10.1016/j.proci.2018.06.095.

Acknowledgements

The principal investigator gratefully acknowledges the contributions of Lisa Fouts, Earl Christensen, Jon Luecke, Seonah Kim, Peter St. John, Mohammad Rahimi, Ray Grout, and Robert McCormick to this project and report.

II.18 Fuel Autoignition Behavior (National Renewable Energy Laboratory)

Brad Zigler, Principal Investigator

National Renewable Energy Laboratory (NREL)
15013 Denver West Parkway
Golden, CO 80401
E-mail: brad.zigler@nrel.gov

Kevin Stork, DOE Technology Development Manager

U.S. Department of Energy
E-mail: Kevin.Stork@ee.doe.gov

Start Date: October 1, 2017	End Date: September 30, 2018	
Project Funding (FY18): \$538,000	DOE share: \$538,000	Non-DOE share: \$0

Project Introduction

Co-development of new, high-performance chemistries and high-efficiency internal combustion engines requires fast, accurate numerical simulations of critical processes to evaluate the interaction between fuel ignition behavior and advanced combustion strategies. These numerical simulations rely on accurate computational fluid dynamics (CFD) linked with fuel chemical kinetic mechanisms to model ignition and combustion performance during the engine cycle. Since fuel composition is complex, chemical kinetic mechanisms are based on surrogate compounds in representative blends. Simulation efficiency also typically requires the use of significantly reduced versions of kinetic mechanisms.

Development of these reduced, yet accurately representative, chemical kinetic mechanisms is enabled by experimental input data and validation through a range of devices, including shock tubes, rapid compression machines, flow reactors, and constant volume combustion chambers (CVCCs). Experimental measurements are especially important to highlight and validate ignition kinetic performance when combining kinetic mechanisms for different chemical classes to represent a fuel blend. Novel fuel blending components can affect ignition performance in non-linear and varying antagonistic or complementary degrees over temperature, pressure, and equivalence ratio space. Fuel kinetic mechanism development and validation therefore benefits from experimental mapping of ignition delay (ID) performance of fuel blends over engine-relevant parametric space. These experimental parametric maps of ID may also be used in simplified engine simulations to provide rapid screening predictions of engine performance with complex fuel blends for which kinetic mechanisms have not yet been developed. Since they utilize the same experimental research tasks and are tightly integrated, this project report combines reporting for both the development of ID data for kinetic mechanism development and the integration of those data in spark ignition (SI) engine autoignition studies under the larger, collaborative multi-lab Co-Optimization of Fuels and Engines (Co-Optima) program.

Objectives

- Develop experimental and simulation tools to characterize fuel ignition behavior in support of advanced combustion engine development, including SI, compression ignition, and multi-mode operation
- Support the development of research fuels, surrogates, blends, and related reduced kinetic mechanisms to further enable co-development of advanced combustion engines and high-performance fuels
- Link bench-scale CVCC-based fuel ignition measurements to single-cylinder research engine studies to enable rapid predictive feedback of engine performance for complex fuel blends
- Develop understanding of fuel chemical and physical properties that enable furtherance of the DOE Co-Optima program research and development program for co-optimization of high-performance fuels and high-efficiency engines

Approach

NREL's ignition kinetics research historically built on continual development and modification of the Ignition Quality Tester (IQT) as a flexible CVCC research platform, both for experiments and coupled simulations for evaluating kinetic mechanisms against experimental data [1–5]. In Fiscal Year (FY) 2017, NREL commissioned another CVCC platform, a fuel ignition tester to provide complementary standard derived cetane number measurements [6]. In FY 2017, NREL spent significant effort to transition most of its bench-scale ignition kinetics research to a newer (internally funded) CVCC platform, the Advanced Fuel Ignition Delay Analyzer (AFIDA) [7]. NREL's AFIDA is a more flexible CVCC research platform than the IQT or fuel ignition tester, covering a broader range of pressures (up to 5 MPa) and temperatures (up to 1,000 K) with a high-pressure (up to 2,000 bar) fuel injection system that significantly reduces the spray physics effects timescales to enable greater focus on the chemical kinetics portion of ID. In FY 2018 NREL extensively characterized internal chamber conditions for the AFIDA and continued development of a CFD model for the AFIDA to utilize with experimental data as part of the kinetic mechanism development feedback loop.

FY 2018 research on gasoline boiling range fuels leveraged NREL's prior development of novel techniques to conduct ID studies over temperature sweeps at various fixed pressures, which are now used by other IQT users. The focus on gasoline boiling range fuels supported SI engine development, as well as other advanced strategies such as gasoline compression ignition. Inherently longer ID times typical of gasoline-range fuels allowed better mixing, reduced spray physics to affect only a small portion of the overall ID (focusing more on chemical kinetics dominated ID), and enabled studies at higher pressures relevant to engine operation. As a result, NREL's flexible AFIDA produced engine-relevant ignition kinetic data for gasoline-range compounds and blends, filling data voids and overlapping some conditions covered by rapid compression machines and shock tubes. FY 2018 research focused on primary reference fuels, toluene reference fuels, and toluene standardization fuels, all blended with various renewable fuel compounds, including Co-Optima boosted SI strategy candidates [8]. NREL also continued development of a modified Livengood-Wu zero-dimensional (0D) knock integral model with parametric experimental ID data to compare autoignition kinetics-based knock limit versus load and temperature to experimental engine data collected [9]. This comparison will help reveal the extent to which octane index captures the true temperature and pressure response of ignition delay for a broad range of functional groups.

NREL's approach includes strong collaboration, including a faculty joint appointment from Colorado School of Mines (Prof. Greg Bogin), a DOE Office of Science-funded Science Undergraduate Laboratory Internship student from Colorado School of Mines (Sam Nichols), a graduate student intern from Colorado State University (Brandon King), and an undergraduate student intern from Metropolitan State University of Denver (Riley Abel) tied to this research. NREL is sharing ID data with other researchers and has been active in applying these techniques to fuel samples shared from other DOE laboratory and industry partners. Experimental data and CVCC simulations with kinetic mechanisms under development are also shared in close collaboration with Lawrence Livermore National Laboratory. These collaborations are critical to integrating AFIDA-based data as part the development feedback loop for kinetic mechanisms, correlating temperature and pressure parametric ID sweeps to engine studies, and developing potential for simple CVCC techniques to provide faster screening and ignition performance insight for biofuel candidate blends.

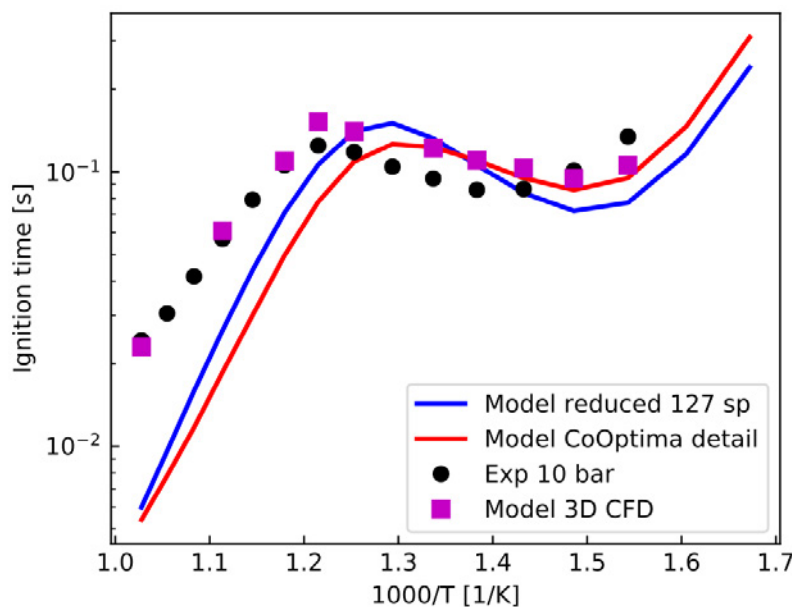
Results

Fuel Autoignition Studies in the AFIDA

NREL made significant progress in FY 2018 characterizing, adapting, modeling, and utilizing the AFIDA for a wide range of fuel autoignition kinetics studies. The research resulted in delivering a Co-Optima milestone for a draft journal article, "Experimental and Numerical Investigation of the AFIDA Constant Volume Chamber as a Research Platform for Chemical Kinetic Model Validation," the first article documenting the development of the AFIDA as an experimental and numerical simulation platform to study ignition kinetics for pure compounds, surrogates, and complex fuel blends. While the AFIDA was originally developed as a CVCC device for a derived cetane number-like measurement, indicated cetane number, with significant improvements over the IQT, NREL has always intended to adapt the AFIDA as a more flexible research platform for ignition kinetics studies, still complementing other devices like shock tubes, rapid compression machines, and flow

reactors. This draft journal article documents the extensive experimental characterization required to adapt the AFIDA as a flexible ignition kinetics research platform, in addition to the development of a numerical model simulation to validate chemical kinetic mechanisms against experimental results. The AFIDA has already proven to address the issues experienced with handling low boiling fractions that limited IQT-based studies for full boiling range gasoline blends.

A multi-dimensional CFD simulation of 1/7 of the reactor (since the injector has seven symmetrical holes) was constructed using CONVERGE, modeling the fuel spray injection, evaporation, mixing, and chemical reaction. Lagrangian-Eulerian coupling was used to model the gas phase spray, and renormalization group k-epsilon Reynolds-averaged Navier-Stokes was used for modeling turbulence. Adaptive mesh refinement technique based on velocity and species concentration gradients was used to resolve spray and the computational domain up to three levels (by factors of two down to 100 μm), with a total mesh size of ~ 15 million cells at instances of highest refinement using 720 cores of NREL's Peregrine high-performance computer. AFIDA experiments were conducted on a range of compounds and surrogate blends and compared against simulations using the Co-Optima mechanism. As illustrated in Figure II.18.1 (with iso-octane at 10 bar), the CFD simulation with the reduced mechanism (purple squares) correlates very well with experimental data (black circles) across the entire temperature sweep. The high fuel system pressure and piezoelectric injector minimize fuel spray physics effects, so much so for longer ignition delay times (beginning ~ 40 ms for some fuels) that a simple 0D simulation can be used for long ignition delay times. For Figure II.18.1, 0D simulations with the detailed Co-Optima mechanism (red line) and a 127-species reduction (blue line) are presented, showing good agreement through the negative temperature coefficient region at around 100 ms. Results with Co-Optima study compounds in blends provide critical feedback to mechanism development, especially with the ability to evaluate mechanisms against experimental data using simple 0D simulations. For example, recent AFIDA experiments and 0D simulations highlighted a predictive error in which a 48-species reduced primary reference fuel kinetic mechanism failed to predict critical negative temperature coefficient behavior for iso-octane, while a 127-species reduction closely matched experimental data. The AFIDA results roughly equal a state of development for the IQT that took several years to reach, and with operation under wider engine-relevant conditions to enable more links with engine simulations.



3D – three-dimensional

Figure II.18.1. Arrhenius plot of ignition delay (log scale) versus inverse temperature ($1,000/\text{K}$) for iso-octane at 10 bar initial pressure in the AFIDA. The AFIDA simulations with full CFD simulation with a 127-species reduced mechanism (purple squares) fit well against the experimental points (black circles). 0D simulations with the detailed Co-Optima mechanism (red line) and the 127-species reduced mechanism (blue line) are also plotted. Note how well the 0D simulations match experimental data for longer ignition delay times. (Figure: Mohammad Rahimi, NREL)

Octane Rating Correlations

NREL also made significant progress in using the AFIDA to quickly generate accurate research octane number (RON) estimates from small fuel samples. A strong correlation to RON was developed using an ignition delay measurement at a single temperature/pressure condition. A weaker correlation to octane sensitivity (S) was made using ignition delay at a second temperature point along the negative temperature coefficient region at the same pressure. When validated against results from a Cooperative Fuels Research (CFR) engine (Figure II.18.2), the AFIDA estimated RON with less than 2% error (85–110 RON) for fuels spanning 65 oxygenated blends, from simple surrogates to full boiling range gasolines. In addition, the automated AFIDA analysis requires less than 1 hour (compared with days for traditional RON testing) and a sample of less than 40 mL (compared with 500 mL or more). Ignition delay at the second temperature point was used to estimate S within brackets (low, medium, high). With the ability to screen small fuel samples for octane number correlation, the AFIDA's flexible capabilities for analysis of diesel- and gasoline-range blends, which also include indicated cetane number calculation and parametric ignition delay mapping for validation of kinetic mechanisms, make it well-suited for assessing emerging fuels for multi-mode engines, a focus for FY 2019 research.

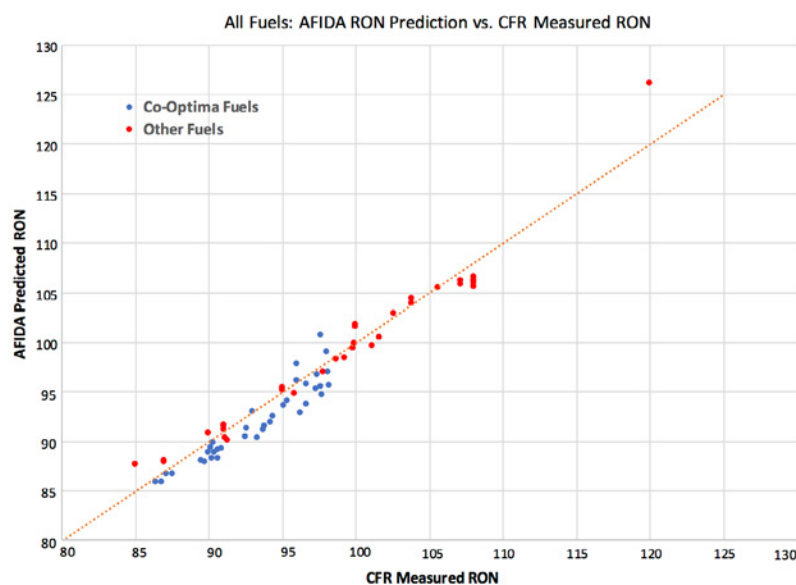


Figure II.18.2. Correlation of RON predicted from AFIDA ignition delay to RON measured by CFR engine method. AFIDA-predicted RON vs. RON measured on the CFR engine, showing excellent agreement. Red points are oxygenated blends in primary reference fuels, toluene standardization fuels, and complex gasoline surrogates. Blue points are oxygenated candidates blended into the core Co-Optima boosted SI fuels. (Figure: Jon Luecke, NREL)

Conclusions

- CVCC ignition kinetics experiments quantify fuel component, surrogate blend, and full boiling range gasoline ignition performance over engine-relevant parametric space.
- Unique AFIDA data complement data from other devices such as shock tubes and rapid compression machines, and provide additional perspective than RON or motor octane number values alone.
- Extensive characterization and experimental methodology development with the AFIDA have demonstrated significantly expanded capability beyond IQT-based studies for high-quality ignition kinetics experiments and simulations.
- AFIDA simulations, both simple 0D and 1/7 chamber CFD, now enable these experiments to be part of the feedback development loop for development of accurate, reduced kinetic mechanisms.

- Rapid AFIDA-based correlations to RON and S enable early-stage screening for compounds or blends for which only small sample volumes may be available.
- The AFIDA now provides measurements for ignition propensity (indicated cetane number) and ignition resistance (RON, S) within one CVCC device, and potential exists to develop additional targeted screening metrics that may be helpful in terms of advanced compression ignition and multi-mode operation.

Key Publications

1. Barraza-Botet, C.L., J. Luecke, B.T. Zigler, and M.S. Wooldridge. 2018. “The Impact of Physicochemical Property Interactions of iso-Octane/Ethanol Blends on Ignition Timescales.” *Fuel* 224 (July): 401–411. <https://doi.org/10.1016/j.fuel.2018.03.105>.
2. Luecke, J., M. Rahimi, B.T. Zigler, and R.W. Grout. “Experimental and Numerical Investigation of the AFIDA Constant Volume Chamber as a Research Platform for Chemical Kinetic Model Validation.” Prepared for submission to *Fuel*.

References

1. Bogin, G.E., Jr., E. Osecky, J.Y. Chen, M.A. Ratcliff, J. Luecke, B.T. Zigler, and A.M. Dean. 2014. “Experiments and Computational Fluid Dynamics Modeling Analysis of Large n-Alkane Ignition Kinetics in the Ignition Quality Tester.” *Energy Fuels* 28: 4781–4794. DOI: 10.1021/ef500769j.
2. Bogin, G.E., Jr., E. Osecky, M.A. Ratcliff, J. Luecke, X. He, B.T. Zigler, and A.M. Dean. 2013. “Ignition Quality Tester (IQT) Investigation of the Negative Temperature Coefficient Region of Alkane Autoignition.” *Energy Fuels* 27: 1632–1642. DOI: 10.1021/ef301738b.
3. Bogin, G.E., Jr., A. DeFilippo, J.Y. Chen, G. Chin, J. Luecke, M.A. Ratcliff, B.T. Zigler, and A.M. Dean. 2011. “Experimental Investigation of n-Heptane Autoignition in the Ignition Quality Tester (IQT).” *Energy Fuels* 25: 5562–5572. DOI: 10.1021/ef201079g.
4. Bogin, G., A.M. Dean, M.A. Ratcliff, J. Luecke, and B.T. Zigler. 2010. “Expanding the Experimental Capabilities of the Ignition Quality Tester for Autoigniting Fuels.” *SAE International Journal of Fuels and Lubricants* Vol. 3, Issue 1: 353–367.
5. Osecky, E.M., G.E. Bogin, Jr., S.M. Villano, M.A. Ratcliff, J. Luecke, B.T. Zigler, and A.M. Dean. 2016. “Investigation of Iso-Octane Ignition and Validation of a Multizone Modeling Method in an Ignition Quality Tester.” *Energy & Fuels* 30 (11): 9761–9771. DOI: 10.1021/acs.energyfuels.6b01406.
6. ASTM D7170-16. 2016. “Standard Test Method for Determination of Derived Cetane Number (DCN) of Diesel Fuel Oils—Fixed Range Injection Period, Constant Volume Combustion Chamber Method.” ASTM International, West Conshohocken, PA, www.astm.org. DOI: 10.1520/D7170-16.
7. Seidenspinner, P., M. Härtl, T. Wilharm, and G. Wachtmeister. 2015. “Cetane Number Determination by Advanced Fuel Ignition Delay Analysis in a New Constant Volume Combustion Chamber.” SAE Technical Paper 2015-01-0798, <https://doi.org/10.4271/2015-01-0798>.
8. Foong, T.M., K.J. Morganti, M.J. Brear, G. da Silva, Y. Yang, and F.L. Dryer. 2014. “The Octane Numbers of Ethanol Blended with Gasoline and Its Surrogates.” *Fuel* 115: 727–739. <http://dx.doi.org/10.1016/j.fuel.2013.07.105>.
9. Livengood, J.C., and P.C. Wu. 1955. “Correlation of Autoignition Phenomena in Internal Combustion Engines and Rapid Compression Machines.” Symposium (International) on Combustion Vol. 5, No. 1. Elsevier.

Acknowledgements

NREL would like to thank Kevin Stork for his support of this research under the Co-Optima program. NREL would also like to thank Philipp Seidenspinner at Analytik-Service Gesellschaft MbH for continued collaboration in expanding the AFIDA as a flexible research platform. Ray Grout also coordinated Mohammad Rahimi's AFIDA simulations within the broader Co-Optima project simulation activities. Thanks also to Jon Luecke, Mohammad Rahimi, Riley Abel, Brandon King, Sam Nichols, and Greg Bogin, Jr., of NREL.

II.19 Modification of PMI to Include Oxygenate Effects (National Renewable Energy Laboratory)

Matt Ratcliff, Principal Investigator

National Renewable Energy Laboratory
15013 Denver West Parkway
Golden, CO 80401
E-mail: matthew.ratcliff@nrel.gov

Kevin Stork, DOE Technology Development Manager

U.S. Department of Energy
E-mail: Kevin.Stork@ee.doe.gov

Start Date: October 1, 2017	End Date: September 30, 2018	
Project Funding (FY18): \$308,000	DOE share: \$308,000	Non-DOE share: \$0

Project Introduction

The project goals were to understand and predict the interactive effects of aromatics and ethanol in gasoline on particulate matter (PM) emissions. The potential of oxygenate-free gasoline to form PM, based on composition, has been successfully modeled [1,2] with the particulate matter index (PMI), shown as Equation 1.

$$PMI = \sum_{i=1}^n \left[\frac{(DBE_{i+1})}{VP(443K)_i} \times Wt_i \right] \quad (1)$$

The double bond equivalent (DBE) represents the tendency for individual fuel components to form soot based on number of rings and unsaturated bonds in the fuel molecule: $DBE = (2C + 2 - H) / 2$. Component vapor pressure at 443 K, or $VP(443 K)$, represents the tendency for individual fuel components to evaporate. Fuel components, especially aromatics ($DBE \geq 4$), having low $VP(443 K)$ increase PMI because their vaporization is relatively slow. They may, therefore, not fully evaporate and mix with air during intake and compression cycle time scales. Locally heterogeneous fuel-air mixtures and/or fuel-rich combustion are responsible for increasing PM emissions.

Ethanol is the most common oxygenate used for gasoline blending, and there are conflicting results in the literature about its effects on PM emissions. Conventional wisdom is that ethanol, with near-zero potential to form PM ($PMI = 0.07$), blended into gasoline dilutes the high-PMI aromatics, thereby decreasing the blend's overall PMI. In many studies where the fuels were "splash-blended," i.e., ethanol was simply added to the gasoline, the PM emissions did indeed decrease [3–5]. However, other studies have shown increased PM under some operating conditions. For example, He and coworkers observed increased PM for an E20 blend (20% ethanol with 80% gasoline) at high load and suggested that ethanol's high heat of vaporization (HOV) slowed fuel evaporation from piston and cylinder surfaces [6]. Similar observations have been made in other studies where blending ethanol into gasoline resulted in higher PM emissions [7–9]. Thus, one objective of this project is to better understand these seemingly contradictory findings by clarifying the interactions between ethanol (and perhaps by extension other low-molecular-weight alcohols), aromatic hydrocarbons in the blend, and engine operating conditions. A second objective of this study is to develop improved models for predicting PM by accurately accounting for fuel property interactions brought about by blending ethanol into gasoline.

Objectives

The research objectives for Fiscal Year 2018 were as follows.

- Quantify PM emissions from a full-factorial designed experimental fuel matrix having the variables of aromatic VP, aromatic concentration, and ethanol concentration

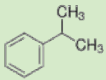
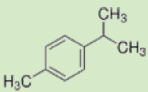
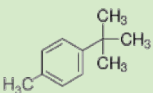
- Analyze PM emissions and fuel property data as well as droplet evaporation model results to identify and characterize fuel property interactions affecting PM
- Develop improved predictive models for PM emissions based on better understanding of fuel property effects and interactions

Approach

A full-factorial experiment was designed to test the hypothesis that increasing fuel HOV (via increasing ethanol content) interacts with aromatics, causing PM emissions to increase. The base gasoline chosen for these experiments was the low-aromatic, high-octane Fuels for Advanced Combustion Engines (FACE) Gasoline B, into which selected boiling point aromatics and ethanol were blended. The aromatic content was held constant on a volumetric basis regardless of ethanol blend level. Aromatics were selected based on their VP (443 K) values, which are shown along with boiling points and structures in Table II.19.1. Table II.19.2 compiles PMI and HOV values for the fuels, which were computed based on their detailed hydrocarbon analysis, a gas chromatography method described in previous publications [10,11].

Differential scanning calorimetry (DSC)/thermogravimetric analysis (TGA) was used to directly measure fuel HOV. A new technique used a mass spectrometer to measure the evolution of selected fuel components in the effluent from the DSC/TGA experiments. The fuels were additionally characterized by the advanced distillation curve method [12] that determines the composition of each distillate fraction by detailed hydrocarbon analysis. Advanced distillation curve analysis provided new insights into the azeotrope interactions between ethanol and hydrocarbons, particularly for the aromatics intentionally blended for this study. The advanced distillation curve results were used to validate a liquid fuel distillation model, which in turn led to development of a single droplet evaporation model. This droplet model was exercised over the range of temperatures, pressures, and time scales relevant to National Renewable Energy Laboratory's single-cylinder gasoline direct injection engine operating conditions.

Table II.19.1. Properties of Aromatics Blended into FACE B Gasoline

Component	Boiling Point (°C)	Vapor Pressure at 443 K (kPa)	Structure	Double Bond Equivalent	Unified YSI
Cumene	153	152		4	188
p-Cymene	177	84.5		4	330
4-t-Butyl Toluene	191	58		4	411

YSI – yield sooting index

Table II.19.2. Measured Compositions of Fuels, HOV, and PMI (computed from detailed hydrocarbon analysis)

FACE B Blends	Ethanol			Added Aromatic			HOV	PMI
	wt%	vol%	mol %	wt%	vol%	mol %	kJ/kg	-
E0 + 10% Cumene	0	0	0	12.50	10.33	10.94	331	0.71
E30 + 10% Cumene	30.57	28.52	49.97	10.58	9.03	6.63	514	0.57
E0 + 10% 4-t-Butyl Toluene	0	0	0	10.60	8.82	7.54	327	1.25
E30 + 10% 4-t-Butyl Toluene	34.95	32.78	55.64	10.81	9.41	5.35	536	1.18
E15 + 15% p-Cymene	16.43	15.21	31.30	16.73	14.26	10.94	429	1.23
E0 + 20% Cumene	0	0	0	23.39	19.68	20.47	336	1.03
E30 + 20% Cumene	33.69	32.28	54.11	22.05	19.34	13.57	537	0.90
E0 + 20% 4-t-Butyl Toluene	0	0	0	22.50	19.15	16.60	327	2.28
E30 + 20% 4-t-Butyl Toluene	31.88	30.34	53.31	20.24	17.88	10.52	518	2.00

PM emissions were measured from the single-cylinder gasoline direct injection engine using (1) an AVL Micro-Soot Sensor and (2) a TSI Fast Mobility Particle Sizer with sample dilution and conditioning provided by a Dekati FPS-4000 and thermodenuder, as previously described [10]. Three engine operating conditions were investigated (see Table II.19.3), including two (A and D) using single injections. The start of injection for single (or first) injection was 280° before top dead center (BTDC). Although occurring relatively early in the intake stroke, this start of injection was previously found to avoid or significantly reduce spray impingement on the piston [6]. Multiple linear regression analyses of the PM emissions and fuel property data were performed to characterize and model fuel property effects on PM emissions. In addition, regression analyses using fuel property interaction terms obtained from the LASSO method [13] were investigated.

Table II.19.3. Engine Operating Conditions for PM Measurements; Intake Air Temperature Fixed at 35 °C

Test Condition	Speed & Load (rpm, bar NMEP)	Intake Manifold Pressure (kPa)	Start of Injection (° BTDC)	Spark Timing (° BTDC)	Target CA50 (° ATDC)
A	2500, 13	105–106	280	6.5	22 ± 2
B	2500, 13	105–106	280, 220	9	22 ± 2
D	1500, 10	76–77	280	15	7.5 ± 1.5

ATDC – after top dead center; CA50 – crank angle for 50% mass of fuel burned; NMEP – net mean effective pressure

Results

Mass spectrometer analysis of the evolving gases during the DSC/TGA/mass spectrometer experiments [14] is shown in Figure II.19.1. The raw ion current mass spectrometer data from the 10% cumene blends include isooctane (a major component of FACE B), xylenes/ethyl benzene, cumene, and ethanol (for fuels containing ethanol) as functions of mass fraction evaporated. Comparing the curves from the ethanol-blended fuel (Figure II.19.1b) with those from the ethanol-free blend (Figure II.19.1a), it is apparent that ethanol interacts with isooctane during its evaporation. Overall, evaporation of isooctane increased while ethanol was present in the liquid and was effectively gone by mass fraction 0.85, as opposed to continuing to the end of evaporation in the ethanol-free blend. This is evidence of azeotrope formation between ethanol and isooctane. Ethanol's apparent facilitation of isooctane evaporation (and presumably for other paraffins in FACE B) resulted in enrichment of the aromatics remaining in the liquid, and their substantial evaporation was delayed to the last 0.3 mass fraction.

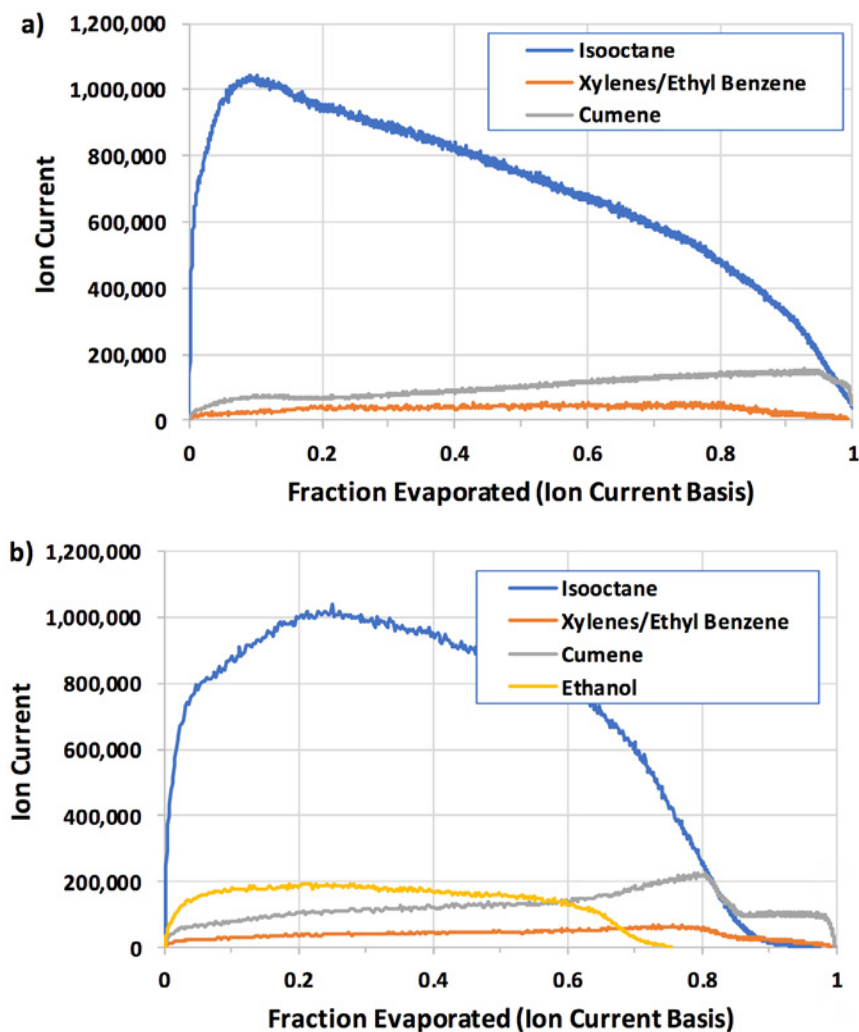


Figure II.19.1. Raw mass spectrometer ion current data for several species: (a) E0-10% cumene blends and (b) E30-10% cumene blends in FACE B gasoline

Figure II.19.2 illustrates the single droplet evaporation simulation results, carried out at an ambient condition of 371 K and 1 atm for the 4-t-butyl toluene blends. This temperature corresponded to the average temperature between start of injection and spark ignition timing, assuming isentropic compression. The addition of ethanol slowed evaporation of the fuel, and fuels containing higher concentrations of 4-t-butyl toluene required more time to evaporate (Figure II.19.2a). Blending ethanol suppressed droplet temperatures, which additionally delayed evaporation (Figure II.19.2b). The transient liquid aromatic mass curves (Figure II.19.2c) show that the addition of ethanol produced droplets having higher liquid aromatic mass near the end of evaporation, lasting longer into the droplet's lifetime than those droplets without ethanol. At a reference time arbitrarily defined by the lifetime of a neat FACE B–E0 droplet (vertical line in Figure II.19.2c), the mass of liquid aromatics remaining in the droplets nearly doubles when the initial amount of 4-t-butyl toluene is doubled (for a given initial ethanol concentration). An additional increase in liquid aromatic mass is observed when the ethanol concentration is increased from 0% to 30% by volume (for a given initial 4-t-butyl toluene concentration). Previous work has credited this enrichment effect to preferential evaporation of ethanol, delaying the evaporation of the heavy fuel fractions, which in this case (and often in commercial gasoline) contains a significant portion of the aromatic compounds in the fuel [15]. The role of non-ideal vaporization was shown to play a minor role. However, for the fuel blends tested here, evaporative cooling of the droplet stemming from ethanol's high HOV lowers VP and slows evaporation more than the increase in VP due to azeotropes. Because of both slowed droplet evaporation as well as the enrichment of the aromatics, the evaporation model predicts an increase in the total aromatic mass after evaporation of the initial gasoline fractions occurs.

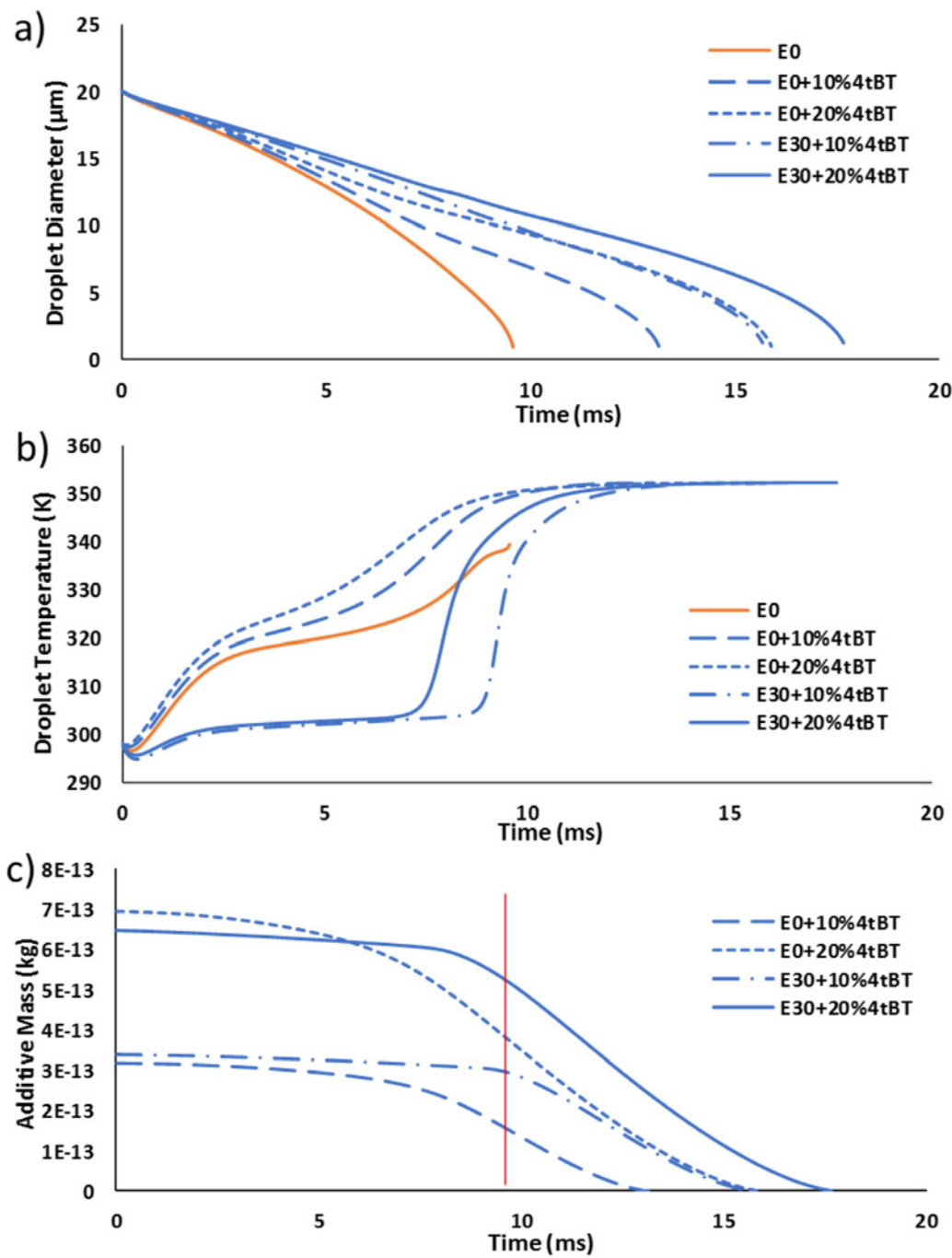
The measured PM mass and total particle number (PN) concentrations from engine test Condition A were well correlated, having $R^2 = 0.94$. Thus, the general trends are valid for both measurements. Figure II.19.3 shows the PN measurements from the 20 vol% aromatic blends and reveals that co-blending ethanol and the lower-VP aromatic 4-t-butyl toluene significantly increased the number of accumulation mode particles, especially in the 35–80 nm range. In contrast, no effects from co-blending ethanol and higher-VP aromatic cumene were observed. These results indicate the complex interactions between the aromatics and ethanol that affect PN (and PM mass) emissions.

The DSC/TGA experimental results demonstrated that the presence of ethanol suppresses and delays the evaporation of the aromatics, while the droplet modeling showed that ethanol increases droplet lifetime and concentrates the aromatics in the droplet at the end of evaporation. On the other hand, co-blending ethanol produces significant dilution of the aromatics on a molar basis, as detailed in Table II.19.2, even for this volumetrically match-blended study. Figure II.19.3 suggests that for the 20 vol% cumene blends within the pressure–temperature environment of Condition A, there was balance between the competing effects of ethanol's dilution of cumene in the E30 blend and ethanol's inhibiting effects on cumene evaporation. This balancing of fuel effects led to similar PN concentrations and size distributions for these cumene blends at Condition A. In contrast, the much less volatile 4-t-butyl toluene appears to have been beyond some threshold of vapor pressure and concentration that produced longer fuel droplet lifetimes for the E30 blend, such that a fuel-rich mixture containing a high aromatic content persisted when the flame front arrived.

Engine operating Condition B (same nominal speed and load as Condition A, but injection split 50:50) resulted in significant reductions of particle emissions in all cases relative to Condition A. Figure II.19.4 compares PN particle size distribution results from the 20 vol% 4-t-butyl toluene blends at Conditions A and B; the latter reduced particle emissions roughly 50%. This reduction is attributed to reduced fuel spray contact with the piston and/or cylinder liner resulting from shorter injection durations and presumably shorter liquid penetration lengths. Similar PN reductions were observed from both 10 vol% and 20 vol% cumene blends when comparing Conditions A and B (not shown). Furthermore, it is noteworthy that at Condition B, PN emissions from E30 + 20% cumene were significantly lower than those from the E0 + 20% cumene blend, indicating the dominance of ethanol's dilution on cumene's molar concentration, over its inhibition of cumene evaporation.

The lower-speed and -load Condition D produced four- to five-fold reductions in PN emissions from the 20% 4-t-butyl toluene blends, compared to Condition A (not shown). From the 20% cumene blends, the PN emissions at Condition D were 10–15% of those at Condition A (not shown), with very slightly lower PN levels arising from the E30 blend. These lower PN emissions observed at Condition D were likely the result of less spray impingement on the piston/cylinder liner due to shorter injector pulse width, additional available

time for evaporation because of the slower engine speed, and less charge cooling associated with the smaller amount of fuel injected.



4tBT – 4-t-butyl toluene

Figure II.19.2. (a) Predicted time-dependent droplet diameter, (b) droplet temperature, and (c) liquid aromatic additive mass during evaporation of droplets of FACE B blends with 4-t-butyl toluene, at constant ambient temperature and pressure of 371 K and 1 atm

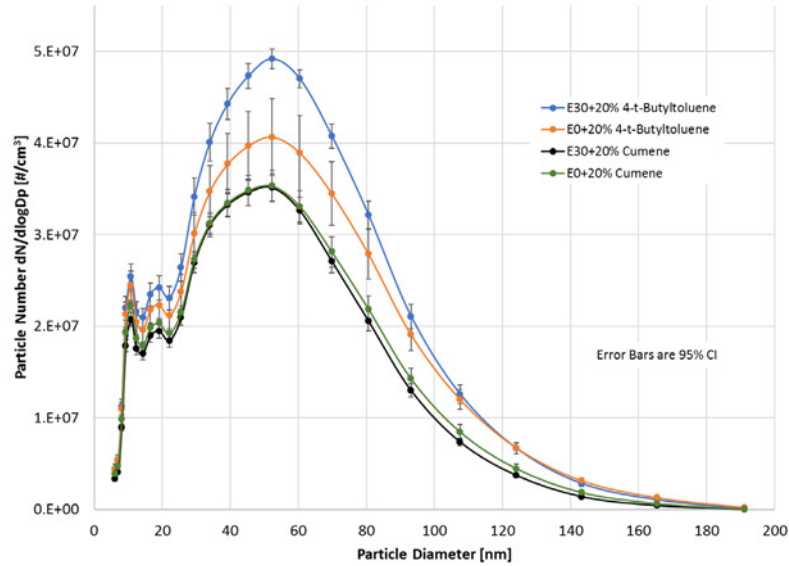


Figure II.19.3. PN concentration as a function of particle diameter at Condition A for fuels blended with aromatics at 20 vol%. Error bars are 95% confidence intervals.

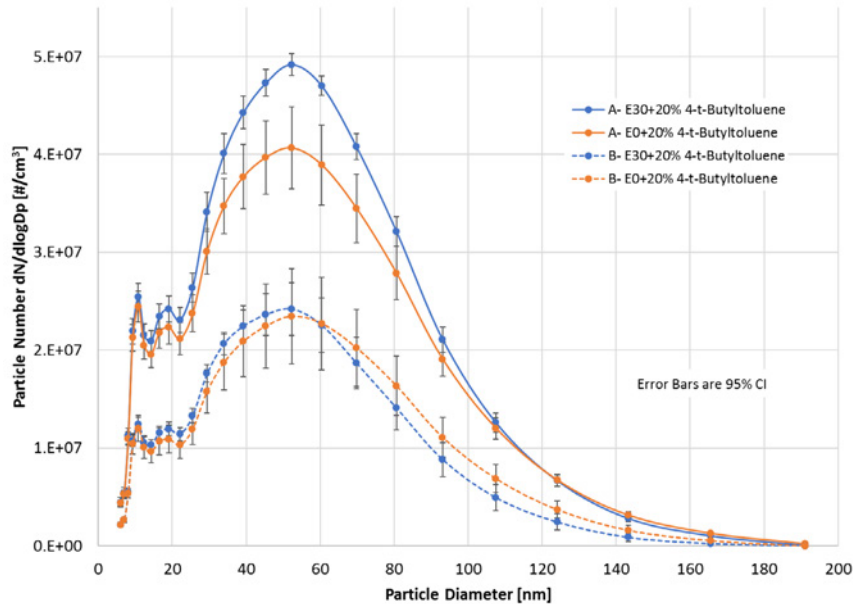


Figure II.19.4. Comparison of particle size distributions between Conditions A and B for the 20 vol% 4-t-butyl toluene blends. Error bars are 95% confidence intervals.

PM emissions correlated poorly with the PMIs for these fuels. Condition A had a linear regression $R^2 = 0.688$, while Conditions B and D had $R^2 = 0.745$ and 0.526 , respectively. These values demonstrate that PMI does not adequately capture relevant fuel properties affecting PM within this dataset. For example, as shown in Table II.19.1, the DBE for all three blended aromatics is 4, while YSI [16] ranged from 188 to 411. Furthermore, PMI does not capture HOV cooling and its impact on fuel droplet lifetime, or the concentration of aromatics into the last fractions of the fuel droplets.

The factorial experimental design allowed the data to be fit to a multiple linear regression model (Equation 2) and then use that model to examine ethanol blending effects, i.e., dilution of aromatics versus HOV and vapor–liquid equilibrium effects. Analysis using ethanol and aromatic concentrations expressed on a mole

percent basis proved most meaningful. The coefficients for aromatic and ethanol molar concentrations, as well as aromatic VP, were found to be statistically significant (p-values < 0.05) for Condition A. With an adjusted $R^2 = 0.838$ (for the PM mass data), this model is a significantly better predictor of PM from fuel composition and properties than PMI for this fuel set. Regression analysis results are summarized in Table II.19.4. Notably, the coefficient on the aromatic concentration term in this linear model is roughly a factor of ten larger than the coefficients for ethanol concentration or VP, highlighting dominance of gasoline aromatic content on PM emissions. The effects of lower aromatic VP or of ethanol blending are secondary in this model.

$$PM = X1 + X2 * (Ethanol\ mol\%) + X3 * (Aromatic\ mol\%) + X4 \quad (2)$$

(Aromatic VP@443 K)

Table II.19.4. Results of Linear Regression Analysis for Condition A Using Mole Percent Concentrations of Ethanol and Aromatics in the Blends

Adjusted R ²	0.838
Ethanol mole% coefficient	0.045
Ethanol mole% p-value	0.012
Aromatic mole% coefficient	0.330
Aromatic mole% p-value	0.004
Aromatic vapor pressure coefficient	-0.033
Aromatic vapor pressure p-value	0.003

While the linear regression model outperformed PMI in predicting PM mass emissions, nonlinear interactions between predictor variables might better explain the observed PM emission results. For example, because the presence of ethanol changes the droplets' distillation characteristics, some nonlinear interaction between the ethanol and aromatic terms is likely required. Because a regression containing all combinations of nonlinear interactions between variables would have far more explanatory variables than the sample size, a regularized regression approach to prevent overfitting was used. Specifically, the LASSO method was used, which penalizes the l1 norm of the regression coefficients and therefore results in sparse solutions containing only a few active explanatory variables [13]. Ten-fold cross-validation was performed to find combined explanatory variables that appeared the most frequently in regressions on subsets of the data. Two variables were selected based on their frequent appearance (Equation 3). The first, ethanol mole percent multiplied by aromatic mole percent divided by aromatic VP, was an active explanatory variable in eight out of the 10 cross-validation splits. The second, added aromatic mole percent multiplied by aromatic YSI [16] divided by aromatic molecular weight, appeared in seven out of the 10 splits. The results of linear regression including only these two combined explanatory variables and an intercept are shown in Figure II.19.5 and Table II.19.5. The R^2 of the regression (0.959) is substantially improved over the linear model without interaction terms.

$$PM = x1 + x2 * \left[\frac{EtOH\% * Aro\%}{AroVP@443K} \right] + x3 * \left[\frac{Aro\ YSI * Aro\%}{Aro\ MW} \right] \quad (3)$$

The first term likely considers the effect of ethanol and aromatic VP shifting the aromatic farther back in the distillation curve. PM could therefore be decreased by decreasing ethanol or aromatic concentrations or choosing an aromatic with a higher VP. The second term considers the kinetic tendency of the aromatic to form soot, as determined by its YSI multiplied by aromatic mass fraction.

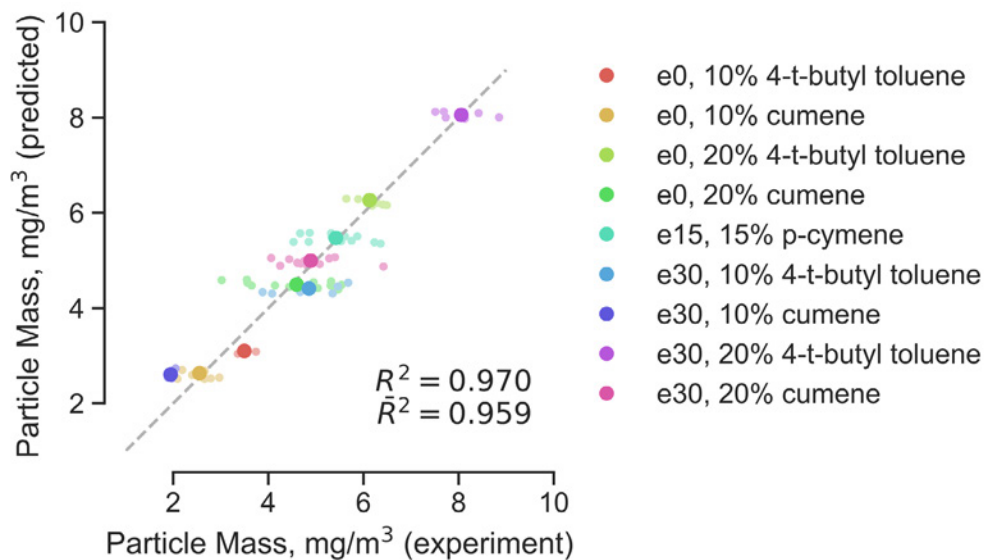


Figure II.19.5. Results of the linear model using optimal combined explanatory variables determined through regularized regression. Large dots indicate the mean experimental PM mass in mg/m³ with individual data points plotted as smaller circles (a slight jitter has been added to the y-values to prevent overlap in this illustration).

Table II.19.5. Regularized Regression Results and Statistics

Regularized regression	
Adjusted R²	0.959
Intercept	0.4646
Variable 1 coefficient	0.3976
Variable 1 p-value	<0.001
Variable 2 coefficient	0.1262
Variable 2 p-value	<0.001

Conclusions

Two patterns of fuel effects on PM/PN emissions emerged from this study. For the low-VP 4-t-butyl toluene blends at Condition A, ethanol’s effects on droplet evaporation dominate, i.e., inhibition of aromatic vaporization and increased droplet lifetime because of evaporative cooling. This effect of ethanol blending on PM was attenuated at Condition B. For the higher-VP 20 vol% cumene blends, the competition between ethanol’s dilution of aromatics (on a molar basis) and the inhibitory droplet evaporation effects appeared approximately balanced at Condition A. But at Condition B, the aromatic molar dilution clearly dominated, as PM from the E30 blend was significantly reduced. For the 10 vol% cumene blends, ethanol’s dilution effects appeared to consistently dominate, with E30 producing lower PM. At the lower load and engine speed Condition D, these fuel property effects and interactions were diminished or eliminated. Additional time for evaporation, coupled with reduced fuel spray impingement on the piston and cylinder liner (the result of shorter injection pulse durations for the lower load, and presumably shorter spray penetration length) are believed responsible for this.

Separate from the increased evaporative cooling effect ethanol blending causes, the formation of azeotropes with paraffins in gasoline leads to delay of aromatics evaporation and, therefore, aromatic enrichment in the liquid spray droplets. The additional evaporative cooling from ethanol blending reduces droplet temperature and therefore increases droplet lifetime. The effect of blending low-VP aromatics combined with the aromatic enrichment and droplet cooling from blending ethanol can result in higher PM emissions under some engine operating conditions, particularly those conditions producing fuel spray impingement and short evaporation period (i.e., high load and high engine speed).

Key Publications

1. Burke, S., R. Rhoads, R. McCormick, M. Ratcliff, and B. Windom. 2018. "Measured and Predicted Vapor Liquid Equilibrium of Ethanol-Gasoline Fuels with Insight on the Influence of Azeotrope Interactions on Aromatic Species Enrichment and Particulate Matter Formation in Spark Ignition Engines." SAE Technical Paper No. 2018-01-0361.
2. Ratcliff, M.A., B. Windom, G.M. Fioroni, P. St. John, S. Burke, J. Burton, E.D. Christensen, P. Sindler, and R.L. McCormick. 2018. "Impact of Ethanol Blending into Gasoline on Aromatic Compound Evaporation and Particle Emissions from a Gasoline Direct Injection Engine." Submitted to *Journal of Applied Energy*.
3. Fioroni, G., L. Fouts, E. Christensen, J. Anderson, and R. McCormick. 2018. "Measurement of Heat of Vaporization for Research Gasolines and Ethanol Blends by DSC/TGA." *Energy and Fuels* 32: 9581–9591.

References

1. Aikawa, K., T. Sakurai, and J.J. Jetter. 2010. "Development of a Predictive Model for Gasoline Vehicle Particulate Matter Emissions." *SAE Int. J. Fuels Lubr.* 3 (2): 610–622. doi:10.4271/2010-01-2115.
2. Aikawa, K., and J.J. Jetter. 2013. "Impact of Gasoline Composition on Particulate Matter Emissions from a Direct-Injection Engine: Applicability of Particulate Matter Index." *Int. J. Eng. Res.* 15 (3): 298–306. doi: 10.1177/1468087413481216.
3. Maricq, M.M., J.J. Szente, and K. Jahr. 2012. "The Impact of Ethanol Fuel Blends on PM Emissions from a Light-Duty GDI Vehicle." *Aerosol Sci. Technol.* 46 (5): 576–583.
4. He, X., J.C. Ireland, B.T. Zigler, M.S. Ratcliff, K.E. Knoll, T.L. Alleman, and J.T. Tester. 2010. "The Impacts of Mid-Level Biofuel Content in Gasoline on SIDI Engine-Out and Tailpipe Particulate Matter Emissions." SAE Technical Paper 2010-01-2125.
5. Fatouraie, M., M.S. Wooldridge, B.R. Petersen, and S.T. Wooldridge. 2015. "Effects of Ethanol on In-Cylinder and Exhaust Gas Particulate Emissions of a Gasoline Direct Injection Spark Ignition Engine." *Energy Fuels* 29: 3399–3412.
6. He, X., M.A. Ratcliff, and B.T. Zigler. 2012. "Effects of Gasoline Direct Injection Engine Operating Parameters on Particle Number Emissions." *Energy Fuels* 26: 2014–2027.
7. Butler, A.D., R.A. Sobotowski, G.J. Hoffman, and P. Machiele. 2015. "Influence of Fuel PM Index and Ethanol Content on Particulate Emissions from Light-Duty Gasoline Vehicles." SAE Technical Paper 2015-01-1072.
8. Storch, M., M. Koegl, M. Altenhoff, S. Will, and L. Zigan. 2016. "Investigation of Soot Formation of Spark-Ignited Ethanol-Blended Gasoline Sprays with Single- and Multi-Component Base Fuels." *Applied Energy* 181: 278–287.
9. CRC Report No. E-94-2. 2017. "Evaluation and Investigation of Fuel Effects on Gaseous and Particulate Emissions on SIDI In-Use Vehicles." March.

10. Ratcliff, M.A., J. Burton, P. Sindler, E. Christensen, G.M. Chupka, L. Fouts, and R.L. McCormick. 2016. "Knock Resistance and Fine Particle Emissions for Several Biomass-Derived Oxygenates in a Direct-Injection Spark-Ignition Engine." *SAE Int. J. Fuels Lubr.* 9 (1): 59–70. doi:10.4271/2016-01-0705.
11. Chupka, G.M., E. Christensen, L. Fouts, T.L. Alleman, M. Ratcliff, and R.L. McCormick. 2015. "Heat of Vaporization Measurements for Ethanol Blends up to 50 Volume Percent in Several Hydrocarbon Blendstocks and Implications for Knock in SI Engines." *SAE Int. J. Fuels Lubr.* doi:10.4271/2015-01-0763.
12. Smith, B.L., and T.J. Bruno. 2007. "Improvements in the Measurement of Distillation Curves. 3. Application to Gasoline and Gasoline + Methanol Mixtures." *Ind. Eng. Chem. Res.* 46: 297–309.
13. Tibshirani, R. 1996. "Regression Shrinkage and Selection via the LASSO." *Journal of the Royal Statistical Society. Series B (Methodological)*. 267–288.
14. Fioroni, G., L. Fouts, E. Christensen, J. Anderson, and R. McCormick. 2018. "Measurement of Heat of Vaporization for Research Gasolines and Ethanol Blends by DSC/TGA." *Energy and Fuels* 32: 9581–9591.
15. Burke, S.C., M.A. Ratcliff, R.L. McCormick, R. Rhoads, and B. Windom. 2017. "Distillation-Based Droplet Modeling of Non-Ideal Oxygenated Gasoline Blends: Investigating the Role of Droplet Evaporation on PM Emissions." SAE World Congress, April 2017. *SAE Int. J. Fuels Lubr.* 10 (1): 69–81. SAE 2017-01-0581.
16. Das, D., P. St. John, C. McEnally, S. Kim, and L. Pfefferle. 2018. "Measuring and Predicting Sooting Tendencies of Oxygenates, Alkanes, Alkenes, Cycloalkanes, and Aromatics on a Unified Scale." *Combustion and Flame* 190: 349–364.

Acknowledgements

Bret Windom and Stephen Burke, Department of Mechanical Engineering, Colorado State University; Gina Fioroni, Peter St. John, Jon Burton, Earl Christensen, Petr Sindler, and Bob McCormick, National Renewable Energy Laboratory.

II.20 Virtual Properties, Reduced Mechanism, Blending of Kinetics Properties, and Modeling of Fuel Properties (National Renewable Energy Laboratory)

Ray Grout, Principal Investigator

National Renewable Energy Laboratory
MS ESIF301
15013 Denver West Parkway
Golden, CO 80401
E-mail: ray.grout@nrel.gov

Kevin Stork, DOE Technology Development Manager

U.S. Department of Energy
E-mail: Kevin.Stork@ee.doe.gov

Start Date: January 10, 2017

End Date: August 15, 2018

Project Funding (FY18): \$15,000

DOE share: \$15,000

Non-DOE share: \$0

Project Introduction

This project is to identify computational surrogates that represent more complicated fuels for the purposes of detailed ignition delay calculations. A barrier to calculating the ignition delay of a fuel numerically is the relatively large number of experiments necessary to develop appropriate chemical mechanisms, typically an assembly of shock tube measurements, rapid compression machine measurements, flow reactor experiments, and so on. For the purpose of screening fuels for ignition properties, various small-volume test devices are in widespread use based on empirical correlation of single-point or small ensembles of measurements with desired characteristics. The U.S. Department of Energy (DOE) Co-Optimization of Fuels and Engines (Co-Optima) initiative is accelerating the introduction of efficient, clean, affordable, and scalable high-performance fuels and engines. The effort is simultaneously tackling fuel and engine research and development to maximize light-, medium-, and heavy-duty vehicle fuel economy and performance, while mapping lower-cost pathways to reduce emissions, leveraging diverse domestic fuel resources, boosting U.S. economic productivity, and enhancing national energy security. Co-Optima uses a composition-agnostic approach to identify new blendstocks that can be combined with conventional petroleum-based fuels to deliver significantly improved performance in advanced internal combustion engines for use in light-duty passenger cars to heavy-duty freight trucks. This property-based approach is a critical success element—identifying the properties needed to enable advanced engines, rather than defining a specific composition or “recipe”—that allows fuel providers the flexibility to provide fuels with these properties into the market in the most practical and economical manner.

An emerging interest within Co-Optima is in examining the autoignition propensity under “beyond research octane number (RON)” and “beyond motor octane number” conditions. This specifically refers to the autoignition characteristics under time-dependent pressure-temperature histories that “bookend” the conditions experienced in an advanced spark ignition/compression ignition engine platform. A current effort is to establish the p-T trajectories that represent the operating conditions relevant to advanced spark ignition/compression ignition engines. Given a pressure-temperature trajectory, there is significant evidence that the ignition properties of a fuel can be captured by a path-independent integral in pressure-temperature space. That is, at ignition [1]:

$$1 = \int_0^{t_{\text{ign}}} \frac{1}{\tau(T(t'), p(t'))} dt' \quad (1)$$

This provides a basis for comparing various fuels based on temperature and pressure time histories relevant to a given engine configuration. A practical difficulty, though, is measuring the ignition delay times across the relevant conditions. Experimental methods include measurements in apparatuses such as shock tubes, rapid

compression machines, and rapid heating devices. Covering the entirety of the relevant conditions typically requires a combination of these devices. While efforts are underway within Co-Optima and elsewhere to reduce the volume of sample required, measurements typically require larger fuel volumes than desirable for early-stage screening. An alternative is to evaluate the ignition delay at the necessary conditions from a homogeneous reactor calculation using an appropriate chemical mechanism. Unfortunately, kinetic mechanism development is also time-consuming and traditionally requires an even larger number of experiments along with measurements such as laminar flame speed and flow reactor speciation.

Objectives

This project is centered around exploring the concept of using an existing chemical mechanism to model a fuel not appearing explicitly in the mechanism inputs, to determine if such a mechanism is sufficiently generic to be able to be used as a surrogate for the actual mechanism.

Overall and Fiscal Year 2018 Objectives

- Identify potential for using a detailed kinetic mechanism as a surrogate for fuels not appearing in the usual inputs for that mechanism
- Demonstrate feasibility of fitting reactant composition to product speciation based on a limited set of notional experiments
- Implement and verify correct operation of relevant analytics pipeline

Approach

The approach is to assemble a computational apparatus to determine parameters in a numerical model of a flow reactor that are consistent with the observables, verify its correct operation, and use it to test the premise above. This is done in the context of a synthetic experiment where a simulation of a flow reactor (corresponding to a fuel kinetics test rig at National Renewable Energy Laboratory) is used to determine the observables. These observables (species concentrations) are then used as targets to determine surrogate composition. Finally, autoignition delays computed using either two- or three-component surrogates are demonstrated to be consistent with those computed from the actual multi-component reactant composition used to generate the targets.

Results

A numerical model, \mathcal{M} , of the flow reactor is constructed:

$$\vec{S} = \mathcal{M}(\vec{\Theta}; t_r, T, \mathbf{C}) \quad (2)$$

where S is a vector of product species at the flow reactor outlet, Θ is the reactant composition at the inlet, and t_r , T , \mathbf{C} are, respectively, the residence time, temperature, and chemical mechanism used to represent the kinetics. In this case, \mathcal{M} consists of a plug flow reactor that has been previously demonstrated to be a reasonable approximation of the flow reactor. Flow reactors, including this one, are designed so that the timescale of radial mixing is short relative to the advective timescale at which fluid is moved through the reactor by the flow; hence, a one-dimensional model is justified. Cantera [2] is used to integrate the species evolution equations in time based on the Co-Optima chemical mechanism and form the model.

The minimization function from the Scipy optimization package (*scipy.optimize.minimize*) with the “Nelder-Mead” method is used to solve for the composition of a surrogate when Θ is restricted to only a few species in the mechanism. That is, it finds the Θ that minimizes the residual:

$$R = \text{norm} \left[\vec{S}_{\text{target}} - \mathcal{M}(\vec{\Theta}; t_r, T, \mathbf{C}) \right] \quad (3)$$

based on the L_2 norm. This project also explored an optimization using a reduced-order model for \mathcal{M} built on the fly to reduce the number of model evaluations; this approach reduced the computational effort but did not otherwise affect the results.

The implementation was verified by using a synthetic dataset created by simulating a flow reactor with 30 mol% n-heptane and 70 mol% iso-octane fuel mixed with 0.5 mol% oxygen and 99.5 mol% nitrogen at equivalence ratio of 1. The reactor pressure is 1 atm with a constant temperature of 1,000 K. The “Co-Optima detailed chemical kinetic model” developed at Lawrence Livermore National Laboratory (S. Wagnon, Co-Optima mechanism, personal communication, 2017) was used; it has most of the necessary components of gasoline fuels and surrogate mixtures. The outputs from this model (in the form of species concentrations after a set time at constant temperature) are then used as targets to identify the initial fuel mixture. The model converges in 32 iterations with total error of the targets being 0.03%. This suggests that the model is correctly implemented and that the four targets listed above are a reasonable set of targets for constraining the surrogate composition.

In the next step, the ability of this technique to obtain useful surrogate mixtures for more complicated fuel mixtures was explored. FACE (Fuels for Advanced Combustion Engines) gasoline fuels [3] are petroleum refined fuels designed to enable detailed analysis of fuel effects in combustion engines. These fuels consist of hundreds of hydrocarbon components, which are usually categorized to n-alkanes, iso-alkanes, aromatics, alkenes, and cycloalkanes. Here, we generate a synthetic dataset using the FACE A fuel. The components and mole fractions for a FACE A multi-component surrogate are given by Sarathy et al. [4], as shown in the first column of Table II.20.1. The RON of this fuel is 84, and the suggested primary reference fuel (PRF) surrogate mixture by the same paper is PRF-84 with 16 mol% n-heptane and 84 mol% iso-octane.

To use this approach to find the best surrogate mixture for the FACE A fuel, two possible sets of components for the surrogate are considered:

1. A PRF, which is a mixture of n-heptane and iso-octane.
2. A toluene primary reference fuel (TPRF), which is a mixture of n-heptane, iso-octane, and toluene.

Table II.20.1. Reduced Component Surrogates for FACE A Fuel Corresponding to Multi-Component Surrogate from Sarathy et al. [4]

mol %	FACE A Surrogate	PRF Surrogate	TPRF Surrogate
n-butane	7	0	0
iso-pentane	15	0	0
2-methylhexane	11	0	0
iso-octane	60	84	76.5
n-heptane	7	16	16.5
toluene	0	0	7

The results of running the optimization using the synthetic data as targets and restricting the resulting surrogate to either [n-heptane, iso-octane] or [n-heptane, iso-octane, toluene] are shown in the right two columns of Table II.20.1. Reassuringly, the PRF matches that recommended by Sarathy et al. [4] with, by definition, RON = 84, consistent with the measured RON of this fuel. For the estimated TPRF, in the right-most column of Table II.20.1, the corresponding RON is 85, which is very close to the original fuel RON of 84.

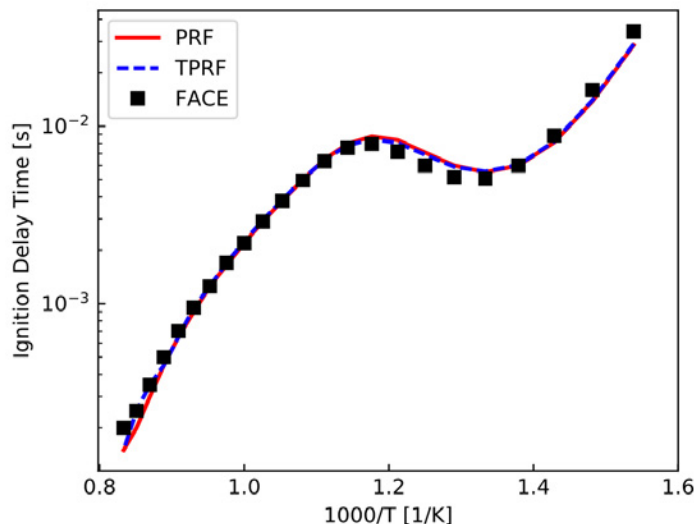


Figure II.20.1. Ignition delay time calculation using FACE A multi-component surrogate, PRF surrogate, and TPRF surrogate

Finally, recalling the objective to find a surrogate that permits evaluation of the ignition delay time shown in Equation 1, Co-Optima mechanism is used to evaluate the ignition delay times for the three surrogates representing the FACE A fuel. Figure II.20.1 shows the comparison for a temperature sweep at 20 atm. The ignition delay times of both the PRF and TPRF surrogate mixtures closely match the original FACE A multi-component surrogate. This provides some confidence that the observables from the flow reactor are sufficient to constrain a simple surrogate that exhibits similar ignition characteristics.

Conclusions

The conclusions of this work are twofold:

- Based on synthetic experiments, flow reactor measurements for a multi-component mixture appear to contain sufficient information to determine a surrogate fuel that results in closely agreeing autoignition characteristics.
- Logical next steps are to use targets obtained from “real” flow reactor measurements and compare to ignition delay prediction experimental data.

References

1. Kasseris, E., and J.B. Heywood. 2012. “Charge Cooling Effects on Knock Limits in SI DI Engines Using Gasoline/Ethanol Blends: Part 2-Effective Octane Numbers.” *SAE International Journal of Fuels and Lubricants* 5 (2012-01-1284): 844–854.
2. Goodwin, D., H.K. Moffat, and R.L. Speth. Cantera, 2017. doi 10.5281/zenodo.170284.
3. Cannella, W., M. Foster, G. Gunter, and W. Leppard. 2014. “FACE Gasolines and Blends with Ethanol: Detailed Characterization of Physical and Chemical Properties.” CRC Report No AVFL-24.
4. Sarathy, S.M., G. Kukkadapu, M. Mehl, W. Wang, T. Javed, S. Park, M.A. Oehlschlaeger, A. Farooq, W.J. Pitz, and C.-J. Sung. 2015. “Ignition of Alkane-Rich FACE Gasoline Fuels and Their Surrogate Mixtures.” *Proceedings of the Combustion Institute* 35 (1): 249–257.

II.21 Scenario Co-Optimizer (Lawrence Berkeley National Laboratory)

Juliane Mueller, Principal Investigator

Lawrence Berkeley National Laboratory
1 Cyclotron Rd., MS 50A-3111
Berkeley, CA 94720
E-mail: JulianeMueller@lbl.gov

Ray Grout, Principal Investigator

National Renewable Energy Laboratory
15013 Denver West Parkway
Golden, CO 80401
E-mail: Ray.Grout@nrel.gov

Kevin Stork, DOE Technology Development Manager

U.S. Department of Energy
E-mail: Kevin.Stork@ee.doe.gov

Start Date: October 1, 2017	End Date: September 30, 2018	
Project Funding (FY18): \$75,000	DOE share: \$75,000	Non-DOE share: \$0

Project Introduction

The scenario co-optimizer is an optimization toolset developed specifically for the Co-Optima program. In its current version, it allows for the simultaneous optimization of fuel costs (minimization) and engine efficiency (maximization), also known as a multi-objective optimization. Within the Co-Optima program, the efficiency for a fuel with a given set of properties is expressed through an evolving merit function, which expresses the increase in efficiency that might be possible relative to fuels currently in the marketplace. Similarly, other quantitative measures are expressed as additional merit functions; synthetic cost data was used as a proxy for these additional quantities. The co-optimizer identifies the tradeoffs between the merit functions (fuel cost and efficiency): as fuel costs increase, efficiency increases, and vice versa. Knowing these tradeoffs enables the decision maker to determine which experiments should be conducted in the laboratory next in order to increase confidence in which fuels have the best efficiency at a given cost. These experiments might otherwise be based on experience and intuition. Thus, the co-optimizer enables improved decision support through prediction capabilities.

The co-optimizer contains several user options, such as different types of merit functions (e.g., analytic merit functions, Gaussian Process [GP] models that are informed by laboratory data, more than two merit functions to optimize simultaneously), constraint handling (e.g., limiting the number of fuels in a fuel blend to specific types), sensitivity analyses (e.g., uncertainty in fuel costs), and black-box expensive optimization (when computationally intensive simulations have to be run as part of the optimization problem). A graphical user interface and user manual exist for the basic bi-objective optimizations and will be further developed for more advanced optimization tasks.

Objectives

The objective for the co-optimizer development for Fiscal Year (FY) 2018 was to extend its capabilities from simple multi-objective optimization of analytically given merit functions to data-informed surrogate optimization that exploits statistical models and other approximation models.

Overall Objectives

- Extend the capabilities of the co-optimizer to solve more difficult (and more realistic) optimization problems

- Assess the co-optimizer capabilities on synthetic problems (proof of concept)
- Demonstrate the co-optimizer capabilities on real-life (laboratory) data

Fiscal Year 2018 Objectives

- Implement capability for simulation optimization
- Model and implement capability for sensitivity analysis
- Develop simple user interface to improve tool usability
- Proof of concept with synthetic cost data and spark ignition merit function (SI-MF) [1]

Approach

The co-optimizer exploits ideas from multi-objective genetic algorithms and surrogate models such as radial basis functions and GP models. Genetic algorithms are based on the idea of survival of the fittest, in which a population of solutions is evolved over several generations by random perturbations and other genetic operations. The fitness of the solutions is based on their merit values. Solutions with better merit values are more likely to evolve. For problems in which analytic merit functions are to be optimized, an off-the-shelf algorithm (python deap library [3]) can be used with only minor modifications for constraint handling. For problems that involve laboratory data, we model the merit functions with surrogate models and then use the genetic algorithm on those. Additional constraint handling is enabled through tailor-made genetic operations. Sensitivity analysis is enabled by user-chosen distributions on uncertain merit function inputs, and uncertainty is propagated through several random realizations from these distributions and optimization. To evaluate the merit function for a given fuel composition, the co-optimizer includes blending models implemented in previous years based on experimental data assembled elsewhere in the Co-Optima program.

Results

In FY 2018, we extended and improved the capabilities of the co-optimizer to solving new classes of optimization problems for the Co-Optima context, including:

- Deterministic optimization and optimization under uncertainty,
- Bi-objective and bi-level optimization, and
- Constrained and unconstrained optimization.

The specific capabilities of the co-optimizer comprise the following.

- Deterministic bi-objective optimization using the SI-MF [1] – optimizes fuels only: maximize SI-MF and minimize fuel costs
- Bi-objective optimization with uncertainty – optimizes fuels only: uncertainty in fuel component costs and in coefficients of the SI-MF; allows for different assumptions for distributions of uncertain inputs
- Bi-objective data-driven optimization – optimizes fuels and engine operating conditions: GP model to approximate experimental data; maximize expected efficiency (net mean effective pressure [NMEP]) and minimize prediction uncertainty
- Simple bi-level bi-objective optimization – optimizes fuels and engine operating conditions: maximize SI-MF and maximize NMEP: given a fuel (higher level), find the best operating conditions (lower level)

The following capability is under construction.

- Bi- and single-objective mixed-data-driven optimization – optimizes fuels and engine operating conditions: uses radial basis functions to inform multi-objective sampling; maximize NMEP and SI-MF

The mentioned capabilities satisfy and exceed the objectives for the FY 2018 co-optimizer development.

All of these capabilities enable the user to compute tradeoff solutions between the objective functions. These tradeoff solutions enable the user to make informed decisions about future experiments to conduct. In particular, with the data-informed methods that rely on approximation models that are built based on laboratory data, having reliable predictions about fuel and engine performance allows targeted experiments and thus savings in experimentation time and resources.

The following is a list of solutions (tradeoff curves) obtained with the co-optimizer for selected problems.

- Bi-objective optimization with uncertainty in one fuel cost component, all other costs are assumed deterministic (for simplicity of illustrating the results)
- Draw 100 random realizations from the distribution of synthetic fuel costs
- Solve 100 bi-objective optimization problems (minimize fuel cost and maximize SI-MF)
- Figure II.21.1 shows the 100 tradeoff curves (all data) obtained from the 100 optimizations together with the mean and median tradeoff curves

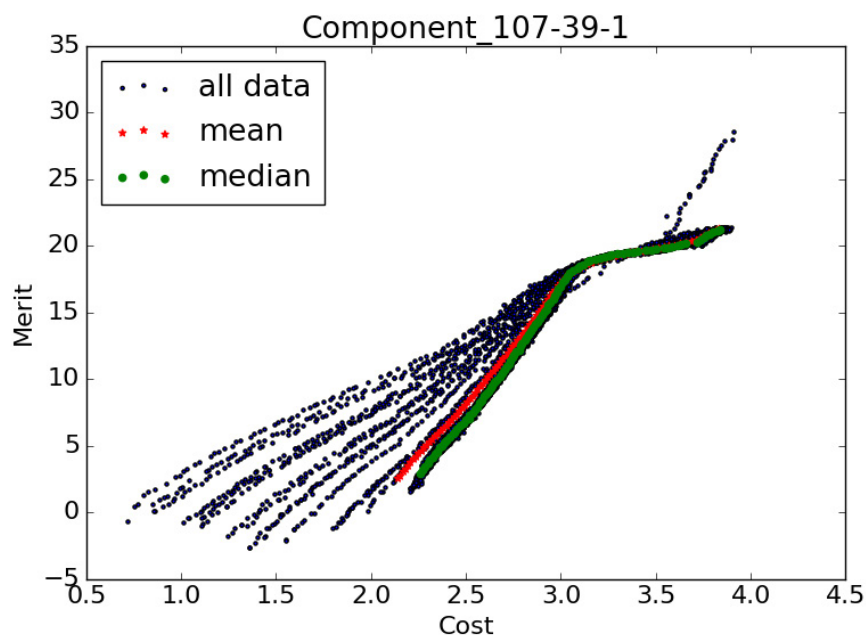


Figure II.21.1. Tradeoff curves for bi-objective optimization with uncertainty in fuel component cost (synthetic cost data used to only show capabilities)

- Bi-objective data-driven optimization
 - The data from Ratcliff et al. [2] was used that measures NMEP for different fuel properties and engine operation conditions.
 - A GP model was built based on this data.
 - The GP model predicts NMEP values at untried fuel property–engine operation conditions combinations and also gives an uncertainty estimate with the predictions.
 - The project simultaneously maximized the predicted NMEP and minimized the prediction uncertainty.
 - Figure II.21.2 shows the resulting tradeoff curves. Low predicted NMEP values have low predicted uncertainty; high predicted NMEP values have high predicted uncertainty.
 - The users select from the shown solutions (dots) the one they subjectively prefer and conduct the corresponding experiment.

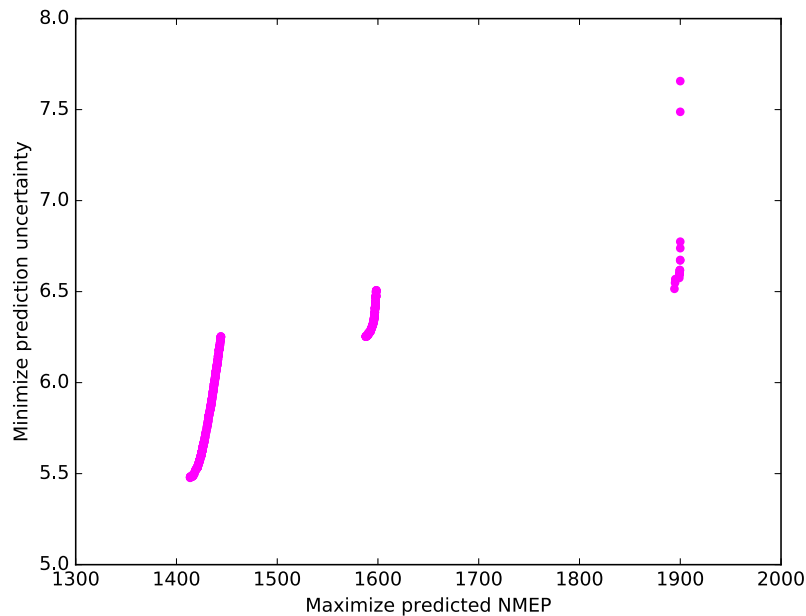


Figure II.21.2. Tradeoff curves for data-informed GP bi-objective optimization

Conclusions

The capabilities of the co-optimizer have been expanded and improved. The project team showed with synthetic as well as real experimental data that it is able to obtain tradeoff curves that inform the users and allow them to make decisions about future experiments. Next steps include using real fuel cost data to redo the analysis (maximize SI-MF, minimize fuel costs), implementing further physical constraints (such as knock limits), improving the bi-level optimization to co-optimize fuels and engine efficiency, and improving collaboration with experimentalists to obtain more data and request new experiments.

Key Publications

1. Co-optimizer release: <https://github.com/rgrout/cooptimizer>

References

1. Miles, Paul. 2018. "Efficiency Merit Function for Spark Ignition Engines: Revisions and Improvements Based on FY16–17 Research." Technical Report. U.S. Department of Energy, Washington, DC. DOE/GO-102018-5041.
2. Ratcliff, Matthew A., Jonathan Burton, Petr Sindler, Earl Christensen, Lisa Fouts, and Robert L. McCormick. 2018. "Effects of Heat of Vaporization and Octane Sensitivity on Knock-Limited Spark Ignition Engine Performance." WCX18: SAE World Congress Experience, (April), Detroit, MI.
3. GitHub, Inc., <https://github.com/DEAP/deap>

Acknowledgements

This is joint work with Ray Grout and Ryan King from National Renewable Energy Laboratory. For our data-informed optimizations, we want to acknowledge Robert McCormick and Matthew Ratcliff (National Renewable Energy Laboratory) for sharing their experimental data with us.

II.22 Fuel Property Blending Model (Pacific Northwest National Laboratory)

J. Timothy Bays, Principal Investigator

Pacific Northwest National Laboratory (PNNL)
902 Battelle Blvd., MS K2-14
Richland, WA 99352
E-mail: tim.bays@pnnl.gov

Kevin Stork, DOE Technology Development Manager

U.S. Department of Energy
E-mail: Kevin.Stork@ee.doe.gov

Start Date: October 1, 2017	End Date: September 30, 2018	
Project Funding (FY18): \$250,000	DOE share: \$250,000	Non-DOE share: \$0

Project Introduction

This project is focused on developing a fundamental attribution of the effects of molecular-level solution structures, such as clustering, hydrogen-bonding networks, and crystallization, on fuel properties in a finished fuel. Understanding and leveraging the effects of oxygenate clusters as a function of concentration and molecular aggregates that form during pressure-induced fuel solidification may yield new approaches to favorably influencing fuel properties in automotive applications. In doing so, this project seeks to facilitate the successful co-optimization of fuels and advanced combustion engines by providing an understanding of changes in properties resulting from the incorporation of potential renewable fuel feedstocks and unconventional hydrocarbon fuels into the domestic fuel supply. This would enhance domestic energy security and economic competitiveness and improve environmental quality.

Objectives

Overall Objectives

- Advance an understanding of the role of molecular-level solution structures, such as clustering, hydrogen-bonding networks, and crystallization, within a fuel on fuel properties (important to current and future engine-combustion strategies)
- Develop predictive models based upon analytical approaches correlating molecular-level solution structures within fuel components to fuel properties and performance

Fiscal Year 2018 Objectives

- Relate nuclear magnetic resonance (NMR) spectroscopic measurements and molecular dynamics simulations of alcohol clusters in model fuel systems to Reid vapor pressure
- Measure the changes in phase behavior resulting from the introduction of complex fuel mixtures on diesel surrogate fuels, created under the auspices of Coordinating Research Council (CRC) Project AVFL-18a, at high pressures simulating those of vehicle fuel injection systems, and attempt to mitigate fuel solidification
- Complete phase change behavior measurements for four CRC diesel surrogate fuels and three Co-Optima diesel surrogate fuels as part of CRC Project AVFL-18a

Approach

The first task of this project uses NMR spectroscopy and molecular dynamics simulations to identify and quantify temperature-dependent, molecular-level solution structures within gasoline and model fuels. NMR diffusion measurements are used to identify oxygenate clustering and hydrogen-bonding network formation. Ethanol clustering in gasoline has previously been observed using this technique, but the reported results provided conflicting information without explanation and provided no links to the impacts that molecular-level

clustering might have on fuel properties [1,2]. In this project, Reid vapor pressure (RVP) was selected as an important fuel property likely to be influenced by molecular aggregation or clustering. To probe cluster formation at shorter time scales than available using NMR, molecular dynamics simulations of parallel systems were undertaken. These simulations provide a great deal of information, including computation of diffusion coefficients, hydrogen-bonding networks, cluster size distributions and lifetimes. Both experiments provide synergistic data and allow researchers to observe molecular clusters and hydrogen-bonding networks in gasoline surrogates consisting of oxygenates in model fuels like *n*-heptane or *iso*-octane, in higher-complexity surrogate fuels, and in the case of NMR, in authentic gasoline samples.

The second task of this project assesses the propensity of fuels to change from a liquid to a solid under pressures representative of fuel injection systems. This was particularly important when trying to avoid unexpected fuel solidification in diesel surrogate fuels, where a high *n*-alkane concentration increases susceptibility to wax crystal formation. Four diesel surrogate fuels created under the auspices of CRC Project AVFL-18a were used to probe these changes [3,4], as were two complex diesel fuels provided by CRC [3,5]. A high-pressure apparatus, custom-built at PNNL, was used to monitor the solid-liquid phase equilibria of each sample, or sample-additive combination. Because the liquid-solid equilibria for the diesel surrogate fuels were sometimes well above room temperature at pressures representative of modern diesel fuel injection systems, efforts were made to forestall solidification to avoid the need to heat fuel systems in order to test the diesel surrogate fuels. These focused on adding diesel cold flow improvers, known to reduce the size of wax crystallites [6], to the five-component V0b surrogate, but the efforts were unsuccessful [7]. During Fiscal Year 2018, additions of complex diesel fuels having different compositions to the V0b surrogate were undertaken with the goal of disrupting wax crystal formation and lowering the diesel surrogate liquid-solid equilibrium temperatures. Studies assessing the temperature-pressure effects on liquid-solid equilibria remain to be undertaken using single-chemical fuel blendstocks, developed under Co-Optima, having concentrations up to 20% in a complex base fuel, once issues regarding system cross-contamination are addressed.

Results

- Task 1: Oxygenate cluster and network formation
 - o Developed a predictive method for determining cluster size in fuel blends to understand how molecular-level solution structures impact fuel properties
 - o Developed models for a molecular-level picture of hydrogen-bonding of alcohols in fuel blends leading to molecular clustering and molecular network formation, which can impact fuel properties
- Task 2: High-pressure liquid-solid equilibria
 - o Assessed changes in the liquid-solid equilibrium values of a five-component diesel surrogate fuel upon adding concentrations of 5–75 vol% of a complex diesel fuel

NMR diffusion measurements, specifically diffusion-ordered spectroscopy, yielded diffusion coefficients for alcohols in single-component gasoline surrogates. Alcohol diffusion coefficients were then correlated with alcohol cluster weights and the average number of molecules per cluster in gasoline surrogates for the following alcohol–surrogate combinations [8,9]: ethanol in *iso*-octane or *n*-heptane and *iso*-butanol in *n*-heptane. As shown in Figure II.22.1, average alcohol cluster size was found to increase with increasing alcohol concentration, to a maximum of approximately six alcohol molecules per cluster. Maximum cluster size was found to occur at 20% ethanol by volume in both *iso*-octane and *n*-heptane, and at 70% *iso*-butanol by volume in *n*-heptane. Clustering was not observed to occur among the gasoline surrogate molecules, *n*-heptane and *iso*-octane. RVP values (blue stars in Figure II.22.1b) were found to correspond to the size and number of ethanol clusters in the ethanol in the *n*-heptane system. At volumes greater than 20% ethanol, where maximum cluster size occurred, the formation of hydrogen-bonding networks was favored, causing cluster size and RVP to decrease.

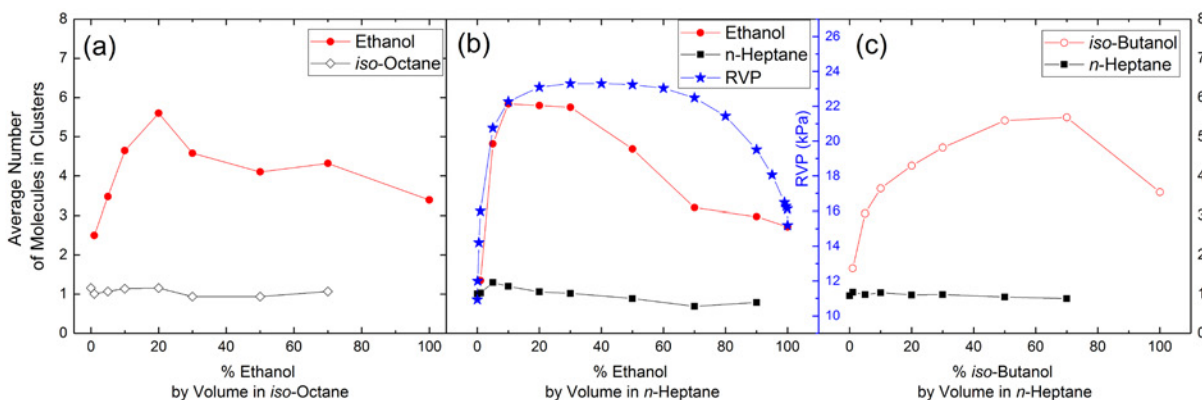
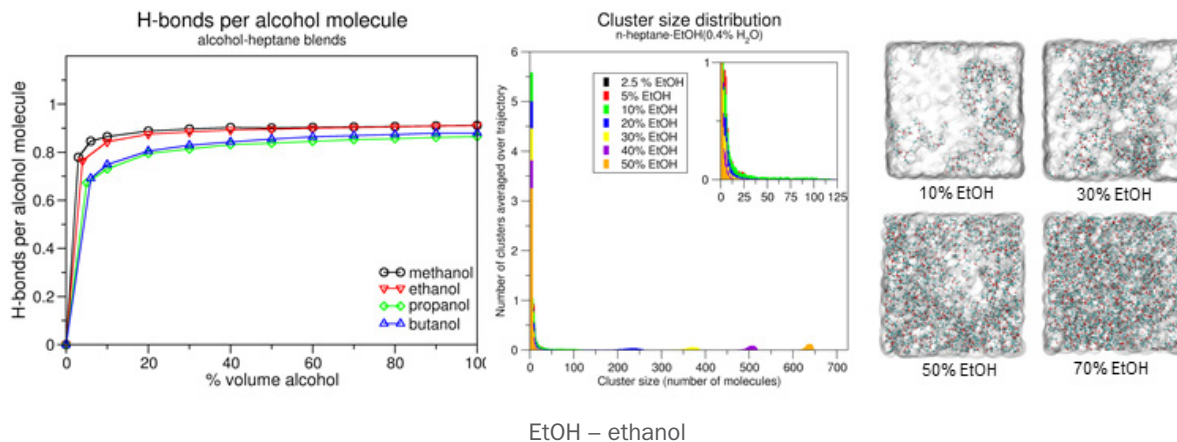


Figure II.22.1. Molecular-level solution structure and Reid vapor pressure. The average number of molecules in clusters was determined by using NMR diffusion measurements in (a) ethanol in *iso*-octane, (b) ethanol in *n*-heptane, and (c) *iso*-butanol in *n*-heptane. Reid vapor pressure for the ethanol–*n*-heptane solution compared with cluster size is shown in (b). (Kee Sung Han)

Molecular dynamics simulations of gasoline surrogate mixtures (methanol in *n*-heptane, ethanol in *n*-heptane, *n*-propanol in *n*-heptane, and *n*-butanol in *n*-heptane) were performed to visualize cluster formation of alcohols in these mixtures and calculate the average number of hydrogen bonds per alcohol molecule, as well as an alcohol molecular cluster size distribution. Figure II.22.2 shows that the number of hydrogen bonds per alcohol molecule tends to increase rapidly up to 20% alcohol by volume and then shows gradual, tapered increases above 20% alcohol. The hydrogen bond number per alcohol molecule tends to decrease with length of the alcohol carbon chain, although that of *n*-propanol is consistently slightly less than that for *n*-butanol. A continuous, broad distribution of ethanol cluster sizes is observed up to 10% ethanol in *n*-heptane. After 10% ethanol in *n*-heptane, the small-cluster distribution attenuates and a large-cluster (much larger, network clusters) distribution appears.



EtOH – ethanol

Figure II.22.2. Hydrogen-bond clustering of alcohols in *n*-heptane determined by molecular dynamics simulations. Left: Number of hydrogen bonds per alcohol with increasing alcohol content. Middle: Ethanol molecule clustering distributions. Right: Molecular depictions of ethanol–*n*-heptane mixtures from molecular dynamics simulations. (Amity Andersen)

In the second task, assessing changes in phase behavior, high-pressure, liquid-solid equilibria were measured for mixtures of V0b and each of two diesel fuels with the goal of dramatically reducing the final melting point of V0b by increasing the complexity of the resulting mixtures. The certification diesel fuel (CFA) and the gas-to-liquid diesel fuel (GTL1) are compositionally very different from each other, as well as from the V0b surrogate (Table II.22.1), and were selected to accentuate any differences in interaction with surrogate V0b [3–5]. Notably, CFA is high in cycloalkanes and low in saturates, whereas GTL1 is composed almost

exclusively of saturates, of which about 46 wt% are *n*-alkanes. The final melting points for both diesel fuels were found to be about 30°C lower than that of V0b at all pressures, with CFA 4°C lower than GTL1 at atmospheric pressure and the difference gradually increasing to about 10°C lower at 275 MPa. Figure II.22.3 shows the changes in the liquid-solid equilibria of several binary fuel mixtures of V0b+GTL1 and V0b+CFA. Each color-coded line, solid (V0b+GTL1) or dashed (V0b+CFA), represents the final melting point at a fixed pressure for that fuel mixture. For equivalent V0b concentrations, several observations can be made from Figure II.22.3:

- In mixtures with V0b, CFA is more effective at lowering the final melting point than GTL1.
- Concentrations greater than 25% GTL1 are required to significantly influence the V0b+GTL1 final melting point, while for mixtures with CFA, changes can be observed at lower concentrations.
- The magnitude of change in the final melting points at each V0b concentration appears to increase with increasing pressure.

Table II.22.1. Composition of Diesel Fuels/Diesel Fuel Surrogate*

Description		CFA [3] (wt %)	GTL1 [5] (wt %)	V0b [4] (wt %)
aromatics	>1-ring aromatics	9.7	0.08	12.3
	1-ring aromatics	21.1	0.47	22.9
cycloalkanes	cycloalkanes	43.5	2.01	0
linear saturates	<i>n</i> -alkanes	13.6	46.4	32.1
	<i>iso</i> -alkanes	11.8	51.5	32.8

* Because of small variations in analyses and rounding, compositions do not add to exactly 100%.

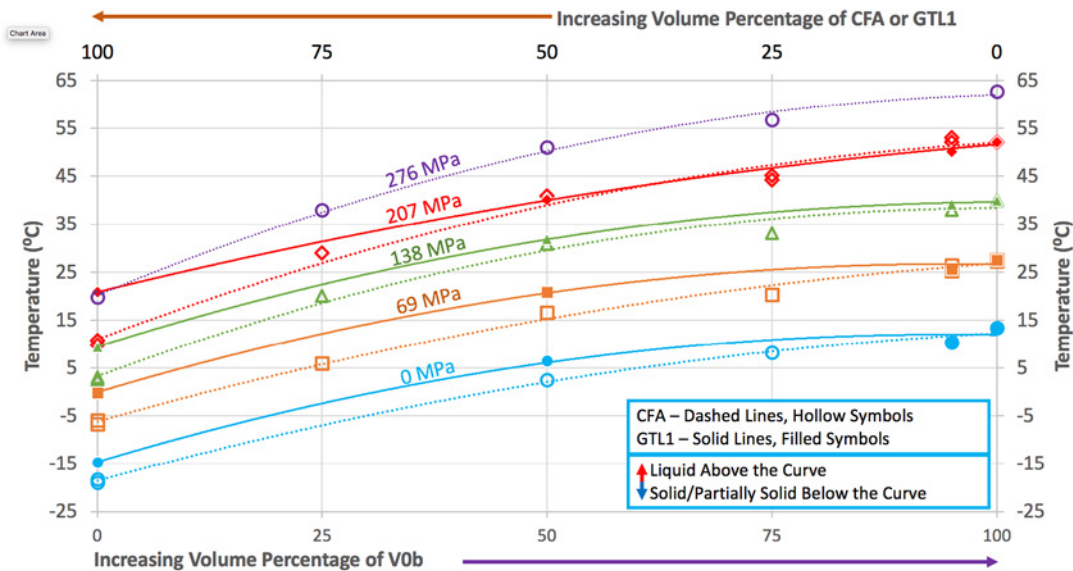


Figure II.22.3. Comparison of the solid-liquid equilibria for mixtures of diesel surrogate fuel V0b with complex diesel fuels, CFA or GTL1. Volume percentages of diesel surrogate fuel V0b are shown along the lower x-axis, increasing from left to right, and volume percentages of diesel fuels CFA or GTL1, as appropriate, are shown along the upper x-axis, increasing from right to left. Data points and trendlines for mixtures of V0b+CFA are shown as hollow symbols and dashed lines, while mixtures of V0b+GTL1 are shown as filled symbols and solid lines. Trendlines are second-order polynomials that represent isobars, distinguished by color, for each set of mixtures. Each material can be expected to remain a liquid at temperatures above its respective trendline at a given pressure. Below its respective trendline, a pure material will solidify, and a multicomponent material will have at least one component freeze out. (Tim Bays and Margaret Jones)

These observations suggest that the composition of the complex fuel affects the degree to which the final melting point of the diesel fuel surrogate is lowered for each mixture. Additional data to fill in compositional gaps will improve the fidelity of these observations.

Conclusions

- Synergistic information from molecular diffusion studies and molecular dynamics simulations show cluster development and hydrogen-bond network formation, which reflect changes in Reid vapor pressure with increasing ethanol concentration.
- Hydrogen-bonding and cluster analyses provided by molecular dynamics simulations provide key insights into the effects of increased alcohol concentrations in gasoline surrogates.
- To date, no acceptable solutions have been identified that lower the high final melting points of some diesel surrogate fuels enough to allow unheated high-pressure fuel lines while maintaining the compositional rigor of the surrogates.

Key Publications

1. Bays, John T., et al. 2017. "Fuel Property Database." In *Advanced Combustion Systems and Fuels, 2017 Annual Progress Report*, edited by Gurpreet Singh, Kenneth C. Howden, Roland M. Gravel, Kevin Stork, and Michael Weismiller. U.S. Department of Energy, Energy Efficiency & Renewable Energy, Vehicle Technologies Office, https://www.energy.gov/sites/prod/files/2018/05/f51/AdvCombSysAndFuels_FY2017_APR_Final.pdf.

References

1. Turanov, A., and A.K. Khitrin. 2014. "Proton NMR Characterization of Gasoline-Ethanol Blends." *Fuel* 137 (December): 335–38.
2. Turanov, A., and A.K. Khitrin. 2016. "Ethanol Clusters in Gasoline-Ethanol Blends." *Industrial & Engineering Chemistry Research* 55, no. 37 (September): 9952–55.
3. Mueller, C.J., W.J. Cannella, T.J. Bruno, B. Bunting, H.D. Dettman, J.A. Franz, M.L. Huber, et al. 2012. "Methodology for Formulating Diesel Surrogate Fuels with Accurate Compositional, Ignition-Quality, and Volatility Characteristics." *Energy & Fuels* 26, no. 6 (June 3): 3284–303.
4. Mueller, Charles, William Cannella, J. Timothy Bays, Thomas Bruno, Kathy DeFabio, Heather Dettman, Rafal Gieleciak, et al. 2016. "Diesel Surrogate Fuels for Engine Testing and Chemical-Kinetic Modeling: Compositions and Properties." *Energy & Fuels* 30, no. 2: 1445–61.
5. Cannella, William, Craig Fairbridge, Rafal Gieleciak, Patricia Arboleda, Timothy Bays, Heather Dettman, Michael Foster, et al. "Advanced Alternative and Renewable Diesel Fuels: Detailed Characterization of Physical and Chemical Properties, CRC Report No. AVFL-19-2." Coordinating Research Council, <http://crcao.com/publications/advancedVehiclesFuelsLubricants/index.html>.
6. Chandler, John, David Daniels, Tony Frank, Roger Gault, Garry Gunter, Dennis Hess, Shailesh Lopes, et al. 2016. "Diesel Fuel Low Temperature Operability Guide, CRC Report No. 671." Coordinating Research Council, <http://crcao.com/publications/advancedVehiclesFuelsLubricants/index.html>.
7. Singh, Gurpreet, Kenneth C. Howden, Roland M. Gravel, Kevin Stork, and Michael Weismiller. 2017. "Advanced Combustion Systems and Fuels, 2017 Annual Progress Report." U.S. Department of Energy, Energy Efficiency & Renewable Energy, Vehicle Technologies Office, https://www.energy.gov/sites/prod/files/2018/05/f51/AdvCombSysAndFuels_FY2017_APR_Final.pdf.
8. Bachmann, S., R. Neufeld, M. Dzemski, and D. Stalke. 2016. "New External Calibration Curves (ECCS) for the Estimation of Molecular Weights in Various Common NMR Solvents." *Chemistry-a European Journal* 22, no. 25 (June): 8462–65.

9. Neufeld, R., and D. Stalke. 2015. “Accurate Molecular Weight Determination of Small Molecules Via DOSY-NMR by Using External Calibration Curves with Normalized Diffusion Coefficients.” *Chemical Science* 6, no. 6: 3354–64.

Acknowledgements

The work necessary to reach the goals of this project was conducted primarily by this project’s co-contributors, Kee Sung Han, Amity Andersen, Katarzyna Grubel, Molly J. O’Hagan, Gregory W. Coffey, Margaret C. Jones, and John C. Linehan. Additionally, the authors are grateful to the Coordinating Research Council, with special thanks to members of the Fuel for Advanced Combustion Engines (FACE) Working Group and project AVFL-18a, for their guidance and support. PNNL clearance number: PNNL-28221.

II.23 Fuel Impacts on Emissions Control Performance and Durability (Oak Ridge National Laboratory)

Josh A. Pihl, Principal Investigator

Oak Ridge National Laboratory
2360 Cherahala Boulevard
Knoxville, TN 37932
E-mail: toopstj@ornl.gov

Kevin Stork, DOE Technology Development Manager

U.S. Department of Energy
E-mail: Kevin.Stork@ee.doe.gov

Start Date: October 1, 2017	End Date: September 30, 2018	
Project Funding (FY18): \$240,000	DOE share: \$240,000	Non-DOE share: \$0

Project Introduction

The overall objective of the Co-Optimization of Fuels and Engines Initiative (Co-Optima) is to cooperatively develop emerging high-performance fuels and advanced engines to bring these technologies to the market sooner to realize a reduction in petroleum consumption. This project aims to investigate the compatibility of Co-Optima fuel candidates with emissions control systems and to identify opportunities for alternative emissions control strategies based on novel fuel chemistry. Specifically, this project is investigating the following questions:

1. Is the catalytic reactivity of Co-Optima candidate fuel components sufficient to allow continued use of current emissions control technologies?
2. Do the Co-Optima candidate fuel components create opportunities for reducing tailpipe emissions and/or aftertreatment system costs based on their reactivities over emissions control catalysts?

Objectives

Overall Objectives

- Develop mathematical terms that capture the impacts of changes in fuel composition on emissions control system performance and durability based on measurable fuel properties for inclusion in the Co-Optima merit functions
- Measure the fuel properties required to evaluate the emissions control merit function terms for Co-Optima blendstock candidates
- Identify and evaluate potential alternative emissions control strategies that exploit the unique chemistry of Co-Optima blendstock candidates

Fiscal Year (FY) 2018 Objectives

- Measure the catalyst light-off of Co-Optima blendstock candidates in the context of fuel blends similar to what would be used in vehicles
- Publish results from prior blendstock light-off measurements

Approach

This research brings together targeted flow-reactor studies and engine-based experiments to evaluate the compatibility of Co-Optima fuel candidates with emissions control systems and identify opportunities for alternative emissions control strategies that make use of novel fuel chemistry. The synthetic exhaust gas flow reactor systems are designed to offer maximum flexibility to mimic exhaust conditions expected in application

and further allow the exploration of the boundary conditions associated with the candidate emissions control systems. Great care has been taken to ensure the results from the flow reactors will correlate well with engine-based studies. The engine-based experiments rely on conventional commercial engines as well as simple genset-based engines for long-term aging efforts. Additionally, a comprehensive suite of materials characterization tools is employed as necessary to understand the impact of fuels and their trace constituents on the material properties of the emissions control system.

Results

FY 2018 Accomplishments

- Successfully measured catalytic light-off temperatures of 13 fuel blends based on a surrogate blendstock for oxygenate blending (BOB) mixed with 10–30% (by volume) of four different Co-Optima fuel component candidates:
 - o Ethanol
 - o Isobutanol
 - o An aromatic mixture (1/3 toluene, 1/3 m-xylene, 1/3 mesitylene)
 - o Di-isobutylene
- Demonstrated that, while the pure Co-Optima candidates have very different catalytic light-off temperatures, for blend levels of 10–30%, the catalytic reactivity is primarily controlled by the BOB, and the Co-Optima candidates do not have a significant impact on light-off for non-methane organic gases (NMOG), CO, and NO_x

In modern gasoline-fueled light-duty vehicles with stoichiometrically operated spark ignition engines, three-way catalysts (TWCs) are very efficient at reducing the emissions of deleterious pollutants such as NMOG, CO, and NO_x to enable compliance with stringent emissions regulations. Most of the NMOG, CO, and NO_x emissions occur during cold-start, when the TWC is below a critical temperature known as the catalyst light-off temperature. Typical strategies adopted to rapidly heat up the catalyst such as injecting additional fuel and delaying spark timing are associated with a fuel penalty, as the engine is not operating at its optimum efficiency during the cold-start period [1,2]. Furthermore, the efficacy of the TWC in controlling emissions of these harmful pollutants is sensitive to the fuel chemistry on the TWC and therefore to the composition of the fuel. Thus, for effective control of emissions of regulated pollutants from light-duty vehicles, the engine and aftertreatment systems must be calibrated to minimize the cold-start period.

Researchers at Oak Ridge National Laboratory have previously derived and reported an expression that estimates the impact of catalytic light-off temperature on vehicle efficiency, thus providing a means for quantification of fuel composition effects on cold-start emissions in terms of measurable fuel properties:

$$merit = 0.008^{\circ\text{C}^{-1}} (T_{C,90,conv} - T_{C,90,COB}) \quad (1)$$

where $T_{C,90,conv}$ and $T_{C,90,COB}$ are the temperatures at which 90% of the conventional fuel and the Co-Optima blend fuel are converted on the TWC, respectively. The constant term is estimated from the fractional increase in fuel consumption rate during cold-start and the catalyst heating rate based on Federal Test Procedure cycle data of several vehicles [3].

Evaluation of the emissions control merit function term requires measurements of the catalytic light-off temperatures for particular Co-Optima fuel blends. During FY 2017, this project measured the catalytic light-off temperature for dozens of individual Co-Optima fuel component candidates. This year, catalyst light-off measurements were conducted with fuel blends containing a surrogate BOB with the composition shown in Table II.23.1 mixed with 10–30% of four of the promising Co-Optima fuel candidates: ethanol, isobutanol, an aromatic mixture (containing 1/3 toluene, 1/3 m-xylene, and 1/3 mesitylene), and di-isobutylene. The catalyst used in these measurements was a dual-zone TWC from a model year 2009 Chevrolet Malibu partial zero-emission vehicle. The catalyst was hydrothermally aged as per industry guidelines delineated in the U.S.

DRIVE (Driving Research and Innovation for Vehicle efficiency and Energy sustainability) Low-Temperature Oxidation Catalyst Test Protocol for 50 h under neutral/rich/lean cycles at 800°C [4].

Table II.23.1. Surrogate BOB Composition

Component	Composition	Description
iso-octane	55%	branched alkane
toluene	25%	aromatic
n-heptane	15%	linear alkane
1-octene	5%	alkene

The fuel light-off measurements were carried out under synthetic engine exhaust conditions on an automated flow reactor system. A vapor delivery module was used to vaporize the liquid fuel. The gas compositions used in the experiments are shown in Table II.23.2. For all the fuel components and blends investigated in this study, λ (ratio of actual air/fuel ratio to stoichiometric air/fuel ratio) was kept constant at 0.999 by adjusting the O₂ concentration to account for the different C, H, and O contents of the fuels. Each light-off measurement with a specific fuel was repeated three times to make sure that the light-off behavior was reproducible.

Table II.23.2. Synthetic Engine Exhaust Gas Composition

Step	Temperature	Gas Composition (Balance N ₂)						
		[O ₂] %	[CO ₂] %	[H ₂ O] %	[CO] ppm	[H ₂] ppm	[NO] ppm	[HC] ppm C ₁
Pretreatment	600°C	-	13%	13%	-	-	-	-
Gaseous HC Light-down	500–100°C	0.72%	13%	13%	5,000	1670	1,000	3,000
Liquid HC Light-off	100–500°C	Varied to adjust λ	13%	13%	5,000	1670	1,000	3,000

HC – hydrocarbon; ppm – parts per million

The catalytic light-off of the surrogate BOB (55% iso-octane, 25% toluene, 15% n-heptane, and 5% 1-hexene) on the hydrothermally aged TWC was considered as the baseline for comparison with the light-off of the Co-Optima blendstock fuel blends. Co-Optima blendstock fuel blends that light off earlier than the BOB surrogate fuel would be considered as promising candidates in terms of reactivity on existing emissions control technology (TWC) and would be likely to meet the current emissions regulations with minimal modification to the existing exhaust aftertreatment architectures. The temperatures at which 50% (T₅₀) and 90% (T₉₀) of the fuel species are converted over the aged commercial TWC in a synthetic exhaust mixture are shown in Figure II.23.1.

Several important observations can be drawn from the data in Figure II.23.1.

- There are no significant trends in T₉₀ with blend composition. The T₉₀s for all the fuel blends essentially fall within experimental error of each other.
- As was previously reported in FY 2017, the reactivity of unblended Co-Optima candidates is sensitive to the chemical structure of the fuel species, as evidenced by the significant changes in T₅₀ for the 100% blend levels (pure components) in Figure II.23.1.
- For the fuel blends, the changes in T₅₀ relative to the BOB are consistent with the T₅₀ trends for the pure components:
 - o Increased levels of ethanol, which had a lower T₅₀ than the surrogate BOB, decreased the T₅₀ of the overall fuel blend to lower temperatures.
 - o Increased levels of isobutanol, the aromatic mixture, or di-isobutylene, all of which had a higher T₅₀ than the surrogate BOB, increased the T₅₀ of the overall fuel blend to higher temperatures.

- However, while these changes in T_{50} were significant relative to the magnitude of the measurement error, the difference in the catalytic light-off temperature between the least reactive Co-Optima candidate fuel blend and the most reactive fuel blend at blend levels of 10–30% is only $\sim 12^\circ\text{C}$, which is probably not large enough to have a significant impact on tailpipe emissions.

The effects of fuel blend light-off on the other regulated pollutants CO and NO_x were also investigated, and the results are presented in Figure II.23.2 and Figure II.23.3, respectively.

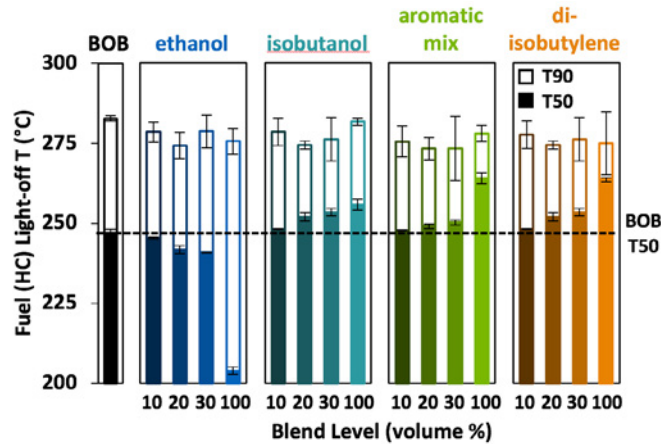


Figure II.23.1. T_{50} and T_{90} of surrogate BOB (baseline); 10%, 20%, and 30% ethanol blended into the BOB; unblended (100%) ethanol; 10%, 20%, and 30% isobutanol blended into the BOB; unblended (100%) isobutanol; 10%, 20%, and 30% of an aromatic mixture blended into the BOB; unblended (100%) aromatic mixture; 10%, 20%, and 30% di-isobutylene blended into the BOB; and unblended (100%) di-isobutylene. Error bars represent 95% confidence intervals calculated from three replicate runs.

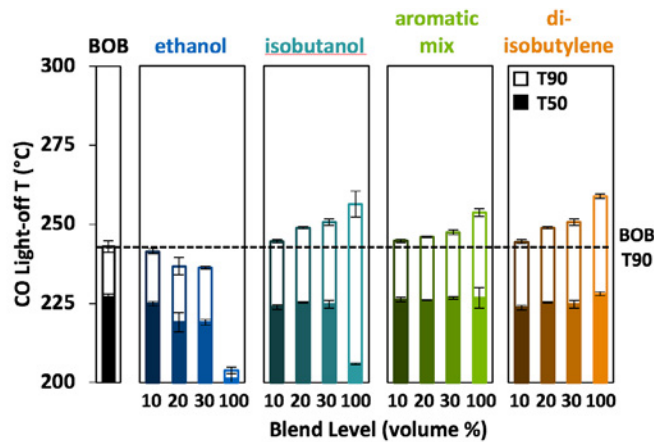


Figure II.23.2. Comparison of CO light-off temperatures (T_{50} and T_{90}) over the hydrothermally aged commercial TWC for all the fuel blends investigated. Error bars represent 95% confidence intervals calculated from three replicate runs.

The trends in CO light-off with blend level shown in Figure II.23.2 are very similar to those observed for light-off of the fuel species in Figure II.23.1, with one major difference: the primary effects are observed in the CO T_{90} , while blend level primarily impacted the T_{50} for the fuel species.

- For the fuel blends, the changes in CO T_{90} relative to the BOB are consistent with the CO T_{90} trends for the pure components:
 - o Increased levels of ethanol, which had a lower CO T_{90} than the surrogate BOB, decreased the CO T_{90} of the overall fuel blend to lower temperatures.

- o Increased levels of isobutanol, the aromatic mixture, or di-isobutylene, all of which had a higher CO T_{90} than the surrogate BOB, increased the CO T_{90} of the overall fuel blend to higher temperatures.
- However, while these changes in T_{90} were significant relative to the magnitude of the measurement error, the difference in the CO light-off temperature between the least reactive Co-Optima candidate fuel blend and the most reactive fuel blend at blend levels of 10–30% is only $\sim 15^\circ\text{C}$, which is probably not large enough to have a significant impact on tailpipe emissions.

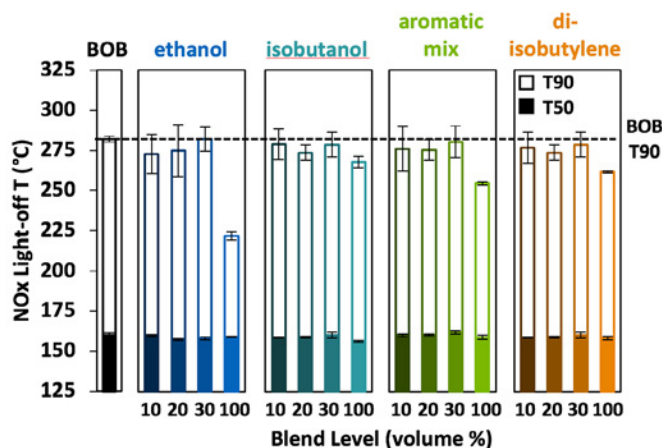


Figure II.23.3. Comparison of NO_x light-off temperatures (T_{50} and T_{90}) over the hydrothermally aged commercial TWC for all the fuel blends investigated. Error bars represent 95% confidence intervals calculated from three replicate runs.

The NO_x T_{50} s shown in Figure II.23.3 are consistent across all the fuels investigated in this study as, at low temperatures, NO_x is reduced by CO and H₂, so there is no effect of the fuel species in the synthetic exhaust mixture. Interestingly, while the NO_x T_{90} s for the unblended fuel candidates vary considerably, the T_{90} s for the fuel blends are all within experimental error of each other. Prior work reported in FY 2017 showed that NO_x T_{90} s follow the fuel T_{90} trends since the experiments are conducted at nearly stoichiometric conditions and high NO_x conversions can be achieved only when the fuel species have completely reacted. The lack of observed trends in NO_x T_{90} for the fuel blends in Figure II.23.3 is consistent with the lack of observed trends in fuel T_{90} for the fuel blends in Figure II.23.1.

In summary, for fuel blends based on a surrogate BOB mixed with 10–30% (by volume) of several different Co-Optima candidates, the cold-start NMOG, CO, and NO_x emissions are not significantly impacted by the Co-Optima candidate. It appears that the catalyst light-off behavior is primarily dictated by the composition of the surrogate BOB, which is the dominant fraction in the fuel blend. Ongoing work is focused on understanding how the composition of the BOB impacts catalytic reactivity of fuel blends.

Conclusions

- Light-off temperatures of fuel blends based on a surrogate BOB mixed with 10–30% (by volume) of four Co-Optima candidates (for a total of 13 fuel blends) have been measured on an aged commercial TWC.
 - o NO_x light-off behavior did not change significantly with fuel composition or blend level.
 - o Changes in fuel T_{50} and CO T_{90} relative to the BOB were consistent with the trends for the pure components:
 - o Increased levels of ethanol, which had lower fuel and CO light-off temperatures than the surrogate BOB, decreased the light-off temperatures of the overall fuel blend.
 - o Increased levels of isobutanol, the aromatic mixture, and di-isobutylene, all of which had higher fuel and CO light-off temperatures than the surrogate BOB, increased the light-off temperatures of the overall fuel blend.

- o The changes in light-off temperatures between the least reactive and most reactive Co-Optima candidate fuels blends were only 12–15°C.
- Fuel blends containing up to 30% of Co-Optima candidates will likely not have a significant impact on cold-start NMOG, CO, and NO_x emissions.
- Ongoing work is focused on measuring the light-off behavior of interacting vs. non-interacting components in fuel blends to gain insights into which species drive the overall light-off of fuel blends.

Key Publications

1. Pihl, Josh, John Thomas, Sreshtha Sinha Majumdar, Shean Huff, Brian West, and Todd Toops. 2018. “Development of a Cold Start Fuel Penalty Metric for Evaluating the Impact of Fuel Composition Changes on SI Engine Emissions Control.” SAE Technical Paper Series.

References

1. Anderson, J., E. Rask, H. Lohse-Busch, and S. Miers. 2014. “A Comparison of Cold-Start Behavior and Its Impact on Fuel Economy for Advanced Technology Vehicles.” *SAE Int. J. Fuels Lubr.* 7 (2). doi:10.4271/2014-01-1375.
2. Kessels, J.T.B.A., D.L. Foster, and W.A.J. Bleuanus. 2010. “Fuel Penalty Comparison for (Electrically) Heated Catalyst Technology.” *Oil & Gas Science and Technology – Rev. IFP*, Vol. 65, No. 1, pp. 47–54.
3. Pihl, Josh, John Thomas, Sreshtha Sinha Majumdar, Shean Huff, Brian West, and Todd Toops. 2018. “Development of a Cold Start Fuel Penalty Metric for Evaluating the Impact of Fuel Composition Changes on SI Engine Emissions Control.” SAE Technical Paper Series.
4. U.S. DRIVE ACEC Tech Team Low Temperature Aftertreatment Working Group. 2016. “Aftertreatment Protocols for Catalyst Characterization and Performance Evaluation: Low Temperature Oxidation Catalyst Test Protocol.” www.cleers.org/acec-lowt.

Acknowledgements

Thanks to Sreshtha Sinha Majumdar and Todd J. Toops of Oak Ridge National Laboratory for contributions to the project.

II.24 Fuel Impacts on ACI PM Formation (Oak Ridge National Laboratory)

Melanie Moses-DeBusk, Principal Investigator

Oak Ridge National Laboratory
1 Bethel Valley Rd.
Oak Ridge, TN 37831-6472
E-mail: mosesmj@ornl.gov

Kevin Stork, DOE Technology Development Manager

U.S. Department of Energy
E-mail: Kevin.Stork@ee.doe.gov

Start Date: November 20, 2017	End Date: September 30, 2018	
Project Funding (FY18): \$350,000	DOE share: \$350,000	Non-DOE share: \$0

Project Introduction

As the Co-Optima program enables higher-efficiency engines with new fuels and combustion approaches, it is critical to evaluate the impact on future vehicle emissions. This effort investigates the effects of fuel chemistry and combustion strategies on emissions and the functionality of the emissions control system to identify potential challenges as well as opportunities created by new fuel compositions.

The key focus of this project is particulate matter (PM) and gaseous hydrocarbon (HC) emissions from Co-Optima spark ignition/advanced compression ignition (ACI) multi-mode engines. The project activity focus is to assess the impacts of base fuel and Co-Optima bio-blendstocks on the generation and composition of gaseous and PM emissions from ACI-mode combustion and the potential strategies and barriers for the mitigation of the emissions with emissions controls. Although ACI engines can have high thermal efficiency, the associated higher work extraction results in lower exhaust temperatures, which are often below the required light-off temperature of the emissions control catalyst. The lower exhaust temperature, combined with the increased HC and CO emissions that result from lower combustion efficiency, further complicate aftertreatment emissions control. Previous research has shown ACI PM to be different than PM formed in conventional spark ignition or mixing-controlled compression ignition processes. This fiscal year, the research focused on improving methods for collecting and quantifying the exhaust constituents that contribute to the measured PM mass. In addition, experiments with some fuels having different fuel properties relevant to Co-Optima, such as research octane number (RON), were performed. Ultimately, the fuels that are identified by Co-Optima will have to work in both spark ignition and ACI modes in the same engine, so understanding PM emissions associated with a given fuel for both types of combustion will be important. The research platform that was used for initial studies is a 1.9 L light-duty diesel base engine modified to enable ACI combustion ranging from homogeneous charge compression ignition (HCCI) to mixing-controlled compression ignition. Different fuel properties are likely to impact the formation of the semi-volatile hydrocarbon phase that contributes greatly to PM mass from ACI engines.

Objectives

The objective is to understand how fuel properties and combustion parameters affect the organic carbon (OC) component of PM from ACI combustion, and, in particular, if the inception of soot formation can be detected.

Overall Objectives

- Identify if a similar formation pathway for elemental-carbon-based PM (soot) production occurs at different levels of air-fuel stratification for a given fuel
- Investigate if trends exist between fuels

Fiscal Year 2018 Objectives

- Collect condensable and solid exhaust PM species as well as gaseous emissions as fuel and air-fuel stratification are changed
- Quantify how air-fuel stratification and fuel RON influence PM mass production
- Quantify the change in HC gaseous emissions as the elemental carbon (EC) component of PM increases

Approach

ACI PM is typically >90% OC; filter smoke meter and microsoot sensor measurements are typically very low, but PM mass is regulated, so understanding the OC component is critical. Therefore, the PM and gaseous emissions were collected from a 1.9 L light-duty engine using filter-based PM sample collections in addition to the typical filter smoke number and microsoot sensor measurements to ascertain the true mass of PM produced and provide samples for further PM chemical speciation efforts. In order to characterize the pathway from OC-PM and gaseous HCs to soot formation (EC-PM) in the PM from ACI combustion, the level of air-fuel stratification was changed from HCCI operation with no stratification to a level of high fuel stratification (HFS). The same fuel and operating conditions (2,000 rpm, 4/5 bar) were maintained. A second fuel was also studied at air-fuel stratification levels within the same range to determine if trends in soot formation pathways in ACI PM vary with fuel properties. The experimental approach included the following tasks.

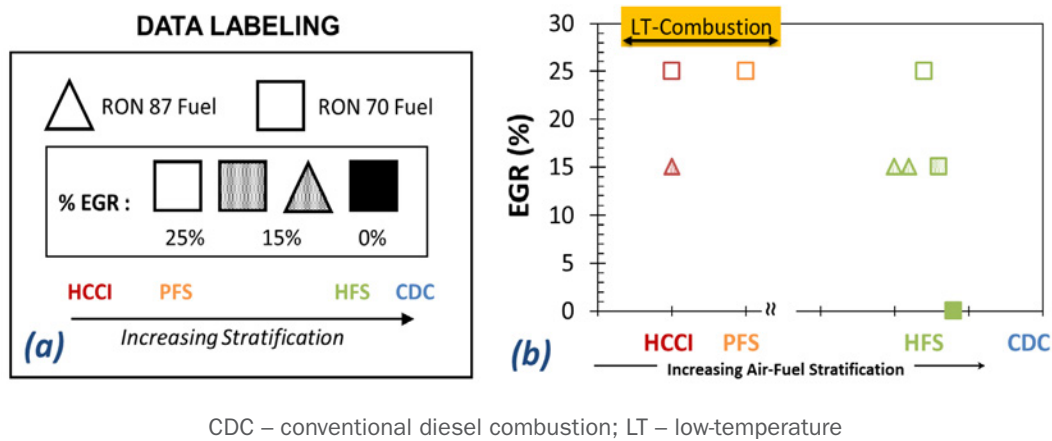
- Characterize shifts in OC composition for fuels with different RONs and, therefore, different chemistries
- Quantify the change in specific oxygenated HC (i.e., aldehydes) speciation across the stratification levels studied
- Study how PM chemical and physical properties correlate with fuel type and ACI operating modes

Results

An ACI engine campaign focused on PM and gaseous emissions sampling was successfully completed this fiscal year. The study was run using two different lower RON, gasoline range fuels over air-fuel stratification levels ranging from HCCI to HFS conditions. The engine had a compression ratio of 16.5, with a variable geometry turbocharger and cooled exhaust gas recirculation (EGR) that was operated at 2,000 rpm and 4/5 bar. Engine operating parameters were adjusted to maintain constant combustion phasing for the two fuels (RON 70 and RON 87) as closely as possible. The RON 87 fuel (anti-knock index 85) was a Co-Optima blendstock for oxygenate blending and was used without further blending. The RON 70 fuel was an even lower RON, gasoline range fuel that contained a lower aromatic content, almost no olefins, and higher saturate content than the RON 87 fuel. The study was designed to understand the conditions and fuel chemistry related to the onset of both soot (EC-PM) and organic PM (OC-PM) formation. The eight conditions tested and how they correlated to each other are presented in Figure II.24.1.

Filter samples of exhaust PM were collected at each of the conditions listed in Figure II.24.1 and were analyzed for mass and carbon compositions. Figure II.24.2 shows the total PM mass calculated on quartz fiber filters and quantified from EC/OC data analyses using the NIOSH method [1]. The NIOSH method is a thermo-optical method used to distinguish between OC and EC for PM collected on filters. A membrane filter used for Environmental Protection Agency regulated PM mass measurements was also collected. The carbon composition was measured at each air-fuel stratification studied. The total PM mass rate was calculated based on the combined mass of EC and OC via the NIOSH method and the total exhaust flow rate. The PM carbon mass was calculated as a mass rate (mg/min) to allow accurate comparison between EGR levels, which had different exhaust flow rates. For the RON 70 fuel, when EGR was kept constant at 25% EGR and the level of air-fuel stratification was reduced, a slight increase of PM mass rate (~10 mg/min) was observed. This is counter to commonly reported reductions in PM formation as air-fuel stratification is reduced. The increase at lower air-fuel stratification levels was also observed for the RON 87 fuel, at 15% EGR, but with a larger increase (~20 mg/min) in the PM mass rate from HFS to partial fuel stratification (PFS). As expected, increasing levels of EGR reduced the level of air-fuel stratification and the total PM mass (RON 70, green squares in Figure II.24.2). Impact of EGR levels was only studied for the RON 70 fuel. A direct fuel

comparison can only be made from this data set for 15% EGR at the HFS level (shaded green \square and Δ , Figure II.24.2), which showed that the RON 70 fuel produced nearly double the total PM compared to the RON 87 fuel under the same conditions.



CDC – conventional diesel combustion; LT – low-temperature

Figure II.24.1. (a) Explains the labeling format for this report in reference to the different conditions studied. The shape indicates which fuel, the shading indicates the % EGR, the color indicates for which type of air-fuel stratification the condition would be classified. (b) A plot of the conditions tested in this project.

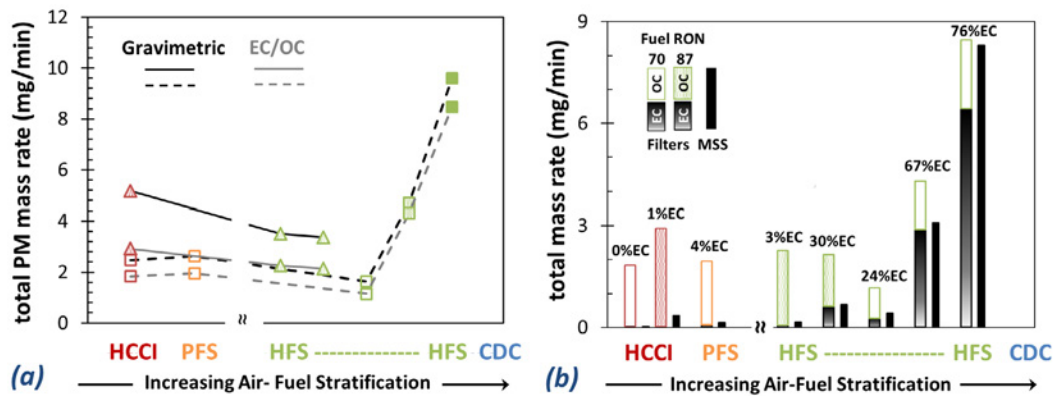


Figure II.24.2. (a) Plot comparison of PM mass rate for each condition tested. PM mass rates were calculated from both gravimetric (black lines) and EC/OC (gray lines) filter analyses. Solid lines indicate RON 87 fuel test points and dashed lines indicate RON 70 fuel test points. (b) Mass rate data from the EC/OC analyses showing fraction speciated as EC (gradient black) and OC (colored) compared to the microsoot sensor mass rate data (solid black to right or comparable EC/OC data). Fuels are differentiated by the OC fill color (RON 70, white; RON 87, shaded color), as indicated in the legend.

Figure II.24.2b shows the PM mass distribution between EC and OC for each ACI condition tested. The elemental carbon contribution is graphed at the bottom of the stacked plot (gradient black fill) with the organic carbon contribution added on top (color and shade coded according to Figure II.24.1a). The fraction of EC in the PM sample is labeled above the corresponding stacked plot in Figure II.24.2b. Less than 5% of the total PM produced in either HCCI or PFS ACI modes was EC-based PM, regardless of the fuel tested. As the air-fuel stratification was increased into the HFS range, an increasing level of EC contribution to the PM mass was measured for both fuels. Figure II.24.2b also compares the mass rate measured by the in-line microsoot sensor to that calculated from the EC/OC analyses. The microsoot sensor method of analysis is designed to measure soot concentration; therefore, the low mass rate measured for the lower air-fuel stratification levels was not surprising considering the nearly 100% OC composition of the PM.

The discrepancy between the gravimetric mass rates and those calculated from the EC/OC analyses (Figure II.24.2a) was likely related to the high mass loading of OC particulate matter, which facilitated condensation of lower boiling gaseous HCs in the exhaust. The difference in mass rate between the two filter-based methods was more significant for RON 87, which also had higher levels of gaseous HCs (Figure II.24.3a).

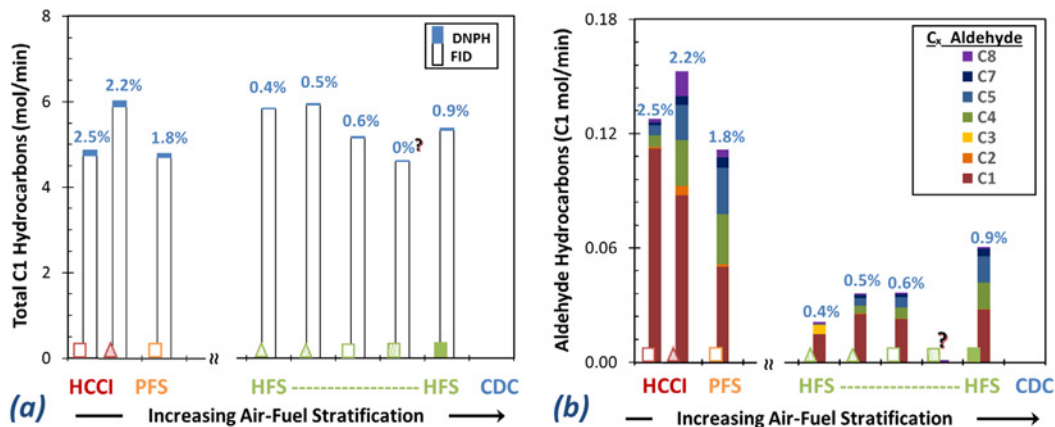


Figure II.24.3. Stacked bar graphs in (a) compare C1 HC emissions in order of increasing air-fuel stratification. The open bars represent the hydrocarbons measured by a FID, and the blue bars represent the aldehyde contribution measured using DNPH cartridges. Percent values above the bars indicate the aldehyde fraction of the total C1 HC emissions. Graph (b) shows breakdowns in the aldehyde composition, measured with DNPH, in terms of C_x (x = number of carbons). No significant presence of aldehydes was measured by DNPH for the RON 70, 15% EGR (HFS) conditions; confirmation of this is still under way. Symbols at the bottom of each bar in (a) and (b) graphs indicate the engine conditions (see Figure II.24.2a).

Gaseous HC emissions are traditionally measured using a flame ionization detector (FID), which is not very sensitive to aldehydes, requiring another method. A diluted exhaust gas was sent through a cartridge containing 2,4-dinitrophenylhydrazine (DNPH), which selectively traps aldehydes and ketones. The DNPH complexed aldehydes were then eluted from the cartridges using the solvent acetonitrile. The concentration of aldehydes was then measured. While the specific aldehyde was confirmed by mass spectroscopy, it was examined on a C1 basis so that its contribution to the total gaseous HC emissions could be combined with the FID data, which is only measured on a C1 basis. Aldehydes accounted for a larger, percent-level fraction of the HC emissions for the conditions with lower levels of air-fuel stratification, which are considered true low-temperature combustion (LT-Combustion, Figure II.24.1); see Figure II.24.3. Virtually no aldehydes were measured by the DNPH analysis for the RON 70, 15% EGR (HFS) condition; more analysis is on-going to confirm the accuracy of this measurement. While some formaldehyde was measured at this condition by Fourier-transform infrared spectroscopy, it was significantly lower than the 25% and 0% EGR conditions, as was the total HCs measured by the FID. Further investigations are needed to confirm these unexpected trends.

The size distribution of the PM generated was also measured at each condition using a TSI engine exhaust particle size (EEPS) in-line analyzer after a two-stage, heated dilution tunnel, see Figure II.24.4. The dilution tunnel included an evaporation section that heated the dilute exhaust to 350°C after the first-stage dilution. The evaporator tube and second-stage dilution remove gaseous condensate from the particle surface, leaving solid (or predominately solid) particles. Figure II.24.4 displays the average EEPS particle size distribution for each condition. A trend in the particle size data that correlates to the level of air-fuel stratification across both fuels was not observed. However, increasing stratification within each fuel set did show an increase in particles, which is shown in Figure II.24.4a for RON 87 fuel and Figure II.24.4b for RON 70 fuel test points.

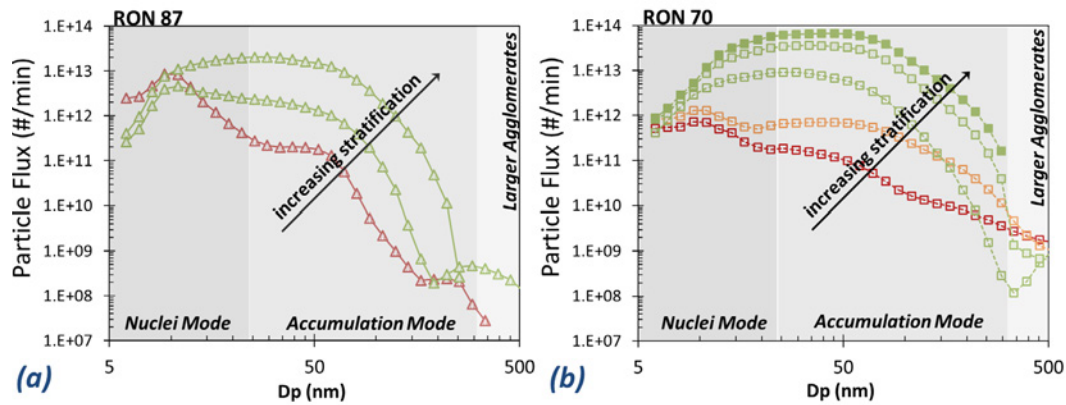


Figure II.24.4. Size distribution plots for particulate flux at each condition tested. (a) RON 87 fuel and (b) RON 70 fuel from EEPS real-time exhaust sampling downstream of 2-stage dilution tunnel, which included a denuder. HCCI (red), PFS (orange), HFS (green). Arrow shows direction conditions with increasing air-fuel stratification.

The total flux of particles at each condition was also seen to increase with increasing air-fuel stratification for a given fuel; see Figure II.24.5a. The fraction of the particle flux that falls within the nuclei mode particles (<25 nm) and accumulation mode particles (≥ 25 nm) is graphically shown in the stacked bar graph of Figure II.24.5b. A trend was also seen within each fuel set that indicated that the lower air-fuel stratification level generates a higher fraction of small sub-25-nm particles.

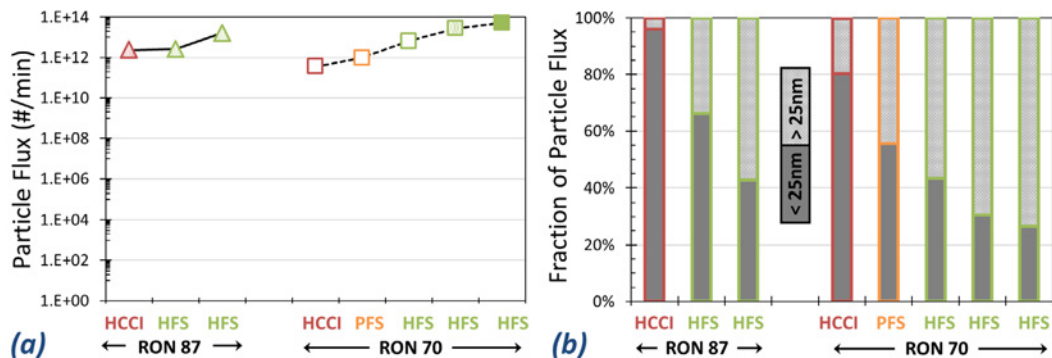


Figure II.24.5. The particle flux (a) sum of all particle sizes measured by EEPS at each engine condition. The stacked bar graph (b) shows the fraction distribution of the total particle flux values associated with sub-25-nm, nuclei mode particulate (bottom, darker gray) and those that fall in the accumulation mode region above 25 nm (top, lighter gray).

Conclusions

The results of this study on the impact of air-fuel stratification during ACI engine operation (2,000 rpm, 4/5 bar) show the following.

- Highest PM mass rate production was seen at the greatest level of air-fuel stratification studied, but HCCI generated higher PM mass rates than some lower stratification HFS conditions.
- Higher mass emissions were seen for the higher RON fuel (RON 87), but mass emissions still followed the same trend as the RON 70 fuel within the same air-fuel stratification.
- Increasing PM was unable to be detected by the on-line PM instrument, microsoot sensor, when EC was low or not present.
- Increasing fractions of EC in the PM composition were observed as the level of air-fuel stratification increased.

- Higher aldehyde concentrations in the gaseous HC emissions were seen for the air-fuel stratification levels that fell within the LT-combustion classification (i.e., HCCI and PFS).
- Increasing particle flux and particulate size were observed with increasing air-fuel stratification for each fuel, suggesting a fuel property impact as well as a stratification influence on particle generation.

Key Publications

1. Moses-DeBusk, M., J.M. Storey, S.A. Lewis, Jr., R.M. Connatser, and S.J. Curran. “Impacts of Air-Fuel Stratification in ACI Combustion on Particulate Matter (PM) and Gaseous Emissions.” 2018 CLEERS Workshop, September 18–20, 2018, Ann Arbor, MI.

Reference

1. Birch, E.M. 2002. “Occupational Monitoring of Particulate Diesel Exhaust by NIOSH Method 5040.” *Appl. Occup. Environ. Hyg.* 17 (6): 400–5.

Acknowledgements

Co-Principal Investigator: John Storey, Oak Ridge National Laboratory

II.25 Kinetic Mechanism Development (Lawrence Livermore National Laboratory)

William J. Pitz, Principal Investigator

Lawrence Livermore National Laboratory (LLNL)
 P. O. Box 808, L-372
 Livermore, CA 94551
 E-mail: pitz1@llnl.gov

Kevin Stork, DOE Technology Development Manager

U.S. Department of Energy
 E-mail: Kevin.Stork@ee.doe.gov

Start Date: October 1, 2016	End Date: September 30, 2018	
Project Funding (FY18): \$800,000	DOE share: \$800,000	Non-DOE share: \$0

Project Introduction

Predictive chemical kinetic models are needed to represent high-performance fuels and their mixtures with conventional fuels (e.g., gasoline and diesel fuels) for Co-Optima. These kinetic models can be used in computational fluid dynamics simulations of advanced combustion engines to predict the behavior of these fuel blends. Enabled by kinetic models, computational fluid dynamics simulations can be used to co-optimize fuel formulations and engines so that goals for engine efficiency, fossil-fuel displacement, and minimizing harmful emissions can be achieved.

Objectives

Overall Objectives

- Develop and improve chemical kinetic models for high-performance fuels (HPFs) and base fuels (e.g., gasoline and diesel) so that the kinetic models accurately predict fuel behavior at engine conditions
- Use chemical kinetic models to simulate combustion properties at boosted spark ignition, advanced compression ignition, and mixing-controlled compression ignition engine conditions

Fiscal Year 2018 Objectives

- Develop and improve chemical kinetic models for HPFs for boosted spark ignition and advanced compression ignition applications
- Develop, improve and validate kinetic models for surrogate components and surrogate mixtures to represent base fuels for gasoline and diesel fuels
- Improve diesel surrogate kinetic model to represent Coordinating Research Council diesel surrogates V0a, V0b, and V1 [1] using rapid compression machine (RCM) experimental data from University of Connecticut

Approach

To develop chemical kinetic models for blends of HPFs and conventional transportation fuels, chemical kinetic models for each fuel of interest are developed and improved, as needed. These fuel component models are developed by identifying the reaction paths and assembling the associated rate constants, thermodynamic data, and transport data. Next, the kinetic models for HPFs are combined with kinetic models for conventional fuels to represent blends of HPFs and conventional transportation fuels. The models are validated by comparison of computed results to fundamental experimental data from RCMs, shock tubes, jet-stirred reactors, flow reactors, and premixed laminar flames. Then the kinetic models are used in multidimensional engine simulation codes to assess fuel property effects in engines. These simulation results can guide and inform efforts to co-optimize fuels and engines for best performance and engine efficiency, and to reduce harmful emissions.

Results

Key accomplishments for Fiscal Year 2018:

- Provided the Co-Optima team with a validated chemical kinetic model for gasoline surrogate fuels with HPFs (22 hydrocarbons and 20 oxygenate components from 9 chemical classes)
- Developed new kinetic models for HPFs cyclopentanone and prenol
- Developed improved kinetic models for HPFs diisobutylene and anisole
- Predicted mixture behavior for blends of cyclopentane and dimethyl ether
- Developed a validated kinetic mechanism and optimized surrogate mixture for a base fuel to represent conventional diesel for mixing-controlled compression ignition engine applications
- Accelerated work flow for kinetic model development by developing an experimental database linked to LLNL zero-order reaction kinetics (Zero-RK) solvers
- Improved and validated gasoline surrogate component models upon which the HPFs and gasoline surrogate mechanisms rely (hexanes: four isomers)
- Successfully simulated Argonne National Laboratory RCM data for a research-grade E10 gasoline (gasoline blend with 10% ethanol) using the LLNL gasoline surrogate model

A new chemical kinetic model for gasoline surrogates, including HPFs, was provided to the Co-Optima team for use in simulating ignition under conditions found in boosted spark ignition, advanced compression ignition, and multimode (spark ignition/advanced compression ignition) engines. This model has been broadly used by the team to generate pressure-temperature ignition delay maps for interpreting engine trajectories for different operating modes, for computing blending effects on research octane number and octane sensitivity of HPFs into different base fuels, and for use in computational fluid dynamics engine simulations after kinetic model reduction.

The LLNL kinetics team has developed two new HPF models: cyclopentanone and prenol. Cyclopentanone is an HPF with high research octane number (101), high octane sensitivity (11), high flame speed, and good blending characteristics. The model for cyclopentanone was developed in collaboration with Massachusetts Institute of Technology; University of Central Florida; National University of Ireland, Galway; and Lund University. The kinetic model included new reaction rates computed from quantum chemistry by Massachusetts Institute of Technology. It has been validated with newly measured ignition delay times (IDTs) from National University of Ireland, Galway (Figure II.25.1 and Figure II.25.2), species concentration histories measured in a shock tube from University of Central Florida, and flame-speed experimental data from University of Central Florida and Lund University, showing good agreement between computed and experimental results.

The second HPF model that has been constructed is for prenol. A new chemical kinetic model for prenol has been developed based on literature reaction rates and thermophysical properties when available. Reaction rates were estimated using reaction rate rules and thermophysical properties via group additivity. This preliminary prenol kinetic model was validated by comparison to literature data on pyrolysis in a jet-stirred reactor. Validation of the model by comparison to RCM ignition data is planned.

The LLNL kinetics team has improved the kinetic model for the HPF diisobutylene, including both isomers. The team updated thermodynamic properties of diisobutylene, incorporated new rates for the unimolecular decomposition of the fuel and fuel radicals, and updated the hydrogen abstraction rates from the fuel. Most importantly, low-temperature reaction paths for diisobutylene have been added, which is expected to allow more accurate simulation of ignition behavior under engine conditions. Thermodynamic data for diisobutylene was updated with the newest group values. The diisobutylene model has been validated by comparison to jet-stirred reactor data and laminar flame speed data. Further improvement in the model is needed to obtain agreement with laminar flame speed data measured by University of Central Florida. Validation of the model by comparison to RCM ignition data is planned.

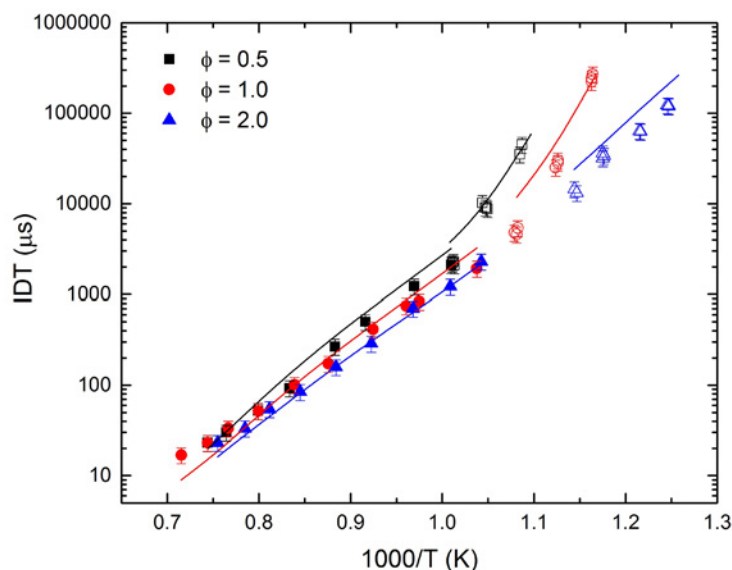


Figure II.25.1. Experimental (symbols) and simulated (lines) ignition delay times of cyclopentanone in air at $\phi = 0.5$, 1.0, and 2.0, and $P = 15$ bar. Solid and open symbols are shock tube and RCM experimental results, respectively [2].

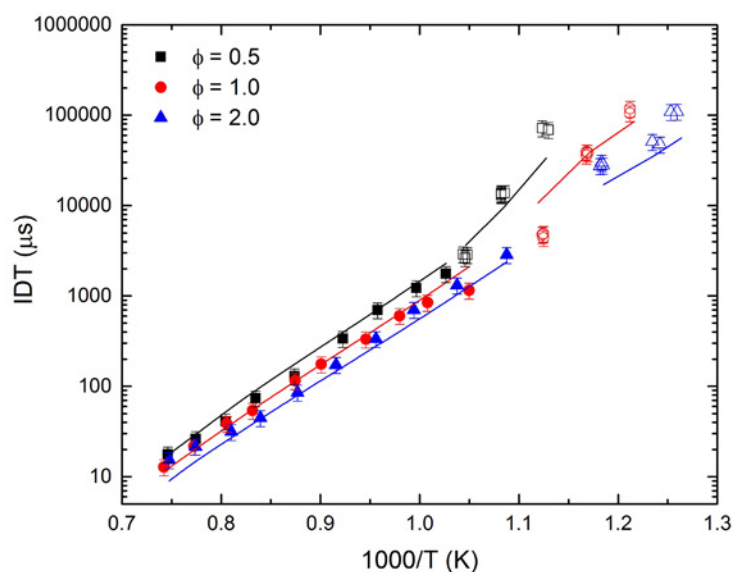


Figure II.25.2. Experimental (symbols) and simulated (lines) ignition delay times of cyclopentanone in air at $\phi = 0.5$, 1.0, and 2.0, and $P = 30$ bar. Solid and open symbols are shock tube and RCM experimental results, respectively [2].

The kinetic model for the HPF anisole was improved and published. Because large amounts of cyclopentadiene radical are formed during anisole pyrolysis and oxidation, the cyclopentadiene submodel reaction pathways and rate constants were updated and validated against flow reactor experiments in literature. Since cyclopentadiene is also an important intermediate in benzene and toluene pyrolysis and oxidation, the improvement of the cyclopentadiene submodel improved the benzene and toluene kinetic models as well.

A detailed chemical kinetic model for diesel was developed based on principles of hierarchy, self-consistency, and modularity. The model describes ignition chemistry for several classes of compounds typically found in diesel fuels, including n-alkanes, iso-alkanes, cycloalkanes, and aromatics. The current model describes the ignition chemistry of hydrocarbons with C1–C20 carbon atoms. The model developed includes about 6,500 species and 18,000 reactions and can be used to model diesel fuels. Simulations from the chemical kinetic model were compared to RCM experiments performed by University of Connecticut on a California diesel

certification fuel. The diesel surrogate model using an LLNL-optimized diesel surrogate mixture numerically emulates the ignition response of the target diesel at varying conditions of pressure, temperature, oxygen concentration, and fuel concentration. This work is planned for a journal publication.

It is critical to predict the behavior of fuel blends to enable the accurate simulation of blending HPFs into base fuels. Towards this goal, the LLNL kinetics team performed a study with National University of Ireland, Galway, on binary blends of cyclopentane and dimethyl ether. Cyclopentane is an unreactive component in gasoline, and dimethyl ether is a simple molecule to represent a reactive fuel component. IDTs in an RCM for cyclopentane/dimethyl ether blends were measured by National University of Ireland, Galway, and compared to predicted IDTs with the LLNL kinetic model. Improvements to the LLNL cyclopentane model were made based on these comparisons.

The LLNL gasoline surrogate kinetic model was used to simulate new experiments performed in the Argonne National Laboratory RCM on a research-grade E10 gasoline with a research octane number of 92 and an octane sensitivity of 7.5. The experiments were performed over a range of temperatures from 740 K to 1,000 K, pressures from 10 bar to 80 bar, and equivalence ratios of 0.67 and 1. A comparison between predicted and measured pressure histories resulting from autoignition in the RCM is shown in Figure II.25.3 for different pressures. The simulation results compare well with experiments for the 1st-stage and 2nd-stage IDTs and for the pressure rise during the 1st-stage ignition, which is an indication of low-temperature heat release.

In a new effort to speed up the work flow in developing and improving kinetic models, an experimental database was developed to be used in tandem with LLNL Zero-RK solvers to allow faster validation of the kinetic models. With Zero-RK solvers developed by the LLNL numerics team, tens of thousands of shock tube and RCM IDT calculations for kinetic model validation can be done in ~20–50 min on high-performance computers. The experimental database was developed by adding initial conditions and IDTs from shock tube and RCM experiments. This experimental database is used by the Zero-RK solvers to compute the IDTs and is used in generating graphical comparisons for kinetic model validation. The experimental database will continue to be expanded in the future.

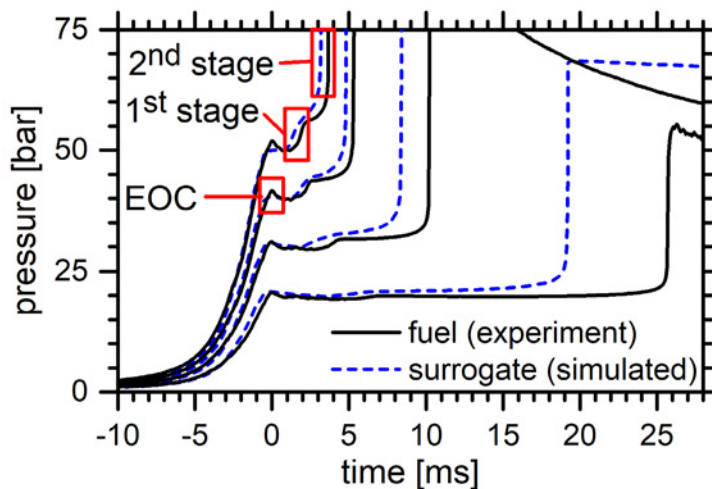


Figure II.25.3. Experimental and simulated pressure histories from the autoignition of an E10 research-grade 87 anti-knock index gasoline at various pressures at the end of compression (EOC) in the Argonne National Laboratory RCM

Conclusions

- Provided the Co-Optima team with a validated kinetic model for gasoline surrogate fuels with HPFs to be used for generating ignition delay maps, for computing blending effects on research octane number and octane sensitivity, and for use in computational fluid dynamics engine simulations after kinetic model reduction

- Developed a new kinetic model for cyclopentanone with contributions from two Co-Optima university partners (Massachusetts Institute of Technology and University of Central Florida)
- Developed and validated a new diesel surrogate model with representative components from all the chemical classes present in diesel fuel
- Developed an improved kinetic model for diisobutylene with updated reaction rates and thermochemistry

Key Publications

1. Zhang, K., N. Lokachari, E. Ninnemann, S. Khanniche, W.H. Green, H.J. Curran, S.S. Vasu, and W.J. Pitz. 2018. “An Experimental, Theoretical, and Modeling Study of the Ignition Behavior of Cyclopentanone.” *Proceedings of the Combustion Institute*. <https://doi.org/10.1016/j.proci.2018.06.097>.
2. Ahmed, A., W.J. Pitz, C. Cavallotti, M. Mehl, N. Lokachari, E.J.K. Nilsson, J.-Y. Wang, A.A. Konnov, S.W. Wagnon, B. Chen, Z. Wang, S. Kim, H.J. Curran, S.J. Klippenstein, W.L. Roberts, and S.M. Sarathy. 2018. “Small Ester Combustion Chemistry: Computational Kinetics and Experimental Study of Methyl Acetate and Ethyl Acetate.” *Proceedings of the Combustion Institute*. <https://doi.org/10.1016/j.proci.2018.06.178>.
3. Kukkadapu, G., D. Kang, S.W. Wagnon, K. Zhang, M. Mehl, M.M. Palacios, H. Wang, S.S. Goldsborough, C.K. Westbrook, and W.J. Pitz. 2018. “Kinetic Modeling Study of Surrogate Components for Gasoline, Jet and Diesel Fuels: C7-C11 Methylated Aromatics.” *Proceedings of the Combustion Institute*. <https://doi.org/10.1016/j.proci.2018.08.016>.
4. Westbrook, C.K., M. Mehl, W.J. Pitz, G. Kukkadapu, S. Wagnon, and K. Zhang. 2018. “Multi-Fuel Surrogate Chemical Kinetic Mechanisms for Real World Applications.” *Physical Chemistry Chemical Physics* 20 (16): 10588–10606.
5. Wagnon, S.W., S. Thion, E.J.K. Nilsson, M. Mehl, Z. Serinyel, K. Zhang, P. Dagaut, A.A. Konnov, G. Dayma, and W.J. Pitz. 2018. “Experimental and Modeling Studies of a Biofuel Surrogate Compound: Laminar Burning Velocities and Jet-Stirred Reactor Measurements of Anisole.” *Combustion and Flame* 189: 325–336.

References

1. Mueller, C.J., W.J. Cannella, T.J. Bruno, B. Bunting, H.D. Dettman, J.A. Franz, M.L. Huber, M. Natarajan, W.J. Pitz, M.A. Ratcliff, and K. Wright. 2012. “Methodology for Formulating Diesel Surrogate Fuels with Accurate Compositional, Ignition-Quality, and Volatility Characteristics.” *Energy & Fuels* 26 (6): 3284–3303.
2. Zhang, K., N. Lokachari, E. Ninnemann, S. Khanniche, W.H. Green, H.J. Curran, S.S. Vasu, and W.J. Pitz. 2018. “An Experimental, Theoretical, and Modeling Study of the Ignition Behavior of Cyclopentanone.” *Proceedings of the Combustion Institute*. <https://doi.org/10.1016/j.proci.2018.06.097>.

Acknowledgements

This work was performed under the auspices of the U.S. Department of Energy by Lawrence Livermore National Laboratory under Contract DE-AC52-07NA27344.

II.26 Fuel Property Blending Model (Lawrence Livermore National Laboratory)

William J. Pitz, Principal Investigator

Lawrence Livermore National Laboratory (LLNL)
 P.O. Box 808, L-372
 Livermore, CA 94551
 E-mail: pitz1@llnl.gov

Kevin Stork, DOE Technology Development Manager

U.S. Department of Energy
 E-mail: Kevin.Stork@ee.doe.gov

Start Date: October 1, 2016	End Date: September 30, 2018	
Project Funding (FY18): \$65,000	DOE share: \$65,000	Non-DOE share: \$0

Project Introduction

The combustion of transportation fuels in internal combustion engines is generally characterized by important properties such as research octane number (RON), motor octane number (MON), cetane number, and flame speed. However, predicting these properties for fuels is challenging because of complex chemical kinetic interactions of fuel components that cause non-linear behavior. To address this issue, the LLNL kinetic modeling team is developing chemical kinetic models that can predict RON, MON, flame speed, and other fuel properties, and can model the complex behavior of these mixtures under conditions in boosted spark ignition, advanced compression ignition, and mixing-controlled compression ignition engines. These accurate and validated chemical kinetic models are critical for developing insight into how fuel properties impact engine performance. To use these chemical kinetic models in multidimensional simulation codes, the models are reduced in size and employed to simulate combustion in engines. These insights and combustion simulations will guide efforts to discover promising high-performance fuels (HPFs) and base-fuel blends that provide the desired engine combustion properties under advanced combustion engine conditions.

Objectives

Overall Objective

- Improve prediction of critical fuel properties relevant to engine efficiency

Fiscal Year 2018 Objectives

- Provide accurate fuel property values for HPF/base-fuel blends
- Identify base-fuel compositions that improve blending behavior with HPFs in terms of RON and/or octane sensitivity (OS)

Approach

Chemical kinetic models for HPFs of interest for blending with gasoline and diesel fuels are developed. Next, these chemical kinetic models are combined with kinetic models for conventional fuels to represent next-generation ground-transportation fuels. Correlations are developed between engine combustion properties (such as RON, MON, OS, and cetane number) and key quantities computed from the chemical kinetic model (such as ignition delay and slope of the ignition delay curve in the low-temperature chemistry region). Using the detailed chemical model and these correlations, key engine combustion properties can be predicted. Also, the kinetic model can be used to interpret the results in terms of the importance of different chemical paths identified by the simulations to help identify how HPF molecular structure affects fuel properties.

Results

Key accomplishments for Fiscal Year 2018:

- Predicted effect of blending Co-Optima HPFs in Co-Optima core gasoline fuels
- Predicted/validated flame speeds for cyclopentanone and for methyl acetate and ethyl acetate
- Developed an optimized surrogate to represent a diesel base fuel for blending studies
- Developed surrogates for Co-Optima core fuels
- Enabled more accurate RON and MON estimates using neural network approach
- Provided pressure–temperature (P–T) ignition delay maps to engine researchers

Fuel surrogate mixtures were developed to represent the five Co-Optima core gasoline fuels. These core fuels were used by the Co-Optima team to test the effect of fuel composition on engine combustion for fuels that have the same octane properties. The research-grade full-boiling gasoline fuels employ different chemical compositions to attain the same nominal RON 98. The chemical classes of compositions are alkylate, aromatic, cycloalkane, olefin, and E30 (gasoline blend with 30% ethanol). All the fuels have a nominal OS of 10 except for the alkylate fuel (OS = 1). The LLNL gasoline + HPFs kinetic model was used with a neural network model developed by the LLNL numerics team to find optimum surrogate mixtures to represent each of the Co-Optima core fuels in terms of RON, MON, distillation curve, hydrogen/carbon ratio, and chemical classes. These surrogate mixture compositions were provided to the Co-Optima team so that the LLNL kinetic model could be used in simulations of experiments on the Co-Optima core fuels.

A computational study was performed to determine the benefits of blending HPFs into the different Co-Optima core fuels. The LLNL gasoline + HPFs kinetic model and a neural network developed by the LLNL numerics team were used to compute RON and OS for blends. The greatest enhancement in blending in RON and OS was predicted when the HPFs were blended into the alkylate fuel (Figure II.26.1). This is an important finding because it shows the strong effect that the chemical composition of the base fuel can have on the blending of HPFs. Other core fuels were predicted to have less enhancement in blending, and their blending gave similar RON and OS.

New diesel surrogate mixtures to represent a diesel base fuel were developed by LLNL to be used for HPF blending experiments on mixing-controlled compression ignition fuel properties. The diesel surrogate mixture was formulated to numerically capture the physical and chemical characteristics of diesel fuel. These surrogate mixtures were designed to match the target diesel fuel in terms of ignition properties (derived cetane number), carbon types, hydrogen/carbon ratio, and distillation curve. In addition, the amount of long-chain n-alkanes was limited in the surrogate formulation to mitigate fuel solidification in high-pressure fuel systems when these surrogates are used in experiments. Using a surrogate matching tool developed by the LLNL numerics team, three surrogates were developed to match a California diesel certification fuel. One of the surrogates has been blended by National Renewable Energy Laboratory for future proposed blending studies of HPFs in a surrogate diesel fuel. The LLNL diesel surrogate kinetic model can be used to simulate these experiments and provide further understanding of the results.

Use of fuels with high laminar flame speeds has been shown to allow increases in spark ignition engine efficiency. Cyclopentanone is an HPF with a high laminar flame speed. The LLNL kinetic team simulated flame speeds for cyclopentanone using a kinetic model improved with high-level fundamental chemistry calculations from Bill Green's group at Massachusetts Institute of Technology. These simulated flame speeds were compared to measured high-quality experimental data on laminar flame speeds from University of Central Florida and Lund University (Figure II.26.2), carbon monoxide time histories from University of Central Florida, and ignition delay times from National University of Ireland, Galway, for the model validation and optimization. The kinetic model has proven to be accurate in predicting the reactivity of cyclopentanone over a wide range of conditions. The newly validated model allows reliable prediction of flame speeds under engine pressures and temperatures. The LLNL kinetic team also simulated laminar flame

speeds of HPFs methyl acetate and ethyl acetate and found good agreement with experimental data from Lund University (Figure II.26.3). These kinetic models can be used for enabling simulations of flame propagation in multidimensional engine simulations to co-optimize HPFs and advanced combustion modes for engine efficiency and performance.

P–T maps of ignition delay have proved useful in exploring P–T trajectories representative of engine operating modes [1]. For boosted spark ignition engine operation, these maps indicate conditions where engine knock will be encountered on an engine trajectory through P–T space. For advanced compression ignition mode of operation, these maps indicate conditions when autoignition is likely to occur along a P–T trajectory. The LLNL kinetics team has provided P–T maps to engine researchers at Oak Ridge National Laboratory so that they can use these maps to interpret their boosted spark ignition and advanced compression ignition engine experiments.

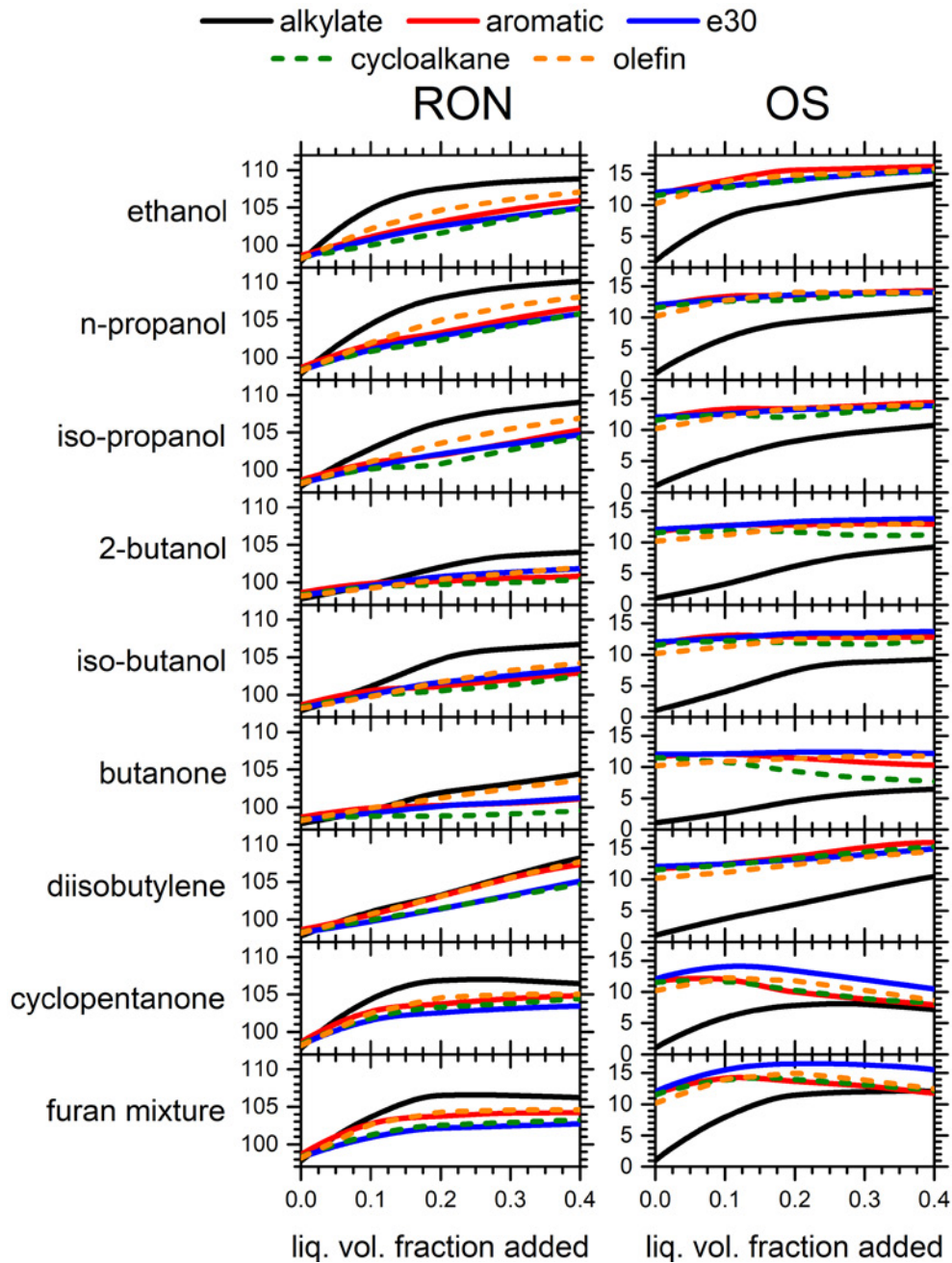


Figure II.26.1. Prediction of RON and OS for the simulated blending of nine HPFs into the Co-Optima core fuels

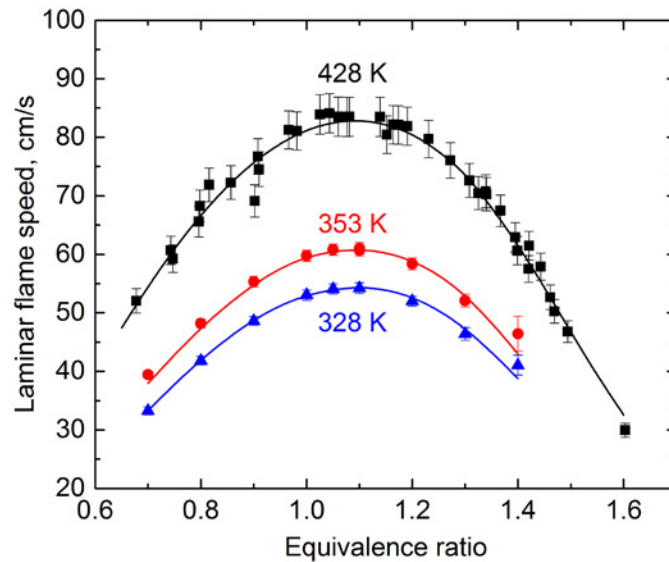


Figure II.26.2. Predicted (curves) and measured (symbols) laminar flame speeds of cyclopentanone at different fuel–air equivalence ratios and unburned gas temperatures. Experiments: University of Central Florida, black symbols; Lund University, red and blue symbols.

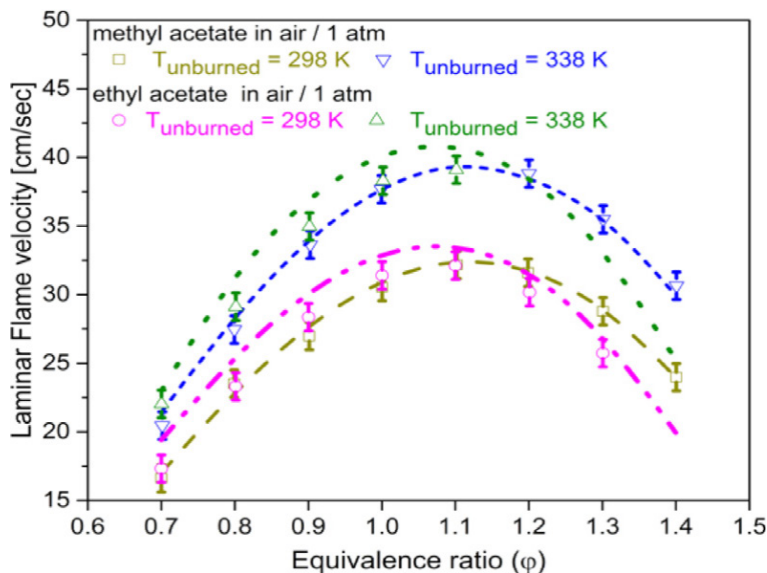


Figure II.26.3. Predicted (curves) and measured (symbols) laminar flame speeds of methyl acetate and ethyl acetate at different fuel–air equivalence ratios and unburned gas temperatures. Experiments: Lund University [2].

Conclusions

- Chemical kinetic models have been developed to predict fuel properties (e.g., ignition delay, RON, OS) for blendstocks blended into gasoline base fuels.
- Maps of ignition delays have been computed over wide temperature and pressure range for blendstocks and Co-Optima core fuels (P–T ignition delay maps).
- Prediction of fuel properties at engine conditions allows engine researchers to evaluate different advanced combustion strategies.
- Diesel surrogate mixtures have been developed to represent a diesel base fuel for HPF blending studies.

Key Publications

1. Ahmed, A., W.J. Pitz, C. Cavallotti, M. Mehl, N. Lokachari, E.J.K., Nilsson, J.-Y. Wang, A.A. Konnov, S.W. Wagnon, B. Chen, Z. Wang, S. Kim, H.J. Curran, S.J. Klippenstein, W.L. Roberts, and S.M. Sarathy. 2018. "Small Ester Combustion Chemistry: Computational Kinetics and Experimental Study of Methyl Acetate and Ethyl Acetate." *Proceedings of the Combustion Institute*. <https://doi.org/10.1016/j.proci.2018.06.178>.
2. Westbrook, C.K., M. Sjöberg, and N.P. Cernansky. 2018. "A New Chemical Kinetic Method of Determining RON and MON Values for Single Component and Multicomponent Mixtures of Engine Fuels." *Combust. Flame* 195: 50–62.
3. Westbrook, C.K., M. Mehl, W.J. Pitz, G. Kukkadapu, S. Wagnon, and K. Zhang. 2018. "Multi-Fuel Surrogate Chemical Kinetic Mechanisms for Real World Applications." *Physical Chemistry Chemical Physics* 20 (16): 10588–10606.

References

1. Szybist, J.P., and D.A. Splitter. 2017. "Pressure and Temperature Effects on Fuels with Varying Octane Sensitivity at High Load in SI Engines." *Combust. Flame* 177: 49–66.
2. Ahmed, A., W.J. Pitz, C. Cavallotti, M. Mehl, N. Lokachari, E.J.K., Nilsson, J.-Y. Wang, A.A. Konnov, S.W. Wagnon, B. Chen, Z. Wang, S. Kim, H.J. Curran, S.J. Klippenstein, W.L. Roberts, and S.M. Sarathy. 2018. "Small Ester Combustion Chemistry: Computational Kinetics and Experimental Study of Methyl Acetate and Ethyl Acetate." *Proceedings of the Combustion Institute*. <https://doi.org/10.1016/j.proci.2018.06.178>.

Acknowledgements

Russell Whitesides of LLNL is acknowledged for the development of the neural network model for RON and MON prediction. This work was performed under the auspices of the U.S. Department of Energy by Lawrence Livermore National Laboratory under Contract DE-AC52-07NA27344.

II.27 Virtual Properties, Reduced Mechanism, Blending of Kinetics Properties, and Modeling of Fuel Properties (Lawrence Livermore National Laboratory)

Matthew J. McNenly, Principal Investigator

Lawrence Livermore National Laboratory
7000 East Avenue
Livermore, CA 94550
E-mail: mcnenly1@llnl.gov

Kevin Stork, DOE Technology Development Manager

U.S. Department of Energy
E-mail: Kevin.Stork@ee.doe.gov

Start Date: October 1, 2017	End Date: September 30, 2018	
Project Funding (FY18): \$375,000	DOE share: \$375,000	Non-DOE share: \$0

Project Introduction

The Central Fuel Hypothesis (CFH) is one of the major hypotheses around which the Co-Optima program is organized. It states that if we identify target values for the critical fuel properties that maximize efficiency and emissions performance for a given engine architecture, then fuels that have properties with those values (regardless of chemical composition) will provide comparable performance. During the performance period, the main purpose of this project is to determine if the CFH applies to the design and performance of blendstocks for oxygenate blending (BOBs) when evaluated by the octane ratings. If the CFH is valid for BOB design, then the blending performance of any blendstock at any volume fraction should only depend on the octane rating of the base BOB, and not on the molecular composition. This would mean that two BOBs with the same research octane number (RON) and motor octane number (MON) should have the same octane ratings when an identical blendstock is added at the same concentration to each. However, if a large difference is observed in the octane numbers of the finished fuels, then the BOB octane rating is not a universal property in the context of the CFH, which indicates that new properties must be included for the CFH to be applied.

If the CFH is not valid for the BOB octane rating, this creates an opportunity to optimize the BOB for a given blendstock. Uncovering this fundamental knowledge could allow the BOB to be designed to maximize the RON and octane sensitivity (RON minus MON) for a given blendstock. Cost information could also be included to optimize for the best octane rating per dollar for a given engine configuration. The understanding will allow for more accurate evaluation of BOB and blendstock combinations for evaluation in the boosted spark ignition merit function [1]. This research demonstrates new Co-Optima tools for stakeholders to evaluate a blendstock's potential with respect to their market estimates. Successful experimental validation of these tools will open the door for model-based fuel optimization, which could help refiners save money and energy designing a BOB for new blendstocks.

Objectives

- Assess the validity of the CFH with respect to using the octane rating of a BOB to capture its blending performance with oxygenates and bio-derived hydrocarbons
- Quantify the potential to optimize the BOB and finished fuel performance using a chemical kinetic model for the inputs to the boosted spark ignition merit function—specifically, the RON and the octane sensitivity
- Coordinate with Co-Optima Fuel Properties Team to test the BOB and blendstock combinations found in the virtual fuel search to have the largest variation in the boosted spark ignition merit score
- Validate the model octane predictions using new test data collected for the ASTM standard measurements for RON (D2699) and MON (D2700)

Approach

The project takes advantage of the latest gasoline surrogate mechanism developed for the Co-Optima program at Lawrence Livermore National Laboratory [2]. This fuel model contains over 2,800 reacting species to resolve ignition phenomena, including 23 hydrocarbon blendstocks commonly found in gasoline. It also contains 20 oxygenates and bio-derived blendstocks, including all tested in the BOB blending study by McCormick et al. [3] as promising candidates for use in advanced spark ignition engines. The blending performance of the BOBs considered here is evaluated by the change in the boosted spark ignition merit function score [1] due to the change in RON and octane sensitivity. The kinetic-based model RON and model MON are computed using a new neural network architecture that takes ignition delay calculations, heat of vaporization, and other readily available fuel properties as inputs [4]. To accelerate the octane prediction model, the ignition delay times are computed using the high-performance combustion solver, Zero-RK, developed at Lawrence Livermore National Laboratory [5].

The CFH for oxygenate blending is tested with virtual BOBs created to have the same octane rating (90.3 RON and 84.7 MON) as the four-component BOB surrogate tested previously for the Co-Optima program [3]. The BOBs are considered “virtual fuels” because the octane blending behavior is simulated using the neural network model. It is not possible to test every possible molecular composition of a BOB to verify the blending performance is independent. Instead, a small, but diverse, set of BOB compositions is considered, which have widely varying concentrations of the different hydrocarbon functional groups. To achieve this diversity, five virtual BOBs are created such that the volume fraction is maximized for each of the PIONA molecular classes while still matching the octane rating of the four-component Co-Optima BOB. Here PIONA stands for paraffins (P), iso-paraffins (I), olefins (O), naphthenes (N), and aromatics (A).

If the CFH is generally applicable for oxygenate blending, then the five virtual BOBs should have similar octane ratings when an oxygenate, or any blendstock, is added to them. The change in merit score is used to quantify how similar the octane ratings are across the BOBs. Based on the merit score formula in [1], the change in merit score due to the octane rating is computed as $\Delta\text{Merit} = 0.625 \Delta\text{RON} + 0.781 \Delta S$, where S is the octane sensitivity. The change in the merit score is scaled so that a value of one represents the potential for a 1% efficiency gain with an engine optimized for the fuel. The reproducibility error of the ASTM standard RON and MON tests produces an uncertainty in ΔMerit of 1.2 (95% confidence). Differences between the merit score across the BOBs are considered negligible below this level. To provide a sense of scale, differences in the merit score on the order of 5.7 are considered substantial, which corresponds to the merit score change that occurs switching from 87 anti-knock index (AKI) gasoline to 93 AKI (98 RON) gasoline [6].

Results

Key accomplishments for Fiscal Year 2018:

- The simulation of the blending performance indicates that the Central Fuel Hypothesis is unlikely to be valid for the BOB octane ratings.
- Strong BOB composition dependencies ($\Delta\text{Merit} > 3$) are found for 11 of the bio-derived blendstocks tested by McCormick et al. [3].
- Six high-performance blendstocks (ethanol, iso-butanol, methylacetate, 3-pentanone, 2-methylfuran, and diisobutylene) with $\Delta\text{Merit} > 3.5$ were selected by the Co-Optima Fuel Properties Team at National Renewable Energy Laboratory for experimental validation.
- The mean absolute error in the neural network octane prediction is 1.6 RON and 1.9 MON for ten new samples created from the virtual BOB compositions.

Five virtual BOBs are created to match the model-based octane rating of the Co-Optima BOB to within 0.1 octane numbers, while maximizing the volume fraction of each of the PIONA classes of molecules. The fuel surrogate designer developed by Whitesides [7] is modified to perform the volume fraction maximization subject to the octane number constraint and three composition constraints. Specifically, the maximum volume fraction of olefins and naphthenes must be less than 25%, and the maximum volume fraction of aromatics must

be less than 50%. These limits are applied to maintain molecular diversity while avoiding the most impractical compositions from the standpoint of large-scale market adoption. Each PIONA class has two molecular representatives, except for the naphthene class, which only has one—cyclopentane. Figure II.27.1 shows the volume percentage of each of the nine hydrocarbons for the five virtual BOBs and the previously tested Co-Optima BOB.

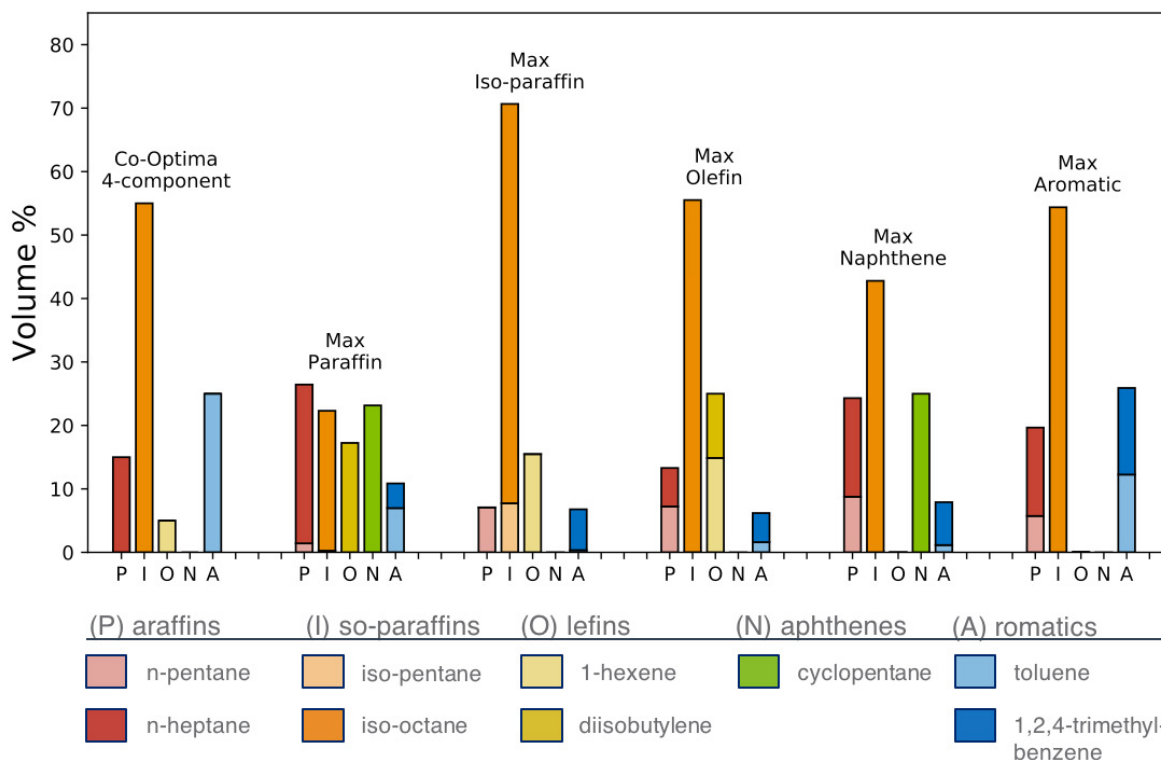


Figure II.27.1. Composition of the four-component Co-Optima BOB and the five virtual BOBs that maximize the volume fraction of each of the PIONA classes. The octane numbers predicted by the neural network match the Co-Optima BOB (90.3 RON and 84.7 MON) to within 0.1 octane numbers.

The RON and MON are computed using the neural network model for the Co-Optima BOB and the five virtual BOBs. Specifically, the octane ratings of 17 high-performance blendstocks studied in McCormick, et al. [3] are calculated for blending levels between zero and 30% (by volume) at 1% increments. From these results, the change in the merit score [1] from the zero blending level is computed to assess the validity of the CFH. The maximum difference between the largest and smallest merit score is then found for each blendstock across the six BOBs. For 11 out of the 17 blendstocks, the maximum merit score change between BOBs is greater than 3.0. A value greater than 3.0 represents more than 50% of the potential engine efficiency gain possible when switching from 87 AKI to 93 AKI gasoline. Once validated experimentally, this is strong evidence that the CFH does not apply to the octane rating of a BOB when used to predict the blending performance of a finished fuel.

Eight blendstocks are found to have a maximum merit score change of 3.5 or greater. Of these, six were recommended for experimental validation by the Co-Optima Fuel Properties Team at National Renewable Energy Laboratory. These include ethanol, iso-butanol, methylacetate, 3-pentanone, 2-methylfuran, and diisobutylene. These blendstocks were selected because they represent a broad range of functional groups and carbon numbers. The change in merit score across the BOBs is shown in Figure II.27.2 for the four blendstocks with the largest variation. The merit score change is plotted relative to the merit score change of the four-component Co-Optima BOB (dashed black line). A gray box on the right-hand side shows the magnitude of the merit score difference between 93 AKI (98 RON) and 87 AKI gasoline, which represents a potential engine efficiency gain of 5.7%. A key observation in Figure II.27.2 is that the virtual BOBs that maximized the

amount of iso-paraffins and olefins tend to produce the greatest merit score benefit, indicating more synergistic octane blending. Further, the virtual BOBs that maximized the amount of paraffins and naphthenes tend to produce the least merit score benefit, indicating more antagonistic octane blending. It is important to note that this general behavior is observed across all 17 high-performance blendstocks, not just those shown in Figure II.27.2.

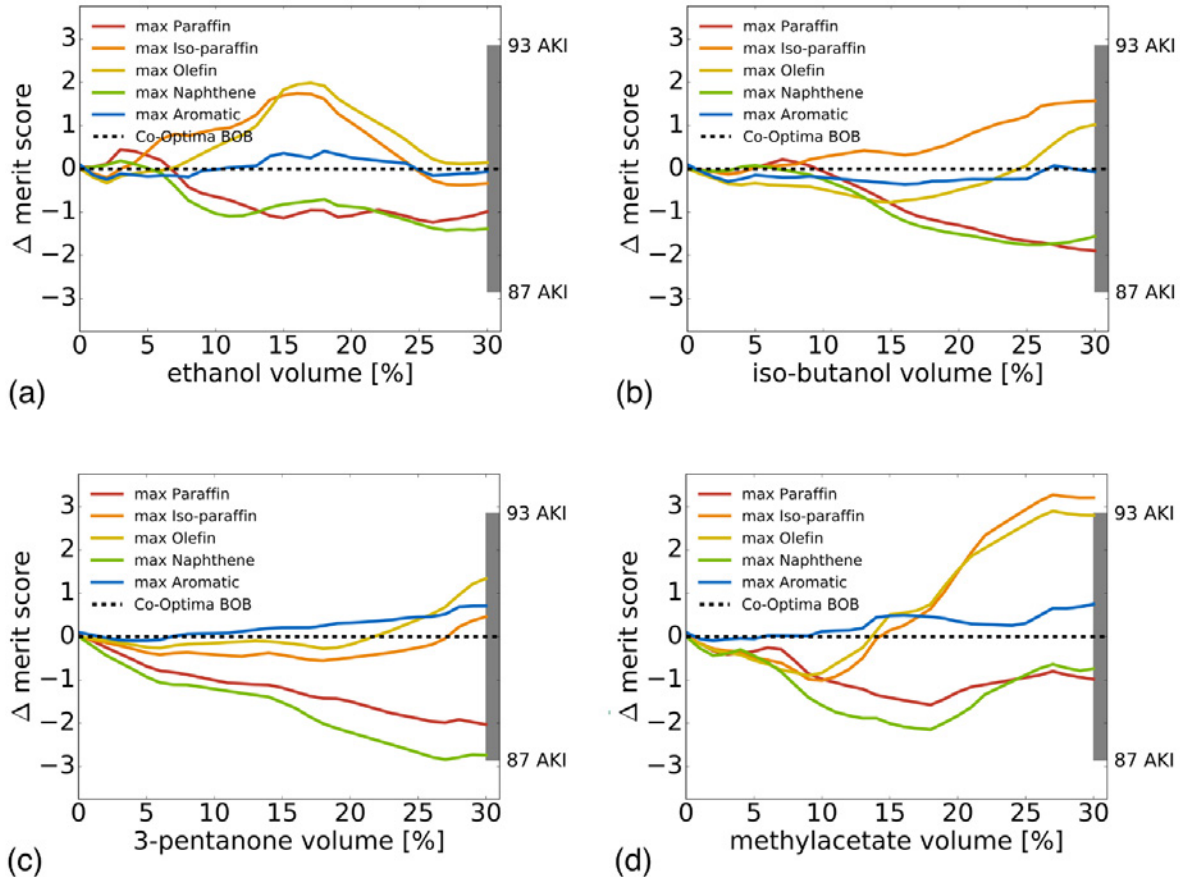


Figure II.27.2. Variation of the merit score across the four-component Co-Optima BOB and the five virtual BOBs as a function of blending level of four blendstocks: (a) ethanol, (b) iso-butanol, (c) 3-pentanone, and (4) methylacetate

The first step of the validation process is to blend and test the five virtual BOB compositions. The neural network octane model has root mean square error of about one octane number for both RON and MON [4]. As a consequence, it is improbable that all five virtual BOBs will have octane ratings within the reproducibility limits of the ASTM tests (0.7 RON and 0.9 MON with 95% confidence). To accelerate the validation process, a total of ten BOBs is tested in the first round: one set of five that matches the compositions in Figure II.27.1, and another set of five for which the RON is predicted to be two octane numbers lower based on the addition of a low-octane component. By using two compositions for each maximized PIONA class, any BOBs that are outside the reproducibility range can be adjusted to the appropriate octane rating using a locally linear blending approximation. Only n-heptane was considered to lower the BOB octane rating originally. However, the model predicted that the addition of n-heptane to the max-iso-paraffin and max-olefin BOBs significantly reduced the synergistic blending performance. N-pentane is used instead to reduce the RON for these two BOBs, with no noticeable reduction in the synergistic behavior predicted by the neural network model.

The model octane number predictions from the neural network are compared to the ASTM standard measurements D2699 and D2700 in Table II.27.1. The mean absolute error across all ten tests is 1.6 RON and 1.9 MON. This agreement is quite good considering these are true predictions for previously untested

fuel compositions with twice as many components as most of the training data for the neural network. Three BOB compositions are found to match the tested octane rating of the four-component Co-Optima BOB: the max-olefin minus 2 RON, max-naphthene, and max-aromatic. While the virtual fuel search did not find all five BOBs in the first round of testing, the model did reasonably well to predict the change in RON due to the addition of a low-octane component. The target change was a difference of 2 RON, and the true change is observed to be between 1.4 and 2.0. Therefore, it is expected that the composition for the max-paraffin and max-iso-paraffin will be found in the next round of testing using the linear approximation.

Table II.27.1. Comparison of the Neural Network Model Predictions for Octane Numbers and the ASTM Standard Measurements D2699 and D2700

BOB	Model RON	RON (D2699)	Model MON	MON (D2700)
Max Paraffin	90.3	89.5	84.6	83.2
Max Paraffin – 2 RON	88.3	87.8	83.3	81.9
Max Iso-Paraffin	90.2	94.0	84.6	88.3
Max Iso-Paraffin – 2 RON	88.2	92.6	82.6	87.3
Max Olefin	90.2	92.5	84.6	86.3
Max Olefin – 2 RON	88.3	90.9	82.8	85.5
Max Naphthene	90.3	89.6	84.6	85.4
Max Naphthene – 2 RON	88.3	87.6	83.4	84.4
Max Aromatic	90.3	90.4	84.6	85.3
Max Aromatic – 2 RON	88.2	88.4	82.8	83.6

Conclusions

This project developed a simulation-based approach to assess the applicability of the CFH when using BOB octane ratings to predict blending performance. Once experimentally validated, the results of this project will open the door for model-based fuel optimization, which could help refiners save money and energy designing a BOB for new blendstocks. There are four key accomplishments from Fiscal Year 2018.

- The simulation of the blending performance indicated that the Central Fuel Hypothesis is unlikely to be valid for the BOB octane ratings.
- Strong BOB composition dependencies ($\Delta\text{Merit} > 3$) were found for 11 of the bio-derived blendstocks tested by McCormick et al. [3].
- Six high-performance blendstocks (ethanol, iso-butanol, methylacetate, 3-pentanone, 2-methylfuran, and diisobutylene) with $\Delta\text{Merit} > 3.5$ were selected by the Co-Optima Fuel Properties Team at National Renewable Energy Laboratory for experimental validation.
- The mean absolute error in the neural network octane prediction was found to be 1.6 RON and 1.9 MON for ten new samples created from the virtual BOB compositions.

Key Publications

1. Whiteside, Russell. 2018. "Prediction of RON and MON of Gasoline Surrogates by Neural Network Regression of Ignition Delay Times and Fuel Properties." AEC Working Group Meeting, Lemont, IL, January 29–February 1.
2. McNenly, Matthew. 2018. "Prediction of RON and MON of Gasoline Surrogates by Neural Network Regression of Ignition Delay Times and Fuel Properties." AEC Working Group Meeting, Lemont, IL, January 29–February 1.

References

1. “Efficiency Merit Function for Spark Ignition Engines: Revisions and Improvements Based on FY16–17 Research and Development.” Technical Report, edited by Paul C. Miles. 2017.
2. Mehl, Marco, Scott Wagnon, Kuiwen Zhang, Goutham Kukkadapu, William Pitz, Charles Westbrook, Yingjia Zhang, et al. 2017. “A Comprehensive Detailed Kinetic Mechanism for the Simulation of Transportation Fuels.” 10th US National Combustion Meeting, paper 1A17, College Park, MD, April 23–26.
3. McCormick, Robert, Gina Fioroni, Lisa Fouts, Earl Christensen, Janet Yanowitz, Evgueni Polikarpov, Karl Albrecht, Daniel Gaspar, John Gladden, and Anthe George. 2017. “Selection Criteria and Screening of Potential Biomass-Derived Streams as Fuel Blendstocks for Advanced Spark-Ignition Engines.” *SAE International Journal of Fuels and Lubricants* 10 (2): 442–460. <https://doi.org/10.4271/2017-01-0868>.
4. Whiteside, Russell. 2018. “Prediction of RON and MON of Gasoline Surrogates by Neural Network Regression of Ignition Delay Times and Fuel Properties.” AEC Working Group Meeting, Lemont, IL, January 29–February 1.
5. McNenly, Matthew, Russell Whitesides, and Daniel Flowers. 2015. “Faster Solvers for Large Kinetic Mechanisms Using Adaptive Preconditioners.” *Proceeding of the Combustion Institute* 35: 581–587. <https://doi.org/10.1016/j.proci.2014.05.113>.
6. Farrell, J., J. Holladay, and R. Wagner. 2017. “Fuel Blendstocks with the Potential to Optimize Boosted Spark-Ignition Engine Performance: Identification of Five Chemical Families for Detailed Evaluation.” Technical Report, National Renewable Energy Laboratory.
7. Whitesides, Russell, and Matthew McNenly. 2017. “Meta-models for Ignition Delay Times with Applications to Surrogate Fuel Mixture Generation.” 10th US National Combustion Meeting, paper 2A18, College Park, MD, April 23–26.

Acknowledgements

Russell Whitesides of Lawrence Livermore National Laboratory is acknowledged for the development of the neural network model for RON and MON prediction. This work was performed under the auspices of the U.S. Department of Energy by Lawrence Livermore National Laboratory under Contract DE-AC52-07NA27344.

II.28 Engine Simulations in Support of Co-Optima (Argonne National Laboratory)

Sibendu Som, Principal Investigator

Argonne National Laboratory (ANL)
9700 S. Cass Avenue
Lemont, IL 60439
E-mail: ssom@anl.gov

Kevin Stork, DOE Technology Development Manager

U.S. Department of Energy
E-mail: Kevin.Stork@ee.doe.gov

Start Date: October 1, 2017	End Date: September 30, 2018	
Project Funding (FY18): \$655,000	DOE share: \$655,000	Non-DOE share: \$0

Project Introduction

Knock is a major bottleneck to achieving higher thermal efficiency in spark-ignited engines. The overall tendency to knock is highly dependent on fuel anti-knock quality as well as engine operating conditions. It is, therefore, critical to gain a better understanding of fuel–engine interactions in order to develop robust knock mitigation strategies. Accurate prediction of engine knock in computational fluid dynamics (CFD) simulations necessitates incorporating both fuel autoignition and flame speed characteristics. Conventional spark ignition turbulent combustion models, however, only account for fuel ignition chemistry in a reliable fashion, while depending on empirical correlations for laminar flame speed. These empirical correlations are valid for only certain simple fuel mixtures and limited pressure-temperature-equivalence ratio ranges, hence cannot be extended to more complex and realistic multi-component fuel blends and engine operating conditions. Therefore, an improved knock modeling framework wherein a laminar flame speed lookup table generated *a priori* from a chemical kinetic mechanism could be used to provide flame speed as an input to the simulation, instead of conventional empirical correlations. In addition, a homogeneous reactor multi-zone model was employed to predict end-gas autoignition ahead of the flame front and post-flame oxidation in the burned zone. This methodology was implemented in a three-dimensional (3D) virtual Cooperative Fuel Research (CFR) engine simulation tool and was demonstrated to be able to capture mean values of combustion phasing, knock onset, and knock intensity with high accuracy. The novel virtual CFR engine model was then leveraged to numerically investigate the validity of Co-Optima central fuel property hypothesis under a representative boosted stoichiometric spark ignition condition using virtual four-component fuel blends having different compositions. It was observed that fuel research octane number and motor octane number were sufficient to provide an indication of knock-limited performance irrespective of fuel composition. However, laminar flame speed was found to affect knock-limited combustion phasing when its variation among the fuel blends was higher than 20%.

Objectives

Overall Objectives

- Develop a virtual CFR engine model based on 3D CFD
- Develop a robust knock modeling approach incorporating fuel effects
- Perform numerical studies of fuel–engine interactions
- Develop a CFD engine model for the Oak Ridge National Laboratory multi-cylinder engine
- Investigate fuel property effects on combustion at practical engine conditions
- Generate virtual engine map for vehicle simulation at practical driving cycles

Fiscal Year 2018 Objectives

- Validate the 3D CFD model against experimental data
- Perform a numerical investigation of Co-Optima central fuel property hypothesis
- Validate the 3D CFD model and develop an efficient approach for knock-limited spark advance (KLSA) prediction
- Investigate fuel property effects with local sensitivity and global sensitivity analysis

Approach

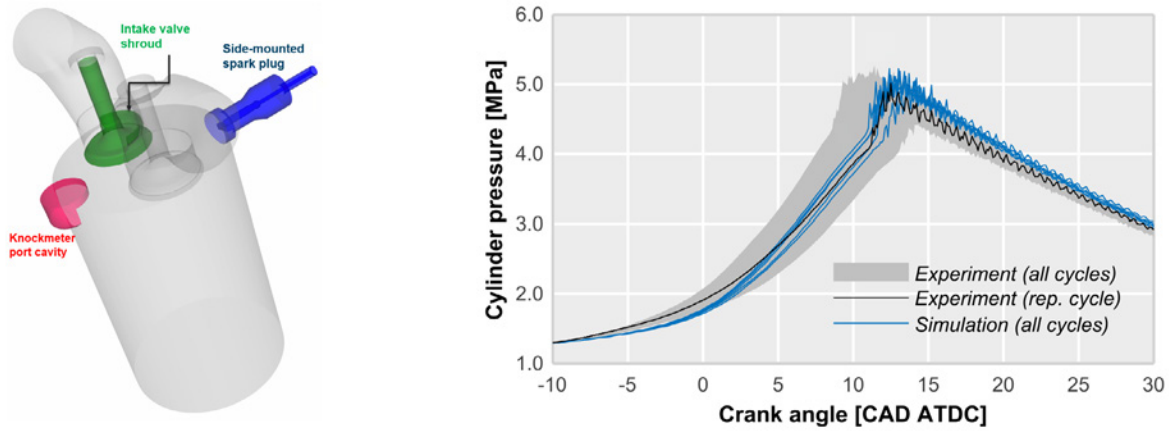
The first phase involved CFD model development and validation. It was carried out in two stages. First, the CFR engine cylinder/head assembly at ANL was scanned to generate a 3D solid geometry file. The solid geometry was then used to develop a surface mesh of the CFR engine. A CFD model was then developed employing the surface mesh and incorporating the combustion model described in the “Project Introduction” section. Next, multi-cycle CFD simulations were performed at different operating conditions (normal spark ignition, light knock, heavy knock), and the numerical results were validated against experimental data available from the Argonne CFR engine. The experiments were performed by Dr. Chris Kolodziej. In addition, boundary conditions for the CFD simulations were obtained from a GT-Power model developed by Seungmok Choi and Chris Kolodziej at ANL. The predictive capability of the CFD model was then assessed with respect to various combustion metrics, such as combustion phasing, knock onset, and knock intensity. In the second phase, a numerical study of central fuel property hypothesis under boosted (beyond research octane number) operating conditions was performed using the validated CFR engine model. Four toluene primary reference fuel–biofuel surrogates with identical research octane number (= 98) and motor octane number (= 90) were generated using a neural network regression model developed by Russell Whitesides and Matthew McNenly at Lawrence Livermore National Laboratory. Three biofuels were included in the analysis: diisobutylene (DIB), anisole, and isobutanol. To perform CFD simulations, reduced kinetic mechanisms were developed in collaboration with Prof. Tianfeng Lu (at University of Connecticut) to model the surrogates’ chemistry. The reduced mechanisms were generated from the Co-Optima detailed mechanism developed by Bill Pitz and coworkers at Lawrence Livermore National Laboratory. Thereafter, spark timing sweeps were numerically performed for the four virtual surrogates. The knock-limited combustion phasing was determined for each surrogate and compared with the corresponding values for other blends.

A CFD model was developed for the Oak Ridge National Laboratory engine using CFD software CONVERGE. The modeled engine was X-ray scanned to provide geometry for the simulation effort. A combustion model developed by Pinaki Pal at ANL was employed, wherein the turbulent flame propagation is modeled by level-set G-Equation model, and end-gas autoignition is modeled by detailed chemical kinetics calculation. Boundary conditions were provided by GT-Power one-dimensional simulation by Dean Edwards at Oak Ridge National Laboratory. The engine model was validated against experiments performed by Scott Sluder at Oak Ridge National Laboratory and was shown to give good predictions for in-cylinder pressure traces, combustion phasing, and cyclic variability with multi-cycle simulations. An efficient approach for KLSA prediction was then developed, wherein the slope change point in maximum knock intensity is used to define knock onset. With the validated CFD model and KLSA prediction approach, the heat of vaporization (HoV) effect on knock mitigation was investigated by numerically varying the HoV value of the baseline case within +/- 10% range. The analysis was then extended to several fuel properties, including density, HoV, heat capacity, and viscosity, by using global sensitivity analysis. Virtual engine maps for 100% and 115% HoV were also generated by CFD simulations and used in Autonomie simulations by Ram Vijayagopal and Ayman Moawad at ANL.

Results

- The technical goal of developing a new knock modeling framework was attained.
- The technical objective of developing and validating the virtual CFR engine model was completed. The CFD model accurately predicted mean values of combustion phasing, knock onset, and knock intensity within the uncertainty of 1 crank angle degree (CAD), 0.5 CAD, and 0.1–0.3 bar, respectively.

- The FY 2018 goal of studying the central fuel property hypothesis using the virtual CFR engine model was achieved, as shown in Table II.28.2. as shown in Figure II.28.1 and Table II.28.1. Figure II.28.2 shows the contour plots for OH, CH₂O, and pressure, clearly showing the regions of knock onset.



ATDC – after top dead center

Figure II.28.1. (left) CFR engine geometry (red: knockmeter port cavity; green: intake valve with 180° shroud; blue: spark plug and cavity). (right) Temporal evolution of in-cylinder pressure for both experiment and simulation (spark timing: -13 CAD ATDC).

Table II.28.1. Mean Knock Characteristics from Experiments and Simulations

Knock characteristic	Experiment	Simulation
Mean knock intensity	2.3 bar	2.57 bar
Mean knock point	11.15 CAD ATDC	11.30 CAD ATDC
Mean combustion phasing	7.6 CAD ATDC	7.4 CAD ATDC

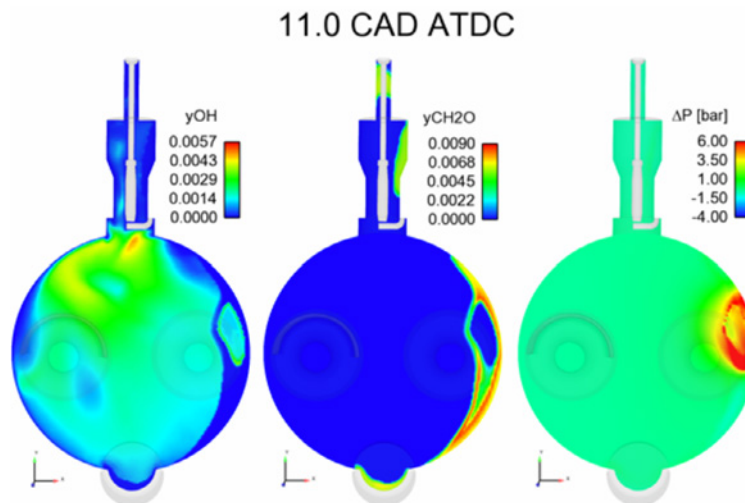


Figure II.28.2. Contour plots of OH and CH₂O mass fractions and local pressure difference on a horizontal cut plane passing through the spark plug electrode, at knock onset. Intake and exhaust valves are located on the left and right sides, respectively. Knockmeter port cavity can be seen at the bottom.

Table II.28.2. Results from the Study of Central Fuel Property Hypothesis: Knock-Limited Combustion Phasing (CA50) of the Virtual Surrogates. The numbers in the first column represent the volume percentage of biofuel in the corresponding four-component surrogate.

Fuel Surrogate	Knock-Limited CA50 (CAD ATDC)
DIB30	20.2
DIB50	20.4
Isobutanol10	19.5
Anisole20	18.0

- A new approach of KLSA prediction using large Mach Courant–Friedrichs–Lewy (CFL) number was proposed, which accounts for cyclic variation and allows at least three times faster simulation turn-around time.
- Local sensitivity analysis of HoV on knock mitigation shows that 10% change in HoV leads to 1.13 CAD change in KLSA for Co-Optima alkylate fuel at 11.5 bar indicated mean effective pressure (IMEP) condition.
- At the same engine condition, global sensitivity analysis shows that HoV is the most important property on indicated thermal efficiency, among other fuel physical properties.

Figure II.28.3 (left) shows the knock intensity predicted by CFD simulation using CFL 50 as a function of spark timing. At each spark timing, 10-cycle simulation was performed, as indicated by the gray dots. The maximum knock intensity is highlighted by the red dot, and its slope change point indicates the KLSA location, which is in good agreement with the corresponding experimental value (green dashed line). The result predicted with CFL 5 is also presented by the blue dot, which shows a consistent prediction of KLSA in spite of the different CFL number used. This approach has also been validated for different fuels and different operating conditions with similar accuracy. The efficient CFD approach allows quick turn-around time for a large amount of simulation in global sensitivity analysis as well as when generating virtual engine maps for vehicle simulation. The global sensitivity analysis is currently focusing on fuel density, HoV, heat capacity, and viscosity, and it requires 800 simulations. The sensitivity index for indicated thermal efficiency is shown in Figure II.28.3 (right). It is seen that the HoV is the most important physical property, which is inconsistent with previous findings on the Sandia direct injection spark ignition engine studied by Noah Van Dam at ANL. Local sensitivity analysis of HoV effects on knock mitigation was also performed by numerically varying the HoV value within 90–110% of the baseline value.

Figure II.28.4 (left) shows maximum knock intensity for different HoVs, and the KLSA locations are indicated by the red dots. A clear trend of knock mitigation by increased HoV is observed, and the slope of linear fit shows that 10% change in HoV results in 1.13 CAD change in KLSA. Focusing on 100% HoV and 115% HoV, simulations were performed at multiple speed and load conditions to generate virtual engine maps that can be used in Autonomie vehicle simulation. Figure II.28.4 (right) shows the improvement in brake specific fuel consumption (BSFC) with higher HoV. It is seen that the largest difference is located in the higher load area, which is less relevant to practical driving conditions, such as Urban Dynamometer Driving Schedule and Highway Fuel Economy Test. However, a greater benefit is the potential for applications of dynamic skip fire or split hybrid vehicles.

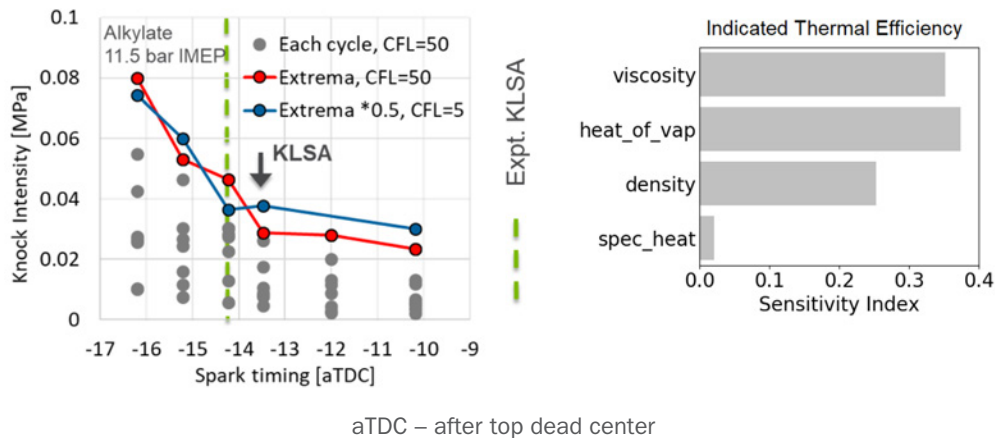


Figure II.28.3. (left) Knock intensity as a function of spark timing. Grey dot: knock intensity from each cycle CFD result with Mach CFL 50; red dot: maximum knock intensity at each spark timing with Mach CFL 50; blue dot: maximum knock intensity divided by two at each spark timing with Mach CFL 5. CFL number controls CFD time-stepping method, and larger value indicates large time step and faster simulation time. (right) Sensitivity index indicated thermal efficiency.

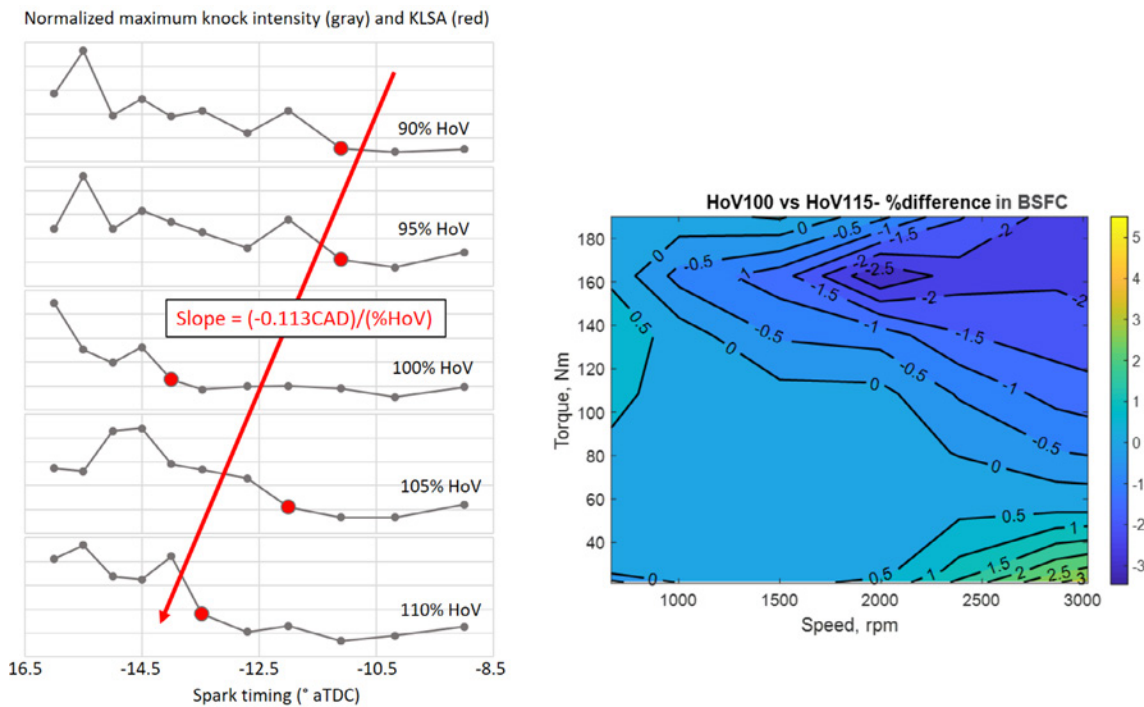


Figure II.28.4. (left) Maximum knock intensity for different HoV values. KLSA predicted by the slope change point is highlighted by red dot. (right) Relative difference in BSFC for two HoVs. Negative value means lower BSFC for 115% HoV.

Conclusions

- The new knock modeling framework allows for numerical study of any fuel blend of interest and accounts for end-gas autoignition and turbulent flame propagation in a robust manner.
- The virtual CFR engine model can accurately predict mean values of combustion phasing, knock onset, and knock intensity under a wide range of engine operating conditions.

- Fuel research octane number and motor octane number are sufficient to provide an indication of knock-limited performance irrespective of fuel composition. However, laminar flame speed can affect knock-limited combustion phasing when its variation from one fuel blend to another is higher than 20%.
- An efficient CFD approach for direct injection spark ignition engines has been proposed and validated against Oak Ridge National Laboratory multi-cylinder engine experiments in terms of pressure traces, combustion phasing, cyclic variability, and KLSA.
- Sensitivity analysis of HoV on knock mitigation shows that 10% change in HoV leads to 1.13 CAD change in KLSA.
- Global sensitivity analysis shows that HoV is the most important physical property for indicated thermal efficiency, which is consistent with findings on the Sandia direct injection spark ignition engine.
- Virtual engine maps have been generated for different HoV values and can be used to investigate the HoV effect in vehicle simulation under practical driving cycles.

Key Publications

1. Pal, Pinaki, Yunchao Wu, Tianfeng Lu, Sibendu Som, Alexandra LeMoine, and Yee Chee See. 2018. "Multidimensional Numerical Simulations of Knocking Combustion in a Cooperative Fuel Research Engine." *Journal of Energy Resources Technology* 140 (10): 102205.
2. Pal, Pinaki, Christopher Kolodziej, Seungmok Choi, Sibendu Som, Alberto Broatch, Josep Gomez-Soriano, Yunchao Wu, Tianfeng Lu, and Yee Chee See. 2018. "Development of a Virtual CFR Engine Model for Knocking Combustion Analysis." SAE Technical Paper (accepted for publication in *SAE International Journal of Engines*).
3. Yue, Z., D. Edwards, S. Sluder, and S. Som. 2018. "Prediction of Cyclic Variability and Knock-Limited-Spark-Advance (KLSA) in Spark Ignition Engines." *Proceedings of the ASME 2018 Internal Combustion Engine Division Fall Technical Conference*, ICEF2018-9605, San Diego, CA, November 2018.
4. Van Dam, N., M. Sjöberg, and S. Som. 2018. "Large-Eddy Simulations of Spray Variability Effects on Flow Variability in a Direct-Injection Spark-Ignition Engine under Non-Combusting Operating Conditions." SAE Technical Paper 2018-01-0196, DOI:10.4271/2018-01-0196.
5. Van Dam, N., K. Kalvakala, E. Boink, Z. Yue, and S. Som. "Sensitivity Analysis of Fuel Physical Property Effects on Spark Ignition Engine Performance." In preparation.

Acknowledgements

This research was funded by DOE's Office of Vehicle Technologies and Office of Energy Efficiency and Renewable Energy under Contract No. DE-AC02-06CH11357. The principal investigator gratefully acknowledges the contributions of Dr. Pinaki Pal for the CFR engine simulations, Dr. Zongyu Yue for Oak Ridge National Laboratory engine simulations, and Dr. Noah Van Dam for Sandia direct injection spark ignition engine simulations under the Co-Optima project. The authors wish to thank Gurpreet Singh, Kevin Stork, Michael Weismiller, and Alicia Lindauer, program managers at DOE, for their support. This research was conducted as part of the Co-Optimization of Fuels & Engines (Co-Optima) project sponsored by the DOE Office of Energy Efficiency and Renewable Energy, Bioenergy Technologies and Vehicle Technologies Offices. The authors would also like to acknowledge the high-performance computing center at the National Renewable Energy Laboratory for computing time on the Peregrine cluster as well as the Laboratory Computing Resource Center at ANL for computing time on the Blues cluster, which were used in this research.

II.29 Characterization of Biomass-Based Fuels and Fuel Blends for Low-Emissions, Advanced Compression Ignition Engines (The University of Alabama)

Ajay K. Agrawal, Principal Investigator

The University of Alabama
Box 870279, 3047 H.M. Comer, 247 7th Ave.
Tuscaloosa, AL 34587
Email: aagrawal@eng.ua.edu

Michael Weismiller, DOE Technology Development Manager

U.S. Department of Energy
E-mail: Michael.Weismiller@ee.doe.gov

Start Date: May 1, 2017

End Date: April 30, 2020

Project Funding: \$630,493

DOE share: \$567,301

Non-DOE share: \$63,192

Project Introduction

The ultimate goal of this project is to accelerate deployment of co-optimized fuels and engines that will reduce fuel consumption and criterion pollutant and greenhouse gas emissions. Specifically, we will acquire combustion measurements in a constant-pressure flow rig (CPFR) with optical access and develop models to predict combustion characteristics based on known fuel and ambient conditions. We are targeting prediction of properties relevant to lean lifted flame combustion, a mixing-controlled low-temperature combustion strategy to reduce soot production in advanced compression ignition engines. Unlike other low-temperature combustion strategies that rely upon chemical kinetics, the combustion or heat release rate in lean lifted flame combustion can be controlled by the fuel injection timing.

Objectives

Overall Objectives

- Experimentally investigate fuel-air mixing and subsequent ignition and combustion processes and properties in different fuel injection regimes, with particular focus on supercritical fuel injection when the surface tension is no longer present. At these conditions, the mixing of the dense supercritical fluid with the ambient air depends mainly upon the influence of turbulence and real-gas effects on thermodynamics and transport properties.
- Identify synergistic opportunities offered by biofuels and their blends with conventional fuels. We seek to analyze the relationship between fuel physical/chemical properties and combustion properties to co-optimize fuels and advanced compression ignition engines.
- Perform experiments in a flexible, modular, and optically accessible flow rig (available at The University of Alabama) with a continuous supply of preheated compressed air to attain the desired pressure and temperature within the chamber volume. The ability to rapidly rinse the test chamber permits acquisition of statistically significant experimental sample sizes and will allow us to collect extensive data sets for a range of test conditions and biofuel blends.
- Utilize a suite of time-resolved optical diagnostics techniques: rainbow schlieren deflectometry technique to examine fuel-air mixing and turbulent flame speed, OH* chemiluminescence to quantify turbulent flame structure, and two-color pyrometry to characterize the soot production.
- Develop a neural network to model functional relationships between fuels' physical/chemical properties and ignition/combustion characteristics. The models will be validated against secondary sets of data not used for the initial development.

Fiscal Year 2018 Objectives

- Integrate time-resolved diagnostics systems to the test facility
- Develop image post-processing techniques
- Develop neural network model framework

Approach

The project will systematically investigate fuel-air mixing and subsequent ignition and combustion processes in trans- and super-critical regimes at diesel conditions. Selected experiments will also be conducted at subcritical conditions for baseline comparisons. Proposed experiments are being conducted in a CPFR with a continuous supply of preheated compressed air to attain the desired pressure and temperature within the chamber volume. In this CPFR, the time between tests is greatly reduced (~ 0.2 Hz) by upstream control of the ambient conditions to create bulk air (or inert gas) flow rates that are minimal compared to the fuel jet velocity. High-fidelity data will be acquired simultaneously by three different optical diagnostics techniques at high temporal and spatial resolutions. These techniques will focus on different regions of the jet/flame and provide not only the time-averaged measurements, but also help delineate the instantaneous flow and chemical features. Phenomena such as autoignition, flame stabilization, and soot formation can be observed simultaneously in real-time, which will improve our understanding and also provide benchmark data for computational fluid dynamics code development.

The fuel property prediction model will be developed as a neural network. A neural network is made up of input nodes (test conditions) and output nodes (combustion properties). Between these input/output node layers are any number of hidden layers where each node represents some weighted and biased transfer function that considers all possible input effects. The remaining hidden layers build on this layering effect to account for all possible first and secondary input-to-output interactions. The gains and biases in the hidden layers are determined by training the network with known data. After validating against other known data not used for training, the network can function as fuel-based combustion property predictor.

Results

- Key milestones have been met, and the project budget is on track
- Refined and optimized optical configuration of the two-color pyrometry system
- Integrated rainbow schlieren deflectometry, OH* chemiluminescence, and two-color pyrometry systems and demonstrated synchronous image acquisition
- Upgraded air compressor support system to expand experimental test range
- Developed the framework for the neural network modeling approach

Two-Color Pyrometer

In the previous year, a preliminary design of a two-color pyrometer system was presented. In the past year, significant effort has gone into developing rigorous understanding of the factors that affect the estimates of spatially and temporally resolved soot temperature. A two-color pyrometer measures light emission at two different wave lengths and relates them to the temperature of a non-black emitter such as a soot particle. The existing system designs use a beam splitter and various mirrors to redirect the image onto a camera. Of particular importance is the refinement of the design to ensure that each image path has the same length and the same number of mirrors. Other designs in literature either ignore these effects or attempt to compensate for these design features in post processing. By eliminating these differences in the optical design of our system, errors associated with optical discrepancies in the two light ray paths are eliminated.

Figure II.29.1 shows the optical system together with sample images of a reacting n-heptane spray captured without the bandpass filters in place. These initial results demonstrate the ability to acquire two (identical) images of sooting spray on a single camera, thereby eliminating the optical distortions introduced by

differences in optical path lengths and, thus, light intensity reaching the camera sensor. Future work will use this system to reduce measurement errors in the experiments.

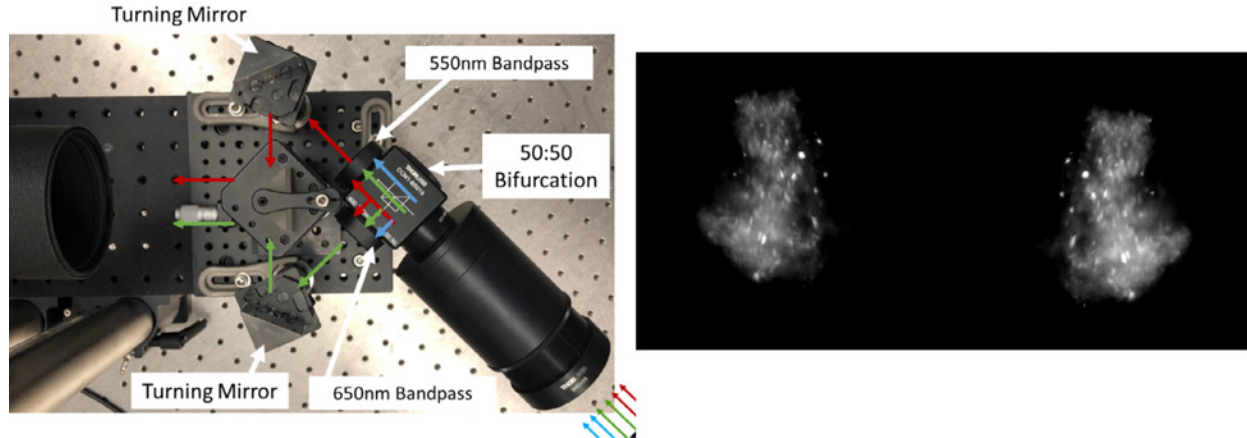


Figure II.29.1. Updated two-color pyrometer design illustrating equal path lengths and equal number of components (left) and sample images of a sooting n-heptane flame with the bandpass filters removed (right). Note the images appear horizontally flipped due to beam splitter reflecting 50% of light and letting 50% pass straight.

Simultaneous Rainbow Schlieren Deflectometry, Two-Color Pyrometer, OH Chemiluminescence Acquisition*

A key aspect enabling the overall project goals is the ability to capture three key optical diagnostics simultaneously at high speed. Figure II.29.2 illustrates how the diagnostics hardware is configured around the CPFR. This includes the two-color pyrometer, OH* chemiluminescence system, and schlieren light source on one side of the chamber, and the schlieren camera on the other side. This configuration was determined to provide the best fields of view and viewing angle for each diagnostic. Further, Figure II.29.3 presents initial results of the simultaneous capture of the three diagnostics applied to a simple Bunsen burner setup. These images were acquired with the setup shown in Figure II.29.2 but with the simple flame instead of the spray inside the actual CPFR to simplify development of the implementation protocols.

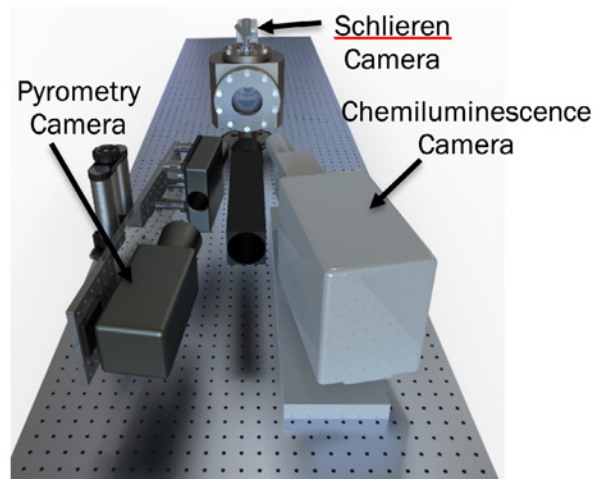


Figure II.29.2. Computer-aided drafting illustration of how the three diagnostics are set up in relation to the CPFR

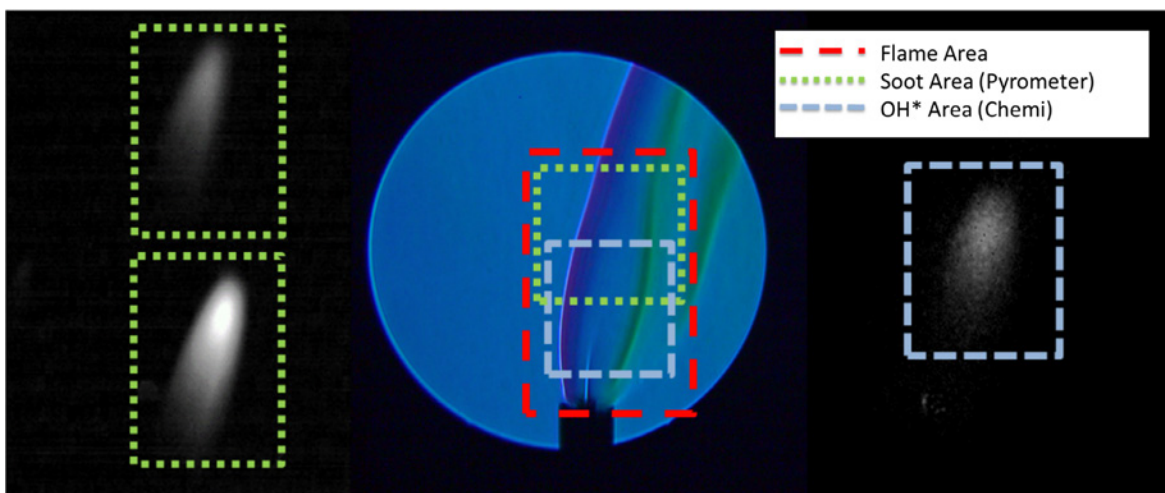


Figure II.29.3. Demonstration of simultaneous two-color pyrometry, rainbow schlieren deflectometry, and OH* chemiluminescence measurements using a simple Bunsen burner

Upgrade of the Air Compressor to Expand the Operating Range of Experiments

In our original system, the operating pressure of the CPFR was limited to 30 bar based on the available compressor capacity. This year, we installed a new compressor to expand the test range capability of the CPFR up to the designed specifications of up to 60 bar and 1,000 K. Figure II.29.4 shows the new compressor, which has been installed and integrated with the CPFR. The compressor fills four large compressed gas cylinders that serve as buffer and storage. This new capacity is important to this project by enabling high-pressure test conditions relevant to modern diesel engines.



Figure II.29.4. New high-pressure air compressor that can supply up to 150 bar continuous air flow and enables testing at the full capacity of the current CPFR at 60 bar

Neural Network Analysis

A neural network model was developed to predict the liquid length of a diesel-like spray under evaporating conditions. While this prediction is well established by Seibers' liquid length model based on fundamental physics, the present model serves to demonstrate that a neural network model can capture the essential physics once well trained. Based on the extensive data set in the Sandia Engine Combustion Network, the neural network was built to predict liquid length based on ambient density, temperature, nozzle diameter, and fuel type (cetane [CET] or hepta-methyl-nonane [HMN]). Most of the liquid data in the Engine Combustion Network is for cetane with a nozzle diameter of 246 μm , while there are a few tests with a larger nozzle diameter and with HMN. The results in Figure II.29.5 show best agreement for the cetane fuel across the density and temperature range while also capturing the nozzle diameter effect. For HMN the network does a reasonable job in the regions where experimental data is available but shows non-physical behavior at low temperature and higher density, where there is no experimental data. This behavior illustrates the need for large data sets that span the expected range of prediction on which the neural networks can be built. As with any model, the ability to extrapolate beyond measured data is limited.

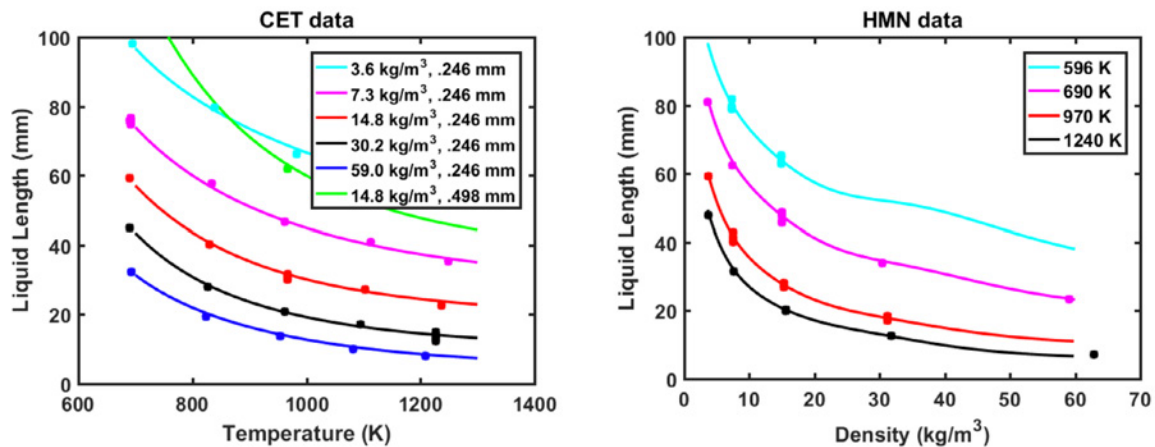


Figure II.29.5. Demonstration of neural network prediction of liquid length data from the Engine Combustion Network hosted by Sandia National Laboratories. Symbols are data from experiments and lines represent predictions from the neural network.

Conclusions

We have expanded capabilities of the CPFR facility to operate at higher pressures than previously possible. The two-color pyrometry system has been developed with a much refined optical setup. The three time-resolved optical diagnostic techniques have been applied independently, and their integration to acquire simultaneous images has been demonstrated. The framework for neural network models has been developed and verified using liquid length data in Engine Combustion Network. We are finalizing test conditions to acquire detailed data using single-component fuels.

Acknowledgements

Professor Joshua Bittle of The University of Alabama is the co-principal investigator for this project. We would like to thank Chuck Mueller of Combustion Research Lab at Sandia National Laboratories for technical guidance and input on various aspects of this project. Thanks also to Ralph Nine, Program Manager at National Energy Technology Laboratory.

II.30 Dynamic Species Reduction for Multi-Cycle CFD Simulations (University of Michigan)

George A. Lavoie, Principal Investigator

University of Michigan
Department of Mechanical Engineering
1231 Beal Avenue
Ann Arbor, MI 48109-2133
E-mail: glavoie@umich.edu

Kevin Stork, DOE Technology Development Manager

U.S. Department of Energy
E-mail: Kevin.Stork@ee.doe.gov

Start Date: April 17, 2017	End Date: September 30, 2018	
Project Funding: \$480,000	DOE share: \$432,000	Non-DOE share: \$48,000

Project Introduction

Full cycle, full chemistry computational fluid dynamics (CFD) simulations form a key part of the Co-Optima program effort of developing suitable fuels for future advanced engines. While full cycle CFD simulations can capture the flow phenomena associated with the intake and exhaust events, single cycle simulations with chemistry are sensitive to the choice of initial conditions and are inadequate to capture prior cycle chemical and/or thermal feedback. Meanwhile, the auto-ignition and compression ignition combustion modes present in both the Virtual Cooperative Fuels Research (CFR) spark ignition engine and advanced compression ignition (ACI) engine configurations are known to be highly sensitive to these effects. Multi-cycle CFD simulations can capture this cyclic feedback but are prohibitively expensive computationally. The existing species reduction methods of reducing this cost rely on user intervention to define the species of interest and suffer from potentially large errors if important intermediate species are erroneously removed from the computation. This project proposes new methods of increasing computational efficiency for multi-cycle simulations while maintaining accuracy by dynamic species reduction (DSR) during open valve events, thereby retaining the species of greatest importance to cyclic feedback effects.

Objectives

The goal of this project is to provide CFD tools that will reduce the computational expense of a full engine cycle simulation with chemistry by 80% relative to the state of the art and enable the Co-Optima team to efficiently perform multi-cycle simulations to capture prior cycle compositional and thermal effects while improving numerical accuracy. Co-Optima's Simulation Toolkit Team is developing engine CFD simulation tools for use in several areas of the program, including facilitating the development of fuel surrogates for bio-fuels and gasoline/bio-fuel blends in a Virtual CFR engine, modeling the research octane number and motor octane number tests, and providing insight for the development of advanced ACI engines.

Overall Objectives

- Develop a method of dynamically reducing the number of species fluxed during gas exchange to reduce the computational expense of the transport equations by 90% while the valves are open
- Improve multi-zone chemistry binning methods to enhance computational efficiency during the expansion stroke, where temperatures are high and the charge composition contains primarily product species

Fiscal Year 2018 Objectives

- Obtain engine and operating conditions for simulation, chemical mechanisms, and surrogates to be used for project simulations

- Obtain CFR and ACI meshes from national lab activities
- Complete baseline ACI and CFR multi-cycle simulations with chemistry active throughout cycle
- Complete implementation of DSR routines into CONVERGE
- Identify CFR and ACI conditions with cyclic coupling
- Validate the DSR model and refine as needed

Approach

Starting with prior work in species reduction and multi-zone binning in the open source KIVA framework, the approach is to develop improved methods and to incorporate them into the CONVERGE CFD code with active collaboration with Convergent Sciences. This is intended to ensure broad accessibility for the computational community, including the Co-Optima fuels project. Collaboration is also ongoing with the computational group at Argonne National Laboratory (ANL), which is providing baseline information on detailed CFD simulations of CFR and ACI engines that will be used as baseline to validate the new computational approaches.

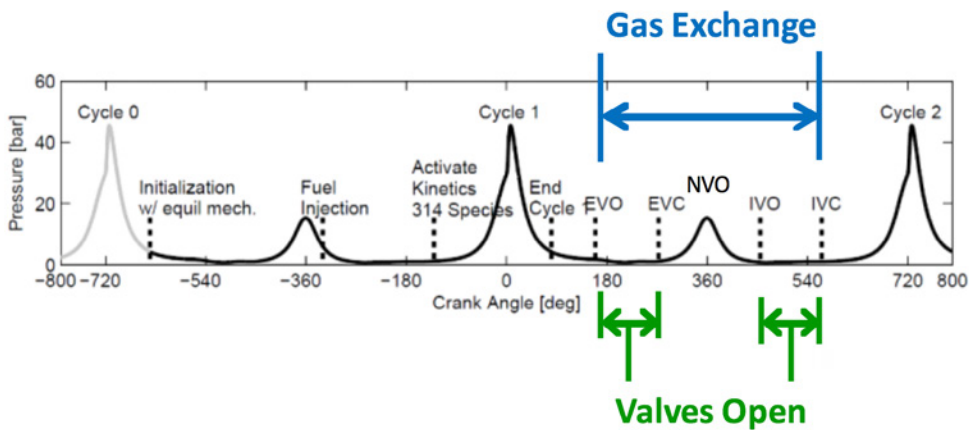
Results

- A chemical kinetic mechanism for primary reference fuel blends currently in use at ANL for Virtual CFR simulations has been provided by ANL.
- Initial simulation conditions based on the Virtual CFR results presented by ANL [1] have been provided to University of Michigan. Operating conditions and results for a boosted spark ignition engine configuration have also been supplied.
- A CONVERGE mesh of the ANL Virtual CFR engine has been provided by ANL as well as an additional mesh for the ACI engine.
- Exploratory full cycle Reynolds-averaged Navier-Stokes simulations have been carried out in KIVA with dynamic species reduction and showed the potential of reducing overall computational cost by 65%.
- Conversion of the KIVA code to the CONVERGE platform is ongoing and expected to be completed in the next quarter.

Exploratory three-dimensional, full cycle Reynolds-averaged Navier-Stokes simulations have been carried out with the dynamic species reduction method at University of Michigan with KIVA-3V modeling an homogeneous charge compression ignition engine using negative valve overlap (NVO) valve events with the fully coupled multi-zone approach [2,3]. A 312-species, four-component gasoline surrogate mechanism [4] was used with a 100,000 cell mesh (at bottom dead center). The project has focused on reducing the cost of the gas exchange calculations, applying the approach at 80° above top dead center main combustion, just before exhaust valve opening, reducing the number of species fluxed and deactivating chemistry calculations while the exhaust valves are open. The species chosen to be eliminated are determined dynamically for each cycle and depend on the state of the charge at that time. Full chemistry is used during the NVO period, and then species reduction is reapplied at intake valve opening (IVO). Figure II.30.1 shows the open valve regions where the species reduction was applied.

Reduction from 312 to approximately 40 species during the open portions of the cycle decreases the cost of the flow calculations by 70% over the entire 720° cycle. By simultaneously deactivating chemistry during the open portions of the cycle, the kinetic expense of the full cycle is reduced by 64%, and the total expense is reduced by 65% relative to a configuration where chemistry is active at all times and all species are fluxed. Despite the reduced compositional fidelity, the DSR approach matched the combustion behavior predicted with all 312 species and chemistry active. The resulting 720° cycle time savings achieved with the KIVA exploratory calculations are summarized in Table II.30.1.

The engine configurations and test conditions to be used in this study have been determined, and the appropriate meshes for the CFR [5] and ACI engines have been received from ANL and are shown in Figure II.30.2. Active simulations will begin with these meshes as soon as the dynamic species mechanism has been successfully transferred into the CONVERGE code.



IVC – intake valve closing; EVC – exhaust valve closing; EVO – exhaust valve opening

Figure II.30.1. Cycle diagram showing gas exchange and open valve periods where species reduction is applied

Table II.30.1. Computational Run-Time Savings Achieved with DSR

Computational Cost (720°)	Full Calculation	DSR and Deactivated Chemistry when Valves Are Open	% Reduction
Flow Time [CPU hr]	223	67	70%
Kinetics Time [CPU hr]	1206	429	64%
Total Time [CPU hr]	1429	496	65%

CPU – central processing unit

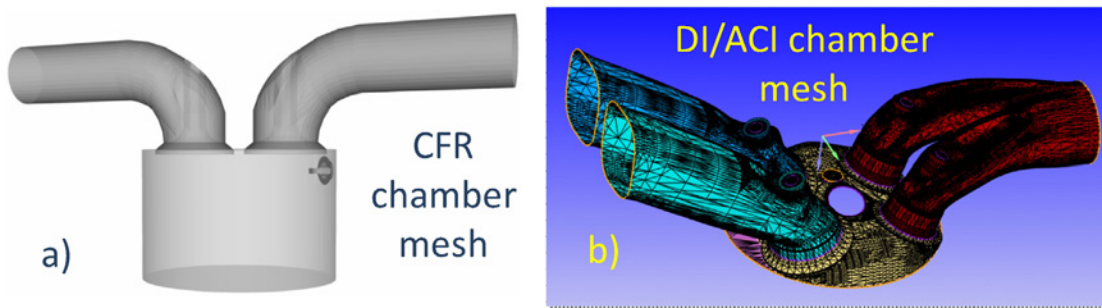


Figure II.30.2. (a) CONVERGE mesh for CFR combustion chamber; (b) Direct injection (DI)/ACI chamber mesh based on Ford 1.6 L, 4-valve pent roof design

Conclusions

- Work so far has demonstrated the potential of DSR to reduce run time by up to 65% for CFD simulations of CFR (spark ignition) and ACI engines with realistic combustion chamber meshes. Greater reduction can be expected with conventional spark ignition valve events, which do not include a negative valve overlap period.
- Full translation of working KIVA code into the CONVERGE framework is expected to be completed in the next quarter.

References

1. Pal, P., Y. Wu, T. Lu, S. Som, Y.C. See, and A. Le Moine. 2017. "Multi-Dimensional CFD Simulations of Knocking Combustion in a CFR Engine." *Proceedings of the ASME 2017 Internal Combustion Engine Division Fall Technical Conference*, Seattle, WA, USA, October 15–18, 2017, paper ICEF2017-3599.
2. Babajimopoulos, A., D.N. Assanis, D.L. Flowers, S.M. Aceves, and R.P. Hessel. 2005. "A Fully Coupled Computational Fluid Dynamics and Multi-Zone Model with Detailed Chemical Kinetics for the Simulation of Premixed Charge Compression Ignition Engines." *International Journal of Engine Research*, Vol. 6, No. 5, 497–512.
3. Kodavasal, J., S. Keum, and A. Babajimopoulos. 2011. "An Extended Multi-Zone Combustion Model for PCI Simulation." *Combustion Theory and Modelling*, Vol. 15, No. 6, 893–910, doi:10.1080/13647830.2011.578663.
4. Mehl, M., W.J. Pitz, C.K. Westbrook, and H.J. Curran. 2011. "Kinetic Modeling of Gasoline Surrogate Components and Mixtures under Engine Conditions." *Proceedings of the Combustion Institute*, Vol. 33, No. 1, 193–200.
5. Pal, P., et al. 2018. "Development of a Virtual CFR Engine Model for Knocking Combustion Analysis." SAE Paper No. 2018-01-0187.

Acknowledgements

Initial simulation configurations and predictions from ANL were provided by Sibendu Som, Pinaki Pal (CFR engine), and Zongyu Yue (DI engine). Convergent Sciences has provided software licenses and technical support to integrate new models into CONVERGE. Integral contributions to this project were provided by Robert J. Middleton and Nicole Sitek of the University of Michigan Department of Mechanical Engineering.

II.31 Micro-liter Fuel Characterization and Property Prediction (Louisiana State University)

Ingmar Schoegl, Principal Investigator

Louisiana State University (LSU)
Mechanical & Industrial Engineering
3261 Patrick F Taylor Hall
Baton Rouge, LA 70803
E-mail: ischoegl@lsu.edu

Michael Weismiller, DOE Technology Development Manager

U.S. Department of Energy
E-mail: Michael.Weismiller@ee.doe.gov

Start Date: March 1, 2017	End Date: February 28, 2020	
Project Funding: \$1,574,444	DOE share: \$1,359,544	Non-DOE share: \$214,900

Project Introduction

The DOE Co-Optima initiative seeks to accelerate the introduction of affordable, scalable, and sustainable high-performance fuels for use in high-efficiency, low-emission engines. Co-optimized fuels and engines offer the opportunity to build on long-term research in both fuels and engines, where advances over the last ten years have identified combustion engine strategies that—especially if optimized to run on new fuels—would offer higher gas mileage and produce less engine-out pollutants than current engines.

The project “Micro-liter Fuel Characterization and Property Prediction” addresses DOE’s stated interest in enabling small-volume (<20 μ L), high-throughput (>100 tests/device/mo) measurements of transportation fuels and blends that are relevant to co-optimized fuels and engines. In this context, the ability to quantify the performance of a fuel in terms of autoignition metrics (e.g., octane number/sensitivity), combustion properties (e.g., flame speed), and physical properties (e.g., volatility and viscosity) is of significant interest. Predictions of fuel performance in a combustion engine require a link to be made between small-volume measurements and combustion behavior of a fuel blend at engine-relevant conditions.

Objectives

The project seeks to establish a foundation for small-volume, high-throughput fuel testing, where relevant fuel metrics are quantified in a micro combustion experiment.

Overall Objectives

- Quantify combustion metrics of transportation fuels (e.g., octane number, flame speed)
- Construct an experimental prototype that can operate at elevated pressures
- Develop prediction models linking small-volume measurements to engine-relevant conditions
- Demonstrate small-volume, high-throughput testing capabilities in blind tests

Fiscal Year (FY) 2018 Objectives

- Demonstrate capability to operate at elevated pressure
- Validate core assumptions (i.e., existence of essential combustion modes at elevated pressure, viability of fuel delivery concept)
- Quantify uncertainty of key measurements

Approach

The approach for micro-liter fuel characterization relies on cyclical combustion events within a heated micro-tube. This combustion mode is known as flames with repetitive extinction and ignition and relies on self-excited instabilities that are sensitive to fuel properties. A total sample volume of 20 mL is stored on a disposable microfluidic chip, dispensed via a micro-electromechanical system droplet generator, and mixed with air to create desired stoichiometry and mass flow rate. Within the micro-tube, a temperature profile (300 K–1,400 K) is established by external heating, whereas the desired operating pressure (25–35 bar) is regulated by a pressure controller downstream of the micro-tube. The time required to capture individual data points lies in the order of 10–20 s, which allows for high-throughput testing. Characteristics of flames with repetitive extinction and ignition are evaluated for sweeps of mass flow rates and/or pressure. Image analysis provides information on ignition, extinction, and flame propagation, which have been shown to be sensitive to fuel octane numbers.

The overall approach aligns with Sub-Topic 5 (“Small Volume, High Throughput Fuel Testing”) of the original funding opportunity announcement. The main objective is to demonstrate the feasibility of micro-liter fuel characterization as a method with smaller sample volumes and higher throughput than conventional approaches (Schoegl/LSU). A broadened scope includes engine-relevant physical fuel metrics (Menon/LSU) and thus encompasses Sub-Topic 1 (“Fuel Characterization and Fuel Property Prediction”) of the original funding opportunity announcement. Small-volume testing requires microfluidic fuel delivery and sensing (Gartia/LSU). It further needs to be validated against data from established experimental methods (Petersen/Texas A&M University), whereas numerical analyses require reduced kinetic models (Lu/University of Connecticut).

Results

Key Accomplishments for Fiscal Year 2018

- Obtained initial experimental evidence that microcombustion measurements differentiate Co-Optima fuel blends based on octane sensitivity at atmospheric pressure
- Confirmed existence of essential combustion modes up to 10 bar in intermediate-pressure setup
- Exceeded pressure range of comparable experiments documented in published work
- Established framework for uncertainty quantification of non-contact temperature measurements, where single-digit Kelvin confidence intervals on a range of 650 K–1,600 K meet project requirements
- Demonstrated feasibility of piezoelectric fuel delivery at moderate pressure of 1–6 bar

Microcombustion at Elevated Pressure. Within the project, the objective of reaching engine-relevant pressures is reached in two steps: (i) an intermediate-pressure setup using components rated at 150 psig is used for 1–10 bar tests, and (ii) a high-pressure setup using components rated for 500 psig is intended for tests up to 25–35 bar. Beyond fuel, pressure, and temperature, microcombustion experiments that involve small-diameter tubes depend on a range of additional parameters that impact combustion characteristics, which creates a large parameter space. As favorable conditions for relevant experimental observations constitute a potentially small subset, an experimental confirmation of the existence of three essential combustion phenomena, i.e., weak flames, flames with repetitive extinction and ignition, and normal flames, is essential.

Microcombustion Experiments. Initial tests of the intermediate-pressure setup equipped with a 1–100 psig pressure regulator showed pressure oscillations for tube pressures larger than 4 bar, thus limiting the experimental range for the first half of FY 2018. Nevertheless, tests run for Co-Optima fuel blends provided by Szybist of Oak Ridge National Laboratory [1] provided first evidence that microcombustion experiments are capable of differentiating between fuels with different octane sensitivity (S). Figure II.31.1 compares the performance of three Co-Optima fuels to 98 Reynolds octane number (RON) E30 (gasoline blend with 30% ethanol); all fuels share a 98 RON, while S of the high-alkylate fuel is significantly lower ($S \approx 1.2$ vs. $S \approx 10.6$). Similar to findings by Oak Ridge National Laboratory [1], fuels with matched RON

and S show comparable combustion characteristics, whereas a deviation in S impacts results. Figure II.31.1 does, however, also indicate that high-accuracy temperature measurements are essential. Measurements use a newly implemented pyrometry technique, where a need for improved algorithms and associated uncertainty quantification is evident (in early FY 2018 measurement uncertainties were estimated at $\pm 20\text{--}30$ K).

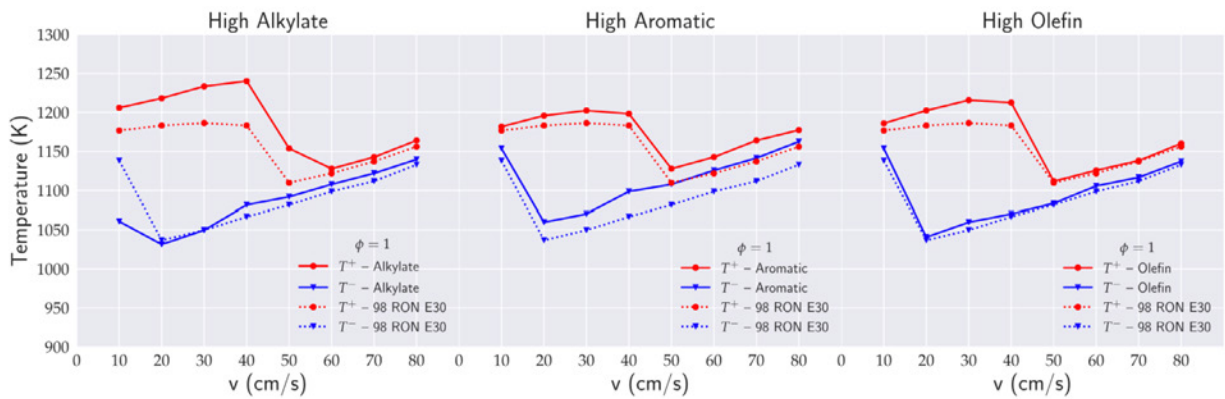


Figure II.31.1. Microcombustion results for Co-Optima fuel blends with matched RON and partially matched octane sensitivity. Fuel samples courtesy of Szybist/Oak Ridge National Laboratory [1]. Results presented at 2018 Annual Merit Review (I. Schoegl/LSU).

After an update of the main pressure controller, the intermediate-pressure setup was operational over the entire 1–10 bar range for the remainder of FY 2018. Experimental tests involved the impact dilution and diameter, where an expected tendency for flashback with increasing pressure was confirmed. Flashback was successfully prevented by reducing O_2 levels from 21% to 12%. All three relevant combustion phenomena were documented for 10 bar in a 1 mm tube. Associated flow velocities were approximately 80% lower than at atmospheric pressure, i.e., no detrimental effect preventing small sample testing was found, as corresponding overall mass flow rates do not vary significantly. Testing did, however, reveal non-negligible effects of thermal gas/wall interactions that have to be quantified in follow-up work. At the end of FY 2018, major components of the high-pressure setup were assembled, with initial tests for updated software and hardware underway.

Qualitative Prediction Model. In mid FY 2018, major efforts were directed towards the development of a simple theoretical model to predict combustion behavior of the micro-tube experiment. This model was developed as a predictive tool to assist in constraining the parameter space for tests at elevated pressure. The newly developed model successfully predicts quenching behavior, transitions between combustion regimes, and temperature levels for normal (strong) flames. The model is qualitative by nature and captures the coupling between heat transfer effects and first-order chemical kinetics (via large activation energy asymptotics). Due to this simplification, the model has inherent limitations in terms of predicting weak flame and ignition phenomena; however, the model provides valuable guidance for scaling up pressure, where predictions are largely consistent with observations. Early results for the model were presented at the 2018 Annual Merit Review. A portion of the results was summarized in a manuscript, where a revision is under review at the time of writing.

Uncertainty Quantification of High Dynamic Range Pyrometry. Non-contact temperature measurements via thin filament pyrometry follow an approach that has originally been developed for high-temperature applications and is based on photographic images of the filament obtained at multiple wavelengths. The project, however, requires the capability of reaching relatively low temperatures for a small-diameter (10–75 μm) silicon carbide filament. One of the stated targets of the project was to measure temperatures with high confidence, where a preferred outcome was single-digit uncertainty at observed temperature levels (650–1,400 K). An initial implementation achieved a low temperature limit of 850 K, with an uncertainty estimated at $\pm 20\text{--}30$ K, which was deemed insufficient, and an improved algorithm was implemented. As experimental validations of measurements are themselves susceptible to uncertainty in benchmark data, a simulation-based approach was chosen for an uncertainty quantification. Work in FY 2018 focused on the image-processing portion, where the emission of radiation, image acquisition by a sensor with inherent noise

characteristics, was simulated, and resulting synthetic images were processed with the updated pyrometry algorithm. Figure II.31.2 shows results, where known and reconstructed temperatures are plotted on horizontal and vertical axes, respectively, i.e., ideal results follow the diagonal. The color coding compares the reconstructed temperature range of a conventional 10-bit camera sensor (green), a high bit count 16-bit sensor (orange), and the high dynamic range (HDR) approach pursued in this project (blue), where the latter combines multiple images with different exposure times. While all tests share the same high temperature limit, HDR clearly outperforms conventional low dynamic range (LDR) approaches. It is noted that while the lowest reconstructed temperatures were around 540 K, the low-temperature region is affected by sensor noise. Above 650 K, confidence intervals were evaluated as smaller than 10 K, meeting project requirements. A corresponding manuscript was in preparation by the end of FY 2018 and submitted by the time of writing.

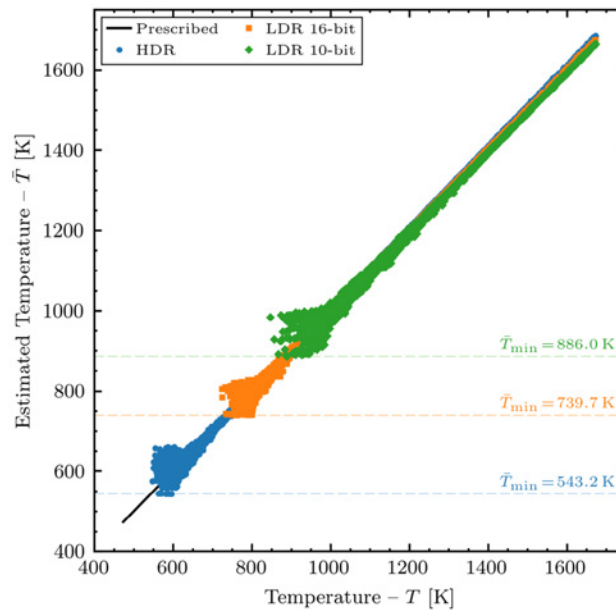


Figure II.31.2. Uncertainty quantification for temperature measurements via pyrometry (Schoegl/LSU)

Nano-liter Fuel Delivery at Elevated Pressures. Microcombustion tests for fuels of interest to Co-Optima involve limited (20 μL) sample size, where it is necessary to supply metered quantities of liquid fuel at nano-liter per second ($\mu\text{L}/\text{min}$) flow rates. While a micro-syringe-based delivery system for low-vapor-pressure fuels was implemented for initial work, a less limiting approach involves the piezoelectric generation of a high-frequency droplet train. The approach provides additional insights into physical fuel properties that are based on droplet metrics. The delivery system produces fine droplets, which vaporize, mix with air, and provide a gaseous fuel-air mixture of desired stoichiometry to the micro-combustor, where engine-relevant pressure capabilities are critical to the success of the project. A piezoelectric droplet-on-demand system was implemented and operated with liquid fuels (isooctane and n-heptane) to generate 50–70 μm -sized droplets at variable frequencies to provide flow rates between 0.5 and 4 $\mu\text{L}/\text{min}$, consistent with the range required by the micro-combustor. Figure II.31.3 illustrates the current operational range of the liquid fuel delivery system at ambient and elevated pressure levels, where markers represent tested conditions. Experiments conducted in FY 2018 aimed at an assessment of the viability of the fuel delivery concept at elevated pressure. In parametric studies, the response of droplet size and velocity to input signal parameters was studied in a vessel rated to 100 psig. Characteristics were evaluated up to 6 bar (87 psig), where elevated pressures reduced droplet velocity but did not interfere with the overall performance of the system, i.e., there is strong evidence that the achievable pressure is limited by the vessel rating and not the droplet generation approach. Based on FY 2018 results, a new setup with a pressure limit of 500 psig with heated air co-flow was designed for FY 2019 testing.

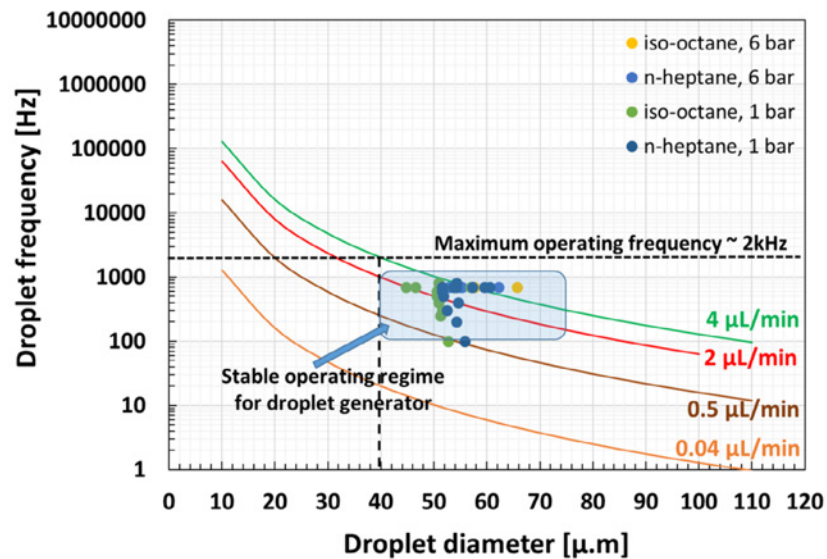


Figure II.31.3. Operating conditions tested for nano-liter fuel delivery at ambient and elevated pressures (S. Menon/LSU)

Milestone Summary

Milestone M1.3 (*Nano-liter Fuel Delivery Baseline*): A piezoelectric delivery system was acquired and installed. Nano-liter delivery of isopropanol and isooctane was demonstrated at atmospheric pressure; the system will be subsequently incorporated into a pressurized environment.

Milestone M1.4 (*Fuel Test Results Linked to Engine-Relevant Metrics*): Experiments and simulations indicate that fuel-specific parameters affect experimental behavior in two ways: (i) flame speed and (ii) ignition behavior. The former is a global phenomenon and thus can be observed at all pressures; available experimental results at low pressure correlate favorably (small shifts correlate with flame speeds of primary reference fuel with varying RON). RON and S have a more pronounced impact on ignition behavior. An experimental approach requires sufficiently short ignition delays, especially in the low-temperature negative temperature coefficient region. At low pressure, corresponding delays cannot be easily reached. Recent results by Szybist (Oak Ridge National Laboratory) [1] as well as McNenly (Lawrence Livermore National Laboratory) [2] show strong evidence for increased sensitivity to RON and S at higher pressure (20 bar).

Milestone M2.1 (*Framework for Co-Optima Fuels Completed*, i.e., selection of fuels to be investigated in year 2): After discussion with project partners, the decision was made to use a 2017 SAE paper by McCormick, et al. [3] as a main point of reference. Relevant portions of the paper are based on a four-component surrogate (isooctane/n-heptane/toluene/1-hexene: RON 90.3/motor octane number [MON] 84.7), where the impact of addition of various blendstocks is investigated. One point of interest is non-linear blending in terms of RON/MON/S, where both synergistic and antagonistic behavior were experimentally documented.

Milestone M2.2 (*Nano-liter Fuel Delivery*): The capability of nano-liter fuel delivery at elevated pressures was demonstrated up to 6 bar (pressure limit of current hardware), where droplet characteristics were documented. Results for high-pressure droplet generation did not provide any evidence of high-pressure limitations.

Conclusions

The following conclusions are derived at the midpoint of the project “Micro-liter Fuel Characterization and Property Prediction.”

- Microcombustion tests in an intermediate-pressure setup show differentiation of octane sensitivity for Co-Optima fuel blends; existence of relevant combustion phenomena was confirmed up to 10 bar.
- A predictive analytical model was developed to guide the selection of experimental parameters and conditions for high-pressure tests.
- Uncertainty quantification for temperature measurements via pyrometry indicates that project requirements with a lower limit of 650 K and single-digit Kelvin confidence intervals are met.
- Nano-liter fuel delivery via piezoelectric droplet generation was demonstrated at intermediate pressure.

The above findings indicate that no major remaining technological hurdles are anticipated. Overall, the project is on track to attain the technical goal for Budget Period II, i.e., “develop models/metrics linking test results to predicted engine performance.” Further, all activities towards meeting FY 2019 goals have been initiated.

Key Publications

1. Pal, Pinaki, Yunchao Wu, Tianfeng Lu, Sibendu Som, et al. 2017. “Multi-Dimensional CFD Simulations of Knocking Combustion in a CFR Engine.” *J. Energy Resour. Technol.*
2. Pinzón, Laura T., Olivier Mathieu, Clayton R. Mulvihill, Ingmar Schoegl, and Eric L. Petersen. “Ethanol Pyrolysis Kinetics Using H₂O Time History Measurements behind Reflected Shock Waves.” *Proc. Combust. Inst.* (in press).
3. Schoegl, Sauer, and Sharma. “Predicting Combustion Characteristics in Externally Heated Microtubes.” *Comb. Flame.* (revision in review).
4. Sauer and Schoegl. “Numerical Assessment of Uncertainty and Dynamic Range Expansion of Multispectral Image-Based Pyrometry.” *Measurement* (submitted).

References

1. Szybist, James P., Scott W. Wagon, Derek Splitter, William J. Pitz, and Marco Mehl. 2017. “The Reduced Effectiveness of EGR to Mitigate Knock at High Loads in Boosted SI Engines.” *SAE Int. J. Engines* 10 (5): 2305–2318. <https://doi.org/10.4271/2017-24-0061>
2. Lapointe, Simon, Clara L. Druzgalski, and Matthew J. McNenly. 2018. “Numerical Study of a Micro Flow Reactor at Engine Pressures: Flames with Repetitive Extinction and Ignition and Simulations with a Reduced Chemical Model.” *Combustion and Flame* 197 (November): 102–110. <https://doi.org/10.1016/j.combustflame.2018.07.020>
3. McCormick, Robert L., Gina Fioroni, Lisa Fouts, Earl Christensen, et al. 2017. “Selection Criteria and Screening of Potential Biomass-Derived Streams as Fuel Blendstocks for Advanced Spark-Ignition Engines.” *SAE Int. J. Fuels Lubr.* 10 (2): 442–460. <https://doi.org/10.4271/2017-01-0868>

Acknowledgements

Shyam Menon and Manas Gartia of Louisiana State University, Eric Petersen of Texas A&M University, Tianfeng Lu of University of Connecticut

II.32 The Development of Yield-Based Sooting Tendency Measurements and Modeling to Enable Advanced Combustion Fuels (Yale University)

Lisa Pfefferle, Principal Investigator

Yale University
205 Mason Laboratory
New Haven, CT 06520-8286
E-mail: lisa.pfefferle@yale.edu

Yuan Xuan, Principal Investigator

The Pennsylvania State University
105 Research East Building
University Park, PA 16802
E-mail: yux19@enr.psu.edu

Kevin Stork, DOE Technology Development Manager

U.S. Department of Energy
E-mail: Kevin.Stork@ee.doe.gov

Start Date: May 1, 2018	End Date: April 30, 2019	
Project Funding: \$1,452,787	DOE share: \$1,307,505	Non-DOE share: \$145,282

Project Introduction

Biofuels can benefit society by reducing emissions of carbonaceous soot particles from motor vehicles. Soot emissions are the second largest source of climate change [1], and they contribute to ambient fine particulate matter (PM_{2.5}) that causes over 3 million deaths worldwide each year [2]. As a consequence of these issues, engine companies are required by regulations to install particulate filters, which can cost up to \$50,000 and require periodic cleaning to remove noncombustible ash [3].

The amount of soot formed in an engine depends strongly on the chemical structure of the fuel; therefore, as biomass-derived fuels begin to replace petroleum-derived fuels, an opportunity exists to achieve lower emissions at lower costs. Biofuels normally contain oxygenated hydrocarbons, and the oxygen atoms in these molecules can hinder the formation of aromatic species that serve as precursors to soot particles [4–6].

To fully exploit this opportunity, stakeholders need information that describes the effects of biofuel composition on soot formation. This information includes (1) lists of possible biofuel components ranked by their measured soot-forming propensities; (2) empirical models that can extend these rankings to potentially interesting biofuel components that have not yet been synthesized and tested; (3) engineering metrics that combine sooting tendencies with other fuel properties—volatility, cetane number, etc.—to predict emissions from specific engine configurations; and (4) validated chemical kinetic models that can be used to computationally simulate soot formation in engines. Major challenges are that these items need to be available from laboratory-scale research in advance of direct engine testing; they need to cover the broad range of biofuel compositions being considered as possible blendstocks; and they need to cover the wide variety of engine configurations available for current and future use (spark ignition, compression ignition, multimode, etc.), each of which has its own unique mixing conditions.

Objectives

Overall Objectives

- Produce a database of measured soot-forming propensities for hydrocarbons from the chemical families that constitute petroleum-derived fuels and possible biomass-derived blendstocks. This database will enable stakeholders to rationally select the biofuels that offer the lowest-cost path to meeting emissions regulations.

- Develop engineering metrics that combine the database of laboratory-scale sooting tendencies with other fuel properties (volatility, heat of vaporization, cetane number, viscosity, etc.) to predict the soot emissions from real combustion engines. These metrics will allow a single sooting tendency database to be applied to a wide range of engine configurations, including spark ignition, compression ignition, and advanced concepts such as multimode.
- Test the ability of detailed chemical kinetic mechanisms to reproduce the measured sooting tendencies. Once these mechanisms have been validated, they can be used in computational fluid dynamics simulations to optimize engine designs to emit the least possible particulates.

Fiscal Year 2018 Objectives

- Measure the sooting tendencies of at least 25 commercially available hydrocarbons and 25 blendstock samples that have been produced by the Co-Optimization of Fuels and Engines (Co-Optima) High Performance Fuels (HPF) Team.
- Determine whether the laboratory-scale sooting tendencies measured in this work apply to the full range of air-fuel equivalence ratios (λ) and pressures that exist in real engines.
- Validate at least one detailed chemical kinetic mechanism for each of the nine specific hydrocarbons in the Co-Optima Tier 3 spark ignition blendstocks [7].

Approach

This project has defined a fundamental fuel property called yield sooting index (YSI) that quantifies the tendency of fuels to form particulates in combustion systems. YSI is determined by adding a small amount of the test fuel to a laboratory-scale methane/air flame and then measuring the flame's maximum soot concentration. The underlying idea is that if the test fuel has a lesser propensity to form soot than another fuel, then it will form less soot when added to the flame, and a smaller soot concentration will be measured.

The YSI methodology offers several benefits. First, each measurement requires only a very small volume of the test fuel (0.1 ml). For perspective, the ASTM International smoke point test requires 100 times as much (10 ml) [8]. This difference allows a wider range of biofuels to be studied, since they are typically produced in milliliter or smaller quantities during the research phase. Second, the YSI approach enables a large number of samples to be processed in a short time. Over 50 fuel samples and specific hydrocarbons were tested during the first year of this project. Third, the YSI flames are well defined and can be computationally simulated with perturbation methods that reduce the computational expense of large kinetic mechanisms. Thus, the YSI data can be used to test kinetic mechanisms of soot formation, even mechanisms that include thousands of species.

Results

During FY 2018, sooting tendencies were measured for more than 100 pure hydrocarbons and 30 fuel samples supplied by the Co-Optima HPF team. Some of these measurements were performed over a range of temperatures and air-fuel equivalence ratios. Sooting tendencies were also simulated for over 30 hydrocarbons, and many of these computations investigated high-pressure flame conditions representative of those that occur in real engines. The following are some of the key results.

- Nitrogen-containing hydrocarbons were identified as a fuel category that combines low particulate emissions with high energy density. Nitrogenates are potential components of biofuels since proteins generally constitute 10%–40% of biomass [9], and all amino acids contain nitrogen atoms. Sooting tendencies were measured for more than 70 nitrogenates from a wide range of chemical families, including amines, amides, imines, nitriles, nitrites, and nitrates. The results depend strongly on the specific chemical form of the nitrogen, and they are significantly smaller than those for the structurally analogous regular hydrocarbons or oxygenated hydrocarbons. Figure II.32.1 illustrates both of these trends for the case of primary and secondary amines. The YSIs for these nitrogenates (orange bars) nearly double from 13 for diethylamine to 23 for isobutylamine, and they are all at least a few YSI units smaller than the YSIs for the corresponding alcohols and ethers (cyan bars).

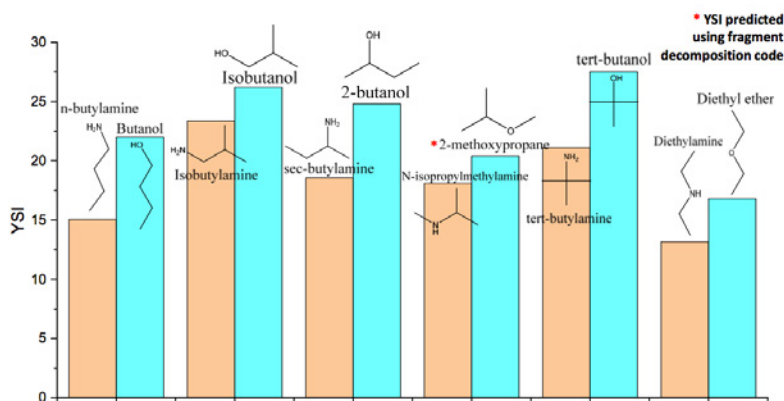


Figure II.32.1. Sooting tendencies of amines ($C_4H_{11}N$ isomers) compared with structurally analogous alcohols and ethers ($C_4H_{10}O$ isomers). The sooting tendencies of the oxygenates were either measured directly or they were estimated with the National Renewable Energy Laboratory (NREL) structure-property model (red asterisks); see Key Publication 1.

- This project has enabled the Co-Optima HPF team to select the biomass-derived blendstocks that offer the lowest soot emissions and target them for further development. For example, sooting tendencies were measured for a series of carboxylic acid-derived blendstocks produced from lignocellulose by NREL. These researchers could produce a broad pool of candidate compositions by varying the processing conditions. Based on the YSI measurements, one of these compositions was chosen as the optimum blendstock. To illustrate the performance of this blendstock, Figure II.32.2 shows soot yields for mixtures of it and an emissions certification diesel fuel; as the proportion of the blendstock increases (moving towards the right side of the figure), the soot yield significantly decreases.

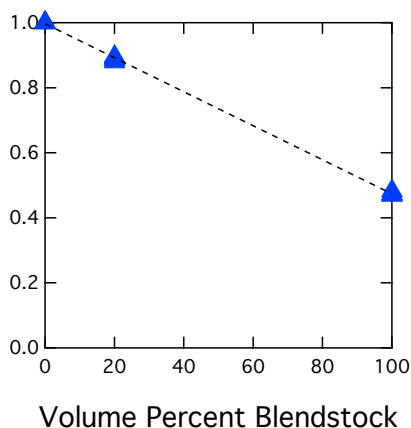


Figure II.32.2. Soot yields for mixtures of a conventional diesel fuel and the optimal NREL acid-upgrading blendstock. The results are normalized to the pure diesel fuel. Each mixture was added to the flame at a fixed flow rate of $100 \mu\text{l}/\text{hour}$.

The ability of the NREL structure-property model to predict YSI was greatly improved by adding new measurements to the underlying database. This model was developed by Peter St. John during FY 2017 (see Key Publication 1) and is regularly used by the Co-Optima HPF team to estimate YSIs of prospective new blendstocks. It uses machine learning to generate predictions for new hydrocarbons from existing measurements; thus, its accuracy depends on the availability of measured data for structurally similar compounds. During FY 2018, data was added for many chemical families of interest to the HPF team. For example, YSIs were measured for a series of dioxolanes supplied by Los Alamos National Laboratory. Figure II.32.3 shows that the predictions with these new measurements (right panel) are much more accurate than with the original database (left panel).

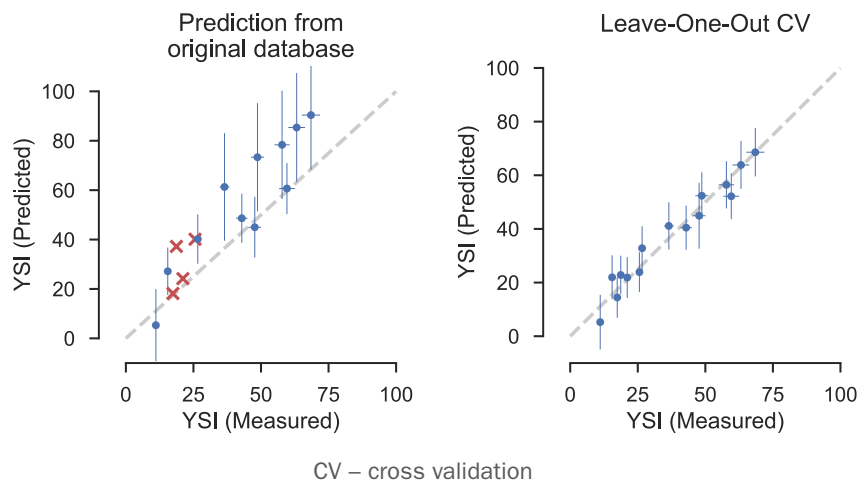


Figure II.32.3. YSIs predicted for dioxolanes and related hydrocarbons with the NREL structure-property model. The panel on the left is with the original database, while the panel on the right shows improved predictions after measurements of the dioxolanes synthesized at Los Alamos National Laboratory were added to the database.

- YSI was demonstrated to be insensitive to flame temperature and to air-fuel equivalence ratio (λ). This was accomplished by measuring YSIs in flames where the base fuel was premixed with nitrogen and/or air, in order to decrease the flame temperature and/or increase λ . The test fuels in these measurements were three cyclic hydrocarbons and three reference jet fuels. Figure II.32.4 shows that the results were uniform across the investigated flame conditions, which proves that YSI is a robust measure of sooting tendency over a wide range of λ and flame temperatures.

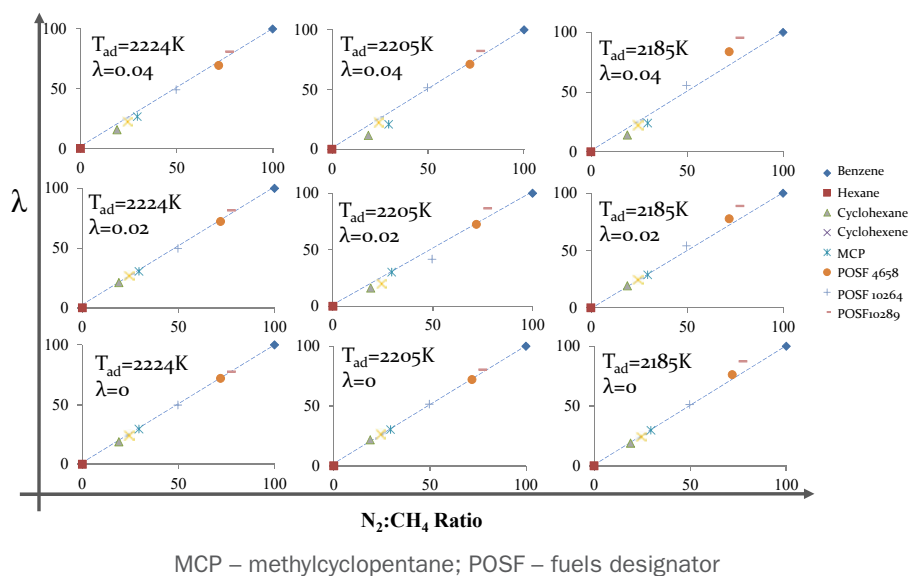


Figure II.32.4. Measured YSI versus reference-case YSI for various air-fuel ratios (λ) and adiabatic flame temperatures (T_{ad}). The reference-case YSI for each fuel is the YSI measured with $\lambda = 0$ and $T_{ad} = 2,224$ K.

- YSI was demonstrated to be insensitive to flame pressure over the range of 1–15 atm. This was accomplished by computationally simulating YSIs for a set of n-alkanes and aromatics at different pressures; these test compounds were chosen because an extensively validated mechanism is available for them [10], so the results are reliable without experimental validation. Figure II.32.5 shows that the YSIs

computed at elevated pressures (colored symbols) agree with the results measured at 1 atm (black symbols and lines). These results illustrate the value of simulations for addressing conditions outside the domain of the experiments; although YSI measurements should be possible at elevated pressure, the high-pressure burner equipment is not currently available.

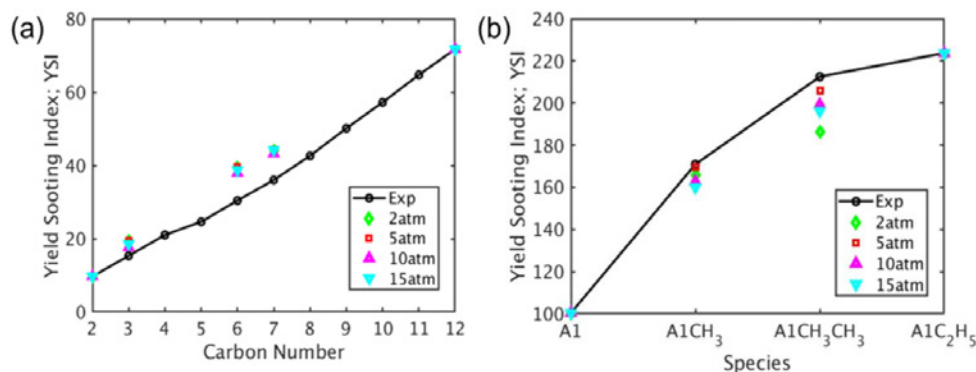


Figure II.32.5. YSIs for n-alkanes (left panel) and aromatic hydrocarbons (right panel) predicted with computational simulations at pressures from 1–15 atm

- A chemical kinetic mechanism has been shown to accurately predict soot formation for the Co-Optima Tier 2 and Tier 3 spark ignition blendstocks [7]. This mechanism was developed by Lawrence Livermore National Laboratory, in collaboration with National University of Ireland Galway and King Abdullah University of Science and Technology [11]. Figure II.32.6 compares the predicted YSIs (vertical axis) to the measured YSIs (horizontal axis); the individual data points (colored symbols) are all close to the black line that indicates perfect agreement.

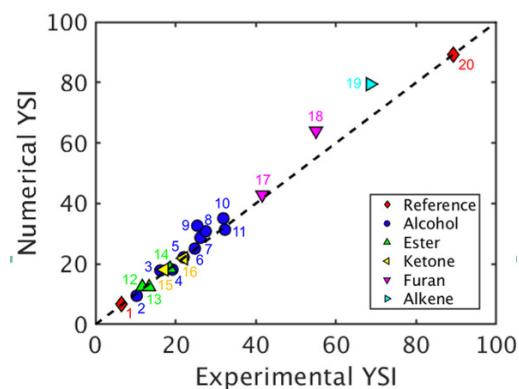


Figure II.32.6. YSI predictions for 20 Co-Optima Tier 2 and Tier 3 blendstocks using chemical-kinetic-based simulations

Conclusions

- Quantitative sooting tendencies were measured for over 100 pure hydrocarbons and 30 fuel samples provided by the Co-Optima HPF team. Several promising categories of low-emissions blendstocks were identified from these measurements. The new results were added to the database underlying the NREL structure-property model, which greatly improved its ability to predict sooting tendencies of biofuel-relevant hydrocarbons.
- Sooting tendencies based on the YSI methodology were shown to be insensitive to air-fuel equivalence ratio, flame temperature, and flame pressure.
- The ability of a detailed chemical kinetic mechanism to predict soot formation was validated for the Co-Optima Tier 2 and Tier 3 spark ignition blendstocks.

Key Publications

1. Das, D.D., P.C. St. John, C.S. McEnally, S. Kim, and L.D. Pfefferle. 2018. “Measuring and Predicting Sooting Tendencies of Oxygenates, Alkanes, Alkenes, Cycloalkanes, and Aromatics on a Unified Scale.” *Combustion and Flame* 190: 349–364.
2. Montgomery, M.J., D.D. Das, C.S. McEnally, and L.D. Pfefferle. “Analyzing the Robustness of the Yield Sooting Index as a Measure of Sooting Tendency.” *Proceedings of the Combustion Institute*, in press. <https://doi.org/10.1016/j.proci.2018.06.105>.
3. Kim, S., G.M. Fioroni, J.-W. Park, D.J. Robichaud, D.D. Das, P.C. St. John, T. Lu, C.S. McEnally, L.D. Pfefferle, R.S. Paton, T.D. Foust, and R.L. McCormick. “Experimental and Theoretical Insight into the Soot Tendencies of the Methylcyclohexene Isomers.” *Proceedings of the Combustion Institute*, in press. <https://doi.org/10.1016/j.proci.2018.06.095>.
4. Jain, A., D.D. Das, C.S. McEnally, L.D. Pfefferle, and Y. Xuan. “Experimental and Numerical Study of Variable Oxygen Index Effects on Soot Yield and Distribution in Laminar Co-Flow Diffusion Flames.” *Proceedings of the Combustion Institute*, in press. <https://doi.org/10.1016/j.proci.2018.05.118>.
5. McEnally, C.S., Y. Xuan, P.C. St. John, D.D. Das, A. Jain, S. Kim, T. Kwan, L.K. Tan, J. Zhu, and L.D. Pfefferle. “Sooting Tendencies of Co-Optima Test Gasolines and Their Surrogates.” *Proceedings of the Combustion Institute*, in press. <https://doi.org/10.1016/j.proci.2018.05.071>.
6. Staples, O., C.M. Moore, J.H. Leal, T.A. Semelsberger, C.S. McEnally, L.D. Pfefferle, and A.D. Sutton. “A Simple, Solvent Free Method for Transforming Bio-Derived Aldehydes into Cyclic Acetals for Renewable Diesel Fuels.” *Sustainable Energy & Fuels*, in press. <http://pubs.rsc.org/en/content/articlelanding/2018/se/c8se00371h#!divAbstract>.

References

1. Bond, T.C., et al. 2013. *J. Geophys. Res. Atmos.* 118: 5380–5552.
2. Gakidou, E., et al. 2017. *Lancet* 390: 1345–1422.
3. U.S. Environmental Protection Agency. “Diesel Particulate Filter General Information.” <https://www.epa.gov/sites/production/files/2016-03/documents/420f10029.pdf>.
4. Westbrook, C., W. Pitz, and H. Curran. 2006. *Journal of Physical Chemistry A* 110: 6912–6922.
5. Pepiot-Desjardins, P., H. Pitsch, R. Malhotra, S.R. Kirby, and A.L. Boehman. 2008. *Combustion and Flame* 154: 191–205.
6. McEnally, C.S., and L.D. Pfefferle. 2011. *Environmental Science & Technology* 45: 2498–2503.
7. Farrell, J., J. Holladay, and R. Wagner. 2018. “Fuel Blendstocks with the Potential to Optimize Future Gasoline Engine Performance.” Technical Report DOE/GO-102018-4970. <http://www.osti.gov/scitech>.
8. ASTM International. 2018. “Standard Test Method for Smoke Point of Kerosene and Aviation Turbine Fuel.” Standard D1322-18. https://compass.astm.org/EDIT/html_annot.cgi?D1322+18.
9. Huber, G.W., S. Iborra, and A. Corma. 2006. *Chemical Reviews* 106: 4044–4098.
10. Blanquart, G., P. Pepiot-Desjardins, and H. Pitsch. 2009. *Combustion and Flame* 156: 588–607.
11. Mehl, M., et al., Paper 1A17, 10th U.S. National Combustion Meeting, 2017.

Acknowledgements

Co-authors: Charles McEnally, Dhruvajyoti Das, Thomas Kwan, Matthew Montgomery, Lance Tan, Junqing Zhu (Yale University); Abhishek Jain, Hyunguk Kwon (The Pennsylvania State University); Gina Fioroni, Thomas Foust, Xiangchen Huo, Nabila Huq, Seonah Kim, Robert McCormick, David Robichaud, Peter St. John, Derek Vardon (NREL); Robert Paton (Colorado State University); Juan Leal, Cameron Moore, Troy Semelsberger, Orion Staples, Andrew Sutton (Los Alamos National Laboratory); Tianfeng Lu, Ji-Woong Park (University of Connecticut); Goutham Kukkadapu, William Pitz, Scott Wagnon, Kuiwen Zhang (Lawrence Livermore National Laboratory)

III. Alternative Fueled Engines

III.1 Single-Fuel Reactivity Controlled Compression Ignition Combustion Enabled by Onboard Fuel Reformulation (Stony Brook University)

Benjamin Lawler, Principal Investigator

Stony Brook University
100 Nicolls Road
Stony Brook, NY 11794
E-mail: benjamin.lawler@stonybrook.edu

Kevin Stork, DOE Technology Development Manager

U.S. Department of Energy
E-mail: Kevin.Stork@ee.doe.gov

Start Date: October 1, 2015	End Date: September 30, 2018	
Project Funding: \$1,128,618	DOE share: \$1,014,352	Non-DOE share: \$114,266

Project Introduction

Reactivity-controlled compression ignition (RCCI) combustion has demonstrated efficiency and emissions improvements compared to both diesel and spark-ignited combustion modes [1–4]. Specifically, RCCI has demonstrated a 20% fuel economy increase compared to spark ignition [3] and a 5% efficiency improvement at certain engine speeds and loads over conventional diesel combustion while maintaining significantly lower engine-out soot and NO_x emissions [4]. However, RCCI is limited in its commercial viability due to the requirement of two separate fuel systems that need to be refilled by the user. To resolve this drawback of RCCI, the proposed innovation uses a single parent fuel with an onboard fuel reformer to create the necessary separation in fuel reactivity to enable RCCI combustion. In this concept, the fuel from the tank would be directed to the engine unaltered, while a separate branch of the fuel stream is directed to an onboard fuel reformer, where the parent fuel is reformed to produce “reformate,” a fuel mixture of H₂, CO, and partially reacted hydrocarbon species whose properties are different from the initial parent fuel. The less reactive fuel is then port fuel injected, and the higher-reactivity fuel is direct injected (DI).

This approach is innovative because fuel reformer technology and RCCI combustion could potentially have a synergistic relationship. The proposed use of an onboard fuel reformer to create the necessary fuel reactivity separation from a single parent fuel would help the future development and potential commercialization of “single-fuel RCCI” and the realization of the previously reported benefits of RCCI.

Objectives

Overall Objectives

- Reform gasoline, diesel, and natural gas to varying levels and characterize the constituent species of their reformate mixtures as well as the autoignition tendency of the reformate mixtures in the form of an effective primary reference fuel (PRF) number
- Evaluate the potential efficiency, emissions, operating range, and burn characteristics of RCCI using a parent fuel and its reformate mixture using computational fluid dynamics (CFD) simulations with detailed chemical kinetics as well as GT-Suite models
- Experimentally test each parent fuel-reformate combination in RCCI and compare reformate RCCI to conventional gasoline-diesel RCCI

Fiscal Year 2018 Objectives

- Utilize the CFD and GT-Suite models that were validated in the previous fiscal year to better understand the combustion chemistry and performance characteristics of single-fuel RCCI
- Experimentally investigate the effects of increasing reactivity separation between the high- and low-reactivity fuels on RCCI combustion by varying the autoignition tendency of the premixed fuel by using various PRF blends as the premixed fuel
- Use the CFD and experimental research engines to determine the operating strategy, operating range, efficiency, and emissions characteristics of single-fuel RCCI using diesel as the DI fuel and the reformat mixture that results from a catalytic partial oxidation reformation of diesel as the premixed fuel

Approach

The goal of this project is to determine the feasibility of RCCI combustion using a parent fuel and its reformat. Three potential parent fuels—diesel, gasoline, and natural gas—will be evaluated since these fuels are most relevant to vehicle applications. The approach to achieve the project goal is to perform a systematic and fundamental evaluation of these parent fuels in this newly conceived realization of RCCI combustion. To do this, the parent fuels were first reformed to varying levels, and the species concentrations of the reformat mixtures, as well their autoignition properties, were characterized. This first step helped determine which parent fuels hold the most promise to enable reformat RCCI. Once the parent fuel and reformat combinations with the largest effective octane separation were determined, CFD and system-level models were used in conjunction with experimental testing to evaluate the potential efficiency, emissions, burn characteristics, and operating range of single-fuel RCCI. The model simulations and the experimental results of reformat RCCI are being compared to RCCI data in the literature to put the results in the greater context of the advanced combustion community and to help evaluate the feasibility and future promise of single-fuel RCCI. Stony Brook University is responsible for all experimental engine testing as well as CFD and system-level modeling. The experimental testing is being conducted at the Engine Combustion Research Laboratory in the Advanced Energy Research and Technology Center at Stony Brook University. The research team has access to several high-performance computing clusters available through the Institute for Advanced Computational Science. Innoveering, LLC, and City College of New York are subcontractors who were responsible for reforming the parent fuels and characterizing the reformat mixtures.

Results

Key accomplishments of Fiscal Year 2018 include the following.

- Used a system-level model with the previously collected experimental fuel reformer results and concurrently collected experimental engine testing to understand the system interactions and system-level efficiency
- Simulated single-fuel RCCI with detailed chemical kinetics using the previously validated CFD model
- Experimentally tested single-fuel RCCI with diesel fuel as the DI fuel and diesel's reformat mixture as the premixed fuel
- Discovered that efficiencies of 44% are achievable with good controllability and low engine-out NO_x emissions in single-fuel RCCI with diesel as the parent fuel based on the combined results of the CFD simulations and experimental testing
- Determined the important considerations for single-fuel RCCI with diesel as the parent fuel in comparison to diesel-gasoline RCCI, which include (1) the reactivity separation is larger with single-fuel RCCI with diesel as the parent fuel; (2) the premixed fuel is gaseous rather than liquid, which displaces some of the air entering the engine; (3) the diluents in the reformat fuel mixture (CO_2 , H_2O , and N_2) displace air and mimic the effects of exhaust gas recirculation (EGR) in the cylinder; and (4) approximately 20% of the lower heating value of diesel is released in the fuel reformer, which lowers the efficiency of the system

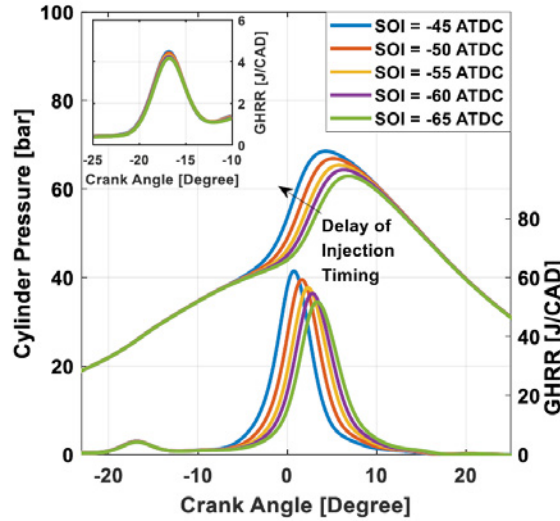
In the previous fiscal years (2016 and 2017), potential parent fuels including gasoline, diesel, and natural gas were reformed in a catalytic partial oxidation reaction with air (i.e., rich equivalence ratios over a catalyst) to produce various gaseous reformat fuel mixtures that corresponded to varying equivalence ratios, pressures, flow rates, and parent fuels. The constituent species of the reformat mixtures were then characterized using gas chromatography–mass spectrometry. With the inlet and outlet species concentrations known, the fraction of the parent fuel’s lower heating value that was released in the fuel reformer could be calculated, which varied based on the flow rate, equivalence ratio, pressure, and parent fuel being reformed. The total range of 6–24% of the fuel’s lower heating value was released in the reformer. Natural gas could vary the full range, from 6% to 24%, depending on the degree of reformation. Gasoline exhibited a smaller range of 15–24%. Reforming diesel fuel released a fairly constant ~16–21% of the fuel’s lower heating value.

Based on the degree of reformation, two representative reformat mixtures were selected for each parent fuel for engine testing and autoignition characterization. Before the autoignition tendency of the reformat mixtures could be characterized, a PRF (blends isooctane and n-heptane) mapping was developed on a Cooperative Fuel Research engine at Stony Brook University. A wide range of PRF blends were autoignited in homogeneous charge compression ignition (HCCI) combustion at different intake temperatures and compression ratios to serve as a reference for the reformat fuel mixtures. Once the mapping was developed, the reformat fuel mixtures were autoignited in HCCI combustion at the same conditions, and based on the compression ratio and intake temperature required to achieve autoignition, an effective PRF number or effective octane number for the reformat fuel mixtures could be determined. The exact value depended slightly on the speciation of each reformat mixture. However, the reformat mixtures generally had an effective octane number of 105–115. Based on this result, it was concluded that the effective octane separation between natural gas and its reformat, or gasoline and its reformat, is not sufficient to enable RCCI combustion. However, the octane separation between diesel and its reformat mixture is sufficiently large to achieve effective control of RCCI combustion with favorable efficiency and emissions levels. For this reason, single-fuel RCCI with diesel fuel and its reformat will be pursued for the remainder of this research effort.

The focus of Fiscal Year 2018 was to use the previous knowledge and constructed and validated models and research engines to evaluate the performance of diesel and its reformat in RCCI combustion. The goal is to benchmark diesel-reformat RCCI against diesel-gasoline RCCI to determine the similarities and differences. Initially, diesel fuel was used with PRF blends to understand how the reactivity separation between the DI and premixed fuels affects the characteristics and performance of RCCI, as it directly relates to the understanding of single-fuel RCCI with diesel fuel and its reformat. By varying the PRF number of the port fuel injected fuel, the reactivity separation between the DI and premixed fuels was varied. An example of the experimental result from testing diesel with PRF80 is shown in Figure III.1.1. From these results, it was concluded that decreasing the premixed fuel’s reactivity results in delayed combustion phasing, lower combustion efficiency, higher thermal efficiency, and an increased sensitivity to the direct injection timing. With these effects well understood, it is anticipated that diesel-reformat RCCI will result in a higher sensitivity to injection timing than diesel-gasoline RCCI due to the larger reactivity separation between the premixed and DI fuels.

After developing a thorough understanding of the effect that increasing reactivity separation has on the operating conditions of RCCI combustion, diesel fuel was used as the DI fuel and diesel’s reformat mixture was used as the premixed fuel in experiments that were conducted on a fully instrumented single-cylinder research engine at Stony Brook University. An example comparison is shown in Table III.1.1 and Figure III.1.2. Generally, the results show that diesel fuel with its reformat is incredibly effective at enabling RCCI combustion in the cylinder with high efficiencies and low emissions. Table III.1.1 and Figure III.1.2 show that similar efficiency and emissions levels are possible with diesel-reformat RCCI as diesel-gasoline RCCI. The experimental testing has shown that the diluents that are present in the reformat mixture due to the partial oxidation reaction have a similar effect as EGR. For example, one of the diesel reformat mixtures consisted of 4.9% H₂, 62.3% N₂, 2.1% CH₄, 7.2% CO, 7.4% CO₂, 1.5% unreacted fuel, and 11.4% H₂O. N₂ is the largest constituent due to the use of air in the catalytic partial oxidation reaction. The presence of CO₂ and H₂O are due to some complete combustion reactions of the fuel that occur within the reformer. Together, the N₂, CO₂, and H₂O have two important effects on the engine operation: (1) to displace the incoming air entering the cylinder and (2) to act as diluents on the thermodynamic cycle and affect the ratio of specific heats of the mixture, in a similar fashion to EGR. In fact, this explains the difference in EGR percentage between the two cases in

Table III.1.1 and Figure III.1.2. The efficiency levels are identical between the two cases. The CO and unburned hydrocarbon (UHC) emissions are lower for the diesel-reformate RCCI case compared to the diesel-gasoline RCCI case, while the NO_x emissions are much higher for the diesel-reformate case. However, this trend is not universal and is simply a product of the two cases being compared in Table III.1.1 and Figure III.1.2.



ATDC – after top dead center; CAD – crank angle degrees; GHRR – gross heat release rate; SOI – start of injection

Figure III.1.1. Single-cylinder engine RCCI results with diesel fuel as the DI fuel and PRF80 as the premixed fuel for varying injection timings as an example result of a fuel reactivity separation study

Table III.1.1. Diesel-Reformate RCCI Compared to Diesel-Gasoline RCCI at an Example Operating Condition

	Premixed Fuel Energy Fraction	EGR	Gross Thermal Efficiency [%]	Indicated Specific NO _x [g/kW-hr]	Indicated Specific CO [g/kW-hr]	Indicated Specific UHC [g/kW-hr]
Diesel-Reformate	41%	0%	43.8	0.22	16.7	12.7
Diesel-Gasoline	64%	35%	43.8	0.01	36.1	17.1

In addition to the experimental testing, CFD modeling and simulations of single-fuel RCCI with diesel and its reformate mixture are being conducted. The CFD model has been validated against the experimental data collected over Fiscal Year 2018 and was used in conjunction with the single-cylinder experimental testing to provide a more complete understanding of the spray, mixing, and combustion processes in single-fuel RCCI. An example of the CFD results is shown in Figure III.1.3, which shows the equivalence ratio distribution and the temperature distribution six crank angle degrees after the direct injection event. Figure III.1.3 shows that there is a distribution of equivalence ratios ranging from the rich equivalence ratios (values larger than 1 shown in yellow-orange-red colors) to the background equivalence ratio of the premixed reformate fuel around 0.5 (shown as the light blue color in the center of the cylinder). Due to the evaporative cooling of the injected diesel fuel, a temperature distribution develops where the rich regions are generally cooler, as can be seen by comparing equivalence ratio distribution and temperature distribution in Figure III.1.3

The CFD results have also been used to help explain some of the experimentally observed phenomena, including the sources of emissions in single-fuel RCCI. In single-fuel RCCI, a portion of the premixed fuel is CO, which is contained in the premixed fuel regions that may or may not reach their autoignition temperature. This can result in CO emissions in single-fuel RCCI, which would instead result in unburned hydrocarbon emissions in diesel-gasoline RCCI. The CFD model will continue to be used in conjunction with the experimental testing to help provide a complete understand of the spray dynamics, evaporation and mixing, and chemical reactions associated with the heat release process in single-fuel RCCI.

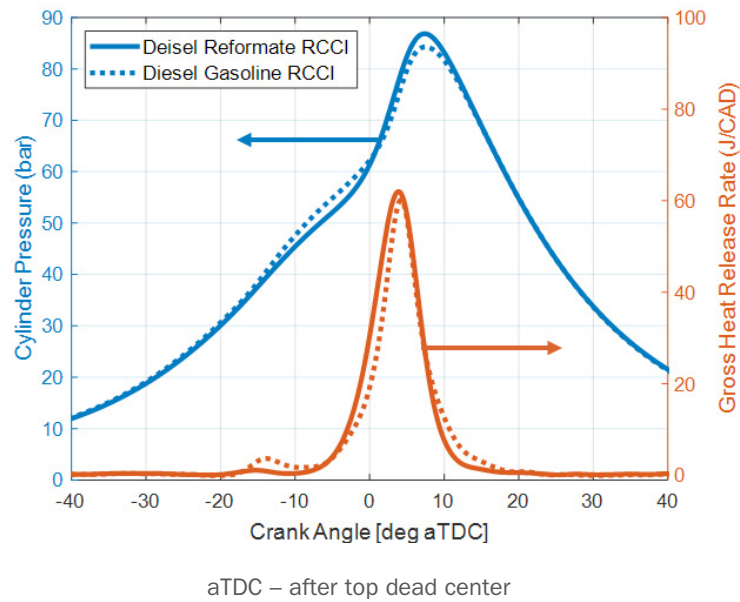


Figure III.1.2. An experimental comparison between diesel-reformatte RCCI and diesel-gasoline RCCI collected on a fully instrumented, single-cylinder research engine

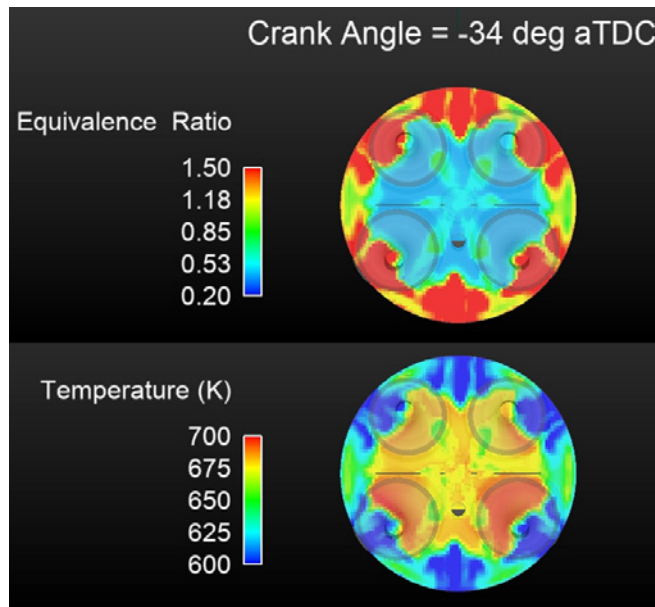


Figure III.1.3. Cut-plane equivalence ratio distribution and temperature distribution from the CFD simulations of single-fuel RCCI combustion with diesel and its reformatte

Conclusions

In summary, the following accomplishments were made during the 2018 fiscal year.

- A system-level model and CFD model with detailed chemical kinetics were used in conjunction with experimental single-cylinder engine testing to develop a complete understanding of the considerations of single-fuel RCCI with diesel as the DI fuel and diesel's gaseous reformatte fuel mixture as the premixed fuel.
- The diluents in the reformatte fuel mixture that result from the catalytic partial oxidation reformation of diesel displace some of the incoming air and act similarly to EGR in the cylinder.

- The efficiencies of single-fuel RCCI and diesel-gasoline RCCI are similar (~44% on this engine), and the emissions characteristics are similar too with some slight differences.
- The larger reactivity separation, the diluents in the reformat mixture, and the fact that the reformat mixture is gaseous are the largest differences between single-fuel RCCI and diesel-gasoline RCCI.
- A catalytic partial oxidation reformation reaction releases approximately 20% of the lower heating value of diesel in the fuel reformer. Future research should focus on better understanding and investigating different reforming strategies to enable single-fuel RCCI.

Key Publications

1. Yang, R., D. Hariharan, S. Zilg, B. Lawler, et al. 2018. "Efficiency and Emissions Characteristics of an HCCI Engine Fueled by Primary Reference Fuels." SAE Technical Paper 2018-01-1255, doi:10.4271/2018-01-1255.
2. Zhou, Y., D. Hariharan, R. Yang, S. Mamalis, and B. Lawler. 2019. "A Predictive 0-D HCCI Combustion Model for Ethanol, Natural Gas, Gasoline, and Primary Reference Fuel Blends." *Fuel* 237: 658–675. ISSN 0016-2361, <https://doi.org/10.1016/j.fuel.2018.10.041>.
3. Yan, Z., D. Hariharan, B. Gainey, S. Mamalis, and B. Lawler. "Investigation into Reactivity Separation between Direct Injected and Premixed Fuels in RCCI Combustion Mode." *Fuel*, In Review.
4. Hariharan, D., R. Yang, S. Mamalis, and B. Lawler. "Effects of Single Versus Two-Stage Heat Release on the Load Limits of HCCI Using Primary Reference Fuels." SAE World Congress, In Review.

References

1. Reitz, Rolf, and Ganesh Duraisamy. 2015. "Review of High Efficiency and Clean Reactivity Controlled Compression Ignition (RCCI) Combustion in Internal Combustion Engines." In *Progress in Energy and Combustion Science* 46: 12–71. ISSN 0360-1285, <https://doi.org/10.1016/j.pecs.2014.05.003>.
2. Kokjohn, S., R. Hanson, D. Splitter, and R. Reitz. 2011. "Fuel Reactivity Controlled Compression Ignition (RCCI): A Pathway to Controlled High-Efficiency Clean Combustion." *International Journal of Engine Research*, Special Issue, Vol. 12, pp. 209–226.
3. Curran, S., Z. Gao, and R. Wagner. 2014. "Reactivity Controlled Compression Ignition Drive Cycle Emissions and Fuel Economy Estimations Using Vehicle Systems Simulations with E30 and ULSD." *SAE Int. J. Engines*.
4. Curran, S., R. Hanson, R. Wagner, and R. Reitz. 2013. "Efficiency and Emissions Mapping of RCCI in a Light-Duty Diesel Engine." SAE Technical Paper 2013-01-0289.

Acknowledgements

The project team would like to recognize and thank Kevin Stork, DOE Vehicle Technologies Office Program Manager, who is serving as the Technology Manager for this project, and Nicolas D'Amico, who is serving as the project manager. Thanks also go out to Sotirios Mamalis of Stony Brook University, Dennis Assanis of the University of Delaware, Dean Modroukas of Innoveering, LLC, and Marco J. Castaldi of City College of New York for their contributions.

III.2 High-Efficiency Cost-Optimized Spark-Ignited Natural Gas (HECO-SING) Engines–2018 (Robert Bosch LLC)

Alex Freitag, Principal Investigator

Robert Bosch LLC
38000 Hills Tech Dr.
Farmington Hills, MI 48331
E-mail: Alexander.Freitag@us.bosch.com

Kevin Stork, DOE Technology Development Manager

U.S. Department of Energy
E-mail: Kevin.Stork@ee.doe.gov

Start Date: January 1, 2016	End Date: November 30, 2018	
Project Funding: \$3,513,514	DOE share: \$1,756,224	Non-DOE share: \$1,757,290

Project Introduction

The abundance of relatively low-cost natural gas in the North American market, along with energy independence, makes natural gas attractive as an alternate fuel. Natural gas also has an advantage over diesel engines in low NO_x emissions production. Natural gas does, however, have some technical challenges in its lower efficiency due to natural gas energy content in comparison to diesel or gasoline, which is also a partial factor in its vehicle storage capacity limitations and thus driving range.

In order to address these challenges, the High-Efficiency Cost-Optimized Spark-Ignited Natural Gas (HECO-SING) Engines project was undertaken. The goal was to increase engine efficiency (fuel economy) while still meeting future emissions requirements in a cost-effective manner. In order to achieve these goals, high-dilution combustion was used with focus on advanced ignition systems, optimized aftertreatment selection, and applied creative engine controls.

Objectives

Overall Objectives

- Develop and demonstrate an HECO-SING heavy-duty engine capable of approaching current near-diesel efficiency while achieving current Environmental Protection Agency (EPA) emission regulations
- Increase engine efficiency through optimized dilution with both exhaust gas recirculation (EGR) and excess air
- Identify key enablers:
 - o Advanced ignition system for robust combustion with high dilution
 - o Lean capable exhaust aftertreatment
 - o Advanced engine and aftertreatment controls (passive selective catalyst reduction [SCR])
- Achieve targets:
 - o EPA17 on-highway emissions
 - o Peak brake thermal efficiency >42%

Fiscal Year 2018 Objectives

- Process ignition imaging and analyze results/correlate image differences to engine results
- Perform simulations of various aftertreatment and control systems/develop recommendation for optimal system

- Develop total cost of ownership (TCO) evaluation balancing performance results versus cost impact (initial system cost plus annual operation costs)
- Develop a projected ignition system wear (maintenance) assessment
- Generate the final project report

Approach

In order to maintain the low cost objective for this project, a passive SCR approach was undertaken to reduce costs of the more expensive active SCR aftertreatment method. To achieve the passive SCR technique, a control strategy switching between a rich operating mode to generate NH_3 (ammonia) in the exhaust system through the three-way catalyst rather than a complex and costly diesel exhaust fluid (urea) dosing, and lean operation to increase engine operating efficiency (lower fuel consumption), was pursued. Optimum balancing of operation in the different operating modes to achieve increased efficiency while maintaining low emissions was the objective.

To achieve the highest efficiency, utilizing advanced ignition systems that could extend the dilution limit boundary was investigated. The ammonia generation mechanism to decompose the oxides of nitrogen (NO_x) created while operating in the lean mode was developed through exhaust gas simulation. EGR was utilized to minimize NO_x while assisting in combustion stability to further expand the combustion dilution operating range. The balance of all parameters and operating conditions for best overall operations to meet project goals is paramount.

In order to focus on the key areas of advanced ignition systems and aftertreatment selection and sizing, the University of Michigan and Pacific Northwest National Laboratory joined with Bosch in the project. The University of Michigan concentration is in the area of researching and selecting advanced ignition systems that may benefit operation in high dilute conditions and developing methods to quantify performance differences between the systems. Pacific Northwest National Laboratory's role is to select and characterize exhaust catalysts and to develop simulation models based on said characterizations, in order to allow Bosch to perform catalyst sizing and control strategies.

Results

- Combustion imaging techniques and methods to analyze and quantify the various ignition systems were developed.
- Simulations of various aftertreatment and control systems were performed. Ability to meet both low NO_x and ultra-low NO_x was achieved while still generating fuel economy improvements, although not to goal level.
- TCO calculations have been completed and included in the final report.
- Projected ignition system wear has been included in the final report.
- Final report was submitted in January 2019.

The process of developing the ignition and combustion imaging progressed from manual binarized images cycle-to-cycle variation (CCV) over 100 cycles, to the flame area over crank angle, to an evolution of thresholding techniques advancing from grayscale to standard Otsu's method, to a University of Michigan adapted two-dimensional (2D) Otsu's method, and to a final iteration that filtered out invalid images based on the objects' size, number of adjacent objects, and the respective objects' location relative to the flame kernel. The final imaging method allowed for the processing of the images to be automated, saving considerable time over the massive number of image files that needed to be processed. To validate the automated imaging process, its results were compared to manual processing over two ignition systems under the same operating conditions. Metrics were also developed out of the processing, allowing for later analysis of the ignition systems in relation to each other and their performance (Figure III.2.1–III.2.4).

In addition to engine imaging assessment, a new bench assessment was added to the project. The bench test allows the chemiluminescence of the ignitor plasma image as well as the combustion flame kernel under

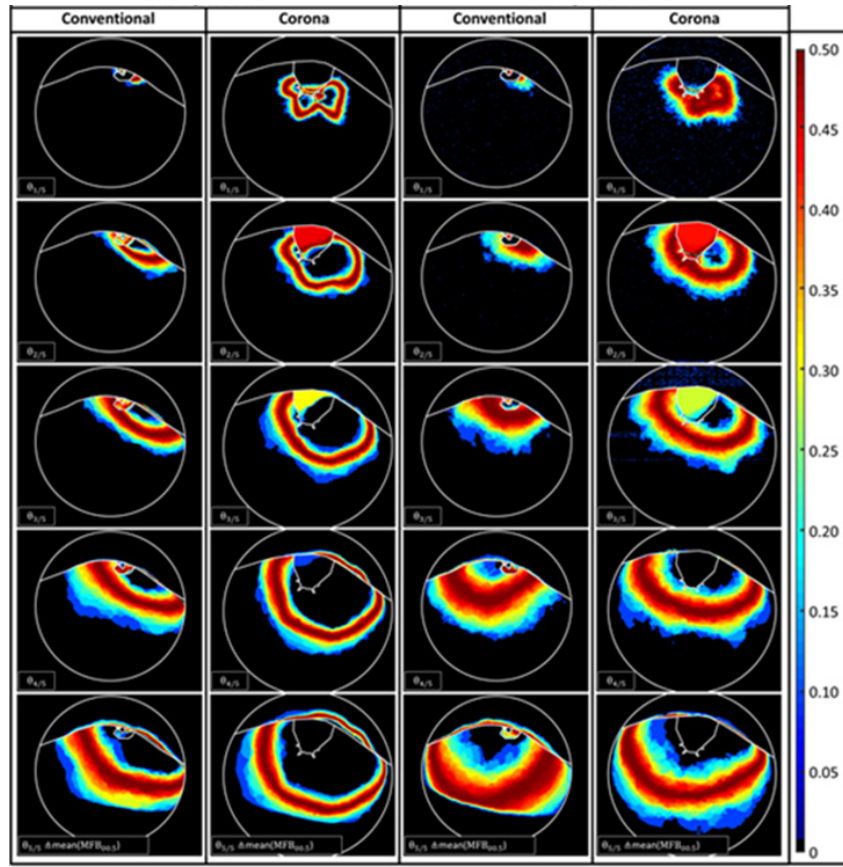


Figure III.2.1. CCV comparison between two ignition systems, each over two operating conditions

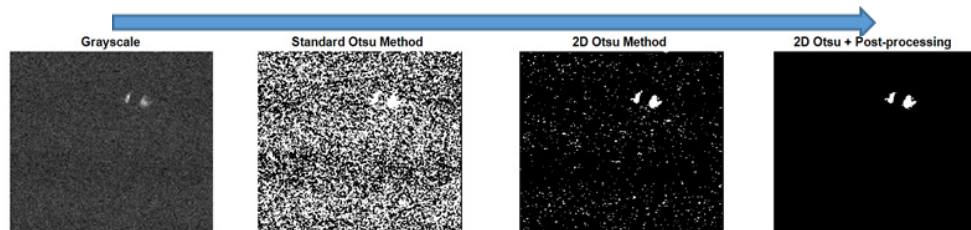


Figure III.2.2. CCV comparison between two ignition systems, each over two operating conditions

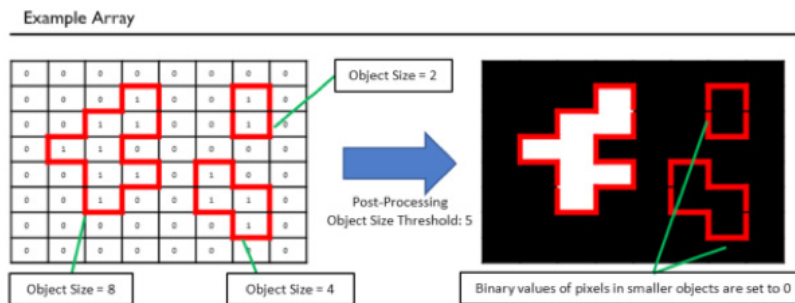
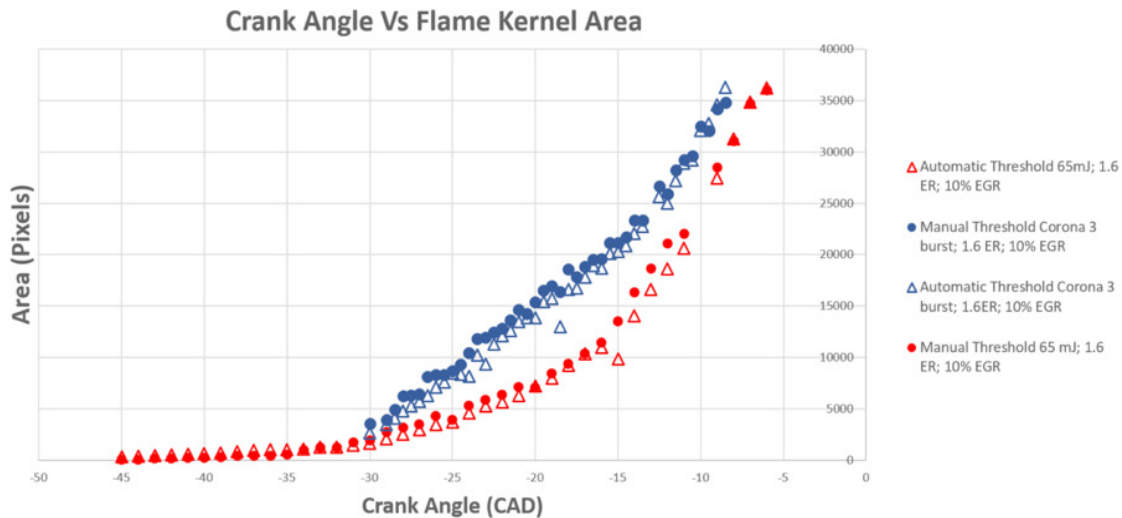


Figure III.2.3. Images are binarized and compared to adjacent pixels and relation to the ignited spark image, to assess if they are valid images or noise



Sanity Check: The automated image processing technique is capable of reproducing binary images that are very similar to manually thresholded images from our Combustion Symposium paper dataset.

Figure III.2.4. Validation of automated to manual ignition processing techniques over two different types of ignition systems (evaluated at the same operating point and condition)

atmospheric conditions to be evaluated. During the engine combustion imaging phase of testing, near-infrared imaging (1,000–1,700 nm range) enabled the tracking of the water emission to identify the burned gas region inside the low-light engine cylinder. With this technique, the identification and study of the early flame kernels in an engine environment could be achieved.

However, by choosing infrared imaging to study flames more rigorously, the ability to detect spark plasmas and corona streamers was compromised because the majority of the signal from these plasmas is in the ultraviolet (UV) and visible bands.

The plasma-to-kernel transition is critical to understanding the entire ignition process. Utilizing UV cameras, the chemiluminescence from hydroxyl radicals (OH^*) in the plasma can be measured. OH^* emits strongly across 280–340 nm wavelengths, with the strongest emissions near 310 nm. An image intensifier was used to enable a high-speed, visible band camera to detect this emission. Since there is no longer access to the engine, these experiments were conducted under atmospheric conditions. A Hencken burner was used in order to provide adequate control over mixture conditions.

An infrared camera has been added to the setup to make simultaneous measurements with the UV camera. That way, infrared-to-UV mapping of signals can be made, and the images that were collected from the engine experiments will be able to be interpreted from an OH^* creation standpoint.

Preliminary UV imaging results with the corona ignition illustrate the plasma-rich corona in OH^* can be seen. Corona streamer outline is captured during the period up to the 350 μs controlled duration. Streamer-to-flame transition is observed, with the following images from the flame. Conventional igniters will be imaged in the same UV band in order to show the impact of OH^* creation differences between the different ignition systems (Figure III.2.5–Figure III.2.6).

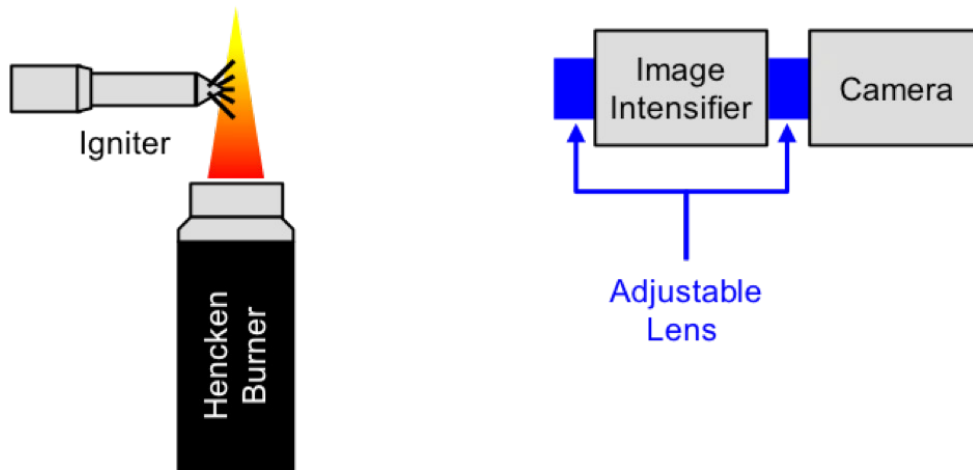


Figure III.2.5. Hencken burner test set-up for igniter plasma imaging under atmospheric conditions

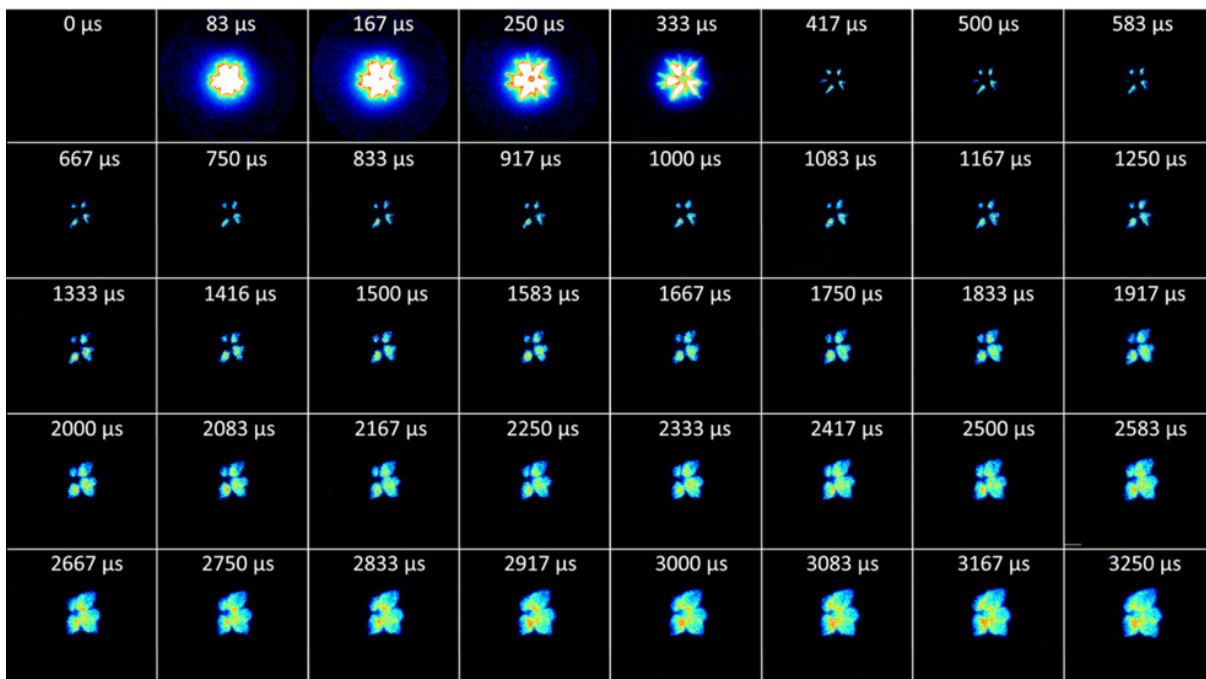


Figure III.2.6. Image of corona plasma during the 350 μ s duration corona generation phase is visible in the UV band with the Hencken burner, while the combustion flame front can be seen in the subsequent images

Aftertreatment simulation utilizing GT Power software has been performed using data generated from Pacific Northwest National Laboratory’s synthetic gas bench that had been developed into an emissions reaction model, along with Bosch engine data. Verification of ammonia generation through a three-way catalyst was performed on the test bench and simulation model. Various combinations of catalyst sizing, pipe length (due to temperature impacts), and operating control strategies have been performed at different target emission levels. Both low and ultra-low NO_x levels have been successfully achieved while still obtaining fuel economy benefits. While efficiency was improved, ability to meet target goals was not achieved with the optimized passive SCR system. However, an alternative configuration not originally planned utilizing active SCR while running full lean in all conditions does appear promising to meet the efficiency goals. The cost impact of the active SCR system versus the efficiency gain will be assessed. (See Table III.2.1.)

Table III.2.1. Aftertreatment Simulation Emissions and Fuel Economy Projected Attainment

Aftertreatment System	NO _x Limit	NO _x Attainment	BSFC improvement - Conventional Ignition	BSFC improvement - Corona Ignition
Passive SCR	0.2 g/hp-hr	0.1458 g/hp-hr	3.31%	4.48%
Passive SCR	0.02 g/hp-hr	0.0193 g/hp-hr	2.35%	3.38%
Active SCR/HiDos	0.02 g/hp-hr	0.0100 g/hp-hr	5.7%	6.85%

BSFC – brake specific fuel consumption; hp-hr – horsepower-hour; HiDos – high use of controlled ammonia dosing

A TCO tool was developed. This tool collected system costs for the multiple unique variations of control systems and aftertreatment and compared their respective efficiency improvements and design operating cost benefits to the initial purchase price of the option on the vehicle (Table III.2.2). The initial outlay vs. the operating improvements generates a payback period for the unique systems to determine best overall financial system (Table III.2.3). Comparison of these systems to the baseline diesel system is established.

Table III.2.2. Partial Example of Early TCO Calculation Tool

HECO-SING TCO calculation sheet 26-Jun-18					
Inputs		Diesel (baseline)	CNG Stoich	CNG Lean Active SCR	Regional CNG Passive SCR High Energy
Regional Distance (miles/year)	65,840	1	1	1	1
Refuse Distance (miles/year)	25,000	0	0	0	0
Diesel Fuel Cost (\$/gallon)	\$2.96	1	0	0	0
NG Fuel Cost (\$/gallon)	\$2.45	0	1	1	1
Urea Cost (\$/gallon)	\$2.27	1	0	1	0
Urea to Fuel Ratio		0.04	0	0.04	0
Maintenance Costs (\$/year)	\$500.00	1	0.5	1	0.5
Fuel Economy (miles/gallon)		5.8	5.28	5.99	5.37
			91%		93%
Operational Costs	\$/year	35,131.84	30,800.76	28,427.59	30,268.73
Fuel cost savings	\$/year		4,331.08	6,704.25	4,843.11
Component Costs \$					
Diesel Fuel Injection System		1	0	0	0
CNG Fuel Injection System		0	0	0	0
Diesel Storage		1	0	0	0
CNG Storage - Regional		0	1	1	1
CNG Storage - Refuse		0	0	0	0
Urea Dosing System		1	0	1	0
SCR Catalyst		1	0	1	1
Three-way Catalyst		0	1	0	1
DOC		1			
cDPF		1			
High-energy ignition system		0	1	1	1
CEI ignition system		0	0	0	0
Corona Discharge ignition system		0	0	0	0
Total fuel system cost	\$	\$3,218.00	\$4,325.00	\$5,068.00	\$4,800.00
Add-on Cost vs Diesel	\$		\$1,107.00	\$1,850.00	\$1,582.00
TCO Calculation	\$	38,349.84	35,125.76		
Payback Period	Years		0.998595634	0.755938546	0.991099453
2-year payback period fuel delta					

CNG – compressed natural gas; NG – natural gas; DOC – diesel oxidation catalyst; cDPF – catalyzed diesel particulate filter; CEI – controlled electronic ignition

Table III.2.3. Preliminary System Payback Scenarios Comparison

NO _x Limit	Control System	Ignition System	TWC	SCR	EGR	DENOX	Payback Period (yrs.)
0.2 g/hp-hr	Passive (Digital L-S)	High Energy	Double brick	Double brick	Yes	No	0.87
0.02 g/hp-hr	Passive (Toggling L-S)	Corona	Double brick	Double brick	Yes	No	0.854
0.02 g/hp-hr	Active High Dose (L)	High Energy	Single OC	Single brick	No	Yes	0.71

L-S – Lean-Stoich (operating either full lean or stoichiometric); L – lean; TWC – three-way catalyst; OC – oxidation catalyst

Conclusions

As the project is winding down, the re-scoped tasks are being completed. Objectives for fuel efficiency were not able to be met per the original concept of utilizing passive SCR, although improvements over baseline were obtained. However, an alternative higher-initial-cost active SCR system (DENOX system) does appear that it might be able to achieve those goals. The ability to achieve the emissions target of low NO_x was reached. Additional effort was expended to determine if even further emissions reductions (ultra-low NO_x) beyond the target objective could be obtained, and it was determined that it was achievable. TCO has been finalized and the lowest payback period has been calculated to be the lean approach with active SCR.

Key Publications

1. University of Michigan provided an oral presentation and paper on “Infrared Borescopic Analysis of Natural-Gas Ignition and Combustion Variability,” at the Society of Automotive Engineers, World Congress Experience in Detroit, MI, on April 10, 2018.
2. University of Michigan provided an oral presentation and paper on “Infrared Borescopic Evaluation of High-Energy and Long-Duration Ignition Systems for Lean/Dilute Combustion in Heavy-Duty Natural-Gas Engines,” at the Society of Automotive Engineers, World Congress Experience on April 12, 2018.
3. University of Michigan provided a poster presentation on their efforts to date at the Princeton-Combustion Institute Summer School on Combustion at the University of Princeton on June 25, 2018.
4. University of Michigan provided an oral presentation and paper on “Time-Resolved Infrared Imaging and Spectroscopy for Engine Diagnostics,” at the 13th International AVL Symposium on Propulsion Diagnostics, Graz, Austria, June 27, 2018.
5. University of Michigan provided an oral presentation at the Combustion Institute’s Combustion Symposium, July 31, 2018, in Dublin, Ireland. A copy of the presentation will be published in the proceedings of the symposium at a later date.
6. Q1 DOE Quarterly Report – 4/26/18
7. Q2 DOE Quarterly Report – 7/19/18
8. Q3 DOE Quarterly Report – 10/31/18
9. Q4 DOE Quarterly Report – 01/31/19
10. Final Report – 01/31/19
11. Princeton-Combustion Institute Summer School on Combustion at the University of Princeton during the week of June 25, 2017.

12. Natural Sciences and Engineering Research Council of Canada - Collaborative Research and Training Experience Program (NSERC CREATE) Combustion Summer School in Toronto during the week of May 21, 2017.
13. Engineering Graduate Symposium at University of Michigan on November 11, 2016.
14. Michigan Institute for Plasma Science and Engineering (MIPSE) Graduate Symposium at University of Michigan on October 5, 2016.
15. Mazacioglu, A., M.C. Gross, and V. Sick. 2018. "Infrared Borescopic Characterization of Corona and Conventional Ignition for Lean/Dilute Combustion in Heavy-Duty Natural-Gas Engines." Presented at 37th International Symposium on Combustion, published in Proceedings of the Combustion Institute, vol. 37, no. 4, pp. 4993–5001, doi:10.1016/j.proci.2018.06.060.

Acknowledgements

Steve White, Principal Project Manager, Robert Bosch LLC
Ahmet Mazacioglu, Doctoral student, University of Michigan
Michael Gross, Assistant Research Scientist, University of Michigan
Margaret Poppe, Undergraduate independent research, University of Michigan
Caleb Sherwood, Undergraduate summer student research, University of Michigan
Andrew Di Mauro, Graduate student research assistant, University of Michigan
Volker Sick, Assoc. VP-Natural Science and Engineering, University of Michigan
Tyler Boggs, Senior Engineer (Simulation), Robert Bosch LLC
Mark Casarella, Manager (Advanced System Development), Robert Bosch LLC
Justin Kern, Principle Engineer (NG), Robert Bosch LLC
Nicholas D'Amico, Project Manager, National Energy Technology Laboratory

III.3 Innovative Dual Fuel Aftermarket Emissions Solution (CALSTART)

Steven Sokolsky, Principal Investigator

CALSTART
48 S. Chester Ave.
Pasadena, CA 91106
E-mail: ssokolsky@calstart.org

Richard K. Whitaker, Principal Investigator

NG1 Technologies
9233 Park Meadows Drive
Lone Tree, CO 80124
E-mail: rwhitaker@ng1techflo.com

Michael Weismiller, DOE Technology Development Manager

U.S. Department of Energy
E-mail: Michael.Weismiller@ee.doe.gov

Start Date: January 1, 2016
Project Funding: \$1,269,320

End Date: March 30, 2019
DOE share: \$998,420

Non-DOE share: \$270,900

Project Introduction

The intent of this project is to develop an advanced emission control system for Class 7 and Class 8 heavy-duty dual fuel vehicles that eliminates or mitigates the negative effects of currently used diesel particulate filter and selective catalytic reduction emissions treatment systems. The project will combine multiple technologies—two exhaust system technologies plus hydrogen injection—working together to increase engine efficiency and reduce most emissions directly within the cylinder.

Objectives

- Initiate baseline and aftermarket testing of the 2012 Mack MP7 UPS stock truck equipped with automatic transmission at Mesilla Valley Transportation, to include fuel cycle testing and emissions testing at BF Goodrich test track
- Deliver the 2012 Mack MP7 UPS stock truck equipped with automatic transmission for vehicle testing at Mesilla Valley Transportation
- Complete engine assembly and install engine to test cell, make adaptations, and tune engine
- Perform single-cell testing for both diesel and dual fuel engines
- Initiate the baseline and diesel iteration testing of the one-cylinder stock engine at VazTec Engine Laboratory
- Perform testing on a comparable one-cylinder diesel engine to validate results and the presence of any increased volumetric air flow realized through the next phases of testing
- Test several exhaust systems to establish a baseline
- Operate multiple vehicles equipped with the TechFlo exhaust combined with the BoostBox hydrogen catalyst for the testing of fuel and emissions
- Compile the data for formal reporting of all fuel and emissions performance improvements into a statistical report

- Establish the test parameters for the setup and use of an engine dynamometer and fuel consumption rate specific to brake specific fuel consumption
- Schedule the delivery of the 2012 Mack MP7 UPS stock equipped with automatic transmission for aftermarket testing that includes dynamometer and vehicle track testing at Penn State University
- Initiate the aftermarket engine testing of the one-cylinder stock engine at VazTec Engine Laboratory
- Perform baseline data collection, single-cylinder engine testing, dynamometer testing, track testing, and field testing of a grant-supplied vehicle; testing of retrofitted existing emissions equipment to determine optimal dual fuel usage; and final technological reporting

Approach

NG1 Technologies along with BoostBox and VazTec project teams traveled to Mesilla Valley Transportation on January 8–22, 2018, to participate in the vehicle testing of the 2012 Mack MP7 UPS stock equipped truck. The vehicle testing consisted of baseline testing of stock equipment, the addition of the aftermarket NG1 TechFlo and BoostBox H2, and the bypass of stock equipment with exclusive use of aftermarket equipment as emissions equipment.

The testing event at Mesilla Valley Transportation included fuel cycle testing and emissions testing on the BF Goodrich test track. The baseline and aftermarket track tests of 5,000+ miles were successfully completed using original equipment manufacturer (OEM) and aftermarket exhaust systems. The 14 days of testing comprised of vehicle setup and track testing measuring fuel consumption and emissions.

Results

- Demonstrated steady improvement in particulate matter (PM) compared to the baseline engine. The average mass concentration of PM in the exhaust was steadily reduced from the baseline level to the point that, at the 5,000-mile test, it was a 64% reduction from the already low baseline level (i.e., 5,000 mile/baseline = 0.36). The 5,000-mile average nitrogen oxide (NO_x) concentration was 77% lower compared to the baseline average (i.e., 5,000 mile/baseline = 0.23). See Figure III.3.1.
- Observed consistency in the data as observed from the Society of Automotive Engineers (SAE) J1264 test performed when compared to the previous reporting period in fuel economy using both the NG1 TechFlo exhaust along with the use of the combined technologies of NG1 and BoostBox.
- Developed a mechanism to reduce the hydrogen production for a single-cylinder engine as per requirements in Task 2.
- Determined the optimal testing equipment for continual on track emissions testing. A combination of a Mobile 5-gas analyzer and a diffusion charger-based PM measurement system was utilized through a third party to make all measurements. These devices and methods have been evaluated by University of California Riverside for use as a standard of on-road measurement for the California Air Resources Board.
- Produced 100% of the required parts: constructed cartridge assemblies and head assemblies, fully assembled engine to accommodate natural gas, and refined emission testing protocol.
- Initiated the baseline engine testing of the one-cylinder stock engine at VazTec Engine Laboratory.

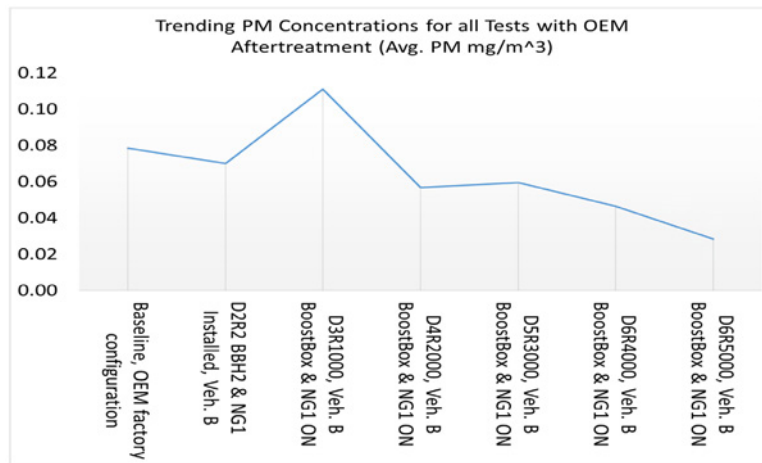


Figure III.3.1. Trending PM concentrations for all tests with OEM aftertreatment average PM mg/m³

Conclusions

NG1 Technologies and Boost Box H2 project teams have compiled a statistical data report of all fuel and emissions performance improvements experienced from September 1, 2016, to September 30, 2018. The data have been derived from operating five Class 8 heavy trucks equipped with the TechFlo exhaust combined with the BoostBox hydrogen catalyst for the testing of fuel and emissions. The results have been derived using city routes and over-the-road methods of traveling, where the same distance to and from a predetermined location has been completed every day for the past 24 months.

The project team is continuing to monitor fuel savings on multiple Class 8 heavy trucks equipped with the BoostBox H2 and NG1 systems. To date, almost 24,000 data points have been collected across multiple vehicles and compiled into Excel formats for statistical analysis and charting. Initial data shows strong correlation that the NG1 improves fuel efficiency compared to the stock vehicles, and the combination of NG1 and BoostBox H2 further improves fuel efficiency above stock vehicles. These results appear to be consistent over the course of the entire data collection period.

- VazTec developed a unique injector control circuit to modify the electronic countermeasure signal to increase the voltage to 65 V, which was needed to properly actuate the piezoelectric crystals in a short burst. Increasing the voltage allowed a 12-volt signal to be maintained until the injection event was complete.
- VazTec used an oscilloscope to line up the injection timing between the electronic countermeasure PC software controls and the given crank timing.
- VazTec used electronic countermeasure control software to run a standardized test mode to verify the injector flow rate with the new 65-volt control circuit.
- VazTec, in conjunction with the NG1 team, initiated a discussion with Cobra Engineering to explore the requirements of increasing the sample size of the single-cell data to a Class 8 truck.
- BoostBox H2 developed a mechanism to reduce the hydrogen production for a single-cylinder engine as per requirements in Task 2. This mechanism was refined in April of 2018 when the system was used at the VazTec facility to create a baseline of a single-cell diesel engine. Additionally, BoostBox H2 has developed a telemetric platform (outside the grant) and integrated that system onto the UPS grant vehicle as an upgrade to the existing platform. This allows the team to remotely monitor the performance of the BoostBox H2 system and provide real-time feedback to the driver or the fleet

Acknowledgements

Thanks to Nicholas D'Amico, Program Manager at National Energy Technology Laboratory.

III.4 Reduced Petroleum Use through Easily-Reformed Fuels and Dedicated Exhaust Gas Recirculation (Southwest Research Institute)

Thomas E. Briggs, Jr., Principal Investigator

Southwest Research Institute
6220 Culebra Road
San Antonio, TX 78238
E-mail: Thomas.briggs@swri.org

Kevin Stork, DOE Technology Development Manager

U.S. Department of Energy
E-mail: Kevin.Stork@ee.doe.gov

Start Date: October 1, 2014

End Date: August 30, 2019

Project Funding: \$394,446

DOE share: \$315,557

Non-DOE share: \$78,889

Project Introduction

This project is focused on improving the efficiency of a gasoline engine by using advanced petroleum and bio-derived fuels in a dedicated exhaust gas recirculation (D-EGR) engine. The D-EGR engine uses one or more of the cylinders to recirculate exhaust gas back to the intake of the engine. This increases the efficiency of the engine by itself but also allows running those cylinders in such a way that they produce hydrogen as one of the byproducts of combustion. Hydrogen enhances combustion so that the compression ratio of the engine can be increased and so it can be optimized to run in a more efficient manner.

Running such an engine on regular gasoline provides significant benefits but becomes limited in how much hydrogen can be produced due to fuel chemistry. By adjusting the chemistry of the fuel, an even more efficient version of the engine can be built, which will support the DOE goal of a 25% improvement in vehicle fuel economy for a typical passenger car.

Objectives

Overall Objectives

- Quantify the impact of fuel chemistry and formulation on D-EGR hydrogen production
- Optimize the operation of a D-EGR engine with purpose-developed fuel
- Demonstrate >25% reduction in petroleum usage for a mid-sized passenger car

Fiscal Year 2018 Objectives

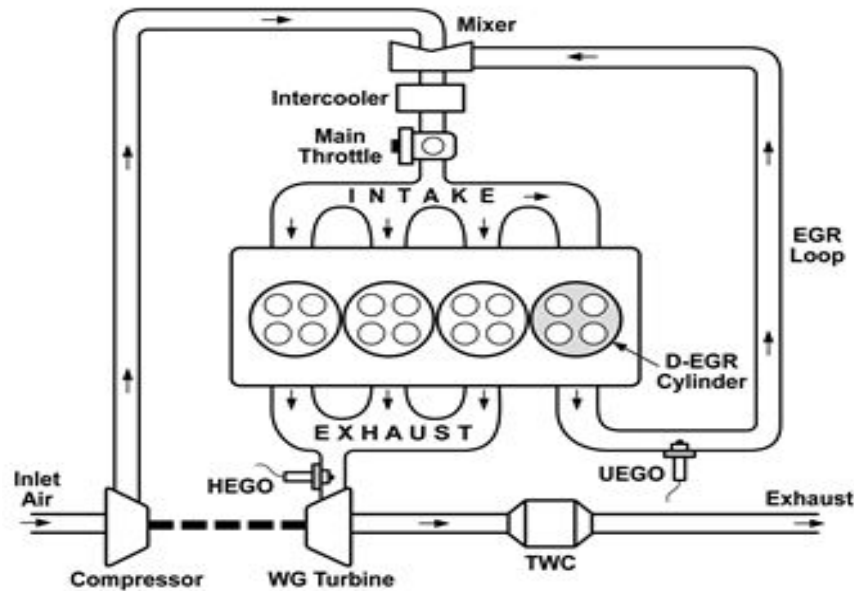
- Quantify impact of fuel chemistry on hydrogen production in the dedicated cylinder of a D-EGR engine
- Demonstrate improved hydrogen production through hardware optimization of a dedicated cylinder

Approach

An existing engine will be modified to function as a D-EGR engine. The operation of the engine on gasoline will then be optimized to ensure that the fuel injection approach and intake/exhaust valve timings are optimal for producing hydrogen using a known fuel. The fuel chemistry will then be adjusted using a combination of refinery products, which are already made (though potentially not used in gasoline), and bio-derived fuel products. The potential improvement in hydrogen production will be demonstrated using these fuels. Learnings from the engine optimization study will then be used to demonstrate an updated engine configuration that can maximize hydrogen production (and hence enable maximized compression ratio and engine efficiency) when using optimized fuels.

Results

An experimental campaign was conducted to evaluate the impact of fuel chemistry on hydrogen production in a single-cylinder engine operated as the dedicated cylinder in a D-EGR combustion system. The overall layout of a D-EGR engine is shown in Figure III.4.1. One of the cylinders is used to provide the EGR gas for the entire engine. This cylinder is run rich of stoichiometric, producing hydrogen and carbon monoxide as combustion byproducts. These compounds enhance the ignitability, flame speed, and knock resistance of the fuel, which can enable higher efficiency. Using fuels that enhance the production of hydrogen, in particular, can further benefit the efficiency of the engine.



TWC – three-way catalyst; HEGO and UEGO – exhaust oxygen sensors

Figure III.4.1. Dedicated EGR engine configuration

Work in Fiscal Year 2018 has investigated the basic chemical effects of fuels using a test matrix of fuels composed of different amounts of n-heptane, iso-octane, toluene, and 1-hexene. Each of these components has a different chemical structure, which should impact the production of hydrogen. The blends also permit a study of the impact of fuel research octane and sensitivity on the dedicated cylinder performance. The studies are still under analysis at the time of publication of this summary but will be used to guide the development of refinery-produced fuels that incorporate bio-components that can demonstrate a production-feasible fuel and engine combination that achieves the project goal of 25% reduction in petroleum consumption from today's baseline engines.

An updated combustion system has also been designed and is being constructed on a test engine platform. A computer model of the engine assembly is shown in Figure III.4.2. The updated engine will have higher in-cylinder tumble flow, a longer piston stroke, and a significant increase in compression ratio, all of which are essential in maximizing the performance of the engine as compared to the baseline combustion system.

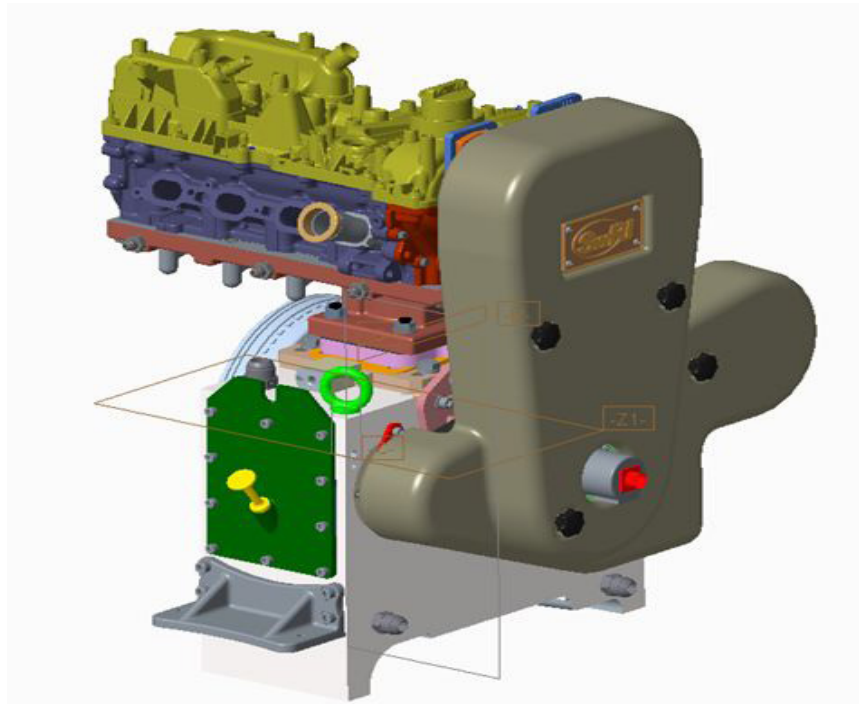


Figure III.4.2. Updated engine configuration for dedicated cylinder testing

Conclusions

The results this year will, when fully analyzed, identify the optimum chemical components of a gasoline fuel optimized for D-EGR combustion. The combined fuel and D-EGR engine system will enable higher compression ratios and extended dedicated cylinder enrichment, both of which will combine with the use of bio-fuel components to yield a major increase in engine efficiency compared to today's engines.

Acknowledgements

The project's principal investigator gratefully thanks Ken Hardman at Fiat Chrysler Automobiles and Nicolas Obrecht at Total for their engineering and in-kind support for this project.

III.5 Improving the Fundamental Understanding of Opportunities Available from Direct Injected Propane in Spark Ignited Engines (Oak Ridge National Laboratory)

James Szybist, Principal Investigator

Oak Ridge National Laboratory
2360 Cherahala Blvd.
Knoxville, TN 37922
E-mail: szybistjp@ornl.gov

Michael Weismiller, DOE Technology Development Manager

U.S. Department of Energy
E-mail: Michael.Weismiller@ee.doe.gov

Start Date: October 1, 2017	End Date: September 30, 2018	
Project Funding (FY18): \$500,000	DOE share: \$500,000	Non-DOE share: \$0

Project Introduction

Spark ignition engine efficiency and operation are fundamentally limited by knock, a process observed via cylinder-pressure measurements as early as the late 1910s [1]. Knock is an unwanted and uncontrolled autoignition of the fuel, which if not avoided can lead to engine damage, and therefore is impermissible in almost all engine applications. It is well known that knock can be reduced through increased octane number fuels. Propane is a high-octane number fuel; however, to date, the intake fumigation or port fuel injection processes used for propane have displaced engine intake air and thus limited the potential of propane as a motor fuel. The goal of this project is to expand the understanding of propane as a motor fuel using direct injection (DI) in advanced spark ignition engines. The results are analyzed by comparing propane to conventional fuels and assessing the efficiency potential that the fuel properties of propane enable relative to conventional fuels.

Objectives

Overall Objective

- Utilize the unique properties of propane to enable higher efficiency in DI engines

Fiscal Year 2018 Objectives

- Design and build a custom long-stroke engine with high compression ratio for use with propane
- Quantify reforming performance with propane over Rh-based catalyst over multiple simulated operating points in a synthetic exhaust flow reactor
- Baseline multi-cylinder engine with propane and compare with gasoline operation

Approach

Oak Ridge National Laboratory has two subtasks as part of the overall effort to increase engine efficiency with DI propane.

Subtask 1: Single-Cylinder Research

Two single-cylinder engine configurations are being explored with DI propane. The first will be with the conventional engine geometry. This will serve as a calibration baseline where efficiency results with direct injected propane will be compared to existing Oak Ridge National Laboratory data with conventional and alternative fuels. In the stock configuration, the engine will have a 9.2:1 compression ratio and a 1:1 stroke-to-bore ratio and is based on a 2.0 L General Motors Ecotec engine equipped with the production side-mounted

direct injection fueling system. The engine was converted to a single-cylinder engine by disabling Cylinders 1, 2, and 3, where Cylinder 1 is closest to the crank snout and Cylinder 4 is closest to the flywheel. The camshaft profiles on Cylinder 4 were unchanged from the stock configuration, and two different engine piston geometries were used, the stock 9.2:1 and a modified 13.6:1 compression ratio (obtained by a modified piston). The engine was operated using standalone laboratory fueling and air handling systems. The engine was controlled through an open setpoint engine controller. The second single-cylinder engine configuration is an advanced engine design with diesel-like compression ratio and a high stroke-to-bore ratio. It has a 13.6:1 compression ratio, but it achieves this through a modified 1.5:1 stroke-to-bore ratio while retaining the stock combustion chamber geometry. The unique aspect of the advanced single-cylinder engine design is that the top dead center engine geometry is identical between the two single-cylinder engine configurations, so there is minimal alteration to the top dead center fluid mechanic scales and quenching effects, minimizing losses typical of conventional reduced clearance volume high-compression-ratio approaches. Moreover, the advanced engine design is specifically oriented towards increased dilution tolerance, where high levels of exhaust gas recirculation (EGR) are possible (greater than 30% cooled external EGR). Using this approach, the work will explore the possibility of achieving diesel engine efficiency parody with stoichiometric dilute DI propane spark ignition combustion. Regardless of the single-cylinder engine configuration, a hydraulic valve train will be used, which has near-infinite control authority, enabling high-efficiency opportunities.

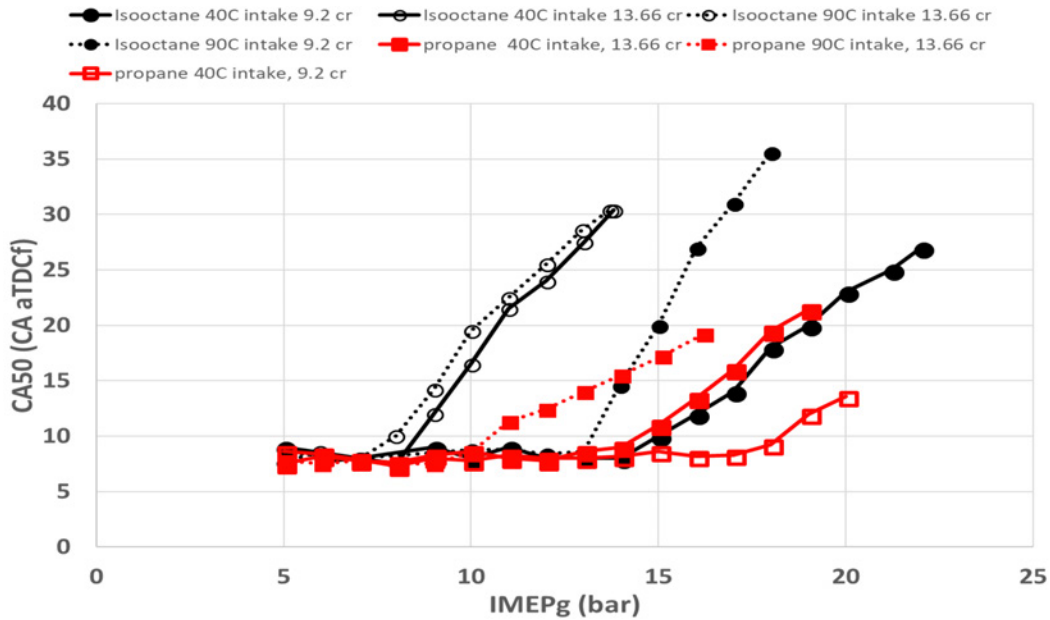
Subtask 2: Multi-Cylinder EGR-Loop Reforming

On the multi-cylinder platform, a catalytic EGR-loop reforming strategy will be investigated. This engine operating strategy has been developed at Oak Ridge National Laboratory with liquid fuels and has demonstrated that high-efficiency fuel reforming is possible, and a fuel consumption decrease of 10% was achieved with this strategy. An isolated cylinder feeds a Rh-based reforming catalyst with a small amount of O₂ present to make the reforming process robust against coking and sulfur deactivation. To guide the engine experiments, a synthetic exhaust flow reactor is being used to define the reforming catalyst boundary conditions suitable for good performance with favorable thermodynamics, including thermochemical recuperation. The strategy is enabled by the reformat extending the dilution limit, which is largely enabled by the high flame speed of the H₂ in the reformat. This was achieved with isooctane and gasoline, where the H/C ratio of the fuel was 1.85–2.125. For propane, the H/C ratio is 2.67, so the potential H₂ yield, dilution tolerance extension, and efficiency benefits with propane are potentially higher. In addition, the initially high octane number of propane combined with the high dilution levels will enable an increase in the compression ratio for an even higher efficiency.

Results

Subtask 1: Single-Cylinder Research

Results with propane and several high-octane “conventional” liquid fuels using the stock (i.e., 1:1 stroke-to-bore ratio) single-cylinder engine configuration are presented in Figure III.5.1, where for brevity only propane and isooctane are shown. The results highlight that at two different compression ratios, there is very different knock-limited performance of propane compared to isooctane. Specifically, propane appears to have increased knock resistance with high compression ratio, but also increased sensitivity to intake temperature. When the intake temperature was 40°C, propane fueling enabled a 4.5-point increase in compression ratio compared to isooctane. However, when the intake temperature was increased to 90°C, the initial knock load of propane was nearly that of isooctane with 9.2 compression ratio with isooctane. The findings illustrate that the thermal sensitivity of propane is high when high compression ratio is used. However, the knock-limited phasing retard for propane was much lower than that of isooctane, where nearly the same loads were achievable with similar combustion phasing once propane was fully retarded. Due to the nature of these intriguing results, the analysis of this data is in the initial stages, but a rigorous investigation of the results and associated reporting of the data is currently underway. Regardless, the findings illustrate that propane expresses very different knock behavior when compared to conventional fuels under similar operating conditions.



cr – compression ratio; CA – crank angle; CA50 – crank angle at 50% mass fraction burned; aTDCf – after top dead center fired; IMEPg – gross indicated mean effective pressure

Figure III.5.1. Knock-limited phasing of propane and isooctane at two compression ratios and various intake temperatures

Based on the results of Figure III.5.1, the custom research engine with similar compression ratio as the high compression (13.66:1 in Figure III.5.1) has been assembled and is being installed for research on propane enabling advanced high-efficiency engine operation. The engine is completely custom and has been designed specifically for high-efficiency operation. The stroke-to-bore ratio of this engine is 1.5:1 and is based on the stock single-cylinder research engine used for the results in Figure III.5.1. The engine installation process is nearing completion, and experiments and analysis on propane as an enabler for this efficiency in this platform are planned for the subsequent year. The custom engine is shown in Figure III.5.2.

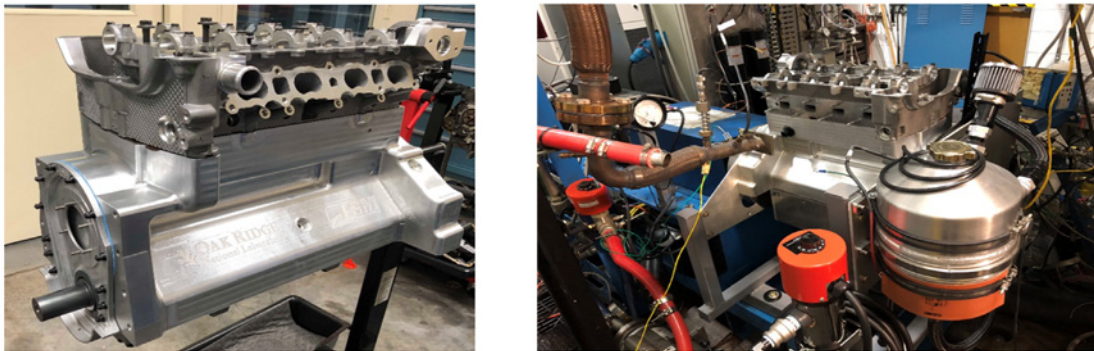


Figure III.5.2. Custom high-efficiency research engine with 1.5:1 stroke-to-bore ratio and high compression ratio

Subtask 2: Multi-Cylinder EGR-Loop Reforming

There were two primary efforts in 2018 associated with this subtask. The first was to evaluate the reforming thermodynamics and performance on a synthetic exhaust flow reactor experiment. This was done using a core sample from the Rh-based catalyst and controlling the feed gas composition, flow rate, and catalyst inlet temperature using a series of mass flow controllers, a water injection system, and a tube furnace. The reforming products were then analyzed and speciated using a series of gas analyzers, including a mass

spectrometer measuring H_2 . This system has been used in the past to measure fuel reforming thermodynamics and performance with liquid fuels. Importantly, for this study, we spanned a wider range of inlet conditions (composition, flow rate, and temperature) to emulate engine operation over a wider range of engine load conditions, spanning from idle to boosted operation.

Figure III.5.3 shows the enthalpy ratio results from the synthetic exhaust flow reactor as a function of inlet O_2 concentration and catalyst equivalence ratio for three different space velocity and temperature conditions, which emulated three different engine operating conditions. It can be seen that at the operating conditions replicating the high-load condition (2,000 RPM, 14.0 bar), the enthalpy ratio is highest. This is because the catalyst temperature at this condition is highest, which provides more favorable thermodynamic conditions for reforming. It should be pointed out that enthalpy ratios greater than unity achieve thermochemical recuperation, which is a form of waste heat recovery where the waste heat in the exhaust is converted to useful chemical energy to be reburned in the engine.

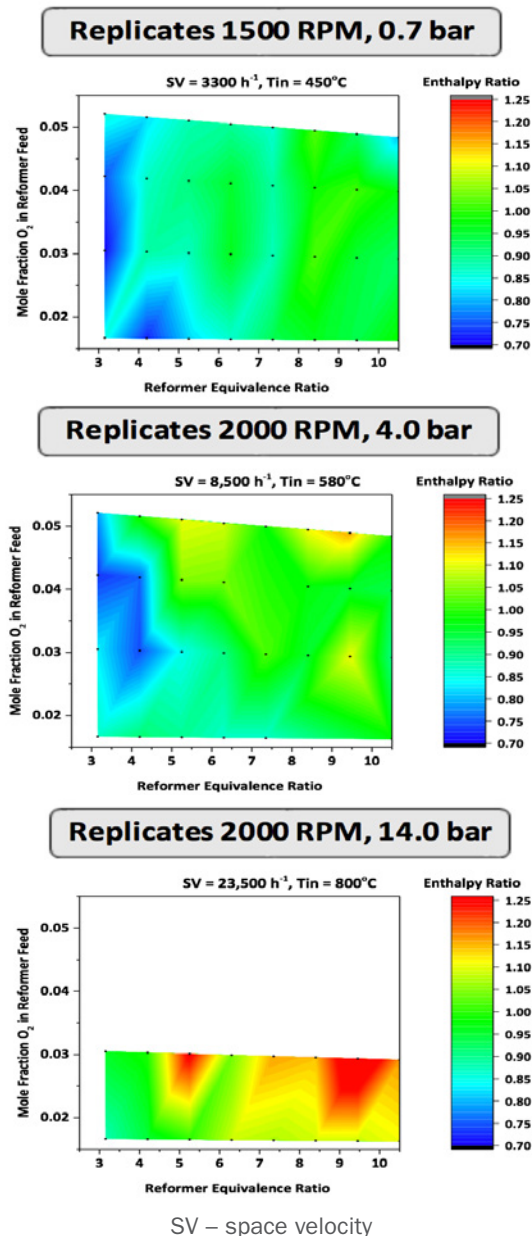


Figure III.5.3. Enthalpy ratio of reformed products to initial products in the synthetic exhaust flow reactor for three different engine conditions

Initial DI engine experiments in the stock configuration to baseline propane operation on the multi-cylinder engine were attempted, but were ultimately not successful initially. The cam-drive DI pump on the multi-cylinder engine could not build fuel rail pressure with the stock configuration because although the propane was under a high pressure, the propane boiled in the DI pump, causing vapor-lock. Thus, experiments in 2018 consisted of conducting multi-cylinder tests with propane by fumigating the propane into the intake system and by pursuing a path to achieving DI propane. To achieve the required hardware modifications, a new propane tank with an internal high-pressure boost pump was acquired. Additionally, a modification was made to the DI pump to provide a bleed hole for the propane vapor to return to the fuel tank. The modified DI pump with the bleed hole for the propane is shown in Figure III.5.4. This pump will be run in the standard and in the reforming engine modes in 2019.

Bleed port machined into DI pump for return propane to prevent vapor-lock

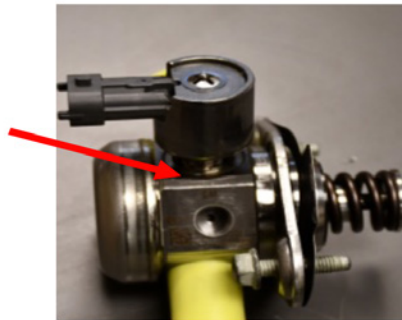
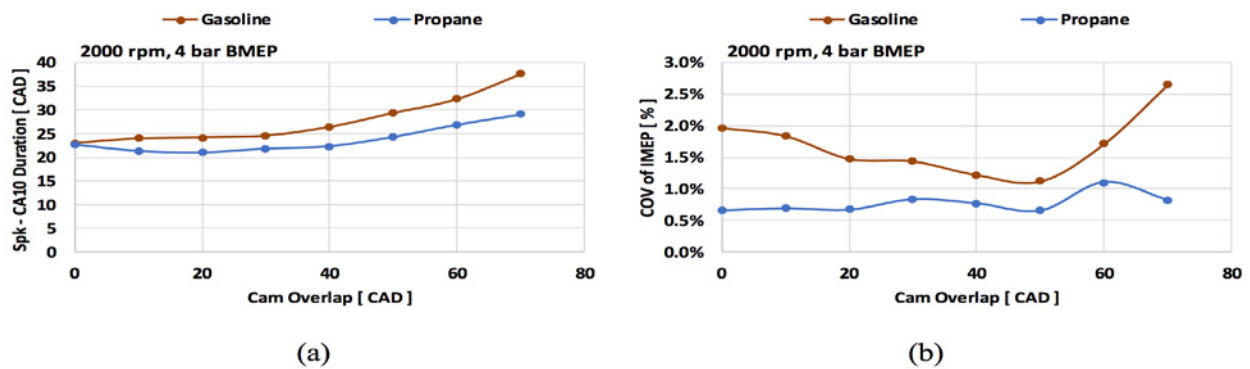


Figure III.5.4. Modified gasoline direct injection pump with bleed port for propane

The engine experiments conducted by fumigating propane into the intake revealed some interesting trends. The propane fuel has a shorter combustion duration, and more specifically, it has a shorter spark-to-CA10 (crank angle at 10% mass fraction burned) duration, as shown in Figure III.5.5a, which indicates a faster initial flame kernel development process. When the initial flame kernel development is faster, combustion stability is improved because there is less time for stochastic turbulence variability to affect the flame kernel [2]. As a result, the combustion variability is lower for the propane fuel than it is for the gasoline, as shown in Figure III.5.5b as the coefficient of variance (COV) of indicated mean effective pressure (IMEP). Faster flame kernel development can be exploited to increase the EGR dilution tolerance [2].



CAD – crank angle degree(s)

Figure III.5.5. (a) Spark-to-CA10 combustion duration and (b) COV of IMEP for both gasoline and propane as a function of the cam overlap at 2,000 rpm and 4 bar brake mean effective pressure (BMEP)

The additional unique feature of the propane is that it had a higher combustion efficiency, meaning that the unburned emissions (CO and HC) were higher. This is shown in Figure III.5.6. The increase in combustion efficiency is substantial, and in some cases is more than a 3% difference. Higher combustion efficiency contributes to a higher engine efficiency by releasing more of the fuel energy in-cylinder and making it available to the engine cycle. Additionally, higher combustion efficiency means that the emissions are easier to treat for an emissions control system.

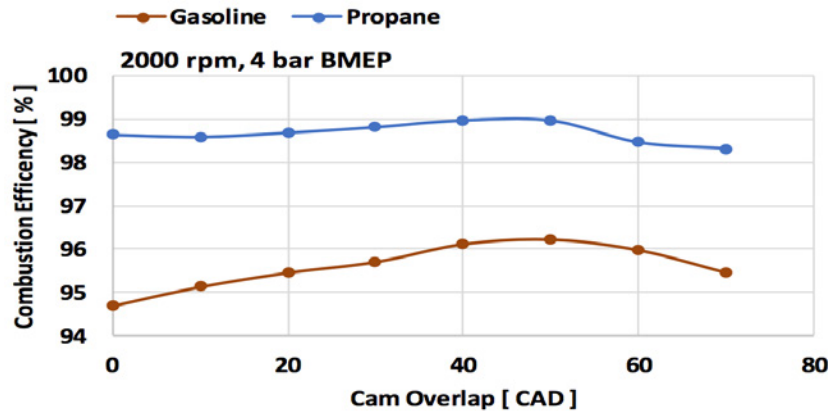


Figure III.5.6. Combustion efficiency for both gasoline and propane as a function of the cam overlap at 2,000 rpm and 4 bar BMEP

Conclusions

- Propane offers unique operation in single-cylinder engines with regards to knock limits, which holds promise for higher efficiency.
- Thermochemical recuperation with propane has been demonstrated over a Rh-based catalyst, which is promising to higher-efficiency engine operation.
- The combustion efficiency and combustion duration with propane in a fumigated engine show distinct advantages over conventional gasoline operation.

References

1. Splitter, D., A. Pawlowski, and R. Wagner. 2016. *Frontiers in Mechanical Engineering*, (1), <https://doi.org/10.3389/fmech.2015.00016>.
2. Szybist, J.P., S.W. Wagnon, D.A. Splitter, W.J. Pitz, and M. Mehl. 2017. "The Reduced Effectiveness of EGR to Mitigate Knock at High Loads in Boosted SI Engines." *SAE Int. J. Engines* 10 (5): 2305–2318, DOI: 10.4271/2017-24-0061.

Acknowledgements

Derek Splitter (Co-Principal Investigator), Melanie Debusk, Josh Pihl of Oak Ridge National Laboratory

III.6 Direct Injection Propane for Advanced Combustion (National Renewable Energy Laboratory)

Brad Zigler, Principal Investigator

National Renewable Energy Laboratory (NREL)
15013 Denver West Parkway
Golden, CO 80401
E-mail: brad.zigler@nrel.gov

Michael Weismiller, DOE Technology Development Manager

U.S. Department of Energy
E-mail: Michael.Weismiller@ee.doe.gov

Start Date: July 1, 2017	End Date: September 30, 2019	
Project Funding (FY18): \$500,000	DOE Share: \$500,000	Non-DOE share: \$0

Project Introduction

Propane, also known as liquefied petroleum gas (LPG) or propane autogas, for on-road transportation is primarily used in spark ignition (SI) engines adapted from existing original equipment manufacturer (OEM) gasoline engines in cars, light-duty trucks, and medium-duty trucks. Similar to natural gas, dual-fuel adaptations of propane fumigated in the intake air stream of a compression ignition (CI) heavy-duty (HD) truck engine have also been attempted but are not currently common in the United States. In light- and medium-duty SI engines, propane is commonly used in a bi-fuel strategy where gasoline is used for the cold start with OEM controls, switching over to propane through additional port fuel injection injectors added to the intake manifold controlled by a piggy-back slave engine control unit using OEM gasoline injector signal inputs after the engine is warmed up. Mono-fuel propane SI engines have also been available, but less common.

Since most propane engines are based on production OEM SI gasoline engines and vehicles, the industry trend for those engines toward direct injection (DI) represents a technology challenge for propane. The combustion strategy enabled by high-pressure, direct fuel injection and unique piston geometries does not adapt well with propane added on with port fuel injection for bi-fuel operation. Converting to mono-fuel operation and flowing propane through the OEM gasoline direct injection (GDI) fuel system is also not a simple engineering problem. NREL is involved in a separate DOE-funded project addressing that technical challenge, as reported in another Annual Progress Report chapter, “Direct Injection 4.3L Propane Engine Research Development and Testing.”

Beyond adapting propane to GDI technology, a longer-term strategy for propane could involve leveraging injection benefits possible with DI to use propane in advanced CI strategies for higher efficiency with low emissions. Expanded transportation use of propane could be enabled, possibly in LPG blends with other similar molecules, in medium- and heavy-duty trucks with advanced CI engines. These truck applications will require high efficiency, could build off current fueling infrastructure technology, and offer low emissions without some of the complex aftertreatment necessary with diesel. This project focuses on early-stage research to understand fundamental challenges and potential for propane blends to support advanced CI using DI.

Objectives

- Adapt NREL’s constant-volume combustion chamber facilities to quantify ignition behavior of propane blends under conditions relevant to advanced CI engine operation
- Develop bench-scale experiments to address technical challenges and characterize injection behavior for flowing propane through existing OEM DI fuel injectors
- Conduct computational fluid dynamics (CFD) simulations to understand mixing behavior differences with propane to guide operating conditions for engine experiments

- Adapt NREL’s new advanced CI single-cylinder research engine (SCRE) to operate with propane blends and demonstrate initial performance under advanced CI strategies
- Develop understanding to link propane blend ignition behavior from constant-volume combustion chamber experiments with SCRE advanced CI performance, guiding potential future research

Approach

As referenced in the Project Introduction, NREL is also working on a separate project with Blossman Services and other partners (including Oak Ridge National Laboratory) to develop a direct injection mono-fuel propane variant of the General Motors 4.3-L V6 GDI engine for a medium-duty, United Parcel Service truck application. That project focuses on higher technology readiness level research and development to adapt propane to a naturally aspirated engine, with only necessary changes from the OEM baseline GDI engine, to support subsequent Environmental Protection Agency certification and commercialization by Blossman. The research NREL is conducting under this project instead has a much lower technology readiness level focus to explore DI of propane with more advanced combustion engine strategies, focusing on increasing efficiency and identifying potential future technology paths.

This research builds on recent gasoline direct injection compression ignition (GDCI) advances by Argonne National Laboratory, Delphi, and Mazda [1–5]. Multi-cylinder engine research and development has been demonstrated for variations of GDCI strategies with gasoline range fuels operating with research octane number (RON) as high as 91–92 [2–4], but with higher efficiencies demonstrated with lower RON (~80) [3]. Fundamental challenges for direct injection of propane under an advanced low-temperature combustion, advanced CI strategy include significantly different fuel spray penetration/breakup/evaporation behavior [6], ignition properties, and fuel system handling issues [7] than gasoline.

Leveraging prior propane system knowledge gained from the separate higher technology readiness level project with Blossman, NREL conducted scale experiments in Fiscal Year (FY) 2018 to understand how propane behaves with the high-pressure DI fuel injector types required for injecting fuel during the compression stroke. In FY 2018, NREL also conducted CFD simulations to model propane injection behavior through DI fuel injectors originally designed for diesel or gasoline range fuels. Since existing kinetic mechanisms do not cover propane blends of interest, NREL is currently adapting the Advanced Fuel Ignition Delay Analyzer (AFIDA) constant-volume combustion chamber platform to conduct experiments on propane blend ignition delay performance under advanced CI-relevant conditions. These ignition kinetics studies build on other related research NREL is performing, as reported in another Annual Progress Report chapter, “Fuel Autoignition Behavior.” Finally, all of these bench-scale experiments and simulations will be integrated in FY 2019 to guide advanced CI engine experiments with propane blends using NREL’s new advanced CI SCRE that is completing construction.

NREL’s approach includes collaboration, including two DOE Office of Science-funded Science Undergraduate Laboratory Internship students: Jacob Barson from Colorado School of Mines (bench-scale DI flow studies) and Owen Brown from University of Colorado-Boulder (CFD studies of propane injection). NREL has also been reviewing this project with industry for technical guidance, including meetings with the propane industry, engine OEMs, and key engine component suppliers.

Results

NREL’s prior related research studying gasoline range ignition kinetics in the AFIDA highlighted issues with flowing low-boiling-range, low-viscosity fuels through a diesel piezoelectric fuel injector. This type of fuel injector is used in the AFIDA, and a similar injector is used in NREL’s new advanced CI SCRE, which is based on the Ford 6.7-L Power Stroke diesel engine. While a DI injector is needed to inject fuel at sufficient pressure to provide adequate mixing during the compression stroke in an advanced CI strategy, it was not yet known if propane blends will need to be injected at very high pressures typical of diesel (~2,000 bar) or moderate pressures typical of GDI (~200 bar). NREL’s research has shown that gasoline boiling range fuels do not allow the internal hydraulic flow control valving in a piezoelectric diesel injector to function properly; propane is expected to be worse. NREL constructed a bench-scale flow rig to study injection flow through the

piezoelectric diesel injector from a Ford 6.7-L engine, as illustrated in Figure III.6.1. Flow studies completed in FY 2018 progressively stepped from diesel to higher volatility with various blends of iso-octane and pentane. Results indicate the piezoelectric injector internal valving does not sufficiently seal to provide adequate injection control. Propane is in progress, including blends with a lubricity improver additive, but results indicate a GDI-type injector may be necessary.

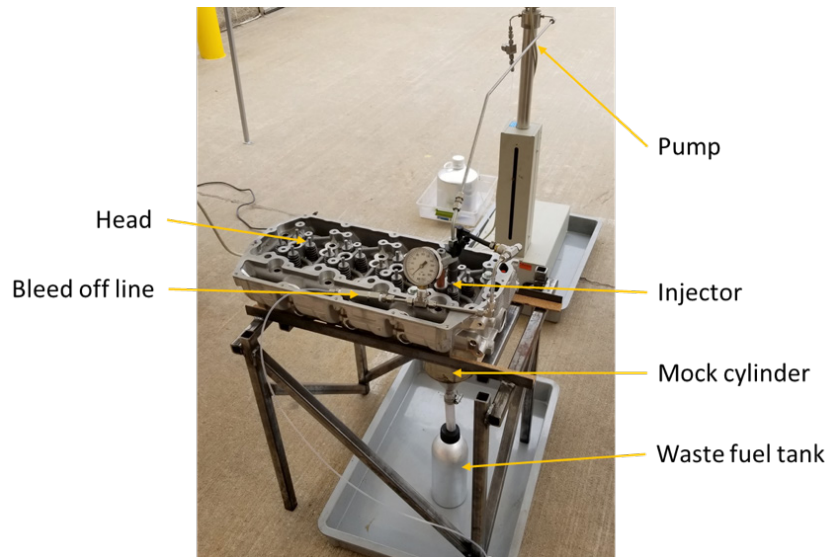


Figure III.6.1. Bench-scale fuel injector flow rig for flow studies through the OEM piezoelectric fuel injector from a Ford 6.7-L diesel engine (Figure: Jacob Barson, NREL)

NREL also completed initial CFD studies of the Ford 6.7-L combustion chamber and production piezoelectric fuel injector to guide subsequent experiments with NREL's new advanced CI SCRE. Fuel injection events with diesel versus propane fuel physical properties were examined to provide guidance on injection pressure and timing, including split events.

NREL is preparing the AFIDA for propane ignition studies in FY 2019 to enable advanced CI operation. Based on the bench-scale studies with a piezoelectric diesel fuel injector, NREL is currently equipping the AFIDA with a new chamber using a GDI injector. The HD-5 transportation fuel specification [8] for LPG will serve as a starting point, but its high pump octane anti-knock index rating (~104–112) [9] and minimum RON (108.2) [10] will likely prevent its direct use for advanced compression ignition strategies. NREL will study ignition behavior of HD-5 LPG and various propane blends to provide guidance on blends that will lower ignition resistance, realizing that current metrics of RON or octane sensitivity may not be sufficient. The propane blend components must maintain LPG-like physical properties, and industry feedback is being gathered to understand potential impacts on transportation LPG fueling infrastructure. The initial focus of propane blends for this GDCI-like study includes propane blended with natural gasolines (~C5–C6), which have RON ~68–72 with very low octane sensitivity [11,12]. Initial linear blend calculations for propane (estimated RON = 110) blended with natural gasoline (estimated RON = 70) provide blends as shown in Table III.6.1.

Table III.6.1. Estimated Volumetric Blending for Propane/Natural Gasoline

Estimated RON	Propane Volume %	Natural Gasoline Volume %
98	70	30
94	60	40
90	50	50
86	40	60
82	30	70

NREL has also reached out to industry to understand more about GDCI studies with naphtha range blends, as light naphtha has a RON in the range of ~68 and heavy naphtha in the range of <40 [13]. Other researchers have evidently also investigated compression ignition of propane blended with cetane improvers, but their recent published work focuses on propane blends with diesel fuel [14,15]. NREL will follow up with those researchers to understand how cetane improvers blended directly with propane were studied, and if this is relevant to GDCI-like combustion.

The most significant portion of NREL's research under this project in FY 2019 will involve SCRE studies of propane blends under advanced, GDCI-like combustion strategies. NREL is currently building a new research-grade metal single-cylinder engine. With support from Ford Motor Company, the engine is based on the production 6.7L Power Stroke diesel engine. The SCRE will have flexible, independent controls to operate under a wide range of low-temperature combustion strategies to study fuels effects. The SCRE will initially use the production piezoelectric diesel injector, but NREL is working with an industry partner to fit a GDI injector into a duplicate cylinder head. The GDI injector may be necessary for advanced CI studies with propane blends, which are planned for summer 2019.

Conclusions

NREL has completed initial lower technology readiness level studies to explore direct injection of propane with more advanced combustion engine strategies, focusing on increasing efficiency and identifying potential future technology paths. Bench-scale injector studies have focused on challenges with controlling injection of propane blends through existing DI injectors. Initial CFD studies have provided guidance on evaporation and mixing differences for propane blends, to help guide engine studies. Initial modifications to the AFIDA are underway to enable propane blend ignition studies. Engine experiments are being planned for propane blends under advanced CI strategies using the new SCRE being commissioned at NREL, with initial results of propane blend potential planned by the end of FY 2019.

References

1. Kolodziej, C., J. Kodavasal, S. Ciatti, S. Som, et al. 2015. "Achieving Stable Engine Operation of Gasoline Compression Ignition Using 87 AKI Gasoline Down to Idle." SAE Technical Paper 2015-01-0832, doi:10.4271/2015-01-0832.
2. Sellnau, M., W. Moore, J. Sinnamon, K. Hoyer, et al. 2015. "GDCI Multi-Cylinder Engine for High Fuel Efficiency and Low Emissions." *SAE Int. J. Engines* 8 (2), doi:10.4271/2015-01-0834.
3. Cho, K., E. Latimer, M. Lorey, D. Cleary, et al. 2017. "Gasoline Fuels Assessment for Delphi's Second Generation Gasoline Direct-Injection Compression Ignition (GDCI) Multi-Cylinder Engine." *SAE Int. J. Engines* 10 (4), doi:10.4271/2017-01-0743.
4. Kolodziej, C., M. Sellnau, K. Cho, and D. Cleary. 2016. "Operation of a Gasoline Direct Injection Compression Ignition Engine on Naphtha and E10 Gasoline Fuels." *SAE Int. J. Engines* 9 (2), doi:10.4271/2016-01-0759.
5. Fujiwara, Kiyoshi. "Briefing on Mazda's Long-Term Vision for Technology Development Technical Overview of SKYACTIV-X." Mazda Motor Corporation, <https://www.scribd.com/document/355807597/mazda-zoom-zoom-2030-skyactiv-x-fujiwara-presentation> (accessed September 2017).
6. Lacey, J., F. Poursadegh, M. Brear, P. Petersen, et al. 2016. "Optical Characterization of Propane at Representative Spark Ignition, Gasoline Direct Injection Conditions." SAE Technical Paper 2016-01-0842, doi:10.4271/2016-01-0842.
7. Kriek, M., M. Günther, S. Pischinger, U. Kramer, et al. 2016. "Future Specification of Automotive LPG Fuels for Modern Turbocharged DI SI Engines with Today's High Pressure Fuel Pumps." *SAE Int. J. Fuels Lubr.* 9 (3), doi:10.4271/2016-01-2255.

8. Gas Processors Association. Liquefied Petroleum Gas specifications and test methods, designation 2140. Tulsa, OK; 1997.
9. https://www.afdc.energy.gov/fuels/propane_benefits.html
10. da Silva, Gabriel, Kai J. Morganti, Tien Mun Foong, Michael J. Brear, Yi Yang, and Frederick Dryer. 2013. “The Research and Motor Octane Numbers of Liquefied Petroleum Gas (LPG).” *Fuel* 108: 797–811, doi:10.1016/j.fuel.2013.01.072.
11. Alleman, T.L., and J. Yanowitz. 2016. “Property Analysis of Ethanol–Natural Gasoline–BOB Blends to Make Flex Fuel.” Technical Report NREL/TP-5400-67243, November 2016.
12. Alleman, T.L., R.L. McCormick, and J. Yanowitz. 2015. “Properties of Ethanol Fuel Blends Made with Natural Gasoline.” *Energy & Fuels* 29 (8): 5095–5102, doi:10.1021/acs.energyfuels.5b00818.
13. Viollet, Y., J. Chang, and G. Kalghatgi. 2014. “Compression Ratio and Derived Cetane Number Effects on Gasoline Compression Ignition Engine Running with Naphtha Fuels.” *SAE Int. J. Fuels Lubr.* 7 (2), doi:10.4271/2014-01-1301.
14. Mancaruso, E., R. Marialto, L. Sequino, B. Vaglieco, et al. 2015. “Investigation of the Injection Process in a Research CR Diesel Engine Using Different Blends of Propane-Diesel Fuel.” SAE Technical Paper 2015-24-2477, doi:10.4271/2015-24-2477.
15. Cardone, M., E. Mancaruso, R. Marialto, L. Sequino, et al. 2016. “Characterization of Combustion and Emissions of a Propane-Diesel Blend in a Research Diesel Engine.” SAE Technical Paper 2016-01-0810, doi:10.4271/2016-01-0810.

Acknowledgements

The principal investigator thanks Jon Luecke, Matt Ratcliff, Jacob Barson, and Owen Brown for their contributions to this project and report. NREL would like to thank Mike Weismiller for his support of this research. Ford Motor Company’s support is greatly appreciated in sharing design information to base NREL’s new advanced CI SCRE on the Ford 6.7-L combustion chamber and architecture. Ford Motor Company also shared design information to enable engine CFD studies. NREL would also like to acknowledge valuable feedback provided to date from various meetings with the propane industry, engine OEMs, and key engine component suppliers.

III.7 Direct Injection 4.3-L Propane Engine Research Development and Testing (Blossman Services, Inc.)

Mark Denton, Principal Investigator

Blossman Services, Inc.
2091 U.S. Highway 70
Swannanoa, NC 28778-9330
E-mail: mldenton@blossmangas.com

Michael Weismiller, DOE Technology Development Manager

U.S. Department of Energy
E-mail: Michael.Weismiller@ee.doe.gov

Start Date: July 18, 2017

End Date: July 17, 2020

Project Funding: \$3,231,643

DOE share: \$2,064,117

Non-DOE share: \$1,167,526

Project Introduction

The goal of this project is to conduct research and develop a dedicated mono-fuel propane-fueled direct injection (DI) engine and emissions control system based on a current production General Motors (GM) EcoTec3 LV3 4.3-L V6 spark ignition, direct injection (SIDI) gasoline/E85 engine, from the Chevrolet Silverado. Led by Blossman Services, the project team also includes Freightliner, National Renewable Energy Laboratory (NREL), Oak Ridge National Laboratory (ORNL), Prins, United Parcel Service (UPS), and the University of Alabama (UA). After demonstrating the prototype DI propane engine and exhaust aftertreatment system is capable of meeting applicable medium-duty engine emissions standards, the engine, fuel system and required exhaust after-treatment will be integrated into a Freightliner P1000 package delivery vehicle. This team will then demonstrate commercial readiness in trial fleet service with UPS.

This new engine/vehicle combination will demonstrate at least a 20% greenhouse gas (GHG) improvement (with a stretch goal of 30%) over the baseline gasoline engine version of the vehicle while meeting all U.S. Environmental Protection Agency (EPA) emissions regulations for the on-highway heavy-duty spark ignition engine and medium-duty and heavy-duty standards. Engine dynamometer, chassis dynamometer, and in-use fleet test data will be incorporated into Autonomie simulations to provide researchers improved tools to assess improvements to the state of the art for propane DI engine technology to reduce GHGs. The 20% GHG improvement over UPS's current 6.0-L V8 port fuel injection (PFI) gasoline engine equipped P1000 will be demonstrated on a custom drive cycle derived from package delivery truck fleet operations.

This project goal requires developing real solutions for the many complications involved when using propane in place of gasoline in SIDI engines. Many of these issues are common with propane usage in DI engines, no matter the engine manufacturer, and some are unique to the specific application chosen. In an effort to maintain focus on fully developing a product with real commercialization potential, the deliverable goal of this project is to develop a propane variant of the GM 4.3-L SIDI V6 engine system that is certification ready and supports a plan to commercialize it for package delivery trucks. Initially planned for the UPS fleet, many other similar engine and chassis types could benefit from this work. Follow-on certification and commercialization in light-duty pickup trucks is also planned.

This project is unique and innovative in two aspects, resulting in a propane-optimized SIDI engine system that will meet fleet user needs and target high-volume commercial applications:

- The DI fuel injection controls will be optimized for mono-fuel propane operation; every effort will be made to keep this propane fuel system a “drop-in” retrofit to the production GM 4.3-L SIDI engine package. This is planned to be accomplished without other significant hardware changes, including using the existing pistons and cylinder heads.

- Since the DI system will be optimized for mono-fuel propane operation, bi-fuel operation with gasoline is unnecessary. The emissions control catalyst system will be developed to meet EPA heavy-duty highway spark ignition emissions standards with propane as a mono-fuel. UPS prefers mono-fuel operation, and this strategy is well aligned with the preferences of other potential fleet users.

Objectives

The overall project objective is to develop a propane-fueled direct injection spark ignition engine and emissions control system based on a current production GM 4.3-L SIDI V6 engine that is certification ready and supports a plan to commercialize it for package delivery trucks. Specific project objectives include:

- Development of propane fuel system, engine hardware, and controls based on recent advances in gasoline direct injection technology that go beyond enabling propane operation and instead allow efficiency and emissions optimization with propane.
- Development of a catalytic emissions control system and catalyst for a propane mono-fuel engine, addressing the cold-start challenge that has required legacy propane systems to retain bi-fuel operation.
- Providing critical, early feedback information to the engine and emissions control industry regarding potential issues for particulate matter on DI propane engines.
- Mapping out of the engineering pathway required for propane DI engine and aftertreatment systems that require minimal changes to an established baseline gasoline engine platform, in recognition that the propane engine market is not yet at critical mass to economically allow for clean-sheet design and independent manufacture.
- Development of the 4.3-L DI engine and emissions control system, and integration into the UPS/Freightliner package delivery truck, ready for certification under the heavy-duty highway spark ignition engine standard, along with evaluation in consideration of the EPA proposed rulemaking for Phase 2 GHG emissions standards and fuel efficiency standards for medium- and heavy-duty engines and vehicles. This directly supports Blossman's commercialization plan to complete certification and take the engine to production in Freightliner MT-45/-55 trucks.
- Demonstration through engine, chassis dynamometer, and in-use fleet operation of at least a 20% GHG improvement over baseline gasoline UPS package delivery truck operation, with a 30% stretch goal.
- Enabling follow-on projects by Blossman to develop and commercialize a propane DI 4.3-L variant of the Silverado/Sierra pickup (Tier 3 emissions), as well as propane DI 5.3-L V8 engine variants.

Approach

This project involves a systems engineering "V-model" of vehicle- and engine-level design targets driving propane-DI-specific hardware and control system research and development, followed by engine- and vehicle-level integration and validation on engine dynamometer, chassis dynamometer, and on-road fleet operation. The project will reach its objectives by focusing on quarterly objectives, total team collaboration, and by making adjustments as needed to reach the stated objectives.

Blossman Services, Inc., serves as the Prime Recipient and project lead responsible for overall management, reporting, budget, collaboration with partners and stakeholders, and primary communication with National Energy Technology Laboratory and DOE.

NREL is responsible for evaluating baseline and prototype vehicles loaned from UPS, developing a UPS-relevant chassis dynamometer drive cycle with the assistance of subcontractor Viatech, studying the baseline engine in and out of the Chevrolet Silverado vehicle, and developing new independent engine control unit integrated engine and aftertreatment controls in direct collaboration with Blossman, UA, and ORNL.

ORNL is responsible for developing new aftertreatment hardware and controls.

UA, as a subcontractor of Blossman, is creating and validating one-dimensional (1D) models to support the development of new engine controls, including sending a graduate student to NREL to assist with experiments.

UPS, who receives no funding, is providing baseline vehicles for analysis to NREL, will purchase new Freightliner vehicle to modify into prototype vehicle and provide to NREL for validation, and will operate prototype vehicle in fleet operation with NREL instrumentation.

Freightliner, who receives no funding, is providing technical support and producing a P1000 vehicle to UPS order specifications, which will be modified into a propane 4.3-L DI prototype by Blossman.

Prins will provide fuel system control hardware and provide technical support to Blossman.

Results

Initial tasks under the systems engineering “V-model” have been completed as follows.

NREL utilized existing data from the Fleet DNA database to develop a custom package delivery truck chassis dynamometer drive cycle to evaluate the baseline 6.0-L gasoline vehicle, against which the 20% GHG reduction will ultimately be evaluated [1]. This custom NREL package delivery drive cycle was developed from almost 1,300 representative days from the 90 vehicles representing package delivery activities in five cities in the United States. As illustrated in Figure III.7.1, the resulting custom cycle has a unique kinetic intensity and average driving speed that better approximates a P1000 duty cycle for UPS than existing standardized chassis dynamometer drive cycles, including the California Air Resources Board (CARB) heavy heavy-duty diesel truck (HHDDT), EPA Urban Dynamometer Driving Schedule (UDDS), or Manhattan bus cycles. NREL then performed fuel consumption and emissions studies of a 2017 Freightliner P1000 UPS truck with a 6.0-L PFI gasoline engine to establish the baseline GHG data.



Figure III.7.1. Kinetic intensity vs. average speed for the NREL package delivery cycle vs. various standard drive cycles

NREL also projected engine performance for the 4.3-L DI engine after propane-specific engineering and development, in part based on prior mapping of the 4.3-L engine on gasoline shared by the EPA [2]. The higher performance level enabled by propane was assumed to match the higher output possible with E85 fuel under the production GM engine control unit operation. NREL and Freightliner then performed vehicle simulations of the P1000 in a heavily loaded gross vehicle weight rating configuration with the projected 4.3-L DI propane engine to ensure the resulting vehicle package meets minimum UPS and Freightliner wide open throttle performance requirements with respect to the 6.0-L PFI gasoline engine baseline. NREL’s vehicle simulations were conducted using Future Automotive Systems Technology Simulator, while Freightliner’s vehicle simulations integrated a more complex transmission model [3].

Blossman supplied NREL with a 2017 Chevrolet Silverado with a 4.3-L DI gasoline/E85 engine, with which NREL has conducted initial engine mapping on a chassis dynamometer before pulling the engine to begin extensive baseline mapping with the original equipment manufacturer production engine control unit calibration on an engine dynamometer. NREL’s subcontractor, Vieletech, is assisting with reverse engineering mapping of the gasoline engine controls to serve as a baseline for propane-specific controls and calibration development using an independent engine controller.

In parallel with NREL’s initial baseline gasoline engine mapping, UA began fuel system simulations with 1D models using GT-SUITE to simulate the gasoline direct injection system used with the 4.3-L DI engine, beginning with the high-pressure pump, through the fuel rails, and out the individual injectors, as illustrated in Figure III.7.2 and Figure III.7.3. This activity included sending a doctoral student under collaborative appointment to NREL over the summer of 2018 to instrument the production 4.3-L DI fuel system and collect critical operating data on gasoline/E85. The UA fuel system 1D simulations and validation on gasoline will feed subsequent 1D propane simulations that will quantify differences in fuel system dynamics expected due to thermodynamic property differences between gasoline/E85 and propane. This knowledge will guide hardware and controls changes required to adapt to propane.

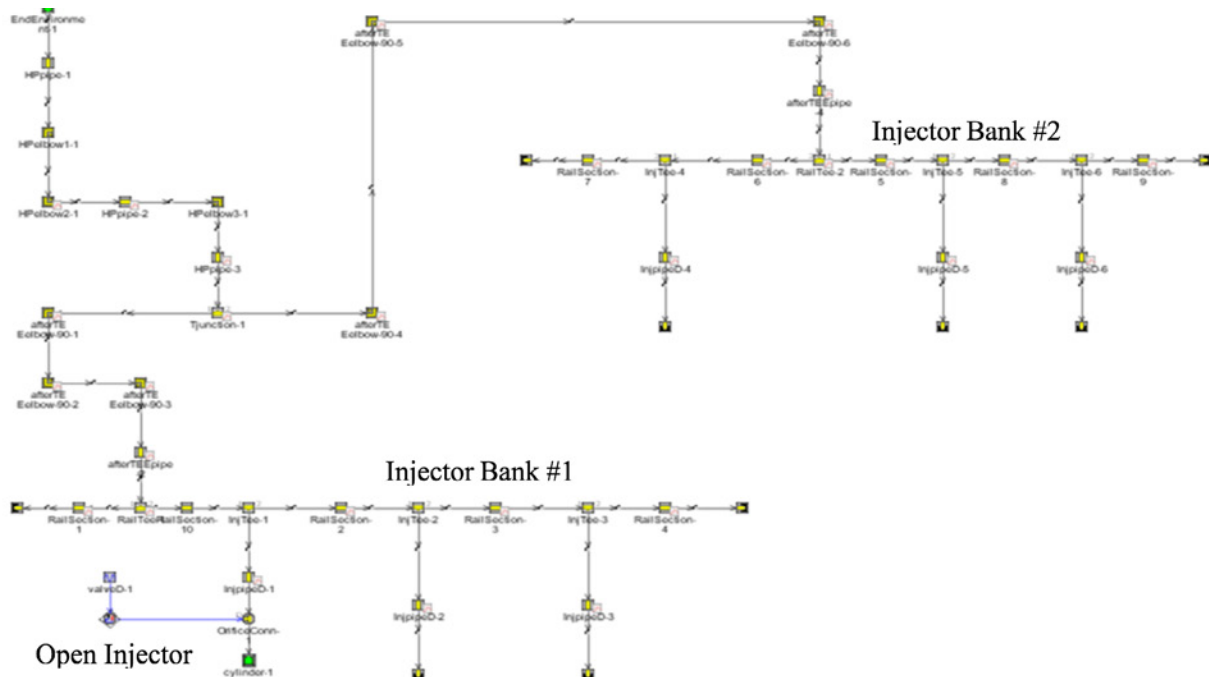


Figure III.7.2. Schematic of the GT-SUITE injection system model developed for the 4.3-L engine

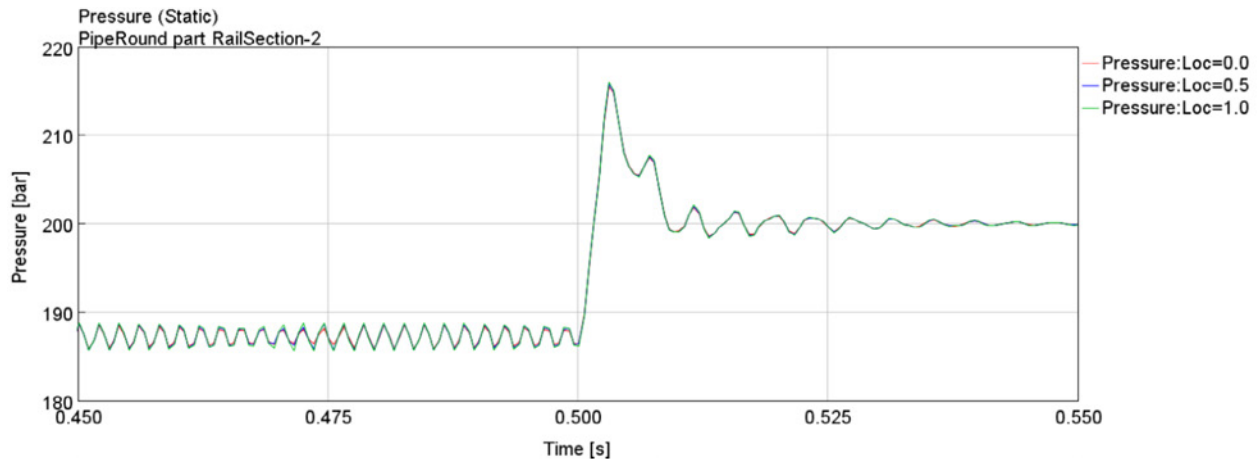


Figure III.7.3. Representative pressure oscillations in Injector Bank #1 of the injection system of the 4.3-L engine for indolene (gasoline) operation at a nominal inlet pressure of 200 bar

In parallel, ORNL has begun development of a propane mono-fuel emissions control system based on a matrix of specially prepared model catalysts provided by industry as well as available industry catalyst components to meet current EPA standards for medium-duty/heavy-duty spark-ignited engines. Three-way catalyst samples from an industry partner have been studied in bench flow reactor studies to study light-off temperature ramps in simulated exhaust gases corresponding to the stoichiometric condition of 0.78% O_2 .

Conclusions

The following specific objectives have been completed on schedule.

- Developed a custom package delivery truck drive cycle
- Used package delivery truck drive cycle to create a GHG baseline using the 6.0-L PFI gasoline variant
- Conducted baseline vehicle-level evaluations to determine GHG targets for the new 4.3-L DI propane engine in the P1000 package delivery truck
- Projected 4.3-L DI propane engine performance and incorporated results in P1000 package delivery vehicle simulations to compare performance against the 6.0-L PFI gasoline baseline
- Began engine baseline studies of a 4.3-L SIDI gasoline engine from Chevrolet Silverado pickup
- Developed 1D models using GT-SUITE to simulate typical gasoline direct injection systems similar to the one used on the GM 4.3-L SIDI gasoline engine
- Began initial aftertreatment three-way catalyst studies to focus on propane mono-fuel operation meeting applicable EPA medium-duty/heavy-duty engine standards

This project is planned to continue in FY 2019 with research and development tied to next-stage objectives related to the following.

- Continued baselining of the 4.3-L DI engine controls on gasoline, to assist with propane-specific development
- Continued simulation and hardware/controls development for the DI propane system
- Development of propane engine control strategy and calibration
- Development of DI propane engine emissions control system and hardware
- Demonstration of 4.3-L DI propane engine and emissions control system performance against emissions targets on an engine dynamometer

Key Publications

1. Zigler, B.T. 2018. "Propane Engine Research Update." Invited presentation at Propane Emissions Summit, Argonne National Laboratory (August).

References

1. "Fleet DNA Project Data." National Renewable Energy Laboratory. Accessed December 2017: www.nrel.gov/fleetdna.
2. Stuhldreher, M. 2016. "Fuel Efficiency Mapping of a 2014 6-Cylinder GM EcoTec 4.3L Engine with Cylinder Deactivation." SAE Technical Paper 2016-01-0662. doi:10.4271/2016-01-0662.
3. Brooker, A., J. Gonder, L. Wang, E. Wood, et al. 2015. "FASTSim: A Model to Estimate Vehicle Efficiency, Cost, and Performance." SAE Technical Paper 2015-01-0973. doi:10.4271/2015-01-0973.

Acknowledgements

This project subcontract is managed under Nicholas D'Amico at the National Energy Technology Laboratory.

IV. Emission Control R&D

IV.1 Joint Development and Coordination of Emission Control Data and Models: Cross-Cut Lean Exhaust Emissions Reduction Simulations (CLEERS) Analysis and Coordination (Oak Ridge National Laboratory)

Josh Pihl, Principal Investigator

Oak Ridge National Laboratory (ORNL)
2360 Cherahala Blvd.
Knoxville, TN 37931
E-mail: pihlja@ornl.gov

Ken Howden, DOE Technology Development Manager

U.S. Department of Energy
E-mail: Ken.Howden@ee.doe.gov

Start Date: October 1, 2015	End Date: September 30, 2018	
Project Funding (FY18): \$650,000	DOE share: \$650,000	Non-DOE share: \$0

Project Introduction

Catalytic emissions control devices will play a critical role in deployment of advanced high-efficiency engine systems by enabling compliance with increasingly stringent emissions regulations. High-efficiency diesel and lean gasoline engines, for example, will require NO_x reduction catalysts with very high conversion efficiencies to meet the U.S. Environmental Protection Agency Tier 3 NO_x emissions standard. Low-temperature combustion strategies, on the other hand, significantly reduce engine-out NO_x, but they generate a challenging combination of high hydrocarbon and carbon monoxide concentrations at low exhaust temperatures that will likely demand novel approaches to emissions control. Design of progressively more complex engine/aftertreatment systems will increasingly rely on advanced simulation tools to ensure that next-generation vehicles maximize efficiency while still meeting emissions standards. These simulation tools will, in turn, require accurate, robust, and computationally efficient component models for emissions control devices. Recognizing this need, the DOE Advanced Engine Crosscut Team initiated the CLEERS activity to support the development of improved computational tools and data for simulating realistic full-system performance of high-efficiency engines and associated emissions control systems. DOE provides funding to ORNL to perform two complementary roles that support this goal: (1) coordination of CLEERS activities that provides a consistent framework for sharing information and supporting pre-competitive collaborative interactions among the emissions control community and (2) focused measurement, analysis, and modeling activities aimed at developing the strategies, data sets, and device parameters needed for better models of catalytic emissions control devices through collaborations with other national labs and partners in academia and industry.

Objectives

Support industry in the development of accurate simulation tools for the design of catalytic emissions control systems that will enable advanced high-efficiency combustion engines to meet emissions regulations while maximizing fuel efficiency through the following activities.

- Coordinate the CLEERS activity for the DOE Advanced Engine Crosscut Team
- Support precompetitive collaborative interactions and provide a consistent framework for sharing information among the emissions control research and development community
- Identify emissions control research and development needs and priorities

- Collaborate with Pacific Northwest National Laboratory to develop mechanistic insights, modeling strategies, benchmark data sets, and representative device parameters for catalytic emissions control devices
- Utilize the CLEERS framework to share the resulting insights, strategies, data sets, and parameters with the emissions control community

Approach

In its administrative role, ORNL coordinates the CLEERS Planning Committee, the CLEERS Focus Group teleconferences, CLEERS public workshops, the biannual CLEERS industry priorities survey, and the CLEERS website (www.cleers.org). ORNL acts as a communication hub and scheduling coordinator among these groups and as the spokesperson and documentation source for CLEERS information and reports. The latter includes preparation and presentation of status reports to the Advanced Engine Crosscut Team, responses to requests and inquiries about CLEERS from the public, and summary reports from the biannual industry surveys.

Measurement, analysis, and modeling activities are conducted in collaboration with Pacific Northwest National Laboratory and include identification of reaction mechanisms occurring over catalytic devices under relevant operating conditions, development of modeling strategies that represent key catalyst processes in a computationally efficient manner, generation of benchmark data sets for model calibration and validation, and measurement of critical device parameters needed for model development. The results of these activities are disseminated through the CLEERS information sharing apparatuses and through publications and presentations. Research directions are guided by the DOE Advanced Engine Crosscut Team, which collectively oversees CLEERS, and by regular CLEERS industry participant priority surveys. ORNL's CLEERS research activities have historically focused on approaches to NO_x reduction in lean exhaust such as lean NO_x traps and urea selective catalytic reduction (SCR), but have recently shifted to include low-temperature aftertreatment technologies such as passive adsorbers for NO_x and hydrocarbons.

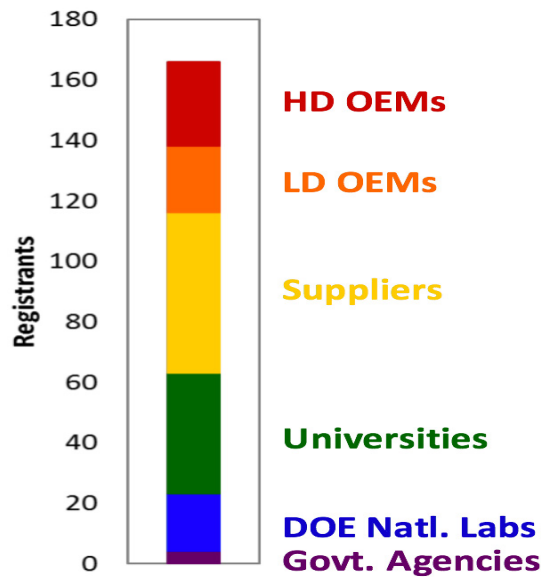
Results

Summary of Fiscal Year (FY) 2018 Accomplishments

- Organized the 2018 DOE Crosscut Workshop on Lean Emissions Reduction Simulation (CLEERS Workshop) in Ann Arbor, Michigan, on September 18–20, 2018
- Facilitated CLEERS Focus Group teleconferences, which continue to have strong domestic and international participation (typically over 40 participants, a majority of which are from industry)
- Provided regular update reports to DOE Advanced Engine Crosscut Team
- Supported the Advanced Combustion and Emission Control Tech Team Low Temperature Aftertreatment Working Group in developing evaluation protocols for low-temperature catalysts
- Conducted extensive experiments to measure the impacts of exhaust gas composition and temperature on the storage and release of NO on a Pd-exchanged zeolite passive NO_x adsorber material; proposed a conceptual mechanism to explain the trends in NO storage capacity

ORNL's CLEERS coordination work during FY 2018 continued to focus on activities that have been identified as high priorities by industrial participants in CLEERS, including the CLEERS Workshop, teleconferences, and the website.

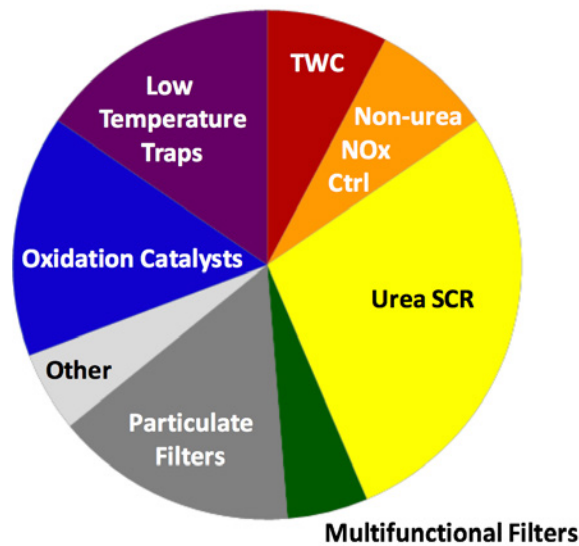
The 2018 (21st) CLEERS Workshop was held September 18–20, 2018, in Ann Arbor, Michigan. The workshop was open to participants from any organization or institution, and workshop registrations once again reached full capacity. Figure IV.1.1 illustrates the broad cross-section of organizations that were represented at the workshop.



OEM – original equipment manufacturer; HD – heavy-duty; LD – light-duty

Figure IV.1.1. 2018 CLEERS Workshop registrations by type of organization

The workshop agenda included four invited speakers, 38 contributed presentations, 24 posters, and an industry panel discussion on “Emission Control Challenges and Opportunities for Hybrid Vehicles.” The presentations covered a wide range of emissions control topics, as illustrated in Figure IV.1.2. Additional details, including many of the workshop presentations, can be found on the CLEERS website (www.cleers.org) under the 2018 Workshop heading.



TWC – three-way catalyst

Figure IV.1.2. 2018 CLEERS Workshop presentation topics

ORNL continued hosting CLEERS Focus Group technical teleconferences in FY 2018. The presentations covered a wide range of research results in emissions control experimentation, modeling, and simulation by members of the CLEERS Focus Group as well as outside experts, including Prof. William Epling (University of Virginia), Andrew “Bean” Getsoian (Ford Motor Company), Petr Kočí (University of Chemical Technology,

Prague), and Yong Miao (General Motors). Teleconference attendance was between 40 and 60 participants, with well over half of those participating from industry.

ORNL also continued to work closely with Pacific Northwest National Laboratory and the industry members of the Advanced Combustion and Emission Control Tech Team Low Temperature Aftertreatment Working Group to support the development of new low-temperature catalyst laboratory evaluation protocols. The protocols for oxidation catalysts, three-way catalysts, and low-temperature storage materials are all available for download from the CLEERS website. Efforts during FY 2018 focused on a fourth protocol for urea SCR catalysts.

ORNL's CLEERS measurement, analysis, and modeling activities during FY 2018 focused on NO storage and release on a passive NO_x adsorber catalyst. Johnson Matthey provided a Pd-exchanged ZSM-5 core sample that was used in a series of synthetic exhaust flow reactor experiments designed to measure the impacts of exhaust composition and temperature on NO storage capacity and release temperature. Data from one of these experiments is shown in Figure IV.1.3. Prior to each experiment, the catalyst was pretreated at 600°C under 10% O₂ and 7% H₂O and then cooled to the desired operating temperature under the same gas mixture. Once the catalyst temperature stabilized, the catalyst was exposed to CO for 5 min (the first step shown in Figure IV.1.3). The catalyst was then exposed to NO until the NO outlet concentration reached a steady state, indicating that the NO storage sites were saturated. The NO was then turned off and the catalyst temperature was ramped from the exposure temperature to 600°C at a rate of 20°C/min. NO storage was quantified by integrating the difference between the inlet and outlet NO concentrations during the uptake process as well as the NO released during the temperature-programmed desorption (TPD). The experimental protocol used in Figure IV.1.3 was repeated dozens of times with different gas concentrations and exposure temperatures as summarized in Table IV.1.1.

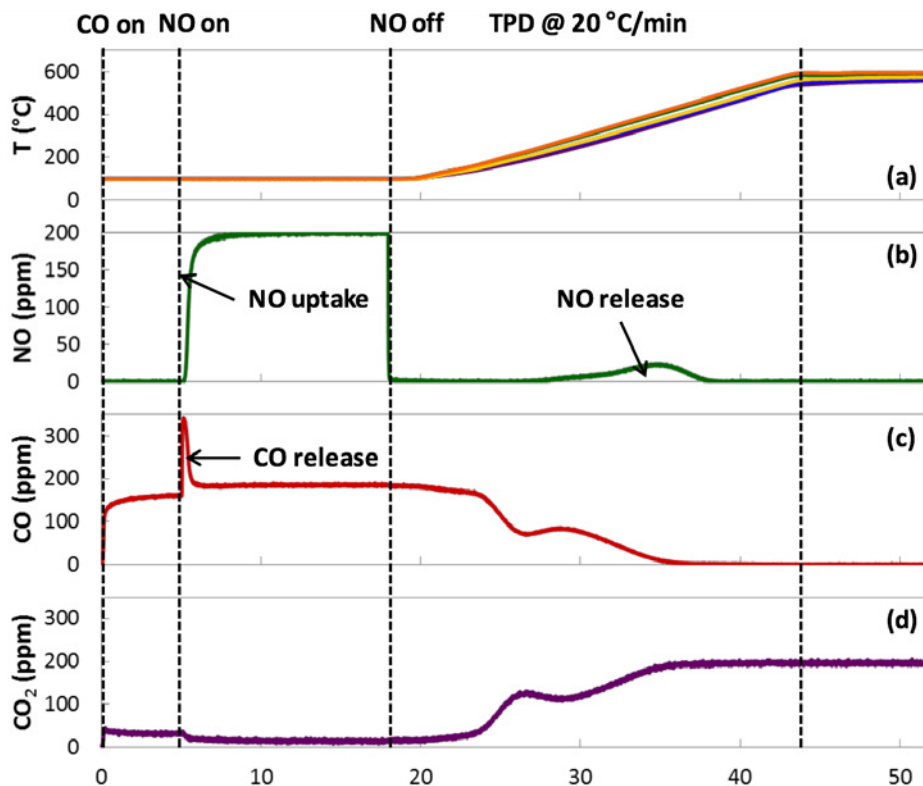


Figure IV.1.3. (a) Core sample temperatures, (b) outlet NO concentration, (c) outlet CO concentration, and (d) outlet CO₂ concentration measured during a synthetic exhaust flow reactor experiment conducted with a Pd-exchanged ZSM-5 catalyst sample

Table IV.1.1. Experiment Parameters

Operating Parameter	Baseline Value	Value Range
NO	200 ppm	(25–1600)
CO	200 ppm	(50–800)
O ₂	10%	(1–13)
H ₂ O	7%	(5–13)
CO ₂	0%	(0–13)
T	100°C	(75–225)

These experiments generated the following observations regarding the impact of various other exhaust constituents on NO storage and release on Pd-exchanged ZSM-5 sample.

- CO₂ concentration had no effect on NO storage capacity or release temperature.
- O₂ concentration had no effect on NO storage capacity and minimal impact on release temperature.
- Increasing H₂O concentration led to a slight decrease in NO storage capacity.
- NO concentration had no effect on NO storage or release temperature (except at extremely low NO concentrations, where release temperature was decreased).
- Increasing CO concentration significantly increased NO uptake but lowered release temperatures at the highest CO concentrations.
- Increasing storage temperature first increased, then decreased NO storage capacity.

Data for a series of experiments conducted with varying CO concentrations while holding all other exposure parameters constant are summarized in Figure IV.1.4. The time for NO to break through clearly gets longer as CO concentration is increased in Figure IV.1.4(a), resulting in higher adsorbed NO in Figure IV.1.4(e). Interestingly, at the highest CO concentrations, the NO desorption profile shifts to lower temperatures in Figure IV.1.4(b). Also, the uptake of NO in Figure IV.1.4(a) is associated with a desorption of CO from the passive NO_x adsorber (PNA) in Figure IV.1.4(c).

These experimental observations are providing insights into the chemical processes by which NO is stored on Pd-exchanged zeolite PNAs. A preliminary mechanistic scheme based on these insights is shown in Figure IV.1.5. Once additional experiments fill in the details of the mechanism, it will be used to guide the development of models for predicting PNA performance and behavior.

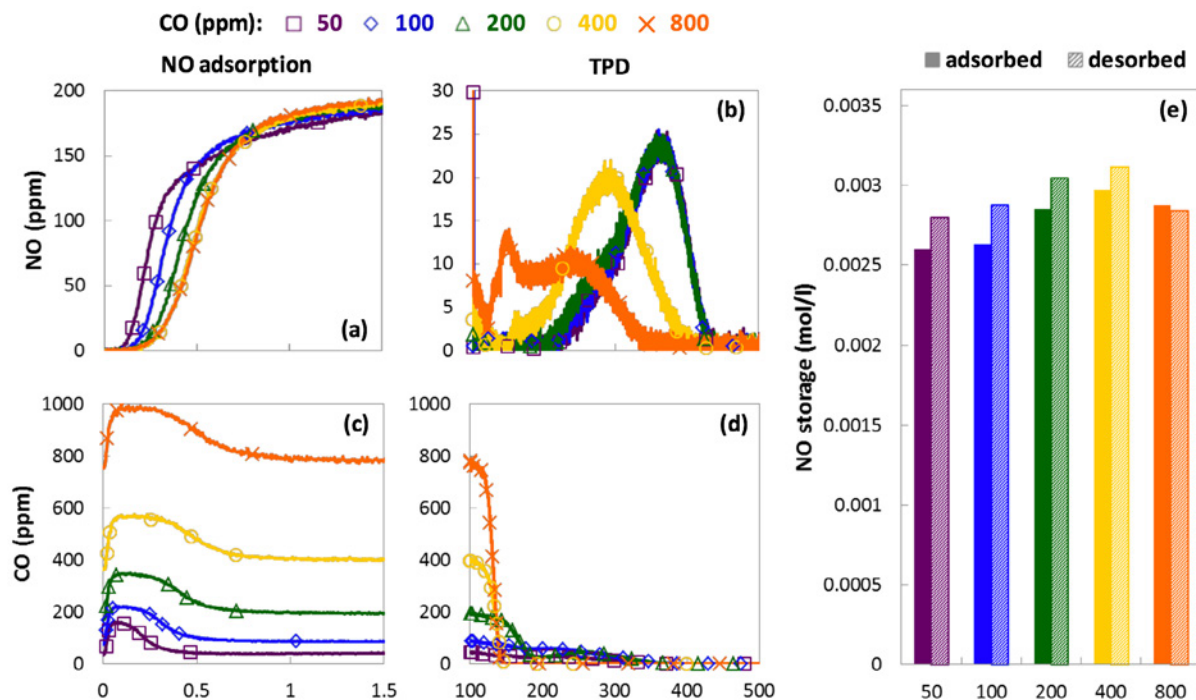


Figure IV.1.4. Impact of changing CO concentration on NO uptake and release measured in a synthetic exhaust flow reactor over a Pd-exchanged ZSM-5 PNA core sample. NO concentration during (a) isothermal uptake and (b) TPD; CO concentration during (c) isothermal NO uptake and (d) TPD; (e) integrated NO adsorption and desorption.

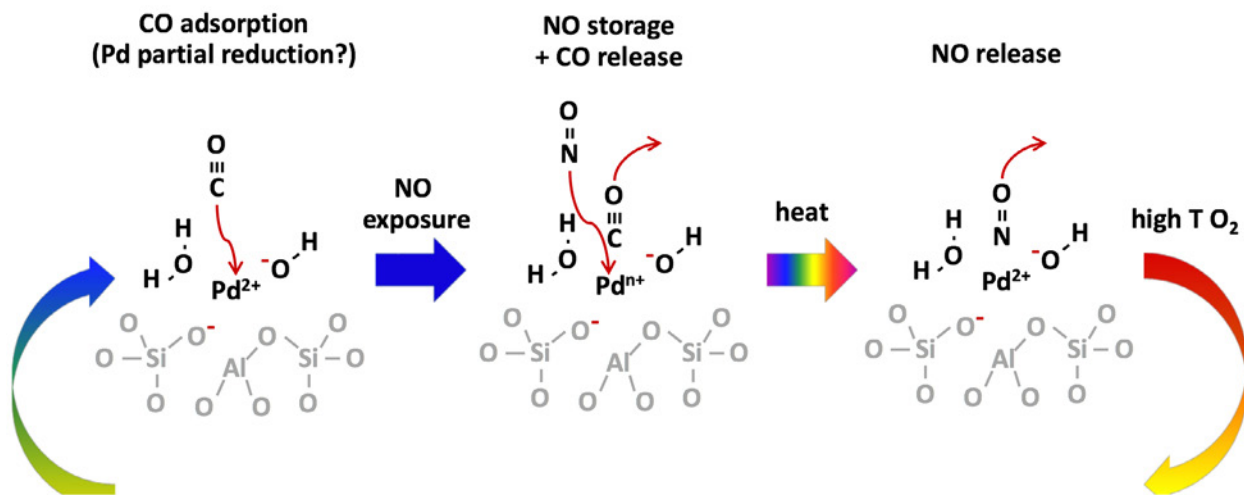


Figure IV.1.5. Schematic of NO storage and release on a Pd-exchanged ZSM-5 PNA

Conclusions

- CLEERS continues to be a valuable resource for the aftertreatment development community, based on the high level of participation in the CLEERS Workshop and Focus Group teleconferences.
- NO storage and release on a Pd-exchanged ZSM-5 passive NO_x adsorber material depend on the exhaust gas composition (particularly H₂O and CO concentrations) and exposure temperature. A preliminary mechanism has been proposed based on these results and will be further refined to incorporate insights from future experiments. Eventually, this mechanism will guide the development of models for simulating PNAs.

Key Publications

1. Rafigh, M., R. Dudgeon, J. Pihl, S. Daw, R. Blint, and S. Wahiduzzaman. 2017. “Development of a Global Kinetic Model for a Commercial Lean NO_x Trap Automotive Catalyst Based on Laboratory Measurements.” *Emission Control Science and Technology* 3 (1): 73–92.

Acknowledgements

The authors gratefully acknowledge Haiying Chen of Johnson Matthey for providing catalyst samples and technical guidance for this work. Thanks also to Vitaly Prikhodko, Sreshtha Sinha Majumdar, Todd Toops, Charles Finney, and Zhiming Gao of ORNL.

IV.2 CLEERS Aftertreatment Modeling and Analysis (Pacific Northwest National Laboratory)

Yong Wang, Principal Investigator

Pacific Northwest National Laboratory (PNNL)
P.O. Box 999, MS K2-12
Richland, WA 99354
E-mail: yong.wang@pnnl.gov

Ken Howden, DOE Technology Development Manager

U.S. Department of Energy
E-mail: Ken.Howden@ee.doe.gov

Start Date: October 1, 2017	End Date: September 30, 2018	
Project Funding (FY18): \$865,000	DOE share: \$865,000	Non-DOE share: \$0

Project Introduction

CLEERS (Cross-Cut Lean Exhaust Emissions Reduction Simulations) is a research and development focus project of the Diesel Cross-Cut Team. The overall objective is to promote the development of improved computational tools for simulating realistic full-system performance of lean-burn engines and the associated emissions control systems. Four fundamental research projects are supported at PNNL through CLEERS: selective catalytic reduction (SCR), passive NO_x absorber (PNA), multi-functional devices, and low-temperature aftertreatment (LTAT). Resources are shared among these efforts in order to actively respond to current industrial needs.

Objectives

- Promote the development of improved computational tools for simulating realistic full-system performance of lean-burn engines and the associated emissions control systems
- Provide the practical and scientific understanding and analytical base required to enable the development of efficient, commercially viable emissions control solutions for ultra-high-efficiency vehicles
- Lead and contribute to the CLEERS activities, e.g., lead technical discussions, invite distinguished speakers, and maintain an open dialogue on modeling issues, and closely work with the Advanced Combustion and Emission Control (ACEC) Tech Team's LTAT team to actively respond to current industrial needs

Approach

This project builds off PNNL's strong base in fundamental sciences by effectively leveraging capabilities from Institute for Integrated Catalysis and Environmental Molecular Sciences Laboratory. Institute for Integrated Catalysis is the largest non-industrial catalysis organization in the United States, and Environmental Molecular Sciences Laboratory is a DOE scientific user facility located at PNNL. The project team closely collaborates with academic research groups from Purdue University, Notre Dame University, University of Houston, and Washington State University, who are funded by National Science Foundation in the emissions control area. The project is oriented strongly towards addressing fundamental issues of broad impact to applications and commercialization by closely working with original equipment manufacturers, TIER 1 suppliers, as well as our partners and sponsors (Oak Ridge National Laboratory, DOE Advanced Engine Cross-Cut Team).

Results

Key accomplishments for Fiscal Year (FY) 2018 include the following.

- The project provided detailed atomic-level understanding on the beneficial or detrimental roles of alkali and alkaline co-cations on the activity and durability of Cu/SSZ-13 SCR catalysts, which can guide further improvement in SCR activity and durability.
- The project prepared Pd/SSZ-13 PNA materials with well-defined structure to provide molecular-level insight into PNA chemistry using combined spectroscopic and density functional theory approach. The project team fundamentally understood the inhibiting role of H₂O and the promotion role of CO on PNA, even in the presence of H₂O, and identified that the maximum NO/Pd ratio of Pd/SSZ-13 is due to stoichiometry of Pd(I/II)-NO and Pd(II)(NO)(CO) complexes. These molecular-level insights provided more accurate descriptions of PNA mechanisms in simulations under CLEERS.
- Low-temperature three-way catalyst test protocol was finalized.
- The team discovered a Pt-based single atom catalyst that exhibits the elusive combination of low-temperature activity and high-temperature durability for CO oxidation.
- The catalyst composition and distribution in a commercial multi-functional exhaust filter were characterized.
- The team effectively disseminated the technical results in 14 peer-reviewed publications in lead scientific journals such as Science, Nature Catalysis, ACS Catalysis, and Journal of Catalysis.

A series of Cu, H/SSZ-13 and Cu, Na/SSZ-13 catalysts were synthesized for the standard NH₃-SCR reaction. The presence of Na⁺ co-cations causes a few effects that are important to SCR. First, their presence lowers Cu-ion exchange capacity, likely because of repulsions between Cu(II)-ions and Na⁺ cations during ion-exchange. Because of this, Cu, H/SSZ-13 catalysts contain higher amounts of isolated Cu-ions and lower amounts of CuO_x clusters, in comparison to Cu, Na/SSZ-13 catalysts with the same total Cu loadings. The presence of CuO_x clusters, beyond a threshold of ~1.0 wt%, is detrimental to hydrothermal stability of the catalysts. The presence of Na⁺ aggravates this adverse effect. However, Na⁺ co-cations provide a beneficial effect of enhancing low-temperature turnover rates of isolated Cu-ion active sites (Table IV.2.1). This effect is believed to be caused by NH₃ adsorption on Na⁺ as a reservoir for reactive NH₃. However, this beneficial effect only leads to catalyst performance enhancement at relatively low Cu loadings (≤1.5 wt%). At higher Cu loadings, this effect is overwhelmed by the detrimental effects (Figure IV.2.1).

Table IV.2.1. Apparent Activation Energy and Turn-Over Rate Summary of Cu, H/SSZ-13, and Cu, Na/SSZ-13 Catalysts. Reaction feed contains 360 ppm NO_x (containing ~20 ppm NO₂), 360 ppm NH₃, 14% O₂, 2.5% H₂O balanced with N₂ at a gas hourly space velocity of 667,000 h⁻¹. Temperatures were varied from 180 °C to 100 °C.

Catalyst	Degreened		Hydrothermally Aged	
	Ea (kJ/mol)	TOR at 180 °C (10 ⁻³ /s)	Ea (kJ/mol)	TOR at 180 °C (10 ⁻³ /s)
1.0wt% Cu, H	42	3.3	43	2.0
2.0wt% Cu, H	68	4.0	58	3.6
3.0wt% Cu, H	78	6.0	47	3.8
4.0wt% Cu, H	63	5.2	68	4.1
1.0wt% Cu, Na	52	7.2	40	4.9
2.0wt% Cu, Na	73	12.1	52	8.4
3.0wt% Cu, Na	65	15.2	62	5.3
4.0wt% Cu, Na	66	10.3	63	1.8

TOR – turn-over rate; Ea – activation energy

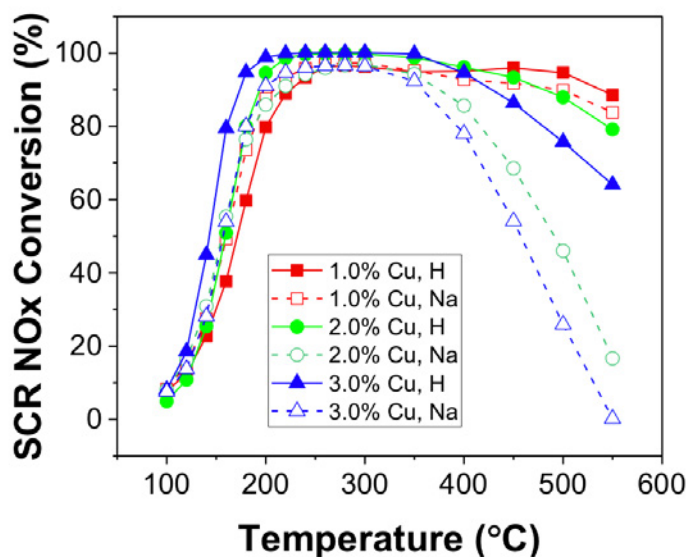


Figure IV.2.1. NO_x conversions as a function of temperature during standard SCR for selected Cu, H/SSZ-13 and Cu, Na/SSZ-13 degreened catalysts. Reactant feed contains 360 ppm NO_x (containing ~20 ppm NO₂), 360 ppm NH₃, 14% O₂, 2.5% H₂O balanced with N₂ at a gas hourly space velocity of 100,000 h⁻¹.

The majority of harmful atmospheric CO and NO_x emissions comes from vehicles' exhaust. Although there has been success addressing NO_x emissions at temperatures above 250°C with the aid of SCR technology that relies on the Cu/SSZ-13 material and sacrificial urea source, emissions during vehicle cold start (when the temperature is below 150°C) are a major challenge. The team provided a direct, simple, and scalable route to highly loaded ionic Pd and Pt in a small-pore siliceous ($3 < \text{Si}/\text{Al} < 12$) zeolite. This route utilizes only wet chemistry and does not require the use of expensive organometallic precursors or organic solvents. The key is to use the NH₄-form of zeolite and the modified incipient wetness method, not the conventional ion exchange. Furthermore, the project reconciles the contradictory literature data in which the Fourier transform infrared spectroscopy characterization for highly loaded Pt and Pd species in Zeolite Socony Mobil-5 (ZSM-5) and other zeolites always indicates the presence of significant amounts of metallic nanoparticles (not well-dispersed Pd or Pt) because (1) H-forms of zeolite are often used for ion exchange, (2) Si/Al ratios greater than 10 are not able to disperse metal as individual atoms due to decreased hydrophilicity of the zeolite micropores, and (3) for Pt, the calcination temperature should not exceed 350°C due to instability of ionic Pt²⁺ above this temperature. This new insight led to the synthesis of Pd/SSZ-13 with up to 2 wt% of atomically dispersed Pd for immediate industrial application as CO and passive NO_x adsorbers. The 1 wt% Pd/SSZ-13 (Si/Al = 6) material synthesized by this new method has an NO/Pd = 1 storage efficiency that translates to a storage capacity of 94 μmol/g. Compared to the state-of-the-art materials described in the open and patent literature, this material exhibits ~50% higher NO storage capacity under industrially relevant conditions than its best reported contender, 1 wt% Pd/BEA, and two times higher than the best reported 1 wt% Pd/SSZ-13. This result brings up the question whether we can further increase the amount of NO_x stored in the Pd-loaded zeolite materials by simply increasing the metal loading. To this end, we prepared additional Pd/SSZ-13 storage materials with metal loadings of 1.9 wt%, 3 wt%, and 5 wt%. We can assume that PNA performance, expressed as NO/Pd ratio, is directly proportional to Pd dispersion since PdO particles do not store NO_x. In fact, we found that for 1.9 wt% Pd/SSZ-13 (Si/Al = 6), the NO/Pd = 1 still holds (Figure IV.2.2). Additional increase in Pd loading to 3 wt%, however, resulted in deviation from this value, as the NO/Pd ratio dropped to 0.9, still a rather high storage efficiency, indicating 90% of Pd is dispersed atomically. Increasing the metal loading to 5 wt% resulted in the decrease in NO/Pd ratio to 0.7. Full utilization of Pd was achieved for materials with Pd loading up to 2 wt%, and the amount of NO stored was 94 μmol/g, 180 μmol/g, 250 μmol/g for 1 wt%, 1.9 wt%, and 3 wt% samples, respectively. Some agglomeration of PdO on the 5 wt% Pd-loaded SSZ-13 (Si/Al = 6) material ultimately led to a decreased NO_x storage efficiency.

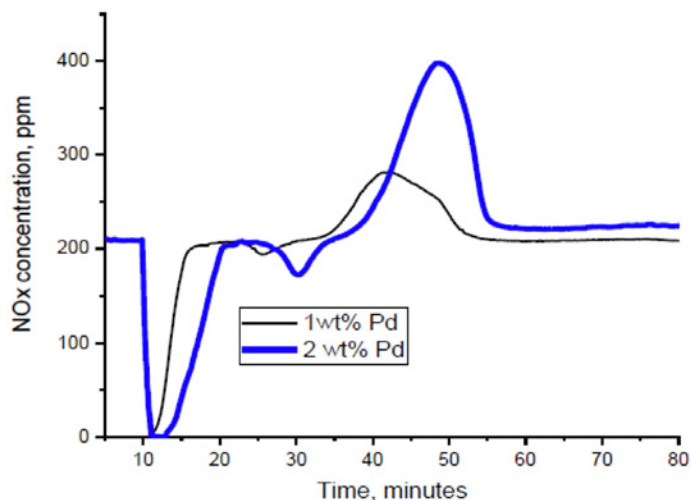


Figure IV.2.2. PNA performance of 1 wt% and 1.9 wt% Pd/SSZ-13 with Si/Al = 6. NO_x adsorption at 100°C for 10 min (after 10 min bypass) followed with temperature-programmed desorption (10°C/min). The feed gas mixture contains 200 ppm of NO_x, 14% O₂, 3% H₂O with 200 ppm CO. Note that for 1.9 wt% Pd/SSZ-13, more time was needed for the NO_x to get back to the initial level due its high effectiveness at abating NO_x; the desorption of NO_x, therefore, was started after ~23 min.

In FY 2018, PNNL supported the activities and mission of the ACEC Tech Team as well as the LTAT group of the ACEC Tech Team. This was predominantly accomplished through (1) routine interaction via bi-weekly LTAT group conference calls and bi-monthly ACEC Tech Team meetings and (2) LTAT catalyst test protocol development; however, activities also included presentations of the highlights of relevant DOE-funded research and preparation of U.S. DRIVE (Driving Research and Innovation for Vehicle efficiency and Energy sustainability) highlights. To review, the low-temperature catalyst test protocols are means to ensure that catalyst discovery is being guided by testing procedure and conditions that are realistic and capture relevant and sufficient performance information. The intent of the protocols is to ensure maximum impact of catalyst discovery and innovation efforts occurring across the technical community towards achieving the goals of U.S. DRIVE and the DOE. This year the LTAT group finalized the Low-Temperature Three-Way Catalyst Test Protocol (Figure IV.2.3), which was reviewed and approved by the ACEC Tech Team and the Advanced Powertrain Technology Leadership Council and has been released to the CLEERS website. Also in FY 2018, the LTAT group is nearing completion of a Low-Temperature NH₃-SCR Catalyst Test Protocol. This protocol has been reviewed by the ACEC Tech Team and will be reviewed by the Advanced Powertrain Technology Leadership Council later this year for expected release to the CLEERS website in early FY 2019.

We have discovered a Pt-based single atom catalyst that exhibits the elusive combination of low-temperature activity and high-temperature durability for CO oxidation. The catalyst is atomically dispersed ionic Pt²⁺ on CeO₂ and is activated via a steam treatment process at 750°C. The synthesis involves a novel approach to trap and stabilize Pt atoms on a CeO₂ surface, resulting in atomically dispersed Pt that enables more efficient use of the precious metal. The catalyst is subsequently treated in high-temperature (750°C) steam to result in a Pt/CeO₂ catalyst that is thermally stable even under harsh hydrothermal conditions. Ultra-high-resolution scanning transmission electron microscopy imaging of Pt/CeO₂ before and after steaming shows that atomic dispersion of Pt/CeO₂ was achieved and retained after thermal and hydrothermal treatment. Additionally, as shown in Figure IV.2.4, the catalytic CO oxidation light-off performance shows excellent low-temperature activity and stability after repeated testing cycles. Activated lattice oxygen, acquired via steam treatment, is believed to be responsible for the extraordinary activity.

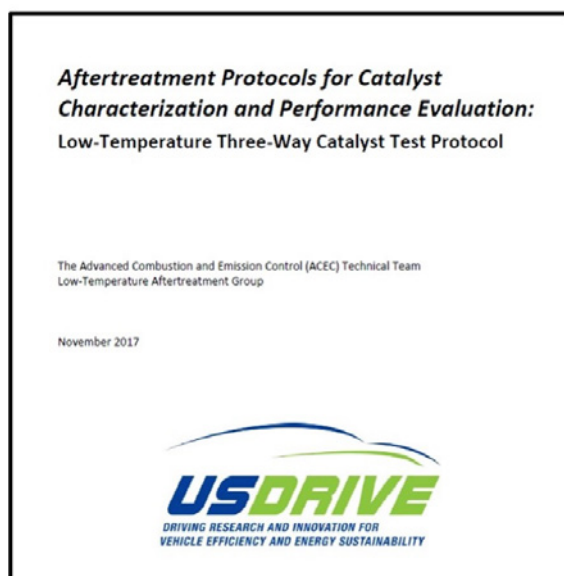


Figure IV.2.3. Low-Temperature Three-Way Catalyst Test Protocol, the third protocol prepared by the LTAT group of the ACEC Tech Team and released to the technical community at <https://cleers.org/low-temperature-protocols>

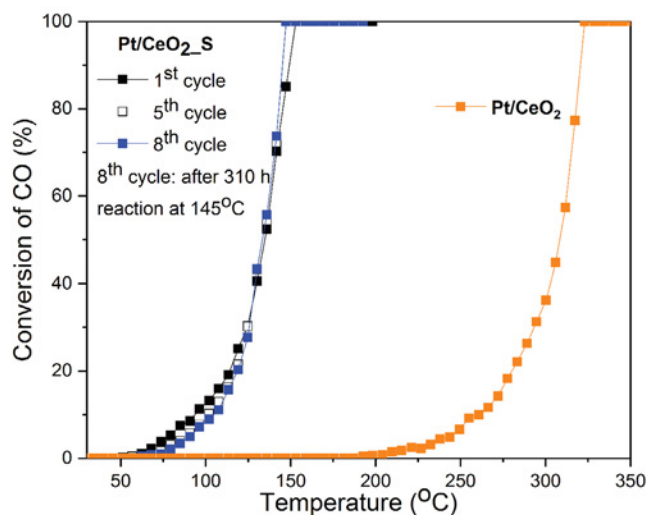


Figure IV.2.4. CO oxidation light-off performance showing excellent low-temperature activity and stability of the hydrothermally treated Pt/CeO₂ catalyst under exhaust conditions ([O₂] = 10%, [CO] = 0.4%, gas hourly space velocity = 200 L (gcat hr)⁻¹)

PNNL continued work on characterization of a commercial SCR-filter unit, which is one of the first examples of a multi-role diesel particulate filter system deployed in the North American market with an integrated NO_x reduction functionality. High-fidelity performance modeling of such devices will likely require detailed information of design features such as location and morphology of the catalyst coating. An array of analyses were performed on multiple filter sections, including mercury porosimetry, electron microscopy, and micro X-ray computed tomography. Catalyst samples were also analyzed using X-ray photoelectron spectroscopy and X-ray diffraction. The catalyst coating likely consists of Cu/SSZ-13, with the possible inclusion of some alumina and zirconia. As previously reported, three distinct axial zones were observed within the filter brick. Mercury porosimetry data corresponding to the three zones is shown in Figure IV.2.5. Two modes can be seen in the pore size distributions. The larger mode presumably corresponds to the pores in the ceramic substrate, and the dotted line represents a hypothetical pore size distribution for the original, uncoated filter,

assuming a porosity of 62%. Section 2 was a band of thick catalyst coating, where practically all of the original substrate porosity had been filled or blocked by the washcoat phase. Here only the small mode was evident, presumably associated with pores in the washcoat phase. Section 1 (at the upstream end of the filter brick) had a lighter coating, while Section 3 (at the downstream end of the brick) had an intermediate level. Both modes were apparent in these regions, indicating that some of the original substrate porosity remained open. X-ray computed tomography images suggest that Section 1 was coated from the upstream end of the brick, Section 3 from the downstream end, and Section 2 from both ends in an overlapping fashion. Pore-scale and device-scale modeling efforts are currently underway to explore the effects of realistic catalyst distribution on multi-functional device performance.

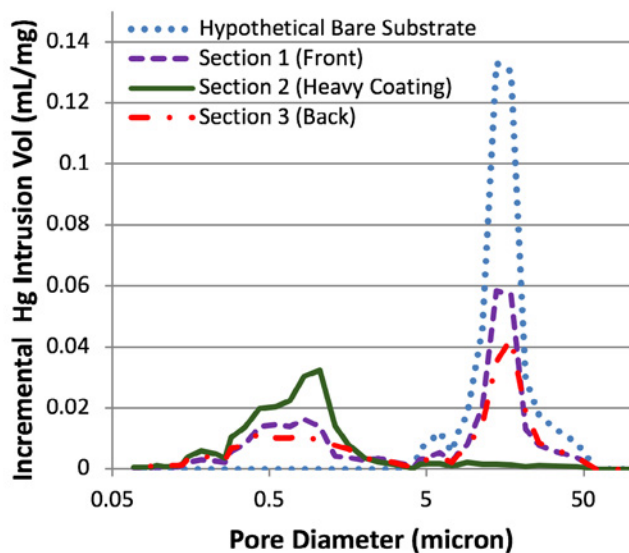


Figure IV.2.5. Pore size distributions in samples from three axial regions in a commercial SCR-filter

Conclusions

- Detailed atomic-level understanding on the beneficial or detrimental roles of alkali and alkaline co-cations on the activity and durability of Cu/SSZ-13 SCR catalysts can guide further improvement in SCR activity and durability.
- Fundamental understanding of the inhibiting role of H₂O and promotion role of CO on PNA, even in the presence of H₂O, provides more accurate descriptions of PNA mechanisms in simulations under CLEERS.
- The low-temperature three-way catalyst test protocol is finalized.
- Pt-based single atom catalyst exhibits the elusive combination of low-temperature activity and high-temperature durability for CO oxidation.
- Catalyst composition and distribution in a commercial multi-functional exhaust filter were characterized.
- Technical results in SCR, PNA, low-temperature aftertreatment, and multifunctional filters were effectively disseminated in 14 peer-reviewed publications in lead scientific journals such as Science, Nature Catalysis, ACS Catalysis, and Journal of Catalysis.

Key Publications

1. Nie, L., D. Mei, H. Xiong, B. Peng, Z. Ren, X. Hernandez, A. DeLaRiva, M. Wang, M.H. Engelhard, L. Kovarik, A.K. Datye, and Y. Wang. 2017. “Activation of Surface Lattice Oxygen in Single-Atom Pt/CeO₂ for Low-Temperature CO Oxidation.” *Science* 358: 1419–1423. DOI: 10.1126/science.aao2109.
2. Song, James, Yilin Wang, Eric D. Walter, Nancy M. Washton, Donghai Mei, Libor Kovarik, Mark H. Engelhard, Sebastian Prodingler, Yong Wang, Charles H.F. Peden, and Feng Gao. 2017. “Toward Rational Design of Cu/SSZ-13 Selective Catalytic Reduction Catalysts: Implications from Atomic-Level Understanding of Hydrothermal Stability.” *ACS Catal.* 7: 8214–8227.
3. Wang, Aiyong, Yilin Wang, Eric D. Walter, Ravi K. Kukkadapu, Yanglong Guo, Guanzhong Lu, Robert S. Weber, Yong Wang, Charles H.F. Peden, and Feng Gao. 2018. “Catalytic N₂O Decomposition and Reduction by NH₃ over Fe/Beta and Fe/SSZ-13 Catalysts.” *J. Catal.* 358: 199–210.
4. Gao, Feng, and Charles H.F. Peden. 2018. “Recent Progress in Atomic-Level Understanding of Cu/SSZ-13 Selective Catalytic Reduction Catalysts.” *Catalysts* 8: 140.
5. Gao, Feng, and János Szanyi. 2018. “The Stream of Change.” *Nature Catalysis* 1: 174–175.
6. Chen, Hai-Ying, Marton Kollar, Zhehao Wei, Feng Gao, Yilin Wang, János Szanyi, and Charles H.F. Peden. “Formation of NO⁺ and Its Possible Roles during the Selective Catalytic Reduction of NO_x with NH₃ on Cu-CHA Catalysts.” *Catal. Today*, in press.
7. Wang, Aiyong, Yilin Wang, Eric D. Walter, Nancy M. Washton, Yanglong Guo, Guanzhong Lu, Charles H.F. Peden, and Feng Gao. “NH₃-SCR on Cu, Fe and Cu+Fe Exchanged Beta and SSZ-13 Catalysts: Hydrothermal Aging and Propylene Poisoning Effects.” *Catal. Today*, in press.
8. Szanyi, János, Donghai Mei, Tamás Varga, Charles H.F. Peden, Iljeong Heo, Se Oh, and Chang Hwan Kim. “Where Does the Sulphur Go? Deactivation of a Low Temperature CO Oxidation Catalyst by Sulphur Poisoning.” *Catalysis Letters*, <https://doi.org/10.1007/s10562-018-2343-2>.
9. Heo, Iljeong, Steven J. Schmiege, Se H. Oh, Wei Li, Charles H.F. Peden, Chang Hwan Kim, and János Szanyi. 2018. “Improved Thermal Stability of a Copper-Containing Ceria-Based Catalyst for Low Temperature CO Oxidation under Simulated Diesel Exhaust Conditions.” *Catal. Sci. Technol.* 8: 1383. DOI: 10.1039/c7cy02288c.
10. Khivantsev, Konstantin, Feng Gao, Libor Kovarik, Yong Wang, and János Szanyi. “Molecular Level Understanding of How Oxygen and Carbon Monoxide Improve NO_x Storage in Palladium/SSZ-13 Passive NO_x Adsorbers: The Role of NO⁺ and Pd(II)(CO)(NO) Species.” *J. Phys. Chem. C*, DOI:10.1021/acs.jpcc.8b01007.

Acknowledgements

Thanks to Feng Gao, Jamie Holladay, Donghai Mei, Ken Rappe, Mark Stewart, Janos Szanyi, and Yilin Wang of Pacific Northwest National Laboratory.

IV.3 Low-Temperature Emission Control to Enable Fuel-Efficient Engine Commercialization (Oak Ridge National Laboratory)

Todd J. Toops, Principal Investigator

Oak Ridge National Laboratory
2360 Cherahala Boulevard
Knoxville, TN 37932
E-mail: toopstj@ornl.gov

Ken Howden, DOE Technology Development Manager

U.S. Department of Energy
E-mail: Ken.Howden@ee.doe.gov

Start Date: October 1, 2016	End Date: September 30, 2018	
Project Funding (FY18): \$340,000	DOE share: \$340,000	Non-DOE share: \$0

Project Introduction

Removing the harmful pollutants in automotive exhaust has been an intense focus of the automotive industry over the last several decades. In particular, the emissions regulations for fuel-efficient diesel engines that were implemented in 2007 and 2010 have resulted in a new generation of emissions control technologies. These catalysts usually reach 90% conversion of pollutants between 200°C and 350°C, but below these temperatures, the catalysts are relatively inactive. Consequently, more than 50% of pollutant emissions occur in the first 2–3 min of the transient drive cycle required for certification and under cold-start or idling conditions. Thus, as emissions regulations become more stringent, meeting the emissions regulations will require increased activity during this warm-up period. To further complicate matters, the increased Corporate Average Fuel Economy standards that will be implemented over the next decade will result in the introduction of more fuel-efficient engines. Higher fuel efficiency will result in less heat loss to exhaust and lower exhaust temperatures, which further necessitates increased emissions control activity at low temperatures. With this in mind, the U.S. DRIVE (Driving Research and Innovation for Vehicle Efficiency and Energy Sustainability) Advanced Combustion and Emissions Control Tech Team has set a goal of achieving 90% conversion of CO, hydrocarbons (HC), and NO_x at 150°C. Higher Pt and Pd loadings may help to increase the catalytic efficiency, but such methods are too expensive for long-term success. Thus, this project focuses on developing new catalytic materials that are active at lower temperatures. In addition, other options to meet the emissions standards such as hydrocarbon and NO_x adsorbers are being pursued; these adsorber materials can trap the pollutants at low temperature for later release and treatment at higher temperatures where catalysts are active.

Objectives

- Develop emissions control technologies that achieve >90% reduction of pollutants at low temperatures (<150°C) to enable fuel-efficient engines with low exhaust temperatures to meet new U.S. Environmental Protection Agency Tier 3 emissions regulations that require ~80% less NO_x and hydrocarbon emissions than current standards
- Identify advancements in technologies that will enable commercialization of advanced combustion engine vehicles
- Understand fundamental surface chemistry mechanisms that either enable or limit low-temperature emissions control

Approach

To reach the goal of 90% conversion at 150°C, a multi-functional approach will be pursued. Currently, there is a large effort being pursued in the Basic Energy Science programs that is focused on studying catalysts with very high activity regardless of the specific application. We initiate contact with these researchers to

investigate their catalysts in the harsh conditions that are present in automotive exhaust, e.g., H₂O, CO₂, CO, HC, NO_x, and hydrothermal aging above 800°C. Often these catalysts show exceptional activity in single-component exhaust streams, but there is significant inhibition from other exhaust species. With this in mind, we are aiming to understand the limitations of each system but also look for synergistic opportunities when possible. This includes using traps to limit exposure of inhibiting species to active catalysts until temperatures are more amenable. Also, mixing catalytic components where the catalysts are limited by different species will be explored. Our efforts will aim to understand the processes at a fundamental level and illustrate any benefits or shortcomings of each catalyst we study, while striving to find compositions that will achieve the very challenging goal of 90% conversion of CO, NO_x, and HC at 150°C. Improving this understanding of the potential advantages and limitations of catalysts will guide the reformulation of new catalysts.

Results

This year we were able to conclude a collaborative study between Oak Ridge National Laboratory, the University of South Carolina (USC), and Solvay. Catalytic support materials with a range of silica (SiO₂) introduced to alumina (Al₂O₃) were provided to USC from Solvay. USC then dispersed Pt and/or Pd on these supports, with catalytic evaluation being performed at Oak Ridge National Laboratory using the low-temperature oxidation catalyst protocols established by the U.S. DRIVE Advanced Combustion and Emissions Control Tech Team [1]. In the fresh state, the catalysts prepared at USC showed remarkable oxidation behavior, as the best one (2% Pt on 20% SiO₂/80% Al₂O₃) was able to achieve 90% conversion at 145°C (T₉₀) of the total hydrocarbons (THC) in the evaluation: C₂H₄, C₃H₆ and C₃H₈ (Figure IV.3.1a). However, upon even mild aging at 700°C for 4 h, these catalysts start to lose effectiveness, and the T₉₀ increases to 159°C. Further aging at 800°C for 50 h, as per the U.S. DRIVE protocol, results in a higher T₉₀ for each evaluated catalyst (Figure IV.3.1b), with the 2% Pt on 20% SiO₂/80% Al₂O₃ catalyst continuing to show the best oxidation behavior. Across all supports, the Pt-based catalysts (✦) show the best oxidation behavior. Another part of the study was to determine optimal silica content in the support. Figure IV.3.2 illustrates that alumina-based supports with 10–30% Si content range showed the lowest/best light-off temperature behavior. One of the samples contained 4% La, which increases the THC light-off temperature.

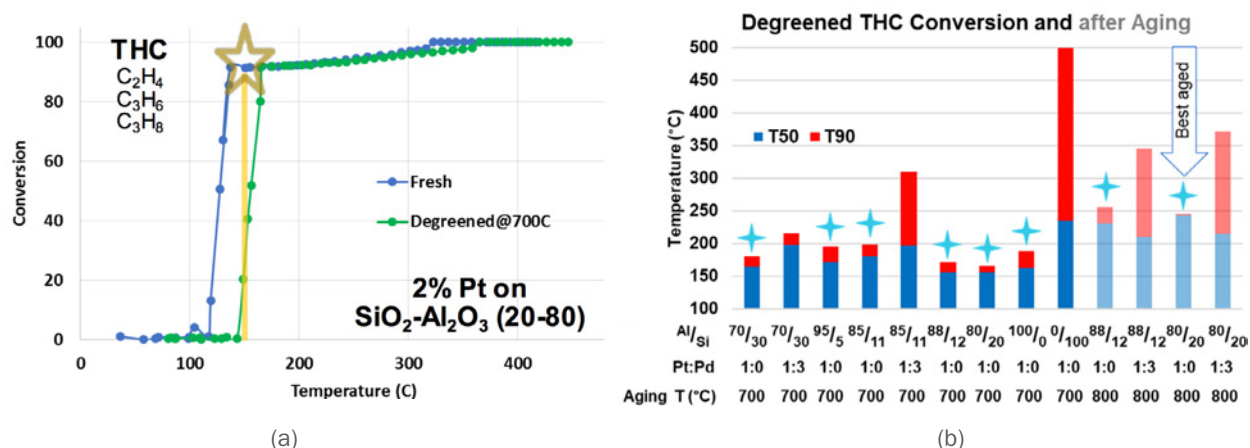


Figure IV.3.1. (a) 2% Pt catalysts supported on a 20% SiO₂/80% Al₂O₃ support from Solvay show exceptionally low THC light-off behavior in the fresh state using the U.S. DRIVE evaluation protocol, but even mildly aging at 700°C for 4 h (degreened) results in lost activity. (b) Of all the samples evaluated, Pt-based catalysts (✦) show the lowest light-off temperatures, while aging up to 800°C continues to degrade performance.

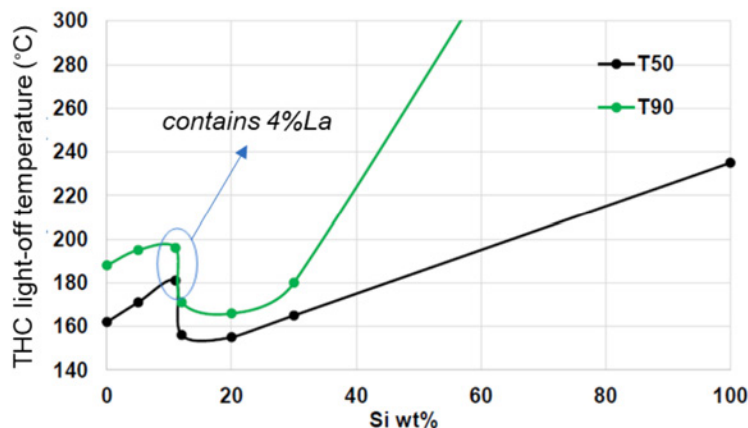


Figure IV.3.2. Varying the Si content of the primarily alumina support material results in a decrease in THC light-off temperature in the 10–30% Si content range. One of the samples contained 4% La, which increases the THC light-off temperature.

Efforts also progressed on the study of trap materials and the impact of aging. Last year we reported that the best trap material for both NO and hydrocarbons was the ion-exchanged Pd/ZSM-5 [2]. Figure IV.3.3a illustrates how well this material trapped hydrocarbons, C_3H_6 and $C_{10}H_{22}$, as well as NO. However, we were unable to complete a full hydrothermal aging evaluation (800°C for 50 h) of this material until this year. Figure IV.3.3b shows that after aging, the Pd/ZSM-5 has maintained the ability to store only $C_{10}H_{22}$, while NO storage has been completely deactivated. This important finding illustrates that even though this catalyst is severely aged, the ability to trap HC is still strong, while another solution will be necessary for NO. A more stable Pd-CHA zeolite will be the focus of research next year for NO trapping.

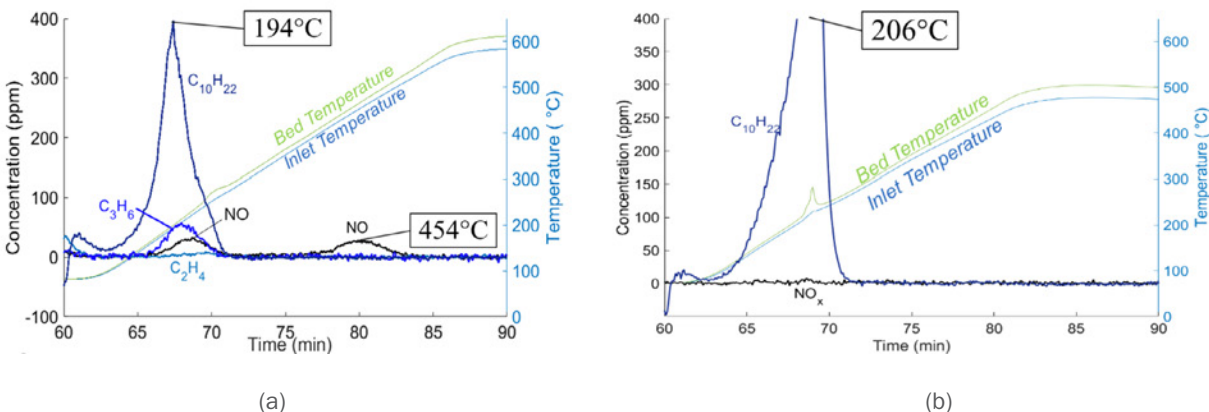
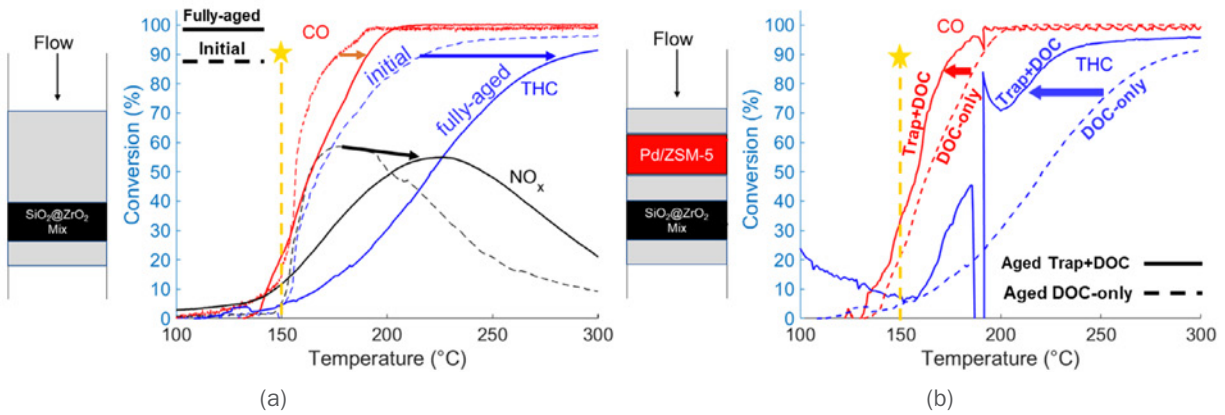


Figure IV.3.3. (a) In the degreened state, the Pd/ZSM-5 stores significant concentrations of C_3H_6 , $C_{10}H_{22}$, and NO following the U.S. DRIVE trapping protocol. (b) Upon aging at 800°C, only $C_{10}H_{22}$ is stored, but it is in large quantities, thus illustrating the ability of ZSM-5 to be useful as a HC trap material.

Other efforts this year have progressed to the study of our most promising materials in combination with each other to overcome drawbacks resulting from use of the individual materials alone. This year we completed a full aging protocol [1] on our best oxidation catalyst that we reported last year [2], a physical mixture of Pt and Pd catalysts dispersed on a novel silica-zirconia core-shell support ($SiO_2@ZrO_2$ mix). Figure IV.3.4a shows how this 50 h aging protocol at 800°C significantly with sulfur exposure degrades the activity of the $SiO_2@ZrO_2$ mix. However, employing a dual-bed configuration and combining this $SiO_2@ZrO_2$ mix with the fully-aged trap material results in significant improvements in T_{90} , as shown in Figure IV.3.4b. To observe how each step of the aging protocol impacted the activity, the T_{90} results are shown in Figure IV.3.5. Here it can be seen that the biggest activity loss for THC activity is the completion of the 50 h aging, as 10 h of aging at 800°C did not have a big impact.



DOC – diesel oxidation catalyst

Figure IV.3.4. (a) Fully hydrothermally aging the oxidation catalysts according to the U.S. DRIVE protocol results in significant losses in activity. (b) Including a hydrothermally aged trap material, Pd/ZSM-5, in front of the oxidation catalyst results in significant improvements of the catalytic activity.

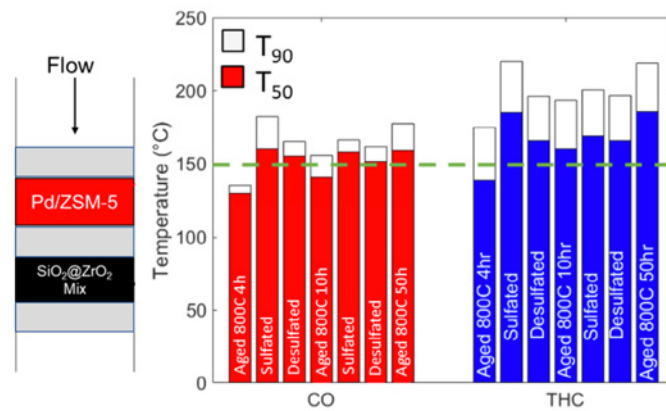


Figure IV.3.5. Summary of T₅₀ and T₉₀ light-off temperatures at each of the different aging steps for the dual-bed Pd/ZSM-5 and oxidation catalyst combination

To understand the impact of the proximity of the trap material and to more closely simulate the temperature ramp observed during cold-start, we implemented a fast ramping protocol at 40°C/min. The previously studied dual-bed configuration shows significant HC trapping during the initial ramp, with greater than 50% of the HC adsorbed below 150°C; this is followed by a large unconverted HC release at 194°C, as shown in Figure IV.3.6a. Arranging these components in a physical mixture within a single packed bed results in greater than 65% HC trapping below 150°C, and at higher temperatures, when the HC is released, there is significantly more HC converted upon the release as the outlet is never higher than the feed concentration (Figure IV.3.6b). This is a clear indication that keeping the trap material near the oxidation catalyst is important for maximum HC reactivity.

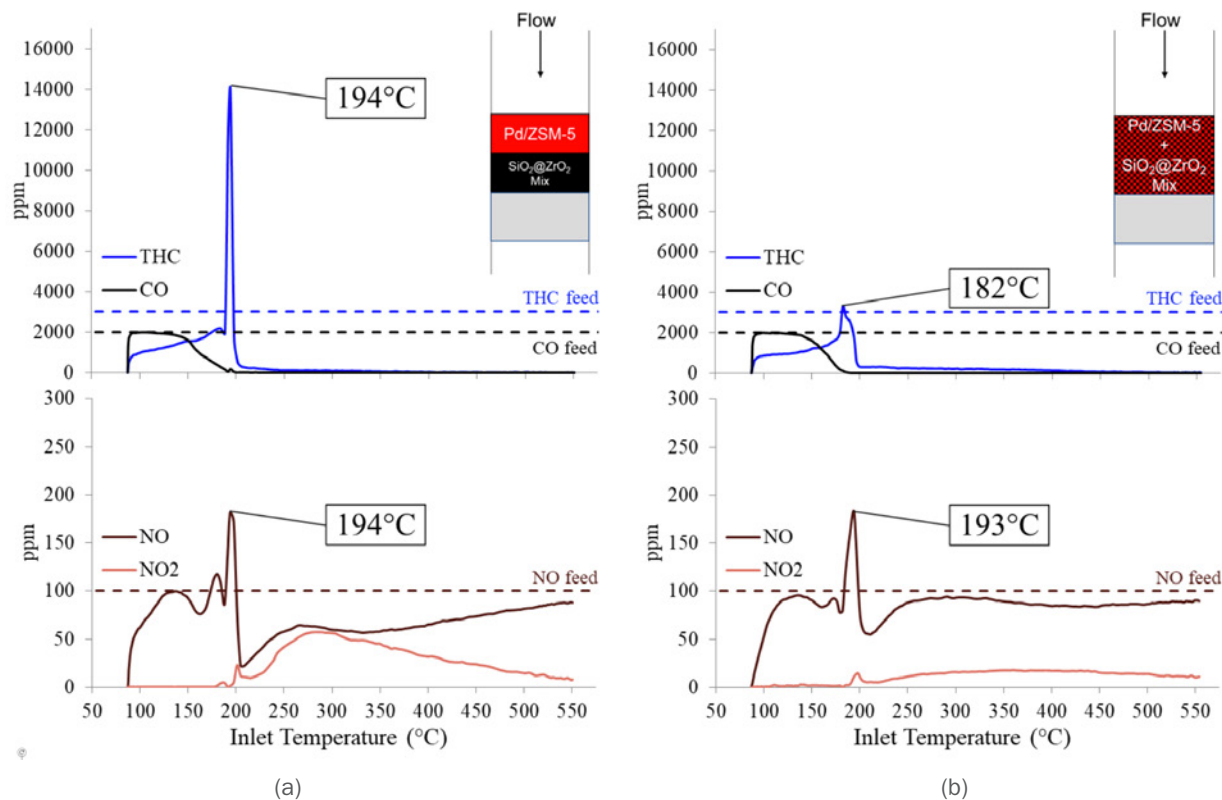


Figure IV.3.6. (a) Dual-bed configuration with Pd/ZSM-5 HC-trap in front of the oxidation catalysts while heating at a rate of 40°C/min. Significant HC quantities are trapped at low temperature and then released at 194°C before being oxidized at higher temperatures. (b) When physically mixing the trap and the oxidation catalyst in the same bed, the released HCs are more readily converted over the oxidation catalyst.

Conclusions

Results this year showed the following:

- 10–30% SiO₂ content in Al₂O₃ improves reactivity of oxidation catalysts through a collaboration with Solvay and USC.
- Trap materials function effectively as oxidation catalysts and improve overall performance.
- Verified aging degrades overall trap functionality, but C₁₀H₂₂ is still trapped efficiently on severely aged samples.
- Combining traps and oxidation catalysts results in good activity even in the most severely aged cases.
- Demonstrated mixed-bed configurations markedly outperform dual-bed configurations.

Key Publications

1. Binder, Andrew J., Todd J. Toops, and James E. Parks II. 2018. “Cu-Co-Ce Ternary Oxide as an Additive to Conventional PGM Catalyst for Automotive Catalysis.” *ChemCatChem* 10 (6): 1263–1266.
2. Choi, Jae-Soon, Josh A. Pihl, Todd J. Toops, and William P. Partridge. 2018. “Reduction of Stored NO_x with CO/H₂ and Hydrocarbons: A Spatial Resolution Analysis.” In *NO_x Trap Catalysts and Technologies: Fundamentals and Industrial Applications*, edited by L. Lietti and L. Castoldi, The Royal Society of Chemistry, Cambridge, UK, Volume 33 (9): 245–278.
3. Toops, Todd J. 2018. “Low-Temperature Emission Control to Enable Fuel-Efficient Engine Commercialization.” 2018 U.S. DOE Vehicle Technologies Office Annual Merit Review, Crystal City, VA (June).
4. Toops, Todd J. 2017. “Approaches to Low-Temperature Emission Control to Enable Fuel-Efficient Engines to Meet Future Regulations.” 2017 Korea Institute of Chemical Engineer’s Annual Meeting (KIChE), (PLENARY LECTURE), Daejeon, South Korea (October 27).
5. Toops, Todd J. 2017. “Approaches to Low-Temperature Emission Control to Enable Fuel-Efficient Engines to Meet Future Regulations.” 17th Hyundai-Kia International Powertrain Conference, (INVITED), Seoul, South Korea (October 25).
6. Toops, Todd J. 2017. “Approaches to Low-Temperature Emission Control to Enable Fuel-Efficient Engines to Meet Future Regulations.” Seoul National University, (INVITED), Seoul, Korea (October 23).
7. Binder, Andrew J., Eleni Kyriakidou, Todd J. Toops, and James E. Parks II. 2017. “Approaching the 150°C Challenge with Passive Trapping Materials and Highly Active Oxidation Catalysts.” 2017 Southeastern Catalysis Society Meeting, Asheville, NC (September 24–25).
8. Binder, Andrew J., Eleni Kyriakidou, Todd J. Toops, and James E. Parks II. 2017. “Approaching the 150°C Challenge with Passive Trapping Materials and Highly Active Oxidation Catalysts.” 2017 CLEERS Workshop, MI (October 3–5).
9. Binder, Andrew J., Eleni Kyriakidou, Todd J. Toops, and James E. Parks II. 2017. “Hydrocarbon and NO Trap/Release Characteristics of Pd/ and Ag/Zeolites with U.S. DRIVE Protocol.” 2017 CLEERS Workshop, MI (October 3–5).

References

1. “Aftertreatment Protocols for Catalyst Characterization and Performance Evaluation: Low-Temperature Oxidation Catalyst Test Protocol,” 2015 www.cleers.org.
2. Toops, Todd J., Eleni A. Kyriakidou, Andrew J. Binder, James E. Parks II, and Jae-Soon Choi. 2018. “Low Temperature Emissions Control.” DOE 2017 Annual Progress Report (April), <https://www.energy.gov/eere/vehicles/downloads/advanced-combustion-systems-fuels-fy2017-annual-progress-report>.

Acknowledgements

Thanks to Shuai Tan, Andrew J. Binder, Eleni A. Kyriakidou, Jae-Soon Choi, and James E. Parks II of Oak Ridge National Laboratory.

IV.4 Emissions Control for Lean-Gasoline Engines (Oak Ridge National Laboratory)

Jim Parks, Principal Investigator

Oak Ridge National Laboratory (ORNL)
2360 Cherahala Blvd.
Knoxville, TN 37932
E-mail: parksjeii@ornl.gov

Ken Howden, DOE Technology Development Manager

U.S. Department of Energy
E-mail: Ken.Howden@ee.doe.gov

Start Date: October 1, 2016	End Date: September 30, 2018	
Project Funding (FY18): \$445,000	DOE share: \$445,000	Non-DOE share: \$0

Project Introduction

Currently, the U.S. passenger car market is dominated by gasoline engine powertrains that operate at stoichiometric air-to-fuel ratios (sufficient fuel is mixed in air such that all of the oxygen in the air is consumed during combustion). Stoichiometric combustion leads to exhaust conditions suitable for three-way catalyst (TWC) technology to reduce NO_x , CO, and hydrocarbon (HC) emissions to extremely low levels. Operating gasoline engines at lean air-to-fuel ratios (excess air) enables more efficient engine operation and reduces fuel consumption; however, the resulting oxygen in the exhaust prevents the TWC technology from reducing NO_x emissions. It is relatively straightforward to operate an engine lean over a significant portion of the load and speed operating range, so, the largest challenge preventing fuel-saving lean combustion in gasoline applications is the control of emissions, primarily NO_x . This project addresses the challenge of reducing emissions from fuel-saving lean gasoline engines in a cost-effective and fuel-efficient manner to enable their market introduction.

In this project, research has been conducted on an emissions control concept known as “passive SCR” [1–3], where SCR stands for selective catalytic reduction. In the passive SCR approach, NH_3 is generated over the TWC under slightly rich engine operation and then stored on a downstream SCR catalyst. After returning to lean operation, the stored NH_3 reduces NO_x that is not converted over the upstream TWC. In this manner, the TWC controls NO_x during stoichiometric and rich operation of the engine, and the SCR catalyst controls NO_x during lean engine operation. Utilizing passive SCR, the project has demonstrated NO_x emission reduction efficiencies over 99.8% on a four-cylinder lean gasoline engine. In addition, experiments have been conducted to identify catalyst material compositions that minimize fuel penalties associated with the technique, and accelerated aging studies have been conducted to understand the durability of the passive SCR approach.

Objectives

Overall Objectives

- Assess and characterize catalytic emissions control technologies for lean gasoline engines
- Identify strategies for reducing the costs, improving the performance, and minimizing the fuel penalty associated with emissions controls for lean gasoline engines
- Identify a technical pathway for a lean gasoline engine to meet U.S. Environmental Protection Agency (EPA) Tier 3 emissions regulations with minimal fuel consumption and cost
- Demonstrate the fuel efficiency improvement of a low-emission lean gasoline engine relative to the stoichiometric gasoline engine case on an engine dynamometer platform

Fiscal Year 2018 Objectives

- Identify engine operating strategies to meet Tier 3 emission levels (0.03 g/mi NO_x + HC) with a passive SCR system (TWC + SCR) over pseudo-transient cycle
- Assess the effect of Ce loading on NH₃ formation on a bench flow reactor
- Determine impacts of sulfur on isolated reactions in three-way catalysts on a bench flow reactor

Approach

This project utilizes the full suite of capabilities available at ORNL's National Transportation Research Center, including a lean gasoline engine on an engine dynamometer, simulated exhaust flow reactors for detailed catalyst evaluations under carefully controlled operating conditions, material characterization tools for catalyst analysis, and vehicle system-level modeling. The combination of catalyst studies on flow reactor and engine platforms is a key component of the project approach. Prototype catalyst formulations are first studied on flow reactors to understand catalytic function and establish operating parameters in a controlled setting; then, select catalyst combinations are studied on the engine platform to characterize performance under realistic exhaust conditions. The engine studies also enable direct measurement of fuel consumption benefits from lean gasoline engine operation as well as measurement of "fuel penalties" imposed by the emissions control system to function properly.

The engine platform for the project is from a Model Year 2008 BMW 120i vehicle sold in Europe. The four-cylinder, direct-injection, naturally aspirated engine operates in multiple modes, including lean (excess air) and stoichiometric combustion. The BMW 120i employs both a TWC for stoichiometric operation and a lean NO_x trap catalyst for NO_x reduction during lean operation. Although this engine and aftertreatment combination met the relevant emissions regulations in Europe, as configured, its emissions are well above the current U.S. emissions standards. Furthermore, the lean NO_x trap catalyst contains high levels of platinum group metals, which add significantly to the overall cost of the vehicle. The goal for this project is to identify emissions control technologies that can meet the EPA Tier 3 emissions standards. In addition to the emissions goal, the project aims to maximize the fuel efficiency benefit from lean gasoline engine operation and minimize system cost.

The catalysts studied in the project were either supplied or recommended by collaborating partner Umicore, a major catalyst supplier to the automotive industry. Other collaborating partners include General Motors for project guidance and the University of South Carolina for research on catalyst aging and durability.

Results

A passive SCR system consisting of a Pd-only TWC (Malibu-1) and a Cu-zeolite SCR catalyst was selected to demonstrate the EPA Tier 3 NO_x + HC emissions on a lean gasoline engine, and to identify challenges and opportunities for further emissions reduction while also minimizing the fuel penalties associated with the passive SCR approach. The Pd-only TWC was selected based on prior bench flow reactor studies that showed high NH₃ selectivity over a wide range of operating conditions compared to other formulations. It is a commercial TWC with primarily Pd as the active catalyst; the catalyst is known as Malibu-1 since it was obtained from the front portion of a super ultra-low emission vehicle Chevrolet Malibu. The demonstration was performed over a six-mode pseudo-transient cycle provided by General Motors. The cycle is a simplified representation of the transient conditions encountered during the federal test protocol used to measure emissions compliance. The BMW four-cylinder lean gasoline engine used in this study is a purpose-built multimode engine. The engine employs a lean combustion mode during part-load operation, and at higher speeds and loads, the engine transitions to a stoichiometric combustion mode. Over the pseudo-transient cycle, the engine exhibited 9.6% fuel consumption benefit using lean/stoichiometric multimode operation relative to stoichiometric-only operation. This fuel consumption improvement is the maximum fuel consumption improvement the engine can achieve under these conditions. However, to control lean NO_x emission with the passive SCR approach, slightly rich engine operation is required in order to generate NH₃ over the TWC; this incurs a fuel penalty. To quantify emissions and fuel penalty of the passive SCR system over the pseudo-transient cycle, several rich strategies were investigated. Simply substituting rich operation for stoichiometric

points (for example, $\lambda = 0.96$ instead of 1.0) resulted in 92% overall NO_x conversion efficiency, which translates to 0.17 g/mi NO_x emissions. This initial operating strategy delivered 6.1% fuel economy benefit, but NO_x + HC emissions were an order of magnitude higher than the EPA Tier 3 emissions of 0.03 g/mi. To improve the NO_x reduction efficiency, the initial strategy was modified to include longer rich times to generate more NH₃, partial preloading of SCR with NH₃, and variable λ control during rich operation. The modified strategy achieved Tier 3 NO_x + HC emissions standards while also showing a reduction in fuel consumption of 5.9% compared to stoichiometric-only operation. CO emissions were twice the EPA Tier 3 levels. Additionally, NH₃ was observed to slip from the SCR, indicating a potential for higher fuel economy benefit. The tail-pipe emissions from the two strategies discussed are depicted in Figure IV.4.1.

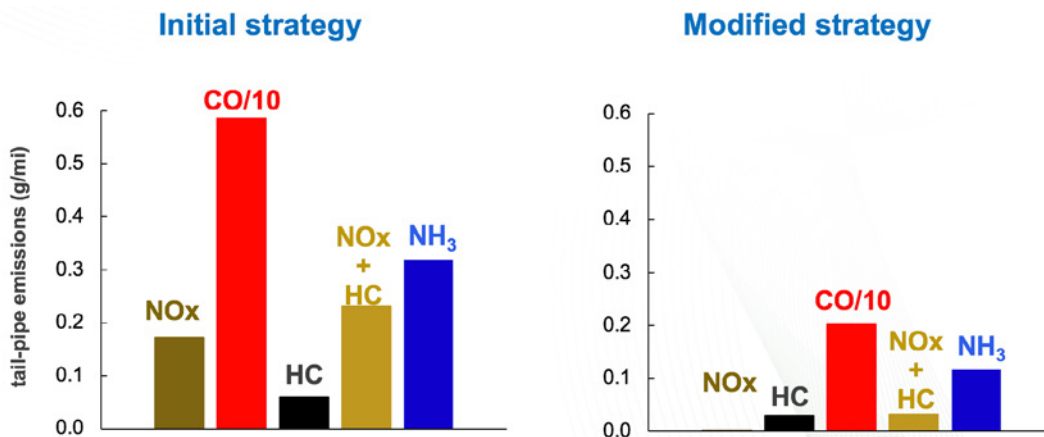


Figure IV.4.1. Tail-pipe emissions from a lean gasoline engine equipped with a passive SCR system over a pseudo-transient drive cycle using different operating strategies

The engine study demonstrated effective NO_x and HC emissions control with significant fuel economy gains due to the lean engine operation. Future work will focus on minimizing the fuel penalty associated with the passive SCR approach by employing advanced catalyst system architecture and adaptive control algorithms that can track system performance while manipulating engine parameters in response to drive cycle demands.

As mentioned earlier, the Pd-only Malibu-1 TWC exhibited higher selectivity of NO_x conversion to NH₃ than other formulations investigated in prior studies. Commercial TWCs often contain other components, which function as catalyst promoters or stabilizers. Ceria, for example, is often included in TWC to assist with three-way functionality under near-stoichiometric conditions, to enhance water-gas-shift (WGS) and steam-reforming reactions, and to function as an oxygen storage component and the basis for on-board diagnostics. Since passive SCR relies on periodic switching between lean and rich operation, the presence of high oxygen storage capacity can potentially delay NH₃ formation on the transition from lean to rich conditions, which would require longer rich time to generate desired levels of NH₃ and lead to higher fuel penalty. It is, therefore, important to understand the effects of oxygen storage components on NH₃ formation. In order to assess the effects of oxygen storage components on NH₃ formation, catalysts with various amounts of Pd and Ce, as listed in Table IV.4.1, were synthesized and evaluated on a bench flow reactor.

Table IV.4.1. Compositions of the Synthesized Catalysts for Evaluation of the Effect of Ce Loading

Name	1Pd	1Pd 0.5Ce	1Pd 1Ce	1Pd 2Ce	1Pd 5Ce	1Pd 10Ce	10Ce
Pd Loading	1.0%	1.0%	1.0%	1.0%	1.0%	1.0%	None
Ce Loading	None	0.5%	1.0%	2.0%	5.0%	10.0%	10.0%

When H₂ was directly available in the feed stream, all of the catalysts exhibited similar performance in converting NO to NH₃ over a wide temperature range. However, in the absence of H₂ in the feed stream, the formation of H₂ from the WGS reaction was found not necessary for converting NO to NH₃ (NO + H₂O + CO),

indicating an alternative pathway of NH₃ formation. The Ce-free catalyst exhibited minimal WGS activity at 350°C, yet over 70% of the NO was converted to NH₃, as shown in Figure IV.4.2. Additionally, adding as little as 0.5% Ce significantly promoted WGS and increased NH₃ formation. This indicates that while WGS is not necessary for NH₃ production, it provides benefits by enhancing NH₃ formation and also consuming CO.

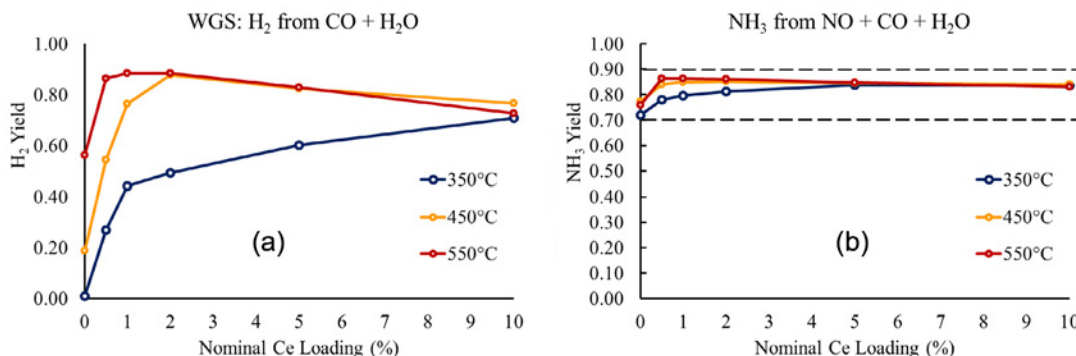


Figure IV.4.2. (a) H₂ production from CO + H₂O and (b) NH₃ production from NO + CO + H₂O using catalysts with different Ce loading. Blue lines are catalyst activities at 350°C, yellow lines are activities at 450°C, and red lines are activities at 550°C.

Another aspect of the project involves durability studies of the catalysts, which is important since regulations require catalyst performance up to full useful life (generally defined as 150,000 mi for a light-duty vehicle). This year durability studies focused on the impact of sulfur, a known catalyst poison, on isolated reactions in Pd-only TWC (Malibu-1) and TWC with NO_x storage components. The TWC with NO_x storage components was provided by Umicore and referred to as ORNL-1 TWC. The ORNL-1 catalyst was included in the durability study because it showed potential to reduce the fuel penalty in the passive SCR system by extending lean operation with storing NO_x on the catalyst and, thereby, preserving NH₃ inventory on the downstream SCR catalyst. Both catalysts were hydrothermally aged for 100 h at 950°C prior to sulfur experiments. When exposed to sulfur, Malibu-1 exhibited stronger deactivation than ORNL-1. This was attributed to the presence of Pt in ORNL-1, which is known to be less susceptible to sulfur poisoning than Pd. When H₂ was directly available in the feed stream, ORNL-1 NH₃ production was largely unaffected by sulfur exposure; however, when CO or HC were used as reductants, strong deactivation was observed, as shown in Figure IV.4.3.

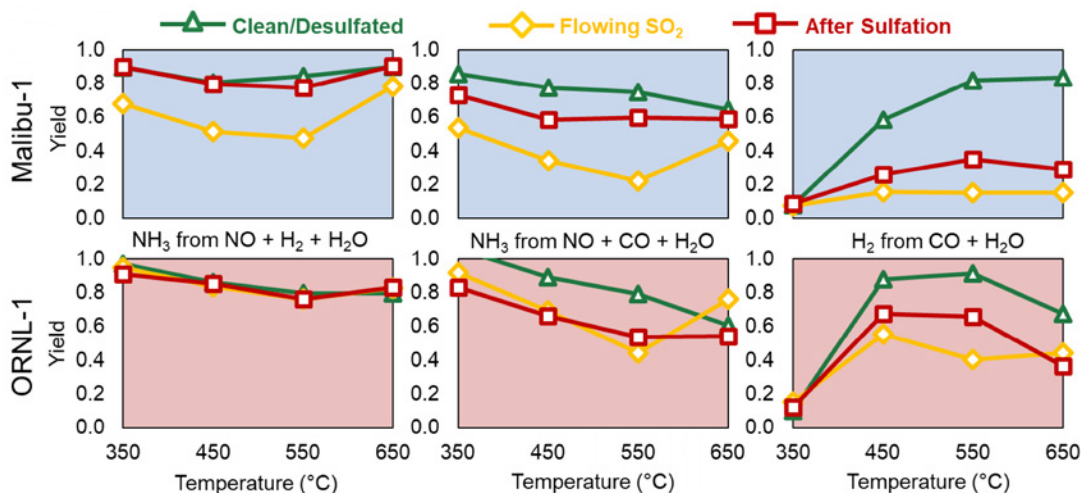


Figure IV.4.3. NH₃ production from NO + H₂ + H₂O (left), NH₃ production from NO + CO + H₂O (middle), and H₂ production from CO + H₂O (right) on Malibu-1 (top) and ORNL-1 (bottom) evaluated clean, while flowing SO₂, and after sulfation

To date, the project has demonstrated that NO_x emissions from lean gasoline engines can effectively be controlled by a passive SCR approach that utilizes NH_3 production over a TWC to reduce NO_x over a downstream SCR catalyst. The results obtained thus far suggest that more efficient NH_3 production and utilization can further increase the fuel economy benefit. Adding a NO_x storage component to the TWC and employing active thermal management of the SCR will be investigated as means to achieve the greater NH_3 production and utilization in the passive SCR system.

Conclusions

- A passive SCR system consisting of a Pd-only TWC (Malibu-1) and a Cu-zeolite SCR catalyst achieved 5.9% fuel efficiency improvement with 0.03 g/mi NO_x + HC emissions on a lean gasoline engine over a pseudo-transient cycle. Future work will focus on minimizing the fuel penalty and further reducing emissions by employing advanced catalyst system architecture and adaptive control algorithms.
- An oxygen storage component (Ce), even though not necessary for NH_3 formation, enhances WGS activity and promotes NH_3 production. However, the presence of high oxygen storage capacity can potentially delay NH_3 formation and lead to higher fuel penalty, which should be considered when selecting optimal amounts oxygen storage components in TWCs for passive SCR applications.
- TWC with NO_x storage component containing Pt as the active catalyst is more resistant to sulfur poisoning than Pd-only TWC. The NH_3 production over TWC with NO_x storage components is largely unaffected when H_2 is present in the feed stream; however, strong deactivation is observed when CO or HC are used as reductants.

Key Publications

1. Prikhodko, V., J. Pihl, T. Toops, and J. Parks. 2018. "Effect of NO_x Storage Component on Ammonia Formation in TWC for Passive SCR NO_x Control in Lean Gasoline Engines." SAE Technical Paper 2018-01-0946, doi:10.4271/2018-01-0946.
2. Lin, Q., P. Chen, and V. Prikhodko. 2017. "Model Predictive Control of a Lean-Burn Gasoline Engine Couple with a Passive Selective Catalytic Reduction System." ASME 2017 Dynamic Systems and Control Conference, DSCC2017-5348, doi:10.1115/DSCC2017-5348.
3. Chen, P., Q. Lin, V. Prikhodko, and J. Parks. 2018. "Non-Uniform Cylinder-to-Cylinder Combustion for Ammonia Generation in a New Passive SCR System." 2018 Annual American Control Conference (ACC), Milwaukee, WI, pp. 19–24. doi: 10.23919/ACC.2018.8431540.

References

1. Li, W., K. Perry, K. Narayanaswamy, C. Kim, et al. 2010. "Passive Ammonia SCR System for Lean-Burn SIDI Engines." *SAE Int. J. Fuels Lubr.* 3 (1): 99–106, doi:10.4271/2010-01-0366.
2. Kim, C., K. Perry, M. Viola, W. Li, et al. 2011. "Three-Way Catalyst Design for Urealess Passive Ammonia SCR: Lean-Burn SIDI Aftertreatment System." SAE Technical Paper 2011-01-0306, doi:10.4271/2011-01-0306.
3. Guralp, O., G. Qi, W. Li, and P. Najt. 2011. "Experimental Study of NO_x Reduction by Passive Ammonia-SCR for Stoichiometric SIDI Engines." SAE Technical Paper 2011-01-0307, doi:10.4271/2011-01-0307.

Acknowledgements

Thanks to Todd Toops, Josh Pihl, and Vitaly Prikhodko of Oak Ridge National Laboratory.

IV.5 Cummins-ORNL SmartCatalyst CRADA: NO_x Control and Measurement Technology for Heavy-Duty Diesel Engines (Oak Ridge National Laboratory)

Bill Partridge, Principal Investigator

Oak Ridge National Laboratory
2360 Cherahala Blvd.
Knoxville, TN 37932
E-mail: partridgewp@ornl.gov

Ken Howden, DOE Technology Development Manager

U.S. Department of Energy
E-mail: Ken.Howden@ee.doe.gov

Start Date: October 1, 2015	End Date: September 30, 2018	
Project Funding (FY18): \$600,000	DOE share: \$300,000	Non-DOE share: \$300,000

Project Introduction

A combination of improved technologies for control of NO_x and particulate emissions is required to efficiently meet increasingly stringent emissions regulations. This Cooperative Research and Development Agreement (CRADA) section focuses on catalyst technologies. Improved catalyst-system efficiency, durability, and cost can be achieved through advanced control methodologies based on continuous catalyst-state monitoring. The overarching goal of this CRADA section is to enable self-diagnosing or smart catalyst systems; these are enabled by basic and practical insights into the transient distributed nature of catalyst performance, improved catalyst models, insights suggesting control methodologies, and instrumentation for improved control. Development and application of enhanced diagnostic tools is required to realize these technology improvements.

Objectives

- Understand the fundamental chemistry of automotive catalysts
- Identify strategies for enabling self-diagnosing catalyst systems
- Address critical barriers to market penetration

Approach

The CRADA applies the historically successful approach of developing and applying minimally invasive advanced diagnostics to resolve spatial and temporal function and performance variations within operating catalysts. Diagnostics are applied to study the detailed nature and origins of catalyst performance variations, including spatial and temporal variations unique to each catalyst function during operating and how these vary with ageing. Measurements are used to assess and guide model development. A combination of measurements and modeling is applied to understand how catalysts function and degrade, develop device and system models, and develop advanced control strategies.

Results

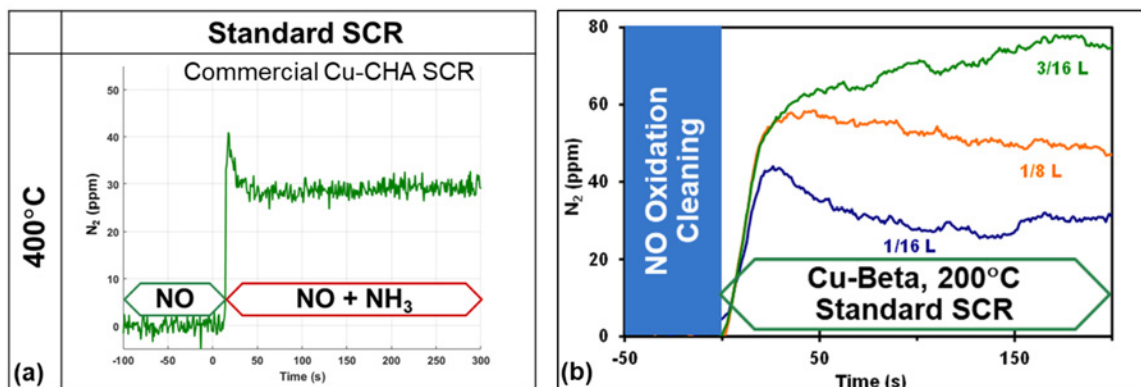
In Fiscal Year 2018, the Catalyst CRADA focused on discovering the origin of Cu selective catalytic reduction (Cu-SCR) onset conversion inflections (CI), which are related to catalyst state but not resolved by existing SCR models. A conceptual model was developed to describe the CI phenomenon. A new experimental protocol and a kinetic model were developed to study CI. Consistencies between the kinetic model and measurements and the conceptual model confirm CI's origin.

- Conceptual model developed describing CI origin
 - o Model based on Cu reduction and oxidation half cycles

- o CI due to half-cycle rate imbalances
- o CI indicates process is limited by the oxidation half cycle
- New Five-Step Protocol developed to probe half-cycle kinetic parameters
 - o Probes individual and combined half-cycle impacts
 - o Can be used with a kinetic model to determine kinetic parameters
- New kinetic model developed describing CI
 - o Model is consistent with measured spatiotemporal and thermal trends
 - o Model is consistent with the conceptual model predictions
- New methodology developed for guiding kinetic model development and determining kinetic parameters
 - o Stoichiometry transients constrain half-cycle formulations
 - o Half-cycle kinetic parameters can be determined via combined protocol and kinetic model application

Conversion Inflections at SCR Onset for Cu-SCR Catalysts

Conversion inflections can occur at SCR onset for different types of Cu-SCR catalysts, as shown in Figure IV.5.1; CI involves rapid, step-like conversion increase at SCR onset to a peak value greater than steady-state (SS) conversion, and slower conversion degradation to the SS value. Such Cu-SCR CI is different from similar transients observed with Fe-SCR catalyst [2], which is attributable to dynamic NH_3 coverage inhibition, in that Cu-SCR CI occurs only at SCR onset and not at SCR termination, and becomes more pronounced with increasing temperature, where NH_3 coverage is lower. Thus, Cu-SCR CI appears to have a different origin compared to similar transients observed with Fe-SCR catalysts. Cu-SCR CI is most apparent at the catalyst front, where NO_x and NH_3 concentrations are highest, are not captured by modern SCR models, and vary with catalyst state [3]. Thus, discovering the origin and nature of these transients could provide a path for improving transient SCR models and on-board Cu-SCR catalyst control. We have published such discovery [4] and summarize it here. Indeed, the work provides an experimental-modeling-based structure for determining Cu-SCR kinetic parameters and guiding model formulation and development.



CHA - chazabite

Figure IV.5.1. SCR-onset conversion inflections for (a) a commercial Cu-CHA SCR catalyst and (b) a model Cu-Beta [1] SCR catalyst

Conceptual Model of CI Origin

The Cu-SCR process can be described as cyclic Cu reduction and oxidation (redox) [4,5], as represented in Figure IV.5.2a, and composed of a reduction half cycle (RHC) and oxidation half cycle (OHC). In the RHC, NO and NH₃ react with oxidized Cu, Cu^{II}, producing N₂ and populating the reduced Cu, Cu^I, state. The OHC completes the Cu redox cycle, consuming additional NO and O₂ and producing N₂. Prior to SCR onset, the Cu partitioning is biased to the Cu^{II} state, as indicated by the blue and red dots. At SCR onset with the Cu^{II} abundance, the RHC creates a conversion step, as shown and labeled SCR-on in Figure IV.5.2e. In cases where the OHC is slower than the RHC, the Cu^{II} is consumed by the RHC faster than it is repopulated by the OHC; correspondingly, the Cu^{II} population drops progressively, and the RHC rate slows accordingly, as shown schematically in Figure IV.5.2b and Figure IV.5.2c. This RHC slowing produces proportional conversion degradation, as labeled in Figure IV.5.2e. At SS, the RHC and OHC rates balance, a steady Cu partitioning has redistributed, and a SS conversion has been reached, as shown in Figure IV.5.2d and Figure IV.5.2e. While Figure IV.5.2 shows the transient half-cycle rate balancing from the perspective of RHC slowing, in fact, the OHC rate increases through the transient proportional to the Cu^I population. For this model, Cu-SCR CI is indicative of an OHC-limited process, and the transient CI nature reflects the kinetic details of the two half cycles.

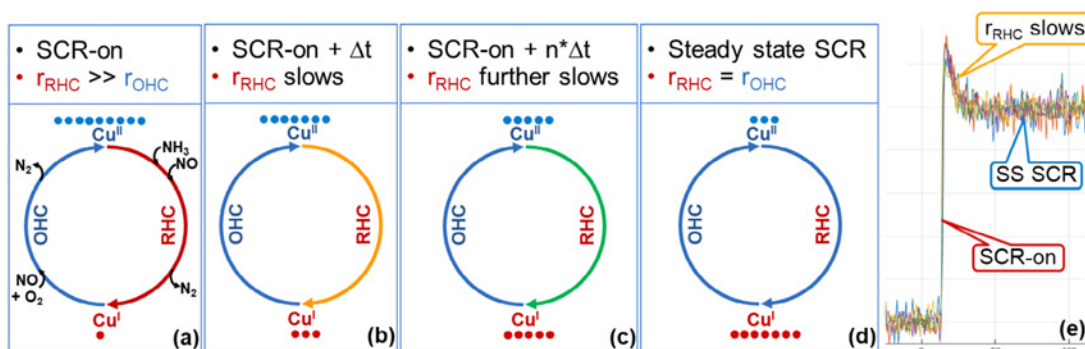


Figure IV.5.2. Conceptual model of Cu-SCR CI origin [4]

Experimental Protocol for Characterizing CI

Figure IV.5.3 shows a standard SCR Five-Step Protocol for characterizing the individual and combined Cu-redox half cycles. The base flow of 5% H₂O, 200 ppm NO, and Ar diluent flows throughout the protocol. To probe the RHC-onset transient, 200 ppm NH₃ is switched on; because the OHC is inactive, the Cu^I concentration reaches the highest value of the protocol at RHC SS. The OHC step involves switching NH₃ off and 0.4% O₂ on. The SCR step involves switching NH₃ back on, and then off for the OHCb step. The OHCb step differs from the OHC step in that the latter starts from a lower Cu^I population. Differing onset transients are observed for the various steps, and some involve differing CI; the details of these transients and their differences reflect the different half-cycle kinetic parameters involved. The protocol provides an analytical method for quantifying the impact of half-cycle kinetic parameters and can be used in conjunction with a corresponding half-cycle kinetic model to determine those parameters.

Kinetic Model Describing CI Transients

A kinetic model based on the RHC and OHC Cu-redox half cycles was formulated for standard and fast SCR, and exercised to study the process and identify consistencies between the model and measurements [4]; highlights of that work are shown here.

The ratio of the RHC and OHC rates, $r_{\text{RHC}}/r_{\text{OHC}}$, is termed the r-ratio and increases with temperature, as shown in Figure IV.5.4a. For r-ratios greater than unity, r_{RHC} is faster than r_{OHC} , and thus CI should be observed based on the conceptual model; for r-ratios less than unity, the process is r_{RHC} -limited and CI is not expected. The positive r-ratio slope indicates that half-cycle rate imbalance increases with increasing temperature, which should enhance CI. Indeed, Figure IV.5.4b shows that CI becomes more distinct with increasing r-ratio, i.e., the

CI peaks become taller, the widths narrower, and the tails faster. Combining the insights of Figure IV.5.4a and Figure IV.5.4b, the model predicts that CI becomes increasingly apparent with increasing temperature, which is consistent with the experimental observations.

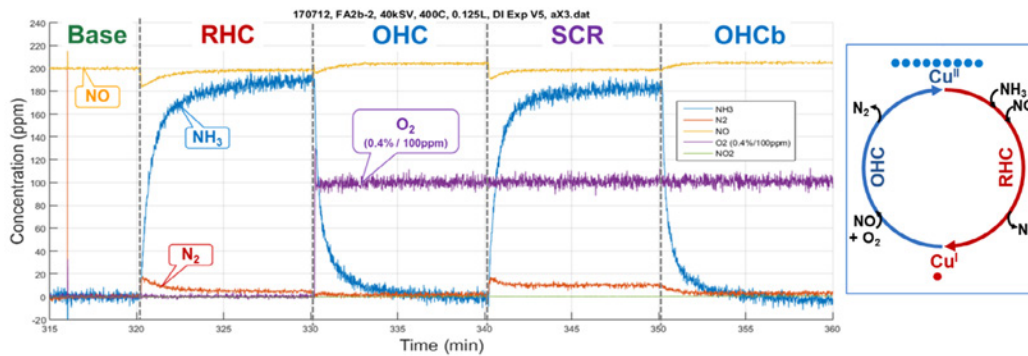


Figure IV.5.3. Five-Step Protocol for characterizing onset transients for the individual and combined Cu-redox half cycles [4]

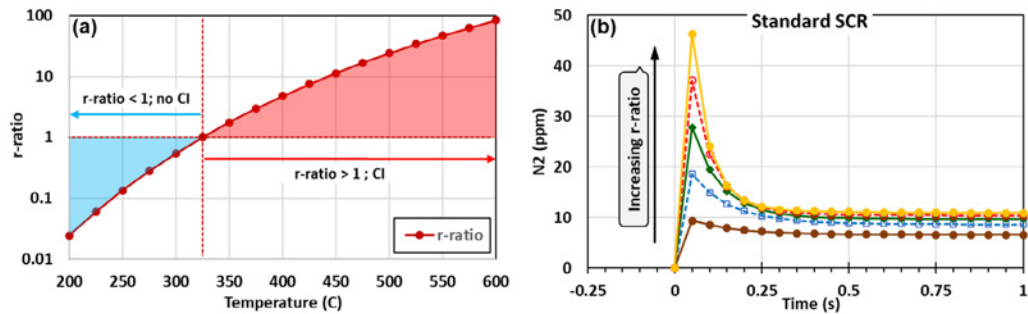


Figure IV.5.4. (a) Variation in r-ratio (r_{RHC}/r_{OHC}) with temperature; (b) variation in N_2 CI with increasing r-ratio

Several important consistencies between the kinetic model and both the conceptual model and experimental measurements are apparent from exercising the model for varying NO feed. Figure IV.5.5 shows kinetic-model results for varying NO feed at constant NH_3 feed; Figure IV.5.5a and Figure IV.5.5b show related N_2 and NO CI, respectively, and Figure IV.5.5c shows the r_{RHC} and r_{OHC} onset transients. Onset CI becomes increasingly distinct with increasing NO concentration, as exists at the catalyst front, and the NO CI transients are similar to the measured spatiotemporal CI variations shown in Figure IV.5.5d. Specifically, NO CI becomes progressively less distinct with increasing NO conversion along the catalyst axis for the field-aged commercial Cu-SCR shown in Figure IV.5.5d. Figure IV.5.5d shows the NO transient at SCR onset at different incremental lengths along the catalyst axis. Moreover, although that catalyst was being fed 200 ppm NO, the feed to the various sections progressively degrades along the catalyst length, e.g., the inlet to the catalyst section 1/8th along the length corresponds to the NO value where the 1/16L and 1/8L (blue and red curves) separate in Figure IV.5.5d, or ca. 175 ppm. Thus, consecutive sections along the catalyst length have progressively lower NO inlet feed and produce progressively less distinct CI. Both of these experimental observations are predicted by the kinetic model, as apparent from comparing Figure IV.5.5b and Figure IV.5.5d. Figure IV.5.5c shows that the half-cycle rates converge at SS for all feed combinations, as predicted by the conceptual model; the convergence occurs fast for increasing NO feed concentration. Moreover, while most of the half-cycle rate convergence is due to RHC slowing, the OHC rate does increase to a lesser extent. Both of these details regarding the half-cycle rate convergence are consistent with the conceptual model.

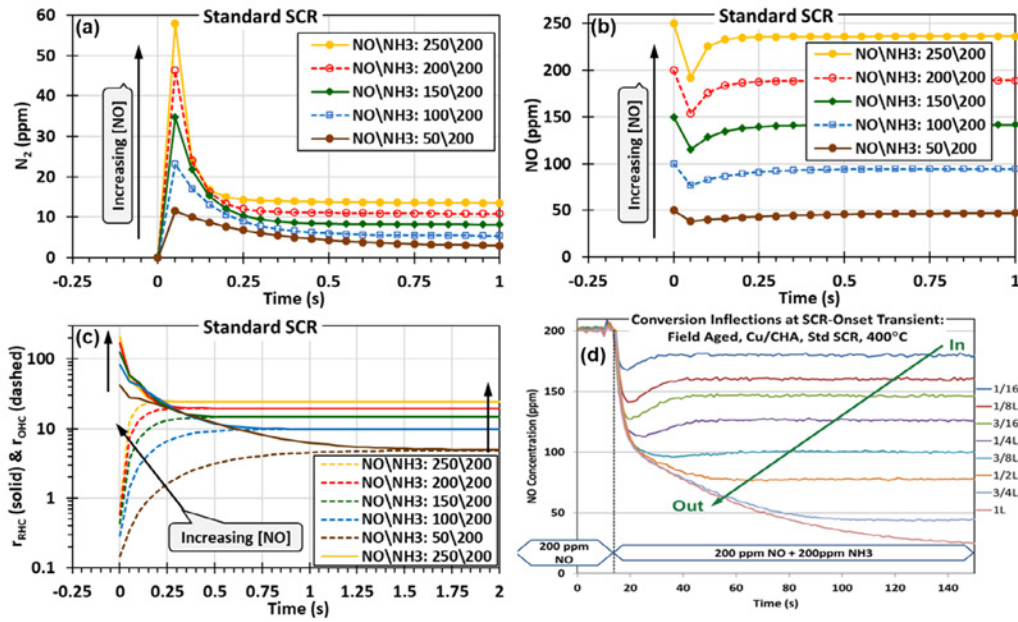


Figure IV.5.5. Kinetic model results for varying NO (50, 100, 150, 200, 250 ppm) at constant 200 ppm NH₃ for (a) N₂, (b) NO CI, and (c) r_{RHC} and r_{OHC}. (d) Spatiotemporal CI distribution for a field-aged commercial Cu-SCR catalyst and 200 ppm standard SCR; L is total catalyst length, e.g., 1/8L is 1/8th along the catalyst length.

Figure IV.5.6 shows onset transients for fast SCR predicted by the kinetic model and how these can be used to guide model formulation. The stoichiometries of the individual half cycles are linked in that they must balance or sum to the net SCR reaction stoichiometry, e.g., specifying the RHC formulation fixes the OHC stoichiometry via the required balance. The fast SCR kinetic model was formulated such that the RHC produces 1 mol of N₂ for every 2 mol of NH₃ and 1 mol of NO consumed, i.e., the N₂-specific NO and NH₃ stoichiometry are 1 mol and 2 mol, respectively [4]. Similarly, the N₂-specific NO and NH₃ stoichiometries for the fast SCR reaction are 0.5 mol and 1 mol, respectively [4]. Figure IV.5.6b shows that the reaction stoichiometry is completely controlled by the RHC at SCR onset and varies through the onset transient to SS values consistent with the fast SCR reaction; the transient reflects the balancing influence of the half-cycle stoichiometries as the half-cycle rates converge. Similar measurements could be used to guide and confirm how the individual half cycles are formulated in the kinetic model, i.e., the measured initial stoichiometry could confirm the RHC stoichiometry, and by the balance requirement, that of the OHC. If the initial values do not agree, then the measured values can be used to guide RHC formulation.

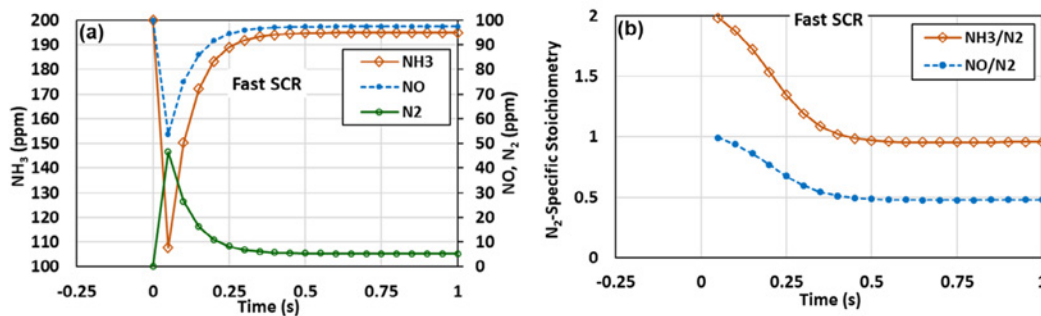


Figure IV.5.6. Kinetic-model predictions of the (a) NO, NH₃ and N₂ onset transients for fast SCR, and (b) corresponding N₂-specific NO and NH₃ transients

Conclusions

The origins of Cu-SCR onset transient were discovered via measurements and modeling and are related to half-cycle rate imbalances in the Cu-redox cycle associated with SCR; specifically, CI occurs when the RHC is faster than the OHC. A Five-Step Protocol was developed and demonstrated to quantify the impact of the individual and combined half-cycle kinetic parameters on onset transients. A conceptual model and a kinetic model were developed describing the CI process. The kinetic model was exercised and demonstrated numerous consistencies with the measurements and conceptual model. The protocol and kinetic model form the basis of a methodology for guiding kinetic-model formulation and determining half-cycle kinetic parameters of fully formulated and model catalysts under operating conditions. Because CI is not captured by existing SCR models, these new insights are relevant to improving catalyst design, specification, and modeling. Through CI's sensitivity to aged state, this new discovery may be used for in-use catalyst-state determination and correspondingly enable improved catalyst control, efficiency, and durability.

Key Publications

1. Partridge, W.P., S.Y. Joshi, J.A. Pihl, and N.W. Currier. 2018. "New Operando Method for Quantifying the Relative Half-Cycle Rates of the NO SCR Redox Cycle Over Cu-Exchanged Zeolites." *Applied Catalysis B: Environmental* 236: 195–204. doi.org/10.1016/j.apcatb.2018.04.071. Archival Journal Publication.
2. Choi, J-S., J.A. Pihl, T.J. Toops, and W.P. Partridge. 2018. "Reduction of Stored NO_x with CO/H₂ and Hydrocarbons: A Spatial Resolution Analysis." In *NO_x Trap Catalysts and Technologies: Fundamentals and Industrial Applications*, edited by Luca Lietti and Lidia Castoldi, 245–278. Cambridge, UK: The Royal Society of Chemistry, Catalysis Series (June).
3. Partridge, W.P., J.A. Pihl, S. Joshi, N. Currier, A. Yezerets, and K. Kamasamudram. 2017. "A New Operando Method for Studying NH₃-SCR Redox-Cycle Kinetics of Cu-Zeolite Catalysts via Spatiotemporally Resolved Measurements." 2017 CLEERS Workshop, Ann Arbor, MI (October 4).
4. Partridge, W.P., J.A. Pihl, S. Joshi, N. Currier, A. Yezerets, and K. Kamasamudram. 2018. "Using SCR Transients to Improve Catalyst Models and Performance." DOE Advanced Engine Crosscut Team, Southfield, MI (May 10).
5. Partridge, W.P., J.A. Pihl, S. Joshi, N. Currier, A. Yezerets, and K. Kamasamudram. 2018. "NO_x Control & Measurement Technology for Heavy-Duty Diesel Engines." 2018 DOE Vehicle Technologies Program Annual Merit Review, Washington, DC (June 20).
https://www.energy.gov/sites/prod/files/2018/06/f52/acs032_partridge_2018_o.pdf

References

1. Auvray, X., et al. 2012. *Appl. Catal. B* 126: 144–152.
2. Colombo, M., et al. 2012. *Appl. Catal. B* 111–112: 106–118.
3. Partridge, Bill, et al. 2017. DOE FY 2017 Advanced Combustion Technologies Annual Report, https://www.energy.gov/sites/prod/files/2018/05/f51/AdvCombSysAndFuels_FY2017_APR_Final.pdf
4. Partridge, W.P., et al. 2018. *Appl. Catal. B* 236: 195–204.
5. (a) Paolucci, C., et al. 2014. *Angew. Chem. Int.* 53: 11828–11833; (b) Paolucci, C., et al. 2016. *J. Am. Chem. Soc.* 138: 6028–6048; (c) Paolucci, C., et al. 2017. *Science* 357: 898–903.

Acknowledgements

Thanks to Saurabh Joshi, Neal Currier, Krishna Kamasamudram, Rohil Daya, and Alex Yezerets of Cummins, Inc., and to Josh Pihl of Oak Ridge National Laboratory.

IV.6 Fuel-Neutral Studies of PM Transportation Emissions (Pacific Northwest National Laboratory)

Mark Stewart, Principal Investigator

Pacific Northwest National Laboratory
902 Battelle Boulevard
Richland, WA 99352
E-mail: mark.stewart@pnnl.gov

David Rothamer, Principal Investigator

University of Wisconsin-Madison Engine Research Center
1500 Engineering Dr., Rm. 127
Madison, WI 53706
E-mail: rothamer@wisc.edu

Ken Howden, DOE Technology Development Manager

U.S. Department of Energy
E-mail: Ken.Howden@ee.doe.gov

Start Date: October 1, 2015	End Date: September 30, 2018	
Project Funding (FY18): \$225,000	DOE share: \$225,000	Non-DOE share: \$0 ¹

Project Introduction

Technologies such as spark ignition direct injection have led to significant gains in the fuel efficiency of engines that run on gasoline and associated fuel blends, but this increased efficiency can come at the price of higher NO_x and/or particulate matter (PM) emissions. As global fuel economy standards increase and emissions limits continue to tighten, major manufacturers are considering exhaust filtration for gasoline vehicles. Deployment of gasoline particulate filters on production vehicles has begun and is anticipated to expand over the next several years in Europe and China in order to meet Euro 6 and China 6 particle number standards.

While gasoline particulate filter deployment for spark ignition direct injection vehicles in the United States is less likely in the near term, gasoline particulate filters remain an option for gasoline PM control, and American manufacturers must continue to study and develop exhaust filter technology in order to remain globally competitive. In addition, other advanced engine technologies, such as compression ignition gasoline engines and reactivity-controlled compression ignition engines, would likely also entail higher particulate emissions than traditional port fuel injected gasoline engines. Exhaust filter manufacturers now offer products designed specifically for advanced gasoline engines, including spark ignition direct injection. Understanding the fundamental relationships between filter system characteristics and ultimate system performance will be critical as manufacturers consider various options moving forward.

Objectives

This project seeks to provide fundamental insight and tools to support the development and optimization of exhaust filter solutions for a variety of future high-efficiency engines, running on a broad spectrum of fuels.

Overall Objectives

- Shorten the time required for development of filtration technologies for future engines
- Develop modeling approaches relevant to the likely key challenge for gasoline particulate filtration: high number efficiency at high exhaust temperatures and low particulate loading

¹ The General Motors Corporation supports this project informally through financial and technical support to the Engine Research Center at the University of Wisconsin-Madison.

- Develop new techniques for exhaust filter media characterization

FY 2018 Objectives

- Develop a specialized capillary flow porometry system for characterization of ceramic exhaust filter media
- Perform detailed three-dimensional (3D) simulations of ultra-fine particle capture in exhaust filters using the lattice-Boltzmann method
- Evaluate methods of improving the standard spherical unit collector filter model
- Develop a new transient filter simulation model based on constricted tube collectors

Approach

General Motors Research has provided components and guidance to develop advanced research engines at the University of Wisconsin-Madison Engine Research Center (ERC). These research engines have been configured to run with a variety of fuels over a wide range of operating conditions. ERC researchers used the Exhaust Filtration Analysis (EFA) system [1], developed at the University of Wisconsin-Madison, to conduct fundamental filtration experiments in realistic exhaust streams using flat wafer samples of various filter substrates. The project team characterized a number of the porous ceramic materials used in the filtration tests through a variety of techniques, which included mercury intrusion porosimetry (MIP), capillary flow porometry (CFP), and micro X-ray computed tomography (CT), in order to understand performance differences between the various products. Existing filtration models based on porosity and pore size alone have thus far been unable to quantitatively predict the observed trends in the behavior of the various filter products examined. Insights from fundamental experiments, filter characterization, and microscale modeling are being incorporated into new empirical expressions and improved device-scale models that can be used by vehicle manufacturers to optimize engine and exhaust systems in future high-efficiency vehicles.

Results

ERC researchers had previously applied CFP to a wide variety of exhaust filter samples, and the technique has shown great promise for providing new insight into structural differences between various filter materials. While MIP provides useful information on pore size distributions throughout a porous material, CFP provides the distribution of controlling constrictions in flow paths passing through a filter wall. These constrictions likely play a key role in determining performance metrics such as permeability and filtration efficiency. CFP could thus provide complimentary information to MIP data, which could help explain differences in performance for media with similar porosity and median pore size. It could also yield a straightforward way to supply pore geometry parameters for more sophisticated filter models.

Despite the clear potential of the CFP approach, there were a number of issues with preliminary data generated by a system designed for general porous media, including poor repeatability, unphysical features, and inability to resolve both large and small constrictions for a range of filter materials. The ERC therefore developed a custom-built CFP system, with flow and pressure transducers sized specifically for characterization of ceramic filter media. Experimentation and literature review also showed that superior results could be obtained by using low-volatility wetting fluids. The new system was validated using ion track etched filter media with known pore size distributions. Figure IV.6.1 shows data generated by the new system for the C1 and A2 filter materials, which have similar porosity and median pore size, but very different distributions of controlling throat sizes, which helps to explain significant differences in filtration behavior. The new system has been used to characterize a wide variety of ceramic filter materials, many of which are included in an extensive filtration performance dataset produced at the ERC using the EFA system [2].

Pacific Northwest National Laboratory had previously obtained micro X-ray CT data for a number of filter substrates for which fundamental filtration data had been gathered using the EFA system. The lattice-Boltzmann method was used to solve for 3D flow fields through the porous filter walls of seven different filter materials, covering a wide range of porosities and median pore sizes. These solutions were then used to perform Eulerian simulations of ultra-fine particle filtration. Results for one example substrate are depicted in Figure IV.6.2. The color scale shows normalized particulate concentration in the cross-section on the right.

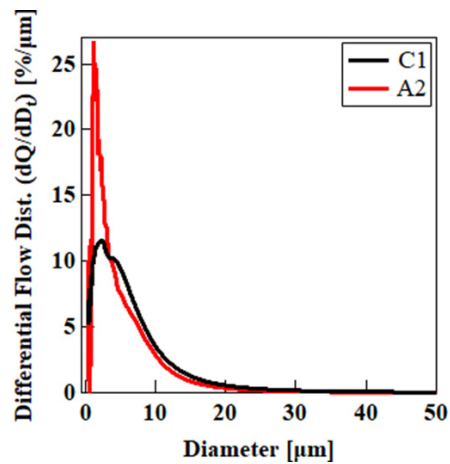


Figure IV.6.1. Comparison of controlling pore size distributions for the C1 and A2 substrates found using a custom-built CFP system

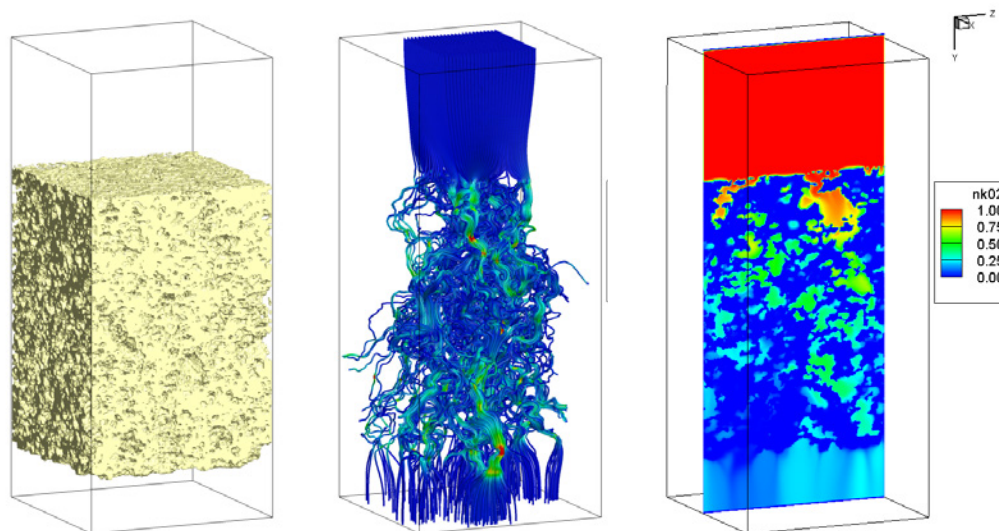


Figure IV.6.2. Reconstructed microstructure (left), flow solution (center), and simulated concentration field (right) for 50-nm particles passing through a C1 filter wall

Although the lattice-Boltzmann simulations represented tiny volumes of reconstructed filter material (roughly one-third square millimeter of wall area), the first-principles simulations did remarkably well at predicting initial filtration efficiency of the seven different substrates at two different wall flow velocities, as measured with the EFA system. Figure IV.6.3 shows a comparison of simulation predictions of initial penetration of 50-nm particles to measured values at a wall flow velocity of 5.5 cm/s. The lattice-Boltzmann simulations captured several interesting trends, such as the difference in initial particle penetration between the C1 and A2 substrates. These results demonstrate that microscale simulations provide a way to study the connection of the 3D structure of various filter materials with their effectiveness at removing ultra-fine particles under various operating conditions. They also allow costly and time-consuming experiments to be supplemented by digital explorations of alternative structures.

Three-dimensional microscale simulations are computationally expensive, however, and the micro X-ray CT data required to model real substrates may not be readily available. There is therefore still a need for simple, device-scale filter models that provide good predictions of filter performance with minimum tuning. A number

of alternative approaches have been explored over the course of this project. One attractive alternative is to make adjustments to the standard spherical unit collector model that has been successfully used for many years for design, optimization, and control of diesel particulate filter systems. Figure IV.6.4 shows the results of one such candidate model, which uses porosity and pore size distribution measured by mercury porosimetry to find a single equivalent spherical unit collector size. A new diffusion capture expression was developed to reproduce the behavior of the class of porous filter materials examined. Another simple model using cylindrical tube collectors was used in [2] to help explain filter performance trends.

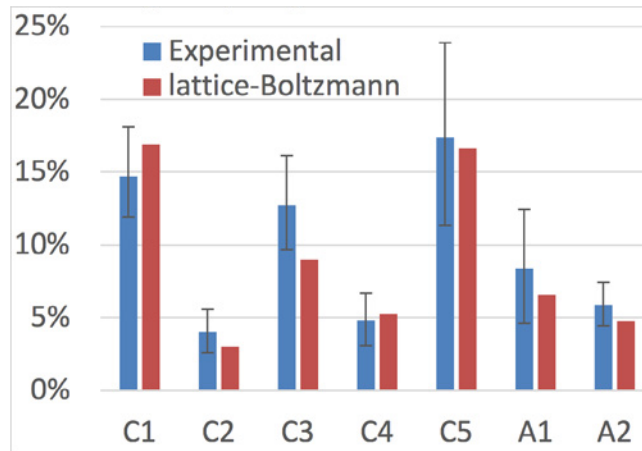


Figure IV.6.3. Comparison between measured initial penetration of 50-nm particles through various filter materials and predictions made by microscale lattice-Boltzmann simulations

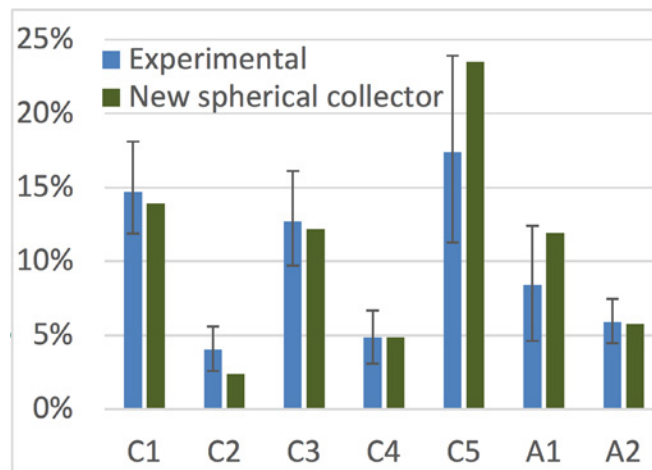


Figure IV.6.4. Comparison between measured initial penetration of 50-nm particles through various filter materials and predictions made by a modified spherical unit collector model

While the modified spherical unit collector model described above has shown promise for prediction of initial filtration efficiency over a range of filter properties, more sophisticated models may be necessary to describe transient filter behavior over a realistic duty cycle. One approach explored previously at the ERC is the Heterogeneous Multiscale Filtration model [3], which uses spherical collectors of multiple sizes to represent the distribution of pores within the filter medium. Another approach developed more recently by ERC researchers is a constricted tube collector model, which seeks to provide higher fidelity and more predictive power by using a collector geometry more closely resembling actual filter pores. Figure IV.6.5 shows that the constricted tube model is able to describe size-resolved filtration efficiency better than the classical spherical

collector filter model. By using information from both mercury porosimetry and CFP to set the size and shape of collectors, the model is also able to predict filtration efficiency and pressure drop as a function of filter loading for a variety of filter media over a range of engine operating conditions.

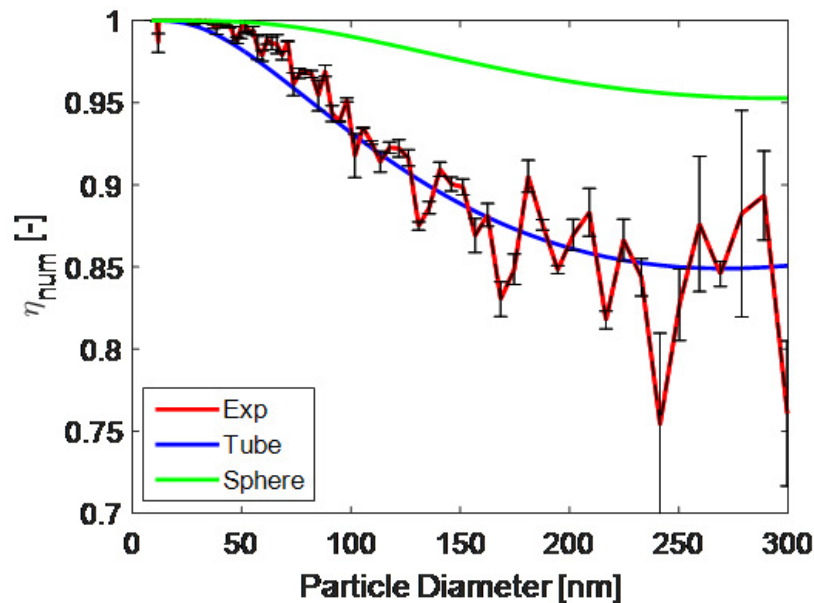


Figure IV.6.5. Size-resolved filtration efficiency predicted by a classical spherical unit collector model and by a new constricted tube collector model compared to experimental data for the C2 filter substrate

Table IV.6.1 summarizes a number of complementary simulation and modeling approaches that have been employed over the course of this research project.

Table IV.6.1. Summary of Simulation and Modeling Approaches Applied throughout the Project

Models Used / Developed	Substrates Examined	Demonstrated Predictions	Notes	Dissemination
Lattice-Boltzmann	C1, C2, C3, C4, C5, A1, A2	Clean removal efficiency for small particles, 2 flow rates	First principles – no tuning, uses X-ray CT data for 3D structure	CLEERS workshop, journal article in preparation
Heterogeneous multiscale filtration	C1, others	Evolving size-resolved efficiency and pressure drop during filtration	Pore size and distribution from MIP, porosity distribution from X-ray CT	Dissertation, multiple peer-reviewed publications
Cylindrical tube	C1, A2	Clean removal efficiency for small particles, 2 flow rates	Pore throat size distribution from CFP	Dissertation, SAE oral, journal article in preparation
Constricted tube	C1, C2, C3, C4, C5	Evolving size-resolved efficiency and pressure drop during filtration	Pore size distribution, shape from MIP, CFP	SAE paper, dissertation, journal article in preparation
New spherical collector	C1, C2, C3, C4, C5, A1, A2	Clean removal efficiency for small particles, 2 flow rates	Pore size distribution from MIP	CLEERS workshop, journal article in preparation

Conclusions

- Capillary flow porometry can provide detailed information about controlling constrictions in the flow paths through ceramic exhaust filter walls, but measurement devices must be sized properly and wetting fluids selected carefully to avoid evaporation effects.
- Three-dimensional microscale Eulerian filtration simulations are able to correctly predict trends in removal efficiency for ultrafine particles by a range of filter media, providing a way to study the connection between structure and performance.
- A modified spherical unit collector model shows promise for improved prediction of filtration efficiency for small particles.
- The constricted tube collector model is capable of predicting size-resolved filtration efficiency and pressure drop as a function of loading for a variety of filter substrates over a range of operating conditions.

Key Publications

1. Gong, J., M.L. Stewart, A. Zelenyuk, A. Strzelec, S. Viswanathan, D. Rothamer, D. Foster, and C. Rutland. 2018. "Importance of Filter's Microstructure in Dynamic Filtration Modeling of Gasoline Particulate Filters (GPFs): Inhomogeneous Porosity and Pore Size Distribution." *Chem Eng J.* 338: 15–26.
2. Yang, Y., C. Rutland, and D. Rothamer. 2018. "Study of the Deep Bed Filtration Using Pore Filtration Model (PFM)." *2018 SAE World Congress.* 2018-01-0956.
3. Yang, Y. 2018. "Fundamental Study on Particle Filtration Process and Gasoline Particulate Filter (GPF) Modeling." Doctoral dissertation. University of Wisconsin, Madison.

References

1. Viswanathan, S., S. Sakai, and D. Rothamer. 2014. "Design & Evaluation of an Exhaust Filtration Analysis (EFA) System." SAE Technical Paper 2014-01-1558, 2014 *SAE World Congress.* Detroit, MI.
2. Viswanathan, S. 2016. "Experimental Investigation of Deep-Bed Filtration of Spark-Ignited, Direct-Injection Engine Exhaust Using Ceramic Particulate Filters." Doctoral dissertation. University of Wisconsin, Madison.
3. Gong, J., and C.J. Rutland. 2015. "PDF-Based Heterogeneous Multiscale Filtration Model." *Environ Sci Technol.* 49: 4970. doi:10.1021/acs.est.5b00329.

Acknowledgements

University of Wisconsin, Madison: Sandeep Viswanathan, Jonathan Molina, Jian Gong, Yangdongfang Yang, Christopher Rutland, Andrea Shen, Todd Fansler, Stephen Sakai, Michael Andrie
 General Motors Corporation: Kushal Narayanaswamy, Paul Najt, Arun Solomon, Wei Li

IV.7 Advanced Emission Control for High-Efficiency Engines (Pacific Northwest National Laboratory)

Yong Wang, Principal Investigator

Pacific Northwest National Laboratory (PNNL)
P.O. Box 999, MS K2-12
Richland, WA 99354
E-mail: yong.wang@pnnl.gov

Ken Howden, DOE Technology Development Manager

U.S. Department of Energy
E-mail: Ken.Howden@ee.doe.gov

Start Date: March 1, 2016	End Date: March 31, 2019	
Project Funding (FY18): \$187,000	DOE share: \$187,000	Non-DOE share: \$0

Project Introduction

This project between Cummins and PNNL focuses on a broad and very important area of critical relevance to DOE and Cummins: advanced emission control for high-efficiency engines. It specifically focuses on three areas: passive NO_x absorbers (PNA), oxidation of methane and short alkanes, and improved understanding of particulates.

The first two areas are based on PNNL's technical leadership in the zeolite-based materials. The third area was completed in Year 1 to leverage the unique single particle laser ablation time-of-flight mass spectrometer capabilities at PNNL to help address Cummins' needs in improving the understanding of particulate properties as a function of engine operating conditions and aftertreatment systems.

Objectives

- Passive NO_x absorbers: develop next-generation materials to address the cold operation, as driven by improved engine efficiency
- Oxidation of methane and short alkanes: address cold-operation emissions arising from compressed natural gas vehicles
- Improved understanding of particulate matter: understand the properties of exhaust particulate matter as a function of engine operating conditions and aftertreatment

Approach

This project takes advantage of the strengths from the partners. In particular, Johnson Matthey is well known in catalyst formulation and upgrading. Cummins is well equipped in its catalysis laboratory with on-engine testing. PNNL has the state-of-the-art catalyst characterizations to provide fundamental understanding of the chemical and physical properties of the catalytic materials.

This partnership will understand the fundamental relationship of particulate properties and engine operation/ aftertreatment utilizing unique approaches for multidimensional real-time in situ characterization of individual exhaust particles, such as single particle laser ablation time-of-flight. It also aims at revealing fundamental aspects of the chemistry and catalytic materials involved in PNA and small alkane catalytic oxidation.

Results

Key accomplishments for Fiscal Year 2018 include the following.

Passive NO_x Absorber

- Finished synthesis, characterization, and evaluation of Pd/SSZ-13 materials with 100% or close to 100% atomic dispersions
- Finished hydrothermal aging tests of these new materials; used transmission electron microscopy imaging and solid-state ²⁷Al nuclear magnetic resonance spectroscopy (NMR) to probe changes of the Pd phase and the zeolite support
- Initiated sulfur poisoning tests of the Pd/SSZ-13 materials and particle-size-dependent investigations of Pd/beta PNA materials

Methane and Ethane Oxidation at Low Temperature

- Synthesized Pd/SSZ-13 catalysts with varying Si/Al ratios; confirmed that by increasing Si/Al ratios, catalyst hydrophobicity increases, leading to higher activity and stability of the catalysts
- Initiated research on Pd loading dependence of Pd/SSZ-13 catalysts

Hydrothermal aging of Pd/SSZ-13 PNA material (Si/Al = 6, 12, and 30; Pd loading = 1.0 wt%) was carried out at 750°C in an air flow containing 10% water vapor for 16 h. NO_x uptake and desorption of these materials were studied using simulated exhaust containing 200 ppm NO_x (185 ppm NO + 15 ppm NO₂), 200 ppm CO, 14% O₂, and 2.5% H₂O balanced with N₂. NO_x uptake was conducted at 100°C for 10 min, followed by ramping to 500°C to release trapped NO_x. As shown in Figure IV.7.1, for all materials, after hydrothermal aging, NO_x storage capacity at 100°C decreases. Desorption profiles also change: while the NO_x release stage at ~250°C does not show great variation, the high-temperature stage above ~400°C clearly decreases. Since the ~250°C stage is attributed to NO release from ionic Pd sites and the ~400°C stage is due to nitrate decomposition, such changes reflect a decrease in oxidation capacity of the PNA materials after hydrothermal aging (NO has to be oxidized to nitrates). This indicates the disappearance of highly oxidizing PdO_x clusters during hydrothermal aging, suggesting that during aging, the atomically dispersed Pd ions are hydrothermally stable while the PdO_x clusters convert to large PdO particles, which no longer have high oxidizing capacities.

As shown in Figure IV.7.2 using the aged Si/Al = 6 material as an example, indeed after hydrothermal aging, large PdO particles measuring 40–50 nm in diameter are detected. These particles have low atomic efficiency to trap NO or convert NO to nitrate species. Figure IV.7.3 presents solid-state ²⁷Al NMR results of fresh and aged PNA materials. Zeolite support degradation during hydrothermal aging is clearly manifested by the generation of penta- and octahedral coordinated Al, which are assigned to framework terminal and extra-framework Al, respectively. It is also seen, by normalizing total Al signals, that for the Si/Al = 12 and 30 materials, some signals are lost during aging. This portion of Al can be assigned to highly distorted, NMR silent Al. Overall, Pd/SSZ-13 PNA materials studied here show decent but clearly not ideal hydrothermal stabilities. Continuous research on improving their hydrothermal stability is currently underway.

Experiments for low-temperature methane combustion were conducted using 600 ppm CH₄, 2.5% H₂O, 6% CO₂, and 10% O₂ with N₂ balance. As shown in Figure IV.7.4, a series of 3 wt% Pd/SSZ-13 catalysts with Si/Al = 6, 12, 24, and 36 display different extents of deactivation on stream. Low-Si/Al-ratio catalysts decrease in the same fashion as Pd/Al₂O₃ commercial catalysts, while high Si/Al catalysts display much improved stability. The Si/Al = 36 sample displays some initial deactivation likely due to agglomeration of some highly unstable PdO species. However, it becomes highly stable after a few hours on stream. This behavior is further demonstrated in Figure IV.7.5, where following repeated uses, the commercial Pd/Al₂O₃ keeps deactivating, yet the Pd/SSZ-13 catalyst with Si/Al = 36 maintains high stability. Via detailed power-law dependence investigations using reaction kinetics and calorimetric studies with H₂O adsorption, it is concluded that high-Si/Al-ratio Pd/SSZ-13 catalysts are much more hydrophobic than low-Si/Al-ratio Pd/SSZ-13 and Pd/Al₂O₃, which greatly inhibits H₂O-induced catalyst deactivation.

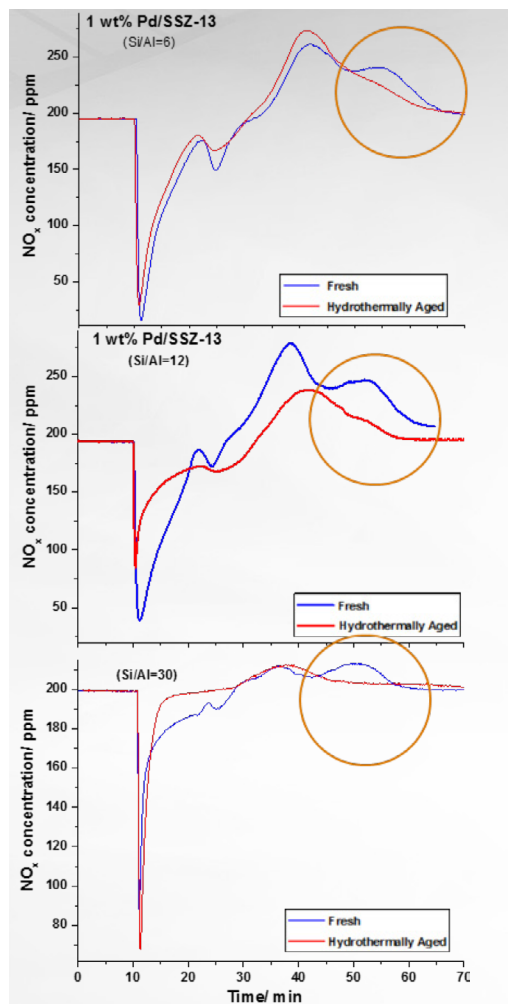


Figure IV.7.1. NO_x uptake and release for 1 wt% Pd/SSZ-13 with Si/Al = 6, 12, and 30, before and after hydrothermal aging

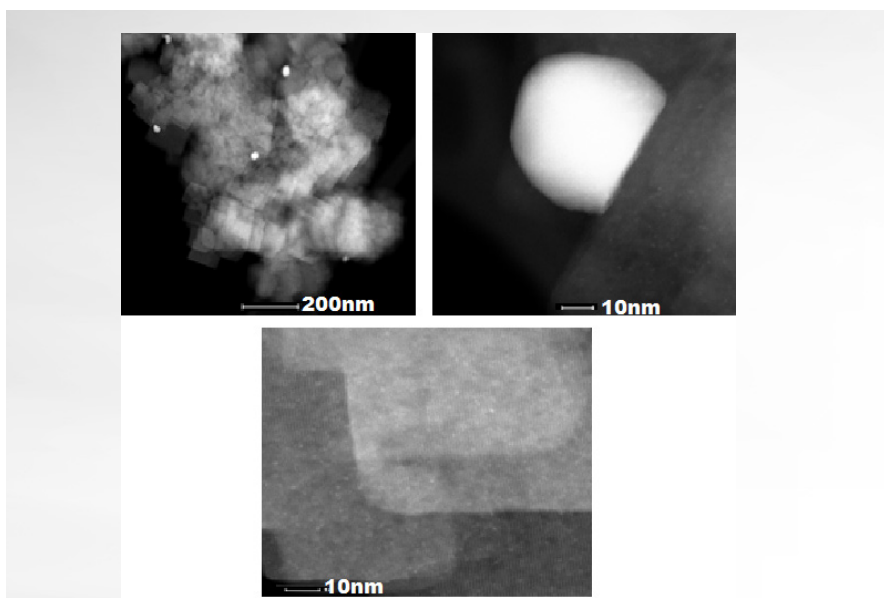


Figure IV.7.2. Transmission electron microscopy images of 1 wt% Pd/SSZ-13 with Si/Al = 6 after hydrothermal aging

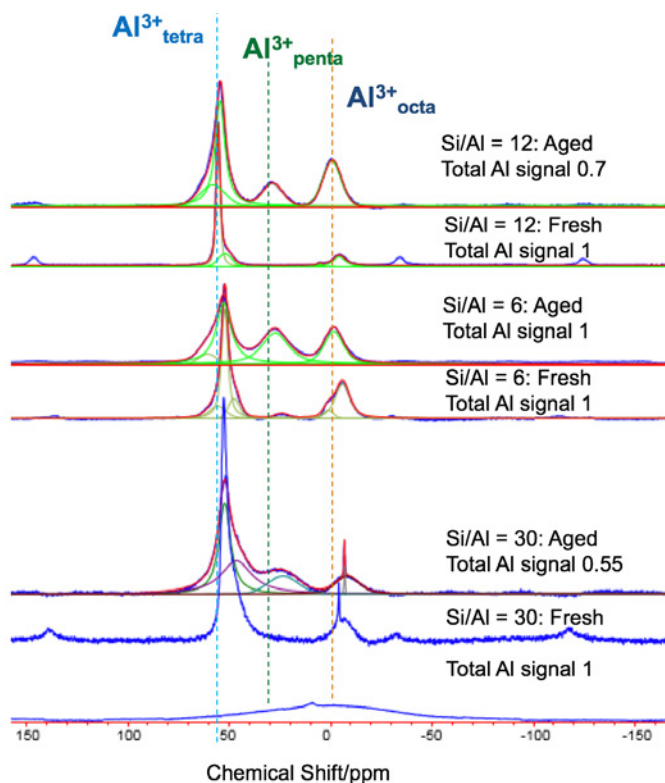


Figure IV.7.3. ²⁷Al NMR spectra of fresh and hydrothermally aged 1 wt% Pd/SSZ-13 with Si/Al = 6, 12, and 30

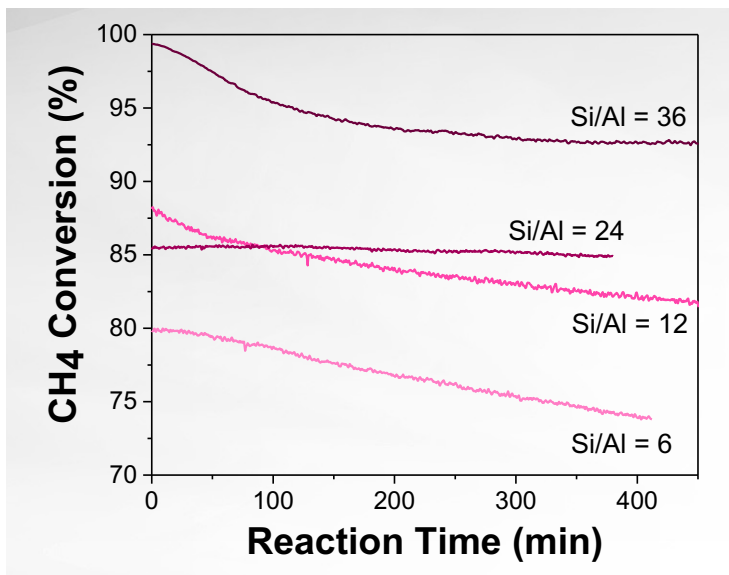


Figure IV.7.4. Methane conversion as a function of time on stream for 3 wt% Pd/SSZ-13 with Si/Al = 6, 12, 24, and 36

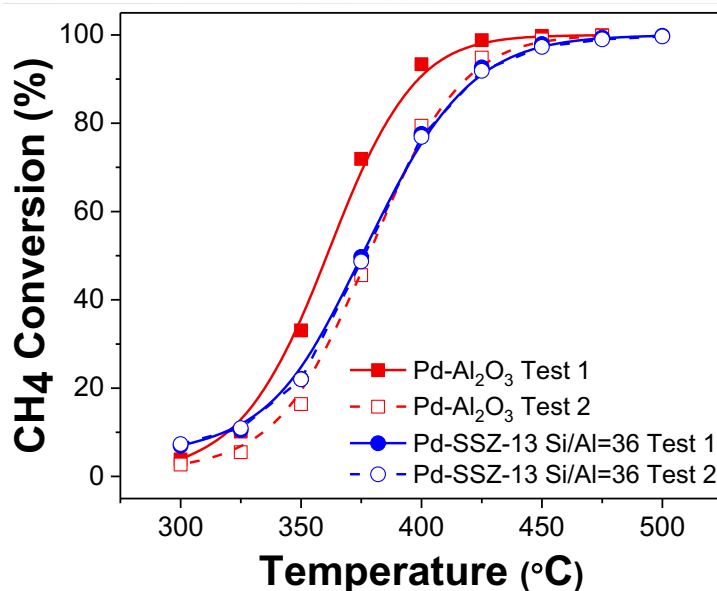


Figure IV.7.5. Comparison of 3 wt% Pd/SSZ-13 (Si/Al = 36) with Pd/Al₂O₃

Conclusions

- For PNA materials, hydrothermal aging causes both Pd agglomeration and SSZ-13 structural degradation. Atomically isolated Pd ions are highly stable during aging, but multinuclear Pd species agglomerate to form large PdO particles.
- In terms of NO_x storage capacity, total NO_x storage capacity decreases after aging. In terms of release temperatures, NO_x release temperatures from isolated Pd sites do not change appreciably, but NO_x release from nitrate decomposition greatly diminishes after aging. This is attributed to the loss of oxidizing capacities of the PNA materials.
- Hydrophobicity of the SSZ-13 material plays a decisive role in the on-stream stability of Pd/SSZ-13 low-temperature combustion catalysts. Catalysts with low Si/Al ratios deactivate with time similar to the commercial Pd/Al₂O₃, but zeolite-supported catalysts with high Si/Al ratios maintain high stability.

Acknowledgements

Thanks to Feng Gao, János Szanyi, Yilin Wang, and Yong Wang of PNNL for contributions to the project.

IV.8 Development and Optimization of Multi-Functional SCR-DPF Aftertreatment for Heavy-Duty NO_x and Soot Emission Reduction (Pacific Northwest National Laboratory)

Kenneth G. Rappé, Principal Investigator

Pacific Northwest National Laboratory (PNNL)
P. O. Box 999
Richland, WA 99352
E-mail: ken.rappe@pnnl.gov

Ken Howden, DOE Technology Development Manager

U.S. Department of Energy
E-mail: Ken.Howden@ee.doe.gov

Start Date: October 1, 2017	End Date: September 30, 2018	
Project Funding (FY18): \$600,000	DOE share: \$300,000	Non-DOE share: \$300,000

Project Introduction

Integrated selective catalytic reduction (SCR) on diesel particulate filter (DPF) (SCR-DPF) technology combines NO_x reduction and soot filtration in a single two-way device by loading an SCR catalyst into the porous wall microstructure of a DPF. Its development is motivated by emission compliance in a manner that reduces aftertreatment system volume/cost and increases packaging flexibility, and enabling a pathway towards improved low-temperature (and overall) NO_x reduction performance particularly for heavy-duty diesel. The challenges faced for successful application of SCR-DPF technology to heavy-duty diesel vehicles are (1) achieving the necessary soot filtration and SCR reaction performance, (2) achieving the necessary SCR durability requirements, and (3) retaining sufficient passive soot oxidation capacity on the DPF for it to be attractive for deployment. The first two challenges have been addressed through the development of advanced ultra-high-porosity substrates and catalyst coating and imaging techniques, and the development of small-pore chabazite (CHA) or CHA-like zeolite-based SCR catalysts with superior thermal durability, and thus have a clear path forward [1–3]. The third challenge is significant because passive soot oxidation (oxidation of soot by NO₂) is a significant contributor to the management of accumulated soot for heavy-duty diesel; it reduces the overall fuel penalty associated with the reduction of soot emissions at the tailpipe.

The reason why passive soot oxidation is a challenge with SCR-DPF technology is because of NO₂ availability, which is the critical oxidant in passive soot oxidation. The fast SCR reaction that consumes NO and NO₂ in equimolar amounts is kinetically dominating in current state-of-the-art Cu-CHA SCR catalysts and is much faster than the passive soot oxidation reaction in the temperature range of interest. Thus, the integration of current state-of-the-art SCR catalyst technology on a DPF results in significantly reduced passive soot oxidation activity due to preferential depletion of the NO₂ by the SCR catalyst. This work is focused on the development of a novel active SCR phase that, when employed in the SCR-DPF configuration, will enable sufficient passive soot oxidation capacity to be attractive for the heavy-duty diesel application while retaining the necessary NO_x reduction performance efficiency.

Objectives

Overall Objectives

- Demonstrate the successful integration of a DPF with a binary catalyst system consisting of an SCR phase and a selective catalytic oxidation (SCO) phase to enable sufficient passive soot oxidation capacity within the device

- Develop an SCR-SCO binary catalyst system that successfully enables the availability of NO₂ for achieving the necessary passive soot oxidation capacity within the integrated device while retaining high NO_x reduction efficiency and minimizing the parasitic oxidation of NH₃ (with O₂)
- Develop the fundamental understanding of the interaction of the SCR and SCO catalyst phases that will lead to an optimized binary catalyst system, identifying the necessary engineering requirements and system limitations for their integration, with a view to proper function and optimal integration
- Develop models that incorporate the SCR catalyst system that can accelerate the optimization of the system by providing SCR operational insight while simultaneously minimizing experimental testing
- Develop the necessary understanding to potentially lead to the design and optimization of four-way devices, which will address particulate matter, hydrocarbons, CO, and NO_x in a single unit

Fiscal Year 2018 Objectives

- Inform on critical catalyst design parameters for a ZrO₂-based SCO phase combined with a Cu-CHA SCR phase, forming an SCR-SCO binary catalyst system, in relation to NO_x reduction performance and SCR durability
- Understand the impact of secondary oxide or heteroatom additives to ZrO₂ employed to improve NO oxidation (to NO₂) behavior on NO_x reduction performance and SCR durability
- Inform on the optimized pathway towards SCO impact on fast-SCR contribution to NO_x reduction

Approach

The work is tasked with developing a novel active SCR catalyst phase that enables superior passive soot oxidation activity and comparable NO_x reduction performance when employed in the SCR configuration in comparison to current state-of-the-art SCR catalyst technology. This is to be accomplished by the integration of an SCO phase to the SCR catalyst, forming an SCO-SCR binary catalyst active phase. The intent of the SCO phase is to increase the NO oxidation (to NO₂) capacity of the active SCR phase, thus generating NO₂ in situ, while retaining or improving upon the NO_x reduction efficiency and SCR durability. The result of a successful SCO-SCR binary catalyst integration will be greater availability of NO₂ to drive passive soot oxidation without compromising durable and efficient NO_x reduction performance. The SCO phase will build off of a ZrO₂-base structure, with variations to its chemistry to potentially include enhanced reducibility and/or oxygen storage (e.g., inclusion of CeO₂), modulation of oxidation capacity (e.g., inclusion of Mn and/or Co), and other potential additives for activity or durability. The targets for a successful binary catalyst active phase are: (1) high NO oxidation capacity to drive passive soot oxidation performance, (2) retaining high NO_x reduction performance and selectivity by not oxidizing NH₃ reductant at unacceptably high levels, and (3) retaining high SCR durability by not inflicting unacceptable damage on the SCR active phase.

PNNL utilizes an extensive suite of standard and specialty analytical tools and test reactors to support steady-state and transient testing that are necessary to provide information on critical catalyst design parameters, enablers, and limitations with the binary catalyst system. PNNL is focused on fundamental understanding of the pathway towards high NO oxidation (to NO₂) capacity of the binary catalyst system in a manner which retains highly efficient and selective NO_x reduction and a durable SCR catalyst phase. PNNL utilizes resources associated with PNNL's Exhaust Emissions Science Lab and leverages the capabilities within the Environmental Molecular Science Laboratory, Institute for Interfacial Catalysis, and Emissions Chemistry & Aerosol Research facility. PACCAR is providing input on preferential direction for SCO phase chemistry and is leading efforts associated with catalyst coating on cores and scaling to the device level.

Results

Work in FY 2018 was focused on developing an understanding of the impact of an SCO phase on the behavior and performance of a Cu-CHA SCR catalyst, including NO_x reduction performance and selectivity and SCR catalyst durability. This included informing on the role of relative proximity of the SCR and SCO catalyst phases, which ranged from solely physical mixing inducing less interaction of the SCO and SCR phases to

more intimate interaction via impregnation and SCO phase growth on the surface of the SCR phase. The reason that informing on SCO-phase impact on SCR performance is important is due to the potential interaction of the SCO phase and the SCR-phase Cu. Current state-of-the-art Cu-CHA SCR catalysts are intimately dependent on intra-framework Cu quantity and behavior, and in particular on low-temperature intra-framework Cu mobility. Interaction of the SCO phase with this intra-framework Cu would expectedly impact SCR-phase performance and durability. Conversely, extra-framework Cu is detrimental to SCR catalyst performance and durability and is a significant contributor towards the primary pathway of hydrothermal degradation of current Cu-CHA SCR catalysts. Extra-framework Cu forms CuO_x clusters on the surface of the zeolite that detrimentally impact SCR selectivity and durability and can dictate end of useful life for SCR catalysts in deployment.

Since the project team is confident that the SCO phase will build off of a ZrO_2 -base structure, ZrO_2 was the initial focus of investigations in FY 2018. As shown in Figure IV.8.1, it was discovered that, with the integration of ZrO_2 with the Cu-CHA SCR catalyst, low-temperature NO_x reduction performance was minimally impacted whereas high-temperature NO_x reduction performance was improved in comparison to Cu-CHA alone. Both of these results were observed even after catalyst aging. The minimal impact of ZrO_2 on the low-temperature NO_x reduction performance informs that (1) there is minimal NO_2 production induced by SCO phase inclusion to contribute to increased NO_x reduction performance through a fast-SCR pathway and (2) there is trivial interaction of the ZrO_2 secondary SCO phase on intra-framework Cu. The former is expected and not surprising, since ZrO_2 itself has very little NO oxidation (to NO_2) activity, and the latter confirms the validity of proceeding with a ZrO_2 -based SCO phase.

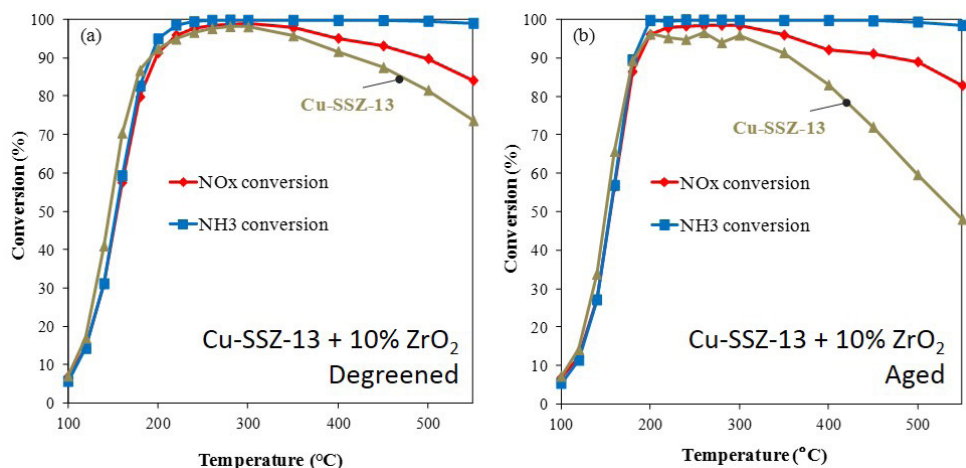


Figure IV.8.1. SCR standard (NO only) performance of Cu-SSZ-13 and Cu-SSZ-13 + 10 wt% ZrO_2 catalyst

The improvement in high-temperature NO_x reduction that resulted from ZrO_2 and Cu-CHA integration increased with catalyst aging and increased with ZrO_2 proximity to the SCR catalyst. With increased aging of Cu-CHA alone, the contribution of non-selective NH_3 oxidation (also known as parasitic NH_3 oxidation) results in decreased NO_x reduction performance at temperatures greater than $\sim 300^\circ\text{C}$ and is also observed in Figure IV.8.1. The binary catalyst with ZrO_2 and Cu-CHA physically mixed resulted in similar NO_x reduction performance to Cu-CHA following degreening, whereas the binary catalyst showed improved performance following aging. This led PNNL to investigate the impact of proximity of the ZrO_2 and Cu-CHA phases. The result of closer proximity of ZrO_2 and Cu-CHA (Figure IV.8.1) is improved NO_x reduction performance observed even after degreening, with even more significantly improved performance after hydrothermal aging.

PNNL discovered that the reasons for improved high-temperature NO_x reduction performance of the binary catalyst system are reaction selectivity and the relative contribution of parasitic NH_3 oxidation. This was further investigated and confirmed through assessment of NH_3 oxidation alone (i.e., by O_2 with NO_x) and is shown in Figure IV.8.2 as a function of relative proximity of the Cu-CHA and ZrO_2 phases. These results show that NH_3 oxidation activity is significantly reduced on these catalysts with increased aging, and the lowest

activity is associated with the closest proximity of ZrO₂ and Cu-CHA. Both of these results suggest that the root of impact of ZrO₂ on Cu-CHA high-temperature performance is associated with a chemical interaction between the Cu-CHA and ZrO₂ phases.

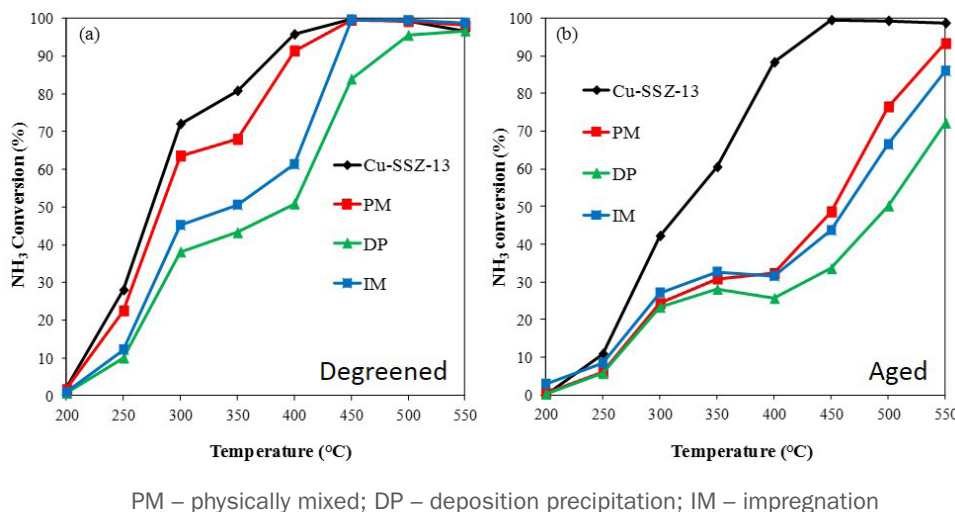


Figure IV.8.2. NH₃ oxidation (by O₂, i.e., without NO_x) activity of Cu-SSZ-13 and Cu-SSZ-13 + 10 wt% ZrO₂ at varying proximity of SCR and SCO catalyst phases

PNNL discovered that the improvement in high-temperature NO_x reduction performance with ZrO₂ integration with Cu-CHA is due to the ability of ZrO₂ to mitigate the NH₃ oxidation activity of extra-framework Cu by taking Cu as a heteroatom into the ZrO₂. This was supported by evidence from temperature-programmed reduction (TPR) and X-ray diffraction (XRD), amongst other techniques. Figure IV.8.3 shows TPR behavior of Cu-CHA + ZrO₂ and compares this behavior with Cu-CHA and ZrO₂ alone. Cu-CHA has a well-known bimodal reduction behavior at 200°C and 360°C associated with framework Cu [Cu(OH)¹⁺ and Cu²⁺], which is also observed in the Cu-CHA + ZrO₂ TPR profile. Similarly, ZrO₂ has a single broad reduction feature centered at ~420°C that is also observed in the Cu-CHA + ZrO₂ TPR profile, albeit at slightly higher temperature, likely due to ZrO₂ monoclinic-tetragonal transformation with stabilized Cu. However, in contrast, Cu-CHA + ZrO₂ exhibits a higher-temperature reduction feature that is not accounted for by Cu-CHA or ZrO₂ alone. This is attributed to the Zr-O-Cu feature of Cu as a heteroatom in ZrO₂.

These results are also supported by XRD analysis (results not shown). XRD analysis shows that the CuO_x features that are visible in the XRD trace of aged Cu-CHA alone are not present in the XRD trace of Cu-CHA + ZrO₂, thus suggesting that CuO_x clusters are not present. Additionally, whereas physically mixed Cu-CHA and ZrO₂ exhibits XRD diffraction features associated with less reactive monoclinic ZrO₂, a closer vicinity of Cu-CHA and ZrO₂ results in diffraction patterns associated with tetragonal ZrO₂. This provides additional evidence of a chemical interaction between Cu-CHA and ZrO₂ and suggests that Cu has inserted into ZrO₂ and helped to stabilize the tetragonal ZrO₂ phase.

PNNL discovered in studies with Cu-CHA + a Ba/ZrO₂ SCO phase evidence of the ability to take advantage of a surface-active NO_x species for participating towards a fast-SCR NO_x reduction mechanism. This was resolved from combined results of NO oxidation and NO_x reduction behavior. Experimental evidence showed no measurable improvement in NO oxidation (to NO₂) activity with the inclusion of varying amounts of Ba. This was compared to the same catalysts that exhibited increased low-temperature NO_x reduction performance with increased Ba loading. These two results are in contrast to one another, as the pathway towards the improved low-temperature NO_x reduction performance is increased fast-SCR contribution by increased NO₂ concentration from oxidation of NO. This suggests that NO₂ desorption is the limiting step in the oxidation of NO to NO₂ on these materials but is not a necessary step for contributing towards a fast-SCR reaction pathway. This is shown for clarity in Figure IV.8.4.

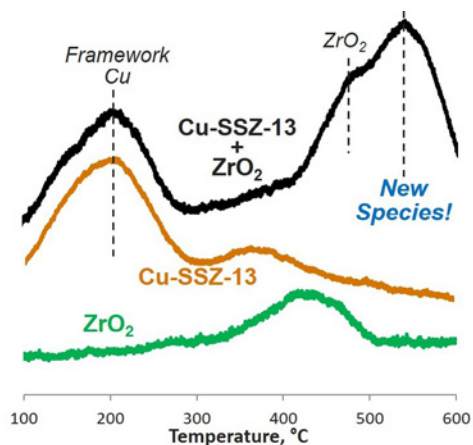


Figure IV.8.3. TPR behavior of Cu-SSZ-13 + 10 wt% ZrO₂ catalyst compared to that of Cu-CHA alone and ZrO₂ alone

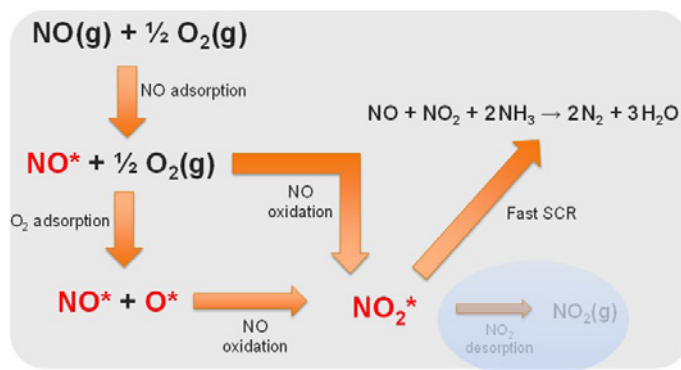


Figure IV.8.4. Pathway towards improved NO_x reduction performance by a surface-active NO_x species

PNNL has also uncovered an aging mechanism that uniquely affects the low-temperature NO_x reduction performance of the Ba/ZrO₂ system versus Cu-CHA or Cu-CHA + ZrO₂. Following high-temperature aging at 800°C, the binary catalyst with Ba in the SCO phase demonstrated reduced low-temperature and comparable high-temperature NO_x reduction activity versus Cu-CHA or Cu-CHA + ZrO₂ that was a direct function of Ba content in the SCO phase. Electron paramagnetic resonance spectroscopy also showed reduced amounts of electron paramagnetic resonance active Cu (i.e., SCR-active intra-framework Cu), which was supported by NH₃ oxidation performance, which also suggested reduced amounts of intra-framework Cu. It is believed that the aging process observed is a thermally induced ion-exchange mechanism, as shown in Figure IV.8.5 for clarity, and its magnitude and propensity to occur is a function of time, temperature, and proximity of the SCO and SCR phases. This is an aging mechanism that the research program must be cognizant of and must consider in regards to SCO phase chemistry and proximity to the SCR phase.

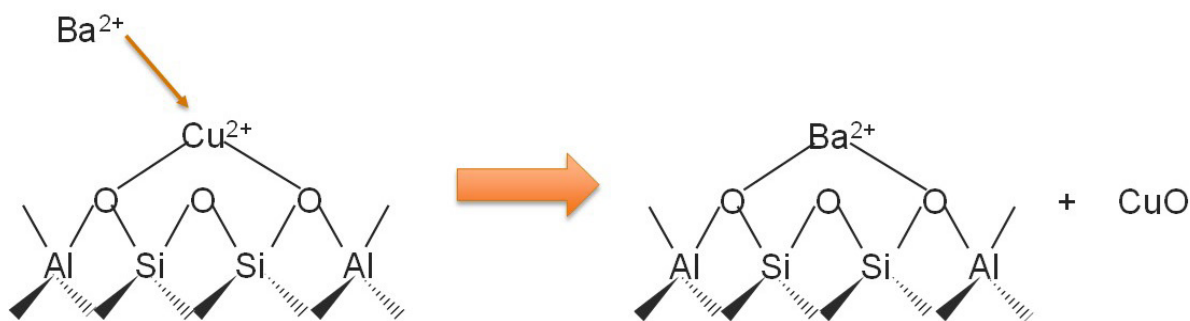


Figure IV.8.5. Thermally induced ion-exchange aging mechanism of Cu-CHA + Ba/ZrO₂ binary catalyst

Conclusions

- Work was focused on understanding important catalyst design parameters and considerations for a binary catalyst system that includes a Cu-CHA SCR phase and a ZrO₂-based SCO phase.
- The integration of ZrO₂ with Cu-CHA SCR catalyst resulted in improved high-temperature NO_x reduction performance and comparable low-temperature NO_x reduction performance in comparison to Cu-CHA.
- ZrO₂ exhibited trivial interaction with intra-framework SCR Cu, whereas ZrO₂ demonstrated the ability to mitigate the NH₃ oxidation activity of extra-framework Cu by taking Cu as a heteroatom into the ZrO₂.
- The ability of ZrO₂ to absorb extra-framework Cu as a heteroatom is significant (1) to catalyst performance in that it greatly improves high-temperature selectivity of the SCR + SCO binary catalyst system by mitigating parasitic NH₃ oxidation and (2) to catalyst durability in that it mitigates the adverse impact that extra-framework Cu has on Cu-CHA structure.
- The ability to take advantage of a surface-active NO_x species towards fast-SCR NO_x reduction was discovered with the binary catalyst system. This is significant in that it is a short-circuiting pathway towards SCO impact on SCR performance that does not require NO oxidation to a gaseous NO₂ product.
- PNNL uncovered a thermally induced ion-exchange aging mechanism associated with Ba and its ability to either interfere with or displace intra-framework Cu, resulting in reduced low-temperature NO_x reduction performance. This is an aging mechanism that will need to be considered moving forward in the work in regards to SCO phase chemistry and proximity to the SCR phase.

References

1. Melscoet-Chauvel, I., C. Remy, and T.H. Tao. 2005. "High Porosity Cordierite Filter Development for NO_x/PM Reduction." *Develop Adv Ceram Compos* 26 (8): 11–19.
2. van Setten, B.A.A.L., M. Makkee, and J.A. Moulijn. 2001. "Science and Technology of Diesel Particulate Filters." *Catal Rev: Sci Eng* 43 (4): 489–564.
3. Beale, A.M., F. Gao, I. Lezcano-Gonzalez, C.H.F. Peden, and J. Szanyi. 2015. "Recent Advances in Automotive Catalysis for NO_x Emission Control by Small-Pore Microporous Materials." *Chem Soc Rev* 44: 7371–7405.

IV.9 Enabling Lean and Stoichiometric Gasoline Direct Injection Engines through Mitigation of Nanoparticle Emissions (University of Minnesota)

William Northrop, Principal Investigator

Department of Mechanical Engineering
University of Minnesota–Twin Cities
111 Church St. SE
Minneapolis, MN 55455
E-mail: wnorthro@umn.edu

Ken Howden, DOE Technology Development Manager

U.S. Department of Energy
E-mail: Ken.Howden@ee.doe.gov

Start Date: October 1, 2015
Project Funding: \$1,311,767

End Date: January 15, 2019
DOE share: \$1,090,654

Non-DOE share: \$221,113

Project Introduction

Gasoline direct injection (GDI) engines have grown in market share in the past decade due to their proven ability to increase fuel economy, especially when combined with dilute/lean operation, boosting, and downsizing strategies; however, high nanoparticle emissions under some conditions may jeopardize many manufacturers' plans for more extensive implementation of GDI. Increasingly stringent particulate mass (PM) and particulate number (PN) standards in the United States and Europe are difficult to meet for modern stoichiometric and lean GDI engines while maintaining low greenhouse gas and other criteria pollutant emissions. The interaction between an engine's design, calibration, and fuel and lubricant formulation defines the composition, mass, morphology, and number of ultrafine particulates emitted. Only by understanding these complex interactions can PN and PM emissions be reduced while maintaining low greenhouse gas and other criteria gaseous emissions.

This project represents a three-way collaboration between a university with an established record in combustion-generated nanoparticle research, a major automotive original equipment manufacturer, and a global fuel provider. It has experimentally explored pathways to reduce nanoparticle emissions from GDI engines using a comprehensive approach that investigated novel fuels to mitigate soot during transient and steady-state operation and to enhance regeneration of gasoline particulate filter (GPF) aftertreatment. This critical research is highly applicable to the Department of Energy goals established by the Advanced Combustion and Emission Control Roadmap to better understand emissions of PM from dilute combustion gasoline engines and to characterize the engine-out and filter-out PM and PN. It also addresses the need to determine the effect of ethanol and fuel chemistry on particulate formation. More broadly, this project provides a comprehensive and innovative approach to address PN and PM emissions as a key risk to implementation of GDI engine technology.

Objectives

This project seeks to develop system-level strategies by seeking synergies between fuel and lubricant properties, engine calibration, and next-generation aftertreatment strategies for PM and PN reduction. In addition, the project aims to develop novel technical solutions that lower emissions while maintaining high engine thermal efficiency. Specific objectives for the overall project and Fiscal Year 2018 are given below.

Overall Objectives

- Efficiently reduce PM and PN emissions of lean and stoichiometric GDI engines used in light-duty vehicles below the European 6 x 10¹¹ solid particles/km limit and the California Air Resources Board 2025 Low Emission Vehicle Program (LEV III) standard of 0.62 mg/km for any imposed driving cycle

- Determine system-level strategies by seeking synergies between fuel and lubricant properties, engine calibration, and next-generation aftertreatment strategies for PM and PN reduction
- Reveal novel technical solutions that have minimal impact on greenhouse gas emissions
- Develop an accurate method for real-time PM measurement using suspended particle instruments

Fiscal Year 2018 Objectives

- Complete a full factorial screening of seven fuels over lean and stoichiometric GDI operating modes
- Reveal fuel and aftertreatment synergies to achieve low PN and PM emissions
- Determine effective density as a function of diameter for lean and stoichiometric GDI particles

Approach

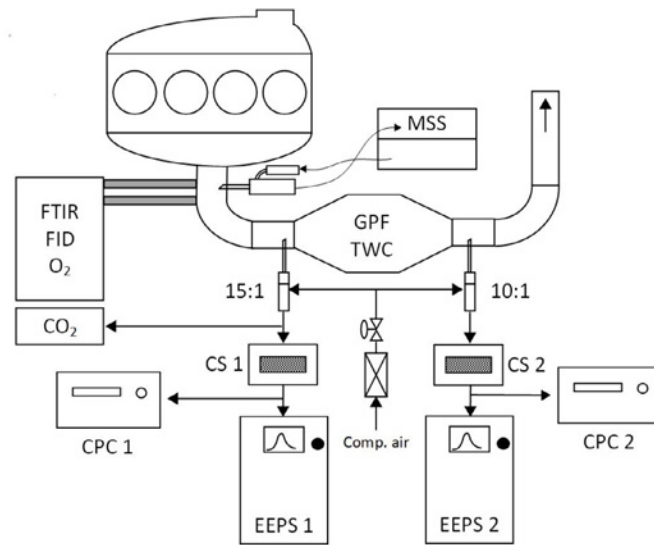
The approach taken in this project was to experimentally characterize PN and PM emissions from stoichiometric and lean GDI operation over a range of fuel properties and with advanced aftertreatment. Nanoparticle emissions (both PN and PM) were characterized using extensive aerosol instrumentation. Instruments used for PN included mobility particle diameter instruments like a scanning mobility particle sizer and engine exhaust particle sizer (EEPS). Since only solid (non-volatile) particles are regulated according to stringent PN standards, a catalytic stripper (CS) technology originally developed at University of Minnesota [1] was used. Other instruments used in the experiments include photoacoustic soot mass analyzer and Fourier transform infrared (FTIR) for gas concentration measurement.

Engine experiments were conducted on a lean-burn GDI engine with a custom fully programmable electronic control unit with the ability to sample emissions from one cylinder for optical experiments and from all four cylinders for fuel characterization work. A range of fuels were provided by project partner BP and three-way catalyst (TWC)-coated GPF provided by project partner FCA. The industrial partners have also worked closely with the university research team to specify engine operating conditions and to refine test plans to ensure the production of vehicle application-relevant results.

Results

The emissions sampling system and measurement instrumentation used in the research project are shown in Figure IV.9.1. Gaseous emissions were measured using an AVL (Graz, Austria) SESAM i60 FT multi-component exhaust measurement system composed of a FTIR spectrometer, a flame ionization detector, and a paramagnetic oxygen detector. PM emissions were measured by an AVL MicroSoot Sensor (MSS), two TSI (Shoreview, Minnesota) EEPS instruments, and two TSI condensation particle counters (CPCs). The MSS measured soot mass concentration upstream of the GPF; the EEPSs simultaneously measured particle size distributions (PSDs) upstream and downstream of the GPF at a rate of 1 Hz using a soot inversion matrix to determine real-time, size-resolved GPF filtration efficiency; and the CPCs measured PN concentration pre- and post-GPF. Two CSs were operated at 300°C in order to remove all volatile and semi-volatile material from the exhaust gas such that the particle emissions measured by EEPSs and CPCs were that of only solid particles.

Seven different fuel formulations were tested in the study to determine the impact of fuel physical properties and chemistry on particle emissions from the three different GDI combustion modes. None of the fuels contained a detergent additive package. The fuels tested are shown in Table IV.9.1 with their fuel identification name, concentration of aromatics, distillation temperature T90, octane number, ethanol (EtOH) concentration, and calculated PM index (PMI) based on Aikawa, et al. [2]. All fuels except the baseline fuel were analyzed by BP using gas chromatography-mass spectrometry to quantify the concentration of more than 300 chemical species. With this analysis, the PMI was calculated for each component present.



FID – flame ionization detector

Figure IV.9.1. Engine and instrumentation schematic showing dilution system and instruments used in the experimental study

Table IV.9.1. Fuel Property Data and PMI

Fuel ID	Aromatics (%)	T90 (°C)	EtOH (%)	RON/MON	Target CA50 (°ATDC)
Baseline	27.0	162	9.9	96.2/85.4 (90.8)	NA
A-1	22.4	160	9.9	95.2/86.5 (90.9)	1.2
A-2	42.9	166	9.9	97.9/87.3 (92.6)	1.8
V-1	29.4	129	9.9	95.1/86.5 (90.8)	0.7
V-2	29.4	187	10.0	96.2/87.2 (91.7)	2.2
E15	28.5	160	15.2	99.1/88.0 (93.6)	1.4
E50	16.7	160	50.0	103.8/88.8 (96.3)	1.1

RON – research octane number; MON – motor octane number; CA50 – crank angle at 50% mass fraction burned; ATDC – after top dead center

The engine was operated in three combustion modes: stoichiometric (S), lean homogeneous (LH), and lean stratified (LS), as given in Table IV.9.2. The combustion modes differed primarily in equivalence ratio and injection strategy. The stoichiometric mode featured two injections during the intake stroke, with two-thirds of the fuel delivered in the primary injection and the remainder in the secondary injection. The lean homogeneous mode featured a primary injection during the intake stroke, where two-thirds of the fuel was injected, followed by a secondary injection delivering the remainder of the fuel and beginning approximately 10 crank angle degrees prior to the spark event. The lean stratified mode featured two injections approximately 20 and 10 crank angle degrees prior to the spark event followed by a small, third injection just after the spark.

Table IV.9.2. Engine Conditions Including Operating Mode and Equivalence Ratio

Condition	Speed (rpm)	T90 (°C) (bar)	EtOH (%)	RON/MON
Steady State 1	1,400	2	S1	1.0
			LH1	0.67
			LS1	0.5
Steady State 2	2,000	4	S2	1.0
			LH2	0.65
			LS2	0.65
Steady State 3	2,000	7	S3	1.0
			LH3	0.69
Steady State 4	2,000	7	S4	1.0
			LH4	0.73

BMEP – brake mean effective pressure; rpm – revolutions per minute

Fuel Effect on Solid Engine-Out PM Emissions

Representing an example of the results from the comprehensive fuel screening experiments, Figure IV.9.2 shows the engine-out PSDs for the lean homogeneous conditions at each engine condition and for each fuel. The fuel label is listed in the legend, with the PMI of that fuel in parentheses. PSDs represent the mean of three five-minute averages taken on the three different test days for each fuel. The error bars are standard deviation of that mean and thus represent the day-to-day repeatability of the engine condition and fuel.

The high-ethanol-content fuel (E50) repeatably produced the highest PM emission for three of the four engine conditions in the lean homogeneous mode. For the LH1 condition, the E50 distribution is similar to that of the other fuels, with a large 10 nm solid nucleation mode and a moderate accumulation mode. At the LH2 condition, the E50 fuel produced significantly lower PM emissions than any other fuel. All other fuels produced similar distributions and concentrations at this condition. However, at the two higher load lean homogeneous conditions, LH3 and LH4, the E50 fuel produced almost an order of magnitude higher accumulation mode concentrations than any other fuel. This is likely a consequence of the late injection employed by the lean homogeneous mode coupled with the high heat of vaporization of ethanol. Because of the greater fuel demand at the higher load conditions, a large quantity of fuel was injected in the late injection, and there was not enough time or enough heat in the cylinder to fully vaporize the fuel prior to combustion. The ethanol was not the source of the high concentration of accumulation mode particles; rather, the high heat of vaporization of the ethanol in the fuel inhibited fuel evaporation, leaving the remaining fuel components with high sooting tendencies in the liquid phase or as highly rich vapor regions as combustion commenced.

It can be seen from the PSDs that the magnitude of the solid nucleation mode, near 10 nm, trends with the magnitude of the accumulation mode. The 10 nm mode particles are thought to be composed of ash derived from metallic lubrication oil additives. It could be expected that, if the formation of these 10 nm ash particles occurred independently from the mechanism through which the accumulation mode soot particles, were formed, the large accumulation mode particles would scavenge the ash particles, and the two modes would be inversely related. Since this is not the case, it is assumed that the mechanisms responsible for the formation of these two modes are related. Namely, it is proposed that wall-wetting induces the formation of both the solid nucleation mode and the accumulation mode. Fuel impingement on cylinder surfaces would dissolve oil films, reducing the viscosity and surface tension of the film, and encourage the ejection of oil droplets from the cylinder wall or piston ring. When the oil is burned during combustion, the metallic ash remains suspended in the gas and forms the 10 nm ash particles. Wall-wetting would also produce soot-forming diffusion flame pool fires, resulting in accumulation mode particles, thus linking the formation of the two modes.

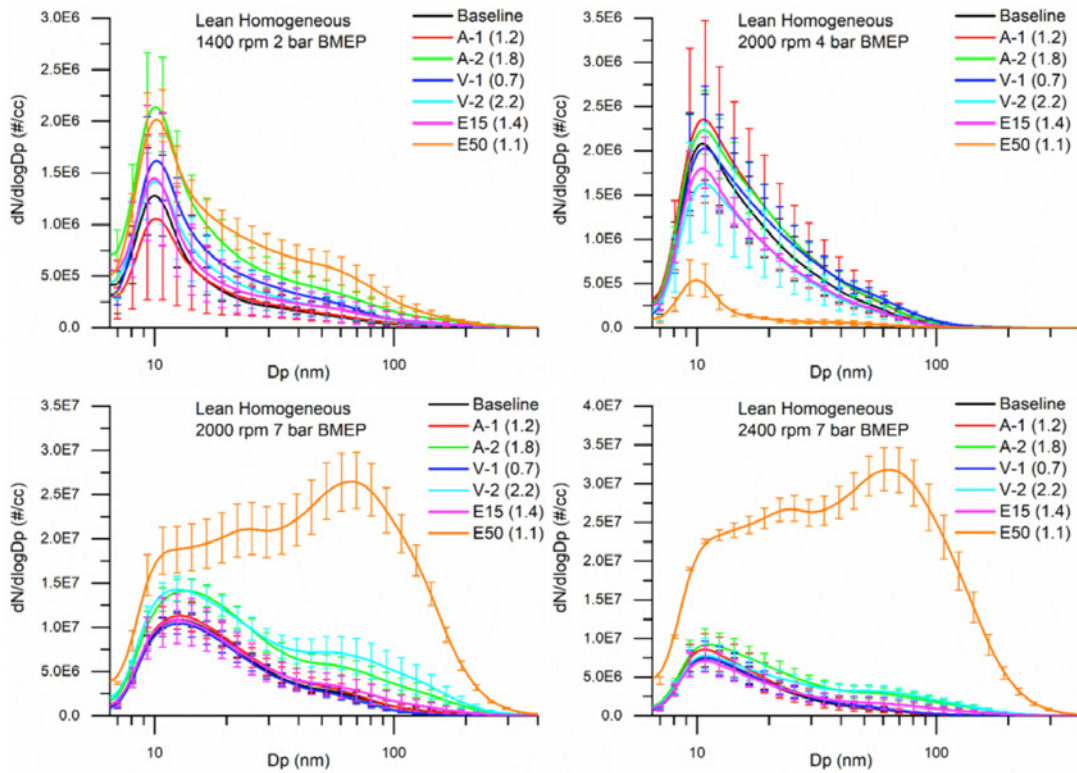


Figure IV.9.2. Engine-out PSDs for the lean homogenous combustion mode at the four different engine conditions for each of the seven fuels tested. From top left to bottom right: LH1, LH2, LH3, and LH4.

When PN and PM mass concentrations were examined at the LH3 and LH4 conditions and the E50 fuel was omitted, the PN and PM mass emissions correlated well with the fuel PMI. Figure IV.9.3 shows the correlation between PN and the PMI for the LH3 condition. The same was found for the LH4 condition (not shown for brevity). PN and PM mass emissions from the lower load lean homogeneous conditions, LH1 and LH2, showed little to no correlation with the PMI. The R square values for the LH1 and LH2 conditions were less than 0.1 and are not shown here for conciseness. These lower load lean homogeneous conditions appear relatively insensitive to fuel formulation.

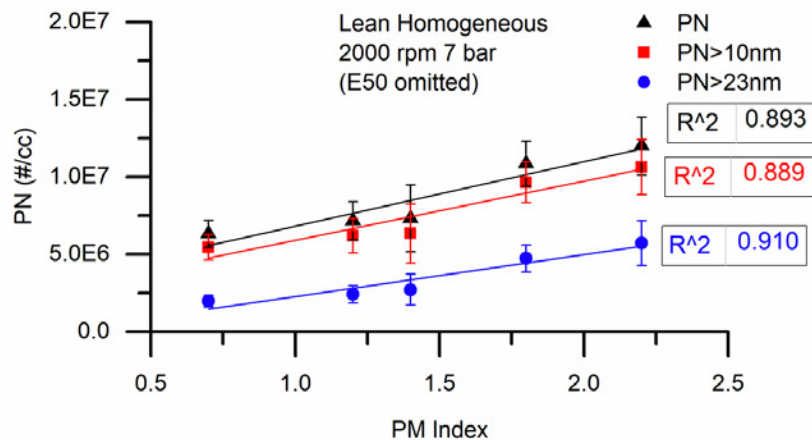


Figure IV.9.3. Correlation between PN and the PMI for the lean homogenous combustion mode at the 2,000 rpm 7 bar BMEP engine condition with the E50 fuel omitted

GPF Filtration Efficiency

Due to the low PM emissions during stoichiometric modes, GPF filtration efficiency is largely unchanged for these engine modes. However, for some lean operating conditions, PM concentrations were sufficient to result in improved efficiency as the filter loaded builds with soot. Figure IV.9.4 shows GPF PN > 23 nm filtration efficiency as a function of unoxidized soot mass loaded per GPF volume for the low-volatility fuel (V2) and E50 at a lean stratified engine condition (LS1) and the lean homogeneous condition (LH3 and LH4) with the addition of a corrected LS1 condition assuming an initial loaded mass of 10 mg/L. Soot load was calculated using the MSS volumetric soot mass concentration and the volumetric exhaust flow rate. The filtration efficiency was calculated using the pre- and post-GPF PSDs measured by the EEPs and is defined as $1 - \text{PN}(D_p)_{\text{out}}/\text{PN}(D_p)_{\text{in}}$ for all particle sizes. The most penetrating particle size for the GPF was between 100 nm and 150 nm. Particles smaller than that were efficiently trapped by diffusion, and particles larger than that were efficiently trapped by impaction and interception.

The corrected LS1 condition reached a higher filtration efficiency with less soot mass compared to the other conditions in which oxidation occurred on the GPF. This loading curve is in the range of what was reported in a study by Liu et al. in which they loaded GPFs of different wash-coat loadings under rich conditions [3]. The engine-out PSD and level of soot loading on the GPF determine the filtration efficiency. The lean homogeneous conditions had PN > 23 nm filtration efficiencies of between 60% and 65% at 7 mg/L, similar to what the LS2 condition had at 1.5 mg/L. This is in part due to greater soot oxidation occurring at the higher temperature LH conditions, but it is mostly caused by the difference in PSDs of the LH and LS modes. The high load LH modes had a greater fraction of particles near the most penetrating particle size compared to the LS condition, so the total filtration efficiency was lower for the same loading conditions, i.e., the same size-resolved filtration efficiency.

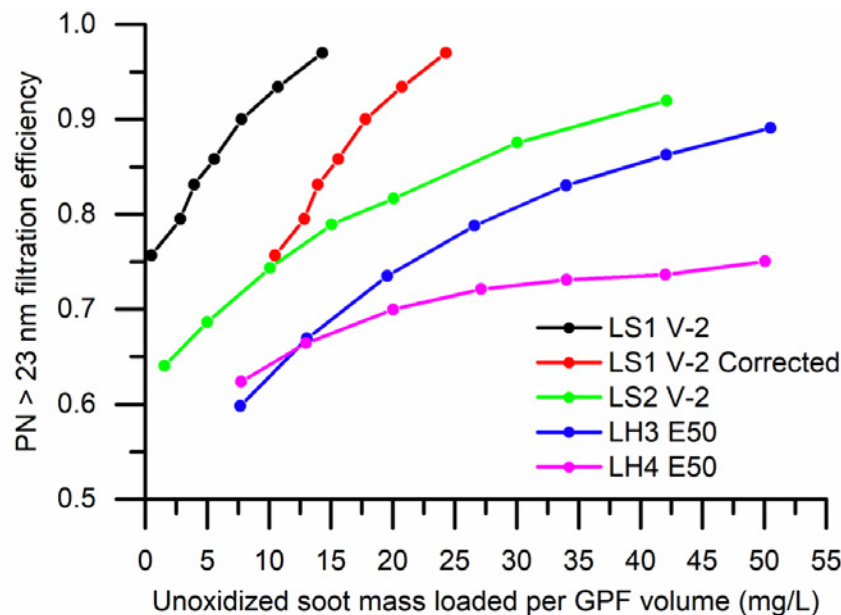


Figure IV.9.4. PN > 23 nm filtration efficiency as a function of non-oxidized soot mass loading on the GPF per filter substrate volume

Conclusions

In Fiscal Year 2018, this project has found that the dominant influence on particle formation is charge composition, which is influenced by fuel properties. However, at either end of the mixture formation spectrum, fuel properties are overshadowed by the prevailing engine conditions. In this work, aside from the E50 fuel, there was minimal fuel influence observed on PM emissions when the charge mixture was homogenous, like in stoichiometric modes, resulting in low particle formation. There was also minimal fuel influence when there was so much fuel stratification that liquid droplets existed when combustion began, resulting in diffusion flames. With moderately stratified charge composition, like in the higher load lean homogeneous conditions, there was a clear correlation between PN and PM mass and the PMI. This indicates that the PMI is only applicable when there is significant accumulation mode particle concentration (soot) and only when the mixture is not overly stratified.

Real-time, size-resolved filtration efficiency was measured for a TWC wash-coated GPF. The work showed that lean combustion modes can induce soot oxidation at relatively low temperatures while increasing engine thermal efficiency through lean operation. Slightly higher temperature conditions or lower soot concentrations than shown here would be useful for performing gradual passive GPF regeneration. Additionally, the lean homogeneous conditions considered in this work represent those that could be used to maintain a desired GPF soot loading level for high filtration efficiency, a safe level of soot loading to avoid thermal runaway if suddenly regenerated, and low pressure drop.

Key Publications

The following peer-reviewed publications resulted from this work in Fiscal Year 2018.

1. Bock, N., J. Jeon, D.B. Kittelson, and W.F. Northrop. 2018. "Solid Particle Number and Mass Emissions from Lean and Stoichiometric Gasoline Direct Injection Engine Operation." *2018 SAE World Congress*, Detroit, MI, 2018-01-0359.
2. Jeon, K., N. Bock, D.B. Kittelson, and W.F. Northrop. 2018. "Correlation of Nanoparticle Size Distribution Features to Spatiotemporal Flame Luminosity in Gasoline Direct Injection Engines." *International Journal of Engine Research*, <https://doi.org/10.1177/1468087418798468>.

References

1. Swanson, J., and D. Kittelson. 2010. "Evaluation of Thermal Denuder and Catalytic Stripper Methods for Solid Particle Measurements." *J. Aerosol Sci.* 41 (12): 1113–1122, doi:10.1016/j.jaerosci.2010.09.003.
2. Aikawa, K., T. Sakurai, and J.J. Jetter. 2010. "Development of a Predictive Model for Gasoline Vehicle Particulate Matter Emissions." *SAE Tech. Pap.* 3 (2): 610–622, doi:10.4271/2010-01-2115.
3. Liu, X., T. Chanko, C. Lambert, M. Maricq, and F. Motor. 2018. "Gasoline Particulate Filter Efficiency and Backpressure at Very Low Mileage." *SAE Tech. Pap.* 1–9, doi:10.4271/2018-01-1259.

Acknowledgements

Beyond the critical industrial partners, BP and FCA, who have provided invaluable assistance to this research, the project team would like to acknowledge James Parks and John Storey at Oak Ridge National Laboratory for their on-going assistance in setting up the test engine.

V. High Efficiency Engine Technologies

V.1 Volvo SuperTruck 2: Pathway to Cost-Effective Commercialized Freight Efficiency (Volvo Group North America)

Pascal Amar, Principal Investigator

Volvo Group North America
 7900 National Service Rd.
 Greensboro, NC 27409
 E-mail: pascal.amar@volvo.com

Ken Howden, DOE Technology Development Manager

U.S. Department of Energy
 E-mail: Ken.Howden@ee.doe.gov

Start Date: October 1, 2016 End Date: September 30, 2018
 Project Funding: \$9,361,258 DOE share: \$4,592,415 Non-DOE share: \$4,768,843

Project Introduction

Volvo’s SuperTruck 2 (ST2) continues to build on the success of the SuperTruck project that demonstrated vehicle freight efficiency improvements in excess of the program goals. Many SuperTruck technologies with customer-acceptable payback (e.g., aerodynamics, powertrain components, tractor light weighting) are now used in commercial trucks, thereby reducing national energy consumption.

Federal data on truck utilization shows that a majority of Class 8 long-haul trucks operate at or below 65,000 lbs gross combined weight, much lower than the maximum combined vehicle weight of 80,000 lbs. This implies that most trucks are under-utilized and are oversized, i.e., heavier and with more powerful engines than needed to meet their actual operational requirements. Volvo’s ST2 will therefore demonstrate an all new complete vehicle concept designed with an integrated approach to maximize freight efficiency.

The project consists of three work packages organized in four sequential phases, as illustrated in Figure V.1.1. During Fiscal Year 2018, the focus shifted from concept selection to technology development and integration.

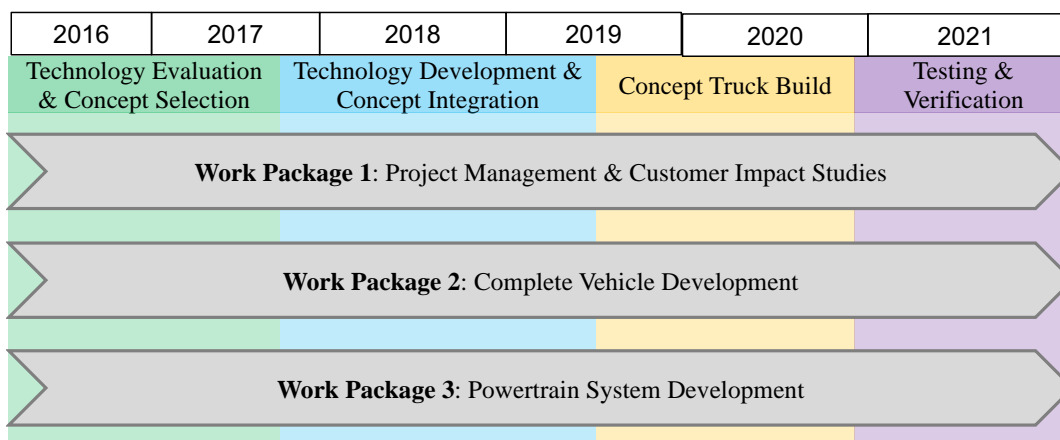


Figure V.1.1. Project schedule and phasing (Volvo)

Objectives

Overall Objectives

- Demonstrate >100% improvement in vehicle ton-miles per gallon compared with a best-in-class 2009 truck, with a stretch goal of 120%
- Demonstrate 55% brake thermal efficiency on an engine dynamometer
- Develop technologies that are commercially cost-effective in terms of a simple payback

Fiscal Year (FY) 2018 Objectives

- Finalize complete vehicle requirements
- Complete road tests with technology mule truck (VEV3)
- Identify all components and technologies for integration in demonstrator

An overview of the main achievements during this fiscal year is presented in the following sections.

Approach

The Volvo SuperTruck demonstrator unveiled in September 2016 served as a research vehicle (VEV3) and was tested on road to support concept selection activities. During FY 2018, this unique truck was deployed on multiple on-road fuel economy tests. The research vehicle was retired as planned upon completion of the tests, and it is now on display at Volvo Trucks' customer experience center in Dublin, Virginia (Figure V.1.2).



Figure V.1.2. Baseline Model Year 2009 vehicle (left) and VEV3 test mule (right) at rest stop during fuel economy test (Volvo)

During FY 2018 Bergstrom joined the project team, bringing with them key expertise in idle reduction technologies. They will perform research and technology exploration on novel ways to reduce fuel consumption when trucks are driving or parked. This addition further broadens the team's area of technical expertise and strengthens its research capabilities.

The powertrain research in this project is guided by two goals: to demonstrate over 100% freight efficiency increase in a vehicle and to demonstrate 55% brake thermal efficiency of the engine in a test cell. These goals differ not only in level of efficiency required by the powertrain solution but also in the size of the design space.

As a consequence, the team is taking a two-pronged approach and will deliver one powertrain shaped as part of a total vehicle optimization toward maximum freight efficiency and another focused on demonstrating 55% brake thermal efficiency. Though the dual path approach may yield two different system-level approaches, significant synergies are expected in the fundamental areas of internal combustion efficiency improvement.

Results

We continued to work with our fleet partners to analyze the operation of their fleets in more detail using Volvo's telematics platform as well as complete vehicle simulation tools. This work has strengthened the collaboration by combining the fleets' invaluable operational experience and Volvo's extensive big data capabilities for customer data analytics. This work allowed us to refine and finalize our technical requirement for the complete vehicle development, which was one of the key objectives for this fiscal year. It also represents the starting point for the technology payback analysis, which will ramp up in the coming reporting periods.

A 24-hour duty cycle was created using truck routes located near Volvo's engineering campus in Greensboro, which was used during multiple test campaigns with our research vehicle. The operational characteristics recorded during these tests were compared with telematics data from our fleet partners to ensure that our tests represent key performance figures from customer operation.

Simulation studies were performed to identify optimization opportunities as a result of downsizing the engine, along with multiple concept evaluations to decide on a microhybrid architecture. Both were completed on schedule, and work will now focus on selection of an energy management strategy.

Vehicle Configuration

All key vehicle parameters were frozen, including wheel base, fifth wheel location, king pin location, vehicle and trailer height, skirting, trailer gap, as well as position of many of the chassis components for a complete vehicle weight distribution that maximizes payload capacity. Weight distribution across all axles was verified using a mule vehicle built last year with the overall characteristics of the ST2 concept. The anticipated weight distribution was confirmed, which allowed the team to freeze the vehicle configuration along with final trailer configuration in early FY 2018.

A new driveshaft was installed on the mule vehicle, which was instrumented for on-track load data acquisition to support the frame design activities ongoing at Metalsa. A new axle was then retrofitted for on-road evaluation to support the supplier's development efforts. Overall frame design progress is on track to complete the final design before the start of FY 2019.

Powertrain System Development

Multiple concept and components studies have been progressing in parallel and are on track, with many achievements to date.

This fiscal year focused on assessing the cooling capacity of the proposed front-end concept and designing a complete cooling package that achieves heat rejection and aerodynamic drag performance targets. A low air-side pressure drop cooling system was analyzed, which enables a compact and lightweight cooling system design as well as a reduction of fan power consumption. Cooling simulations were completed, and detailed design for these components has begun.

A comprehensive system simulation study was performed to select a 48 V microhybrid architecture. A 48 V integrated starter generator connected to the rear gear train of the engine was chosen as the best concept for the freight efficiency demonstrator powertrain. This approach provides best tradeoff between fuel economy benefit and system cost, and it enables other advanced concepts including enhanced stop/start functionality.

A Penn State learning factory project in collaboration with Chalmers University designed a prototype electrified coolant pump system for ST2 during FY 2018. The project completed with a successful demonstration of a functional prototype proving that powertrain cooling needs can be met utilizing a cost-effective off-the-shelf 48 V motor in an industry standard frame size within a realistic packaging envelope.

A key tool in this work stream is a single-cylinder research engine at the University of Michigan, which provides test data for comparison with Volvo multi-cylinder engine tests, for validation of Volvo advanced engine models, as well as for piston design and combustion studies. In FY 2018, the team at University of Michigan completed the testing of four pistons with various thermal barrier coatings. Analysis of the results is

ongoing, and the findings will guide the next phase of tests. Work has also begun to update this research engine with a variable valve control system with independent authority over each valve. The system is installed and will be commissioned next reporting period.

Combustion system optimization testing has also begun to further optimize the wave piston design that was developed as part of SuperTruck 1. Work focuses on studying the impact of the wave shape, height, floor shape, and interaction with injector flow rate and umbrella angle. This testing will yield an improved fundamental understanding of the wave piston combustion system, with direct applications on ST2 engines.

The main objective of Oak Ridge National Laboratory's effort is to evaluate exhaust after-treatment system architectures, component formulations, and control strategies that would enable the ST2 engines to achieve applicable emission levels. The key challenge is that engines operating at high brake thermal efficiency will have low exhaust temperatures downstream of the final expansion, requiring after-treatment components optimized for low-temperature operation or placement of after-treatment components upstream of the final expander. Exhaust after-treatment system evaluations therefore require a synthetic exhaust flow reactor capable of operating at elevated pressures. For FY 2018 much of the work at Oak Ridge National Laboratory focused on commissioning a flow reactor system, which was modified during FY 2017 to handle higher pressures; see Figure V.1.3. Delays were encountered due to component failures, but Oak Ridge National Laboratory worked with the suppliers to resolve the issues before they could have an impact on the overall project schedule.



Figure V.1.3. Synthetic exhaust gas flow reactor rig at Oak Ridge National Laboratory (Volvo)

Aerodynamics

Simulation iterations continued at a good pace during FY 2018. The aerodynamic performance of the ST2 concept was evaluated as the design evolved for manufacturing feasibility. The latest design is on track to meet or exceed the aero drag reduction targets for the project. Recent design iterations focused on the front end of the vehicle in order to optimize the shape of the hood while maximizing heat rejection and incorporating styling characteristics.

A headlamp concept and supplier were selected, and development has begun with integrating the efficient headlamp design into the aerodynamic shape of the hood.

A final road test campaign was conducted in June 2018 to validate the latest changes to the trailer aerodynamic devices against the simulated improvements.

Advanced Lightweight Concepts

Metalsa kicked off the design phase, building on flexible roll forming, integration of components, new joining technologies, and the use of lightweight materials. The SuperTruck 2 chassis modeling team evaluated several concepts for stiffness and modal frequencies, focusing on rail and reinforcement thickness, cross member shape and placement in order to achieve a design that minimizes weight while meeting stiffness and frequency requirements. Modeling also progressed on the virtual truck used to generate baseline load scenarios and check modeling assumptions against data acquired on the mule truck.

In a collaborative effort with Virginia Technological Institute, Metalsa developed a fully parametric geometry generation tool that outputs designs complying with a set of flexible roll form manufacturing limits. This allowed design exploration through both traditional manual iterations as well as optimization-assisted methods.

Concept Trailer Development

The Wabash team continued its concept trailer development plan, which includes aerodynamics, light weighting, and connectivity. During FY 2018, the work focused on refining the geometry of commercially available aerodynamic devices through computational fluid dynamics simulations and road testing in order to match the performance of Volvo's SuperTruck 1 idealized trailer configuration. The optimization of a new boat tail was completed in complete vehicle simulations.

Wabash National modified the baseline trailer devices to match the designs optimized through computational fluid dynamics and provided a trailer, which was tested with the research vehicle in order to confirm the expected aerodynamic improvements. The team also designed and tested a lightweight sidewall panel, which was retrofitted onto the baseline trailer using structural adhesive bonding for the panel connection. The resultant weight saving was approximately 300 lbs while keeping the trailer material cost and performance durability nearly constant.

A new task was initiated to investigate an electro-mechanical wheel end concept that could provide power during operation or regenerate power during braking.

Low Rolling Resistance Tires

Michelin identified tire technologies that are combined by the project team in design events to deliver a 275/80R22.5 for the drive axle. The design optimization was carried out through computer simulations of tire models that predicted the tire endurance performance, rolling resistance, wear, and adherence. The optimization yielded the mold profile shape, tire components, and internal architecture. The tire mold has been delivered, and tires are scheduled to be delivered by the end of 2018.

Hotel Mode

Bergstrom, who joined the team during FY 2018, has performed a technology evaluation and created a development plan to deliver a heating, ventilation, and air conditioning (HVAC) concept that supports the overall freight efficiency objectives of the program.

An energy storage study was conducted to translate the data from tests and simulations into a set of system requirements as well as a battery cell chemistry recommendation. A vendor was selected, and the team kicked off the detailed design activities for a prototype system that will be delivered and installed on the demonstrator during next fiscal year.

Complete Vehicle Energy Management

The complete vehicle energy management system that was developed in SuperTruck 1 is the starting point for concept development in this project. Data collected during on-road testing in FY 2018 was used to calibrate our new energy management models, which the team used to initiate a series of simulations to define the final size and configuration of the new system consisting of HVAC, microhybrid components, energy storage, etc. Work is progressing on schedule to finalize the energy management strategy and start defining the software modifications, which will be required to control the new components integrated into the ST2 demonstrator.

Conclusions

- All objectives to date were met according to the original schedule and on budget.
- The research vehicle, formerly known as Volvo's SuperTruck 1, was deployed on multiple road tests before it was retired this year, a key milestone of this fiscal year.
- The cab design is frozen and aerodynamic optimization almost complete.
- Detailed design work was kicked off for multiple key components, including the energy storage system, the lightweight frame, the low-pressure drop cooling system, and the advanced HVAC system.
- Tire optimization work has already delivered mold profile shape, tire components, and internal architecture for the drive tires.

V.2 Cummins/Peterbilt SuperTruck II (Cummins Inc.)

Michael Ruth, Principal Investigator

Cummins Inc.
P.O. Box 3005
Columbus, IN 47201-3005
E-mail: michael.j.ruth@cummins.com

Ken Howden, DOE Technology Development Manager

U.S. Department of Energy
E-mail: Ken.Howden@ee.doe.gov

Start Date: October 1, 2017	End Date: September 30, 2021	
Project Funding: \$9,500,000	DOE share: \$4,700,000	Non-DOE share: \$4,800,000

Project Introduction

The trucking industry is faced with numerous challenges to reduce petroleum consumption while meeting stringent criteria emissions regulations and providing customer value. The United States has approximately 3.5 million Class 8 vehicles on the road, consuming 4.5 million barrels of petroleum per day. If only half of the fleet implemented half of the benefits proposed, at \$3.85/gal, the nation would see a fuel savings over \$30 billion annually and reduce petroleum consumption by over 0.5 million barrels per day. This reduction would have a positive impact on the environment by eliminating 200,000 metric tons of CO₂ per day.

The Cummins-led SuperTruck II project goals are to design, develop, and demonstrate a very-high-efficiency engine that is optimized around the drive cycle that will yield a very high increase in vehicle freight efficiency. The baseline for comparison will remain the 2009 vehicle, where the demonstration will be done with similar vehicle specifications. The engine will maintain compliance with the current heavy-duty diesel emission regulation for line haul vehicles, while the vehicle system will remain compliant with the current greenhouse gas regulatory requirements.

Objectives

- Demonstrate a *minimum* of 55% brake thermal efficiency (BTE) using 65 mph cruise conditions on an engine dynamometer test
- Utilize the same engine system demonstrated on the dynamometer in a vehicle and operating on real-world drive cycles
- Achieve a *minimum* of 125% freight ton efficiency (FTE) over a relevant drive cycle (FTE = miles per gallon [mpg] x tons of freight)
- Track, promote, and report on cost-effective solutions, prioritizing solutions that have an approximate three-year payback period utilizing a relevant customer counsel for understanding customer acceptance and expectations

Approach

The approach for meeting the 55% BTE target is via careful dissection of the diesel cycle and reduction of losses via waste heat recovery (WHR). The engine will be tuned to take advantage of ideal conditions for the aftertreatment effectiveness, therefore reducing the inefficiency of the exhaust gas recirculation (EGR) injection timing systems. The closed cycle efficiency will be optimized for high expansion ratio via rapid heat release and insulated surfaces. The open cycle will be optimized by using low-pressure EGR, ideal valve events, and a fixed-geometry turbocharger with the ultimate in tip clearance and efficiency. The mechanical efficiency of the engine system will be developed to use low-viscosity oil with variable lube and cooling pumps, all while running the engine at a low enough speed to minimize spin and pumping losses. The WHR

system will be a two-loop system harvesting both low-quality heat from the coolant and charge cooler and high-quality heat from the EGR coolers and tailpipe boiler. The WHR system will be the primary cooling system for the engine under the cruise operating conditions and only require a small radiator for sustained high-load conditions.

The powertrain will integrate the WHR and an energy recovery system (motor/generator) onto the Eaton automated transmission for compactness and efficiency reasons. During flat-road and uphill operations, this system can input power to the system to reduce fuel consumption. As the vehicle operates downhill, the engine can be decoupled from the powertrain, leaving the controls to apply power from the WHR system as needed and/or to recover energy from the system through the motor/generator, to be stored in an onboard battery.

The vehicle will achieve the high FTE with the combination of low motive resistance and light weighting. Bridgestone will be supplying tires that can meet customer requirements for longevity yet reduce rolling resistance well beyond the current commercially available tires via compound development and siping design. The vehicle structure will include a new weight-saving, composite design that will incorporate a kneeling suspension that will aid in the reduction of aerodynamic load. The vehicle design will incorporate aerodynamic features to improve drag in all wind conditions via moving surfaces that react to changing winds detected by the onboard Lidar system. Finally, the drive axle will incorporate an advanced control system that will ensure good low-speed traction with state-of-the-art low-parasitic, high-speed operation.

Results

The following lists the key accomplishments for Fiscal Year 2018. The accomplishments listed below are fundamental steps required to complete the objectives of the project.

The team has:

- Completed design and procurement of the CERD, a transmission-coupled motor/generator with provisions for a WHR turbine connection for future system coupling.
- Completed testing of the CERD in a powertrain test cell.
- Demonstrated a base engine performance of 49% BTE on a new engine platform.
- Completed build of a mule vehicle to be used for powertrain technology development.
- Completed layout and design of a comprehensive WHR system.
- Completed build of mule tires that represents approximately 50% of the goal for rolling resistance improvement over the 2009 baseline.

The powertrain design will include a mild hybrid system that couples an electric motor to the transmission power take-off shaft. A re-designed rear transmission housing will integrate the CERD internal hardware for a more structurally robust design, while the two-stage parallel axis gear train and belt drive will enable combined operation of the WHR turbine and motor generator at peak efficiency. The initial system will only include the electric motor.

The internal gear train is designed for high efficiency at high speeds, minimized transmission control complication, and optimized inertia. The bearings required to support the gear train will provide a balance between durability and low power loss. A normally closed multi-plate wet clutch is intended to reduce power consumption in the open state.

The hybrid system was tested for the first time at the powertrain test cell at Oak Ridge National Laboratory. This testing brings together new hardware and software, which had only been verified for functionality separately. The testing had three main objectives: to (1) verify mechanical functionality of the integrated CERD hybrid powertrain; (2) verify supervisory controls against system requirements, while validating new transmission integration and interface; and (3) provide data for comparison and validation of the detailed and simple controls simulation environments.

The conventional, non-hybrid powertrain was exercised through several relevant routes to establish baseline behaviors. The powertrain was also run through the cycle average mapping tests as part of the test methods for greenhouse gas regulations. Following the baseline, the CERD system was installed.

In a testament to the power of detailed preparation using simulation on the supervisory and transmission controls, initial testing of the hybrid powertrain successfully completed vehicle launch, gear shifts, hybrid propulsion, hybrid regeneration, state of charge balancing, generator mode, and other base vehicle functionalities without software changes other than minor interface corrections. With each passing test, the power envelope of the motor/generator was also increased (reduced safeguarding). To date, learnings from the powertrain testing have been tremendous. Critical calibrations have been fine-tuned for better performance of the system. As well, software interface bugs were identified and fixed. The test cell testing also revealed a couple of issues with new electronic hardware that are being investigated and corrected.

Cummins is utilizing a new platform engine for the SuperTruck II project. The engine design is substantially shorter than the previous, production engine, accommodating improved aerodynamic design of the vehicle. As well the engine is more than 300 lbs lighter, contributing to the freight efficiency. The best demonstrated performance at cruise condition to date has been 49% BTE. Technologies included in this demonstration included high-compression-ratio, high-heat-release-rate combustion system; insulated exhaust manifold; reduced-clearance compressor and turbine; and a variable-flow oil pump. Cummins has a goal to reach 50% BTE without the use of WHR and low-pressure EGR by the conclusion of 2018. Several technologies have yet to be employed in this effort.

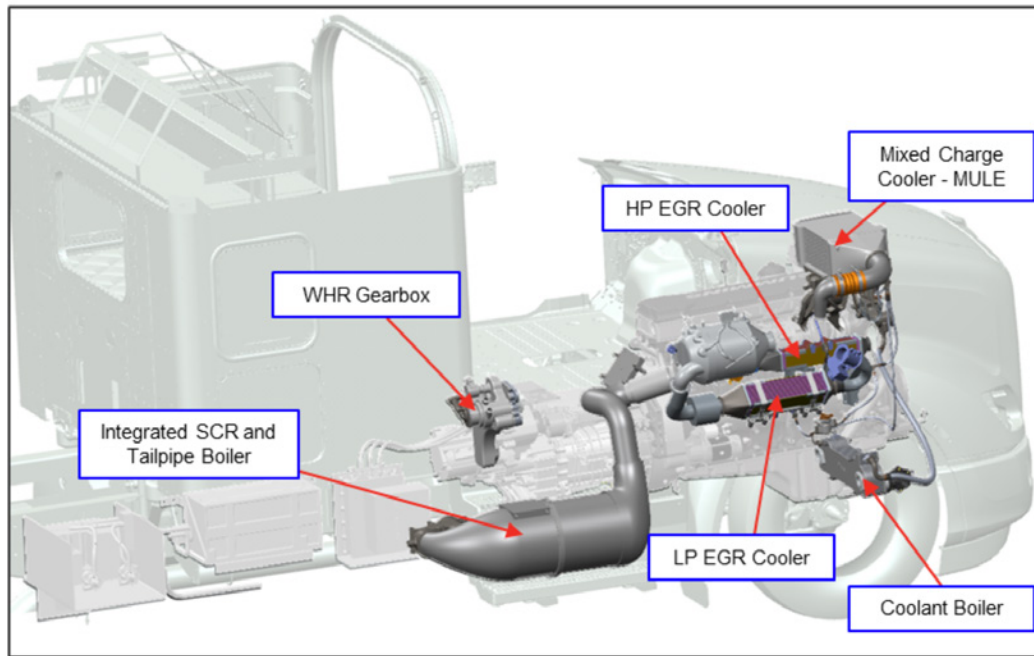
The mule vehicle build, initially planned for June 2018, was delayed due to availability of chassis system parts. The long lead time is the result of the unique design of the hybrid aluminum/steel chassis, which facilitates a strong and lightweight chassis system but required significant tooling and processing.

Once out of the production sequence, the engineering team has fit prototype parts which include (1) chassis height control hardware and plumbing, (2) full camera systems (virtual mirrors), (3) electric power steer assist, (4) solar panel battery charger, and (5) tandem axle disconnect controls. Upon completion of engineering shake-down and troubleshooting, the truck will undergo a series of evaluations to assess the ride quality of the lightweight chassis, functionality of the chassis ride height adjustment, and interactions associated with the disconnect tandems (6x4 to 6x2). It is expected to take three to four weeks to gain a representative sample size of drivers into the truck while making corrections and/or adjustments as data is obtained.

Following completion of the engineering evaluations, the truck will be transported to Bendix (Elyria, Ohio) for several weeks of brake stability/control system calibration. Finally, the vehicle will be sent to Cummins Technical Center for use as the powertrain development mule.

At Cummins the mule will receive several hardware updates. Mule 2.0 will be the result of the up-fit of the mild hybrid CERD and the associated cooling package. Following the up-fit, the truck will be used to develop control algorithms for the Advanced Cycle Efficiency Manager, a vital enabler of the demonstrator vehicle path to target.

The Cummins and Peterbilt design teams have integrated the WHR system to fit the application given the limitations of both the mule and demonstrator vehicle. As a system, the WHR consists of heat exchangers, pumps, turbine, and control valves and sensors. Figure V.2.1 highlights the complexity of the system and its fit into the mule vehicle. The system has been designed to initially be applied without a power turbine. The application will be fitted with an orifice in place of the turbine in order to test the least complex arrangement and allow engineers to balance heat and flow prior to the addition of the turbine and CERD controls for the turbine. The turbine and turbine gear box will be added to the transmission assembly, where the turbine power will be transferred to the powertrain via a belt drive that powers the power take-off shaft (CERD).



SCR – selective catalytic reduction; HP – high pressure; LP – low pressure

Figure V.2.1. Mule vehicle WHR system integration. This system will be applied in stages in late 2019, finishing in 2020.

Steer, drive, and trailer tires were delivered to Peterbilt for the mule truck build. The level of technology for these tires represents approximately 50% of the Bridgestone goal for rolling resistance improvement over the 2009 baseline.

An area of primary focus in the tire development has been the evaluation of different mixer technologies. The intent of the new mixer technology is that it is expected to yield improved rolling resistance versus wear balance. The team has also been working to incorporate silica into the tread compound. This path also facilitates maintaining desired wear characteristics while reducing rolling resistance. In 2017, multiple rounds of mixing were completed. Results from an initial wear test were received and analyzed in January. The data shows the new mix technologies under evaluation will allow the team to effectively manage the wear tradeoff associated with the new silica technology. This technology was utilized in the mule vehicle tire build.

Conclusions

The Cummins-led SuperTruck II team has completed the second year of the planned five-year project. In the first two years, the team has concluded many goals and set the direction for the remainder of the project. The following bullet list summarizes those conclusions.

- The mild hybrid system design and preparation (simulation and bench component testing) has led to a successful demonstration of the concept in a powertrain test environment.
- The original path to target for the 50% engine BTE has proven accurate on an individual technology basis. Work continues to be able to realize the technology benefits when built into one system.
- The new engine platform chosen to demonstrate the high BTE performance has proven to be beneficial from a capability standpoint.
- Input from the customer (Walmart) on tire wear concerns is being acted upon to ensure the benefits of reduced rolling resistance are not lost in wear.

- Data from nearly 275,000 mi of Walmart routes out of three distribution centers have shown the average highway Walmart route looks very similar to the Denton, Maryland–Vernon, Texas round trip, which also looks very similar to the overall U.S. highway system from a distance-grade perspective.
- Analysis shows a diminishing return as the capacity of the motor/generator is larger than 30 kW.
- Analysis indicates an energy storage system greater than ~3 kWh would yield no benefit.
- Target compression ratio for future development will be centered on 22:1.
- Charge-to-fuel ratio for future development will be targeted at greater than 34:1 but not greater than 39:1.
- Increases in injection rate in testing have defined the limit in burn rate as the increasing slope and peak have shown max values even as injection rate is increased, indicating other parameters in the combustion chamber must be explored in order to increase the burn rate.
- Tire effect of compound on wear and rolling resistance can have a profound impact on customer tire acceptance. Feedback from Walmart has indicated tire life, including rebuilds, must be considered in total lifecycle costing models.

Key Publications

1. DOE quarterly progress report, Q1 – January 30, 2017
2. DOE quarterly progress report, Q2 – April 30, 2017
3. 2017 Annual Merit Review – June 8, 2017
4. DOE quarterly progress report, Q3 – July 30, 2017
5. DOE quarterly progress report, Q4 – October 30, 2017
6. DOE quarterly progress report, Q5 – January 30, 2018
7. DOE quarterly progress report, Q6 – April 30, 2018
8. 2018 Annual Merit Review – June 21, 2018
9. DOE quarterly progress report, Q7 – July 30, 2018
10. DOE quarterly progress report, Q8 – October 30, 2018

Acknowledgements

Ken Damon (Peterbilt), Nicole Downing (Eaton), Reubin Close (Bridgestone), Ralph Nine (National Energy Technology Laboratory Program Manager)

V.3 Development and Demonstration of a Fuel-Efficient Class 8 Tractor and Trailer SuperTruck (Navistar, Inc.)

Russell Zukouski, Principal Investigator

Navistar, Inc.
2701 Navistar Drive
Lisle, IL 60531
E-mail: russ.zukouski@navistar.com

Ken Howden, DOE Technology Development Manager

U.S. Department of Energy
E-mail: Ken.Howden@ee.doe.gov

Start Date: October 1, 2016	End Date: November 1, 2021	
Project Funding: \$55,595,000	DOE share: \$20,000,000	Non-DOE share: \$35,595,000

Project Introduction

The objective of the SuperTruck 2 engine project is to research, develop, and demonstrate a heavy-duty engine that can meet 2010 federal emissions standards and can achieve 55% brake thermal efficiency (BTE) demonstrated in an operational engine at a 65-mph cruise point on a dynamometer. In addition, the technologies applied to this engine should be commercially cost effective.

Objectives

Overall Objectives

- Attain greater than or equal to 55% BTE demonstrated in an operational engine at a 65-mph cruise point on a dynamometer
- Develop engine technologies that are commercially cost effective
- Contribute to greater than 100% improvement in vehicle freight efficiency relative to a 2009 baseline

Fiscal Year 2018 Objectives

- Evaluate cylinder deactivation technology to achieve elevated exhaust temperatures efficiently
- Improve air system efficiency for SuperTruck 2 engines
- Investigate novel fuel system configuration to increase combustion burn rates
- Identify organic Rankine cycle (ORC) waste heat recovery system that contributes to achieving 55% BTE
- Evaluate new technologies for engine thermal management
- Continue gasoline compression ignition investigation at Argonne National Laboratory

Approach

The work will include component and system-level consideration of base engine architecture, air system, combustion and fuel system, advanced aftertreatment, thermal management, and waste heat recovery. It will involve analysis, development, testing, and down-selection of individual and system-level engine technologies as well as integration of the final selected technologies into a prototype engine.

Results

Cylinder Deactivation

A cylinder deactivation system was installed on an engine for evaluation. During the deactivation of a cylinder, the opening of its intake and exhaust valves was disabled, and the fuel injection was turned off. The remaining active cylinders had to work harder to maintain the power, resulting in an increase of exhaust temperature. In addition to the increase of exhaust temperatures, test results showed improvements in brake specific fuel consumption (BSFC) at very light loads with three cylinders deactivated (3 CDA); however, such BSFC improvement decreased and became negative as the load increased over a threshold (Figure V.3.1a). A GT-Power simulation was employed to understand the root cause to this phenomenon. The simulation was able to reproduce the crossover behavior (Figure V.3.1b). The simulation showed that, due to the increase in fueling among the active cylinders, the air-fuel ratio (AFR) was reduced as compared to the baseline. The reduction in AFR resulted in an increase in cylinder temperature. The thermal efficiency increased with the increase in cylinder temperature; so did the cylinder heat rejection. The simulation indicated that BSFC improvement became negative when the increase in heat rejection outpaced the gain in thermal efficiency due to the reduction in AFR (Figure V.3.1c).

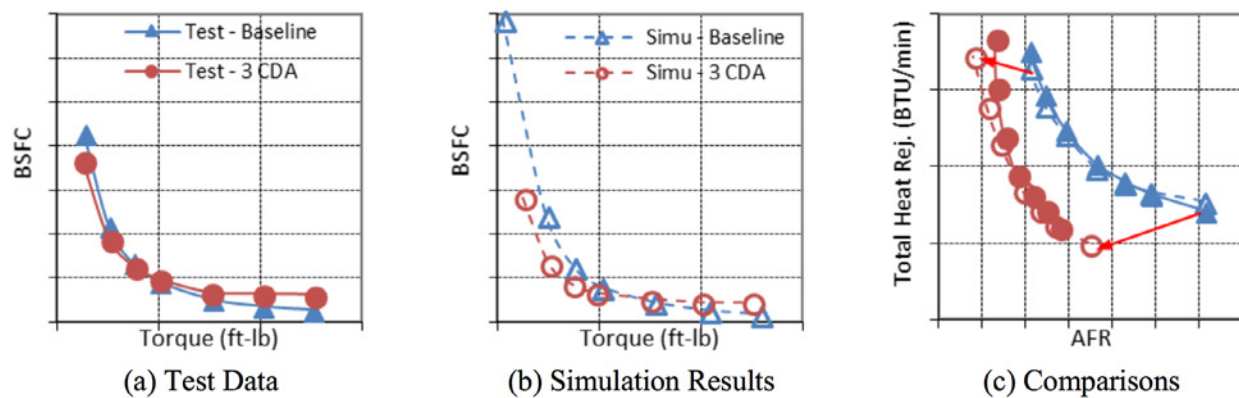


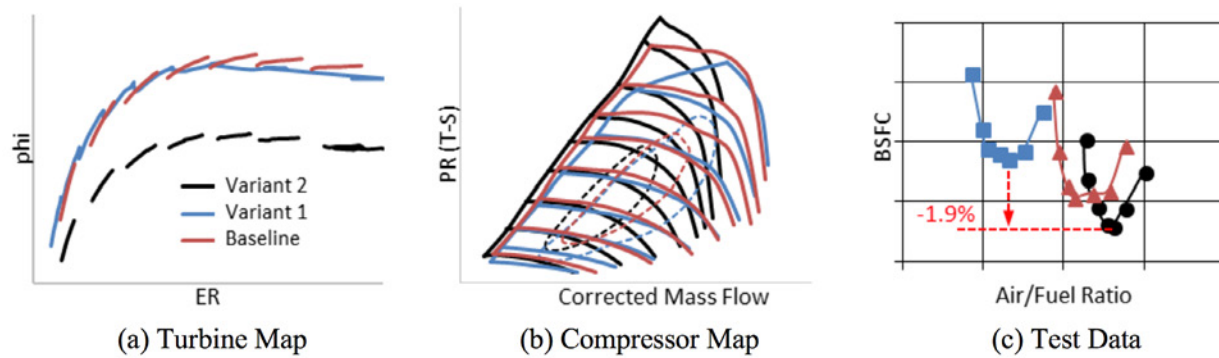
Figure V.3.1. Effects of cylinder deactivation on BSFC

The engine calibration and control implementation for cylinder deactivation were optimized and completed. An analysis was carried out to project the impact of cylinder deactivation on the fuel economy at three different vehicle operating conditions: (1) bobtail city cycle, (2) loaded city cycle, and (3) Illinois flatland cycle. The analysis showed that the city cycle fuel economy improved between 1% and 1.5% with cylinder deactivation, while the Illinois flatland fuel economy was neutral or slightly improved.

Air System

Two variants of high-efficiency turbocharger were procured and evaluated. Figure V.3.2 depicts the comparison of turbine and compressor maps of these two variants with the baseline. All three turbochargers could deliver combined efficiency greater than 60%, with Variant 2 being the highest. The best BSFC is associated with the turbocharger providing the highest combined efficiency. These results were shared with the supplier for optimization of the original HET turbocharger in SuperTruck 1. A plus version was designed and assembled for testing the next fiscal year. The wastegate was eliminated from this new HET Plus turbocharger.

Furthermore, it is necessary to more fully utilize the exhaust pulse energy to improve turbine efficiency, especially at low engine speed regimes. As an initial attempt to gauge the sensitivity, a prototype exhaust manifold was fabricated with 4130/4140 steel. This fabricated manifold has approximately 30% reduction in volume from the baseline manifold. The preliminary testing shows a slight increase in the pumping mean effective pressure, thus, higher BSFC. Further testing is planned for exhaust pulse energy optimization, including the casting of a larger-volume exhaust manifold.



ER – expansion ratio (turbine); PR – pressure ratio (compressor)

Figure V.3.2. Turbocharger optimization

Combustion System

Navistar continued to investigate the opportunities of reducing the combustion duration for thermal efficiency improvement. The focus has been on the advanced fuel injection configurations with three-dimensional model simulation. The boundary conditions for this model were based on the 50% BTE data from the SuperTruck 1 program. The simulation was carried out using software from Convergent Science. The key parameters of the fuel injection configurations include number of holes and nozzle flow rates. Figure V.3.3 shows the comparisons of indicated specific fuel consumption (ISFC) of various fuel injection configurations with the baseline. These results were communicated with Bosch to identify feasible configurations for procurement and testing.

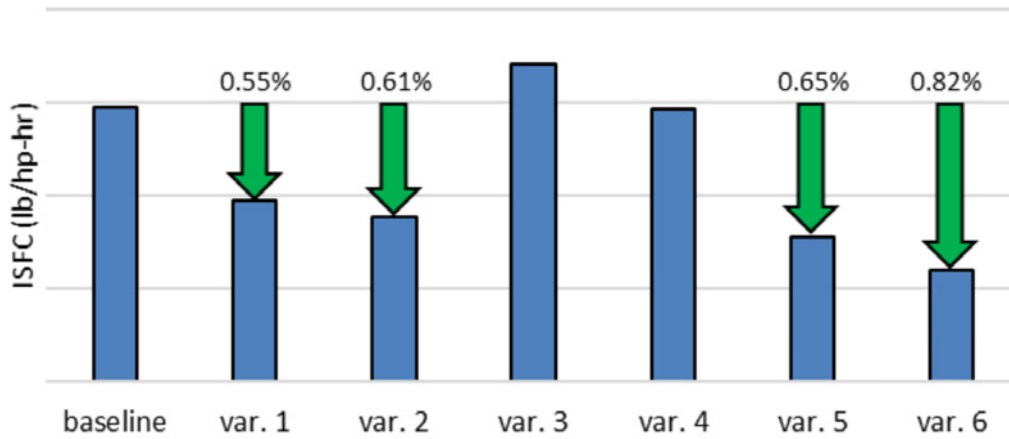


Figure V.3.3. Advanced fuel injection strategy simulation

Waste Heat Recovery–ORC

To achieve 55% BTE, waste heat recovery plays a critical role. Navistar has selected ORC technologies as the prime path for waste heat recovery. To maximize ORC system efficiency, energy recovery from all available waste heat was considered. Based on the temperature characteristics of the heat sources, the ORC system was divided into high-temperature (HT) and low-temperature (LT) loops. After analyzing many possible configurations, an intent ORC system was selected (Figure V.3.4). In addition, five working fluids were simulated, and a candidate was identified.

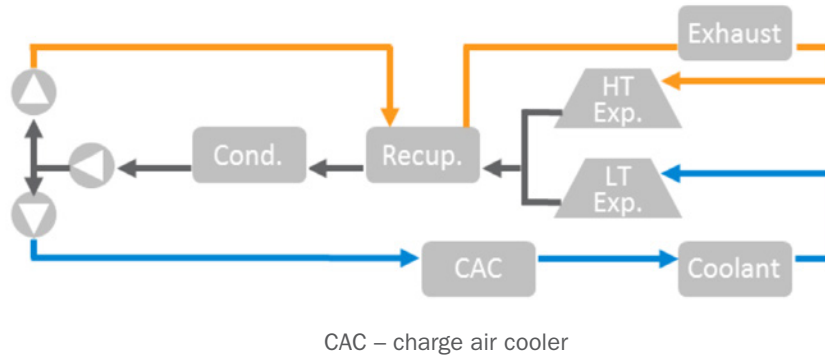


Figure V.3.4. Schematic of intent ORC system

Moreover, an analysis was carried out to project the impact of system variants on freight efficiency. The weight of the SuperTruck 1 vehicle ORC system, which represented one of the system variants, an HT loop ORC system, was used as a base input. The analysis showed that the loss of freight efficiency due to added weight is significantly more than the BSFC improvement from the HT loop ORC system. Such loss-to-improvement ratio is basically the same even if a dual loop ORC system is implemented for the vehicle. This is a significant challenge to be overcome in the future.

Thermal Management

The energy balance analysis had shown a significant amount of heat rejection to engine coolant. A low-heat-transfer liner was procured and investigated to minimize the heat loss to coolant. The investigation was done with an external oil cooler platform. The oil cooler was cooled with processed water to control the oil temperature. The testing was carried out such that the engine coolant flow was progressively decreased, and the system response was monitored at selected engine modes. The results showed that block heat rejection was reduced as expected. However, an increase of oil heat rejection was observed. As a result, the BSFC remains similar between the baseline and the low-heat-transfer liner.

Thereafter, a new high-temperature piston was designed and provided by a supplier. This new piston allowed its combustion bowl surface temperature to be elevated up to 100°C higher than the baseline piston. The new piston was installed on an engine. The test data showed that the high-temperature piston resulted in higher exhaust temperature but worse BSFC. Further investigation with simulation is needed to understand the root cause. In addition, testing was performed with variation of oil temperatures. The test results showed that an increase of 100°F oil temperature would result in approximately 1% BTE gain (Figure V.3.5). However, the slope appeared to be the same for both high-temperature and baseline pistons. In additional testing, two sizes of oil jet were evaluated for the high-temperature piston: the baseline jet and a reduced-diameter jet. The results showed that the reduction in oil jet flow had very little impact on the BTE or any other energy components. Note that the oil pump remained the same, and the smaller oil jet diameter resulted in an increase of oil pressure.

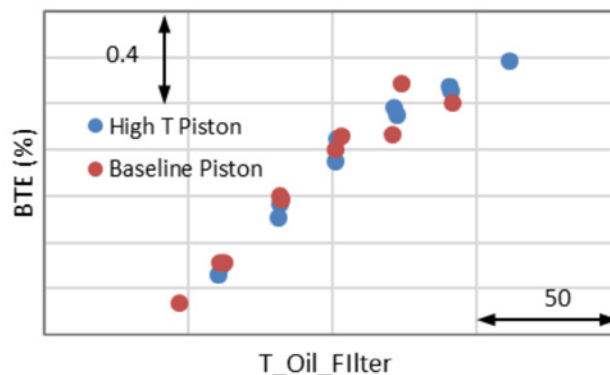


Figure V.3.5. Effects of oil temperature on BTE of high-temperature and baseline pistons

Gasoline Compression Ignition at Argonne National Laboratory

Gasoline compression ignition is a combination of two advanced combustion strategies: partial fuel stratification and partially premixed combustion. A key factor of gasoline compression ignition is to increase the premixed combustion portion. Two fuel injection strategies could be used to increase the portion of premixed combustion: early/late pilot injection and port fuel injection (PFI)/direct injection (DI) strategy. The gasoline fuels selected for investigation were Environmental Protection Agency Tier II certification gasoline (EEE) and E85 gasoline, which was blended in-house with 85 vol% dry ethanol and 15 vol% EEE. A lubricity improver was blended into the gasoline fuels to protect the high-pressure diesel injection system. Testing showed that E85 performed best with the PFI/DI strategy, while the EEE worked better with the pilot injection strategy. To increase early pilot injection without wetting the liner wall, a new injector with narrower spray angle than the baseline injector was investigated. This new injector has larger nozzle hole diameter due to the reduced number of holes, but the overall nozzle flow remains the same as the baseline injector. Injection pressure was swept with the new injector for all three fuels. BTE was not significantly affected during the injection pressure sweep due to the trade-off between shortened combustion duration and increased friction loss, due to increase of injection pressures.

Figure V.3.6 depicts the efficiency breakdown and loss comparison of peak BTE condition for all three fuels: regular diesel combustion, EEE with late pilot injection, and E85 with PFI/DI strategy. E85 PFI/DI strategy exhibited the highest BTE among the three fuels investigated. Diesel and EEE showed a comparable efficiency, which was similar to the findings with the baseline injector. Overall, the new injectors exhibited 0.4%–0.7% reduction in BTE for all fuels investigated, attributed to the deteriorated mixing process.

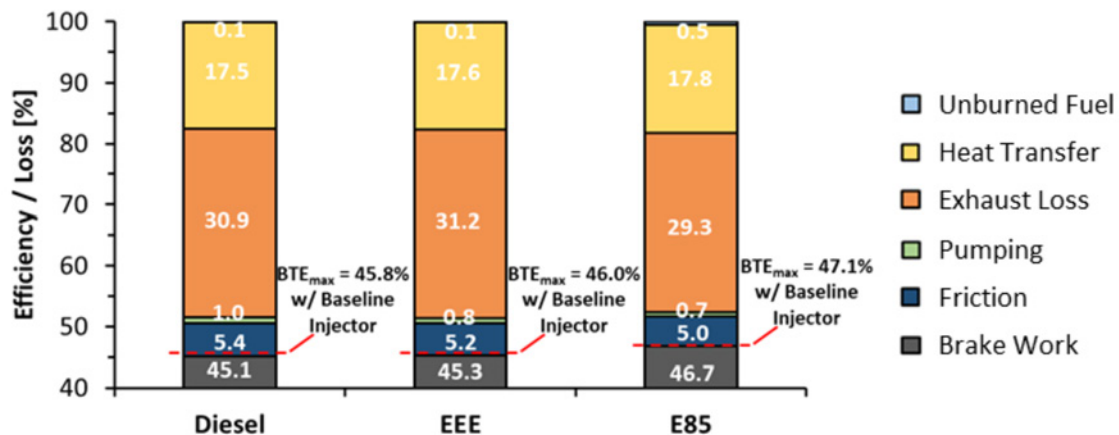


Figure V.3.6. Efficiency breakdown and loss comparison at peak BTE for diesel, EEE, and E85 with a new injector

Conclusions

- A cylinder deactivation system was evaluated on a dyno. Testing showed increase of exhaust temperatures and improvement of BSFC at very light loads. Analysis showed 1%–1.5% fuel economy improvement in the city cycle but neutral fuel economy in the Illinois flatland. The engine was calibrated, and controls were implemented. The system is ready for vehicle testing.
- Improvement/optimization work for both air system and combustion system were continued throughout this fiscal year. BSFC continued to improve with the increase of turbocharger combined efficiency. An advanced fuel injection configuration, which delivered the most ISFC reduction, was identified via three-dimensional simulation.
- Analysis of the ORC system and its working fluid for 55% BTE engine dyno demonstration was completed. The final system comprised both HT and LT loops. In addition, the impact of ORC system weight on vehicle freight efficiency was evaluated. The weight had a significantly negative impact on vehicle freight efficiency, much more than the BSFC improvement.

- Two new power cylinder components, low-heat-transfer liner and high-temperature piston, were evaluated to reduce the in-cylinder heat rejection. An increase of exhaust temperatures was observed; however, no BTE gain was measured.
- Gasoline compression ignition investigation continued at Argonne National Laboratory. Injection strategies were optimized for different gasoline fuels. E85 gasoline with PFI/DI strategy delivered the best BTE.

Key Publications

1. Rajkumar, M., R. Vojtech, and J. Cigler. 2018. "Effect of Thermal Management on Engine Performance." SAE Technical Paper 2018-01-0224.
2. Vojtech, R. 2018. "Advanced Combustion for Improved Thermal Efficiency in an Advanced On-Road Heavy Duty Diesel Engine." SAE Technical Paper 2018-01-0237.
3. Wang, B., M. Pamminger, R. Vojtech, and T. Wallner. 2018. "Impact of Injection Strategies on Combustion Characteristics, Efficiency and Emissions of Gasoline Compression Ignition Operation in a Heavy-Duty Multi-Cylinder Engine." *International Journal of Engine Research* 1–15, doi:10.1177/1468087418801660.
4. Wang, B., M. Pamminger, and T. Wallner. 2018. "Effects of Port Fuel and Direct Injection Strategies and Intake Conditions on Gasoline Compression Ignition Operation." *Proceedings of the ASME 2018 Internal Combustion Fall Technical Conference*, ICEF2018-9723.
5. Pamminger, M., B. Wang, C. Hall, R. Vojtech, and T. Wallner. "The Impact of Water Injection and EGR on Combustion and Emissions in a Heavy-Duty Compression-Ignition Engine Operated on Diesel and Gasoline." *International Journal of Engine Research*, under review.

V.4 Improving Transportation Efficiency through Integrated Vehicle, Engine, and Powertrain Research – SuperTruck 2 (Daimler Trucks North America)

Justin Yee, Principal Investigator

Daimler Trucks North America
 4555 N Channel Ave.
 Portland, OR 97217
 E-mail: Justin.Yee@daimler.com

Ken Howden, DOE Technology Development Manager

U.S. Department of Energy
 E-mail: Ken.Howden@ee.doe.gov

Start Date: January 1, 2017	End Date: January 1, 2022	
Project Funding: \$40,000,000	DOE share: \$20,000,000	Non-DOE share: \$20,000,000

Project Introduction

The objective of the SuperTruck 2 (ST2) project is to develop and demonstrate a greater than 100% improvement in overall freight efficiency on a heavy-duty Class 8 tractor-trailer measured in ton-miles per gallon. In addition, the project team will design and demonstrate an engine capable of achieving 55% brake thermal efficiency (BTE). Daimler Trucks North America will achieve these targets through the application of several advanced vehicle system technologies and advanced engine technologies.

The ST2 project is broken into five phases (see Figure V.4.1), of which the project is coming towards the end of Phase 2. The first half of this phase has focused on the overall vehicle architecture, running simulations, and developing the conceptual system design. The second half of this phase has been the detailed design work, defining the computer-aided design surfaces, laying out of components, and defining the control algorithms. At the end of Phase 2, the team is releasing computer-aided design models, drawings, and software to build the first integration truck, called A-Sample. The donor vehicle has already been built and delivered, and the project team will begin modifications in the fourth quarter of 2018.

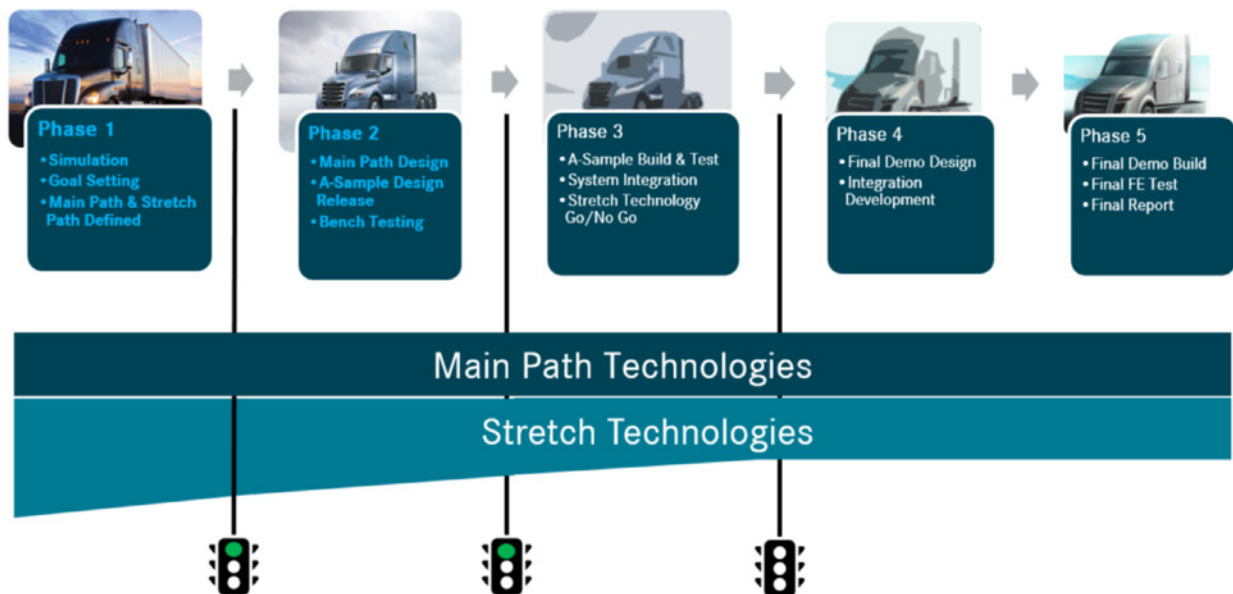


Figure V.4.1. Phases of SuperTruck 2 project

Objectives

Overall Objectives

There are two main objectives for the ST2 project.

- The first objective is to meet or exceed the vehicle freight efficiency target for the ST2 project, specified as 100% freight efficiency improvement over a baseline vehicle (same vehicle as used in SuperTruck 1, a 2009 Cascadia). Daimler Trucks North America has specified that they will exceed the target with a vehicle that demonstrates 115% freight efficiency.
- The second objective that must be met is to demonstrate, in a test cell, a running technology engine that meets or exceeds a 55% BTE rating.

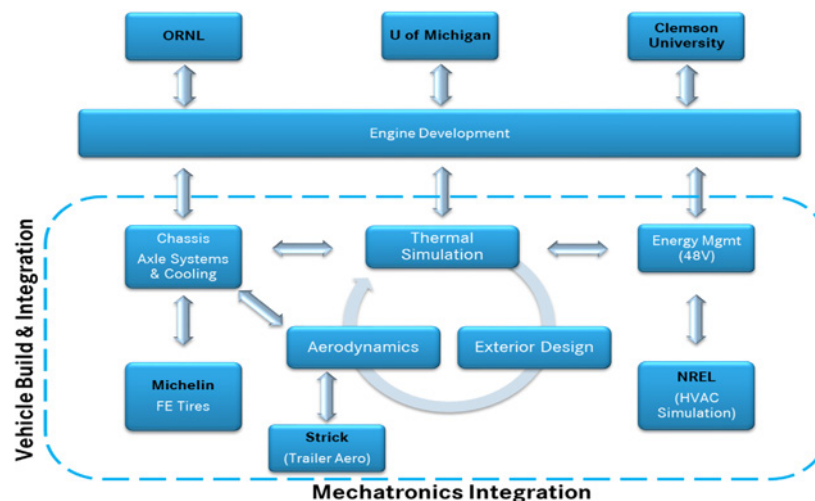
Fiscal Year 2018 Objectives

- Selection and scope of work defined for each of the work stream areas
- Simulation of multiple concepts for the engine, vehicle cooling, and aerodynamics performed
- Design engineering for A-Sample (75% complete), long-lead-time items released for prototype build
- A-Sample build schedule solidified and identified resources moved into the project
- First program audit completed and action items to remain compliant completed
- Agreement on the final ST2 validation testing cycle achieved

Approach

In Phase 2 of the ST2 project, individual system simulations were used to define the fuel consumption reduction benefits of each of the different work streams. Computational fluid dynamics was used to research multiple areas of the vehicle, thermal simulation was used to determine the architecture of the cooling system, and Matlab Simulink was used to define the 48-V power net design.

In order to achieve system-level improvements in the four topics of aerodynamics, exterior design, cooling, and 48-V power net design, we had to create a new collaboration model. The different work streams needed to work together to create a more optimized design; this new methodology and the interface to the engine development are shown in Figure V.4.2. Collaboration with the two federally funded national laboratories, Oak Ridge National Laboratory (ORNL) and National Renewable Energy Laboratory (NREL), as shown in Figure V.4.2, was also important to solve some of the system issues using thermal simulation.



HVAC – heating, ventilation, and air conditioning; FE – fuel efficient

Figure V.4.2. ST2 collaboration model

Investigation of the aerodynamic trade-off of split cooling was performed. The increase in aero drag has been accounted for in the end fuel efficiency number reported in Figure V.4.5. It is important to know the trade-offs between competing technologies.

A digital mock-up became the driving vehicle towards space claim and component packaging. Before the designs could be released, all components were modelled and checked for interference in the digital mock-up. One of the results of packaging space was having to move the 48-V belt recuperation motor to the right-hand side (cold side) of the engine. This change could have side benefits for the belt recuperation motor in that it will run cooler and have an improvement on bearing life.

With the focus of ST2 on the long-haul vehicle, we re-examined the test routes of SuperTruck 1. The city route only accounted for 2% of the freight efficiency, and with SuperTruck 2 not having a large high-voltage hybrid system, it was proposed and accepted by DOE that we will remove the city route in the test cycle. The end result is shown in Figure V.4.3, with the two driving routes covering 14 hours of the 24-hour cycle.

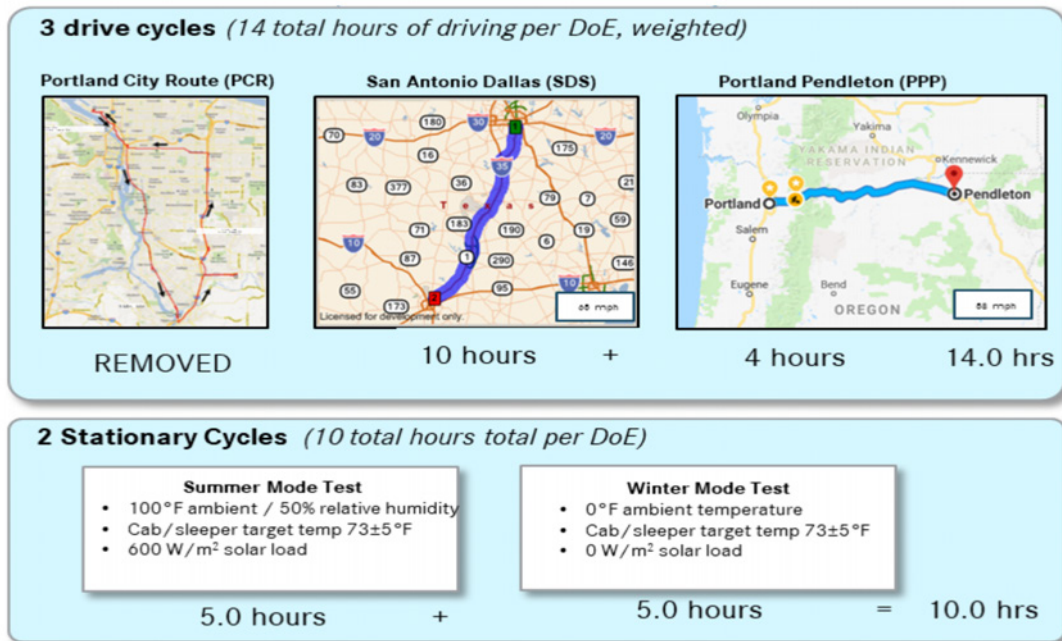


Figure V.4.3. ST2 updated validation methodology

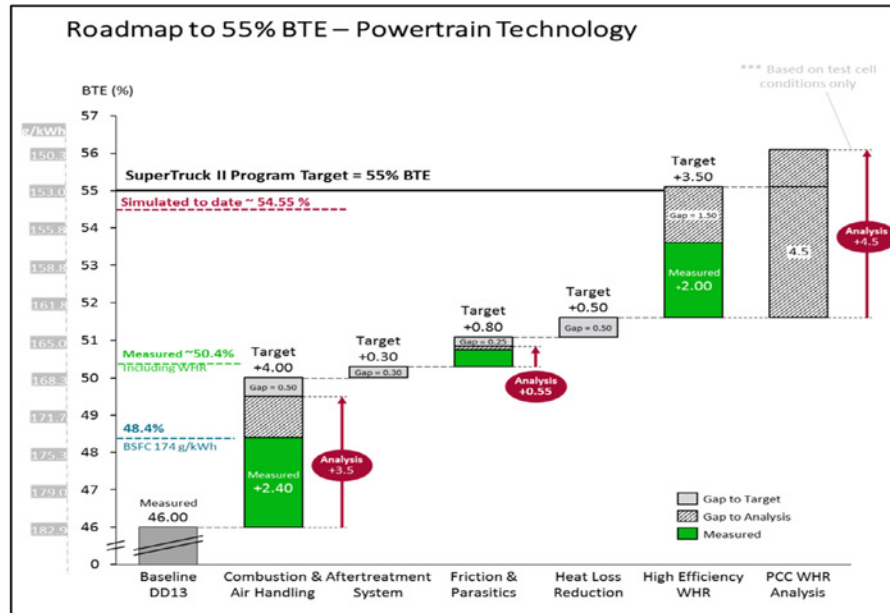
Results

The engine roadmap developed and refined during Year 1 of the project (see Figure V.4.4) shows the pathway towards 55% BTE and the five main technical areas under focus. Year 2 of the project (the current reporting period) led to:

- Further analysis (both one-dimensional and computational fluid dynamics) of several engine systems, including the combustion system, air system, engine friction, and in-cylinder heat loss.
- Technical roadmap refinement.
- Procurement initiation of key engine, transmission, and rear axle components.
- Experimental evaluation of engine and aftertreatment systems in the Detroit test cell.
- Build-up of a ST2 Detroit tinker truck to enable the evaluation of powertrain-specific fuel efficiency measures and their direct impact on over-the-road fuel economy.

- Continued development of predictive engine and aftertreatment system control algorithms, which have shown the potential for measurably improving engine thermal management.

In addition to the high BTE performance engine, a more reliable and less risky variant is being tested for fuel efficiency performance. It improves the torque performance of the existing DD15 (Detroit 15-L diesel engine) to allow for down-speeding but does not require split cooling; hence, it could be a lower-cost alternative. This variant will run on the Portland-Pendleton route for evaluation.



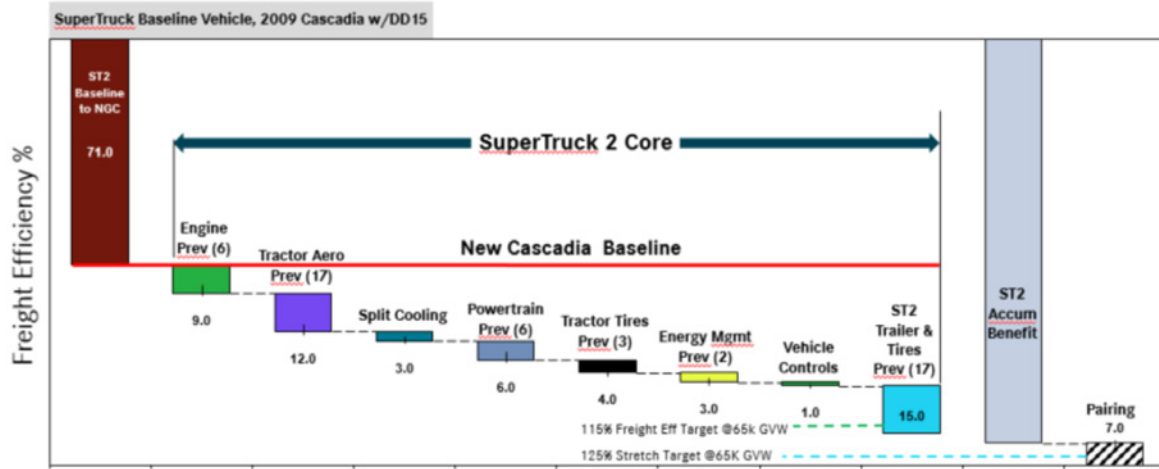
BSFC – brake specific fuel consumption; DD13 – Detroit 13-L diesel engine; WHR – waste heat recovery; PCC – phase change cooling

Figure V.4.4. Detroit roadmap to reach the 55% BTE target

Developing from the initial ST2 work stream targets, the teams have focused on determining how to meet those project goals. Ideation, simulation, and design development have led to the following measured performance results.

- Engine (in vehicle) Simulated 9% freight efficiency
- Tractor Aerodynamics Simulated 12% freight efficiency
- Split Cooling Simulated 6% freight efficiency
- Powertrain Simulated 6% freight efficiency
- Tractor Tires Simulated 3% freight efficiency
- Energy Management Simulated 2% freight efficiency
- Vehicle Controls Simulated 1% freight efficiency
- Trailer Aero & Tires Calculated 15% freight efficiency

Figure V.4.5 shows a summary of the simulation results. In Phase 3 of the project, the team will be validating the simulation results by physical measurements and feeding the knowledge gained back into the design for the final demonstrator. Some designs will be tested independently on a tinker truck, while the aero components will be tested on a closed track. The closed track is necessary when measuring very small improvements in aerodynamic performance.



NGC – next-generation Cascadia; GVW – gross vehicle weight

Figure V.4.5. Daimler Trucks North America updated pathway to reach 115% freight efficiency target

A-Sample Prototype Build

As previously mentioned, the second half of this phase has focused on completing the design of our first mule vehicle called A-Sample. Unlike the SuperTruck 1 project, we will not be running a full validation test on A-Sample. The purpose of this truck will be to optimize the integration of the different systems, so a higher focus will be on software integration than mechanical. Many of the systems will have fuel consumption measurements taken separately, so it is not necessary to take a combined measurement at this time. This method will also reduce the exterior modifications and extra development costs to make the exterior roadworthy. Instead, aero will be measured independently as well as the early developments on the engine.

As of writing this report, the A-Sample design release is in process, and prototype manufacturing is starting. Even trying to minimize the changes, 24% of the base vehicle requires new bills of material. Of those 115 bills of material, 48 have all new prototype content (see Figure V.4.6).

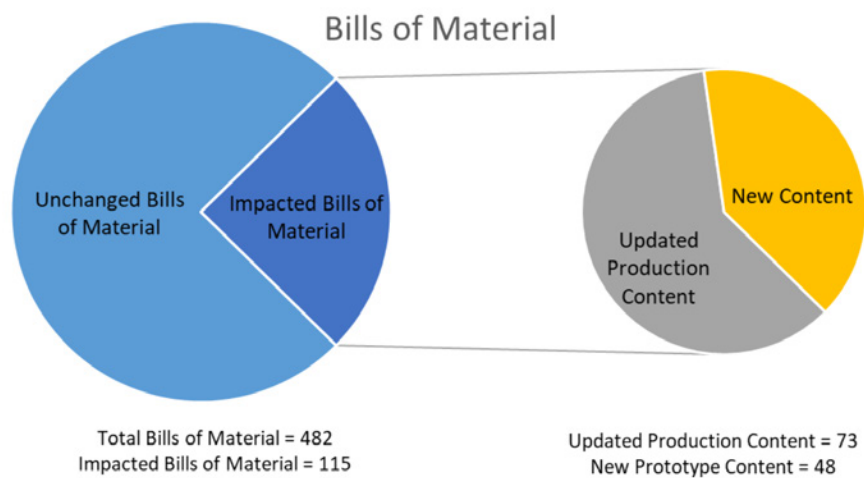


Figure V.4.6. A-Sample impacted bills of material

Conclusions

The SuperTruck 2 project is on a successful path towards meeting the target of 115% freight efficiency improvement over a 2009 Cascadia, and the engine team is on schedule to meet their goal of a 55% BTE demonstrator engine.

- Concept development and first simulations are complete for both the engine and the vehicle project.
- Working teams have completed the first prototype designs, and some technologies are already in prototype assembly and validation phases.
- Collaboration with outside suppliers is in place.
 - o Oak Ridge National Laboratory
 - o National Renewable Energy Laboratory
 - o University of Michigan
 - o Michelin Tire Corporation: tire concepts are complete, moving into the next phase of prototype hard tooling
- Scope definition is 75% complete in preparation for Phase 2 design work.

SuperTruck 2 is different than the first project in that it tries to find solutions that, while not currently economically feasible, have a pathway towards future production. Investigation of the implementation issues up front allows us to stretch the organization to look at solutions that would otherwise not have been considered. Funding this research in the early stages is of large importance due to the high risk of the technologies. It allows exploration into technologies that, if implemented, have potential to significantly reduce CO₂ on a large scale.

Acknowledgements

Thanks to Jeff Girbach, principal investigator in engine research, of Daimler Trucks North America for integral contributions to the project.

V.5 Development and Demonstration of Advanced Engine and Vehicle Technologies for Class 8 Heavy-Duty Vehicle – SuperTruck II (PACCAR Inc.)

Carl Hergart, Ph.D., Principal Investigator

PACCAR Inc.
12479 Farm to Market Road
Mount Vernon, WA 98273
E-mail: Carl.Hergart@paccar.com

Ken Howden, DOE Technology Development Manager

U.S. Department of Energy
E-mail: Ken.Howden@ee.doe.gov

Start Date: October 1, 2017	End Date: September 30, 2022	
Project Funding: \$40,000,000	DOE share: \$20,000,000	Non-DOE share: \$20,000,000

Project Introduction

PACCAR Inc., through Kenworth Truck Company, PACCAR Technical Center, and PACCAR Engine Company, and its partners (National Renewable Energy Laboratory, AVL NA, and Eaton Corp.) are collaborating in the design and development of a very-high-efficiency engine with advanced combustion, reduced friction, advanced air management, and waste heat recovery. This engine will be integrated into a high-efficiency powertrain system enhanced through accessory electrification and advanced controls. The powertrain will be incorporated into a highly aerodynamic and lightweight tractor-trailer combination. The vehicle concept includes advancements in rolling resistance, thermal management, and auxiliary components. Representative customer driving routes have been selected and will be used for development and optimization of the integrated vehicle controls package. Testing of engine, powertrain, and vehicle will demonstrate that the project goals have been met.

The combination of technologies is forecasted to provide greater than 100% improvement in vehicle freight efficiency at an affordable cost and with a short payback time. This level of fuel efficiency improvement applied over the entire Class 7/8 vehicle fleet in the United States will have a tremendous positive impact on the operating efficiency of truck fleets and significantly reduce fossil fuel energy dependency.

Objectives

The objective of this project is to research, develop, and demonstrate a Class 8 long-haul tractor-trailer combination that meets prevailing federal emissions standards and applicable safety and regulatory requirements while achieving the following goals.

Overall Objectives

- Achieve greater than 100% improvement in vehicle freight efficiency (on a ton-mile-per-gallon basis), with a stretch goal of 120%, relative to a 2009 baseline
- Demonstrate 55% engine brake thermal efficiency (BTE) in an operational point representative of cruise conditions
- Demonstrate same or improved vehicle performance (acceleration and gradeability) relative to a 2009 baseline
- Foster rapid market adoption of new technologies by providing cost effectiveness as expressed in terms of a simple payback

Fiscal Year 2018 Objectives

- Determine the engine power required for the SuperTruck II vehicle to meet performance targets while meeting or exceeding the performance of the 2009 baseline vehicle
- Assess the average road load required for the SuperTruck II vehicle in order to complete representative drive cycles and the Environmental Protection Agency Phase 2 greenhouse gas regulatory cycles
- Define the appropriate level of powertrain electrification/hybridization needed in order to achieve the required freight efficiency improvement target, while optimizing the balance between system cost and added weight of components
- Select the drive and duty cycles for the demonstration of freight efficiency improvement
- Complete simulation and analysis of engine, powertrain, and vehicle to define technical path

Approach

The project has been approached in three distinct but related areas: engine, powertrain, and vehicle. The engine portion will use a PACCAR MX-11 engine (introduced in North America in 2016 and manufactured in Columbus, Mississippi) as a baseline. The team is optimizing the combustion system, including the fuel injection parameters and the piston bowl geometry, in order to maximize the efficiency of the combustion process. Revisions to the air handling system including port geometry, manifold design, and turbocharger are also underway. Methods to reduce parasitic loads are being investigated. Recognizing that a significant portion of the heat generated during combustion is available in the exhaust, waste heat recovery will be used to reclaim energy from multiple sources around the engine.

The powertrain portion incorporates the recently launched PACCAR automated transmission, seamlessly integrated with the MX-11 engine and configured in a 4x2 axle architecture. The truck will feature low-rolling-resistance tires, hybrid electric power for accessories with energy storage capability, and predictive powertrain management (predictive route, real-time traffic, and route optimization).

The vehicle design includes significant aerodynamic improvements such as tractor wheel well close-outs, camera-based mirrors, optimized windshield curvature and A-pillars, as well as reduced tractor-trailer gap, among other things. The tractor and trailer are also undergoing significant light-weighting along with reduced energy use for auxiliary loads.

Results

Figure V.5.1 shows a characterization of various drive cycles in terms of the terrain. HDCC (heavy-duty composite cycle) refers to PACCAR's standard fuel economy cycle. PCC is the acronym for the predictive cruise control feature in PACCAR vehicles. Superimposed onto the plot is the energy storage required to recover braking energy over the route. Short hills generate small amounts of energy, whereas longer hills require more substantial energy storage.

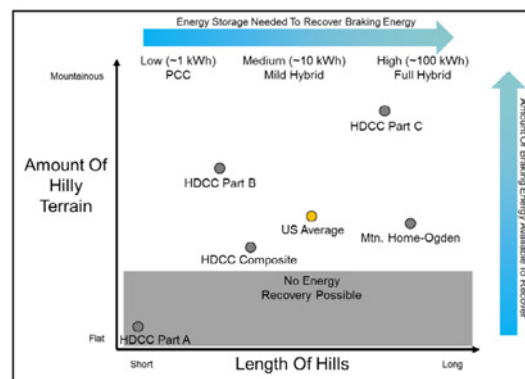


Figure V.5.1. Route selection to evaluate SuperTruck technologies

The amount of grades over a specific route will determine the benefit of having energy storage capability on the truck. As a result of a thorough analysis of multiple routes and the U.S. average, it was concluded that a mild hybrid platform with energy storage of approximately 10 kWh represents an optimum in terms of providing significant fuel efficiency without adding excessive cost and weight to the system. Leveraging National Renewable Energy Laboratory’s extensive route databases combined with customer input, a route in North Dakota, representative of the U.S. average, was selected as the route over which the project’s freight efficiency benefit was measured.

Vehicle Design

Through careful consideration, targeting line-haul and regional applications, and leveraging insight into changing fleet operations, candidate vehicle concepts have been selected. The selected concepts are forecasted to achieve our internal stretch goal of greater than 120% freight efficiency improvement, as shown in Figure V.5.2.

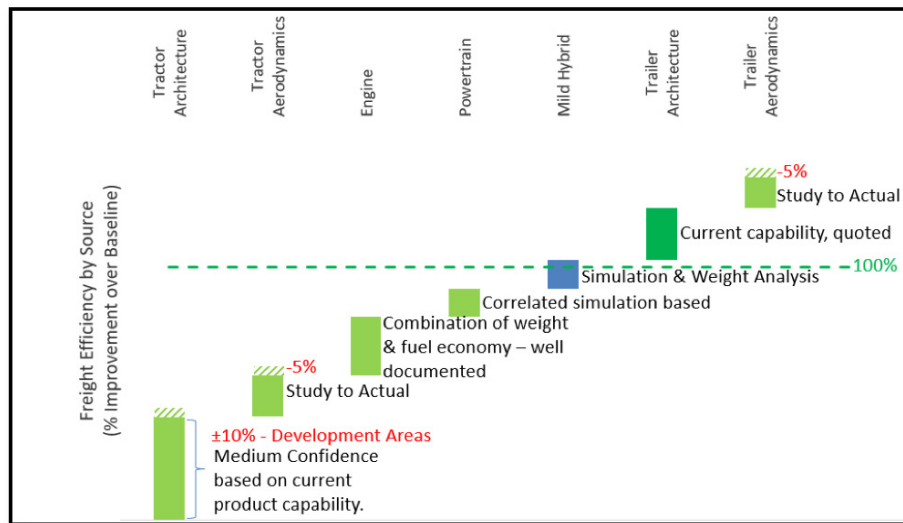


Figure V.5.2. Forecasted freight efficiency

During the first year, concepts have been identified and selected for vehicle size and shape; interior amenities; electric heating, ventilation, and air conditioning (HVAC); electrical architecture; aerodynamics package; powertrain package; dual-loop cooling system; chassis and suspension strategy; and tire strategy.

The chosen cab and sleeper shape was driven by aerodynamic performance while balancing needs of occupant space, windshield manufacturing capability, feasible wiper solutions, and user accessibility. Interior content and amenities consider both expectations of current product and forecasted future market needs for fleets running more regional operations.

An HVAC system strategy has been defined that includes reduced solar transmission, reduced conductive losses, and improved hardware efficiency. Solar treatment solutions, insulation materials, and an efficient hardware package have been identified for further testing and quantification of benefit.

Major aerodynamic treatments for the tractor and trailer have been selected with the guidance that the tractor is forward and backward compatible with existing trailer fleets. Similarly, the team is approaching trailer aerodynamics with the intent that trailers can be retrofitted. Figure V.5.3 shows the evolution in calculated reduction in aerodynamic drag as a function of concept iterations.

The vehicle powertrain package consists of an improved MX-11, 11-liter engine; PACCAR automated transmission; PTO (Power Take Off)-driven mild hybrid system; and advanced efficiency axle.

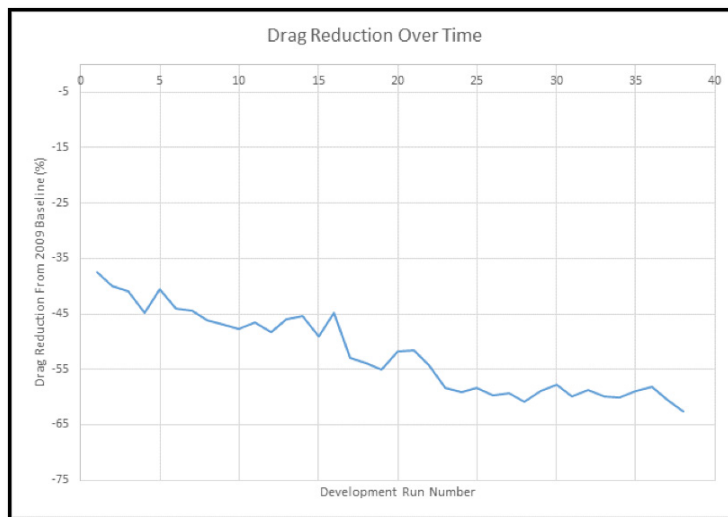


Figure V.5.3. Aerodynamic development (computational fluid dynamics)

Vehicle electronics will be a blend of 12 V for traditional and low loads with major power consumers utilizing 48 V supplied by the PTO-driven motor. A major development during this period has been the definition and simulation of a feasible dual-circuit coolant system utilizing electric fans.

Leveraging the full vehicle redesign opportunity, the chassis concept includes centralized mass and integrated mounting, which eliminates redundant brackets. As these additional mounting features for items such as fuel tanks and battery boxes account for nearly 20% of the total chassis weight, they present a desirable path to chassis weight reduction without compromising strength or stiffness. Several chassis concepts were evaluated and down-selected to a single primary concept. Utilizing new manufacturing techniques for the frame rails, additional geometry flexibility is afforded and incorporated into the new design.

Tire development efforts started with an investigation into desired sizes for load rating, packaging, and aerodynamic performance, which were then evaluated against rolling resistance projections and applicable efficient technologies that could be leveraged or developed. Additional development efforts are underway to refine the tire designs and resulting performance, with prototype evaluation targeted in 2020.

The above development efforts have resulted in the following key achievements.

- Forecasted aerodynamic drag reduction of over 60%
- Forecasted combined average coefficient of rolling resistance reduction of more than 20%
- Forecasted combination weight reduction of over 25%
- Path to achieve greater than 100% freight efficiency improvement

Hybrid Design Criteria

A hybrid system layout has been selected, and the team is in the process of right-sizing the energy storage system. During this period, the team also made important decisions regarding the controls strategies for the hybrid powertrain. The team employed a hybrid selection methodology that included evaluation criteria such as freight efficiency contribution, serviceability, cost of commercialization, and customer payback to arrive at an initial concept, as shown in Table V.5.1. Freight efficiency was evaluated using vehicle modeling techniques, while commercialization costs and customer payback time were informed using Kenworth's customer council and its network of suppliers and dealers. Basic control systems in the vehicle model have been upgraded to include predictive cruise control, energy storage system cycling, and electrically driven air conditioning systems.

Table V.5.1. Hybrid Technology Approach Risk Assessment

eMotor Power	15 kW	30 kW	45 kW	60 kW	90 kW	120 kW	120kW
Battery (e = energy, p = power)	e 10 kWh	e 10 kWh	p 10 kWh	p 10 kWh	p 10 kWh	p 10 kWh	e 60 kWh*
System Voltage	48 V	48 V	650 V	650 V	650 V	650 V	650 V
Integration	PTO	PTO	PTO	Integrated	Integrated	Integrated	Integrated
Contribution to ST-II Freight Efficiency	G	G	G	G	G	G	R
Customer Payback	G	Y	R	R	R	R	R
GHG2 Credit Potential	G	G	G	G	G	G	G
Serviceability	G	G	Y	Y	Y	Y	Y
Volume Potential	G	G	Y	R	R	R	R
Customer Cost	G	Y	Y	Y	R	R	R
Commercialization Cost	Y	Y	Y	R	R	R	R
Proof Of Concept Cost	G	G	Y	R	R	R	R
Zero Emission Zone Capable	R	R	R	R	R	R	G

GHG2 – U.S. Environmental Protection Agency Phase 2 greenhouse gas standards; ST-II – SuperTruck II

Highlights of the work performed by the powertrain team include:

- Development and validation of vehicle simulation model.
- Integration of the hybrid system and preliminary energy management.
- Evaluation of the effects of battery size and downhill speed overshoot.
- Development of cost and weight trade-offs.
- Analysis of the hybrid benefit over multiple drive cycles.

PACCAR SuperTruck data analysis of multiple real-world applications and geographic information from the major U.S. trucking routes were used to determine the road load point to demonstrate the 55% BTE engine goal for the project. In Figure V.5.4, the truck velocity is shown vs. grade percentage, which is the information that governs the power requirement of the vehicle. ST2 refers to SuperTruck II.

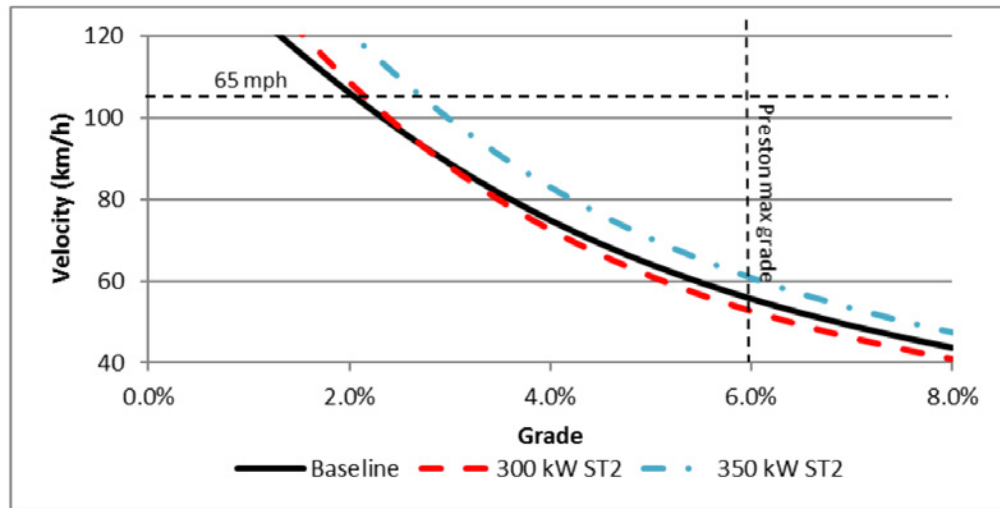


Figure V.5.4. Vehicle velocity vs. grade to determine power requirement

Engine Design

The roadmap for selecting engine technologies required to meet the 55% BTE goal is shown in Figure V.5.5. The baseline engine is estimated to achieve a peak of 47% BTE. The technologies selected to achieve the 55% BTE goal include improved combustion efficiency (where in Figure V.5.5 CR and PFP denote compression ratio and peak firing pressure, respectively), improved air management, reduced friction and parasitic losses, and the use of a waste heat recovery system.

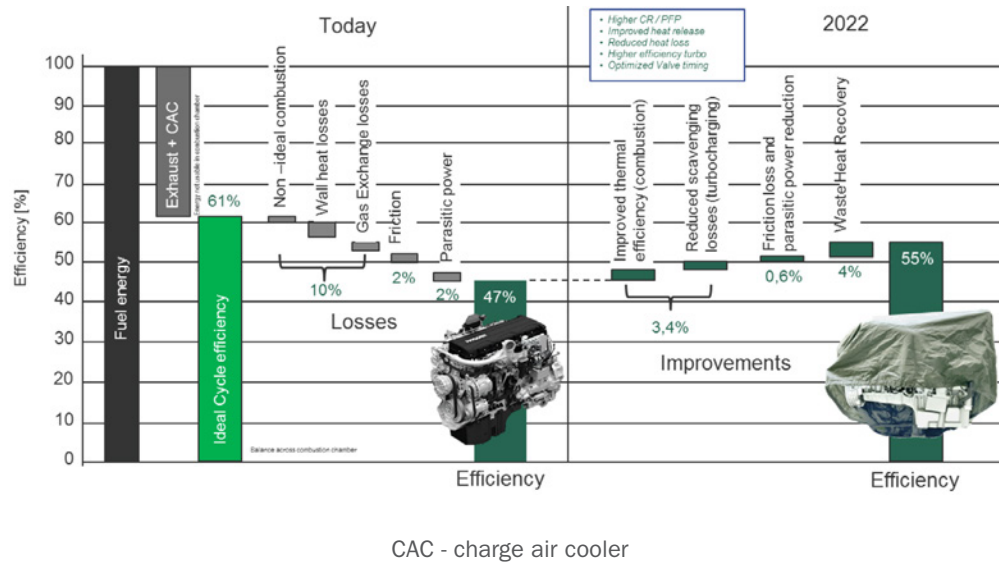


Figure V.5.5. Engine roadmap to 55% BTE

Engine simulations have produced a recipe for meeting the BTE goal for the engine. Design constraints posed by the air handling system have been identified, and work has begun to resolve them. Detailed one-dimensional and three-dimensional models of the MX-11 engine have been developed, calibrated, and refined during this period.

One-dimensional and three-dimensional engine analyses completed so far include the following.

- Crank and valvetrain friction
- Dual-loop exhaust gas recirculation flow paths
- Optimum sources for waste heat recovery
- Effect of valve timings and lift profiles
- Combustion system investigation with compression ratio and injector configuration variants
- Effects of longer stroke, example images of which are shown on the left and center images of Figure V.5.6
- Impact of thermal barrier coatings on combustion efficiency
- Optimization of valve port geometry, as illustrated by the right image in Figure V.5.6
- Turbocharger matching involving high-efficiency turbomachinery and increased boost conditions

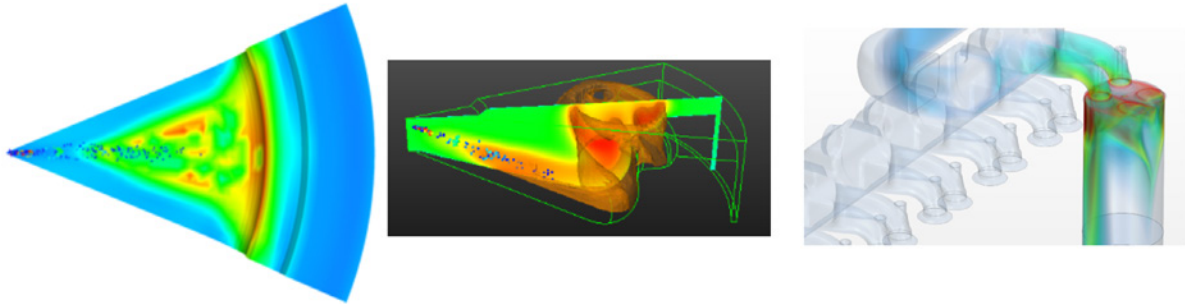


Figure V.5.6. Simulation results of in-cylinder combustion and port flow optimization

Conclusions

The PACCAR-led team has used simulation and analysis to develop recipes for engine, powertrain, and vehicle to meet the project objectives. These recipes include the following.

- Vehicle improvements
 - o Significantly improved aerodynamics of the tractor and trailer
 - o Light-weighting of the tractor (including the engine) and trailer to maximize freight efficiency
 - o Advanced electronics and driver assistance
- Powertrain technology improvements
 - o 48 V mild hybrid system has been selected based upon a variety of factors to maximize both energy and freight efficiency
 - o Electrified accessories enable maximum flexibility of the mild hybrid
- Engine technologies to reach 55% BTE
 - o Improved combustion system to reduce heat transfer
 - o Advanced turbocharging to improve gas exchange
 - o Reduced friction and parasitic losses
 - o Waste heat recovery

A demonstration route has been selected, leveraging tools and resources developed by the U.S. Department of Energy at its national laboratories. Big data analytics were used to develop the road load point for the demonstration of the 55% BTE engine in a dynamometer.

Key Publications

2018 Annual Merit Review Presentation, June 21, 2018

Acknowledgements

Ralph Nine, National Energy Technology Laboratory Project Manager

V.6 Ultra-Efficient Light-Duty Powertrain with Gasoline Low-Temperature Combustion (Delphi Technologies, PLC)

Keith Confer, Principal Investigator

Delphi Technologies
3000 University Drive
Auburn Hills, MI 48326
E-mail: keith.confer@delphi.com

Ken Howden, DOE Technology Development Manager

U.S. Department of Energy
E-mail: Ken.Howden@ee.doe.gov

Start Date: October 1, 2014	End Date: March 31, 2019	
Project Funding: \$24,112,162	DOE share: \$9,392,865	Non-DOE share: \$14,719,297

Project Introduction

Low-temperature combustion approaches have the potential to provide significant fuel economy benefit for internal combustion engines. Gasoline direct-injection compression ignition (GDCI) is a particular approach to realizing low-temperature combustion operation. GDCI is currently a moderately mature combustion technology, due in large part to advances made during a previous program funded through the Department of Energy (Advanced Technology Powertrain) opportunity and led by Delphi (Advanced Technology Powertrain's contract DE-EE0003258).

The current project is addressing a number of technical risks and issues that must be overcome for GDCI to become a production-viable technology. These are (1) further refinement of the GDCI combustion system to achieve near-ideal air/fuel mixture preparation for high efficiency and low hydrocarbon (HC) and CO emissions, (2) demonstration of low-temperature combustion transient control with high exhaust gas recirculation (EGR) levels during real-world transient driving maneuvers, and (3) development of an aftertreatment system that is effective in dealing with the low temperature challenges of a highly efficient engine.

The ultimate deliverable for this project is to demonstrate a 35% fuel economy improvement over a baseline vehicle with a port fuel injection engine, while simultaneously meeting Tier 3 emissions levels.

Objectives

Overall Objectives

- Refine the GDCI combustion system for high efficiency and low HC and CO emissions
- Demonstrate low-temperature combustion transient control
- Develop an aftertreatment system that is effective in dealing with the low temperature challenges of a highly efficient engine

Fiscal Year 2018 Objectives

- Characterize benchmark gasoline direct injection (GDI) spark ignition (SI) engine
- Characterize and map Generation (Gen) 3 GDCI engine on performance dynamometer
- Develop improved strategies for high-load GDCI operation

- Perform Gen 3 vehicle simulation for fuel economy and emissions
- Refine controls, algorithms, and software for the Gen 3 GDCI vehicle

Approach

This project has substantially expanded upon the existing success in developing GDCI combustion technology. Further optimization of the combustion process, supported by component development, has focused on improved brake thermal efficiency (BTE) and reduced emissions. A key focus area has been the continued development of the injection process and fuel sprays to reduce engine-out HC and CO, which are especially challenging for low-temperature combustion, while also improving thermal efficiency. Controls development has targeted improved ignition timing and combustion control, with an emphasis on transient operation and cold starting. System and controls optimization work has demonstrated robust operation over an expanded range of operating conditions, including ambient temperature and variations in gasoline composition. To meet stringent Tier 3 emissions targets, a new aftertreatment system has been developed in combination with advanced controls and fast warm-up strategies to deliver an optimized solution for GDCI.

A Gen 2 GDCI development level engine was designed and built, and used to develop refined controller hardware, including improved sensor, actuator, and control algorithms. The Gen 2 GDCI engine was retrofitted into the development vehicle and used for refinement of GDCI controls and calibration. Development of the final Gen 3 GDCI engine, Gen 3 GDCI demonstration vehicle, control systems, and aftertreatment is based on the work done on the Gen 2 GDCI engine.

The Gen 3 and Gen 3X GDCI engines were designed and built specifically for this project based on experience from the earlier engines. These engines, when combined with refined control systems and project-specific exhaust aftertreatment, are planned to meet Tier 3 emissions levels.

Results

During the past year:

- Dynamometer mapping of the Gen 3 GDCI engine was performed.
- “Wet-less” injection strategy was demonstrated.
- Injector sprays for wet-less strategy were characterized.
- The baseline GDI engine was mapped for use as a comparison to the GDCI engine.
- GDCI-diffusion burn strategy was developed for high-load conditions.
- The Gen 3X engine was built and tested, yielding a minimum brake specific fuel consumption (BSFC) of 194 g/kW (43% BTE), with BSFC < 210 (40% BTE) over a wide load range.
- Gen 3 vehicle build and controls integration were completed.
- Vehicle simulation (Argonne National Laboratory) was completed showing 36%–51% improvement in combined federal test procedure fuel economy.

Dynamometer Mapping of Gen 3 GDCI Engine

A new calibration procedure was developed for mapping of the Gen 3 GDCI dynamometer engine and produced very good results. Tests were completed at 800 rpm, 1,000 rpm, and 1,500 rpm over a range of loads from idle up to 11 bar indicated mean effective pressure (IMEP). Results were semi-optimized for minimum BSFC within constraints for combustion noise, stability, and emissions. As well, best points were selected for wide operating ranges of key control variables such as EGR, intake air temperature, and manifold absolute pressure. This leads to a robust combustion system that can compensate for deviations from the ideal calibration map during aggressive transients.

One key finding was that exhaust temperatures could be maintained at high temperatures down to low engine loads. This was accomplished by use of the “Phi-EGR” strategy, which avoids excessively lean operation and maintains global equivalence ratio, Phi, at higher levels than previously tested. This improved “burn out” in the combustion chamber and increased combustion efficiency significantly.

New Gen 3 fuel injectors were developed with spray characteristics optimized using computational fluid dynamics simulation for wet-less injection with minimum smoke emissions. These new injectors were tested at 1,500 rpm, 4 bar IMEP on the Gen 3 engine. Very low smoke was measured even for very late injection timings. The use of GDCI late injection timings significantly improved robustness of the combustion process. Sensitivity of combustion phasing to intake air temperature was reduced, and injection timing authority was increased relative to GDCI early injection. These new injectors represent an important technological step for GDCI combustion.

Injector Spray Characterization

Spray chamber tests of the latest prototype GDI fuel injectors were conducted at University of Wisconsin-Madison. This injector spray is the outcome of extensive simulations and development and is a key element of the GDCI wet-less combustion system. Testing was done up to 500 bar, and backlit and Schlieren tests showed that fuel vaporization was very fast, with liquid penetration less than 20 mm at chamber pressure and temperature of 40 bar and 650°C, respectively.

Gen 3X Engine Build and Test

A new version of the Gen 3 GDCI engine, called Gen 3X, was completed (see Figure V.6.1) and installed on the dynamometer at Delphi Technologies. The main features of the engine are:

- Single-stage, variable inlet compressor, variable nozzle turbine turbocharger (and eliminating the supercharger).
- Simplified thermal management with fast air-blend system.
- Two-step valvetrain for exhaust rebreathing (previously continuously variable).
- Higher compression ratio of 16.8.
- GDCI-diffusion combustion strategy for high load.
- Prototype GDI fuel system and injectors for preferred spray characteristics for GDCI combustion.

This Gen 3X GDCI engine version is targeted to be less complex and less costly than the Gen 3 engine and to have lower fuel consumption and higher output.

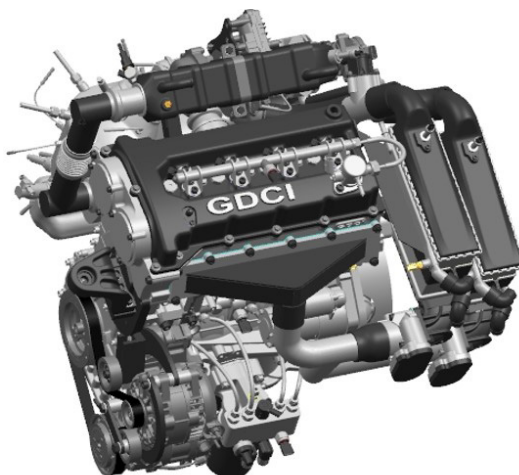
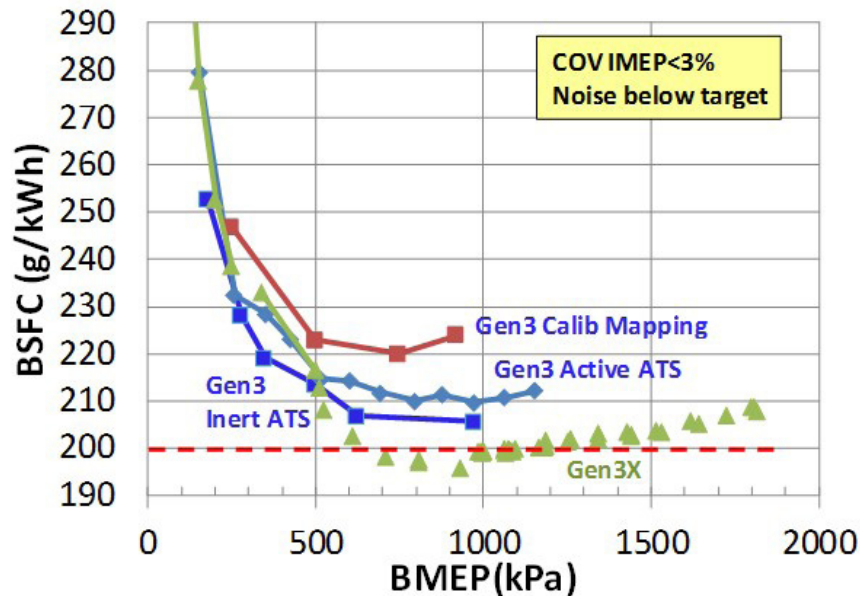


Figure V.6.1. Gen 3X GDCI engine

Break-in tests were completed and a load sweep was conducted at 1,500 rpm. BSFC as a function of brake mean effective pressure (BMEP) is shown in Figure V.6.2. In this comparison, there are two versions of the Gen 3 engine (Gen 3 and Gen 3X), and the Gen 3 version was tested under three different conditions.

Of the Gen 3 test conditions, the first tests with inert exhaust aftertreatment system (ATS) exhibited minimum BSFC of 205 g/kWh. However, with an active ATS system, about a 2% penalty was observed, as can be seen in the plot of Figure V.6.2. This was attributed to oxidation of fuel in the gasoline oxidation catalyst ahead of the EGR system. Without an active ATS, this unburned HC and CO would be returned to the combustion system to make torque. The upper curve in Figure V.6.2 shows the results of detailed calibration mapping. As can be seen, there is a significant fuel consumption penalty on the Gen 3 engine when all these constraints are applied.

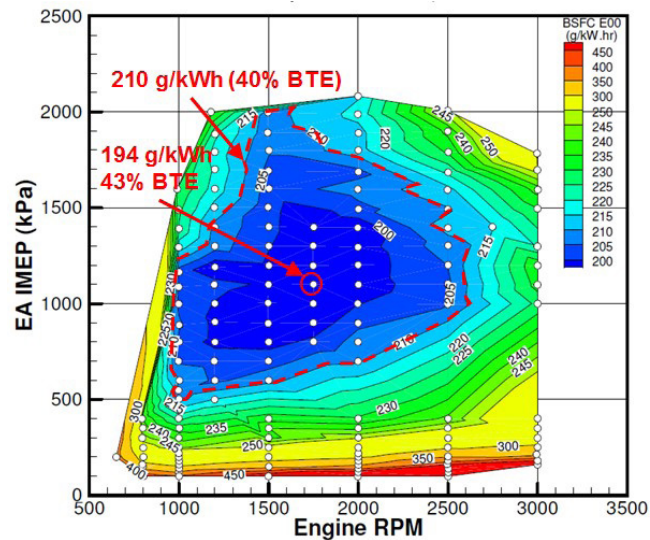
The bottom curve in Figure V.6.2 shows data for the new Gen 3X engine. This data is the best achieved in this project. Minimum BSFC was 195 g/kWh at 9 bar BMEP. The engine utilized a new GDCI-diffusion combustion strategy for higher loads. Double injections were used with a two-stage, GDCI-diffusion combustion strategy. The first stage was an ultra-clean GDCI combustion event. The second stage utilized a GDCI-diffusion combustion, which extended the burn duration and reduced combustion noise.



COV IMEP – coefficient of variation in indicated mean effective pressure

Figure V.6.2. Preliminary load sweep at 1,500 rpm for the Gen 3X GDCI engine

Preliminary calibration mapping of the Gen 3X engine was conducted on the engine with full lean control and without EGR. The BSFC contour plot is shown in Figure V.6.3. Tests were run at 650 rpm for idle and up to 3,500 rpm in this test (data plotted up to 3,000 rpm). Load ranged from 1 bar to 21 bar IMEP. For IMEP of 4 bar and below, single injections with GDCI combustion were used with heavy exhaust rebreathing and elevated intake air temperature up to 75°C. For 5 bar IMEP and above, double injections were used with the new two-stage GDCI-diffusion combustion strategy. Minimum BSFC for this test was 194 g/kWh (43% BTE) measured at 1,750 rpm, 12 bar IMEP. Notably, BSFC of 210 g/kWh (40% BTE) is a very large portion of the operating map from 5 bar to 20 bar IMEP. This is very important for engine down-speeding and up-loading to achieve the best vehicle fuel economy.



EA IMEP – electronically assisted indicated mean effective pressure

Figure V.6.3. Initial BSFC contour map for Gen 3X GDCI engine

Exhaust temperatures were favorable for a lean, low-temperature combustion engine and demonstrated that exhaust temperatures can be elevated to levels needed for selective catalytic reduction (SCR) lean NO_x reduction systems. Testing of a full exhaust aftertreatment system was not completed at the time of this report, but non-methane HC was close to the Tier 3, Bin 30 target of 10 ppm for the upper load range, and CO was approximately five times below the Tier 3, Bin 30 target of 50 ppm for the entire map down to 2–3 bar IMEP. However, as load increased, and the fraction of fuel burned in two-stage GDCI-diffusion combustion strategy increased, both NO_x and smoke increased. New tests are planned for the fourth quarter of 2018 to address the higher NO_x and smoke emissions for the higher load range.

Gen 3 Demonstration Vehicle

The build of the Gen 3 demonstration vehicle was completed in the first quarter of 2018 (Figure V.6.4), and a warm-idle demonstration of the vehicle was conducted for visitors from DOE on March 19, 2018. Subsequent to the idle demonstration, the engine was removed from the vehicle and transferred to the engine dyno lab for calibration mapping testing (replacing previous dyno engine, which was damaged during testing).



Figure V.6.4. Engine compartment of completed Gen 3 vehicle

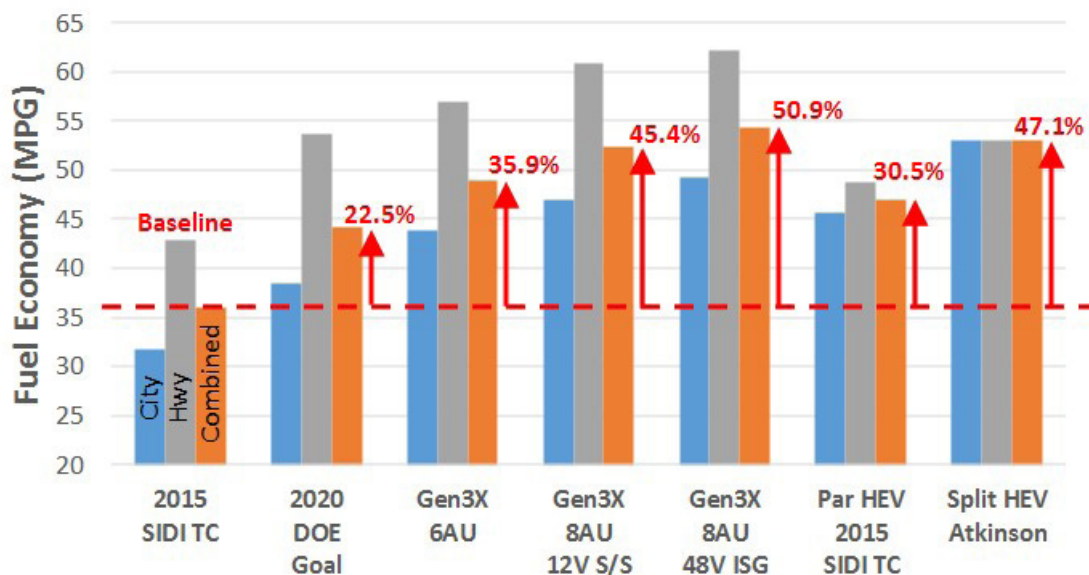
Gen 3 Engine Controls

During this past year, the GDCI engine controls were updated to include new control hardware, algorithms, and software to support all Gen 3 content, including the SCR system and urea dosing system. The control system provides rapid algorithm development flexibility while offering improved data acquisition capabilities and a reduction in the number of add-on hardware input/output boxes. Additional insight to the combustion control system response has been gained via the development of a Charge Reactivity Index Model that provides a single numeric index of air charge reactivity.

Simulations were also performed to test new strategies for rapid cold start warmup of the aftertreatment system. Results showed that exhaust gas temperatures of over 500°C could be achieved by combining rebreathing with high back pressure at moderate loads. This is important to rapidly light off the pre-turbo catalyst, oxidation/HC trap catalyst, and the SCR catalyst just after the cold start.

Vehicle Simulation Completed

Vehicle simulations were conducted at Argonne National Laboratory using the 2.2 L Gen 3X engine map for a mid-sized passenger car, small and medium sport utility vehicles, and a pickup truck. Objectives were to simulate the GDCI Gen 3X engine with six-speed automatic transmission (6AU), eight-speed automatic transmission with 12 V start/stop (8AU), and eight-speed automatic transmission with 48 V integrated starter generator (8AU 48V ISG), and compare results to baseline SI engines and full hybrid powertrains. Results showed that combined federal test procedure fuel economy could be improved by 36% to 51% over the baseline SI turbo engine (Figure V.6.5). In some cases, the Gen 3X GDCI engine exceeded the fuel economy of SI engines with parallel and power-split full hybrid technologies in this study.



TC – turbocharger; S/S – start/stop; HEV – hybrid electric vehicle; SIDI – spark ignition direct injection

Figure V.6.5. Simulated vehicle fuel economy results for the 2.2 L Gen 3X GDCI engine with various powertrain technologies compared to baseline engine and full hybrid engines (Argonne)

Conclusions

- GDCI engine technology has evolved to exceptional fuel efficiency of 43% BTE and excellent torque characteristics in a production-feasible powertrain. Key to this development are a high-pressure direct injection system, a wet-less injection process, and a new GDCI-diffusion combustion process in combination with an advanced single-stage turbocharger. Robustness of the combustion system and ease of operation and control were greatly improved.

- Vehicle simulations at Argonne predicted that combined federal test procedure fuel economy could be improved by 36%–51% over a contemporary SI engine baseline. This is comparable to or exceeds the fuel economy of power-split hybrid and parallel hybrid powertrains.
- An aftertreatment system was developed for 2025 Tier 3, Bin 30 regulations using a close-coupled oxidation catalyst and an SCR catalyst. Exhaust temperatures were sufficiently high at low loads to maintain high catalyst conversion efficiency. Dynamometer tests are underway to confirm emissions compliance.

Key Publications

1. Sinnamon, J., K. Aggoune, M. Sellnau, and K. Hoyer. 2018. “Transient Control of Thermal and EGR Systems for Third Generation GDCI Multi-Cylinder Engine.” (SAE 2018-01-0902) Presented at the 2018 SAE World Congress, Detroit, MI, April 11, 2018.
2. Malaczynski, G., and M. Foster. 2018. “Wavelet Filtering of Cylinder Pressure Signal for Improved Polytropic Exponents, Reduced Variation in Heat Release Calculations and Improved Prediction of Motoring Pressure & Temperature.” (SAE 2018-01-1150) Presented at the 2018 SAE World Congress, Detroit, MI, April 11, 2018.
3. Sellnau, M., K. Hoyer, W. Moore, M. Foster, et al. 2018. “Advancement of GDCI Engine Technology for US 2025 CAFE and Tier 3 Emissions.” (SAE 2018-01-0901) Presented at the 2018 SAE World Congress, Detroit, MI, April 11, 2018.

Acknowledgements

The project team would like to thank the U.S. Department of Energy for its continued support of this project with special thanks to Gurpreet Singh, Ken Howden, and Ralph Nine (National Energy Technology Laboratory). Thanks also to Dr. Peter Olin and Mark Sellnau of Delphi Technologies.

V.7 Lean Miller Cycle System Development for Light-Duty Vehicles (General Motors LLC)

Paul A. Battiston, Principal Investigator

General Motors LLC
800 Glenwood Ave.
Pontiac, MI 48340
E-mail: paul.a.battiston@gm.com

Ken Howden, DOE Technology Development Manager

U.S. Department of Energy
E-mail: Ken.Howden@ee.doe.gov

Start Date: January 1, 2015	End Date: December 31, 2019	
Project Funding: \$20,672,201	DOE share: \$8,268,880	Non-DOE share: \$12,403,321

Project Introduction

In order to accomplish the government objective of achieving breakthrough thermal efficiencies while meeting U.S. Environmental Protection Agency emissions standards, this project focuses on combining two enabling technologies in a gasoline engine: lean combustion and Miller cycle. Lean combustion requires a more complex exhaust after-treatment system than a traditional three-way catalyst system [1]. The Miller cycle concept provides knock mitigation, increased expansion of combustion gases to extract additional work, reduced pumping losses, and increased efficiency.

The objective of the project is to research, develop, and demonstrate the new lean Miller cycle (LMC) combustion concept. The lean Miller strategy will be integrated with engine downsizing, advanced thermal management, stop/start, and friction reduction to maximize efficiency to achieve a 35% improvement in fuel economy over a production baseline vehicle. A lean after-treatment exhaust system will be developed to meet Tier 3 emissions standards. The overall system will be demonstrated in a vehicle.

Objectives

Overall Objectives

- Demonstrate a new combustion concept combining lean stratified operation with Miller cycle in a gasoline engine
- Integrate with engine downsizing, advanced thermal management, 12-Volt stop/start, friction reduction mechanisms, and a lean after-treatment exhaust system
- Demonstrate a vehicle with a fuel economy improvement of more than 35% over an existing production baseline vehicle while meeting Tier 3 emissions standards

Fiscal Year 2018 Objectives

- Finalize calibration on a single-cylinder engine (SCE) of the final combustion hardware set deployed to a multi-cylinder engine (MCE)
- Finalize hardware procurement for the first MCE design and build two engines
- Finalize control architecture for a steady-state dyno engine and commission MCE on dyno to support validation of fuel efficiency projections
- Refine simulation toolsets to project cycle fuel economy and emissions potential
- Design and procure MCE upgrades and after-treatment systems for transient development phases

Approach

The challenges of the combustion and after-treatment will be addressed systematically. The first step is SCE testing, which establishes the requirements for the combustion system. This central injection, lean combustion system requires very high levels of exhaust gas recirculation (EGR) to mitigate NO_x emissions; such a highly “dilute” system presents a combustion challenge. Computational fluid dynamics is being used to analyze in-cylinder flows and spray interaction and design options for optimizing thermodynamic efficiency. This highly dilute system also presents a boost and after-treatment challenge due to the low-temperature lean exhaust and potential high cost of components. One-dimensional (1D) modeling is being used to investigate options for boost, EGR, and exhaust after-treatment systems and provide realistic boundary conditions for the SCE testing. 1D modeling will also be used to predict MCE performance and combined with vehicle simulation tools to predict cycle fuel economy and tailpipe emissions potential.

These fundamentals will then be integrated into an MCE and after-treatment system. The engine will be optimized and calibrated on an engine dynamometer. The final demonstration will be in a vehicle, where emissions, drivability, and performance will be confirmed. Decision gates are set up annually to assess progress and determine whether or not to continue the investigation.

Results

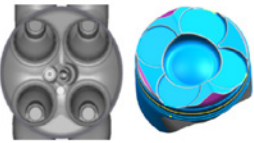
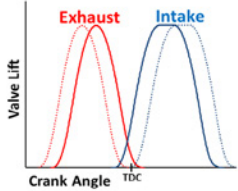

Significant progress was made in MCE procurement, build, and initial dyno development of the first MCE variant to demonstrate steady-state fuel efficiency against targets. Key accomplishments are as follows.

- Optimized calibration on SCE of the final combustion hardware set deployed to the MCE
- Demonstrated the potential to achieve the DOE brake thermal efficiency targets of 26% and 35% at 2,000 rpm part-load test conditions
- Commissioned the first MCE in an engine dyno test cell to support steady-state testing
- Demonstrated the potential to achieve 46% fuel efficiency improvement over a baseline vehicle based on 1D MCE model and vehicle fuel economy simulations
- Finalized and initiated procurement of the MCE and lean after-treatment system to support transient dyno and vehicle development

SCE Calibration Refinement

Calibration optimization was accomplished on the SCE for the down-selected combustion hardware set deployed to the MCE. Table V.7.1 highlights key features of the final MCE hardware set. The combustion solution set improves combustion efficiency and combustion stability by utilizing an injector design coupled with multi-pulse injection strategies to minimize spray collapse and manage flame front equivalence ratio and flame turbulence by applying small injection pulses timed with ignition. Flame containment in the piston bowl and reduced wall wetting are also accomplished with this strategy.

Table V.7.1. Combustion System Hardware Set for Multi-Cylinder Engine

	<p>Open chamber with high tumble works well with closely-spaced multiple pulse strategies without need of port throttle</p> <p>12:1 CR, spray-guided bowl-in-piston optimized with chamber for light-load lean-stratified combustion</p>
	<p>LIVC best compromise between light-load stratified and WOT torque and power</p> <p>Injector design meets spray/control requirements Closely-spaced small pulses 35MPa injection pressure</p> 

CR – compression ratio; LIVC – late intake valve closing; WOT – wide open throttle; TDC – top dead center

SCE testing was extended into the first quarter of 2018 in order to refine the calibration of the final MCE intent hardware set and provide a starting point for MCE development. The strategy is to run naturally aspirated, lean stratified combustion with external EGR up to 6 bar brake mean effective pressure (BMEP), then transition to stoich-homogeneous operation. EGR and air-fuel ratios over 30% and 30:1, respectively, were typical at the lean stratified key points. The engine will target naturally aspirated operation to approximately 8 bar BMEP. Figure V.7.1 highlights the results of the calibration refinement. Additional efficiency gains were realized across the drive cycle weighted key points while maintaining combustion stability and $\text{NO}_x < 10 \text{ g/kg fuel}$. The efficiency gains were estimated to improve fuel economy by approximately 2% on the city drive cycle over the original calibration. Hydrocarbons in LMC mode remains a challenge below 2 bar BMEP. Calibration strategies for exhaust heating and rich operation for passive ammonia formation were also explored at select light-load key points to guide MCE calibration development. Multi-pulse injection strategies were investigated on the SCE at full load. A 6% improvement in torque output was achieved running a triple vs. single pulse injection strategy.

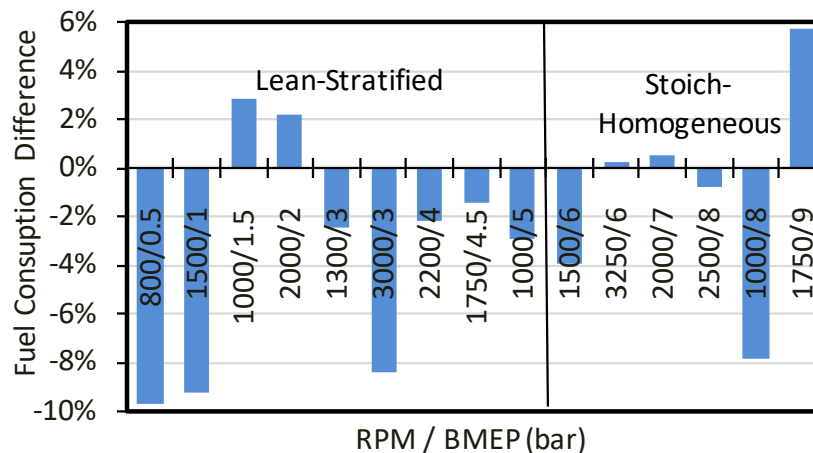


Figure V.7.1. Fuel consumption improvement achieved during SCE calibration optimization on final MCE hardware set

MCE Commissioning and Calibration Development

Figure V.7.2. highlights the first engine build equipped with a clutched fixed-drive ratio supercharger and its dyno installation. First fire was successfully accomplished on August 22, 2018, with commissioning of cell and steady-state engine controls completed by mid-September. Two minor issues were addressed during the commissioning effort. This included a malfunction in the positive crankcase ventilation system and a failure of the supercharger drive pulley assembly. Both issues were resolved with a recovery plan executed. Due to the pulley failure, testing focused on the naturally aspirated key points through the end of the reporting period. A re-designed pulley assembly was available in October.

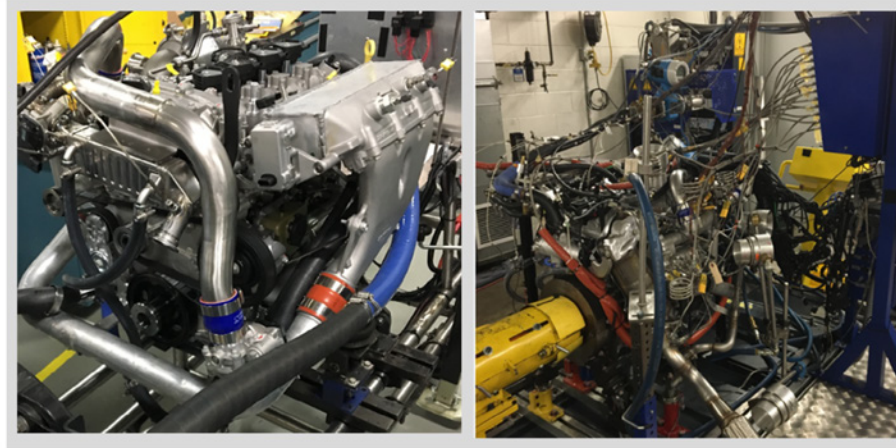


Figure V.7.2. First steady-state engine (fixed-drive supercharger) and dyno installation

Calibration development began on the MCE by establishing stoichiometric-homogeneous baselines with and without external EGR. Naturally aspirated key points were explored, producing brake specific fuel consumption (BSFC) responses within 3% of comparative stoichiometric Miller cycle (SMC) engines of similar displacement and base architecture. The application of external EGR was then explored to improve efficiency while maintaining emissions and combustion stability. The gain at each naturally aspirated key point depended on the combustion system’s tolerance for external EGR beyond the residual dilution established by the cam phasing strategy. The extent of efficiency gains are shown in Figure V.7.3. A mean BSFC gain of 1.5% was estimated across the naturally aspirated key points, with maximum gains recorded up to 4%. Lean stratified testing will begin in early October. The MCE key point results will be leveraged to correlate the 1D MCE model to feed fuel economy and tailpipe emissions projections over the vehicle drive cycle.

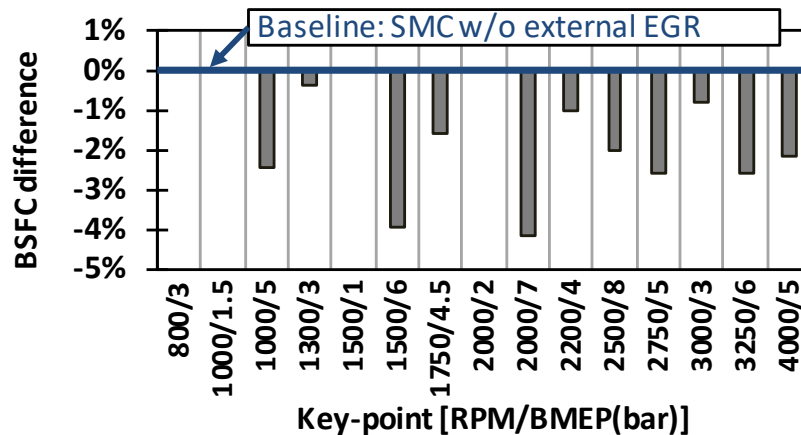


Figure V.7.3. BSFC reduction of LMC engine running in SMC mode with external EGR, naturally aspirated key points

Efficiency and Fuel Economy Projections

Brake thermal efficiency potential was demonstrated on the SCE at the 2,000 rpm part-load points. SCE results achieved 32% (26% target) and 35% (35% target) brake thermal efficiency for the 2 bar and 20% full-load BMEP points, respectively, meeting or exceeding the 2020 DOE stretch targets. The 1D MCE model was correlated to the results from the calibration optimization on the SCE. BSFC maps were generated and used within vehicle simulations to predict the fuel economy potential on the city drive cycle. This process will be repeated as empirical results become available from MCE testing. Figure V.7.4. projects the fuel economy potential over the Environmental Protection Agency's 23-cycle Federal Test Procedure (FTP) based on the vehicle simulation method described above for the reference vehicle equipped with start-stop (SS) and 8-speed automatic transmission. An 11% margin is projected over the 35% fuel economy improvement target to the baseline vehicle equipped with a 3.5 L V6 port fuel injection (PFI) engine. Results for the LMC variants do not account for fuel economy penalties associated with drive quality compromises, catalyst heating, and passive NH₃ formation for a passive lean-NO_x after-treatment. Projections will be refined as MCE results become available in the fourth quarter.

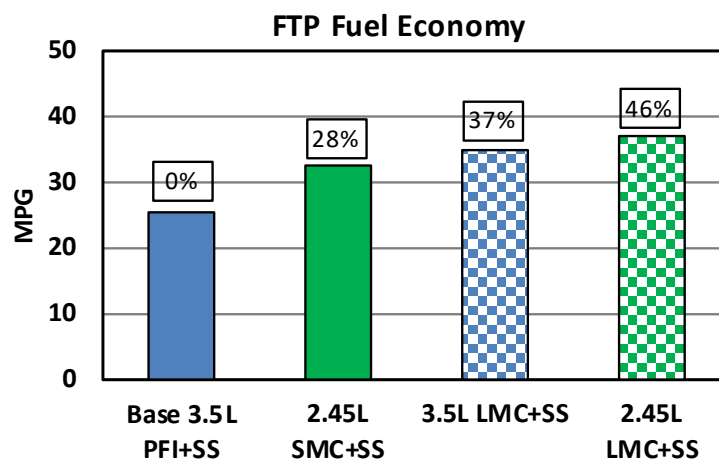


Figure V.7.4. Cycle fuel economy predictions based on weighted test points

Transient Development Hardware Package

The first MCE design was revisited to improve the transient performance and reduce friction parasitics associated with the fixed-drive supercharger. This engine design was intended for steady-state engine dyno operation to validate engine efficiency predicted on the SCE. 1D MCE analysis projected friction parasitics compromising efficiencies over the boosted key points and full-load performance. A 48-V electric compressor from BorgWarner (eBooster[®]) was identified as a solution to lower friction parasitics over a mechanical supercharger while providing continuously variable boost control and packaging flexibility, which could be leveraged to improve transient performance. 1D models for the eBooster[®] system and a 48-V generator model were incorporated into the 1D MCE engine model. 1D analysis projected an average reduction in friction mean effective pressure of 30% over the mechanical supercharger across the boosted operating range. This should also improve fuel efficiency on the vehicle drive cycle over the original mechanical-supercharger-based engine. Figure V.7.5 highlights the changes made to the first supercharger-equipped MCE build. Design was also completed for a modular after-treatment package to support transient dyno development in later phases of the project. The after-treatment system is capable of active urea dosing and passive ammonia formation under rich engine operation. Procurement of the new transient engine hardware is 90% complete. After-treatment hardware procurement is dependent on passing of the next go/no go gate in late November 2018. Finally, a vehicle packaging study was completed that incorporated the transient engine package along with the supporting 48-V architecture to support its operation.

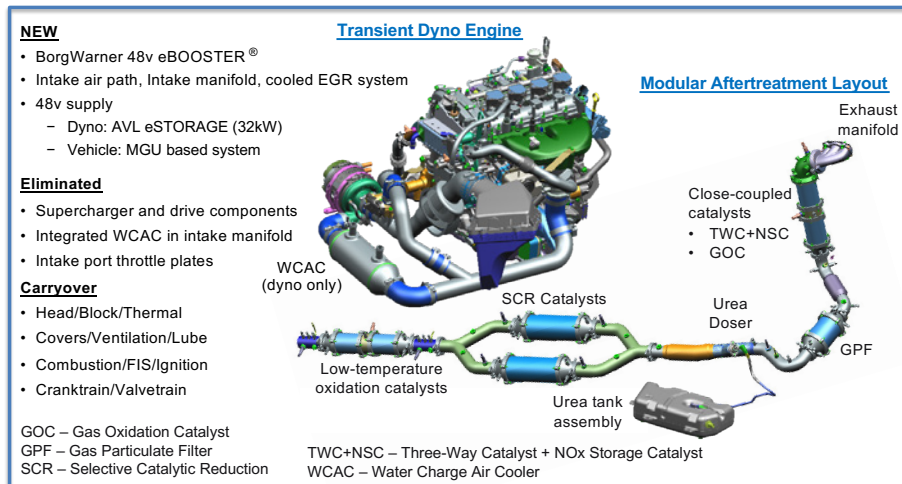


Figure V.7.5. Transient dyno hardware package

Conclusions

The LMC system scope of work includes analysis, single cylinder, multi-cylinder, and vehicle development. It will include full after-treatment and controls development to meet performance targets and Tier 3 emissions standards. Progress over the past year included the following.

- Refined calibration strategies on the SCE to maximize efficiency for the combustion hardware set deployed to the MCE
- Defined calibration strategies to support MCE development, including exhaust heating for catalyst light-off, rich combustion operation for passive ammonia formation, and multi-pulse injection strategies at full load
- Built and dyno commissioned the first MCE equipped with a fixed-drive mechanical supercharger to support steady-state testing to validate efficiency projections
- Completed MCE calibration to define SMC baseline at steady-state key points
- Demonstrated potential to achieve project cycle fuel economy target from 1D MCE correlated to SCE steady-state results and vehicle simulations
- Designed and initiated procurement of transient-capable engine and after-treatment package

1D modeling will continue and be correlated to MCE test results to predict fuel economy and emissions potential over the emissions drive cycle. The gate decision to pursue transient controls and calibration development leading to a final transient-capable package for vehicle development is planned for the end of November 2018.

Key Publications

2018 Annual Merit Review presented on June 21, 2018.

References

1. Smith, Stuart R. "Lean Gasoline System Development for Fuel Efficient Small Cars." DOE Final Report, Cooperative Agreement DE-EE0003379, November 25, 2013.

Acknowledgements

The author wishes to acknowledge Arun Solomon, General Motors LLC, for contributions to this project.

V.8 Cummins 55% BTE Project (Cummins Inc.)

Lyle Kocher, Principal Investigator

Cummins Inc.
1900 McKinley Avenue
Columbus, IN 47201-6414
E-mail: lyle.e.kocher@cummins.com

Ken Howden, DOE Technology Development Manager

U.S. Department of Energy
E-mail: Ken.Howden@ee.doe.gov

Start Date: December 1, 2015	End Date: June 30, 2018	
Project Funding: \$10,100,000	DOE share: \$4,500,000	Non-DOE share: \$5,600,000

Project Introduction

The successful development of a high-efficiency diesel engine system could significantly reduce petroleum usage in the United States and provide energy security for the future. The project's efforts directly address the Vehicle Technologies Office's goal of achieving 55% brake thermal efficiency (BTE) and prevailing emissions compliance. The project accelerates the development of the high-efficiency-enabling technologies to shorten their time to market.

The landscape of advanced heavy-duty engines includes both high-temperature diffusion combustion and low-temperature premixed combustion. The low-temperature combustion engines are capable of demonstrating low engine-out constituent emissions and high thermal efficiencies. The high thermal efficiency is predominately due to a short combustion duration and low in-cylinder heat loss from the distributed premixed reactions. However, low-temperature combustion engines suffer from controllability issues due to the lack of a direct combustion trigger and knock issues due to fuel and temperature stratification in the cylinder. These barriers currently prohibit low-temperature combustion engines from entering the heavy-duty market. High-temperature conventional diesel combustion engines are easily controllable and do not suffer from knock but emit higher levels of constituent emissions such as NO_x and particulate matter. The emissions can be treated through the application of low-pressure exhaust gas recirculation and a close-coupled selective catalytic reduction on filter catalyst system. Efficiency improvements for the high-temperature combustion engines can be achieved by mimicking the best traits of a low-temperature combustion engine: short combustion duration and low in-cylinder heat loss. These efficiency improvements are being leveraged in this project. The implementation of the low-pressure loop exhaust gas recirculation system allows for the usage of a larger, more efficient turbocharger since all the low-pressure exhaust gas recirculation flow will go through the turbocharger. The efficiency of the engine system can be further improved through the addition of a waste heat recovery (WHR) system.

Objectives

Overall Objectives

- Use a diesel engine system to demonstrate in a test cell peak engine efficiency of 55% BTE
- Develop and demonstrate an advanced, highly integrated combustion and after-treatment system to achieve 2010 emissions compliance

Fiscal Year 2018 Objectives

- Demonstrate in a test cell peak engine efficiency of the diesel engine system
- Demonstrate emissions compliance of the system
- Complete the final technical report

Approach

The approach integrates advances in the areas of combustion, engine design, waste heat recovery, fuel injection, turbocharging, and aftertreatment to provide an optimized and integrated total engine system. Achieving 55% BTE will require virtually all engine systems to be improved with thorough effort placed on the interaction between the systems. When examining the entire system, opportunities can be created to take advantage of technologies to benefit multiple engine systems. Starting with the combustion system, a low-heat-rejection combustion chamber is desired to minimize the in-cylinder heat losses. The low-heat-rejection design will be achieved through piston material changes to low-thermal-conductivity materials and use of thermal barrier coatings. The low-heat-transfer (LHT) piston will operate with higher surface temperatures and thus have lower in-cylinder heat losses. Additionally, the LHT piston will be able to operate with reduced piston oil cooling flow. This represents a savings of up to 40% of the lube flow and will allow a smaller, lower-parasitic lube pump to be utilized. The LHT pistons will also have higher exhaust temperatures for better turbocharger and after-treatment performance. Similar symbiotic system-level opportunities are available through the use of a close-coupled aftertreatment system and the addition of a low-pressure exhaust gas recirculation loop. An integrated system designed to opportunistically take advantage of these interactions is critical to achieving the overall efficiency goals.

Results

The improvements in the base engine have allowed for the previous demonstration of 50% BTE without WHR. The engine is paired with a low-pressure-drop after-treatment system. The system was tested over the emissions cycles and demonstrated compliance over the ramped model cycle supplemental emissions test (RMCSET) and hot federal test procedure (FTP) cycles. The project's final emissions cycle values are shared below in Table V.8.1. The system-out brake specific NO_x (BSNO_x) values over the RMCSET meet the limit of 0.27 g/kWh for a heavy-duty engine. Similarly, the hot FTP met the regulation. Due to the time available, the project was unable to develop the cold start thermal management calibration for the system, but the project team was confident that a suitable calibration could be developed using this system hardware.

Table V.8.1. RMCSET and FTP Cycle NO_x Summaries

Cycle	BSNO _x g/kWh
None	
RMCSET	0.20
Hot FTP	0.22

The development of an advanced WHR system to aid in achieving maximum engine thermal efficiency was a critical aspect of the 55% BTE project. To improve energy recovery, Cummins designed, produced, and demonstrated a unique dual-entry-turbine WHR system based on organic Rankine cycle technology. At the final engine demonstration point, the system provided 19.3 kW of net mechanical power back to the engine, as shown in Table V.8.3, improving engine BTE by 4.30 percentage points and exceeding the original performance estimates for the system. The available heat for the WHR system at this point is shown in Table V.8.2. This was accomplished while using R1233zd(E) as the working fluid; R1233zd(E) is a non-toxic, non-flammable, next-generation refrigerant with low global warming potential and near-zero ozone depletion potential (reported values of 1.0 and 0, respectively).

Table V.8.2. WHR Heat Values for Best BTE Test Point

	High-Pressure Loop Heat kW	Low-Pressure Loop Heat kW	Recuperator Heat kW
Best BTE Point	75.5	90.1	23.9

Table V.8.3. WHR Power Values for Best BTE Test Point

	Wheel Power kW	Gearbox & Pump Loss Power kW	Net Power kW
Best BTE Point	23.0	3.7	19.3

Despite exceeding estimated performance predictions, analysis of the final performance data indicated a number of possible areas for improvement of the WHR system. These improvements were beyond the scope of the current 55% BTE project, but if fully realized, WHR net power produced at the final demonstration conditions could be increased an additional 2.8 kW, resulting in a total BTE benefit of 4.96 percentage points. Many of these potential improvements, as well as the successful WHR developments demonstrated during the 55% BTE project, will be carried on to future Cummins WHR systems, including those deployed under the Cummins SuperTruck 2 program.

The project concluded the planned engine system demonstration in pursuit of the goal of demonstrating a peak system BTE of 55%. The engine system included a high-efficiency diesel engine integrated with a state-of-the-art WHR system and an advanced after-treatment system capable of meeting the current emissions standards. While the ultimate project goal of 55% BTE was not fully achieved due to hardware issues during the final testing phase, the project demonstrated a significant increase in reported engine system BTE for a heavy-duty-sized engine. The previous demonstrations in the DOE-funded SuperTruck 1 program ranged between 50–51% BTE. The Cummins 55% BTE project demonstrated 53.6% BTE. See Table V.8.4.

Table V.8.4. Demonstrated Peak BTE System Efficiency Breakdown

	Engine BTE %	WHR ΔBTE %	System BTE %
Best BTE Point	49.3	4.3	53.6

Additionally, the project established a revised path-to-target showing how the system could be improved to reach the ultimate project goal of 55% BTE with some minor modification to the engine system. The changes in the revised path-to-target were unable to be completed during the course of this project due to time and money constraints placed on the project. This revised path is shared in Figure V.8.1, where each incremental improvement is bounded by a low side and high side estimated delta BTE (ΔBTE) improvement.

Working through the identified improvements, the WHR tailpipe boiler system resulted in more engine backpressure than had originally been planned. In the final demonstration, this additional backpressure caused the engine BTE to be reduced below previously demonstrated levels. Steps to reduce this were identified but were not implemented prior to completion of testing. On the turbocharge side, the demonstrated turbine and compressor efficiencies were slightly lower than the original project targets. In addition, due to the late changes in planned turbomachinery, the original plans for a roller-element bearing turbine housing were unable to be realized. Early evaluations of LHT pistons did not fully realize original closed cycle efficiency expectations; however, with piston design improvements, additional efficiency gains are expected.

On the waste heat recovery side, as the engine efficiency is increased, the waste heat available to the WHR system is reduced. Despite that, improvements were identified that could have been realized on the original test cell installation but again were unable to be implemented. These improvements included resizing the WHR system pulley to correct the WHR turbine speed to target the peak turbine efficiency and applying additional insulation to the exhaust system and refrigerant lines. While these items could have been implemented on the original installation, additional improvements also could have been realized with a system redesign. These include a redesign of the WHR turbine nozzle and blade geometry and changes to the plumbing to reduce pressure losses.

The final line item in the revised path to 55% BTE includes significant improvements to the turbocharger that would be in-line with current industry state of the art. The cumulative effect of these improvements is estimated to yield a BTE between 55% and 56%.

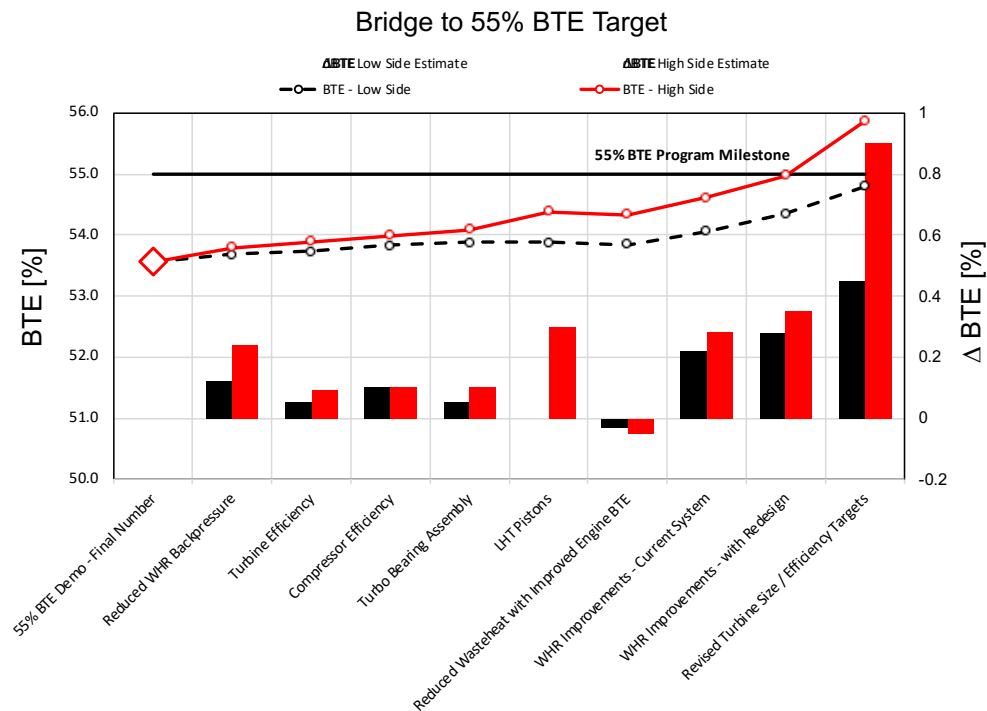


Figure V.8.1. Revised path to 55% BTE from project's demonstrated peak BTE

Conclusions

The Cummins 55% BTE project has been successfully completed. The project demonstrated a peak system BTE of 54%. While the project fell a little short of the 55% BTE goal due to time and monetary constraints, the project developed a revised path-to-target that would meet the 55% BTE target. The project also demonstrated that the system could meet emissions compliance over the RMCSET and hot FTP cycles. The project ran out of time to develop the cold FTP calibration but didn't see any issues that would prevent a successful calibration from being developed. The following progress was made.

- Demonstrated 54% BTE in a heavy-duty truck engine with WHR
- Demonstrated 50% BTE in a heavy-duty truck engine without WHR
- Demonstrated +4.3% ΔBTE from the WHR system
- Demonstrated emission compliance over RMCSET and hot FTP cycles

Key Publications

1. Q4 2017 – 55BTE Program Quarterly Research Performance Progress Report, 01/30/2018.
2. Q1 2018 – 55BTE Program Quarterly Research Performance Progress Report, 04/30/2018.
3. Q2 2018 – 55BTE Program Quarterly Research Performance Progress Report, 07/30/2018.
4. Q3 2018 – Final Scientific/Technical Report, 9/30/2018

V.9 A High Specific Output Gasoline Low-Temperature Combustion Engine (General Motors)

Hanho Yun, Principal Investigator

Propulsion System Research Lab., General Motors
800 N. Glenwood Dr.
Pontiac, MI 48034
E-mail: Hanho.yun@gm.com

Ken Howden, DOE Technology Development Manager

U.S. Department of Energy
E-mail: Ken.Howden@ee.doe.gov

Start Date: October 1, 2014	End Date: December 31, 2017	
Project Funding: \$3,499,000	DOE share: \$1,749,500	Non-DOE share: \$1,749,500

Project Introduction

In this project, the team proposed to develop and demonstrate a downsized boosted, lean, low-temperature combustion (LTC) engine system capable of demonstrating a 15–17% fuel economy improvement relative to a contemporary naturally aspirated, stoichiometric, combustion engine consistent with relevant emissions constraints. The project will focus on the integration, development, and demonstration of the overall engine system performance potential over the Federal Test Procedure (FTP) and US06 (Supplemental Federal Test Procedure) drive cycles as well as the harsh conditions associated with real-world driving on a transient engine dynamometer using a fully functional multi-cylinder engine.

The project will focus on maximizing internal combustion engine fuel economy potential by combining lean LTC over the majority of the drive cycle to maximize work extraction while minimizing NO_x emissions, advanced cylinder-pressure-based controls along with variable valve lift technology for precise in-cylinder composition control, downsizing and turbocharging for reduced parasitic losses, and a novel plasma-based ignition technology to enhance combustion robustness and controllability through in-cylinder reactive species generation.

The project is currently in Budget Period 2.

Objectives

The objective of this project is the development of a high-output, low-temperature gasoline combustion engine system demonstrating a 15–17% fuel economy improvement relative to a contemporary stoichiometric combustion engine.

Overall Objectives

- Develop a gasoline combustion engine system to demonstrate a 15–17% fuel economy improvement relative to a contemporary stoichiometric combustion engine using marketplace gasoline (RD587)
- Be consistent with relevant emissions constraints (target: super ultra-low emissions vehicle 30 regulation)
- Integrate the enabling technologies (gasoline LTC combined with downsizing and boosting technology, low-temperature plasma ignition, physics-based model-based control, passive ammonia selective catalytic reduction system lean after-treatment system) synergistically

Fiscal Year 2018 Objectives

- Conduct homogeneous stoich spark ignition combustion assessment of the LTC engine with the prototype controller

- Develop and demonstrate LTC performance at key steady-state points in conjunction with the novel low-temperature plasma ignition system
- Develop LTC control system architecture and calibration control system models and algorithms
- Develop and demonstrate full LTC engine calibrations and a simplified combustion control system

Approach

Budget Period 1: Multi-cylinder engine and prototype controller design, build, and testing

Design modification and procurement activities for the LTC multi-cylinder engine and prototype controller, including build and installation of the baseline engine into a dynamometer test cell.

Go/No-Go Decision #1 approval required to continue to Phase 2

Budget Period 2: LTC combustion and controls development, steady-state condition

LTC multi-cylinder engine combustion and controls development and testing using the low-temperature plasma ignition system.

Go/No-Go Decision #2 approval required to continue to Phase 3

Budget Period 3: Develop/demonstrate full integrated engine, combustion, and controls capability

Final integration and demonstration phase. This phase will turn to refining the transient controls and calibration packages. All dynamometer-based multi-cylinder testing will have been completed and a 100% verified dynamometer-based calibration developed.

Results

- Homogeneous stoichiometric calibration was completed using base engine.
- These data will serve as the reference baseline for the upcoming lean LTC system development.
- Also, some of the high load points will be used even in LTC transient test.
- Physics-based control was successfully developed, calibrated, and implemented.
- Transient operation was verified through FTP drive cycle testing, including Urban Dynamometer Driving Schedule (UDDS) and Highway Fuel Economy Test (HWFET) (Figure V.9.1).

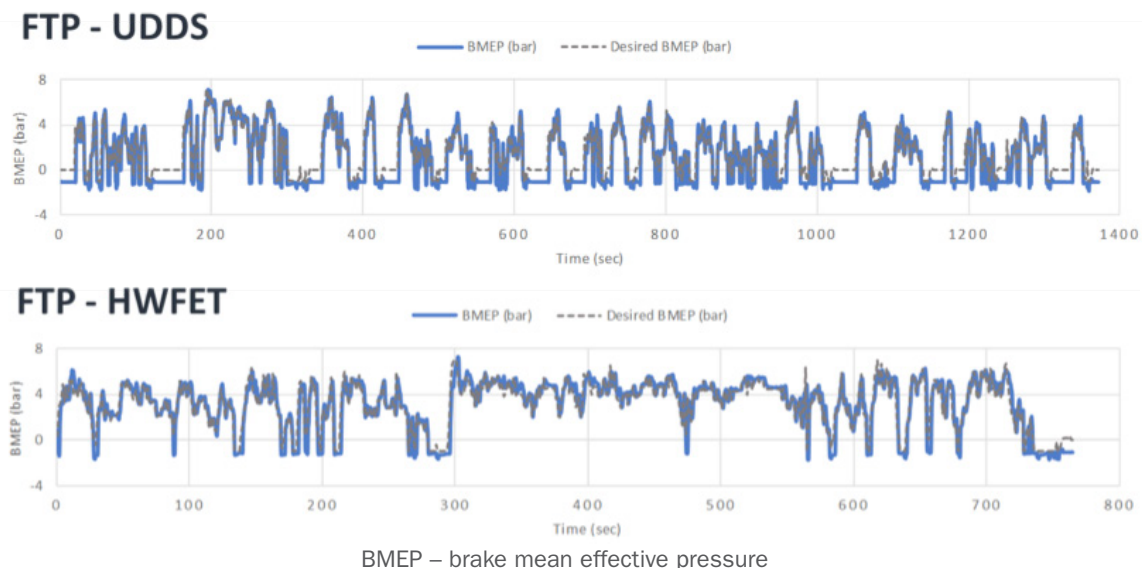
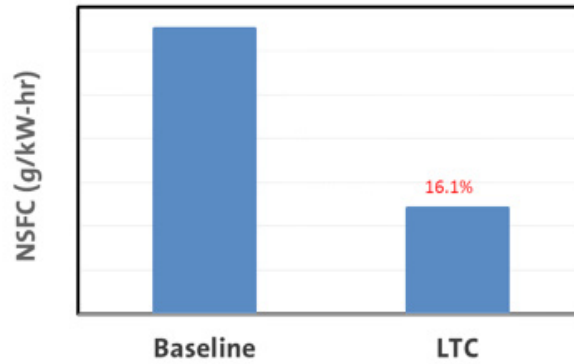


Figure V.9.1. UDDS and HWFET drive cycle test results

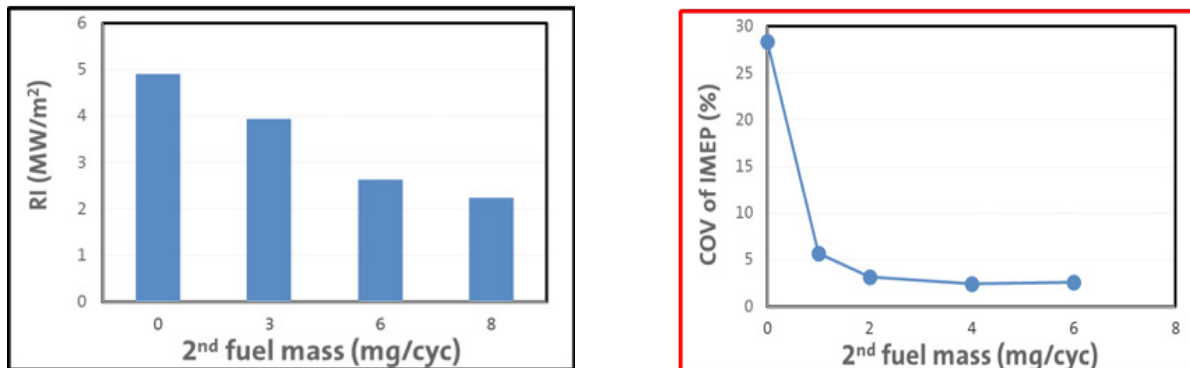
- An efficiency gain of LTC was achieved at 2,000 rpm, 2 bar net mean effective pressure condition (LTC shows 16% gain over stoich., see Figure V.9.2).



NSFC – net specific fuel consumption

Figure V.9.2. Efficiency gain of LTC

- The emission index of nitrous oxide was 0.2 g/kgf.
- An ignition timing control methodology, which has been considered as one of the barriers of LTC, was successfully developed.
- It was determined that a slow-response parameter such as intake temperature cannot be chosen as a control parameter.
- Injection timing was selected at low and medium load during negative valve overlap operation.
- Spark timing was chosen at high load during negative valve overlap operation since double injection strategy was applied.
- Combustion noise can be controlled by adjusting the fuel mass injected for second injection during high load negative valve overlap operation (Figure V.9.3). This will help reduce the combustion noise during transient operation when the measured dilution level does not reach the target dilution.
- Significant improvement of combustion stability was realized by applying double injection strategy during positive valve overlap LTC operation.
- Optimal fuel mass for second injection should be selected considering NO_x emission.



RI – ringing intensity; COV – coefficient of variation; IMEP – indicated mean effective pressure

Figure V.9.3. Effects of fuel mass injected for second injection

- Combustion stability during negative valve overlap LTC operation can be improved using groundless barrier discharge ignition system. Higher voltage and duration help to enhance the auto-ignitability of the mixture by generating ozone (Figure V.9.4).

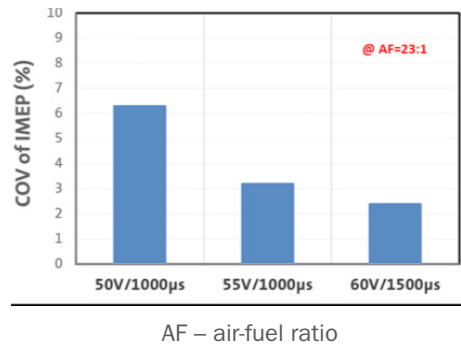


Figure V.9.4. Coefficient of variation of IMEP at 50 V/1,000 µs, 55 V/1,000 µs, and 60 V/1,500 µs

- Combustion stability during positive valve overlap LTC operation can be improved using a groundless barrier discharge ignition system. Higher voltage helps to enhance the initial flame kernel development (Figure V.9.5).

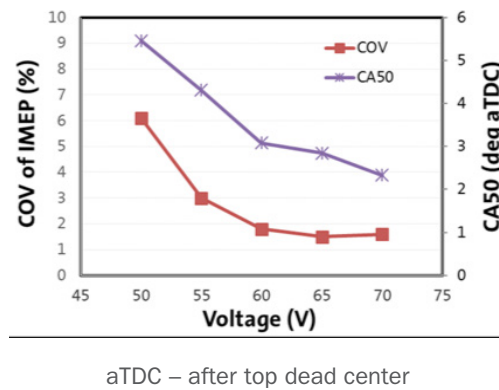


Figure V.9.5. Coefficient of variation of IMEP and crank angle at 50% mass fraction burned for voltage from 50 V to 70 V

- Higher igniter-by-igniter variation over the spark plug system might be related to the durability issue (Figure V.9.6).

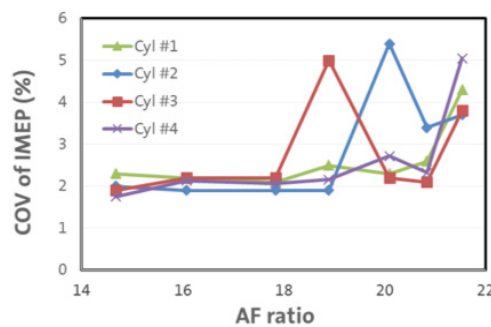


Figure V.9.6. Igniter-by-igniter variation

- Twelve igniters have failed in less than two months. Even though benefits have been found, a conventional spark plug system will be used for future LTC tests.

Conclusions

- Complete the development of homogeneous stoichiometric spark ignition calibration and controls
- Successfully demonstrate FTP cycle test (both UDDS and HWFET) for homogeneous stoichiometric spark ignition operation
- Verify the efficiency benefits of LTC
- Develop the methodology of combustion phasing control for various modes of LTC
- Extend the lean LTC regime using multiple injection, exhaust gas recirculation, and valving strategy
- Complete the evaluation of groundless barrier discharge ignition system for all multi-mode LTC regimes

Acknowledgements

The author would like to thank Ralph Nine, Ken Howden, and Gurpreet Singh for support of this project.

V.10 Solenoid Actuated Cylinder Deactivation Valve Train for Dynamic Skip Fire (Delphi Technologies, PLC)

Hermes Fernandez, Principal Investigator

Delphi Technologies, PLC
5500 W. Henrietta Rd.
W. Henrietta, NY 14586
E-mail: Hermes.fernandez@delphi.com

Robert Wang, Principal Investigator

Tula Technology, Inc.
2460 Zanker Rd.
San Jose, CA 95131
E-mail: wangr@tulatech.com

Ken Howden, DOE Technology Development Manager

U.S. Department of Energy
E-mail: Ken.Howden@ee.doe.gov

Start Date: January 1, 2017	End Date: July 1, 2019	
Project Funding: \$3,472,676	DOE share: \$1,736,338	Non-DOE share: \$1,736,338

Project Introduction

Delphi Technologies, PLC, and Tula Technology, Inc., are developing an advanced combustion strategy known as dynamic skip fire (DSF). The basis of this strategy is to selectively deactivate cylinders based on engine load and speed to minimize fuel consumption. Cylinder deactivation requires intake and exhaust valve as well as fuel injector deactivation to reduce engine pumping work and improve efficiency. Existing hydraulically actuated valve train hardware has been used on development engines and vehicles to prove out the fuel economy benefits of DSF. Hydraulic actuation has proven difficult to implement for production-level programs due to the complexity of adding four independent hydraulic circuits to an existing cylinder head for a four-cylinder engine.

The purpose of this project is to develop solenoid actuated valve train hardware which will allow DSF technology to be more easily commercialized with current overhead cam production engines. Additional benefits expected from this project include a faster and more repeatable switching response, leading to improved system reliability as well as a larger operating window for DSF.

Objectives

Overall Objectives

- The main objective of this project is to improve engine fuel efficiency by developing a production-feasible electrically actuated cylinder deactivation valve train, which will enable internal combustion engines to employ this combustion strategy.
- The project is expected to enable the realization of 8–10% fuel economy improvement above stock operation of a non-cylinder-deactivation four-cylinder engine, while maintaining production-level noise, vibration, and harshness targets and emissions.
- This project will enable DSF technology to be more easily implemented into production engines by eliminating the complex hydraulic circuit packaging that is currently required to individually deactivate cylinders. This will allow broader market adaptations, especially on overhead cam engines.

Fiscal Year 2018 Objectives

- Demonstrate actuator control. Design, build, and demonstrate an actuation system capable of meeting performance and durability targets for DSF combustion strategy. Actuation system includes engine control module, actuator driver module (ADM), and direct solenoid actuators.
- Confirm operation of the deactivation system. Use the actuation system along with the switchable valve train to confirm the ability to deactivate and reactivate engine valves in a motored cylinder head. The full system must be integrated into the selected production cylinder head and meet all performance and durability targets for DSF combustion strategy.
- Baseline dyno engine performance. Document steady-state fuel economy of the selected production engine in order to establish a baseline for fuel economy improvement.
- Control system functionality. Confirm that the deactivation system meets the modeled switching speed requirements on a motored cylinder head and effectively deactivates cylinders as planned.

Approach

Delphi and Tula are working together to improve engine fuel efficiency by researching, designing, developing, building, and testing a production-feasible electrically actuated cylinder deactivation valve train, which will maximize the fuel economy benefit of Tula's DSF technology.

Tula has conducted engine and vehicle simulations to characterize cylinder deactivation and project fuel economy improvement, and to define deactivation requirements. State-of-the-art software, such as GT-Suite, Matlab, and Simulink, were utilized for engine and vehicle performance and noise, vibration, and harshness simulation and analysis work. Tula will also participate in engine testing and provide guidance on control strategies to minimize noise, vibration, and harshness, as well as fuel consumption.

Delphi is responsible for all aspects of the design and development of the deactivation roller finger followers, electrical actuators, controls, and engine management system optimization and testing. A packaging study was conducted to understand the available space for the electrical actuators, as well as mounting and interfaces to the deactivation roller finger followers. Concepts were generated and design simulations were used to select both the deactivation roller finger follower and an electrical actuation concept. The build of both the selected concept and its control hardware and software is currently underway. Build is completed for the deactivating roller finger followers and is in process for the direct acting solenoids. Once the builds are completed, the valve train hardware and controls will be installed on a four-cylinder dynamometer engine. Steady-state and transient engine calibrations will then be optimized. Fuel usage and emissions at key Federal Test Procedure steady-state speed-load points and simulated Federal Test Procedure operation will be documented. Data analysis will be completed, and results will be reported.

Results

Major FY 2018 accomplishments include:

- Completion of all required deactivating roller finger follower (DRFF) valve train analysis, hardware print release, and build of engine-level valve train components.
 - o DRFF probe hardware testing revealed undesirable locking mechanism friction from the selected concept. A new locking mechanism was developed and evaluated to have significantly reduced friction. Figure V.10.1 shows friction comparisons between the initial lever design and the new control rod design.

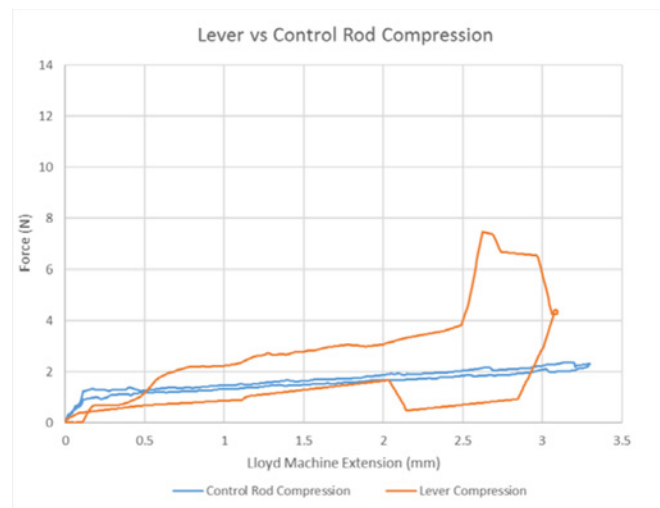


Figure V.10.1. Locking mechanism friction comparison

- o Finite element analysis was performed on the new design with a few iterations required to meet stress and stiffness targets. Tolerance analysis was completed on the new design, and kinematic and dynamic analyses were rerun with a slightly reduced mass for the new DRFF design. Prints were released, and a hardware order was placed upon completion of all analysis.
- o The hardware order was completed, and all components required for this project were assembled and inspected. The final engine DRFF hardware is shown in Figure V.10.2.



Figure V.10.2. Final engine build DRFF hardware

- Completion of engine and vehicle simulations to characterize cylinder deactivation and to project fuel economy, Milestone M1.1.
 - o Solenoid probe hardware testing identified a couple of issues that required several build–test–evaluation–redesign iterations. Initially, the team identified a high part-to-part solenoid force variation. Investigation revealed friction due to poor guidance of the moving rod/armature sub-assembly to be the major cause of the friction-related force variation. Our first attempt to remedy the friction issue resulted in a design with consistently high force, but unsatisfactory durability.
 - o Our fifth-generation solenoid design was finally able to meet force and durability requirements and was released for engine-level hardware build. Figure V.10.3 shows force test results for the Generation (GEN) 5 solenoid tested new and at 1M, 7M, and 50M cycles. Our full vehicle life cycle target is 50M cycles.

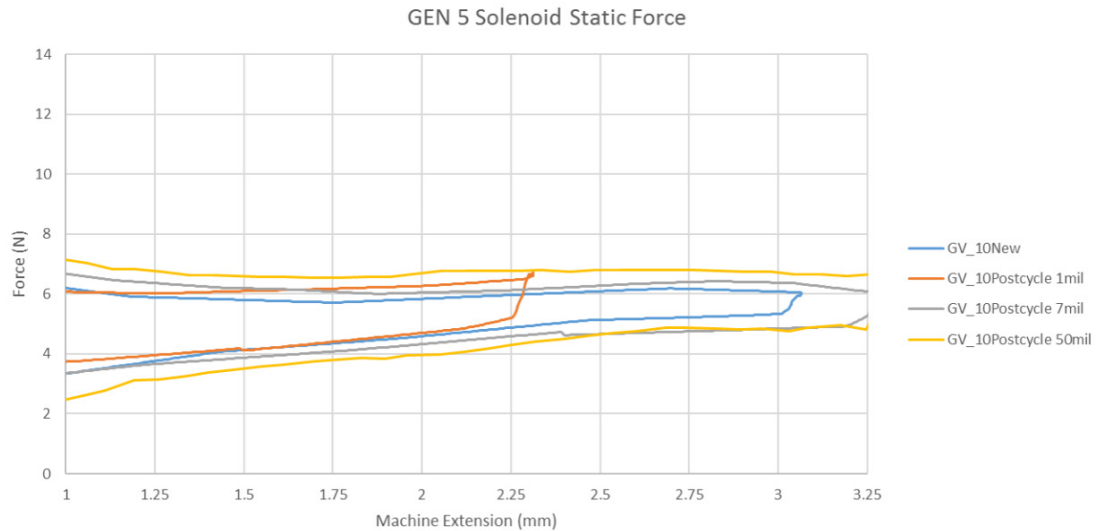


Figure V.10.3. GEN 5 solenoid force vs. stroke throughout durability test

- Complete modification of all required development cylinder heads to accommodate valve train and actuation hardware.
 - The production VW EA888 cylinder head received minor modifications in order to accommodate the selected DSF valve train hardware. The main modification was the choice of replacing the production upper cam bearing assembly with a custom fabricated part. The production upper bearing assembly is integrated into the cam cover, which was believed would make the many assembly and disassembly cycles performed during development difficult. For this reason, the upper bearing assembly was separated from the cam cover. Separate solenoid holders were added. Some modifications were made to the positive crankcase ventilation structure to accommodate the space requirement for the aft intake solenoid. Bulkhead wire connectors with protective metal conduit were added as a development-level wiring design. All cylinder heads required for this project were modified and received. Figure V.10.4 below shows one of our fully modified head assemblies running on a test stand during one of our durability tests. Note that a clear Plexiglas cam cover is used in place of aluminum covers for ease of inspection during this test.

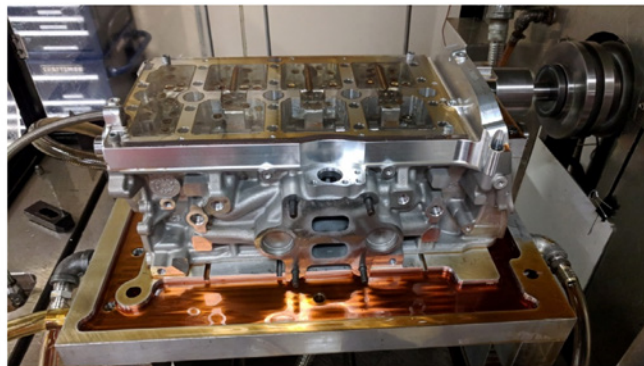


Figure V.10.4. Complete DSF cylinder head assembly on test stand

- Design, build, and verification of an ADM capable of driving direct solenoid actuators.
 - ADM requirements were completed based on solenoid and full system design. The ADM architecture design was analyzed, and the hardware build was completed. All hardware required for this project was built. Bench testing was completed to determine whether the ADM was capable of meeting system response as well as fault detection requirements. This hardware was used for previously discussed solenoid durability development testing and has proven to be very reliable. A picture of an ADM is shown in Figure V.10.5.



Figure V.10.5. Actuator driver module

- FiniWiring harnesses to connect the engine control module to the ADM were completed. Wiring harnesses to connect the ADM to the cylinder head bulkhead connectors were also completed and are being used in durability testing.
- Procurement, build, and setup of engine for baseline dyno testing.
 - A VW EA888 GEN 3 engine was procured for this project. The engine was assembled, instrumented, and installed into a dyno cell for baseline testing. The intent of baseline testing is to establish baseline fuel economy for comparison with DSF modified engine tests to be conducted next budget period. Figure V.10.6 shows the baseline engine installed in a dyno cell.

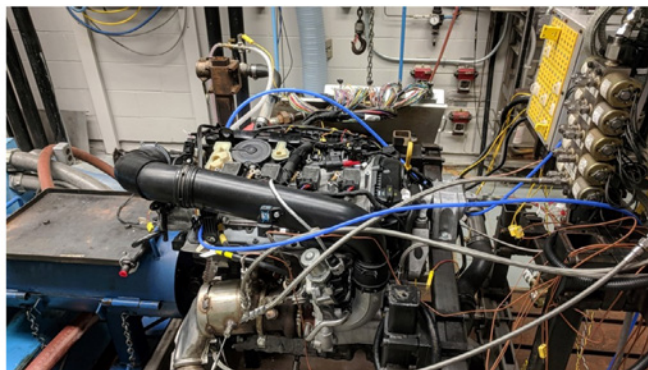


Figure V.10.6. Baseline engine installed in dyno cell

Conclusions

- Up-front DRFF probe hardware build and test cycles were effective in identifying problems ahead of final engine-level hardware build. The project team was able to identify a friction issue with enough time to create and evaluate a redesign ahead of placing a large order. This process led to lower risk of having to resolve final build hardware issues. To date, testing has not found any performance or durability issues with our final build hardware.
- Similar probe hardware build and test cycles performed on the solenoid have proven to be even more beneficial, and they have uncovered a few issues ahead of final engine-level hardware build. A limited number of parts of a new GEN 5 design have been tested, which have met all performance and durability requirements. Hardware has been received for the full engine-level build, but as of this writing, the hardware has not yet been assembled and tested.
- The ADM design has proven to effectively drive solenoids in the application at temperature extremes (140°C) and low voltage (10 VDC) over several million cycles. The team is awaiting completion of the final solenoid assembly in order to complete evaluation of the full system.

Key Publications

1. S-N/A, Docket No. DP-324785, eDEAC Z STRAP patent application submitted on 07/09/2018. Robert M. Mariuz, Kevin R. Keegan, Peter Charles, and Hermes A. Fernandez are the inventors.
2. S-N/A, Docket No. DP-324738, NON MAGNETIC CENTERING SLEEVE, submitted on 04/19/2018. Kevin R. Keegan, Hermes A. Fernandez, Robert M. Mariuz, Catherine C. Vavonese, and Jacob Daniels are the inventors.
3. S-N/A, Docket No. DP-324748, CONTROL ROD TRIGGER, submitted on 05/02/2018. Kevin R. Keegan, Hermes A. Fernandez, Robert M. Mariuz, Catherine C. Vavonese, and Peter R. Charles are the inventors.
4. S-149,210, iEdison Invention 10042275-18-0002, Docket No. DP-324592, SIDE LOCK MECHANISM FOR ROCKER FINGER FOLLOWER, originally submitted on 11/15/2017, resubmitted on 1/24/2018. Robert Mariuz, Kevin R. Keegan, Hermes A. Fernandez, and Richard B. Roe are the inventors.

Acknowledgements

Ralph Nine, Program Manager, National Energy Technology Laboratory

V.11 Temperature-Following Thermal Barrier Coatings for High-Efficiency Engines (HRL Laboratories, LLC)

Dr. Tobias Schaedler, Principal Investigator

HRL Laboratories, LLC
3011 Malibu Canyon Road
Malibu, CA 90265
E-mail: taschaedler@hrl.com

Ken Howden, DOE Technology Development Manager

U.S. Department of Energy
E-mail: Ken.Howden@ee.doe.gov

Start Date: January 1, 2017	End Date: December 31, 2019	
Project Funding: \$2,800,000	DOE share: \$1,400,000	Non-DOE share: \$1,400,000

Project Introduction

Temperature-following insulation allows surfaces to cool down rapidly during the intake and compression stroke of a combustion engine. This helps with volumetric efficiency and compression work and mitigates engine knock. During combustion, the temperature-following coating insulates the chamber to reduce heat rejection into the cooling system and thereby increases efficiency.

Over the entire cycle, the benefits of conventional insulation are negated by the increased compression work and higher tendency for engine knock. When temperature-following insulation is used, improvements can be seen over a metal surface in compression and expansion. This allows in-cylinder insulation to provide all the benefits of lower heat rejection, but with none of the volumetric efficiency or knock drawbacks.

Objectives

Overall Objectives

- Increase internal combustion engine efficiency by 4–8% with temperature-following thermal barrier coatings (TBCs)
- Add less than ~\$250 in cost to a four-cylinder engine with new coated parts
- Decrease heat loss from the combustion chamber
- Develop TBCs with extremely low thermal conductivity and heat capacity based on high-temperature alloy microshells
- Apply these TBCs to valve faces, piston crowns, and exhaust port liners, and subsequently test in single-cylinder engine

Fiscal Year 2018 Objectives

- Demonstrate >2% efficiency gain and TBC survival of first-generation valves, pistons, and exhaust ports in successful engine test
- Define scalable low-cost process for microshell fabrication
- Define process to coat valves, pistons, and port liners

Approach

Thermal conductivity and volumetric heat capacity were independently varied to determine the material properties necessary for maximizing the temperature swing. High levels of porosity were determined to be necessary to decrease the volumetric heat capacity, density, and thermal conductivity.

It was determined that 90–95% porosity was necessary to achieve a large enough surface temperature swing. HRL developed hollow nickel-alloy microsphere TBCs. These microspheres can be sintered together to form high-temperature metal matrices with over 90% porosity. Engine parts are coated and sent to General Motors Research and Development to utilize the test facility. A single-cylinder test cell is used to test parts with these coatings and evaluate improvements in efficiency as well as coating durability.

Results

Task 1: Modeling

Modeling results, detailed in the 2018 first quarter report, show that a poor bond in a piston or punctures and damage to the sealing layer will cause substantial efficiency losses. Significant efforts have been taken during this budget period to mitigate these issues and are detailed in the quarterly reports.

Task 2: Coating Development

Improvements have been made to the thermal microshell coating to improve packing density and surface sealing, as shown in Figure V.11.1 and Figure V.11.2. This progress is applicable to piston and valve coating and surface sealing. Details are given in the quarterly technical reports.

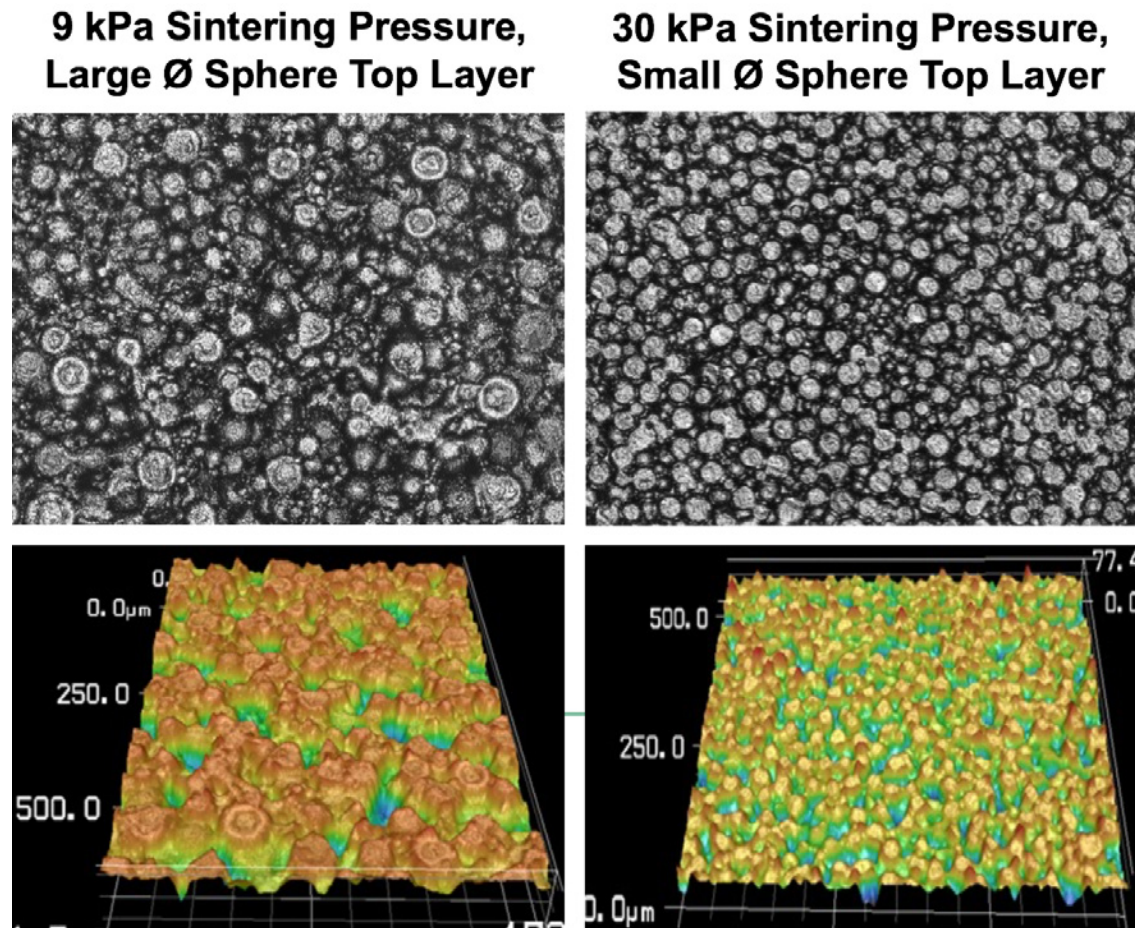


Figure V.11.1. Surface roughness is greatly improved by filtering spheres for size and using a top layer of small-diameter spheres sintered under pressure; this results in a more robust sealing layer

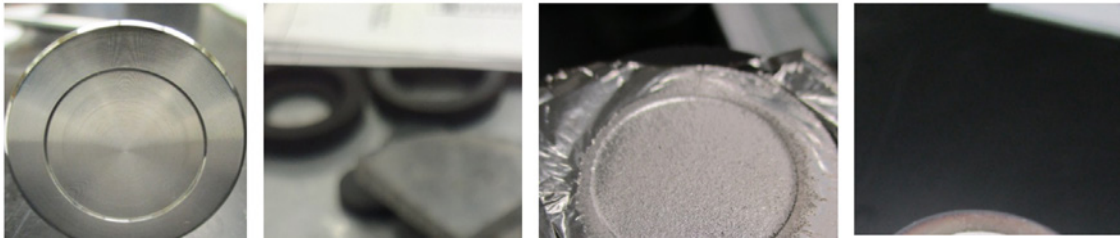


Figure V.11.2. Valve prototypes with microshell TBC applied to the face were fabricated by (1) machining stainless steel valves with a pocket in the face, (2) filling the pocket with nickel microspheres and sintering, (3) bonding a nickel foil to the surface, and (4) final heat treatment and clean-up

The process for coating exhaust ports evolved to produce a liner with less surface roughness, shown in Figure V.11.3. More on this process can be found in the third quarter report.



Figure V.11.3. Exhaust port liner coating process begins with (1) plating a core with solid nickel to form a shell once the core is dissolved, (2) spraying the shell with a TBC microshell and binder slurry and sintering, and (3) spraying over the TBC with a ceramic protective coating and curing

Task 3: Testing

Engine test results during the second quarter showed that the surface roughness of the unsealed exhaust port resulted in higher heat losses than an uncoated port liner, shown in Figure V.11.4. The third quarter was spent developing a better method for coating exhaust port liners that results in a smooth surface, discussed under Task 2. Details on engine tests can be found in the quarterly reports.

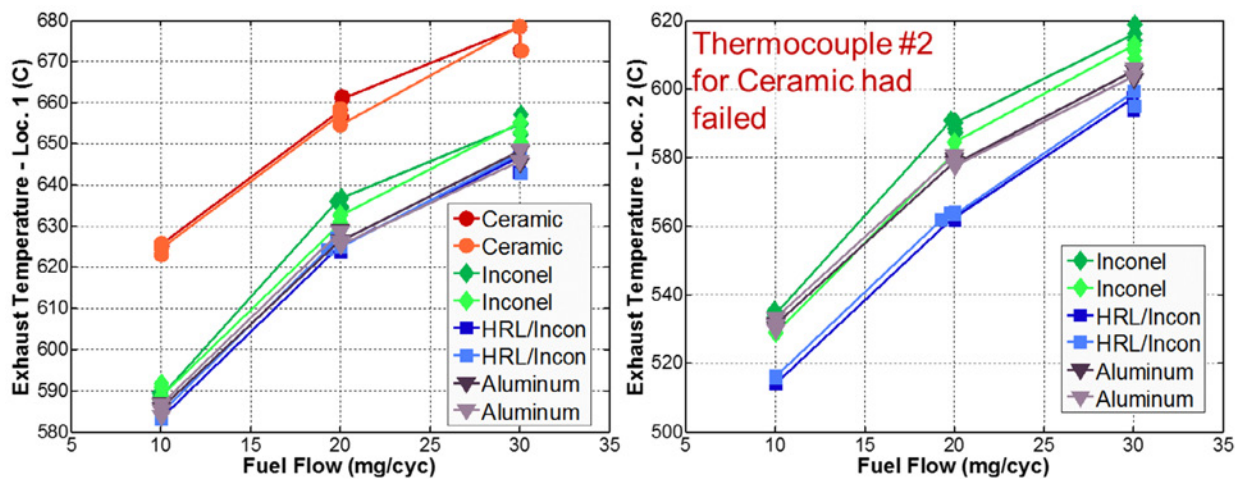


Figure V.11.4. Exhaust temperatures in the center (left) and near the wall (right) at the exhaust port exit

Several iterations of Generation 2 exhaust valves were tested by General Motors during the third quarter, shown in Figure V.11.5, with improved results compared to Generation 1. Results are detailed in the third quarter report.

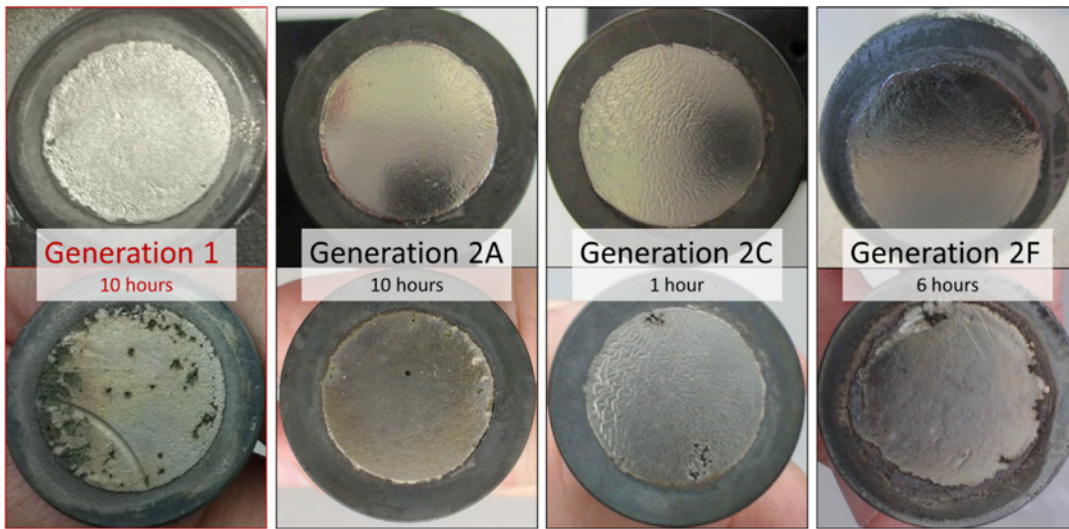


Figure V.11.5. Pre- and post-test conditions of Generation 2 coated valves vs. Generation 1

Project Schedule Status

The three milestones M1.3.3, M2.2.1, and M2.2.2 have been accomplished on schedule as shown in Table V.11.1. Details on how the milestones were accomplished are given in the quarterly technical reports. Milestone M2.2.3 is in progress and on track to be completed on time. The go/no-go milestone was scheduled for December 15, 2018, but engine tests of coated pistons failed before efficiency could be determined due to debonding of the coating. Difficulties in brazing coatings to the aluminum piston crown further delayed tests. Therefore, a no-cost extension for the second budget period through June 30, 2019, was requested. This will allow additional engine tests with improved aluminum pistons as well as steel pistons.

Table V.11.1. Milestone Status

Milestone	Type	Anticipated		Actual		% Complete
		Start	Completion	Start	Completion	
M1.3.3 Successful engine test	Go/No-Go	9/30/17	12/15/17	3/10/17	12/30/17	100%
M2.2.1 Scalable low-cost process for microshell fabrication defined	Technical	1/1/18	6/30/18	1/1/18	6/30/18	100%
M2.2.2 Process to coat valves, pistons & port liners defined	Technical	1/1/18	9/30/18	1/1/18	9/30/18	100%
M2.2.3 Scalable low-cost process to seal coatings defined	Technical	1/1/18	12/15/18	1/1/18		60%
M2.2.1 Scalable low-cost process for microshell fabrication defined	Go/No-Go	6/1/18	12/15/18	6/1/18		0%

Conclusions

Results Summary

- Developed TBC material with desired thermal properties: low thermal conductivity and heat capacity
- Determined through testing that further development is needed to improve TBC structural properties and part integration
- Improved TBC structural properties by order of magnitude and currently developing better methods for part integration; validated through valve testing
- Started development of promising alternative sealing layer methods

Next Steps

- Fabricate pistons for testing using improved TBC structural properties and part integration methods
- Demonstrate actual efficiency gains from TBC with piston test
- Develop exhaust port liners for testing and continue work on improving sealing method

Key Publications

Invention Disclosure: “A Method to Cast Thermal Barrier Coatings in Sand or Granular Media Casting Processes.” Michael Walker, Paul Najt, and Russell Durrett. Submitted August 2018.

VI. Lubricant Technologies

VI.1 Power Cylinder Friction Reduction through Coatings, Surface Finish, and Design (Ford Motor Company)

Arup K. Gangopadhyay, Principal Investigator

Ford Motor Company
2101 Village Rd.
Dearborn, MI 48121
E-mail: agangopa@ford.com

Ali Erdemir, Principal Investigator

Argonne National Laboratory
9700 Cass Avenue, Building 212
Argonne, IL 60439
E-mail: erdemir@anl.gov

Michael Weismiller, DOE Technology Development Manager

U.S. Department of Energy
E-mail: Michael.Weismiller@ee.doe.gov

Start Date: January 1, 2015	End Date: December 31, 2018	
Project Funding: \$1,070,000	DOE share: \$820,000	Non-DOE share: \$250,000

Project Introduction

Approximately 7–10% of the total energy input in a vehicle is lost due to mechanical friction [1]; therefore, there are great opportunities for friction reduction. In an engine, about 60% of the total frictional losses occur at the interface between the cylinder and pistons and piston rings, and about 30% at the bearings [2]. The goal of this study is to demonstrate friction reduction potential using advanced high-porosity plasma transfer wire arc (HP PTWA) coatings, surface finish, and design on power cylinder systems containing cylinder bore, piston rings, piston skirt, bearings and crankshaft, and advanced engine oils. Experience through years of research in this area leads us to believe that full benefit potential can be realized only by considering a systems approach.

This project developed (a) a process for depositing and honing HP PTWA coatings to achieve different porosity levels with improved surface finish on free-standing cylinder liners and engine blocks; (b) various techniques for characterizing coatings, including porosity area percent, porosity size distribution, oxide content, etc.; (c) a method for achieving micro-polishing crankshaft journals; (d) a technique for depositing nano-composite VN-Cu and VN-Ni coatings on piston ring and piston skirts; (e) a method for laboratory friction and wear assessment for generating a Stribeck curve; (f) a method for evaluating friction reduction potential of HP PTWA coatings and micro-polished journals using a motored cranktrain rig; and (g) a method for evaluating wear (durability) of HP PTWA coating and ring coatings using a radio tracer method.

Objectives

Overall Objectives

- Demonstrate deposition of HP PTWA coatings at various porosity levels on liners and engine blocks with improved surface finish
- Develop and demonstrate deposition of nano-composite coatings on piston rings and skirts
- Demonstrate friction benefits of micro-polished crank journals

- Demonstrate friction benefits through laboratory bench, motored cranktrain and engine, fired single-cylinder engine, and chassis roll dynamometer (vehicle) tests
- Demonstrate durability of HP PTWA coatings using radio tracer method technique

Fiscal Year 2018 Objectives

- Demonstrate friction benefits of HP PTWA coatings in engine cranktrain
- Demonstrate friction benefit of ring face coating technologies in laboratory bench, motored single-cylinder, and motored engine cranktrain tests
- Demonstrate friction benefit in a motored engine

Approach

The project goal of delivering 4% fuel economy improvement over current (2014) technologies can be achieved through a technology bundle comprising (a) deposition of low-friction coating (HP PTWA) on cylinder bores, (b) low-friction nano-composite coatings for piston rings and skirts, (c) improved surface finish on cylinder bores and crankshafts, and (d) novel engine oil formulation (polyalkylene glycol), an outcome of a previous DOE-funded project.

Achieving the project goals necessitated partnering with key suppliers, including (a) Comau for deposition of bore coatings, (b) Gehrung for cylinder bore honing of HP PTWA coatings, (c) Paramount for mechanical roughening treatment prior to coating deposition, (d) NETZSCH for assessment of coating thermal properties, (e) Mahle and KS for low-friction piston skirt and piston ring coatings, (f) Southwest Research Institute for single-cylinder fired engine tests, and (g) The Dow Chemical Company for novel polyalkylene glycol engine oil.

Results

The efforts were primarily focused on two areas: deposition and honing of HP PTWA coatings on free-standing 92.5 mm liners of varying porosity levels and friction evaluations on (i) laboratory ring-on-liner reciprocating machines, (ii) cranktrains, and (iii) full engines under motoring conditions. The liner diameter represents one of the current production engines. It was observed that although the engine blocks had high porosity levels, they were lower than the target values. This was believed to be due to the use of a different plasma torch, which may have different spray characteristics. Porosity analysis of coupons deposited by different plasma torches was completed and found no significant difference. Therefore, the focus was shifted to identifying suitable honing conditions to reach targeted porosity levels. A design matrix was created to address this in a few phases. Initial results were encouraging. Additional honing conditions were identified and several liners were coated and are currently being honed. This will be followed by detailed porosity analysis. Once the exact honing conditions are identified, cast iron liners will be processed for single-cylinder fired engine friction evaluation, and additional aluminum engine blocks will be processed for chassis roll friction evaluations and wear measurements on HP PTWA coating and piston rings using radiotracer methods.

Laboratory Bench Test Friction Assessment

Sections were cut from liners for coating characterization and friction evaluation using a Plint TE-77 reciprocating laboratory test rig, where a section of a ring reciprocated against a liner section at various temperatures (30°C, 50°C, 80°C, 120°C), loads (50 N, 100 N, 150 N), and frequency (2 Hz, 5 Hz, 10 Hz, 20 Hz, 30 Hz) in the presence of GF-5 SAE 5W-20 engine oil. Figure VI.1.1 shows the coefficient of friction (COF) as a function of engine oil viscosity and reciprocating speed for HP PTWA coating against various ring face coatings obtained from one of our suppliers (different from those reported in the 2017 annual report). The HP PTWA liner section was mirror polished, an outcome of the honing process. The data clearly indicate HP PTWA coatings offer friction reduction opportunities with different ring face coatings. In contact with diamond-like carbon (DLC) coatings, reduced COF was observed under the boundary lubrication regime (low $\mu_{v,max}$ values), whereas physical vapor deposition (PVD) and nitride coatings showed reduced COF under mixed lubrication regime. Nitride coating performed best with HP PTWA coating compared to the baseline material pair (cast iron liner and production ring).

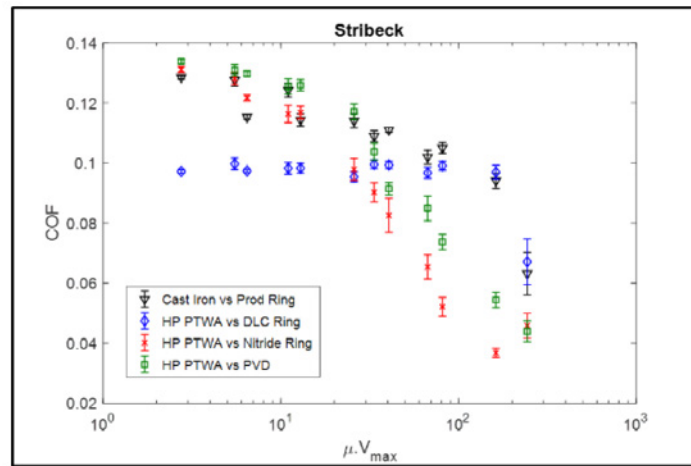
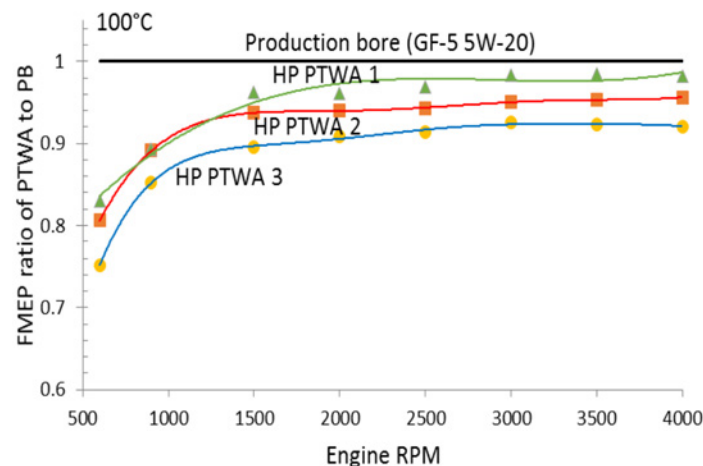


Figure VI.1.1. HP PTWA coating shows friction benefits with DLC, PVD, and nitride ring face coatings

Motored Cranktrain Friction Assessment

Cranktrain friction was evaluated using a block from an I-4 engine. The friction contributions on this rig are from the bearings (main and connecting rod), piston skirt, and piston rings in contact with cylinder bore. GF-5 SAE 5W-20 engine oil was used at 40°C, 60°C, 100°C, and 120°C. Engine blocks with HP PTWA coatings having various porosity levels were evaluated against current production piston rings. The blocks were carefully assembled to maintain a fixed piston-to-bore clearance and nominal bearing clearance to avoid confounding of friction results. Figure VI.1.2 shows improvement in friction torque (as friction mean effective pressure [FMEP]) as a function of engine speed at 100°C oil temperature for engine blocks with different HP PTWA coatings in contact with production piston rings. The black line represents friction torque for cast iron block with production piston rings. The results indicate HP PTWA blocks offer up to 25% friction reduction depending on engine speed and choice of HP PTWA block. Similar results were obtained at other engine oil temperatures. Figure VI.1.3 shows the effect of ring face coating on FMEP at 100°C oil temperature. PVD and nitrided rings showed up to 20% friction reduction with production cast iron liner at higher engine speeds. Both PVD and nitride rings exhibited excellent (up to 30%) friction reduction against HP PTWA 3, particularly at lower engine speeds, which is particularly important as engine speed is reduced with the use of higher-speed transmissions.



PB – production bore; RPM – revolutions per minute

Figure VI.1.2. Cranktrain friction as a function of engine speed at 100°C oil temperature for various HP PTWA coatings

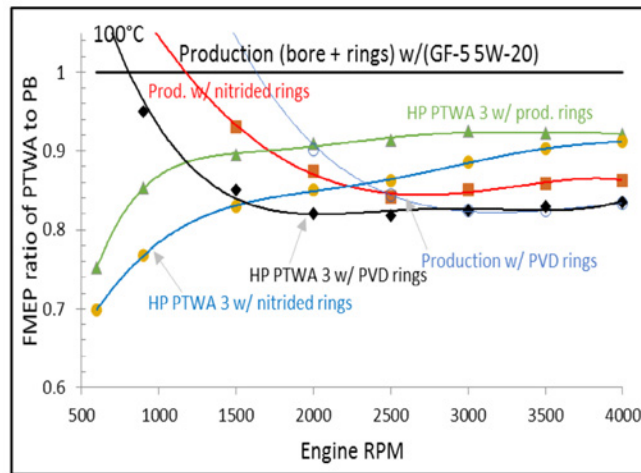


Figure VI.1.3. Cranktrain friction as a function of engine speed at 100°C oil temperature for various piston ring face coatings with HP PTWA 3 coating

Motored Single Cylinder Friction Assessment

Friction force measurements were conducted under unpressurized conditions using the motored single-cylinder rig. The measurements were done with current production cast iron liner (92.5 mm bore diameter) with different ring face coatings, including Argonne National Laboratory produced VN-Cu nano-composite coating, at various temperatures. Results in Figure VI.1.4 show friction force measured as a function of crank angle at 750 rpm and 100°C oil temperature using GF-5 SAE 5W-20 oil. Crank angles 0–180 represent piston motion in one direction, while crank angles 180–360 represent motion in opposite direction. The area under the curve represents friction force for one complete rotation of the crankshaft. The friction force for the production ring is 7.12 N, while that of PVD, nitrided, and VN-Cu coatings are 11.2 N, 3.38 N, and 10.2 N, respectively. The higher friction force with PVD coating compared to the production rings is consistent with motored cranktrain friction data, where higher friction torque was observed with this coating at lower engine speed, but significant improvements were observed at higher engine speeds. Nitrided coating showed the lowest friction among all ring coatings.

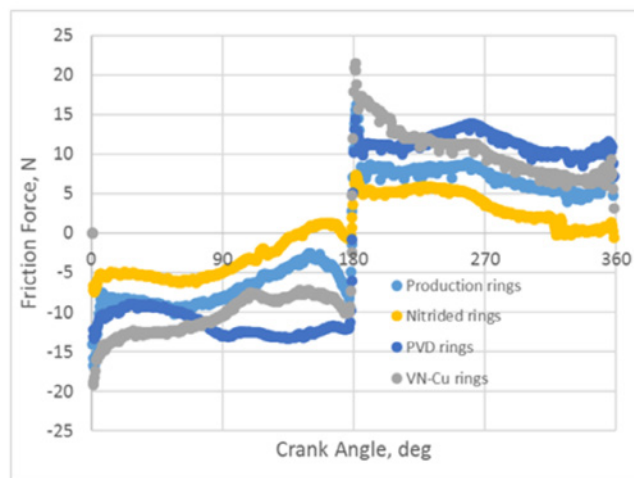


Figure VI.1.4. Cranktrain friction as a function of engine speed at 100°C oil temperature for various piston ring face coatings with HP PTWA 3 coating

Motored Engine Friction Assessment

Figure VI.1.5 shows motored engine friction results obtained for various HP PTWA coatings and compared with production cast iron block with production piston rings using GF-5 SAE 5W-20 oil at 100°C. HP PTWA 3 showed an average (over engine speed range investigated) 5.1% lower friction.

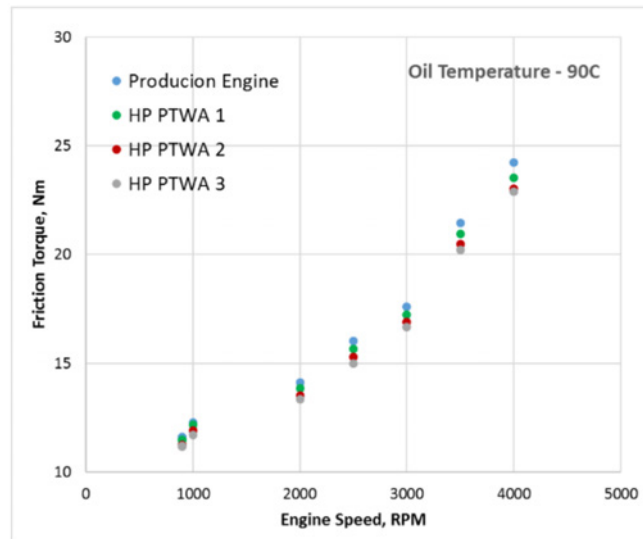


Figure VI.1.5. Motored engine friction tests showed HP PTWA coatings offer friction benefit

Conclusions

- HP PTWA coatings showed up to 5.1% friction benefit over cast iron liner block in motored engine tests.
- Ring face coatings offer additional friction benefits with HP PTWA coatings.

References

1. Pinkus, O., and D.F. Wilcock. 1977. "Strategy for Energy Conservation through Tribology." New York, ASME.
2. Kiovsky, T.E., N.C. Yates, and J.R. Bales. 1994. "Fuel Efficient Lubricants and the Effect of Base Oils." *Lubrication Engineering* 50 (4): 307.

Acknowledgements

Thanks to Osman Eryilmaz of Argonne National Laboratory for integral contributions to the project.

VI.2 Integrated Friction Reduction Technology to Improve Fuel Economy Without Sacrificing Durability (George Washington University)

Stephen Hsu, Principal Investigator

George Washington University
323C Exploration Hall, 20101 Academic Way
Ashburn, VA 20147
E-mail: Stevehsu@gwu.edu

Michael Weismiller, DOE Technology Development Manager

U.S. Department of Energy
E-mail: Michael.Weismiller@ee.doe.gov

Start Date: October 1, 2014	End Date: September 30, 2019	
Project Funding: \$2,000,000	DOE share: \$1,000,000	Non-DOE share: \$1,000,000

Project Introduction

The use of petroleum-based fuels to propel vehicles to transport people and goods is the major oil use in the United States, resulting in imports of about 10 M barrels of oil per day in 2016. Improving the fuel economy of cars and trucks will reduce United States dependence on foreign oil. The new corporate average fuel economy standard has raised the fuel economy of cars and light trucks from 27.5 mpg in 2012 to 54.5 mpg by 2025. This project supports the energy independence goal.

In a worldwide effort to improve fuel economy, Japanese automakers have introduced a new class of ultra-low-viscosity lubricants to reduce drag and improve fuel economy. This new class has three viscosity grades: 0W-16 (defined by 2.3 mPa.sec viscosity at 150°C), 0W-12, and 0W-8. The technical concern for the low-viscosity oils is that the resultant thin oil film thickness may cause wear. This project aims to (1) develop a prototype 0W-20 low-viscosity oil and demonstrate that it can improve fuel economy by 2%, is backward compatible, and is suitable for use by current cars and light trucks; (2) develop a prototype 0W-16 ultra-low-viscosity oil and demonstrate that it can improve fuel economy by 2% against current commercial oils; and (3) develop engine durability test protocols to evaluate engine durability using 0W-16 oils.

Objectives

Overall Objectives

- Develop 0W-20 and 0W-16 low-viscosity lubricants that will improve fuel economy by 2%
- Conduct industrial standard engine tests to verify fuel efficiency
- Measure engine durability while using the ultra-low-viscosity lubricant
- Develop and measure the effects of surface textures and coatings on engine durability

Fiscal Year 2018 Objectives

- Fabricate surface textures on the new 2018 platform engine for fuel economy testing
- Develop vehicle test protocols to confirm fuel economy improvement using the new engine

Approach

- A vertically integrated technical research team was formed with members from engine manufacturer, oil marketer, and additive companies to develop a comprehensive strategy to achieve the objectives. The team formed includes General Motors (GM), Valvoline, Afton, and Vanderbilt. Many other additive companies agree to provide experimental additive chemistries.

- Valvoline and GM participate in this project actively and provide advice and engine testing. Valvoline provides formulation guidance and oil testing, and GM provides new engines and test development.
- George Washington University conducts basic and applied research in additive evaluation, additive interactions, and microencapsulation of additives and surface texture (design and fabrication techniques).

The team was initially organized in 2014 at the beginning of the project. Subsequently, many industrial and academic organizations have collaborated with this effort. Over 120 additive components and base oils have been received from industrial partners and collaborators. Four generations of formulations were developed and tested. The 0W-20 was first tested in ASTM Sequence Engine Dynamometer test IV-E and achieved 2.4% fuel economy improvement against current commercial lubricants, meeting the key goal. The 0W-16 is intended for future engine platforms, which have evolved rapidly since 2014. In order to comply with this new reality, the team decided to switch the test engine from the 2009 V-6 engine to the new modern V-8 engine equipped with most of the fuel-efficient technologies. This prompted a one-year request of no-cost extension in 2017. The new engine has incorporated many new materials technologies and posed many challenges in surface texture fabrication. To overcome these challenges, the team requested a second extension in 2018. This report describes the new vehicle testing protocols and the completion of surface texturing of engine parts.

Results

For Fiscal Year 2018, under the second revised project management plan, the key objectives are to (1) overcome the technical challenges in fabricating textures on engine components which already have grooves and organic-inorganic coatings and (2) confirm that the ASTM Sequence VI-E engine test results showing that low-viscosity lubricants improve the fuel economy are valid for a 2018 engine equipped with current fuel-efficient technologies.

Key accomplishments:

- A chassis engine dynamometer test was used to measure fuel economy difference among the 5W-30 (the prevalent current lubricant used in the United States), the 0W-20 “GF-6A” low-viscosity formulation, and the 0W-16 “GF-6B” formulation using Environmental Protection Agency (EPA) cycles. Results confirm fuel economy improvement of the low-viscosity lubricants.
- Surface textures were completed on new V-8 engine parts, and the parts were delivered to GM.

DOE Technical Targets and Objective

The 2015 technical target of 2% fuel economy increase for cars and light trucks (the legacy fleet) was attained via advanced lubricants without sacrificing engine durability.

Technical Details

The research team has developed three generations of 0W-16 oil formulations. Some were tested in the ASTM Sequence VI-E engine dynamometer fuel economy tests and compared to the baseline oil (GF-5 5W-30 commercial oil). We have engine test data on the baseline oil (GF-5 5W-30), GF-6A 0W-20 formulation, and the GF-6B 0W-16 formulations. The 0W-20 oil achieved 2.4% fuel economy improvement in Sequence VI-E while the 0W-16 showed 2.1% fuel economy improvement. Both test results met the proposed targets mandated by the DOE solicitation.

At the same time, the auto industry is going through unprecedented change in an attempt to reach the corporate average fuel economy standards of 54.5 mpg by 2025. Materials and engine designs changed rapidly and by 2018, engines and vehicle technologies no longer bear any resemblance to the Sequence VI test engines (2009 Cadillac V-6 engine). Therefore, the team decided to change the engine to the 2018 platform engine, a V-8 engine with advanced fuel-efficient technologies. The test engine used is the Gen-V 5.3 L V-8 in a Silverado vehicle. The engine has been updated to enhance its fuel efficiency. It has many fuel economy technologies, such as direct injection, active fuel management (cylinder deactivation), and dual-equal camshaft phasing (variable valve timing) that support an advanced combustion system. The engine components also have many

coatings and surface treatments, including directionally aligned shallow grooves on some of the bearings and improved hard coatings on rings.

To evaluate the fuel efficiency of the oil formulations in a vehicle, an oil flush/fill routine is necessary before and after the fuel economy test of the oil. SAE 5W-30 GF-5 oil was used as the baseline oil. Five candidate oils were tested against the baseline: GF-6A (0W-20), three GF-6B (0W-16) oils, and one commercial 0W-16 oil. The test sequence consists of baseline oil, candidate oil, and baseline oil tests to ensure valid statistical comparisons. If the engine severity shifts, the bracketing baseline oil test results would reveal variations in the baseline oil test results. While this is technically correct, the cost of all these engine tests is very significant.

The fuel efficiency test cycle consists of five tests, one per day for five days. Each day, the test starts with a cold start FTP-75 (EPA city driving cycle), followed by a double highway test cycle (FFE), and finally by a high-speed, high-acceleration test cycle, the US06 test cycle. The US06 Supplemental Federal Test Procedure was developed to address the shortcomings with the FTP-75 test cycle in the lack of aggressive, high-speed and/or high-acceleration, rapid-speed-fluctuation test cycles. To evaluate the fuel efficiency of the oil formulations in this engine, the engine was installed in a Silverado light truck. The test follows oil flush/fill routine steps before and after the fuel economy test. Note this is a short-duration test with high precision to identify the effect of lubricant chemistry on fuel economy. Summary test results are shown in Table VI.2.1. This new generation of low-viscosity-potential GF-6B oils does show fuel economy improvements when compared to the baseline oil, 5W-30 GF-5 current commercial premium oil.

We have tested three George Washington University 0W-16 oil formulations. They all showed improvement in cold start city driving cycle but much less improvement in highway test cycle (still showing improvements). In the US06 driving cycle, the 0W-20 maintained 1.1% fuel economy gain, but the low-viscosity oils showed very little improvement if any. There were potentially two factors in play during the tests using this V-8 L83 engine: (1) cylinder deactivation of the engine and (2) increased surface contacts resulting in higher friction under high-load, high-temperature test cycles such as the highway and US06 test cycles.

Table VI.2.1. Percent Improvement of Fuel Efficiency of 0W-16 Formulations

	FTP City Cycle mpg	FFE Highway mpg	Combined Mpg	US06 mpg
Baseline GF-5 5W-30	23±0.05	36±0.04	27.5±0.04	20±0.14
GW G1 "GF-6A" 0W-20	+1.11%	+0.39%	+0.87%	+0.87%
GW G1 "GF-6B" 0W-16 (A)	+1.33%	+0.47%	+0.99%	+0.87%
GW G2 "GF-6B" 0W-16 (B)	+1.66%	+0.08%	+0.95%	+0.87%
GW G3 "GF-6B" 0W-16 (C)	+1.05%	+0.92%	+1.16%	+0.87%
Top Tier com. 0W-16 oil	+1.16%	-0.02%	+0.76%	+0.87%

This engine chassis dynamometer test uses two separate ways to measure fuel consumption: metered fuel pump and tailpipe carbon analysis. The variations of the engine tests are monitored by running baseline oil before and after a candidate oil run. The fuel economy test severity shifts are monitored, and the candidate performance is adjusted based on the baseline oil performance. The accuracy of the results is estimated at ±5% of the results. The principle causes for variations are graduate shift in engine build, air moisture content, and wear-in of the engine sliding components.

As can be seen from Table VI.2.1, a total of six candidate oils were tested. Because of the test precision correction, a total of 16 baseline oil samples were tested to ensure valid comparison. The test results, in general, all show fuel economy improvements under the normal EPA fuel economy testing protocols. The

combined city and highway column summarizes the overall fuel economy test results of a particular oil formulation under EPA fuel economy test protocol. As one can see, there are some trade-offs between city and highway cycles for some formulations. GW G2 sample has the highest city driving cycle fuel economy gains (+1.66%) but also has the lowest highway performance (+0.08%). GW G3 has the highest combined fuel economy gain (+1.16%). This balance between city driving cycle and highway driving cycle is evident for all the oils. This balance may be attributed to the kind of friction modifiers being used and the balance between organic friction modifier and solid film friction modifier.

The US06 test is outside of the EPA fuel economy testing procedure. It is included in this test sequence to explore the test cycle to be used in the durability test later on in the program. In the US06 test cycle, 0W-16 oils did not show much improvement over the baseline oil.

Surface Texture Fabrication

The fabrication of surface textures on engine components has been presented in detail in the 2017 annual report. We are using a once-through soft mask to couple with electrochemical etching on engine parts. The one-step soft mask was developed in 2017, and many of the engine parts have not been textured due to additional interference from existing coatings and surface textures (simple shallow grooves in the direction of sliding). The soft mask can be used to impart complex location-specific texture for smooth surface. The presence of micro-grooves and organic/inorganic coatings tends to increase the overall surface roughness. This tends to create air bubbles trapped between the mask and the surface when the mask is applied to bearings and other concave surfaces. After much research and trials, small jigs were designed and used to put the soft mask on the surface, which is pre-coated with a monolayer of either hydrophilic or hydrophobic molecular layer. This approach has proven to be effective, and all the engine parts were successfully textured.

Conclusions

Based on the work accomplished this year, the following conclusions can be drawn.

- Vehicle chassis engine dynamometer tests were conducted to examine the use of ultra-low-viscosity oils. In general, the ultra-low-viscosity lubricants tested all show fuel economy improvement. This is significant in translating the ASTM engine sequence test results to modern engines equipped with most of the fuel-efficient technologies. The exact amount of fuel economy improvement will depend on engine design, materials used, duty cycles, and driving habits.
- For the new modern engine, all the parts used in tribological interfaces were textured and delivered to GM for testing fuel economy. This will be a definitive testing of the effect of surface texture on engine fuel economy.

Acknowledgements

The author wishes to acknowledge Tim Cushing, General Motors Company, and Gefei Wu, Valvoline, for their contributions to this project.

VII. System-Level Efficiency Improvement

VII.1 Improved Tire Efficiency through Elastomeric Polymers Enhanced with Carbon-Based Nanostructured Materials (Oak Ridge National Laboratory)

Georgios Polyzos, Principal Investigator

Oak Ridge National Laboratory
One Bethel Valley Road
Oak Ridge, TN 37831-6054
E-mail: polyzosg@ornl.gov

Gurpreet Singh, DOE Program Manager

U.S. Department of Energy
E-mail: Gurpreet.Singh@ee.doe.gov

Start Date: October 1, 2017	End Date: September 30, 2018	
Project Funding (FY18): \$230,000	DOE share: \$222,000	Non-DOE share: \$8,000

Project Introduction

In the United States, road vehicles account for more than 80% of motorized transportation and are considered to be the driving force for the steep growth in oil demand [1]. Several studies have indicated the importance of the tire rolling resistance for significant reductions in fuel consumption. The rolling resistance can be responsible for up to 25% of the energy required to drive at highway speeds [2], and a 10% reduction in tire rolling resistance yields fuel savings of 1%–2% [1,3]. The above-referred results are in excellent agreement with the research conducted for the California Energy Commission, which concluded that approximately 1.5%–4.5% of fuel consumption could be saved by using low-resistance tires [4]. In response to a Vehicle Technologies Office funding opportunity announcement, we proposed to develop innovative nanocomposite materials that will reduce the fuel consumption by reducing the tire rolling resistance. The targeted fuel consumption reduction will be at least 4% compared to the state of the art, while maintaining traction and wear resistance.

In materials science of elastomers, the influence of manufactured nanomaterial filler particles is of utmost significance for the performance of innovative rubber products, i.e., passenger and commercial tires with ultra-low rolling resistance but high traction. Advances in both performance areas are imperative for the development of improved tire efficiency to meet DOE's fuel consumption reduction target of 4%, all while maintaining or improving wear characteristics of the tire. Recent research efforts focus mainly on the development of composite tires based on carbon black and silica. The project goal is to replace existing fillers (such as carbon black and silica) with higher-performance materials (viz., graphene and silica nanofibers). The proposed approach capitalizes on the recent advances in nanomaterial and graphene synthesis and functionalization by our group and suggests a promising avenue for the amalgamation of cutting-edge nanotechnologies that can be utilized toward DOE's technical targets. The project will enable fabrication and testing of scalable structures, which are anticipated to demonstrate unprecedented improvements in the rolling and wear resistance of tires used in the automotive industry. The successful implementation of the project will deliver scalable composite materials and will provide processing conditions that can be utilized in advanced tire manufacturing for breakthrough fuel savings.

Objectives

The objective of the project is to reduce the hysteretic losses of elastomers that are used for manufacturing vehicle tires. Composite elastomers based on graphene and silica nanofibers will be developed. The filler material should not compromise the wear and tear resistance of the tire.

Overall Objectives

- Improve tire efficiency and meet DOE's fuel consumption reduction target of 4%
- Optimize the viscoelastic properties of the composite elastomer
- Reduce the rolling resistance of the tire

Fiscal Year 2018 Objectives

- Scale up the synthesized filler material
- Disperse the filler material in the elastomer matrix using industrial techniques
- Test the properties of the composite elastomers using industrial techniques

Approach

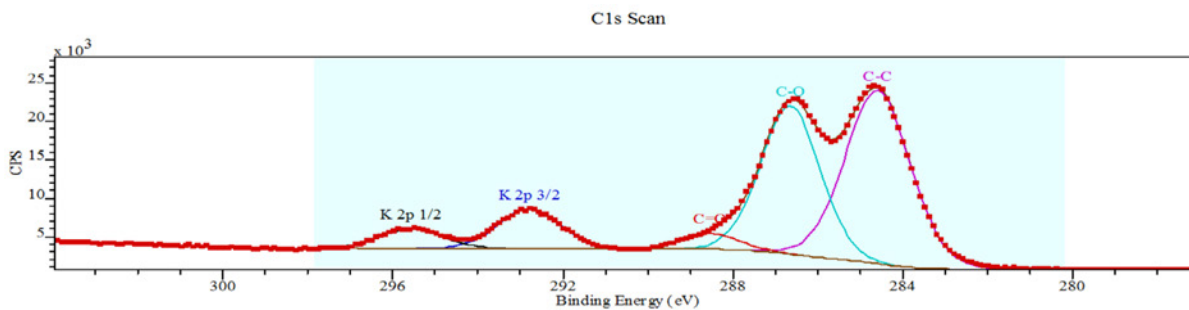
Graphene oxide (GO) nanoplatelets were functionalized with organic coupling agents based on sulfur (S) and methyl groups. The chemical composition of the fillers was investigated. The nanoplatelets were exfoliated in styrene-butadiene-rubber and styrene-butadiene-styrene (SBS) elastomers. Composite elastomers were fabricated at several filler weight contents. Mixing procedures were developed in order to achieve good dispersion of the filler material in the elastomers. We collaborated with a major tire manufacturer. The mechanical and abrasion resistance properties of the synthesized elastomers were studied.

Results*Key Accomplishments for Fiscal Year 2018*

- Sulfur groups were chemically bonded on the surface of GO filler material.
- The functionalized GO nanoplatelets were successfully reduced (rGO).
- Mixing techniques were developed to synthesize composite elastomers.
- Nano-indentation measurements were performed on composite elastomers.
- A 10-fold increase in the Modulus values was achieved for certain graphene composite elastomers.
- Abrasion testing was performed on the elastomers.
- The graphene fillers improved the wear resistance of the composite elastomer according to Taber abrasion testing.
- Safety data sheets were generated for all synthesized materials.

To improve the vulcanization of the composite tire elastomers, we introduced sulfur groups on the GO nanoplatelets by chemically attaching organic coupling agents based on S. The filler material was successfully reduced with hydrazine. The reduction was performed to decrease the oxygen content of the surface of the fillers and enhance their mechanical performance. After the hydrazine reduction, the filler material was washed with distilled water and dried in a vacuum oven. X-ray photoelectron spectroscopy (XPS) and X-ray diffraction techniques were used to characterize the surface chemistry of the prepared fillers.

XPS was used to study the covalent bond formation between the organic coupling agents and the GO. The results are summarized in Figure VII.1.1, Figure VII.1.2, and Figure VII.1.3. In brief, the C1s XPS spectra in Figure VII.1.1 and Figure VII.1.2 clearly indicate that the oxygen content of the rGO fillers decreases after the reduction process (the peak intensity at 287 eV, which is assigned to the C–O bonds, decreased in the rGO sample). In Figure VII.1.3, the peak around 400 eV, in the N1s high-resolution XPS spectrum, is attributed to the amide bond formation between GO and the coupling agent. The coupling agent was successfully covalently bonded to the GO surface.



CPS – count per second

Figure VII.1.1. High-resolution C1s XPS analysis of the functionalized GO fillers before the reduction

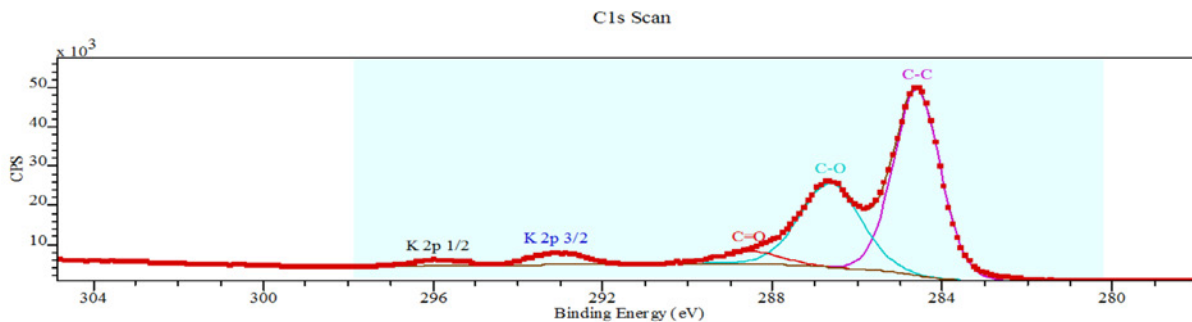


Figure VII.1.2. High-resolution C1s XPS analysis of the functionalized GO fillers after the reduction

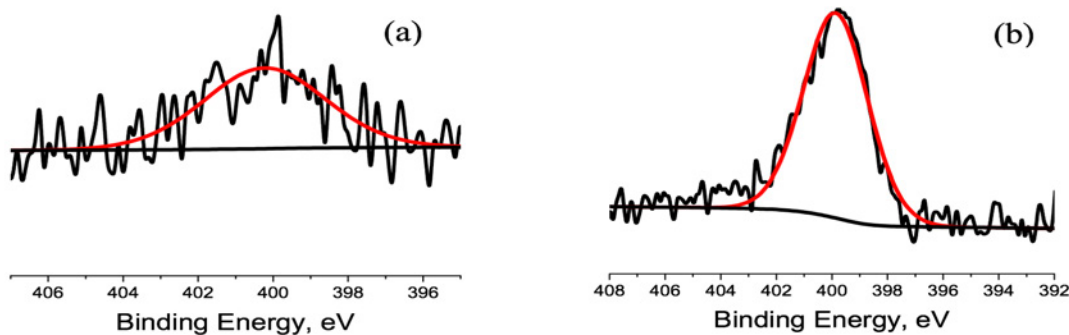


Figure VII.1.3. High-resolution N1s XPS analysis of the functionalized GO fillers (a) before and (b) after the reduction

The GO fillers were dispersed in SBS elastomer. The mixing was performed in solvent, and ultrasonic agitation was applied to assist the filler dispersion. The synthesized samples are shown in Figure VII.1.4. Nano-indentation measurements were performed on 100 different areas in each sample. The Modulus values were calculated from the maximum load versus displacement plots. The maximum Modulus improvement was approximately one order of magnitude. Similar values were obtained from the tensile (Instron) measurements.

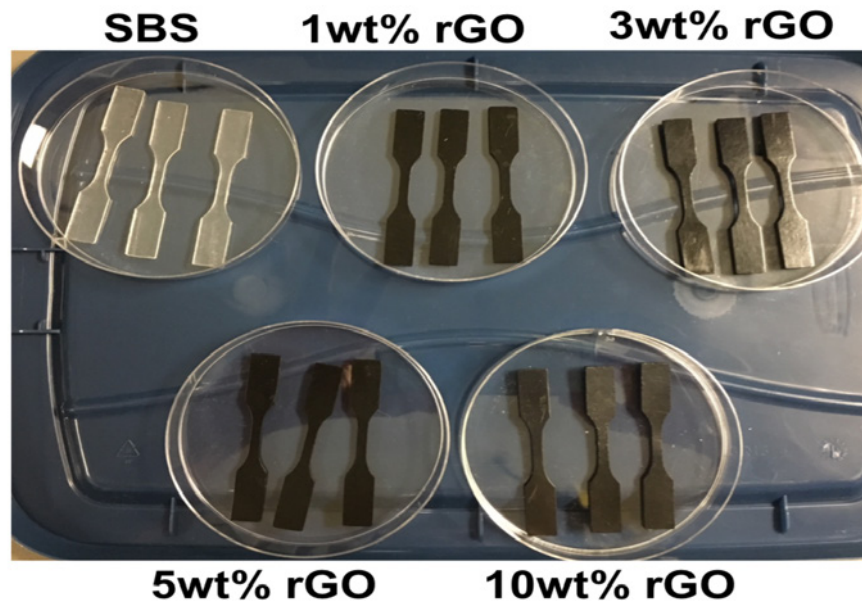


Figure VII.1.4. SBS samples filled with rGO at several weight contents

The wear resistance of composite SBS-GO elastomers was evaluated using a Taber 5135 rotary platform abrasion tester. Abrasive wear experiments were performed on samples turning against two abrading CS10 wheels at 60 rpm. The samples were subjected to 100 consecutive abrading cycles. Scanning electron microscopy and atomic force microscopy techniques were used to characterize the abraded surface of the unfilled SBS and SBS-GO samples. Scanning electron microscopy images of the abraded SBS and SBS-GO surfaces are shown in Figure VII.1.5. The unfilled SBS surface was abraded significantly. SBS fragments were detached from the surface and are aggregated on the surface of the sample. The abrasion of the SBS-GO was minimal. The surface indentations are shallow (a few micrometers in depth). The graphene fillers improved the wear resistance of the composite elastomer. This can be attributed to the strong interactions between the polymer elastomer matrix and the filler material.

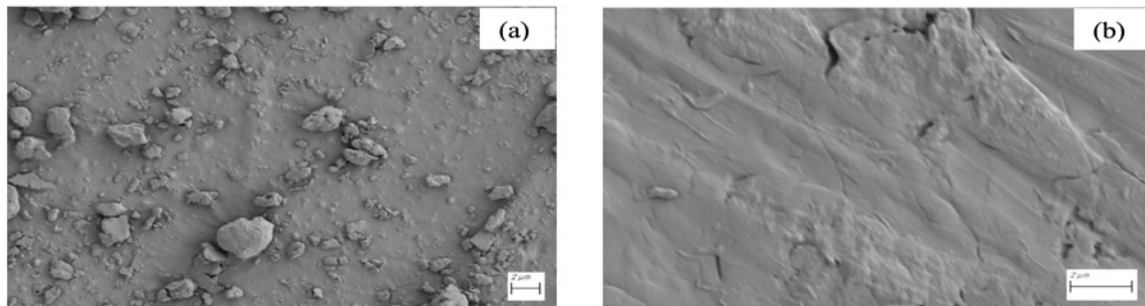


Figure VII.1.5. Scanning electron microscopy images of the abraded surface of (a) unfilled SBS and (b) SBS-GO samples after 100 abrading cycles

Conclusions

The reinforcement of the elastomer is associated with the good dispersion of the filler material. The optimum dispersion was achieved using liquid mixing in solvent followed by ultrasonic agitation.

- The maximum Modulus improvement was approximately one order of magnitude according to nano-indentation and tensile measurements.
- The graphene fillers improved the wear resistance of the composite elastomer. This can be attributed to the strong interactions between the polymer elastomer matrix and the filler material.

Key Publications

1. U.S. Patent Application entitled “Nanocomposite Additives Based on Graphene Sheets and Silica Nanofibers.” Serial No. 16/000,975. Filed: June 6, 2018.
2. Voylov, D.N., V. Bocharova, N. Lavrik, I. Vlassiuk, G. Polizos, A. Volodin, Y.M. Shulga, A. Kisliuk, T. Thiyagarajan, D.D. Miller, R. Narayanan, B.G. Sumpter, and A.P. Sokolov. “Noncontact Mode Tip-Enhanced Raman Spectroscopy: Applications and Prospects.” (Under review).
3. One publication in preparation.

References

1. Carpenter, J.A. Jr., J. Gibbs, A.A. Pesaran, L.D. Marlina, and K. Kelly. 2008. “Road Transportation Vehicles.” *MRS Bulletin* 33: 439–444.
2. Lindemuth, B.E. 2006. “An Overview of Tire Technology.” Chapter 1 in *The Pneumatic Tire*. U.S. Department of Transportation, National Highway Traffic Safety Administration, February 2006.
3. Markel, T., A. Brooker, V. Johnson, K. Kelly, M. O’Keefe, S. Sprik, and K. Wipke. 2002. “ADVISOR: A Systems Analysis Tool for Advanced Vehicle Modeling.” *J. Power Sources* 110: 255–266.
4. California Energy Commission, Fuel-Efficient Tires and CEC Proceeding Documents Page, www.energy.ca.gov/transportation/tire_efficiency/documents/index.html (accessed January 2008).

Acknowledgements

The author acknowledges Jaehyeung Park and Jaswinder Sharma of Oak Ridge National Laboratory for their contributions to this project.

VII.2 Advanced Non-Tread Materials for Fuel-Efficient Tires (PPG Industries, Inc.)

Lucas Dos Santos Freire, Sr., Principal Investigator

PPG Industries, Inc.
440 College Park Dr.
Monroeville, PA
E-mail: dossantosfreire@ppg.com

Gurpreet Singh, DOE Program Manager

U.S. Department of Energy
E-mail: Gurpreet.Singh@ee.doe.gov

Start Date: October 1, 2016	End Date: September 30, 2019	
Project Funding: \$1,143,464	DOE share: \$914,771	Non-DOE share: \$228,693

Project Introduction

Precipitated silica is an amorphous particle produced commercially by the acid neutralization of a sodium silicate solution. It is primarily used as a reinforcing filler for synthetic rubber tires. Amorphous silica is known to provide a variety of benefits in tire rubber compounds, including the capability to significantly reduce rolling resistance when compared to carbon black (CB). Much emphasis has been placed on incorporating fuel-efficient silicas into tire tread compounds since the tread is often the single largest contributor to fuel consumption. However, although approximately 50% of the fuel-efficiency impact of a tire is ascribed to the tread, the remaining 50% is attributed to the energy dissipation of non-tread components. Of the non-tread tire components, roughly 20% of the energy losses are attributed to the sidewall, in many cases making it the next largest contributor to fuel-efficiency after the tread. For this reason, the sidewall is an excellent candidate to evaluate new reinforcing materials for non-tread compounds.

Agilon® silicas are a new generation of pre-treated silicas which can overcome the problem of mixing silicas with natural rubber (NR), the main rubber in non-tread compounds. These silicas have been shown to provide dramatic improvements in rolling resistance compared to CB in NR-based compounds. The work in this area has been published and presented in industry magazines, conferences, and the 2017 and 2018 DOE Annual Merit Review and has been well received [1,2,3,4]. In this work, we will develop sidewall compounds containing non-treated and treated silica fillers. While the main objective is to improve rolling resistance, performance parameters relevant to non-tread components have to be taken into account. Ozone resistance, additives migration, and conductivity are some of the parameters that are taken into account in this project.

Objectives

The objective of the project is to develop a new silica filler that can increase tire fuel efficiency by 2% while maximizing key performance properties in non-tread tire components compared to current CB-filled sidewall compounds. To achieve these goals, the developed compounds will be required to maintain or improve resistance to degradative forces while reducing compound hysteresis by approximately 25%.

Overall Objectives

- Predictive model that maps reinforcing filler characteristics to trends in sidewall performance
- Model sidewall compound that exhibits at least a 25% reduction in energy loss compared to CB, with no more than a 5% loss of resistance to degradative forces (targeting better performance)

Fiscal Year 2018 Objectives

- Develop a database with custom-made silica fillers to enable statistical analysis of the results
- Identify the surface chemistry and morphology variables that optimize the wide range of required sidewall performance metrics

Approach

The first step of this project was to understand the tradeoffs in performance of different commercially available materials in model sidewall compounds and identify trends toward improved fuel-efficiency indicators and resistance to degradative forces. This was performed by systematically selecting representative commercial silica and CB fillers to provide a significant range in filler morphology and surface chemistry, and then evaluating their performance in a model sidewall formulation. Akron Rubber Development Laboratory, Inc., facilities were used to perform certain sidewall-specific tests, such as ozone resistance and antioxidants migration.

During the last year, similar systematic studies varying the silica morphology and surface chemistry were performed. First, a series of silica fillers with a wide range of known silica reactants was prepared and evaluated. Then, selected chemistries were used to synthesize silica prototypes with different morphologies, which were also evaluated. Finally, the model sidewall compound will be optimized during the final year of the project, together with the optimum filler developed to achieve the final project goal of developing a compound with 25% reduction in energy loss while maintaining other compound properties similar to the CB control.

Results

Earlier, ten commercial reinforcing fillers (three CBs, four non-functionalized precipitated silicas, and three functionalized precipitated silicas) were compounded in a model sidewall formulation, and results were analyzed to establish a baseline performance of compounds containing commercially available fillers. During the last year, ten prototype silica samples, pretreated with different chemical treatments, were synthesized and compounded in a model sidewall formulation. The silicas were treated with a variety of industry-standard silanes as the coupling agents. The selected chemistries were reacted onto the silica surface, holding the morphology constant, using the Agilon® treatment process. Compounding was performed using a 1.25 L internal mixer with two wing tangential rotors. The model formulation comprised a 50/50 blend of NR and polybutadiene. The total filler loading was 50 phr. These compounds were evaluated for:

- Energy loss as measured by hysteresis ($\tan \delta$), loss modulus, and heat build-up;
- Resistance to degradative forces as measured by fatigue to failure, crack growth, tear strength, and ozone resistance;
- Impact on the extraction/migration/diffusion characteristics of a widely-used anti-degradant protection package; and
- Additional important criteria including measurements of processing, extrusion, curing, and filler dispersion.

Selected data is summarized in Table VII.2.1. There are small differences among the fillers, but these differences can be used to select the best filler for the next step of the project. The fillers TO0517-1, -2, -8, -9, and -10 show a small advantage in hysteresis ($\tan \delta$ at 60°C) over the other prototypes. This is critical to achieve the rolling resistance goal of the project. Some of these silicas also show good dispersion (>80%) and hardness. Cycles to failure on the flex fatigue test is also an important parameter for sidewall compounds, since these compounds are constantly subjected to cyclic loads through the operation of a tire. TO0517-2 has the best resistance of all the compounds. Most of the other properties in Table VII.2.1, such as tensile strength, elongation, viscosity, etc., are comparable for all the samples.

This energy loss/fuel-efficiency improvement cannot be obtained at the expense of resistance to degradative forces. Processing and extrusion performance are additional important criteria that were determined. The results, not shown here, did not raise any concerns for the silica prototypes. This type of data will be discussed later when discussing the final silica prototype selected to move forward for the following year of the project. The information shown in Table VII.2.1 was used to select the chemical treatment to proceed to the next part for the project. Based on Table VII.2.1 and the processing and degradation resistance data not shown, filler TO0517-2 was selected because it seems to show the best balance of properties. It provides the best hysteresis and flex fatigue of all the fillers, and at the same time, it did not show any significant deficiencies in any of the parameters measured.

Table VII.2.1. Compound Data of Silica Prototypes with Different Surface Treatments

	T00517-1	T00517-2	T00517-3	T00517-4	T00517-5	T00517-6	T00517-7	T00517-8	T00517-9	T00517-10
S'max (in-lbs)	10.1	10.0	10.5	9.8	9.5	8.2	8.2	8.2	9.4	9.3
S'min (in-lbs)	1.3	1.3	1.3	1.3	1.3	1.2	1.2	1.3	1.2	1.1
ΔS (in-lbs)	8.8	8.7	9.2	8.6	8.2	7	7	6.9	8.2	8.2
T50 (min)	3.9	3.8	8.7	8.8	8.2	7.7	8.1	7.5	6.6	5.8
ML1+4	40	40	39	41	41	41	40	40	40	36
Stress (psi)	3,008	2,969	2,891	2,962	2,920	2,931	2,917	2,910	2,866	2,984
Strain (%)	714	720	723	768	760	783	786	783	731	755
300% mod. (psi)	835	776	767	670	683	598	626	626	669	623
Hardness	55	55	57	54	55	52	51	51	53	52
Dispersion (%)	83	82	88	88	67	80	76	77	82	69
G' @60°C, MPa	1.64	1.62	1.7	1.73	1.65	1.49	1.42	1.3	1.53	1.51
tan (δ) @ 60°C	0.115	0.114	0.121	0.133	0.131	0.137	0.126	0.115	0.116	0.112
tan (δ) @ 0°C	0.176	0.176	0.184	0.199	0.201	0.199	0.191	0.193	0.194	0.191
G' @30°C, MPa	2.39	2.59	3.07	3.27	2.55	2.57	2.36	2.26	2.65	2.65
Tear strength	39	41	46	48	43	45	51	38	48	36
Flex fatigue (cycles to failure)	162,800	187,500	162,500	154,600	106,900	169,400	131,600	126,600	102,000	164,500

Once the best surface treatment was selected, six silica prototypes treated with the treatment used in T00517-2 were prepared, varying the silica morphology. Mainly, variations in silica surface area, porosity, and pore size distribution were explored. The silica samples were compounded in the same sidewall model formulation, and compound data is shown in Table VII.2.2. Also, a control compound containing N550 CB was used in the study. LD0632-3 shows the lowest hysteresis of all the compounds. The six silica samples have comparable mechanical properties (tensile strength and elongation), viscosity, cure parameters, and hardness. There is some variation in tear strength among the prototypes. When comparing to the CB control, all parameters are comparable, except that the silica compounds have slightly higher hardness and dynamic stiffness (G'). This can be adjusted in the next stage of the project. Also, while LD0623-2 has tear strength close to the CB control, the rest of the compounds have lower tear strength. This can also be improved later, when reducing the hardness of the compounds through compound optimization.

Parameters related to the resistance of the compounds to degradation are shown in Table VII.2.3. It can be seen that all silica compounds have better flex fatigue resistance than the CB control. The hardness after aging remains slightly higher than the CB control. Furthermore, the mechanical properties measured after applying different aging protocols are slightly better than the CB control, similarly to before aging. Because of this, there are no concerns that any of these silica prototypes would have any significant problems after aging.

Table VII.2.2. Compound Data of Silica Prototypes with Different Morphologies

	N550	LD0632-1	LD0623-2	LD0632-3	LD0632-6	LD0632-7	LD0632-8
S'max (in-lbs)	7.7	8.8	8.6	9.3	9.0	9.4	7.3
S'-min (in-lbs)	1.2	1.1	1.2	1.1	1.2	1.3	1.1
ΔS (in-lbs)	6.6	7.6	7.3	8.1	7.8	8.1	6.2
T50 (min)	6.4	4.6	4.7	4.6	4.7	4.9	4.6
T90 (min)	12.4	9.3	9.5	9.2	9.6	9.7	9.5
Tensile strength (psi)	2,655	2,903	3,022	2,886	2,889	2,887	2,683
Elongation (%)	743	716	749	683	701	692	783
100% mod. (psi)	199	208	199	213	205	214	163
300% mod. (psi)	862	818	760	845	800	803	532
Hardness	53	56	56	57	56	58	54
tan δ at 5%	0.196	0.181	0.182	0.171	0.178	0.176	0.181
G' @ 30 °C (MPa)	1.27	1.53	1.56	1.56	1.52	1.53	1.43
Tear strength (M/mm)	211	154	198	120	144	138	150

The effect of the filler selection on migration of the antioxidant (N-(1,3-dimethylbutyl)-N'-phenyl-p-phenylenediamine, 6-PPD) and wax in the compound was also studied, and the diffusion constants for 6-PPD and wax were determined. This was performed because the silica introduced in place of CB can interact with the antioxidant package and affect the degradation of the compound. To perform these experiments, two rubber compounds were prepared, consisting on the model sidewall compound with and without antioxidants. A two-layer laminate comprised of a 0.25 in thick layer of the compound with 6-PPD and wax was placed next to a 0.25 in layer of the compound without 6-PPD and wax. The 6-PPD concentration was measured after curing at 160°C for 19 min and, subsequently, after aging 36 d at 50°C. A scheme showing how this experiment was set up for the measurement of concentrations at different places in the laminate is shown in Figure VII.2.1. The diffusion coefficients were measured for 6-PPD using the measured concentration gradient after curing and after aging. Diffusion coefficients during curing and aging were determined based on the concentration profiles measured. Table VII.2.3 shows that a silica, such as LD0623-3, can slow down the migration of 6-PPD and wax during curing, which is a desirable property. Later, during service, the antioxidants still have a good migration rate to protect the tire.

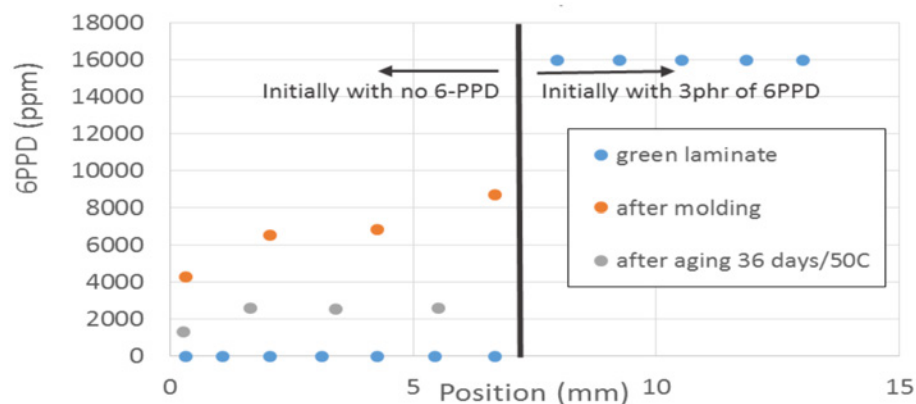


Figure VII.2.1. Example of sampling data for determination of diffusion coefficients

Table VII.2.3. Resistance to Degradation of Silica Prototypes with Different Morphologies

	N550	LD0632-1	LD0623-2	LD0632-3	LD0632-6	LD0632-7	LD0632-8
Flex fatigue (cycles to failure)	105,180	192,400	147,560	156,200	113,120	167,160	105,200
Hardness after ozone aging	56	60	60	60	59	59	57
Tensile strength after ozone aging (psi)	2,654	2,913	2,975	2,797	2,909	2,917	2,561
Elongation after ozone aging (%)	637	595	629	575	599	613	641
Dynamic belt flex aging, stress (psi)	1,767	2,250	1,974	1,839	1,817	1,905	1,743
Dynamic belt flex aging, strain (%)	517	568	532	468	483	476	507
Dynamic tension after ozone aging, stress (psi)	1,807	1,955	2,030	2,060	2,134	2,106	1,900
Dynamic tension after ozone aging, elongation (%)	483	492	500	469	490	486	544
Crack growth rate	2.4	10.7	10.8	12.3	9.8	11.8	7.5
Crack growth, crack length after 80 h in ozone (mm)	1.94	4.33	4.19	2.42	3.41	2.9	2.3
6-PPD diff. coeff. during molding (1/m ² -min)	0.17	0.16	0.19	0.10	0.25	0.42	0.24
Wax diff. coeff. during molding (1/m ² -min)	0.30	0.28	0.31	0.24	0.25	0.36	0.32
6-PPD diff. coeff. during aging (1/m ² -min)	0.12	0.31	0.088	0.42	0.64	~0	0.55
Wax diff. coeff. during aging (1/m ² -min)	0.69	0.61	0.73	0.77	0.90	0.52	0.61

Conclusions

A range of silica prototypes with variations in surface chemistry and morphologies were prepared and tested in a model sidewall rubber compound. Traditional performance parameters were determined, as well as parameters related to resistance to compound degradation. The experimental plan allowed:

- Identification of the surface chemistry and morphology variables that optimize the wide range of required sidewall performance metrics.
- Development of a database with custom-made silica fillers and their compound performance.
- Development and evaluation of different tools to determine compound degradation performance.

The data generated showed that silica technology including surface functionalization shows promise in producing an improved overall performance balance, with lower hysteresis than CB compounds, while maintaining the resistance to degradation.

References

1. Okel, Tim, and Justin Martin. 2014. "Innovating the Silica Surface for Improved NR Truck Tire Vulcanisates." Presentation at Tire Technology International, Cologne, Germany, February 2014.
2. Okel, Tim, and Justin Martin. 2014. "Functionalized Silicas for Improved NR Truck Tire Vulcanisates." *Rubber World* 249 (2): 19–24.
3. Okel, Tim, and Justin Martin. 2013. "Bringing Innovation to the Surface: Functionalized Silicas for Improved Natural Rubber Truck Tire Vulcanisates." 184th Technical Meeting of the American Chemical Society Rubber Division, October 2013, paper #33.
4. Okel, Tim, et al. 2011. "Agilon Performance Silicas in Natural Rubber Truck Tire Tread Compounds." 180th Technical Meeting of the American Chemical Society Rubber Division, October 2011, paper #70.

VIII. Index of Principal Investigators

A

Agrawal, Ajay	I.21, II.29
Amar, Pascal	V.1
Arienti, Marco	II.8

B

Battiston, Paul	V.7
Bays, Tim	II.22
Briggs, Tom	III.4
Busch, Stephen	I.1

C

Carrington, David	I.15
Confer, Keith	V.6
Curran, Scott	II.9

D

Dec, John	I.4, II.7
Denton, Mark	III.7
Dos Santos Freire, Lucas	VII.2

E

Edwards, Dean	I.16
Ekoto, Isaac	I.5
Erdemir, Ali	VI.1

F

Farrell, John	II.1
Fernandez, Hermes	V.10
Fioroni, Gina	II.17
Freitag, Alex	III.2

G

Gangopadhyay, Arup	VI.1
Gaspar, Dan	II.1
Genzale, Caroline	I.24

Goldsborough, Scott	I.8, II.15
Grout, Ray.....	II.20, II.21
H	
Haworth, Dan	I.17
Hergart, Carl.....	V.5
Hsu, Stephen	VI.2
K	
Kim, Seung Hyun.....	I.22
Kocher, Lyle.....	V.8
Kokjohn, Sage.....	I.20
Kolodziej, Chris	I.9, II.14
L	
Lavoie, George.....	II.30
Lawler, Ben.....	III.1
Lee, Chia-Fon	I.18
Lee, Seong-Young.....	I.19
M	
McNenly, Matt	II.27
Moen, Chris.....	II.1
Moses-DeBusk, Melanie.....	II.24
Mueller, Charles.....	II.16
Mueller, Juliane.....	II.21
Musculus, Mark	I.2
N	
Northrop, William	IV.9
P	
Parks, Jim.....	IV.4
Partridge, Bill.....	IV.5
Pfefferle, Lisa.....	II.32
Pickett, Lyle	I.3, II.6
Pihl, Josh.....	II.23, IV.1

Pitz, William J.....	I.13, II.25, II.26
Polyzos, Georgios	VII.1
Powell, Christopher F.....	I.7, I.24, II.13
R	
Rappé, Ken.....	IV.8
Ratcliff, Matt.....	II.19
Rockstroh, Toby	II.12
Rothamer, David	IV.6
Ruth, Michael.....	V.2
Ryan, Emily	I.23
S	
Scarcelli, Riccardo	I.10
Schaedler, Tobias	V.11
Schoegl, Ingmar	II.31
Sick, Volker	I.17
Sjöberg, Magnus	II.5
Sluder, Scott	II.2
Sokolsky, Steve.....	III.3
Som, Sibendu	I.6, I.18, I.21, II.28
Splitter, Derek	II.10, II.11
Stewart, Mark.....	IV.6
Szybist, Jim.....	I.11, I.17, II.3, II.4, III.5
T	
Toops, Todd.....	IV.3
W	
Wagner, Robert	II.1, V.10
Wang, Yong	IV.2, IV.7
Whitaker, Richard	III.3
Whitesides, Russell	I.14
Wissink, Martin.....	I.12

X

Xuan, Yuan..... II.32

Y

Yee, JustinV.4

Yun, HanhoV.9

Z

Zigler, Brad II.18, III.6

Zukouski, Russ.....V.3

IX. Project Listings by Organizations

Argonne National Laboratory

I.6	Advancements in Fuel Spray and Combustion Modeling with High Performance Computing Resources	68
I.7	Fuel Injection and Spray Research Using X-Ray Diagnostics	75
I.8	RCM Studies to Enable Gasoline-Relevant Low Temperature Combustion	81
I.9	Advances in High Efficiency Gasoline Compression Ignition	88
I.10	Advanced Ignition Systems for Gasoline Direct Injection (GDI) Engines.....	93
I.18	Model Development for Multi-Component Fuel Vaporization and Flash Boiling	141
I.21	Development and Validation of Physics-Based Submodels of High Pressure Supercritical Fuel Injection at Diesel Conditions	160
I.24	Turbulent Spray Atomization Model for Diesel Engine Simulations	178
II.12	Fuel Properties Enhancing Multi-Mode ACI/SI Engine Operation	253
II.13	X-Ray Imaging of GDI Sprays with Alcohol Blends	259
II.14	Fuel Properties Effects on Auto-Ignition in Internal Combustion Engines	263
II.15	RCM for Kinetic Mechanism Development	270
II.28	Engine Simulations in Support of Co-Optima	347
VI.1	Power Cylinder Friction Reduction through Coatings, Surface Finish, and Design	530

Blossman Services, Inc

III.7	Direct Injection 4.3-L Propane Engine Research Development and Testing	406
-------	--	-----

Boston University

I.23	Development and Multiscale Validation of Euler-Lagrange-Based Computational Methods for Modeling Cavitation within Fuel Injectors	172
------	---	-----

CALSTART

III.3	Innovative Dual Fuel Aftermarket Emissions Solution	389
-------	---	-----

Cummins Inc.

V.2	Cummins/Peterbilt SuperTruck II	473
V.8	Cummins 55% BTE Project	510

Daimler Trucks North America

V.4	Improving Transportation Efficiency through Integrated Vehicle, Engine, and Powertrain Research – SuperTruck 2	484
-----	--	-----

Delphi Technologies, PLC

V.6	Ultra-Efficient Light-Duty Powertrain with Gasoline Low-Temperature Combustion	497
V.10	Solenoid Actuated Cylinder Deactivation Valve Train for Dynamic Skip Fire	519

Ford Motor Company

VI.1	Power Cylinder Friction Reduction through Coatings, Surface Finish, and Design	530
------	--	-----

General Motors LLC

V.7	Lean Miller Cycle System Development for Light-Duty Vehicles.....	504
V.9	A High Specific Output Gasoline Low-Temperature Combustion Engine.....	514

George Washington University

VI.2	Integrated Friction Reduction Technology to Improve Fuel Economy Without Sacrificing Durability	535
------	---	-----

Georgia Institute of Technology

I.24	Turbulent Spray Atomization Model for Diesel Engine Simulations	178
------	---	-----

HRL Laboratories, LLC

V.11	Temperature-Following Thermal Barrier Coatings for High-Efficiency Engines	525
------	--	-----

Lawrence Berkeley National Laboratory

II.21	Scenario Co-Optimizer	309
-------	-----------------------------	-----

Lawrence Livermore National Laboratory

I.13	Chemical Kinetic Models for Advanced Engine Combustion	111
I.14	Model Development and Analysis of Clean and Efficient Engine Combustion.....	116
II.25	Kinetic Mechanism Development	331
II.26	Fuel Property Blending Model	336
II.27	Virtual Properties, Reduced Mechanism, Blending of Kinetics Properties, and Modeling of Fuel Properties	341

Los Alamos National Laboratory

I.15	2018 FEARCE Development: A Robust and Accurate Engine Modeling Software	121
------	---	-----

Louisiana State University

II.31	Micro-liter Fuel Characterization and Property Prediction	362
-------	---	-----

Michigan Technological University

I.19	Spray–Wall Interaction at High-Pressure and High-Temperature Conditions.....	146
------	--	-----

National Renewable Energy Laboratory

II.1	Co-Optima.....	183
II.17	Flow Reactor Autoignition Kinetic Mechanism Development and Validation and Understanding How Fuels Blend for Autoignition	282
II.18	Fuel Autoignition Behavior	288
II.19	Modification of PMI to Include Oxygenate Effects.....	294
II.20	Virtual Properties, Reduced Mechanism, Blending of Kinetics Properties, and Modeling of Fuel Properties	305
II.21	Scenario Co-Optimizer	309
III.6	Direct Injection Propane for Advanced Combustion.....	401

Navistar, Inc

V.3 Development and Demonstration of a Fuel-Efficient Class 8 Tractor and Trailer SuperTruck..... 478

NG1 Technologies

III.3 Innovative Dual Fuel Aftermarket Emissions Solution 389

Oak Ridge National Laboratory

I.11 Stretch Efficiency for Combustion Engines: Exploiting New Combustion Regimes..... 99

I.12 Neutron Imaging of Advanced Transportation Technologies 105

I.16 Accelerating Predictive Simulation of Internal Combustion Engines with High Performance Computing..... 129

I.17 Development and Validation of Predictive Models for In-Cylinder Radiation and Wall Heat Transfer 135

II.1 Co-Optima 183

II.2 Engine Efficiency Potential of High-Octane Renewable Fuels in Multi-Cylinder Engines 190

II.3 Developing a Better Understanding of Octane Index 196

II.4 Characterizing BOB Impacts and Limits within Octane Index 203

II.9 Multi-Mode SI/ACI: Stratification/Fuel/Dilute 235

II.10 Fuel Effects on Low Speed Pre-Ignition 240

II.11 Fuel Property Effects on Abnormal Combustion..... 246

II.23 Fuel Impacts on Emissions Control Performance and Durability 319

II.24 Fuel Impacts on ACI PM Formation 325

III.5 Improving the Fundamental Understanding of Opportunities Available from Direct Injected Propane in Spark Ignited Engines 395

IV.1 Joint Development and Coordination of Emission Control Data and Models: Cross-Cut Lean Exhaust Emissions Reduction Simulations (CLEERS) Analysis and Coordination 412

IV.3 Low-Temperature Emission Control to Enable Fuel-Efficient Engine Commercialization..... 426

IV.4 Emissions Control for Lean-Gasoline Engines 432

IV.5 Cummins-ORNL SmartCatalyst CRADA: NO_x Control and Measurement Technology for Heavy-Duty Diesel Engines 437

VII.1 Improved Tire Efficiency through Elastomeric Polymers Enhanced with Carbon-Based Nanostructured Materials 539

PACCAR Inc.

V.5 Development and Demonstration of Advanced Engine and Vehicle Technologies for Class 8 Heavy-Duty Vehicle – SuperTruck II 490

Pacific Northwest National Laboratory

II.1	Co-Optima.....	183
II.22	Fuel Property Blending Model	313
IV.2	CLEERS Aftertreatment Modeling and Analysis	419
IV.6	Fuel-Neutral Studies of PM Transportation Emissions	443
IV.7	Advanced Emission Control for High-Efficiency Engines	449
IV.8	Development and Optimization of Multi-Functional SCR-DPF Aftertreatment for Heavy-Duty NO _x and Soot Emission Reduction	454

PPG Industries, Inc.

VII.2	Advanced Non-Tread Materials for Fuel-Efficient Tires	544
-------	---	-----

Robert Bosch, LLC

III.2	High-Efficiency Cost-Optimized Spark-Ignited Natural Gas (HECO-SING) Engines–2018	381
-------	---	-----

Sandia National Laboratories

I.1	Light- and Medium-Duty Diesel Combustion	30
I.2	Heavy-Duty Low-Temperature and Diesel Combustion and Heavy-Duty Combustion Modeling	36
I.3	Spray Combustion Cross-Cut Engine Research	45
I.4	Low-Temperature Gasoline Combustion (LTGC) Engine Research	51
I.5	Gasoline Combustion Fundamentals	60
II.1	Co-Optima	183
II.5	Advanced Light-Duty SI Engine Fuels Research	209
II.6	Effect of Properties/Injection Schedule on Fuel Spray Mixing	216
II.7	Low-Temperature Gasoline Combustion (LTGC) Engines: Fuel Effects and Fuel Co-Optimization	221
II.8	Thermophysical Property Impact on Spray Formation.....	229
II.16	Mixing-Controlled Compression-Ignition Combustion and Fuel-Effects Research: Ducted Fuel Injection	277

Southwest Research Institute

III.4	Reduced Petroleum Use through Easily-Reformed Fuels and Dedicated Exhaust Gas Recirculation	392
-------	---	-----

Stony Brook University

III.1	Single-Fuel Reactivity Controlled Compression Ignition Combustion Enabled by Onboard Fuel Reformation	375
-------	---	-----

The Ohio State University

I.22	Development of a Physics-Based Combustion Model for Engine Knock Prediction	166
------	---	-----

The Pennsylvania State University

I.17 Development and Validation of Predictive Models for In-Cylinder Radiation and Wall Heat Transfer 135

II.32 The Development of Yield-Based Sooting Tendency Measurements and Modeling to Enable Advanced Combustion Fuels 368

The University of Alabama

I.21 Development and Validation of Physics-Based Submodels of High Pressure Supercritical Fuel Injection at Diesel Conditions..... 160

II.29 Characterization of Biomass-Based Fuels and Fuel Blends for Low-Emissions, Advanced Compression Ignition Engines 353

Tula Technology, Inc.

V.10 Solenoid Actuated Cylinder Deactivation Valve Train for Dynamic Skip Fire 519

University of Illinois at Urbana-Champaign

I.17 Development and Validation of Predictive Models for In-Cylinder Radiation and Wall Heat Transfer 135

I.18 Model Development for Multi-Component Fuel Vaporization and Flash Boiling 141

University of Michigan

II.30 Dynamic Species Reduction for Multi-Cycle CFD Simulations 358

University of Minnesota

IV.9 Enabling Lean and Stoichiometric Gasoline Direct Injection Engines through Mitigation of Nanoparticle Emissions 460

University of Wisconsin

I.20 Development and Validation of a Lagrangian Soot Model Considering Detailed Gas Phase Kinetics and Surface Chemistry..... 154

IV.6 Fuel-Neutral Studies of PM Transportation Emissions 443

Volvo Group Trucks North America

V.1 Volvo SuperTruck 2: Pathway to Cost-Effective Commercialized Freight Efficiency..... 467

Yale University

II.32 The Development of Yield-Based Sooting Tendency Measurements and Modeling to Enable Advanced Combustion Fuels 368

(This page intentionally left blank)

U.S. DEPARTMENT OF
ENERGY

Office of
**ENERGY EFFICIENCY &
RENEWABLE ENERGY**

For more information, visit:
energy.gov/eere/vehicles

DOE/EE-1833 April 2019